

IntechOpen

Trends in Telecommunications Technologies

Edited by Christos J Bouras



**TRENDS IN TELECOMMUNICATIONS
TECHNOLOGIES**

Edited by
CHRISTOS J. BOURAS

Trends in Telecommunications Technologies

<http://dx.doi.org/10.5772/180>

Edited by Christos J Bouras

© The Editor(s) and the Author(s) 2010

The moral rights of the and the author(s) have been asserted.

All rights to the book as a whole are reserved by INTECH. The book as a whole (compilation) cannot be reproduced, distributed or used for commercial or non-commercial purposes without INTECH's written permission.

Enquiries concerning the use of the book should be directed to INTECH rights and permissions department (permissions@intechopen.com).

Violations are liable to prosecution under the governing Copyright Law.



Individual chapters of this publication are distributed under the terms of the Creative Commons Attribution 3.0 Unported License which permits commercial use, distribution and reproduction of the individual chapters, provided the original author(s) and source publication are appropriately acknowledged. If so indicated, certain images may not be included under the Creative Commons license. In such cases users will need to obtain permission from the license holder to reproduce the material. More details and guidelines concerning content reuse and adaptation can be found at <http://www.intechopen.com/copyright-policy.html>.

Notice

Statements and opinions expressed in the chapters are those of the individual contributors and not necessarily those of the editors or publisher. No responsibility is accepted for the accuracy of information contained in the published chapters. The publisher assumes no responsibility for any damage or injury to persons or property arising out of the use of any materials, instructions, methods or ideas contained in the book.

First published in Croatia, 2010 by INTECH d.o.o.

eBook (PDF) Published by IN TECH d.o.o.

Place and year of publication of eBook (PDF): Rijeka, 2019.

IntechOpen is the global imprint of IN TECH d.o.o.

Printed in Croatia

Legal deposit, Croatia: National and University Library in Zagreb

Additional hard and PDF copies can be obtained from orders@intechopen.com

Trends in Telecommunications Technologies

Edited by Christos J Bouras

p. cm.

ISBN 978-953-307-072-8

eBook (PDF) ISBN 978-953-51-5877-6

We are IntechOpen, the world's leading publisher of Open Access books Built by scientists, for scientists

4,200+

Open access books available

116,000+

International authors and editors

125M+

Downloads

151

Countries delivered to

Our authors are among the
Top 1%

most cited scientists

12.2%

Contributors from top 500 universities



WEB OF SCIENCE™

Selection of our books indexed in the Book Citation Index
in Web of Science™ Core Collection (BKCI)

Interested in publishing with us?
Contact book.department@intechopen.com

Numbers displayed above are based on latest data collected.
For more information visit www.intechopen.com



Meet the editor



Christos Bouras is Professor in the University of Patras, Department of Computer Engineering and Informatics. Also he is a scientific advisor of Research Unit 6 in Computer Technology Institute and Press - Diophantus, Patras, Greece. His research interests include Analysis of Performance of Networking and Computer Systems, Computer Networks and Protocols, Mobile and Wireless Communications, Telematics and New Services, QoS and Pricing for Networks and Services, e-learning, Networked Virtual Environments and WWW Issues. He has extended professional experience in Design and Analysis of Networks, Protocols, Telematics and New Services. He has published more than 450 papers in various well-known refereed books, conferences and journals. He is a co-author of 9 books in Greek and editor of 2 in English. He has been member of editorial board for international journals and PC member and referee in various international journals and conferences. He has participated in R&D projects.

Preface

This book is the culmination of an effort to gather world-class scientists, engineers and educators engaged in the fields of telecommunications to meet and present their latest activities. Telecommunication is the assisted transmission of signals over a distance for the purpose of communication. Having drastically transformed the human way of living, telecommunications are considered the revolution of our times, and the catalyst for present and future technological and scientific developments. Being a very active research field, new advances in telecommunications are constantly changing the landscape and introduce new capabilities and enhanced ways of communication. Literature in the field is extensive and constantly enlarged. This book therefore intends to increase the dissemination level of the latest research advances and breakthroughs by making them available to a wide audience in a compact and friendly to the user way. It furthermore aims to provide a particularly good way for experts in one aspect of the field to learn about advances made by their colleagues with different research interests.

The main focus of the book is the advances in telecommunications modeling, policy, and technology. In particular, several chapters of the book deal with low-level network layers and present issues in optical communication technology and optical networks, including the deployment of optical hardware devices and the design of optical network architecture. Wireless networking is also covered, with a focus on WiFi and WiMAX technologies. The book also contains chapters that deal with transport issues, and namely protocols and policies for efficient and guaranteed transmission characteristics while transferring demanding data applications such as video. Finally, the book includes chapters that focus on the delivery of applications through common telecommunication channels such as the earth atmosphere.

This book is useful for researchers working in the telecommunications field, in order to read a compact gathering of some of the latest efforts in related areas. It is also useful for educators that wish to get an up-to-date glimpse of telecommunications research and present it in an easily understandable and concise way. It is finally suitable for the engineers and other interested people that would benefit from an overview of ideas, experiments, algorithms and techniques that are presented throughout the book.

Bringing this book to the publication stage is the reward of the effort put by the editors, contributors and reviewers of all the presented chapters. We would therefore like to acknowledge the valuable contributions of all the authors of the chapters contained in this book, who decided to offer their insights and expertise in order to help assemble, in our opinion, a highly useful and quality book. We would also like to thank the publishing house, which supported this effort and helped make the result available to a wide audience all over the world.

Patras, 17th March, 2010

Christos J. Bouras
Professor
University of Patras and RACTI

Contents

Preface	IX
1. A Novel PFC Circuit for Three-phase utilizing Single Switching Device Keiju Matsui and Masaru Hasegawa	001
2. Advanced Modulation Formats and Multiplexing Techniques for Optical Telecommunication Systems Ghafour Amouzad Mahdiraji and Ahmad Fauzi Abas	013
3. A Survey on the Design of Binary Pulse Compression Codes with Low Autocorrelation Maryam Amin Nasrabadi and Mohammad Hassan Bastani	039
4. Virtual Multicast Petr Holub and Eva Hladká	063
5. The Asymmetrical Architecture of New Optical Switch Device Mohammad Syuhaimi Ab-Rahman and Boonchuan Ng	087
6. Adaptive Active Queue Management for TCP Friendly Rate Control (TFRC) Traffic in Heterogeneous Networks Rahim Rahmani and Christer Åhlund	109
7. Queues with session arrivals as models for optimizing the traffic control in telecommunication networks Sergey Dudin and Moon Ho Lee	123
8. Telecommunication Power System: energy saving, renewable sources and environmental monitoring Carmine Lubritto	145
9. Propagation Models and their Applications in Digital Television Broadcast Network Design and Implementation Armoogum V., Soyjaudah K.M.S., Mohamudally N. and Fogarty T.	165
10. Interference Modeling for Wireless Ad Hoc Networks Altenis V. Lima-e-Lima, Carlos E. B. Cruz Pimentel and Renato M. de Moraes	185

11. Energy Saving Drives New Approaches to Telecommunications Power System Rais Miftakhutdinov	201
12. Directional Routing Protocol in Wireless Mobile Ad Hoc Network L.A.Latiff, N. Fisal, S.A. Arifin and A. Ali Ahmed	235
13. Free Space Optical Technologies Davide M. Forin, G. Incerti, G.M. Tosi Beleffi, A.L.J. Teixeira, L.N. Costa, P.S. De Brito Andrè, B. Geiger, E. Leitgeb and F. Nadeem	257
14. Novel multiple access models and their probabilistic description Dmitry Osipov	297
15. Performance analysis of multi-server queueing system operating under control of a random environment Che Soong Kim, Alexander Dudin, Valentina Klimenok and Valentina Khramova	317
16. Interdomain QoS paths finding based on overlay topology and QoS negotiation approach Şerban Georgică Obreja and Eugen Borcoci	345
17. Dual Linearly Polarized Microstrip Array Antenna M. S. R Mohd Shah, M. Z. A Abdul Aziz, M. K. Suaidi and M. K. A Rahim	367
18. A Time-Delay Suppression Technique for Digital PWM Control Circuit Yoichi Ishizuka	389
19. Layer 2 Quality of Service Architectures Christos Bouras, Vaggelis Kapoulas, Vassilis Papapanagiotou, Leonidas Pouloupoulos, Dimitris Primpas and Kostas Stamos	399
20. Secrecy on the Physical Layer in Wireless Networks Eduard A. Jorswieck, AnneWolf, and Sabrina Gerbracht	413
21. Performance Analysis of Time-of-Arrival Mobile Positioning in Wireless Cellular CDMA Networks M. A.Landolsi, A. H. Muqaibel, A. S. Al-Ahmari, H.-R. Khan and R. A. Al-Nimnim	437
22. Mobility and Handoff Management in Wireless Networks Jaydip Sen	457
23. GPS Total Electron Content (TEC) Prediction at Ionosphere Layer over the Equatorial Region Norsuzila Ya'acob, Martina Abdullah and Mahamod Ismail	485
24. Performance Evaluation Methods to Study IEEE 802.11 Broadband Wireless Networks under the PCF Mode Vladimir Vishnevsky and Olga Semenova	509
25. Next Generation Optical Access Networks: from TDM to WDM Ll. Gutierrez, P. Garfias, M. De Andrade, C. Cervelló-Pastor and S. Sallent	537

26. Building energy efficiency design for telecommunication base stations in Guangzhou 561
Yi Chen, Yufeng Zhang and Qinglin Meng
27. Dynamic Space-Code Multiple Access (DSCMA) System: A Double Interference Cancellation Multiple Access Scheme in Wireless Communications System 583
Chee Kyun Ng, Nor Kamariah Noordin, Borhanuddin Mohd Ali, and Sudhanshu Shekhar Jamuar
28. Video Streaming in Evolving Networks under Fuzzy Logic Control 613
Martin Fleury, Emmanuel Jammeh, Rouzbeh Razavi, Sandro Moiron and Mohammed Ghanbari
29. The Development of Crosstalk-Free Scheduling Algorithms for Routing in Optical Multistage Interconnection Networks 643
Mohamed Othman, and Tg Dian Shahida Raja Mohd Auzar
30. Traditional float charges: are they suited to stationary antimony-free lead acid batteries? 665
T. M. Phuong Nguyen, Guillaume Dillenseger Christian Glaize and Jean Alzieu
31. Neighbor Discovery: Security Challenges in Wireless Ad hoc and Sensor Networks 693
Mohammad Sayad Haghghi and Kamal Mohamedpour
32. New Trends in Network Anomaly Detection 715
Yasser Yasami and Saadat Pourmozaffari
33. An Efficient Energy Aware Routing Protocol for Real Time Traffics in Wireless Sensor Networks 735
Amir Hossein Mohajerzadeh and Mohammad Hossein Yaghmaee
34. Quality of Service Differentiation in WiMAX Networks 753
Pedro Neves, Susana Sargento, Francisco Fontes, Thomas M. Bohnert and João Monteiro

A Novel PFC Circuit for Three-phase utilizing Single Switching Device

Keiju Matsui and Masaru Hasegawa
Chubu University
Japan

1. Introduction

For consumer or industrial applications, electrical appliances use various types of rectifier, which give rise to distorted input current due their non linear characteristics. Problems are created by the various harmonics, generated in the power system. Under such circumstances, IEC guideline was instituted ten and several years ago, and has recently been superseded.(JISC.2005). With the spread of the use of such nonlinear equipments, it is anticipated that we can not avoid the problems due to harmonics. With the relatively increased capacity of industry applications, PWM rectifiers can be expected to be used in three phase and single phase applications. (Takahashi. 1985, IEEJ Committee. 2000). Also in office environments, OA equipments, inverter type fluorescent lamps and inverter type air-conditioners are frequently used, surely bringing harmonic problems with them. Under such conditions, various new type PFC schemes are presented and discussed. (Takahashi.1900,Fujiwara.1991,Takeuchi2005). Methods intending to improve the current towards a sinusoidal waveform by using switching devices will incur high cost performance and yet troublesome noise problems. Certain applications require a switch-less scheme to maintain the electromagnetic environmental standards. (Yamamoto. 2001, Takeuchi. 2007). Also in the future, main stream methods will intend to achieve sinusoidal waveforms. From thinking about research stream until now, more simplified method or low cost scheme would be discussed and developed in a similar manner also in the future. On the basis of the perceived requirements, in this paper, we propose and discuss a novel PFC circuit for three phase, employing a single switch in such a manner as to render the waveform as sinusoidal as possible.

2. Operational Principle

2.1 Prasad-Ziogas Circuit

Figure 1 shows a conventional circuit, comprising a three-phase circuit, using single switching device. (Prasad & Ziogas. 1991). The principle of operation is such that the three phase circuit is periodically shorted by a single switching device at a high frequency, so that the input current waveform is created in proportion to input voltage waveform. The input current waveform becomes synchronized with the input voltage, so that the circuit scheme

is constructed as PFC circuit. In this paper, this circuit is named the PZ (Prasad-Ziogas) circuit, one of these individuals being famous for contributions toward power electronics development.

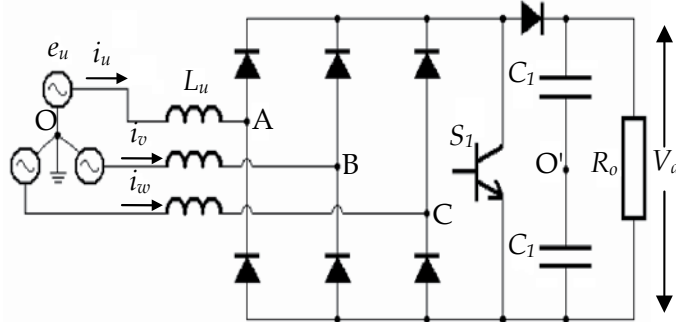


Fig. 1. Three-phase single switch PFC circuit by Prasad-Ziogas.

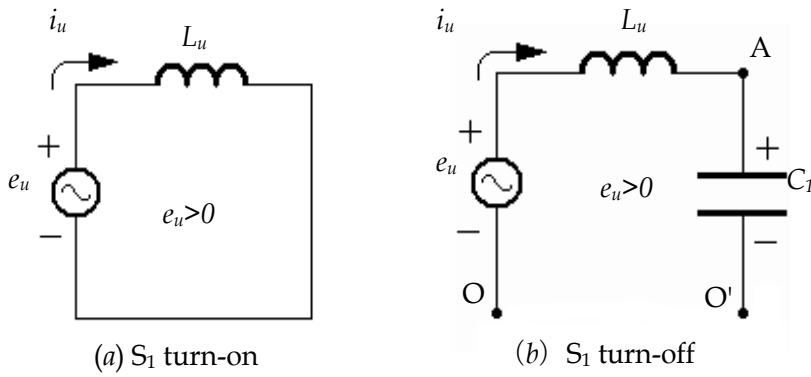


Fig. 2. Equivalent circuit for Prasad-Ziogas.

Figure 2 shows the equivalent circuit of the PZ circuit. These characteristics may be explained as follows; In Figure 2 (a), when S_1 turns-on, the equivalent circuit is established as shown, where the operation will be explained as a current-discontinuous mode for simplicity of circuit analysis. In Figure 2 (b), the terminal voltage across O and O' of fictional neutral point can be derived from Figure 1, the amplitude being $E_0/6$ with an operational frequency three times supply frequency, where E_0 is the output dc link voltage. In Figure 2 (a), when S_1 is turned on, circuit equation can be established as follows;

$$e_u = L_u \frac{di_u}{dt} \quad (1)$$

The analogous equations can be described also in phase v and phase w. From Eq. (1), the input current is increasing in proportion to amplitude of e_u at S_1 turn-on. (see Figure 3 (b) and (c)). When the switch is turned-off, the equivalent circuit is established as shown in Figure 2 (b), where, by analogy with the other phases, the equations become as follows;

$$\begin{aligned}
 e_u - v_{AO} &= L_u \frac{di_u}{dt} \\
 e_v - v_{BO} &= L_v \frac{di_v}{dt} \\
 e_w - v_{CO} &= L_w \frac{di_w}{dt}
 \end{aligned}
 \tag{2}$$

From these equations, it is clear that each phase current is decreasing in proportion to $e_u - v_{AO}$ etc. These waveforms are shown for the S_1 -off period in Figure 3. If the current waveforms are decreasing, as shown by the dashed lines, the resultant current values could be obtained in proportion to the input voltage values. However, the terms for attenuation, such as $e_u - v_{AO}$, are nonlinear. (see Figure 4 showing v_{AO}). Actual waveforms are attenuated by means of the terms like $e_u - v_{AO}$ etc. (Murphy. 1985). If e_v , for an example, has a small value, the degree of attenuation may be small, so that a gently decaying dashed line would be obtained, as shown. In this example case, however, the attenuation term is $e_v - v_{BO}$, so that the attenuation degree becomes severe. As a result, the sharply decaying solid line can be obtained, because of significant attenuation, producing nonlinear waveforms.

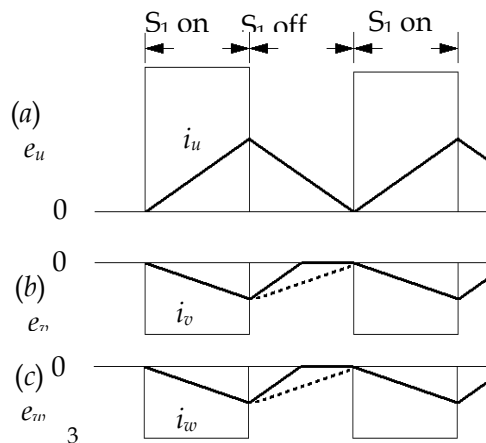


Fig. 3. Input current waveforms at S_1 switching.

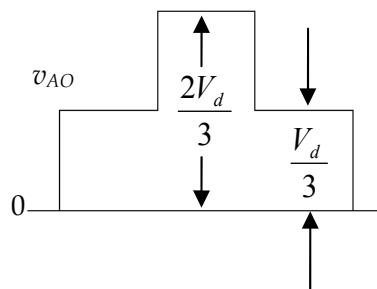


Fig. 4. Conceptual voltage waveform, v_{AO} .

Figure 4 shows conceptual waveform as v_{AO} . When S_1 is turned-off, the corresponding diode conducts. Depending on whether the amplitude of $v_{AO}=2V_d/3$ or $V_d/3$, where V_d is the output voltage, the degree of attenuation at S_1 turn-off is varied.

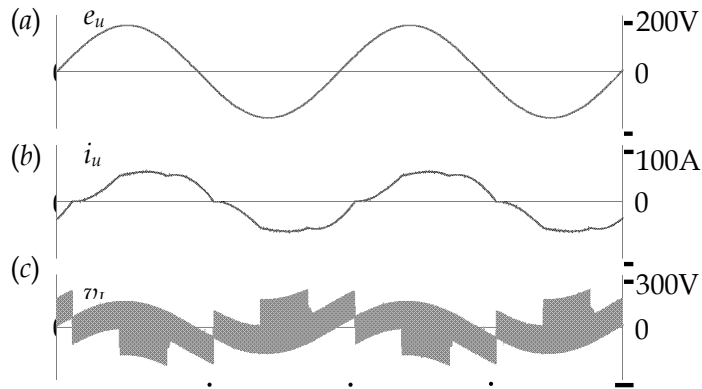


Fig. 5. Explanation of distorted input current waveform in conventional method.

Figure 5 shows the operational waveforms for Figure 1 from circuit simulation. From these figures, the reasons for waveform distortion in the conventional input current can be explained to a certain extent. From the phase voltage, e_u , in Figure 5 (a), the input current waveform, i_u , appears as in Figure 5 (b), using single device switching. It can be found that the envelope of a six stepped waveform v_{AO} appears and the distortion of i_u is generated as in Figure 5 (b). The term $e_u - v_{AO}$ in (2) appears as an envelope of the applied voltage across the input inductor in Figure 5 (c). From equation $v_L = L_u di_u / dt$, it can be seen that the integral of v_L becomes the input current, i_u , so that the improvement scheme for input current waveform can be determined from observing the inductor voltage wave, v_L , to a certain extent.

2.2 Operation Principle of the Proposed Circuit

Figure 6 shows one of the proposed types of, three-phase, single switch converter. In this paper, we will discuss the boost type converter. In the future, however, it may be possible that a buck type converter could be realized under adequate discussion. Thus, this paper title does not restrict the concept to the boost type converter. The circuit configuration originates from the above mentioned Prasad-Ziogas circuit. The notable feature is that several electrolytic capacitors are parallel-connected to rectifying diodes. By means of this configuration, the input voltage circuit is always connected to either dc output bus, so that continuity and improvement of the input current can be realized. In such a way, a boosted dc voltage, utilizing the PFC scheme, can be obtained in comparison to the conventional circuit. The circuit operation can be roughly divided into six periods, where each period is 60 degrees. From the operation waveforms in Figure 7 and the operational periods shown in Figure 8, the circuit operation can be discussed. To simplify the analysis of the operation, we will assume a unity power factor of phase, u , where fundamental voltage and current components are almost synchronized with each other.

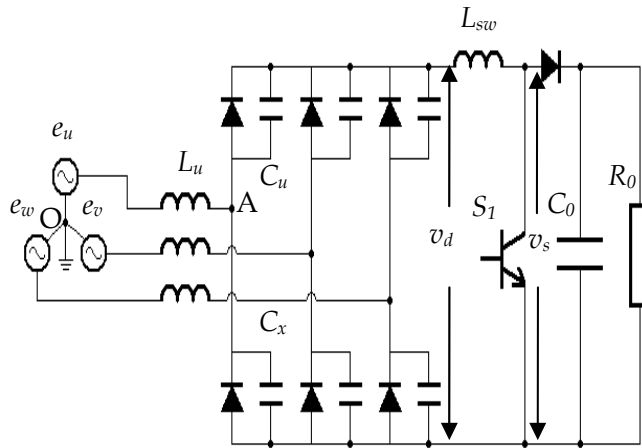


Fig. 6. Proposed circuit configuration.

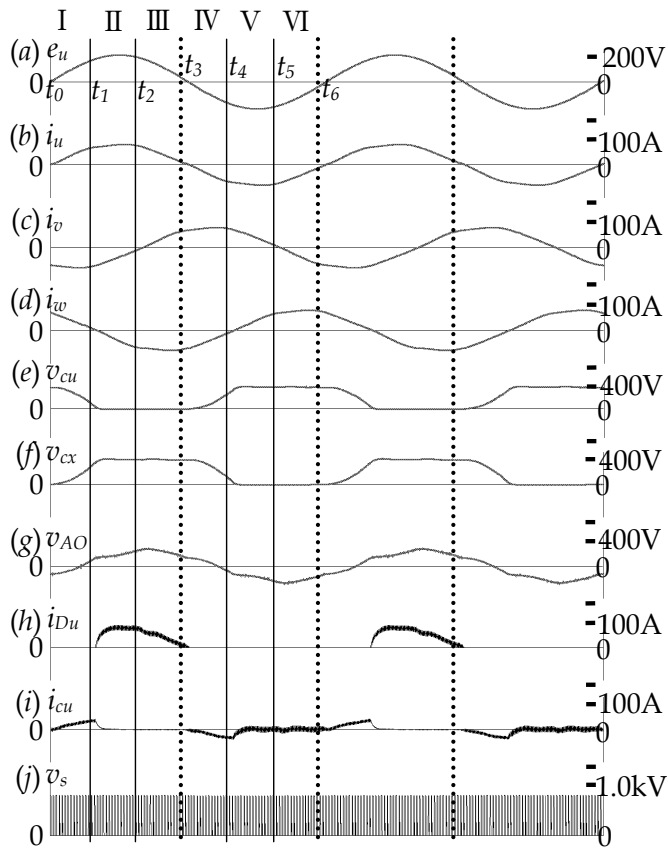


Fig. 7. Waveforms for proposed circuit.

(a) period I ($t_0 < t < t_1$)

The voltage in phase u is gradually increasing from $e_u=0$. In usual three phase circuit, the current at small values of supply voltage can not be rising due to a large dc link voltage, so that the current becomes zero for usual circuits, or suppressed to fairly reduced value, even in the Prasad-Ziogas circuit. In the proposed circuit, however, the capacitor voltage, v_{cu} , is gradually discharged from being fully charged at the dc link voltage. (see Figure 7 (e)). During this discharging period, diode current, i_{Du} , does not flow. In the other phases, v and w, diodes, D_v and D_w , conduct, although parallel-capacitor currents do not flow. The capacitor charge and discharge currents, i_{cu} and i_{cx} , each of which are connected to the constant dc link voltage, are equal, i.e., $|i_{cu}| = |i_{cx}| = |i_u/2|$. These results can be derived from the equation $C_u \times dv_{cu}/dt = -C_x \times dv_{cx}/dt$. In Figure 7 (h), (i) and (b), these results can be seen as $i_{Du} + 2i_{Cu} = i_u$. The diode current in phase w is decreasing toward zero as e_w decreases. When this voltage polarity is reversed, and the D_w current is commutated to D_z circuit, this period comes to an end.

(b) period II ($t_1 < t < t_2$)

As the capacitor, C_z , in parallel with D_z , is charged to $v_{cz}=v_d$, this period starts from the beginning of the discharge current i_{cz} . The current, D_u , in phase u and the current, D_y , in phase v continue to flow, supplying the dc bus. At the end of this period, the voltage, e_v , is reversed and i_v is greater than zero.

(c) period III ($t_2 < t < t_3$)

The voltage, e_v , begins to rise and the commutation from D_y to D_v commences. The capacitor voltage, v_{cv} , is varied in a similar manner to v_{cu} in period I. The current, i_v , rises from the zero point of e_v . In phase u, the current, i_{ur} , is decreasing toward zero according to the decrease in e_{ur} when this period comes to an end.

In the subsequent period of negative e_{ur} , an analogous operation is repeated such as a commutation of D_u to C_x and D_x etc. A remarkable characteristic of this strategy is that there is no discontinuity of the input current wave, as compared to the conventional three phase diode circuit having 120 degree current wave. In the proposed method, on the other hand, one terminal is always connected to either dc link circuit through a capacitor, achieving a continuous and improved waveform. In this paper, the boost chopper strategy has been considered and discussed, such that the stored charge is forced to flow from capacitors, so that the functions of charge and discharge become more efficient and smoothing of the input current becomes more effective. As an indication of the improvement of input current waveform, the v_{AO} waveform is shown in Figure 7 (g). This waveform can be derived from the conventional six step inverter circuit by an analogous procedure. In the proposed circuit, however, due to the intermediate capacitors, the v_{AO} waveform becomes smoothed, as shown in Figure 7 (g). Through such improved waveforms, instead of usual six step wave v_{AO} as in Figure 4, input current waveform can be improved, as shown in Figure 7 (b).

3. Operational Characteristics

By employing circuit constants in Table 1, various characteristics can be resolved. The operational waveforms in Figure 7 can be resolved by using these circuit constants. Figure 9

shows the relationship between output power and THD. The characteristics are compared between the conventional and

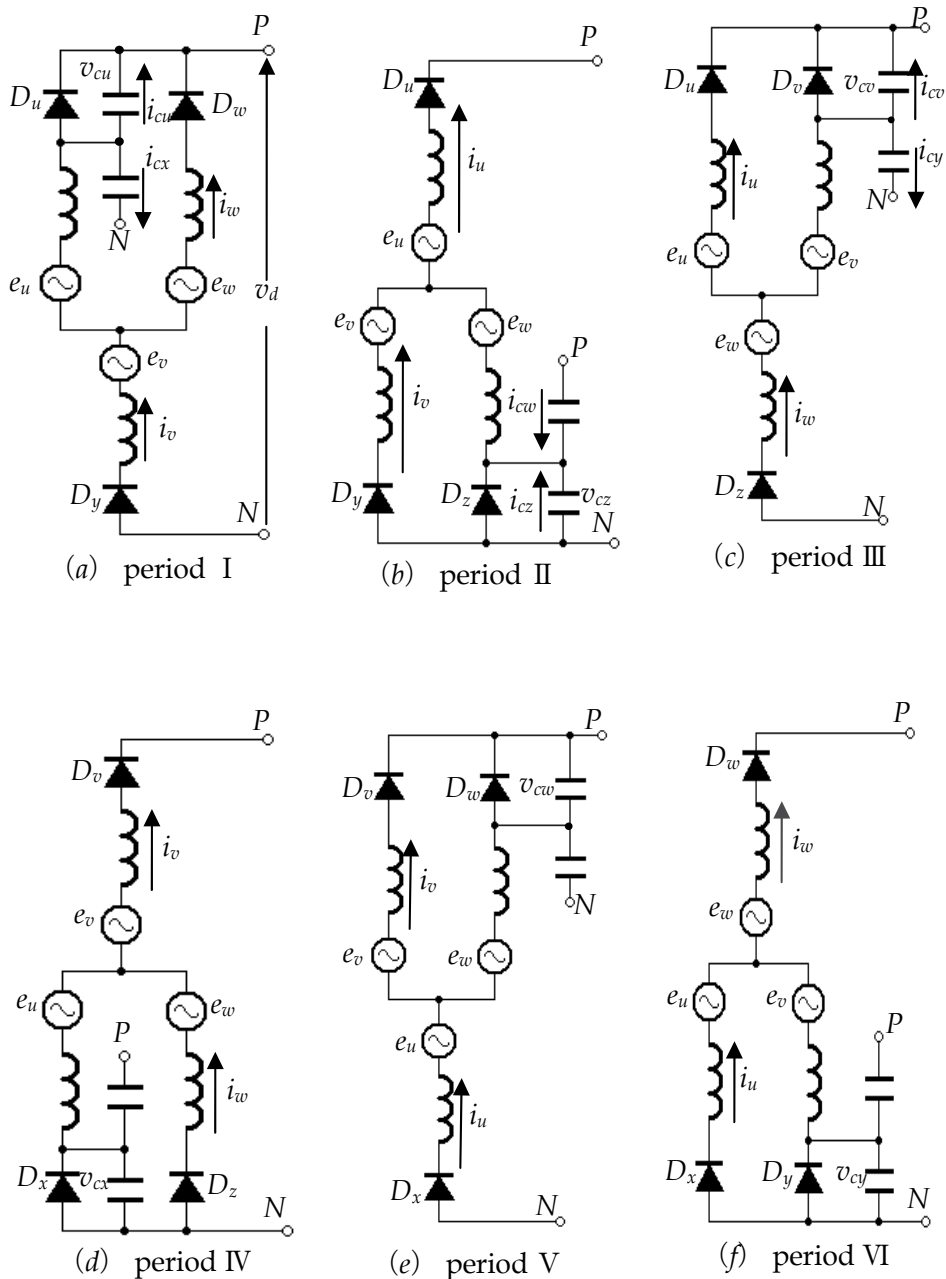


Fig. 8. Operating circuit.

proposed methods, where the input inductors are taken as parameter. In the reduced power region of conventional circuit, the THD is deteriorated. In a region of increased power of the circuit, the harmonics are relatively suppressed due to the function of the input inductor, and the THD can be improved. For the proposed circuit, in this manner, the THD can be entirely suppressed and improved.

L_L : Line inductance	0.25 mH
R_s : Line resistance	0.2 Ω
L_{in} : Input filter inductance	
proposed	5 mH
conventional	3 mH
L_{sw} : Switching inductance	0.2 mH
C_a : Auxiliary capacitance	150 μ F
C_o : Output capacitance	6000 μ F
R_o : Load resistance	
proposed	42 Ω
conventional	22 Ω
f_{sw} : Switching frequency	20 kHz
v_s : Supply line voltage	200 V
f_s : Supply frequency	60 Hz

Table 1. Circuit constants

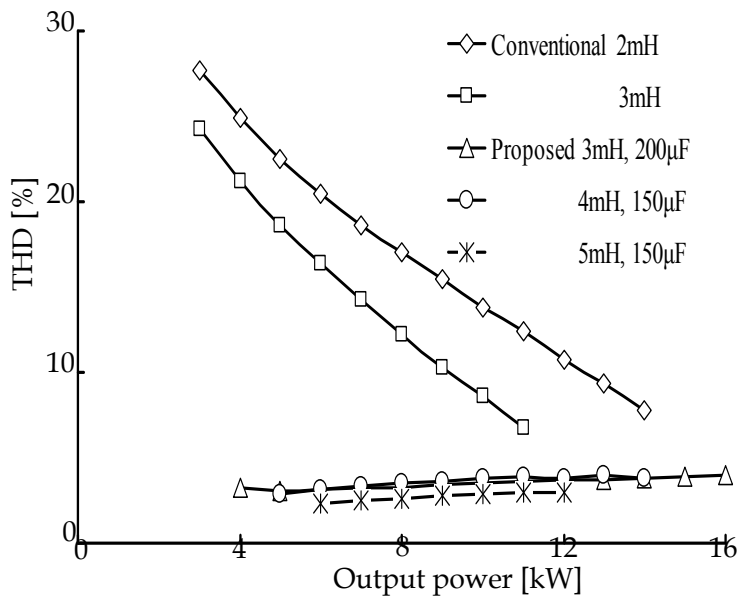


Fig. 9. Relationship between output power and THD.

In a region of more increased power for the conventional method, we might expect that a more improved THD could be obtained, but the actual result is to the contrary. Because voltage drop across the input inductor is significant in the increased power region, a more increased power can not be obtained. Due to an LC resonant operation, where the stored electric charge in the C is charged and discharged, a little increased power can easily be obtained, offering one remarkable feature of this strategy.

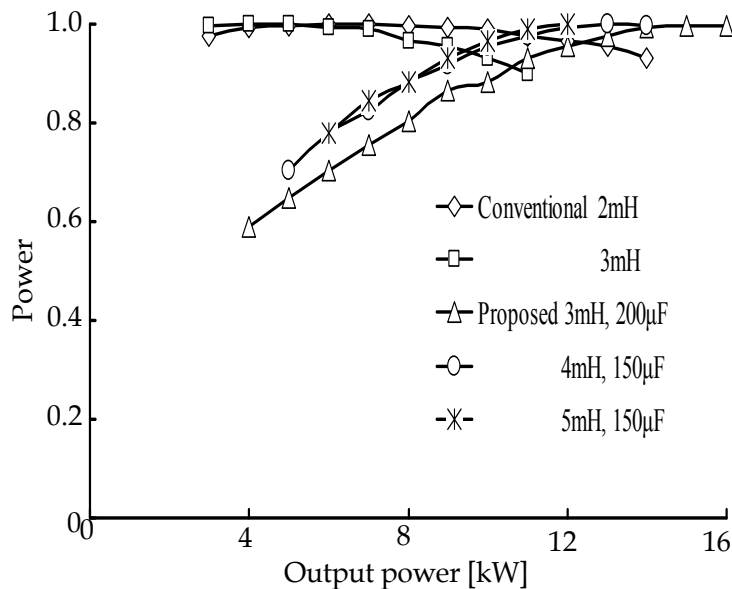


Fig. 10. Relationship between output power and power factor.

Figure 10 shows the relationship between the output power and power factor using the same circuit constants from Table 1. In the conventional circuit, as the output power is increased, the power factor is reduced a little. The reason is that the voltage drop across the input inductor is fairly significant. In the proposed method, however, though the THD characteristic is much improved, the power factor characteristic is a little deteriorated. For this reason, it could be said that this strategy is unsuitable for an application requiring the avoidance of reduced power factor over a variable wide power range. Rather, it is suitable for an application requiring constant output power or extended operation term with constant power.

Figure 11 shows the relationship between auxiliary capacitance, C_a , and the THD. Results at $C_a=0$ are represented for Prasad-Ziogas circuit, where THD is 12% of deteriorated value. Employing the proposed auxiliary capacitance, however, as the value of capacitance is increased, the THD characteristic is fairly improved, where output power is adjusted so as to maintain unity power factor. Consequently, as the capacitance is increased, the input current and the power are also increased, as shown by dotted line in Fig 11. Such increased current can partly contribute an improvement in the THD.

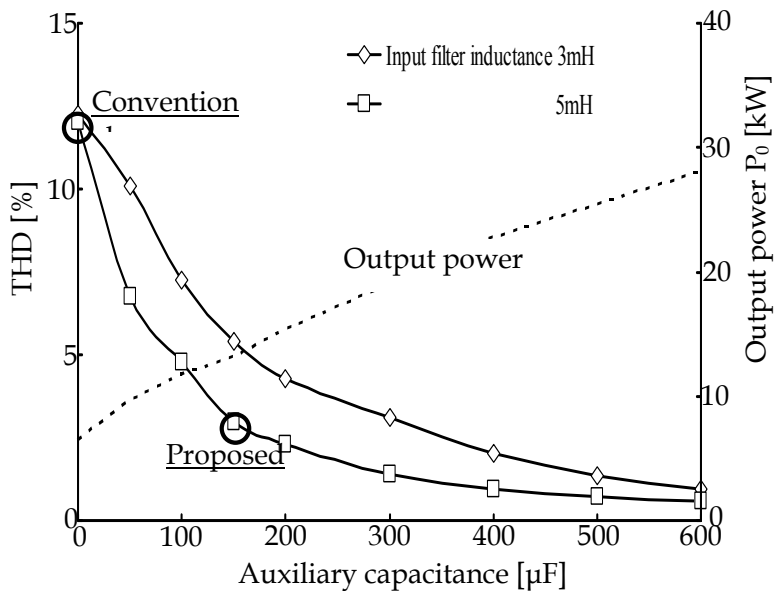


Fig. 11. Relationship between auxiliary capacitance and THD.

4. Development to Buck-converters

This paper discussed about boost type converters, but those type ones can be easily develop toward any type of converters. In this section, we will discuss about the application for buck type converter in single phase. Figure 12 shows such proposed circuit for buck converter, where previously mentioned auxiliary intermediate capacitors are installed. In this circuit configuration, the intended characteristics could be realized. The basic circuit is constructed by the conventional buck-converter. The distinctive feature of the discussed circuit is to be described as follows: Previously mentioned relatively large capacitors such as electrolytic ones are parallel-connected to diodes in a similar way. By means of those connections, the input circuit is always connected to either terminal of the dc link circuit, such as positive or negative one, which makes possible the input current continuity and the improvement of input current waveform. In general, for buck-type converter when the PFC circuits are designed both for three-phase and single-phase, it might be difficult to construct the suitable PFC ones, even with fairly large inductions or transforms. The distinctive feature of the proposed strategy employs a very simple way, in which some electrolytic capacitors are merely parallel-connected. By means of this parallel connection of capacitors, non-linearity of input current waveform becomes linear one, which brings the waveform improvement. In the usual buck chopper circuit having the constant dc link voltage, the output current does not flow in a certain period. This feature brings non-sinusoidal waveforms. In a case of the proposed circuit, the dc link voltage is constructed by the sum of series-connected double capacitor voltage such as $v_{C1} + v_{C2}$. As a result, due to assistance of each capacitor charge and discharge operation, the input current always continues to flow, though the dc link voltage v_R becomes constant, so that each appearance should be in sinusoidally wave.

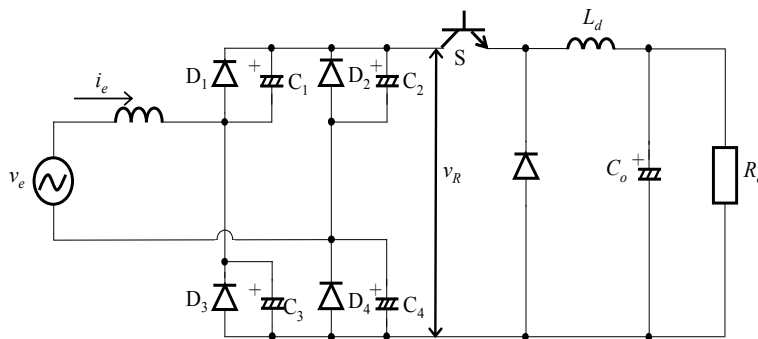


Fig. 12. Development to buck-converter.

5. Conclusions

An improved circuit strategy has been proposed and discussed, based on an extension of the Prasad-Ziogas circuit, offering significant improvement in the THD characteristic. The results have been presented and compared. The proposed circuit uses single switching device like the conventional one and the characteristics can be improved sufficiently by using a simple auxiliary capacitor connection. In this way, a three phase PFC circuit can be realized in a simple manner. Another feature in the proposed circuit is the ability to obtain a fairly increased power capacity, making the circuit suitable for high capacity converter.

However, the circuit employs several capacitors in the series current path. As a result, a somewhat reduced power factor region is observed, particularly in the lower output power region. Consequently, the circuit is unsuitable for an application requiring a wide variable power range and a reduced power operation for a long period.

In the future, after further consideration and discussion, a novel buck-type converter using proposed method might be realized.

6. References

- Converter-circuit and Control-strategy Committee on IEEJ. (2000). Current Circumstances and Trends of PFC Converter-circuit and Control Strategies. *Technical Report of Institute of Electrical Engineers in Japan*, No.785
- Fujiwara, K. & Nomura, H. (1995). A Power Factor Correction for Single-Phase Diode Rectifiers without employing PWM Strategy. *IPEC-Yokohama '95*, pp.1501 -1506
- JISC.(2005). Electromagnetic compatibility (EMC) - Part 3-2: Limits. *JISC61000-3-20*. PFC Circuit Investigation Committee on IEEJ. (2000).
- Murphy, J. M. D. & Turnbull, F. G. (1988). *Power Electronic Control of AC Motors*. Pergamon Press, p.112
- Prasad, A. R. & Ziogas, P. D. (1991). An Active Power Factor Correction Technique for Three-Phase Diode Rectifiers, *IEEE Trans. Power Electronics*, Vol.6, No.1, pp.83-92
- Takahashi, I. & Ikeshita, W. (1985). Improvement of Input Current Waveforms of a Single-Phase Rectifier Circuit. *IEEJ Trans*. Vol.105-B, No.2, pp.82-90

- Takahashi, I. Hori, K.(1997). Improvement of Input Current Waveforms of a Single Phase Diode Rectifier by Passive Devices. *IEEJ Trans.* Vol.117-D, No.1, pp.13 - 18
- Takeuchi, N. & Matsui, K. (2007). A Discussion on PFC Circuit Using Ladder Type Filter. *Industry Applications Society of the Institute of Electrical Engineers of Japan* , Vo.I, No.98, pp.519-522.
- Yamamoto, I. & Matsui, K. (2001). A Power Factor Correction with Two-Input Current Mode using Voltage Doubler Rectifier. *IEEJ Trans. IA*, Vol.121-D, No.2, pp.225 - 230

Advanced Modulation Formats and Multiplexing Techniques for Optical Telecommunication Systems

Ghafour Amouzad Mahdiraji¹ and Ahmad Fauzi Abas²
*¹UCSI University & ²Universiti Putra Malaysia
Malaysia*

1. Introduction

Since ancient times, one of the principal needs of people has been to communicate. This need created interest in devising communication systems for sending messages from one place to another. The advent of high performance computer processors brought many advantages for digital communications over that of analog. These benefits include more features, easy storage and faster processing. These caused huge amount of information, which is increasing exponentially every year, to be carried over communication networks.

Various types of communication system appeared over the years. Among the basic motivations behind each type are to improve the transmission fidelity, increase the data rate, and increase the transmission distance between stations. All these facilities are achievable utilizing optical fiber communications. Optical fiber offers several advantages over the traditional media (e.g., twisted wire pair and coaxial cable). Its decisive advantages are huge bandwidth and very low attenuation and noise (Arumugam, 2001). The first, results in higher bit rate, and the second, results in longer transmission distance. These potentials can be further pushed by utilizing multiplexing techniques and/or advanced modulation formats.

The invention of wavelength division multiplexing (WDM) (G. E. Keiser, 1999) contributes great benefit to the optical fiber communication systems especially after the introduction of Erbium-doped fiber amplifier (EDFA). Using WDM, about forty channels can be accommodated in the C-band at 100 GHz (0.8 nm) channel spacing. Based on this condition, up to 1.6 Tb/s transmission capacity has been reported (Zhu et al., 2001). More channels can be transmitted using ultra-dense WDM technique by considering channel spacing of as close as 12.5 GHz (Ciaramella, 2002; Sang-Yuep, Sang-Hoon, Sang-Soo, & Jae-Seung, 2004). Using such channel spacing, up to 2.5 Tb/s transmission is reported (Gyo-Sun et al., 2007) by multiplexing 256 12.5 Gb/s channels, and transmitted over 2000 km standard single mode fiber (SSMF). Larger transmission capacity can be achieved by utilizing the S- and L-bands (Freund et al., 2005; Seo, Chung, & Ahn, 2005). Using triple bands (S + C + L), 10.92 Tb/s transmission is experimentally reported (Fukuchi et al., 2001) by using 273 WDM channels and 50 GHz spacing.

Higher transmission capacity can be achieved with higher bit rate per WDM channel. Time division multiplexing (TDM) is the most commonly used for multiplexing high number of lower bit rate channels to form a higher bit rate. For example, a 40 Gb/s data stream can be achieved by multiplexing four 10 Gb/s data using electrical TDM (ETDM) (Dong-Soo, Man Seop, Yang Jing, & Nirmalathas, 2003; Krummrich et al., 2002; Lach, Bulow, Kaiser, Veith, & Bouchoule, 1998; Lee, Garthe, Pettitt, & Hadjifotiou, 1997; Miyamoto, Yoneyama, Otsuji, Yonenaga, & Shimizu, 1999; Yoneyama et al., 1999). Using such system, 3.2 Tb/s (80×40 Gb/s) bidirectional WDM/ETDM transmission over 40 km SSMF is experimentally reported (Scheerer et al., 1999). The feasibility to realize transmission systems, subsystems, and electronic and optoelectronic components operating at bit rates beyond 40 Gb/s has been demonstrated in numerous papers (Andre, Kauffmann, Desrousseaux, Godin, & Konczykowska, 1999; Derksen, Moller, & Schubert, 2007; Elbers, 2002; Jansen et al., 2007; Kauffmann et al., 2001; Lach & Schuh, 2006; Lach et al., 2007; Schuh et al., 2005). Recently, up to 107 Gb/s full-ETDM transmission is experimented in laboratory and tested over installed fiber in the field (Derksen et al., 2007; Jansen et al., 2007; Lach et al., 2007).

WDM channels capacity can be doubled using polarization division multiplexing (PDM) technique (Hinz, Sandel, Noe, & Wust, 2000; Hinz, Sandel, Wust, & Noe, 2001; Martelli et al., 2007; Sandel, Wust, Mirvoda, & Noe, 2002; Suzuki, Kubota, Kawanishi, Tanaka, & Fujita, 2001; Yan, Zhang, Belisle, Willner, & Yao, 2007). Combining PDM with WDM system, 10.2 Tb/s (256×42.7 Gb/s) transmission in C + L bands is experimentally demonstrated, which offers 1.28 b/s/Hz SE (Bigo et al., 2001).

Further improvement in WDM network capacity can be realized by using advanced modulation formats. Amongst different types of available modulation formats, differential quaternary phase-shift keying (DQPSK) transmission is currently under serious consideration for high-speed long-haul optical transmission systems due to its reduced optical bandwidth and high tolerance to chromatic dispersion (CD) relative to traditional binary systems (A. F. Abas, 2006; Cho, Grigoryan, Godin, Salamon, & Achiam, 2003; Christen, Nuccio, Xiaoxia, & Willner, 2007; A. H. Gnauck, Winzer, Dorrer, & Chandrasekhar, 2006; Morita & Yoshikane, 2005; Schubert et al., 2006; Weber et al., 2005; Weber, Ferber et al., 2006; Yoshikane & Morita, 2004). Using the mentioned technique, WDM channel capacity can be doubled with requiring transceivers operating at the same baud rate. This improves the spectral efficiency (SE) of WDM system. Using WDM and carrier-suppressed-return-to-zero (CS-RZ) DQPSK format, 4 Tb/s (50×85.4 Gb/s) with 70 GHz spacing has been experimentally tested (Yoshikane & Morita, 2004). Using that configuration, 1.14 b/s/Hz spectral efficiency (SE) was achieved. Elsewhere, using RZ-DQPSK, 5.12 Tb/s (64×85.4 Gb/s) with 50 GHz channel interval and 1.6 b/s/Hz SE was experimentally demonstrated (Morita & Yoshikane, 2005).

Combining DQPSK with PDM, quadruples WDM channel capacity (Ahmad Fauzi Abas, Hidayat, Sandel, Milivojevic, & Noe, 2007; Charlet et al., 2008; Pardo et al., 2008a; Renaudier et al., 2008; Savory, Gavioli, Killely, & Bayvel, 2007; Wree et al., 2003). With this configuration, Gnauck et al. (Alan H. Gnauck et al., 2007; A. H. Gnauck et al., 2008), demonstrated a record of 25.6 Tb/s transmission over 240 km using 160 WDM channels with 50 GHz grid in the C + L bands. In their experiment, they employed 85.4 Gb/s RZ-DQPSK modulation and polarization multiplexing to attain 160 Gb/s in each WDM channel, resulting in a SE of 3.2 b/s/Hz in each band (Alan H. Gnauck et al., 2007; A. H. Gnauck et al., 2008). This was the record in optical communication systems in 2008.

Recently, Zhou et al. (Zhou et al., 22-26 March 2009) has reported 320×114 Gb/s PDM-RZ-8 quadrature amplitude modulation (QAM)dense WDM transmission with channel spacing of 25 GHz over 580 km ultra-low-loss SMF-28. This is a record capacity of 32 Tb/s till 2009.

Duty cycle division multiplexing (DCDM) is another newly reported multiplexing technique that can support multiple users per WDM channel (Mahdiraji et al., (In Press)). In this technique, the multiplexed signals have a rising edge transition at the beginning of the multiplexed symbol. This unique property has never been reported in other multiplexing techniques and modulation formats. Considering that property, the technique allows aggregate bit rate to be recovered at symbol/ baud rate. Based on our knowledge, this is the latest multiplexing technique reported to date.

In the following sections, details on principles, operation and implementation of various modulation format and multiplexing techniques are presented.

2. Modulation Formats

Modulation is a process to form the baseband signal using high frequency carrier signal to become more suitable for transmission over long communication link. Advanced modulation formats improves the channel utilization and capacity. There are various types of multiplexing techniques and modulation formats commonly used in optical fiber communication system, which will be further discussed in the following Subsections.

2.1 Amplitude Shift Keying

In optical fiber communication systems, the baseband signals are modulated onto high frequency optical carriers. Various types of modulation can be used for that purpose. Amplitude modulation (AM) or amplitude-shift keying (ASK) or on-off keying (OOK) is the simplest and commonly used technique in optical fiber communication systems, where AM is referred to analog signals, and ASK and OOK referred to digital signals. In this technique, the baseband signal is multiplied by a carrier frequency, thus (assuming binary signaling), the binary 0 is transmitted with 0 W and binary 1 with $A W$. At the receiver, the demodulation can be easily performed using a photodetector, which converts the optical signal to the electrical signal, resulting in the original transmitted pattern. Figure 1 shows example of a ASK modulation format.

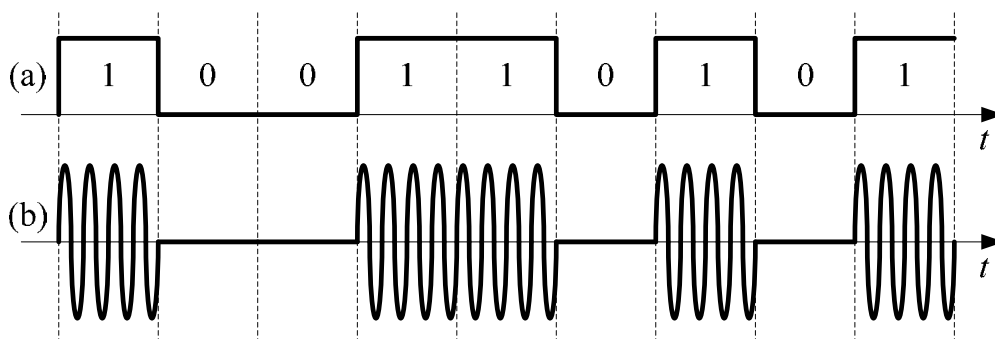


Fig. 1. Example of ASK modulation format, (a) binary signal, and (b) ASK modulated signal

In advanced communication systems, instead of transmitting single bit per symbol, using two level binary signals, more than one bit per symbol can be achieved, which it results in higher transmission capacity. This technique is called multilevel signaling. The number of signal level M , follows the rule of $M = 2^b$ where the b is the number of bits per symbol, thus called M -ary signaling. In ASK, the value of $M = 4$ (4-ary ASK) is mostly used to double the transmission capacity while maintaining the spectral width (Avlonitis, Yeatman, Jones, & Hadjifotiou, 2006; Cimini & Foschini, 1993; Muoi & Hullett, 1975; Walklin & Conradi, 1999). The 8-ary ASK is also studied over fiber optic communication for tripling the transmission capacity (Walklin & Conradi, 1999). The improvement in channel capacity was obtained at the cost of power penalty in the OSNR and system receiver sensitivity. For example, receiver sensitivity of 4-ary ASK coded with NRZ and RZ signaling experienced around 3.8 dB and 6.6 dB penalty in comparison to binary NRZ and RZ respectively (Avlonitis et al., 2006). This is due to the fragmentation of the main eye to the several smaller eyes for the 4-ary ASK.

2.2 Phase Shift keying

In phase modulation, binary data are modulated onto the optical carrier referring to the phase difference between binary 0 and 1. This technique is called phase-shift keying (PSK) or BPSK for binary PSK. Example of BPSK modulation is shown in Figure 2. In this example, binary 1 is signed as $\sin(\omega t)$ and binary 0 is signed as $\sin(\omega t + \pi)$ or $-\sin(\omega t)$.

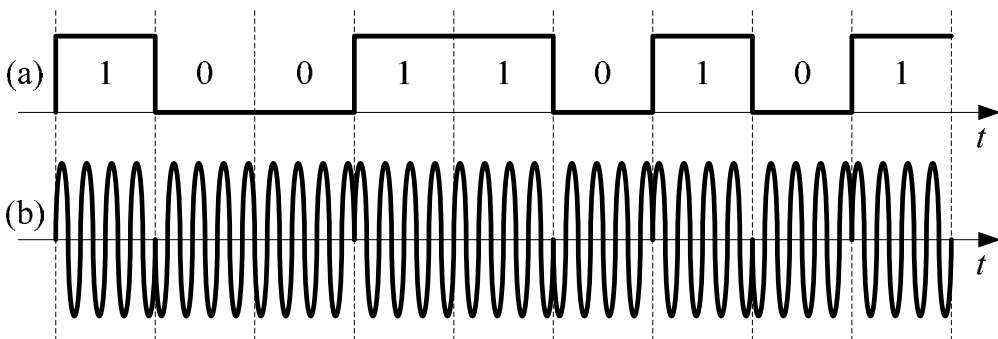


Fig. 2. Example of BPSK modulation format, (a) binary signal, and (b) BPSK modulated signal

In the early days, PSK did not receive much interest due to its demodulator's complexity. Instead, differential PSK (DPSK) had received more interests (Ho, 2005). In DPSK, the data are first encoded differentially as the differential encoder shown in Figure 3(a). The encoded data are then modulated onto optical carrier using a phase modulator (PM) or Mach-Zehnder modulator (MZM), which externally changes the optical phase from its original phase to a relatively π phase shift. In response to the driving baseband signal (Ho, 2005), MZM is preferable to PM due to better chromatic dispersion tolerance. Figure 4 shows example of DPSK, which Figure 4(a) shows the binary signal, and 4(b) is the DPSK modulated signal.

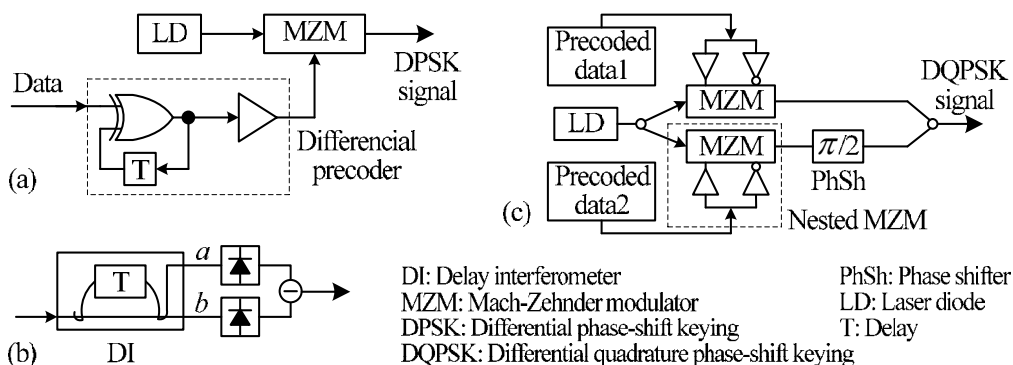


Fig. 3. DPSK transceiver, (a) DPSK transmitter, (b) DPSK balanced receiver, and (c) DQPSK transmitter

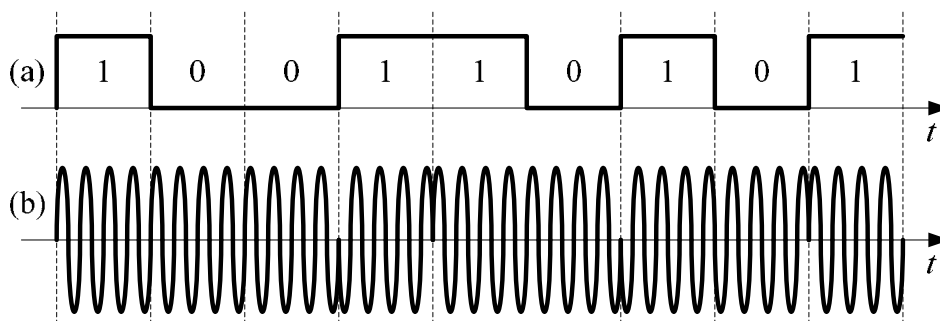


Fig. 4. Example of DPSK modulation format, (a) binary signal, and (b) DPSK modulated signal

At the receiver, since DPSK can not directly be demodulated, a delay interferometer (DI) is inserted in the optical path at the receiver to convert the differential phase modulation into intensity modulation. As shown in Figure 3(b), a DI splits the received signals into two paths, which experience one-bit delay to let two neighboring bits interfere at the DI output. At port *a* (the destructive port), the two optical fields interfere destructively whenever there is no phase change, and constructively whenever there is a phase change between subsequent bits, thus converting phase modulation into intensity modulation (Winzer & Essiambre, 2006).

Maintaining good interference is the most critical aspect in the design of DPSK receivers (Ho, 2005; Winzer & Essiambre, 2006; Winzer & Hoon, 2003). Due to energy conservation within the DI, the second DI output port *b* (the constructive port) yields the logically inverted data pattern. In principle, one of the two DI output ports is sufficient to detect the DPSK signal (single-ended detection). However, the 3-dB sensitivity advantage of DPSK is only seen for balanced detections (Ho, 2005; Winzer & Essiambre, 2006). A balanced detection (as shown in Figure 3(b) made with two photodetectors) considers the difference between ports *a* and *b* signal providing a larger signal than that of a single-branch receiver (Ho, 2005).

In advanced communication systems, similar to the M -ary ASK, M -ary DPSK are used instead of binary DPSK. The most reports are on $M = 4$, which called 4-ary DPSK or differential quadrature PSK (DQPSK). DQPSK is the only true multilevel modulation format (more than one bit per symbol) that has received appreciable attention in optical communications so far (A. F. Abas, 2006; Cho et al., 2003; Christen et al., 2007; A. H. Gnauck et al., 2006; Kawanishi et al., 2007; Morita & Yoshikane, 2005; Nasu et al., 2008; Schubert et al., 2006; van den Borne et al., 2008; Weber et al., 2005; Weber, Ferber et al., 2006; Yoshikane & Morita, 2004). It experiences four phase shifts, 0 , $+\pi/2$, $-\pi/2$, and π ($\sin(\omega t)$, $\sin(\omega t + \pi/2)$, $\sin(\omega t - \pi/2)$, and $\sin(\omega t + \pi)$), for data modulation, and operates at a symbol rate of half the aggregate bit rate. Figure 3(c) shows a schematic of DQPSK based on (Winzer & Essiambre, 2006), consisting of a continuously operating laser source, a splitter to divide the light into two paths of equal intensity, two nested MZMs operated as PMs, an optical $\pi/2$ phase shifter in one of the paths, and a combiner to produce a single-output signal. Figure 5 shows example of a QPSK/DQPSK modulated signal. In this example, the binaries 00, 01, 10, and 11 are signed with 0° , 90° , 270° , and 180° respectively. The QPSK and DQPSK modulated signal are the same. The different is referred to the encoder before the modulator. If the encoder is a differential encoder, then the modulated signal is DQPSK, otherwise it is QPSK.

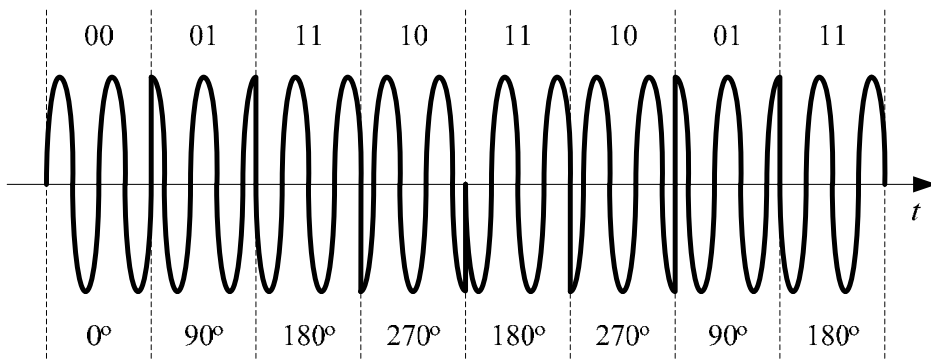


Fig. 5. Example of QPSK/DQPSK modulated signal

At the receiver, DQPSK signal first splits into two equal parts, and detected by two balanced receivers of the form depicted in Figure 3(b). The two balanced receivers are used in parallel to simultaneously demodulate the two binary data streams contained in the DQPSK signal. Note that, the delay produced by DI has to be equal to the symbol duration for DQPSK demodulation, which is twice the bit duration. In general, feedback-controlled DI tuning within the receiver is needed for both DPSK and DQPSK (Winzer & Essiambre, 2006). In DQPSK, the reduction of bandwidth is beneficial for achieving high SE in WDM systems, as well as for increasing tolerance to CD.

The higher bandwidth reduction or higher channel capacity can be achieved by increasing the value of M . This is achieved by combination of the amplitude and phase modulation which is called M -ary-quadrature amplitude modulation (QAM). In fact, the QAM (or 4-ary QAM) is produced by two PSK/DPSK signals, thus, it is the same as QPSK/DQPSK. Higher value of M , for example $M = 16$, which means 4 bits per symbol, is produced by utilizing 4 different amplitude levels combined with 8 different phase levels. In theory, this will lead to

32 states, allowing us to encode 5 bits per symbols ($2^5 = 32$). However, only 16 of these states are used to encode 4 bits ($\log_2(16) = 4$) per symbol (Lathi, 1998; Zahedi, 2002). Using QAM technique, 20-Msymbol/s using 128-QAM with coherent transmission over 500 km (Nakazawa, Yoshida, Kasai, & Hongou, 2006), and 1-Gsymbol/s using 64-QAM coherent transmission over 150 km optical fiber has been reported (Jumpei, Kasai, Yoshida, & Nakazawa, 2007; Yoshida, Goto, Kasai, & Nakazawa, 2008). In M -ary signaling, since there is b number of bit information per symbol, therefore, one symbol error produced b number of errors. This is called error propagation, which is more serious at higher value of b and M .

2.3 Duobinary

Optical duobinary (DB) has attracted great attention in recent years. The two main advantages attributed to this modulation format are increased tolerance to the effects of CD and improved SE (Ibrahim, Bhandare, & Noe, 2006; Lender, 1964; Said, Sitch, & Elmasry, 2005; Wei et al., 2002; Yonenaga & Kuwano, 1997; Yonenaga, Kuwano, Norimatsu, & Shibata, 1995). The fundamental idea of DB modulation (electrical or optical) that were first described by Lender (Lender, 1964) is to deliberately introduce intersymbol interference (ISI) by overlapping data from adjacent bits. This correlation between successive bits in a binary signal leads the signal spectrum to be more concentrated around the optical carrier (Said et al., 2005). This is accomplished by adding a data sequence to a 1-bit delayed version of itself, which can be obtained by passing the binary signal through the delay-and-add filter as shown in Figure 6(a) (Said et al., 2005). For example, if the (input) data sequence is $x(nT) = (0, 0, 1, 0, 1, 0, 0, 1, 1, 0)$, we would instead transmit the (output) data sequence $y(nT) = (0, 0, 1, 0, 1, 0, 0, 1, 1, 0) + (*, 0, 0, 1, 0, 1, 0, 0, 1, 1) = (0, 0, 1, 1, 1, 1, 0, 1, 2, 1)$. Here the sign * denotes the initial value ($z(nT)$) of the input sequence, which is assumed to be zero. Note that while the input sequence is binary and consists of 0s and 1s, the output sequence is a ternary sequence consisting of 0s, 1s, and 2s. Mathematically, DB results in $y(nT) = x(nT) + x(nT - T)$, where T is the bit period and n in the number of bit sequences (in above example n is 10). At the receiver, the input sequence $x(nT)$ can be recovered from the received $y(nT)$ based on $z(nT) = y(nT) - z(nT - T)$ (detail refer to (Ramaswami & Sivarajan, 2002)).

There is one problem with this scheme, however; a single transmission error will cause all further bits to be in error, until another transmission error occurs to correct the first one! This phenomenon is known as error propagation (Ramaswami & Sivarajan, 2002). The solution to the error propagation problem is to encode the actual data to be transmitted in a differential form. For example, the $x(nT)$ is encoded into $d(nT) = (0, 0, 1, 1, 1, 1, 0, 1, 0, 1)$. To see how differential encoding solves the problem, observe that if sequences of consecutive bits are all in error, their differences will still be correct. However, such an approach would eliminate the bandwidth advantage of DB signaling (Ramaswami & Sivarajan, 2002). The bandwidth advantage of DB signaling can only be exploited by using a ternary signaling scheme.

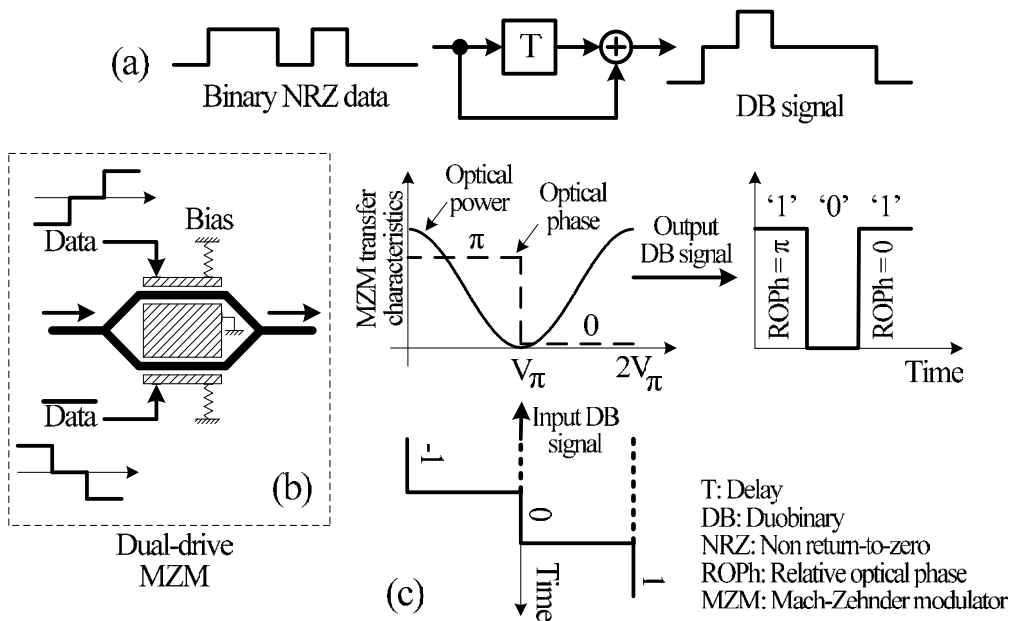


Fig. 6. Generating DB signal, (a) digital filter for electrical DB signal, (b) dual-derive MZM and (c) MZM bias and derive conditions for optical DB signal

The primary version of DB, which used three level signal, increases the sensitivity penalty (Said et al., 2005). To avoid the penalty, the three level DB signals need to be encoded in both the amplitude and the phase of the optical carrier (Yonenaga & Kuwano, 1997; Yonenaga et al., 1995). Such a scheme is called optical AM-PSK (Ramaswami & Sivarajan, 2002) and most studies of optical DB signaling today are based on AM-PSK. If the data is differentially encoded before the DB filter, the carrier phase information becomes redundant, and hence, the received data can be decoded using a conventional binary direct-detection receiver (Yonenaga & Kuwano, 1997; Yonenaga et al., 1995). This DB signal can be generated by applying a baseband, three-level electrical DB signal to a dual-drive MZM (Figure 6 (c)) that is biased at maximum extinction ratio, as shown in Figure 6(b) (Yonenaga & Kuwano, 1997; Yonenaga et al., 1995). Conceptually, the carrier is a continuous wave signal, a sinusoid denoted by $a \cos(\omega t)$. The three levels of the ternary signal correspond to $-a \cos(\omega t) = a \cos(\omega t + \pi)$, $0 = 0 \cos(\omega t)$, and $\cos(\omega t)$, which is denoted by -1, 0, and +1, respectively. These are the three signal levels corresponding to 0, 1, and 2, respectively, in $y(nT)$. The AM-PSK signal retains the bandwidth advantage of DB signaling.

3. Multiplexing Techniques

Multiplexing is an essential part in a communication system where multiple users transmit data simultaneously through a single link, whether the link is a coaxial cable, a fiber, radio or satellite. Multiplexing is widely employed in communication systems due to its capability to increase the channel utilization or the transmission capacity and decrease system costs. Figure 7 depicts the multiplexing function in its simplest form. There are n inputs to a multiplexer. The multiplexer multiplex or combine these inputs in a way so that they are

separable. The demultiplexer performs opposite process as multiplexer to separate the multiplexed data, and delivers them to the appropriate output lines. If each input to the multiplexer carrying k bps digital data, the total data rate or the aggregate rate of the link is nk . There are various types of multiplexing techniques commonly used in optical fiber communication system, which working principles are discussed in the following Subsections.

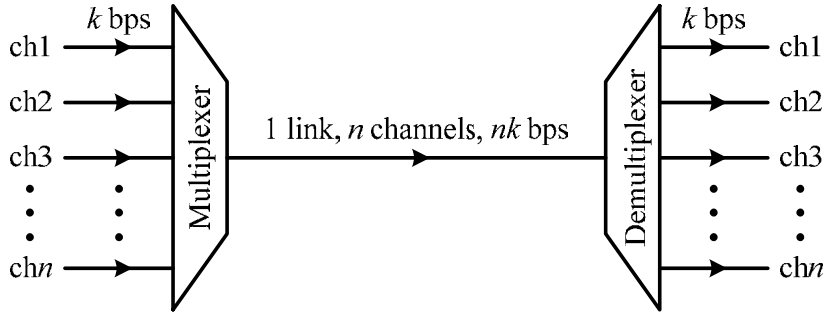


Fig. 7. Multiplexing

3.1 Time Division Multiplexing

Several low bit rate signals can be multiplexed, or combined to form a high bit rate signal by sharing the time. Because the medium is time shared by various incoming signals, this technique is generally called time division multiplexing (TDM). For those implemented in electrical domain, they are called electrical TDM (ETDM). Example of TDM system for multiplexing two channels is shown in Figure 8. In TDM systems, if n number of users with the same pulse width of T s (seconds) is multiplexed, the pulse width of the multiplexed signals is T/n . In TDM, the multiplexer and demultiplexer needs to operate at frequency equal to the total aggregate bitrate, which is n times faster than the bit rate of a single user.

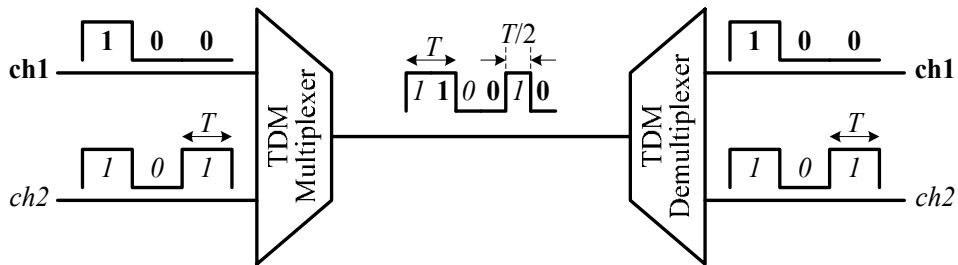


Fig. 8. Example of a TDM system for multipleing two channels

The multiplexer typically interleaves the lower speed streams to obtain the higher speed stream. The interleaving can be performed on a bit-by-bit (Figure 8) or packet-by-packet basis. Framing is required for both cases because at the receiving terminal, the incoming digital streams must be divided and distributed to the appropriate output channels. For this purpose, the receiving terminal must be able to identify the timing of each bit correctly. This requires the receiving system to uniquely synchronize in time with the beginning of each frame, with each slot in a frame, and each bit within a slot. This is accomplished by adding

framing and synchronization bits to the data bits. These bits are part of the so-called overhead bits.

Optical time division multiplexing (OTDM) has a similar concept to electrical TDM, only that it is implemented in optical domain. Figure 9 illustrates the basic concept of point-to-point transmission system using bit-interleaved OTDM. In this system, access nodes share different channels that operate at a fraction of the media rate. For example, the channel rates could vary from 100 Mb/s to 10 Gb/s, whereas the time-multiplexed media rate is around 100 Gb/s. In Figure 9, a laser source produces a regular stream of very narrow RZ optical pulses at a repetition rate R . This rate typically ranges from 2.5 Gb/s to 10 Gb/s, which corresponds to the bit rate of the electronic data tributaries feeding the system. An optical splitter divides the pulse train into n separate streams. In Figure 9, the pulse stream is 10 Gb/s and $n = 4$. Each of these channels is then individually modulated by an electrical tributary data source at a bit rate R . The modulated outputs are delayed individually by different fractions of the clock period, and interleaved through an optical combiner to produce an aggregate bit rate of nR . At the receiving end, the aggregate pulse stream is demultiplexed into the original n independent data channels for further signal processing. In this technique, a clock-recovery mechanism operating at the base bit rate R is required at the receiver to drive and synchronize the demultiplexer (G. Keiser, 2000).

OTDM requires very narrow RZ pulses to be able to interleave data of different users within a bit interval. These narrow pulses require higher spectral width. In addition, this system becomes vulnerable to CD and polarization mode dispersion (PMD) as well as creating the need for a higher optical signal-to-noise ratio (OSNR) in the wavelength channels due to the very short pulses. A higher OSNR is obtained by employing a higher signal power and will make the system more sensitive to fiber nonlinearity (Weber, Ludwig et al., 2006).

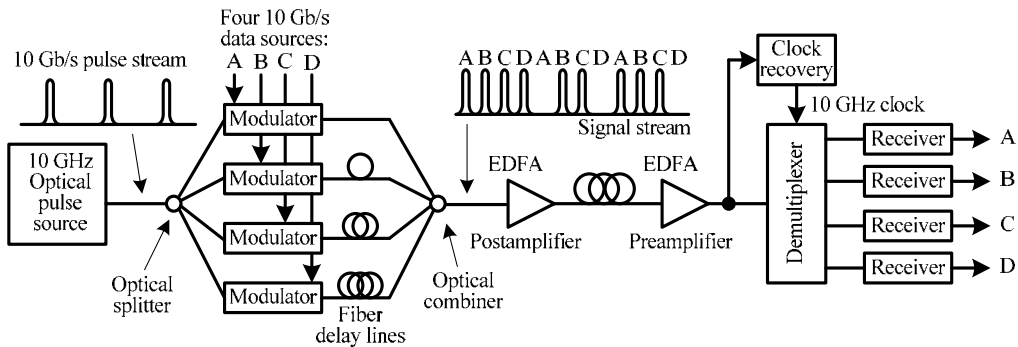


Fig. 9. Example of an ultrafast point-to-point transmission system using OTDM technique (G. Keiser, 2000)

3.2 Wavelength Division Multiplexing

In wavelength-division multiplexing (WDM) systems, different independent users transmit data over a single fiber using different wavelengths (G. E. Keiser, 1999; Palais, 2005). Conceptually, WDM scheme, which is illustrated in Figure 10, is similar to frequency division multiplexing (FDM) used in microwave radio and satellite systems. At the transmitter side, n independent users' data are modulated onto n high frequency carriers, each with a unique wavelength (λ). These wavelengths can be spaced based on ITU-T

standards. A wavelength multiplexer combines these optical signals and couples them into a single fiber. At the receiving end, a demultiplexer is required to separate the optical signals into appropriate channels. This is done with n optical filters, whereby their cut-off frequency is set based on the transmitted light source frequency. The total capacity of a WDM link depends on how close the channels can be spaced in the available transmission window. In late 1980s, with the advent of tunable lasers that have extremely narrow linewidth, one then can have very closely spaced signal bands. This is the basis of dense WDM (DWDM) (G. Keiser, 2000; G. E. Keiser, 1999). Figure 10 shows a typical WDM network containing various types of optical filter such as post-amplifier or booster, in-line amplifier and preamplifier.

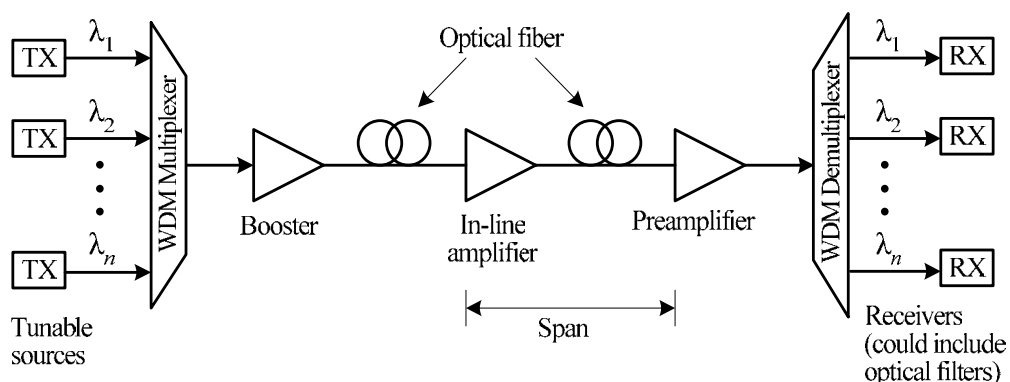


Fig. 10. Implementation of a typical WDM network

The major disadvantage of WDM is the low channel utilization and spectral efficiency because one wavelength is required per user. Therefore, for multiplexing n users, n wavelengths or light sources with n filters are required, which increase the cost of the system. The goal of all other multiplexing techniques and modulation formats are to increase channel utilization and/or channel capacity of the WDM systems.

3.3 Orthogonal Frequency Division Multiplexing

Orthogonal frequency division multiplexing (OFDM) is a special form of a multi-carrier modulation (MCM) or subcarrier multiplexing (SCM). In MCM, information of different users is modulated with different waveforms, which are called subcarriers. The channel spacing between subcarriers has to be multiple of symbol rate, which reduces the spectral efficiency (Shieh, Bao, & Tang, 2008). A novel approach which overlaps between subcarriers by reducing the channel spacing employing orthogonal signal set is called OFDM. A fundamental challenge of OFDM is on the number of subcarriers, where a large number of them are needed so that other channel treats sub-channels as a flat channel. This leads to an extremely complex architecture involving many oscillators and filters at both transmitting and receiving ends (Shieh, Bao et al., 2008). A family of OFDM was first proposed by Weinstein and Ebert (Weinstein & Ebert, 1971), in which OFDM modulation/ demodulation was implemented by using inverse discrete Fourier transform (IDFT)/discrete Fourier transform (DFT) (Weinstein & Ebert, 1971). This made OFDM attractive to be investigated for

applications in the optical domain because of its resilience to the channel dispersion (Shieh & Athaudage, 2006; Shieh, Bao et al., 2008). The most critical assumption for OFDM is the linearity in modulation, transmission, and demodulation. Consequently, a linear transformation is the key goal for the OFDM implementation. This is realized in coherent optical OFDM (CO-OFDM) with challenges in designing a linear modulator (RF-to-optical up-converter) and demodulator (optical-to-RF down-converter) (Shieh, Bao et al., 2008; Shieh, Yi, Ma, & Yang, 2008). A generic CO-OFDM system can be divided into five functional blocks including (Shieh, Bao et al., 2008; Shieh, Yi et al., 2008) (i) the RF OFDM transmitter, (ii) the RF-to-optical (RTO) up-converter, (iii) the optical channel, (iv) the optical-to-RF (OTR) down-converter, and (v) the RF OFDM receiver as shown in Figure 11.

In the RF OFDM transmitter, the input digital data is converted from serial to parallel into a block of bits consisting of information symbols. This information symbol will be mapped into a two-dimensional complex signal. The subscripts of the mapped complex information symbol correspond to the sequence of the subcarriers and OFDM blocks. The time-domain OFDM signal is obtained through IDFT and a guard interval is inserted to avoid the channel dispersion. The digital signal is then converted into analog form through a digital-to-analog converter (DAC) and filtered with a low-pass filter (LPF) to remove the alias sideband signal. The subsequent RTO up-converter transforms the baseband signal into the optical domain using an optical in-phase/quadrature (I/Q) modulator comprising a pair of Mach-Zehnder modulators (MZMs) with a 90° phase offset. The baseband OFDM signal is directly up-converted to the optical domain and propagates inside the optical medium. At the receiver, the optical OFDM signal is then fed into the OTR down-converter where it is converted to a RF OFDM signal. In the RF OFDM receiver, the down-converted signal is first sampled with an analog-to-digital converter (ADC). Then the signal needs to go through sophisticated three-level synchronization before the symbol decision can be made. The three levels of synchronization are (i) DFT window synchronization where the OFDM symbol is properly delineated to avoid intersymbol interference; (ii) frequency synchronization, namely, frequency offset needs to be estimated, compensated, and preferably, adjusted to a small value at the start; (iii) the subcarrier recovery, where each subcarrier channel is estimated and recovered (Shieh, Yi et al., 2008). Assuming successful completion of DFT window synchronization and frequency synchronization, the sampled value of RF OFDM signal passed through the DFT. The third synchronization of the subcarrier recovery involves estimation of the OFDM symbol phase (OSP), and the channel transfer function. Once they are known, an estimated value, which is calculated by the zero-forcing method is used for symbol decision or to recover the transmitted value, which is subsequently mapped back to the original transmitted digital bits (Shieh, Bao et al., 2008; Shieh, Yi et al., 2008).

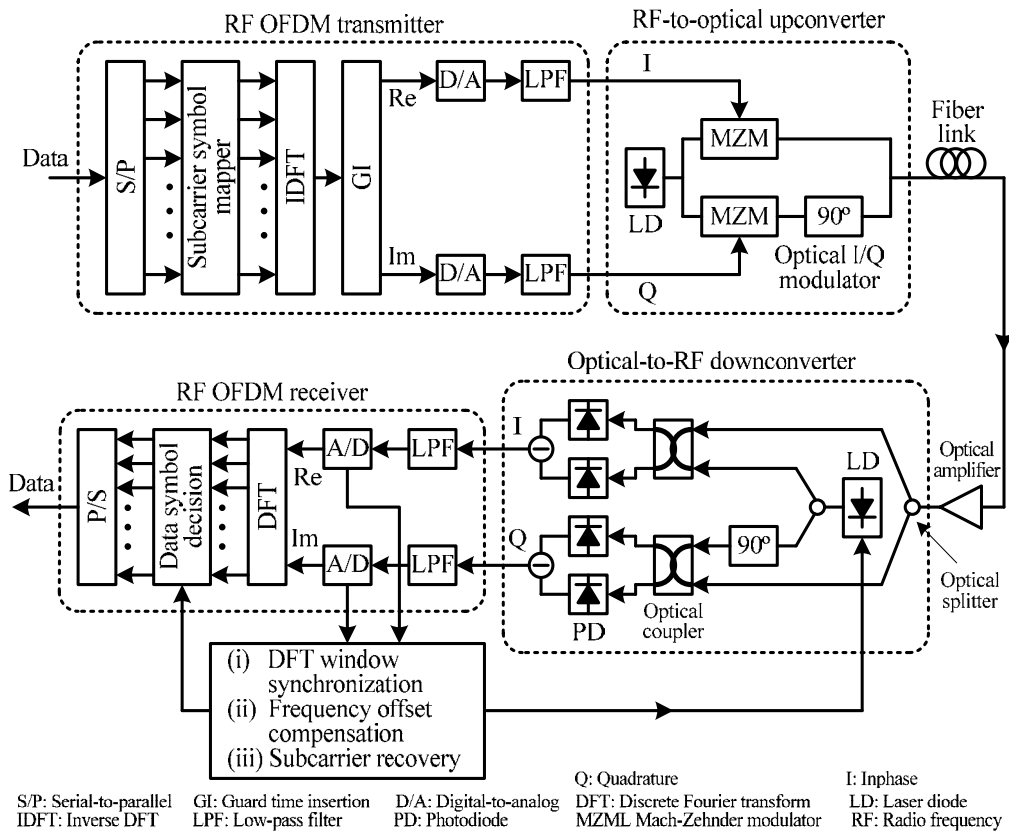


Fig. 11. Conceptual diagram for a generic CO-OFDM system with direct up-down conversion architecture (Shieh, Yi et al., 2008)

CO-OFDM has advantages in mitigating CD effects (Shieh & Athaudage, 2006; Shieh, Yi et al., 2008), as it transmits a high data rate divided into several low subcarrier channels resulting in longer signal pulse width. Also, the spectra of OFDM subcarriers are partially overlapped, resulting in high optical spectral efficiency. On the other hand, CO-OFDM requires very accurate synchronizations (Shieh, Bao et al., 2008; Shieh, Yi et al., 2008), very sensitive to nonlinear effects (Shieh, Bao et al., 2008), very complex and costly.

3.4 Polarization Division Multiplexing

Polarization division multiplexing (PDM) is a method for doubling the system capacity or spectral efficiency, in which two independently modulated data channels with the same wavelength, but orthogonal polarization states are simultaneously transmitted in a single fiber (Hayee, Cardakli, Sahin, & Willner, 2001; Martelli et al., 2008; Nelson & Kogelnik, 2000; Nelson, Nielsen, & Kogelnik, 2001; Yao, Yan, Zhang, Willner, & Jiang, 2007). At the receiver end, the two polarization channels are separated and detected independently. Figure 12 shows a simple sketch of a polarization multiplexed system. As shown in this figure, the multiplexer requires a polarization beam combiner (PBC) to combine two channels with orthogonal polarizations. State of polarization is controlled accurately with very high speed

optical polarization controller (PC). At the receiver, the polarization demultiplexer operates opposite of the multiplexer, in which a dynamic PC controls the polarization state before the polarization beam splitter (PBS) separates the two data streams.

The main advantage of PDM is that, it can be applied on existing fiber system without having to change any part of transmission hardware or software (Yao et al., 2007). It can also be used together with modulation format like DQPSK (Alan H. Gnauck et al., 2007; A. H. Gnauck et al., 2008) or QPSK (Charlet et al., 2008; Pardo et al., 2008a, 2008b) to quadruple system capacity and increase SE. Even though polarization multiplexing is straightforward, separating the two channels with acceptable crosstalk at the receiving end is not trivial because the polarization state of the multiplexed channels changes rapidly with time. Therefore, coherent crosstalk due to misaligned signal in reference to the input state of polarization in the polarizers or polarization beam splitters arises. In addition to that, PMD is another impairment for PDM (Nelson & Kogelnik, 2000; Nelson et al., 2001). Different techniques have been proposed to mitigate this impairment such as monitoring of clock tone or pilot tones (Chraplyvy et al., 1996; Hill, Olshansky, & Burns, 1992), multi-level electronic detection (Han & Li, 2006; Hayee et al., 2001), cross-correlation detection of the two demultiplexed channels (Noe, Hinz, Sandel, & Wust, 2001), and coherent detection (Charlet et al., 2008; Jansen, Morita, Schenk, & Tanaka, 2008; Pardo et al., 2008a), but they add to the system complexity and cost (Yao et al., 2007).

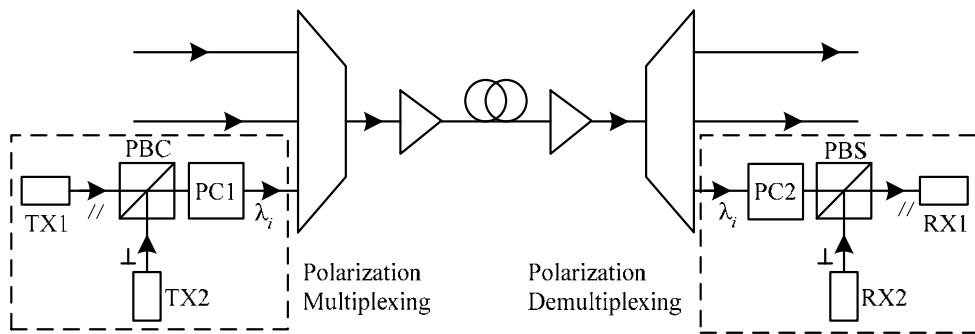


Fig. 12. Schematic of a simple polarization division multiplexing system (Nelson & Kogelnik, 2000; Yao et al., 2007)

3.5 Duty-Cycle Division Multiplexing

Duty cycle division multiplexing (DCDM) is a new multiplexing technique introduced recently by (Abdullah, Abdalla, F. Abas, & Mahdiraji, 2007). In this technique, different users sign with different RZ duty cycles and then combine together synchronously to form a multilevel step shape signal. The multiplexing process can be Performed either in electrical domain (E-DCDM) or optical domain (O-DCDM). Figure 13(a) shows example of an E-DCDM system for multiplexing three users. Data of the User 1 to 3 (U1, U2, and U3), each with let say 10 Gb/s pulse at pseudo random binary signal (PRBS) $2^{10}-1$, are curved with three RZ modulators (RZ1, RZ2, and RZ3), which produces different duty cycles (DCs). The three RZ modulators operate synchronously based on a central clock. The i th RZ modulator has a DC of $T_i = (i \times T_s)/(n + 1)$, where T_s represents the symbol duration and n is the number of user. Thus, data of U1 is curved with RZ1 which is set at 25% DC (U25); data of U2 is curved with RZ2 set at 50% DC (U50); and finally, data of U3 is curved at 75% DC

(U75). The signals with different DCs are then multiplexed synchronously using an electrical adder and then modulated with a laser diode (LD) signal, using an intensity modulator (IM). Figure 13(b) shows the eye diagram of the modulated signal obtained from the receiver.

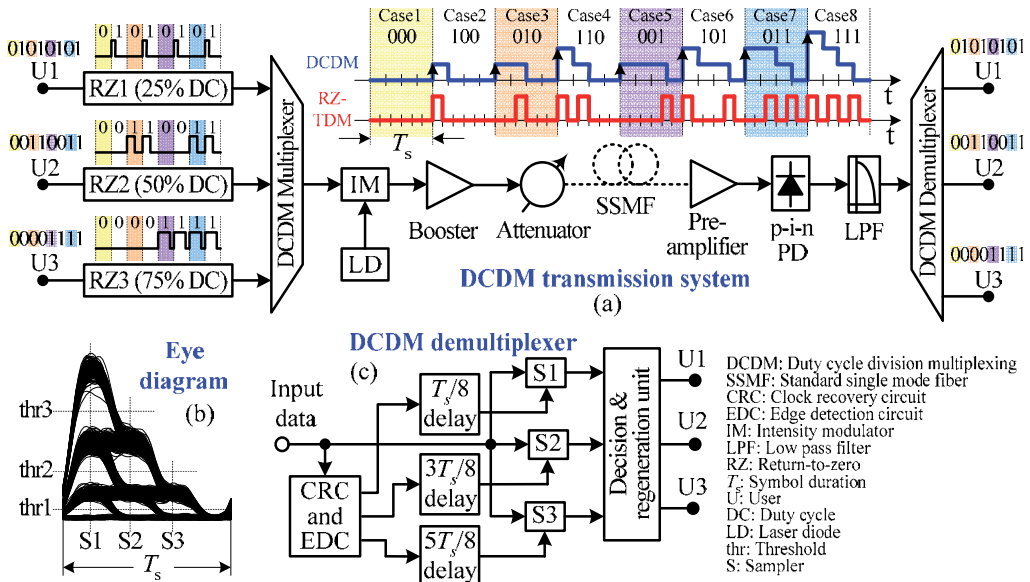


Fig. 13. (a) Schematic of E-DCDM system, (b) eye diagram, and (c) demultiplexer

The main advantage of DCDM is the inherent self-symbol synchronized system. As highlighted in Figure 13(a), there is one and only one rising edge transition in each multiplexed symbol (except the case that all user send bit 0), which located at the beginning of the symbol. Comparing these properties with RZ-TDM, they can only support the bit synchronization and required external symbol synchronization scheme. For comparison purpose, three-user RZ-TDM signal is shown in Figure 13(a). Another unique advantage of DCDM is the impulse transitions in the multiplexed signal spectrum. Figure 14(a) shows modulated spectra of 3×10 Gb/s DCDM, where the modulation is performed using a LD operated at 1550 nm. It can be seen that DCDM has multiple impulse transitions in its spectra. In general, the number of impulses are equal to the number of multiplexing users with spacing equal to the single user bit rate or the symbol rate, which in Figure 14(a) the transitions repeated every 10 GHz. Comparing this against RZ-TDM shows that it has only one impulse transition, which is located at frequency equal to the channel aggregate bit rate, which it is 30 GHz away from the carrier frequency (Figure 14(b)). DCDM provides smaller spectra width in comparison to RZ-TDM.

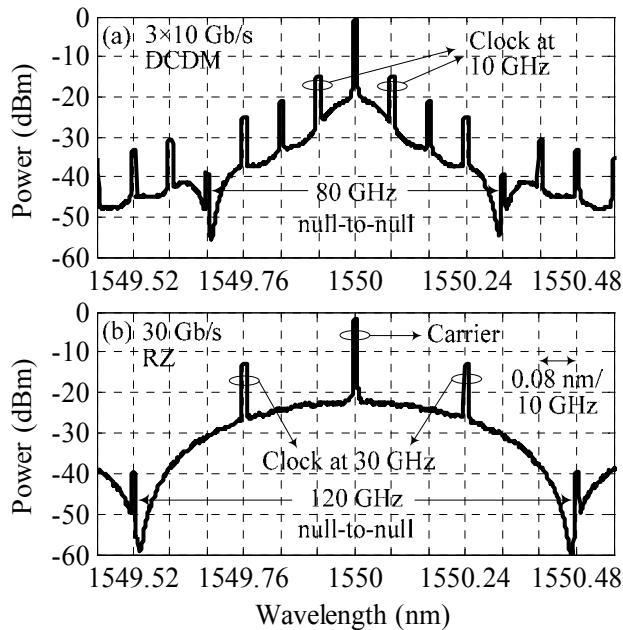


Fig. 14. Modulation spectra of 3×10 Gb/s DCDM and 30 Gb/s RZ-TDM

DCDM demultiplexer operates in electrical domain. Considering Figure 13(a), at the receiver side, the optical signal is first detected by a P-i-N photodiode (PD) and passed through a low-pass filter (LPF) followed by the demultiplexer. In the demultiplexer (Figure 13(b)), a clock recovery circuit (CRC) and edge detection circuit (EDC) is used to recover the clock and detect the beginning of each multiplexed symbol. A 10 GHz clock is recovered referring to the impulse transition available in the signal spectra (Figure 14(a)). On the other hand, considering the 10 GHz recovered clock, the beginning of each multiplexing symbol can be detected using the EDC. Three sampling circuits are synchronized with the recovered clock or the detected edges. By putting appropriate delay lines for each sampler as shown in Figure 13(b), the first, second, and third sampler (S_1 , S_2 , S_3) take samples at $T_s/8$, $3T_s/8$, and $5T_s/8$ s per symbol respectively. The frequency of all samplers is equal to the symbol rate (10 GHz). Outputs of the samplers are fed into the decision and regeneration unit. In this unit, the sampled values are compared against three threshold values thr_1 , thr_2 , and thr_3 , and the decision is performed based on the operations shown in Table 1. Regarding to the rules in that table, for U25, the decision is made based on the information taken from the two consecutive sampling points, S_1 and S_2 . If amplitudes of those two adjacent sampling points are equal, bit 0 is regenerated (rules 1 to 3 from Table 1 and cases 1, 3, 5, and 7 from Figure 13(a)). On the other hand, when the amplitude at S_1 is one level greater than S_2 , bit 1 is regenerated (rules 4 to 6 from Table 1 and cases 2, 4, 6, and 8 from Figure 13(a)). The same method is used for U50, which utilizes information extracted from S_2 and S_3 . Finally, U75 is recovered from only S_3 by comparing amplitude of S_3 against thr_1 .

Rules for U1						Cases	
1	if	$(S1 < thr_1)$	&	$(S2 < thr_1),$	then	$U1 = 0$	1
2	if	$(thr_1 \leq S1 < thr_2)$	&	$(thr_1 \leq S2 < thr_2),$	then	$U1 = 0$	3, 5
3	if	$(thr_2 \leq S1 < thr_3)$	&	$(S2 \geq thr_2),$	then	$U1 = 0$	7
4	if	$(thr_1 \leq S1 < thr_2)$	&	$(S2 < thr_1),$	then	$U1 = 1$	2
5	if	$(thr_2 \leq S1 < thr_3)$	&	$(thr_1 \leq S2 < thr_2),$	then	$U1 = 1$	4, 6
6	if	$(S1 \geq thr_3)$	&	$(S2 \geq thr_2),$	then	$U1 = 1$	8
Rules for U2						Cases	
1	if	$(S2 < thr_1)$	&	$(S3 < thr_1),$	then	$U2 = 0$	1, 2
2	if	$(thr_1 \leq S2 < thr_2)$	&	$(S3 \geq thr_1),$	then	$U2 = 0$	5, 6
3	if	$(thr_1 \leq S2 < thr_2)$	&	$(S3 < thr_1),$	then	$U2 = 1$	3, 4
4	if	$(S2 \geq thr_2)$	&	$(S3 \geq thr_1),$	then	$U2 = 1$	7, 8
Rules for U3						Cases	
1	if	$(S3 < thr_1),$	then	$U3 = 0$			1, 2, 3, 4
2	if	$(S3 \geq thr_1),$	then	$U3 = 1$			5, 6, 7, 8

Table 1. Data recovery rules for three-DCDM users

The main disadvantage of DCDM system is that it required high OSNR in comparison to the binary signalling such as RZ or NRZ. This is due to the fragmentation of the main eye to several smaller eyes (Figure 13(b)) similar to the multilevel amplitude signalling. Performance of DCDM is improved using optical multiplexer by adding the cost in multiplexer, which required one modulator for each multiplexing user. In terms of transmitter and receiver complexity, DCDM has simple transmitter and receiver. At the same time, DCDM allows high speed aggregate bit rate to be recovered at symbol or baud rate, which made DCDM receiver very economic. Furthermore, this technique allow more users to be allocated in a WDM channel, which contributes towards improvement in SE.

4. Comparison between Multiplexing Techniques and Modulation Formats

Table 2 shows a comparison between different modulation formats and multiplexing techniques at 40 Gb/s. The comparison is made based on transmitter (Tx) and receiver (Rx) complexity, optical signal-to-noise ratio (OSNR), chromatic dispersion (CD), null-to-null modulated bandwidth (MBW) and clock recovery frequency (CRF).

Multiplexing techniques improve transmission capacity of optical networks. TDM with a simple transmitter and receiver can improve channel utilization by expending spectral bands or bandwidth. This technique is limited by the electronics technology (for example, based on today technology, the maximum aggregated bit rate per single channel reported is 114 Gb/s). PDM can double the channel capacity with the same spectral band as required by TDM systems. However, it suffers from channel crosstalk due to PMD and requiring very high speed polarization controllers, which increase the system complexity and the cost. OFDM improves channels capacity by allowing hundreds of low speed channels to form a single channel with very complex transmitter and receiver and requiring 3 stages of precise synchronizations. DCDM with simple transceivers can support multiple channels per WDM channel with requiring smaller spectral bandwidth in comparison to the RZ-TDM. It also facilitates symbol synchronization and allows high speed transmission to be recovered at low speed clock. However, it suffers from the high OSNR requirement.

40Gb/s Modulation & multiplexing techniques	Tx complexity	Rx complexity	OSNR (dBm)	CD (ps/nm)	MBW (GHz)	CRF (GHz)	
NRZ-TDM	1 M	1 PD	Sim: 16.5 (E-3), 19.8 (E-9) Exp: ~23.3 (E-9)	54	80	40	
50% RZ-TDM	2 Ms	1 PD	Sim: 14.4 (E-3), 18.3 (E-9) Exp: ~21 (E-9)	48	160	40	
67% CS-RZ-TDM	2 Ms	1 PD	Sim: 14.9 (E-3), 15.1 (E-3), 18.8 (E-9)	42	120	40	
DB			Sim: 22.4 (E-9)		40		
NRZ-DPSK	1 M	1 DI + 2 PDs	Sim: 11.7 (E-3), 13.5 (E-3), 18.5 (E-9) Exp: ~20 (E-9)	74	80	40	
50% RZ-DPSK	2 Ms	1 DI + 2 PDs	Sim: 11.1 (E-3), 15.6 (E-9) Exp: ~18 (E-9)	50	160	40	
NRZ-DQPSK	2 Ms	2 DIs + 4 PDs	Sim: 13.2 (E-3), 15 (E-3), 13.4 (E-3), 20.5 (E-9) Exp: ~24.5 (E-9)	168	40	20	
50% RZ-DQPSK	2 Ms	2 DIs + 4 PDs	Sim: 12.2 (E-3), 15 (E-3), 17.7 (E-9), 20.2 (E-9) Exp: ~23.3 (E-9)	161	80	20	
RZ-DQPSK-PDM	3PCs, 2 Ms, 1PM, 1RZ-PG, 2PBS, 1PBC	PS, PBS, 2DIs, 4PDs, PC	Exp: 13.7 (E-9)		40	10	
NRZ-16-QAM	3 PCs, 1 M	2 PDs, 3 PCs, Pol, TFL	Sim: 20.9 (E-9)		20	10	
E-DCDM (2 × 20 Gb/s)	1 M	1 PD	Sim: 17.8 (E-3), 21.74 (E-9)	62	120	20	
E-DCDM (4 × 10 Gb/s)	1 M	1 PD	Sim: 21.6 (E-3), 26.4 (E-9)	58	100	10	
E-DCDM (7 × 5.71 Gb/s)	1 M	1 PD	Sim: 27 (E-3), 31.4 (E-9)	52	91.4	5.71	
WDM: Wavelength division multiplexing		NRZ: Non return-to-zero		RZ: Return-to-zero		M: Modulator	
DQPSK: Differential quadrature phase shift keying		CD: Chromatic dispersion		DB: Duobinary		Num: Numerical	
QAM: Quadrature amplitude modulation		RS: Receiver sensitivity		Tx: Transmitter		Rx: Receiver	
PDM: Polarization division multiplexing		PS: Polarization stabilizer		Exp: Experimental		Pol: Polarizer	
CRF: Clock recovery frequency		DI: Delay interferometer		PD: Photodetector		OOK: On off keying	
PBC: Polarization beam combiner		PC: Polarization controller		PG: Pulse generator			
PBS: Polarization beam splitter		TFL: Tunable fiber laser		MBW: Modulated bandwidth			

Table 2. Performance and complexity comparison between different multiplexing techniques and modulation formats at 40 Gb/s aggregation bit rate (Daikoku, Yoshikane, & Morita, 2005; Essiambre, Winzer, & Grosz, 2006; Jumpei et al., 2007; Leibrich, Serbay, Baumgart, Rosenkranz, & Schimmler, 24-28 September 2006; Martelli et al., 2008; Ohm & Freckmann, 2004)

Advanced modulation formats such as QASK, QAM, QPSK, QDPSK and DB double channel capacity of optical network with requiring the same spectral band as TDM. However, they have complex and costly transmitter and receiver. Beside all these techniques, WDM allows the use of available spectra in optical domain but only at one channel per wavelength.

Combining WDM with individual or combination of the techniques mentioned above and/or other techniques can increase the transmission capacity tremendously and improve spectral efficiency of the optical fiber communication systems. Overall, the goal of all multiplexing techniques and modulation format are to increase spectral efficiency of WDM networks. To date, PDM and DQPSK and combination of these two techniques achieved the most attention from the communication society. At the same time, DCDM has some attractive and unique properties that have not been discovered in other techniques. This technique has the potential to become an alternative multiplexing technique but it required more investigation on the practical and experimental systems.

5. Conclusion

The main objective in the communication systems is to transmit as much as possible information in as low as possible bandwidth and cost. Different modulation formats such as M-ary ASK, QPSK/DQPSK, QAM and DB are proposed to improve WDM channel capacity. M-ary ASK improves the channel capacity by transmitting more than one bit per signal element utilizing different signal levels or multilevel signals. QPSK/DQPSK utilizes multiple phases for transmit more than one bit per signal element. QAM improve channel capacity by transmitting more than one bit per signal element utilizing different phases and different amplitudes. DB use either three amplitude levels or two amplitudes (like binary signals) and one redundant phase element instead of the third level. All the advanced modulation schemes are limited to double or triple the channel utilization but all of them improve the channel capacity or the spectral efficiency. On the other hand, different multiplexing techniques such as TDM, WDM, OFDM, PDM and DCDM are proposed to improve the channel utilization. In TDM, different users share the same WDM channel by allocating each user different time slot. Using WDM, the available optical spectrum can be to utilize to support multiple numbers of users. In this technique, each user is assigned a wavelength as the carrier signal. In OFDM, utilizing IDFT many different RF signals can be assigned as the carrier for many low bit rate users. PDM allows two users to be carried over two different polarizations, vertical and horizontal polarizations. In DCDM, different users signed with different RZ duty cycles to share the same WDM channel. Except PDM, all other multiplexing techniques can support multiple users. Eventhough multiplexing techniques improve the channel utilization, but all of them except PDM, failed to improve the spectral efficiency of the link. PDM act like modulation schemes that can double the channel capacity or the spectral efficiency. Amongst all these multiplexing techniques and modulation schemes, PDM and QPSK/DQPSK or combinations of them have obtained the most attention in the communication systems. Finally, DCDM can reduce the clock recovery frequency significantly.

6. References

- Abas, A. F. (2006). *Chromatic Dispersion Compensation in 40 Gbaud Optical Fiber WDM Phase-Shift-Keyed Communication Systems*. Universität Paderborn.
- Abas, A. F., Hidayat, A., Sandel, D., Milivojevic, B., & Noe, R. (2007). 100 km fiber span in 292 km, 2.38 Tb/s (16×160 Gb/s) WDM DQPSK polarization division multiplex transmission experiment without Raman amplification. *Optical Fiber Technology*, 13(1), 46-50.
- Abdullah, M. K., Abdalla, M. F., F.Abas, A., & Mahdiraji, G. A. (2007). *Duty-cycle Division Multiplexing (DCDM): A Novel and Economical Optical Multiplexing and Electrical Demultiplexing technique for High Speed Fiber Optics Networks*. Paper presented at the Wireless and Optical Communications Networks, 2007. WOCN '07. IFIP International Conference on.
- Andre, P., Kauffmann, N., Desrousseaux, P., Godin, J., & Konczykowska, A. (1999). *InP HBT circuits for high speed ETDM systems*. Paper presented at the Circuits and Systems, 1999. ISCAS '99. Proceedings of the 1999 IEEE International Symposium on.
- Arumugam, M. (2001). Optical fiber communication -- An overview. *Pramana - Journal of physics*, 57(5 & 6), 849-869.
- Avlonitis, N., Yeatman, E. M., Jones, M., & Hadjifotiou, A. (2006). Multilevel amplitude shift keying in dispersion uncompensated optical systems. *Optoelectronics, IEE Proceedings -*, 153(3), 101-108.
- Bigo, S., Frignac, Y., Charlet, G., Idler, W., Borne, S., Gross, H., et al. (2001). *10.2 Tbit/s (256x42.7 Gbit/s PDM/WDM) transmission over 100 km TeraLight™ fiber with 1.28 bit/s/Hz spectral efficiency*. Paper presented at the Optical Fiber Communication Conference and Exhibit, 2001. OFC 2001.
- Charlet, G., Renaudier, J., Mardoyan, H., Tran, P., Pardo, O. B., Verluise, F., et al. (2008). *Transmission of 16.4Tbit/s Capacity over 2,550km Using PDM QPSK Modulation Format and Coherent Receiver*. Paper presented at the Proc. OFC/NFOEC, San Diego, California.
- Cho, P. S., Grigoryan, V. S., Godin, Y. A., Salamon, A., & Achiam, Y. (2003). Transmission of 25-Gb/s RZ-DQPSK signals with 25-GHz channel spacing over 1000 km of SMF-28 fiber. *Photonics Technology Letters, IEEE*, 15(3), 473-475.
- Chraplyvy, A. R., Gnauck, A. H., Tkach, R. W., Zyskind, J. L., Sulhoff, J. W., Lucero, A. J., et al. (1996). 1-Tb/s transmission experiment. *IEEE Photonics Technology Letters*, 8, 1264-1266.
- Christen, L., Nuccio, S. R., Xiaoxia, W., & Willner, A. E. (2007). *Polarization-Based 43 Gb/s RZ-DQPSK Receiver Design Employing a Single Delay-Line Interferometer*. Paper presented at the Lasers and Electro-Optics, 2007. CLEO 2007. Conference on.
- Ciaramella, E. (2002). Nonlinear impairments in extremely dense WDM systems. *Photonics Technology Letters, IEEE*, 14(6), 804-806.
- Cimini, L. J., Jr., & Foschini, G. J. (1993). Can multilevel signaling improve the spectral efficiency of ASK optical FDM systems? *Communications, IEEE Transactions on*, 41(7), 1084-1090.
- Daikoku, M., Yoshikane, N., & Morita, I. (2005). *Performance comparison of modulation formats for 40 Gbit/s DWDM transmission systems*. Paper presented at the Optical Fiber Communication Conference, 2005. Technical Digest. OFC/NFOEC.

- Derksen, R. H., Moller, M., & Schubert, C. (2007). *100-Gbit/s Full-ETDM Transmission Technologies*. Paper presented at the Compound Semiconductor Integrated Circuit Symposium, 2007. CSIC 2007. IEEE.
- Dong-Soo, L., Man Seop, L., Yang Jing, W., & Nirmalathas, A. (2003). Electrically band-limited CSRZ signal with simple generation and large dispersion tolerance for 40-Gb/s WDM transmission systems. *Photonics Technology Letters, IEEE*, 15(7), 987-989.
- Elbers, J. P. (2002). *High-capacity DWDM/ETDM transmission*. Paper presented at the Optical Fiber Communication Conference and Exhibit, 2002. OFC 2002.
- Essiambre, R.-J., Winzer, P. J., & Grosz, D. F. (2006). Impact of DCF properties on system design. *Journal of Optical and Fiber Communications Reports*, 3, 221-291.
- Freund, R., Molle, L., Raub, F., Caspar, C., Karkri, M., & Weber, C. (2005). *Triple-(S/C/L)-band WDM transmission using erbium-doped fibre amplifiers*. Paper presented at the Optical Communication, 2005. ECOC 2005. 31st European Conference on.
- Fukuchi, K., Kasamatsu, T., Morie, M., Ohhira, R., Ito, T., Sekiya, K., et al. (2001). *10.92-Tb/s (273 x 40-Gb/s) triple-band/ultra-dense WDM optical-repeated transmission experiment*. Paper presented at the Optical Fiber Communication Conference and Exhibit, 2001. OFC 2001.
- Gnauck, A. H., Charlet, G., Tran, P., Winzer, P., Doerr, C., Centanni, J., et al. (2007). *25.6-Tb/s C+L-Band Transmission of Polarization-Multiplexed RZ-DQPSK Signals*. Paper presented at the Proc. OFC/NFOEC, Anaheim, California.
- Gnauck, A. H., Charlet, G., Tran, P., Winzer, P. J., Doerr, C. R., Centanni, J. C., et al. (2008). *25.6-Tb/s WDM Transmission of Polarization-Multiplexed RZ-DQPSK Signals*. *J. Lightwave Technology*, 26(1), 79-84.
- Gnauck, A. H., Winzer, P. J., Dorrer, C., & Chandrasekhar, S. (2006). Linear and nonlinear performance of 42.7-Gb/s single-polarization RZ-DQPSK format. *Photonics Technology Letters, IEEE*, 18(7), 883-885.
- Gyo-Sun, H., Un-Seung, P., Sung-Ho, K., Youngchul, C., Jae-Seung, L., & Byoung-Whi, K. (2007). *2.5-Tb/s (256 x 12.4 Gb/s) Transmission of 12.5-GHz-Spaced Ultra-dense WDM Channels over a Standard Single-Mode Fiber of 2000 km*. Paper presented at the Optical Fiber Communication and the National Fiber Optic Engineers Conference, 2007. OFC/NFOEC 2007. Conference on.
- Han, Y., & Li, G. (2006). Experimental demonstration of direct-detection quaternary differential polarization-phaseshift keying with electrical multilevel decision. *Electronics Letters*, 42, 109-111.
- Hayee, M. I., Cardakli, M. C., Sahin, A. B., & Willner, A. E. (2001). Doubling of Bandwidth Utilization Using Two Orthogonal Polarizations and Power Unbalancing in a Polarization-Division-Multiplexing Scheme. *IEEE Photonics Technology Letters*, 13(8), 881-883.
- Hill, P. M., Olshansky, R., & Burns, W. K. (1992). Optical polarization division multiplexing at 4 Gb/s. *IEEE Photonics Technology Letters*, 4(5), 500-502.
- Hinz, S., Sandel, D., Noe, R., & Wust, F. (2000). Optical NRZ 2 x 10 Gbit/s polarisation division multiplex transmission with endless polarisation control driven by correlation signals. *Electronics Letters*, 36(16), 1402-1403.
- Hinz, S., Sandel, D., Wust, F., & Noe, R. (2001). Interference detection enabling 2 x 20 Gbit/s RZ polarisation division multiplex transmission. *Electronics Letters*, 37(8), 511-512.
- Ho, K.-P. (2005). *Phase-modulated optical communication systems*: Springer, USA.

- Ibrahim, S. K., Bhandare, S., & Noe, R. (2006). Performance of 20 Gb/s quaternary intensity modulation based on binary or duobinary modulation in two quadratures with unequal amplitudes. *Selected Topics in Quantum Electronics, IEEE Journal of*, 12(4), 596-602.
- Jansen, S. L., Derksen, R. H., Schubert, C., Zhou, X., Birk, M., Weiske, C. J., et al. (2007). *107-Gb/s full-ETDM transmission over field installed fiber using vestigial sideband modulation*. Paper presented at the Optical Fiber Communication and the National Fiber Optic Engineers Conference, 2007. OFC/NFOEC 2007. Conference on.
- Jansen, S. L., Morita, I., Schenk, T. C. W., & Tanaka, H. (2008). Long-haul transmission of 16×52.5 Gbits/s polarization-division-multiplexed OFDM enabled by MIMO processing (Invited). *Journal of Optical Networking*, 7(2), 173-182.
- Jumpei, H., Kasai, K., Yoshida, M., & Nakazawa, M. A. N. M. (2007). *1 Gsymbol/s, 64 QAM coherent optical transmission over 150 km with a spectral efficiency of 3 bit/s/Hz*. Paper presented at the Proc. OFC/NFOEC, Anaheim, California.
- Kauffmann, N., Blayac, S., Abboun, M., Andre, P., Aniel, F., Riet, M., et al. (2001). InP HBT driver circuit optimization for high-speed ETDM transmission. *Solid-State Circuits, IEEE Journal of*, 36(4), 639-647.
- Kawanishi, T., Sakamoto, T., Miyazaki, T., Izutsu, M., Higuma, K., & Ichikawa, J. (2007). *80 Gb/s DQPSK modulator*. Paper presented at the Optical Fiber Communication and the National Fiber Optic Engineers Conference, 2007. OFC/NFOEC 2007. Conference on.
- Keiser, G. (2000). *Optical fiber communications* (3rd edition ed.): McGraw-Hill.
- Keiser, G. E. (1999). A review of WDM technology and applications. *Optical Fiber Technology*, 5, 3-39.
- Krummrich, P. M., Gottwald, E., Weiske, C. J., Schopflin, A., Kotten, I., & Lankl, B. (2002). *40 Gbit/s ETDM for long haul WDM transmission*. Paper presented at the Lasers and Electro-Optics Society, 2002. LEOS 2002. The 15th Annual Meeting of the IEEE.
- Lach, E., Bulow, H., Kaiser, M., Veith, G., & Bouchoule, S. (1998). *40 Gbit/s TDM field test over 111 km installed G.652 fiber*. Paper presented at the Optical Communication, 1998. 24th European Conference on.
- Lach, E., & Schuh, K. (2006). Recent Advances in Ultrahigh Bit Rate ETDM Transmission Systems. *Lightwave Technology, Journal of*, 24(12), 4455-4467.
- Lach, E., Schuh, K., Junginger, B., Veith, G., Lutz, J., & Moller, M. (2007). *Challenges for 100 Gbit/s ETDM Transmission and Implementation*. Paper presented at the Optical Fiber Communication and the National Fiber Optic Engineers Conference, 2007. OFC/NFOEC 2007. Conference on.
- Lathi, B. P. (1998). *Modern Digital and Analog Communication Systems*: Oxford university press.
- Lee, W. S., Garthe, D., Pettitt, G. A., & Hadjifotiou, A. A. (1997). *40-Gbit/s TDM transmission over 160 km (2 x 80 km) of standard nondispersion-shifted fiber*. Paper presented at the Optical Fiber Communication. OFC 97., Conference on.
- Leibrich, J., Serbay, M., Baumgart, S., Rosenkranz, W., & Schimmler, M. (24-28 September 2006, 24-28 September 2006). *Receiver sensitivity of advanced modulation formats for 40 Gb/s DWDM transmission with and without FEC*. Paper presented at the 32nd European Conference and Exhibition on Optical Communication (ECOC), Cannes, France.

- Lender, A. (1964). Correlative Digital Communication Techniques. *Communication Technology, IEEE Transactions on*, 12(4), 128-135.
- Mahdiraji, G. A., Abdullah, M. K., Mokhtar, M., Mohammadi, A. M., Abdullah, R. S. A. R., & Abas, A. F. ((In Press)). Duty-Cycle-Division-Multiplexing: Bit Error Rate Estimation and Performance Evaluation. *Optical Review*.
- Martelli, P., Boffi, P., Ferrario, M., Marazzi, L., Parolari, P., Pietralunga, S. M., et al. (2008). *Endless Polarization Stabilizer for High Bit-rate Polarization-Division Multiplexed Optical Systems*. Paper presented at the OFC/NFOEC.
- Martelli, P., Boffi, P., Ferrario, M., Marazzi, L., Parolari, P., Righetti, A., et al. (2007). *Uncompensated 20 Gb/s Duobinary Polarization Division Multiplexing Transmission over 200 km*. Paper presented at the Lasers and Electro-Optics, 2007. CLEO 2007. Conference on.
- Miyamoto, Y., Yoneyama, M., Otsuji, T., Yonenaga, K., & Shimizu, N. (1999). 40-Gbit/s TDM transmission technologies based on ultra-high-speed ICs. *Solid-State Circuits, IEEE Journal of*, 34(9), 1246-1253.
- Morita, I., & Yoshikane, N. (2005). *Merits of DQPSK for ultrahigh capacity transmission*. Paper presented at the Lasers and Electro-Optics Society, 2005. LEOS 2005. The 18th Annual Meeting of the IEEE.
- Muoi, T., & Hullett, J. (1975). Receiver Design for Multilevel Digital Optical Fiber Systems. *Communications, IEEE Transactions on [legacy, pre - 1988]*, 23(9), 987-994.
- Nakazawa, M., Yoshida, M., Kasai, K., & Hongou, J. (2006). 20Msymbol/s, 64 and 128 QAM coherent optical transmission over 525km using heterodyne detection with frequency-stabilised laser. *Electronics Letters*, 42(12), 710-712.
- Nasu, Y., Oguma, M., Takahashi, H., Inoue, Y., Kawakami, H., & Yoshida, E. (2008). *Polarization insensitive MZI-based DQPSK demodulator with asymmetric half-wave plate configuration*. Paper presented at the Optical Fiber communication/National Fiber Optic Engineers Conference, 2008. OFC/NFOEC 2008. Conference on.
- Nelson, L. E., & Kogelnik, H. (2000). Coherent crosstalk impairments in polarization multiplexed transmission due to polarization mode dispersion. *Optical Express*, 7(10), 350-361.
- Nelson, L. E., Nielsen, T. N., & Kogelnik, H. (2001). Observation of PMD-Induced Coherent Crosstalk in Polarization-Multiplexed Transmission. *IEEE Photonics Technology Letters*, 13(7), 738-740.
- Noe, R., Hinz, S., Sandel, D., & Wust, F. (2001). Crosstalk detection schemes for polarization division multiplex transmission. *Journal of Lightwave Technology*, 19, 1469-1475.
- Ohm, M., & Freckmann, T. (2004). *Comparison of different DQPSK transmitters with NRZ and RZ impulse shaping*. Paper presented at the Advanced Modulation Formats, 2004 IEEE/LEOS Workshop on.
- Palais, J. C. (2005). *Fiber optic communications* (5th edition ed.): Pearson Prentice Hall.
- Pardo, O. B., Renaudier, J., Mardoyan, H., Tran, P., Charlet, G., & Bigo, S. (2008a). *Investigation of design options for overlaying 40Gb/s coherent PDM-QPSK channels over a 10Gb/s system infrastructure*. Paper presented at the Optical Fiber communication/National Fiber Optic Engineers Conference, 2008. OFC/NFOEC 2008. Conference on.
- Pardo, O. B., Renaudier, J., Mardoyan, H., Tran, P., Charlet, G., & Bigo, S. (2008b). *Investigation of design options for overlaying 40Gb/s coherent PDM-QPSK channels over a 10Gb/s system infrastructure*. Paper presented at the OFC/NFOEC.

- Ramaswami, R., & Sivarajan, K. N. (2002). *Optical Networks: A Practical Perspective*. Morgan Kaufmann
- Renaudier, J., Charlet, G., Salsi, M., Pardo, O. B., Mardoyan, H., Tran, P., et al. (2008). Linear Fiber Impairments Mitigation of 40-Gbit/s Polarization-Multiplexed QPSK by Digital Processing in a Coherent Receiver. *Lightwave Technology, Journal of*, 26(1), 36-42.
- Said, M. M. E., Sitch, J., & Elmasry, M. I. (2005). An electrically pre-equalized 10-Gb/s duobinary transmission system. *Lightwave Technology, Journal of*, 23(1), 388-400.
- Sandel, D., Wust, F., Mirvoda, V., & Noe, R. (2002). Standard (NRZ 1 x 40 Gb/s, 210 km) and polarization multiplex (CS-RZ, 2 x 40 Gb/s, 212 km) transmissions with PMD compensation. *Photonics Technology Letters, IEEE*, 14(8), 1181-1183.
- Sang-Yuep, K., Sang-Hoon, L., Sang-Soo, L., & Jae-Seung, L. (2004). Upgrading WDM networks using ultradense WDM channel groups. *Photonics Technology Letters, IEEE*, 16(8), 1966-1968.
- Savory, S. J., Gavioli, G., Killey, R. I., & Bayvel, P. (2007). *Transmission of 42.8Gbit/s polarization multiplexed NRZ-QPSK over 6400km of standard fiber with no optical dispersion compensation*. Paper presented at the OFC/NFOEC 2007 - Optical Fiber Communication and the National Fiber Optic Engineers Conference 2007.
- Scheerer, C., Glingener, C., Farbert, A., Elbers, J. P., Schopflin, A., Gottwald, E., et al. (1999). 3.2 Tbit/s (80 x 40 Gbit/s) bidirectional WDM/ETDM transmission over 40 km standard singlemode fibre. *Electronics Letters*, 35(20), 1752-1753.
- Schubert, C., Ludwig, R., Ferber, S., Schmidt-Langhorst, C., Huettl, B., & Weber, H. G. (2006). *Single Channel Transmission Beyond 1 Tbit/s*. Paper presented at the Lasers and Electro-Optics Society, 2006. LEOS 2006. 19th Annual Meeting of the IEEE.
- Schuh, K., Junginger, B., Rempp, H., Klose, P., Rosener, D., & Lach, E. (2005). *85.4 Gbit/s ETDM transmission over 401 km SSMF applying UFEC*. Paper presented at the Optical Communication, 2005. ECOC 2005. 31st European Conference on.
- Seo, H. S., Chung, W. J., & Ahn, J. T. (2005). A novel hybrid silica wide-band amplifier covering S+C+L bands with 105-nm bandwidth. *Photonics Technology Letters, IEEE*, 17(9), 1830-1832.
- Shieh, W., & Athaudage, C. (2006). Coherent optical orthogonal frequency division multiplexing. *Electronics Letters*, 42(10).
- Shieh, W., Bao, H., & Tang, Y. (2008). Coherent optical OFDM: theory and design. *Optical Express*, 16(2), 841-859.
- Shieh, W., Yi, X., Ma, Y., & Yang, Q. (2008). Coherent optical OFDM: has its time come? [Invited]. *Journal of Optical Networking*, 7(3), 234-255.
- Suzuki, K., Kubota, H., Kawanishi, S., Tanaka, M., & Fujita, M. (2001). High-speed bidirectional polarisation division multiplexed optical transmission in ultra low-loss (1.3 dB/km) polarisation-maintaining photonic crystal fibre. *Electronics Letters*, 37(23), 1399-1401.
- van den Borne, D., Jansen, S. L., Gottwald, E., Schmidt, E. D., Khoe, G. D., & de Waardt, H. (2008). *DQPSK modulation for robust optical transmission*. Paper presented at the Optical Fiber communication/National Fiber Optic Engineers Conference, 2008. OFC/NFOEC 2008. Conference on.
- Walklin, S., & Conradi, J. (1999). Multilevel signaling for increasing the reach of 10 Gb/s lightwave systems. *Lightwave Technology, Journal of*, 17(11), 2235-2248.

- Weber, H. G., Ferber, S., Kroh, M., Schmidt-Langhorst, C., Ludwig, R., Marembert, V., et al. (2005). *Single channel 1.28 Tbit/s and 2.56 Tbit/s DQPSK transmission*. Paper presented at the Optical Communication, 2005. ECOC 2005. 31st European Conference on.
- Weber, H. G., Ferber, S., Kroh, M., Schmidt-Langhorst, C., Ludwig, R., Marembert, V., et al. (2006). Single channel 1.28 Tbit/s and 2.56 Tbit/s DQPSK transmission. *Electronics Letters*, 42(3), 178-179.
- Weber, H. G., Ludwig, R., Ferber, S., Schmidt-Langhorst, C. A., Kroh, M. A., Marembert, V. A., et al. (2006). Ultrahigh-Speed OTDM-Transmission Technology. *Lightwave Technology, Journal of*, 24(12), 4616-4627.
- Wei, X., Liu, X., Chandrasekhar, S., Gnauck, A. H., Raybon, G., Leuthold, J., et al. (2002). *40 Gb/s Duobinary and Modified Duobinary Transmitter Based on an Optical Delay Interferometer*. Paper presented at the Optical Communication, 2002. ECOC 2002. 28th European Conference on.
- Weinsten, S. B., & Ebert, P. M. (1971). Data transmission by frequency-division multiplexing using the discrete Fourier transform. *IEEE Transactions on Communication*, 19, 628-634.
- Winzer, P. J., & Essiambre, R. J. (2006). Advanced Modulation Formats for High-Capacity Optical Transport Networks. *Lightwave Technology, Journal of*, 24(12), 4711-4728.
- Winzer, P. J., & Hoon, K. (2003). Degradations in balanced DPSK receivers. *Photonics Technology Letters, IEEE*, 15(9), 1282-1284.
- Wree, C., Hecker-Denschlag, N., Gottwald, E., Krummrich, P., Leibrich, J., Schmidt, E. D., et al. (2003). High spectral efficiency 1.6-b/s/Hz transmission (8 x 40 Gb/s with a 25-GHz grid) over 200-km SSMF using RZ-DQPSK and polarization multiplexing. *Photonics Technology Letters, IEEE*, 15(9), 1303-1305.
- Yan, L. S., Zhang, B., Belisle, A., Willner, A. E., & Yao, X. S. (2007). *Automatic All-Optical Detection in Polarization-Division-Multiplexing System Using Power Unbalanced Transmission*. Paper presented at the Lasers and Electro-Optics, 2007. CLEO 2007. Conference on.
- Yao, X. S., Yan, L.-S., Zhang, B., Willner, A. E., & Jiang, J. (2007). All-optic scheme for automatic polarization division demultiplexing. *Optical Express*, 15(12), 7407-7414.
- Yonenaga, K., & Kuwano, S. (1997). Dispersion-tolerant optical transmission system using duobinary transmitter and binary receiver. *Lightwave Technology, Journal of*, 15(8), 1530-1537.
- Yonenaga, K., Kuwano, S., Norimatsu, S., & Shibata, N. (1995). Optical duobinary transmission system with no receiver sensitivity degradation. *Electronics Letters*, 31(4), 302-304.
- Yoneyama, M., Miyamoto, Y., Otsuji, T., Hirano, A. A., Kikuchi, H. A., Ishibashi, T. A., et al. (1999). *Fully electrical 40-Gbit/s TDM system prototype and its application to 160-Gbit/s WDM transmission*. Paper presented at the Optical Fiber Communication Conference, 1999, and the International Conference on Integrated Optics and Optical Fiber Communication. OFC/IOOC '99. Technical Digest.
- Yoshida, M., Goto, H., Kasai, K., & Nakazawa, M. (2008). 64 and 128 coherent QAM optical transmission over 150 km using frequency-stabilized laser and heterodyne PLL detection. *Optics Express*, 16(2), 829-840.

- Yoshikane, N., & Morita, I. (2004). *1.14 b/s/Hz spectrally-efficient 50 x 85.4 Gb/s transmission over 300 km using copolarized CS-RZ DQPSK signals*. Paper presented at the Optical Fiber Communication Conference, 2004. OFC 2004.
- Zahedi, E. (2002). *Digital Data Communication*: Prentice Hall.
- Zhou, X., Yu, J., Huang, M.-F., Shao, Y., Wang, T., Magill, P., et al. (22-26 March 2009). *32Tb/s (320x114Gb/s) PDM-RZ-8QAM transmission over 580km of SMF-28 ultra-low-loss fiber*. Paper presented at the OFC/NFOEC.
- Zhu, B., Leng, L., Nelson, L. E., Knudsen, S., Bromage, J., Peckham, D., et al. (2001). *1.6 Tb/s (40 × 42.7 Gb/s) transmission over 2000 km of fiber with 100-km dispersion-managed spans*. Paper presented at the Optical Communication, 2001. ECOC '01. 27th European Conference on.

A Survey on the Design of Binary Pulse Compression Codes with Low Autocorrelation

Maryam Amin_Nasrabadi* and Mohammad_Hassan Bastani†

**BasamadAzma Co., †Sharif University of Technology
Iran*

1. Introduction

Simple pulsed radar is limited in range sensitivity by the average radiation power and, in range resolution by the pulse length. The design of any radar always involves a compromise between the two constraints. Waveform design aims to seek an appropriate harmony that best suits the relevant application. The pulse compression theory has been introduced in order to get a high range resolution as well as a good detection probability.

One of the basic types of pulse compression is binary phase coding which encodes the transmitted pulse with information that is compressed (decoded) in the receiver of the radar.

The study of the peak sidelobe level (PSL) binary sequences occurs as a classical problem of signal design for digital communication and, in equivalent guise, in analytic number theory. It has also become a notorious problem of combinatorial optimization. For years mathematicians, engineers, physicists and chemists have sought a systematic way to construct long binary sequences with low PSL.

In this Chapter, we describe pulse compression technique in radar waveform design. In order to make the presentation self-contained, we start by providing a short summary of waveform design and an introduction to principle behind pulse compression by compiling the basic tools required for analyzing and comparing different radar signals.

After that, we talk about binary sequence, its desired properties and general types of methods for finding and generating such waveforms. We keep on by an overview and introducing the existing methods and search routine done.

We conclude the chapter with a brief survey of the results exhibited yet for low autocorrelation binary sequences. We mention a table of complete results presented and also introduce a histogram to unscramble them visually and predict the future.

2. Why is pulse compression needed?

One of the most important usages of radar is range finding which is done through measuring time delay, Δt ; it takes a pulse to travel the two-way path between the radar and the target.

$$R = \frac{c\Delta t}{2} \quad (1)$$

Where, c is denoted as speed light.

In general, a pulsed radar transmits and receives a train of pulses, as illustrated by Figure 1.

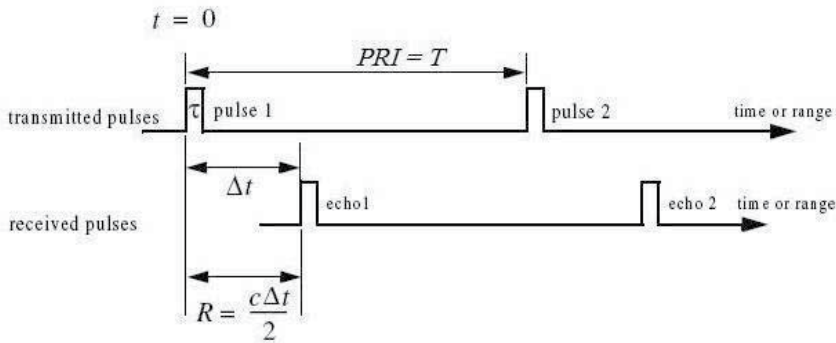


Fig. 1. Illustrating range.

By definition, Range Resolution is the ability to detect targets close proximity to each other as distinct objects only by measurement of their ranges (distances from radar) which usually expressed in terms of the minimum distance by which two targets of equal strength at the same azimuth and elevation angles must be spaced to be separately distinguishable. Resolution in the range domain ΔR corresponds to the resolution τ in the time domain, and is set by the pulsewidth according to $\Delta R = c\tau/2$ (for pulse-compression waveform, τ is the pulsewidth after pulse compression).

Without pulse compression, the instantaneous bandwidth of radar receiver, B , is equal to pulse bandwidth which is usually set to $1/\tau$; thus

$$\Delta R = \frac{c\tau}{2} = \frac{c}{2B} \quad (2)$$

In general, radar users and designers alike seek to minimize ΔR in order to enhance the radar performance. As suggested by equation (2), in order to achieve fine range resolution one must minimize the pulse width or maximize the bandwidth.

On the other hand, as illustrated in Figure 1., during each PRI¹ the radar radiates energy only for τ seconds and listens for target returns for the rest of PRI.

Let P_{av} , P_t and E_p stand for average transmitted power, peak transmitted power and pulse energy, respectively. So,

¹ Pulse Repetition Interval

$$P_{av} = P_t \left(\frac{\tau}{T} \right) \quad (3)$$

$$E_p = P_t \cdot \tau = P_{av} \cdot T \quad (4)$$

With regard to equations (3) and (4) and also Figure 1., above solutions will reduce the average transmitted power. Furthermore, in accordance with Radar Equation (equation (5)), maximum range and thus detection probability will decrease.

$$R_{\max} = \left(\frac{P_t G^2 \lambda^2 \sigma}{(4\pi)^3 K T_e BFL (SNR)_{\min}} \right)^{1/4} \quad (5)$$

So, it seems that the only way to account for these problems and have good range resolution is increasing the peak transmitted power, whereas there are technical limitations for the maximum peak power, such as maximum high voltage or power from the output stage, or waveguide breakdown. So, the only approach for achieving fine range resolution while maintaining adequate average transmitted power is using pulse compression techniques (Mahafza & Alabama, 2000; Skolnik, 2001) which is the main subject of this chapter and will be expatiated.

For clarity, consider this example:

Example:

Desired resolution: $R = 15$ cm

Required bandwidth: $B = 1$ GHz

Required pulse energy: $E = 1$ mJ

By using equation (4), two solutions are as follows:

Brute force approach:

Raw pulse duration: $\tau = 1$ ns

Required peak transmitted power: $P = 1$ MW!

Pulse compression approach:

Pulse duration: $\tau = 0.1$ ms

Required peak transmitted power: $P = 10$ W

It is good to mention that, required range resolution for a given radar is dependent on its performance (detection, recognition, identification, etc.). For example, see table R26 in (Barton & Leonov, 1998) about resolution required for target interpretation tasks.

3. Pulse compression

Pulse compression allows radar to use long waveforms in order to obtain high energy and simultaneously achieve the resolution of a short pulse by internal modulation of the long pulse. This technique can increase signal bandwidth through frequency or phase coding. Although, amplitude modulation is not forbidden but usually is not used. The received echo is processed in the receiver matched filter to produce a short pulse with duration $1/B$, where

B is bandwidth of compressed pulse. This technique is of interest when the radar is not able to generate enough required power. So, a concise summary for pulse compression is gathering two opposite benefits "High Range Resolution" and "high detection probability" concurrently. It can be stated that "radar pulse compression" is a substitute for "short pulse radar", although, each one has its own advantages and difficulties.

Some privileges of short-pulse radar are as follows (Skolnik, 2001):

- range resolution
- range accuracy
- clutter reduction
- interclutter visibility
- glint reduction
- multipath resolution
- multipath height-finding
- target classification
- doppler tolerance
- ECCM
- Minimum range

and some defects of short-pulse are given below:

- Interference with other frequency bands
- Limited maximum range

Pulse compression has all advantages related to short pulse except short minimum range. Furthermore, this technique has obviated limitation in average transmitted power belonging to short pulse. In other hand, it has two disadvantages:

- Increased complexity for generating, transmitting and processing which cause more expense.
- Appearing sidelobes in compressed pulse which result in decreased range resolution.

A twin good and bad effect of pulse compression technique can be shown by Figure 2.

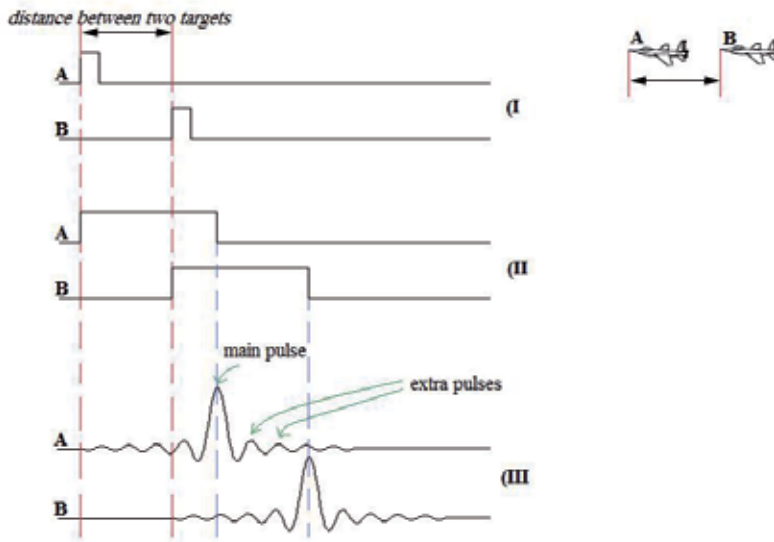


Fig. 2. Resolving targets in range (I) two resolved targets by short-pulse (II) two unresolved targets by long-pulse (III) two resolved target by using pulse compression with long-pulse

Consider two targets which can receive and reflect radar pulse. If these two reflected pulses are narrow enough, they will be separated; A-pulse and B-pulse are indicated reflected pulse from target A and B respectively (Figure 2-I). But, if these pulses are wide, they may overlap and may not be separable (Figure 2-II). If these wide pulses are passed through compression filter, two narrow pulses will be generated which can be distinguished easily (Figure 2-III). This is an efficacy of pulse compression but, one must tolerate a bad effect along with this advantage which is appearing extra pulses around the main one at the output of compression filter (Figure 2-III). This is obvious that if these side pulses have large amplitude, the radar will mistake.

Another parameter needed to introduce is pulse compression ratio which is define here:

$$\text{Pulse compression ratio} = \frac{\text{uncompressed pulse width}}{\text{compressed pulse width}}$$

And can be stated as follow:

$$\text{pulse compression ratio} = B\tau \tag{6}$$

In equation (6), B and τ are denoted as pulse bandwidth and compressed pulse width and usually $B\tau \gg 1$.

4. Different types of pulse compression technique

There are various kinds of pulse compression technique which can be categorized in two general sets. In order to be familiar to these categorizes, some common types of them are considered and since these signals have been discussed in details in many literatures, only a synoptic account of them is cited including its benefits and difficulties. For more information, the reader is referred to (Barton & Leonov, 1998; Skolnik, 2001; Farnett & Stevens, 1991; Levanon & Mozeson, 2004).

4.1 Frequency Modulation

These waveforms can entail linear (LFM) or nonlinear (NLFM) modulation of the frequency of the transmitted waveform. The summary of general characteristics of them given here (Nathanson & Cohen, 1999 ; Barton & Leonov, 1998; Farnett & Stevens, 1991):

4.1.1 Linear frequency modulation (Chirp)

Advantages:

- It is quite insensitive to doppler shifts.
- It is the easiest waveform to generate.
- There is a variety of hardware being available to form and process it.

Disadvantages:

- It has range-doppler cross coupling, resulting in measurement errors unless one of the coordinates (range or doppler) is determined.
- Range sidelobes are high, compared with nonlinear FM and phase-coded waveforms. To reduce sidelobe level, weighting is usually required, resulting 1-to-2-db loss in signal to noise ratio.

4.1.2 Nonlinear frequency modulation

- It has very low range sidelobes without necessitating the use of special weighting for their suppression, and hence has no signal-to-noise ratio loss as does the LFM waveform.
- It is more sensitive to doppler frequency shifts.
- It is complex and its generation techniques has been developed limitedly.

4.2 Phase coding

This waveform is one in which intrapulse modulation is obtained by subdividing the pulse into subpulses of equal duration, each having a particular phase. The phase of each subpulse is set in accordance with a given code or code sequence. Common characteristics of phase coded radar are as follows (Barton & Leonov, 1998; Farnett & Stevens, 1991):

- In comparison with LFM waveforms, they have lower range sidelobes.
- They are preferred in jamming conditions, as the coding of the transmitted signal gives an additional degree of protection against ECM.
- Their resolution performance in a dense target environment or in presence of distributed clutter can be rather poor.

- The implementation of phase coded waveforms is more complex than that of the LFM waveforms.

This modulation can be categorized in two subsets:

4.2.1 Polyphase coding

This waveform uses codes with the number of discrete phase values greater than two. Some properties of this modulation are:

- The range sidelobes of polyphase coded waveforms can be lower than those of the binary coded ones of the same length, but the performance of these waveforms deteriorates rapidly in the presence of doppler frequency shift.
- Generation and processing of polyphase-coded waveforms use technique similar to those of frequency-coded waveforms, but their range sidelobe parameters are much better than for unweighted FM waveforms.

4.2.2 Binary coding

It is the most widely used phase coded waveform which employs two phase. In this type of pulse compression method, a long pulse with duration τ is divided into N "subpulse", each with duration τ_n , where

$$\tau_n = \frac{\tau}{N} \quad (7)$$

The phase of each segment is set to 0° and 180° in accordance with the sequence of element in the phase code, as indicated in Figure 3.

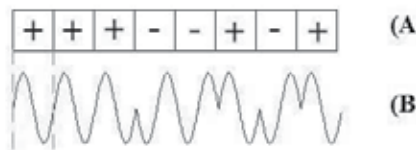


Fig. 3. Binary coded waveform.

(A) binary sequence (modulator). (B) phase coded signal.

If these phases are selected randomly, the resulted waveform will be a noise modulated one and if they are chosen in accordance with some special patterns, the generated binary coded signal will have better function and the goal of this chapter is finding such sequences (Barton & Leonov, 1998; Farnett & Stevens, 1991; Skolnik, 2001).

By using binary coded waveform, the effective width of matched filter output pulse is τ_n and its amplitude is N times greater than primary one. Thus, pulse compression ratio is

$$\text{pulse compression ratio} = B\tau = \frac{\tau}{\tau_n} = N \quad (8)$$

Where, B is bandwidth of modulated pulse and can be calculated by

$$B = \frac{1}{\tau_n} \quad (9)$$

The duration of matched filter output is indeed 2τ . i.e.; in addition to main peak with width τ_n the output of this filter spreads over a 2τ period in both sides of the main lobe. These extra pulses are named time sidelobes.

Table 1. is shown a brief comparison between LFM and Biphas-coded signals (Skolnik 2001). Also, the reader can refer to a table including summary of performance of various pulse compression implementation in (Farnett & Stevens, 1991) and a good and depth overview of HRR¹ radar and comparison between several modulations mentioned in previous sections in (Cohen, 1991; Levanon & Getz, 1994).

Property	LFM	Binary phase coded pulses
Time sidelobes	Good when weighting on receive, and when a loss of about 1 dB can be tolerant	Can be equal to $1/2N$, and are not easy to improve; poor doppler sidelobes
Doppler	Doppler tolerant	Requires filter bank
Ambiguity diagram	Ridge	Thumbtack (but with high sidelobes in plateau)
Pulse compression filter	Single filter can be used for transmit and receive; usually analog for high resolution	Single filter can be used for transmit and receive, but with input at opposite end; usually digital
Complexity	Less complex, especially if Stretch can be used	More complex, (requires filter bank)
Application	High resolution (wide bandwidth)	Long pulses
Other	Range-doppler coupling; has been more widely used than other pulse compression	Bandwidth limited by availability of A/D converter; erroneously thought to be less susceptible to ECM spoofing

Table 1. Comparison of linear FM and Binary phase-coded pulse compression waveforms

¹ High Range Resolution

5. Matched filter

Matched filter have a principle position in pulse compression technique, so before starting to talk about main question, its properties and characteristics are considered briefly.

The most unique characteristic of the matched filter is that it produces the maximum achievable instantaneous SNR¹ at its output when a signal plus additive white noise is present at the input. The peak instantaneous SNR at the receiver output can be achieved by matching the radar receiver transfer function to the received signal and this peak value can be calculated by

$$SNR = \frac{2E}{N_o} \quad (10)$$

Where, E and N_o are denoted as input signal energy and input noise power respectively.

Thus, we can draw the conclusion that the peak instantaneous SNR depends only on the signal energy and input noise power, and is independent of the waveform utilized by the radar.

For this peak instantaneous SNR, matched filter impulse response is:

$$h(t) = s_i^* (\tau - t) \quad (11)$$

Where, s_i(t) is radar transmitted signal. Equation (11) indicates that the peak occurs at τ second after entering signal to matched filter.

Now, consider a radar system that uses signal s_i(t), and assume that a matched filter receiver is utilized. The matched filter input signal can then be represented by

$$x(t) = Cs_i(t - t_1) + n_i(t) \quad (12)$$

Where C is constant, t₁ is an unknown time delay proportional to target range, and n_i(t) is input white noise.

The matched filter output y(t) can be expressed by the convolution integral between the filter's impulse response and x(t),

$$y(t) = \int_{-\infty}^{+\infty} x(u)h(t - u)du \quad (13)$$

And by using equation (11), the matched filter output signal can be written

$$y(t) = \int_{-\infty}^{+\infty} x(u)s_i^* (\tau - t + u)du = \overline{R}_{xs_i} (t - \tau) \quad (14)$$

¹ Signal to Noise Ratio

Where $\overline{R}_{x_s_i}(t - \tau)$ is cross-correlation between $x(t)$ and $s_i(t-\tau)$.

Therefore, the matched filter output can be computed from the cross-correlation between the radar received signal and a delayed replica of the transmitted waveform. If the input signal is the same as the transmitted signal, the output of the matched filter would be the autocorrelation function of the received (or transmitted) signal.

In practice, replicas of the transmitted waveforms are normally computed and stored in memory for use by the radar signal processor when needed (Mahafza & Alabama, 2000; Skolnik, 2001).

In pulse compression technique, initially a long pulse is generated and modulated in transmitter and in receiver, a matched filter is used to compressed signal. The matched filter output is compressed by factor equal to $B\tau$ which is proportional to bandwidth and pulsewidth. i.e.; by utilizing long pulse and wide band modulation, it is possible to gain high compression ratio. Therefore, in using pulse compression, it is good to apply a modulation which can maximize compression ratio while having low sidelobe in compressed signal.

Sidelobe suppression technique can be used on the compressed pulse spectrum in order to reduce the side lobe levels. Usually, the cost associated with such an approach is a loss in the main lobe resolution, and a reduction in the peak value (i.e., loss in the SNR). For more information, the reader can see (Mahafza & Alabama, 2000; Baden & Cohen, 1990; Ackroyd & Ghani, 1973; Rihaczek & Golden, 1971).

6. Autocorrelation function

Since, this function have a critical position in this matter, before continuing to talk about the problem, it is good to review its definition and some important characteristics which researchers are used.

Consider a real binary sequence of length N ,

$$\{a_k\}_{k=0}^{N-1}, \quad a_k = \pm 1 \quad (15)$$

Some definitions related to these codes are as follow (Levanon & Mozeson, 2004; Golay, 1977):

1. Its ACF¹,

$$R(n) = \sum_{i=0}^{N-|n|-1} a_i a_{i+|n|}, \quad n = 0, \pm 1, \dots, \pm(N-1) \quad (16)$$

2. ML² which is defined as the absolute maximum value of ACF,

¹ AutoCorrelation Function

² MainLobe

$$ML = \max_n(R(n)) \quad (17)$$

3. Sidelobes which are described as maximum values of ACF except absolute one.
4. PSL which is denoted as maximum of sidelobes,

$$PSL = \max_{n \neq 0}(|R(n)|) \quad (18)$$

5. E which means energy of a sequence,

$$E = 2 \sum_{n=1}^{N-1} R^2(n) \quad (19)$$

6. ISL¹ which is another parameter for measuring sidelobe levels,

$$ISL = 10 \log_{10} \left(\frac{E}{N^2} \right) \quad (20)$$

7. MF² which is first defined by Golay,

$$MF = \frac{N^2}{E} \quad (21)$$

8. ACF is an even function,

$$R(n) = R(-n) \quad (22)$$

9. ACF is a finite length sequence,

$$R(n) = 0, |n| \geq N \quad (23)$$

10. The absolute maximum value of ACF is at the origin,

$$R(n) \leq R(0), \forall n \quad (24)$$

11. ACF's value for all N-bit sequences at the origin is equal and independent on codes' elements,

¹ Integrated Sidelobe Level

² Merit Factor

$$R(0) = N \quad (25)$$

12. ACF has a limitation on its values,

$$|R(n)| \leq N - |n|, \forall n \quad (26)$$

And

$$1 \leq PSL \leq (N - 1) \quad (27)$$

Another concept which is introduced is Allomorphic forms and psl-preserving operations. Each binary sequence can be stated in 4 forms in terms of autocorrelation function. If $R_a(n)$ is referred to ACF of sequence a_k , these three codes have ACF equal to $R_a(n)$:

- Inverse-amplitude or complement:

$$\{b_k\}, \quad b_k = -a_k, \quad 0 \leq k \leq (N - 1) \quad (28)$$

- Inverse-time or reverse:

$$\{c_k\}, \quad c_k = a_{N-k-1}, \quad 0 \leq k \leq (N - 1) \quad (29)$$

- Complement of reverse:

$$\{d_k\}, \quad d_k = -a_{N-k-1}, \quad 0 \leq k \leq (N - 1) \quad (30)$$

Then,

$$R_a(n) = R_b(n) = R_c(n) = R_d(n), \forall n \quad (31)$$

As PSL is related to the absolute value of ACF, there are some other forms that can have the PSL equal to a_k :

$$\{e_k\}, \quad e_k = (-1)^k a_k, \quad 0 \leq k \leq (N - 1) \quad (32)$$

$$\{f_k\}, \quad f_k = (-1)^{k+1} a_k, \quad 0 \leq k \leq (N - 1) \quad (33)$$

$$\{g_k\}, \quad g_k = (-1)^k a_{N-k-1}, \quad 0 \leq k \leq (N - 1) \quad (34)$$

$$\{h_k\}, \quad h_k = (-1)^{k+1} a_{N-k-1}, \quad 0 \leq k \leq (N - 1) \quad (35)$$

Such that,

$$R_e(n) = R_f(n) = R_g(n) = R_h(n) = (-1)^n R_a(n), \forall n \quad (36)$$

7. Problem definition

Now, everything is ready in order to introduce main problem and its offered solutions. As proved before, the output of the matched filter is the autocorrelation function of the input signal (without any doppler shift frequencies and considering noise). So, a good criterion for choosing biphasic codes is that their autocorrelation have sidelobes as minimum as possible. Barker sequences are one of these optimum codes whose peak sidelobe levels are equal to 1. One of these codes is shown in Figure 4.A and its autocorrelation is drawn in Figure 4.B. As indicated, level of these sidelobes is -22.3 dB below the main peak.

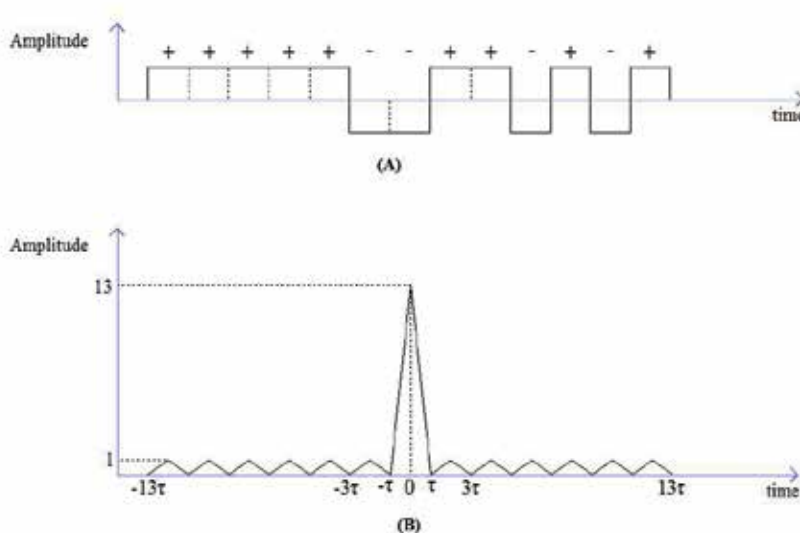


Fig. 4. Complex envelope of transmitted signal which is modulated by Barker sequence (A) Barker sequence (B) complex envelope of matched filter output

Up to now, a few numbers of these codes have been discovered as the longest found one has only 13 elements which is not appropriate for practical usage in radar. It has been shown that there is not any odd-length Barker code longer than 13. It has remained an open question for even-length Barker codes, but it is assumed that there is not any even-length one longer than 4.

Since, most practical applications require peak-to-sidelobe ratio much greater than 13, a compilation of sequences with the lowest possible sidelobes at the longer length is needed. Finding optimal sets of M phases (or codes) for different radar applications has kept radar engineers busy from the early days of radar. The number of possibilities of generating phase codes of length M is unlimited. The criteria for selecting a specific code are the resolution

properties of the resulting waveform, frequency spectrum, and the ease with which the system can be implemented. Sometimes the design is even more complicated by using different phase codes for the transmitted pulse and the reference pulse used at the receiver (possibly even with different lengths). This can improve resolution at the expense of a suboptimal signal-to-noise ratio.

The problem of finding a code that leads to a predetermined range–Doppler resolution is very complicated. A manageable problem is finding a code with a good correlation function. So, it is needed to search for codes whose autocorrelation functions have sidelobes as low as possible.

There are several parameters for measuring the sidelobe levels which are used in different conditions. The matched-filter peak sidelobe level ratio is often used to characterize the level of interference expected from point targets. For volume or surface clutter the interference level is characterized by the matched-filter integrated sidelobe level ratio. The science (or art) of designing radar signals is based on finding signals that yield a matched-filter response that matches a given application. For example, if closely separated targets are to be detected and distinguished in a low-SNR scenario, a radar signal having a matched-filter response that exhibits a narrow mainlobe (the peak) and low sidelobes is required. The mainlobe width and sidelobe level requirements are a function of the expected target separation and expected target RCS difference.

Now, the problem can be written in mathematical format:

It is desired to find N -bit binary sequences whose PSLs or ISLs have the minimum value among all 2^N existing codes.

These codes are often called MPS¹ codes. Finding such these codes is classified in optimization problems and so far, no accurate and analytical solution has been found for it.

- General solutions for this optimization problem are not known (Lindner 1975).
- The search for the least autocorrelated binary sequence resembles the search of the needle in the haystack (Militzer et al.,1998).
- There is no known analytical technique to construct sequences with minimum PSL (Deng & Fan, 1999).
- Although one can identify minimum PSL sequences by conducting an exhaustive search, no general-setting solution for identifying least autocorrelated binary sequences of arbitrary bit length have been described in the literature (Ferrara, 2006).

8. A survey of the methodologies and inquiries

The search methods of finding binary sequences of desired length and PSLs are categorized in two general classes:

- Exhaustive or Global
- Partial or Local

which have their own advantages and disadvantages and are used in accordance with designer's goal.

¹ Minimum Peak Sidelobe

8.1 Global search

Finding MPS codes involves exhaustive computer search. The only disadvantage of this method is that it takes long time, but it associates with these benefits:

1. It can reach to the absolute minimum, despite existing local ones.
2. It is able to find all optimum solutions.
3. It does not need to define any intermediate criteria and can directly search on the base of main one.

So, if all optimum solutions are required, the only key is global search. Of course, there are some limitations for this method too. Calculating of autocorrelation function for each sequence needs $N^2/2$ binary multiplications and $N^2/2$ normal summations. So, total amount of calculations needed to compute ACFs for all N -bit binary sequences are $2^N \cdot N^2/2$ binary multiplications and the same number for normal summations. i.e.; if one bit is added to a code, the needed search time will be doubled minimally. Therefore, for large N , elapsing cpu time becomes very huge, unless special computers are used. Of course, this kind of computers has its own limitations.

The above computations are related to *simple* full search. i.e., at first, all N -bit sequences whose number is 2^N are generated and their ACF are computed. Then, optimum codes are selected.

8.2 Local search

The only advantage of this method is that it requires relatively short time. But, it suffers from these difficulties:

1. Although it finds rather reasonable answers, it can not guarantee that it is able to reach optimum ones. Since, it involves in local minimums.
2. Even if it can find some optimal answers, it is not determined whether it has found all optimum ones or not.
3. The approximation methods usually consider a primary code, then determine next codes by using an intermediate criterion. They find new code by using previous one in this manner. The intermediate criterion must satisfy the main one. In different approach, these criteria are referred to as different names like "evaluation functions", "fitness functions", "error functions", etc. In such methods, the intermediate criteria lead to a better solution, but it can be told that up to now, no such criterion have been found so that is able to navigate the search routine to the best solution. So, definition of the intermediate criterion has important position in these methods.

However, even with the most powerful computers, enumeration algorithms are only able to globally search for the best sequences with rather small length within a reasonable amount of time. Therefore, for longer length effective optimization method should be adopted to search sequences with good rather than the best aperiodic ACF properties.

8.3 History of scientific endeavors

In 1975, Lindner searched all binary sequences up to length 40 in simple-full search method and by utilizing a fast special minicomputer constructed for extensive investigation of the

correlation functions of binary sequences. It took about 50 days. For error detection purposes, inverse-amplitude and inverse-time sequences were not excluded. He summarized his results in a table and introduced several good parameters for each code length which can be used as selection criteria (Lindner, 1975). Although, he has searched all N-bit codes till length 40, he has discarded inverse-time and inverse-amplitude sequences in stating the number of optimum codes. Later on, he published his detailed results in a restored version in 2006 which included almost all optimum found sequences. The obvious important benefits of such this table can be stated in two items:

1. Before starting to search for optimum codes, by referring to this table, one can be informed the optimum PSL of each length.
2. The number of optimum reported codes can be a good criterion to check the validity and accuracy of full search algorithms.

In none-simple exhaustive method, by considering some concepts and characteristics of autocorrelation function (usually allomorphic forms), only a portion of N-element code configuration space is searched.

In 1986, Kerdoc et al. searched sequences of length 51 and found that their minimum attainable PSL is equal to 3. As Lindner, they utilized a special-purpose digital hardware designed for the task. Also, they tried to found longest binary codes which have PSLs equal to 3, 4 and 5. They claimed that there is not any code longer than 51 with PSL equal to 3 and so far, it has remained correct (Kerdoc et al., 1986).

In 1990, Cohen et al. searched all binary sequences from bit length 41 through 48. They employed psl-preserver concept to reduce the search space. Also, they introduced an innovative and recursive algorithm to search a smaller number of codes. They used PSL as selection criterion and enumerated all MPSL codes in these lengths. They completed the efforts of Kerdoc and his co-authors and noted that there are no length 49 or 50 biphasic codes with peak sidelobes of three or less. As Lindner, they have excluded inverse-time and inverse-amplitude sequences in stating the number of optimum codes, but there is a difference between these two routines. Cohen has not searched them at all (Cohen et al., 1990).

In 1996, Mertens searched all binary sequences up to length 48 again, but his criterion was minimum possible energy (E_{\min}) or maximizing MF. He used psl-preserver concept to reduce search time. He compiled a table of sequences with minimum energy and suggested an asymptotic value for MF in large code length (Mertens, 1996).

In 1998, Militzer et al. introduced an evolutionary algorithm and tried to determine the most suitable values for the optimization parameters of the strategy. They used MF as a criterion and showed their highest values for some lengths of skew-symmetric sequences. They compiled a table for comparison their found MF with the highest ones which others have reported (Militzer et al., 1998).

In 1999, Deng and Fan presented another new evolutionary algorithm to generate sequences with low PSL. They obtained a list of sequences of length 49-100 which were better than the other letters in most lengths at that time (Deng & Fan, 1999).

In 2001, Coxson et al. searched binary sequences up to length 69. They exploited all psl-preserver operations and therefore, were able to reduce search space more than before. They introduced a new algorithm which is induced from Cohen's one (Cohen et al., 1990) and exhibited a new version for Lindner's and Cohen's tables. They enumerated the MPSL codes

of each length up to 48 again after excluding all allomorphic forms of a code. Also, in accordance with Kerdoc claim, they tried to provide examples of PSL=4 codes for each length between 49 and 69 but their examples are correct only up to 60 (Coxson et al., 2001).

In 2004, Coxson et al. exhibited an efficient exhaustive algorithm which exploited all psl-preserver operations too. Also, they introduced a fast method for computing the aperiodic autocorrelation function. They established its ability by finding examples of PSL=4 codes for each length from 61 through 70. Also they searched all 64-bit sequences and found all MPSL codes and exhibited all balanced ones in a table. It is the longest power of two codes that have been fully searched (Coxson & Russo, 2004).

Next, Levanon and Mozeson provided a summary of optimal PSLs for lengths up to 69 (Levanon & Mozeson, 2004).

In 2006, Ferrara described an integer programming method for generating low autocorrelation binary codes at arbitrary bit lengths. He compared PSL values and MFs (for bit length 71 through 100) of the sequences obtained with this method to the best literature-based minimal-PSL sequences and compiled a table of best minimum-PSL binary sequences for bit lengths 71 through 100. His record of length 74 was better than the other found codes (Ferrara, 2006).

In 2008, Nunn and Coxson updated table of best minimum-PSL binary sequences from bit lengths 71 through 105. For bit lengths 71 to 82, codes with PSL 4 were found. Under the generally accepted assumption that no PSL-3 binary codes exist for lengths greater than 51, they established, with near certainty, that the optimal PSL for lengths 71-82 is 4 by searching until a single PSL-4 code is discovered for each of these lengths. PSL-5 codes were produced for all lengths from 83 to 105 (Nunn & Coxson, 2008).

8.4 The authors' efforts

The problem of finding best possible PSLs for binary sequences has triggered the authors' interest from year 2005.

The first exhibited method combined several contents and gained its efficiency from Genetic algorithm. It used some other orders of allomorphic forms which reduced search spaces more than the ordinary algorithms which only use three psl-preserver concepts. Although it was a partial search method, it does not involve in local minimum. Also, it could be implemented by a simple scheme for partitioning and parallelizing the search by the fixed upper bound on PSL. Since, it used genetic algorithm, it was possible to optimize found codes by several factors simultaneously included in fitness function. Although the presented result for this algorithm is not good (a 126-bit code with PSL 11), it seems to be able to find better codes by using the better simulation (Amin & Bastani, 2006).

The other suggested approach belonged to Global search. It utilized a branch-and-bound search strategy and PSL-preserver concept. Also, it used some rules and properties of autocorrelations which reduces the configuration space more. A fast recursive method for computing ACFs of binary sequences was presented. In addition, this algorithm could be implemented in parallel mode. All these items lead to less elapsed cpu time and faster execution. For example, it was fast enough to search all codes up to length 50 without requiring any special computer or workstation. Also, this method could be easily modified for local search (Amin & Bastani, 2007).

The recent published method was based on Local one and introduced a new innovative evolutionary algorithm inspired by the Genetic algorithm (Amin & Bastani, 2006) and

Length-Increment one (Amin & Bastani, 2007). Same as other evolutionary algorithm, at first it starts by an initial population and the better the initial codes, the faster the execution is. But, it uses some rules and lemmas which results in not depending on primary population. This proposed algorithm is fast enough to yield optimum or near optimal codes, especially in long length codes. This algorithm was used to generate optimum codes longer than 200, but in a test execution on length shorter than 100 in a matter of hours, the authors were surprised by the results which were very better than others mentioned in literatures. It was able to improve 11 records of previous best mentioned PSLs. So, the authors decided to publish these found records without trying to improve them more. At that time, the paper of Dr. Coxson (Nunn & Coxson, 2008) had been accepted but the authors could not gain access to their results. Later on, I saw mentioned paper and its results. I think it is one of our proposed method excellences that some of its fast found PSLs still have remained as minimum as accessible ones. Also, a histogram for MPSL have been represented which help to visualize the results and predict longer ones. By the histogram, it is expected, not proved, that longer codes have better mainlobe to sidelobe ratio, thus better compression ratio (Amin & Bastani, 2008).

9. Results

The summary of best found PSLs is exhibited in Table 2. These results are accurate for lengths up to 82 and for upper ones, all reported values are relative and it is the Nunn's and Coxson's opinion that many of these codes (of length 83-105) are themselves optimal for PSL.

Codes with a peak sidelobe of 2 were reported for $N \leq 28$ except ones which Barker codes have been found. The MPS codes reported for $28 < N \leq 48$ and $N = 51$ have a sidelobe level of 3, and the MPS codes of length $N = 50$ and $52 \leq N \leq 82$ have a sidelobe level of 4 and the best found PSL for all upper length to 105 is 5.

As all codes of length 1-48 and 64 have been searched exhaustively and all MPSL codes of these lengths have been found, it is possible to mention the number of best optimal existing codes. These numbers are stated after excluding all allomorphic forms of codes.

Table 2. gives a single MPS code for each length. For $M \leq 48$ the listed codes are those that have, from all those with minimum peak sidelobe, the minimum integrated sidelobe (Levanon & Mozeson, 2004).

Table 2. lists codes in Hexadecimal. Each hexadecimal digit represents four binary bits, and the convention is made that, upon base conversion, any unnecessary binary digits are removed from the left side of the sequence.

Length	PSL	Example	Number
2	1	3	1
3	1	6	1
4	1	E	1
5	1	1D	1
6	2	34	4
7	1	72	1
8	2	97	8
9	2	0D7	10

10	2	167	5
11	1	712	1
12	2	977	16
13	1	1F35	1
14	2	1483	9
15	2	182B	13
16	2	6877	10
17	2	0774B	4
18	2	190F5	2
19	2	5BB8F	1
20	2	5181B	3
21	2	16BB83	3
22	3	0E6D5F	378
23	3	38FD49	515
24	3	64AFE3	858
25	2	12540E7	1
26	3	2380AD9	242
27	3	25BBB87	388
28	2	8F1112D	2
29	3	164A80E7	283
30	3	2315240F	86
31	3	2A498C0F	251
32	3	01E5AACC	422
33	3	0CCAA587F	139
34	3	333FE1A55	51
35	3	00796AB33	111
36	3	3314A083E	161
37	3	0574276F9E	52
38	3	003C34AA66	17
39	3	13350BEF3C	30
40	3	2223DC3A5A	57
41	3	038EA520364	15
42	3	04447B874B4	4
43	3	005B2ACCE1C	12
44	3	0FECECB2AD7	15
45	3	02AF0CC6DBF6	4
46	3	03C0CF7B6556	1
47	3	069A7E851988	1
48	3	156B61E64FF3	4
49	4	012ABEC79E46F	-
50	4	025863ABC266F	-
51	3	0E3F88C89524B	-
52	4	0945AE0F3246F	-
53	4	0132AA7F8D2C6F	-

54	4	0266A2814B3C6F	-
55	4	04C26AA1E3246F	-
56	4	099BAACB47BC6F	-
57	4	01268A8ED623C6F	-
58	4	023CE545C9ED66F	-
59	4	049D38128A1DC6F	-
60	4	0AB8DF0C973252F	-
61	4	005B44C4C79EA350	-
62	4	002D66634CB07450	-
63	4	04CF5A2471657C6F	-
64	4	4090A2E9E63237C2	1859
65	4	002DC0B0D9BCE5450	-
66	4	0069B454739F12B42	-
67	4	20506C9AB1E909CC2	-
68	4	009E49E3662A8EA50	-
69	4	026FDB09A83A118E15	-
70	4	1A133B4E3093EDD57E	-
71	4	63383AB6B452ED93FE	-
72	4	E4CD5AF0D054433D82	-
73	4	1B66B26359C3E2BC00A	-
74	4	36DDBED681F98C70EAE	-
75	4	6399C983D03EFDB556D	-
76	4	DB69891118E2C2A1FA0	-
77	4	1961AE251DC950FDDBF4	-
78	4	328B457F0461E4ED7B73	-
79	4	76CF68F327438AC6FA80	-
80	4	CE43C8D986ED429F7D75	-
81	4	0E3C32FA1FEFD2519AB32	-
82	4	3CB25D380CE3B7765695F	-
83	5	711763AE7DBB8482D3A5A	-
84	5	CE79CCCD8B6003C1E95AAA	-
85	5	19900199463E51E8B4B574	-
86	5	3603FB659181A2A52A38C7	-
87	5	7F7184F04F4E5E4D9B56AA	-
88	5	D54A9326C2C686F86F3880	-
89	5	180E09434E1BBC44ACDAC8A	-
90	5	3326D87C3A91DA8AFA84211	-
91	5	77F80E632661C3459492A55	-
92	5	CC6181859D9244A5EAA87F0	-
93	5	187B2ECB802FB4F56BCCECE5	-
94	5	319D9676CAFEADD68825F878	-
95	5	69566B2ACCC8BC3CE0DE0005	-
96	5	CF963FD09B1381657A8A098E	-
97	5	1A843DC410898B2D3AE8FC362	-

98	5	30E05C18A1525596DCCE600DF	-
99	5	72E6DB6A75E6A9E81F0846777	-
100	5	DF490FFB1F8390A54E3CD9AAE	-
101	5	DF490FFB1F8390A54E3CD9AAE	-
102	5	2945A4F11CE44FF664850D182A	-
103	5	77FAAB2C6E065AC4BE18F274CB	-
104	5	E568ED4982F9660EBA2F611184	-
105	5	1C6387FF5DA4FA325C895958DC5	-

Table 2. Best-known binary codes.

It seems that for any peak sidelobe level there is a limit of the maximal value of N for which a binary sequence with that sidelobe level exists. Now, it is possible to update Kerdoc's table in Table 3.

PSL	Code Length (N)	Example
1	13	1F35
2	28	DA44478
3	51	71C077376ADB4
4	82	3CB25D380CE3B7765695F
5	105	1C6387FF5DA4FA325C895958DC5

Table 3. Longest-known binary codes for PSLs from one to five.

MPSL histogram for binary sequences up to length 105 is drawn in Figure 5. This histogram shows that, the longer the code, the smaller the PSL ratio and the best record is related to length. So, it is expected, not proved, that longer codes have better mainlobe to peak sidelobe ratio, thus better compression characteristic.

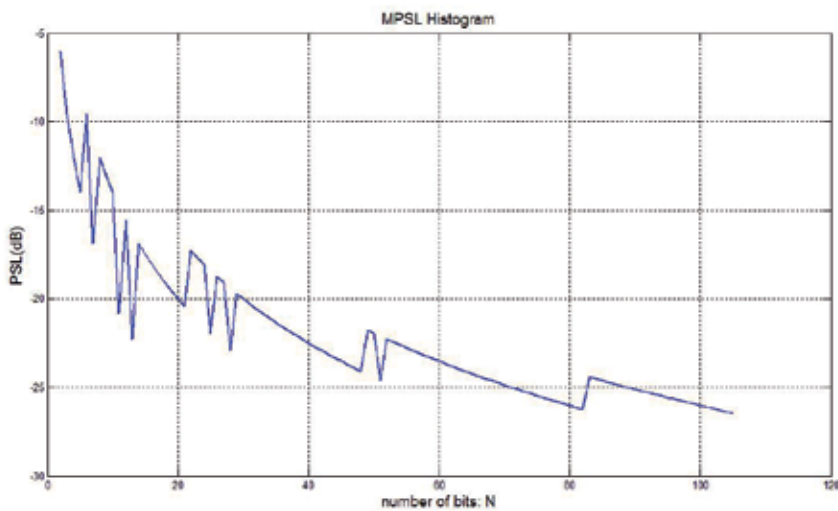


Fig. 5. MPSL Histogram in dB (absolute and relative values)

10. References

- Amin_Nasrabadi, M.; Bastani, M. H. (2006), A new approach for long low autocorrelation binary sequence problem using genetic algorithm, *Proceedings of CIE International Conference on Radar*, Vol. II, pp. 1898-1900, 0-7803-9582-4, China, October 2006, Shanghai.
- Amin_Nasrabadi, M.; Bastani, M. H. (2007), Exhaustive search for long low autocorrelation binary codes using Length-Increment algorithm, *Proceedings of IET International Conference on Radar Systems*, pp. 1-4, 978-0-86341-848-8, Edinburgh, UK, October 2007, Edinburgh.
- Amin_Nasrabadi, M.; Bastani, M. H. (2008), Best known PSLs for binary sequences from bit length 71 through 100. *Proceedings of International Symposium on Telecommunications*, pp. 697-700, 978-1-4244-2751-2, Iran, August 2008, Tehran.
- Ackroyd, M. H.; Ghani, F. (1973). Optimum mismatched filters for sidelobe suppression. *IEEE Transactions on Aerospace and Electronic Systems*, Vol. AES-9, No. 2, (March 1973) pp. 214-218, 0018-9251.
- Baden, J. M.; Cohen, M. N. (1990). Optimal peak sidelobe filters for biphasic pulse compression, *Proceedings of IEEE International Radar Conference*, pp. 249-252, Arlington, VA, USA, May 1990, Arlington.
- Barton, D. K.; Leonov, S. A. (1998). *Radar technology encyclopedia*, Artech House, 0-89006-893-3, Boston.
- Cohen, M. N.; Fox, M. R. & Baden, J. M. (1990). Minimum peak sidelobe pulse compression codes, *Proceedings of the IEEE International Radar Conference*, pp. 633-638, Arlington, VA, USA, May 1990, Arlington.
- Cohen, M. N. (1991). An overview of high range resolution radar techniques, *Proceedings of National Telesystems Conference*, pp. 107-115, 0-7803-0062-9, Atlanta, GA, USA, March 1991, Atlanta.
- Coxson, G. E.; Hirschel, A. & Cohen, M. N. (2001). New results on minimum-PSL binary codes, *Proceedings of IEEE National Radar Conference*, pp. 153-156, 0-7803-6707-3, Atlanta, GA, USA, May 2001, Atlanta.
- Coxson, G. E.; Russo, J. (2004). Efficient exhaustive search for optimal-peak-sidelobe binary codes, *Proceedings of the IEEE Radar Conference*, pp. 438-443, 0-7803-8234-X, Philadelphia, PA, April 2004, Philadelphia.
- Deng, X.; Fan, P. (1999). New binary sequences with good aperiodic autocorrelations obtained by evolutionary algorithm. *IEEE Communications Letters*, Vol. 3, No. 10, (October 1999) pp. 288-290, 1089-7798.
- Farnett, E. C.; Stevens, G. H. (1991). Pulse compression radar, In: *Radar Handbook*, Skolnik, M. I., (Ed.), pp. 10.1-10.39, McGraw-Hill, 0-07-057913-X, Singapore.
- Ferrara, M. (2006). Near-optimal peak-sidelobe binary codes. *Proceedings of IEEE National Radar Conference*, pp. 400-403, 0-7803-9496-8, Syracuse, NY, April 2006, Syracuse.
- Golay, M. J. E. (1977). Sieves for low autocorrelation binary sequences. *IEEE Transactions on Information Theory*, Vol. IT-23, No. 1, (January 1977) pp. 43-51, 0018-9448.
- Kerdoc, A. M.; Mayer, R. & Bass, D. (1986). Longest binary pulse compression codes with given peak sidelobe levels, *Proceedings of the IEEE*, Vol. 74, No. 2, pp. 366-366, February 1986.

- Levanon, N.; Getz, B. (1994). Comparison between linear FM and phase-coded CW radars. *IEE Proceedings Radar, Sonar & Navigation*, Vol. 141, No. 4, (August 1994) pp. 230-240, 1350-2395.
- Levanon, N.; Mozeson, E. (2004). *Radar signals*, John Wiley & Sons, 0-471-47378-2, New Jersey.
- Lindner, J. (1975). Binary sequences up to length 40 with best possible autocorrelation function. *Electronics Letters*, Vol. 11, No. 21, (October 1975) pp. 507-507, 0013-5194.
- Mahafza, B. R.; Alabama, H. (2000). *Radar systems & analysis and design using Matlab*, Chapman & Hall/CRC, 1-58488-182-8, USA.
- Mertens, S. (1996). Exhaustive search for low-autocorrelation binary sequences. *Journal of Physics A: Mathematical and General*, Vol. 29, No. 18, (September 1996) pp. L473-L481, 0305-4470.
- Militzer, B.; Zamparelli, M. & Beule, D. (1998). Evolutionary search for low autocorrelated binary sequences. *IEEE Transactions on Evolutionary Computation*, Vol. 2, No. 1, (April 1998) pp. 34-39, 1089-778X.
- Nathanson, F. E.; Cohen, M. N. (1999). Frequency-modulated pulse compression waveforms, In: *Radar design principles: signal processing and the environment*, Nathanson, F. E.; Reilly, J. P. & Cohen, M. N., (Ed.), pp. 583-634, SciTech, 9781891121098, New Jersey.
- Nunn, C. J.; Coxson, G. E. (2008). Best-known autocorrelation peak sidelobe levels for binary codes of length 71 to 105. *IEEE Transactions on Aerospace and Electronic Systems*, Vol. 44, No. 1, (January 2008) pp. 392-395, 0018-9251.
- Rihaczek, A.; Golden, R. (1971). Range sidelobe suppression for Barker codes. *IEEE Transactions on Aerospace and Electronic systems*, Vol. AES-7, No. 6, (November 1971) pp.1087-1092, 0018-9251.
- Skolnik, M. I. (2001). *Introduction to radar systems*, Tata McGraw-Hill, 0-07-044533-8, New Dehli.

Virtual Multicast

Petr Holub and Eva Hladká
Masaryk University and CESNET z. s. p. o.
Czech Republic

1. Introduction

The ability of the Internet to facilitate collaboration leads to widespread use of various video-conferencing and more advanced collaborative environments. As a result, synchronous multimedia transmissions have become more common. Various communication patterns emerged: from many-to-many low-bandwidth streams for large scale collaboration over slow links to few-to-few extreme-bandwidth streams as seen in collaboration based on high-definition (HD) Holub et al. (2006), Jo et al. (2006) or even post-HD video Shimizu et al. (2006). These applications require Internet to become more active, the classical passive transmission service is no longer sufficient.

Multimedia streams are processed within the network, allowing, e.g., to establish a collaborating group where most members are connected to the high-bandwidth network links while a minority has rather limited connection. If the network is capable of processing—compressing, down-sampling, etc.—the data at the appropriate nodes (where the high and low throughput network links interconnect), the communication quality should not be reduced to the lowest common throughput denominator. The network must be able to support complex communication patterns and to process data internally. Robustness and failure resilience is another area, where more support at the network level is expected. While classical transport protocols like TCP support reliable data transmission, they are not appropriate for synchronous multimedia environment, where delays are unacceptable. It may be undesirable to wait for a timeout and then ask for a datagram retransmission, the network and applications themselves must be able to detect and immediately mitigate any data corruption or loss. Up to now, new requirements were served by different infrastructures tailored for a specific purpose. Nowadays, we need to merge them together in a network that uses packet transmission as its basis protocol—to do this successfully, new models, approaches, and techniques are necessary.

The theoretical model of the virtual multicast naturally follows from graph-based model of computer networks. The graph model of computer network can easily be extended to multi-graphs, which allow multiple line to connect any individual nodes. Although most computer networks are bi-directional, working a semi-duplex or full duplex regime, orientation can be added for explicit description of direction of flows (multiple edges used to represent the bi-directionality). As another step, we can add labels to the edges, representing some important properties like throughput or latency of each link. Labels on nodes can denote their properties, like different capabilities, latency of passing (bridging) data between edges of the node (the internal latency), size of internal buffers, etc. We can also speak about *internal* network, which is a part of the graph without any leaf node. It is also easy to identify end—i.e. leaf—elements.

Such a model is appropriate to study most usual flow patterns in contemporary computer networks, namely the sender–receiver one. In this case, we have one node sending and exactly one node receiving a particular data flow. The basic network problem is finding a route between the communicating nodes, additional constraint is to guarantee available bandwidth and eventually other properties like overall latency or jitter. The route is usually the one composed from the smallest number of edges—the so called *shortest* path—but in some case any path could fit—this is the case, e.g., in the interdomain routing. The mechanism for creating a route can work on a flow basis—we speak about *connection oriented* networks—or on a datagram basis—the case of IP network. In the later case stability of the route is becoming additional important parameter that could influence the behavior of the whole flow (e.g., there is no reordering of datagrams within a flow in the connection oriented networks). Each path has one sending, one receiving, and zero or several *internal* nodes that are responsible for forwarding data.

However, as the networks were exposed to larger number of more sophisticated applications, more complex communicating patterns emerged. The first one is a multicast, with still one sender but multitude of receivers. A simple extension is a communicating mesh, where every member of such a communicating group (the multicast group) could become a sender. Yet more complex communication patterns are seen in the *peer to peer* networks, where we may have multiple partially overlaid multicast groups communicating in parallel, it may use flooding, different cases of wave communication patterns, etc.

All the more complex communication patterns can still be expressed in our simple graph model using the sender–receiver paradigm. Multicast can be modeled by a set of sender to receiver flows, but to express it correctly some kind of *coordination (synchronicity)* must be added to the model (data delivery to all receivers is expected to happen at the same time). Also, even in networks with unlimited bandwidth the simultaneous sending of all streams by just one element stress it above the optimal level (reducing efficiency of the communication scenario).

To deal with such complex communicating patterns more effectively, we have to extend our routing algorithm to find not paths, but whole subgraphs of the original graph. Flows going through such subgraph are more efficient than collection of individual send–receiver flows. The subgraphs represent *overlay networks*, that are specialized to transfer the particular flow pattern in the most efficient way.

When mapped back to the underlying network, the subgraphs extend the requirements on the internal path nodes. Simple forwarding (taking data from one link and sending them to another) is no longer sufficient, data must be duplicated and further processed to fit the communicating subgraph (overlay network) requirements. At the theoretical level this is just a simple extension, but propagating it back to the network proved to be very difficult, if not impossible work.

As an example, let's briefly discuss the IP multicast. It has been established as a family of protocols at the beginning of 80s in the last century Cheriton & Deering (1985); Deering & Cheriton (1990). IP multicast is based on a family of multicast routing protocols (how to create the appropriate subgraph of the network) and its implementation requires support at each network element both for routing and also for multicast forwarding. The IP multicast includes nodes that do datagram duplication—they must be able to forward incoming data to two or even more output links. IP multicast does not guarantee delivery of datagrams, does not provide any feedback to sender, it is in fact very simple extended forwarding scheme. All vendors of routers officially support multicast, yet it is not available on large parts of the Internet and

the situation is not expected to change in the future. Although simple, multicast still can interfere with the basic sender–receiver communication patterns, imposes more load on routers (duplication is more complicated than simple forwarding) and the multicast routing protocols can introduce instability into the basic routing. As the result, multicast may not work properly or could be switched off by network administrators if they suspect it to be the cause of a problem they have with the network¹ Diot et al. (2000); Dressler (2003a;b); El-Sayed et al. (2003).

If the IP multicast situation is far from satisfactory, what we can anticipate with more complex extensions, where data have to be not only transmitted but also processed during transmission?

We must change the paradigm—instead of expecting the underlying network to provide all the advanced functionality and increasing complexity above sustainable levels, more *isolation* and *independent deployment* of support for complex communication (and data processing) patterns is the possible answer. The isolation is provided by the overlay networks, that take care of all the new functionality by themselves. The independence of deployment is achieved through the *user empowered* approach. The overlay networks are constructed and managed (often just temporarily) by their own users, without any need for specific support from network and its administrators.

Several years ago we started to build a network environment based on the user-empowered approach for transport and processing data in IP networks. We used the concept of active networks and designed and developed an *Active Element*—a programmable network node designed for synchronous data distribution and processing, configurable without administrator’s right—and used it as the basic building block for construction of complex communication patterns.

The initial phase of our research was influenced by the network-centric view. We designed an active router Hladká & Salvet (2001a), an extension of the classical router that allows users to define their own processing over individual data streams. The active network paradigm which introduced the active network elements, opened also the door to more user oriented approach. The active routers (and similar active network elements) are expected to be setup and operated by system administrators, with users “only” injecting smaller or larger programs to process their data within the network. Although the concept of active networks has been proved to provide the new functionality necessary to fulfill new requirements of data transmission and processing within the network, the whole idea collided with the conservative approach of network vendors and administrators. As the multicast experience demonstrated, it is very difficult to introduce new properties as they can interact in unpredictable way with the simpler, previously introduced protocols. Also, security concerns could not be overemphasized. A network programmable by end users is ripe for being taken completely by a hacker; this risk seen too high to be outweighed by the potential of new features.

At the same time as the active networks were developed, another paradigm that proved the value in giving control to end users emerged—the peer to peer networks. They completely

¹ To further illustrate this problem, we have performed a quick survey of Internet2 Bigvideo group mailing list archive (<https://mail.internet2.edu/wws/arc/bigvideo/>). This list was in operation from May 2003 to May 2006. It focused on education and problem solving for users of high-end video technologies in advanced academic networks like the one operated by Internet2. The list was not limited to Internet2 community and there was a significant international contribution. As a majority of the advanced video tools use multicast, 212 of total 625 messages, i.e., 34% was spent on multicast testing and debugging.

abandon the network-centric view, implementing in fact many already available network protocols once again, providing complete orthogonality (and independence) on the underlying network. The peer to peer networks are classical *overlay networks*, taking as granted only limited number of very simple properties of the underlying network and providing all the higher level functionality—searching, routing, etc.—by themselves.

However, the complete independence on the underlying network leads to inefficiency. The classical peer to peer networks could place their nodes only on the periphery of the network, where the users' stations are connected. The data distribution pattern required by the content (which the peer to peer network understood) may fit very poorly into the actual underlying network topology, overloading some lines while leaving other unused. Also, reliability of the peer to peer network is usually based on an overwhelming redundancy, when the same data is distributed, processed, and stored by many nodes—again a clear contradiction to the network-centric approach where the efficiency (the cost of the infrastructure) is one of the ruling paradigms.

We can see that the network-centric approach is highly efficient, but very slow in adopting new features and rather unfriendly to users. On the other hand, pure user-centric overlay approach, as represented by basic peer to peer networks is very inefficient (consuming more resources than needed in the optimal case), but it is able to introduce new features fast and can provide exactly the services the users are looking for. Another reason for that huge success is also their single purpose—the peer to peer networks are not trying to solve all the users' requirements, they focus on one service or just a small set of similar interconnected services.

Is it possible to take the positive from both approaches and leave out their negatives? Several years ago we decided to try this combination, moving from the network-centric to the user-centric approach, but not abandoning the network orientation completely. We extended the active router model to fit into the user-centric paradigm. The original active router and its implementation was based on Unix operating system and exploited both the kernel and user components. Its installation and deployment thus required system administrator's privileges that ordinary user may not have. As the next step, we completely redesigned the active router to become Active Element (AE), working in the user space of any operating system only. We obtained a fully user controlled element, that can be installed on any machine user has access to, without any specific privileges (e.g., on a server that is more strategically placed within the network than end user desktop machine). However, the AE design still followed basic network-centric pattern, being an evolutionary successor of active router, and thus became a keystone for the distribution and processing infrastructure, not a node in a peer to peer network. We still differentiate between an infrastructure and clients, but we put both into users' hands.

The user controlled Active Element is a very strong and flexible component to build different distribution schemes. We started with an infrastructure for virtual multicast. We used this infrastructure to study properties of the serial communication schema for group synchronous communication instead of the parallel communication model of the native multicast. While we had clearly demonstrated its advantages, especially in the area of security and reliability, the limited scalability remained the major disadvantage and it became our natural next research target. Instead of using just a single AE to do all the processing and distribution, we designed a network of AEs with distinct control and data planes. This separation allowed us to use the peer to peer principles at the control plane, taking advantage of the properties of peer to peer networks like robustness and very high scalability. The inherent low efficiency of peer to peer networks does not play significant role, as the amount of control data is al-

ways limited. The result is an easily configurable and fault tolerant network of AEs with a reasonably high throughput capabilities.

However, the scalability is not one dimensional issue. While the network of AEs addressed the scalability in terms of number of clients supported, very high quality video (e.g., that used in the cinema theaters) generates so huge amount of data that may not be processed by a single AE. Therefore, we extended our work on scalability to increase the AE processing capacity through their internal parallelization. The parallelized AE runs on a cluster with fast internal interconnect and is capable of processing in near real time even 10 Gbps data stream.

All this research and development would not be complete without an actual deployment. Putting the AEs and their networks into production use provided a very valuable continuous feedback on their design while experimentally testing their properties. The AEs were used to build an infrastructure for collaborative environment used by several geographically distributed groups of researchers. Requirements from these groups initiated further research into support of advanced communication and collaboration features like moderating or subgrouping. The AEs started to play a role of directly controlled user tool to support these advanced properties. This confirmed the strength of the general concept of user empowered building blocks for data processing and distribution networks.

In another environment we used the idea of overlay network with AEs capable to provide new functionality for the stereoscopic video streams synchronization. A simple software implementation running on commodity hardware is able to synchronize two streams of stereoscopic digital video (DV, 25 Mbps) format successfully even when the original streams are highly desynchronized. The penalty of the synchronization is increased latency, as the “faster” stream must wait for data in the slower stream, plus some processing latency is added to the final perceived delay. While this delay may be problematic in interactive implementation, we demonstrated that the AE-based synchronization element can be easily used for synchronized unidirectional stereoscopic streaming to multiple end users even in highly adverse and desynchronizing network conditions Hladká et al. (2005). While the stereoscopic streaming may not be too common, this concept is usable for synchronization of stereo or multichannel (e.g., 5.1) audio streams or for synchronization of separately sent audio and video streams.

The real strength of the AEs and the whole concept of controllable overlay networks is demonstrated in the multi-point High Definition (HD) video distribution. If the HD video is to be used for a synchronous collaborative environment, uncompressed streams must be sent over the network. However, the required throughput of 1.5 Gbps per each stream was too high to be sent reliably over a native multicast in heterogeneous network over multiple administrative domains (even if it was available). The optimized AEs are able to replicate even such high demanding streams in near real time and were used to build infrastructure that supported one of the world first multipoint videoconferences using uncompressed HD video Holub et al. (2006). Later, improved AEs grouped into a network became key infrastructure for a virtual classroom that ran full semester and connected 6 sites on two continents Matyska, Hladká & Holub (2007). The Active Element network processed up to 18 Gbps bi-directional bandwidth, fully confirming the usability of the AE design.

In this chapter, we present several classes of solutions following our long term research in this field. The simplest solution to user-empowered data distribution and processing is a central Active Element (AE) described briefly in Section 2, which is a programmable modular active element, that can be run in the network easily without requiring any administrative privileges. The AE distributes and optionally also processes the incoming data, which allows for unique per-user processing capabilities—something that is impossible to do with traditional

data distribution systems like multicast. As any centralized solution, it has its positives and shortcomings: while it is easy to setup and deploy, it has limited robustness and scalability, both with respect to number of streams and the bandwidth of a single stream. When more clients are collaborating or when higher robustness is needed, the AEs may be deployed as static or dynamic self-organizing AE networks shown in Section 2.1. This field has been studied thoroughly from the data distribution efficiency and robustness point of view by many groups previously and the most relevant body of work is referenced in Section 2.1. Our view here is, however, more general, focusing not only on mere multicast-like data distribution, but also on the possibilities enabled by additional data processing, operation in adverse networking environments, self-organization, etc. Another step forward needs to be taken when bandwidth of a single stream exceeds capacity of any single AE in the AE network. Utilizing properties of real-time multimedia applications and data distribution protocols, we have designed a distributed AE described in Section 2.2 that can be deployed on tightly coupled clusters—but this solution becomes very complex when not only the data distribution but also data processing is required. We demonstrate applications which have been built on top of these technologies for synchronous data distribution and processing in Section 3. Related work is summarized in Section 4 and we conclude with some remarks on directions for future research in Section 5.

2. Active Elements

The Active Element (AE) Hladká et al. (2004) is a programmable element designed for synchronous data distribution and processing while minimizing the latency of the distribution. The word “reflector” is also being used in this context, which only refers to data distribution capabilities. Since our approach is far more general and close to idea of active networks, we have resorted to using the Active Element name. The architecture of the AE is flexible enough to allow implementation of required features while leaving space for easy extensions. If the data is sent to all the listening clients and all the clients are also actively sending, which is a standard scenario for collaborative group of participants, the number of data copies is equal to the number of the clients, and the limiting outbound traffic grows with $n(n - 1)$, where n is the number of sending clients.

From general point of view the AE is a user-controlled modular programmable router working on the application layer. It runs entirely in user-space of the underlying operating system and thus it works without the need for administrative privileges on the host computer. AEs are based on our active router concept described in Hladká & Salvat (2001b), building on the same principles of modularity, but adding the user-empowered approach. The AE architecture is shown in the Figure 1.

Data processing architecture.

Data routing and processing part of the AE comprises *network listeners, shared memory, a packet classifier, a processor scheduler, number of processors, and a packet scheduler/sender*.

The network listeners are bound to one UDP port each. When a packet arrives to the listener it places the packet into the shared memory and adds reference to a *to-be-processed queue*. The packet classifier then reads the packets from that queue and determines a path of the data through the processor modules. It also checks with routing AAA module whether the packet is allowed or not (in the later case it simply drops that packet and creates event that may be logged). Zero-copy processing is used in all simple processors (packet filters), minimizing processing overhead (and thus packet delay). E. g. for simple data multiplication, the data

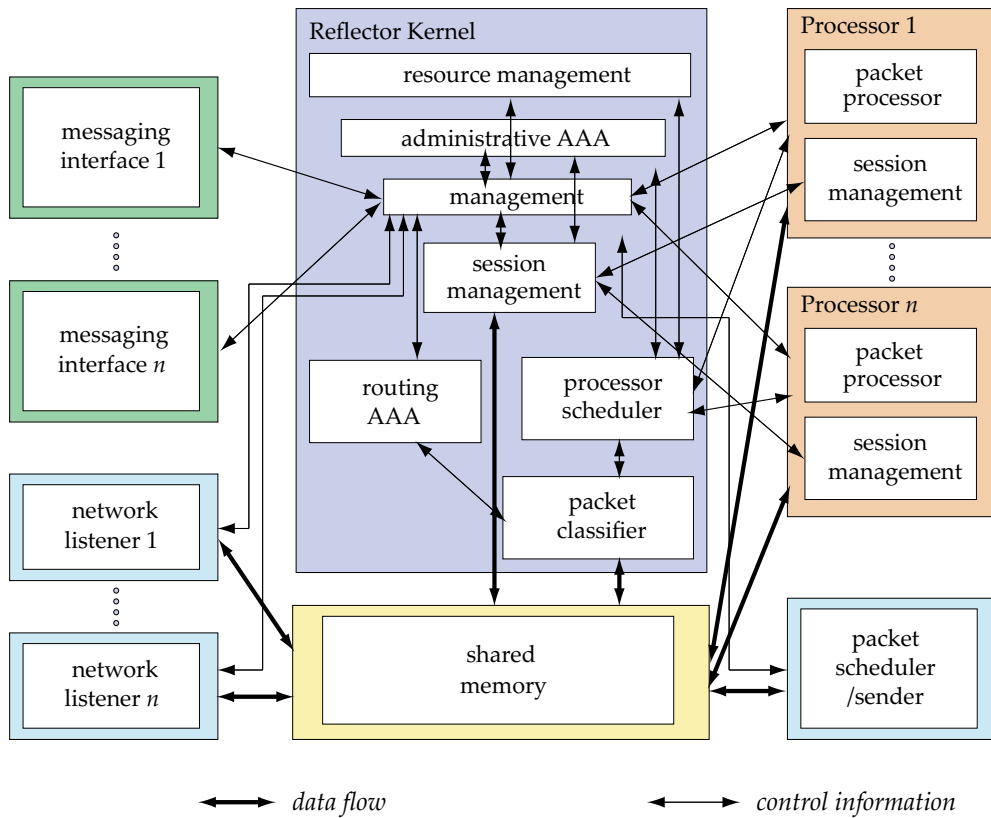


Fig. 1. Architecture of Active Element with its individual modules and interactions.

are only referenced multiple times in the packet scheduler/sender queue before they are actually being sent. Only the more complex modules may require processing that is impossible without use of packet copies.

The *session management* module follows the processors and fills the distribution list of the target addresses. The filling step can be omitted if data passed through a special processor that filled the distribution list structure and marked data attribute appropriately (this allows client-specific processing). Processor can also poll session management module to obtain up to date list of clients for specified session. Session management module also takes care of adding new clients to the session as well as removing inactive (stale) ones. There are two ways of adding clients for a session at the AE: implicit mode and explicit mode. In the implicit mode, when new client sends packets for the first time, session management module adds client to the distribution list (data from forbidden client has already been dropped by packet classifier). This mechanism is designed to work with the multimedia systems like Mbone Tools suite. The explicit mode requires some specific action to be taken by the user or application to register for the session at the AE, be it RTSP protocol Schulzrinne et al. (1998) or direct interaction through one of native messaging interfaces of the AE. Information about the last activity of a client is also maintained by the session module and is used for pruning stale clients periodically in the

implicit mode. Even when distribution list is not filled by the session management module, packets must pass through it to allow addition of new clients and removal of stale ones.

When the packet targets are determined by the router processor a reference to the packet is put into the *to-be-sent queue*. Then the packet scheduler/sender picks up packets from that queue, schedules them for transmission, and finally sends them to the network. Per client packet scheduling can also be used for e. g. client specific traffic shaping.

The *processor scheduler* is not only responsible for the processors scheduling but it also takes care of start-up and (possibly forced) shutdown of processors which can be controlled via administrative interface of the AE. It checks resource limits with routing AAA module while scheduling and provides back some statistics for accounting purposes.

Architecture of management.

Communication with the AE from the administrative point of view is provided using *messaging interfaces, management module, and administrative AAA module* of the AE. Commands for the management module are written in a specific *message language*.

The administrative part of the AE can be accessed via secure messaging channels such as HTTP with SSL/TLS encrypted transport or SOAP with GSI support. The user can authenticate using various authentication procedures, e. g., combination of login and password, Kerberos ticket, or X.509 certificate. Authorization uses access control lists (ACLs) and is performed on a per-command basis. Authentication, authorization, and accounting for the administrative section of the AE is provided by an administrative AAA module. Each of these interfaces unwraps the message if necessary and passes it to the management module. A message language for communication with the management module is called Reflector Administration Protocol (RAP) described in Denmark et al. (2003).

Prototype implementation and performance evaluation.

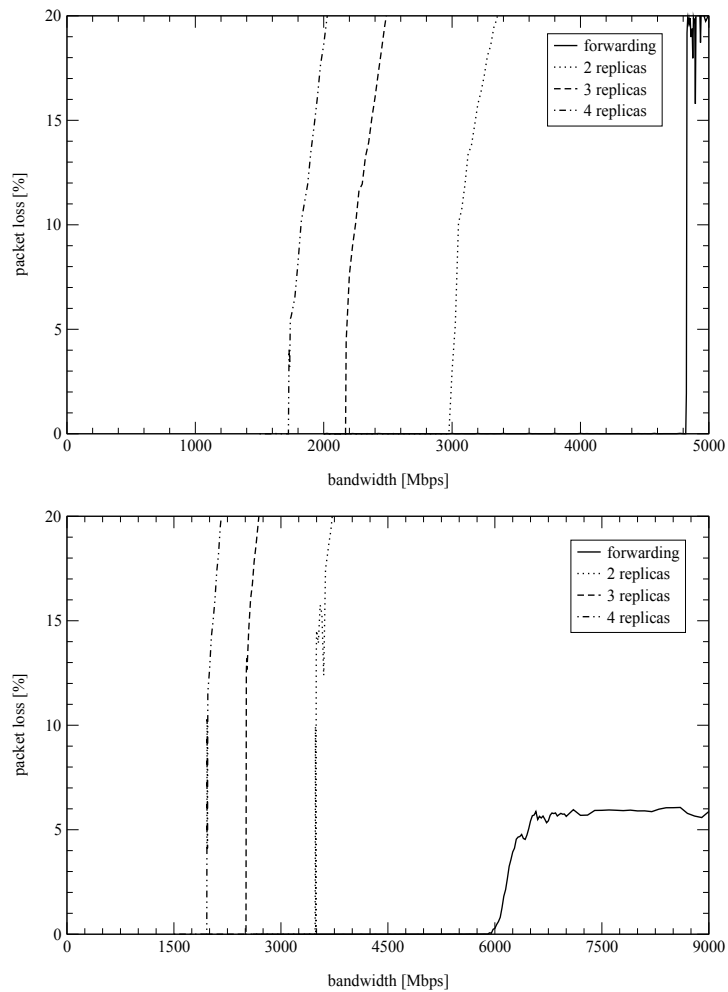
In order to evaluate the behavior of AE on recent high-performance infrastructure, we have set up a testbed comprising sender and receiver machines (each $2 \times$ AMD Opteron 2.4 GHz, 2 GB memory, Linux 2.6.9 SMP kernel) and a machine running the AE ($2 \times$ dual core Intel Xeon 3.0 GHz, 8 GB memory, Linux 2.6.19 SMP kernel). The sender machine was equipped with Chelsio T110 and both the receiver and the AE machine with Myricom Myri-10GE NICs. All the three machines were connected to a 10GE Cisco 6506 switch.

The performance was measured using two implementations of the AE: the full featured complex version described above² (denoted as AE) and a high-performance simplified version including only one receiving and one sending thread, which was designed for HD video distribution Holub et al. (2006) (thus denoted as HD-AE). The performance is summarized in Fig. 2. The results indicate that even the more complex version is capable of distributing the uncompressed HD video for up to 4 participants when Jumbo frames are used, which is necessary for this application anyway.

2.1 AE Networks

As the scalability of AE is limited especially with respect to the number of data streams (clients), the concept of single AE has been extended to a network of AE Holub et al. (2005) while preserving its processing capabilities through modularity and retaining the user-empowered approach to maximum extent. Its architecture features separated data distribution plane and control plane: while the data distribution is optimized for maximum performance and minimum latency, the control plane has to provide maximum robustness even at

² The AE concept has been implemented in C language for Unix-like operating systems under code name RUM2. <http://miro.cesnet.cz/software/software.cz.html>.



replica(s)	AE		HD-AE	
	1500 B	8500 B	1500 B	8500 B
1	1450	4820	2700	6100
2	1000	2975	1660	3490
3	775	2170	1140	2510
4	600	1725	825	1960

Fig. 2. Performance of the modular full-featured AE compared to highly simplified version optimized for HD video distribution (HD-AE). Stabilization in the upper right graph is because of sender card saturation above 6.5 Gbps. The table below the graphs shows maximum stream bandwidth [Mbps] distributed with less than 0.1% packet loss for both standard and Jumbo frame sizes.

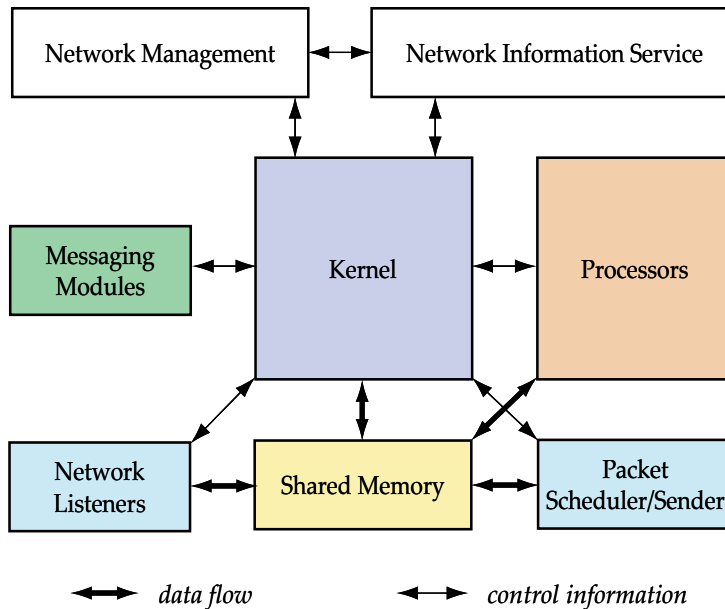


Fig. 3. Architecture of Active Element with Network Management and Network Information Service modules.

cost of performance. The control plane is responsible for management actions of the AE network like monitoring, reconstruction of the network after node or network link failure and has to survive all the perturbations. Thus we have chosen a P2P architecture of the control plane which exhibits very strong resilience. The data plane on the other hand may be dynamically rebuilt based on the information from the control plane; even the data distribution model may change.

The AEs has networking capability, i.e., inter-element communication. The network management is implemented via two modules dynamically linked to the AE: Network Management (NM) and Network Information Service (NIS) as shown in Fig. 3. The NM takes care of building and managing the network of AEs, joining new content groups and leaving old ones, and reorganizing the network in case of link failure. The NIS gathers and publishes information about the specific AE (e.g., available network and processing capacity), about the network of AEs, about properties important for synchronous multimedia distribution (e.g., pairwise one-way delay, RTT, estimated link capacity), and also information on content and available formats distributed by the network.

The data distribution plane is designed using loadable plug-ins to enable incorporating various distribution models. A number of suitable models has been proposed previously by many independent groups in the past, most of which fall into one of the two categories: (1) mesh first distribution models like Narada Chu et al. (2000), Delaunay triangulation Liebeherr & Nahas (2001), Bayeux Zhuang et al. (2001), and (2) tree first models like YOID Francis (2000), TBCP Mathy et al. (2001), HMTP Zhang et al. (2002), SHDC Mathy et al. (2002), NICE Banerjee et al. (2002), Overcast Jannotti et al. (2000), ZIGZAG Tran et al. (2003). Some other models may also be found in El-Sayed et al. (2003); Li & Shin (2002).

Given the data processing capabilities of the AE, the usefulness of AE networks goes beyond pure data distribution models. AEs in the network can be specialized in performing various transformation of the data based on user request (e.g., AE running on host with enough CPU power and sufficient network capacity can perform transformation of the data from high-bitrate to low-bitrate). However, combinations of data distribution and data processing makes makes scheduling problem particularly hard and first approaches have only been studied recently using self-organizing CoUniverse platform Liška & Holub (2009).

Prototype implementation of the AE networks with P2P control plane based on JXTA-C³ has been demonstrated in Procházka et al. (2005). A few simple optimizations to default JXTA settings improved the performance significantly for synchronous applications with a limited number of participants where down-time minimization is required despite increasing communication overhead, thus making it suitable control-plane middleware.

The AE network is also designed to facilitate communication in adverse networking environments, i.e., environments where the network communication is obstructed by firewalls, network address translators (NATs) and proxy servers. The data may be tunneled over TCP instead of usual UDP, it may even mimic using HTTP and tunnel the data over HTTP proxy. The AE may also be augmented by employing a VPN Holub et al. (2007) such as OpenVPN⁴, which boosts pervasivity, as it allows even tunneling through HTTP and SOCKS proxy servers. VPN also enables deployment of strong authentication and very secure data encryption protocols. Similar approaches have also been described in Alchaal et al. (2002). The solution that integrates these features directly into AE modules Bouček (2002); Salvet (2001) has significant advantages despite having a more demanding implementation: it allows for dynamic failure recovery properties in case of AE node failure or network link failure, as the client may join the AE network using another AE node that is still available and reachable.

2.2 Distributed Active Element

Another scalability issue regarding both single AE and AE networks is scalability with respect to the bandwidth of each individual data stream. In order to improve on this, we have designed a distributed AE Holub (2005); Holub & Hladká (2006), intended to be run on tightly coupled clusters with low latency network interconnection for the control plane and high-bandwidth interfaces for the data plane. The distributed AE splits a single stream into multiple sub-streams, which are processed in parallel—thus possibly introducing packet reordering. This is significantly different from general purpose load distribution systems like LACP IEEE 802.3ad protocol, which have to avoid the packet reordering and therefore a single data stream is processed sequentially⁵. The distributed AE includes distribution unit to distribute the data to the parallel processing units, and aggregation unit, which aggregates the data from the parallel units.

Limited synchronization and FCT. The basic idea behind distributed AE utilizes the fact, that most of the synchronous multimedia applications use non-guaranteed data transport like UDP and thus they need to adapt to some packet reordering. However, significant data reordering may either not be adapted upon or it results in latency increase as substantial buffer-

³ <http://www.jxta.org/>

⁴ <http://openvpn.net/>

⁵ This is done by using data flow identifiers hash to assign each data flow to a specific link of the of the aggregated link group. Thus each single data flow must not exceed capacity of the single link.

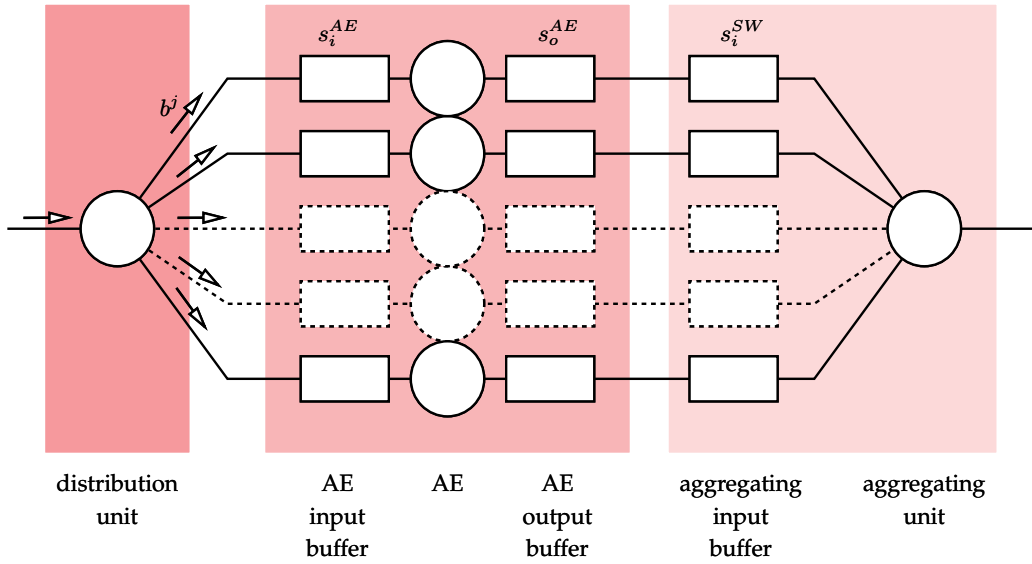


Fig. 4. Model of the ideal distributed AE with ideal aggregation unit.

ing is necessary to reorder the packets. Without any explicit synchronization, the maximum packet reordering can be

$$n(s_i^{AE} + s_o^{AE} + s_i^{SW} + 1)$$

where n is number of parallel paths and s_i^{AE} , s_o^{AE} , s_i^{SW} are buffer sizes on input of the AE, output of AE, and input of the aggregation unit respectively, as shown in Figure 4.

In order to decrease packet reordering introduced by the distributed AE, we have introduced a distributed algorithm for achieving less packet reordering compared to no explicit synchronization. The nodes are ordered in a ring with one node elected as a master node and they circulate a token which serves as a barrier so that no node can run too much ahead with sending data. After reception of the token containing the current "active" round number, each non-master node passes on the token immediately and may send only the data from the round marked in the token until it receives the token again. When the master node receives the token from the last node in the ring, it finishes sending the current round, increments the round number in the token and passes on the token. The mechanism is called *Fast Circulating Token* (FCT) since the token is not held for the entire time period of data sending as usual in the token ring networks.

Because of real world implementation of data packet sending in common operating systems, we assume that sending procedure for a single packet is non-preemptive. Further we assume that token reception event processing has precedence over any other event processing in the distributed AE. However, as the data sending is non-preemptive, if the token arrives in the middle of data packet sending, it will be handled just after that packet sending is finished. After more detailed analysis Holub (2005), it can be shown the maximum reordering induced by an ideal distributed AE with FCT egress synchronization and ideal aggregating unit is

$$n(s_i^{SW} + 3),$$

when all queues operate in FIFO tail-drop mode. Thus the receiving application can adapt its buffer size to this upper bound. On custom hardware, the FCT protocol can be adapted to provide no packet reordering at all (called Exact Order Sending). More in-depth analysis can be found in Holub (2005); Holub & Hladká (2006).

Prototype implementation and experimental evaluation. Prototype implementation of the distributed AE is implemented in ANSI C language for portability and performance reasons. The implementation comprises two parts: a load distribution library and the distributed AE itself.

Because of lack of flexible enough load distribution hardware unit, we have implemented it as a library, which allows simple replacement of standard UDP related sending functions in existing applications and allows developers to have defined type of load distribution—either pure round robin or load balancing.

Each parallel AE uses threaded modular implementation based on architecture described above. Internal buffering capacity of each AE node has been set to 500 packets. Explicit synchronization using FCT protocol has been implemented using MPICH implementation⁶ of MPI built with low-latency Myrinet GM 2.0 API⁷ (so called MPICH-GM). Prototype implementation has been tested on Linux.

For cost-effective prototype implementation, the aggregation unit was implemented as commodity switch with sufficient capacity of internal switching fabrics.

The experimental results obtained on 10GE infrastructure, revealing that the distributed AE is capable of completely saturating sender machine in a testbed similar to the one used for AE performance evaluation above. Up to 8 parallel units were used for the measurement, connected using Gigabit Ethernet NICs into GE ports of the Cisco 6506. Myrinet-2000 NICs and switch were used for the low-latency interconnection. Packet distribution was implemented as user-land UDP library and the aggregation was performed by the Cisco 6506 switch. When the FCT protocol is used, the experimental evaluation showed the maximum packet reordering is below 15 for 8 parallel units, which makes it comparable to long-haul networks of good quality. Without the FCT, the maximum reordering was up to 111 for the same setup, i.e., one magnitude worse. Typical results can be seen in Figure 5.

The distributed AEs can also be incorporated into an AE network using the same approach described in the previous chapter. However, because of running on more complicated infrastructure, the setup and start is more complex than for a single AE and thus the system has worse fail-over behavior compared to the network of simple AEs. Another complication of the distributed AE is in the processing of the passing data, which requires development of parallel programming paradigms similar to MIT StreamIt Thies et al. (2002). The processing may follow one of two possible approaches: (1) a context is maintained within one parallel unit only (requires either that all the data requiring the same context to be processed in are processed with one parallel unit only, or per-packet processing without a context is used), or (2) the context is maintained within a subset of parallel nodes using the low-latency interconnection of the cluster. These approaches will be further investigated in the future.

⁶ <http://www-unix.mcs.anl.gov/mpi/mpich/>

⁷ <http://www.myri.com/scs/GM-2/doc/html/>

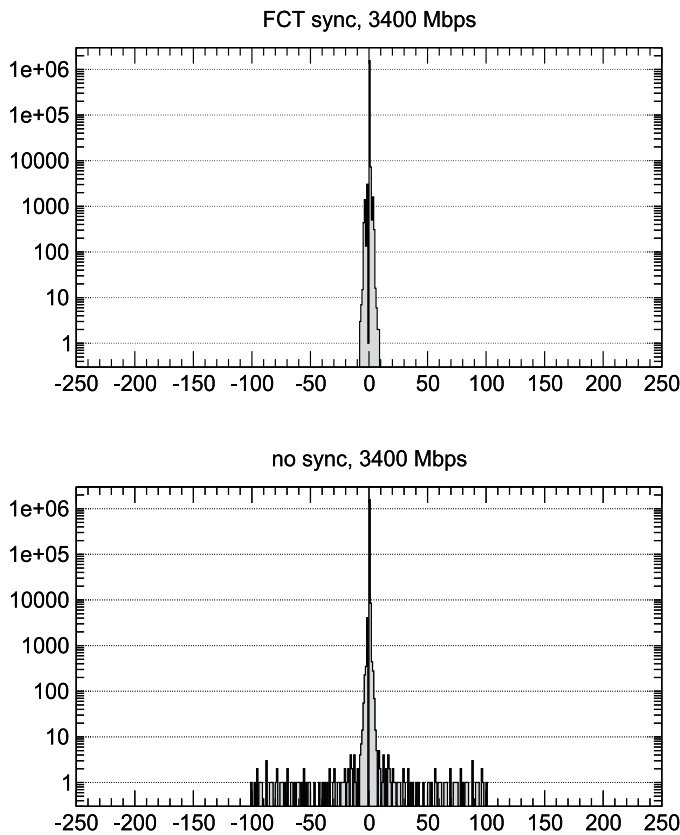


Fig. 5. Packet reordering distribution with FCT and without synchronization, for 8 parallel units and 3.4 Gbps per data flow.

3. Applications

Applications of virtual multicast range from simple user-empowered data distribution to complex data parallel data processing tasks and per-user data processing. Overlay network creating virtual multicast can be also used to distribute data strongly protected environments. These use cases are further discussed in this chapter.

3.1 Data Distribution

The AEs have been used routinely by different groups for collaboration, mostly with MBone Tools⁸, DVTS⁹, and uncompressed HD video based on UltraGrid Holub et al. (2006). A recent demonstration of uncompressed HD video with bandwidth usage of 1.5 Gbps per data stream at SuperComputing |06 conference¹⁰ used a network with 3 optimized HD AEs in StarLight (Chicago, USA) and achieved sustained aggregated data rate of 18 Gbps without any packet

⁸ <http://www-mice.cs.ucl.ac.uk/multimedia/software/>

⁹ <http://www.sfc.wide.ad.jp/DVTS/>

¹⁰ https://sitola.fi.muni.cz/igrid/index.php/SuperComputing_2006

loss. As an alternative setup, we have also used a combination of an AE with multiplication on optical layer (optical multicast), which is, however, far from user-empowered as it requires both direct access to Layer 1 network and installation of specialized hardware directly into the network. The high-performance static AE network has also been used in production for uncompressed HD video distribution for a distributed class on high-performance computing taught by prof. Sterling at Louisiana State University Matyska, Holub & Hladká (2007). In this case, dedicated λ -circuits spanning 5 institutions across the USA and one in the Czech Republic were used and, therefore, a static configuration was the most appropriate as the circuit topology was also statically configured. The 1.5 Gbps streams were distributed up to 7 locations as shown in Figure 6.

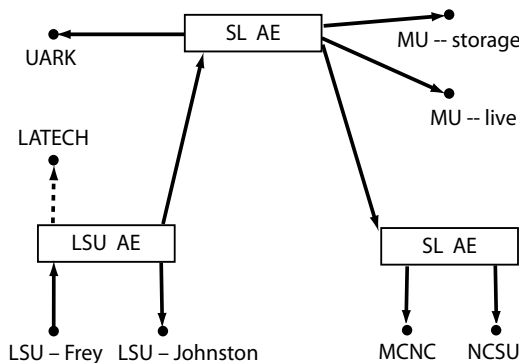


Fig. 6. Data distribution for LSU HPC Class by prof. Sterling based on uncompressed HD video with 1.5Gbps per stream.

With much lower bandwidth per stream but many more clients served, another AE network is also used for streaming data distribution using VLC at the Masaryk University to get the live video feeds from the lecturing halls even over networks without multicast support. Furthermore, it is used for tunneling the data to the student dormitories which have very adverse networking environments. This AE network also supports transcoding as described below.

3.2 Stream transcoding

Typical application of processing on an AE is stream transcoding. For live video stream distribution from several lecturing halls at the Masaryk University, a transcoding processor for the video and audio streams has been implemented as an AE module Liška & Denemark (2006). It uses VideoLAN Client¹¹ (VLC) as the actual transcoding back-end, thus giving us a large variety of supported formats for both input and output. The transcoding module communicates with VLC in three ways: the source data is delivered using Unix standard I/O, the transcoded data is received from VLC using a local UDP socket in order to receive the data appropriately packetized, while a local telnet interface is used for remote control of VLC.

For the specific application, the distribution schema is shown in Fig. 7. There are basically two types of video stream sources: an MPEG-2 hardware encoder such as Teracue ENC-100 or a regular MPEG-4 streaming PC with video capture card and VideoLAN Client installed.

¹¹ <http://www.videolan.org>

In both cases the video stream is generated as a standard MPEG Transport Stream (MPEG-TS) at 2 Mbps and sent using unicast to the AE for further processing. The original data is available to the students either using unicast (AE) or multicast from the AE, or they can watch transcoded video from the gateway AE. Students then use VLC again for rendering the streams at their computers. This allows us to provide students at the high-speed networks with the maximum quality video, while students with slower networks (e.g., in dormitories) are also supported and may participate in the class using transcoded streams with a lower bitrate. Depending on the settings, the transcoding can consume a considerable amount of processing power and therefore the transcoding AE has significantly lower distribution capacity. As a result it is set up at the beginning of the low bandwidth link working as a gateway or bridge only, while another AE is used to actually distribute the transcoded data at large.

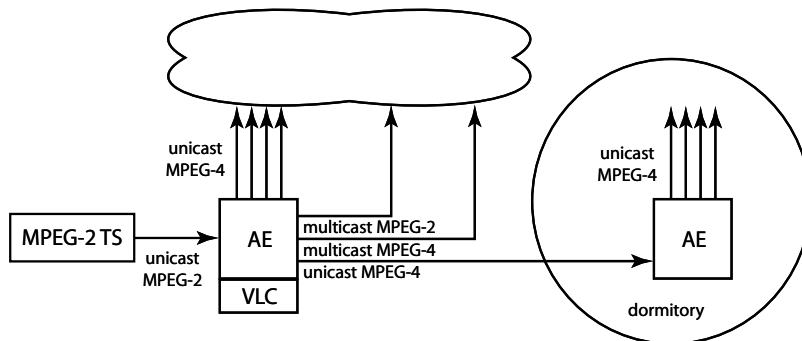


Fig. 7. Video stream distribution schema for the live streaming from lecturing halls.

Performance evaluation

In order to evaluate efficiency and scalability of this solution, we have performed a series of performance and latency measurements.

For performance measurements, we have used the following testbed: the AE was running on a computer with the dual-core Pentium D at 3 GHz, 1 GB RAM, and a Gigabit Ethernet (GE) NIC Broadcom NetXtreme BCM5721. Client computers were furnished with two Intel Xeon 3 GHz processors, 8 GB RAM, and a GE NIC BCM 5708. The testbed was interconnected using two HP Procurve GE switches (2824 and 5406zl). All the computers were running Linux kernel version 2.6. We have optimized buffer settings on NIC to 1 MB to improve the performance. For transcoding, VLC 0.8.6b with ffmpeg library using libavutil 49.4.0, libavcodec 51.40.2, and libavformat 51.11.0 was used. Source video for transcoding was in MPEG-2 format with full PAL resolution (768×576) at 6 Mbps bitrate. MPGA audio accompanied the video and both streams were encapsulated in MPEG Transport Stream format. The output stream was MPEG-4 with 576×384 resolution at 1 Mbps bitrate, audio bitrate 128 kbps, all encapsulated again in MPEG TS. Scalability and resource utilization is shown in Figure 8.

We have also performed a similar experiment for H.264 output video with full PAL resolution at 2 Mbps bitrate using x264 library¹², but this didn't work as the conversion used 100% CPU capacity which resulted in visible packet loss in the image.

¹² <http://www.videolan.org/developers/x264.html>

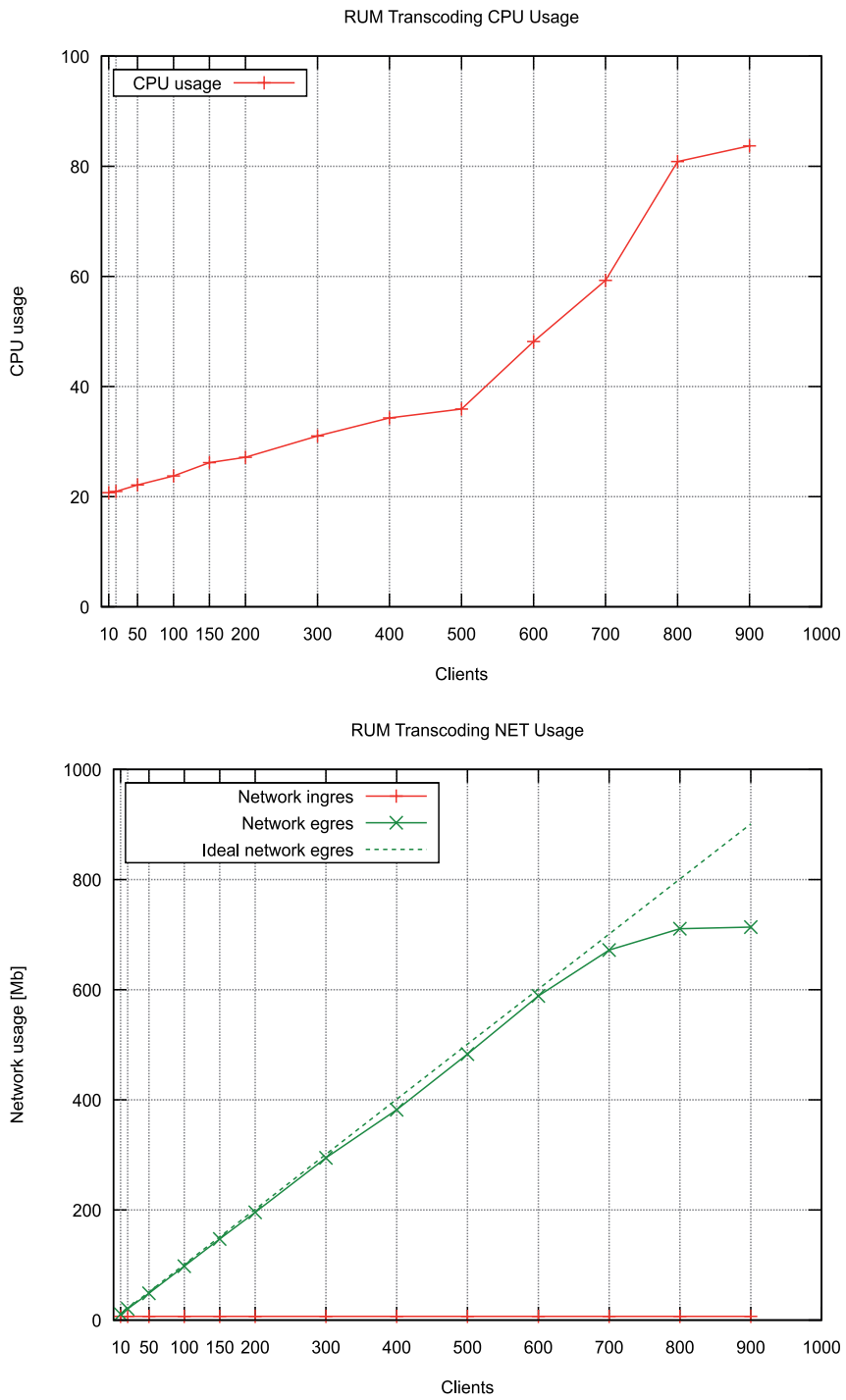


Fig. 8. Performance characteristics of transcoding AE (1 MB buffer or NIC).

<i>Output encoding</i>	<i>Measure latency [ms]</i>
MPEG-4	1220 ± 20
MPEG-4, keyint = 1	1240 ± 20
MJPEG, keyint = 1	1200 ± 20
H.263, keyint = 1, res. 704×576	1180 ± 20

Table 1. Transcoding AE latency measurements results.

Using the same setup, we have measured also the latency of the transcoding AE. The results are summarized in Table 1. Obviously, this implementation of transcoding provides too much latency for interactive video communication, but it is perfectly valid for streaming purposes described above. The latency can be decreased to tens of milliseconds when implemented directly as an AE module, not dependent on external transcoding tool—the latency added by a simple AE module that just passes on the raw data in zero copy mode is 0.238 ms on given infrastructure.

3.3 Video stream composition

Large group collaboration may easily result in too many windows at client sites (typical scenario for AccessGrid¹³), and clients may not have sufficient power or desktop space to render them all. In cases like this, it may be advantageous to down-sample the video streams and compose several of them into a single stream directly on the AE. The same technique is implemented in MCUs for H.323/SIP, but it was unavailable for Mbone Tools. The first version of video compositor Holer (2003) has been adapted to fit into the modular AE architecture as a processor. This processor is based on the VIC tool McCanne & Jacobson (1995) and thus it supports exactly the same set of video formats and the result is seen in Fig. 9. Up to four video streams can be composed into one output stream. Input video formats are auto-detected, the processor is able to work with different formats simultaneously. The output video format is configurable by the end user.



Fig. 9. Example of video stream composition at AE using VIC video clients.

¹³ <http://www.accessgrid.org/>

3.4 Operation in Adverse Networking Environments and Security

The real-time communication for healthcare purposes is unique because of the two classes of interconnected requirements: security and ability to operate even in heavily protected networking environments. The security is necessary as the specialist often need to communicate very sensitive patients data. Because of the security requirements, the healthcare institutions are usually trying to implement the most restrictive networking scenarios. E.g., we have been collaborating with a hospital that has its network protected by a firewall and hidden behind a NAT, that allows only HTTP traffic, which has to pass through two tiers of proxies. However, even the specialists from this hospital need to communicate with their colleagues. The AE approach combined with VPNs have been deployed successfully for several healthcare related projects and we were able to include even the institute mentioned above. As shown in Holub et al. (2007), the OpenVPN approach only has a minimal impact on the performance of collaborative tools. Another important feature that we are developing in this field is efficient aggregation of individual media streams—not only the video streams as discussed above—as some of the institutions, especially in developing countries, have only very limited Internet connection capacity.

4. Related work

Distribution of multimedia data over IP network leads to a multicast schema Almeroth (2000). However, as the native multicast solution is not always appropriate (e.g., for many small groups which is characteristic for interactive collaboration as it has been designed for small number of large groups), reliable, or even available, other distribution schemes were developed following the approach of multicast virtualization El-Sayed et al. (2003); Li & Shin (2002), e.g., Mtunnel Parnes et al. (1998) and UMTF Finlayson (2003). While many theoretical concepts for data distribution were developed namely during 1998–2003 period (see the data distribution models referenced in Section 2.1), the practical approaches are still usually based on a central distribution unit or static topologies like the H.323 MCUs or reflectors provided in the Virtual Room Videoconferencing System (VRVS)¹⁴. The successor of VRVS called Enabling Virtual Organizations (EVO)Galvez (2006) is based on a self-organizing system of reflectors, again not empowering the end-user with tools to change the distribution topology. High-performance dynamic data distribution system used for distribution of 200 Mbps compressed 4K video streams designed by NTT is called Flexcast Shimizu et al. (2006). Another application-level multicast called Host Based Multicast (HBM) has been proposed in El-Sayed (2004). The HBM author also investigated a combination of an IPsec based VPN environment—while useful for data protection, it doesn't improve on adaptability of HBM for adverse networking environments. Other simpler UDP packet reflectors include rcbidge Buchhorn (2005), reflector¹⁵, and Alkit Reflex¹⁶. However, all these systems are primarily focused on pure data distribution and most of them even neglect the user-empowered view, thus differing significantly from our highly modular and user-empowered AE based on active network concept.

Another relevant field of work is parallel stream-oriented processing and programming of such systems, which is of high importance for the distributed AE. A parallel programming paradigm, that might be suitable for distributed AE programming, has been proposed in MIT

¹⁴ <http://www.vrvs.org/>

¹⁵ <http://www.cs.ucl.ac.uk/staff/s.bhatti/teaching/z02/reflector.html>

¹⁶ <http://w2.alkit.se/reflex/>

StreamIt system Thies et al. (2002). It enables efficient parallelization of the data processing based on sent data structure and processing dependencies. Its suitability and possible adaptation will be further investigated.

5. Future work

In this chapter, we have explained basic principles of multicast virtualization, presented a framework of Active Elements, designed for user-empowered synchronous data distribution and processing. Depending on target environment and the streams that are being distributed, the AEs may be deployed as a single central entity, or as a network of AEs for increased scalability with respect to number of clients and increased failure resiliency, or as a distributed AE to improve scalability with respect to the bandwidth of individual data stream. We have demonstrated a number of applications both for data distribution and processing.

In the future, there are at least several areas to focus on. Utilizing a single AE, we would like to introduce multi-level QoS approach to provide strict user and stream separation. This is especially important when an AE is used for data processing. We would like to use a virtualization-based approach to achieve this, and the virtual machines may also be used for “programming” the AE, as the user may “inject” the whole virtual machine into the AE. For the AE network, we would like to develop more complex signaling protocols to improve diagnostics (e.g., failure information needs to be distributed not only inside the AE network, but also to the influenced users in some way). The virtual machine approach will also be used to simplify migration of the processing modules in the AE network. Last but not least, we will further investigate programming paradigms suitable for the distributed AE to enable truly parallel stream processing.

This field of data distribution in overlay networks has been thoroughly examined by several research groups between 1998 – 2003; some were examining the data distribution perspective, while others were also looking at security issues. We provide a much broader view of the field extending it with active network and user-empowered approaches. We have demonstrated that while the research interest in this field dropped since 2003, new useful techniques can still be invented and there are many practical applications worth analyzing.

Larger networks of AEs that are specialized in their functionality for data distribution as well as processing goes beyond human capacity to manage such system. Thus we are researching application of self-organization principles to application orchestration Liška & Holub (2009), that could include not only AE and their networks, but also other components ranging from individual applications running at users’ computers to allocation of network circuits.

Acknowledgments

This project has been kindly supported by the research intent “Optical Network of National Research and Its New Applications” (MŠM 6383917201) and “Parallel and Distributed Systems” (MŠM 0021622419). We would like to appreciate various colleagues that worked in various stages of multicast virtualization projects, namely Jiří Denemark, Luděk Matyska, and Tomáš Rebok.

6. References

Alchaal, L., Roca, V. & Habert, M. (2002). Offering a multicast delivery service in a programmable secure IP VPN environment., *Networked Group Communication, Fourth In-*

- ternational COST264 Workshop, NGC 2002, Boston, MA, USA, October 23-25, 2002, Proceedings, ACM, pp. 5–10.*
- Almeroth, K. C. (2000). The evolution of multicast: From the Mbone to inter-domain multicast to Internet2 deployment, *IEEE Network* **14**(1): 10–20.
- Banerjee, S., Bhattacharjee, B. & Kommareddy, C. (2002). Scalable application layer multicast., *Proceedings of the ACM SIGCOMM 2002 Conference on Applications, Technologies, Architectures, and Protocols for Computer Communication, August 19-23, 2002, Pittsburgh, PA, USA, ACM, pp. 205–217.*
- Bouček, T. (2002). *Kryptografické zabezpečení videokonferencí (Securing videoconferences using cryptography)*, Master's thesis, Military Academy of Brno, Czech Republic.
- Buchhorn, M. (2005). Designing a multi-channel-video campus delivery and archive service, *The 7th Annual SURA/ViDe Conference, Atlanta, GA, USA.*
- Cheriton, D. R. & Deering, S. E. (1985). Host groups: a multicast extension for datagram internetworks, *Technical report*, Stanford University, Stanford, CA, USA.
- Chu, Y.-H., Rao, S. G. & Zhang, H. (2000). A case for end system multicast, *ACM SIGMETRICS: Measurement and Modeling of Computer Systems*, pp. 1–12.
- Deering, S. E. & Cheriton, D. R. (1990). Multicast routing in datagram internetworks and extended LANs, *ACM Transactions on Computer Systems* **8**: 85–110.
- Denemark, J., Holub, P. & Hladká, E. (2003). RAP – Reflector Administration Protocol, *Technical Report 9/2003, CESNET.*
URL: <http://www.cesnet.cz/doc/techzpravy/>
- Diot, C., Levine, B. N., Lyles, B., Kassem, H. & Balensiefen, D. (2000). Deployment issues for the IP multicast service and architecture, *IEEE Network* **14**(1): 78–88.
- Dressler, F. (2003a). Availability analysis in large scale multicast networks, *15th IASTED International Conference on Parallel and Distributed Computing and Systems (PDCS2003)*, Vol. I, pp. 399–403.
- Dressler, F. (2003b). *Monitoring of Multicast Networks for Time-Synchronous Communication*, Ph.d. thesis, University of Erlangen-Nuremberg.
URL: <http://www7.informatik.uni-erlangen.de/dressler/publications/dissertation.pdf>
- El-Sayed, A. (2004). *Application-Level Multicast Transmission Techniques Over The Internet*, PhD thesis, INRIA Rhône-Alpes, France.
URL: http://www.inrialpes.fr/planete/people/elsayed/phd/phd_final_080304.pdf
- El-Sayed, A., Roca, V. & Mathy, L. (2003). A survey of proposals for an alternative group communication service, *IEEE Network* **17**(1): 46–51.
- Finlayson, R. (2003). The UDP multicast tunneling protocol. IETF Draft <draft-finlayson-umtp-09.txt>.
URL: <http://tools.ietf.org/id/draft-finlayson-umtp-09.txt>
- Francis, P. (2000). YOID: extending the internet multicast architecture. Unpublished report for ACIRI, <http://www.aciri.org/yoid/docs/index.html>.
- Galvez, P. (2006). From VRVS to EVO (Enabling Virtual Organizations), *TERENA Networking Conference 2006, Catania, Italy.*
- Hladká, E., Holub, P. & Denemark, J. (2004). An active network architecture: Distributed computer or transport medium, *3rd International Conference on Networking (ICN'04)*, Gosier, Guadeloupe, pp. 338–343.
- Hladká, E., Liška, M. & Rebok, T. (2005). Stereoscopic video over ip networks, in P. Dini & P. Lorenz (eds), *International Conference on Networking and Services 2005 (ICNS'05)*, IEEE, p. 6.

- Hladká, E. & Salvet, Z. (2001a). An active network architecture: Distributed computer or transport medium, in P. Lorenz (ed.), *Networking – ICN 2001: First International Conference Colmar, France, July 9-13, 2001, Proceedings, Part II*, Vol. 2094 of *Lecture Notes in Computer Science*, Springer-Verlag, Heidelberg, pp. 612–619.
- Hladká, E. & Salvet, Z. (2001b). An active network architecture: Distributed computer or transport medium, in P. Lorenz (ed.), *Networking – ICN 2001: First International Conference Colmar, France, July 9-13, 2001, Proceedings, Part II*, Vol. 2094 of *Lecture Notes in Computer Science*, Springer-Verlag, Heidelberg, pp. 612–619.
- Holer, V. (2003). *Slučování videostreamů (Videostream Merging)*, Bachelor thesis, Faculty of Informatics, Masaryk University Brno, Brno, Czech Republic.
- Holub, P. (2005). *Network and Grid Support for Multimedia Distribution and Processing*, PhD thesis, Faculty of Informatics, Masaryk University Brno, Czech Republic.
- Holub, P. & Hladká, E. (2006). Distributed active element for high-performance data distribution, *NPC 2006: Network and Parallel Computing*, Tokio, Japan, pp. 27–36.
- Holub, P., Hladká, E. & Matyska, L. (2005). Scalability and robustness of virtual multicast for synchronous multimedia distribution, *Networking - ICN 2005: 4th International Conference on Networking, Reunion Island, France, April 17-21, 2005, Proceedings, Part II*, Vol. 3421/2005 of *Lecture Notes in Computer Science*, Springer-Verlag Heidelberg, La Réunion, France, pp. 876–883.
- Holub, P., Hladká, E., Procházka, M. & Liška, M. (2007). Secure and pervasive collaborative platform for medical applications, *Studies in Health Technology and Informatics* **126**: 229–238. IOS Press, Amsterdam, The Netherlands.
- Holub, P., Matyska, L., Liška, M., Hejtmánek, L., Denemark, J., Rebok, T., Hutanu, A., Paruchuri, R., Radil, J. & Hladká, E. (2006). High-definition multimedia for multiparty low-latency interactive communication, *Future Generation Computer Systems* **22**(8): 856–861.
- Jannotti, J., Gifford, D. K., Johnson, K. L., Kaashoek, M. F. & O’Toole, J. J. W. (2000). Overcast: reliable multicasting with on overlay network, *OSDI’00: Proceedings of the 4th conference on Symposium on Operating System Design & Implementation*, USENIX Association, Berkeley, CA, USA, pp. 197–212.
- Jo, J., Hong, W., Lee, S., Kim, D., Kim, J. & Byeon, O. (2006). Interactive 3D HD video transport for e-science collaboration over UCLP-enabled GLORIAD lightpath, *Future Generation Computer Systems* **22**(8): 884–891.
- Li, Z. & Shin, Y. (2002). Survey of overlay multicast technology. Unpublished report for Networks Lab, UC Davis, <http://networks.cs.ucdavis.edu/~lizhi/papers/ECS289.pdf>.
- Liebeherr, J. & Nahas, M. (2001). Application-layer multicast with delaunay triangulations, *Global Telecommunications Conference, 2001. GLOBECOM ’01. IEEE*, pp. 1651–1655 vol.3.
- Liška, M. & Denemark, J. (2006). Real-time transcoding and scalable data distribution for video streaming, *Technical Report 30/2006*, CESNET, Praha, Czech Republic.
URL: <http://www.cesnet.cz/doc/techzpravy/2006/rum-streaming/>
- Liška, M. & Holub, P. (2009). Couniverse: Framework for building self-organizing collaborative environments using extreme-bandwidth media applications, *Euro-Par 2008 Workshops - Parallel Processing. Las Palmas de Gran Canaria, Spain*, Vol. 5415 of *Lecture Notes in Computer Science*, Springer-Verlag, Berlin/Heidelberg, pp. 339–351.

- Mathy, L., Canonico, R. & Hutchison, D. (2001). An overlay tree building control protocol, *Lecture Notes in Computer Science* **2233**: 76–87.
- Mathy, L., Canonico, R., Simpson, S. & Hutchison, D. (2002). Scalable adaptive hierarchical clustering, *NETWORKING '02: Proceedings of the Second International IFIP-TC6 Networking Conference on Networking Technologies, Services, and Protocols; Performance of Computer and Communication Networks; and Mobile and Wireless Communications*, Springer-Verlag, London, UK, pp. 1172–1177.
- Matyska, L., Hladká, E. & Holub, P. (2007). Collaborative framework for distributed distance learning, *Proceedings of the 8th International Conference on Information Technology Based Higher Education and Training (ITHET '07)*, Kumamoto, Japan.
- Matyska, L., Holub, P. & Hladká, E. (2007). Collaborative framework for distributed distance learning, *Proceedings of the 4th High-End Visualization Workshop*, Obergurgl, Tyrol, Austria, pp. 40–45.
- McCanne, S. & Jacobson, V. (1995). vic: A flexible framework for packet video, *Proceedings of ACM Multimedia'95*, San Francisco, CA, USA, pp. 511–512.
- Parnes, P., Synnes, K. & Schefstrom, D. (1998). Lightweight application level multicast tunneling using mtunnel, *Computer Communication* **21**(15): 1295–1301.
- Procházka, M., Holub, P. & Hladká, E. (2005). Active element network with P2P control plane, *IWSOS 2006: 1st International Workshop on Self-Organizing Systems*, Vol. 4124/2006 of *Lecture Notes in Computer Science*, Springer-Verlag Heidelberg, University of Passau, Germany, p. 257.
- Salvet, Z. (2001). Enhanced UDP packet reflector for unfriendly environments, *Technical Report 16/2001*, CESNET, Praha, Czech Republic.
URL: <http://www.cesnet.cz/doc/techzpravy/2001/16/>
- Schulzrinne, H., Rao, A. & Lanphier, R. (1998). Real Time Streaming Protocol (RTSP). RFC 2326.
- Shimizu, T., Shirai, D., Takahashi, H., Murooka, T., Obana, K., Tonomura, Y., Inoue, T., Yamaguchi, T., Fujii, T., Ohta, N., Ono, S., Aoyama, T., Herr, L., van Osdol, N., Wang, X., Brown, M. D., DeFanti, T. A., Feld, R., Balser, J., Morris, S., Henthorn, T., Dawe, G., Otto, P. & Smarr, L. (2006). International real-time streaming of 4K digital cinema, *Future Generation Computer Systems* **22**(8): 929–939.
- Thies, W., Karczmarek, M. & Amarasinghe, S. (2002). StreamIt: A language for streaming applications, *Proceedings of the 11th International Conference on Compiler Construction*, Vol. 2304/2002 of *Lecture Notes in Computer Science*, Springer-Verlag Heidelberg, Grenoble, France, pp. 179–196.
- Tran, D. A., Hua, K. A. & Do, T. T. (2003). ZIGZAG: An efficient peer-to-peer scheme for media streaming, *INFOCOM*.
- Zhang, B., Jamin, S. & Zhang, L. (2002). Host multicast: A framework for delivering multicast to end users., *IEEE INFOCOM '02*, New York, NY.
- Zhuang, S. Q., Zhao, B. Y., Joseph, A. D., Katz, R. H. & Kubiawicz, J. D. (2001). Bayeux: an architecture for scalable and fault-tolerant wide-area data dissemination, *NOSS-DAV '01: Proceedings of the 11th international workshop on Network and operating systems support for digital audio and video*, ACM Press, New York, NY, USA, pp. 11–20.

The Asymmetrical Architecture of New Optical Switch Device

Mohammad Syuhaimi Ab-Rahman and Boonchuan Ng
Universiti Kebangsaan Malaysia (UKM)
Malaysia

1. Introduction

The explosive growth of data and combusting traffic have led to a demanding of flexible, efficient, survivable, and multifunctional device to support all of network functions, management and testing. The sophisticated technologies today had led to realize any complex design in optical architecture that has become impossible for some years ago. The waveguide technologies become the first player in developing the new architecture of optical switch device. The most optical devices today are built by symmetrical architecture. Therefore, they can perform bi-directionally with the same function to both side of incoming signal.

The introducing of new optical switching device named optical cross add and drop multiplexing (OXADM) which has an asymmetrical architecture and can perform bi-directionally function as the previous using the combination concept of optical cross connect (OXC) and optical add and drop multiplexing (OADM). Its enable the operating wavelength on two different optical trunks to be switched to each other while implementing add and drop function simultaneously. With the asymmetrical architecture, its enable the operating wavelength on two different optical trunks to be switched to each other and implementing accumulating function simultaneously. Here, the operating wavelengths can be reused again as a carrier of new data stream. The wavelength transfer between two different cores of fiber will increase the flexibility, survivability, and also efficiency of the network structure. To make device operational more efficient, micro-electromechanical system (MEMS) switches are used to control the mechanism of operation such as wavelength add/drop and wavelength routing operation. As a result, the switching performed within the optical layer will be able to achieve high-speed restoration against failure/degradation of cables, fibers and optical amplifiers.

The OXADM architecture consists of 3 parts; selective port, add/drop operation, and path routing. Selective port permits only the interest wavelength going through and acts as filter. With the switch configuration, add and drop function can be activated in second part of OXADM architecture. The 'accumulation' feature is found in the third part. The functions of OXADM include node termination, drop and add, routing, multiplexing, and also providing mechanism of restoration for point-to-point (P2P), ring, and mesh metropolitan as well as fiber-to-the-home (FTTH) access network.

The OXADM also provide survivability through restoration against failure by means of dedicated and shared protection that can be applied in wavelength division multiplexing (WDM) ring metropolitan network. In other application, OXADM can also work as any single device such as multiplexer, demultiplexer, OXC, OADM, wavelength selective coupler (WSC), and wavelength roundabout (WRB). With such the excellent features, the OXADM is expected to be unique, universal, and with a high reliability that is used to overcome the various functions in WDM communication network today.

The experimental results showed the value of crosstalk and return loss for OXADM is bigger than 60 dB and 40 dB respectively. The results also showed the value of insertion loss was less than 0.06 dB under ideal condition, the maximum length that can be achieved is 94 km. In the transmission using SMF-28 fiber, with the transmitter power of 0 dBm and sensitivity -22.8 dBm at a P2P configuration with safety margin, the required transmission is 71 km with OXADM. The optical signal-noise-ratio (OSNR) measurements for every function of OXADM are also proposed with the values are bigger than 20 dB.

2. Wavelength Routed Networks Switching

Optical networks are high-capacity telecommunications networks based on optical technologies and components that provide routing, grooming, and restoration at the wavelength level as well as wavelength-based services. As networks face increasing bandwidth demand and diminishing fiber availability, network providers are moving towards a crucial milestone in network evolution: the optical network. Optical networks based on the emergence of the optical layer in transport networks, provide higher capacity and reduced costs for new applications such as the Internet, video and multimedia interaction, and advanced digital services (IEC, 2007).

The explosive growth of data, particularly internet traffic, has led to a dramatic increase in demand for transmission bandwidth imposing an immediate requirement for broadband transport networks. Currently telecommunications networks widely employ WDM in single-mode (SM) optical fibers to interconnect discrete network locations and offer high capacity, high-speed and long reach transmission capabilities. The information transmitted in the optical domain is transferred through simple P2P links terminated by Synchronous Digital Hierarchy (SDH) or Synchronous Optical Network (SONET) equipment forming ring and mesh network topologies. This solution requires a number of intermediate service layers introducing complex network architectures. Such a scenario provides unnecessarily high switching granularity, numerous optoelectronic conversions and complicated network management resulting in poor scalability for data services and slow service turn up with high installation, operation and maintenance cost. With the recent technology evolution in the area of optical communications, the WDM transport layer is migrating from simple transmission links into elaborate networks providing similar functionality to that of the SDH/SONET layer, with improved features, higher manageability, lower complexity, and cost-effective. Integrated WDM networks performing switching (Ramaswami, 2001) and routing are deployed in order to overcome the need for multi-layer network architectures (Tzanakaki et al., 2002). In such network scenarios, high capacity optical routes are set in the transport layer forming connections between discrete points of the network topology. In wavelength routed networks switching is performed through OADM and OXC nodes.

2.1 Optical Add/Drop Multiplexers (OADM)

OADM is element that provides capability to add and drop traffic in optical network. The function of an OADM is to insert (add) or extract (drop) one or more selected wavelengths at a designated point in an optical network (Keiser, 2003). An OADM can be passive or active device that located at sites supporting one or two (bi-directional) fiber pairs and enable a number of wavelength channels to be dropped and added reducing the number of unnecessary optoelectronic conversions, without affecting the traffic that is transmitted transparently through the node (Mukherjee, 2006).

The features that an OADM should ideally support are listed below:

- Drop capability of any channel and insertion capability of a channel on any unused wavelength
- Dynamic reconfiguration supporting fast switching speed (\sim ms)
- Variable add/drop percentage up to 100%
- Scalable architecture in a modular fashion
- Drop and continue functionality enabling network architectures such as dual homing rings
- Span and ring protection capabilities
- Minimum performance degradation in terms of noise, crosstalk, filtering, etc for add, drop, and through paths

The OADM enhances the WDM terminals by adding several significant features (see Figure 1). The OADM systems have the capacity of up to 40 optical wavelengths. They efficiently drop and add various wavelengths at intermediate sites along the network for solving a significant challenge for existing WDM (IEC, 2007).

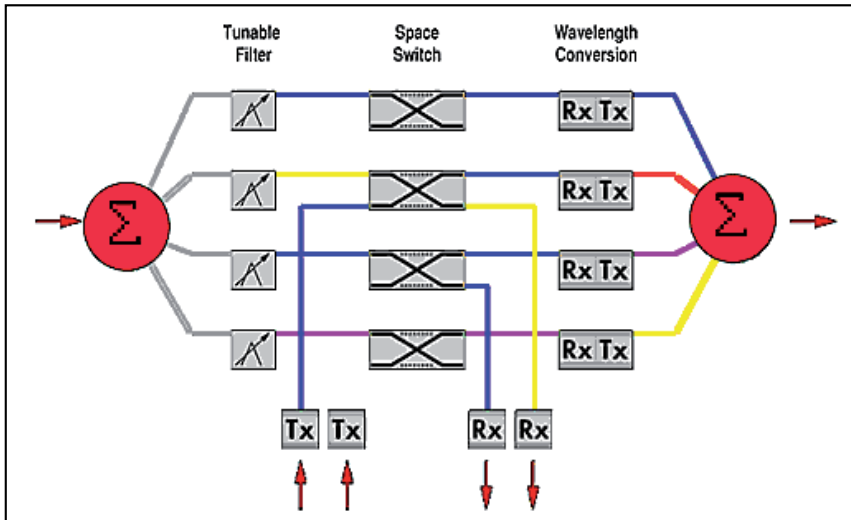


Fig. 1. OADM functionality (IEC, 2007).

Most important, OADM technology introduces asynchronous transponders to allow the optical-network element to interface directly to high revenue generating services. It is now possible for asynchronous transfer mode (ATM), frame relay (FR), native local area networks (LANs), high-bandwidth Internet protocol (IP), and others to connect directly to

the network via a wavelength in the optical layer. Transponder technology also extends the life of older lightwave systems by accepting its bandwidth directly into the optical layer, converting its frequency to an acceptable standard, and providing protection, and restoration. The OADM also is the foundation of optical bidirectional line switched rings (OBLSRs), which are described in the next module (IEC, 2007).

An OADM can be used in both linear and ring network architectures and in practice operate in either fixed or reconfigurable mode. In fixed OADMs the add/drop and express (through) channels are predetermined and can only be manually rearranged after installation. In reconfigurable OADMs the channels that are added/dropped or pass transparently through the node can be dynamically reconfigured as required by the network. These are more complicated structures but more flexible as they provide provisioning on demand without manual intervention, therefore they can be set up on the fly to allow adding or dropping of a percentage of the overall traffic. The reduction of unnecessary optoelectronic conversions through the use of OADMs introduces significant cost savings in the network (Tzanakaki et al., 2003).

An OADM allows the insertion or extraction of a wavelength from a fiber at a point between terminals. An OADM can operate either statically or dynamically. Some vendors call a dynamic device a reconfigurable OADM (R-OADM). A static version obviously is not as flexible and may require a hardware change if a different wavelength needs to be dropped or added. For example, a static OADM might use two optical circulators in conjunction with a series of fixed-wavelength fiber Bragg gratings (FBG). A dynamic or R-OADM results if the gratings are tunable. Although a dynamic feature adds greater flexibility to a network, this versatility also requires more careful system design. In particular, tunable (wavelength-selectable) optical filters may be needed at the drop receivers, and the OSNR for each wavelength must be analyzed more exactly (Keiser, 2003).

The technology of choice is determined by the functional and the performance requirements of the node. R-OADM can be divided into two categories partly and fully reconfigurable. In partly reconfigurable architectures there is capability to select the channels to be added/dropped, but there is a predetermined connectivity matrix between add/drop and through ports restricting the wavelength assignment function. Fully reconfigurable OADMs also provide the ability to select the channels to be added/dropped, but also offer flexible connectivity between add/drop and through ports, which enables flexible wavelength assignment with the use of tunable transmitters and receivers (Tzanakaki et al., 2003).

R-OADM can be divided into two main generations. The first is mainly applied in linear network configurations and does not support optical path protection while the second is applied in ring configurations and provide optical layer protection to support network survivability. The two most common examples of fully R-OADM: Wavelength selective (WC) and broadcast select (BS) architectures are illustrated in Figure 2b & 2c. The WS architecture utilizes wavelength (de)multiplexing and a switch fabric interconnecting all express and add/drop ports; while the BS is based on passive splitters/couplers and tunable filters (Mukherjee, 2006).

The tunable filtering, present in the through path, should provide selective blocking of any dropped channels and can be achieved using technologies such as acousto-optic filters or dynamic channel equalizers (DCEs) based on diffraction grating and liquid crystal or MEMS technologies (Tzanakaki et al., 2003). The overall loss introduced by the through path of the BS solution is noticeably lower than the loss of the WS approach, significantly improving the

OSNR of the node and therefore its concatenation performance in a practical transmission link or ring network. In addition, the BS design offers superior filter concatenation performance, advanced features such as drop and continue, and good scalability in terms of add/drop percentage (Mukherjee, 2006).

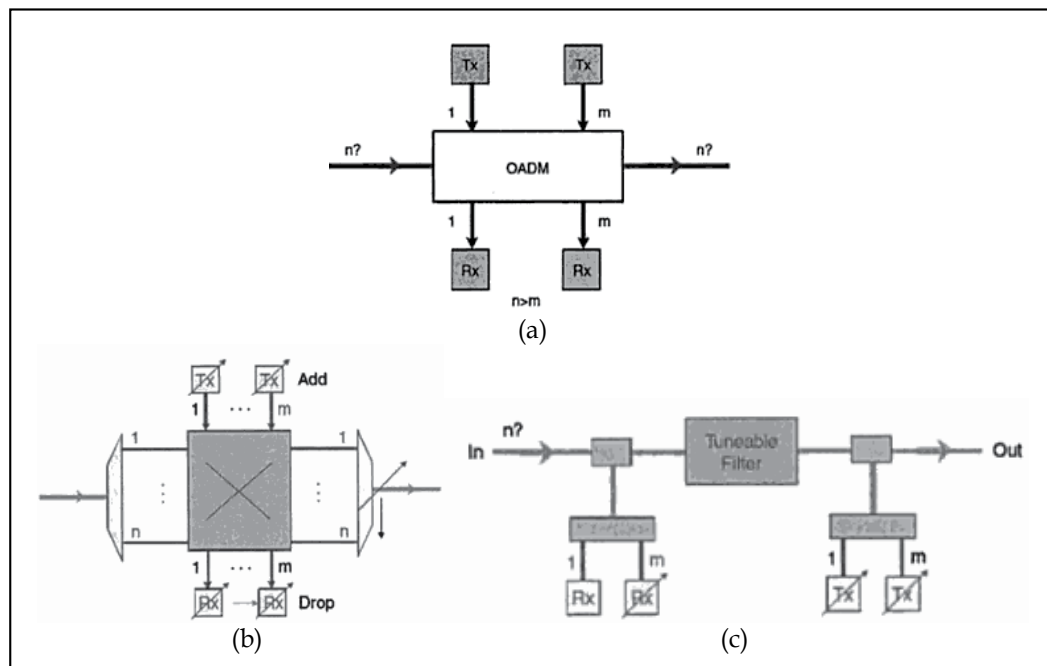


Fig. 2. (a) Generic OADM architecture, (b) WS OADM architecture, and (c) BS OADM architecture

Figure 3 showed a simple OADM configuration that has four input and four output ports. Here the add and drop functions are controlled by MEMS-based miniature mirrors that are activated selectively to connect the desired fiber paths. When no mirrors are activated, each incoming channel passes through the switch to the output port. Incoming signals can be dropped from the traffic flow by activating the appropriate mirror pair. For example, to have the signal carried on wavelength λ_3 entering port 3 dropped to port 2D; the mirrors are activated as shown in Figure 3. When an optical signal is dropped, another path is established simultaneously, allowing a new signal to be added from port 2A to the traffic flow. There are many variations on optical add/drop device configurations depending on the switching technology used. However, in each case the operation is independent of wavelength, data rate, and signal format (Keiser, 2003).

Depending on whether an engineer is designing a metropolitan area network (MAN) or a long-haul network, different performance specifications need to be addressed when implementing an OADM capability in the network. In general, because of the nature of the services provided, changes in the add/drop configuration for a long-haul network tend to occur less frequently than in a MAN. In addition, the channel spacing is much narrower in a long-haul network, and the optical amplifiers which are used must cover a wider spectral band. For an interesting analysis of the Erbium Doped Fiber Amplifier (EDFA) performance

requirements and the link power budgets used for an OADM capability in a MAN environment (Keiser, 2003).

Wideband long-haul networks are essentially a collection of P2P trunk lines with one or more OADMs for inserting and extracting traffic at intermediate points. Figure 4 depicted a generic long-haul Dense WDM (DWDM) network. Such networks typically are configured as large rings in order to offer reliability and survivability features. For example, if there is cable cut somewhere, the traffic that was supposed to pass through that fault can be routed in the opposite direction on the ring and still reach its intended destination. As shown in Figure 4 are three 10 Gbps DWDM rings and the major switching centers where wavelengths can be regenerated, routed, added, or dropped. The links between DWDM nodes have optical amplifiers every 80 km to boost the optical signal amplitude and regenerators every 600 km to overcome degradation in the quality of the optical signals. Extended-reach long-haul networks allow path lengths without regenerators of several thousand kilometers. Also illustrated are typical services between two end-users, such as SONET/SDH, Gigabit Ethernet, or IP traffic (Keiser, 2003).

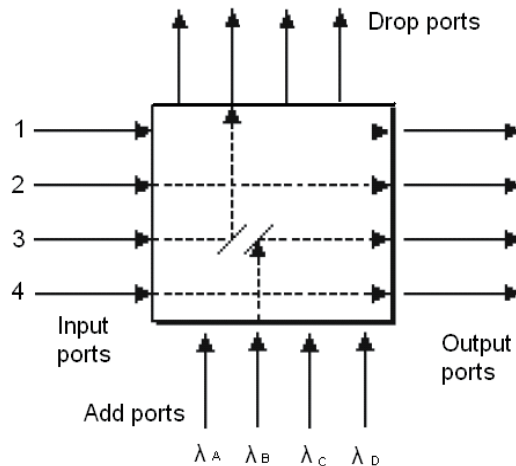


Fig. 3. Example of adding and dropping wavelengths with a 4x4 OADM device that uses miniature switching mirrors

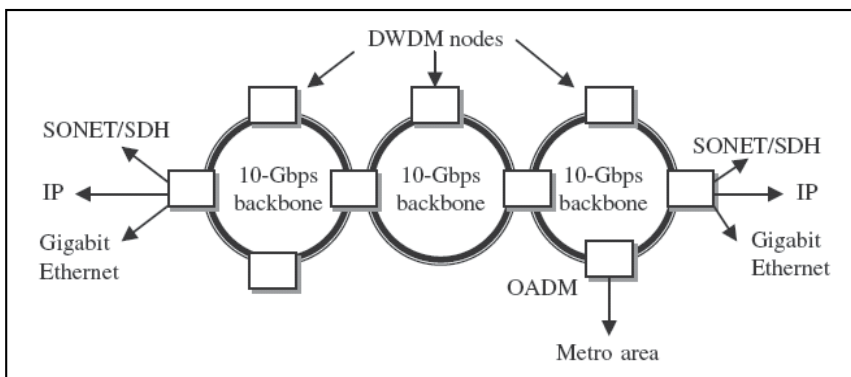


Fig. 4. A generic long-haul DWDM network which is configured as a set of large rings

2.2 Optical Cross-Connect (OXC)

OXC switches optical signals from input ports to output ports. These type of elements are usually considered to be wavelength insensitive, i.e., incapable of demultiplexing different wavelength signals on a given input fiber. OXC is located at nodes cross-connecting a number of fiber pairs and also support add and drop of local traffic providing the interface with the service layer. A basic cross-connect element is the 2x2 cross point element. A 2x2 cross point element routes optical signals from two input ports to two output ports and has two states: cross states and bar states (see Figure 5). In the cross state, the signal from the upper input port is routed to the lower output port, and the signal from the lower input port is routed to the upper output port. In the bar state, the signal from the upper input port is routed to the upper output port, and the signal from the lower input port is routed to the lower output port (Mukherjee, 2006).

To support flexible path provisioning and network resilience, OXCs normally utilize a switch fabric to enable routing of any incoming channels to the appropriate output ports and access to the local client traffic. The features that an OXC should ideally support are similar to these of an OADM, but additionally OXCs need to provide:

- Strictly non-blocking connectivity between input and output ports
- Span and ring protection as well as mesh restoration capabilities

Efficient use of fiber facilities at the optical level obviously becomes critical as service providers begin to move wavelengths around the world. Routing and grooming are key areas that must be addressed. This is the function of the OXC, as shown in Figure 6.

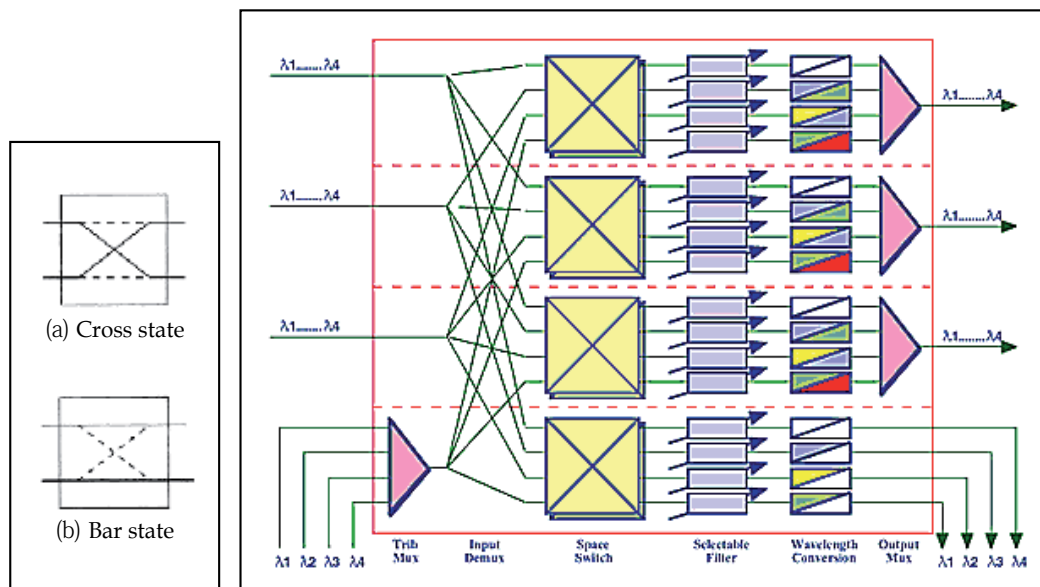


Fig. 5. OXC state

Fig. 6. OXC block diagram (IEC, 2007)

In the optical domain, where 40 optical channels can be transported on a single fiber, a network element is needed that can accept various wavelengths on input ports and route them to appropriate output ports in the network. To accomplish this, the OXC needs three building blocks as illustrated in Figure 7:

1. Fiber switching - the ability to route all of the wavelengths on an incoming fiber to a different outgoing fiber
2. Wavelength switching - the ability to switch specific wavelengths from an incoming fiber to multiple outgoing fibers
3. Wavelength conversion - the ability to take incoming wavelengths and convert them (on the fly) to another optical frequency on the outgoing port; this is necessary to achieve strictly non-blocking architectures when using wavelength switching (IEC, 2007).

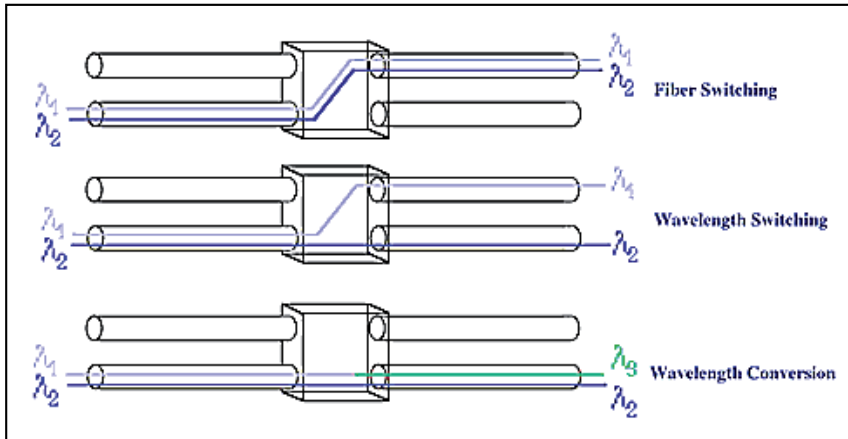


Fig. 7. Switching and conversion with OXC (IEC, 2007).

3. Optical Cross and Add/Drop Multiplexers (OXADM)

OXADMs are elements which provide the capabilities of add and drop function and cross connecting traffic in the network, similar to OADM and OXC (Caraglia, 2003; Mutafungwa, 2000; Tsushima, 1998; Tzanakaki, 2003). OXADM consists of three main subsystem; a wavelength selective demultiplexer, a switching subsystem, and a wavelength multiplexer. Each OXADM is expected to handle at least two distinct wavelength channels each with a coarse granularity of 2.5 Gbps or higher (signals with finer granularities are handled by logical switch node such as SDH/SONET digital cross connects or ATM switches). There are eight ports for add and drop functions, which are controlled by four lines of MEMS-optical switch. The other four lines of MEMS switches are used to control the wavelength routing function between two different paths (see Figure 8). The functions of OXADM include node termination, drop and add, routing, multiplexing and also providing mechanism of restoration for P2P, point-to-multipoint (P2MP), ring, and mesh metropolitan. With the setting of the MEMS optical switch configuration, the device can be programmed to function as another optical switch such as multiplexer, demultiplexer, coupler, wavelength converter (with fiber grating filter configuration), OADM, WRB, and etc for the single application.

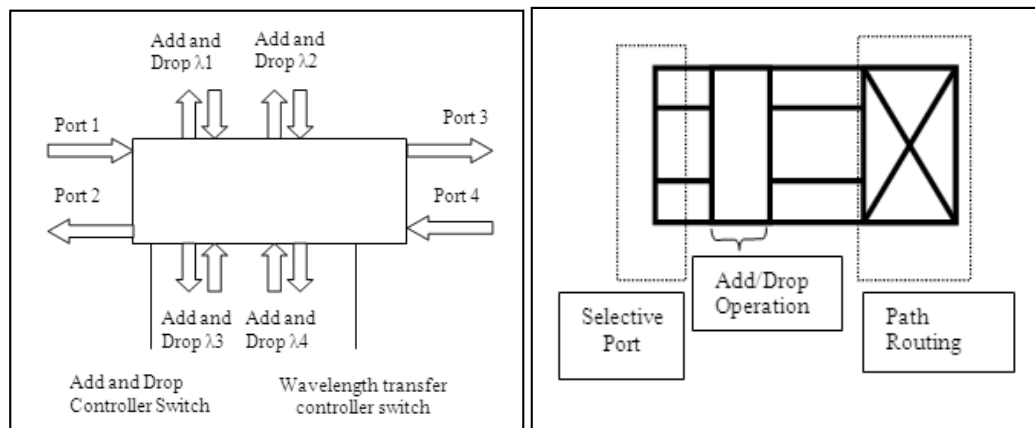


Fig. 8. The block diagram of OXADM architecture Fig. 9. The classification of OXADM

3.1 OXADM Optical Hybrid Device

The designed 4-channels OXADM device is expected to have maximum operational loss of 0.06 dB for each channel when device components are in ideal condition. The maximum insertion loss when considering the component loss at every channel is less than 6 dB. In the transmission using SMF-28 fiber, with the transmitter power of 0 dBm and sensitivity -22.8 dBm at a point-to-point configuration with safety margin, the required transmission is 71 km with OXADM without regeneration (Rahman et al., 2006).

The OXADM architecture consists of 3 parts; selective port, add/drop operation, and path routing. Selective port permits only the interest wavelength going through and acts as filter. With the switch configuration, add and drop function can be activated in second part of OXADM architecture. The signals are then re-routing to any port of output. The signals can also be accumulated on one path and exit at any output port. The partition of OXADM architecture is depicted in Figure 9.

3.2 OXADM Optical Switch

The control switch for OXADM optical switch is used to change the path of incoming from the input port. When the control switches in 'off' state, no switching occurs and the signal pass through the device as seen from the Figure 10a. But when the control switch B is 'on' state, the signal from the Input 1 will be switch to Output 2 (see Figure 10b). In contrast to the control switch B is in reverse state, the accumulation function occurs which multiplex all the signals from the inputs together and exit at the Output 2. This will be the same if the control switch A is in 'on' state but the output is at Output 1. If both switches are in 'on' state, the signal will be switched to exchange their output port and works as an OXC device. The functional of an OXADM optical switch can be summarized through the truth functional table shown by Table 1. The incoming signals from the back will be switched to neighbor output port or pass through the device. This is shown in Figure 11.

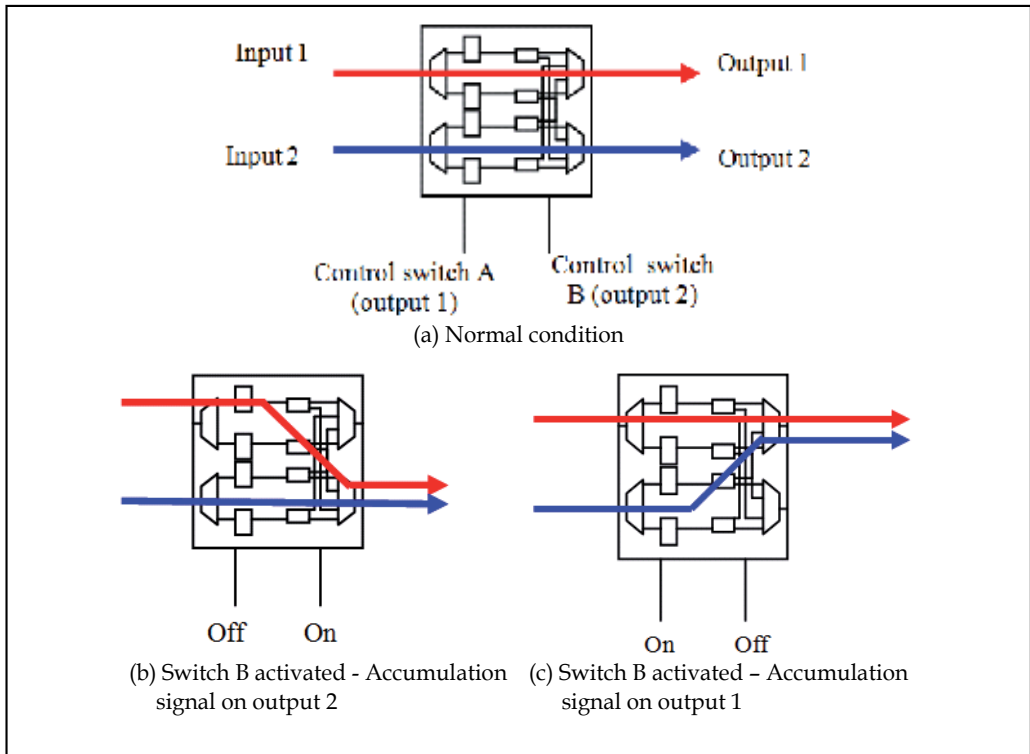


Fig. 10. OXADM optical switch works as re-configurable output port multiplexer

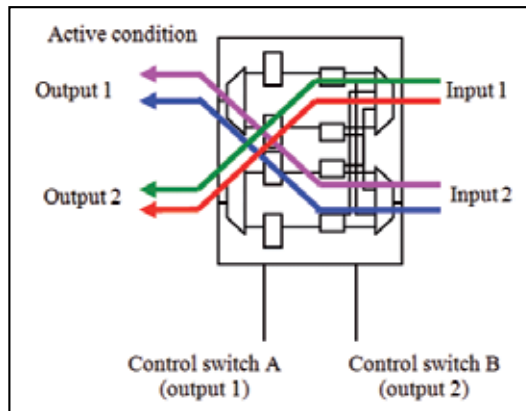


Fig. 11. OXADM optical switch works as 2x2 demultiplexer. When the switch is activated, the signal will be switched to any output port.

Switch A	Switch B	Output 1	Output 2
0	0	λ_A	λ_B
1	0	$\lambda_A + \lambda_B$	X
0	1	X	$\lambda_A + \lambda_B$

0 = Off

1 = On

 λ_A = Signal enters input 1 λ_B = Signal enters input 2

X = No signal

Table 1. The truth table of OXADM optical switch

3.3 OXADM Multifunctional Switch

OXADM can also work as any single device such as multiplexer, demultiplexer, OXC, OADM, WSC, and WRB.

1. Demultiplexer - There are two configuration of demultiplexer using OXADM, with interleaver and without interleaver. The function of interleaver is to separate the incoming signal before entering the OXADM ports (Figure 12ai). In contrast, the signal will enter the back port and has automatically routed to their respective path (Figure 12aii).
2. Multiplexer - The input signals enter the add ports of OXADM and the multiplexed signal out of the signal via output port (Figure 12b).
3. OADM - The separated wavelengths out of the interleaver have a capability to add/drop function before they are combined and exit one of the output ports of OXADM (Figure 12c).
4. WSC - Two WSC devices will be produced by OXADM. The signal will enter the input port and will be separated out through the drop port of OXADM (Figure 12d).
5. OXC - The concept is similar to OADM but the OXADM also offer the function of cross-connect the signals. The function is almost the same with OXC device (Figure 12e).
6. WRB - The new invented device that offer the management function of wavelengths. Different with circulator in which the inputs and outputs are built separately (Figure 12f).

3.4 Other Application

FTTH is a simple, inexpensive, ideal, and attractive many parties in optical communication today. A number of factors are increasing the interest among network service providers in offering the triple play services of high-speed data access, voice, and video. Most importantly, subscribers are finding a growing number of applications that drive their desire for higher bandwidth, including Internet access, interactive games, and video delivery. Since the fiber offers a vast amount of bandwidth that can be utilized for communication, one of utilizing this is signal multiplexing. Due to the large bandwidth and the associated high bit rates, the multiplexing process is beyond the capabilities of pure electronic methods and has to be implemented optically as well. As the reach of fiber is being extended to the access network it is economically attractive to share fibers between

different end-users without adding active components in the network (Menif and Fathallah, 2007).

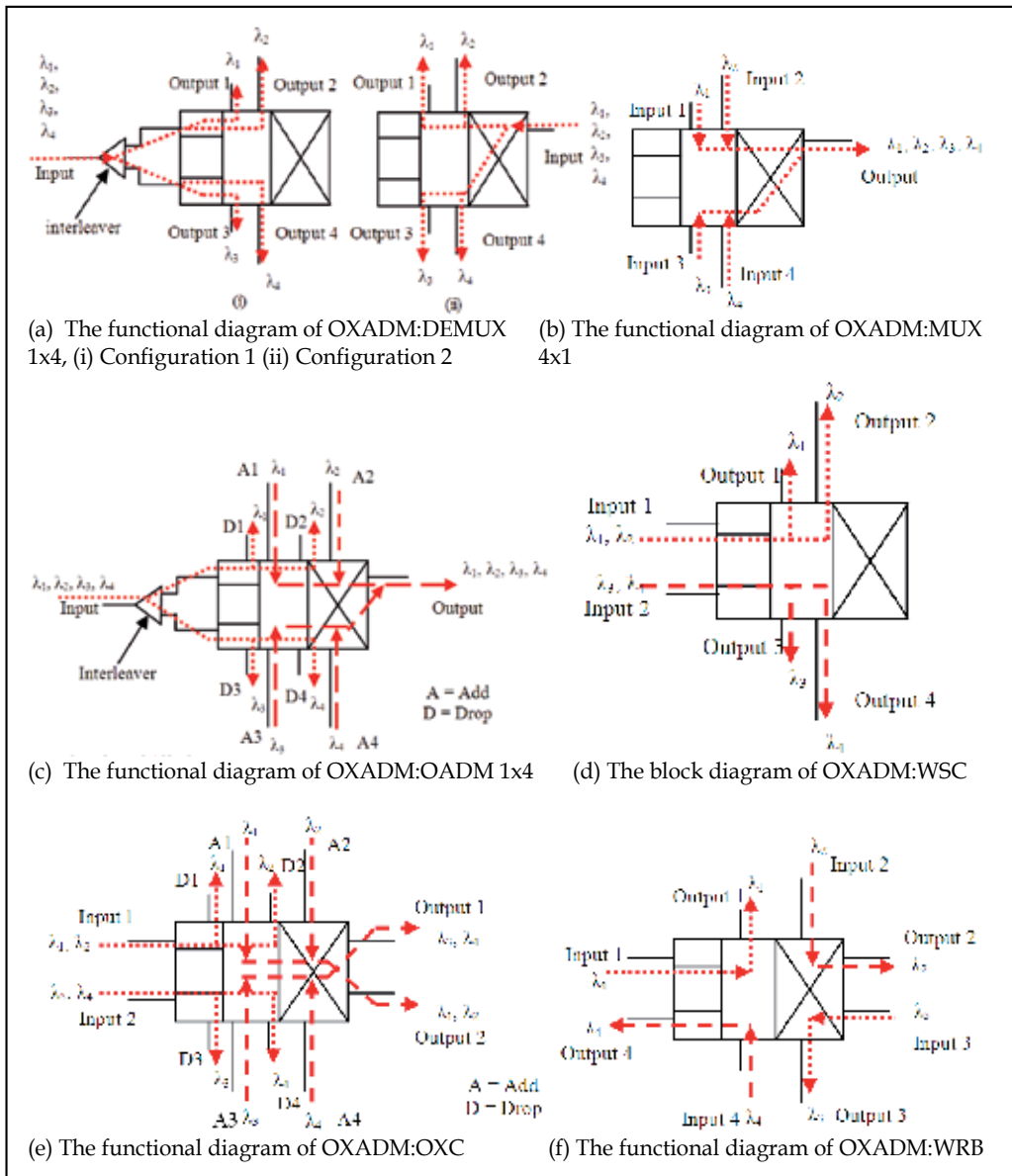


Fig. 12. OXADM multifunctional switch

It involves the full installment of fiber from central office (CO) till to customer houses which is called premises. Recently, installation of FTTH technology has started to accelerate as a strong alternative to the existing broadband access technologies based on copper pairs (Digital Subscriber Line, DSL) and coax (cable modems). This worldwide acceleration is largely due to both the considerable decrease in capital expenses (CAPEX) of introducing

FTTH connectivity and its “future proof” nature in providing ever increasing user bandwidth requirements (Yuksel et al., 2008). This technology ensures low operational expenditures (OPEX) due to all elements in used are the passive optical device with small number used. The maximum distance achievable is 20 km with gigabit of transmission rate. FTTH consists of 3 significant elements: optical line terminal (OLT), optical splitter, and optical network unit (ONU). The designed OXADM is can also used as the wavelength management in OLT architecture for excellently FTTH. It has 4 inputs terminal which represent the 4 different signal carriers to be multiplexed and exit at Output 1. Three wavelengths are used typically 1310 nm for data/voice upstream transmission and 1490 nm for the downstream data/voice transmission. Meanwhile 1550 nm is used to transmit downstream video signal.

Since the possible wavelength for communication is 1200-1600 nm, 1625-1650 nm wavelength regions is commonly considered for in-service monitoring purpose without affecting the services to other end-users. Additional wavelength 1625 nm will be adding up to the system to carries the troubleshooting signal for line status monitoring purposes. In the downstream direction (OLT to users), packets are broadcast by the OLT and extracted by their destination ONUs based on their media access control (MAC) address. In the upstream direction (users to OLT), each ONU will use a time shared channel (TDM) arbitrated by the OLT. OLT is function to aggregates Ethernet traffic from remote ONU devices through passive optical splitters. The signals then are sent to the customer premises. This can be defined in Figure 13 with the wavelength allocation highlighted.

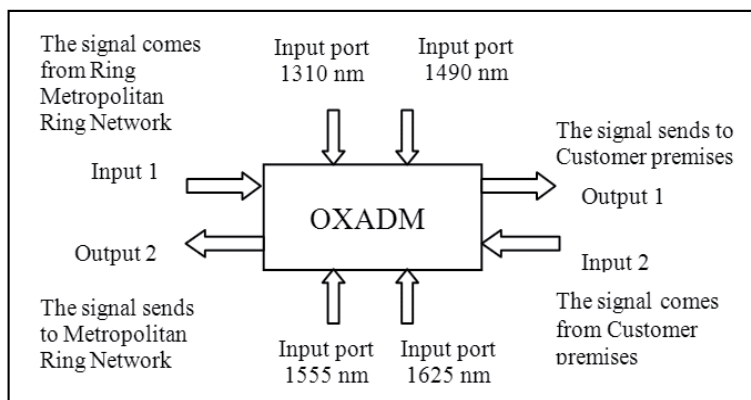


Fig. 13. OXADM function as the wavelength management element in OLT in FTTH

3.5 Device Comparison

The OXADM device will be compared with two existing switching devices; directional coupler (DC) switch and OXC. The non-selective DC switch has two states and one control element. It has fixed number of input and output port that is two. The wide bandwidth signal comes from the input port with switch to either one of output ports. It works bi-directional with symmetrical function (Palais, 2005). Figure 14 showed the mechanism of switching for directional coupler switch in normal (a) and active condition (b) & (c). The application of DC switch is to control the signal path in WDM network and optical storage; and can also perform the function of OADM in optical distributed network

OXC is the directional coupler witch but with many ports. The functional of OXC is cross-connecting between output and input port (see Figure 15) (Mutafungwa, 2001). Same with OXADM, the OXC is selective device but it does not have ‘accumulation’ feature. In contrast with OXADM, OXC works bi-directional with symmetrical function. The application of OXC is as a switching device in mesh network configuration and also in optical storage. Table 2 summarized the differences of OXADM as compared with DC and OXC.

Features	OXADM	DC	OXC
Selective	Yes	No	Yes
Accumulation	Yes	No	No
Scalability	Yes	No	Yes
Symmetrical function	No	Yes	Yes

Table 2. Comparison between OXADM, DC, and OXC

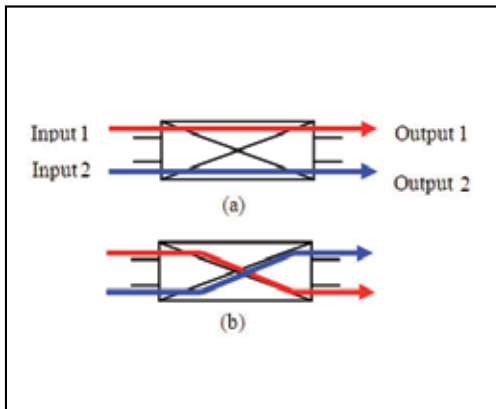


Fig. 14. Switching mechanism of DC optical switch, a) normal (b) activate

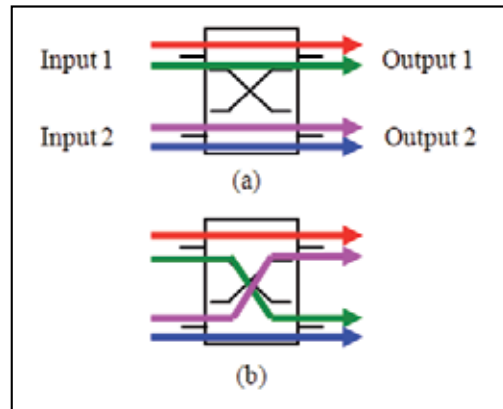


Fig. 15. Switching mechanism of OXC, a) normal (b) activate

4. Experimental Results and Discussions

4.1 Experimental Setup

Two parameters have been studied experimentally to ensure the interference of uninterested signal is minimized. Figure 16 presented the experimental set up to measure the crosstalk at two ports of OXADM and the results have been redrawn in Figure 17 and 18 respectively. The crosstalk value is bigger than 60 dB means the interested wavelength is in safety level and the transmitted data can be interpreted at any receiver end.

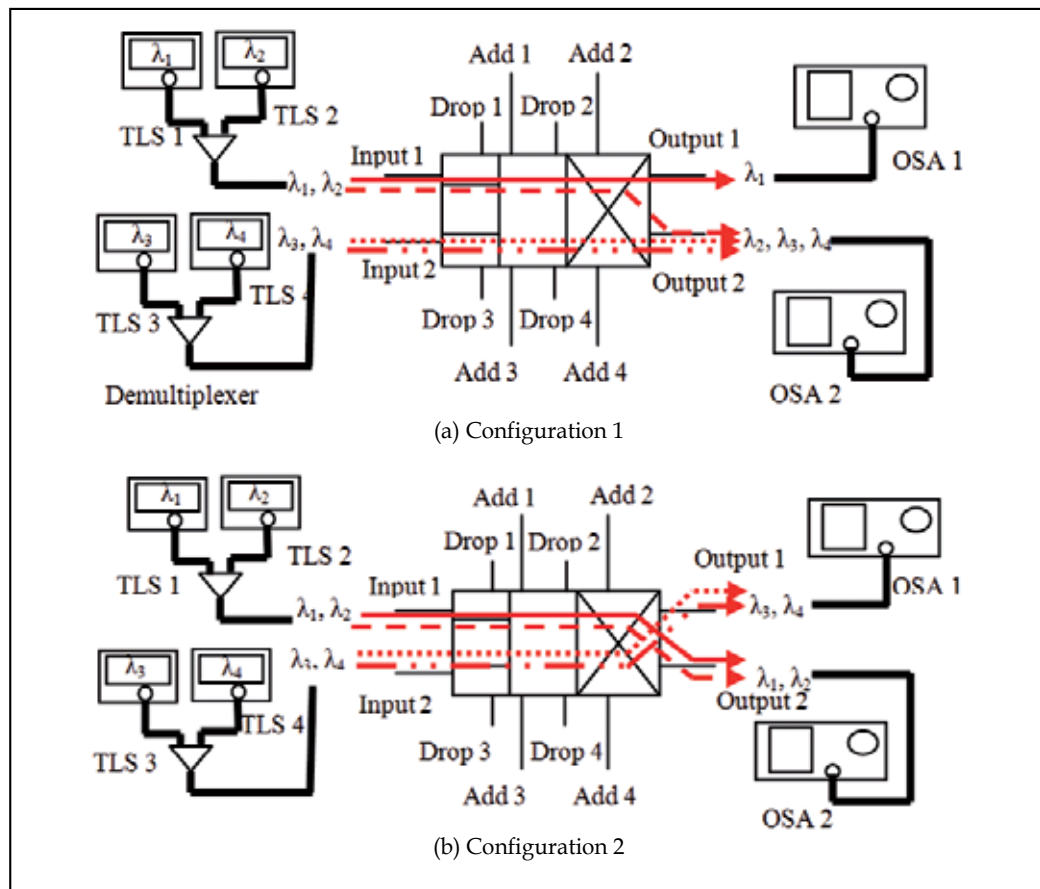


Fig. 16. Crosstalk measurement set up

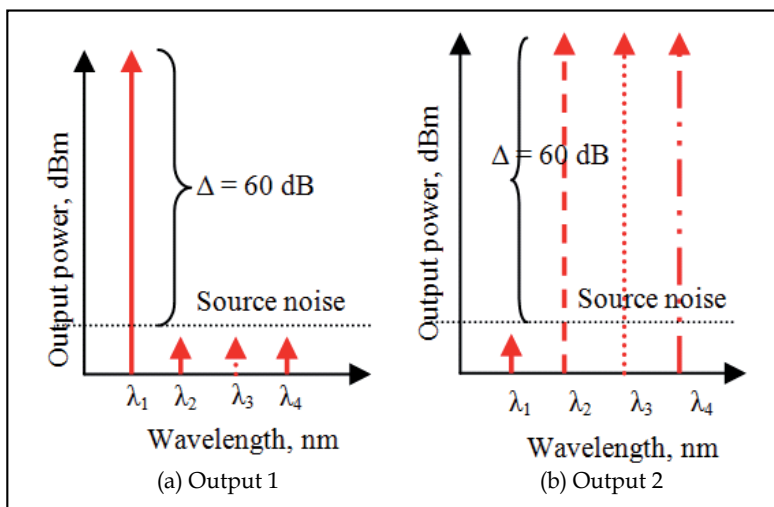


Fig. 17. Redrawing of measured output port at every port for configuration 1

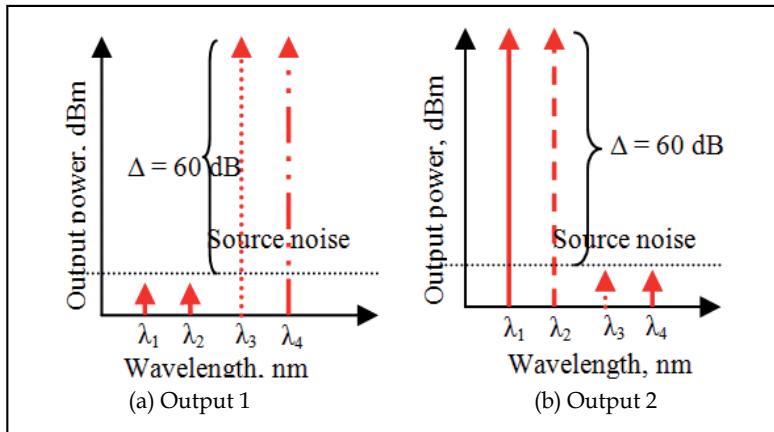


Fig. 18. Redrawing of measured output port at every port for configuration 2

The other parameter should be considered for bi-directional device is return loss. Return loss is the disturbance of uninterested signal against the direction of interested signal. This can be explained using Figure 19. The return loss is measured by using set up in Figure 20 and the result is shown in Figure 21. The return signal coming out from the input port is routing to OSA 3 using optical circulator. The value is 40 dB which is higher than minimum safety value. Both experimental have shown that the OXADM optical switch has a good and acceptable value of crosstalk and return loss.

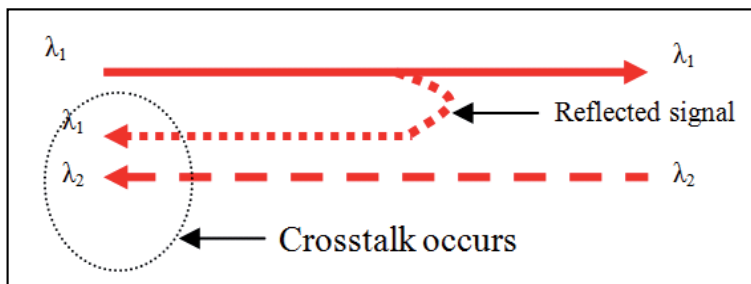


Fig. 19. Return loss or leak reflected signal which contributes to crosstalk phenomena in bi-directional device.

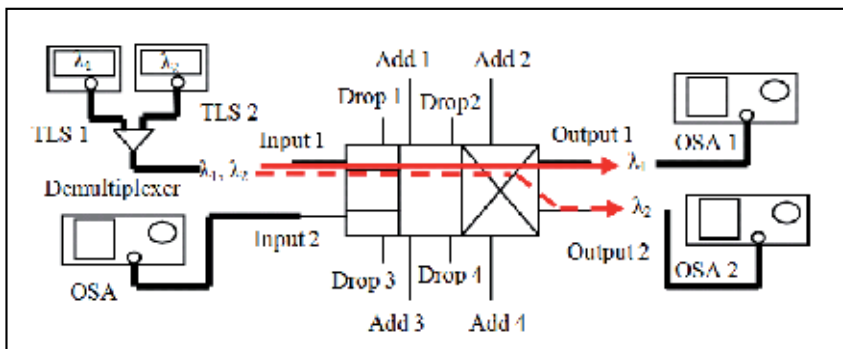


Fig. 20. Return loss measurement set up

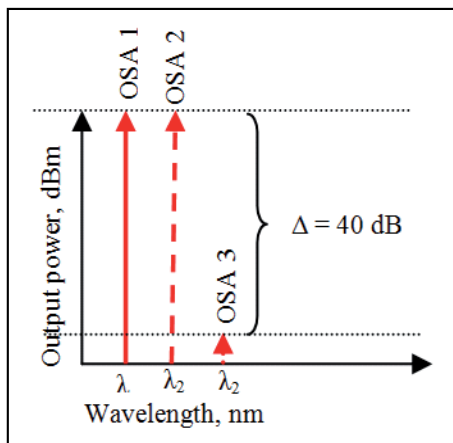


Fig. 21. Redrawing of measured output port at every port for configuration 2 for return loss measurement

4.2 Experimental Results

The OXADM device is characterized by using two tunable light sources and two optical spectrum analyzers. The designed 4-channel OXADM device is expected to have maximum operational loss of 0.6 dB for each channel when device components are in ideal condition. The maximum insertion loss when considering the component loss at every channel is 6 dB. The testing is carried out for every single function of OXADM. The function includes bypass, path exchange and accumulation. The single operating wavelength test (wavelength is 1510 nm), the results show the OSNR value for bypass function is 20 dB and path exchange is also 20 dB. Each measurement result is indicated in Figure 22 till 24.

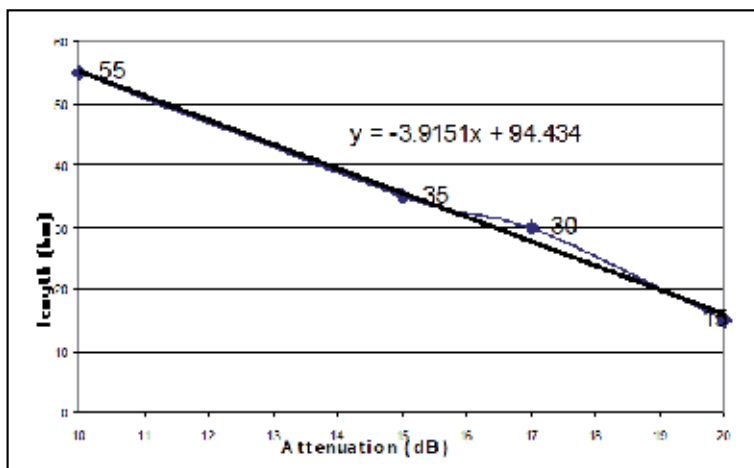


Fig. 22. The decrement of kilometers occurs by increasing the attenuation of OXADM which represent the device losses

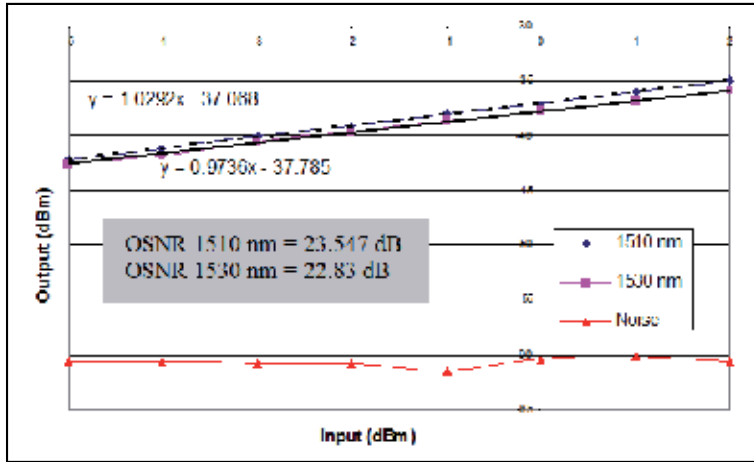


Fig. 23. The measured output power at two operating wavelength for bypass operation

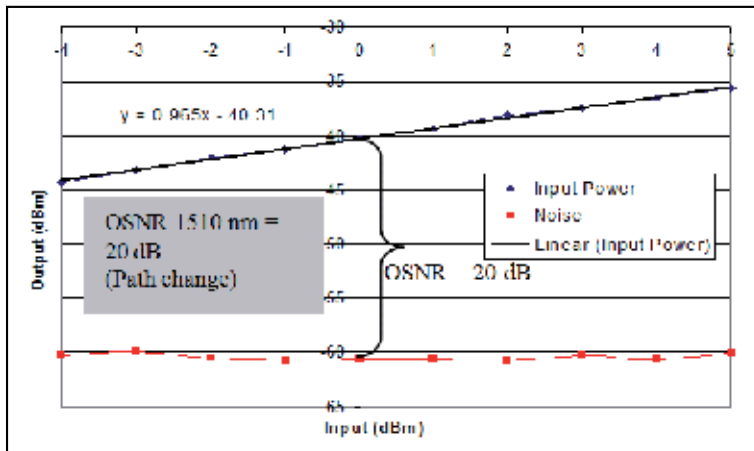


Fig. 24. The measured output power for path exchange operation

The path splitting function (accumulation function in reverse mode as Figure 10b and 10c) is also applied and the result shown in Figure 25 with OSNR > 24 dB. For backward operation as depicted in Figure 26, the OSNR values for cross-connecting function (as Figure 11) are bigger than 22 dB. This can be defined that the level of signal is 20 dB higher than noise level for all single functions of OXADM optical switch. The 20 dB reference indicates the acceptable value for the signal to noise ratio in data communication.

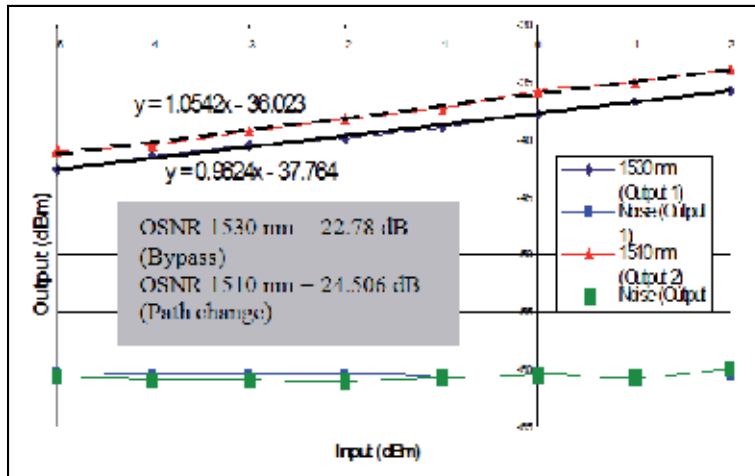


Fig. 25. The measured output power two operating wavelength for path splitting operation (accumulation function in reverse mode)

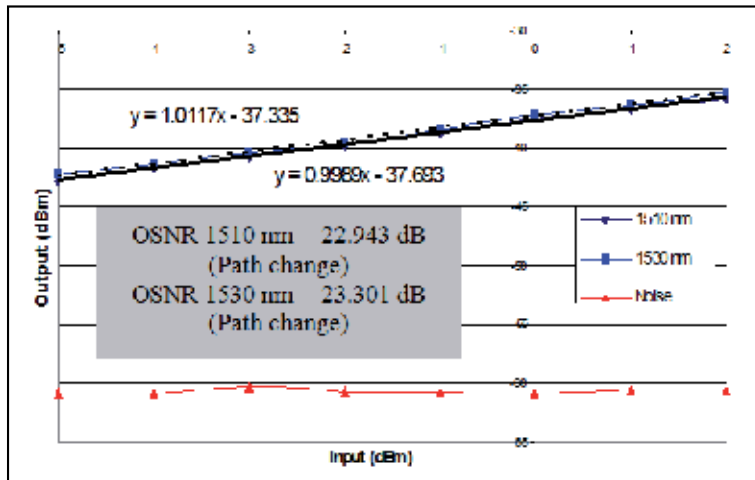


Fig. 26. The measured output power at two operating wavelengths for path exchange operation

5. The Developed Prototype

A prototype was designed and developed to enable us to evaluate the performance in an actual propagation environment as illustrated in Figure 27 and 28.

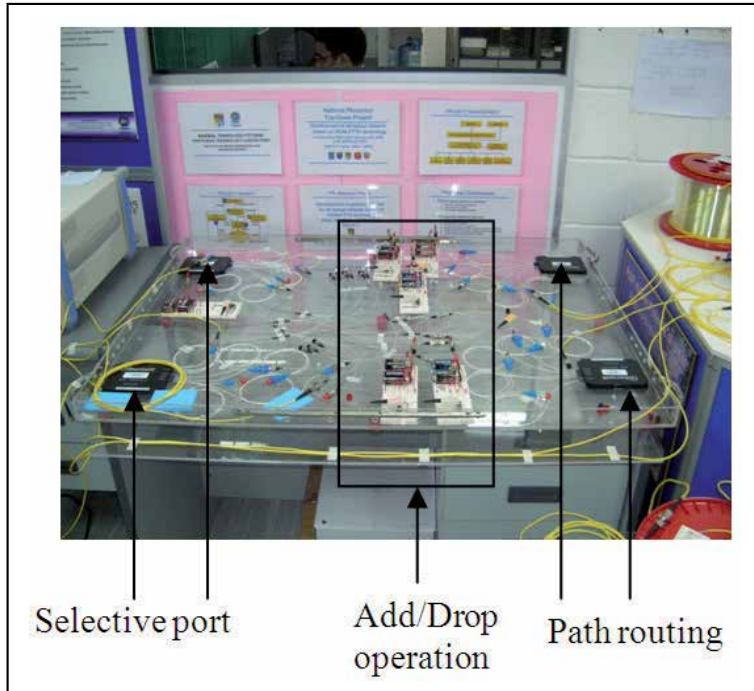


Fig. 27. Photographic view of OXADM device set up

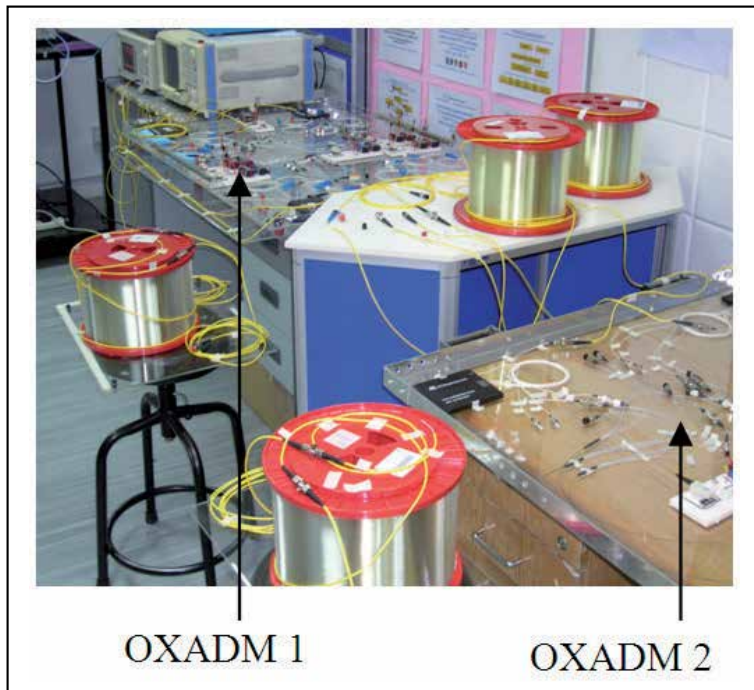


Fig. 28. Photographic view of two OXADM device prototypes set up in P2P network

6. Conclusion

A new switching device which utilizes the combined concepts of OADM and OXC operation is presented through the development of OXADM. The experimental results show the value of crosstalk and return loss is bigger than 60 dB and 40 dB respectively. In our previous results have also shown the value of insertion loss was less than 0.06 dB under ideal condition, the maximum length that can be achieved is 94 km. While when considering the loss, with the transmitter power of 0 dBm and sensitivity -22.8 dBm at a P2P configuration with safety margin, the required transmission is 71 km with OXADM. The OXADM switching mechanism has been explained and compare with other existing optical switch; DC optical switch and OXC. The OXADM optical device is particularly designed for WDM metro application. It can be used as restoration switch in FTTH network. OXADM can also work as any single device such as demultiplexer, multiplexer, OADM, OXC, WSC, and WRB. In other application, the OXADM can also provide survivability through restoration against failure by means of dedicated and shared protection that can be applied in WDM ring metropolitan network.

Acknowledgement

This project is supported by Ministry of Science, Technology and Innovation (MOSTI), Government of Malaysia, through the National Top-Down Project fund and National Science Fund (NSF). The authors would like to thank the Photonic Technology Laboratory in Institute of Micro Engineering and Nanoelectronics (IMEN), Universiti Kebangsaan Malaysia (UKM), Malaysia, for providing the facilities to conduct the experiments. The OXADM had firstly been exhibited in 19th International Invention, Innovation and Technology Exhibition (ITEX 2008), Malaysia, and was awarded with Bronze medal in telecommunication category.

7. References

- Caraglia, C.; Haffaouz, S.; Zantvoort, J.V.; Leijtens, X. & Smit, M. (2003). A Photonic Integrated Add-Drop Multiplexing for a 1.6 Tbits/s Optical Ring Network, *Proceeding Symposium IEEE/LEOS Benelux Chapter*, Enshede, pp. 69-72, 2003
- International Engineering Consortium. (2007). Optical Networks, *White Paper*, 2007, Available: http://www.iec.org/online/tutorials/opt_net/index.asp
- Keiser, G. (2003). *Optical Communications Essentials*, McGraw Hill, New York, US, ISBN: 0-07-143353-8
- Menif, M. & Fathallah, H. (2007). An Encoder/decoder Device Including a Single Reflective Element for Optical Code Division Multiple Access System. *Journal of Optical Communications*, Vol. 28, No. 3 (2007) 172-174, ISSN: 0173-4911
- Mukherjee, B. (2006). *Optical WDM Networks (Optical Networks)*, Springer, ISBN: 978-0-387-29055-3
- Mutafungwa, E. (2001). An Improved Wavelength-selective All Fiber Cross-connect Node, *Proceedings of 2001 IEEE Workshop on High Performance Switching and Routing*, pp. 93-96, ISBN: 0-7803-6711-1, Dallas, TX, USA, 2001

- Tsushima, H.; Hanatani, S.; Kanetake, T.; Fee, J.A. & Liu, S.A. (1998). Optical Cross-connect System for Survivable Optical Layer Networks, *Hitachi Review*, Vol. 47, No. 2, (1998) 85-90, ISSN: 0018-277X
- Palais, J.C. (2005). *Fiber Optic Communication*, Prentice Hall, New Jersey, ISBN: 978-0130085108
- Rahman, M.S.A.; Husin, H.; Ehsan, A.A. & Shaari, S. (2006). Analytical Modeling of Optical Cross Add and Drop Multiplexing Switch, *Proceedings of 2006 IEEE International Conference on Semiconductor Electronics*, pp. 290-293, ISSN: 0-7803-9731-2, Kuala Lumpur, Malaysia, 2006
- Ramaswami, R. (2001). All-Optical Crossconnects in the Transport Network, *Proceedings of 2001 Optical Fiber Communication Conference and Exhibit (OFC 2001)*, Vol. 3, pp. WZ1-WZ1, ISBN: 1-55752-655-9, Anaheim, CA, USA, March 2001
- Tzanakaki, A.; Wright, I. & Sian, S.S. (2002). Wavelength Routed Networks: Benefits and Design Limitations, *Proceedings of Cybernetics and Informatics (SCI2002)*, Orlando, Florida, July 2002
- Tzanakaki, A.; Zacharopoulos, I. & Tomkos, I. (2003). Optical Add/drop Multiplexers and Optical Cross-connects for Wavelength Routed Network, *Proceedings of 5th International Conference on Transparent Optical Networks (ICTON 2003)*, pp. 41-46, ISBN: 0-7803-7816-4, Warsaw, Poland, June 2003
- Yuksel, K.; Moeyaert, V.; Wuilpart, M. & Mégret, P. 2008. Optical layer monitoring in passive optical networks (PONs): a review. *Proceedings of 10th Anniversary International Conference on Transparent Optical Networks (ICTON 2008)*, pp. 92-98, ISSN: 978-1-4244-2626-3, Athens, Greece, June 2008

Adaptive Active Queue Management for TCP Friendly Rate Control (TFRC) Traffic in Heterogeneous Networks

Rahim Rahmani^a and Christer Åhlund^b

*^aMid Sweden University, ^bLuleå University of Technology
SWEDEN*

1. Introduction

Proposals to handle differentiated and guaranteed services in Internet have not provided the benefits that users and operators are expecting. Its complexity, with a large number of interconnected networks, is difficult to handle in an efficient way. This is due to the resource heterogeneity in terms of technologies and the inconsistent implementation of quality of services (QoS) in different networks. Despite several research activities in the area of QoS, Internet is still basically a best-effort network, which it is likely to stay, also in the far future. Streaming-based servers utilizing UDP for the underlying transport need to use some form of congestion control [1] to ensure the stability of Internet as well as the fairness to other flows, like those using TCP. The TCP-Friendly Rate Control (TFRC) is such a congestion control scheme appropriate for UDP. In this paper we target the question of how to optimize network and user-perceived performance in a best-effort network. In particular, we focus on the impact of end-to-end performance of the queue management scheme utilized in a wireless network.

The first of the basic assumptions in this study is that the wireless last hop constitutes the bottleneck of the end-to-end (E2E) path. TFRC is intended for applications such as streaming media, where a relatively smooth sending rate is of importance. TFRC measures loss rate by estimating the loss event ratio [2], and uses this measured rate to determine the sending rate in packets per RTT. When a bottleneck is shared with large-packet TCP flows, this has consequences for the rate achievable by TFRC. In particular a low bandwidth small-packet TFRC flow, sharing a bottleneck with high-bandwidth large-packet TCP flows, may be forced to slow down, even though the nominal rate of the TFRC application in bytes per second is less than the total rate of the TCP flows. This is fair only if the network limitation is defined by the number of packets per second, instead of bytes per second. In the TFRC protocol the small-packets are intended for flows that need to send frequent small quantities of information. It intends to support applications better, which should not have their sending rates in bytes per second decreased because of the use of small packets. This is restricted to applications, which do not send packets more often than every 10 ms. The TFRC Small-Packet (TFRC-SP) variant is motivated partly by the approach in Ref. [3], with

the argument that it is reasonable for voice over IP (VoIP) flows to assume that the network limitation is in bytes rather in packets per second, that the sending rate is the same in bytes per second as for a TCP flow with 1500 byte packets, and that the packet drop rate is the same. An application using TFRC-SP can have a fixed packet size or may vary its packet size in response to congestion.

Wireless channels suffer from bursty error losses reducing TFRC throughput, because TFRC incorrectly interprets packet loss as a sign of congestion. The maximum increase of TFRC rate, given fixed RTT, is estimated to be 0.14 packets per RTT and 0.22 packets per RTT with history discounting [4]. It takes four to eight RTTs for TFRC to halve its sending rate in the presence of persistent congestion.

Active Queue Management (AQM) intends to achieve high link utilization without introducing an excessive delay into the E2E path. For good link utilization it is necessary for queues to adapt to varying traffic load. The AQM has been subject to extensive research in the Internet community lately, and a number of methods to control the queue size have been proposed. An increase in RTT not only degrades the control performance of an AQM algorithm, but also leads to instability in the network.

The work described in this chapter examines throughput, aggressiveness, and smoothness of TFRC with varying bandwidth. A dynamic model of TFRC enables applications to address the basic feedback nature of AQM.

To demonstrate the generality of the proposed method an analytic model is described and verified by extensive simulation of different AQM.

2. Adaptive AQM (AAQM) Algorithm

AAQM is a light weight algorithm aimed at maximizing the flow of packets through the router, by continuously computing the quotient between the number of arriving and departing packets. The algorithm applies probabilistic marking of incoming packets to keep the quotient between arriving and departing packets just below 1 to minimize the queue length and maximize the throughput. Minimizing the queue length means minimizing the delay and packet loss.

2.1 Formal description

This part contains a more formal description regarding how the AAQM algorithm works. The goal of the AAQM algorithm is to keep the packet arrival rate as close to the packet departure rate as possible in order to maximize the flow of packets through the queue. The packet arrival rate is determined by the end systems sending packets and can for this reason be controlled by probabilistic marking of arriving packets. The packet departure rate is determined by the packet size and bandwidth of the outgoing link. The packet arrival rate is denoted by A and the packet departure rate is denoted by B , both of which are measured over T seconds. The utilization U of the flow of packets through the queue is defined by equation (1).

$$U = \frac{A}{B}, \quad B \neq 0 \quad (1)$$

If in the equation above, $U > 1$ the queue grows, which can result in a queue overflow and packet loss. Similarly, if, in the equation above, $U < 1$ the queue shrinks, which could result in a link underutilization and wasted bandwidth. Therefore to maximize the flow, U should be as close to 1 as possible. The required benefit is that when $U=1$ a packet arrives for each departing packet causing the link to be fully utilized, and if U is just below 1 the queue will simultaneously shrink minimizing both loss and delay. Now, if the total running time of the algorithm is divided into N non-overlapping time slots of size T seconds then the utilization of each time slot n is given by equation (2).

$$U_n = \frac{A_n}{B_n}, \quad B_n \neq 0, n = 1 \dots N \quad (2)$$

Now the packet marking probability P will be adjusted depending on the value of U during each time slot n . If $U > 1$ then P can be increased to reduce the arrival rate and thus decrease U . Likewise, if $U < 1$ then P can be decreased to increase the arrival rate and thus increase U . Equation (3) shows how the packet marking probability is adjusted.

$$P_{n+1} = P_n + f(U_n), \quad n = 1 \dots N \quad (3)$$

$$P_0 = 0$$

The function f is given by equation (4) and, depending on U , increases or decreases the packet marking probability P .

$$f(x) = \begin{cases} -P_1, & x < 1 \\ P_2, & x > 1 \end{cases} \quad (4)$$

T , P_1 and P_2 are constants that need to be determined beforehand.

2.2 Parameter Tuning

Of the variables described above only P_1 , P_2 and T are user adjustable. Two sets of recommended values for these parameters are presented in Table 1. The first row of parameters in Table 1 gives the algorithm a little better utilization at the cost of higher loss and delay. In the second row of parameters gives the algorithm a little lower utilization but improved loss and delay characteristics. The recommended parameters have been found by performing several simulations using NS[13] of the network using different parameter settings.

P_1	P_2	T
0.700	0.900	0.010
0.700	1.000	0.010

Table 1. Recommended AAQM Parameter.

When tuning the algorithm for use in a network some basic aspects must be kept in mind. A larger T will give a larger time interval over which the quotient U is computed. This will

in turn lead to a better prediction of the flow through the queue but on the downside it will also lead to a slower reaction to changes in the flow. Slow reactions to changes in the flow can lead to high delay and packet loss. When choosing P_1 and P_2 it should be kept in mind that $P_1 < P_2$ leads to low utilization, delay and packet loss. Similarly $P_1 > P_2$ gives high utilization, delay and packet loss.

3. Simulation setup

We use the methods presented in [9] for the study of the average queue time to have a well-tuned AQM

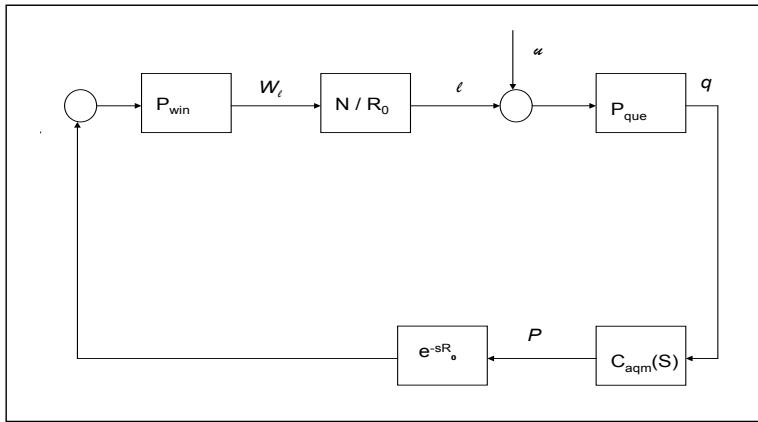


Fig. 1. Linearization of AQM with long-lived TCP traffic l and unresponsive traffic u .

with a queue averaging time less than RTTs. Figure 1 presents a block diagram of the linearized AQM feedback system, where $C_{aqm}(s)$ denotes the transfer function of the AQM controller, w_l the congestion window size in packets, R_0 the round-trip time, N the number of long-lived TCP connections, P_{win} the window size, and P_{que} the queue transfer function. The symbol l is used for long-lived TCP traffic (FTP) and u for unresponsive flows when describing how these flows impact on the queue length q , loss probability p , and arrival rates of both l and u . In this work we focus on randomly created short and long-lived flows as well as their impact on AQM. For applications needing to maintain a slowly changing sending rate, the equation-based congestion control is the most appropriate. This kind of application is the source of short-lived flows. It is assumed that they never escape the slow start phase of TCP, so their window sizes are increasing exponentially rather than linearly as during TCP's congestion-control phase. As a model of a short-lived flow we used the sending rate of TFRC [4] which is a rate based congestion control mechanism ensuring fairness when it co-exists with TCP flows [4]. Its throughput equation is a version of the throughput equation for conformant TCP Reno [4]:

$$X = \frac{B}{RTT \sqrt{\frac{2bp}{3}} + t_{RTO} \left(3 \sqrt{\frac{3bp}{8}} p(1 + 32p^2) \right)}, \quad (5)$$

where X is the transmission rate in byte/sec, as a function of the packet size B in bytes, RTT is the round-trip time in seconds, p the steady-state loss event rate, t_{RTO} is the TCP retransmission timeout value in seconds, and b the number of packets acknowledged by a single TCP acknowledgement. TFRC uses this equation to adjust the sender rate to achieve the goal of TCP friendliness.

The sender can calculate the retransmit timeout value t_{RTO} using the usual TCP algorithm:

$$t_{RTO} = SRTT + 4 * RTT_{var}, \quad (6)$$

where RTT_{var} is the variance of RTT , and $SRTT$ is the round trip time estimate. Different TCP congestion control mechanisms use different clock granularities to calculate retransmit timeout values, so it is not sure that TFRC accurately can model a typical TCP flow. Unlike TCP, TFRC does not use this value to determine whether to retransmit or not. Hence the consequences of this inaccuracy are less serious. In practice the simple empirical heuristic of $t_{RTO} = 4RTT$ works reasonably well to provide fairness with TCP [4]. For the dynamics of the model for TFRC behavior, we use the simplified and modified model presented in [10]. This model ignores the TCP timeout mechanism and is described by the nonlinear differential equation:

$$\dot{X}(t) = \frac{1}{R(t)} - \frac{X(t)}{2} \cdot \frac{X(t-R(t))}{R(t-R(t))} p(t-R(t)), \quad (7)$$

$$Q = \begin{cases} -C + \frac{N(t)}{R(t)} X(t), & q > 0 \\ \max\left\{0, -C + \frac{N(t)}{R(t)} X(t)\right\}, & q = 0 \end{cases} \quad (8)$$

where X is the average packet rate (packets/s). The RTT is calculated as $R(t) = q(t)/C + T_p$, where q is the average queue length (packets), C is the link capacity (packets/s), and T_p is the propagation delay. The parameter p is the probability of a packet mark, the $1/R(t)$ term models additive increase of the packet rate, while the $X(t)/2$ term models multiplicative decrease of the packet rates in response to a packet marking p . Eq. (8) models the bottleneck queue length using the accumulated differences between packet arrival rates $N(t)X(t)/R(t)$ and the link capacity C , where $N(t)$ is the load factor (number of traffic sessions).

For linearization of Eqs. (7) and (8) and the estimation of some of the parameters Ref. [10] defines plant dynamics of the AQM feedback control as:

$$P(s) = \frac{C^2/2N}{\left(s + \frac{2N}{R^2C}\right)\left(s + \frac{1}{R}\right)}, \quad (9)$$

In Eq. (5) $C^2/2N$ is the high-frequency plant gain, which is an important parameter in the design of AQM control schemes, since it affects the stability, transient response, and steady-state performance. The variation of the queue length depends on the input rate, output rate, and the AQM controller.

The design of adaptive AQM algorithm should be based on the mean RTT [11] since realistic network conditions have heterogeneous flows with different RTTs. The link capacity C is measured by keeping track of departed packets, and an estimate of the TFRC load N/R is inferred from measurements of the dropping probability p . The TFRC throughput $N/RC = \sqrt{p/2}$ provides a mean for estimating N/R .

For the parameterization of AQM dynamics the generalized fluid description of AQM dynamics relating instantaneous queue length q and loss probability p from [12] is used which is described as follow:

$$\begin{aligned}\chi_{am} &= f_{\theta}(\chi_{am}, q), \\ p &= g(\chi_{am}, q),\end{aligned}\tag{10}$$

Where χ_{am} denotes AQM state and f and g describe the AQM dynamic behavior. In RED [5], χ_{am} is the average queue length (RED bases its decision whether to mark a packet or not on the average queue length). In REM [6] χ_{am} is the marking probability and the link price and in BLUE [7] χ_{am} is the packet loss and link utilization history used to manage congestion.

In AAQM [8] χ_{am} is the quote between the numbers of arrived and departed packets within a timer event. This kind of event occurs at fixed, evenly spaced, time intervals, see [8]. The quote is used as the utilization factor of the queue. For tuning of the AAQM the control parameters of the AAQM (P_1, P_2, T) are linked to the network parameters N, R and C . In the absence of knowledge of these parameters we can develop an on-line estimation of the link capacity C and the TFRC load N .

The link capacity \hat{C} is estimated using the model in [12] extended with computation of the packet arrival rate. The degree of TFRC traffic utilization of the link changes depending on the competing traffic, and to smooth the TFRC capacity \hat{C} a low-pass filter (LPF) and the fluid mechanism is used:

$$\dot{\theta}_C = -K_C \theta_C + K_C \hat{C},\tag{11}$$

where θ_c denotes the estimated capacity and K_c the filter time constant. To estimate the TFRC load we use the TFRC fluid model presented by Eqs. (7) and (8) and derive the following steady-state TFRC relationship:

$$0 = \frac{1}{R} - \frac{X_0^2}{2R} P_0,\tag{12}$$

$$0 = \frac{N}{R} X_0 - C,\tag{13}$$

Where X_0 is the equilibrium congestion packet rate and P_0 is the equilibrium drop probability. From formulas (12) and (13) we can obtain $\sqrt{p_0/2} = N/RC$. In the same way as we estimated the link capacity, we can smooth the estimate of the N/RC by using the LPF:

$$\dot{\theta}_{rc}^n = -K_{rc}^n \theta_{rc}^n + K_{rc}^n \sqrt{p/2},\tag{14}$$

Where θ_{rc}^n is the smoothed estimate of the N/RC and K_{rc}^n the filter time constant. For self-tuning AQM uses the parameters estimated in Eqs. (11) and (14) described as:

$$\begin{aligned} \chi_{am} &= f\theta(\chi_{am}, q), \\ p &= g\theta(\chi_{am}, q), \end{aligned} \tag{15}$$

Where f_θ and g_θ show the explicit dependency of AQM dynamics using the estimate variables $\theta = (\theta_C, \theta_{rc}^n)$.

When the 802.11 MAC layer approaches saturation, contention delays induced by deferred count-down timers, an increased contention window and retransmissions affecting the performance of TFRC and TCP [16]. TFRC is unaware of the MAC layer congestion, rendering in that the TFRC sender may overestimate the maximum sending rate. This congests the MAC layer, and the wireless network consequently reaches a sub-optimal stable state with respect to the throughput and round-trip time [17][18]. Because of the lack of interaction between TFRC and the 802.11 MAC layer, a Rate Estimator (RE) is added to TFRC [17]. The RE approximates the saturation capacity of the MAC layer, and by limiting the sending rate, MAC layer congestion can be avoided.

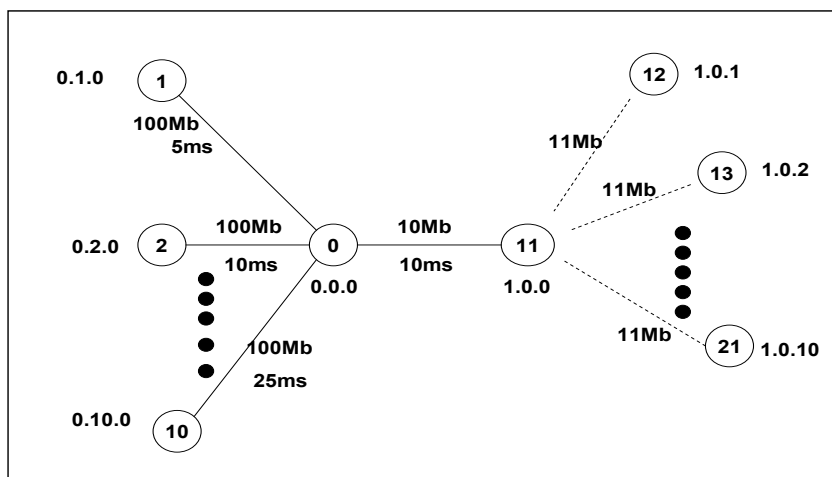


Fig. 2. Configuration of the simulated network

4. Simulations

The simulation results presented obtained using the NS-2 simulation tool [13]. Figure 2 depicts the topology used. The solid lines symbolize wired links and the dashed lines wireless links. Nodes numbered 1-10 are fixed; those numbered 12 - 21 are mobile, and the node numbered 11 is the 802.11b base station (infrastructure mode). The link between the nodes number 0 and 11 represents the virtual bottleneck link running the AQM algorithms. An access point has two interfaces an 802.11 wireless interface to transmit/receive frames on the air and a wired interface. The disparity in channel capacity of these two interfaces makes

the access point a significant potential bottleneck link. The virtual bottleneck represents an access point.

Data are originating at the nodes numbered 1 - 10 and received by the nodes numbered 12 - 21. Each link carries both a TFRC and a TCP flow using a Pareto traffic generator (to generate aggregate traffic that exhibits a long-range dependency). The traffic generators start randomly after one second of the simulation to avoid a deterministic behavior and lasts for 100 seconds. Each simulation was run 30 times with different seeds for the random number generator. TCP-SACK [14] is used with Selective Acknowledgments (SACK), allowing a receiver to acknowledge out-of-order segments selectively. The TFRC flows are modeled as short-lived small packets web flows, and the TCP flows as a mix of short-lived flows and long-lived FTP flows. The sources of the short-lived web flows are modeled according to Ref. [15].

In table 2 the different parameters settings used are listed. The TFRC and TCP timer granularity used, i.e. the tick value, is set to 500 ms, and the TCP minimum retransmission timeout to 1 s. The throughput at the bottleneck link, the queue size (in packets), and the drop probability are used for performance evaluation throughout the simulations.

Queues	Queue sizes (packets)	Numbers of web sessions
BLUE	5	400
Drop-Tail	10	800
RED	50	1600
REM	100	
AAQM		

Table 2. List of parameter settings used in different scenarios and packetsize 14 bytes.

The parameter settings used in the AQM algorithms are shown in Tab. III. For Blue the values were obtained from Ref. [7], for RED from Ref. [5], for REM from Ref. [6], and for AAQM from Ref. [8].

BLUE	freeze_time=10 ms	D1=0.001	d2=0.0002	
RED	Wq=0.002	minth=20% of the queue size	maxth=80% of the queue size	maxp=1
REM	Gamma=1	Phi=1.001	Bo=20	Updtime=0.0
AAQM	P1=0.700	P2=1.000	T=0.010	

Table 3. Parameter setting for the simulated aqm

5. Performance evaluation

To achieve satisfactory control performance, the design goals of AQM algorithms are responsiveness and stability. Bursty sources are used for the performance evaluation with varying queue sizes managed by the AQM algorithms. The bursts generated require an AQM algorithm to efficiently and quickly adapt to the current situation to maintain a high overall throughput and to avoid dropping more packets than necessary. As a result the drop rate and throughput are compared for the different algorithms.

Figures 3 and 4 depict the results for the drop rate and overall throughput respectively. Four queue sizes are used 5, 10, 50 and 100 packets. The curves are plotted using a 95% confidence interval

Figures 3 shows that Drop-Tail (DT) exhibits a high drop rate. This is due to the fact that all packets are dropped when the queue is full so it affects all flows. All sources will then decrease its sending rate at approximately the same time. This also means that all sources will increase the sending rate about the same time rendering in full queues once more and this will create oscillation. and beyond a high drop rate low throughput is also exhibited.

Figures 3(a) and 3(b) show AAQM and RED have similar drop rate but in figures 3(c) and 3(d) RED has higher drop rate than AAQM.

The instantaneous queue length of RED is controlled in range of \min_{th} and \max_{th} . In order to be effective a RED queue must be configured with a sufficient amount of buffer space to accommodate an applied load greater than the link capacity from the instant in time when the applied load decreases at the bottleneck link in response to congestion notification. RED must ensure that congestion notification is given at a rate which sufficiently suppresses the transmitting sources without underutilizing the link. When a large number of TCP flows are active the aggregate traffic generated is extremely bursty. Bursty traffic often defeats the active queue management techniques used by RED since queue length grow and shrink rapidly before RED can react. Exactly that happens in figures 3(c), 3(d), 4(c) and 4(d).

On the other hand the queues controlled by REM and BLUE are often empty. When the link capacity is low AAQM regulates the queue length, where REM and BLUE oscillate between an empty buffer and its limit of queue size. As a result REM and BLUE show poor performance under a wide range of traffic environments.

Drop-Tail and REM must be configured with a sufficient amount of buffer space in order to accommodate an applied load greater than the link capacity from the instant that congestion is detected, using the queue length trigger, to the instant when the applied load decreases in response to congestion notification.

In general, the bias against bursty traffic and the tendency towards global synchronization can be eliminated by maintaining a stable packet loss over time. The steady-state control performance of each AQM algorithm was evaluated and the packet loss rate studied at three different traffic loads.

As shown in figure 3 and figure 4 the flow dynamics are severely oscillating and it takes a long time to stabilize to a steady-state. The AAQM controller is able to compensate the oscillatory of the flow dynamics and given satisfactory control performance such as a fast and stable control dynamics. AAQM show the most robust steady-state control performance, independent of traffic loads, in terms of relatively small mean value of the packet loss rate as well as its variance.

In the experiments we allowed the AQM schemes to converge to steady state when there were 400 web sessions, then we increased the web session number to 800 and 1600 to study

the performance of the AQM schemes when the number of short flows increases. From figures 4(a) and 4(b) it can be seen that AAQM has 1% better throughput than RED when the number of sessions is 1600, and much higher throughput than BLUE, REM and DropTail. In figure 4(c) AAQM has 3% better throughput than RED, and from figure 4(d), it can be seen that AAQM has 36% better throughput than RED.

The results from Figures 3 and 4 show that AAQM has the best responsiveness to congestion as well as the most robust steady-state control.

6. Related work

The work presented in [9] studies the effects of unresponsive flows on AQM. It shows that the queue averaging time is a result of a trade-off between AQM responsiveness and the robustness of the uncontrolled flows. The average queue time results in a smooth or stable congestion feedback, which introduces jitter in the queuing delay due to variation in the unresponsive flows. Three types of flow types were considered: short-lived TCP, Markov on-off UDP, and traffic with long-range dependencies (e.g. ftp). Our work instead focuses on short-lived flows and uses a more realistic model for VoIP traffic by using TFRC-SP. Also [9] does not study the impact of unresponsive flows on the AQM algorithms, while we do. Our focus is on the responsiveness of UDP flows with co-existent TCP flows.

The work presented in [19] surveys two adaptive and proactive AQM algorithms using a classical proportional-integral-derivative feedback control to achieve stability and responsiveness. The TCP flows are modeled as long-lived FTP flows. In our work the flows are modeled as the mix of long-lived flows and short-lived flows to fulfill the design goal of an adaptive AQM to interact with a realistic flow composition.

In reference [22] the authors argue in favor of rate-based AQM for high-speed links. Also in that work a proportional-integral controller for the AQM scheme is used. The design goal was to match the aggregate rate of TCP flows to the available capacity while minimizing the queue size. We study the integration of TFRC-SP and UDP in co-existence with TCP in heterogeneous networks.

The work presented in [23] uses a token-bucket model as a virtual queue (VQ) with a link capacity less than the actual link capacity. If a packet arrives, it is placed in a queue in the VQ if there is space available. Otherwise the packet is dropped. Accordingly the algorithm is able to react at an earlier stage, even before the queue grows, making it very sensitive to the traffic load and round trip time. However, the utility functions are much different from ours due to the AQM control parameters. AAQM uses control law and link utilization in order to manage congestion. The action of the control law in AAQM is to mark incoming packets in order to maintain the quotient between arriving and departing packets as close to one as possible.

The study in reference [24] focused just on the RED and the parameter setting of RED was based on heuristics. It also studied RED against disturbances on the wireless access network. Only one type of flow types was considered: short-lived TCP. We study UDP in co-existence with TCP and their impact on DT, RED, REM, BLUE and AAQM.

The work presented in [25] by using proxy AQM between access point for WLAN and wired network. The proxy reduces the overhead of the access point by implementing the AQM functionality at the gateway. In the work they extended the RED/ARED scheme to a

proxy mode by calculating the average queue length and updating p_{ma} of ARED. They measured only a number of TCP flows.

In reference [26] a channel-aware AQM scheme is presented. This new approach provides congestion signals for flow control not only based on the queue length but also the channel condition and the transmission bit rate. For the performance evaluation of the new AQM in multi-rate WLAN the bit rate of the wireless node in manuals fixed at different levels (in sequence of 2M, 1M, 11M, and 5.5 Mbps). Two TCP flows were considered. The main idea in the work was to design an AQM for flow control in multi-rate WLAN.

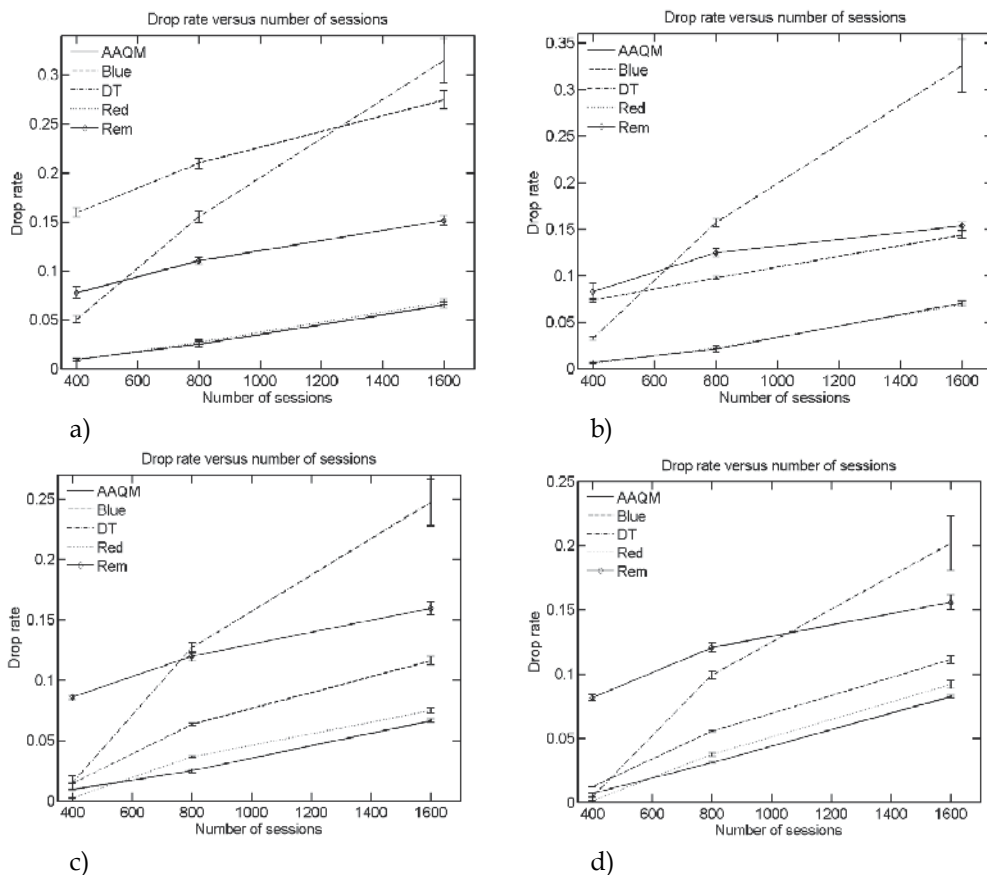


Fig. 3. Packet loss rate for a packet size of 14 bytes; (a) queue size 5 packets, (b) queue size 10 packets, (c) queue size 50 packets, (d) queue size 100 packets.

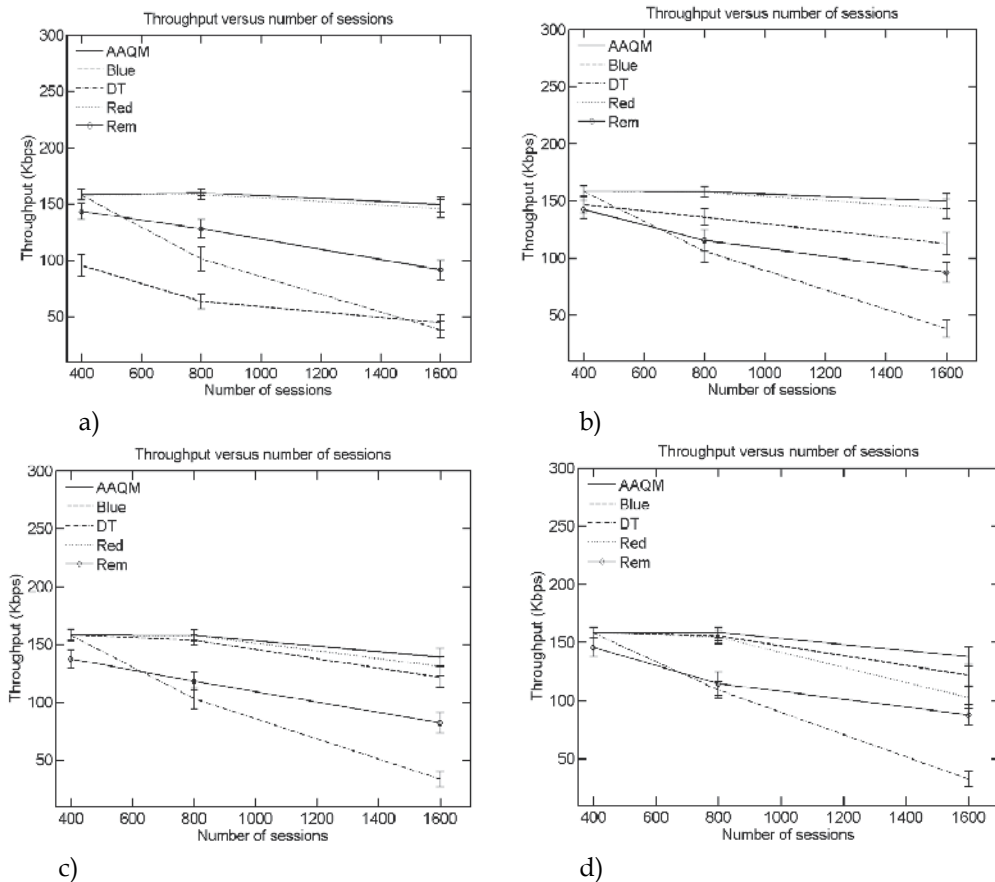


Fig. 4. Throughput of the link for a packet size of 14 bytes; (a) queue size 5 packets, (b) queue size 10 packets, (c) queue size 50 packets, (d) queue size 100 packets.

7. Conclusions and future work

The present work studies AQM algorithms for competing small-packet TFRC flows and TCP flows in heterogeneous networks. We investigate the effects caused by unresponsive flows using TFRC on the AQM performance that is measured using responsiveness and stability. Through simulations it is shown that with suitable design of the AQM scheme the end-to-end performance can be maintained for TFRC flows consisting of small packets. It is shown that the control performance of Drop-tail, RED, and BLUE are very sensitive to the traffic load and round trip time. With REM the links suffer in utilization as the buffer size increases. In particular AAQM shows a stable queue length with low and smooth packet loss rates independent of the traffic load.

Future works will particularly investigate the integration of the Guaranteed TFRC (GTFRC) [20] with the DCCP protocol [21] and co-existence of DCCP with the Stream Control Transmission Protocol (SCTP). The impact of these protocols on the AQM performance and QoS will be studied in heterogeneous networks. An additionally study will be focused on optimization of the buffer space requirements.

8. References

- [1] S. Floyd, "Congestion Control Principles" RFC2914, September 2000.
- [2] M. Handley, J. Padhye, S. Floyd, and J. Widmer, "TCP Friendly Rate Control (TFRC): Protocol Specification". RFC3448, January 2003.
- [3] RFC 3714.
- [4] S. Floyd, M. Handley, J. Padhye, and J. Widmer. "Equation-based congestion control for unicast application". In proc. of ACM SIGCOMM'00, Aug. 2000.
- [5] Sally Floyd and Van Jacobson, "Random Early Detection Gateways for Congestion Avoidance", IEEE/ACM Transactions on Networking, vol. 1, Number 4, August 1993.
- [6] Sanjeewa Athuraliya, "A Note on Parameter Values of REM with Reno-like Algorithms", Networking Laboratory, Caltech, March 2002.
- [7] Wu-chang Feng, Dilip Kandlur, Debanjan Saha and Kang Shin, "BLUE: A New Class of Active Queue Management Algorithms", Department of EECS, University of Michigan, Ann Arbor, MI 48105.
- [8] R. Rahmani, "Adaptive Active Queue Management in Heterogeneous Networks" in 26th ITI 2004, Croatia, June 2004.
- [9] C.V. Hollot, Y. Liu, V. Misra, D. Towsley "Unresponsive flows and AQM Performance", In Proceedings IEEE, 2003.
- [10] V. Misra, W. Gong, and D. Towsley, "Fluid based analysis of a network of AQM routers supporting TCP flows with an application to RED," in Proceedings of ACM/SIGCOMM, 2000.
- [11] C. Hollot, V. Misra, D. Towsley, and Gong, "Analysis and design of controllers for AQM routers supporting TCP flows," IEEE Transactions on Automatic Control, vol. 47, no. 6, 2002.
- [12] H. Zhang, C. Hollot, D. Towsley, and V. Misra, "A self-tuning structure for adaptation in TCP/AQM networks," Department of computer sciences, UMass, Amherst, Tech. Rep., July 2002.
- [13] The NS-2 Simulator available at <http://www.isi.edu/nsnam/ns/>.
- [14] RFC 2018.
- [15] Anja Feldmann, Anna C., P. Huang and W. Willinger "Dynamics of IP traffic: A study of the role of variability and the impact of control" sigcomm99, pub acm, pages 301-313, <http://www.acm.org/sigcomm/sigcomm99/papers/session8-3.html>.
- [16] Saikat Ray, Jeffrey Carruthers, and David Starobinski, "RTS/CTS-induced Congestion in Ad-Hoc Wireless LANs" in Proceedings of IEEE WCNC, Mar. 2003, pp. 1516-1521.
- [17] Mingzhe Li, Choong-Soo Lee, Emmanuel Agu, Mark Claypool, and Robert Kinicki, "Performance Enhancement of TFRC in Wireless Ad Hoc Networks, Distributed Multimedia Systems (DMS)", September 2004.
- [18] henghua Fu, Xiaoqiao Meng, and Songwu Lu, "A Transport Protocol For Supporting Multimedia Streaming in Mobile Ad Hoc Networks", IEEE JSAC, December 2004.
- [19] S. Ryu, C. Rump, C. Qiao "Advances in Active Queue Management (AQM) Based TCP Congestion Control" Telecommunication Systems Journal Kluwer publisher 25:3,4, p 317-351, 2004.

- [20] E. Lochin, L. Dairaine, G. Jourjon "gTFRC: a QoS-aware congestion control algorithm", The 5th International Conference on Networking (ICN'2006) Mauritius - April, 2006.
- [21] S. Floyd, E. Kohler, J. Padhye : " Profile for DCCP Congestion Control ID 3: TFRC Congestion Control ", RFC 4342, IETF (2006).
- [22] J. Aweya, M. Ouellette, D. Y. Montuno, K. Felske, "Rate-based proportional-integral control scheme for active queue management" International Journal of Network Management John Wiley & Sons Publisher 16: p 203-231, 2006.
- [23] S. Kunniyur, R. Srikant, " An Adaptive Queue(AVQ) Algorithm for Active Queue Management" ACM Transactions on Networking Vol.12 No.2 April 2004.
- [24] F. Zheng, J. Nelson, " An H_∞ approach to congestion control design for AQM routers supporting TCP flows in wireless access networks" Computer Networks vol. 51 p 1684-1704, 2007.
- [25] S. Yi, M. Kappes, S. Grag, X. Deng, G. Kesidis, C. R. Das, " Proxy-RED: An AQM Scheme for Wireless Local Area Networks" 0-7803-8784-8/\$20.00 2004, IEEE.
- [26] Y. Xue, H. V. Nguyen, K. Nahrstedt " CA-AQM: ChannelAware Active Queue Management for wireless Networks" ICC 2007, IEEE.

Queues with session arrivals as models for optimizing the traffic control in telecommunication networks

Sergey Dudin ¹ and Moon Ho Lee ²

¹*Belarusian State University*

Belarus

²*Chonbuk National University*

Korea

1. Introduction

Many problems in routing, scheduling, flow control, resources allocation and capacity management in telecommunication, production, and transportation networks can be solved with help of queueing theory. Typically, a user of a network generates not a single item (packet, job, pallet, etc) but a whole bunch of items and service of this user assumes sequential transmission of all these items. This is why the batch arrivals are often assumed in analysis of queueing systems. It is usually assumed that, at a batch arrival epoch, all requests of this batch arrive into the system simultaneously. However, the typical feature of many nowadays networks is that requests arrive in batch, while arrival of requests belonging to a batch is not instantaneous but is distributed in time. We call such batches as sessions. The first request of a session arrives at the session arrival epoch while the rest of requests arrive one by one in random intervals. The session size is random and it may be not known a priori at the session arrival epoch. Such a situation is typical, e.g., in modeling transmission of video and multimedia information. This situation is also typical in IP networks, e.g., in World Wide Web with Hypertext Transfer Protocol (HTTP) where a session can be interpreted as a HTTP connection and a request as a HTTP request. This situation is also discussed in literature with respect to the modeling the Scheme of Alternative Packet Overflow Routing (*SAPOR*) in *IP* networks.

In this scheme, the session is called as *flow* and represents a set of packets that should be sequentially routed in the same channel. When a packet arrives, it is determined (e.g. by means of *IP* address) if the packet is a part of a flow, already tracked. If the packet belongs to an existing flow, the packet is marked for transmission. If the flow is not yet tracked and the channel capacity is still available, the packet is admitted into the system and flow count is increased. Otherwise the flow is routed on the overflow link (or is dropped at all) and the packet is rejected in the considered channel. Tracked flows are cleared after they are finished. Clearing of an inactive flow is done if no more packets belonging to this flow are received within a certain time interval. Tracking and clearing of flows is performed by

means of a token mechanism. The number of tokens, which defines the maximal number of flows that can be admitted into the system simultaneously, is very important control parameter. If this number is small, the channel may be underutilized. If this number is too large, the channel may become congested. Average delivering time and jitter may increase essentially and Grade of Service becomes bad. So, the problem of defining the optimal number of tokens is of practical importance and non-trivial. In (Kist et al., 2005), performance measures of the *SAPOR* scheme of routing in *IP* networks are evaluated by means of computer simulation.

Analogous situation also naturally arises in modeling information retrieving in relational data bases where, besides the CPU and disc memory, some additional "threads" or "connections" should be provided to start the user's application processing. In this interpretation, session means application while requests are queries to be processed within this application and tokens are threads or connections.

In the paper (Lee et al., 2007), the Markovian queueing model with a finite buffer that suits for analytical performance evaluation and capacity planning of the *SAPOR* routing scheme as well as for modelling the other real-world systems with time distributed arrival of requests in a session is considered. To the best of our knowledge, such kind of queueing models was not considered and investigated in literature previously. In (Lee et al., 2007), the problem of the system throughput maximization subject to restriction of the loss probability for requests from accepted sessions is solved. In the paper (Kim et al., 2009), the analysis given in (Lee et al., 2007) is extended in three directions. Instead of the stationary Poisson arrival process of sessions, the *Markov Arrival Process (MAP)* is considered. It allows catching the effect of correlation of flow of sessions. The presented numerical results show that the correlation has profound effect on the system performance measures. The second direction is consideration of the *Phase type (PH)* service process instead of an exponential service time distribution assumed in (Lee et al., 2007). Because *PH* type distributions are suitable for fitting an arbitrary distribution, this allows to take into account the service time distribution and variance of this time in particular, carefully. The third direction of extension is the following one. It is assumed in (Lee et al., 2007), that the loss (due to a buffer overflow) of the request from the accepted session never causes loss of a whole session itself. More realistic assumption in some situations is that the session might be lost (terminates connection ahead of schedule). E.g., it can happen if the percentage of lost voice or video packets (and quality of speech or movie) becomes unacceptable for the user. To take such a possibility into account in some extent, it is assumed in this paper that the loss of a request from the admitted session, with fixed probability, leads to the loss of a session to which this request belongs. Influence of this probability is numerically investigated in the paper (Kim et al., 2009).

In the present paper, the modification of model from (Kim et al., 2009) to the case of an infinite buffer is under study. In contrast to the model with a finite buffer considered in (Kim et al., 2009) where the problem of the throughput maximization was solved under constraint on the probability of the loss of a request from an accepted session, here we do not have such a loss. So, the problem of the throughput maximization is solved under constraint on the average sojourn time of requests from the accepted sessions. In section 2, the mathematical model is described in detail. Stability condition, which is not required in the model (Kim et al., 2009) with a finite state space but is very important in the model with an infinite buffer space, is derived in a simple form. This condition creates an additional

constraint in maximization problem. The steady state joint distribution of the number of sessions and requests in the system is analyzed by means of the matrix analytical technique and expressions for the main performance measures of the system are given in section 3. Section 4 is devoted to consideration of the request and the session sojourn time distribution. Section 5 contains numerical illustrations and their short discussion and section 6 concludes the paper.

2. Mathematical model

We consider a single server queueing system with a buffer of an infinite capacity. The requests arrive to the system in sessions. Sessions arrive according to the Markov Arrival Process. Sessions arrival in the *MAP* is directed by an irreducible continuous time Markov chain $\nu_t, t \geq 0$, with the finite state space $\{0, \dots, W\}$. The sojourn time of the Markov chain $\nu_t, t \geq 0$, in the state ν has an exponential distribution with the parameter $\lambda_\nu, \nu = \overline{0, W}$. After this sojourn time expires, with probability $p_k(\nu, \nu')$, the process $\nu_t, t \geq 0$, transits to the state ν' , and k sessions, $k = 0, 1$, arrive into the system. The intensities of jumps from one state into another, which are accompanied by an arrival of k sessions, are combined into the matrices $D_k, k = 0, 1$, of size $(W + 1) \times (W + 1)$. The matrix generating function of these matrices is $D(z) = D_0 + D_1 z, |z| \leq 1$. The matrix $D(1)$ is the infinitesimal generator of the process $\nu_t, t \geq 0$. The stationary distribution vector δ of this process satisfies the equations $\delta D(1) = \mathbf{0}, \delta \mathbf{e} = 1$. Here and in the sequel $\mathbf{0}$ is the zero row vector and \mathbf{e} is the column vector of appropriate size consisting of 1's. In case the dimensionality of the vector is not clear from the context, it is indicated as a lower index, e.g. $\mathbf{e}_{\overline{W}}$ denotes the unit column vector of dimensionality $\overline{W} = W + 1$.

The average intensity λ (fundamental rate) of the *MAP* is defined as

$$\lambda = \delta D_1 \mathbf{e}.$$

The variance v of intervals between session arrivals is calculated as

$$v = 2\lambda^{-1} \delta (-D_0)^{-1} \mathbf{e} - \lambda^{-2},$$

the squared coefficient c_{var} of variation is calculated by

$$c_{var} = 2\lambda \delta (-D_0)^{-1} \mathbf{e} - 1,$$

while the correlation coefficient c_{cor} of intervals between successive group arrivals is given by

$$c_{cor} = (\lambda^{-1} \delta (-D_0)^{-1} D_1 (-D_0)^{-1} \mathbf{e} - \lambda^{-2}) / v.$$

For more information about the *MAP*, its special cases and properties and related research see (Fisher & Meier-Hellstern, 1993), (Lucantoni, 1991) and the survey paper by S.

Chakravarthy (Chakravarthy, 2001). Usefulness of the *MAP* in modeling telecommunication systems is mentioned in (Heyman & Lucantoni, 2003), (Klemm et al., 2003). Note, that the problem of constructing the *MAP*, which fits well a real arrival process, is not very simple. However, this problem has practical importance and is intensively solving. For relevant references and the fitting algorithms see, e.g., (Heyman & Lucantoni, 2003), (Klemm et al., 2003), (Asmussen et al., 1996) and (Panchenko & Buchholz, 2007).

Following (Kist et al., 2005), we assume that admission of sessions (they are called *flows* in (Kist et al., 2005) and called *threads, connections, sessions, exchanges, windows*, etc. in different real-world applications) is restricted by means of *tokens*. The total number of available tokens is assumed to be K , $K \geq 1$. Further we consider the number K as a control parameter and solve the corresponding optimization problem.

If there is no token available at a session arrival epoch the session is rejected. It leaves the system forever. If the number of available tokens at the session arrival epoch is positive this session is admitted into the system and the number of available tokens decreases by one. We assume that one request of a session arrives at the session arrival epoch and if it meets free server, it occupies the server and is processed. If the server is busy, the request moves to the buffer and later it is picked up for the service according to the First Come - First Served discipline.

After admission of the session, the next request of this session can arrive into the system in an exponentially distributed with the parameter γ time. The number of requests in the session has the geometrical distribution with the parameter θ , $0 < \theta < 1$, i.e., probability that the session consists of k requests is equal to $\theta^{k-1}(1-\theta)$, $k \geq 1$. The average size of the session is equal to $(1-\theta)^{-1}$.

If the exponentially distributed with the parameter γ time since arrival of the previous request of a session expires and new request does not arrive, it means that the arrival of the session is finished. The token, which was obtained by this session upon arrival, is returned to the pool of available tokens. The requests of this session, which stay in the system at the epoch of returning the token, must be completely processed by the system. When the last request is served, the sojourn time of the session in the system is considered finished.

The service time of a request is assumed having *PH* distribution. It means the following. Request's service time is governed by the directing process η_t , $t > 0$, which is the continuous time Markov chain with the state space $\{1, \dots, M\}$. The initial state of the process η_t , $t \geq 0$, at the epoch of starting the service is determined by the probabilistic row-vector $\boldsymbol{\beta} = (\beta_1, \dots, \beta_M)$. The transitions of the process η_t , $t \geq 0$, that do not lead to the service completion, are defined by the irreducible matrix S of size $M \times M$. The intensities of transitions, which lead to the service completion, are defined by the column vector $\mathbf{S}_0 = -\mathbf{S}\mathbf{e}$. The service time distribution function has the form $B(x) = 1 - \boldsymbol{\beta}e^{Sx}\mathbf{e}$. Laplace-

Stieltjes transform $\int_0^\infty e^{-sx} dB(x)$ of this distribution function is $\boldsymbol{\beta}(s\mathbf{I} - S)^{-1}\mathbf{S}_0$. The average

service time is given by $b_1 = \boldsymbol{\beta}(-S)^{-1}\mathbf{e}$. The matrix $S + \mathbf{S}_0\boldsymbol{\beta}$ is assumed to be irreducible. The more detailed description of the *PH*-type distribution and its partial cases can be found, e.g., in the book (Neuts, 1981). Usefulness of *PH* distribution in description of service

process in telecommunication networks is stated, e.g., in (Pattavina & Parini, 2005) and (Riska et al., 2002).

It is intuitively clear that the described mechanism of arrivals restriction by means of tokens is reasonable. At the expense of some sessions rejection, it allows to decrease the sojourn time and jitter for admitted sessions. This is important in modeling real-world systems because the quality of transmission of accepted information units should satisfy imposed requirements of Quality of Service. Quantitative analysis of advantages and shortcomings of this mechanism as well as optimal choice of the number of tokens requires calculation of the main performance measures of the system under the fixed value K of tokens in the system. These measures can be calculated based on the knowledge of stationary distribution of the random process describing dynamics of the system under study.

3. Stationary distribution of the system states

Let us assume that the number $K, K \geq 1$, of tokens is fixed and let

- i_t be the total number of requests in the system, $i_t \geq 0$,
- k_t be the number of sessions having token for admission to the system, $k_t = \overline{0, K}$,
- ν_t and η_t be the states of the directing processes of the *MAP* arrival process and *PH* service process, $\nu_t = \overline{0, W}, \eta_t = \overline{1, M}$,

at the epoch $t, t \geq 0$.

Note that when $i_t = 0$, i.e., requests are absent in the system, the value of the component η_t , which describes the state of the service directing process, is not defined. To avoid special treatment of this situation, without loss of generality, we assume that if the server becomes idle the state of the component η_t is chosen randomly according to the probabilistic vector β and is kept until the next service beginning moment.

It is obvious that the four-dimensional process $\xi_t = \{i_t, k_t, \nu_t, \eta_t\}, t \geq 0$, is the irreducible regular continuous time Markov chain.

Let us enumerate the states of this Markov chain in lexicographic order and refer to (i, k) as macro-state consisting of $M_1 = (W + 1)M$ states $(i, k, \nu, \eta), \nu = \overline{0, W}, \eta = \overline{1, M}$.

For the use in the sequel, introduce the following notation:

- $\gamma^- = \gamma(1 - \theta), \gamma^+ = \gamma\theta, \Gamma^- = \gamma^- I_{M_1}, \Gamma^+ = \gamma^+ I_{M_1}, \Gamma = \gamma I_{M_1}$;
- $\tilde{C}_K = \text{diag}\{0, 1, \dots, K\}$ is the diagonal matrix with the diagonal entries $\{0, 1, \dots, K\}$, $C_K = \tilde{C}_K \otimes I_{M_1}$;
- $R_K = \text{diag}\{1, \dots, K\} \otimes I_{M_1}$; I is an identity matrix, O is a zero matrix;
-

$$A = \begin{pmatrix} O & O & O & \dots & O & O \\ \Gamma^- & -\Gamma & O & \dots & O & O \\ O & 2\Gamma^- & -2\Gamma & \dots & O & O \\ \vdots & \vdots & \vdots & \ddots & \vdots & \vdots \\ O & O & O & \dots & K\Gamma^- & -K\Gamma \end{pmatrix}, E^+ = \begin{pmatrix} 0 & 1 & 0 & \dots & 0 \\ 0 & 0 & 1 & \dots & 0 \\ \vdots & \vdots & \vdots & \ddots & \vdots \\ 0 & 0 & 0 & \dots & 1 \\ 0 & 0 & 0 & \dots & 0 \end{pmatrix};$$

•

$$A_1 = \begin{pmatrix} -\Gamma & O & \dots & O & O \\ \Gamma^- & -2\Gamma & \dots & O & O \\ O & 2\Gamma^- & \dots & O & O \\ \vdots & \vdots & \ddots & \vdots & \vdots \\ O & O & O\dots & (K-1)\Gamma^- & -K\Gamma \end{pmatrix}, \tilde{E} = \begin{pmatrix} 0 & 0 & 0 & \dots & 0 \\ 0 & 0 & 0 & \dots & 0 \\ \vdots & \vdots & \vdots & \ddots & \vdots \\ 0 & 0 & 0 & \dots & 0 \\ 0 & 0 & 0 & \dots & 1 \end{pmatrix};$$

- $\delta_{i,j}$ is Kronecker delta, $\delta_{i,j}$ is equal to 1, if $i = j$ and equal to 0 otherwise;
- \otimes is the symbol of Kronecker product of matrices;
- \oplus is the symbol of Kronecker sum of matrices;
- \mathbf{b}^T denotes transposed vector \mathbf{b} .

Let Q be the generator of the Markov chain $\xi_t, t \geq 0$, with blocks $Q_{i,j}$ consisting of intensities $(Q_{i,j})_{k,k'}$ of the Markov chain $\xi_t, t \geq 0$, transitions from the macro-state (i,k) to the macro-state $(j,k'), k, k' = \overline{0, K}$. The diagonal entries of the matrix $Q_{i,i}$ are negative and the modulus of the diagonal entry of $(Q_{i,i})_{k,k}$ defines the total intensity of leaving the corresponding state (i, k, ν, η) of the Markov chain. The block $Q_{i,j}, i, j \geq 0$, has dimension $K_1 \times K_1$, where $K_1 = (K + 1)M_1$.

Lemma 1. Generator Q has the three block diagonal structure:

$$Q = \begin{pmatrix} Q_{0,0} & Q_0 & O & O & \dots \\ Q_2 & Q_1 & Q_0 & O & \dots \\ O & Q_2 & Q_1 & Q_0 & \dots \\ \vdots & \vdots & \vdots & \vdots & \ddots \end{pmatrix}$$

where non-zero blocks $Q_{i,j}$ are defined by

$$\begin{aligned} Q_{0,0} &= A + I_{K+1} \otimes D_0 \otimes I_M + \tilde{E} \otimes D_1 \otimes I_M, \\ Q_1 &= A + I_{K+1} \otimes (D_0 \oplus S) + \tilde{E} \otimes D_1 \otimes I_M, \\ Q_0 &= \gamma^+ C_K + E^+ \otimes D_1 \otimes I_M, \\ Q_2 &= I_{K+1} \otimes I_{W+1} \otimes \mathbf{S}_0 \boldsymbol{\beta}. \end{aligned}$$

Proof of the lemma consists of analysis of the Markov chain $\xi_t, t \geq 0$, transitions during the infinitesimal interval of time and further assembling the corresponding transition intensities into the matrix blocks. Value γ^- is the intensity of a token releasing due to the finish of the session arrival, γ^+ is the intensity of a new request in the session arrival.

Let us investigate the Markov chain $\xi_t, t \geq 0$, defined by the generator Q . To this end, at first we should derive conditions under which this Markov chain is ergodic (positive recurrent).

Theorem 1. Markov chain $\xi_t = \{i_t, k_t, v_t, \eta_t\}, t \geq 0$, is ergodic if and only if the following inequality is fulfilled:

$$\mu > \Lambda = \gamma^+ \sum_{k=0}^K k \mathbf{x}_k \mathbf{e}_{W+1} + \sum_{k=0}^{K-1} \mathbf{x}_k D_1 \mathbf{e}_{W+1}, \quad (1)$$

where μ is the average service rate defined by

$$\mu^{-1} = b_1 = \boldsymbol{\beta}(-S)^{-1} \mathbf{e}$$

and $\mathbf{x} = (\mathbf{x}_0, \dots, \mathbf{x}_K)$ is the vector of the stationary distribution of the system $MAP/M/K/0$ with the MAP arrival process, defined by the matrices D_0 and D_1 and the average service rate γ^- .

Proof. It follows from (Neuts, 1981) that the ergodicity condition of the Markov chain $\xi_t = \{i_t, k_t, v_t, \eta_t\}, t \geq 0$, is the fulfillment of inequality

$$\mathbf{y} Q_2 \mathbf{e} > \mathbf{y} Q_0 \mathbf{e}, \quad (2)$$

where the row vector \mathbf{y} is solution to the system of linear algebraic equations of form

$$\mathbf{y}(Q_0 + Q_1 + Q_2) = \mathbf{0}, \mathbf{y} \mathbf{e} = 1. \quad (3)$$

It is easy to verify that

$$Q_0 + Q_1 + Q_2 = B \otimes I_M + I_{(K+1)(W+1)} \otimes (S + \mathbf{S}_0 \boldsymbol{\beta}),$$

where B is the generator of the Markov chain, which describes behavior of the $MAP|M|K|0$ system with the MAP arrival process defined by matrices D_0 and D_1 and average service rate γ^- :

$$B = \begin{pmatrix} D_0 & D_1 & O & \dots & O & O \\ \gamma^- I & D_0 - \gamma^- I & D_1 & \dots & O & O \\ 0 & 2\gamma^- I & D_0 - 2\gamma^- I & \dots & O & O \\ \vdots & \vdots & \vdots & \ddots & \vdots & \vdots \\ O & O & O & \dots & K\gamma^- I & D(1) - K\gamma^- I \end{pmatrix}.$$

According to the definition, vector \mathbf{x} satisfies equations

$$\mathbf{x} B = \mathbf{0}, \mathbf{x} \mathbf{e} = 1. \quad (4)$$

By direct substitution into (3), it can be verified that the vector \mathbf{y} , which is solution to the

system (3), can be represented in the form $\mathbf{y} = \mathbf{x} \otimes \boldsymbol{\psi}$, where $\boldsymbol{\psi}$ is the unique solution of the system of linear algebraic equations

$$\boldsymbol{\psi}(S + \mathbf{S}_0\boldsymbol{\beta}) = \mathbf{0}, \boldsymbol{\psi}\mathbf{e} = 1. \quad (5)$$

By substituting vector $\mathbf{y} = \mathbf{x} \otimes \boldsymbol{\psi}$ into inequality (2), after some transformations we get inequality (1). Theorem 1 is proven.

In what follows we assume that condition (1) is fulfilled. Then the following limits (stationary probabilities) exist:

$$\pi(i, k, v, \eta) = \lim_{t \rightarrow \infty} P\{i_t = i, k_t = k, v_t = v, \eta_t = \eta\}, i \geq 0, k = \overline{0, K}, v = \overline{0, W}, \eta = \overline{1, M}.$$

Let us combine these probabilities into the row-vectors

$$\begin{aligned} \boldsymbol{\pi}(i, k, v) &= (\pi(i, k, v, 1), \pi(i, k, v, 2), \dots, \pi(i, k, v, M)), \\ \boldsymbol{\pi}(i, k) &= (\boldsymbol{\pi}(i, k, 0), \boldsymbol{\pi}(i, k, 1), \dots, \boldsymbol{\pi}(i, k, W)), \\ \boldsymbol{\pi}_i &= (\boldsymbol{\pi}(i, 0), \boldsymbol{\pi}(i, 1), \dots, \boldsymbol{\pi}(i, K)), \quad i \geq 0. \end{aligned}$$

The following statement directly stems from the results in (Neuts, 1981).

Theorem 2. The stationary probability vectors $\boldsymbol{\pi}_i, i \geq 0$, are calculated by

$$\boldsymbol{\pi}_i = \boldsymbol{\pi}_0 R^i, \quad i \geq 0,$$

where the matrix R is the minimal non-negative solution to the equation

$$R^2 Q_2 + R Q_1 + Q_0 = O,$$

and the vector $\boldsymbol{\pi}_0$ is the unique solution to the system of linear algebraic equations

$$\boldsymbol{\pi}_0(Q_{0,0} + R Q_2) = \mathbf{0}, \boldsymbol{\pi}_0(I - R)^{-1} \mathbf{e} = 1.$$

Having stationary probability vectors $\boldsymbol{\pi}_i, i \geq 0$, been computed, we can calculate different performance measures of the system. Some of them are given in the following statements.

Corollary 1. The probability distribution of the number of requests in the system is computed by

$$\lim_{t \rightarrow \infty} P\{i_t = i\} = \boldsymbol{\pi}_i \mathbf{e}, \quad i \geq 0.$$

The average number L of requests in the system is computed by

$$L = \sum_{i=0}^{\infty} i \boldsymbol{\pi}_i \mathbf{e} = \boldsymbol{\pi}_0 R (I - R)^{-2} \mathbf{e}.$$

The probability distribution of the number of sessions in the system is computed by

$$\lim_{t \rightarrow \infty} P\{k_t = k\} = \sum_{i=0}^{\infty} \boldsymbol{\pi}(i, k) \mathbf{e} = \boldsymbol{\pi}_0 (I - R)^{-1} (\mathbf{e}^{(k)} \otimes \mathbf{e}), \quad k = \overline{0, K},$$

where the column vector $\mathbf{e}^{(k)}$ has all zero entries except the k th one, which is equal to 1, $k = \overline{0, K}$.

The average number Z of sessions in the system is computed by

$$Z = \sum_{k=1}^K \sum_{i=0}^{\infty} k \boldsymbol{\pi}(i, k) \mathbf{e} = \boldsymbol{\pi}_0 (I - R)^{-1} \sum_{k=1}^K k (\mathbf{e}^{(k)} \otimes \mathbf{e}).$$

The distribution function $R(t)$ of a time, during which arrivals from an arbitrary session occur, is computed by

$$R(t) = (1 - \theta) \sum_{l=1}^{\infty} \int_0^t \theta^{l-1} \frac{\gamma (\gamma y)^{l-1}}{(l-1)!} e^{-\gamma y} dy = 1 - e^{-\gamma(1-\theta)t}.$$

The average number T of requests processed by the system at unit of time (throughput) is computed by

$$T = \sum_{i=1}^{\infty} \sum_{k=0}^K \sum_{v=0}^W \sum_{\eta=1}^M \boldsymbol{\pi}(i, k, v, \eta) (\mathbf{S}_0)_{\eta} = \boldsymbol{\pi}_0 R (I - R)^{-1} (\mathbf{e}_{(K+1)(W+1)} \otimes \mathbf{S}_0).$$

Remark 1. In contrast to the model with a finite buffer, see (Lee et al., 2007) and (Kim et al., 2009), where the arriving session can be rejected not only due to the tokens absence but also due to the buffer overloading, distribution of the number of sessions in the model under study does not depend on the number of requests in the system. It is defined by formula

$$\lim_{t \rightarrow \infty} P\{k_t = k\} = \mathbf{x}_k \mathbf{e}, \quad k = \overline{0, K},$$

where the vectors $\mathbf{x}_k, k = \overline{0, K}$, are the entries of the vector $\mathbf{x} = (\mathbf{x}_0, \dots, \mathbf{x}_K)$ which satisfies the system (5). However, distribution $\boldsymbol{\pi}(i, k), i \geq 0, k = \overline{0, K}$, does not have multiplicative form because the number of requests in the system depends on the number of sessions currently presenting in the system.

Remark 2. It can be verified that the considered model with the infinite buffer has the steady state distribution of the process $\xi_t = \{i_t, k_t, v_t, \eta_t\}, t \geq 0$, coinciding with the steady state distribution of the queueing model of the *MAP/PH/1* type with the phase service time distribution having irreducible representation $(\boldsymbol{\beta}, S)$ and the *MAP* arrival process defined by the matrices \tilde{D}_0 and \tilde{D}_1 having the form

$$\tilde{D}_0 = \begin{pmatrix} D_0 & O & O & \dots & O & O \\ \gamma^- I & D_0 - \gamma I & O & \dots & O & O \\ 0 & 2\gamma^- I & D_0 - 2\gamma I & \dots & O & O \\ \vdots & \vdots & \vdots & \ddots & \vdots & \vdots \\ O & O & O & \dots & K\gamma^- I & D(1) - K\gamma I \end{pmatrix}, \tilde{D}_1 = \begin{pmatrix} O & D_1 & O & \dots & O & O \\ O & \gamma^+ I & D_1 & \dots & O & O \\ 0 & O & 2\gamma^+ I & \dots & O & O \\ \vdots & \vdots & \vdots & \ddots & \vdots & \vdots \\ O & O & O & \dots & O & K\gamma^+ I \end{pmatrix}.$$

It is easy to verify that the fundamental rate of this MAP is equal to Λ which is defined in (1). So, stability condition (1) is intuitively clear: the average service rate should exceed the average arrival rate. Note that the first summand in expression $\Lambda = \gamma^+ \sum_{k=0}^K k \mathbf{x}_k \mathbf{e}_{W+1} + \sum_{k=0}^{K-1} \mathbf{x}_k D_1 \mathbf{e}_{W+1}$, for the rate Λ represents the rate of requests from already accepted sessions, i.e., the rate of requests who are not the first in a session. The second summand is the rate of the sessions arrival.

Theorem 2. The probability $P_b^{(loss)}$ of an arbitrary session rejection upon arrival is computed by

$$P_b^{(loss)} = \sum_{i=0}^{\infty} \boldsymbol{\pi}(i, K) \frac{(D_1 \otimes I_M)}{\lambda} \mathbf{e} = \mathbf{x}_K \frac{D_1}{\lambda} \mathbf{e}.$$

The probability $P_c^{(loss)}$ of an arbitrary request rejection upon arrival is computed by

$$P_c^{(loss)} = \sum_{i=0}^{\infty} \boldsymbol{\pi}(i, K) \frac{(D_1 \otimes I_M)}{\tilde{\Lambda}} \mathbf{e} = \mathbf{x}_K \frac{D_1}{\tilde{\Lambda}} \mathbf{e}$$

where $\tilde{\Lambda} = \Lambda + \mathbf{x}_K D_1 \mathbf{e}$.

Proof of formula for probability $P_b^{(loss)}$ accounts that the session is rejected upon arrival if and only if the number of sessions in the system at this epoch is equal to K . So

$$P_b^{(loss)} = \frac{\sum_{i=0}^{\infty} \boldsymbol{\pi}(i, K) (D_1 \otimes I_M) \mathbf{e}}{\sum_{i=0}^{\infty} \sum_{k=0}^K \boldsymbol{\pi}(i, k) (D_1 \otimes I_M) \mathbf{e}} = \sum_{i=0}^{\infty} \boldsymbol{\pi}(i, K) \frac{(D_1 \otimes I_M)}{\lambda} \mathbf{e}.$$

Rejection of a request can occur only if this request is the first in a session and the number of sessions in the system at this session arrival epoch is equal to K . So

$$P_c^{(loss)} = \frac{\sum_{i=0}^{\infty} \boldsymbol{\pi}(i, K) (D_1 \otimes I_M) \mathbf{e}}{\sum_{i=0}^{\infty} \sum_{k=0}^K \boldsymbol{\pi}(i, k) (D_1 + k\gamma^+ I) \otimes I_M \mathbf{e}} = \sum_{i=0}^{\infty} \boldsymbol{\pi}(i, K) \frac{D_1 \otimes I_M}{\tilde{\Lambda}} \mathbf{e}.$$

4. Distribution of the sojourn times

Let $V_b(x)$, $V_c(x)$ and $V_c^{(a)}(x)$ be distribution functions of the sojourn time of an arbitrary session, an arbitrary request, which is the first in a session, and an arbitrary request from the admitted session, which is not the first in this session, in the system under study, and $v_b(s)$, $v_c(s)$ and $v_c^{(a)}(s)$, $Re s > 0$, be their Laplace-Stieltjes transforms (LSTs):

$$v_b(s) = \int_0^{\infty} e^{-sx} dV_b(x), v_c(s) = \int_0^{\infty} e^{-sx} dV_c(x), v_c^{(a)}(s) = \int_0^{\infty} e^{-sx} dV_c^{(a)}(x).$$

Formulae for calculation of the LSTs $v_c(s)$ and $v_c^{(a)}(s)$ are the following:

$$\begin{aligned} v_c(s) &= \frac{1}{\lambda} [\boldsymbol{\pi}_0 (D_1 \otimes I_M) \mathbf{e} \boldsymbol{\beta} (sI - S)^{-1} \mathbf{S}_0 + \sum_{i=1}^{\infty} \boldsymbol{\pi}_i (D_1 \otimes I_M) (\mathbf{e}_{(K+1)(W+1)} \otimes ((sI - S)^{-1} \mathbf{S}_0)) (\boldsymbol{\beta} (sI - S)^{-1} \mathbf{S}_0)^i] = \\ &= \frac{1}{\lambda} [\boldsymbol{\pi}_0 (D_1 \otimes I_M) \mathbf{e} \boldsymbol{\beta} (sI - S)^{-1} \mathbf{S}_0 + \boldsymbol{\pi}_0 R (\boldsymbol{\beta} (sI - S)^{-1} \mathbf{S}_0) \times \\ &\times (I - R (\boldsymbol{\beta} (sI - S)^{-1} \mathbf{S}_0))^{-1} (D_1 \otimes I_M) (\mathbf{e}_{(K+1)(W+1)} \otimes ((sI - S)^{-1} \mathbf{S}_0))], \\ v_c^{(a)}(s) &= \frac{1}{\sum_{k=1}^K \sum_{i=0}^{\infty} k \gamma^+ \boldsymbol{\pi}(i, k) \mathbf{e}} \sum_{k=1}^K k \gamma^+ [\boldsymbol{\pi}(0, k) \mathbf{e} \boldsymbol{\beta} (sI - S)^{-1} \mathbf{S}_0 + \\ &+ \sum_{i=1}^{\infty} \boldsymbol{\pi}(i, k) (\mathbf{e}_{W+1} \otimes ((sI - S)^{-1} \mathbf{S}_0)) (\boldsymbol{\beta} (sI - S)^{-1} \mathbf{S}_0)^i]. \end{aligned}$$

Formulae for the average sojourn time V_c of an arbitrary request, which is the first in a session, the average sojourn time V_c^* of an arbitrary non-rejected request, which is the first in a session, and the average sojourn time $V_c^{(a)}$ of an arbitrary request from the admitted session, which is not the first in this session, are as follows:

$$\begin{aligned} V_c &= \frac{1}{\lambda} [\boldsymbol{\pi}_0 (D_1 \otimes I_M) \mathbf{e} b_1 + \sum_{i=1}^{\infty} \boldsymbol{\pi}_i (D_1 \otimes I_M) ((\mathbf{e}_{(K+1)(W+1)} \otimes (-S)^{-1} \mathbf{e}) + \mathbf{e} i b_1)] = \\ &= \frac{\boldsymbol{\pi}_0}{\lambda} [(I + R(I - R)^{-2}) (D_1 \otimes I_M) \mathbf{e} b_1 + R(I - R)^{-1} (D_1 \otimes I_M) (\mathbf{e}_{(K+1)(W+1)} \otimes (-S)^{-1} \mathbf{e})], \\ V_c^* &= \frac{V_c}{1 - P_b^{(loss)}}, \\ V_c^{(a)} &= \frac{\sum_{k=1}^K k \gamma^+ [\boldsymbol{\pi}(0, k) \mathbf{e} b_1 + \sum_{i=1}^{\infty} \boldsymbol{\pi}(i, k) ((\mathbf{e}_{W+1} \otimes (-S)^{-1} \mathbf{e}) + \mathbf{e} i b_1)]}{\sum_{k=1}^K \sum_{i=0}^{\infty} k \gamma^+ \boldsymbol{\pi}(i, k) \mathbf{e}}. \end{aligned}$$

If the service time distribution is exponential, expression for the average sojourn time V_c of an arbitrary arriving request, which is the first in a session, becomes simpler:

$$V_c = \frac{\pi_0}{\lambda} b_1 (I - R)^{-2} D_1 \mathbf{e}.$$

Derivation of formula for calculation of the *LST* $v_b(s)$ is more involved. Recall that the sojourn time of an arbitrary session in the system lasts since the epoch of the session arrival into the system until the moment when the arrival of a session is finished and all requests, which belong to this session, leave the system. We will derive expression for the *LST* $v_b(s)$ by means of the method of collective marks (method of additional event, method of catastrophes), for references see, e.g., (Kasten & Runnenburg, 1956) and (Danzig, 1955). To this end, we interpret the variable s as the intensity of some virtual stationary Poisson flow of catastrophes. So, $v_b(s)$ has meaning of probability that no one catastrophe arrives during the sojourn time of an arbitrary session.

We will tag an arbitrary session and will keep track of its staying in the system. Let $v(s, i, l, k, \nu, \eta)$ be the probability that catastrophe will not arrive during the rest of the tagged session sojourn time in the system conditional that, at the given moment, the number of sessions processed in the system is equal to $k, k = \overline{1, K}$, the number of requests is equal to $i, i \geq 0$, the last (in the order of arrival) request of a tagged session has position number $l, l = \overline{0, i}$, in the system, and the states of the processes $\nu_t, \eta_t, t \geq 0$, are ν, η . Position number 0 means that currently there is no one request of the tagged session in the system.

It follows from the formula of total probability that if we will have functions $v(s, i, l, k, \nu, \eta)$ been calculated the Laplace-Stieltjes transform $v_b(s)$ can be computed by

$$v_b(s) = P_b^{(loss)} + \frac{1}{\lambda} \sum_{i=0}^{\infty} \sum_{k=0}^{K-1} \sum_{\nu=0}^W \sum_{\eta=1}^M \sum_{\nu'=0}^W \pi(i, k, \nu, \eta) \lambda_{\nu} p_{\nu, \nu'}^{(1)} \times v(s, i+1, i+1, k+1, \nu', \eta). \quad (6)$$

The system of linear algebraic equations for functions $v(s, i, l, k, \nu, \eta)$ is derived by means of formula of total probability in the following form:

$$\begin{aligned} v(s, i, l, k, \nu, \eta) = & [\lambda_{\nu} \sum_{\nu'=0}^W p_{\nu, \nu'}^{(1)} ((1 - \delta_{k, k}) v(s, i+1, l, k+1, \nu', \eta) + \\ & + \delta_{k, k} v(s, i, l, k, \nu', \eta)) + \lambda_{\nu} \sum_{\nu'=0}^W p_{\nu, \nu'}^{(0)} v(s, i, l, k, \nu', \eta) + \\ & + (1 - \delta_{i, 0}) (S_0)_{\eta} \sum_{\eta'=1}^M \beta_{\eta'} [v(s, i-1, l-1, k, \nu, \eta') (1 - \delta_{l, 0}) + v(s, i-1, 0, k, \nu, \eta') \delta_{l, 0}] + \\ & + (1 - \delta_{i, 0}) \sum_{\eta'=1}^M (S)_{\eta, \eta'} v(s, i, l, k, \nu, \eta') + \gamma^+ v(s, i+1, i+1, k, \nu, \eta) + \\ & + \gamma^+ (k-1) v(s, i+1, l, k, \nu, \eta) + \gamma^- (k-1) v(s, i, l, k-1, \nu, \eta) + \end{aligned} \quad (7)$$

$$+\gamma^-[(sI - S)^{-1}\mathbf{S}_0]_\eta(\boldsymbol{\beta}(sI - S)^{-1}\mathbf{S}_0)^{l-1}(1 - \delta_{i,0}) + \delta_{i,0}]] \times \\ \times (s + \lambda_\nu - S_{\eta,\eta} + k\gamma)^{-1}, l = \overline{0}, i, i \geq 0, k = \overline{1}, K, \nu = \overline{0}, W, \eta = \overline{1}, M.$$

Let us explain formula (7) in brief. The denominator of the right hand side of (7) is equal to the total intensity of the events which can happen after the arbitrary time moment: catastrophe arrival, transition of the directing process of the *MAP*, transition of the directing process of the *PH* service process, and expiring the time till the moment of possible request arrival from sessions already admitted into the system. The first term in the square brackets in (7) corresponds to the case when a new session arrives. The second term corresponds to the case when transition of the directing process of the *MAP* occurs without new session generation. The third term corresponds to the case when service completion takes place. The fourth term corresponds to the case when the transition of the directing process of the *PH* service process occurs without the service completion. The fifth term corresponds to the case when the new request of the tagged session arrives into the system. In this case, the position of the last request of the tagged session in the system is reinstalled from l to $i + 1$. The sixth term corresponds to the case when the new request from another session, which was already admitted to the system, arrives. The seventh term corresponds to the case when some non-tagged session terminates arrivals. The eighth term corresponds to the case when the expected new request of the tagged session does not arrive into the system and arrival of requests of the tagged session is stopped. This session will not more counted as arriving into the system and the tagged request finishes its sojourn time when the last request, who is currently the l th in the system, will leave the system. Number $((sI - S)^{-1}\mathbf{S}_0)_\eta$ defines the probability that catastrophe will not arrive during the residual service time conditional that the directing process of the *PH* service is currently in the state η . The number $\boldsymbol{\beta}(sI - S)^{-1}\mathbf{S}_0$ defines probability that catastrophe will not arrive during the service time of an arbitrary request.

Let us introduce column vectors

$$\mathbf{v}(s, i, l, k, \nu) = (v(s, i, l, k, \nu, 1), \dots, v(s, i, l, k, \nu, M))^T, \\ \mathbf{v}(s, i, l, k) = (\mathbf{v}(s, i, l, k, 0), \dots, \mathbf{v}(s, i, l, k, W))^T, \\ \mathbf{v}(s, i, l) = (\mathbf{v}(s, i, l, 1), \dots, \mathbf{v}(s, i, l, K))^T, \\ \mathbf{v}(s, i) = (\mathbf{v}(s, i, 0), \dots, \mathbf{v}(s, i, i))^T, \mathbf{v}(s) = (\mathbf{v}(s, 0), \mathbf{v}(s, 1), \dots)^T.$$

System (7) of linear algebraic equations can be rewritten to the matrix form as

$$-(sI - \hat{Q}_{i,i})\mathbf{v}(s, i, l) + \hat{Q}_{i,i+1}\mathbf{v}(s, i + 1, l) + \hat{Q}_{i,i-1}\mathbf{v}(s, i - 1, l - 1)(1 - \delta_{0,l}) + \hat{Q}_{i,i-1}v(s, i - 1, 0)\delta_{0,l} + \\ + I_K \otimes \Gamma^+\mathbf{v}(s, i + 1, i + 1) + \gamma^- \mathbf{e}_{K(W+1)} \otimes ((sI - S)^{-1}\mathbf{S}_0)(\boldsymbol{\beta}(sI - S)^{-1}\mathbf{S}_0)^{l-1} = \mathbf{0}_{KM_1}^T, l = \overline{0}, i, i \geq 0, \quad (8)$$

where

$$\hat{Q}_{i,i} = A_1 + I_K \otimes (D_0 \oplus S)(1 - \delta_{i,0}) + \tilde{E} \otimes ((D_1 \otimes I_M)) + I_K \otimes (D_0 \otimes I_M)\delta_{i,0}, i \geq 0,$$

$$\begin{aligned}\hat{Q}_{i,i+1} &= \gamma^+ C_{K-1} + E_K^+ \otimes (D_1 \otimes I_M), i \geq 0, \\ \hat{Q}_{i,i-1} &= I_{K(W+1)} \otimes \mathbf{S}_0 \boldsymbol{\beta}, i \geq 0, \hat{Q}_{0,-1} = O.\end{aligned}$$

Let us introduce notation:

$\Omega(s)$ is three block diagonal matrix with non-zero blocks

$$\Omega_{i,j}(s), j = \max\{0, i-1\}, i, i+1, i \geq 0,$$

defined by

$$\begin{aligned}\Omega_{i,i}(s) &= -I_{i+1} \otimes (sI - \hat{Q}_{i,i}), \Omega_{i,i-1} = D_3^{(i)} \otimes \hat{Q}_{i,i-1}, \\ \Omega_{i,i+1} &= D_1^{(i)} \otimes \hat{Q}_{i,i+1} + D_2^{(i)} \otimes I_K \otimes \Gamma^+.\end{aligned}$$

Here the matrix $D_1^{(i)}$ of size $(i+1) \times (i+2)$ is obtained from the identity matrix I_{i+1} by means of supplementing from the right by the column $\mathbf{0}_{i+1}^T$. The matrix $D_2^{(i)}$ of the same size has the last column consisting of 1's and other columns consisting of 0's. The matrix $D_3^{(i)}$ of size $(i+1) \times i$ is obtained from the identity matrix I_i by means of supplementing from above by the row $(1, 0, \dots, 0)$.

Vector $\mathbf{B}(s)$ is defined by

$$\mathbf{B}(s) = (\mathbf{B}_0(s), \dots, \mathbf{B}_N(s), \dots)^T$$

where

$$\begin{aligned}\mathbf{B}_i(s) &= \gamma^- (\mathbf{e}_K \otimes \mathbf{e}_{M_1}, \mathbf{e}_K \otimes \mathbf{e}_{W+1} \otimes (sI - S)^{-1} \mathbf{S}_0, \mathbf{e}_K \otimes \mathbf{e}_{W+1} \otimes ((sI - S)^{-1} \mathbf{S}_0) \boldsymbol{\beta} (sI - S)^{-1} \mathbf{S}_0, \dots, \\ &\quad \mathbf{e}_K \otimes \mathbf{e}_{W+1} \otimes ((sI - S)^{-1} \mathbf{S}_0) (\boldsymbol{\beta} (sI - S)^{-1} \mathbf{S}_0)^{i-1})^T, i \geq 0.\end{aligned}$$

Using this notation we can rewrite the system (7) to the form

$$\Omega(s) \mathbf{v}(s) + \mathbf{B}(s) = \mathbf{0}^T. \quad (9)$$

It can be verified that the diagonal entries of the matrix $\Omega(s)$ dominate in all rows of this matrix. So the inverse matrix exists. Thus we proved the following assertion.

Theorem 3. The vector $\mathbf{v}(s)$ consisting of conditional Laplace-Stieltjes transforms LST $v(s, i, l, k, \nu, \eta)$, $l = \overline{0, i}$, $i \geq 0$, $k = \overline{1, K}$, $\nu = \overline{0, W}$, $\eta = \overline{1, M}$, is calculated by

$$\mathbf{v}(s) = -\Omega^{-1}(s) \mathbf{B}(s). \quad (10)$$

Corollary 2. The average sojourn time V_b of an arbitrary session is calculated by

$$V_b = -\sum_{i=0}^{\infty} \sum_{k=0}^{K-1} \boldsymbol{\pi}(i, k) \frac{(D_1 \otimes I_M)}{\lambda} \frac{\partial \mathbf{v}(s, i+1, i+1, k+1)}{\partial s} \Big|_{s=0},$$

where column vectors $\frac{\partial \mathbf{v}(s, i+1, i+1, k+1)}{\partial s} \Big|_{s=0}$ are calculated as the blocks of the vector $\frac{d\mathbf{v}(s)}{ds} \Big|_{s=0}$ defined by

$$\frac{d\mathbf{v}(s)}{ds} \Big|_{s=0} = \Omega^{-1}(0) \left(-\frac{d\mathbf{B}(s)}{ds} \Big|_{s=0} + \mathbf{v}(0) \right),$$

where $\mathbf{v}(0) = -\gamma^{-1} \Omega^{-1}(0) \mathbf{e}$.

Corollary 3. The average sojourn time $V_b^{(accept)}$ of an arbitrary admitted session is calculated by

$$V_b^{(accept)} = \frac{V_b}{1 - P_b^{(loss)}},$$

where $P_b^{(loss)}$ is probability of an arbitrary session rejection upon arrival.

5. Optimization problem and numerical examples

It is obvious that the most important from economical point of view characteristic of the considered model is the throughput T of the system because it defines the profit earned by information transmission. If the number K that restricts the number of sessions, which can be served in the system simultaneously, increases the throughput T of the system increases and the probability $P_b^{(loss)}$ of an arbitrary session rejection upon arrival decreases. So, it seems to be reasonable to increase the number K as much as possible until stability condition (1) is violated. However, such performance measures as the average sojourn time of an arbitrary request and jitter are also very important because they should fit requirements of Quality of Service. These performance measures become worse if the number K grows. Evidently, it does not make sense to admit too many sessions into the system simultaneously and provide bad Quality of Service (average sojourn time and jitter) for them. So, the system manager should decide how many sessions can be allowed to enter the system simultaneously to fit requirements of Quality of Service and to reach the maximally possible throughput.

Thus, one should solve, e.g., the following non-trivial optimization problem:

$$T = T(K) \rightarrow \max \tag{11}$$

subject to constraints (1) and

$$V_c^* \leq V, \tag{12}$$

where V is the maximal admissible value of the sojourn time of the first request from non-rejected session and is assumed to be fixed in advance.

This optimization problem can be easily solved by means of computer, based on presented above expressions for the main performance measures of the system, by means of enumeration, i.e., increasing the value K until constraints (1) and (12) are violated. The

optimal value of K in the optimization problem (1), (11), (12) will be denoted by K^* . Corresponding computer program allows to validate the feasibility of such an optimization algorithm and to illustrate the dependencies of the system characteristics on the system parameters and the value of K . In what follows several illustrative examples are presented. Before to start description of these examples, let us mention that numerous experiments show that the famous Little's formula holds good for the system under study in the form $\lambda L = V_c$, where L is the average number of requests in the system and V_c is the average sojourn time of an arbitrary request which is the first in a session.

5.1. Dependence of probabilities P_b^{loss} of an arbitrary session loss and P_c^{loss} of an arbitrary request loss on the number K of tokens and correlation in the sessions arrival process

The experiment has two goals. One is to illustrate quantitatively the dependence of probabilities P_b^{loss} of an arbitrary session loss and P_c^{loss} of an arbitrary request loss on the number K of tokens. The second goal is to show that for several different arrival processes having the same average rate but different correlation this dependence is quite different. This explains the importance of consideration of the model with the *MAP* arrival process of sessions, which can be essentially correlated in real telecommunication networks, instead of analysis of simpler model with the stationary Poisson arrival process of sessions.

We consider six different *MAPs* having the same fundamental rate $\lambda = 1$. The first *MAP* is the stationary Poisson arrival process. Variation coefficient of inter-arrival times is equal to 1. Four other *MAPs* have the variation coefficient equal to 2 but different coefficients of correlation of successive intervals between sessions arrival. These four *MAPs* are described as follows.

- *MAP* (*IPP* – *Interrupted Poisson Process*) flow with correlation coefficient equal to 0 is defined by the matrices

$$D_0 = \begin{pmatrix} -0.4 & 0.16 & 0.24 \\ 1.3 & -69.4 & 68.1 \\ 1.3 & 1.3 & -270 \end{pmatrix}; D_1 = \begin{pmatrix} 0 & 0 & 0 \\ 0 & 0 & 0 \\ 100.2 & 167.2 & 0 \end{pmatrix}.$$

- *MAP* flow with correlation coefficient equal to 0.1 is defined by the matrices

$$D_0 = \begin{pmatrix} -2.66 & 0.12 & 0.12 \\ 0.13 & -0.5 & 0.08 \\ 0.14 & 0.08 & -0.32 \end{pmatrix}; D_1 = \begin{pmatrix} 2.3 & 0.08 & 0.04 \\ 0.09 & 0.18 & 0.02 \\ 0.5 & 0.01 & 0.04 \end{pmatrix}.$$

- *MAP* flow with correlation coefficient equal to 0.2 is defined by the matrices

$$D_0 = \begin{pmatrix} -3.16 & 0.12 & 0.12 \\ 0.1 & -0.45 & 0.09 \\ 0.12 & 0.11 & -0.39 \end{pmatrix}; D_1 = \begin{pmatrix} 2.84 & 0.06 & 0.02 \\ 0.02 & 0.21 & 0.03 \\ 0.02 & 0.04 & 0.1 \end{pmatrix}.$$

- *MAP* flow with correlation coefficient equal to 0.3 is defined by the matrices

$$D_0 = \begin{pmatrix} -5.11 & 0.08 & 0.07 \\ 0.029 & -0.446 & 0.04 \\ 0.06 & 0.08 & -0.35 \end{pmatrix}; D_1 = \begin{pmatrix} 4.85 & 0.09 & 0.02 \\ 0.007 & 0.333 & 0.037 \\ 0 & 0.05 & 0.16 \end{pmatrix}.$$

- The sixth MAP has correlation coefficient equal to -0.16 and the squared correlation coefficient equal to 1.896. It is defined by the matrices

$$D_0 = \begin{pmatrix} -3.607 & 0 \\ 0 & -0.617 \end{pmatrix}; D_1 = \begin{pmatrix} 0.347 & 3.26 \\ 0.478 & 0.139 \end{pmatrix}.$$

The service time distribution is Erlangian of order 2 with intensity of the phase equal to 16. The rest of the parameters are the following: $\gamma = 2, \theta = 0.9$.

Figures 1 and 2 illustrate the dependencies of probability P_b^{loss} of an arbitrary session loss and P_c^{loss} of an arbitrary request loss on the number K of tokens for the listed above different MAP s with the same fundamental rate but the different correlation.

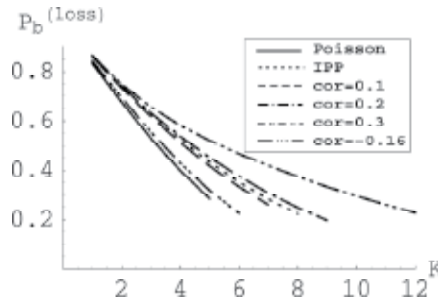


Fig. 1. Dependence of probability P_b^{loss} of arbitrary session loss on the number of tokens K

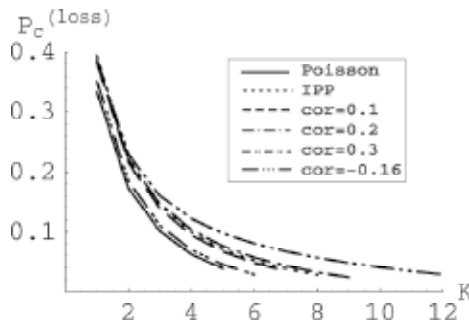


Fig. 2. Dependence of probability of an arbitrary request loss on the number of tokens K

One can pay attention that the curves corresponding to the different MAP s terminate at the different points, e.g., the curve corresponding to the stationary Poisson process terminates at the point $K = 5$, the curve corresponding to the MAP s having correlation coefficient 0.3 terminates at the point $K = 12$. The reason of termination is that the stationary distribution existence condition violates for K larger than 5 and 12 correspondingly.

It is worth to mention, that the previous analysis of different queues with the Batch Markovian Arrival Process given in many papers shows that usually the stability condition depends on the average arrival rate, but does not depend on correlation. In the model under study, stability condition (1) depends on correlation as well. This has the clear explanation: stability condition includes the stationary distribution of the corresponding MAP/M/K/0

queueing system which describes the behavior of the number of busy tokens. As it is illustrated in (Klimenok et al., 2005), this distribution essentially depends on the correlation in the arrival process.

Conclusion that can be made based on these numerical results is the following: higher correlation of the session's arrival process implies higher value of P_b^{loss} and P_c^{loss} but larger number of sessions which can be simultaneously processed in the system without overloading the system. *IPP* process violates this rule a bit. This is well known very special kind of arrival process. It has zero correlation. Intervals where arrivals occur more or less intensively alternate with time periods when no arrivals are possible. Such irregular arrivals make the *IPP* violating the conclusion made above. Note that the system with the negative correlation in the arrival process has characteristics close to characteristics of the system with the stationary Poisson process. While the more or less strong positive correlation changes these characteristics essentially.

5.2. Dependence of the throughput of the system on the number of tokens and correlation in the sessions arrival process

Let us consider the same system as in the previous experiment and consider optimization problem (11), (12) where the limiting value of the average sojourn time for the first request in non-rejected session is assumed to be $V = 40$. Figure 3 illustrates the dependence of the throughput T of the system on the number of tokens K . As it is expected, the throughput T is the increasing function of K for all arrival processes. However, the shape of this function depends on the correlation in the sessions arrival process. The lines corresponding to the different *MAP*s terminate when condition (12) is not hold true. So, as it is seen from Figure 3 the optimal value K^* of tokens is equal to 5 when the arrival process is the stationary Poisson or has the negative correlation or is equal to 0.1 and is equal to 6 for the rest of the arrival processes.

It is seen from Figures 1-3 that positive correlation has the negative impact on the system performance. Although the number of simultaneously processed requests can be larger, loss probability is higher and the throughput of the system is lesser.

Dependence of the average sojourn time V_c^* for the first request in non-rejected sessions on the number of tokens in these examples is presented on Figure 4.

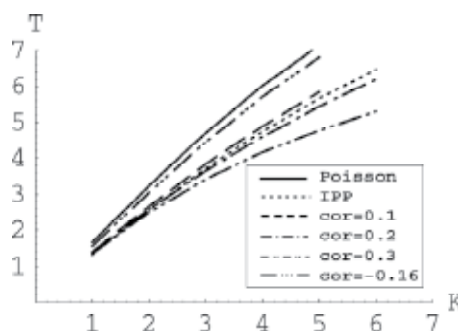


Fig. 3. Dependence of the throughput T of the system on the number of tokens under restriction $V_c^* < 40$

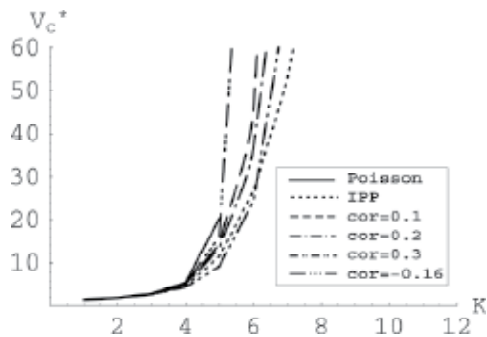


Fig. 4. Dependence of V_c^* on K

It is seen that the average sojourn time V_c^* sharply increases when the number of tokens K approaches the value $K=5$ or $K=6$, depending on correlation in the arrival process. For the model with the stationary Poisson arrival process stationary distribution does not exist for $K=6$.

5.3. Dependence of the optimal number of tokens on the session size, arrival and service rates

The goal of this experiment is to illustrate the dependence of the optimal number of tokens on the session size, average arrival and average service rates.

Firstly, let us clarify the impact of the session size. We assume that the *MAP* process of sessions is defined by the matrices

$$D_0 = \begin{pmatrix} -6.88 & 0.0008 \\ 0.0008 & -0.22 \end{pmatrix}; D_1 = \begin{pmatrix} 6.8 & 0.0792 \\ 0.016 & 0.2032 \end{pmatrix}.$$

This *MAP* has the average rate equal to 1.37, correlation coefficient 0.4 and the squared variation coefficient 9.4. As in the previous examples, the service time distribution is assumed to be Erlangian of order 2 with the intensity of the phase equal to 16.

On Figure 5, we vary the parameter θ , which characterizes the distribution of the number of requests in a session, in the interval $[0.1;0.8]$. This implies that the average session size varies in the interval $[1.111;5]$. Parameter V defining the limiting value of the average sojourn time for the first request in non-rejected sessions is assumed to be equal to 0.8.

On Figure 6, we vary the parameter θ in the interval $[0.8;0.98]$. This implies that the average session size varies in the interval $[5;50]$. Parameter V is assumed to be equal to 8.

As it is expected, the optimal number K^* is non-increasing function of θ . When θ increases from 0.1 to 0.8 the number K^* decreases from 8 to 1 under restriction $V_c^* < 0.8$. If we take θ greater than 0.8, restriction $V_c^* < 0.8$ is not fulfilled even only 1 session is allowed to enter the system. If we weaken this restriction to the restriction $V_c^* < 8$, four sessions can be processed in the system simultaneously for θ equal to 0.8. Situation when restriction $V_c^* < 8$ is not fulfilled even only 1 session is allowed to enter the system occurs for θ greater than 0.98.

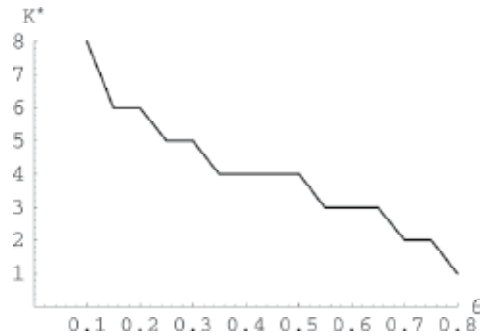


Fig. 5. Dependence of the optimal number K^* of tokens on the parameter θ under restriction $V_c^* < 0.8$

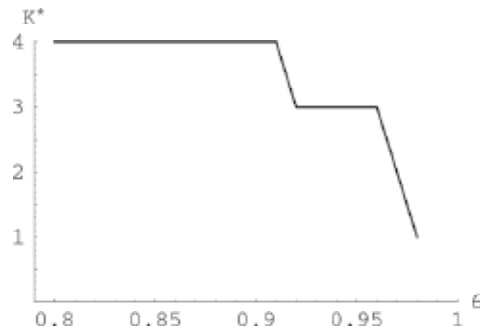


Fig. 6. Dependence of the optimal number K^* of tokens on the parameter θ under restriction $V_c^* < 8$

In the next example, we illustrate the impact of the average arrival rate. We consider the *IPP* process defined above and vary the average arrival rate in the interval [1;11] by means of multiplication of the matrices D_0 and D_1 by the corresponding factor. The service time distribution is assumed to be Erlangian of order 2 with the intensity of the phase equal to 30. Parameter V defining the limiting value of the average sojourn time is assumed to be equal to 4. Figure 7 shows the dependence of the optimal number K^* of tokens on the average arrival rate λ .

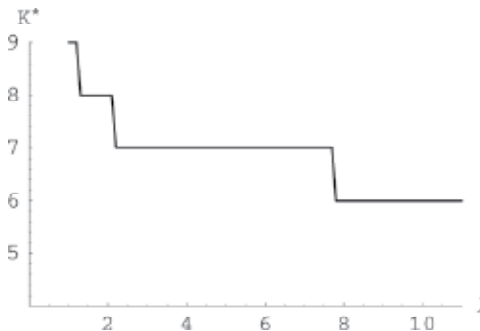


Fig. 7. Dependence of the optimal number K^* of tokens on the average arrival rate λ

As it is expectable, the optimal number K^* of tokens decreases when λ is increasing. The same dependence takes place for other *MAP* s, only the points of the jumps of the lines are different.

In the last example, we illustrate the impact of the average service rate. We consider the *IPP* process defined above having the average arrival rate $\lambda = 1$. The service time distribution is assumed to be Erlangian of order 2 with intensity of the phase varied to get the average service rate in the interval $[3.5;20]$. Parameter V defining the limiting value of the average sojourn time is assumed to be equal to 5.

Figure 8 shows the dependence of the optimal number K^* of tokens on the average service rate μ .

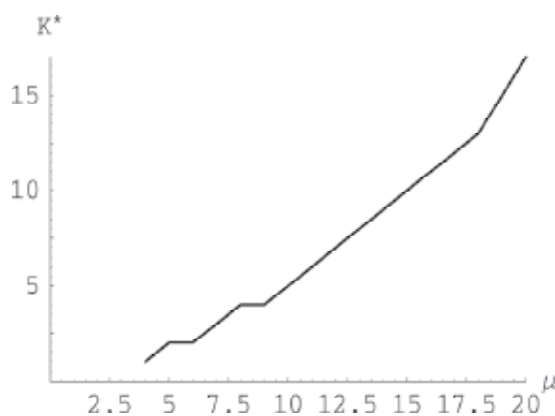


Fig. 8. Dependence of the optimal number K^* of tokens on the average service rate μ

As it is expectable, the optimal number K^* of tokens increases when μ is increasing. The same dependence takes place for other *MAP* s, only again the points of the jumps of the lines are different.

6. Conclusion

In this paper, the novel infinite buffer queueing model with session arrivals distributed in time is analyzed. Ergodicity condition is derived. Joint distribution of the number of requests in the system and number of currently admitted sessions is computed. The sojourn time distribution of an arbitrary request and arbitrary session is given in terms of the Laplace-Stieltjes Transform. Usefulness of the presented results is illustrated numerically. Validity of Little's formulas is checked by means of numerical experiment.

Results are planned to be extended to the systems with many servers, non-geometrical session size distribution, and heterogeneous arrival flow.

Acknowledgement

This work was supported by World Class Univ. R32-2008-000-20014-0 NRF and KRF-2007-521-D00330, Korea.

7. References

- Asmussen, S.; Nerman, O. & Olsson, M. (1996) Fitting phase-type distributions via the EM algorithm. *Scandinavian Journal of Statistics*, Vol. 23, pp. 419-441.
- Chakravarthy, S.R. (2001) The session Markovian arrival process: a review and future work, in: A. Krishnamoorthy, et al. (Eds.). *Advances in Probability Theory and Stochastic Process: Proc., Notable Publications*, pp. 21-49.
- Danzig, D. (1955) Chaines de Markof dans les ensembles abstraits et applications aux processus avec regions absorbantes et au probleme des boucles. *Ann. de l'Inst. H. Poincare*, Vol. 14, pp. 145-199.
- Fisher, W. & Meier-Hellstern, K.S. (1993) The Markov-modulated Poisson process (MMPP) cookbook. *Performance Evaluation*, Vol. 18, pp. 149-171.
- Heyman, D.P. & Lucantoni, D. (2003) Modelling multiple IP traffic streams with rate limits, *IEEE/ACM Transactions on Networking*, Vol. 11, pp. 948-958.
- Kasten, H. & Runnenburg, J. Th. (1956) Priority in waiting line problems, *Mathematisch Centrum*, Amsterdam, Holland.
- Klemm, A.; Lindermann, C.; & Lohmann, M. (2003) Modelling IP traffic using the session Markovian arrival process. *Performance Evaluation*, Vol. 54, pp. 149-173.
- Klimenok, V.; Kim, C.S.; Orlovsky, D. & Dudin, A. (2005) Lack of invariant property of Erlang loss model in case of the MAP input. *Queueing Systems*, Vol. 49, pp. 187-213.
- Kim, C.S.; Dudin, S. & Klimenok, V. (2009) The MAP/PH/1/N queue with time phased arrivals as model for traffic control in telecommunication networks. *Performance Evaluation*, Vol. 66, pp. 564-579.
- Kist, A.A.; Lloyd-Smith, B. & Harris, R.J. (2005) A simple IP flow blocking model. Performance Challenges for Efficient Next Generation Networks. *Proceedings of 19th International Teletraffic Congress*, 29 August - 2 September 2005, Beijing, pp. 355-364.
- Lee, M.H.; Dudin, S. & Klimenok, V. (2007) Queueing Model with Time-Phased Session Arrivals. In: *Managing Traffic Performance in Converged Networks Proceedings 20th International Teletraffic Congress*, Ottawa, Canada, June 2007. Berlin: Springer. *Lecture Notes in Computer Science*, Vol. 4516. pp. 716-730.
- Lucantoni, D.M. (1991) New results on the single server queue with a session Markovian arrival process. *Communications in Statistics-Stochastic Models*, Vol. 7, pp. 1-46.
- Neuts M.F., (1981) *Matrix-geometric solutions in stochastic models*. Baltimore, The Johns Hopkins University Press.
- Panchenko, A. & Buchholz, P. (2007) A hybrid algorithm for parameter fitting of Markovian Arrival Process, in: Al-Begain K, Heindl A, Telek M. (Eds.). *14th Int. Conf. "Analytical and stochastic modelling technique and applications"*. Prague, 2007, pp. 7-12.
- Pattavina, A. & Parini, A., (2005) Modelling voice call inter-arrival and holding time distributions in mobile networks, in: Performance Challenges for Efficient Next Generation Networks - *Proc. of 19th International Teletraffic Congress*, Aug.-Sept. 2005, pp. 729-738.
- Riska, A.; Diev, V. & Smirni, E. (2002) Efficient fitting of long-tailed data sets into hyperexponential distributions, *Global Telecommunications Conference (GLOBALCOM'02, IEEE)*, 7-21 Nov. 2002, pp. 2513-2517.

Telecommunication Power System: energy saving, renewable sources and environmental monitoring

Carmine Lubritto
*Department of Environmental Science,
II University of Naples
ITALY*

1. Introduction

The considerable problems deriving from the growth of energetic consumptions and from the relevant environmental “emergency” due to the emissions of greenhouse gases, push people to find out new solutions and new technologies for the production of primary energy fit for fulfilling the urging and growing energetic demands.

The global climate change, which is due to increased CO₂ and other green house gases concentration levels in atmosphere, is considered one of the most important global emergency that requires immediate and effective policies (IPCC,2007). The CO₂ emissions are mostly due to the use of fossil fuels as energy source. Thus in the future the use of fossil fuels has to be decreased. This can be obtained by improving energy efficiency and by using large scale renewable energy sources.

This is also true in the telecommunication applications, which has seen, in the last years, a remarkable increase in the number of installations present on the whole territory - sometimes located in hardly reachable areas - and the relevant growth of energetic consumptions, because of growing interest about new and reliable services in mobility calls with an increase of the BTS operation hours and traffic management, in order to guarantee the quality of the service anywhere and anytime.

As an example, in the last years the development of the telecommunications sector has resulted in a significant increase of the number of Base Transceiver Station (BTS) on the Italian territory: according to the official database of the non ionizing radiation observatory of the National Agency for Environment (ISPRA,2007), the BTS present in Italy are about 60.000. On the other hand it has been shown (Roy, 2008) that the energetic consumptions of a typical operator network varies between 1.5 TWh to 9 TWh for a year. What is alarming is what we are faced in the future. On the wired line side it is expected a relevant growth of the number of broadband subscribers with a power per subscriber rate that is 4 to 8 times the traditional consumption, while on the wireless side the number of connected device with high speed data services is growing. By extrapolation, it has been estimated (Roy, 2008) that the telecom industry consumed last year about 1% of the global energy consumption of the

planet, that is the equivalent energy consumption of 15 million US homes and also the equivalent CO₂ emissions of 29 million cars.

Therefore, the reduction of the energetic consumptions of a Telecommunications Power Systems represents one of the critical factors of the telecommunication's technologies, both to allow a sizeable saving of economic resources to the mobile communications system management and to realize "sustainable" development actions. In other words improving the energy efficiency of telecom networks is not just a necessary contribution towards the fight against global warming, but with the rapidly rising prices of energy, it is becoming also a financial opportunity.

Therefore clear and defined approaches must be taken to optimize actions of energy savings. A telecom network is just like an eco-system: one cannot just apply any energy savings actions without looking at the impacts on the other system components (Roy, 2008). It has been proposed an "Energy Logic Method" which might be applied to both a wireless and a wired line network. This approach is based on a holistic method to energy savings and provides a complete roadmap of recommendations and quantifies their savings, reviewing also the different impacts.

Starting from these considerations the research project "Telecommunication power systems: energy saving, renewable sources and environmental monitoring" was launched by the Department of Environmental Sciences of the Second University of Naples (DSA-SUN) and the Institute for the Environmental Research (ISPRA), with the participation of the Italian suppliers of mobile telecommunications (H3G, Vodafone, Telecom and Wind) and their technological partners (Ericsson).

The general goal of the research project is to study a set of solutions which may allow:

- a) to obtain a rationalization of the consumptions of a BTS through the intervention on energy saving;
- b) to produce, in the sites where the BTS are located, energy coming from renewable sources - aiming to reduce the emissions of polluting agents in the atmosphere;
- c) to implement intelligent monitoring systems for the energy consumptions and the relevant impacts on the environment.

It has been evaluated, from a technical and economical point of view, the feasibility of some solutions , including:

- Energetic auditing for a radio-telecommunication station in different operational contexts (urban and rural areas, different periods in the year, different working load, etc.);
- Interventions of efficiency and energy saving such as reduction of transmission apparatus consumptions, optimization of air conditioning consumptions, efficiency in the temperature control system;
- Evaluation and development of interventions and technical solutions based on the production of a part of the energy used by radio-telecommunication apparatus, through the use of photovoltaic cells on the infrastructures themselves;

- Analyses of possible uses of other renewable sources (e.g. wind micro turbines) generating energy usable for telecommunication power systems located in areas not reached by the electricity network;
- Analyses of the social and environmental advantages in the introduction of technologies based on renewable sources for covering a part of the energy requirements of radio-telecommunication installations;
- Simulation studies useful to estimate the amount of energy that can be saved using a software system that helps to use the BTS-GSM transmission power in a more efficient way according to the telecommunication traffic features.
- Environmental monitoring of the sites where prototypal solutions has been installed, aimed to compare the conditions before and after the intervention.

2. Wireless network energy consumption

The typical wireless network can be viewed as composed by three different sections:

- the Mobile Switching Center (MSC), that take care of switching and interface to fixed network;
- Radio Base Station (RBS), which take care of the frequency interface between network and mobile terminals;
- Mobile terminals, which is the subscriber's part, normally limited to the handheld device.

It is estimated that over 90% of the wireless network energy consumption is part of the operator's operating expenses (Scheck, 2008).

The key elements are the radio base stations because of the number of base stations is relative high with relative high energy consumption. On the other hand as the number of core network elements is low, the total energy consumption due to core network is relative low. Finally the energy consumption of mobile terminals is very low due to the mobile nature.

With these premises the ways to decrease energy consumptions of cellular network and thus to reduce cost and CO₂ emissions are:

- Minimizing BTS energy consumption;
- Use of renewable energy sources.

Moreover could also be considered a minimization of number of BTS sites in order to reduce energy consumption: in this case the network design play an important role to implement a telecom network with correct capacity and minimum number of sites at optimum locations.

The model used in this paper for a typical Radio Base Station is shown in figure 1. It is the same model analyzed and presented in the literature (Roy,2008; White Paper Ericsson 2007; Lubritto, 2008). Analysing the proposed scheme it result that the system takes 10.3 kW of electricity to produce only 120 watts of transmitted radio signals and to process the incoming signals from the subscriber cell phones, with a total efficiency (output power/input power) of about 1.2%.

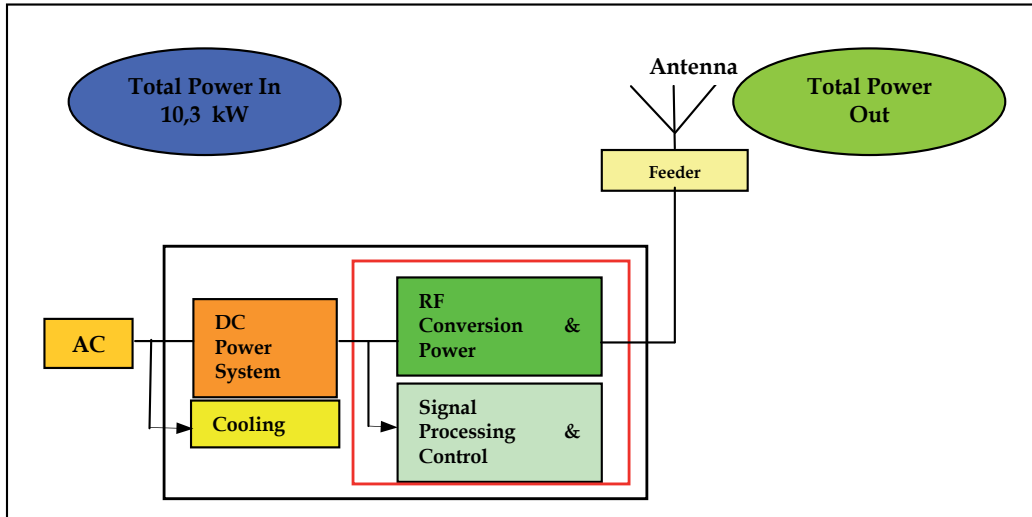


Fig. 1. RBS Block Diagram

In figure 2 is shown the energy allocation per function within the RBS (Roy, 2008). More than 60% of the power is consumed by the radio equipment and amplifiers, 11% is consumed by the DC power system and 25% by the cooling equipment, an air conditioning unit, typical of many such sites. The Radio Equipment and the Cooling are the two major sections where the highest energy savings potential resides.

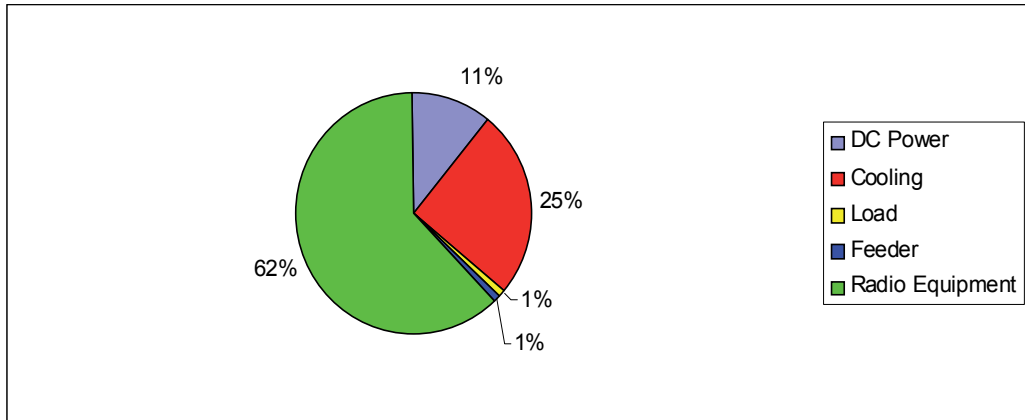


Fig. 2. Percent BTS Energy per function

In the framework of the energy saving, it is very important to consider a cascade effect that represents in aggregate a benefit of 28 times: for example, saving 1W in the feeder cables saves 17.3 watts of modulation and amplification losses, 3.3W of rectification losses and 7.1W of associated cooling energy (Roy, 2008).

2.1 BTS Energy Savings Strategies

In the last years many Energy Savings Strategies for Wireless Network, applied both to the radio equipment and to the cooling and power equipment. have been proposed (Roy, 2008, White Paper Ericsson, 2007; Louhi, 2007; Cucciatti, 2006; Lubritto, 2008)

1. Remote Radio Units: consists in moving the RF converters and power amplifiers from the base of the station to the top of the tower close to the antenna and connecting them via fiber cables. This strategy offers the higher potential energy savings: most radio manufacturers now offer this topology.

2 Radio Standby Mode The second strategy is very easy to implement and typically consists of a software and basic hardware upgrade. Often termed ECO Mode or Power Saving Mode, this strategy consists of turning radio transmitters and receivers off when the call traffic goes down, typically during the night. When the ECO Mode is implemented, the power consumption can be reduced by up to 40% under low traffic. Overall, this strategy will reduce the consumption of the radio equipment between 10 to 20%, plus its associated power conversion and cooling energy requirements. Overall this translates into cascaded savings in the order of 6 to 7%.

3 Passive Cooling The third area of focus is the cooling. Such cooling requires, usually 1/3 of the heat produced inside the RBS. It is also a noisy and maintenance intensive solution. Depending on the geographic location, other cooling techniques such as free ventilation, forced fan cooling with hydrophobic filtering or heat exchangers will change significantly the energy consumption, and often yield a lower total cost of ownership. It is estimated that passive cooling can provide energy savings above 10%.

4 Advanced Climate Control for Air Conditioners If an air conditioner remains necessary, one can minimize its consumption operating at a higher temperature at opportune moments. By doing so, the energy consumption is reduced for two reasons, one that the higher set point means that the unit will be turned on less frequently, and two that it will run more efficiently due to the higher temperature at the air exchange. A total savings of 3-4% can safely be obtained without major availability impacts.

5 DC Power System ECO Mode The last two strategies relate to the DC power plant. Evidently, at this stage, we have already reduced the load through the previous measures and introduced the radio ECO mode to further reduce the load during low traffic periods. An advanced system controller scheme can ensure that rectifiers will operate at their peak efficiency over virtually all conditions

6 Higher Efficiency Rectifiers Last strategy is the use of higher efficiency rectifiers.

When all strategies are considered, total savings above more than 58% are possible (Roy,2008):

- On the radio side, going to a Remote Radio concept and applying the Radio ECO functionality will reduce the energy consumption by 40%.

- On the infrastructure side, the cooling costs can be improved by optimizing the use of the air conditioner or preferably, by migrating to a more passive approach. These will take to down by an additional 3% and 11% respectively, cumulatively down by 54%.
- Finally, the last 4% of reduction will come from the DC plant by implementing energy management to keep the rectifiers at their peak efficiency level and by opting for higher efficiency rectifiers.

In the paragraph 3.2 results of specific studies concerning Radio Standby Mode Strategy will be presented.

2.2 Renewable energy sources

As mentioned above a second way to reduce cost and CO₂ emissions is the evaluation and development of interventions and technical solutions based on the production of a part of the power energy used by radio-telecommunication apparatus, through the use renewable sources (e.g. photovoltaic cells, wind micro turbines or new alternative power based on fuel cells) installed on the infrastructures themselves or usable from off-grid telecommunications power systems. The use of alternative energy sources has been studied in particular for sites that are beyond the reach of an electricity grid, or where the electricity supply is unreliable or sites remote enough to make the regular maintenance and refueling of diesel generators prohibitive (Morea, 2007; Boccaletti, 2007). The choice of alternative energy source will depend on local conditions, BTS typology and energy consumption.

Solar and wind power can provide virtually free energy. Solar power is a mature technology and can be used for low- and medium capacity sites. Apart from having very low environmental impact, solar-powered sites also have the advantage of being very low-maintenance, with a technical lifetime of 20 years or so, and much more reliable than diesel generator-powered systems. Also, solar power scales with the load, so the size of the solar installation can be matched to actual needs without unnecessary capacity.

On the other side a micro-wind turbine can support a traditional RBS site without too large impact on cost, where on average a wind velocity is about 5 m/s. In most case a hybrid solution combining of solar and wind is the actually the most feasible solution for autonomous BTS site. Anyway the size of solar cell and wind turbine have to be defined based on BTS load and on-site availability solar and wind. In the paragraph 3.4 a typical hybrid solution for off-grid BTS is presented.

Finally fuel cells are increasingly being considered as a viable alternative site energy solution for telecoms. They can be deployed in place of diesel generators, and partly replace batteries, at remote sites with long back-up requirements. In addition to improving energy efficiency, they can also improve network up-time and reliability. Moreover environmental advantage in terms of special waste disposal will be obtained by using fuel cell in substitution of backup battery.

3. Telecommunications power systems and energy saving

Energetic auditing of a BTS is the most important step in the understanding of energy management of wireless telecommunication power system. With this aim it has been realized a campaign of measurements for a radio-telecommunication apparatus starting from on-site measurements, performed in collaboration with Italian companies of mobile communications systems (Vodafone, H3G, Telecom and Wind), which take into account different technologies (GSM, UMTS, DCS+GSM+UMTS), different typologies of apparatuses (outdoor, room, shelter), different locations (North, Centre, South of Italy) and different working loads.

Thanks to the collaboration of the Italian mobile telecommunication providers, it has been possible to retrieve data coming from a statistic sample of around 100 radio base stations located on the whole national territory, that corresponds to more than 1000 monitoring days. All the field measurements are performed by using specific monitoring systems (Pizzuti, 2008).

For carrying out the statistic analyses and the correlations we considered separately the following characteristics of the systems:

- Systems typologies (Shelter, Room, Outdoor)
- Systems technologies (UMTS, GSM, DCS)
- Localization (North, Centre and South)

and the following functioning parameters:

- Energy consumption (Wh)
- Instantaneous Power (W)
- Internal temperature (°C)
- External temperature (°C)
- Phone traffic for cells (erlang)

A specific database has been built containing all data related to: energetic consumptions, BTS localization, typology and technologies, environmental parameters.

3.1 Energetic consumptions associated to a radio base station

Aim of our studies is to find statistic correlations between the energetic consumptions and the operational parameters of the BTS. Moreover we are interested to study both the energetic consumption correlated to the transmission function of the apparatuses and the energetic consumptions related to the cooling of the equipments and infrastructures. To achieve this goal, we made statistical analysis by using the software "R" of the "R-Foundation for Statistical Computing" R-foundation for statistical computing" (www.r-project.org/foundation/).

From these analysis one can establish the following:

- The average yearly consumption of a BTS is ca. 35500 kWh compatible with the average consumption of 10 Italian families. If we consider that in Italy there are 60.000 BTS (data 2007 coming from the NIR Observatory - ISPRA), the total average yearly consumption of all the BTS systems present in Italy is ca. 2,1 TWh/year; which is the 0,6 % of the whole national electrical consumption (data source: TERNA 2007). In terms of economical and environmental impact, the data correspond to ca. 300M€ yearly energy costs and ca. 1,2 Mton of CO_{2eq} emitted in the atmosphere every year.

- If we carry out analyses on the average energy consumptions associated to the different technologies, we will note that the GSM energy consumptions are considerably higher than the UMTS technology - as it is expected because of the different mode of operation of the two technologies (Table 1)

Energy Consumption/technology		
Technology	kWh/day	kWh/year
UMTS	72,97	26268
GSM	111,35	40085

Table 1. Energy consumption for GSM and UMTS technology

- To evaluate the daily energy consumptions and the contributions due to the transmission and air-conditioning, in the following graph is represented the daily trend of the energy consumptions of a BTS. We can clearly distinguish two different trends: a constant energy consumption value of about 800Wh for the nighttime and the morning, and an oscillating trend, with an average value of about 1100Wh for the hottest hours and the late evening. This trend is comprehensible if we consider that in the first case the consumption is due only to the transmission functions (constant trend), whereas in the second case at the transmission functions are added the conditioning energy consumption, with a “saw tooth” trend generated by the switching on/off of the air-conditioning systems. We can therefore divide the energy consumptions in two contributions; i.e.: approx. 2/3 of the consumed daily energy are due to the transmission, whereas 1/3 of the energy is used for feeding the conditioning systems.

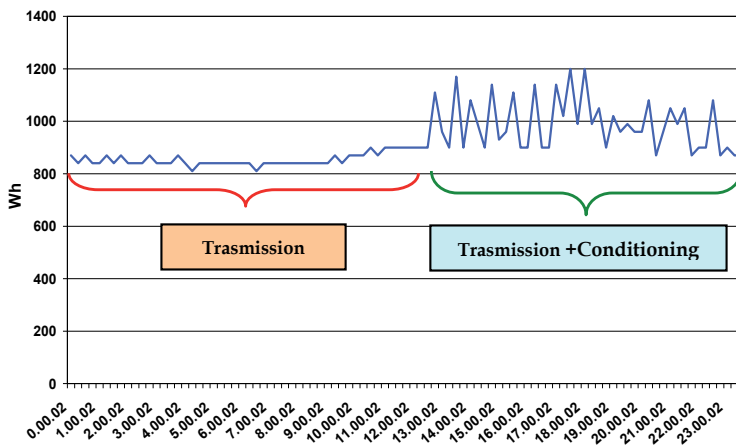


Fig. 3. Daily Energetic Consumption of a BTS

In order to verify our latter statement in figure 4 we show the power distribution considering four selected days:

- 15th December 2007: it represents the coldest day during the monitoring period in which the internal temperature ranges from a minimum of 2,8°C to a maximum of 9,5 °C (the blue line);
- 19th December 2007, it represents a typical day of the coldest period in which the temperature ranges from a minimum of 7,0°C to a maximum of 17,6 °C (the violet line);
- 24th May 2008, it represents a typical day of the hottest period in which the temperature varies from a minimum of 15,5°C to a maximum of 37,3 °C (the green line);
- 27th May 2008, it represents the hottest day of the monitoring period in which the temperature ranges from a minimum of 21,8°C to a maximum of 42,5°C (the red line).

There is a clear difference among the distribution functions on the coldest days (blue and violet line), in which the instant power is presumably due only to the transmission function and show a peak in correspondence of defined power values, and the distribution functions on the warmest days (red and green lines), in which there are both the transmission and air conditioning contributions .

In this way we can esteem an energetic consumption connected to the transmission functions and another connected to the air-conditioning functions which are 2/3 and 1/3 of the total energetic consumption, respectively.

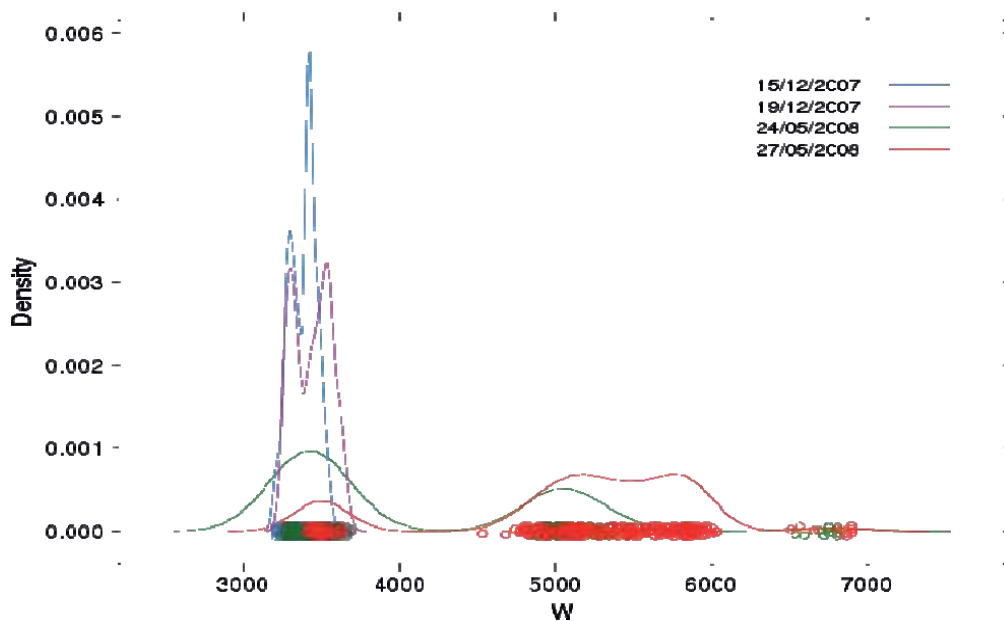


Fig. 4. Density of states plotted as a function of power distribution

In figure 5 we plot the variation of the energetic consumptions versus the external temperature, for different BTS typology (shelter, room, outdoor) and BTS technology (UMTS and GSM).

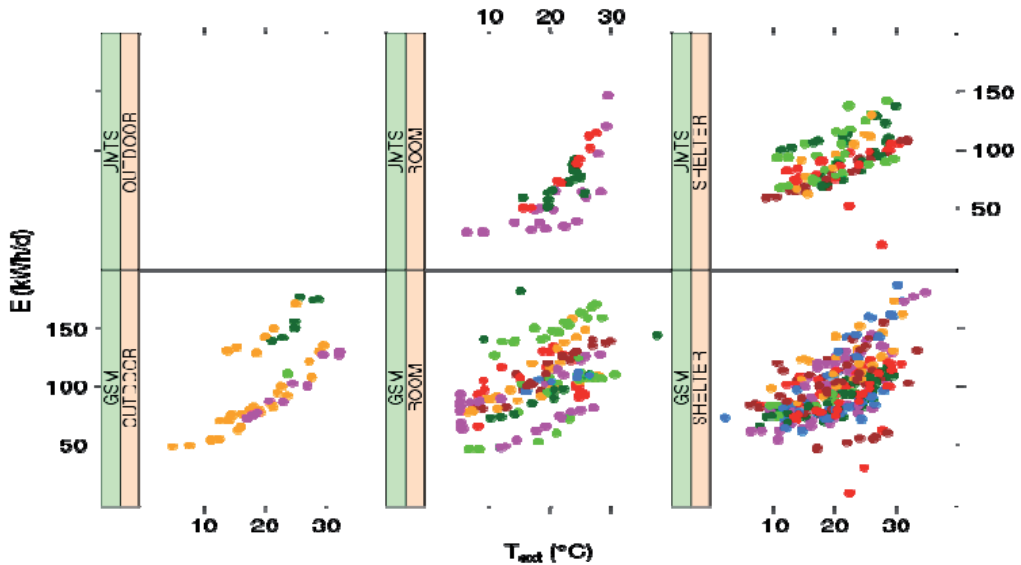


Fig. 5. Energetic Consumption versus external temperature

A “universal trend” of the energy consumption versus the temperature is discovered independently both from the technology used and from the typology of BTS. Furthermore the higher dispersion of the consumption data in the room and shelter typologies, in comparison with the outdoor one, can be comprehensible if we consider that in the first two cases there is a higher thermal dispersion - with a consequent increase of the consumptions - which is needed to air-condition the equipments as well as the environment where they are implemented.

In figure 6 we plot the energy consumptions as a function of a different time of the year, for different BTS technology (GSM and UMTS) and BTS typology of site (outdoor, room, shelter). First of all we find a similar behaviour during the months with a greater energetic consumption in summer respect to the winter, as expected.

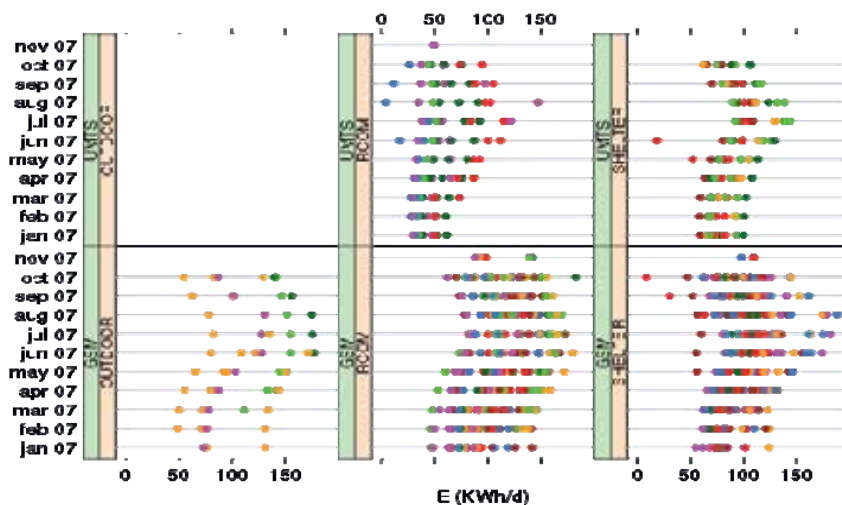


Fig. 6. Energetic consumptions versus. time of the year

Moreover comparing the graphs for the room and shelter typology, it is clear that the UMTS technology has on average lower energetic consumption of GSM technology, because of the different characteristic of the mobile communication standards. No difference was found for energetic consumptions versus the time of year for the three BTS typologies.

For understanding an eventual correlation between the energy consumptions data and the numbers of phone calls of a BTS, we show in figure 7, the energy consumptions as a function of call traffic (in erlang). There seems to be no correlation between these two parameters; that means that at the moment any intervention which may regulate BTS turning on/off when the call traffic goes down, is realized.

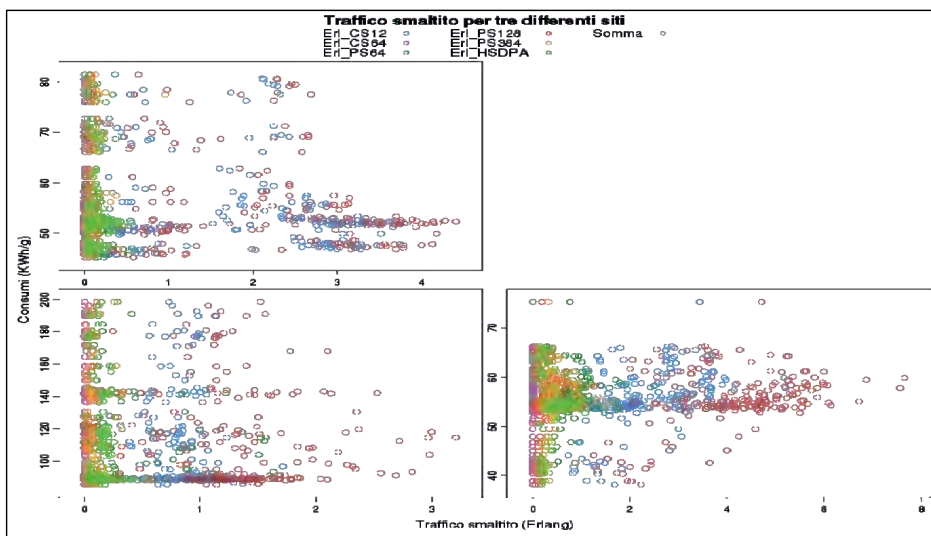


Fig. 7. Energy consumption vs traffic for three different sites

3.2 Energy saving

Starting from the statistical analyses on the BTS energy consumptions, it is useful to study the possible interventions for optimizing and saving energy consumptions. Our aim is to individuate useful interventions both for saving action on conditioning systems and on transmission consumption.

Regarding the saving of energy consumptions relevant to the air-conditioning we studied two possible intervention strategies; the first one was based on "intelligent" algorithms for the optimization and dynamical regulation of the air-conditioning functions, the second one was founded on the local cooling of the single electronic equipment, avoiding to air-condition the environment where they were located. Both hypotheses were based on the fact that inside the shelter the thermo-dynamic parameters (temperatures, humidity, etc.) can assume values ranges larger than in areas frequented by people. Therefore both the use of air-conditioning intelligent systems and the local cooling technologies are useful strategies for saving energy, basing on the possibility to eliminate useless conditioning actions of the environment and mechanical parts. One can estimate that such interventions can achieve an energy saving from 5% to 10% of the air-conditioning consumptions.

For optimizing the consumptions coming from the transmission functions we studied and tested a software feature launched by Ericsson that helps to use the BTS-GSM transmission power in a more efficient way (Hjorth, 2008). These algorithms can correlate the phone traffic of a BTS and the energy consumptions. During periods of low network traffic, the feature effectively puts transceivers that are not being used in standby mode - overcoming the traditional practice of having radio equipment continually turned on, which results in energy being wasted.

Depending on the network traffic pattern, the feature algorithm parameter settings and on the type of apparatus, this innovation can save between 5 and 20 percent of the energy per BTS when a base station is in use, while still providing the same services and quality to end users.

The study has been carried out with a two fold approach:

- The direct investigation of test BTS in order to have direct hints about the feasibility of the project, the practical problems, and the real savings. To reach this goal on field measurements have been carried out in an operating BTS during periods in which the feature was either activated or not activated.
- However, it is not feasible and practically unreliable to explore all the BTS power consumption and to measure the power saved with different configurations of the feature algorithm. Thus a simulation study has been carried out. The best parameters ensuring good communications and best savings have been pointed out.

A comparison between on field measurements and simulations have been realized, in order to optimize the parameters used in the "BTS power saving algorithms".

Parameters useful in this kind of analysis are telephone traffic, BTS typology and location, number of transmitters. Measurements of energetic consumptions and other environmental parameters have been realized in a suburban BTS (provider Telecom Italia Mobile) located in Agliana (Toscana), composed by 3 GSM transmitter and 3 DCS transmitter. On this BTS the "power saving" function has been activated as experimental on field test of "power saving algorithms"

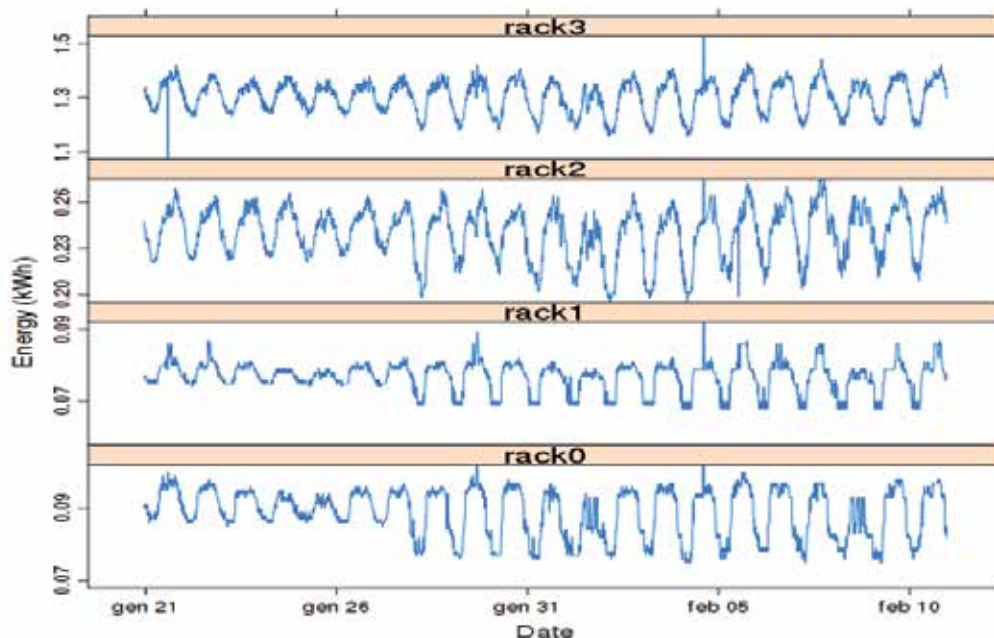


Fig. 8. BTS energetic consumption at the experimental site - Agliana

The results obtained by our monitoring are presented in the following figure 8, where we reported the energy consumption of the basic radio station for three weeks; in two of those

was activated the “Power Saving” function. Rack 0-Rack 2 represents the energy consumption of each DCS transmitter, Rack3 shows the energy consumption of all GSM transmitters. It is clear that average value of energetic consumptions are lower in the days in which the power saving function is active: a decrease of more than 10% of energetic consumption is evident starting from the second period.

In the following graph (figure 9) it is presented the measured energy in the same day of the week (Thursday), in the condition of power saving function ON (red line) and OFF (blue line).

The considerable energy saving achieved during the nighttime - when the call traffic goes down and the “power saving” algorithm can switch off many transmission supporters - is here very remarkable. On the contrary, during the daytime, the curves trend coincides, since the high traffic does not allow the switch off of any transmitters.

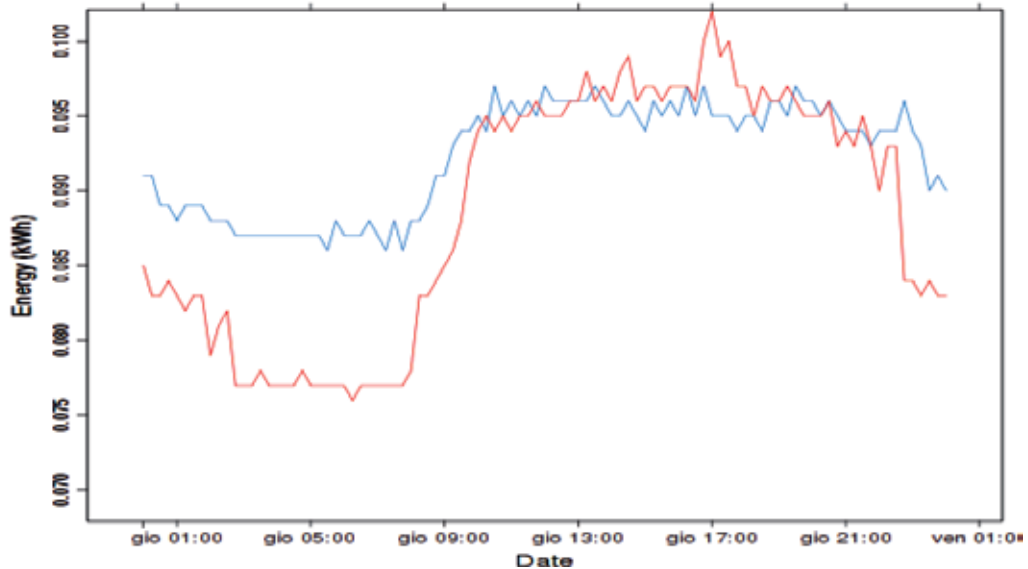


Fig. 9. Comparison of the measured daily energetic consumption in a day with Power Saving ON (red line) and OFF (blue line).

The data of the experimental measures have been compared to the simulation analyses realized through a specific software which has been implemented (Lubritto,2009).

The simulation software takes as input the available measured data (average number of telephone calls started every ten seconds, the average length of calls, the cell parameters, the parameters of the Power Savings algorithm) then it uses a Montecarlo algorithm for simulation of telephone traffic.

The number of calls started every 10 seconds is supposed to follow a Poisson distribution with a varying average value during the day. Length of calls follow an exponential distribution with a given average. Both average values, measured every hour, are taken from the collected data. The convolution of the two distributions gives the number of active calls for any given time. However, the maximum number of calls in the cell is fixed by the number of channel available.

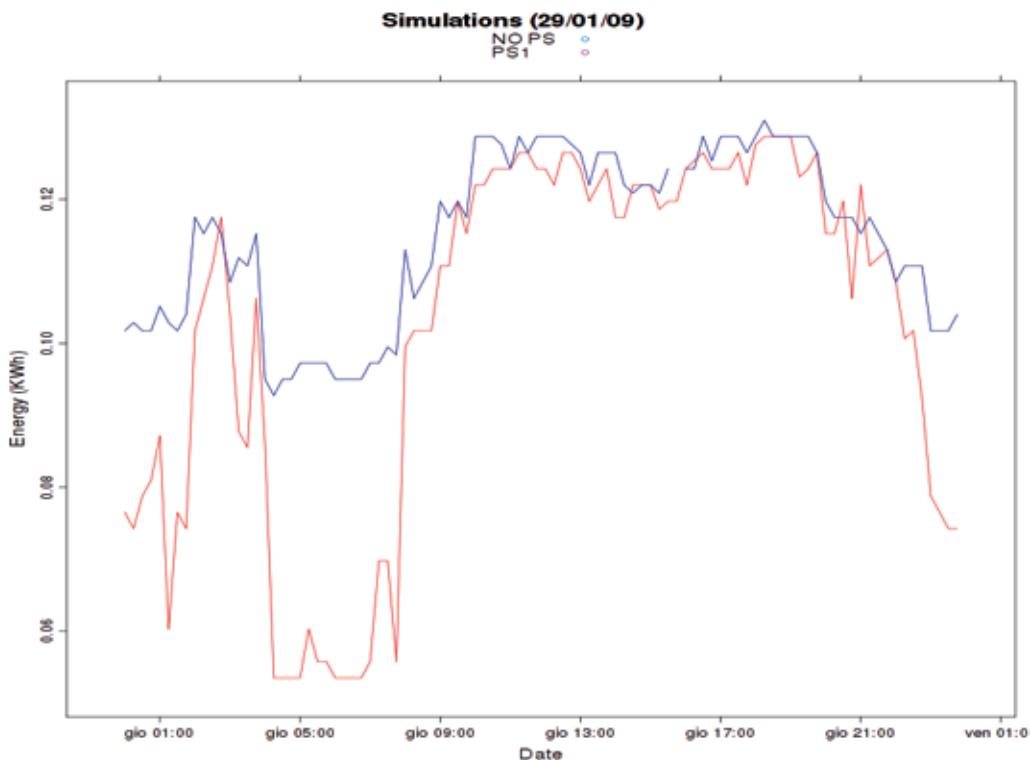


Fig. 10. Comparison of the simulated energy consumption in a day – with (red line) and without (blue line) Power Saving features on.

In the above figure 10 we reported the values obtained by the simulation in a day; the blue lines indicate the consumptions without Power Saving and the red lines indicate the activation of the Power Saving. As it is evident, the simulation software faithfully reproduces the data achieved by the field measurements.

The similarity with on field measurements is acceptable: here too the savings are evident in periods of low traffic when there is the possibility to switch off the unused channels, as for the measured data.

After established the goodness of the simulation algorithm, we can analyze the Power Savings optimization parameters. In such a way we address the set of parameters giving the maximum power saving, and thus lower environmental impact, while still guaranteeing the communication quality.

The study has to be carried out with the following criteria:

- [1] the intervals were chosen to cover the entire space of the suggested parameters;
- [2] for each set of parameters were we took an average of many runs;

The resulting optimal set of parameters depends on the average communication load and available channels, so should be site specific or at least cover "classes" of sites, with similar load and operating behaviour. Optimal parameter sets for the sites under survey have already been created, and an improvement in energy saving of about of 3% is expected.

The saving obtained through the introduction of the “Power Saving” algorithms might change from 10% up to 15% of the transmission consumptions, according to the typology and the location of the basic radio station. With the same algorithm we succeeded in obtaining the Power Saving parameters set that maximizes the energy saving, increasing it of a further 3%.

In conclusion, if we sum up the contributions of the energy saving to the air-conditioning functions and the transmission functions, – considering the feedback processes of the two components – we obtain a total yearly energy saving of 20% of the total consumptions (i.e. 7000 KWh per year) with an economical advantage of approximately 1000 €/year saved for each BTS, that means a further environmental advantage in avoiding to emit, for each year and BTS, 4 Ton of CO_{2eq} in the atmosphere.

4. Telecommunications power systems and renewable energy

In order to introduce clean technology in the telecommunications power system management, one has to consider the use of renewable sources technologies (photovoltaic, wind, hybrid systems) installed on telecommunication systems infrastructures. We analyzed the most advanced technological solutions in the photovoltaic sector (single crystal, multi-crystal panels, amorphous silicon, thin films) and in the further renewable sources, useful for producing the energy in situ in consideration of the functioning conditions and the structural features of a radio-telecommunication station.

We chose to analyze the interventions in locations with different testing conditions for each provider, in order to plan and realize photovoltaic systems for basic radio stations in urban and rural areas (raw-land), to forecast the use of combustible cells for substituting the batteries of a microcell site and to analyze the use of different renewable sources for grid-off BTS (not connected to the electrical net), fed by generators

Therefore it has been realized an experiment in which use of photovoltaic systems and other renewable sources for different typologies of contexts (urban and rural areas) and for apparatuses not reached by the electricity network (stand-alone apparatuses), has been tested.

Two rural sites in which a photovoltaic plant has been built in with provider Vodafone, in order to understand how to use infrastructure of the BTS to obtain a total or partial architectural integration of the photovoltaic plants on the shelter or support pole. It has been shown that their energetic productivity depend on the geographical location, on the surface available to implement the photovoltaic plants and on the effects of shadow.

In two of these pilot sites, photovoltaic plants have been realized both on shelter and on the infrastructures; the area of PV modules varies from 16 to 20 m², limited by the available site space, to guarantee a production of 2.0 and 2,5 kWp. Figures 11 and 12 show the installation on the two sites.



Fig. 11. Photovoltaic system installed on the BTS infrastructure (Vodafone)



Fig. 12. Photovoltaic system installed on the BTS infrastructure (Vodafone)

These sites came into operation on 01/01/2008 and, according to data provided by VODAFONE the two photovoltaic systems have produced, up to 30/05/2008, respectively 1100 and 1200 kWh; this implies an annual estimated production of 2640 and 2880 kWh. A further important element of the application - made by the involved provider - was to activate and complete the whole proceeding in order to obtain incentivizing by Italian electricity Authority (i.e. "Conto Energia" fund). It is to be noted that such an application gives an environment advantage of approximately of 3 Ton of not emitted CO_{2eq} /year for each BTS, apart all reduction of the pollution coming from further physical agents.

In order to carry out specific controls on these pilot sites and to be able to compare the conditions of energetic consumption pre and post installation of the photovoltaic panels, a

monitoring station has been used that allows to check operational parameters such as electric consumption, external and inside temperature and other environmental parameters. On these same sites we studied further technological solutions in the photovoltaic field. In particular very important is to evaluate the possibility to implement further photovoltaic technologies (amorphous, thin film) and to evaluate the technical feasibility and the investment advantage for each solution.

A very convenient and realistic solution – from the technical and commercial point of view – apart from the use of single and multi crystal panels - is the usage of panels based on the amorphous and thin film.

In the amorphous solution one can consider an efficiency of about half of the crystalline, well compensated by an implementing cost of 70% less than the crystalline solution. Using the aforementioned option we get a 6 years payback time.

In the case of the thin film solution, we have to consider a reduction of efficiency of approx. 10% less than the amorphous solution. Furthermore the considered (sub-vertical) exposure affects the energy production reducing it of the 30%. Beside this negativity, we noticed a net gain in the installation costs, which is ca. 55% higher than the crystalline solution. Finally, we could calculate the GSE government incentive basing on a system architectonically integrated. With these hypotheses there would be 6 years payback time.

In general, in order to implement photovoltaic energy systems for feeding radio base stations in a total or in a partial way in urban areas one have to take into account the presence of obstacles which could cause shadowing effects and the real presence of useful areas.

A very interesting application of renewable energy source with telecommunication systems sector is the situation when BTS is located far from the electrical network (grid-off systems). In order to analyze innovative technologic solutions for producing energy close to the BTS, we used as experimental site the BTS located in Sardinia on Gardaininu Mount (Nuoro, provider TIM), for which to completely fulfill the BTS energetic requirements (approx. 35500 kWh a year), we considered to implement a micro-wind system (overhead generators with an energy power up to 20 kW) coupled to a 4.5 kW photovoltaic system. Therefore it is convenient to implement an hybrid solution composed by :

- a photovoltaic system with panels mounted on a support between the transmission tower and the south side of the external border, since we noticed an available surface of ca. 50 m² was present;
- a micro-Wind system (power of 20kW), for which one can estimate energy production starting from wind average speed and hours of productivity in the specific site;

In the aforementioned site in Sardinia, the annual average speed of the wind is 5 m/s (CESI Wind Atlantis,2007) and the annual productivity is 2000 hours. Consequently electric energy power production is 31567 kWh, and, the payback time is little more than 5 years.

5. Telecommunications power systems and environmental monitoring

In the framework considered in the present chapter, it becomes very important to study the relation between energetic aspect, environmental impacts and radio-telecommunication power systems.

One can consider at least three different relevant contexts:

- Impact of BTS on the landscape
- Electromagnetic pollution generated by the BTS

- Environmental impact coming from further polluting agents (emission of greenhouse gases, noise, etc.)

Regarding the impact on the environment, it is fundamental to build BTS integrated in their territorial context. The possibility to use the structures of the plants (support poles, shelter, etc.) in order to realize energy production systems deriving from renewable sources could be an useful way to satisfy such request. It is evident that up to now such problems have not been faced, but we believe it essential to define the right prescriptions in order to minimize the impact of the BTS on the environment and, at the same time, to implement innovative power energy solutions.

Besides, the possibility to decrease the emission quantity of the greenhouse gases deriving from the BTS functioning is strictly joined to the introduction of the distributed production system of renewable energy. In fact, the use of solutions based on renewable energy, especially in grid-off conditions, can considerably reduce the impact on the environment caused by the station and the feeding generators management. The usage of a micro-wind or photovoltaic systems may avoid the implementing of feeding systems - which should be fed with fuel every day with the relevant high use of vehicles. That would mean a remarkable reduction of the emissions in the atmosphere.

Even more important is the impact on the environment and on the population of the electromagnetic fields generated by the transmission systems. Especially during last years, such a problem has attracted the attention of single citizens and of the entire civil community, because of the considerable diffusion on the territory of low frequency electromagnetic fields sources (power lines) and of high frequency sources (radio-television stations and mobile phone stations). From a technical point of view, we should note that the field level in an area can considerably change according to the status of the existing transmitters, to the emitted power (at its turn variable according to the users' need) and to the further territorial characteristics, such as the presence of buildings and/or other obstacles which determine reflections/refractions changeable in time. Basing on these premises and considering the hypothesized energy power saving strategies, we evaluated the feedback on the minimization of the electromagnetic fields emitted by the BTS. It is easy to understand that the use of a "power saving" system can give a valid contribution to the reduction of the BTS emissions. In fact, switching off the transmitters when the traffic goes down, means to get a null emission of the electromagnetic fields and a reduction of the daily average value emitted by the radio base stations. If we consider that, following to the activation of the "power saving" algorithm there is a switch off of 70% of transmitters during nighttime (from 24 to 8), we can estimate a daily average reduction of the electromagnetic emissions of 15-20%.

Acknowledgments

I would like to thank my colleagues and collaborator (in no particular order)- Salvatore Curcuruto, Antonio D'Onofrio, Antonio Petraglia, Carmela Vetromile, Maria Logorelli, Giuseppe Marsico, Floriana Caterina, Laura Miglio - for fruitful discussions and for the many hours of working together on research project. This research project has been funded by ISPRA.

6. References

- Boccaletti C.; Fabbri G. & Santini E. (2007). *Innovative Solutions for Stand Alone System Powering*, *Proceedings of INTELEC*, pp. 294-301, 978-1-4244-1628-8, Rome (Italy), September 2007, IEEE, Rome
- Efrainsson L. (2008). *Halve the Power Related Costs for a Cluster of Diesel – Fed Telecom Sites*, *Proceedings of INTELEC*, pp. 397-400, 978-1-4244-2056-8, San Diego (CA), September 2008, IEEE, San Diego
- Hjorth P. ; Lovehagen N. , Malmodin J. & Westergren K. (2008). *Reducing CO₂ Emissions from Mobile Communications – BTS Power Savings and Tower Tube*, *Ericsson Review* n. 1,
- Ikebe H. ; Yamashita N. & Nishii R. (2007). *Green Energy for Telecommunications*, *Proceedings of INTELEC*, pp. 750-755, 978-1-4244-1628-8, Rome (Italy), September 2007, IEEE, Rome
- IPCC, Fourth Assessment Report (AR4) *Climate Change 2007 – International Panel of climate Change*, 2007
- ISPRA, Non Ionizing Database - *Italian Agency for Environmental Protection*, 2007
- Louhi J. T. (2007). *Energy Efficiency of Modern Cellular Base Stations*, *Proceedings of INTELEC*, pp. 475-476, 978-1-4244-1628-8, Rome (Italy), September 2007, IEEE, Rome
- C. Lubritto, A. Petraglia, C. Vetromile, F. Caterina, A. D’Onofrio, M. Logorelli, G. Marsico, S. Curcuruto “*New Energy*” for Telecommunications Power System in *Proceedings of INTELEC*, pp. 443-445, 978-1-4244-1628-8, Rome (Italy), September 2007, IEEE, Rome
- C. Lubritto, A. Petraglia, C. Vetromile, F. Caterina, A. D’Onofrio, M. Logorelli, G. Marsico, S. Curcuruto “*Telecommunications power systems: energy saving, renewable sources and environmental monitoring*”- in *Telecommunications Networks*, *Proceedings of INTELEC*, pp. 120-126, 978-1-4244-2056-8, San Diego (CA), September 2008, IEEE, San Diego.
- C. Lubritto, A. Petraglia, C. Vetromile, F. Caterina, A. D’Onofrio, M. Logorelli, G. Marsico, S. Curcuruto, L. Miglio, F. Cenci “*Simulation analysis and test study of BTS power saving techniques*” – Extended Abstract INTELEC 2009 – 18-22 /October/2009 Incheon South Korea.
- Masone M. (2007). *Environmental Certification for Service Networks and Data Centers*, *Proceedings of INTELEC*, pp. 756-759, 978-1-4244-1628-8, Rome (Italy), September 2007, IEEE, Rome
- Morea F. ; Viciguerra G. , Cucchi D. & Valencia C. (2007). *Life Cycle Cost Evaluation of Off-Grid PV-Wind Hybrid Power Systems*, *Proceedings of INTELEC*, pp. 439-441, 978-1-4244-1628-8, Rome (Italy), September 2007, IEEE, Rome
- Pizzuti F. ; Rega G. & Grossoni M. (2008). *Site Power Saving*, *Proceedings of INTELEC*, pp. 84-89, 978-1-4244-2056-8, San Diego (CA), September 2008, IEEE, San Diego.
- Roy S. N. (2008). *Energy Logic: A Road Map to Reducing Energy Consumption in Telecommunications Networks*, *Proceedings of INTELEC*, pp. 90-98, 978-1-4244-2056-8, San Diego (CA), September 2008, IEEE, San Diego
- White Paper Ericsson (2007). *Sustainable Energy Use in Mobile Communications White Paper EAB-07:021801 Ericsson AB 2007*.

Propagation Models and their Applications in Digital Television Broadcast Network Design and Implementation

Armoogum V., Member IEEE, *University of Technology, Mauritius*
Soyjaudah K.M.S., *University of Mauritius, Mauritius*
Mohamudally N., *University of Technology, Mauritius*
Fogarty T., *London South Bank University*

1. Introduction

In this work, we will discuss the importance of propagation models when designing new broadcast networks. We will hence consider the Island of Mauritius as a case study. Mauritius is a tropical island, located in the Southern Hemisphere with geographic coordinates 20° 17' S, 57° 33' E and has two climates. A humid and subtropical climate dominates and becomes more effective below the 400-meter level on most of the south-eastern side of the island as well as below 450 meters on the leeward side. Above these altitudes, the climate is more temperate (Metz 1994). The island has two seasons. Summer is hot and wet and lasts from November to April. The warmest months are January and February with average temperatures of 35 °C in the lowlands and 32 °C on the central plateau. The problem with warm weather is that cyclones are frequent. Cyclones, with strong winds and heavy rain, can occur between November and April. Mauritius will normally experience about three or four cyclones a year during this period, each usually lasting two to three days. Winter season, which is influenced by the south-east trade wind, is from May to October. During this period the weather is cool and dry. The average temperature is 22 °C in the lower parts of Mauritius and 16 °C on the plateau and Plaines Wilhems. Rainfall ranges from 90 cm per year in the western lowlands to 500 cm in the central plateau with an average of 200 cm per year overall (Metz 1994). Humidity is frequently high in Mauritius and is above 80% in the south and the central plateau. Hence, the effects of climate can be investigated to know the degree of signal degradation.

The original motivation for this work came from a report by Pather (2000), in which he described the penetration of digital television in Mauritius and how this would affect the life of people. He predicted at that time that analogue television broadcasting would become part of history and hence there would be no alternative than to venture within the digital arena. He added that interactive digital television and T-Services would form part of everyday life, as was the case for NTSC, SECAM and PAL fourty years ago. This new technology would give better quality of service (QoS) and would be more economical.

Since the first proposal in 1990 for digital systems by General Instrument Corporation (GIS: Company History online n.d.), there has been significant development in this area. The United States, Europe and Japan developed their own standards between 1993 and 1994. In this work we constrain our attention on the DVB-T standard used in European countries and in Mauritius. The DVB-T standard was produced in 1997 following several measurements and testing by various projects. Digital television is now an integral part of the information superhighway that is being built to deliver large amounts of information at very low cost compared to analogue technology and can be fully integrated into completely digital transmission networks. Digital television can deliver more programs than traditional analog television over one transmission channel and can be manipulated and treated in various ways which were never possible with analog television. We can therefore store digital images on computers and discs and play them continuously over digital networks without signal degradation until a certain threshold value is reached. Pictures can be modified, compressed, stored and transmitted. One advantage of the digital format is that it can be integrated with telephone conversations as well as computer data and then transmitted from one network to other broadcast networks. Furthermore, any program can be stored on multimedia servers (soap and movie, fillers and jingles, advert, songs) and retrieved instantly for broadcast to a single or multiple viewers on demand. However, having good Quality of Service (QoS) and cheaper services do not mean that the problems of transmission and reception of digital signal broadcasting are completely solved. A correctly-formatted DTV signal is exposed to various factors which can detriment the sound or picture quality before it reaches the intended customers. For that reasons, many organizations and researchers are working on various areas such as transmitter and antenna models, propagation and coverage failures, compression techniques and standards in order to overcome implementation problems in view of setting frameworks and standards for digital television implementation. In this study, we constrain our attention to propagation models, coverage areas and failures.

2. Problem Statement

Following the liberalisation of the airwaves by the Government of Mauritius in 2002 and the official launching of digital terrestrial television in October 2005, there are now more private radio companies and will, in the near future, be more private television companies operating in the country. The digital TV (DTV) signal, just like the analogue signal, suffers from noise giving rise to problems such as 'ghosts' or tidal effects. A decoder in general is able to tolerate loss in field strength. Independently of the threshold noise level that the decoder can tolerate, our aim is to design a propagation model such that the signal despite suffering from maximum attenuation does not go below the threshold level for the decoder, as once the bit error rate crosses 2×10^{-4} , a total loss of signal is obtained. The digital coverage, therefore, has to be studied to obtain good QoS.

In the coming decades, the number of channels which will beam into homes and the number of potential signal paths to the consumer will multiply. Due to a more sophisticated multi-channel environment, there will be an even larger number of separate processes and switching stages through which a radio or television signal will pass and, at any moment, one signal may fail or detrimentally affect the picture or sound quality. Hence, the opportunity for faults and failures occurring between the broadcaster and the consumer is

increasing. It will become more and more difficult for a broadcast engineer to know whether a signal, after passing through all these separate processes and transmission paths, will reach the consumer in a correct audio and picture format. An alternative solution to the problems needs to be found.

3. Propagation Models

3.1 Overview

The common approaches to propagation modelling include:

- (i) Physical models
Physical models of path loss make use of physical radio waves principles such as free space transmission, reflection or diffraction.
- (ii) Empirical models
Empirical models use measurement data to model a path loss equation. Examples of empirical propagation models include the ITU-R and the Hata models. Empirical models use what are known as predictors or specifiers in general statistical modelling theory (Saunders 2005). To conceive these models, a correlation was found between the received signal strength and other parameters such as antenna heights, terrain profiles etc through the use of extensive measurement and statistical analysis.

Prediction of path loss is an important element of system design in any communication system. In the radio and TV broadcast systems, the prediction of path loss is very important as the environment is constantly changing with time. The question that is always asked is how to calculate the path loss with maximum accuracy. One solution is to use a propagation model. A reliable propagation model is one which calculates the path loss with small standard deviation. This will, hence, help network engineers and planners to optimise the cell coverage size and to use the correct transmitted powers. Suitable models must be chosen for prediction. An accurate and reliable prediction method helps to optimize the coverage area, transmitter power and eliminates interference problems of other radio transmitters. All the prediction methods are divided into empirical and deterministic/physical models.

The choice of the coverage prediction model depends on the propagation environment and the coverage area. In communications, propagation takes place through multiple diffraction, reflection and scattering among others from an extremely large number of objects. Since it is very difficult to locate scatterers deterministically, characterisation of the signal within the coverage zone is done statistically. For this reason, prediction models have been developed using empirical or statistical methods. The accuracy of a particular model in a given environment depends on the fit between the parameters required by the model and those available for the area concerned (Rama Rao et al. 2000). Examples of these models are Ikegami (Tapan et al. 2003), Ibrahim and Parsons (Tapan et al. 2003), Free-Space (Friis 1946 cited in Saunders 205 and Tapan et al. 2003), Extended COST-231 (COST 231 Final Report 1999 cited in Tapan et al. 2003), Perez-Vega and Zamanillo's model (Perez-Vega and Zamanillo 2002), Plane Earth Loss (Perez-Vega and Zamanillo 2002), Hata model (Hata 1980), Lee model (Lee 1985), COST231 Walfisch-Ikegami model (Ikegami et al. 1984), Walfisch-Bertoni model (Walfisch and Bertoni 1988), and ITU-R (ITU Report 1998, p.370).

3.2 Applications of Propagation models

The prediction techniques or models described in this study are most often implemented for practical planning within computer software. The development of such software has been motivated and enabled by a number of factors (Saunders 2005):

- (i) The enormous increase in the need to plan digital broadcast systems for TV services and cellular systems accurately and quickly
- (ii) The development of fast and affordable resources
- (iii) The development of graphical information systems, which index data of terrain, clutter and land usage in an easily accessible and manipulated form giving better frequency management etc.

Such techniques have been implemented in a wide range of commercially available and company-specific planning tools. Some of the prediction tools are listed in Table 1. Although most are based on combined empirical and simple physical models, it is anticipated there will be a progressive evolution in the future towards more physical or physical-statistical models as computing resources becomes cheaper and cheaper, as clutter data improves in resolution and as researchers develop more efficient path loss prediction algorithms.

Tools	Description
PACE	The original propagation systems is now integrated into Vodafone Geographical Information System
ASTRIX	Advanced SysTem for RadioInterface eXploration is intended for macrocells. It incorporates path loss models Okumura-Hata, Blomquist-Ladell, Walfisch-Bertoni and diffraction loss models Deygout and Epstein-Peterson. It treats also 3D terrain scattering.
PathPro	It treats propagation models COST 231 microcell and macrocell, Hata and Longley-Rice.
CelPlanner	It incorporates propagation models Lee-Picquenard, Okumura-Hata, COST 231 and Korrowajczuk.
CRUMPET	It incorporates the propagation model UK Army EMC Agency PR03.
Planet	It incorporates propagation models Okumura-Hata and Walfisch-Ikegami.
NetPlan	It incorporates propagation models Walfisch-Ikegami COST 231-Hata and Walfisch-Xia

Table 1: Prediction Tools (Source from Saunders 2005)

3.3 Survey of various propagation models and their technical background

The two basic propagation models (Free-Space and Plane Earth Loss) have all the mechanisms which are encountered in macrocell prediction. Many researchers use these models and predict the total signal loss. Other models require detailed knowledge of the location, dimension and parameters for every tree or building and terrain feature in the area to be covered. The models are complex and yield an unnecessary amount of details as the network designer is not interested in the particular locations covered, but the overall extent of the coverage area. One appropriate way of removing these complexities is to adopt an empirical model. These models use, as parameters, the received signal strength, frequency, antenna heights and terrain profiles, derived from a particular environment through the use of extensive measurement and statistical analysis. The models can then be used to design systems operated in similar environments to the original measurements.

3.3.1 The Okumura-Hata model

The simple modeling of path loss is still dominated by the Hata empirical model (Hata 1980), where the propagation results are fitted to a simple analytical expression, which depends on antenna height, environment, frequency and other parameters. Hata's method is basically an extension of Okumura's method (which is somewhat cumbersome due to numerous correction factors) and employs propagation curves instead of parametric equations. It is a model based upon an extensive series of measurements made in and around Tokyo city between 200 MHz and 2 GHz. Predictions are made via a series of graphs. The thoroughness of work has made the model the most widely used macrocell prediction model and is often regarded as a standard against which researchers can benchmark new approaches. The model for urban areas has been standardised in 1997 for international use as Rec ITU-R P.529 model (ITU Report 1997). The Hata model does not have any of the path-specific corrections which are available in Okumura's model. Okumura takes urban areas as a reference and applies correction factors for conversion to the classification of terrain. Hence the model will involve dividing the prediction area into a series of clutter and terrain categories as follows:

- (i) Open area: Open space, no tall trees or buildings in path, plot of land cleared for 300-400 m ahead, e.g. farm land, rice fields, open fields;
- (ii) Suburban area: Village or highway scattered by trees and houses, some obstacles near the receiving antenna but not very congested;
- (iii) Urban area: Build up city or large town with buildings and houses with two or more storages, or larger villages with close houses and tall and thickly grown trees.

The negative side of the Okumura-Hata model is that it is valid only for frequency between 150 MHz and 1500 MHz, with base antenna height between 30 m to 200 m and receiving antenna between 1 m and 10 m. However, this model will not be a problem to use in this research as measurements are taken within the ranges mentioned above. Another problem encountered by this model is that in some countries measurements have been in disagreement with the predictions. The reason cited is the difference in characteristics of Tokyo city. Kozono and Watanabe (1977) have tried to modify the model by including a measure of building density, but such approach has not found common acceptance. The third problem is that the model has been developed for only three categories of land usage (rural, sub-urban and urban) as in practice the classification of land usage of a country (e.g. Mauritius, England, India) can exceed 10 categories.

3.3.2 Other Standard Models

In this study, the Lee model (Lee 1985), and the approximate model Extended COST 231-Hata (COST 231 Final Report 1999 cited in Rama Rao 2000) are considered apart from the Hata and Free Space model as explained in the previous section. Approximate models COST 231/Walfisch-Ikegami (1984) and Walfisch-Bertoni (1988) have some restrictions because they do not include information on the environment. Hence, the risk of incorrect prediction is high since there are no correction factors for conversion according to the terrain classification. Moreover, COST 231/Walfisch-Ikegami model is valid for frequency between 800 and 2000 MHz, that is, it is not applicable to macrocells but to microcells. In a later stage in 1999, COST 231 was improved and a new model was created which is adopted for various terrains. The model which was derived from Hata is known as Extended COST

231-Hata model (COST 231 Final Report 1999). The Walfisch–Bertoni model considers the impact of rooftops and building height by using diffraction to predict average signal strength at street level. These methods describe urban propagation loss as a sum of three terms: free space losses, rooftop to street losses and multiple diffraction losses. The approaches of Walfisch–Ikegami and Walfisch–Bertoni are restricted by definition to radio paths that are obstructed by buildings. The models account for local terrain slope in the vicinity of the receiving antenna and do not incorporate terrain roughness factors and do not treat obstructing terrain features such mountains and gorges. Finally, the empirical model developed by Blomquist-Ladell (1974) has some limitation since it includes only the sum of free space loss, the sum of smooth spherical earth loss, obstacle diffraction loss, urban loss and vegetation loss. It does not include loss due to reflection, climates and seasons.

Research on propagation models and path loss have been carried out in the past by several researchers like Grosskopf (1987) in Germany, Rama Rao et al. (2000) and Prasad (2006) in India, The Perez-Vega-Zamanillo (2002) in Spain and Hosseinzadey (2003) in Iran among many others. The Perez-Vega-Zamanillo model is a simple propagation model for the VHF and UHF bands. The model is a computational form of the data provided by the FCC F(50,50) propagation curves. The model is not frequency dependent in the band of interest and can be used to predict the path-loss for television broadcasting. One disadvantage is that it does not provide information on issues such as fade margins, angles of arrival, or delay spread, which must be estimated by another way.

The model developed by Grosskopf (1987) has no classification of urban, suburban and open areas or correction factors which are very important for a model. His technique is to predict path loss for only hilly and mountainous land in Germany. Prasad (2006) has done intensive work where field strength measurements are taken over Indian subcontinent and the calculated path loss is compared with other models including the Perez-Vega-Zamanillo (2002) one. However, no model was proposed from the observations and results.

3.4 Factors to improve accuracy of models

Below are factors that can be considered to improve accuracy of propagation models:

- (i) Reflection is the result of digital TV signal hitting on obstructions with properties (thickness, length) much larger than the wavelength of the radio wave (e.g. smooth surface of walls and hills/mountains).
- (ii) Diffraction occurs when radio waves strikes the edges or corners of obstacles. These act as secondary sources re-radiating into the shadow region. It is due to the diffraction effect that radio frequency energy travels in dense urban environments where there is no clear Line-of-Sight between two antennas (e.g. from edges such as building rooftops and mountaintops).
- (iii) Scattering occurs when the properties of the object interacting with the radio wave is on the order of the colliding wavelength (e.g. from rough surfaces such as sea, rough ground and the leaves and branches of trees).
- (iv) Absorption (e.g. by walls, foliage and by atmosphere)
- (v) Refraction (e.g. due to atmospheric layers or layered and graded materials)
- (vi) The directional characteristics of both the transmitter and the receiver antennas. (Saunders 2005).

All these factors are called multiplicative noise. It is more conventional to subdivide these factors as path loss, shadowing or slow fading and fast fading or multipath fading.

Shadowing

Shadowing is the loss of field strength typically contributed to a diffracted wave emanating from an obstacle between transmitter antenna and receiver antenna (Saunders 2005). As passing through a shadow area requires considerable time, the name 'slow fading' is commonly used. The shadow effect is modeled with a log-normal distribution of the mean signal.

Fast Fading (Multipath Propagation)

As radio waves are reflected or diffracted or scattered by trees, hills and mountains, buildings and other obstacles, they establish various transmission paths from the transmitter to the receiver antennas. Many reflections are produced in an urban environment and few reflections in rural areas. The multipath creates the most difficult problem in the digital broadcast environment.

3.5 The Technical Background of Propagation Models

This section provides methods for predicting path loss used in macrocells (above 1 km). The models presented here treat the path loss associated with a given macrocell as dependent on distance between a transmitter and a receiver, provided that the environment is fairly uniform. The free space propagation model is discussed briefly whereas the plane earth loss model is not treated in this work as the latter will require detailed knowledge of the location, dimension and constructive parameters of every tree, building and terrain feature in the area to be covered. It will be too complex and will yield an unnecessary amount of details since the broadcasting designer, network engineer and planner will not be interested in the particular locations being covered, but rather in the overall extent of the coverage area (Saunders 2005).

In the design of any broadcasting system, the fundamental task is to predict the coverage of the proposed system. Digital television service coverages are characterised by a very rapid transition from near perfect reception to no reception at all (Smith 2003). Hence, it becomes critical to be able to define which areas are going to be covered and which are not. As it is the case for Mauritius, it becomes necessary to increase the transmitter powers or to provide a large number of transmitters in order to guarantee coverage to the last few percent of the worst served small areas.

A wide variety of techniques have been developed over the years to predict coverage using what are known as propagation models (Saunders 2005). Propagation, in this context, means the transmission of signals from the transmitter to the receiver. En route from the transmitter to the receiver, the signal gets weaker and may experience shadow or multipath effects (Ong et al 2004).

As said by Saunders (2005), based on the path loss information, to improve reception in a particular situation the following factors can be considered:

- (i) Use a more directional receiving antenna with a higher gain
- (ii) Find a better position for the receiver-antenna
- (iii) Use of a low-noise antenna amplifier (as in the case of fixed antenna reception).

In general terms, path loss occurs when the transmitted signal suffers a loss proportional $1/R^2$, where R is the distance between transmit and receive antennas.

3.5.1 Free Space Propagation Model

The free space propagation model is used to predict received signal strength when the transmitter and receiver have a clear, unobstructed line-of-sight path between them (Friis 1946). As with most large-scale radio wave propagation models, the free space model predicts that received power decays as a function of the Transmitter-Receiver separation distance raised to some power (i.e. a power law function) (Saunders 2005).

The free space power received by a receiver antenna which is separated from a radiating transmitter antenna by a distance d , is given by the Friis free space equation (Friis 1946),

$$P_r(d) = \frac{P_t G_t G_r \lambda^2}{(4\pi)^2 d^2} \quad (1)$$

where P_t is the transmitted power, $P_r(d)$ is the received power, G_t is the transmitter antenna gain, G_r is the receiver antenna gain, d is the T-R separation distance in meters and λ is the wavelength in meters.

The Friis free space equation shows that the received power falls off as the square of the Transmitter-Receiver (T-R) separation distance. This implies that the received power decays at a rate of 20 dB/decade with distance.

The path loss, which represents signal attenuation as a positive quantity measured in dB, is defined as the difference (in dB) between the effective transmitted power and the received power, and may or may not include the effect of antenna gains (ITU Report 1998).

The path loss for the free space model when antenna gains are included is given by:

$$\begin{aligned} PL (dB) &= 10 \log \frac{P_t}{P_r} \\ &= -10 \log \left[\frac{G_t G_r \lambda^2}{(4\pi)^2 d^2} \right] \end{aligned} \quad (2)$$

Equation (3.2) can be expanded to give an equation in terms of distance, d (km) and frequency of operation, f (MHz):

$$\begin{aligned} PL (dB) &= -10 \log_{10} (G_t) - 10 \log_{10} (G_r) - 20 \log_{10} \left[\frac{(c \times 10^{-3})}{4\pi \times f \times 10^6} \right] - 20 \log_{10} (1/d) \\ &= -G_t (dB) - G_r (dB) + 32.44 + 20 \log_{10} (d / km) + 20 \log_{10} (f / MHz) \end{aligned} \quad (2.1)$$

where c is the speed of light ($3 \times 10^8 \text{ ms}^{-1}$)

3.5.2 Okumura-Hata path loss model

The Okumura-Hata model (1980) is an empirical formulation of the graphical path loss data provided by Yoshihisa Okumura, and is valid from 150 MHz to 1500 MHz. The Hata model

is, basically, a set of equations based on measurements and extrapolations from the curves derived by Okumura. Hata presented the urban area propagation loss as a standard formula, along with additional correction factors for application in other situations such as suburban and rural.

Only four parameters are required in the Hata model. Hence, the computation time is very short. This is an advantage of the model. However, the model neglects the terrain profile between the transmitter and receiver, that is, hills or other obstacles between the transmitter and receiver are not considered. This is because both Hata and Okumura made the assumption that the transmitters would normally be located on hills. Figure 1 shows a typical scenario for Hata-Okumura model.

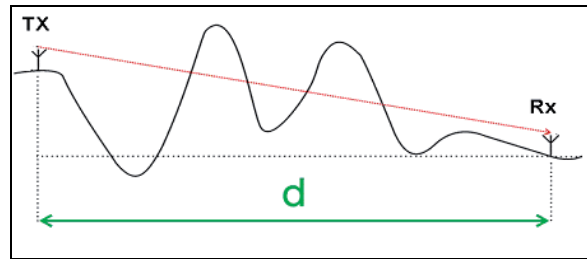


Fig. 1. Scenario for Hata model

The above model assumes a direct line-of-sight path from transmitter (tx) to receiver (rx) but the actual path is obstructed by two hills. Hence, the prediction would be too optimistic.

The standard Hata formula for median path loss in urban areas is given by:

$$L(urban)(dB) = 69.55 + 26.16 \log f_c - 13.82 \log h_{tx} - a(h_{rx}) + (44.9 - 6.55 \log h_{tx}) \log d \quad (3)$$

where:

f_c is the frequency (in MHz) from 150 MHz to 1500 MHz,

h_{tx} is the effective transmitter antenna height (in m) ranging from 30m to 200m,

h_{rx} is the effective receiver antenna height (in m) ranging from 1 m to 10 m,

d is the T-R separation distance (in km),

$a(h_{rx})$ is the correction factor for effective antenna height which is a function of the size of the coverage area.

To obtain the path loss in a suburban area, the standard Hata model formula in equation (3) is modified to:

$$L (dB) = L (urban) - 2 [\log (f_c / 28)]^2 - 5.4 \quad (3.1)$$

For a terrain category such as the north of Mauritius, the antenna correction factor is given by:

$$a(h_{rx}) = (1.1 \log f_c - 0.7)h_{rx} - (1.56 \log f_c - 0.8) \text{ dB} \quad (4)$$

3.5.3 Extended COST-231 Hata model

This model (COST 231 Final Report 1999 cited in Tapan et al. 2003 and Zreikat and Al-Begain n.d.) is derived from the Hata model and depends upon four parameters for the prediction of propagation loss: frequency, height of a received antenna, height of a base station and distance between the base station and the received antenna.

From equation (3), the urban model is given by:

$$L(\text{urban})(dB) = 46.33 + 33.9 \log f_c - 13.82 \log h_{tx} - a(h_{rx}) + (44.9 - 6.55 \log h_{tx}) \log d \quad (5)$$

The path loss in a suburban area is given by:

$$L(dB) = L(\text{urban}) - 2 [\log(f_c / 28)]^2 - 5.4 \quad (5.1)$$

where $a(h_{rx})$ is obtained from equation (4).

3.5.4 Lee Model

The Lee model (1985) is a power law model with parameters taken from measurements in a number of locations. The model is expressed as follows:

$$L(\text{suburban})(dB) = 10n \log d - 20 \log h_{tx} - P_o - 10 \log h_{rx} + 29 \quad (6)$$

where $n = 3.84$ and $P_o = -61.7$. Here it has been assumed that h_{tx} is the effective base station height.

3.5.5 Rec ITU-R P.370 Propagation prediction method

Prediction of the coverage provided by a given transmitting station is normally done on the basis of the field strength for the wanted signal predicted.

Rec ITU-R P.370 (ITU Report 1998) is a commonly agreed field strength method for broadcasting services. The propagation curves given in this recommendation represent field strength values in the VHF and UHF bands as a function of various parameters.

The power received at a distance d , P_r is given by:

$$P_r = \frac{|E|^2}{120 \pi} A_e$$

$$P_r(dB) = 20 \log_{10} E - 10 \log_{10} (120 \pi) + 10 \log_{10} A_e \quad (7)$$

$$P_r(dB) = 2E_{\min} - 10 \log_{10} (120 \pi) / \Omega + A_e(dBm^2)$$

where:

E_{\min} is the equivalent minimum field strength at receiving place

A_e is the effective antenna aperture (dBm^2)

120π is the value of intrinsic impedance of free space (ohms).

However, the above equation relates electric field (with units of V/m) to received power (with units of watts). Often, this equation is used to relate the received power level to a receiver input voltage, as well as to an induced electric field at the receiver antenna.

In situations where practical values of field strengths are available in $dB\mu V/m$ from measurements, the corresponding path loss in dB can be calculated as follows if the values for transmitted power and effective receiver antenna aperture are known:

$$PL (dB) = P_t (dB) - P_r (dB)$$

$$PL(dB) = P_t(dB) - E_{\min} - A_e(dB) + 10\log_{10}(120\pi)$$

$$PL(dB) = P_t(dB) - 2E_{\min}(dB\mu V/m) + 240 - A_e(dB) + 10\log_{10}(120\pi) \quad (7.1)$$

where $E_{\min} = E_{\min} (dB\mu V/m) - 120$.

4. Comparative Field Strength and Path Loss Analysis – A Case Study

4.1 Data Collection, Experimental Details and Methodology

Measurement locations are divided into three groups for each region, that is, three concentric circles CC1N, CC2N and CC3N for the north and CC1S, CC2S and CC3S for the south. The radius determines the horizontal distance between the measured point (receiver antenna) and the transmitter. The radii of CC1N/CC1S, CC2N/CC2S and CC3N/CC3S are 5 km, 10 and 15 km respectively. Points are selected on the circles as shown in Figure 2 and determined the measuring sites. It should be noted that at each measuring site, three to four times, measurements were taken every five minutes for a period of 20 minutes. The exercise are conducted at 78 locations sites in the North (26 for CC1N, 26 for CC2N and 26 for CC3N) and at 99 locations sites in the South (33 for CC1S, 33 for CC2S and 33 for CC3S)

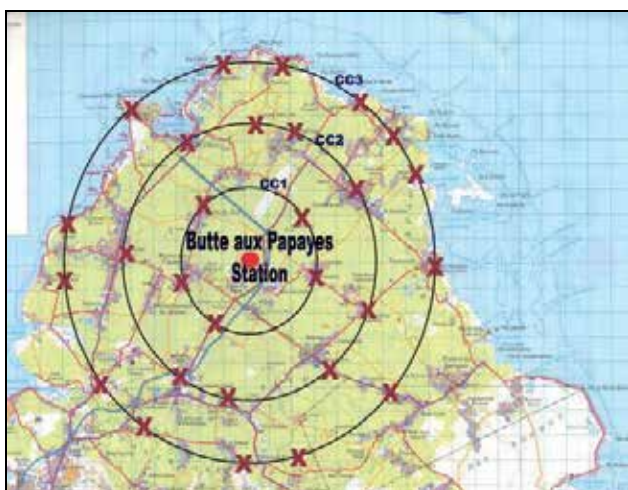


Fig. 2. View of one part of Mauritius

A measuring vehicle is used to carry the equipment and the measurements are done manually. As shown in Figure 3, the vehicle is stopped at each site and the log periodic antenna from Fracarro (Antennas online 2007, Fracarro Antenna online 2007) is raised up to a height and is properly oriented towards the transmitter to achieve maximum signal strength. The measurements are conducted around the relay station and are repeated for two receiving antenna heights of 4 m and 6 m. Once the received signal has been captured the field strength, the BER value, the minimum Carrier to Noise (C/N) and CSI are recorded for digital TV signal. Measurements were taken at antenna heights 4 m and 6 m.



Fig. 3. The Measuring Vehicle

4.2 Signal Strength and Interference

The aim of this work is to study the variation of the received field strength, carrier-to noise and Bit Error Rate for different locations in the northern region of Mauritius (Fogarty, Soyjaudah and Armoogum 2006). Similar works have been carried out in various countries (India, Spain, Canada, Korea) as explained by Rama Rao et al. (2000), by Prasad (2006), by Arinda et al. (1999a, 1999b), by Assia Semmar *et al.* (2006), by Sung Ik Park et al. (2007) and more recently by Martinez et al. (2009). All these studies have analysed the quality of digital TV signal reception. In Mauritius, this exercise is important so as to give a realistic picture of the situation. Few measurements at UHF frequencies for digital television have been made. The experiment (Figure 4) shows that at a distance of 5 km the field strength is high enough (minimum threshold value is 53 dB μ V/m) for the COFDM component of the AFSM to decode picture to achieve a BER lower than 2×10^{-4} . For both regions, almost all locations will have high performance of digital transmission. For an ideal case, that is, a topography of flat earth with Line-Of-Sight propagation, the received field strength at all locations over concentric circle CC1 must be constant. At a distance of 10 km and more, the cell covered by the base station does not include all the measuring points since the received signal strength is less than 53 dB μ V/m (the signal level and quality at some points are not high enough to decode the information stream). However, for both regions at a certain constant distance round the station, the graph obtained shows that the field strength is varying with location. This may be explained by the fact that due to Non Line-Of Sight (NLOS), there may be different diffraction losses due to different buildings in the north or due to dense forests and mountains (knife-edge) in the south in the path linking the base station and the location of interest. Multipath effects may also be the cause, giving rise to a graph of varying field strength with location.

The field strength in the south decreases more than that of the north. Besides, when comparing the standard deviations, the C/N deviates too much from the mean values in the south, indicating that there are more obstructions in the south. Though the south is classified as a rural area compared to the northern area (sub urban), there are more factors affecting the signal in that region.

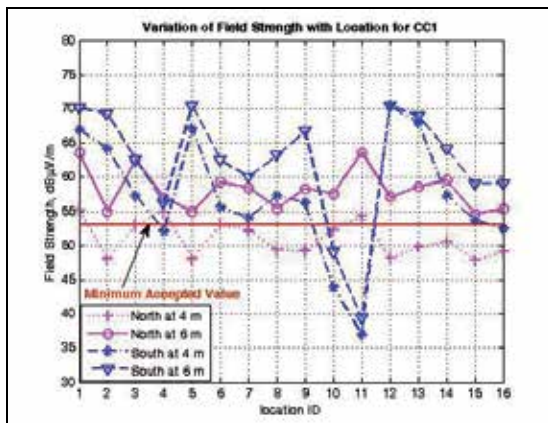


Fig. 4. Variation of Field strength for various antenna heights in the North and South at a distance of 5 km from transmitter

4.3 Path Loss Analysis

The main aim is to study the variation of the path loss at various locations in the south and compare them with those from the north (Armoogum et al. 2007a, Armoogum et al. 2007b). In theory, the path loss at a constant distance from a transmitter is the same for any point around it. For both areas, as depicted in Figure 5, the path loss is not constant at various locations for a constant distance around the transmitter which therefore indicates about the irregularity of both terrains of the island. The path loss for an antenna height of 6 m is lower than that of 4 m as a result of a reduction of multipath effects with a higher antenna.

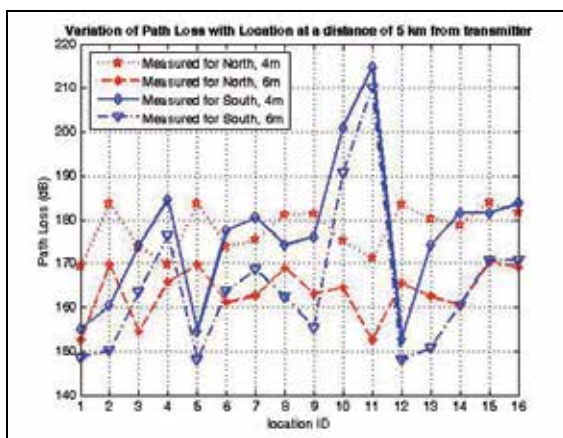


Fig. 5. Variation of Path Loss for both regions at 5 km from transmitter

4.4 Comparative Study of Pass Loss with Various Existing Propagation Models and Selecting the Best One(s)

The measured pass loss is compared with models such as Free-Space, Okumura-Hata, Extended COST-231 and Lee. The aim is find out which of the model(s) gives/give better agreement with the measured pass loss. From figures Figure 6 and Figure 7, it is clear that the Lee model and the Free-Space model deviate too much from the measured values, which implies that these models are not suitable for modelling the south of Mauritius. For both regions, the path loss using Okumura-Hata model and Extended COST-231 are much closer to each other and give better agreement with the measured values. The slight difference between these two models can be considered negligible.

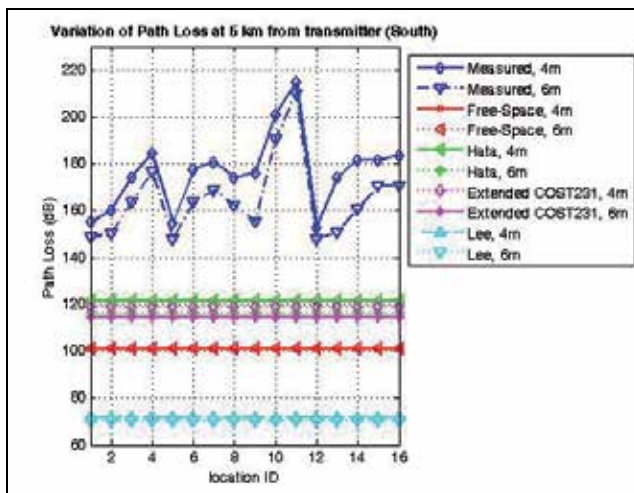


Fig. 6. Variation of Path Loss in the South using various propagation models at 5 km from transmitter

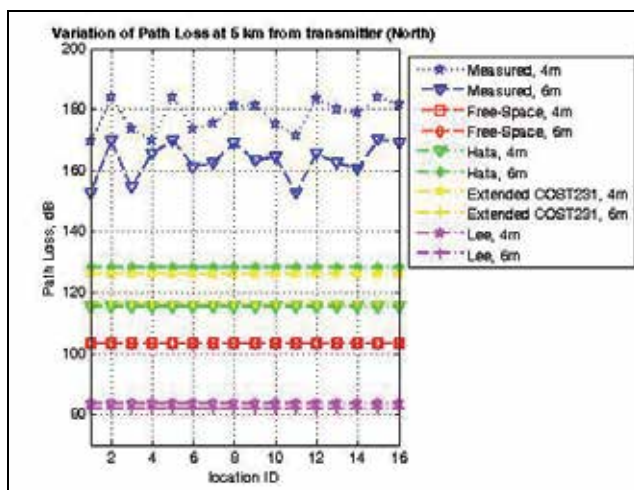


Fig. 7. Variation of Path Loss in the North using various propagation models at 5 km from transmitter

There is no need to transform the two models into a discrete-time mode as the signal strength depends only upon the power transmitted and received. The results show that the analogue models can be used in digital broadcast systems. These models can be used to develop a novel digital model for Mauritius. Since the north and the south of Mauritius are inhomogeneous ones and consist of rural, sub-urban and urban areas unevenly located, we can take sub-urban areas as a reference and applies correction factors for conversion to the classification of terrain.

Using equations (3) and (3.1) from Section 3.5, the digital Hata-Okumura model is given by:

$$L(dB) = 69.55 + 26.16 \log f_c - 13.82 \log h_{tx} - a(h_{rx}) + (44.9 - 6.55 \log h_{tx}) \log d - 2[\log(f_c/28)]^2 - 5.4 \quad (4.1)$$

Using equations (5) and (3.5.1) from Section 3.5, the digital Extended COST-231 Hata model is given by:

$$L(dB) = 46.33 + 33.9 \log f_c - 13.82 \log h_{tx} - a(h_{rx}) + (44.9 - 6.55 \log h_{tx}) \log d - 2[\log(f_c/28)]^2 - 5.4$$

5. Proposed way for Modelling Broadcast Networks

The best way to design new broadcast networks or optimize existing networks is to develop new models or improving existing ones. This section provides a new definition for the types of terrain of Mauritius (a case study) and secondly proposed the techniques that could be used in developing new models.

5.1 Redefining the Classification of Land Usage for Mauritius

The first problem with the empirical models is the classification of environment in which the system is operating. Once the real classification through the analysis parts is known, better results are obtained if the appropriate category of terrain is reviewed. The categories must be numerous so that the properties of different locations classed within the same category are not too variable. A proposed definition of categories is depicted in Table 2.

5.2 The Approaches

The two empirical models stated in Section 4 are fundamental for the prediction of path loss. The new models may thus be developed as means of improving accuracy using two approaches: deterministic empirical-physical approach or empirical-statistical approach using some statistical parameters.

What are Physical and Statistical approaches?

The physical approach:

A Digital TV wave signal can be reflected or refracted when hitting a surface. In these cases the Snell's laws of reflection and refraction will be applied. Rays can hit different types of surface. In Mauritius, there are dry land, average ground, wet ground, sea water and fresh

water and the reflection will differ according to the conductivity and relative dielectric constant. These values are available in ITU Report-527 (ITU Doc. 1992). These reflection processes are so far applicable to smooth surfaces and are termed specular reflection. When the surface is rougher, the reflected signals become scattered from a larger number of positions on the surface, hence, reducing the field strength and increasing the attenuation. Refraction also occurs due to atmospheric layers. A higher permittivity (the denser medium) causes the transmitted signal to bend more toward the surface normal. This change of direction changes the velocity of the signal with respect to refractive index and might cause delay spread. In many situations in Mauritius, diffraction over obstructions such as hills, mountains and buildings may be treated as if they are absorbing knife-edges (single knife-edge and multiple knife edge diffraction). Using physical approach means modelling all the above factors.

The statistical approach:

The region is divided into small homogeneous areas and categories. The smaller the sector, the more homogeneous will be the area. A forecasting technique is used to predict path loss from 0 to 15 km (interpolation) and above (extrapolation). Mathematical equations are derived for each homogeneous area. Finally, a general Mathematical equation is derived for similar homogeneous areas, that is, for a specific category of land.

For the development of novel models, it is believed that the empirical-statistical approach is better for the following reasons

- (i) The physical approach will lead to entirely incorrect predictions when considering fields in the shadow region behind an obstruction.
- (ii) Using the physical approach, it would be very difficult to get the exact parameters of obstructions (size of buildings, heights, distance between buildings, density of forests, types of soil etc).
- (iii) The empirical-statistical model is more economical as the physical models involve a large number of expensive input data requirements.

Category	Details
0	Reservoirs, Lakes and Sea ¹ .
1	Open Rural Area with Plantation (Sugar cane and Tea).
2	Open Rural Area with Forest in between.
3	Dense Forested Area.
4	Mountainous region
5	Hilly and Mountainous Forested Area.
6	Sub Urban Area - Small villages ² of low-density houses of up to two storeys, with some open areas and trees.
7	Sub Urban Area - Big villages ³ with houses of up to two storeys and industries (industrial zones) and with some open space and trees in between.
8	Urban Area - Big villages or towns with buildings of up to four storeys
9	Higher Urban Area - Town ⁴ with buildings of up to four storeys and closed to each other.
10	Dense Urban Area - Town with buildings very closed to each other in which some of them are up to eight storeys.
11	Very Dense Urban Area - Big town or cities ⁵ with buildings very closed to each other in which most of them are eight storeys and above.

Table 2. Classifications of Land Usage for Mauritius

6. Conclusion

The increasing demand of various fixed and mobile services has placed considerable pressure on the limited frequency spectrum. For the efficient utilisation of this resource, as well as for performance assessment of the existing systems, modeling and coverage predictions are essential. A reliable model of predicting path loss helps in reducing load on base stations and helps in designing digital broadcasting networks including TV services. We have considered Mauritius Island as a case study. From the observations and results obtained, it is concluded that the existing empirical models are not accurate and therefore cannot be used in Mauritius since the focus here is on small area propagation and for tropical, mountainous regions. The first limitation of existing models is that they are developed for limited categories of land (open area, sub-urban and urban areas). The table of classification of land usage was defined for Mauritius. For qualitative classification, the categories are numerous so that the properties of different locations classed with the same category are not too variable. Analysis and comparisons of field strength and height gain analysis in North and South were conducted to find out the types of terrain of Mauritius and the reasons why TV signals suffer a loss. The path loss analysis was conducted and tested using several models. Extended COST-231 and Okumura-Hata give better agreement in regions of Mauritius. Before developing novel models, the regions were divided into small homogenous areas and categorised. Two techniques are proposed for the development of new propagation models.

7. Future Work

In section 5, the technicalities toward the development of new models are not discussed. Then, performance analysis and testing need to be done using new measured data. The usual goal of performance analysis and testing is to determine the places of Mauritius where the models work properly and the places there are high deviations. An extensive work needs to be conducted for this purpose.

Models are widely used in prediction tools such as ASTRIX or CRUMPET. Computer applications have to be developed for the prediction of path loss, the designing of broadcast networks or optimizing existing network.

Some of the functionalities of these software tools with the integrated models are as follows:

- (i) Design new broadcast networks,
- (ii) Perform coverage prediction for various types of communication systems in order to design optimize networks of transmitters,
- (iii) Analyze interference problems,
- (iv) Explore new coverage scenarios,
- (v) Diagnose difficult coverage situations,
- (vi) Evaluate new transmitter and receiver concepts.
- (vii) Visualize and analyze predicted performance, as well as compare simulation with experimental data.

Finally, to obtain a high quality image, these applications can be used with a geographical information system (GIS) storing the geographical locations of points for every 10 m² and their corresponding categories as the main fields.

8. References

- Anderson, J. 2005. *Digital Transmission Engineering*. 2nd Edition. Wiley Publication.
- Antenna [Online] 2001. Available at www.fracarro.com/NR/rdonlyres/7456FB27-45EF-489D-8373-F8E23BB3CCAD/0/Antennas.pdf. [Accessed 2007].
- Armoogum, V. Soyjaudah, K.M.S. Mohamudally, N. and Fogarty, T. 2007. Height Gain Study for Digital Television Broadcasting at UHF Bands in two Regions of Mauritius. *Proceedings of the 2007 Computer Science and IT Education Conference*, pp. 017-025, ISBN 9789990387476.
- Armoogum, V. Soyjaudah, K.M.S. Mohamudally, N. and Fogarty, T. 2007. Comparative Study of Path Loss with some Existing Models for Digital Television Broadcasting for Summer Season in the North of Mauritius at UHF Band. *IEEE The Third Advanced International Conference on Telecommunications (AICT-07)*, ISBN 0-7695-2443-0.
- Armoogum, V. Soyjaudah, K.M.S. Mohamudally, N. and Fogarty, T. 2007. Path Loss Analysis between the north and the south of Mauritius with some Existing Models for Digital Television Broadcasting for Summer Season at UHF Bands. *Proceedings of the 8th IEEE AFRICON 2007*, ISBN 0-7803-8606-X.
- Arrinda, A. Ma Velez, M. Angueira, P. de la Vega, D. and Ordiales, J. L. 1999. Digital Terrestrial Television (COFDM 8k System) Field Trials And Coverage Measurements In Spain. *IEEE Transactions On Broadcasting*, 45(2), No. 2, pp. 171-176.
- Arrinda, A. Ma Velez, M. Angueira, P. de la Vega, D. and Ordiales, J. L. 1999. Local-Area Field Strength Variation Measurements Of The Digital Terrestrial Television Signal (COFDM 8k) In Suburban Environments. *IEEE Transactions On Broadcasting*, 45(4), pp. 386-391.
- Assia Semmar, Jean-Yves Chouinard, Viet Ha Pham, Xianbin Wang, Yiyang Wu, and Sébastien Lafèche 2006. Digital Broadcasting Television Channel Measurements and Characterization for SIMO Mobile Reception. *IEEE Transactions On Broadcasting*, 52(4), pp. 450-463.
- BBC 1998. AC106 Verification and Launch of Advanced Television in Europe (VALIDATE), Project Report.
- Blomquist, A. and Ladell, L. 1974. Prediction and calculation of transmission loss in different types of terrain, *FOA report*.
- CEPT 1997. The Chester 1997 Multilateral Coordination Agreement relating to Technical Criteria, Coordination Principles and Procedures for the introduction of Terrestrial Digital Video Broadcasting (DVB-T).
- COST 231 Final Report 1999. Digital Mobile Radio: COST 231 View on the Evolution Towards 3rd Generation Systems, Commission of the European Communities and COST Telecommunications, Brussels.
- ETSI (European Telecommunications Standards Institute) 1997. Digital Video Broadcasting (DVB), Framing structure, Channel coding and Modulation for Digital Terrestrial Television (DVB-T), ETS 300 744.
- ETSI (European Telecommunications Standards Institute) 1997. Digital Video Broadcasting (DVB), Implementation guidelines for DVB services. *Transmission aspects, ETS 101 190*.

- Fogarty, T. Soyjaudah, K.M.S. and Armoogum, V. 2006. Signal Strength Variation Measurements of Digital Television Broadcasting for Summer Season in the North of Mauritius at UHF Bands, *Conference Proceeding of the 3rd International Conference on Computers and Device for Communication*, pp. 89-92.
- Fracarro Antenna [Online] 2001. Available at www.tvantenna.com.au/FARCARRO%20ANTENNAS [Accessed 2007].
- Friis, H.T. 1946. The Free Space Transmission equation. *Proc. IRE*, vol. 34, p.254.
- Gaudrel, R. Betend, C. 1997. DIGITAL TV BROADCAST Field Trials on the Experimental Network of Rennes, Internal VALIDATE document from CCETT, FT.CNET/DMR/DDH.
- GIS Company History [Online] n.d. Available at <http://www.fundinguniverse.com/company-histories/General-Instrument-Corporation-Company-History.html>, [Accessed on June 2006].
- Grosskopf, R. 1987. Comparison of different methods for the prediction of the field strength in the VHF range. *IEEE Trans. Ant. Propagation*, 35(7), pp. 852-859.
- Hata, M. 1980. Empirical formula for propagation loss in land mobile radio services. *IEEE Trans. Veh. Technol.*, 29(no issue number), pp. 317-325.
- Homayoon, O. and Shahram Hosseinzadeh 2003. Determination of the effect of Vegetation on Radio wave Propagation by the Parabolic Equation Method, *Proceeding of 2nd International Symposium of Telecommunications, IST2003*, pp.340-344 Isfahan Iran.
- Ikegami, F. Yoshida, S. Takeuchi, T. and Umehira, M. 1984. Propagation factors controlling mean field strength on urban streets. *IEEE Trans. Ant. Prop.*, vol. 32 (no issue number), pp. 822-829.
- International Telecommunication Union, ITU-R recommendation P.529-2 1997. Prediction methods for the terrestrial land mobile service in VHF and UHF bands.
- International Telecommunication Union, ITU-R recommendation P.370 1998. Prediction methods for the terrestrial land mobile service in VHF and UHF bands, 1998.
- International Telecommunication Union 1992. ITU-R Recommendation 527-3: Electrical Characteristics of the surface of the Earth, Geneva 1992.
- ITU Geneva 1989. Final Acts of the Regional Administrative Conference for the Planning of VHF/UHF Television Broadcasting in the African Broadcasting Area and Neighbouring Countries.
- Kozono, S. Watanabe, K. 1977. Influence of Environmental buidings on UHF Land mobile radio propagation, *IEEE Trans. Commun.*, 25(10), pp.1133-1143.
- Lee, W.C.Y. 1985. Estimation of local average power of a mobile radio signal. *IEEE Trans. Veh. Technol.*, 34(1), pp. 22-27.
- Martínez, A. Zabala, D. Peña, I. Angueira, P. Vélez M.M. Arrinda, A. de la Vega, D. and Ordiales, J.L. 2009. Analysis of the DVB-T Signal Variation for Indoor Portable Reception. *IEEE Transactions On Broadcasting*, 55(1), pp. 11-19.
- Metz H. C., [Online] 1994. Ed. Mauritius: A Country Study. Washington: GPO for the Library of Congress, 1994. Available at <http://countrystudies.us/mauritius/7.htm> [Accessed on May 2006].
- Ong, J. T. Rao, S. V. B. Shanmugam, G. Hong Y. 2003, Results of the Mobile DTV Measurements in Singapore, Nanyang Technological University, Singapore, Conference Publication.

- Ong, J.T. Rao, S.V.B. Hong Y. Shanmugam, G. 2004. Height Gain Measurements for DTV Reception in Singapore. *IEEE Transactions On Broadcasting*, 50(4), pp. 396-398.
- Pather, A. August 2000. The move to Digital Broadcasting – Challenges Ahead, MultiCarrier (Mauritius) Limited.
- Parsons, J.D. and Ibrahim, M.F. 1983. Signal strength prediction in built-up areas – Part 2: Signal variability. *IEE Proc.*, vol. 130, no. 5, pp. 385-391.
- Perez-Vega, C. and Zamanillo, J.M. 2002. Path Loss Model for Broadcasting Applications and Outdoor Communication Systems in the VHF and UHF Bands. *IEEE Transactions On Broadcasting*, 48(2), pp. 91-96.
- Prasad, M.V.S.N. 2006. Path Loss Deduced From VHF and UHF Measurements Over Indian Subcontinent and Model Comparison. *IEEE Transactions On Broadcasting*, 52(3), pp. 290-298.
- Prasad, M.V.S.N. and Iqbal, A. 1997. Comparison of some Path Loss Prediction Methods with VHF&UHF Measurements. *IEEE Transactions On Broadcasting*, 43(4), pp. 459-486.
- Rama Rao, T. Vijaya Bhaskara Rao, S. Prasad, M.V.S.N. Mangal Sain, Iqbal, A. and Lakshmi, D. R. 2000. Mobile Radio Propagation Path Loss Studies at VHF/UHF Bands in Southern India. *IEEE Transactions On Broadcasting*, 46(2), pp. 158-164.
- Regional Radiocommunication Conference for planning of the digital terrestrial broadcasting service (RCC-04). *ITU-R Report*, Geneva 2004.
- Saunders, S. R. 2005. *Antenna and Propagation for Wireless Communication Systems*. Wiley.
- Smith, D. 2003. *Digital Transmission Systems*. 3rd Edition. Kluwer Academic Publishers.
- Sung Ik Park, Yong-Tae Lee, Jae Young Lee, Seung Won Kim, and Soo In Lee 2007. Field Test Results of the E-VSB System in Korea, *IEEE Transactions On Broadcasting*, 53(1) pp. 14-22.
- Tapan, K. S. Zhong, J. Kyungjung, K. Abdellatif, M. and Magdalena Salazar-Palma 2003. A Survey of Various Propagation Models for Mobile Communication. *IEEE Antennas and Propagation Magazine*, 45(3), No. 3.
- Walfisch, J. Bertoni, H. L. 1988. A Theoretical Model of UHF Propagation in Urban Environments. *IEEE Transactions On Antennas And Propagation*, 36(12), pp. 1788-1796.
- Zreikat, A. and Al-Begain, K. n.d. Simulation of 3G Networks in Realistic Propagation Environments, *I.J. of SIMULATION*, 4(3&4), ISSN 1473-804x online, 1473-8031.

Interference Modeling for Wireless Ad Hoc Networks

Altenis V. Lima-e-Lima*, Carlos E. B. Cruz Pimentel*
and Renato M. de Moraes**

* *University of Pernambuco (UPE), Recife, Brazil*

** *University of Brasília (UnB), Brasília, Brazil*

1. Introduction

Interference effects constrain scalability performance of ad hoc networks as Gupta and Kumar (Gupta & Kumar, 2000) showed that the throughput capacity of a fixed wireless network decreases when the number of total nodes n increases. More specifically, they showed that the node throughput decreases approximately like $1/\sqrt{n}$. Grossglauser and Tse (Grossglauser & Tse, 2001) presented a two-phase packet forwarding technique for mobile ad hoc networks (MANETs), utilizing *multiuser diversity* (Knopp & Humblet, 1995), in which a source node transmits a packet to the nearest neighbor, and that relay delivers the packet to the destination when this destination becomes the closest neighbor of the relay. The scheme was shown (Grossglauser & Tse, 2001) to increase the throughput capacity of MANETs, such that it remains constant as the number of users in the network increases, taking advantage that communication among nearest nodes copes the interference due to farther nodes.

On the other hand, detailed and straightforward models for interference computation in dense ad hoc networks have not been extensively studied. Grid models have been proposed to compute interference (Gobriel et al., 2004), (Liu & Haenggi, 2005), which take advantage of the regular placement of the nodes. This orderly topology is a good starting point for static networks; however, it does not apply for MANETs. Also, some previous works have assumed a transmission or a reception range for communication among nodes without considering the effect from the entire network (Tobagi & Kleinrock, 1975), (Deng et al., 2004). This approximation can be good for low density networks, but it may imply in inaccurate results for dense networks. One problem with such approximation is the difficulty in finding an analytical description for the random topology inherent to ad hoc networks. In other cases, analytical models use graph theory (Rickenbach et al., 2005), (Qin-yun et al. 2005). While they are good for higher layer analysis, like routing, such models may not be appropriate for a more detailed communication channel study because they do not consider physical parameters like Euclidean distance, fading and path loss, for example.

This chapter analyzes an improved channel communication model, from the model proposed by Moraes et al. (Moraes et al., 2008) that permits to obtain the measured signal to noise and interference ratio (SNIR) by a receiver node, and consequently its spectral Shannon capacity (or spectral efficiency) (Cover & Thomas, 1991) at any point in the network when it communicates with a close neighbor. This model considers Euclidean distance, path loss and Rayleigh fading. The nodes are assumed to move according to a random mobility pattern and the parameter θ represents the fraction of sender nodes in the network. Monte-Carlo simulations (Robert & Casella, 2004) are used to validate the model. Furthermore, previous works had assumed the receiver node located at the center of the network (Lau & Leung, 1992), (Shepard, 1996), (Hajek et al., 1997). The results presented here are more general which shows that the received SNIR and spectral efficiency tend to a constant as n increases if a node communicates with its close neighbors when the path loss parameter α is greater than two, regardless of the position of the node in the network, i.e., wherever the receiver node is at the center, or at the middle, or at the boundary of the network area. For the case where α equals two, the limit SNIR and spectral efficiency go to zero; however, they decay very slowly making local communication still possible for a finite n . Another study performed here presents an autonomous technique for node state determination (sender or receiver) for each node in the network as function of the θ parameter.

The remaining of this chapter is organized as follows. Section 2 introduces the network model. Section 3 presents the average number of feasible receiving neighbor nodes as a function of the network parameters. Section 4 explains the interference and spectral efficiency computation. Section 5 shows the results. Section 6 explains the autonomous technique for node state determination. Finally, Section 7 concludes the chapter summarizing the main results obtained.

2. Model

The modeling problem addressed here is that of a wireless ad hoc network with nodes assumed mobile. The model consists of a normalized unit circular area (or disk) containing n nodes, and resembles the Grossglauser and Tse's model (Grossglauser & Tse, 2001). Therefore, information flow in the network follows the two-phase packet relaying technique as described in (Grossglauser & Tse, 2001). The position of node i at time t is indicated by $X_i(t)$. Nodes are assumed to move according to the *uniform mobility model* (Bansal & Liu, 2003). This model satisfies the following properties (Bansal & Liu, 2003): (a) the position of the nodes are independent of each other at any time t ; (b) the steady-state distribution of the mobile nodes is uniform; (c) the direction of the node movement is uniformly distributed in $[0, 2\pi)$, conditional on the position of the node.

Any node can operate either as a sender or as a receiver. At a given time t , a fraction of the total number of nodes n in the network, n_s , is randomly chosen by the scheduler as senders, while the remaining nodes, n_r , operate as possible receiving nodes (Grossglauser & Tse, 2001). A sender density parameter θ is defined as $n_s = \theta n$, where $\theta \in (0, 1)$, and $n_r = (1 - \theta)n$. Section 6 describes a technique that allows the nodes to adjust their communication status (sender or receiver) in order to the network attain $n_s = \theta n$.

A node j at time t is capable of receiving data at a given transmission rate of W bits/sec from sender node i if (Grossglauser & Tse, 2001), (Gupta & Kumar, 2000)

$$SNIR = \frac{P_i(t)g_{ij}(t)}{N_0 + \frac{1}{L}\sum_{k \neq i} P_k(t)g_{kj}(t)} = \frac{P_i(t)g_{ij}(t)}{N_0 + \frac{1}{L}I} \geq \beta, \quad (1)$$

where the summation is over all sender nodes $k \neq i$, $P_i(t)$ is the transmitting power of sender node i , $g_{ij}(t)$ is the channel path gain from node i to node j , β is the SNIR level necessary for reliable communication, N_0 is the noise power spectral density, L is the processing gain of the system, and I is the total interference at node j . In order to facilitate the analysis, let us assume that no processing gain is used, i.e., $L = 1$, and that $P_i = P \forall i$. The channel path gain is considered to be a function of the distance, fading and path loss, so that

$$g_{ij}(t) = \frac{\chi_{ij}^2}{|X_i(t) - X_j(t)|^\alpha} = \frac{\chi_{ij}^2}{r_{ij}^\alpha}, \quad (2)$$

where χ_{ij}^2 is the Rayleigh fading from node i to node j , r_{ij} is the Euclidean distance between nodes i and j , and α is the path loss parameter.

The goal is to find an equation relating the total interference measured by a receiver node that is communicating with a neighbor node as a function of the number of total users n in the network. More precisely, we aim to obtain an expression for Eq. (1) as a function of n and calculate the limit of the SNIR and consequently the limiting spectral efficiency, as n goes to infinity.

3. Feasible Receivers Near a Sender

In order to obtain the interference generated by nodes outside the neighborhood of a receiver node, we first need to find the average radius size containing a sender node and how many feasible receivers are within this range.

If the density of nodes in the disk is

$$\rho = \frac{n}{\text{total area}} = \frac{n}{1} = n, \quad (3)$$

then the average radius for one sender node (r_0), for a uniform node distribution, is given by

$$1 = \theta \rho \pi r_0^2 = \theta n \pi r_0^2 \Rightarrow r_0 = \frac{1}{\sqrt{\theta n \pi}}. \quad (4)$$

Hence, the average number of receiving nodes, called \bar{K} , within r_0 , assuming a uniform node distribution (Shepard, 1996), is

$$\bar{K} = nR\pi r_0^2 = (1 - \theta)n\pi \left(\frac{1}{\sqrt{\theta n\pi}}\right)^2 = \frac{1}{\theta} - 1, \tag{5}$$

which is constant for a given θ . Eq. (5) is a benchmark for obtaining the average number of receiving nodes as a function of the network parameter θ .

Thus, the radius r_0 defines a cell (radius range) around a sender where \bar{K} receiver nodes are nearby on average. The feasibility that all of those \bar{K} nodes successfully receive the same data being transmitted by the sender is the subject of the next section.

4. Interference and Capacity Computation

In the previous section, the average radius r_0 containing one sender with \bar{K} receiver nodes around on average was obtained. Suppose that one of the \bar{K} receiving nodes is at the neighborhood¹ distance r_0 . We want to show how the SNIR measured by this receiver behaves as the number of total nodes in the network (and therefore the number of total interferers) goes to infinity. We are interested in determining whether feasible communication between the sender and the farthest neighbor (with distance r_0) is still possible, even if the number of interferers grows.

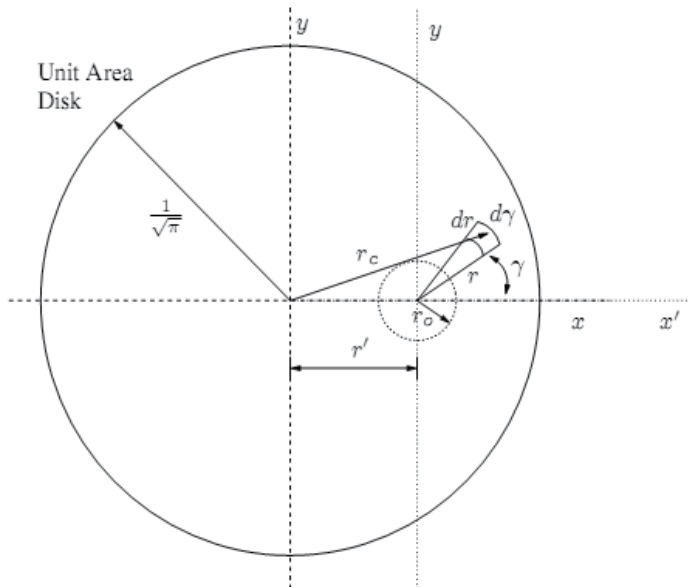


Fig. 1. Snapshot of the unit area disk at a given time t . At this time, the receiver node being analyzed is located at distance r' from the center while the sender is at distance r_0 from the receiver node.

¹ This represents the worst case scenario, because the other $\bar{K} - 1$ neighbors are located either closer or at the same distance r_0 to the sender, so they measure either a stronger or the same SNIR value.

For a packet to be successfully received, Eq. (1) must be satisfied. Hence, consider a receiver at any location in the network for a given time t . Its distance from the center r' is shown in Figure 1, where $0 \leq r' \leq \frac{1}{\sqrt{\pi}} - r_0$.

Let us assume that the sender is at distance r_0 from this receiver and transmitting at constant power P , so that the power P_0 measured by this receiver is given by

$$P_0 = \frac{P\chi_0^2}{r_0^\alpha}, \quad (6)$$

where χ_0^2 is the Rayleigh fading from sender to receiver.

In order to obtain the overall expected interference at the receiver caused by all transmitting nodes in the disk, let us consider a differential element area $rdrd\gamma$ that is distant r units from the receiver and r_c units from the center of the network (see Figure 1). As consequence of the uniform mobility model, the steady-state distribution of the nodes is uniform (Bansal & Liu, 2003). Thus, the probability density function of the distance r_c to the center of the network is given by (Lau & Leung, 1992)

$$f_{R_c}(r_c) = \begin{cases} 2\pi r_c & \text{if } 0 \leq r_c \leq \frac{1}{\sqrt{\pi}} \\ 0 & \text{otherwise.} \end{cases} \quad (7)$$

Because the nodes are uniformly distributed in the disk, the transmitting nodes inside the differential element of area generate, at the receiver, the following amount of interference²

$$dI = \frac{P\chi^2}{r^\alpha} \theta \rho r dr d\gamma = \frac{P\chi^2}{r^{\alpha-1}} \theta n dr d\gamma. \quad (8)$$

The total interference is obtained by integrating Eq. (8) over the disk area and the result depends on the value of α . Accordingly, the following two cases are considered.

A. The case $\alpha > 2$

For some propagation environments (Rappaport, 2002) the path loss parameter is modeled to be always greater than two, i.e., $\alpha > 2$. In this case, the SNIR at the receiver located at distance r' from the center for a total of n nodes in the network is given in the following lemma.

Lemma 1. *At a given time t , for a receiver node located at distance r' from the center in a unit area disk network containing n mobile nodes uniformly distributed, where $\alpha > 2$, and assuming the sender located at distance r_0 from this receiver, then the receiver SNIR is given by*

² Because the nodes are uniformly distributed in the disk and n grows to infinity, we approximate the sum in Eq. (1) by an integral.

$$SNIR_{r'}(n) = \frac{Pe^{(\delta\sigma_s)^2}}{\frac{N_0}{(\theta n\pi)^{\frac{\alpha}{2}}} + \frac{2Pe^{(\delta\sigma_s)^2}}{\alpha - 2} q_{r',\alpha,\theta}(n)} \quad (9)$$

where $\delta = \frac{\ln(10)}{10}$, σ_s is the standard deviation of the attenuation Gaussian random variable in decibels due to shadowing (Akl et al., 2001), and

$$q_{r',\alpha,\theta}(n) = \left[1 - \frac{\int_0^\pi \left[\sqrt{\frac{1}{\pi} - (r' \sin \gamma)^2} - r' \cos \gamma \right]^{2-\alpha} d\gamma}{\pi^{\frac{\alpha}{2}} (\theta n)^{\frac{\alpha-2}{2}}} \right]^{-1}. \quad (10)$$

Proof of Lemma 1. By integrating Eq. (8) over the area of the disk, for $\alpha > 2$, we obtain the interference at the receiver located at a distance r' from the center for a total of n nodes in the network. Hence,

$$\begin{aligned} E[I_{r'}(n)] &= \int_{\text{disk area}} dl = E \left[\int_0^{2\pi} \int_{r_0}^{r_m(r',\gamma)} \frac{P\chi^2}{r^{\alpha-1}} \theta n dr d\gamma \right] \\ &= Pe^{(\delta\sigma_s)^2} \theta n \int_0^{2\pi} \frac{r^{2-\alpha}}{2-\alpha} \Big|_{r_0}^{r_m(r',\gamma)} d\gamma \\ &= \frac{Pe^{(\delta\sigma_s)^2} \theta n}{\alpha - 2} \int_0^{2\pi} \left\{ \frac{1}{r_0^{\alpha-2}} - \frac{1}{[r_m(r',\gamma)]^{\alpha-2}} \right\} d\gamma. \end{aligned} \quad (11)$$

r_m is the maximum radius that r can have and is a function of the location r' and the angle γ (see Figure 1). To find this function, we can use the boundary disk curve (or circumference) equation expressed as a function of the x-axis and y-axis shown in Figure 1, i.e.,

$$x^2 + y^2 = \left(\frac{1}{\sqrt{\pi}} \right)^2. \quad (12)$$

Define $x = x' + r'$, $x' = r_m \cos \gamma$, and $y = r_m \sin \gamma$. Then, Eq. (12) becomes

$$(r_m \cos \gamma + r')^2 + (r_m \sin \gamma)^2 = \left(\frac{1}{\sqrt{\pi}} \right)^2 \Rightarrow r_m(r', \gamma) = \sqrt{\frac{1}{\pi} - (r' \sin \gamma)^2} - r' \cos \gamma. \quad (13)$$

By substituting this result in Eq. (11), we arrive at

$$E[I_{r'}(n)] = \frac{2Pe^{(\delta\sigma_s)^2} \theta n}{\alpha - 2} \left[\frac{\pi}{r^{\alpha-1}} - f_\alpha(r') \right], \quad (14)$$

where

$$f_\alpha(r') = \int_0^\pi \frac{d\gamma}{\left[\sqrt{\frac{1}{\pi} - (r' \sin \gamma)^2} - r' \cos \gamma \right]^{\alpha-2}} \quad (15)$$

is a constant for a given position r' . For the case in which $\alpha = 4$, Eq. (15) reduces to

$$f_4(r') = \frac{\pi^2}{1 - 2\pi r'^2 + \pi^2 r'^4}. \quad (16)$$

The SNIR can be obtained by using Eqs. (1), (4), (6), and (14) to arrive at

$$\begin{aligned} SNIR_{r'}(n) &= \frac{E[P_0]}{N_0 + E[I_{r'}(n)]} = \frac{P e^{(\delta\sigma_s)^2}}{\frac{N_0}{(\theta n \pi)^{\frac{\alpha}{2}}} + \frac{2P e^{(\delta\sigma_s)^2}}{\alpha - 2} \cdot \frac{1}{1 - \frac{1}{\pi^{\frac{\alpha}{2}} (\theta n)^{\frac{\alpha-2}{2}}} \cdot f_\alpha(r')}}} \\ &= \frac{P e^{(\delta\sigma_s)^2}}{\frac{N_0}{(\theta n \pi)^{\frac{\alpha}{2}}} + \frac{2P e^{(\delta\sigma_s)^2}}{\alpha - 2} \cdot q_{r',\alpha,\theta}(n)} \end{aligned} \quad (17)$$

Where

$$q_{r',\alpha,\theta}(n) = \left[1 - \frac{1}{\pi^{\frac{\alpha}{2}} (\theta n)^{\frac{\alpha-2}{2}}} f_\alpha(r') \right]^{-1}, \quad (18)$$

which finishes the proof. ■

From Eq. (9), taking the limit as $n \rightarrow \infty$, we obtain

$$\begin{aligned} SNIR &= \lim_{n \rightarrow \infty} \frac{P e^{(\delta\sigma_s)^2}}{\frac{N_0}{(\theta n \pi)^{\frac{\alpha}{2}}} + \frac{2P e^{(\delta\sigma_s)^2}}{\alpha - 2} \cdot q_{r',\alpha,\theta}(n)} \\ &= \begin{cases} \frac{\alpha - 2}{2} & \text{if } 0 \leq r' < \frac{1}{\sqrt{\pi}} - r_0 \\ \frac{\alpha - 2}{2} q_{r',\alpha,\theta}(n)(n \rightarrow \infty) & \text{if } r' = \frac{1}{\sqrt{\pi}} - r_0, \text{ i. e.,} \\ & \text{the network boundary.} \end{cases} \end{aligned} \quad (19)$$

From Eq. (10), $q_{r',\alpha,\theta}(n \rightarrow \infty) = q_{r',\alpha}(n \rightarrow \infty)$ because θ is a scale factor on n and it does not change the limit. Thus,

$$q_{r',\alpha,\theta}(n \rightarrow \infty) = \begin{cases} 1 & \text{if } 0 \leq r' < \frac{1}{\sqrt{\pi}} - r_0 \text{ and } \alpha > 2 \\ 1.47 & \text{if } r' = \frac{1}{\sqrt{\pi}} - r_0 \text{ and } \alpha = 3 \\ 1.33 & \text{if } r' = \frac{1}{\sqrt{\pi}} - r_0 \text{ and } \alpha = 4 \\ 1.27 & \text{if } r' = \frac{1}{\sqrt{\pi}} - r_0 \text{ and } \alpha = 5 \\ 1.23 & \text{if } r' = \frac{1}{\sqrt{\pi}} - r_0 \text{ and } \alpha = 6. \end{cases} \quad (20)$$

Therefore, from Eqs. (19) and (20), for $\alpha > 2$, the $SNIR$ tends to a constant as $n \rightarrow \infty$.

From Lemma 1, the spectral efficiency (C) is straightly obtained and is given (in units of bits/s/Hz) by (Cover & Thomas, 1991)

$$C = \log_2[1 + SNIR_{r'}(n)] = \log_2 \left[1 + \frac{P e^{(\delta\sigma_s)^2}}{\frac{N_0}{(\theta n \pi)^{\frac{\alpha}{2}}} + \frac{2P e^{(\delta\sigma_s)^2}}{\alpha - 2} \cdot q_{r',\alpha,\theta}(n)} \right]. \quad (21)$$

Accordingly, from Eqs. (9), (20) and (21), we conclude that the limiting spectral efficiency goes to a constant as $n \rightarrow \infty$ for $\alpha > 2$.

B. The case $\alpha = 2$

For the free space propagation environment (Rappaport, 2002), the path loss parameter is modeled to be equal to two, i.e., $\alpha = 2$. Thus, the total expected interference at the receiver located at distance r' from the center for a total of n nodes in the network is obtained by the following lemma, which proof is analogous to Lemma 1.

Lemma 2. *At a given time t , for a receiver node located at distance r from the center in a unit area disk network containing n mobile nodes uniformly distributed, where $\alpha = 2$, and assuming the sender located at distance r_0 from this receiver, then the receiver $SNIR$ is given by*

$$SNIR_{r'}(n) = \frac{P e^{(\delta\sigma_s)^2}}{\frac{N_0}{\theta n \pi} + \frac{2P e^{(\delta\sigma_s)^2}}{\pi} \cdot \int_0^\pi \ln \left[(\sqrt{\pi\theta n}) \left(\sqrt{\frac{1}{\pi} - (r' \sin \gamma)^2} - r' \cos \gamma \right) \right] d\gamma}. \quad (22)$$

Consequently, the spectral efficiency is obtained (in units of bits/s/Hz) by (Cover & Thomas, 1991)

$$C = \log_2 \left[1 + \frac{P e^{(\delta\sigma_s)^2}}{\frac{N_0}{\theta n \pi} + \frac{2P e^{(\delta\sigma_s)^2}}{\pi} \cdot \int_0^\pi \ln \left[(\sqrt{\pi\theta n}) \left(\sqrt{\frac{1}{\pi} - (r' \sin \gamma)^2} - r' \cos \gamma \right) \right] d\gamma} \right]. \quad (23)$$

From Eq. (22), it is straightforward that $SNIR_{r'}(n) \rightarrow 0$ as $n \rightarrow \infty$. Therefore, the limiting spectral efficiency goes to zero as $n \rightarrow \infty$ for $\alpha = 2$.

5. Results

In this section, the analytical results elaborated in Section 4 are compared with Monte-Carlo simulations (Robert & Casella, 2004).

Figure 2 shows the spectral efficiency as function of n for $\alpha = 3, \theta = 1/3$ for distinct values of r' . Also, Figure 2 shows that the spectral efficiency remains constant when n goes to infinity and its does not depend on r' if $0 \leq r' < \frac{1}{\sqrt{\pi}} - r_0$, and has the same value for any position of the receiver node, whether the position is at the center, close to the boundary, or at the middle region of the radius disk. Nevertheless, if the receiver node is at the boundary ($r' = \frac{1}{\sqrt{\pi}} - r_0$), then the limiting spectral efficiency is still a constant when n scales to infinity but it has a greater value.

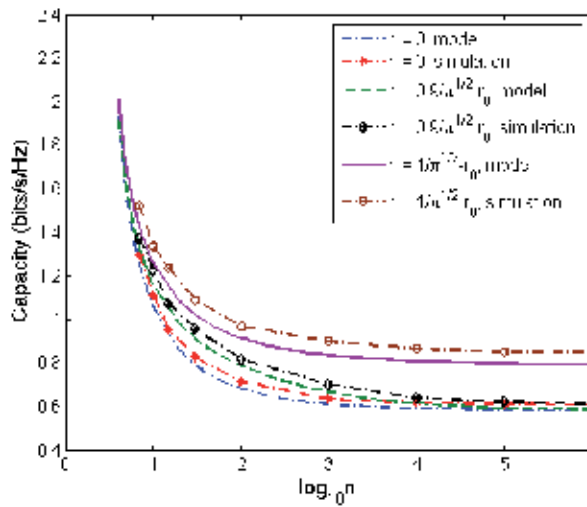


Fig. 2. Spectral efficiency curves as a function of n for $\alpha = 3, \theta = 1/3, P = 1W, \sigma_s = 6$ and $N_0 = 5$ for the receiver node located at different positions in the network. In the legend, *model* is used for Eq. (21), while *simulation* is used for Monte-Carlo simulation.

Figure 3 illustrates the spectral efficiency behavior for different values of N_0 when $P = 1W$. As expected, the capacity diminishes when noise increases; however, the limiting capacity is the same regardless of noise because the interference effect dominates the denominator of Eq. (1) as $n \rightarrow \infty$.

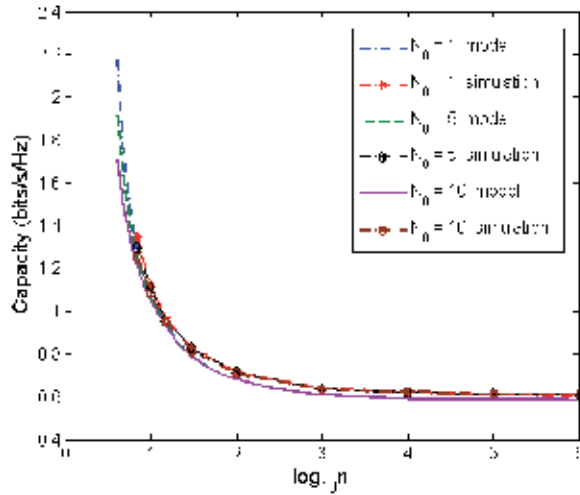


Fig. 3. Spectral efficiency curves as a function of n , for $\alpha = 3, \theta = 1/3, P = 1W$ and $\sigma_s = 6$, for different values of N_0 . In the legend, *model* is used for Eq. (21), while *simulation* is used for Monte-Carlo simulation.

Figure 4 confirms that the limiting spectral efficiency does not depend on θ as observed in Section 4-A.

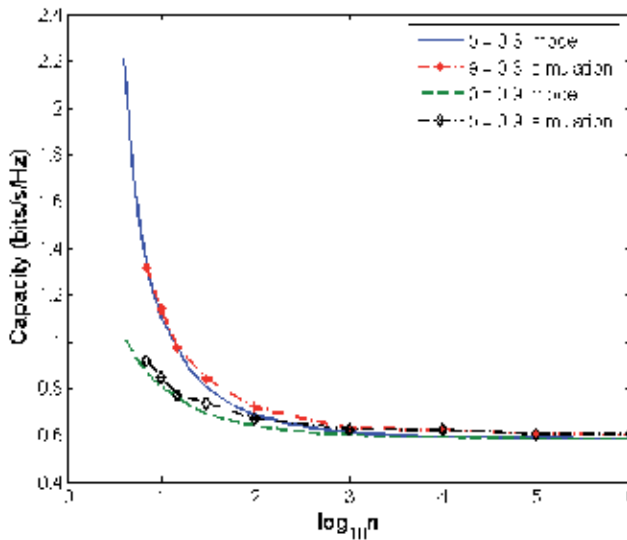


Fig. 4. Spectral efficiency curves as a function of n , for $\alpha = 3, N_0 = 5, P = 1W$ and $\sigma_s = 6$, for different values of θ . In the legend, *model* is used for Eq. (21), while *simulation* is used for Monte-Carlo simulation.

Figure 5 shows the spectral efficiency as function of n for different values of σ_s . It also illustrates that the capacity tends to a constant value as n scales to infinity regardless of σ_s .

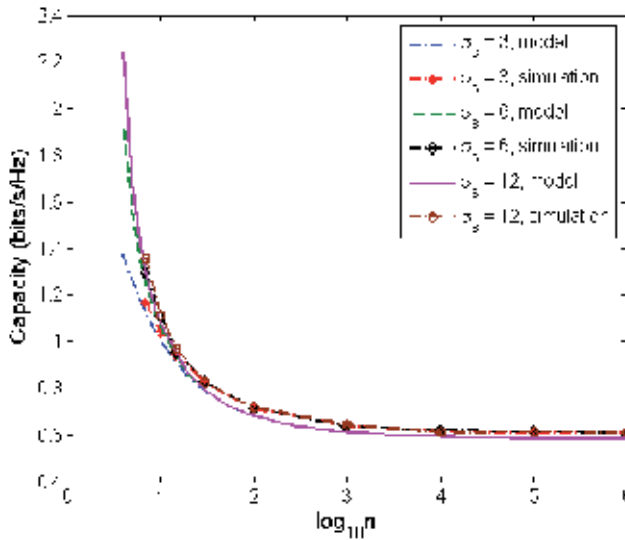


Fig. 5. Spectral efficiency curves as a function of n , for $\alpha = 3, N_0 = 5, P = 1W$ and $\theta = 1/3$, for different values of σ_s . In the legend, *model* is used for Eq. (21), while *simulation* is used for Monte-Carlo simulation.

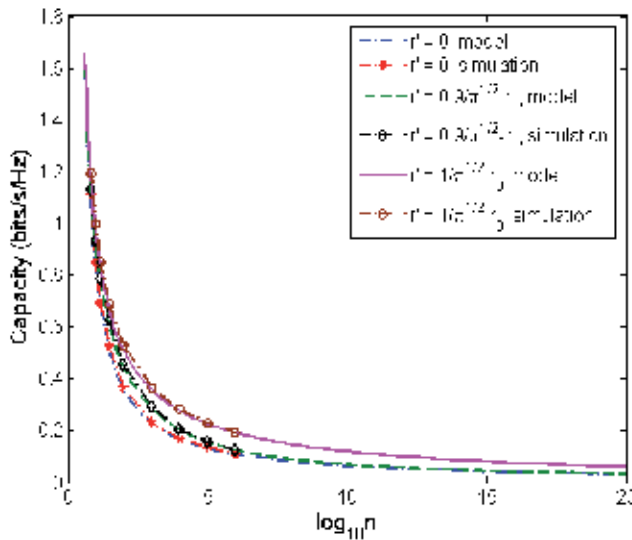


Fig. 6. Spectral efficiency curves as a function of n for $\alpha = 2, \theta = 1/3, P = 1W, \sigma_s = 6$ and $N_0 = 5$ for the receiver node located at different positions in the network. In the legend, *model* is used for Eq. (23), while *simulation* is used for Monte-Carlo simulation.

Figure 6 shows curves for spectral efficiency as function of n when $\alpha = 2$. Although the limiting capacity goes to zero as already observed in Section 4-B, the decay is not fast. We see that the spectral efficiency for a receiver node reaches 0.04 bits/s/Hz as the number of interferers approaches 10^{20} , i.e., the capacity falls very slowly, and it can allow feasible

communication between neighbor nodes for a finite number of users n . In addition, the capacity is about 0.066 bits/s/Hz for a receiver at the boundary of the network for this same number of interferers. Note that we have plotted points up to $n = 10^{20}$ for the model, while the simulations were plotted up to $n = 10^6$ due to computer limitation.

6. A Technique to Attain a Desired Value for The θ Parameter

Another challenge associated with this study is how a node can efficiently set its state (sender or receiver) in order to the network attain a given θ . The work presented by Grossglauser and Tse (Grossglauser & Tse, 2001), and supplemented by Moraes (Moraes et al., 2007) shows analytically and by simulation that the maximum throughput for a wireless ad hoc network is achieved when the fraction of sender nodes (θ) is approximately $1/3$ of the total nodes in the network. However, to the best of our knowledge, there are no studies in the literature on MAC protocols that seek this distribution autonomously and in a distributed way.

The technique suggested here consists of a simplified part of a MAC layer protocol. Similar to the Traffic Adaptive Medium Access (TRAMA) protocol (Rajendran et al., 2003), our scheme has the requirement to be synchronized with cyclical periods of contention followed by transmission in which some nodes are capable of taking control of close neighbors, as found in IEEE 802.15.4 - ZigBee (ZigBee Alliance, 2009). This technique, restricted only to the contention period, is intended to be autonomous and able to distribute the states of the nodes according to the θ parameter.

Considering the node distribution as described in Section 2 and that each node has its unique identification (ID), the node with the lowest ID controls the network and it is called the coordinator node of the network.

The communication among nodes follows cycles which are divided in contention and transmission phases. The contention period is divided in following three phases, respectively. The announcement is the period in which each node sends its packet identification number. The dissemination is the phase when the coordinator node sends its identification to all nodes of the domain. Finally, there is the distribution phase where the node coordinator sends a random sequence indicating the status (sender or receiver) that each node in the network must assume during the following transmission period according to the θ parameter previously scheduled.

Figure 7 presents the results of a simulation implemented in JAVA (Java, 2009), using the shuffle method of Class Collections (JavaClassCollections, 2009) for the random distribution of the states (sender and receiver), which are displayed as fraction of times that three nodes randomly chosen, over 100 cycles, were senders. It is observed that the three randomly chosen nodes tend to converge their sender fraction of times to $\theta = 1/3$ as expected.

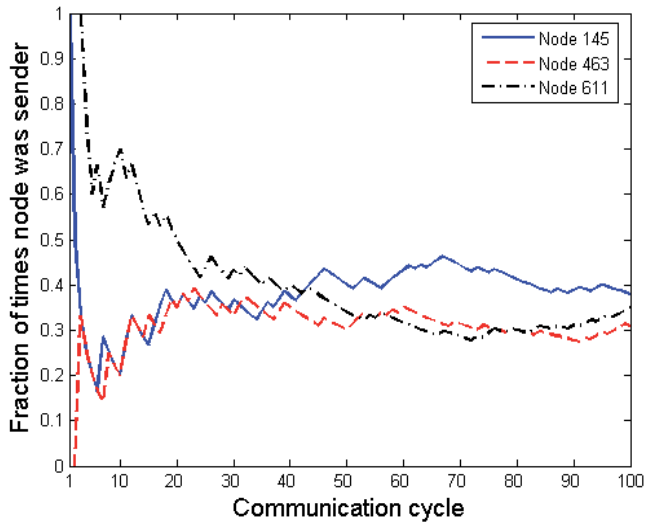


Fig. 7. Evolution of the fraction of times that three randomly chosen nodes were sender over the simulated cycles for $\theta = 1/3$ and $n = 1000$.

The technique suggested here does not consider other medium access issues like channel admission control, collision resolution, node failure, etc., which is subject of future work.

7. Conclusions

We have analyzed interference effects and spectral Shannon capacity (or spectral efficiency) for mobile ad hoc networks using a communication channel model, which considers Euclidean distance, path loss, fading and a random mobility model. We found that, for a receiver node communicating with a close neighbor where the path loss parameter α is greater than two, the resultant signal to noise and interference ratio (SNIR) and consequently the spectral efficiency tend to a constant as the number of nodes n goes to infinity, regardless of the position of the receiver node in the network. Therefore, for the studied model, communication is feasible for near neighbors when the number of interferers scales. Furthermore, for the receiver nodes located at the boundary of the circular network, we show that they suffer less interference than those located inside attaining higher capacity. Also, for the case where α is equal to two, the capacity was shown to go to zero as n increases; however, the decay is very slowly making local communication still possible for a finite n . Model and Monte-Carlo simulation results present good agreement and validate the interference and Shannon capacity investigation performed.

It was also proposed a technique for autonomous and distributed allocation of states (sender or receiver) of nodes based on the parameter θ . Future work can consider MAC layer issues like admission control and collisions, as well as power control and other types of mobility which results in other distributions of nodes in the network, and how they affect the capacity.

Acknowledgements

This work was supported in part by PIBIC/POLI, by Fundação de Amparo à Ciência e Tecnologia do Estado de Pernambuco (FACEPE) and by Conselho Nacional de Desenvolvimento Científico e Tecnológico (CNPq), Brazil.

8. References

- Akl, R., Hedge, M., Naraghi-Pour, M., & Min, P. (2001). Multicell CDMA Network Design, *IEEE Transactions on Vehicular Technology*, vol. 50, no. 3, pp. 711-722.
- Bansal, N. & Liu, Z. (2003). Capacity, delay and mobility in wireless ad-hoc networks, *Proc. of IEEE Infocom*, San Francisco, CA.
- Cover, T. M. & Thomas, J. A. (1991), In: *Elements of Information Theory*. John Wiley & Sons.
- Deng, J., Han, Y. S., Chen, P. N. & Varshney, P. K. (2004). Optimum transmission range for wireless ad hoc networks, *Proc. of IEEE WCNC*, Atlanta, GA.
- Gobriel, S., Melhem, R. & Mossé, D. (2004). A unified interference/collision analysis for power-aware ad hoc networks, *Proc. of IEEE Infocom*, Hong Kong.
- Grossglauser, M. & Tse, D. (2001). Mobility increases the capacity of wireless ad-hoc networks, *Proc. of IEEE Infocom*, Anchorage, AK.
- Gupta, P. & Kumar, P. R. (2000). The capacity of wireless networks, *IEEE Transactions on Information Theory*, vol. 46, no. 2, pp. 388-404.
- Hajek, B.; Krishna, A. & LaMaire, R. O. (1997). On the capture probability for a large number of stations, *IEEE Transactions on Communications*, vol. 45, no. 2, pp. 254-260.
- Java Class Collections (2009). On <http://java.sun.com/j2se/1.3/docs/api/java/util/Collections.html>
- Java Language (2009). On <http://java.sun.com>
- Knopp, R. & Humblet, P. A. (1995). Information capacity and power control in single-cell multiuser communications, *Proc. of IEEE ICC*, Seattle, WA.
- Lau, C. T. & Leung, C. (1992). Capture models for mobile packet radio networks, *IEEE Transactions on Communications*, vol. 40, no. 5, pp. 917-925.
- Liu, X. & Haenggi, M. (2005). Performance analysis of rayleigh fading ad hoc networks with regular topology, In *Proc. of IEEE Globecom*, St. Louis, MO.
- Moraes, R. M. de, Buarque, C. E. & Araujo, F. P. (2008). Shannon Capacity for a Simple Communication Channel Model in Dense MANETs, *Proc. Of IEEE IWCMC*, Crete, Greece.
- Moraes, R. M. de, Sadjadpour, H. & Garcia-Luna-Aceves, J. J. (2007). Taking full advantage of multiuser diversity in mobile ad hoc networks. *IEEE Transactions on Communications*, vol. 55, pp. 1202-1211.
- Qin-yun, D.; Xiu-lin, H.; Hong-yi, Y. & Jun, Z. (2005). On the capacity of wireless ad-hoc network basing on graph theory, In: *Lecture Notes in Computer Science*, vol. 3421/2005, pp. 353-360.
- Rajendran, V. ; Obraczka, K. & Garcia-Luna-Aceves, J. J. (2003). Energy-Efficient, Collision-Free Medium Access Control for Wireless Sensor Networks, *Proceedings of ACM SenSys 03*, Los Angeles, CA.
- Rappaport, T. S. (2002). In: *Wireless Communications: Principles and Practice*. Prentice Hall.

- Rickenbach, P. von; Schmid, S.; Wattenrofer, R. & Zollinger, A. (2005). A robust interference model for wireless ad-hoc networks, *Proc. of IEEE WMAN*, Denver, CO.
- Robert, C. P. & Casella, G. (2004). In: *Monte Carlo Statistical Methods*. Springer-Verlag.
- Shepard, T. J. (1996). A channel access scheme for large dense packet radio networks, *Proc. of ACM SigComm*, San Francisco, CA.
- Tobagi, F. & Kleinrock, L. (1975). Packet switching in radio channels: Part ii - the hidden terminal problem in carrier sense multiple-access and the busy-tone solution, *IEEE Transactions on Communications*, vol. COM-23, no. 12, pp. 1417-1433.
- ZigBee Alliance (2009). IEEE 802.15.4, ZigBee standard. On <http://www.zigbee.org>

Energy Saving Drives New Approaches to Telecommunications Power System

Rais Miftakhutdinov
Texas Instrument Inc.
United States of America

1. Introduction

Steady growth in the telecommunication industry providing data, voice and video is very likely to continue in the foreseeable future. This growth is supported by expansion into the new markets, especially in Asia, accelerated widespread of wireless and broadband technology, and strong demand for more efficient, power saving solutions. As the result of the growth, the telecommunication infrastructure becomes significant energy consumer and contributor to greenhouse emissions. Based on International Telecommunication Union estimation, the information and communication technology contributes 2-2.5 per cent into the worldwide greenhouse gas emissions (<http://www.itu.int/themes/climate/index.html>). To reduce the impact on global warming, more efficient distribution, conversion and use of electrical energy by telecommunication industry is required. Worldwide movements for energy saving and “Green power” generation and distribution, have resulted in number of voluntary initiatives and mandatory regulations by international and government organizations for increased efficiency of electronic equipment including data and telecommunication power systems. Examples of such organizations and initiatives are United States ENERGY STAR® program, German Blue Angel, Japan Environment Association, European Code of Conduct and others (http://www.energystar.gov/index.cfm?c=ent_servers.enterprise_servers; Mammano, 2006). The focus of this chapter is efficient and low power consumption DC power systems for a central office and base station of telecommunication infrastructure. According to (Fasullo et al., 2008) telecommunication industry consumes 160 Billion kWh each year, and majority of this electrical energy passes through DC power distribution system.

Telecommunication DC power systems have come long way from simple rectifier/battery system to complex switching power supplies, from centralized power to distributed architecture (Thorsell, 1990). At the same time, required tasks and functional complexity of power systems continue to grow. To effectively reduce the overall system power consumption per required functionality, all design levels from system architecture level down to each specific function and component must be optimized. This chapter limits its scope to energy saving considerations of power system at facility level, then down to power distribution in a rack, or cabinet, and finally focuses on the specific power conversion topologies and control algorithms implemented in power supplies.

At the facility level, intensive research and evaluation of 380-V DC distribution bus is reported to replace traditional 208 V (230 V) AC mains (Pratt et al., 2007; Akerlund et al., 2007). At the cabinet level, intermediate bus architecture (IBA) has become widespread to address increased requirements for supply voltage quality, accurate power sequencing, flexibility and availability of power system (Morrisson, 2002; White, 2003; Miftakhutdinov, 2008a). Currently, demand for high efficiency over wide output power range and low power consumption reshapes the telecom power distribution system once again. Typical cabinet level power system includes AC/DC front end power supply providing system bus voltage that can be -48 V, 24 V, 12 V or 130 V depending on specific system and application. The same power supply in most cases is used as a charger for the backup battery. Driven by government regulations and market demand, the telecom and server power supply is now required to be efficient over output power range from 10% (sometimes even 5%) up to 100% (http://www.energystar.gov/index.cfm?c=ent_servers.enterprise_servers).

Efficiency was always important for data and telecommunication power supply to achieve high power density and improve thermal performance. So far, only high efficiency at maximum load was required because it determines reliability, size and cost of equipment and cooling. Currently, the focus is shifted to energy saving and high efficiency over the entire output power range.

Overall, the design procedure includes power system architecture selection and identifying power conversion topologies and related control strategy. Use of the best in class components is also critical to meet the design goals. In the chapter, all these critical stages of telecom power system design are discussed in details including comparison of alternative solutions.

Optimal control algorithm is critical not only to meet static and dynamic requirements of telecom power system. It also opens new opportunities to increase the efficiency by transitioning into different optimal power saving modes depending on system conditions. Here, the flexibility, programmability and auto tuning capability of digital controllers must be weighted against the lower cost, simple, and usually faster analog control ICs. Promising control strategies along with the examples of advanced analog and digital controllers addressing new requirements for high efficiency will be provided in the chapter.

The interface between IC controller and power stage, that includes power switch drivers, current, voltage, and temperature sensing, auxiliary bias supply, has critical role and deserve careful consideration as well.

The chapter discusses requirements for telecom rectifiers and front-end server power supplies: the key functional parts of any data- and telecommunication power system.

Special attention is provided to intermediate bus converters (IBC) that are the enabling part of any IBA. The IBC requirements and parameters, popular topologies, design challengers are discussed in details. The design examples and test results of 600-W unregulated IBC converter with 48-V input and 5:1 transfer ratio are provided to illustrate and verify the recommended design approaches and solutions.

2. Strive for Efficiency and Power Saving

2.1 Energy Saving Trends and Regulations

High efficiency was always critical requirement for data and telecom power system as precondition to achieve high power density and improve thermal parameters. So far, only

the efficiency at maximum load was usually being taken into consideration. This is because the size, cost, temperature profile of components and their cooling selection is determined at the maximum output power, where power losses are the highest. However, currently the paradigm is shifted and the new requirements focus primarily on energy saving. Therefore, it is critical to have high efficiency even at mid and light loads, where, as it turned out, power system operates significant amount of time. Driven by government regulations and market demand, the data and telecommunication power supply efficiency is now specified from 10% (sometimes 5%) up to 100% of its output power range. At the same time, the power supply and entire system must not exceed the power consumption limits specified for idle operation modes. One example is ENERGY STAR®, which is a joint program of the U.S. Environmental Protection Agency and the U.S. Department of Energy. The program sets efficiency and power consumption recommendations and regulations for different types of electronic equipment. The version 1 of ENERGY STAR® Program Requirements for Computer Servers was effective starting May 15, 2009 (http://www.energystar.gov/ia/partners/product_specs/program_reqs/computer_server_prog_req.pdf). Table 1 below shows related efficiency requirements at 10%, 20%, 50% and 100% output power of single-output AC/DC and DC/DC converters.

Rated Output Power	10% Load	20% Load	50% Load	100% Load
≤ 500 W	70%	82%	89%	85%
501 – 1000 W	75%	85%	89%	85%
> 1000 W	80%	88%	92%	88%

Table 1. Efficiency requirements for single output AC/DC or DC/DC server power supply

For AC/DC Server Power Supply the ENERGY STAR® Program also defines the minimum Power Factor Coefficient as 0.9 for loads from 50% to 100%. This practically means mandatory use of active power factor corrector block in power supply. The Program also limits maximum power dissipated at Idle State to 55 W for single processor based standard server. By definition, during the Idle Operational State, the operating system and other software have completed loading and the server is capable of completing workload transactions, but not processing of any useful work. Adding redundant power supplies to the system allows extra 20 W of power per each additional power supply. Another words only 20 W power can be consumed by the power supply at no load condition.

Similar power saving programs are currently implemented or under development worldwide by government organizations like German Blue Angel, Japan Environment Association, European Code of Conduct and others (Mammano, 2006). It becomes widespread practice that large data and telecommunication providers sometimes set even stronger efficiency and power saving requirements to power system manufactures in attempt to reduce the cost of service and stay competitive.

2.2 Power System Architecture at Facility Level

To meet new efficiency and power saving requirements all system and design levels must be reviewed and optimized. These levels include general power system architecture, power stage topologies for each power conversion, optimal power stage component selection and control algorithms providing optimal and efficient operation of the entire system.

Typical power system of data center at the facility level is shown in Figure 1. Such system generates uninterruptable 208 V AC line. There is double power conversion from DC to AC in UPS and from AC back to DC in the front-end power supply.

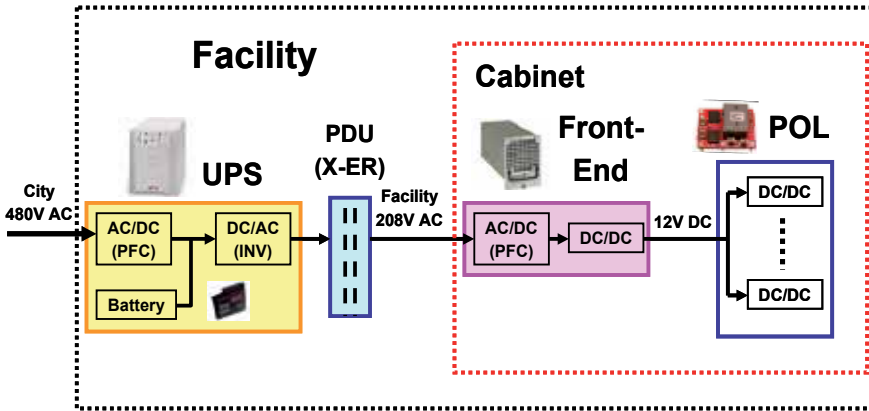


Fig. 1. Typical power system of data center

If to replace AC uninterruptable distribution power line at facility level by the DC line, as it is shown in Figure 2, more than 7% overall efficiency improvement (Pratt et al., 2007) and 10% to 30% saving in cost of operation (Akerlund et al., 2007) can be achieved.

Advantages of the power system with DC distribution bus at facility level are obvious from the power saving view however, some safety and technical questions must be resolved including certified DC power distribution units and availability of UPS with high voltage DC output. The European Standard EN 300 132-3 issued by ETSI includes DC bus up to 400 V as an option for powering telecommunication equipment, thus setting guidelines for development and use of such power architecture (ETSI, 2003).

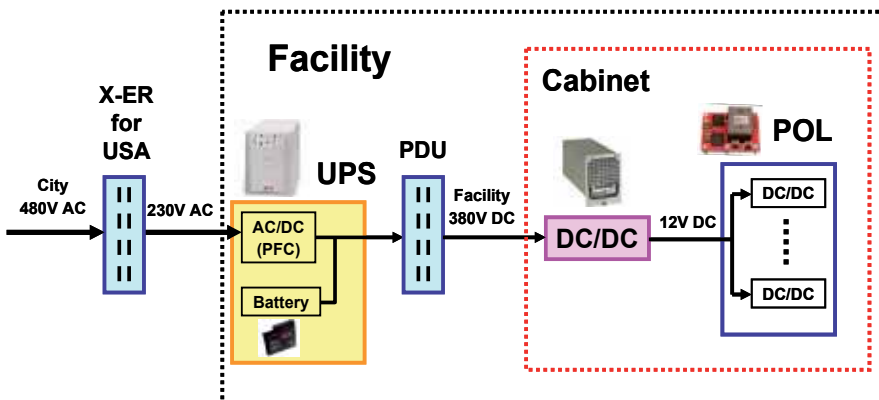


Fig. 2. Power system with 380 V DC distribution bus at facility

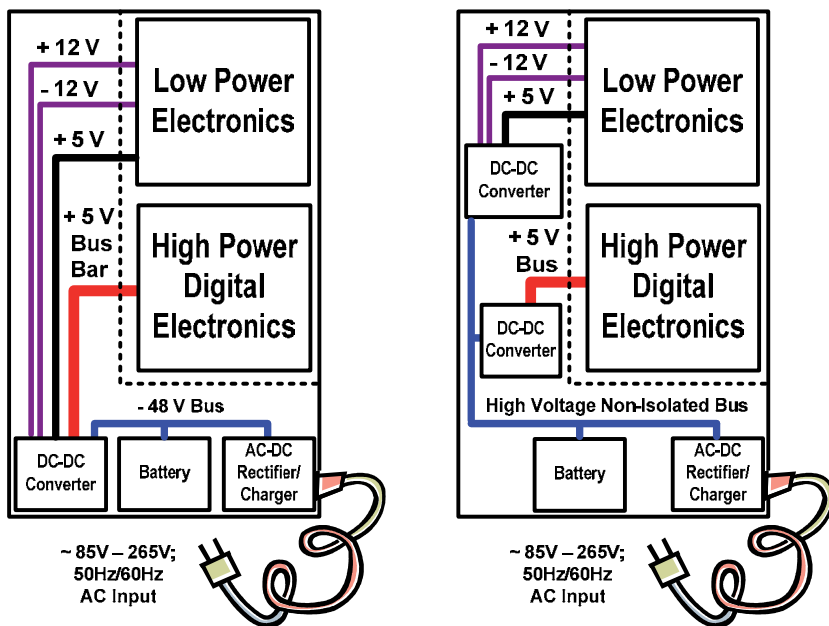
3. Evolution of Telecommunication Power System at Cabinet Level

Power distribution systems for tele- and data-communication equipment at cabinet level have undergone dramatic changes within last two decades because of fast progress of

modern digital-processing technology, requiring high quality supply voltages with specific power sequencing. significant increase in economic losses in case of service interruption was another key factor demanding highly reliable, flexible and available power system. And the most recent changes are driven by push for the efficient, “green” power with the reduced cost of ownership. The evolution of cabinet power system from centralized power to distributed power architecture (DPA) and then to the intermediate bus architecture (IBA) as subset of DPA is the focus of this section.

3.1 Centralized Power System

Originally, the only voltage needed for telecommunication electromechanical switching systems was -48 V provided by AC/DC rectifiers and back up batteries. Since 1960s, the transition from electromechanical relays to electronic semiconductor switchers added to power system the DC/DC converters generating $+5\text{ V}$ and $\pm 12\text{ V}$ from -48V supply. These centralized power supplies, typically located in the bottom of a rack or cabinet, included AC/DC front-end rectifier/charger, a power backup battery and DC/DC converter. Large and costly supply bus bars routed the required voltages to each shelf inside the cabinet, which contained replaceable line cards with switching, diagnostic and monitoring equipment. Figure 3 shows typical configuration of centralized power systems that were dominant till mid 1980s (Thorsell, 1990, Ericsson Inc., 1996)



(a) Centralized power system

(b) Multilocation centralized power system

Fig. 3. Different types of centralized power system with battery backup

In multilocation centralized power systems, the DC/DC converters were physically located in different places, thus requiring safety shielding because of the presence of the high-voltage bus. The centralized power system is still used in “silver” box power supplies for

low end desktop and server computers, but it has become obsolete in relatively large telecommunication power distribution systems because of the following reasons:

- Centralized, custom power supplies require longer time to market and lack flexibility for quick modification.
- Failure of any part of the power system means failure for the electronic equipment in the whole cabinet.
- Custom, bulky power-delivery bus bars are expensive.
- Static and dynamic regulation of the supply voltage is poor and varies from shelf to shelf

3.2 Distributed Power Architecture

A dramatic step happened in early 1990s when the market largely adopted distributed power architecture (Tabisz et al., 1992; Lindman & Thorsell, 1996). The bulky centralized power supplies were replaced by AC/DC rectifier/charges providing -48-V backplane voltage to each shelf and line card. The line cards allow hot-swap replacement to reduce failure downtime. Each line card includes a number of -48-V input isolated DC/DC modules, that provide all required voltages to the electronic functional blocks (Figure 4).

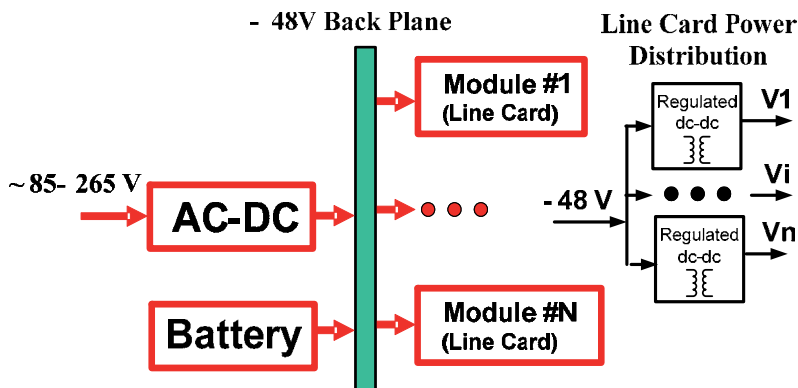


Fig. 4. Example of distributed power architecture

The introduction of distributed power architecture (DPA) was driven by the following:

- A trend towards digital processing blocks with increased power consumption, lower voltages, and specific power sequencing
- A broad market introduction of modular, high density, and reliable isolated DC/DC converters at a reasonable cost
- A demand for a more flexible, shorter design cycle power distribution systems allowing quick changes and updates
- A need for systems with high reliability and availability that supported hot swapping and had lower maintenance costs

3.3 Hybrid Power System

DPA-based systems addressed new power requirements, but the system cost remained relatively high. When the required number of supply voltages per line card exceeded the

initial four to five, the excessive number of isolated DC/DC converters was questioned (Narveson, 1996). In this paper there was suggestion to use only one isolated DC/DC converter. This converter provides most power demanding supply voltage in the system and also supplies non-isolated point-of-load (POL) regulators, which provide the remaining supply voltages to electronic blocks. This architecture, commonly called hybrid power system (Figure 5), was the first step towards the IBA. The hybrid power system reduces power distribution costs and allows placing POLs right next to the related load, thus reducing the impact of supply plane parasitics and improving high di/dt transient response. If power sequencing is needed, an additional switch can be added between the isolated converter output and the electronic load (Figure 5).

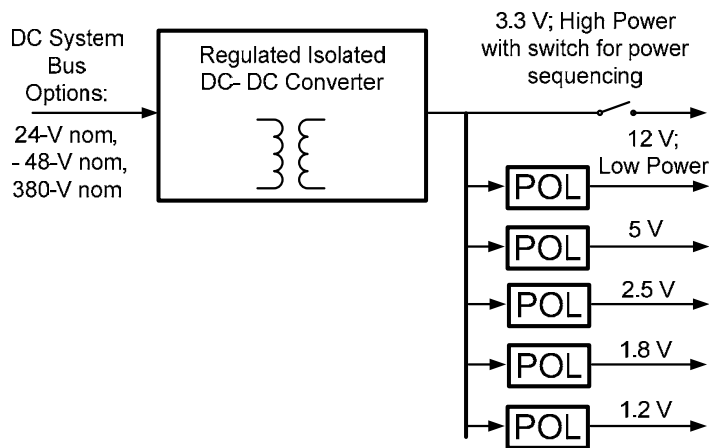


Fig. 5. Hybrid power system

The hybrid power system is preferable solution when one of the output voltages requires relatively high power. In this case, a single regulated isolated converter improves the efficiency of the whole system when the converter's output voltage is 3.3 V or higher. With the 3.3-V bus voltage, the hybrid system's overall output power might be limited to about 200 W. This limit is suggested because high currents circulating through the power and ground planes can cause significant losses and EMI issues as the system power increases.

3.4 Intermediate Bus Architecture

Driven by digital- and analog-IC industry demands for the low-level supply voltages in the 0.5-V to 3.3-V range and for the low-cost POLs, since early 2000s the market adopted the IBA (Morrison, 2002; White, 2003, Mills, 2004). In many applications, the IBA-based power system includes a front-end AC/DC power supply with a typical output of -48 V, 24 V, 12 V or 130 V. In some data-communication and medical equipment the input DC voltage can be 380 V taken directly from a power factor corrector output (Zhu & Dou, 2006) This voltage is supplied to an input of intermediate bus converter, that provides isolation and conversion to the lower level intermediate bus voltage, typically within 5 to 14 V. This intermediate bus voltage is supplied to non-isolated, POL regulators that provide high quality voltages for a variety of digital and analog electronic functional blocks (Figure 6).

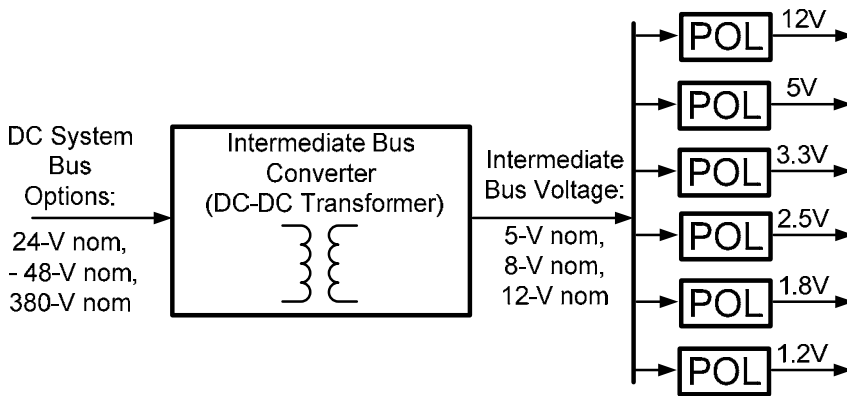


Fig. 6. Example of intermediate bus architecture

The following are advantages of IBA:

- System cost is reduced because only one isolated converter is needed and low cost, standardized, non-isolated POL regulators are available in the market.
- IBC circuit can be made simple because typically intermediate bus voltage variation is relaxed.
- Quality of supply voltages is increased because non-isolated POLs are located next to the electronic functional blocks.
- System is flexible for modifications and updates.
- Overall system reliability is higher.
- Housekeeping, power sequencing, diagnostics, optimized power saving modes are easier to implement because all major control signals are on the secondary side.

The following are challengers that IBA needs to address:

- The IBC must have highest efficiency and power density to provide a competitive edge for IBA versus DPA.
- The overall line card power can be limited because of high currents circulating through ground and bus-voltage planes.
- Parallel operation of highly efficient unregulated bus converters can be difficult.
- Specialized IBC controller ICs are needed to address specific IBC requirements.

3.5 Comparison and Trade-Offs of IBA versus DPA

IBA is a continuation of DPA at the line card level. An optimal choice between IBA and standard DPA for each specific case depends on many factors, including the number of supply voltages, the required voltage and power levels, the system-bus input voltage range, and the specified static and dynamic regulation for supply voltages. It is obvious that cost and efficiency are the most significant trade-off. Table 2 shows the pros and cons between IBA- and DPA-based systems in very general terms. A detailed analytical comparison is needed to make the right design decision. Examples of such analysis can be found in literature (Sayani & Wanes, 2003).

System Requirement		IBA	DPA
Input Voltage Range	Wide	—	Best
	Narrow	Best	—
Number of Outputs	<4	—	Best
	≥4	Best	—
One Regulated Output Demands Most of the Power		—	Good
		Hybrid system could be the best in such case	
Cost		Best	—
Efficiency		Better	Best
Load Supply Voltage Quality		Best	Good
Power Density		Best	Good

Table 2. Comparison of IBA versus DPA for different system requirements

3.6 Selection of Optimal Bus Voltage

Optimal selection of intermediate bus voltage is critical for the overall performance and lowest cost of IBA based power distribution system. For higher bus voltages, IBC is more efficient; however, POL regulators perform more efficiently at lower bus voltages. A lower bus voltage means higher currents circulating through the power and ground planes, thus adding additional losses. Obviously, there are some trade-offs to consider when defining a bus voltage optimized for the lowest overall power losses.

In general, the power losses, P_{tot} , associated with any switching power conversion can be expressed as

$$P_{tot} = P_{const} + K_v \times V^2 + R_{eq} \times I^2 \quad (1)$$

where P_{const} is nearly-constant power losses consumed by the control and housekeeping circuits; $K_v \times V^2$ is the power losses associated with the switching process (a function of switching voltage, frequency and in some cases, the load current); K_v is a coefficient measured in W/V^2 that reflects module losses dependence on the switching voltage; $R_{eq} \times I^2$ is the conduction power losses that are dependent on load current, I , and equivalent resistances, R_{eq} , of the components and traces. It is assumed that the switching frequency is constant.

The optimal bus voltage has to be analyzed for each design case because the selected IBC converter and POL regulators differ in terms of their power losses dependence from the bus voltage and current. The following example of bus-voltage optimization is for a DPA consisting of an unregulated IBC converter and POLs providing five different output voltages. It is assumed that for the bus voltage ranges from 5 V up to 15 V, the MOSFET switches for the selected IBC converter and POL modules remain the same. The key optimization parameters are shown in Table 3. These data is taken from the IBC converter and the POL modules available in the market. The parameters R_{eq} and K_v are specific for the selected modules and might be different for other practical examples.

Module	Vout, V	Iout, A	Pout, W	Pconst, W	Req, mΩ	Ploss(I), W	$K_V, \frac{W}{V^2}$
POL #1	0.7	60	42	0.46	2.5	9	0.038
POL #2	1.0	120	120	0.92	1.25	18	0.076
POL #3	1.5	60	90	0.46	2.5	9	0.038
POL #4	2.5	60	150	0.46	2.5	9	0.038
POL #5	3.3	30	99	0.23	5	4.5	0.019
Total	-	-	501	2.53	-	49.5	0.209
Bus Plane	-	-	-	-	2	Pplane(Vbus)	-
IBC	Vbus	Ibus	Pbus(Vbus)	0.5	4	Req x Ibus ²	0.056

Table 3. IBA power system parameters for optimal bus voltage analysis

The sum of the constant losses of each POL module (2.53W) and the sum of the output-current related losses (49.5W), can be used to define the total losses in the POLs as function of V_{bus} :

$$P_{pol}(V_{bus}) = 2.53W + 0.209 \frac{W}{V^2} \times V_{bus}^2 + 49.5W \quad (2)$$

The bus-voltage power and ground planes have a resistance, R_{bus} , equal to $2m\Omega$, and the overall output power, $P_{out\ total}$, is equal to 501 W. Thus, the plane losses are defined as function of V_{bus} :

$$P_{bus}(V_{bus}) = R_{bus} \times \left(\frac{P_{pol}(V_{bus}) + P_{outtotal}}{V_{bus}} \right)^2 \quad (3)$$

IBC converter V_{bus} -dependent losses, $P_{ibc}(V_{bus})$, are shown in Equation (4) after substituting the related parameters from Table 3 and the Equations (2) and (3):

$$P_{ibc}(V_{bus}) = 0.5W + 0.056 \frac{W}{V^2} \times V_{bus}^2 + 4m\Omega \times \left(\frac{P_{bus}(V_{bus}) + P_{pol}(V_{bus}) + P_{outtotal}}{V_{bus}} \right)^2 \quad (4)$$

Therefore, total IBA-based power system losses can be defined as:

$$P_{total}(V_{bus}) = P_{pol}(V_{bus}) + P_{bus}(V_{bus}) + P_{ibc}(V_{bus}) \quad (5)$$

Figure 7 shows power losses plots as a function of bus voltage. The optimal bus voltage for minimal overall power losses can be chosen from the plot. In this particular case, the curve showing total power losses is relatively flat in the region of minimum losses for bus-voltages between 8 and 10.5 V. With this wide optimal bus-voltage range, the unregulated IBC converter can be good fit depending on its input voltage range.

The optimal bus voltage is usually lower for the higher switching frequencies of POLs and the lower total system power. This trend supports a balance between the voltage-dependent losses like switching losses and the current-dependent losses like conduction losses.

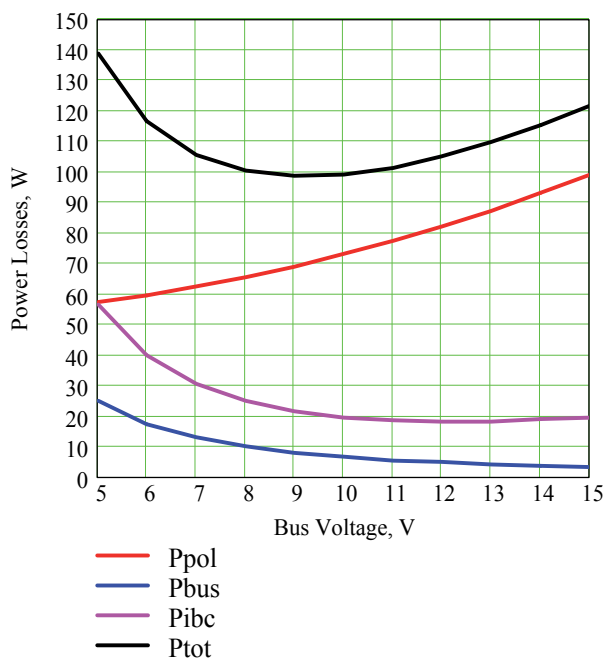


Fig. 7. Power losses over bus voltage

4. Telecom Rectifier and Front-End Server Power Supply

Practically every telecom rectifier, or server power supply have the following key functional blocks, which are usually associated with any over 500 W AC/DC power supply:

- EMI filter
- Power factor corrector (PFC) with hold up capacitor
- Isolated post-PFC DC/DC converter
- Auxiliary bias or standby power supply
- Fan and its regulator

Regulations and specifications define the overall efficiency of AC/DC power supply. It is the responsibility of designer, based on previous designs and future forecast, identify the efficiency and power losses of each functional block to meet the total efficiency goals.

4.1 Power and Efficiency Distribution

For a power and efficiency distribution analysis between the key functional blocks of AC/DC power supply the following approach can be used. Usually the EMI filter and PFC are considered together because it is convenient from the test procedure as well. The output of the PFC (typically 400 V) supplies the main isolated DC/DC converter and the standby power supply. The typical standby power-supply output-power range Can be from 5 W up to 30 W depending on application. It is much lower than the output power of main DC/DC converter. But, the efficiency and power consumption of standby power supply can not be neglected, because the regulations specify the efficiency down to 10% or even 5% of

maximum output power. The fan regulator is usually supplied from the output of DC/DC converter and thus, it is included into the efficiency of converter. Table 4 below is an example of power and efficiency distribution analysis between the PFC, main DC/DC converter and standby power supply. It is fulfilled for 12-V, 660-W output server power supply.

Rated Output Power	10% Load	20% Load	50% Load	100% Load
Efficiency from Table 1	75%	85%	89%	85%
Overall Power Consumption	89 W	158 W	376 W	788 W
PFC Efficiency	95.3%	96.4%	97.6%	97.7%
PFC Output Power	85 W	152 W	367 W	770 W
Standby Power	6 W	7 W	10 W	10 W
Standby Power Efficiency	80%	82%	85%	85%
Standby Power Consumption	7.5 W	8.5 W	12 W	12 W
DC/DC Input Power	77.5 W	143.5 W	355 W	758 W
DC/DC Output Power	66 W	132 W	330 W	660 W
DC/DC Efficiency Goal	85.2%	92.7%	93%	87.1%

Table 4. Power and efficiency analysis of 660-W server power supply

4.2 Power Factor Corrector

Efficiency of power factor corrector (PFC) depends significantly on input AC line range (Cohen & Lu, 2008). Typically, for the more than 500-W PFC, the boost converter based power stage remains the most popular option. The boost converter achieves its highest efficiency at high input line, and the efficiency gradually degrades at lower input voltages. The efficiency and power factor specified by ENERRGY STAR® test procedure for the single output server power supplies has to be confirmed by measurements at 230 Vrms AC line (http://www.energystar.gov/ia/partners/product_specs/program_reqs/computer_server_prog_req.pdf). However, if the design targets the 85 to 265 Vrms universal range, all critical thermal and electrical parameters of PFC have to be verified in the whole operating range. Usually, the output power capability rated at 230-Vrms input voltage, for the same front-end AC/DC power supply is de-rated for the 115-Vrms AC line.

Currently the interleaved PFC and bridgeless PFC are two major directions where most of the research and development is focused. The interleaved PFC is already established solution in mass production supported by available in the market controllers from different vendors (see in <http://focus.ti.com/docs/prod/folders/print/ucc28070.html>). Typical application diagram of the two-phase interleaved, continuous current mode PFC using UCC28070 from Texas Instruments is shown in Figure 8.

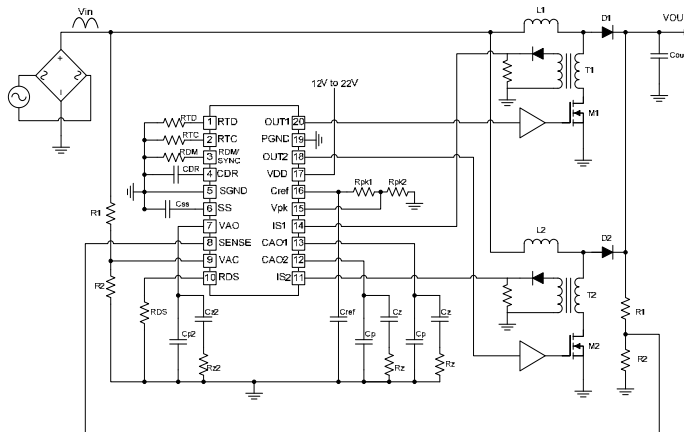


Fig. 8. Two-phase interleaved PFC converter using UCC28070 controller

Advantages of interleaved PFC include:

- Reduced input current ripple because of ripple cancellation effect caused by 180° phase shifted operation;
- Reduced EMI filter because of lower input current ripple;
- Lower RMS current through the output capacitor because of ripple cancellation effect. This means less number of capacitors is needed, or increased reliability when the output capacitance can not be reduced because of required hold up time;
- Better, equalized temperature profile because the power dissipated components are spread between phases. This also results in the higher overall efficiency.

The first bridgeless PFC circuit has been patented as far as in 1983 (Mitchell, 1983), but the concept is still mostly at the research stage. The practical implementation has been limited by the high voltage MOSFET and diode performance, EMI issues, difficulties of voltage and current sensing. Latest achievements in components technology, especially availability of CoolMOS™ transistors and Silicon Carbide diodes, renewed interest to the bridgeless PFC (Hancock, 2008). The analytical and experimental comparison of few different bridgeless PFC topologies is provided in (Huber et al., 2008). The analysis claims that the bridgeless PFC with two boost circuits (Souza & Barbi, 1999) shown in Figure 9 has the efficiency advantages and less EMI issues versus other bridgeless PFC topologies. In general, publications claim up to 1% efficiency improvement when using the bridgeless PFC versus standard approach.

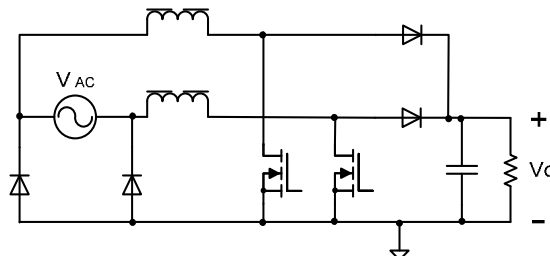


Fig. 9. Bridgeless PFC with two boost circuits (Souza & Barbi, 1999)

4.3 Isolated DC/DC Converter for Front-End Power Supply

The isolated DC/DC converter topology selection is critical for total efficiency of front-end power supply. Zero voltage switching (ZVS) enabling topologies are preferable in such applications because of the relatively high input voltage usually, from 350 to 420-V range. Attractive solutions include phase shifted full-bridge, asymmetrical half-bridge, LLC resonant converter and variations of these topologies (Zhang et al., 2004; Miftakhutdinov et al., 1999; Fu et al., 2007).

For the interleaved topology, the asymmetrical half-bridge converter suits best because of its relative simplicity (Miftakhutdinov et al., 1999). One possible example of interleaving with four phases is shown in Figure 10.

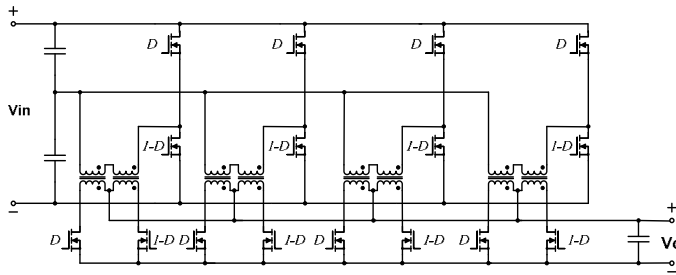


Fig. 10. Four phases interleaved asymmetrical half-bridge.

The LLC resonant topology is recently gaining popularity as post-PFC isolated DC/DC converter (Figure 11).

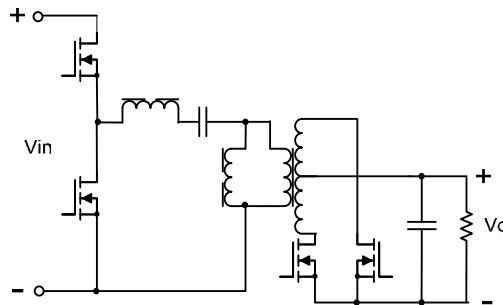


Fig. 11. LLC resonant converter power stage

Its main advantage is ZVS for the primary side switches and zero current switching (ZCS) for the secondary side synchronous rectifier MOSFETs (Fu et al., 2007). Variable switching frequency, special attention to light load operation and difficulties with interleaving limit this topology to sub-kW range.

One implementation of classical phase shifted bridge topology using specialized analog controller is shown in Figure 12. The efficiency improvement of this circuit is achieved by using synchronous rectification, adaptive control algorithm providing ZVS condition over wide operating range, accurate adaptive timing of control signals for primary and secondary power FETs and light load management block providing the highest efficiency and power savings at low output power conditions.

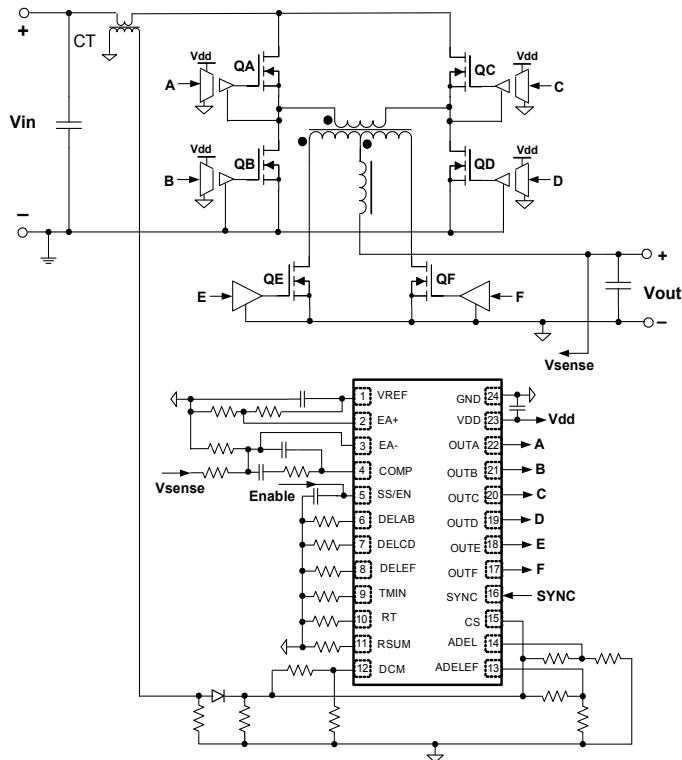


Fig. 12. Phase shifted full-bridge converter with advanced analog controller

4.4 Control Algorithms for High Efficiency

Optimal control algorithm is critical not only to meet static and dynamic requirements of telecom power system, but it also opens new opportunities to increase efficiency by transitioning into optimal power saving modes depending on system conditions. When selecting the controller, the flexibility, programmability and auto tuning capability of digital controllers have to be weighted versus lower cost, simple and generally faster analog control ICs. The list of most popular power saving control strategies is provided below.

- Interleaving of few phases for better current and temperature distribution at maximum output power and gradual phase shedding when the load is reduced (Figure 10);
- Synchronous rectification using MOSFETs with the diode emulation technique at light load to avoid current circulation. It could be beneficiary to switch off the drive circuit of rectifier MOSFETs at very light load where the drive losses exceed the conduction losses. Performance of synchronous rectifier significantly depends on accurate timing between primary and secondary side switches (Figure 12);
- Proper use of zero voltage (ZVS) and zero current (ZCS) switching technique to reduce switching losses in power MOFETs. This requires optimal adaptive or predictable set of delays between switching events depending on operation conditions (Figs. 10 - 12);

- Optimal adjustment of intermediate bus voltage, drive voltage and other system parameters to maintain highest efficiency at different operation conditions;
- Smooth transition between operation modes to maintain highest efficiency depending on operating conditions, for example from continuous mode to discontinuous, from fixed frequency to frequency foldback etc (Figure 12);
- Proper use of pulse skipping or burst mode at light load or no load to reduce the power consumption (Figure 12)

This list shows benefits of wide use of digital controllers to address power saving technique because of their programmability and flexibility. The digital controllers for power supplies are available from few vendors at reduced cost that make these devices competitive with analog controllers, even for relatively low power applications in sub-kW range (see in <http://focus.ti.com/docs/prod/folders/print/tms320f28023.html>). Specifically designed for these applications high end analog controllers also have their niche. Analog controller ICs remain popular in mature, high volume applications where the operating conditions are well known and established, and thus, cost is more critical than programmability and flexibility (Figure 12).

4.5 Design Considerations and Component Selection

Optimal selection of power stage components provides foundation for high efficiency power system design. Magnetics and power switches are major contributors into the total power losses budget. In this chapter the main focus is on power MOSFETs and high voltage diodes where the significant progress has been achieved lately. The new super junction technology for high voltage MOSFETs significantly reduces $R_{ds(on)}$, drain-source and gate-source capacitances providing lower conduction losses and switching losses (Bjoerk et al., 2007). Still accurate ZVS condition analysis over operating conditions remains critical to ensure the highest efficiency. Because of significant non-linear behavior of drain-source capacitance, the super junction MOSFETs, like CoolMOS™, require new analytical model to estimate switching losses and determine ZVS conditions. The following Equation (6) is adequate for energy calculation stored in the output capacitance of high-voltage regular MOSFETs (Miftakhutdinov, 2008a)

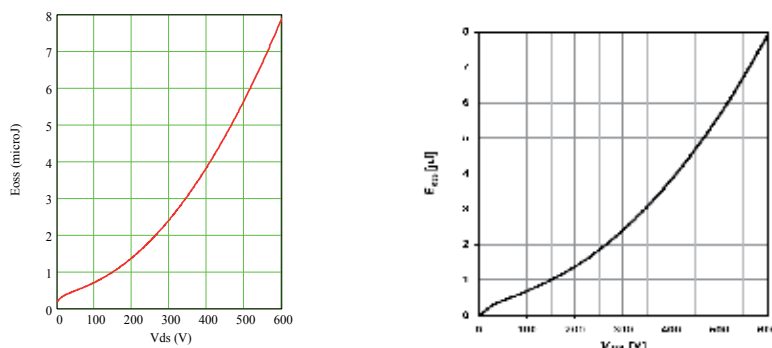
$$E_{cds} = \frac{2}{3} \cdot C_{oss} \cdot \sqrt{V_{ds(oss)}} \cdot V_{ds}^{\frac{3}{2}} \quad (6)$$

Here, E_{cds} is the energy, C_{oss} is the output capacitance at $V_{ds(oss)} = 25V$ from datasheet, and V_{ds} is the voltage where the energy should be calculated. The new super junction MOSFETs require different model because of significant non-linear behavior of drain-source capacitance. The following approximated Equation (7) provides good practical results for super junction FETs:

$$E_{cds} = \frac{C_{oss}}{K_c} \cdot (V_{ds(oss)})^2 \cdot \ln\left(\frac{V_{ds} + 5V}{V}\right) + \frac{C_{init} \cdot (V_{ds})^2}{2} \quad (7)$$

where $K_c = 2.2$ and $C_{init} = 40$ pF for SPA11N60FCD type MOSFET from Infineon.

The plots in Figure 13 compare calculated energy using Equation (7) with the plot provided in the datasheet.



a) analytically derived plot b) experimental plot from datasheet

Fig. 13. Energy E_{oss} over V_{ds} for SPA11N60FCD type MOSFET

The pairing of super junction MOSFETs with silicon carbide diodes in PFC applications results in significant power losses reduction (Miesner et al., 2001). The use of silicon carbide diodes practically eliminated the need for complicated snubbers in PFC boost power stage. This is because these Schottky type diodes have very fast recovery time versus the p-n junction silicon diodes. Regardless of the extra cost of such diode, the industry widely accepts silicon carbide diodes for PFC applications because the overall efficiency gain could be 3% or higher.

5. Intermediate Bus Converter

This section discusses major requirements to IBC converters, compares key parameters of the available in the market products, considers preferable topologies and focuses on design challenges that must be taken into account. An example of practical implementation based on the IBC controller UCC28230 is also provided and supported by test results. Additional analysis and design information related to IBC as part of IBA can be found in publications (Barry, 2004; Miftakhutdinov & Sheng, 2007; Miftakhutdinov et al., 2008; Miftakhutdinov, 2008a; Miftakhutdinov, 2008b)

5.1 Major Requirements and Parameters of Modern IBCs

IBA includes an additional DC/DC conversion stage provided by IBC to supply intermediate bus voltage. It is important for the IBC to be highly efficient with high power density at the lowest possible cost. The first bus converters in the market were slightly modified versions of fully regulated DC/DC modules. However, the IBC's strict requirements in a short time have made it a stand-alone, specialized product in module manufacturer' portfolios. A list of major IBC parameters follows:

- Efficiency: 96% to 97% typical
- Power density: >250 W/inch³
- Cost: \$0.1 to \$0.2 per watt

- Input voltage range:
 - 43 to 53 V for servers and storage
 - 38 to 55 V for enterprise systems
 - 36 to 60 V for narrow telecom range
 - 36 to 75 V for wide telecom range
 - 380 to 420 V for data center high-voltage systems
- Power range: 150 to 600 W and higher
- Mechanical form factor:
 - 1/4 brick for > 240 W of output power
 - 1/8 or even 1/16 brick for < 240 W output power
- Most popular transfer ratios: 4:1, 5:1 and 6:1 for -48-V nominal input voltage
- Switching frequency: relatively low at 100 to 200 kHz
- Most popular power stage topologies: Full-bridge, half-bridge, and push-pull
- Secondary-side rectification: Almost entirely uses synchronous MOSFETs, self- or control-driven
- Control approaches: Fully regulated, semi-regulated, or unregulated

Because of the growing popularity of IBA, the IBCs for different power levels and transfer ratios are readily available from different vendors. Table 5 shows the major parameters of currently available IBCs in the market. This data is based on review of products from the popular vendors in the first half of 2008.

Manu- facturer	Model	Input, V	Form Fact. Brick	Pout, W	Trans. Ratio	Output, V	Eff., %	Density, W/inch ³
Tyco	EUK240S9R0	36-60	1/8	240	5:1	6.5-11.5 unreg.	95.5	272
Tyco	QBK033AOB	36-60	1/4	396	4:1	11.4-12.6 reg.	94.5	285
Ericsson	PKM 4402NG PI	38-55	1/4	587	5:1	7.1-11.0 unreg.	96.4	403
Ericsson	PKM400B PI	36-75	1/4	286	4:1	11-12.5 reg.	95.9	191
Delta	Q48SB9R650NRFA	36-57	1/4	500	5:1	6.8-11.5 unreg.	96.4	312
Delta	ES8SB9R625NRFA	38-55	1/8	240	5:1	7-11 unreg.	96.5	258
Delta	V48SB12013NFRA	38-55	1/16	150	4:1	8.9-13.75 unreg.	95.2	347

Table 5. Major parameters of modern IBC converters

5.2 Control Approaches

Depending on the input voltage range and the requirements for output voltage tolerances, the IBC can be regulated with the feedback loop taken from its output; semi-regulated with the input voltage feed-forward circuit; or unregulated (Barry, 2004; Ericsson Inc., 2005).

The IBC with a closed feedback loop requires an additional isolation barrier for feedback signal transfer. It is more expensive than semi-regulated because of more complex control circuit and less efficient than unregulated IBC because it operates in a wide duty cycle range. However, full regulation is justified for the hybrid power system where the IBCs

output is the supply voltage for the most power consuming load. If the power sequencing is needed, an additional switch can be added between the IBC output and the load as it is shown in Figure 5 (Ericsson Inc., 2005).

The semi-regulated IBC with input feed-forward control is usually a lower cost solution than the fully regulated converter, but it also has lower density and efficiency than the unregulated converter. This is because the semi-regulated IBC is designed to operate over a wide duty cycle range, even at steady state. The semi-regulated IBC is usually used in a system with a relatively wide input voltage range.

The unregulated IBC provides the solution with the highest efficiency and power density and the lowest cost because it operates at almost 100% duty cycle at steady state. There is no additional communication through the isolation barrier except for the energy transfer through the power transformer. The size of the transformer and output and input filters is small because converter operates at maximum duty cycle. However, overstresses during transient conditions like start up, current limiting, and shut down need to be addressed during the design.

5.3 Major IBC Topologies

IBCs usually employ forward type full-bridge, half-bridge and push-pull topologies with the synchronous MOSFET rectification technique to achieve highest efficiency. Figure 14 shows three such IBCs in their very simplified forms.

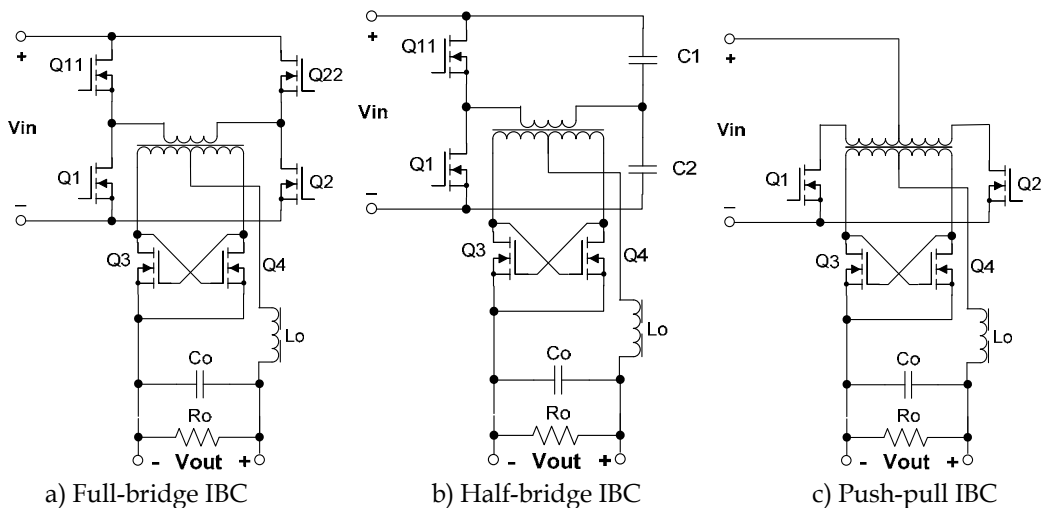


Fig. 14. Popular power stage topologies for IBC

Using a self-driven synchronous MOSFET rectifier is a very popular choice, especially for unregulated converters, but practical solutions might require additional control windings and snubber circuits for improved efficiency and reliability. For the high power applications and, especially for the fully regulated and semi-regulated converters, the control driven MOSFET rectifiers can be preferable. The advantages of using control driven rectifiers are a simplified power transformer and a gate drive voltage that is independent from input voltage and load current variations. A detailed review, classification and comparison of synchronous rectification techniques can be found in Reference (Miftakhutdinov, 2007).

The double-ended topologies shown in Figure 14 are preferred for bus converter applications because they can operate at almost 100% duty cycle applied to the output filter, thus significantly reducing the size of the output inductor. Currently available IBCs usually operate at about 100 kHz switching frequency. IBCs with 48-V (nominal) input voltage can operate in the hard switching mode, but the zero voltage switching technique is preferred for the IBCs with 400-V (nominal) input voltage. The full-bridge topology is preferred for a 250-W or higher output power. The half-bridge topology provides a low cost solution for the output power range below 250 W. The bridge based topologies have primary MOSFETs with a drain-to-source voltage rating equal to the input voltage, with some reliability margin. These topologies are better choice for input voltages higher than 24 V. For a 24-V or lower input, the push-pull topology is attractive because of simple drive circuit of primary MOSFETs. However, the center tapped primary winding is a drawback for the planar transformer in push-pull topology.

Table 6 provides a general comparison of IBC topologies. However, to select the right topology during practical design, detailed calculations and a review of power system specifications are needed for each specific case.

Topology	Full-Bridge	Half-Bridge	Push-Pull
Primary MOSFETs	$V_{ds} = V_{in}$	$V_{ds} = V_{in}$	$V_{ds} > 2V_{in}$
Transformer	Good utilization	Issue with 5:1 transfer ratio because planar transformer has to be 2.5:1	Poor utilization
Rectifier MOSFETs	Primary winding clamping to zero is possible	No primary winding clamping ability	No primary winding clamping ability
Output inductor	The Same		
Cycle-by-cycle current limit	Only a problem if a DC blocking capacitor is used	Inherent issue	Not a problem

Table 6. Comparison of popular IBC topologies

5.4 Using a Resonant Converter as an Unregulated IBC

Recently, high frequency resonant topologies for IBC application have been suggested and their high performance reported (Ren et al., 2005). In this research the resonant topology has been successfully used for a 48-V input, 12-V, 500-W output IBC at switching frequency up to 800 kHz and the 95.5% efficiency achieved. Nevertheless, the resonant IBC approach has not yet become mainstream in the industry.

5.5 Unregulated IBC Design Challenges

The design of unregulated IBC with self-driven MOSFET rectification has its own challenges and trade offs. The design goal is to achieve the highest efficiency and power density at the lowest cost. The challenges include the following:

- High ripple current during transitional states
- Start up problems
- Optimal synchronous rectification
- Reverse energy flow and self-oscillation
- Parallel operation issues
- Flux balancing of power transformer

A. Operation at Transitional States

At steady state, an unregulated converter operates at almost 100% duty cycle with very low output inductor current ripple. However, during soft start or cycle-by-cycle current limiting, the duty cycle varies from 0% to 100%, which can cause significant ripple increase in the middle of this range. This ripple can overstress the power stage and limit the start up capabilities of the IBC, especially when there is a large output capacitance. The output inductor's peak-to-peak ripple current, ΔI_L , is defined for the whole duty cycle range with Equation (8):

$$\Delta I_L = \frac{V_{in} \times D \times (1-D)}{2 \times N_{tr} \times L_o \times F_{sw}}, \quad (8)$$

where $F_{sw} = 1/T_{sw}$ is the switching frequency, $D = T_{on}/(0.5 \times T_{sw})$ is the duty cycle after rectification, $N_{tr} = W_{pr}/W_{sec}$ is the transformer's turns ratio, W_{pr} is the primary winding turns, W_{sec} is the secondary winding turns, L_o is the inductance of the output inductor, and V_{in} is the voltage applied to the transformer's primary winding. Note that duty cycle calculations and related equations assume a D value between 0 and 1. The following discussion and plots refer to duty cycle in percent, which is $D \times 100$. The plots in Figure 15 show that the output inductor's ripple current is very low in the vicinity of $D = 0$ and 100%, but can reach 120 A at $D = 50\%$.

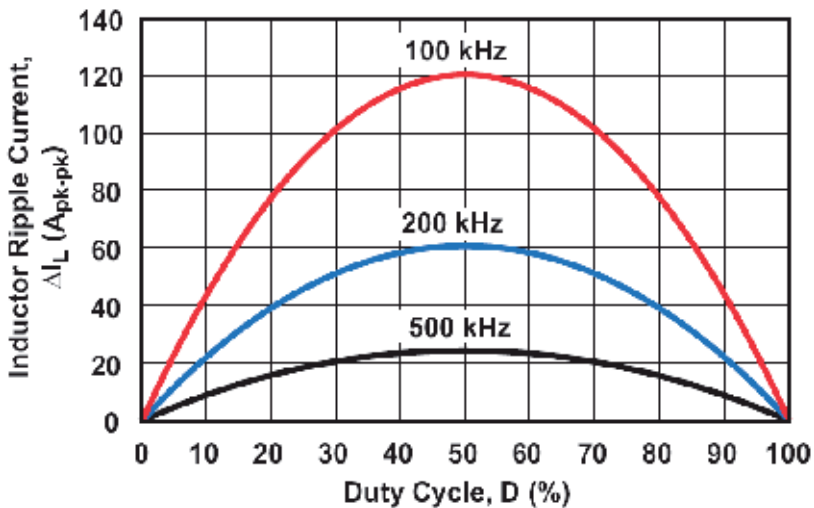


Fig. 15. Output inductor's ripple current versus duty cycle for $V_{in} = 50$ V, $N_{tr} = 5$, $L_o = 0.1$ μ H, and 100, 200 and 500 kHz switching frequencies in accordance with Equation (8)

Thus, the size and cost of power stage components, especially of the output inductor, become significantly higher when this increased transitional ripple and peak current has been taken into account.

One way to avoid the issue of high ripple current is to use a special frequency control circuit that limits the output inductor's ripple current during duty cycle transitions between 0% and 100%. The desired change in switching frequency over the duty cycle range is

$$F_{sw} = k \times D \times (1 - D), \quad (9)$$

where k is a constant based on circuit implementation. Substitution Equation (9) into Equation (8) gives the inductor ripple current as

$$\Delta I_L = \frac{V_{in}}{2 \times N_{tr} \times L_o \times k}. \quad (10)$$

The result is that the switching frequency changes as the duty cycle changes to maintain the inductor's ripple current at a constant value. This idea has been implemented in Texas Instruments UCC28230/1 controller

(<http://focus.ti.com/docs/prod/folders/print/ucc28230.html>).

A measured plot of the switching frequency change versus the duty cycle is shown in Figure 16. In this case, the nominal switching frequency is set at about 100 kHz.

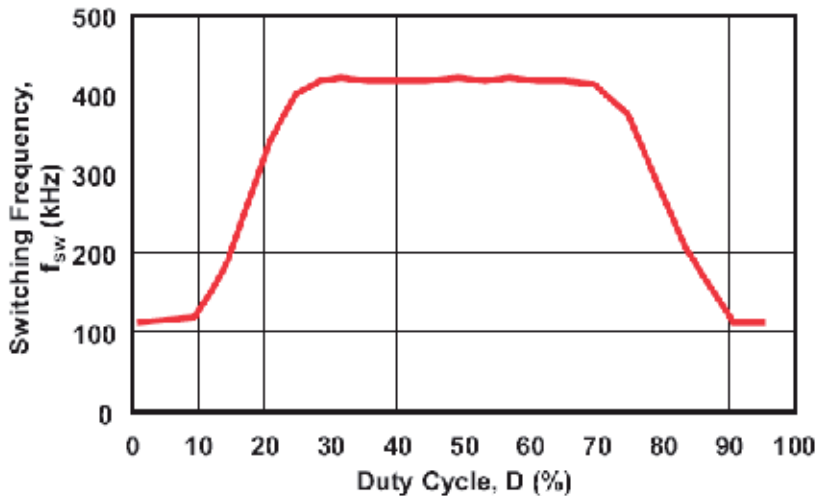


Fig. 16. Measured switching frequency versus duty cycle with frequency control circuit

The frequency is maintained constant at steady state operation when the duty cycle is above 90 % or less than 10%. During start up or cycle-by-cycle current limiting, the duty cycle varies significantly such that the inductor's ripple current reaches a maximum value at 50 % duty cycle. The frequency control circuit maintains the maximum frequency at about 420 kHz when the duty cycle is between 30 % and 70 %. The higher frequency significantly reduces ripple current and allows the output inductor to be approximately 25% of the value needed without the frequency control circuit. When the frequency control circuit is used, inductor selection is based on a maximum frequency of 420 kHz at 50% duty cycle instead of on 100 kHz as it would be without frequency control.

B. Start Up Problems

The ripple increase described in previous section also impacts IBC start up. The inductor's ripple current increase during start up may activate the over-current protection circuit,

possibly causing the converter not to start at all. Increasing the over-current limit threshold and adding more filtering are not recommended for correcting a start up problem. If a real over-current or output short circuit occurs, these methods of correction will probably overstress the converter. To meet reliability and current stress margin requirements for the power stage components, a much larger output inductor must be selected or the switching frequency must be increased to reduce the ripple (Figure 15).

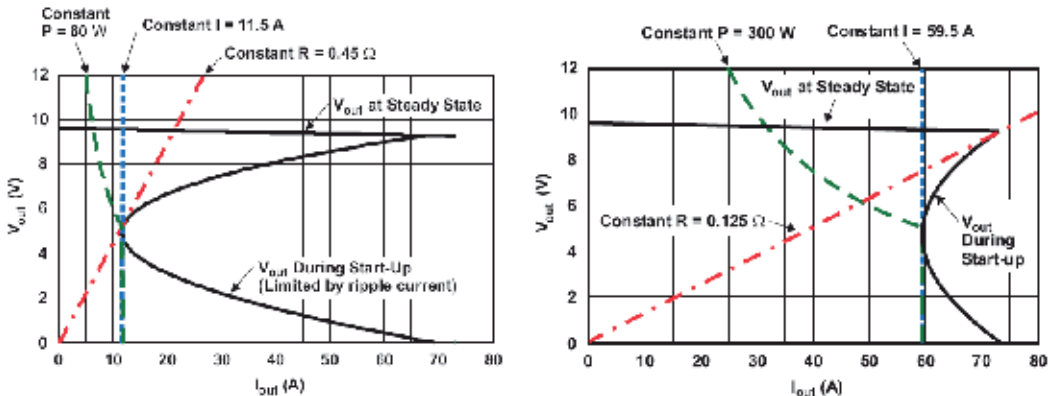
To further illustrate the start up issue, the plots in Figure 17 of output voltage versus average load current are presented based on the following analysis. During the cycle-by-cycle current limiting, the inductor's average output current, I_{out} , and converter's output voltage, V_{out} , can be described by Equations (11) and (12):

$$I_{out} = I_{o\ lim} - \frac{N_{tr} \times V_{in} \times D}{4 \times L_m \times F_{sw}} - \frac{V_{in} \times D \times (1 - D)}{4 \times N_{tr} \times L_o \times F_{sw}}, \tag{11}$$

where $I_{o\ lim}$ is the output current limit and L_m is the primary magnetizing inductance of the power transformer. For any I_{out} range the output voltage, V_{out} , can be determined as follows:

$$V_{out} = \frac{(V_{in} - I_{out} \times R_{pr} / N_{tr}) \times D}{N_{tr}} - I_{out} \times R_{sec} \tag{12}$$

where R_{pr} is the equivalent series resistance of the power stage primary side, and R_{sec} is the equivalent series resistance of the secondary side.



a) Without frequency control $F_{max} = 100\text{ kHz}$ b) With frequency control $F_{max} = 420\text{ kHz}$
 Fig. 17. IBC start up capability at 75 A current limit threshold and 100-kHz nominal switching frequency

The plots in Figure 17a show the output voltage versus the average load current at steady state and during start up operation with cycle-by-cycle current limiting. These plots were determined after substituting Equation (11) into Equation (12) with the following conditions: $V_{in} = 48\text{ V}$, $F_{sw} = 100\text{ kHz}$, $N_{tr} = 5$, $L_o = 0.1\ \mu\text{H}$, $L_m = 75\ \mu\text{H}$, $I_{o\ lim} = 75\text{ A}$, $R_{pr} = 25\text{ m}\Omega$ and $R_{sec} = 4\text{ m}\Omega$.

Also included in Figure 17a are the load curves for the resistive load of 0.45Ω , a constant current load of 11.5 A, and a constant power load of 60 W. The constant-resistance and constant-current load curves are touching the start up V_{out} versus I_{out} curve without crossing it. With the constant-power mode replicating POL regulator behavior, it is assumed that the POL regulator starts operating and draws current only after V_{out} exceeds the under voltage lockout threshold (UVLO) set at 5 V. Until then, the POL regulator does not draw any current. Thus, the load curves indicate the maximum start up load current of the converter designed for 60-A nominal output with a current limit set at 75 A. Obviously, the fold back type of behavior of V_{out} versus I_{out} limits the start up capability of this unregulated IBC. The load curves cross the steady state V_{out} (upper) plot at 21 A for the constant-resistance mode, at 11.5 A for the constant-current mode, and at 5 A for the constant-power mode. The start up performance of the converter is reduced dramatically because of the inductor's large ripple current at 50% duty cycle. Without the frequency control circuit suggested earlier, the only way to override this limitation is to either increase the output inductance or increase the nominal switching frequency. Either way, power losses and converter cost increase.

Figure 17b illustrates the advantage of a start-up frequency-control circuit. The conditions are the same as for Figure 17a except that the converter operates at 420 kHz for most of the start-up time and at 100 kHz when it reaches the steady-state condition. With the same 0.1- μ H output inductor, the start-up capability is significantly improved over that shown in Figure 17a where $F_{sw(max)} = 100$ kHz. The load curves cross the steady-state V_{out} curve at 75 A for constant-resistance mode, at 59.5 A for constant-current mode, and at 32 A for constant-power mode.

This start-up analysis is based on the assumption that the IBC's output capacitance is not very large. Obviously, if the allowable start-up time is short and the output capacitor is large, an additional current to charge the high capacitance must be taken into account. The frequency-control circuit increases the average charge current available for start-up even with a large output capacitor. The average charge current, I_{ch} , for the output capacitor, C_{out} , that satisfies the selected soft-start time, t_{ss} , can be determined by Equation (13):

$$I_{ch} = C_{out} \times \frac{V_{in}}{t_{ss} \times N_{tr}} \quad (13)$$

Figure 18 shows the IBC's average output current required for charging different output capacitances for the selected soft-start time. These curves do not account for the extra current drawn by the load. The effects of different output capacitances can be estimated with and without a frequency-control circuit by comparing the plots in Figs. 17 and 18. With the frequency-control circuit, a charge current of at least 59.5-A is available per Figure 17b. A 10-A portion of this current can be used to charge the 10,000- μ F output capacitor within 10 ms per Figure 18. The remaining 49.5-A current is available to the load. Without the frequency-control circuit, the available current per Figure 17a is only 11.5 A. This current is barely sufficient to charge the 10,000- μ F output capacitor within 10 ms. If the load draws more than 1.5 A in addition to the capacitor's charge current, the converter will not start because the over-current protection circuit will be activated due to the large ripple current.

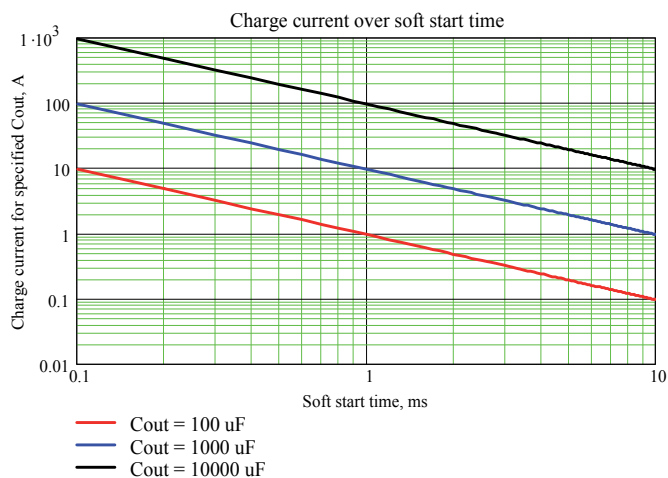


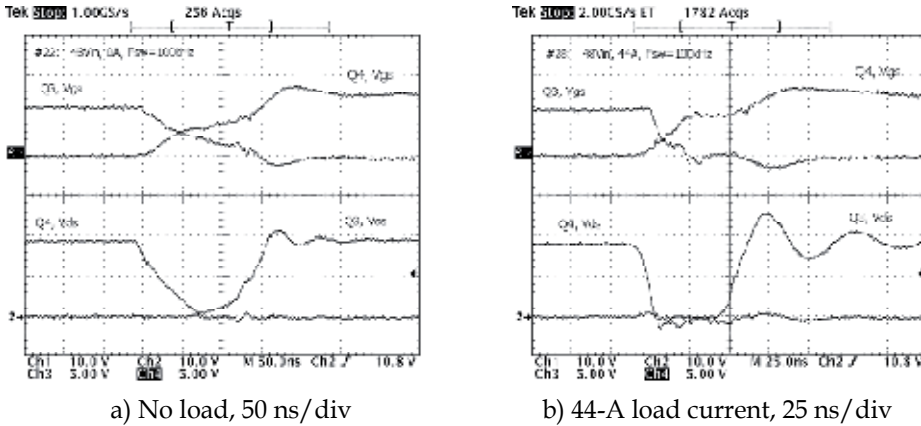
Fig. 18. IBC's required charge current for different output capacitances at selected soft start time

C. Optimal Synchronous Rectification Technique

For IBCs with a 12-V or lower output voltage, the synchronous-rectification technique is mandatory to achieve the required efficiency. Compared to Schottky diodes, low-RDS(on) rectifier MOSFETs can increase IBC efficiency by more than 5%. There are many publications and patented solutions for how to drive the rectifier MOSFETs. Most designs can be divided into self-driven, control-driven, and diode-emulator categories.

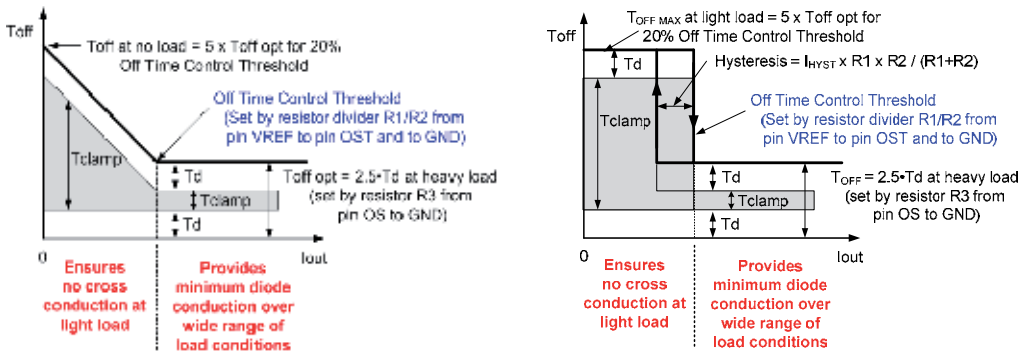
Classification of synchronous rectification and additional details can be found in Reference (Miftakhutdinov, 2007). For the unregulated IBC, a self-driven rectification approach that uses a secondary-side transformer winding (Figure 14) or an additional control winding is quite popular because of its simplicity. The proper timing in either self-driven or control-driven synchronous rectifiers is critical to reduce power losses. To avoid overshoot, it is important that the conducting rectifier MOSFET on the secondary side turn off before the primary-side MOSFET is turned on. This is achieved by proper OFF-time switching control of primary-side MOSFETs for half-bridge (Figure 14b) and push-pull (Figure 14c) topologies. For the full-bridge topology (Figure 14a), the OFF time is specified to be the time between primary current switching of MOSFETs on one diagonal to MOSFETs on the other diagonal. The optimal OFF time, $T_{off(opt)}$, depends on power-stage parameters and the load current.

With light loads, the optimal OFF time is longer. This relationship is illustrated in the drain-source and gate-source switching waveforms of the synchronous-rectifier MOSFETs shown in Figure 19a for no load and in Figure 19b for nominal current conditions.



a) No load, 50 ns/div
 b) 44-A load current, 25 ns/div
 Fig. 19. Secondary side MOSFET rectifier switching waveforms

Optimal switching of rectifier MOSFETs over a wide load-current range is possible when the OFF time is allowed to increase to some degree at light loads but is kept as short as possible with nominal loads. A special OFF-time control circuit can be designed to allow the desired output-current threshold to be set such that the OFF time, T_{off} , starts increasing and reaches its maximum at no-load condition (Figure 20). This increase can be implemented in a linear manner as shown in Figure 20a, or as a step function with hysteresis as shown in Figure 20b. The method can vary depending on the specific design and application. Texas Instruments' specialized UCC28230/1 bus-converter controller implements a comparator based approach as shown in Figure 20b. This controller has dedicated pins (OS and OST) to allow programming of the nominal OFF time, T_{off} , and the output current threshold so the OFF time steps up to the new $T_{off}(max)$ value at the desired current level. The gray area designated "Tclamp" in Figure 20 represents the time when both rectifier MOSFETs are turned off. The purpose of T_{clamp} is to prevent reverse energy flow, which is described in detail in the following Section D.



a) Linear approach of controlling off time
 b) Step change approach of controlling off time
 Fig. 20. Setting T_{off} , T_d and T_{clamp} versus load current with off time control circuit

Since the control circuit of unregulated IBC does not have direct access to the secondary side, so the primary current sensing with a current sense transformer or resistor is usually used to monitor the output current indirectly. Primary side current sensing includes not only the

reflected load current, but also magnetizing current. However, in most applications, the magnetizing current is only a small percentage of total current and can be ignored. The impact of increasing off time at light load to the output voltage V_{out} is shown by Equation (14):

$$V_{out} = \frac{V_{in}}{N_{tr}} \times \frac{T_s - T_{off}}{T_s} - I_{out} \times R_{out} \tag{14}$$

For the comparator based approach shown in Figure 20b, the output voltage, V_{out} , can jump a few hundred millivolts (with hysteresis) as shown in Figure 21. This jump is not desirable if IBC's operate in parallel with droop current sharing. For such applications, the off time control circuit can be disabled to allow constant-slope output voltage.

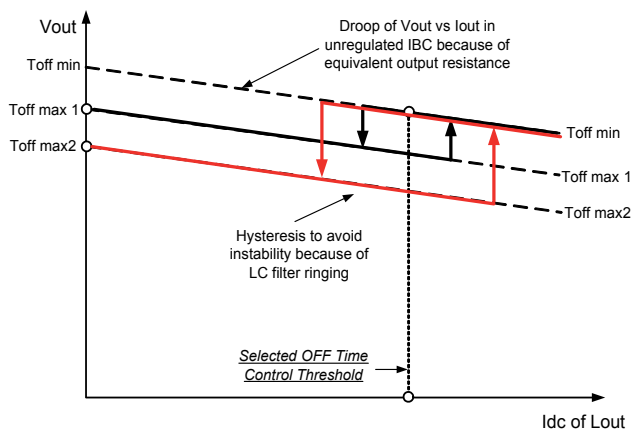


Fig. 21. Impact of comparator based off time control circuit on output voltage (not to scale)

The impact on V_{out} of changing off time is different for linear based off time control circuit. Depending on the gain of the control circuit shown in Figure 20a and the output impedance of the IBC, the slope of V_{out} versus I_{out} below the off-time-set threshold can be positive, negative or zero (Figure 22).

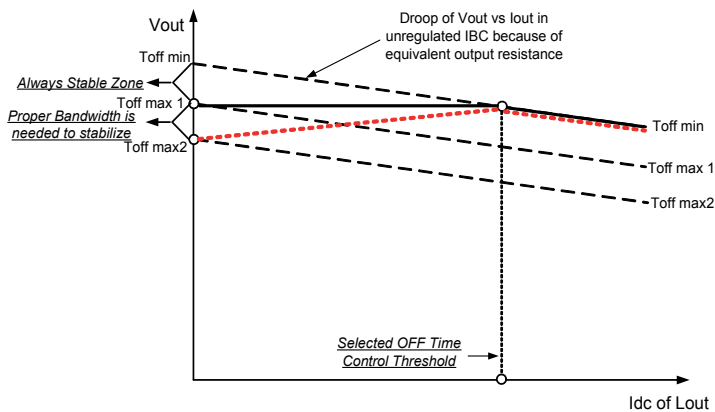


Fig. 22. Impact of linear based off time control circuit on output voltage (not to scale)

D. Reverse Energy Flow and Self-Oscillation

All topologies shown in Figure 14 are capable of transferring energy in the reverse direction, that is, from the output to input. This is because MOSFETs can conduct current in either direction when turned on. This is not true for a converter using a diode rectifier. During shutdown or a sudden input voltage drop, it is possible for the self-driven MOSFET rectifier to start oscillating and pumping energy backwards, thus causing large current and voltage spikes at the rectifier MOSFETs (Bottrill, 2007). The reverse current flow is also possible during quick converter re-start because the output bus capacitor has not been completely discharged from the previous operation. Another potential condition for reverse energy flow is the parallel operation of several bus converters.

One possible way to address this issue is to forcibly turn off the secondary side rectifier MOSFET during primary-side MOSFET off time. To understand this technique let us refer to Figs. 23 and 24. In this implementation, the controller uses additional output signals O1_DIN and O2_DIN, to turn off rectifier MOSFETs during T_{off} time as shown in Figure 23. Figure 24 shows the controller's push-pull outputs, O1_D and O2_D, driving the high side MOSFETs in the full-bridge power stage, and complementary 1-D outputs, O1_DIN and O2_DIN, driving the low side MOSFETs via external drivers. There is always dead time, T_d , between the D and 1-D pulses that is necessary to avoid shoot-through currents in each leg on primary side. If the duty cycle is less than maximum, there is the overlapping time, T_{CLAMP} , when the primary winding is shorted by the lower MOSFETs because they are both in the ON state (Figs. 23 and 24). This specific timing algorithm has been implemented in UCC28230/1 controllers (<http://focus.ti.com/docs/prod/folders/print/ucc28230.html>).

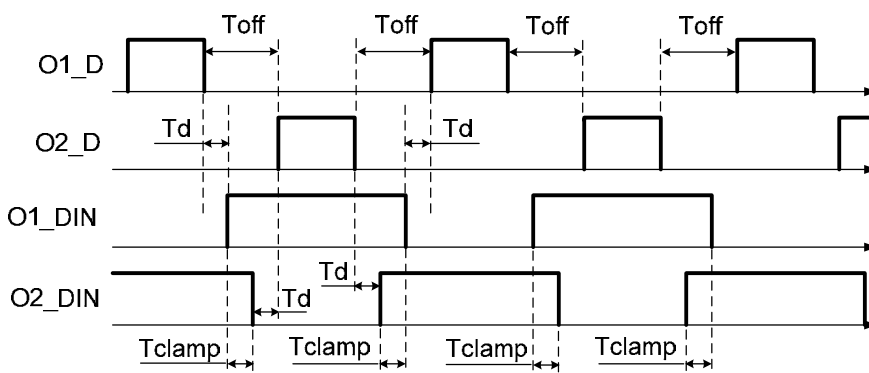


Fig. 23. Timing of UCC28230 controller's output signal

As mentioned earlier, this timing technique addresses the problem of reverse current flow during output pre-bias start up, shut down, input voltage drop, or parallel operation. For the half-bridge (Figure 14b) or push-pull (Figure 14c) IBC topologies, the primary winding of the power transformer can not be shorted by the primary power MOSFETs. To turn off the secondary side rectifier MOSFETs during the T_{CLAMP} interval, an external pulse transformer can be used as shown in Figure 25. In this case the synchronous rectifier scheme uses the control-driven technique for the unregulated IBC.

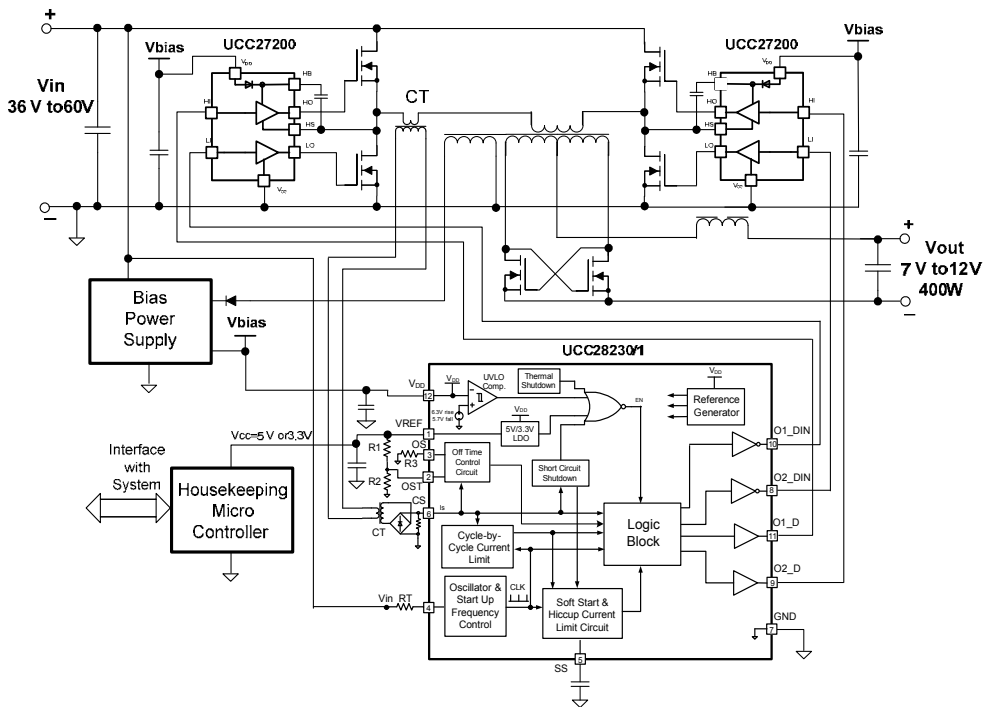


Fig. 24. Simplified diagram of typical full-bridge unregulated IBC

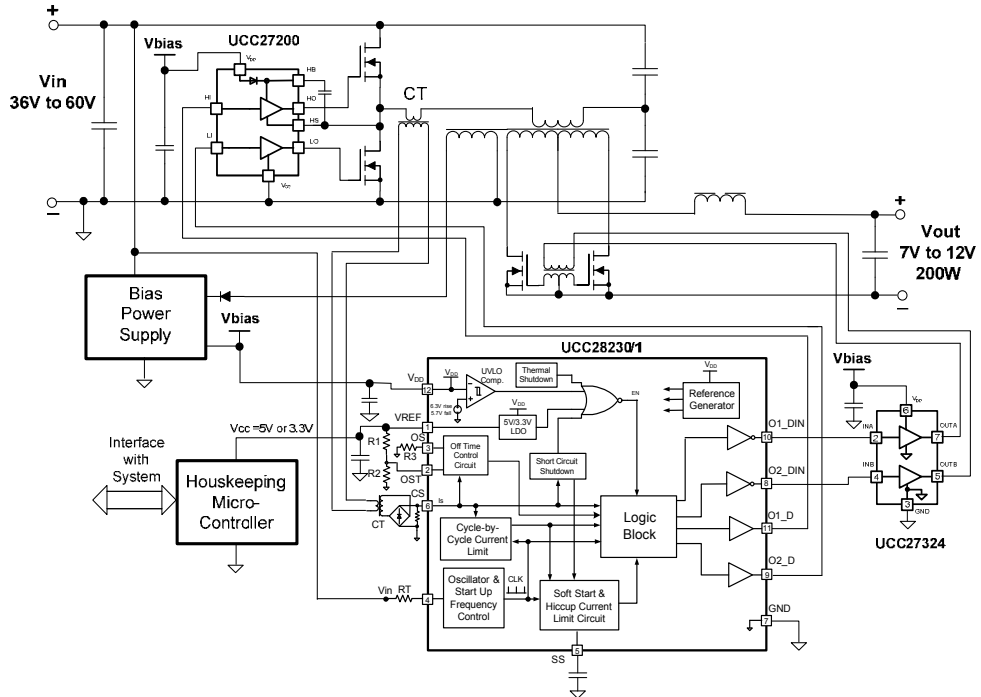


Fig. 25. Typical half-bridge unregulated IBC with control driven synchronous rectifier

E. Parallel Operation Issues

Parallel operation of IBCs is desirable in cases when the physical height is limited or when there may be a future need to easily upgrade to higher power levels. Paralleling can also be used for N+1 redundancy, but in this case, diodes in series with the outputs are needed to isolate a failed converter from the rest of the system. It is impossible to use any kind of active current-sharing technique with unregulated converters in parallel. The only option is to use a droop-current-sharing mechanism that depends on the output impedance of the converters sharing the current. Obviously, an accurate droop-current-sharing approach becomes more difficult as new IBC designs become more efficient. Additional problems related to sharing steady-state current can occur if all parallel IBCs do not start simultaneously. These problems include power circulation and tripping the over current protection circuit. Maintaining the secondary-side rectifier MOSFETs in the off state during the 1 - D cycle previously described is one way to prevent reverse current flow during parallel operation of unregulated IBCs.

F. Flux Balancing of Power Transformer

To reduce switching losses, unregulated IBCs use a relatively low 100- to 200-kHz switching frequency. The power transformers in the topologies shown in Figure 14 are expected to operate with a symmetrical B-H loop with no flux unbalancing for smaller size and reduced losses. One option to avoid flux unbalancing is using the gapped transformer. However, this approach increases a magnetizing current. Another option is to use a DC blocking capacitor in series with the primary winding of full-bridge converter shown in Figure 14a. For the half-bridge topology, this capacitor is already present as a necessary part of the power stage (Figure 14b). The potential issue with the DC blocking capacitor is that during cycle-by-cycle current limiting, significant variations in pulse amplitudes applied to the primary winding each half-cycle might occur. This pulse variation occurs because significant DC voltage can build up across the blocking capacitor that maintains volt-second balance of the transformer each half-switching cycle. Unequal amplitude pulses to the transformer windings cause over voltage stresses at the secondary side rectifier MOSFET. In many cases, careful layout and symmetrical matched output pulses from the controller and drivers can eliminate the need for DC blocking capacitor in the full-bridge converter. The simplest way to avoid unbalancing in a push-pull converter is to use cycle-by-cycle current limiting or a gapped transformer, because the DC blocking capacitor can not be used with this topology.

5.6 Experimental Results

The described advanced control improvements to an unregulated IBC were verified with a DC/DC module that had a 600-W output, a 48-V input, a 5:1 turns ratio, and a quarter-brick form factor. The controller used for these experiments was the UCC28230/1. More details about this controller can be found in (Texas Instruments, 2008. <http://focus.ti.com/docs/prod/folders/print/ucc28230.html>) The measured module efficiency, power losses, and output voltage are shown in Figs. 26, 27, and 28, respectively. In this example, the off time was set to a fixed time period. For this reason the output voltage shown in Figure 28 has an almost constant slope. The input-voltage measurements were $V_{in1} = 38$ V, $V_{in2} = 44$ V, $V_{in3} = 48$ V, and $V_{in4} = 53$ V. A comparison to the old controller that had an identical power stage, revealed an efficiency improvement of at least 1% over the full load-current range.

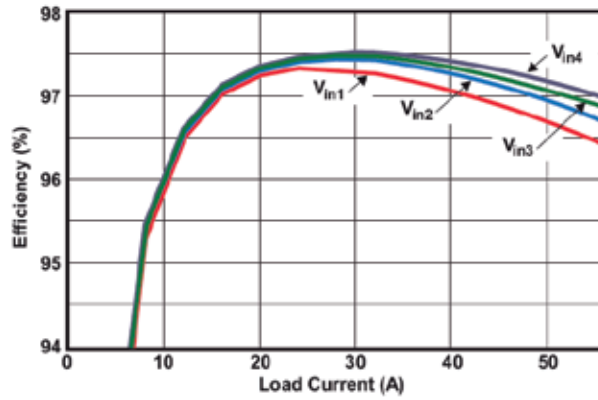


Fig. 26. Efficiency at 38V, 44V, 48V and 53V inputs over 0A to 56A output current range

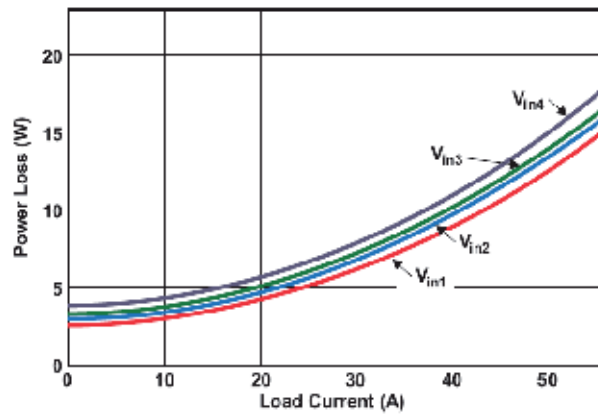


Fig. 27. Power losses at 38V, 44V, 48V and 53V inputs over 0A to 56A output current range

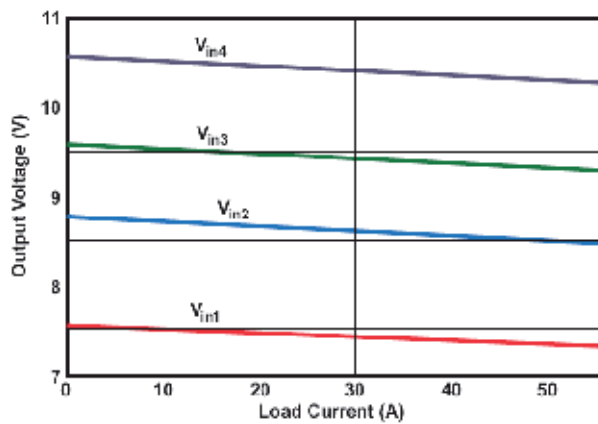


Fig. 28. Output voltage versus load current measurements

6. Conclusion

General market trends and new regulations to the telecommunication power system are discussed. It was shown, that to meet the new efficiency and power saving requirements, all system and design levels must be considered. Therefore, the focus was on review and comparison of the efficient, power saving solutions from the facility-level power system, to the cabinet level, followed by discussion of the specific requirements and solutions for the key functional blocks.

At the facility level, the new high voltage DC bus distribution system and its pros and cons have been described and compared. At the cabinet level, the brief history of power system evolution was shown. Pros and cons of different distribution power architectures were provided. Advantages and challenges of the evolving intermediate bus architecture were discussed in details including the optimal bus voltage analysis and selection.

The chapter discussed the requirements for telecom rectifiers and front-end server power supplies: the key functional parts of any data- and telecommunication power system.

Special attention was provided to the intermediate bus converters that are an enabling part of any IBA. Their requirements, key parameters, popular topologies, and design challenges were discussed in depth. The design example and test results of 600-W unregulated IBC converter with 48-V input and 5:1 transfer ratio was provided to illustrate and verify the recommended design approaches and solutions.

7. References

- Akerlund, J.; Boije af Gennas, C.; Olsson, G. & Rosin, D. (2007), One year operation of a 9 kW HVDC UPS 350 V at Gnesta Municipality data center, *Proceedings of 29th International Telecommunications Energy Conference, INTELEC'2007*, pp. 40-45, ISBN: 978-1-4244-1628-8, Rome, Italy, September 2007, IEEE
- Barry, M. (2004). Design issues in regulated and unregulated intermediate bus converters, *Proceedings of 19th Applied Power Electronics Conference, APEC'2004*, Vol. 3, pp.1389-1394, ISBN: 0-7803-8269-2, Anaheim, CA, USA, February 2004, IEEE
- Bjoerk, F.; Hancock, J. & Devoy, G. (2007). CoolMOS™ CP- How to make most beneficial use of the latest generation of super junction technology devices, *Infineon Application Note, AN-CoolMOS-CP-01*, February 2007
- Bottrill, J. The effects of turning off a converter with self-driven synchronous rectifiers, *Bodo's Power Systems*, May 2007, pp.32-35
- Cohen, I. & Lu, B. (2008). High power factor and high efficiency – you can have both, *Texas Instruments Power Supply Design Seminar*, Topic 1, SEM-1800, 2008
- ENERGY STAR® program requirements for computer servers, version 1.0, http://www.energystar.gov/index.cfm?c=ent_servers.enterprise_servers
- Ericsson Inc., (1996). A designers' guide to distributed power architectures using DC/DC power modules, *Published by Ericsson Components AB*, 1996.
- Ericsson Inc., (2005). Selection of architecture for systems using bus converters and POL converters, *Design Note 023*, Ericsson Inc., May 2005
- ETSI (2003) Environmental Engineering (EE) EN 300 132-3 Standard, Power supply interface at the input to telecommunication equipment; Part 3: Operated by rectified current source, alternating current source or direct current source up to 400 V, 2003

- Fasullo, G.; Kania, M. & Pitts, A. (2008). The Green revolution in DC power systems, *Proceedings of 30th International Telecommunications Energy Conference, INTELEC'2008*, pp. 1-7, ISBN: 978-1-4244-2056-8, San Diego, CA, USA, September 2008, IEEE
- Fu, D.; Lu, B. & Lee, F. (2007). 1MHz high efficiency LLC resonant converters with synchronous rectifier, *Proceedings of 38th Power Electronics Specialists Conference, PESC'2007*, pp. 2404-2410, ISBN: 1-4244-0655-2/07, Orlando, FL, USA, June 2007
- Hancock, J. (2008). Bridgeless PFC boosts low line efficiency, *Power Electronics Technology*, February 2008, pp.14-20
- Huber, L.; Jang, Y. & Jovanovic, M. (2008). Performance evaluation of bridgeless PFC boost rectifiers, *IEEE Transactions on Power Electronics*, vol.23, no.3, pp. 1381-1390, ISSN: 0885-8993, May 2008.
- ITU, (2009). International Telecommunication Union web site, <http://www.itu.int/themes/climate/index.html>
- Lindman, P. & Thorsell, L. (1996). Applying distributed power modules in telecom systems, *IEEE Transactions on Power Electronics.*, vol. 11, no. 2, pp. 365-373, ISSN: 0885-8993(96)01921-7, March 1996
- Mammano, R. (2006). Improving power supply efficiency - The global perspective, *Texas Instruments Power Supply Design Seminar*, Topic 1, SEM-1700, 2006
- Miesner, C.; Rupp, R.; Kapels, H.; Krach, M. & Zverev, I. (2001). ThinQ!™ Silicon Carbide Schottky Diodes: An SMPS Circuit Designer's Dream Comes True! *Infineon white paper*, Ordering No. B112-H7804-X-X-7600, September 2001
- Miftakhutdinov, R.; Nemchinov, A.; Meleshin, V. & Fraidlin, S. (1999). Modified asymmetrical ZVS half-bridge DC-DC converter, *Proceedings of 14th Applied Power Electronics Conference, APEC'1999*, Volume 1, pp. 567-574, ISBN: 0-7803-5160-6, Dallas, TX, USA, March 1999, IEEE
- Miftakhutdinov, R. (2007). Synchronous rectification technique: classification, review, comparison, *Proceedings of Power Electronics Technology Conference on CD-Rom*, Dallas, TX, USA, October 2007, <http://home.powerelectronics.com>
- Miftakhutdinov, R. & Sheng, L. (2007). New generation intermediate bus converter, *Proceedings of Power Electronics Technology Conference on CD-Rom*, Dallas, TX, USA, October 2007, <http://home.powerelectronics.com>
- R. Miftakhutdinov and L. Sheng, J. Liang, J. Wiggernhorn and H. Huang, (2008). Advanced control circuit for intermediate bus converter, *Proceedings of 23th Applied Power Electronics Conference, APEC'2008*, pp. 1515-1521, ISBN: 978-1-4244-1873-2, Austin, TX, USA, February 2008, IEEE
- Miftakhutdinov, R. (2008a). Power distribution architecture for tele- and data communication system based on new generation intermediate bus converter, *Proceedings of 30th International Telecommunications Energy Conference, INTELEC'2008*, Session 34-1, pp. 1-8, ISBN: 978-1-4244-2056-8, San Diego, CA, USA, September 2008, IEEE
- Miftakhutdinov, R. (2008b). Improving system efficiency with a new intermediate-bus architecture, *Texas Instruments Power Supply Design Seminar*, Topic 4, SEM-1800, 2008
- Mills, F. M. (2004). An alternative power architecture for next generation systems, *Proceedings of 4th International Power Electronics and Motion Control Conference, IPESC'2004*, pp.67-72, ISBN: 7 - 5605 - 1869 - 9, Xian, China, August 2004, IEEE

- Mitchell, D. M. (1983). AC-DC converter having an improved power factor, U.S. Patent 4 412 277, October 25, 1983
- Morrison, D. (2002). Distributed power moves to Intermediate Bus Voltage, *Electronic Design*, pp. 55-62, 16 September, 2002
- Narveson, B. (1996). How many isolated DC-DC's do you really need?, *Proceedings of 11th Applied Power Electronics Conference, APEC'1996*, Volume 2, pp.692-695, ISBN: 0-7803-3044-7/96, San Jose, CA, USA, March 1996, IEEE
- Pratt, A.; Kumar, R. & Aldridge, T.V. (2007). Evaluation of 400V DC distribution in telco and data centers to improve energy efficiency, *Proceedings of 29th International Telecommunications Energy Conference, INTELEC'2007*, pp. 32-39, ISBN: 978-1-4244-1628-8, Rome, Italy, September 2007, IEEE
- Ren, Y.; Xu, M.; Sun J. ; & Lee, F. (2005). A family of high power density unregulated bus converters, *IEEE Transactions on Power Electronics*, Vol. 20, No. 5, pp. 1045-1054, ISSN: 0885-8993, September 2005, IEEE
- Sayani, M. & Wanes, J. (2003). Analyzing and determining optimum on-board power architectures for 48V-input systems, *Proceedings of 18th Applied Power Electronics Conference, APEC'2003*, Volume 2, pp.781-785, ISBN: 0-7803-7768-0, Miami Beach, FL, USA, February 2003, IEEE
- Souza, A. & Barbi, I. (1999). High power factor rectifier with reduced conduction and commutation losses, *Proceedings of 21th International Telecommunications Energy Conference, INTELEC'1999*, Session 8.1, pp.1-5, ISBN: 0-7803-5624-1, Copenhagen, Denmark, June 1999, IEEE
- Tabisz, W.; Jovanovic, M. & Lee, F. (1992). Present and future of distributed power systems, *Proceedings of 7th Applied Power Electronics Conference, APEC'1992*, pp.11-18, ISBN: 0-7803-0485-3/92, Boston, MA, USA, February 1992, IEEE
- Texas Instruments, Datasheet: Two-phase, interleaved CCM PFC controller, UCC28070, <http://focus.ti.com/docs/prod/folders/print/ucc28070.html>
- Texas Instruments, Datasheet: Advanced PWM Controller for Bus Converters, UCC28230/1 TI Document, SLUS 814, April 2008
<http://focus.ti.com/docs/prod/folders/print/ucc28230.html>
- Texas Instruments, Datasheet: TMS320F28023 Piccolo™ microcontroller, <http://focus.ti.com/docs/prod/folders/print/tms320f28023.html>
- Thorsell, L. (1990). Will distributed on-board DC/DC converters become economically beneficial in telecom switching equipment?, *Proceedings of 12th International Telecommunications Energy Conference, INTELEC'1990*, pp. 63-69, Cat. No.90CH2928-0, Orlando, FL, USA, October 1990, IEEE
- White, R. (2003). Emerging On-Board Power Architectures, *Proceedings of 18th Applied Power Electronics Conference, APEC'2003*, Volume 2, pp.799-804, ISBN: 0-7803-7768-0, Miami Beach, FL, USA, February 2003, IEEE
- Zhang, J. ; Xie, X.; Wu, X. & Qian, Z. (2004). Comparison study of phase-shifted full bridge ZVS converters, *Proceedings of 35th Power Electronics Specialists Conference, PESC'2004*, pp. 533-539, ISBN: 0-7803-8399-0, Aachen, Germany, June 2004, IEEE
- Zhu, J. & Dou, S. (2006). Intermediate bus voltage optimization for high voltage input VRM, *Proceedings of 7th International Conference on Electronic Packaging Technology, ICEPT'2006*, pp.1-4, ISBN: 1-4244-0620-X/06/, Shanghai, China, August 2006, IEEE

Directional Routing Protocol in Wireless Mobile Ad Hoc Network

L.A.Latiff¹, N. Faisal², S.A. Arifin³ and A. Ali Ahmed⁴,
^{1,2,3}Telematics Research Group, Universiti Teknologi Malaysia, Malaysia
⁴Yemen University of Science and Technology, Yemen

1. Introduction

Advancement in wireless communication technology and portable computing devices such as wireless handhelds, Personal Digital Assistants (PDA) and other mobile information terminals have led to a revolutionary change in our information society towards the era of mobile computing. The ubiquitous access to a variety of digital devices and multimedia tools makes it possible to create, analyze, synthesize and communicate knowledge using a rich variety of media forms. Additionally, the mobile devices are getting smaller, cheaper, more convenient, and more powerful and have contributed to the explosive growth of the mobile computing equipment market. Vast interest and concerted work in developing and enhancing wireless and mobile network protocols are being driven by the ever increasing demand for an anytime and anywhere Internet access.

To date, the type of network that have been widely deployed is based on a centralized approach which requires a network point of access, commonly called the Access Point (AP) that act as a gateway for the mobile device to the Internet. Even though these infrastructure-based networks provide the path for mobile devices connectivity, time and potentially high cost are required to set up the necessary infrastructure (Xue & Ganz, 2003). Also due to the limited radio range, the devices must be in the vicinity of an AP in order to be connected. It is important to note that when a natural catastrophe, war, or geographic isolation occurs, communication may break down; thus, unavailability of the network connection (Milanovic et al.,2004). Hence, the provision of required connectivity and network services at this instance becomes a real challenge. With this scenario, ad hoc technology emerges with the aim to solve this problem.

1.1 MANET Features

Mobile Ad Hoc Network (MANET) is a large collection of mobile nodes which are equipped with wireless communication devices. These devices communicate peer-to-peer in a network with no fixed infrastructure even when moving. Nodes in MANET can serve as hosts and routers where communication between nodes beyond their transmission radius can be achieved via several hops as inherent in collaborative communication of

neighbouring nodes. Due to its portability, MANET nodes depend on batteries for their source of energy (Sun, 2001).

The wireless media used will remain to have a significantly lesser capacity compared to the wired media (Macker & Corson, 1997). Also, the communication media, which is shared with neighbours that are within communication range, warrants implementation of a multiple access protocol to support systematic and efficient sharing.

Each mobile device in MANET is an autonomous node (Macker & Corson, 1997) and this means that nodes not only perform basic processing abilities to initiate and receive data as a host, it also performs routing functions. The routing algorithm in MANET can be a single-hop or multihop which has different link layer attributes and routing protocols. Single-hop communication is simpler in terms of structure and implementations but has lesser functions and applications compared to multi-hop communication. In multi-hop communication, the destination is beyond the transmission coverage of the source and hence the packets are forwarded via one or more intermediate nodes. Figure 1 shows a MANET network consisting of nodes and their transmission ranges. As shown in Figure 1, Node 2 and Node 3 are neighbours of Node 1 whilst Node 4 and Node 5 are not. Therefore, data transmission to Node 4 and Node 5 will have to be relayed by Node 2.

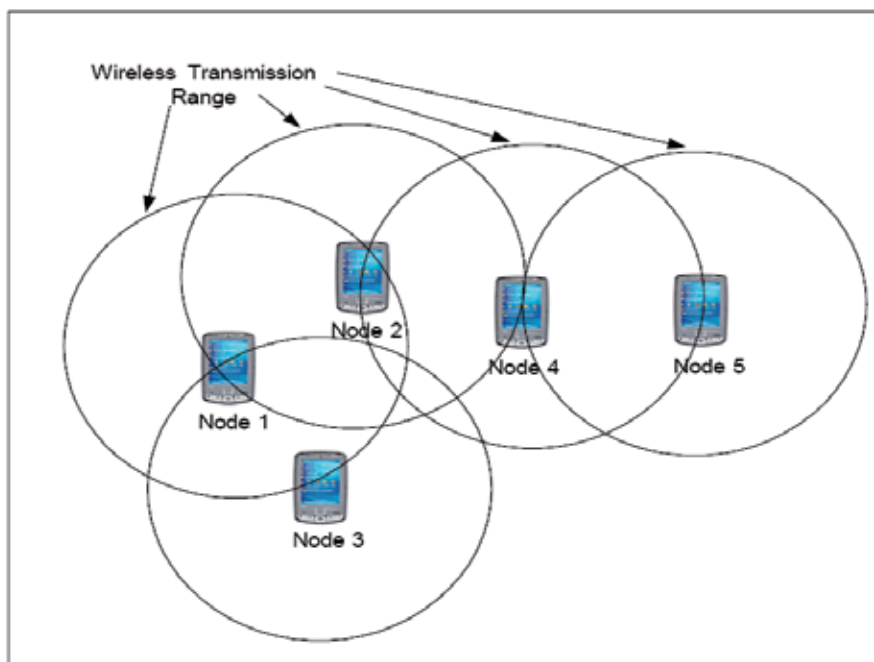


Fig. 1. MANET nodes and their transmission ranges

Since nodes in MANET use batteries as their source of energy which is easily depleted, it is required to extend the longevity of nodes by utilizing effective and energy-saving algorithm.

In MANET, nodes are free to move randomly. Hence, the topology of the network is ever changing and the communication link created between a source and destination pair may vary with time (Agrawal & Zeng, 2003). Nodes must be able to establish and maintain the routes as they move to allow applications services to operate without interruptions. Therefore, the control and management of the network must be distributed among the mobile nodes to support multi-hop communication beyond the transmission range of a node.

These characteristics do pose challenges to the roll-off of MANET which have motivated a concerted time and effort of researchers in proposing new, innovative and improved routing protocols for MANET. The important issues in routing are reaching the destination in minimum time at minimum cost.

1.2 Routing Protocols in MANET

Topology in MANET is very dynamic and ever-changing where nodes are free to join or leave arbitrarily. The goal of mobile ad hoc networking is to extend mobility into the realm of autonomous, mobile, wireless domains, where a set of nodes themselves form the network routing infrastructure in an ad hoc fashion (Macker & Corson, 1997). Traditional routing protocol used in wired network cannot be applied directly to wireless and mobile network. Several considerations are needed before we embark on the development of a routing protocol for a wireless network which is non-trivial due to nodes' high mobility.

Generally, there are two different stages in routing; they are route discovery and data forwarding. In route discovery, route to a destination will be discovered by broadcasting the query. Then, once the route has been established, data forwarding will be initiated and sent via the routes that have been determined. Through broadcasting, all nodes that receive the query will broadcast to all neighbours and hence, large number of control messages is transmitted. It will be further compounded if the nodes move and new route need to be recomputed. Frequent route discovery and in some instances, additional periodic updates will cause more bandwidth being utilized and thus more energy wastage. Hence, to conserve the power consumption, route relaying load, battery life, reduction in the frequency of sending control messages, optimization of size of control headers and efficient route reconfiguration should be considered when developing a routing protocol (Chlamtac et al., 2003).

Over the past several years, many routing protocols have been proposed and can be categorized into topology-based (Royer & Toh, 1999) and position-based protocols (Giordano et al., 2004). Topology-based routing protocols route packets based on information about the network links while position-based routing protocols uses physical information about the participating nodes to decide on how to route packets. Topology-based protocols can be further divided into proactive, reactive and hybrid routing protocols. The network links are determined long before routing process in proactive protocols, when routing in reactive protocols and a combination of before and when routing in hybrid protocols. In the position-based protocols, location information of the destination are known and used. There are two sub-divisions in position-based routing protocols, namely

greedy forwarding and restricted flooding. In greedy forwarding, nodes that have the best progress will be selected and data packet will be forwarded to these nodes. Ideally, this process is repeated until the packet arrives at the destination. Note there is no route discovery in greedy forwarding. Restricted flooding, on the other hand, will mitigate broadcast storm problem where only nodes in the direction of the destination will participate in the route discovery until the route to destination is found. The participation of nodes in routing will optimize broadcasting in MANET. Restricted flooding will broadcast messages to a selected number of nodes which is usually more than one that are located closer to the destination. It will significantly reduce not only energy but also reduce the probability of packet collisions of messages rebroadcast by neighbours using the same transmission channel (Stojmenovic, 2002; Mauve et al, 2001; Giordano et al, 2004). Figure 2 shows the categorization of routing protocols in MANET.

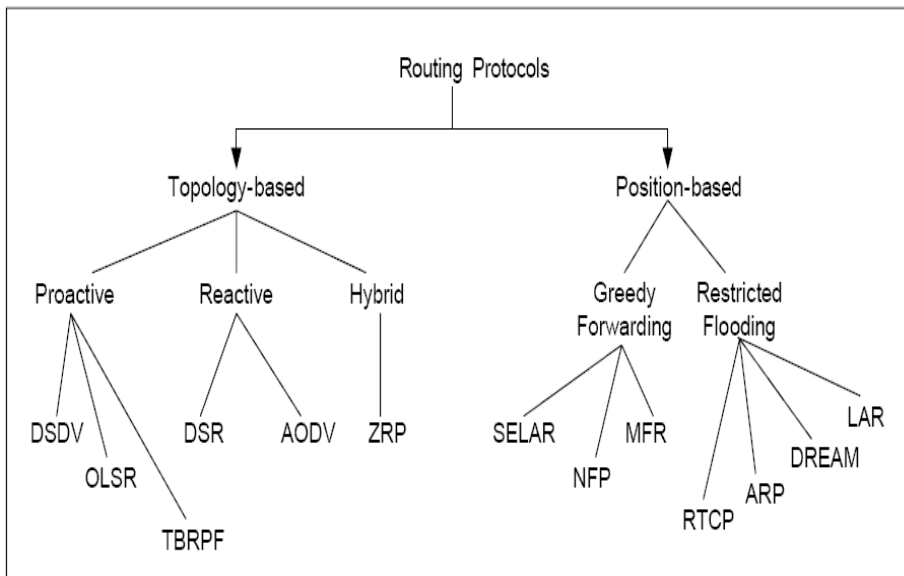


Fig. 2. Categorization of MANET Routing Protocols

2. Literature Review

With the advent of Global Positioning System (GPS) and MANET environment-based self-positioning (Latiff et al, 2005) and remote-positioning system (Li et al, 2000; Ali et al, 2004), location information can be easily disseminated to the requesting node as required in the position-based routing protocol. Besides availability of location information, complexity of mathematical computations and issues pertaining to the implementation of the said protocols should also be considered. Complex computational iterations will result in processing delay and hence, higher latency while many routing packets transversing in the network will result in high energy consumption and high probability of packet collisions. Hence, position-based routing that restricts the broadcast region will reduce routing

messages periodically transmitted that has information of the sending node location information must be implemented. Hence, knowledge of the local topology will have to be maintained in a neighbours table at each node. This will require storage of neighbour information which meant additional cost. Also, these approaches will also require complex computation at the nodes and hence, will incur delay at the intermediate nodes.

2.2 Restricted Flooding

The main approach in restricted flooding is to limit the flooding region which can be based on distance, angle and distance covered by the next intermediate node. Using distance, only nodes that are nearer to the destination will participate in the route discovery. Nodes that are further away from source will not participate. LAR (Ko & Vaidya, 2000) calculates distance from the destination based on location information of the destination that will be extracted from the request packet while (Cartigny et al, 2003) uses the relative neighborhood graph (RNG) with local information of distance to neighbours and distances between neighbours to decide whether its participation has better coverage compared to other nodes. This will minimize the total energy consumption while still maintaining the whole network coverage through broadcasting. (Ali et al, 2005) calculates distances to all nodes in the network and will compare the distance information of the source to the destination extracted from the request packet to determine its participation.

On the other hand, ARP (Kumar Bankar & Xue, 2002) and DREAM [Basagni et al, 1998] uses the angle made from the straight line drawn from source to destination as the restricted region whereby all nodes in this region will participate in the route discovery. However, DDB (Heissenbutte et al, 2004) uses the location information of the destination node and also of the intermediate node which are inserted in the request packet. With this additional information, an intermediate node can calculate the estimated additional covered area that it would cover with its transmission which is based on Dynamic Forwarding Delay (DFD). The concept of DFD is to determine when to forward the packet and node with more area covered will be given a smaller delay to broadcast and hence, will broadcast it first. All the proposed protocols require quite complex mathematical computation of the distance, angle and coverage at all intermediate nodes to determine the nodes' participation. Information of the source and destination are required and must be inserted in the incoming packet.

In MANET, route discovery is initiated by total flooding of route request (RREQ) messages that consume a large portion of the already limited bandwidth in MANET. As illustrated in Figure 4, RREQ is broadcasted to all neighbours whereby frequent broadcast causes network congestion and degrades the performance of routing protocol. This could be proved by several performance observations that the number of RREQ in the network increases linearly with the node population (Perkins, 2004). The ratio of control packet over data packet even reaches 5000 in one of the experiments.

As such, we suggest utilizing restricted flooding mechanism to optimise the route establishment phase of AODVbis. Restricted flooding is broadcasting messages to a selected number of nodes which is more than one that are located in an area in the vicinity of the destination. Position information of the destination can be obtained from any location

service while position location of the destination can be obtained with the aid of GPS or any other self-positioning system proposed for MANET. Then if these information are piggy-backed in the query packet, nodes will calculate its location with reference to the source and destination and will then decide to broadcast the query or not. Figure 5 illustrates that the same network topology shown in Figure 4 but with limited flooding. RREQ packets will be broadcast by nodes located in the request zone which is a quadrant drawn with respect to source node coordinates. Nodes participation is denoted by shaded circles with arrows indicating the direction of broadcast while lesser-toned circles indicate non-participating nodes. With this unique approach of using quadrant as the broadcast region, we proposed Quadrant-based Directional Routing Protocol or Q-DIR.

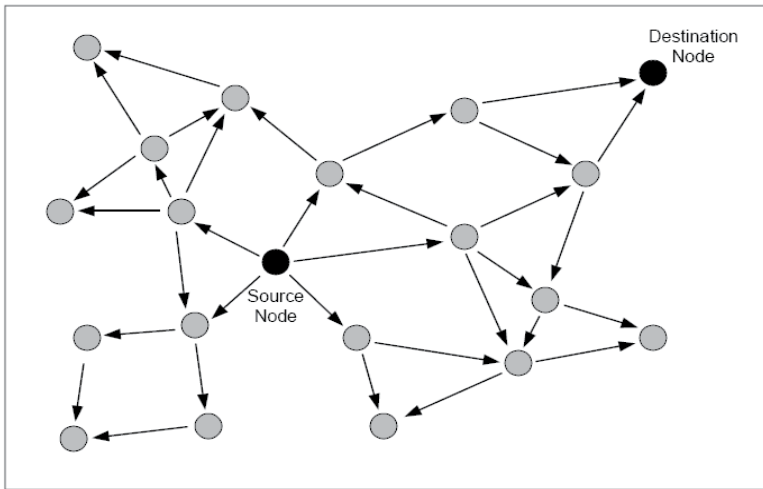


Fig. 4. RREQs broadcast based on Total Flooding.

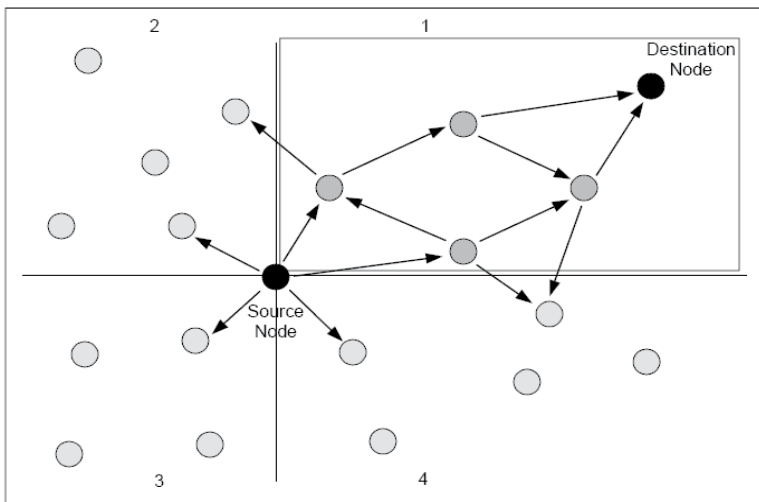


Fig. 5. RREQ broadcast based on Restricted Flooding.

2.3 Quadrant-based Directional Routing Protocol (Q-DIR)

Q-DIR is a limited flooding routing protocol that concentrates on a specified zone using location information provided by a location service. It restricts the broadcast region to all nodes in the same quadrant as the source and destination and does not require maintenance of a separate neighbours table at each node as in (Ko & Vaidya, 2000; Kumar Banka & Xue, 2002; Cartigny et al, 2003; Heissenbutte et al, 2004). Q-DIR determines the quadrant of the current node based on the coordinates of source, destination and the current node that will direct the packet towards the destination. Even though (Cartigny et al, 2003) uses all these information to determine the distance or area covered, it requires trigonometric computations which will further incur delay if computed in kernel space.

Decision to broadcast or discard will be done as the RREQ packet is received by the node. Unlike LAR scheme 2 (Ko & Vaidya, 2000), geocast-enhanced AODVbis (Ooi, 2005; Latiff et al, 2006), nodes in Q-DIR do not keep a distance table or a neighbours table which must be updated frequently. Keeping a distance table is much like a table-driven proactive routing concept. The size of the table will increase for a larger network because nodes need to have distance information of itself to every other node in the network which will vary from node to node. This will pose a constraint to the maximum number of nodes in the network as the memory allocation to store distance information of every node in the network at each node is limited and scarce.

In Q-DIR, the RREQ packet which contains the coordinates of the source and destination will be the only information the current node needs to decide to participate in the routing or not. The decision to participate at each node is made immediately as the node receives the RREQ packet and a neighbours table is not required to make the decision.

Q-DIR will significantly reduce not only energy but also reduce the probability of packet collisions of messages rebroadcast by neighbours using the same transmission channel. This will result in reduced routing overhead especially in a dense network.

3. Development of Q-DIR in Ns-2

In Q-DIR operation, the location information of the source and destination nodes is piggy-backed in the route request (RREQ) packet and then broadcasted. Upon receiving the RREQ, intermediate nodes will compare using a simple mathematical comparison based on the coordinates of source, destination and the current node that directs the packet towards the destination and as illustrated in Figure 6. This mathematical processing will be done in the kernel environment to eliminate the cross-over from user to kernel space and vice versa. Hence, the decision to participate is made immediately.

Quadrant of me compared to source?
 Quadrant of destination compared to source?
 If same, FORWARD
 If not, DROP.

Fig. 6. Q-DIR decision at each intermediate node.

Once the decision to broadcast has been made, the intermediate node will insert its location by replacing the source node coordinates and append its address and sequence number at the end of the RREQ packet. It will then broadcast the packet. The process will repeat at each intermediate node until it reaches the destination. The replacement of the source node location information with the intermediate node coordinates will make the packet more directed towards the destination since the comparison now is based on the previous node. Upon receiving the RREQ, destination node will send a route reply message (RREP) back to source via the path taken to reach the destination that was appended in the RREQ as it traverses across the network. There is no need for the route discovery to the source node. Figure 7 shows the format of the RREQ packet in Q-DIR where the source and destination nodes location information are inserted are highlighted.

0	1	2	3	4	5	6	7	0	1	2	3	4	5	6	7	0	1	2	3	4	5	6	7
Type				D/G		Reserved						Hop Count											
RREQ ID																							
X_s				Y_s				X_d				Y_d											
Destination IP Address																							
Destination Sequence Number																							
Originator IP Address																							
Originator Sequence Number																							
Path Node IP Address																							
Path Node Sequence Number																							
(additional path node IP address and sequence number pairs) ...																							

Fig. 7. RREQ format in Q-DIR.

There are several open source network simulators such as Commnet, OMNeT++ but Network Simulator-2 (Ns-2) has been found to be a widely used tool for simulating inter-network topologies and to test and evaluate various networking protocols (CMU Monarch Project, 2006). It is a discrete event simulator written in C++ and uses Massachusetts Institute of Technology (MIT) Object Tool Command Language (OTcl) as a command and configuration interface. The most important characteristic of a discrete-event approach is that the components of an actual network are represented within the software and real events are simulated by the operation of the software.

Ns-2 can be installed on both Windows and Linux platforms. For Q-DIR, the simulation work is done on a Red Hat Linux platform (Chakeres et al, 2005) The compiler used in Q-DIR is the ns-allinone-2.28 version (CMU Monarch Project, 2006). The underlying protocol is AODVbis which has the path accumulation feature (Gwalani et al, 2003). The Dynamic MANET On-demand - University of Murcia (DYMOUM) (Ros & Ruiz, 2004) is based on DYMO which is an internet draft dated June 2005. DYMO enables reactive, multi-hop routing between participating node that wish to communicate. The basic operation of DYMO is similar to AODVbis which are route discovery and route management and the

differences are in the new packet format, generic packet handling, unsupported element handling and optional path accumulation. DYMOUM has There are three types of elements that have been defined in DYMO. They are RE (Routing Element), RERR and UERR (Unsupported-element Error) and RE can be further divided into RREQ and Route Reply (RREP). From the description given, DYMO can be used as the underlying protocol in this work. DYMO is reactive and implements route discovery and path accumulation. Even though it uses a generic element structure but basically has the needed RREQ, RREP and RERR packets as in the AODVbis routing protocol. Any modification work should be done in the C++ hierarchy.

3.1 RREQ packet format

As shown in Figure 8, to modify the RREQ packet, the source and destination coordinates are declared as a double precision integer. In the DYMOUM source file, when a new RREQ is generated by the source node, the `NS_CLASS re_create_rreq ()` procedure will create the RREQ packet. The RREQ packet requires location information of the source node; therefore the following syntax will extract the source coordinates from the ns-2 environment which is searched by using the node address.

```
Node*node=Node::get_node_by_address(re_node_addr.s_addr);
((MobileNode *)node)->getLoc(&x,&y,&z);
```

To extract the destination coordinates, a declaration of the following were made at the beginning of the source file that permits calling for those information using Tcl hooks in the ns-2 platform. Description of the declaration for Tcl hooks will be described in the following section.

```
extern dst_x, dst_y;
```

```
/* dymo_re.c */
RE *NS_CLASS re_create_rreq(struct in_addr target_addr,u_int32_t
target_seqnum,struct in_addr re_node_addr,u_int32_t re_node_seqnum,u_int8_t prefix,
u_int8_t g,u_int8_t ttl, u_int8_t thopcnt)
{
    RE *re;
    /* declare variable type for coordinates and get info of node using s_addr */
    double x=0,y=0,z=0;
    Node *node=Node::get_node_by_address(re_node_addr.s_addr);
    ((MobileNode *)node)->getLoc(&x, &y, &z);

    re
        = (RE *) dymo_socket_new_element();
    re->m
        = 0;
    re->h
        = 0;
    re->type
        = DYMO_RE_TYPE;
    re->a
        = 1;
    re->i
        = 0;
    re->res1
        = 0;
    re->res2
        = 0;
    re->ttl
        = ttl;
    re->len
        = RE_BASIC_SIZE + RE_BLOCK_SIZE;
    re->thopcnt
        = thopcnt;
    re->target_addr
        = (u_int32_t) target_addr.s_addr;
    re->target_seqnum
        = htonl(target_seqnum);
    /* add new field for x and y coordinates of source and destination in RREQ packet */
    re->dst_x=dst_x; /* x-coord for destination */
    re->dst_y=dst_y; /* y-coord for destination */
    re->src_x=x; /* x-coord for source */
    re->src_y=y; /* y-coord for source */

    re->re_blocks[0].g
        = g;
    re->re_blocks[0].prefix
        = prefix;
    re->re_blocks[0].res
        = 0;
    re->re_blocks[0].re_hopcnt
        = 0;
    re->re_blocks[0].re_node_addr
        = (u_int32_t) re_node_addr.s_addr;
    re->re_blocks[0].re_node_seqnum
        = htonl(re_node_seqnum);
    return re;
}
```

Fig. 8. Declaration of additional fields to the RREQ packet.

3.2 Tcl Hooks

Ns-2 consists of two hierarchies: compiled C++ hierarchy and the OTcl that make use of objects in C++ through OTcl linkages that have a one-to-one correspondence to each other. The objects that have already been linked are “*no_path_acc_*”, “*reissue_rreq*”, and “*s_bit*”. Therefore, to link the coordinates of the destination node that will be declared in the tcl script in the OTcl environment, links for both objects have to be created and the declarations are as shown in Figure 9. This *ns-2.28/dymoum-0.1/ns/dymo_um.cc* file has other links to the C++ hierarchy that are relevant to the DYMO configuration but will not be shown here. The variables for *dst_x* and *dst_y* in the header file *dymo_um.h* to enable referencing by *dymo_um.cc* have been declared. To enable calling DYMOUM from the tcl script, the agent DYMOUM (Agent/DYMOUM), *dst_x* and *dst_y* in the *ns-default.tcl* file in ns-2 library are inserted.

```

/* dymoum-0.1/ns/dymo_um.cc */
NS_CLASS DYMOUM(nsaddr_t id): Agent(PT_DYMOUM), qtimer_(this), initialized_(0), pq_len(0)
{
    /* Enable usage of some of the configuration variables from Tcl.
    Note: Do NOT change the values of these variables in the constructor
    after binding them! The desired default values should be set in
    ~ns/tcl/lib/ns-default.tcl instead */
    bind_bool("no_path_acc_", &no_path_acc);
    bind_bool("reissue_rreq_", &reissue_rreq);
    bind("dstx", &dst_x);
    bind("dsty", &dst_y);
    .
    .
    .
    .
    .
}

```

Fig. 9. Binding of Tcl objects to the C++ hierarchy

3.3 Processing RREQ

As described in Section 3, processing of RREQ consists of two events. They are Generating RREQ when the current node has data to send and initiates the route discovery for a certain destination and Receiving RREQ that is implemented at the intermediate nodes that receives the query broadcast. In the same *dymo_re.c* file previously mentioned, in the function **NS_CLASS re_process()**, variables such as temporary fields to store coordinates of current node and value of quadrant are declared. Then, the syntax to search for the current node coordinates and store these information in *mynode_x* and *mynode_y* will be made as shown in Figure 10.

```

void NS_CLASS re_process(RE *re, struct in_addr ip_src, u_int32_t ifindex)
{
    struct in_addr node_addr;
    rtable_entry_t *entry;
    int i;
    /* declare variable type for x and y coordinates field in packet received */
    double mynode_x, mynode_y;
    int quaddest, quadsrc;
    double x=0, y=0, z=0;
    /* get info of current node using address from ns */
    Node *node=Node::get_node_by_address(ip_src.s_addr); /* current node
address*/
    printf("process current node=%d\n", ip_src.s_addr);
    ((MobileNode *)node)->getLoc(&x, &y, &z);
    mynode_x=x; mynode_y=y; /* put the coordinates into mynode_x and
mynode_y */
    /* to check for correct info extracted from ns */
    printf("srcx=%f, srcy=%f, dstx=%f, dsty=%f, myx=%f, myy=%f\n",
re->src_x, re->src_y, re->dst_x, re->dst_y, mynode_x, mynode_y);
    .
    .
    .
}

```

Fig. 10. Declaration of variables in *dymo_re.c*.

When receiving RREQ, nodes will compare the quadrant of destination and current node and the codes are be inserted right after the declaration of the variables in function **NS_CLASS re_process()**. The coordinates of the source are denoted by *src_x* and *src_y*, while the coordinates of destination are denoted by *dst_x* and *dst_y*. The current node coordinates are denoted by *mynode_x* and *mynode_y*. If the quadrant of the source is equal to the quadrant of destination, the current node will broadcast the request. The code for this receiving RREQ is shown in Figure 11.

```

if ((re->dst_x >= re->src_x) && (re->dst_y >= re->src_y)) quaddest = 1;
if ((re->dst_x >= re->src_x) && (re->dst_y < re->src_y)) quaddest = 4;
if ((re->dst_x < re->src_x) && (re->dst_y >= re->src_y)) quaddest = 2;
if ((re->dst_x < re->src_x) && (re->dst_y < re->src_y)) quaddest = 3;
printf("Quadrant of destination compared to previous node is %3d\n", quaddest);

if ((mynode_x >= re->src_x) && (mynode_y >= re->src_y)) quadsrc = 1;
if ((mynode_x >= re->src_x) && (mynode_y < re->src_y)) quadsrc = 4;
if ((mynode_x < re->src_x) && (mynode_y >= re->src_y)) quadsrc = 2;
if ((mynode_x < re->src_x) && (mynode_y < re->src_y)) quadsrc = 3;
printf("My quadrant compared to previous node is %3d\n", quadsrc);
if (quaddest != quadsrc)
{
    printf("I am not in the same quadrant as destination. DROP packet.\n");
    return;
}
else printf("I am in the same quadrant as destination. FORWARD packet.\n");

```

Fig. 11. Code for broadcast decision at each node.

4. Verification of Q-DIR

4.1 Network Model

A network model N-1 as shown in Figure 12 is used which consist of 6 nodes and the coordinates are carefully chosen so that there will be at least 2-hops transmission to the destination. The imaginary x - and y -axis are drawn to show in which quadrant the nodes are located with reference to their immediate neighbours.

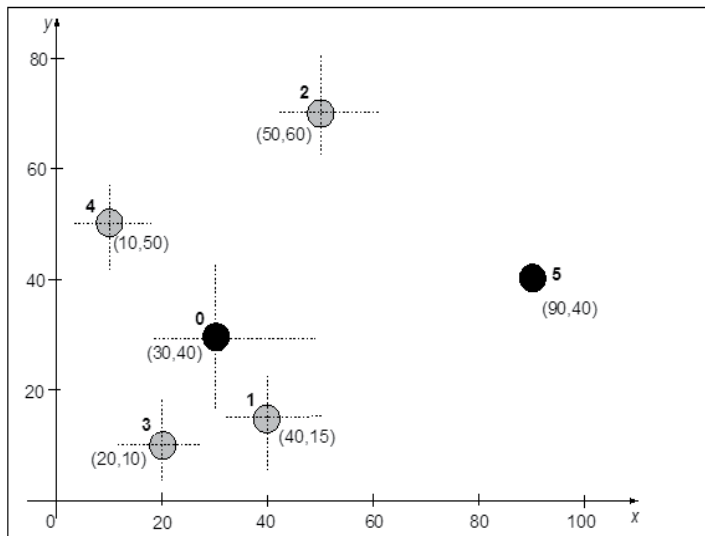


Fig. 12. Topology N-1

For topology N-1, the 1-hop neighbours of node 0 are nodes 1, 2, 3 and 4 while the neighbours of node 5 are 1 and 2. The configuration parameters used for both Q-DIR and AODVbis routing are shown in Table 1. The values can be modified depending on the network and its environment. The maximum number of hops between nodes have been set to 10 while the estimated average of one hop traversal time is set to 0.6 s. From I-D (Perkins et al, 2003), for correct operation, the route delete period must be greater than both (Allowed HELLO loss* HELLO interval) and the total traversal time.

The MAC layer protocol used is IEEE 802.11 DCF CSMA/CA. The data rate have been set to 2 Mbps and the network protocol is IP. The path loss model used is the log-normal path loss model (Rappaport, 2002) and the value for n is 2.4 and the standard deviation σ is 4. To simulate in ns-2, the receive threshold power has to be determined first in order to set the transmission range to 30 meters for all 1-hop neighbours. The default transmitted power is 0.28318 W. The receive threshold power calculated is 1.20475e-08 watts and the packet rate is set to 1 packet/sec while the packet size is set at 64 bytes and 512 bytes with a CBR (Constant Bit Rate) traffic pattern.

<i>Configuration Parameters</i>	<i>Value</i>
<i>Maximum number of possible hops between two nodes</i>	10
<i>Average one hop traversal time</i>	60 milliseconds
<i>Route discovery time</i>	2400 milliseconds
<i>Route delete period</i>	4800 milliseconds
<i>Number of RREQ tries</i>	3
<i>Total traversal time</i>	1200 milliseconds
<i>HELLO interval</i>	1000 milliseconds
<i>Allowed HELLO loss</i>	2

Table 1. Simulation Configuration Parameters.

4.2 Results

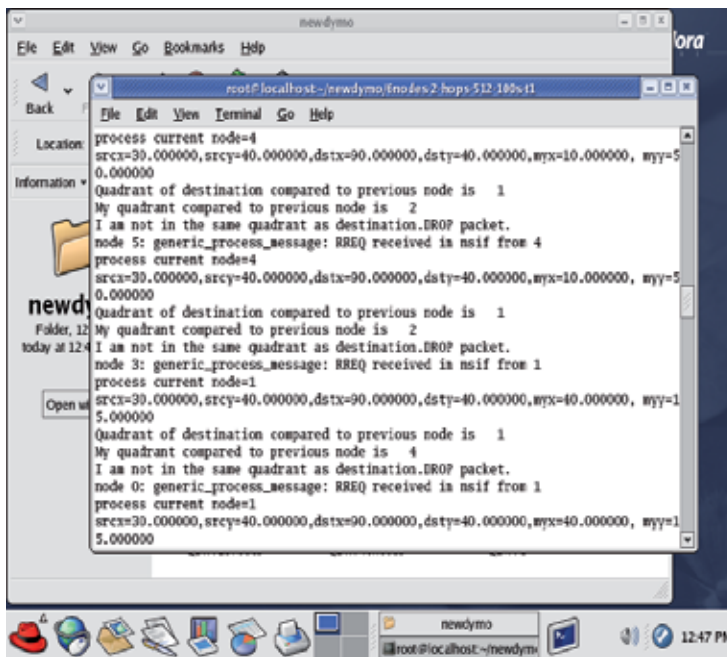
The simulation for topology N-1 was run and results show that for N-1, nodes 1, 2, 3 and 4 will all receive the RREQ packet from source node 0 destined for destination node 5. However, nodes 1, 3, and 4 will drop the packet since they are in different quadrant from the source and destination. Figure 13(a) shows the snapshot of the message displayed on the screen when running the simulation. The snapshot shows that node 1 and 3 drop the RREQ received from source node 0 while Figure 13(b) shows that node 4 drops the packet from source node 0. On the other hand, from Figure 13(c), node 2 forwards the packet to destination node 5 since it is in the same quadrant as destination compared to source.

```

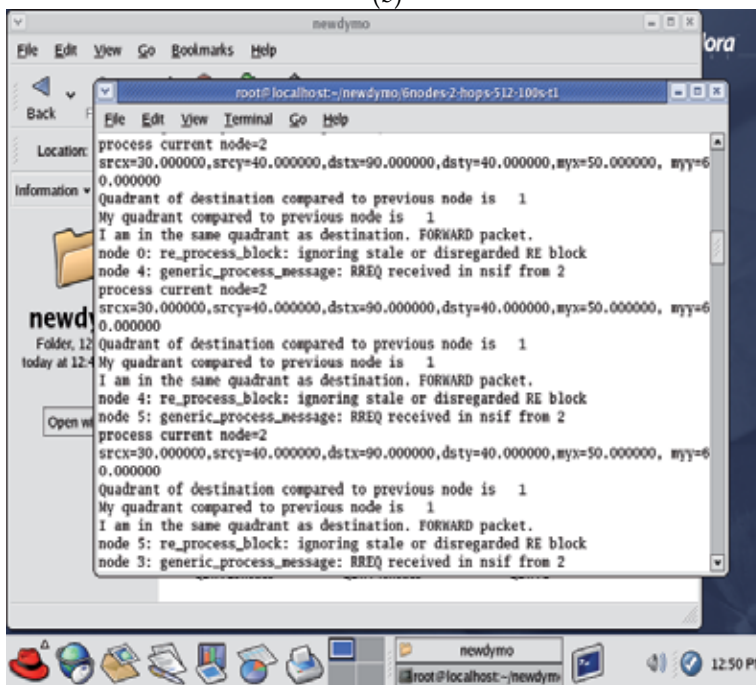
File Edit View Terminal Go Help
process current node=3
srcx=30.000000,srcy=40.000000,dstx=90.000000,dsty=40.000000,myx=20.000000,myy=1
0.000000
Quadrant of destination compared to previous node is 1
My quadrant compared to previous node is 3
I am not in the same quadrant as destination.EROP packet.
node 0: generic_process_message: RREQ received is nsif from 3
process current node=3
srcx=30.000000,srcy=40.000000,dstx=90.000000,dsty=40.000000,myx=20.000000,myy=1
0.000000
Quadrant of destination compared to previous node is 1
My quadrant compared to previous node is 3
I am not in the same quadrant as destination.EROP packet.
node 4: generic_process_message: RREQ received is nsif from 1
process current node=1
srcx=30.000000,srcy=40.000000,dstx=90.000000,dsty=40.000000,myx=40.000000,myy=1
5.000000
Quadrant of destination compared to previous node is 1
My quadrant compared to previous node is 4
I am not in the same quadrant as destination.EROP packet.
node 2: generic_process_message: RREQ received is nsif from 1
process current node=1
srcx=30.000000,srcy=40.000000,dstx=90.000000,dsty=40.000000,myx=40.000000,myy=1
5.000000

```

(a)



(b)



(c)

Fig. 13. RREQ packet broadcasting decision for Topology N-1 (a) Node 1 and 3 drop. (b) Node 4 drops. (c) Node 2 broadcasts.

5. Performance of Q-DIR in Dense Network

The study to evaluate the performance of Q-DIR in a large and densely populated network were conducted and it is hoped that results will show that Q-DIR with reduced collisions, and less contention of bandwidth, less routing overhead and consequently, power consumption is inherent and reflects that this new routing protocols is implementable and economical.

5.1 Dense Network Model

Figure 14 shows a network model of 49 nodes that forms a 7 by 7 grid model where the distance from adjacent nodes are 30m. Based on this grid model, the density is 1 node per 661m². In the network model, the x- and y-axis of the Cartesian coordinate system have been drawn to denote in which quadrant the nodes are located. The source and destination are denoted by the letter S and D respectively and destination node is at the top right edge of the grid. The simulation configuration parameters used in the simulation are as shown in Table 1.

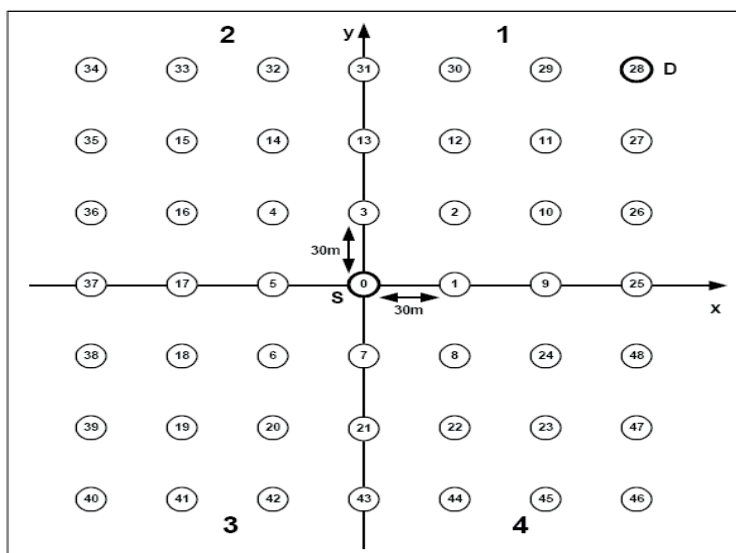


Fig. 14. Simulation Network Model of 49 nodes

5.2 Performance Metrics

Two protocols were simulated and they are AODVbis which is a total flooding protocol and Q-DIR which is based on restricted flooding. The performance metric used are as follows:

- *normalized routing overhead* - The number of routing packets transmitted per data packet received at the destination.
- *Effective energy consumption per data packet received* - The total energy consumption in the network for every data packet successfully received by the destination. This is the metric on the effectiveness of energy consumption when routing data packets.

5.3 Simulation Results

A. Effect of Varying Simulation Time

The simulation time was varied from 100s to 800s in steps of 100s. The number of routing packets that are broadcast and the corresponding data packet received at the destination in the network are counted for both AODVbis and Q-DIR routing protocol. Figure 15 shows the normalized routing overhead graphs for both protocols. As the simulation time increases to 800s, both protocols show reduced routing packets and leveled to a constant as it approaches 800s. The average normalized routing overhead in AODVbis is 338 packets while in Q-DIR, the average normalized routing overhead is 128 packets per data packet received. It is observed that 160% more routing packets are transmitted in AODVbis compared to Q-DIR due the higher number of node participations in the network in AODVbis.

Figure 16 shows graph for effective energy consumed per data packet received for both protocols. Both protocols shows a reduced energy consumption as the simulation time increases. The average effective energy is 2.43 J in AODVbis and 1.48 J in Q-DIR. Q-DIR consumes 64% less energy to send packets since only a quarter of the number of nodes participated in the routing process which is a limited flooding protocol based on quadrant.

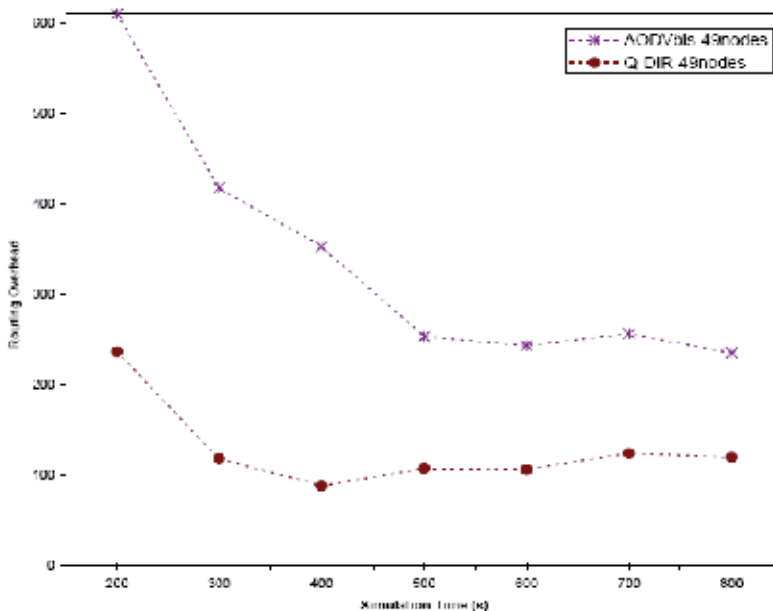


Fig. 15. Normalized routing overhead with simulation time.

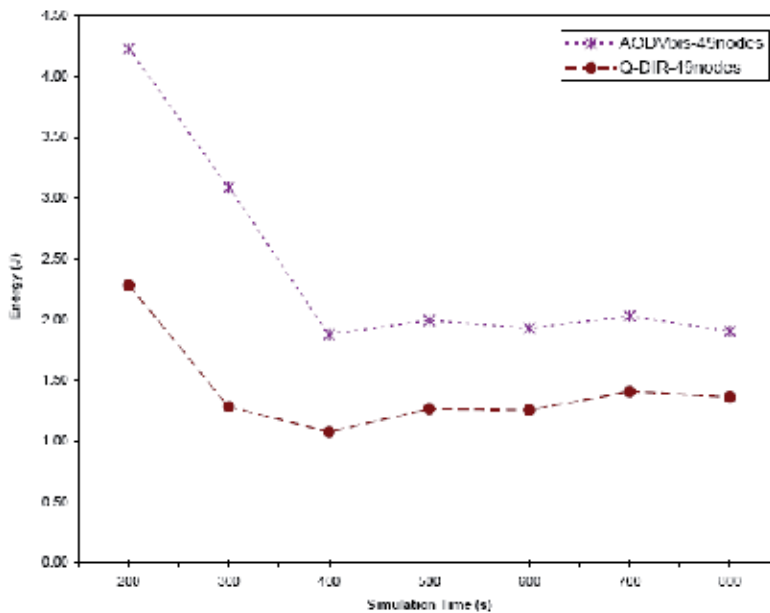


Fig. 16. Effective energy consumed per data packet received in Q-DIR.

B. Effect of Varying Packet Rate

Both AODVbis and Q-DIR routing protocols are simulated in the 49 nodes topology for a simulation time of 400s because the performance of both protocols remains constant. The transmission rate was varied in steps of 32 kbits/s with initial rate of 16 kbits/s to a maximum of 144 kbits/s. Figure 17 shows the average normalized routing overhead for both protocols which increases as the transmission rate increases. The graph for AODVbis shows large fluctuations as the transmission rate increases. AODVbis sends out an average of 255.664 normalized routing packets compared to Q-DIR which sends out only 108.08 packets. The large fluctuations in AODVbis are due to the total flooding algorithm of AODVbis and hence the routes taken vary for different transmission rate. However, the graphs in Q-DIR remain consistent throughout due to the directed flooding based on quadrant.

Figure 18 shows the graphs for effective energy consumed per data packet received for both AODVbis and Q-DIR protocols. The effective energy for AODVbis fluctuates as the transmission rate increases but for Q-DIR, it remains constant. Again, the fluctuation in AODVbis is due to different route taken at different transmission rate. AODVbis consumes an average of 1.574 J of energy while Q-DIR consumes only 1.084 J of energy which 45% less energy consumed compared to AODVbis. Based on this trend in energy consumption, less power is consumed if only a section or an area of a network participates in the routing.

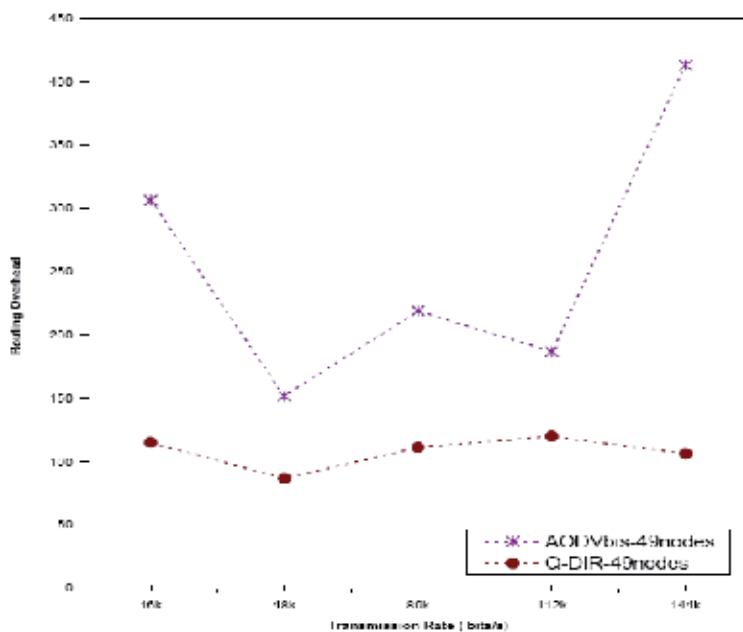


Fig. 17. Normalized routing overhead for 49 nodes.

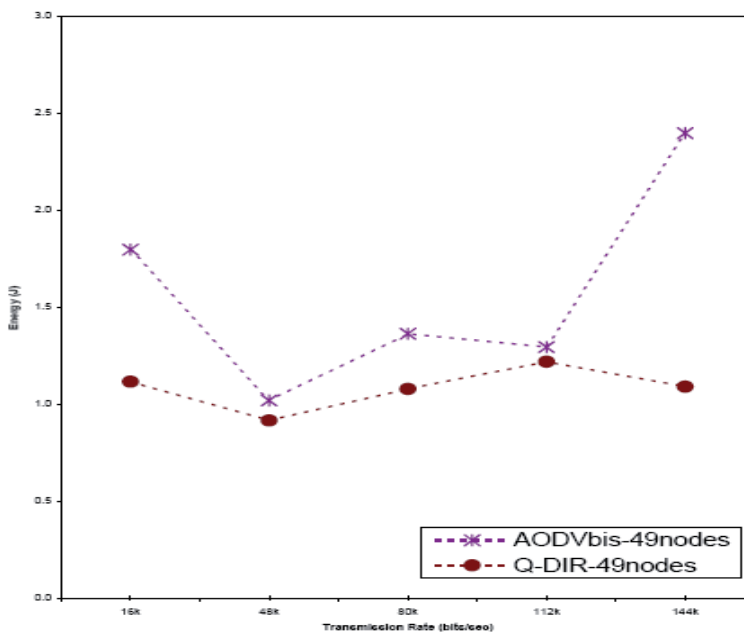


Fig. 18. Effective energy consumed per data packet received

6. Conclusion

This paper has presented the performance of Q-DIR which is a restricted flooding algorithm which uses location information of the source, destination and the intermediate node to determine the broadcasting decision. Nodes that are in the restricted broadcast region will broadcast while other nodes which are out of this region will ignore the RREQ packet. The simple mathematical comparison is implemental in the kernel environment which does not incur processing delay due the crossing from user to kernel space and vice versa. The simulation results shows that implementing Q-DIR reduces the power by 160% as the simulation time is increased and by 45% as the transmission rate increases compared to AODVbis. The restricted flooding and directional routing reduces the number of participating nodes as the RREQ traverses in the network towards the destination node and hence reduced routing overhead and power consumption are achieved in Q-DIR.

7. References

- Agrawal, D.P. and Zeng, Qing-An. (2003). *Introduction to Wireless and Mobile Systems*. USA:Brooke/Cole-Thomson Learning.
- Ali, A., Latiff, L.A., Faisal, N. (2004). GPS-free Indoor Location Tracking in Mobile Ad Hoc Network (MANET) using RSSI. RFM 2004, Malaysia.
- Ali, A., Latiff, L.A., Ooi, Chia-Ching, and Faisal, N. (2005). Location-based Geocasting and Forwarding (LGF) Strategy in Mobile Ad Hoc Network (MANET) *ICT 2005*, Cape Town, South Africa, May 2005.
- Basagni, S., Chlamtac, I. and Syrotiuk, V.R. (1998). A Distance Routing Effect Algorithm for Mobility (DREAM). *ACM/IEEE International Conference on Mobile Computing and Networking*. Oct. 1998. 76-84.
- Cartigny, J., Simplot, D. and Stojmenovic, I. (2003). Localized minimum-energy broadcasting in ad hoc networks. *INFOCOM 2003*. 30 March-3 April 2003. 3:2210 - 2217.
- Chakeres, I. D., Royer, E.M. and Perkins, C. E. (2005). Dynamic MANET On-demand (DYMO) Routing . *Internet Draft of IETF MANET WG*. draft-ietf-manet-dymo-02.txt. June 2005.
- Chang, J. and Tassiluas, L. (2000). Energy Conserving Routing in Wireless Ad Hoc Networks. *Proceedings of IEEE INFOCOM 2000*. 22-31.
- Chlamtac, I., Conti, M. and Liu, J. J. (2003). Mobile Ad-hoc Networking: Imperatives and Challenges. *Elsevier Ad Hoc Networks Journal*. 2003. Vol. 1(1): 13-64.
- Department of Computer Science, Rice University. (2006). *CMU Monarch Project*. <http://www.monarch.cs.cmu.edu/>. Accessed June 2006.
- Giordano, S., Stojmenovic, I. and Blazevic, L. (2004). Position-based Routing Algorithm for Ad Hoc Networks: A Taxonomy. In: *Ad Hoc Wireless Networking*. X. Cheng, X Huang and D.Z. Du (Eds.). 103-136. Kluwer Publishers.
- Gwalani, S., Belding-Royer, E.M. and Perkins, C.E. (2003). AODV-PA:AODV with Path Accumulation. *International Conference on Communications*. May 2003. 26(1):527-531.
- Heissenbuttel, M., Braun, T., Walchli, M. and Bernoulli, T. Broadcasting in Wireless Multihop Network with Dynamic Forwarding Delay Concept. *Technical Report IAM-04-010*. Institute of Computer Science and Applied Mathematics University of Berne, Switzerland, December 2004.

- Hou, T.C. and Li, V.O.K. (1986). Transmission Range Control in Multihop Packet Radio Networks. *IEEE Transactions. In Communications*. 34(1):38-44.
- Ko, Y.B. and Vaidya, N.H. (2000). Location-Aided Routing (LAR) in Mobile Ad Hoc Networks. *ACM/Baltzer Wireless Networks Journal*. 2000. 6:307-321.
- Kranakis, E., Singh, H. and Urrutia, J. (1999). Compass Routing on Geometric Networks. *Proceeding of the 11th Canadian Conference on Computational Geometry*. Vancouver, Canada.
- Kumar Banka, R. and Xue, G. (2002). Angle routing protocol: location aided routing for mobile ad-hoc networks using dynamic angle selection. *MILCOM 2002 Proceedings*. 7-10 Oct 2002. 1:501-506.
- Latiff, L.A., Ali, A., Ooi, C.-C. and Fisal, N. (2005). Development of an Indoor GPS-free Self-Positioning System for Mobile Ad Hoc Network (MANET). *MICC-ICON 2005*, Malaysia.
- Latiff, L.A., Ali, A., Ooi, C.-C. and Fisal, N. (2006). Implementation of a Quadrant-based Directional Routing Protocol (Q-DIR) in Wireless Mobile Ad Hoc Network. *IASTED NCS 2006*. 29-31 Mac 2006. Chiang Mai, Thailand. IASTED. 2006.
- Li, J., Jannotti, J., De Couto, D.S.J. , Karger, D.R. , Morris, R. (2000). A Scalable Location Service for Geographic Ad Hoc Routing. *Mobicom 2000*.
- Macker, J. and Corson, S. (1997). Mobile Ad Hoc Networks (MANET). 1997. <http://www.ietf.org/html.charters/manet-charter.html>
- Mauve, M., Widmer, A. and Hartenstein, H. (2001). A Survey on Position-based Routing in Mobile Ad Hoc Network. *IEEE Network*. 15(6):30-39.
- Milanovic, N., Malek, M., Davidson, A. and Milutinovic, V. (2004). Routing and Security in Mobile Ad hoc Network. *IEEE Computer Journal*. 37(2). 61-65.
- Ooi, C.-C. (2005). *Implementation of Geocast-Enhanced AODVbis Routing Protocol in MANET*. M.Sc. Thesis, UTM;2005.
- Perkins, C.E., Royer, E. M and Chakeres, I. (2003). Ad hoc On Demand Distance Vector-bis (AODVbis) routing. *Internet Draft of IETF MANET WG*. October 2003.
- Perkins, C.E. (2004). Convergence in Ad hoc Networking Protocol. *The IASTED International Conference on WNET 2004*. July 2004.
- Rappaport, T.S. (2002). *Wireless Communications: Principles and Practice*. 2nd Edition. USA. Prentice Hall. 2002.
- Ros, F. J. and Ruiz, P. M. Implementing a New Manet Unicast Routing Protocol in NS2. December 2004. <http://www.masimum.dif.um.es/nsrt-howto/html/nsrt-howto.html>.
- Royer, E.M and Toh, C.K. (1999). A Review of Current Routing Protocol for Ad-Hoc Mobile Wireless Network. *IEEE Personal Communications*. pp. 46-55, April 1999.
- Stojmenovic, I. (2002). Position-based Routing in Ad Hoc Networks. *IEEE Communications Magazine*. 40(7). 128-134.
- Sun, J.Z. (2001). Mobile Ad Hoc Networking An Essential Technology for Pervasive Computing, *Intl. Conference on Info-tech & Info-net*. Beijing, China.
- Xue, Q. and Ganz, A. (2003). Adaptive Routing in Ubiquitous Mobile Access Networks. *Proceedings of IEEE VTC*. 6-9 October, 2003. Orlando, Florida: IEEE. 3070-6074.

Free Space Optical Technologies

Davide M. Forin, G. Incerti

University of Rome Tor Vergata –Italy

G.M. Tosi Beleffi

ISCOM, Italian Ministry of Economic Development Comm. Department, Rome – Italy

A.L.J. Teixeira, L.N. Costa, P.S. De Brito André

Instituto de Telecomunicações, Aveiro, Portugal

B. Geiger, E. Leitgeb and F. Nadeem

Graz University of Technology

1. Introduction (D. Forin – G.M. Tosi Beleffi – B. Geiger – E. Leitgeb)

Free Space Optics (FSO), also known as Optical Wireless or Lasercom (i.e. Laser Communications), is a re-emerging technology using modulated optical beams to establish short, medium or long reach wireless data transmission. Most of the attention on FSO communication systems it was initially boost by military purposes and first development of this technology was dedicated to the solution of issues related to defense applications.

Today's market interest to FSO refers to both civil and military scenarios covering different situations and different environments, from undersea to space. In particular, due to the high carrier frequency of 300 THz and the consequently high bandwidth, the most prominent advantage of Free Space Optical (FSO) communication links may be their potential for very high data rates of several Gbps (up to 40 Gbps in the future (J. Wells, 2009)). Other advantages like license-free operation, easy installation, commercial availability, and insensitivity to electromagnetic interference, jamming, or wiretapping make FSO interesting for applications like last mile access, airborne and satellite communication (L. Stotts et al, 2009), temporary mobile links and permanent connections between buildings. Mainly, the adoption of FSO is needed when a physical connection is not a practicable solution and where is requested to handle an high bandwidth. As a matter of fact, FSO is the only technology, in the wireless scenario, able to grant bandwidth of several Gigabits per second. The interest in this technology is also due to the low initial CAPEX (Capital Expenditure) requirement, to the intrinsic high-level data protection & security, to the good flexibility and great scalability innate in this solution. For these reasons FSO possible applications cover today, as mentioned, a wide range. Thus this technology generates interest in several markets: the first/last mile in dense urban areas, network access for isolated premises, high-speed LAN-to-LAN (Local Area Networks) and even chip-to-chip connections, transitional and temporary network connection, undersea and space communication. Furthermore FSO can be used as an alternative or upgrade add-on to existing wireless technologies when the climatic conditions permit its full usage.

In spite of the growing interest in space and undersea applications, in fact, the terrestrial FSO still remains of primary significance and the performance of such links is highly dependent on different weather conditions. Atmospheric effects affect the distance and the availability of the optical wireless links so not all the geographical sites are suitable for this kind of broadband solution. Links as long as 7 km are in operation, but prior to the deployment of wireless optical links the average weather condition must be evaluated to estimate the expected outage time on the link in that area. The outage will depend on the link length and on the persistence of adverse weather conditions. So in general, it can be affirmed that short enough links, hundreds of meters, will be operational also with the worst possible weather conditions.

Besides commercially available opaque systems, where the optical signal is terminated to an electronic receiver and subsequently sent through the atmosphere by means of a dedicated laser, a new configuration, known as fully transparent, is under study. The bandwidth achievable in these last systems is comparable to the optical fiber one. Being absent any kind of optical to electrical bottleneck (OEO). For transparency, in fact, is meant launching and collecting power directly through single mode optical fibers. Such new extremely high bandwidth wireless systems, although still in the research stage, are gaining more and more interest especially in the last mile scenarios. Last but not least, compared to a microwave link, an FSO link can support higher bit rates and its operational frequencies are license-free in all jurisdictions apart for an year low cost fee that must be paid to the reference PA (Public Administration). The Authors want to outline that the work carried out in this chapter has been done in the framework of the European funded FP7 NoE BONE Project (WP13) and the COST IC0802 Action.

2. History of Free Space Communications (G.M. Tosi Beleffi)

Telegraphy is a word coming from ancient greek and means in Italian “scrivere a distanza” while in English sounds more or less like “writing to a distant place”. The human being has from the very beginning tried to increase his capabilities to communicate with his far away fellow men and so to transmit. Under this point of view, the mythology is full of interesting examples with the most famous and known that is Hermes, the Gods messenger, able to move faster than the wind and responsible to carry informations to the Gods.

First experiences in the ancient past can be found in the IVth century b.C. (before Christ), where Diodoro Crono reports on a human chain used by the Persian king Dario I (522-486 b.C) to transmit informations from the Capital to the Empire’s districts.

In the IVth Century b.C., Enea il Tattico, reports on an hydraulic telegraph probably invented by the Chartaginians. During the Roman and Greek age, was used to place in geographical key points “fire towers” to be switched on in case of security breaches and/or attacks on the borders. Eschilo (525-456 a.C.) reports in the Oresteia that the news about the falls of Troy arrived to Argo passing through the Cicladi islands covering, more or less, 900 km (Eschilo, 458 b.C.). This sort of tradition remained, for example, on the Italian territory assuming and adopting different schemes, fire or mechanical systems, depending on the time period, the geography and the geopolity (Pottino, 1976).

In the Center-South of Italy, in particular, the use of fire based signals during night and of smoke based signals during the daylight on the top of towers or hills, afterwards called communications by the usage of *fani*, has been quite common in the XVI and XVII Centuries

a.C. (Agnello, 1963). During the day one smoke signal means the presence of one enemy vessel, in the night was switched on a bundle of dry woods and moved up and down to inform about the exact number of the enemy vessels. Several testimonies report on different communications links and distances. The most interesting one has been established in 1657 between the city of Messina and the Malta island with mid span vessels used to cover the Mediterranean sea (Castelli, 1700).

The use of mechanical systems to implement optical wireless systems is due to Claude Chappe in 1792 (Huurdean, 2003). Chappe introduces the "optical telegraph" in France. The system was based on a regulator, 4.5m long and 0.35m wide, to which two indicators were attached. This systems was placed on the top of stations in LOS (Line Of Site) at 9 km each. Telescopes and human repeaters were, of course, needed to move the regulator and the indicators via three cranks and wire ropes. The time usage was short because the system was able to work only during the daylight and with good weather conditions. On the other hand, it was long reach considering an average coverage in France equal to around 4830km, with 29 cities connected using around 540 towers. Security was ensured by transmitting secret codes with short preambles, this also to understand the accuracy of the transmission. Chappe introduced, infact, a particular code in 1795, to increase the transmission speed. This system helped to reduced the time to exchange informations from several days to minutes and has been adopted in 1794. The subsequent studies on the electricity, the results from Volta (1745-1827) and from Ampere (1775-1836) on the electrical pile and the introduction of the electrical telegraph in 1838 (Morse), will carry to the dismissal of the Chappe system around the mid of 1800. The Chappe system was introduced also in other European countries connecting the cities of Amsterdam, Strasbourg, Turin, Milan and Brussels.

At the end of the 19th century, Alexander Graham Bell experienced with excellent results the so called Photophone (Michaelis, 1965) (Bova and Rudnicki, 2001). This system worked using the sound waves of the voice to move a mirror, responsible to send pulses of reflected sunlight to the receiving instrument. In particular Bell modulated with his voice, by the use of an acousto-optic transducer, a lens-collimated solar beam. Bell used to consider this invention to be his best work, even better than "his demonstration of the telephone". Although Bell's Photophone never became a commercial reality, it demonstrated the basic principle of optical communications.

Wireless Optical Communications, becomes from this point and year by year more important boosting the research worldwide. We can in this case divide the wireless optical experiments in three main areas depending on the time periods: in the 60s arrives the laser concepts and rises up the idea of wireless communications, in the 90s becomes popular the idea of ground to satellite and satellite to ground laser communications still using red and green sources, after 2000 the explosion of the Free Space Optical technologies (FSO) faces civil and military applications ranging from standard telecommunications up to intersatellites & interplanets experiments and using different wavelengths from 1 up to 10 microns.

For these reasons, essentially all of the engineering of today's FSO communications systems, has been studied over the past 40 years, at the beginning for defense applications and afterwards for civil ones. By addressing the principal engineering challenges FSO, this aerospace/defense activity established a strong foundation upon which today's commercial FSO systems.

In particular, the realization of the first LASER, based on ruby, in 1960 by Maiman opened wider possibilities for the communications involving beams propagating over long distances in atmosphere. Low loss optical fibers (less than 20 dB/km), in fact, will arrive only in the 70s. In 1960s NASA started to perform preliminary experiments between the Goddard Space Center and the Gemini 7 module. In 1968 the first experiment about FSO transmission of 12 phone channels along 4km had been demonstrated in Rome (Italy) by researchers from the Istituto P.T, CNR and Fondazione Ugo Bordoni under the management of Prof. Sette, Physics Institute University La Sapienza. A red laser source (0.8 microns) was used to connect two buildings between the Colombo and Trastevere Streets in Rome (Unknown, 1968). In the same year Dr. E. Kube in Germany published on the viability of free space optical communications considering both green (0.6 microns) and red (0.8 microns) laser sources (Kube, 1968). The introduction of semiconductor light sources working at room temperature, by Alferov in 1970, were decisive for a further development of integrated and low cost FSO systems. On the point of view of the research, the first experiment using a quantum cascade laser (Capasso 1994) can be considered fundamental today speaking about new transmission wavelengths for FSO (up to 10 microns). Between 1994 and 1996 years the first demonstration of a bidirectional space to ground laser link between the ETS-VI satellite and the Communications Research Laboratory (CRL) in Koganey (Tokio) has been accomplished. 1Mbps using 0.5 microns and 0.8 microns emitting lasers. With the ongoing intensive and worldwide studies on FSO communications, especially re started after the September 11 tragedy where the communications were supported by free space optics links, the related scenarios changed extremely fast covering today different applications and environments like the followings: atmosphere, undersea, inter satellites, deep space. We can in fact report on the SILEX experiment (Semiconductor Intersatellite Link Experiment) in 2001 demonstrating bidirectional GEO-LEO and GEO-ground communications. ARTEMIS satellite (GEO) using a semiconductor laser at 0.8 microns directly driven at 2 Mbps with an average output of 10mW towards a Si-APD on SPOT-4 satellite (LEO). In the same year, the GeoLite (Geosynchronous Lightweight Technology Experiment) experiment successfully demonstrated a bidirectional laser communication between GEO satellites, ground and aircraft. We cannot forget afterwards the MLCDC (Mars Laser Communication Demonstration) program started in 2003 and ended in 2005 with the aim of covering the distance between Earth and Mars planets using an optical parametric amplifier with an average output of 5W and photon counting detectors working at 1.06 microns (Majumdar and Ricklin, 2008).

3. Basic principles of the optical wireless communications (E. Leitgeb – B. Geiger – F. Nadeem - A.L.J. Teixeira, P. Andre)

3.1 Introduction

Free Space Optical communication links transmit information by laser light through an atmospheric channel. Relying on infrared light, these communication systems are immune to electromagnetic interference (EMI), jamming, or wiretapping. Furthermore, they do not cause EMI themselves and operate at frequency bands (around 300 THz) where the spectrum is unlicensed. As a further advantage, FSO and fiber equipment can be combined without intermediate conversion, since both the air and the material used for fiber cables have good transmittance at the established wavelengths, namely 850 nm and 1550 nm. Currently, all-

optical fiber/FSO systems are a well populated field of research, developing solutions for signal regeneration, transmission, and reception without an intermediate electronic signal. FSO systems can be installed faster and cheaper than their wireless radio counterparts, making them interesting for short-term installations for events, military purposes and disaster recovery. Consequently, a multitude of FSO equipment is commercially available for interconnection with standard fiber or Ethernet components. Acting as an alternative to other wireless radio or high-bandwidth wired links (fiber optics, Gigabit Ethernet), it has to fulfill general requirements such as low bit error rate (BER < 10⁻⁹) and high reliability.

As already mentioned, a prerequisite for these requirements is an unobstructed line-of-sight, especially in long-distance outdoor environments. A major drawback therefore is the susceptibility of FSO links to certain weather conditions, where especially fog causes severe attenuation of the laser beam and subsequent total link loss. Even moderate continental fog can result in an attenuation of 130 dB/km, whereas dense maritime fog can account for attenuations up to 480 dB/km (E. Leitgeb et al, 2006; M.S. Awan et al, 2008).

Rain attenuation has very little effects on the availability of FSO systems, but these effects strongly depend on the rain rate R . According to (T. Carbonneau and D. Wisley, 1998) and the references therein an adequate relationship between rainfall and attenuation would be

$$\tau_{rain} = \exp(-(0.05556 + 0.00848 \cdot R - 3.66 \times 10^{-5} \cdot R^2) \cdot l) \quad (1)$$

For light to moderate rain rates of $R = 5$ mm/h as they are occurring in the continental climate of middle Europe the attenuation is only approx. 3 dB/km. Peak attenuations due to tropical rain falls of $R = 100$ mm/h would result in higher attenuations (approx. 30 dB/km), but such weather conditions occur rarely and only in burst in Europe and the United States (J. Wells, 2009; H.Alma and W. Al-Khateeb, 2008). Similar considerations hold for heavy snowfall (more than 5 cm over 3 hrs), where attenuations of more than 45 dB/km have been measured (R. Nebuloni and C. Capsoni, 2008). Depending on seasonal and geographic peculiarities, these values can vary to some extent. It may also happen that certain weather events occur simultaneously, i.e. heavy rain in combination with fog, or fog in combination with snowfall (V. Kvicera, 2008).

Another phenomenon occurring influencing FSO communication links is related to scintillations and air turbulences. Air cells with different temperatures randomly distributed along the link cause focusing and defocusing of the link due to changes in the refractive index. Amplitude and frequency of these scintillation depend on the size of cells compared to the diameter of the optical beam (S. S. Muhammad, 2005; A. Chaman Motlagh, 2008). FSO systems usually cope with such variations in the optical received signal strength (ORSS) by using multiple beams (so-called multi-beam systems) or by using saturated amplifiers (M. Abtahi and L. Rusch, 2006). More detailed investigations can be found in (S. S. Muhammad, 2005) and the references there.

Other problems affecting visibility are mostly related to the narrow beam FSO systems use (usually at the order of a few milli radians): sand, dust, birds, et cetera flying through the beam cause momentary link losses, whereas misalignment due to tower sway or thermal effects can be coped by auto-tracking systems (J. Wells, 2009). The sun itself acts as a noise source, which may completely overdrive the receivers (W. Kogler, 2003) if they are directly exposed to sunlight. Soiling and aging of the components, especially lenses and mirrors,

finalize the list of effects on FSO link availability. Summarizing, most of these effects can be overcome by either granting a certain link margin (snow and rain attenuation, fluctuations due to scintillation) or by adding complexity to the system (multi-beam and auto-tracking systems). Fog, on the other hand, is the only remaining condition harmful for availability, making carrier class availability (99.999%) for FSO systems highly questionable.

Depending on the geographic areas, fog mainly occurs during fall and winter months on a persistent basis, whereas outages during summer and spring are caused by thunderstorms (E. Leitgeb, 2004). Fig. 1 shows the average unavailability throughout the year in Graz, Austria. Moreover, diurnal changes affect the probability of fog as Fig. 2 shows; it is low during noon where the sun clears up the sky and high during dusk, dawn and the night (E. Leitgeb, 2004).

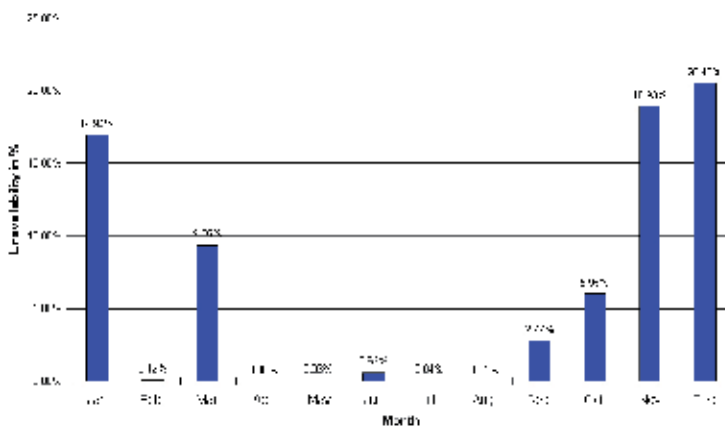


Fig. 1. Average unavailability throughout the year (based on measurements from Oct. 2000 to Sep. 2001 (with the permission of E. Leitgeb, 2004))

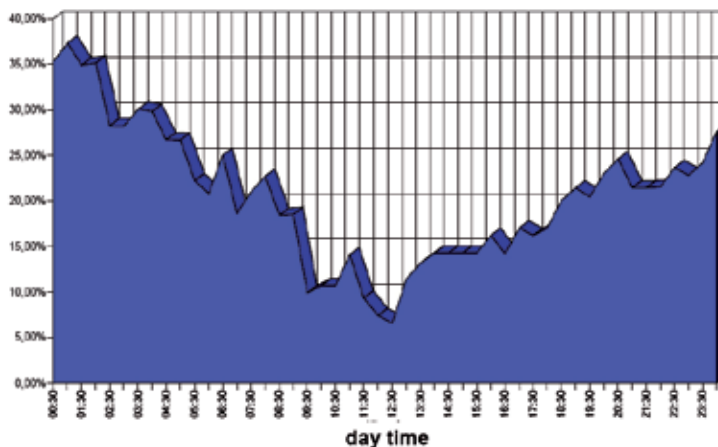


Fig. 2. Probability of failure during the daytime (based on measurements from Dec. 2000 (with the permission of E. Leitgeb, 2004))

Due to the complexity connected with phase or frequency modulation, current free-space optical communication systems typically use intensity modulation with direct detection

(IM/DD). Like in fibre optics communications systems, the performance characteristics for a free space optical communications system are dependent on the propagation medium. However, in this case the propagation medium is randomly changed, and susceptible to atmospheric conditions, resulting in alterations to the beam propagation constants.

In order to get a clearer picture of the behavior of FSO systems a numerical model for the atmosphere is going to be presented [Andre, 2003]. This propagation model was incorporated in a commercial available photonic simulator and used to predict the behaviour of a point to point free space data link as function of the climacteric variables.

3.2 Atmosphere Model

As, referred, atmospheric effects can degrade free space data links by two mechanisms: (i) reduction in the detected optical power level due to atmospheric attenuation and (ii) random optical power fluctuations in the received beam which result in beam deformation, scintillation effects and beam wander (Kim, 1998). All these factors can become impairing to the communications if their influence is significant. For that it is going to be presented each of the contributing parts model and therefore a complete evaluation with effects will be made for better understanding of the real effects in the system.

A. Atmospheric attenuation

The atmospheric attenuation results from the interaction of the laser beam with air molecules and aerosols along the propagation. Similar to other waves, the optical beam power has an exponential decay with propagation distance. At a given distance from the emitter, l , the optical transmittance is:

$$\tau = \tau_a + \tau_s = \frac{P(l)}{P(0)} = \exp(-\alpha \cdot l) \quad (1)$$

where α is the overall attenuation coefficient, determined by four individual processes: molecular absorption, molecular scattering, aerosol absorption and aerosol scattering.

The molecular absorption includes the absorption by water, CO₂ and ozone molecules. The aerosol absorption results from the finely dispersed solid and liquid particles in the atmosphere, such as ice and dust, with a maximum radius of 20 μm . A simple approach to calculate absorption, assumes that variations in the transmission are caused by changes in the water content of the air. The precipitable water, w (in millimetres), encountered by the light beam is (Wichel, 1990):

$$w = 10^{-3} \cdot \rho \cdot l \quad (2)$$

where ρ is the absolute humidity in g/m³. This value can be related with the relative humidity percentage (RH) and with the temperature in degrees Celsius, T , by:

$$\rho = RH \cdot (-0.74 + 90.96 \cdot \exp(T/13.67)) \cdot \exp(-85.4 \cdot \exp(T/13.52)) \quad (3)$$

The absorptive transmittance can be then calculated for any transmission window, by the following empirical expressions (Wichel, 1990):

$$\tau_a = \exp(-A_i \cdot w^{1/2}), \quad w < w_i \quad (4)$$

$$\tau_a = k_i \cdot \left(\frac{w_i}{w}\right)^{\beta_i}, \quad w > w_i \quad (4a)$$

The values typical values of the constants used are listed in table 1 (these are also used in calculations following).

Window boundaries (nm)	Ai	ki	βi	Wi
720 - 940	0.0305	0.800	0.112	54
940 - 1130	0.0363	0.765	0.134	54
1130 - 1380	0.1303	0.830	0.093	2
1380 - 1900	0.211	0.802	0.111	1.1
1900 - 2700	0.350	0.814	0.1035	0.35
2700 - 4300	0.373	0.827	0.095	0.26
4300 - 6000	0.598	0.784	0.122	0.165

Table 1. Constants used in expressions (4) and (4a).

Another attenuation process is the scattering, where there is no power loss, and there is only a directional distribution. The two dominate scattering mechanisms are the Rayleigh scattering, when the wavelength of the light is higher than the particle size, and the Mie scattering when the particle size is comparable with the wavelength of the radiation. An empirical relationship sometimes used to describe the scattering transmittance is [Wichel, 1990]:

$$\tau_s = \exp(-l \cdot (C_1 \cdot \lambda^{-\delta} + C_2 \cdot \lambda^{-4})) \quad (5)$$

where, C_1 and δ are constants determined by the aerosol concentration and size distribution and $C_2 = 0.00258 \text{ m}^3$ accounts the Rayleigh scattering. These two constants can be related with the visual range, V , in kilometres at 550 nm [1]:

$$C_1 = \frac{3.91}{V} \cdot 0.55^\delta \quad (6)$$

For a very good visibility, δ can take a value of 1.6, and for average visibility it have a value of ≈ 1.3 . If the visual range is inferior to 6 km, then the exponent δ can be obtained by:

$$\delta = 0.585 \cdot V^{1/3} \quad (7)$$

The presence of precipitation (rain or fog) increases the scattering coefficient. The transmittance can be related with the rainfall rate (R) in mm/hr, by:

$$\tau_{rain} = \exp(-(0.05556 + 0.00848 \cdot R - 3.66 \times 10^{-5} \cdot R^2) \cdot l) \quad (8)$$

The propagation of a laser beam in dense fog or clouds much difficult and attenuations as high as $\approx 50 - 150$ dB/km can be found (Strickland, 1999).

The total attenuation to be considered in (1) is the sum of the several partial attenuation factor (eqs (4), (5) and (8))

The geometrical beam expansion, resulting from the beam divergence, is also responsible for a reduction of the optical power coupled to the receiver. It must be also take into account the optical miss alignment between the emitter and the receiver, for systems without auto-tracking (Kim, 1998).

B. Turbulence

The atmospheric turbulence arises when air parcels at different temperatures are mixed by wind and convection. This effect produces fluctuations in the density and therefore in the air refractive index. The parameter that describe the disturbances caused by turbulence is the refractive index structure coefficient, C_n , which usually varies between $5 \times 10^{-7} \text{ m}^{-1/3}$ and $8 \times 10^{-9} \text{ m}^{-1/3}$ for situation of strong and weak turbulence, respectively.

The value of C_n can be estimated by (Strohbehn, 1978):

$$C_n^2 = \left(\frac{h^{4/3}}{3000^{4/3}} \right) \cdot \frac{\left(\frac{79 \times 10^{-6} \cdot P}{(T + 273.15)^2} \right)}{5.49 \times 10^{-13}} \quad (9)$$

$$\left(\left(2.2 \times 10^{-53} \cdot 3000^{10} \cdot \left(\frac{v \cdot \sin(\theta)}{27} \right)^2 \right) \cdot e^{-3} + 10^{-16} \cdot e^{-2} \right)$$

where h is the height in meters, P the air pressure is milibars, v is the wind speed in m/s and θ the angle between the beam and the wind.

The dominant turbulence scale size leads to different effects: (i) if the scale of the turbulence cells is larger than the beam diameter then the dominant effect is the beam wander, that is the rapid displacement of the beam spot, (ii) if the scale of the turbulence cells is smaller than the beam diameter then the dominant effect is the beam intensity fluctuation or scintillation.

The radial variance of beam wander can be described by (Zhu, 2002):

$$\sigma_r^2 = 1.90 \cdot C_n^2 \cdot (2 \cdot w)^{-1/3} \cdot l^3 \quad (10)$$

where w is the spot size at the transmitter.

The scintillation is described by a log-intensity distribution (Clifford, 1981), with a variance given by [Wichel, 1990]:

$$\sigma_i^2 = 1.23 \cdot C_n^2 \cdot \left(\frac{2\pi}{\lambda} \right)^{7/6} \cdot l^{11/6} \quad (11)$$

The effect of scintillation can be smoothed by spatial averaging using a width detector area, multiple apertures detector or a spatial diversity with several receivers or emitters (Kim, 1997).

The presence of atmospheric turbulence is also responsible for the beam spreading, contributing to the beam divergence, which is given by [Wichel, 1990]:

$$a_t = 2.01 \cdot \lambda^{-1/5} \cdot C_n^{6/5} \cdot l^{8/6} \quad (12)$$

C. Thermal Blooming

The molecular absorption by the air of the beam energy, will lead to a temperature gradient in the medium that induces density and index refraction changes. In the presence of air flow (wind) results in a density wavefront destruction which leads in a beam bender directed to the air flow.

The displacement of the beam at the receiver is (Strohbehn, 1978):

$$u = - \frac{5 \cdot (\gamma - 1) \cdot (n - 1) \cdot l \cdot \left(\frac{\langle I_0 \rangle}{w} \right)^2}{6 \cdot \gamma \cdot P \cdot 100 \cdot |\nu \cdot \sin(\theta)|} \quad (13)$$

where γ is the ratio of specific heats (with a value of 1.4 in air), n is the refractive index of the air and I_0 is the beam optical power at the transmitter.

III. Simulation

In this subsection, and for sake of understanding of the modeling described above, a set of simulations is presented based on the atmospheric model described in the previous section. This model was implemented through Matlab in a commercial available photonic simulator, VPI from Virtual Photonics™.

The free space optical communications system used as reference for these simulations had the following parameters. The propagation distance was 1000 m, oriented in a 158° heading. The optical power of the beam at the emitter was 40 mW and at a 780 nm wavelength, with a radius of 10 cm and a divergence of 1 mrad. The optical beam is modulated at 2.048 Mb/s (E1) with an optical extinction ratio of 15 dB. The use of this low bitrate allows us to later compare these results with some experimental ones (Almeida, 2001). For the receiver we have considered a photodiode based O-E converter with a 0.85 responsivity and a 1.4 Mbit/s bandwidth pulse reformatting electrical filter, preceded by a 6 dB attenuator to account the miss alignment losses.

We obtained, for several values of temperature and relative humidity, the attenuation of for 1 km path link. These results can be observed in figure 3.

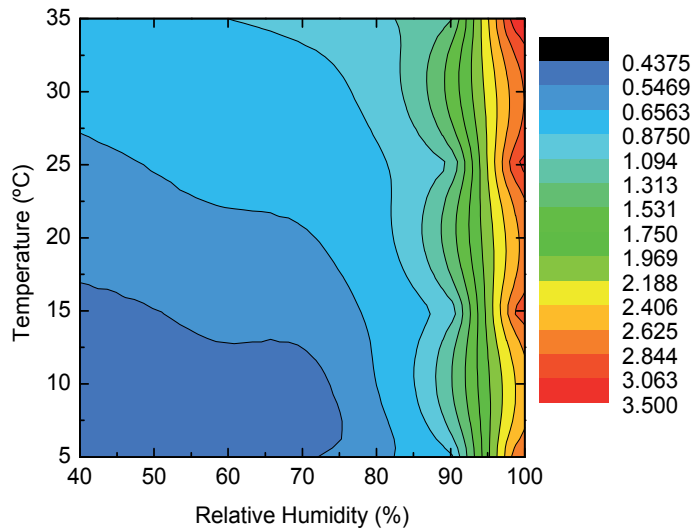


Fig. 3. Optical attenuation for one km path link as a function of the temperature and relative humidity.

It is clear, from figure 3 that the effect of temperature and humidity in the losses, due to absorption and scattering is important. The total attenuation vary from ≈ 0.5 dB/km to 3.5 dB/km.

The effect of rain fall can also be analyzed with this model. Keeping the values of temperature and relative humidity constant, 25 °C and 80 % respectively, the attenuation was obtained as function of the rain fall rate, as displayed in figure 4.

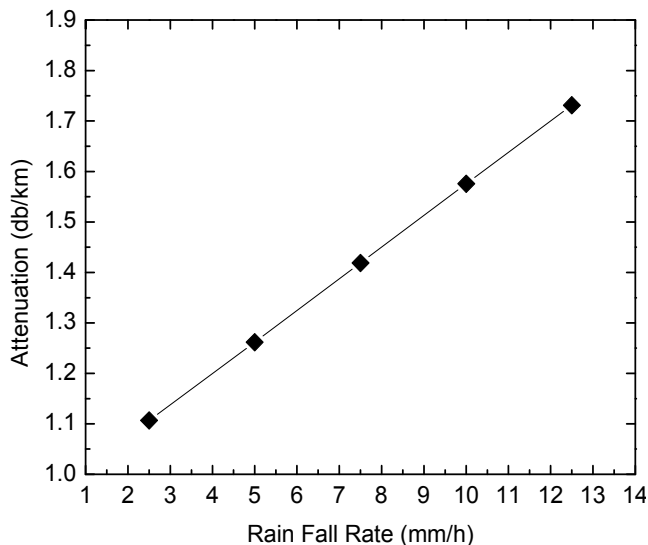


Fig. 4. Optical attenuation for 1 km path link due to rain. The line is a visual guide.

The introduction of turbulence in the atmosphere model will result in the observation of scintillation on the received power. In figure 5 is shown the BER (bit error rate) of the received data for 1 km path direct optical link as function of the received optical power and for several values of the refractive index structure coefficient.

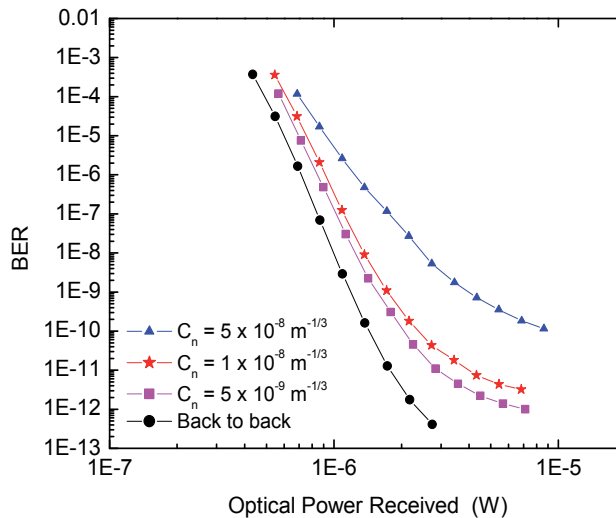


Fig. 5. BER versus the received optical power for several values of C_n . The lines are visual guides.

From the previous figure it is clear that the power penalty depends on the value of C_n , as it can be observed in the eye diagrams of figure 6, obtained for a received power of -22 dBm and for several values of C_n . The eye diagram of figure 6 a) corresponds to a high turbulent medium with a C_n value of $1 \times 10^{-7} \text{ m}^{-1/3}$, 6 b) is a situation of medium turbulence with C_n of $5 \times 10^{-8} \text{ m}^{-1/3}$, while 6 c) is obtained in a low turbulence medium with a value of $1 \times 10^{-9} \text{ m}^{-1/3}$ for C_n .

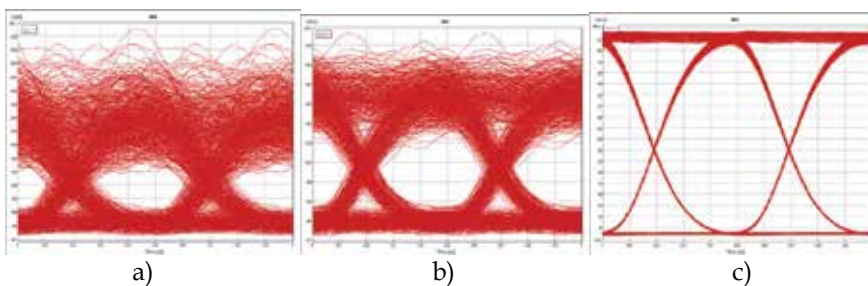


Fig. 6. Eye diagrams obtained for several values of the refractive index structure coefficient: a) $1 \times 10^{-7} \text{ m}^{-1/3}$, b) $5 \times 10^{-8} \text{ m}^{-1/3}$, c) $1 \times 10^{-9} \text{ m}^{-1/3}$.

A reasonable good approach to estimate the BER of a FSO system is to consider only the attenuation (discarding the scattering and thermal blooming but considering the beam wander), then the BER can be written as:

$$BER = \frac{1}{2} \operatorname{erfc} \left(\frac{RP_R}{2\sqrt{2}\sigma^2} \right) \quad (14)$$

Where R is the detector responsivity, P_R the optical power at the detector and σ the receiver thermal noise. The impact of the C_n factor in the BER can be observed in the figure 7, where experimental C_n factor measured in Rio de Janeiro along the day in February 2003. For the receiver it was considered a typical configuration with $R=0.9$ A/W and a receiver diameter of 13 cm, the optical power at the emitter is 10 mW for a link length of 1 km.

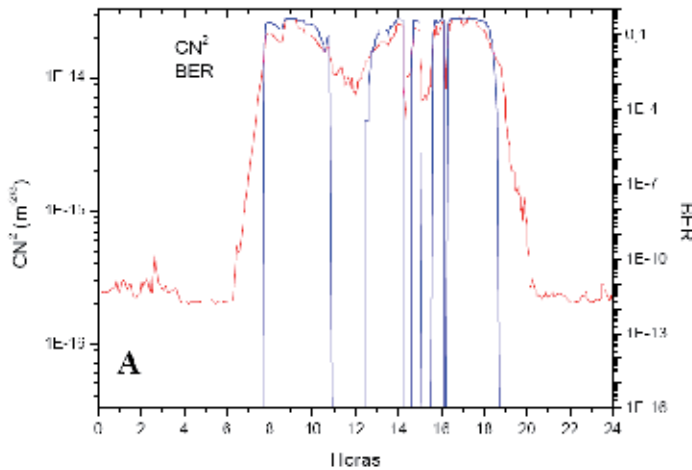


Fig. 7. C_n influence in the BER for 1 km link.

4. Hybrid network infrastructures: FSO & RF (B. Geiger – E. Leitgeb – F. Nadeem)

4.1 Introduction

Relying on an unobstructed line-of-sight, FSO links are strongly influenced by atmospheric conditions reducing or influencing visibility, such as fog, precipitation, haze, and scintillation. Fog, as one can expect, is the most critical effect affecting attenuation and, subsequently, availability of the FSO link. Attenuation is caused by scattering, resulting from the fact that the size of the fog particles is in the order of the wavelength of optical and near-infrared waves (as they are used for FSO). Consequently, link distances in coastal or metropolitan environments which are prone to fog are limited to a few hundred meters.

Radio Frequency (RF) links on the other hand show almost negligible fog attenuation if the carrier frequency is chosen accordingly, while they usually suffer from other precipitation types like rain and wet snow. Combining these two technologies to an FSO/RF hybrid network may increase overall availability significantly, guaranteeing quality-of-service and broadband connectivity regardless of atmospheric conditions.

Several types of hybrid system concepts have been introduced in the literature (L. Stotts et al, 2009; S. Bloom and W. S. Hartley; H. Izadpanah et al, 2003; T. Elbatt et al, 2001; F. Nadeem et al, 2009; E. Leitgeb et al, 2004; J. Pacheco de Carvalho et al, 2008; S. Vangala

et al, 2007; A. Akbulut et al, 2005; S. Gurumani et al, 2008; J. Derenick et al, 2005; T. Kamalakis et al, 2005; W. Kogler et al, 2003; F. Nadeem et al, 2009; S.D. Milner et al, 2004; O.I. Kim and E. Korevaar, 2001; H. Wu et al, 2004; S. Vangala and H. Pishro-Nik, 2007), focusing on increasing availability, bandwidth efficiency, or minimizing system complexity. Resulting from these focuses, hybrid systems can be categorized in three different groups: Redundant, load-balancing, and switch-over hybrids.

4.2 Description of the RF Communication Links

As already mentioned, FSO links are strongly influenced by fog attenuation and consequently suffer from long periods of total link loss (E. Leitgeb, 2005). On the other hand, FSO systems provide very high data rates without the requirement of licensing. As a consequence, the RF link for a hybrid FSO/RF system has to be chosen according to the following requirements:

- The RF link should be available whenever the FSO link is not, i.e. it should not be influenced by fog or other weather effects reducing visibility.
- The RF link should provide a similar bandwidth as the FSO link, so that the hybrid system does not suffer from performance degradation.
- The RF link should be operated in a frequency band which does not require licensing, so that this advantage of FSO systems is not lost in a hybrid setup.

Unfortunately, some of these requirements are contradictory. High data rates, or equivalently, bandwidths require high carrier frequencies, which on the other hand either show strong attenuation due to fog or would result in a prohibitively high system complexity. Moreover, these systems operate in license-free, but regulated bands and are thus subject to stringent transmission power restrictions limiting the possible link margin considerably. A higher geometrical loss further adds to the availability issues. Especially during times when rain and fog occur simultaneously, as it often happens in continental climate, both links are suffering from weather effects (E. Leitgeb et al, 2004; E. Leitgeb et al, 2005). Scintillations have little or no effect on RF links, since they are not susceptible to changes in the refractive index rather than changes in humidity (S.S. Muhammad, 2005). A more complete discussion of weather effects on RF links is available in (H. Wu et al, 2004; ITU-R, 2005). Commercially available bands with very high available bandwidths are centered around 60 GHz and 70/80 GHz, respectively. While the former, license-free band cannot be exploited for long link distances due to an oxygen absorption peak (15 dB/km), the latter provides an interesting field of research for hybrid systems. Peak attenuation due to moderate rain are usually well below 5 dB/km, whereas fog attenuation is as small as 0.4 dB/km for a fog density of 0.1 g/m³ – under these conditions a FSO system would suffer from 225 dB/km (S. Bloom, 2005). Currently available equipment operating in the 70/80 GHz band can provide carrier class availability disregarding weather conditions over a distance of 2-3 km achieving 1 Gbps. Unfortunately, this band can only be used after obtaining a low-cost license. Spectra currently unregulated by the ITU lying at 275 GHz are unreachable with current technologies (J. Wells, 2009).

Lower frequency bands (e.g. the license-free ISM bands at 2.4 and 5 GHz), on the other hand, provide much less bandwidth to the user, leading to a greatly decreased bandwidth performance of the overall hybrid system. However, these systems are not susceptible to fog

at all (ITU-R, 2005) and also show much smaller influence of rain and snow than systems operating with carrier frequencies beyond 20 GHz (H. Wu et al., 2004). Multi-user interference, as it is common in license-free bands at lower frequencies, which are accessible by low-cost technologies, can be mitigated by using directional links.

These bands, which also host users of IEEE 802.11a/b/g/n compliant equipment, are of particular interest since they allow building a hybrid FSO/RF system with commercially available equipment for the RF part as well. Especially the IEEE 802.11a standard is interesting for FSO/RF hybrids, since it is operating in the less populated 5 GHz band and allows a higher transmit power of up to 30 dBm EIRP. Although the standard claims possible data rates of up to 54 Mbps, usual limits for long-range directional links are around 20 Mbps. Moreover, the use of this technology offers the possibility of an upgrade to IEEE 802.11n compliant equipment, claiming data rates of up to 600 Mbps with MIMO functionality. Future studies will show if this technology can also be used for long-range directional links and thus build the RF component of the proposed hybrid systems.

4.3 Overview of Hybrid Systems introduced in the literature

Hybrid systems can be classified into three categories:

- **Redundant systems:** These systems duplicate data and transmit it simultaneously over both the RF and the FSO link. As a consequence, the data rate of both links has to be equal, resulting in either a requirement for very high frequencies on the RF link or a relatively high FSO underutilization. Moreover, systems which duplicate and recombine data are necessary. Redundant systems provide a high reliability, but suffer from the fact that both links have to be active all the time, wasting a significant amount of energy.
- **Switch-Over systems:** These systems transmit data only over one link, which is chosen according to link availability. Usually, since the FSO link allows higher data rates, it is chosen as a primary link whereas the RF link acts a backup. Consequently, data rates of both links need not be identical, if one accepts a reduced bandwidth during fog events. Switch-over systems require multiplexers on both ends, algorithms choosing the active link, synchronization, and accurate, timely measurement data of the optical signal strength. However, these algorithms save energy by transmitting over one link only, and can be connected to standard network equipment without protocol overhead (F. Nadeem et al., 2009).
- **Load-Balancing systems:** These most sophisticated algorithms distribute traffic among the links according to the quality of their connectivity, thus exploiting the full available bandwidth each time. Besides a measurement of the link quality, these systems require recombination systems on either sides of the hybrid link, often resulting in either significant protocol overhead (F. Nadeem et al., 2009) or high-complexity codes which automatically distribute data among different links.

In the literature a wide field of hybrid systems can be found: AirFiber (S. Bloom, 2009), a US-based company pioneered redundant transmission over FSO and RF links, the latter one being a millimeter wave (MMW) link with a carrier frequency at 60 GHz. Data rates of approx. 100 Mbps were achieved, but availability was well below the expectations. Wu et al. (H. Wu et al., 2004) analyzed FSO and RF link separately and concluded that by using a hybrid network link margin can be reduced significantly to achieve carrier class availability.

The FSO link was using a 1550 nm laser source, the RF link was operated in the 60 GHz MMW band. Link distance was 1500 m.

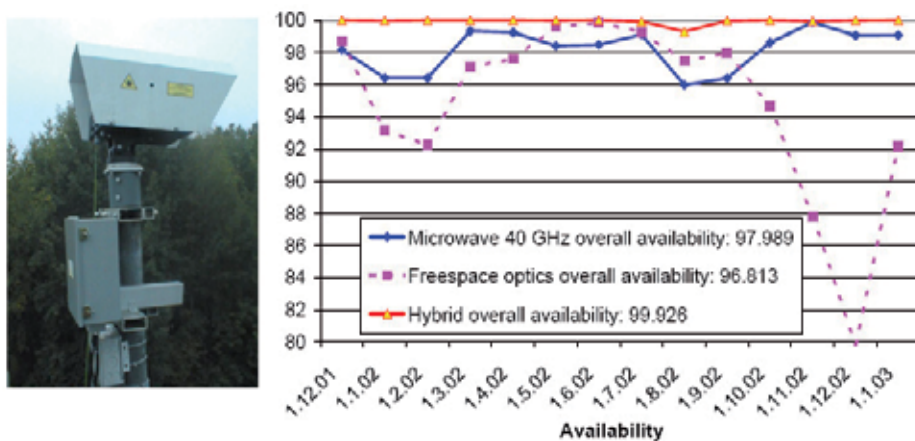


Fig. 8. Redundant hybrid system and availability measurements (with the permission of E. Leitgeb et al, 2004)

Kim and Korevar (I.I. Kim and E. Korevaar, 2001) studied the distance limitation of FSO systems for both carrier and enterprise applications and showed that carrier class availability can be achieved for much longer link distances if the FSO link is combined with an RF back-up transmitting data redundantly. Leitgeb et al. performed an experiment in Graz, Austria, over 15 months during 2002-2003, where data was sent simultaneously over two FSO/RF links (E. Leitgeb et al 2004). The RF link was designed with a carrier frequency of 40 GHz, the FSO system transmitted using a 850 nm laser with a data rate of 155 Mbps. The availability was measured over this time for each individual link and for the hybrid combination. The redundant transmission achieved an availability of 99.93% (see Fig. 8.) Hashmi et al. (S. Hashmi and H. Mouftah, 2004) also proposed a redundant hybrid system, calculating it based on rain data only for an FSO and a MMW link in the 60 GHz band. They also mentioned that the hybrid system could be used in an asymmetric uplink/downlink scenario where different traffic demands have to be served.

Akbulut et al (A. Akbulut et al 2005) developed an experimental hybrid FSO/RF switch-over system between the two of five campuses of Ankara University, Turkey, located at different locations in the city. The optical link provided a 155 Mbps full duplex connection by using a laser source at 1550 nm over a distance of 2.9 km. The RF link was compliant to IEEE 802.11b WLAN, operated at 2.4 GHz linking the two terminals at 11 Mbps. The switch-over algorithm was a power hysteresis. Pacheco de Carvalho et al. (J. Pacheco de Carvalho, 2008) installed a similar system at the University of Aveiro, Portugal, where a 1 Gbps laser link was backed up by a 75 Mbps (nominal) WiMAX (IEEE 802.16) link. The laser link was operated at 1550 nm, switching was implemented on the network layer via switching between static routes. Power hysteresis was employed, and the link distance was 1.14 km.

Milner and Davis (S.D.Milner and C.C. Davis, 2004) proposed a switch-over system for tactical operations in a general manner, considering protocols for switching between links as well as for traffic re-distribution after a change in the network topology. Their intention was to use two 1550 nm FSO systems in combination with an RF link operated in the Ku-band

(12-18 GHz). Kamalakis et al. (T. Kamalakis et al., 2005) installed a hybrid switch-over system at the University of Athens, Greece, using a 1 Gbps FSO link and a 100 Mbps MMW link operated at 95 GHz over a distance of 800 m. Also, (L. Stotts et al., 2009) report about switch-over systems.

Dynamic load balancing is also proposed in literature: ElBatt and Izadpanah (H. Izadpanah et al., 2003; T. ElBatt and H. Izadpanah, 2001) proposed a load balancing system distributing traffic among one FSO and several RF links. In this work, however, it is assumed that the amount of traffic on the FSO link affects its availability. Vangala and Pishro-Nik (S. Vangala and H. Pishro-Nik, 2007; S. Vangala and H. Pishro-Nik, 2007) use special non-uniform low-density parity check codes to distribute traffic among different links, showing increased link utilization and availability, while BER could be reduced significantly. Finally, Nadeem et al (F. Nadeem et al., 2009; F. Nadeem et al., 2009) analyzed both switch-over and load-balancing systems based on standard Ethernet equipment with minimum hardware extension. A 155 Mbps FSO system with a 850 nm laser was used in combination with an IEEE 802.11a link. It was shown that availability almost achieves carrier class values of 99.999%.

4.4 Hybrid FSO/RF switch-over system

Switch-over (SO) systems, as they were introduced in Section IV can be illustrated by Fig. 9: Depending on the strength and availability of the links, only one of them is used for transmission. While the FSO link is the primary link, the RF link acts as a back-up. In this section the interested reader will find an overview of the problems in designing such an SO system together with some possible solutions. In particular, synchronization between the switches/multiplexers on both sides, SO algorithms and possible applications will be analyzed.

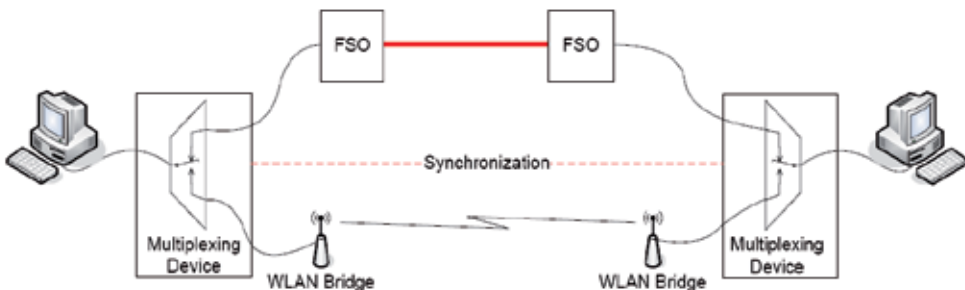


Fig. 9. Application setup of FSO-WLAN switch-over system (with the permission of (F. Nadeem et al., 2009))

For the simulations, a commercial WLAN link with a carrier frequency in the 5 GHz ISM band will be considered. The WLAN link was built with two embedded PCs using high-gain grid antennas and miniPCI WLAN cards with fairly high receiver sensitivity (depending on the antennas, distances of over 50 km can be covered). The FSO system is a GoC MultiLink 155/2 system. It supports data rates of 155 Mbps over distances up to 2 km and uses 4 transmitters at 850 nm. The properties of the FSO and the WLAN system are given in Table 2. It is further assumed that the transceivers of both links are able to provide status information.

Spec.	FSO	WLAN
TX wavelength/frequency	850 nm	5.20-5.825 GHz
TX technology	VCSEL	Semiconductor amplifier
TX power	2 mW (+ 3 dBm)	1.26mW (1 dBm)
TX aperture diameter	4 x 25 mm lens	30 dBi
Beam divergence	2.5 mrad	
RX technology	Si-APD	Semiconductor amplifier
RX acceptance angle	2 mrad	30 dBi
RX aperture	4 x 80 mm lens	
RX sensitivity	- 41 dBm	-94 dBm
Spec. Margin	7 dB/km	14 dB/km

Table 2. Properties of FSO and WLAN Systems (with the permission of F. Nadeem et al, 2009)

Since FSO is the primary link switching is exclusively determined by the ORSS: As soon as the ORSS indicates a total link loss for FSO, an SO operation to the WLAN link is performed. Similarly, as soon as the optical system restores connectivity, data packets are transmitted over this link only.

Switching and Synchronization: Switching itself can be done on almost all layers of the OSI reference model, although it is done preferably on the lower layers 1-3. Hardware multiplexers, virtual LAN switches or commercially available Ethernet routers are only a few possible switches to name. Switching on the physical layer (PHY) has the advantage of fast reconfigurations of the links, at least if the connected wireless systems are capable of such quick changes. If both links are providing Ethernet compliant interfaces only, fast physical layer switching may be problematic; connecting a CAT5 cable to an Ethernet device always requires a so-called auto-negotiation phase where the devices determine link speed, duplex mode and other transmission parameters. This negotiation takes some time, usually in the order of 1-2 seconds. Consequently, during this time data cannot be transmitted, resulting in a relatively long link loss time (LLT). As it was shown in (F. Nadeem et al, 2009) LLT is around 1.62 s for a self-made hardware multiplexer.

Moreover, it may occur that packets are cut in halves and lost during the switch-over process. On the other hand, switching on the physical layer has the advantage of a completely transparent link between the two networks to be connected via the hybrid system. Switching on the medium access (MAC) layer also provides a transparent link, if the wireless connections allow it. FSO equipment usually operates on the PHY layer and thus is protocol independent. WLAN equipment can at least be configured in a way that it is transparent to the MAC layer (bridging or WDS bridging modes), so that source and destination MAC addresses are unchanged over the link. Switching on MAC layer, e.g. by reconfiguring a virtual LAN (VLAN), has the advantage that no physical re-connections and subsequent auto-negotiation phases are necessary, significantly reducing LLT. (F. Nadeem et al, 2009) reports LLTs of 1.29 s for a commercially available VLAN device. In some cases, however, the VLAN device requires a soft re-boot after configuration, slightly prolonging the LLT (F. Nadeem et al, 2009). However, more sophisticated devices use a store and forward algorithm which at least guarantees that every packet arriving at the multiplexer is forwarded – if not over the active link. Switching on network layer can be done via routers and can rely on both physical measurements of the ORSS or interface statistics of the router ports, such as BER and packet

loss (J. Pacheco de Carvalho et al, 2008). In the former case the router needs special hardware extensions or interfaces to some measurement equipment, in the latter the router has to be capable of running a custom-made program. Furthermore, switching based on physical signal strengths has the advantage that it does not rely on actual errors, but allows for implementation of a more or less generous link margin. Switching itself is usually done by changing the route metrics (J. Pacheco de Carvalho et al, 2008) of the different links according to the measurements. Consequently, all packets are transmitted, although not all may reach its destination. Moreover, one can expect that depending on the type of link status information available reactions on changes in the ORSS are delayed. Links switched on the network layer are usually not transparent to lower layers. In order to provide full connectivity, synchronization between the different multiplexers has to be ensured. Assuming that the channel is reciprocal one may state that both sides of the system will always measure the same ORSS and therefore chose the same link as active automatically. However, usually one does not want to base a hybrid system designed to achieve maximum reliability on that assumption. Moreover, using a side channel for transmitting information about which link to take is questionable as well, because that very channel has to be made reliable itself. Of course, one can feed such information into both the FSO and the RF link, but that certainly adds to the complexity of the system. Besides, it was the main intention of the SO system that at each time instant only one link has to be active. Finally, an asymmetric scenario, where one of the multiplexers chooses the link according to the ORSS would be possible. The other multiplexer accepts packets from either link, but responds only over the very link from where the last packet arrived. Such a self-synchronizing setup, as it was introduced in (F. Nadeem, 2009) has the disadvantage that it inherently relies on quasi-continuous transmission from the network on the side of the active multiplexer – a condition which is usually fulfilled by higher-layer protocols, such as TCP. In any case, despite all considerations about synchronization and switching, the overall hybrid network still has to be considered unreliable; the difference, however, is that the availability is increased significantly.

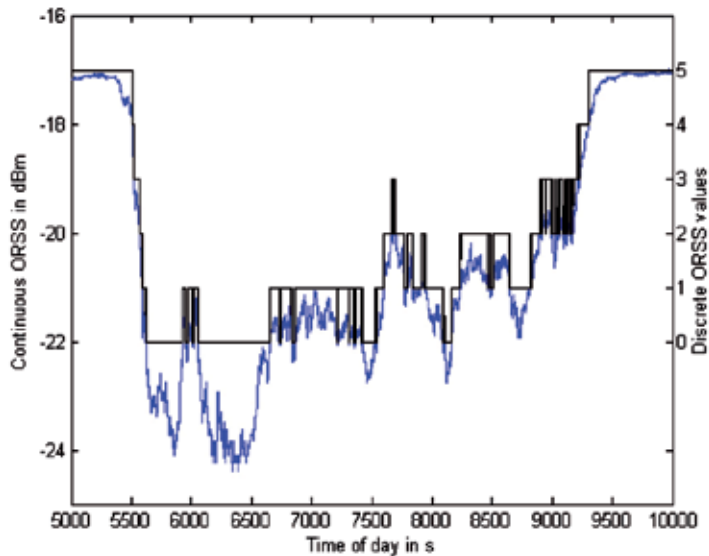


Fig. 10. Comparison of discrete and continuous ORSS values. (with the permission of B. Flecker, 2006) Fog event from October 25th, 2005, 03:00 to 11:00.

Switch-Over Algorithms: After deciding upon the layer on which switching is performed, upon the data which is determining the active link, and the synchronization method, the designer of the hybrid SO system has to take a multitude of switch-over algorithms into consideration.

Remembering the advantages of physical measurements describing the link status we will put special emphasis on SO systems switching based on those measurements. This, however, rises an important question: Can it be guaranteed that the FSO system (which purely determines the active link) provides link status information in an accurate, timely manner? It can be taken as granted that the system itself measures and uses ORSS information, but is this information accessible to the user over a certain interface? The MultiLink 155/2 system for example indicates the ORSS continuously with a LED bar (discrete amplitude as shown in Fig. 10), but provides this data over an RS232 interface on a per-second basis only (discrete time). Somewhere within the system, however, the time and amplitude continuous ORSS will be available (as also shown in Fig. 10). Thereby one can assume that the previous assumption of link status information provided to the user can be justified, even if hardware reconfiguration are necessary. As one can see in Fig. 10, especially during the gradient from clear sky conditions to foggy weather there are many variations in the ORSS. These variations, as one can expect, cause a certain threshold to be crossed multiple times. If now the SO system is designed to employ a straightforward threshold comparison (TC) algorithm, it would suffer from frequent switching between the links due to these variations. Since after each switching operation a certain time is required to restore the link completely (so called link loss time, or LLT), frequent switching would cause reduced bandwidth and availability. Consequently, other algorithms coping with these variations have to be evaluated – it is the purpose of this section to introduce some of them and compare their performance.

a) Power Hysteresis (PH): A power hysteresis defines two thresholds and two states: a lower and an upper threshold, WLAN and FSO operation. If during FSO operation the lower threshold is crossed, WLAN is activated. If during WLAN operation the upper threshold is crossed, FSO is activated – it's as simple as that to prevent the system from switching back and forth. The width of the hysteresis (i.e. the distance between upper and lower threshold) depends on the amplitude of variations and has to be optimized with respect to actual system measurements. To maximize availability, the lower threshold has to be set to values equal to or greater than the receiver sensitivity of the FSO device. b) Time Hysteresis (TH): Relating variations in the ORSS to bouncing of electrical contacts, one can also use techniques called debouncing to cope with these variations. Such techniques usually employ a wait period T during which the ORSS are evaluated and during which after every threshold crossing the wait period is restarted. Consequently, only if the signal does not cross the threshold for a certain time, an SO operation is performed. The duration of the wait period in that case is determined by the frequency and the amplitude of the variations. To maximize availability, the wait period can be set to different values for crossing the threshold in either directions; in the limiting case, the wait period can even be omitted for switching from FSO to WLAN. c) Filtering: Treating variations in the ORSS as noise, methods for noise mitigation come into view. Most prominently, low-pass filtering can be named as such a method. Different realizations of low-pass filters in the analog (RC-network) and digital (moving average filter, raised-cosine filter, etc.) domain are possibilities to cope with this unwanted noise. Filters are characterized by their order, pass

and stop band characteristics, and by their cut-off frequency. These characteristics have to be designed with respect to the frequency of the variations. It is of vital importance that the frequency of these variations is in the stop band, while the highest occurring frequency in climatic changes still lies in the pass band to allow for a timely reaction on an emerging fog event.

Moreover, combinations of these methods can be considered (e.g. filtering and hysteresis methods, power hysteresis and debouncing, etc.). Unfortunately, seasonal and diurnal, as well as geographic peculiarities make a general design or general optimization of parameters impossible. The reader will understand that the design of a SO system in a coastal area with dense fog conditions differs from a system in a metropolitan area, where moderate fog can be expected. The following simulations therefore focus on the continental, metropolitan climate of Graz, which is characterized by moderate, persistent fog events during fall and winter and strong rainfall during summer.

Simulations and Results: For the simulation, measurement data was taken from (B. Flecker et al, 2006). For parameter optimization the particular fog event depicted in Fig. 10 was used. The benefit of focusing on one fog event is based on the fact that the influence of LLT after switching is increased compared to the influence on an all-year average availability. Moreover, as it can be seen in Fig. 1, fog events mainly occur during fall and winter, making a separate analysis of these seasons sensible. Assuming little or no unavailability during the summer months, simulation data can be extrapolated. Receiver sensitivity of the FSO system was set to -22 dBm. For this value, a significant number of threshold crossings occurred which allows an optimization of the algorithms. Using this sensitivity, the fog event under consideration yielded an FSO availability of only 67.43%. Link loss time after switching was set to 3 s in order to include an additional margin to link re-establishment. For bandwidth simulations, bandwidths of the FSO and WLAN link were set in accordance to (F. Nadeem et al, 2004) to 91.9 Mbps and 18.8 Mbps, respectively. The WLAN link was assumed to be active whenever FSO was inactive. This assumption holds for fall and winter periods where FSO outages are usually caused by fog only and where rain is rarely occurring simultaneously. During summer months where strong rainfall in combination with severe fog affects both links this assumption may not be valid anymore (E. Leitgeb et al, 2004).

As one can imagine, finding the best algorithm parameters is related to finding a trade-off between availability and bandwidth efficiency. While WLAN may be available throughout the year, its bandwidth is prohibitively low. Consequently, the simulations are limited by a minimum bandwidth of 60 Mbps. A more complete evaluation of simulation results and a comprehensive discussion of this topic can be found in (F. Nadeem et al, 2009).

a) **Threshold Comparison:** Pure threshold comparison (TC) is done by comparing the ORSS to the RX sensitivity and switching based on the outcome of this comparison. TC yields an increase in availability to 98.62% while achieving best bandwidth performance (see Table 3). This can be explained by the fact that TC uses the FSO link whenever it is available, and the outstanding bandwidth of this link compensates for relatively high unavailabilities due to LLTs. However, for maximizing availability this may not be the best of all choices as Fig. 11 shows. b) **Power Hysteresis:** For all simulations, the width of the power hysteresis was set to 1 dB and the lower threshold was varied. Fig. 12 shows that availability can be increased significantly by increasing the lower threshold to values much greater than the receiver sensitivity. The only problem is that by increasing this threshold FSO underutilization increases and, subsequently, bandwidth efficiency is low. E.g. to obtain a minimum

bandwidth of 60 Mbps, the lower threshold has to be below -21.7 dBm. In these regions, also the beneficial effects of filtering cannot be exploited anymore, because the time to react on changes in the ORSS due to fog increases.

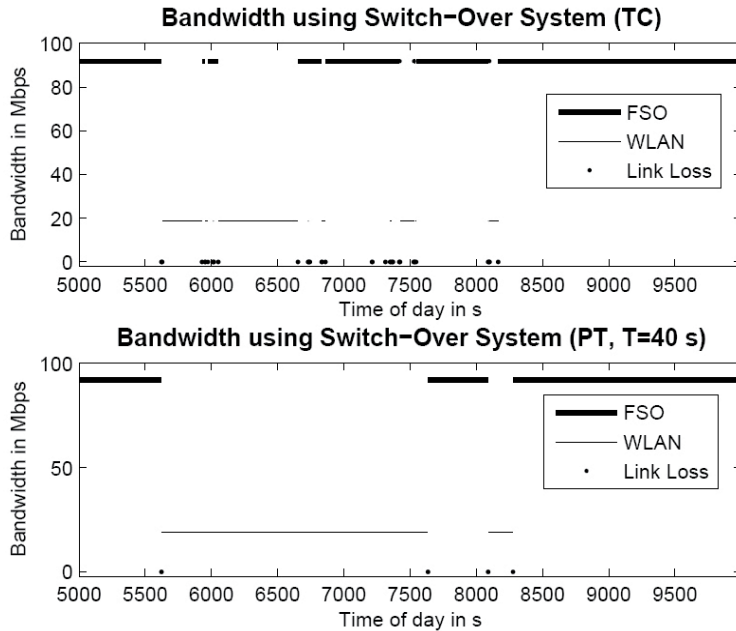


Fig. 11. Bandwidth for different switch-over methods (with the permission of F. Nadeem et al, IET submitted 2009)

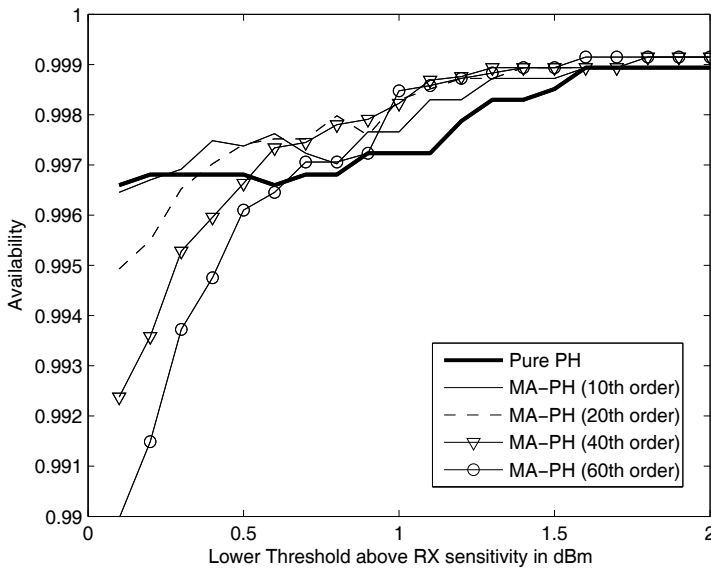


Fig. 12. Availability for pure PH and MA-PH (with the permission of F. Nadeem et al, 2009)

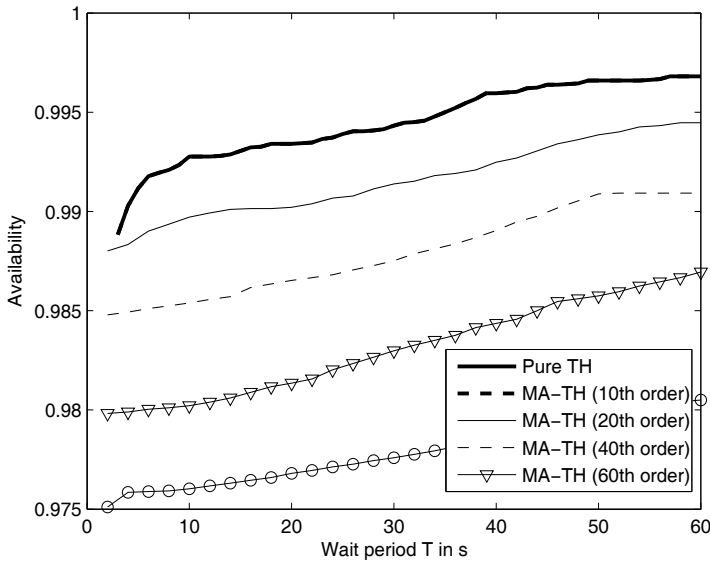


Fig. 13. Availability for pure TH and MA-TH (with the permission of F. Nadeem et al, 2009)

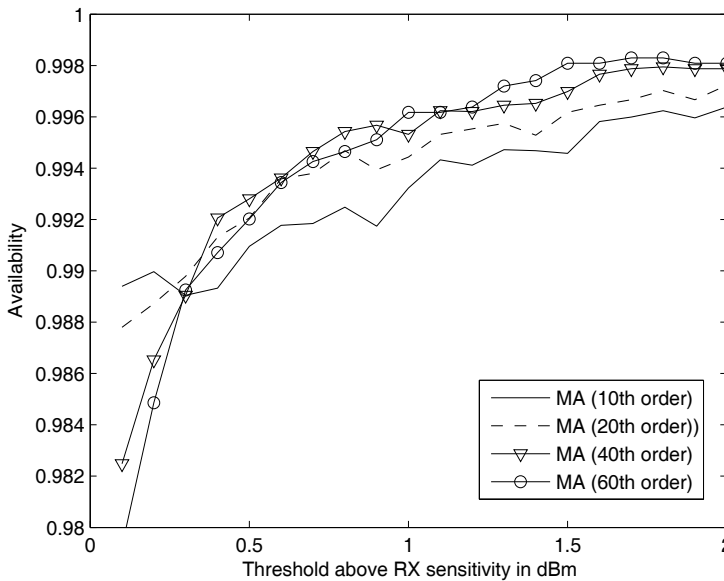


Fig. 14. Availability for different filter orders (with the permission of F. Nadeem et al, 2009)

c) Time Hysteresis: For the time hysteresis the threshold was set to the receiver sensitivity, and the wait period T was varied as a simulation parameter. As seen in Fig. 13, availability can be increased significantly. Moreover, FSO underutilization is low, so the minimum bandwidth of 60 Mbps is achieved for all depicted values of T. Filtering beforehand is

counter-productive. d) Filtering: For filtering, the threshold was increased in steps starting from the receiver sensitivity. As the only filter type, a moving average (MA) filter was considered, where the order N of the filter automatically determines its cut-off frequency (other filter types are discussed in (F. Nadeem et al, 2009)). Fig. 14 shows that availability increases with increasing thresholds. Interesting, though, might be the fact that higher orders (i.e. lower cut-off frequencies) perform better than lower ones, as long as the threshold is set to values high enough. High-order filters perform smoothing, but do not allow timely reactions on critical changes in the ORSS. Consequently, high availability is only achievable with a combination of smoothing and a large margin to the receiver sensitivity.

This in turn leads to FSO underutilization and limits maximum threshold values to -21 dBm to obtain a minimum bandwidth of 60 Mbps. In these regions, however, lower filter orders outperform higher orders.

e) Combined Power and Time Hysteresis: For the combined power and time hysteresis the lower threshold was set to the receiver sensitivity and the width of the hysteresis was 1 dB. The wait period of the time hysteresis portion was varied. As it can be seen in Fig. 15 and Table 3, pure PT delivers best results in term of availability. Furthermore, minimum bandwidth of 60 Mbps can be achieved for wait periods below 40 s, where availability still has values above 99.8%. Extending this simulation to the whole measurement campaign, availabilities of 99.988% can be achieved, as it is shown in Table 3. Simulations proved that by doubling this period to $T = 80$ s, availability could be increased to 99.997%. Taking these values into consideration one can see that carrier class availability becomes a graspable goal, even for hybrid switch-over systems.

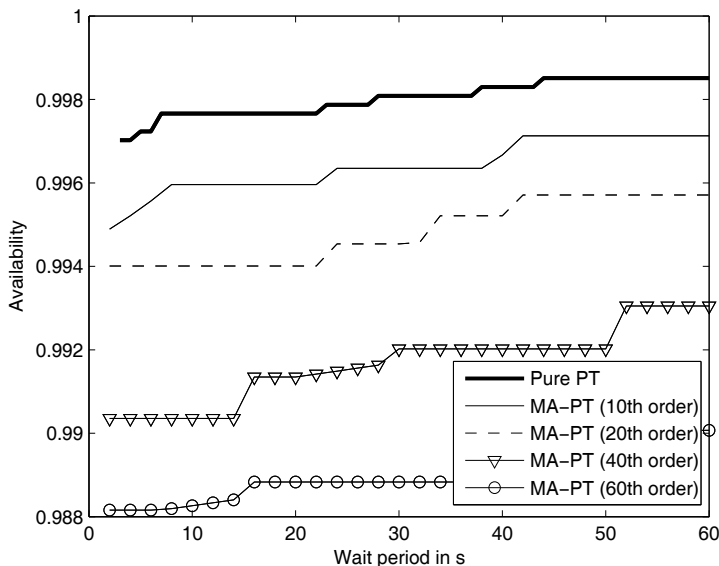


Fig. 15. Availability for pure PT and MA-PT (with the permission of F. Nadeem et al, 2009)

		Pure FSO	TC	PT (T=40 s)
Results for fog event				
Availability	%	67.43	98.62	99.83
Link Loss	%	38.62	1.38	0.17
Bandwidth (HDX)	Mbps	61.96	67.30	60.97
FSO underutilization	%	0	≈ 0	9.61
Results for overall campaign				
Availability	%	90.71	99.76	99.97
Link Loss	%	9.29	0.24	0.03
Bandwidth (HDX)	Mbps	83.36	84.97	83.74
FSO underutilization	%	0	≈ 0	1.35
Results for whole year (extrapolated)				
Availability	%	96.13	99.90	99.988
Link Loss	%	3.87	0.10	0.012
Bandwidth (HDX)	Mbps	88.34	91.83	91.79
FSO underutilization	%	0	≈ 0	0.56

Table 3. Performance comparison of different switch over methods (with the permission of F. Nadeem et al IET submitted 2009)

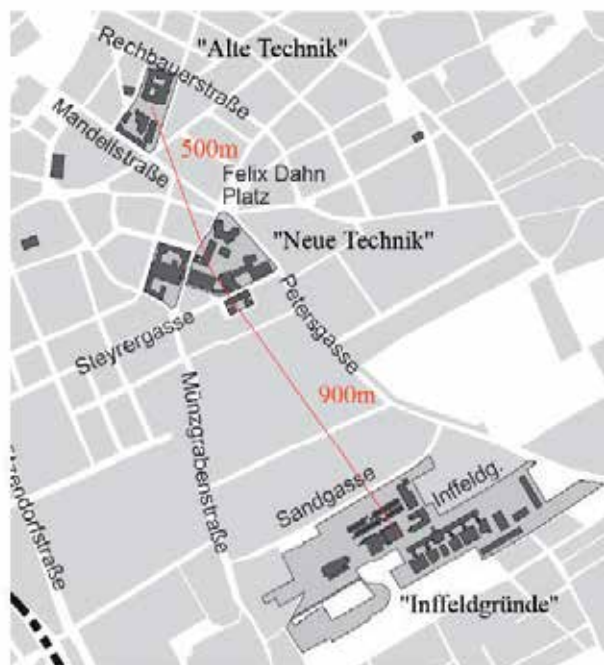


Fig. 16. Map of the campus of the Technical University of Graz

An Application: Interconnection of different sites of the campus Finally, to conclude about hybrid switch-over systems, a possible application scenario shall be introduced, where different sites of the campus of Graz University of Technology will be interconnected. Such an application is widely evaluated in the literature (J. Pacheco de Carvalho et al, 2008; A. Akbulut et al, 2005), but only (F. Nadeem et al, 2009) considers not only availability of the different links but also traffic demands of the different sites. In Fig. 16 one can see the

location of the main sites of the campus, which are known as “Alte Technik”, “Neue Technik” and “Inffeldgründe”. The latter one is the largest, housing many offices and student computer rooms. Moreover, one can see that the distance between the sites never exceeds 2 km, making the use of directional WLAN links and FSO links possible. For evaluation purposes, characteristics described in Table 2 were considered. Moreover, it was assumed that the line-of-sight for the FSO and for the WLAN link is free. As already mentioned availability of the FSO link is generally high during the summer months, and during the winter months only during daytime (cf. Fig. 1 and Fig. 2) for the continental climate of Graz. Traffic demands were recorded using the Multi-Router-Traffic-Grapher (MRTG), where green bars indicate incoming and blue lines indicate outgoing traffic.

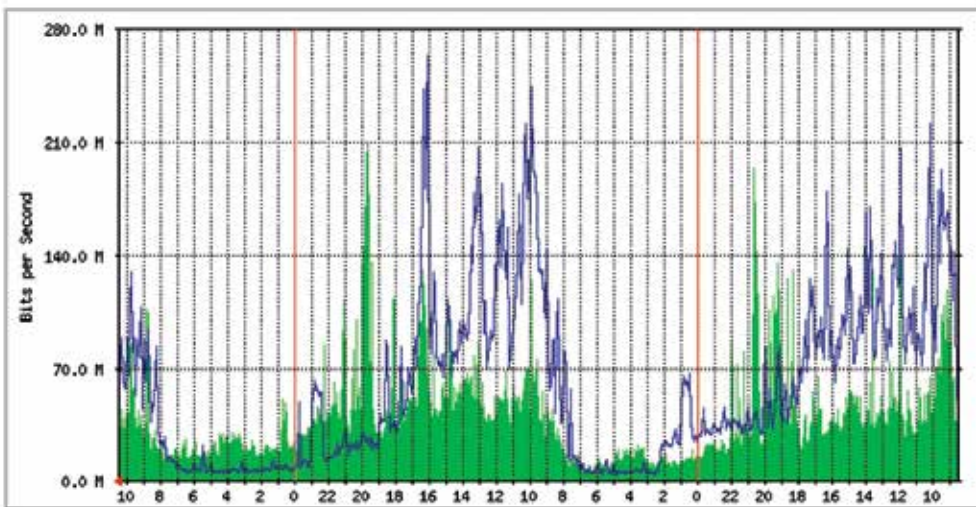


Fig. 17. Traffic data recorded for “Inffeldgasse” (with the permission of F. Nadeem et al, 2009)

Traffic recordings were made during December 2008, assuming that the average availability due to fog is similar as in Fig. 1. Fig. 17 shows the traffic demands for campus “Inffeldgasse” on December 3rd, 2008. It can be seen that peak traffic demands are occurring between 10 am and 4 pm, medium traffic was caused from 8 am to 10 am and from 4 pm to 6 pm, whereas traffic during the night time is low. Obviously, the major traffic requirements coincide with office and lecture hours. These considerations do not only hold for a particular day, but throughout the year – naturally, on holidays and weekends, traffic demands are much lower. Moreover, one can see that this peak of incoming traffic at 8 pm occurs every day, which is most likely related to an automatic backup. Scheduling such events more properly, traffic demands can be distributed accordingly. Simulations were performed using a set of measurements of the years 2000 and 2001 (J. Tanczos, 2002). Link bandwidth was set to 155 Mbps for FSO and to 15 Mbps for WLAN, respectively. For the WLAN link a slightly lower bandwidth was taken, assuming that the Fresnel zones may be partially blocked by surrounding buildings and trees. Link loss time was neglected, since it affects the average bandwidth only very little. A more complete discussion of these things can be found in (F. Nadeem et al, 2009). Comparing Fig. 18 with Fig. 17, the diurnal changes in the traffic requirements are reflected in the average as well. Furthermore, one can see from Fig. 18 that

the proposed hybrid FSO/WLAN switch-over system can satisfy traffic demands on average. Unfortunately, peak traffic demands of campus “Inffeldgasse” exceed even the available bandwidth for FSO, let alone WLAN. However, by using multiple links of each technology, or newer, more sophisticated equipment (such as Gigabit FSO equipment and IEEE 802.11n standard compliant WLAN links), traffic demands could be satisfied in a highly reliable manner over wireless links.

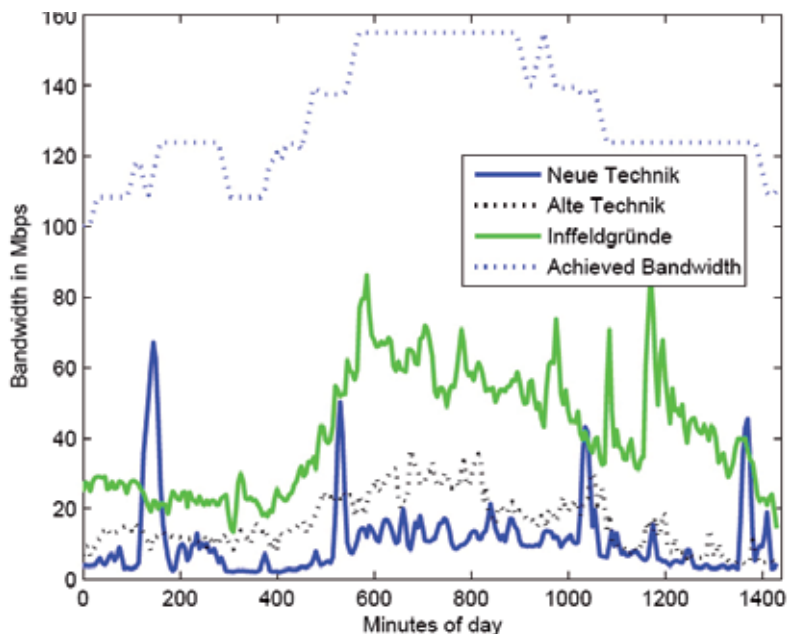


Fig. 18. Average required and achieved bandwidth (with the permission of F. Nadeem et al, 2009)

5. Blue sky applications: inter satellite, inter planetary, under sea, chip to chip FSO communications (G. Incerti – G.M. Tosi Beleffi)

The today increase of the networks complexity, with several devices and subsystems intensively used, involves an aggressive use of the bandwidth management thus to guarantee an high rate and security, especially in military scenarios. In fact, the military applications requires more strictly features respect to the civilian applications. The bandwidth offered by the optical cables is very high and for this reason the optical fibres are also used in military area. Inside airplanes, UAVs, vessels, cars and so on. Several informations and data can run through the same optical fibre and an high rate can be transmitted and managed. We started with this introduction on military purposes because this is the first market that boost the optical wireless, from the paper to the real implementation. FSO communication, infact, is a valid solution especially in military situations because of the previously mentioned ability to guarantee a confidential transmission with a huge bandwidth.

Challenge	Mitigation approach	Description
Pointing, acquisition, and tracking	RF/FSO hybrids Adaptive optics	-RF system facilitates coarse acquisition and tracking -An RF channel can serve as control channel for FSO data link -Adaptive optics systems achieve very fine beam steering and tracking
Weather/ environment	Path redundancy RF/FSO hybrids	-Path redundancy and topology control are implemented in an FSO network to counteract link obscuration -Environmental obscuration for optical may be permissible for RF or vice versa
Turbulence	Adaptive optics Channel coding/Diversity	-Adaptive optics correct beam distortion -Channel coding/diversity improve BER through forward error correction
Eye safety Eye safety	Infrared wavelengths Adaptive optics	-Infrared wavelengths such as 1550 nm are more eye safe than visible wavelengths -Adaptive optics reduce the need for increased power by correcting beam for improved SNR
Networking	RF/FSO hybrids QoS techniques	-RF system provides channel for topology control, link monitoring, and broadcasting network status -Differentiated services protocols sort data by priority to counter capacity changes -Application layer QoS algorithms prioritize data

Table 4. FSO mitigation approach (Juan C. Juarez et al., 2006)

The limited scenario offered by the radio frequency (RF) spectrum available for military use, contributed to the exploration of alternative systems able to convey the secret informations generated by military devices and/or systems. RF based systems reach only hundreds of Mbps per link and the RF beam cover an high area, in terms of spatial aperture, thus increasing the eavesdropping percentage. On the contrary, FSO systems can guarantee robust optical link with a very small beam size. Granting, at the same time, a huge bandwidth in the order of Gbps. Confining the data flow in a small spatial portion represent an advantage because becomes very difficult to detect the beam and subsequently drop some information from one or more miscreants. Furthermore, several beams, close to each other, can be used at the same time to transport the information without any kind of interference and or interaction.

The precision in the pointing and tracking steps is still a challenge especially in complex and variable scenarios like, for example, the sea one. Mounting FSO on vessels, infact, means, first of all, that a fast tracking system should be implemented. Maintaining, of course, a minimum power budget and the numeric aperture already set. In particular, for the military applications, is required an high degree of accuracy to obtain an alignment of laser beam with the receiver (Juan C. Juarez et al., 2006).

In order to win the challenges induced by the adoption of FSO systems in the communication scenario, sometime is possible to discover the presence of RF backup lines, as supporting elements of the optical counterpart. This is commonly referred as an hybrid communication system. The hybrid system shares a common aperture and the use of FSO with RF system permit to facilitate principal function like for example control signalling,

tracking, acquisition and signals discovery. The RF beam is used to search the other device (neighbour discovery) or to start the acquisition step. The RF beacon is used also as control signalling and to rehabilitate the communications in case of optical channels fades.

In order to minimize the dependence from a single link, reconfigurable FSO links can be accomplished. Path redundancy and topology control are two ways to set up a fast and smart network able to counteract in case of path obscuration. Moreover, to compensate the environment effects without increase the total beam power, the adoption of adaptive optics such as deformable mirrors, is considered a proper solution. In the following figure, are illustrated several static and mobile nodes. This is a real scenario in which an FSO link can be established in a few time.

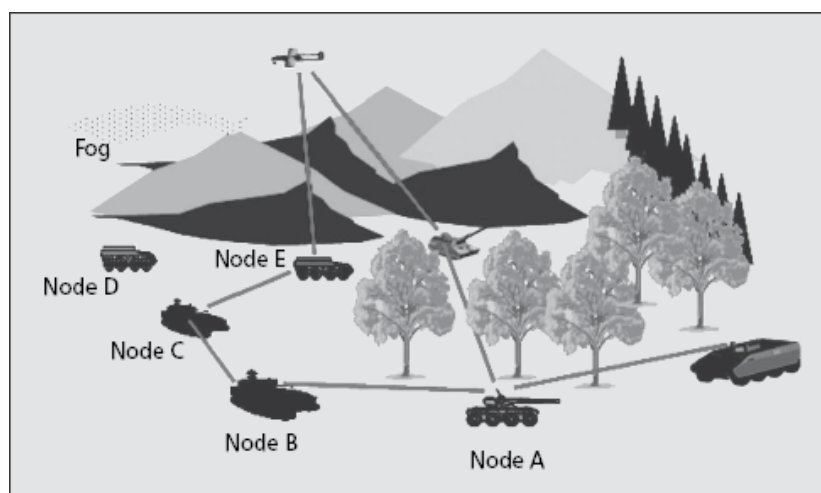


Fig. 19. Topology of a battlefield scenario using FSO system to connect all partners (Juan C. Juarez et al., 2006)

Referring to the picture, node C has two optical heads and must be able to manage the optical beams. Moreover, it is near at the B, D, E nodes; thus node C must be able to take a decision in which direction must point its optical beam. This kind of decision can be managed considering operational aspects; distance from the other devices, rate and traffic demand, distance between the end users, and environment measurement because weather conditions could limit the optical link. In this case, node C is able to send the beam through another path using another nodes. How shown in the picture, node D result isolated because the dense fog does not allow to established a FSO link with the airborne node. Thus, the only way result node C but its optical heads are both in use. The idea of the optical reconfigurable network is to establish a link between nodes C and D instead of node B. Node B will be reached from node.

The quickness in term of time to install, together with a small size, make this kind of technology able to operate in different segments, like for example, the rehabilitation of link in case of terroristic attacks or disaster recovery due to natural catastrophic events (E. Leitgeb et al., 2005).

FSO technology is used also in several non conventional scenarios like:

- **Aerospace communications:** a laser beam can directionally guarantee a link between two satellites, between the earth and a satellite platform, and vice versa, without any kind of interference and, at the same time, achieving an high data rate. Several experiments have been performed demonstrating that the FSO technology is mature to accomplish such kind of challenges. On the inter satellite side. In 2008 has been demonstrate an optical link between two LEO orbiting satellites, Terra SAR-X and NFIRE, at 5.5 Gbps on a total distance of 5500km and at a speed of 25000 km/h. On the downstream side. The KIODO (KIrari's Optical Downlink to Oberpfaffenhofen) project demonstrated a downlink stream from the OICETS LEO Japanese satellite. In 2006, 5 trials performed successfully achieving a BER of 10⁻⁶ with a modulated optical signal at 50 Mbps and 847nm (N. Perlot et al, 2007). The FP6 CAPANINA (Communications from Aerial Platform Networks delivering Broadband for ALL) project regarded the downlink between a stratospheric balloon at 22 km and a transportable ground station in Kiruna, Sweden at 1.25 Gbps (M. Knapex et al 2006). In 2008 a 2.5 Gbps experiments using a 1W laser at 1064nm with a BPSK modulation format between a LEO satellite and a ground station has been demonstrated (E. Leitgeb et al, 2009).

FSO has been also used to establish links between satellites and aircrafts or between aircrafts or even between satellite, aircrafts and ground stations realizing an ad hoc optical broadband wireless airborne network. The LOLA (Liaison Optique Laser Aéroportée) programme, for example, in 2006 demonstrated the first two way FSO link between the ARTEMIS GEO satellite and a Mystere 20 airplane flying at 9000m. At the receiver side an accurate hemispherical broadband pointing system and a CMOS sensor for detection and tracking, with a pointing accuracy better than 1 micron rad, was used (Cazaubiel et al, 2005). Real time data communications, video and audio, demonstrated via a 50 Mbps transmission with a link acquisition time under the second in 2006 and 2007.
- **Deep Space Communications:** ultra-long distance can be reached with the FSO system, thanks to the recent developments in this field, in order to allow the link with deep space. A great number of studies investigate about the beam divergence and the geometrical loss to obtain the features to established high data rate FSO link between Earth-Satellite, Earth-Moon, Earth-Mars and Earth to celestial bodies within the solar system. To obtain a detector able to work with very low power, new technologies propose devices such as low noise photon-counting detector to be placed on the planets in the form of fields array. The link budget description is based on EIRP (effective isotropic radiated power), Space losses and PDE (photodetection efficiency. Furthermore problems can arise from laser to optics coupling and turbulence in high atmosphere if passed. Modulation formats are based on pulse pattern modulation (PPM), at wavelengths ranging from 1064nm and 1550nm via YDFA technology (D. Caplan et al, 2007). Dimensioning these parameters, an FSO system can be used for deep space mission since the optical beam can cover large distances and go through the space to reach the destination (Harris Alan et al., 2006). In particular the MLCD project expected performances are 1Mbit/s farthest Mars and 30 Mbit/s nearest Mars. Increased performances can support data rate up to 1Gbit/s maximum Mars distance, 100 Mbit/s Jupiter and 10 Mbit/s Uranus (D. Boroson, C. Chen, B. Edwards, 2005).

- **Undersea communications:** FSO is used to transport information from fixed or mobile sea-platforms to other stations without deploying any cable. Using a particular wavelength it is possible to cover small distances (around 100 m) but with transmission rate around 10Mb/s. The disadvantage is that the sea offers an attenuation greater than the attenuations offered by the air. Submarine Laser Communications (SLC) is implemented to achieve high data rate transmissions also in case of emergency between two platforms or between a platform and an airborne system. SLC is used for communication with deeply submerged submarine using an FSO laser at particular wavelength. Often it is used green or blue wavelengths, thus the radiation is placed in visible spectrum. For undersea application, particular type of lasers are used such as xenon chloride (XeCl) laser shifted in the visible spectrum. Each submarine receiver, has the ad-hoc detector to capture the optical laser beam. Several tests was made to study the performances of undersea laser link and also aircraft to submarine transmission system was implemented. An aircraft flying at 40.000 feet was connected with a submarine using a double wavelength: blue wavelength for uplink and green wavelength for the downlink stream. There was also clouds between aircraft and submarine but the detector installed on board of the submarine was able to detect the signal since a special optical receiver was applied. In this way, the use of the blue-green optical wavelength for undersea applications confirmed the use of these optical frequencies in the sea field. The disadvantage of this kind of laser is that its time operational life is not so long; but the technology, today permit to have solid-state lasers. This kind of solution permit to have a longer operational life laser and also with its efficiency is improved. The smaller cost respect to normal gas lasers, permit also the use of these devices in deep space scenario.
- **Air to Earth communications:** to prolong the band of the RF technology used today for several airplanes carrier to monitor, perform surveillance actions and for GIS (Geographic Information System) applications (Juan C. Juarez et al., 2006). NASA JPL, on this side, demonstrated a 2.5 Gbps FSO link between an UAV and a ground station studying in particular the atmospheric fades and the problems related to the pointing systems (G. Ortiz et alt, 2003).
- **Inter island communications:** With the DOLCE study, ESA funded project, an inter island free space communication has been demonstrated covering 142 km between La Palma and Tenerife at 10 Mbps with a 1W MOPA (Master Oscillator Power Amplifier) using a 32 PPM (Pulse Position Modulation) and a simple Si-APD as receiver placed on a OGS (Optical Ground Station) (G. Baister et alt, 2009). On the same link, the ROSA project performed experiments to investigate an optical telemetry system for the mars sample return mission (T. Dreischer, 2008).
- **Inter optical communications subsystems:** board to board and chip to chip optical wireless interconnections become a reality in the last years (Hirabayashi K. et alt, 1997). The main reasons have been the need to compensate the board to board bottlenecks and to increase the backplane interconnections speed. Especially in chip to chip wireless interconnections, the main problem arise from design and package issues. Other challenges are focused to the development of ultra low driving devices for VCSEL arrays, commonly used in board to board interconnections, and to the increase of alignment tolerance. Experiments demonstrated that is possible to

establish more than 1000 channels per printed circuit board using a 1mm pitch optical beam array having at 1Gbps per channel, thus a throughput per board up to 1 Tbps (Hirabayashi, Yamamoto, Hino 2004).

6. Techno economic analysis (Tosi Beleffi – Forin)

A correct approach, in the techno economic analysis of a FSO based scenario, must focus on the main market drivers that, today, are mainly related to the civil telecommunications. Undersea, inter planetary, inter satellites or military based communications, infact, still are in the research or prototyping field where, everyone knows, the costs are not in principle, especially at the beginning, strictly taken into account for a mass production. This preamble is important to justify the fact that this sub chapter will be mainly devoted to the civil telecommunication applications where the competition of different actors is today increasing the market portfolio thus lowering the overall costs.

The demand for broadband infrastructures, mainly driven today by the request for new multimedia applications, is pushing the Operators to implement specific strategies characterized by a continuous and slow migration to the so called FTTx family (Fiber to The Curb/Cabinet/Building/Home) where the final step is constituted by the FTTH (Fiber To The Home). In the future, infact, is expected that we will have an exact replica of the PSTN network but with fibres instead of the copper. Each end user will have a single or a pair of fibres directly connected with the CO (Central Office).

Today the main effort is, for what has been previously mentioned, devoted to the development of new burying strategies to lower the CAPEX that, in the fibre optical based infrastructures, are mainly due to the fibre installation. The installation costs of a 36 fibre optical cable, in a typical urban area environment, are, for example, divided between the dig (12%), the cable and the cable lying (14%) and the civil works for surface footway (74%) (A.L.Harmer, 1999). For these reasons a tremendous proliferation of new techniques has been experienced: trench, micro trench, dig, micro dig, one day dig, Teraspan, aerial cables. Several Operators and Municipalities are today performing demo trials to demonstrate the possibility to put the fibre cables in the sewer pipes, inside the urban lighting systems or even in the gas pipes. All these different approaches can, in principle, reduce the installation costs, depending of course on the particular case and/or situation, in average of a 30-40% respect to a standard trench approach.

But what can happen if must be crossed a river, a railway or connected a neighbour island?

In this scenario, which can be the role of the FSO?

It should be considered that nothing is so simple as reported with the pen on the paper. In the case of digs, still many problems are present especially under the regulatory point of view and, most important, for the huge amount of authorizations that has to be requested to the Regions, Provinces, Municipalities and Districts. Is not so simple, costless and fast, infact, taking a excavator and start to dig along a street. On the other side, it must be pointed out that gas pipes, urban lighting systems, sewer pipes, water systems can be in principle used to host optical fibres but still remain critical infrastructures, under the security point of view, and so the fully access to them is still difficult.

We start to understand that the development and the diffusion of the broadband to the end user is not only a matter of digging the fibre. Is a more complex problem where mixed wireless and wired infrastructures can and must coexist. This to limit the digital divide,

increase the broadband to all, taking care of the costs, both CAPEX and OPEX (Operational Expenditures). Depending on the geography, in fact, a particular technology can be better than a different one, being wired or wireless. This opens the way to the implementation of mixed infrastructures and to the deployment of different technologies like: WiMax, WiFi, SDH Radio, LMDS, WDCMA/UMTS, UTRAN, GSM, FSO, Satellite, xDLS, Fibre, Coax. Considering the FSO technology as a point to point based system, we can start to define and differentiate it respect to other possible competitors like the Fibre, the Microwave links, the XDSL and the COAx (see table 5).

	FSO	Microwave radio	Optical Fibre	Coaxial cable	xDSL
Speed	Gpbs	Mbps	Independent	Mbps	Mbps
Installation	Moderate	Difficult	Difficult	Moderate	Difficult
Uses	P2P/P2MP short and long reach	P2P short reach	P2P/P2MP short and long reach	Campus, multi drop short reach	Phone and data, access telecom sector
Advantages	Price vs performances, security	Speed vs installation	Huge Available bandwidth, security	Better than other copper media.	Low cost, is already present.
Disadvantages	Dependent on the climatic conditions	Can be intercepted	Installation costs	Costs	Speed limited by interference and cable quality
Security	Good	Poor	Very good	Good	Good
Maintenance	Low	Low	Low	Moderate	High
Skills	Moderate	High	High	Moderate	Moderate

Table 5. Comparison between different P2P networks

From table 5 we can start to figure out, respect to other P2P technologies, the sector of influence that can be covered by the FSO technology. In order to understand which broadband technology can be the most efficient in terms of CAPEX and OPEX, we have to go deeper in the problem considering also the following economic factors like: cost per line, average return per user, mean time before failure (MTBF), mean time to repair (MTTR), warranty by vendor, upgradable characteristics, operation and maintenance costs, manufactured respect to which standard.

Going deeper and deeper in the analysis we can make a simple calculation pointing out the main media/devices needed to set up a point to point link (see Table 6). In this case we can see that the main characteristics of a point to point optical wireless link are to be wideband, easy and fast to install as well as low cost respect to the other technologies. The mix made by cost per bandwidth per easy to use/install is the winner. The main drawback is of course due to the climatic conditions encountered that limit, in case, the maximum distance/bit rate achievable. Adding a RF (Radio Frequency) link, increases the costs but increases also the availability.

TECHNOLOGY	MAIN COSTS	LICENCES	NOTES
FSO	From 13k€ @ 155 Mbps to 19k€ @ 1.2 Gbps (up to 3.6 km). From 22k€ @ 155 Mbps (up to 5.7km) to 33k€ @ 1.2 Gbps (up to 5.3km) (source: vendor).	Is not needed a licence. An unatum per year is due to the reference / control PA.	Fast installation both indoor and outdoor. Radio backup is needed to increase the availability up to 99,999%.
RF	From 20k€ to 30k€ depending on the length (1-10km) working @ 18, 26 or 38 GHz can transmit up to 300 Mbps. (source: vendor).	Is needed a licence. Example: For 28MHz in the 7GHz bandwidth along 20km costs around 5k€. (source: PA)	Fast installation, limited bandwidth. High time window if is considered the time needed to have the licence.
FIBRE	In the case of a P2MP system that is the most cost effective in terms of CAPEXs respect to a pure FTTH. A standard GPON OLT (with 4 G-Ethernet ports), a 1:16 splitter, an ONU serving 48 VDSL2 end users, 15 ONTs with 2 G-Ethernet ports and VOIP [Everything compliant with the ITU G.984 standard] has a total cost of around 26k€. (Source: vendor). Around 70€/m for the dig and 10€/m for the cable in urban environment. In river basin the installation plus the cable (120 fibres) can go down at around 16€/m. (Source: PA).	Dark fibres can be rented in average from 5 to 15 €/m with a 15 year based contract (source: consulting center). Free ducts can be also rented at around 12,3€/m (source: company).	Slow installation, dig is needed with or without trench. The bandwidth is virtually unlimited. Today the new dig techniques can lower the costs up to 40% depending on several factors. (source: operator)
xDSL	The costs can vary from 14k€ for an IP DSLAM serving 64 users (modems included) up to 40k€ for an IP DSLAM serving up to 1024 end users (modem included). In this last case the average bit/rate per client is at around 10-15 Mbps over 1.2 km - access network segment. (Source: consulting center).	Copper line/client in unbundling regime is in average at 7,5€ (source: operator). A twisted pair can vary from 80€ to 225€ depending on the cable quality. (source: operator). Installation costs are in average at 80-85€/m. (source: consulting center).	Maximum available bandwidth is limited by interferences. Major costs due to copper maintenance Other voices (CO apparatus rental, CO apparatus maintenance, et alt).

Table 6. Main costs per technology. All these costs do not include installation&maintenance.

It can be also pointed out that, especially where the duct availability is limited, FSO can provide an economically favourable alternative to both FTTH/FTTC scenarios (T. Rokkas et

alt, 2007). Using a particular tool originated from several EU projects (IST-TONIC Techno-ecoNomiCs of IP optimised networks and services, and the CELTIC ECOSYS Techno-Economics of integrated communication SYStems and services), a geometric area model has been obtained to calculate the number of network elements required (Cabinet, Local Exchange, Central Office, Fiber Cables) to reach the end user premise. Based on this geometric area, taking a MTBF of 10 years and a MTTR of 8h and considering the duct availability, has been demonstrated a Net Present Value (NPV) for FSO Local Exchange (LE) better than FTTC and FTTH, in case of no duct availability. The fibre based scenarios are better than the FSO LE building alternative if the duct availability is greater than 70% (T.Rokkas et Alt, 2007).

Last but not least, analyzing the world market from the very beginning is interesting to see that in principle the society consider, in general, communications not as a fad but as a necessity. The global consumption of fiber optic components in communication networks exploded from only 2.5\$ million in 1975 to 15.8\$ billion in 2000 (J.D. Montgomery, 1999). Continued growth to 739\$ billion in 2025 is expected. In particular, from 2000 to 2025, the average annual growth rate has been predicted (J.D. Montgomery, 1999), not considering the actual negative conjuncture, to 12% for fiber optic cable, 21% for active components, 19% for passive components, 15% for other components. Analyzing data more close to the current time period we can outline that the global fiber optic connector and mechanical splice consumption in 2006 was \$1.401 billion and by the year 2011, the worldwide consumption value is forecasted to reach \$3.462 billion (ElectroniCast, 2008). Fiber optic collimating lenses market in Japan/pacific Rim lead the global consumption (number of units used) with 46.7%, 37.9% in North America. Europe with a market share close to 15% is forecasted to experience a flat growth trend considering the manufacturing outsourcing strategies. Fiber optic collimating lens assemblies market in North America lead the global consumption volume (number of units used) with 40%, 35% in Japan Pacific Rim. Europe is forecasted to increase due to the value-added building of sub assemblies and equipment (ElectroniCast, 2008). Furthermore, the laser product market continued to expand at a healthy rate in 2008 with fiber laser sales almost reached \$300 million in revenue (Strategies Unlimited, 2009). Bank of America forecast 21% growth in 2010 for the semiconductor market mainly driven by electronic equipment sales. Global electronic equipment revenue will rise by 4.9% in 2010 after a 9.8% decline in 2009, respect to 2008, while the global semiconductor revenue is set to loose 23% in 2009 respect to 2008 (D. Manners, 2009). It must be pointed out that, in this case, the main electronic equipment categories are: automotive, data processing, wired communications, wireless communications, consumer and industrial. The automotive decline from 2008 to 2009 had a major impact on the overall electronic equipment sales.

Analyzing the data, it can be affirmed that despite the global crisis, the telecom market is holding up the shock and is representing a real answer for the Governments. Focusing the telecom sector, especially in the part related to FSO technologies/components, all the data analyzed demonstrate a good vitality with both capital expenditures, consumes and revenues. On this point it is expected from GE and 10GE technology to be the next driver for the FSO companies. 10 Gbps Ethernet lines becomes reality not only within campus or high rise networks but also to all that customers involved in applications like redundant data centres, medical imaging and HDTV editing. The costs of 10G FSO systems will certainly tied by the adoption of the 10GE technology and by it corresponding decrease in the cost curve. The trade-off for the 10G FSO will be, for example, from the receiver side point of

view on the balance between the size/sensitivity of the InGaAs receivers (suitable at 1550nm) and the tracking/focusing system. FEC, DWDM, laser driver and preamplifiers at the receiver will certainly must be taken into account to accomplish an economy of scale for 10G FSO (I. Kim, 2009).

7. Conclusion (All)

Communications and transmissions are two fundamental concepts that follow the human being from the beginning. Free Space Optics is only one of the several choices that we have today in the complex and mixed telecommunication environment (WiFi, WiMax, LTE, Fibre, Coax, GSM, UMTS, et al). With its inherent characteristics like ease of installation, fast ROI, low CAPEX, intrinsic security, broad band and with its wide applications range, from under sea to deep space, free space optics represents today a solution that all the telecom actors have to take into account. Especially now that 10/100 G Ethernet technology is appearing at the horizon.

8. References

- F. Nadeem, B. Geiger, E. Leitgeb, M. S. Awan, S. S. Muhammad, M. Loeschnig, and G. Kandus (2009) *Comparison of link selection algorithms for fso/rf hybrid network*, IET, submitted 2009.
- I. Kim (2009) *10G FSO systems position technology for the future*, Lighthwave, PennWell July 2009.
- L. Stotts, L. Andrews, P. Cherry, J. Foshee, P. Kolodzy, W. McIntire, M. Northcott, R. Phillips, H. Pike, B. Stadler, and D. Young (2009) *Hybrid optical rf airborne communications*, Proceedings of the IEEE, vol. 97, no. 6, pp. 1109-1127, June 2009.
- E. Leitged, M.S. Awan, P. Brandl, T. Plank, C. Capsoni, R. Nebuloni, T. Javornik, G. Kandus, S. Sheik Muhammad, F. Ghassenlooy, M. Loschnigg, F. Nadeem (2009) *Current Optical Technologies for wireless access*, Proc. Of IEEE CONTEL Conference, Zagreb Croatia 8-10 June 2009.
- J. Wells (2009), *Faster than fiber*, IEEE Microwave Magazine, vol. 10, no. 3, pp. 104-112, May 2009.
- F. Nadeem, B. Geiger, M. S. Awan, E. Leitgeb, and G. Kandus (2009) *Evaluation of switch-over methods for hybrid FSO-WLAN systems*, in Wireless VITAE, Aalborg, May 2009, pp. 565-570.
- F. Nadeem, B. Geiger, M. Henkel, E. Leitgeb, M. S. Awan, M. Gebhart, S. Hranilovic, and G. Kandus (2009) *Comparison of wireless optical communication availability data and traffic data*, in VTC Spring, Barcelona, April 2009, pp. 1-5.
- F. Nadeem, B. Geiger, M. Henkel, E. Leitgeb, M. Löschnig, and G. Kandus (2009) *Switch-over implementation and analysis for hybrid wireless network of optical wireless and GHz links*, in WTS, Prag, April 2009, pp. 1-6.
- F. Nadeem, M. Henkel, B. Geiger, E. Leitgeb, and G. Kandus (2009) *Implementation and analysis of load balancing switch over for hybrid wireless network*, in WCNC, Budapest, April 2009, pp. 1-6.
- G. Baister, K. Kudielka, T. Dreischer, M. Tüchler (2009), *Results from the DOLCE (Deep Space Optical Link Communications Experiment) Project*", Proc. of SPIE Vol. 7199 71990B-1.
- D. Manners (2009) *Semiconductor sales to grow 10% in Q3, says iSuppli*, ElectronicsWeekly.com

- Strategies Unlimited (2009) *Fiber and industrial Laser Market review and forecast*, OM-46 Third Edition 2009.
- S. Bloom and W. S. Hartley (2009), *The last-mile solution: hybrid FSO radio*, <http://www.systemsupportolutions.com/whitepapers.htm>.
- ElectroniCast (2008) *Fiber Optic Connector and Mechanical Splice Global Market & Technology Forecast (2007-2012)*, Global Summary.
- ElectroniCast (2008) *Fiber Optic Communication Collimator Lens & Lens assemblies global market forecast (2007-2012)*, Global Summary.
- T. Dreischer, "ROSA Final Presentation (RF-Optical System Study for Aurora)", ESA Contract No. 20371/07/NL/EK Final Presentation, ESTEC, 2nd December 2008
- S. Gurumani, H. Moradi, H. H. Refai, P. G. LoPresti, and M. Atiquzzaman (2008) *Dynamic path reconfiguration among hybrid fso/rf nodes*, in GLOBECOM, November 2008, pp. 1-5.
- M. S. Awan, E. Leitgeb, S. S. Muhammad, Marzuki, F. Nadeem, M. S. Khan, and C. Capsoni, *Distribution function for continental and maritime fog environments for optical wireless communication*, in CSNDSP, July 2008, pp. 260-264.
- J. Pacheco de Carvalho, H. Veiga, P. Gomes, and A. Reis (2008) *Experimental development and study of Wi-Fi and FSO links*, in CSNDSP, July 2008, pp. 137-141.
- V. Kvicera, M. Grabner, and O. Fiser (2008) *Visibility and attenuation due to hydrometeors at 850 nm measured on an 850 m path*, in CSNDSP, July 2008, pp. 270-272.
- A. Chaman Motlagh, V. Ahmadi, Z. Ghassemlooy, and K. Abedi (2008) *The effect of atmospheric turbulence on the performance of the free space optical communications*, in CSNDSP, July 2008, pp. 540-543.
- R. Nebuloni and C. Capsoni (2008) *Laser attenuation by falling snow* in CSNDSP, July 2008, pp. 265-269.
- H. Alma and W. Al-Khateeb (2008) *Effect of weather conditions on quality of free space optics links (with focus on malaysia)* in ICCCE, May 2008, pp. 1206-1210.
- A.K. Majumdar, J.C. Ricklin (2008) *Free Space Laser Communications Principles and Advances*, Springer ISBN 978-0-387-28652-5.
- S. Vangala and H. Pishro-Nik (2007) *A highly reliable fso/rf communication system using efficient codes*, in Global Telecommunications Conference, 2007. GLOBECOM '07. IEEE, Nov. 2007, pp. 2232-2236.
- D. Caplan, M. Stevens, B. Robinson, S. Constrantine, D. Boroson *Ultra-Long Distance Free Space Laser Communications*, CLEO Conference 2007, Baltimore USA.
- Perlot, N. et al, "Results of the Optical Downlink Experiment KIODO from OICETS Satellite to Optical Ground Station Oberpfaffenhofen (OGSOP)", Proceedings of SPIE, Vol. 6457, 2007.
- T. Rokkas, T. Kamalakis, D. Katsianis, D. Varoutas and T. Sphicopoulos (2007), *FBusiness prospects of wide-scale deployment of free space optical technology as a last mile solution: a techno-economic evaluation*, Journal of Optical Networking Vol.6 No.7, July 2007.
- S. Vangala and H. Pishro-Nik (2007) *Optimal hybrid RF-wireless optical communication for maximum efficiency and reliability*, in CISS, March 2007, pp. 684-689.
- Markus Knapek, Joachim Horwatha, Nicolas Perlot, Brandon Wilkerson (2006) *The DLR Ground Station in the Optical Payload Experiment (STROPEX) - Results of the Atmospheric Measurement Instruments*, Proc of SPIE, ISSN 0277-786X CODEN PSISDG.

- Harris Alan, Sluss James J., Refai Hazem H., Lopresti Peter G., (2006). *Analysis of beam steering tolerances and divergence for various long range FSO communication links*, proceedings of SPIE, the international Society for Optical Engineering, ISSN 0277-786X.
- Juan C. Juarez, Anurag Dwivedi, A. Roger Hammons, Steven D. Jones, Vijitha Weerackody, Robert A. Nichols, (2006). *Free-Space Optical Communications for Next-Generation Military Networks*, IEEE Communications Magazine, November 2006.
- M. Abtahi and L. Rusch (2006) *Mitigating of scintillation noise in FSO communication links using saturated optical amplifiers*, in MILCOM, October 2006, pp. 1-5.
- E. Leitgeb, S. S. Muhammad, B. Flecker, C. Chlestil, M. Gebhart, and T. Javornik (2006) *The influence of dense fog on optical wireless systems, analysed by measurements in Graz for improving link-reliability*, in ICTON, July 2006, pp. 154-159.
- B. Flecker, M. Gebhart, E. Leitgeb, S. S. Muhammad, and C. Chlestil (2006) *Results of attenuation-measurements for optical wireless channel under dense fog conditions regarding different wavelengths*, in SPIE, 2006, pp. 1-11.
- Cazaubiel, V. et al., "Le terminal optique aeroporté sur lola", Proceedings of OPTRO 2005 Conference, Paris, France, May 2005
- Don M Boroson, Chien-Chung Chen, Bernard Edwards *Overview of the Mars Laser Communications Deminstration Project*, IEEE LEOS Vol 19 N.5 Oct. 2005.
- D. Grace, M. Mohorcic, M. H. Capstick, M. Bobbio Pallavicini, M. Fitch (2005) *Integrating Users into the Wider Broadband Network via High Altitude Platforms*, IEEE Wireless Communications, Vol. 12, No. 5, October 2005.
- J. Derenick, C. Thorne, and J. Spletzer (2005), *On the deployment of a hybrid free-space optic/radio frequency (FSO/RF) mobile ad-hoc network*, in IROS, August 2005, pp. 3990-3996.
- T. Kamalakis, I. Neokosmidis, A. Tsipouras, T. Sphicopoulos, S. Pantazis, and I. Andrikopoulos (2005) *Hybrid free space optical/millimeter wave outdoor links for broadband wireless access networks*, in PIMRC, 2005, pp. 1-5.
- CAPANINA project website www.capanina.org 2005
- Arun K. Majumdar and Jennifer C. Ricklin, (2005). *Free-Space laser communication performance, principles and advantages*, pp.9-56, Springer, New York, 2005.
- E. Leitgeb, S. S. Muhammad, C. Chlestil, M. Gebhart, and U. Birnbacher (2005) *Reliability of FSO links in next generation optical networks*, in ICTON, July 2005, pp. 394-401
- Osorio, José Alberto Huanachín Osorio (2005) *Simulação e desenvolvimento de um enlace de „Free-Space Optics“ no Rio de Janeiro e a relação com a ITU-T G826*, Master Thesis, PUC - Rio de Janeiro, 2005.
- S. S. Muhammad, P. Köhldorfer, and E. Leitgeb (2005) *Channel modeling for terrestrial free space optical links*, in ICTON, July 2005, pp. 407-410.
- A. Akbulut, H. Ilk, and F. Ari (2005) *Design, availability and reliability analysis on an experimental FSO/RF communication system*, in ICTON, July 2005, pp. 403-406.
- ITU (2005) *Attenuation due to clouds and fog*, recommendation ITU-R P840-3.
- E. Leitgeb, S. Sheikh Muhammad, M. Gebhart, Ch. Chlestil, U. Birnbacher, O. Koudelka, P. Schrotter, A. Merdonig, Gorazd Kandus, (2005). *Hybrid wireless networks combining WLAN, FSO and satellite technology for disaster recovery*, *Proceedings of 14th IST Mobile & Wireless Communications Summit*, Dresden, Germany, 19-23 June 2005. (COBISS.SI-ID19153703).

- S. Bloom (2005) *The physics of free-space optics*, May 2005, white Paper, Air Fiber.
- H. Wu, B. Hamzeh, and M. Kavehrad (2004) *Achieving carrier class availability of FSO link via a complementary RF link*, in ACSSC, November 2004, pp. 1483–1487.
- S. Hashmi and H. Mouftah (2004) *Integrated optical/wireless networking*, in Electrical and Computer Engineering, 2004. Canadian Conference on, vol. 4, May 2004, pp. 2095–2098 Vol.4.
- E. Leitgeb, M. Gebhart, U. Birnbacher, W. Kogler, and P. Schrotter (2004) *High availability of hybrid wireless networks*, Proceedings of the SPIE, vol. 5465, pp. 238–249, 2004
- Hirabayashi K., Yamamoto T., Hino S. (2004) *Optical backplane with free-space optical interconnections using tunable beam deflectors and a mirror for bookshelf-assembled terabit per second class asynchronous transfer mode switch*, Optical Engineering 37(2004), pp 1332-1342, Donal O'Shea Ed.
- S. D. Milner and C. C. Davis (2004), *Hybrid free space optical/RF networks for tactical operations*, in MILCOM, 2004, pp. 409–415.
- H. Izadpanah, T. ElBatt, V. Kukshya, F. Dolezal, and B. K. Ryu (2003) *High-availability free space optical and RF hybrid wireless networks*, IEEE Wireless Communications, pp. 45–53, April 2003.
- W. Kogler, P. Schrotter, U. Birnbacher, E. Leitgeb, and O. Koudelka (2003), *Hybrid wireless networks - high availability with combined optical / microwave links*, in Telecommunications and Mobile Computing, Mar. 2003, pp. 1–3.
- Ortiz, G.G. et al, “*Design and development of robust ATP subsystem for the Altair UAV-to-ground lasercomm 2.5-Gbps demonstration*”, Proceedings of the SPIE Vol. 4975, 2003.
- A.A. Huurdeman, (2003). *The worldwide history of telecommunications* John Wiley & Sons ISBN 0-471-20500-2
- A Paulo S. B. André, António L. J. Teixeira, João L. Pinto (2003) *Simulation of Laser Beam Propagation Through the Atmosphere for Optical Communications Proposes*, Proceedings of ConfTele 2003, Portugal.
- Zhu, Xiaming Zhu, Joseph M. Kahn (2002) “*Free-Space Optical Communication Through Atmospheric Turbulance Channels*”, IEEE Transactions on Communications, vol. 50, pp. 1293-1300, August 2002.
- J. Tanczos (2002) *Untersuchungen der Verfügbarkeit optischer Freiraumübertragungstrecken*, Master's thesis, Technical University of Graz, 2002.
- T. ElBatt and H. Izadpanah (2001) *Design aspects of hybrid rffree space optical wireless networks*, in Broadband Communications for the Internet Era Symposium digest, 2001 IEEE Emerging Technologies Symposium on, 2001, pp. 157–161.
- Almeida, Rui Sérgio Rainho de Almeida, José Luís de Jesus Ferreira Santo (2001) *Sistemas de Transmissão/Recepção sem fios por Raios Infravermelhos*, University of Aveiro, Aveiro, Portugal, Graduation Project, 2001.
- B. Bova, S. Rudnicki, (2001). *The Story of Light*, Sourcebook ISBN 1-4022-0009-9
- I. I. Kim and E. Korevaar (2001) *Availability of free space optics (FSO) and hybrid FSO/RF systems*, <http://www.freespaceoptic.com/WhitePapers/SPIE2001b.pdf>.
- J.D. Montgomery (1999) *Fifty year of fiber optics*, Nasua, N.H. Lightwave/Penn Well Corp.
- A.L.Harmer, (1999) *Communication cables and related technologies*, IOS Press, EuroCable 1999, p.170.

- Strickland, Brian R. Strickland, Michael J. Lavan, Eric Woodbridge, Victor Chan (1999) *Effects of fog on the bit-error rate of a free-space laser communication system*, Applied Optics, vol. 38, pp. 424-431, January 1999.
- Kim, Isaac I. Kim, Eric Woodbridge, Victor Chan, Brian R. Strickland (1998) Proceedings of SPIE, vol. 3266, pp. 209-220, 1998.
- T. Carbonneau and D. Wisley (1998) *Opportunities and challenges for optical wireless; the competitive advantage of free space telecommunications links in today's crowded market place*, in SPIE Conference on Optical Wireless Communications, 1998, pp. 119-128.
- Hirabayashi K., Yamamoto T., Hino S.Kohama Y., Tateno K. (1997) *Optical beam direction compensating system for board-to-board free space optical interconnection in high-capacity ATM switch*, Journal of Lightwave technology Vol15, N.5, pp.874-882.
- Kim, Isaac I. Kim, Harel Hakakha, Prasanna Adhikari, Eric Korevaar, Arun K. Majumbar (1997) *Scintillation reduction using multiple transmitters*, Proceedings of SPIE, vol. 2990, pp. 102-113, 1997.
- Wichel, Hugo Weichel (1990) *Laser Beam Propagation in the Atmosphere*, Washington: Tutorial Texts, 1990.
- Clifford, S. F. Clifford, R. J. Hill (1981) *Relation between irradiance and log-amplitude variance for optical scintillation described by the K distribution*, Journal of the Optical Society of America A, vol. 71, pp. 1112-1114, January 1981.
- Strohbehm, J. W. Strohbehm ed., (1978) *Laser Beam Propagation in the Atmosphere* New York: Springer-Verlag, 1978.
- G. Pottino, (1976). *I Cartaginesi in Sicilia* Palermo, Italy.
- Unknown, (1968) *Da Trastevere alla Colombo le telefonare del futuro*, Column on "Il Messaggero", Italian National Newspaper, 11 June 1968 Rome, Italy.
- E.Kube, (1968). *Information Transmission by light beams through the atmosphere*, Journal Nachrichtentechnik 19 (1969) II.6
- A.R.Michaelis, (1965). *From Semaphore to Satellite*, International Telecommunication Union, Geneva, p.18.
- G.Agnello, (1963). *Le torri costiere di Siracusa nella lotta anticorsara* Archivio storico di Siracusa, Vol I-IV, p.25, Siracusa, Italy.
- V. Castelli, (1700). *Dizionario enciclopedico siculo*, B.C. Palermo, Italy
- Eschilo, (458 b.C.). *Oresteia (Agamennone-Coefore.Eumenidi)*, prol. 15-30.

Novel multiple access models and their probabilistic description

Dmitry Osipov

*Institute for Information Transmission Problems Russian Academy of Science
(Kharkevich Institute)
Russia*

1. Introduction

Nowadays as both the number of subscribers of the wireless services and the amount of data transmitted via the aforesaid services are growing rapidly multiple access techniques are becoming of special urgency for specialists in the field. Frequency Hopping technique appears to be one of the most promising paradigms for the next-generation multiple access system design.

In conventional frequency hopping the entire available frequency band is divided into N subbands (following the terminology used in (Zigangirov, 2004) we shall further on refer to the set of all subbands available to the user as a **hopset**). Each user's transmitter chooses one of the N subbands in a pseudorandom manner and transmits a signal via the chosen subband using a conventional modulation technique (for the most part FSK is used). In the multiple access theory it is common to refer to each change of the subband in use as a **hop**. The process of switching between the subbands (which can be also interpreted in terms of assigning subbands to the users) is called **frequency hopping**. Frequency Hopping can be easily combined with the OFDM technique, which enables to reduce the distortion considered by both fadings and impulse noise (Note that OFDM is the fundamental technique for the most of the advanced telecommunications systems).

Frequency hopping (assigning subbands to the users) can be either coordinated (this means that when choosing a code sequence for each user, we use knowledge about other users; therefore, this scheme is mostly used for the downlink transmission) or uncoordinated. The uncoordinated frequency hopping has a number of advantages (enables to realize random multiple access, is well protected from eavesdropping or intentional jamming, and does not require elaborated protocols, which are inevitable in a system with coordinated subcarrier assignment) and is used, as a rule, for the uplink transmission. We shall consider uplink transmission, and, hence, uncoordinated subcarrier assignment strategies. In turn, these strategies can be divided into two groups. Methods of the first group exploit code sequences specially designed for multiple access systems and satisfying certain requirements. The second group includes methods where subcarrier numbers are assigned to users pseudo-

randomly. In what follows a FH CDMA system using a method from the second group will be considered.

The proposed chapter is aimed at introducing to the readers a novel class of FH CDMA systems; these are Dynamic Hopset Allocation FH CDMA (DHA FH CDMA) systems. This class has been initially introduced in (Zyablov & Osipov, 2008). As can be seen from its name the main difference between the conventional FH CDMA and the proposed class of Dynamic Hopset Allocation FH CDMA is that the hopset allocated to each user varies in time.

2. DHA FH: transmission technique

Let us now consider the basics of the DHA FH CDMA in more detail. Consider a multiple access system where K active users transmit data to the base station through a channel divided with the help of the OFDM technology into Q frequency subchannels; the transmission is asynchronous and uncoordinated (the latter means that neither of the users has information about the others). It is assumed that all the users transmit binary β -tuples. In the course of the transmission of each consecutive tuple the subchannel number generator assigned to the user under consideration chooses (in a random manner) $q = 2^\beta$ subchannels out of Q subchannels. Each tuple (or a part of the tuple) that is to be transmitted by the aforesaid user within the frame is mapped into the number of the subchannel, via which the signal is transmitted.

In what follows we shall assume that in the system under consideration optimal power control is used. The latter means that the amplitudes of all the signals from distinct users are equal at the receiver side. Furthermore we shall assume that in the system under consideration optimal phase estimation and prediction mechanism is used (i. e. phases of all the signals from distinct users are known to the base station). Hereinafter we shall consider a multiple access system, which uses an Additive White Gaussian Noise channel. In this case near optimal power control and phase estimation can be done fairly easily since both transmission ratio and phase of the signal from a certain user depend only on the distance between the transmitter and the receiver. The latter can be measured either by using pilot sequences or by analyzing information obtained from the downlink channel (which seems preferable since it is more convenient for implementing open loop power control and enables to avoid other users interference). Note, however, that in either case the transmitted signal is affected at least by the background noise, thus even in this case only near optimal power control and phase estimation can be maintained.

It is assumed that the base station is equipped with the subchannel numbers generator synchronized with that of the active user. The latter means that within the scope of the reception of the respective tuple subchannel numbers generator of the base station produces the very same subchannel numbers vector that has been generated by the subchannel numbers generator of the user under consideration. Note that this assumption is not restrictive since synchronized generators are an essential part of any conventional FH CDMA system. Thus we simply replace a generator producing random numbers with a generator producing random vectors.

Assume now that there is an eavesdropper, who intends to reconstruct the signals sent by the active users. In the conventional FH CDMA system eavesdropping is considered to be a complicated task since it is preassumed that the hopping sequences are not known to the eavesdropper. However even if the hopping sequence is not known to the user it is still possible to reconstruct the transmitted signal. Note that the DHA FH CDMA system is much more eavesdropping proof than the conventional one (since to reconstruct a tuple an eavesdropper needs not only to detect, which subchannel has actually been used to transmit a signal, but also to detect its position in the hopset, the latter being known only to the active user under consideration).

However, the introduction of the aforesaid new class of FH CDMA systems results in the emergence of a whole complex of problems. The problem of giving a suitable probabilistic description appears to be one of the most urgent ones. The present chapter is aimed at solving this problem. The latter is to be done using characteristic function apparatus. Since the probabilistic description depends on the reception strategy two different strategies, i. e. threshold reception and MAXP reception, will be considered. For each of the above mentioned reception strategies an analytical expression will be given. The results to be obtained will enable to get new insights into the whole complex of problems of novel types of CDMA systems study and development.

3.1 DHA FH OFDMA system with threshold reception: system model and probabilistic description

A receiver, equipped with a subchannel number generator synchronized with the subchannel number generator of this user, compares values of projections of signals received through these subchannels onto a direction denoted by the phase of the signal from the respective user at the receiver side with a certain threshold (in what follows, we shall assume that the base station knows the phases of complex transmission coefficients of all the subchannels; i. e., the system exploits an ideal estimation and prediction mechanism for frequency characteristics of the channel). If threshold crossing is detected in only one subchannel, a tuple corresponding to the subchannel where the threshold crossing was registered, is accepted. Otherwise, an erasure decision is made. If a symbol other than the transmitted one is accepted, we say that an error has occurred. The block diagram of the DHA FH CDMA system with a threshold receiver is shown in Figure 1.

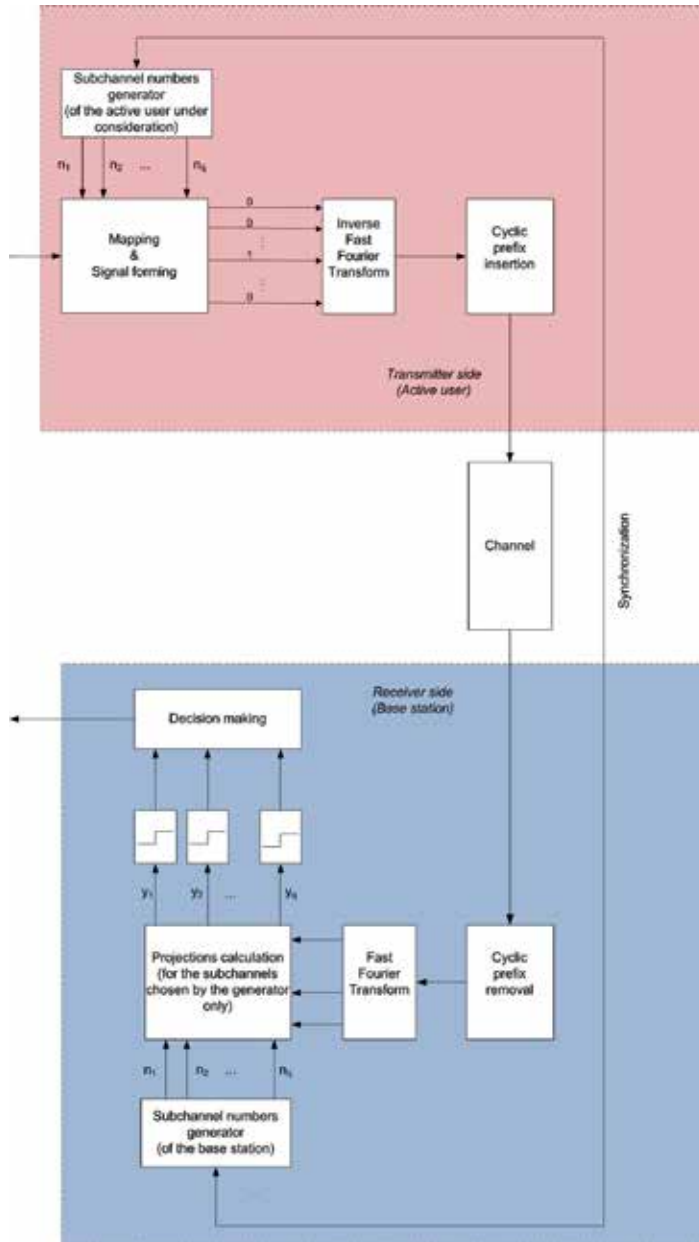


Fig. 1. DHA FH OFDMA system with threshold reception: block diagram.

Due to the above-made assumption on the availability of an ideal power control in the system, the signal of each user at the receiver end can be represented by a vector of a unit amplitude with a random phase uniformly distributed on the circle $[0, 2\pi]$. Since all the users transmit data asynchronously, the duration of interaction of a fixed user with other active users (we call them "interfering" users) is a random variable uniformly distributed on $[0, T]$. Therefore, components of the noise from each "interfering" user can be represented

by vectors with amplitudes uniformly distributed on $[0,1]$ and random phases uniformly distributed on $[0,2\pi]$.

Let us consider the projection of an output of the j -th subchannel onto a unit-amplitude vector with phase φ_j (here φ_j is the phase of the signal from the user under consideration at the receiver end.) The projection is of the form:

$$y_j = a_j + \sum_{k=1}^{K_j} r'_{jk} \cdot \cos(\varphi_{jk}) + n'_j \tag{3.1}$$

where a_j is the amplitude of the signal transmitted by this user through this subchannel

$$a_j = \begin{cases} 1 & j = j^* \\ 0 & j \neq j^* \end{cases}$$

K_j is the number of "interfering" users in the j -th subchannel; r'_{jk} is the amplitude of the noise caused by the interaction with the k -th "interfering" user, which is uniformly distributed on $[0,1]$; $\varphi_{jk} = \varphi_j - \varphi_k$, where φ_k is the phase of the noise caused by the interaction with the k -th "interfering" user, which is uniformly distributed on the circle $[0,2\pi]$; φ_j is the phase of the transmitted symbol at the receiver end, which is uniformly distributed on the circle $[0,2\pi]$; and n'_j is the projection of a vector corresponding to the white Gaussian noise.

Since the components of the white noise have the same variance, the value of the projection of the corresponding vector onto any direction is also normally distributed with the same variance. Since the phases of both the noise and the transmitted symbol are uniformly distributed on the circle $[0,2\pi]$, the phase difference φ_{jk} is also uniformly distributed on $[0,2\pi]$.

Since for parameters that adequately describe modern multiple access systems, the probability of a collision of multiplicity greater than two is much less than the probability of a collision of multiplicity two (see Appendix A.) further on only collisions of multiplicity two will be considered; the occurrence probability of such a collision is set to be equal to the collision occurrence probability

$$p_j = 1 - p_0. \tag{3.2}$$

where p_0 is the probability of no collision. Since transmission is asynchronous, during the time when a user transmits a symbol, each of the other active users chooses two subchannels. Therefore, the probability of no collision is given by

$$p_0 = \left(\frac{Q-1}{Q}\right)^{2(K-1)} \tag{3.3}$$

and the projection is given by:

$$y_j = a_j + \lambda \cos(a) + n'_j. \tag{3.4}$$

An expression for the density function of the value of the projection of the noise from the k -th “interfering” user onto a given vector follows from a formula due to (Feller, 1971) and is of the form:

$$f(z) = \frac{1}{\pi} \ln \left(\frac{1 + \sqrt{1 - z^2}}{|z|} \right). \tag{3.5}$$

Finding an analytic expression for the density function of y_j directly (for instance, using the convolution theorem) presents considerable difficulties. By definition (Lukacs, 1987), the characteristic function of a random variable $Z = \lambda \cdot \cos(a)$ is the expectation of the function $y = \varphi_\xi(\lambda, a) = e^{i\xi Z(\lambda, a)}$. This expectation can be defined in a straightforward manner:

$$g_Z(\xi) = \int_{-\infty}^{\infty} \int_{-\infty}^{\infty} \varphi_\xi(\lambda, a) \cdot f(\lambda, a) d\alpha d\lambda \tag{3.6}$$

here

$$f(\lambda, a) = \begin{cases} \frac{1}{2\pi} & \lambda \in [0, 1] \wedge a \in [0, 2\pi] \\ 0 & \text{otherwise} \end{cases} \text{ is the joint probability density function.}$$

Taking into account the domain of definition of the function, the characteristic function can be represented as follows:

$$g_Z(\xi) = \int_0^1 \int_0^{2\pi} \frac{e^{i\xi\lambda \cos(\alpha)}}{2\pi} d\alpha d\lambda. \tag{3.7}$$

Note that

$$J_0(\xi\lambda) = \frac{1}{2\pi} \int_0^{2\pi} e^{i\xi\lambda \cos(\varphi)} d\varphi. \tag{3.8}$$

is nothing but the zero-order Bessel function of the first kind of the variable $v = \xi\lambda$ (Watson, 1945). Integrating the series expansion of this function term by term, we obtain:

$$g^1(\xi) = \int_0^1 \left(1 + \sum_{k=1}^{\infty} (i)^{2k} \frac{(\xi\lambda)^{2k}}{2^{2k} (k!)^2} \right) d\lambda = 1 + \sum_{k=1}^{\infty} (i)^{2k} \frac{\xi^{2k}}{(2k+1)2^{2k} (k!)^2}. \tag{3.9}$$

By a property of characteristic functions, the desired density function of the variable y is of the form:

$$f(y, a, \sigma) = \int_{-\infty}^{\infty} e^{-i\xi y} g_Z(\xi) \cdot \chi(\xi, a, \sigma) d\xi, \quad (3.10)$$

where $\chi(\xi, a, \sigma)$ is the characteristic function of a normal distribution with mean a and variance σ . Taking into account $\int_{-\infty}^{\infty} e^{-i\xi y} \cdot \xi^n \cdot \chi(\xi, a, \sigma) d\xi = \frac{1}{(-i)^n} \frac{d^n \eta(y, a, \sigma)}{dy^n}$ we obtain

$$f_s(y, a, \sigma) = \sum_{k=1}^{\infty} \frac{1}{(2k+1)2^{2k}(k!)^2} \frac{d^{2k} \eta(y, a, \sigma)}{dy^{2k}}. \quad (3.11)$$

here $\eta(\xi, a, \sigma)$ is the probability density function of a normal distribution with mean a and standard deviation σ

This function characterizes the density function of the value of the projection of a subchannel output provided that a collision of multiplicity two occurred in the subchannel (i. e., there was one “interfering” user) and that the user under consideration transmitted a signal of amplitude a through this subchannel.

Thus, the conditional density function of the variable at the output of a subchannel, through which the user transmitted a symbol of amplitude a , is of the form:

$$\mu(y, a, \sigma) = \eta(y, a, \sigma)p_0 + (f(y, a, \sigma)(1 - p_0)). \quad (3.12)$$

Below we are using the obtained probability density function to solve the detection problem in the described system.

3.2 DHA FH OFDMA system with threshold reception: threshold choice and analytical expressions for error and erasure probabilities

Symbol detection in the described system boils down to choosing between two hypotheses:

H0: the user did not transmit any symbol through this subchannel ($a = 0$);

H1: the user transmitted a symbol through this subchannel ($a = 1$).

The maximum likelihood condition implies that:

$$\begin{aligned} \text{if } \frac{f_s(y|1)}{f_s(y|0)} \geq \frac{p_a(0)}{p_a(1)} \quad H_1 \text{ is accepted} \\ \text{if } \frac{f_s(y|1)}{f_s(y|0)} < \frac{p_a(0)}{p_a(1)} \quad H_0 \text{ is accepted} \end{aligned} \quad (3.13)$$

where $L = \frac{f_s(y|1)}{f_s(y|0)}$ is the likelihood ratio, and $p_a(1) = \frac{1}{q}$, $p_a(0) = 1 - p_a(1) = \frac{q-1}{q}$

a priori probabilities. Hence we obtain,

$$\frac{f_s(y|1)}{f_s(y|0)} = q - 1 . \quad (3.14)$$

Our goal is to find the threshold value y . The value will be found by solving the nonlinear equation (3.14) numerically.

Direct computation of the likelihood ratio on the left-hand side of (3.14) seems to be difficult. At the same time, numerical values of the conditional density function at any point can be computed using finitely many terms of the above-given expansion. To estimate these values to a given degree of accuracy, it suffices to find an expansion term, whose absolute value at a given point is less than the accuracy parameter and check that the same holds for the subsequent term too. Thus, the threshold finding problem is reduced to solving a nonlinear equation (3.14) which can be done numerically using specialized software packages. The solution of the equation (3.14) \hat{y} is the optimal (in a maximum a posteriori sense) threshold value.

Hereinbefore we have treated the process of assigning subchannels to the users in terms of series of random trials. Strictly speaking, when considering a set of subchannels, we are to consider the parameters of each consecutive test run as dependant on outcomes of the previous test runs. Consider the i -th subchannel of the q subchannels chosen by the subchannels number generator. Let us assume that k users were transmitting in $i-1$ previously considered subchannels. The probability of collision is to be estimated as

$$p'_i = \left(\frac{Q-i-1}{Q-i} \right)^{2(K-1)-k} .$$

However, since $i < q \ll Q$ and $k < K$

$$\left(\frac{Q-i-1}{Q-i} \right)^{2(K-1)-k} \approx \left(\frac{Q-1}{Q} \right)^{2(K-1)} .$$

Thus, in what follows we shall assume that the probability of collision in a certain subchannel does not depend on the situation in other subchannels.

The error probability is the probability that the threshold is not crossed in the subchannel, through which the user under consideration has transmitted a symbol and at the same time the threshold is crossed in one of the subchannels, where this user has not transmitted any signal (and only in it). This probability can be written as:

$$p_{err} \approx (q-1) \cdot \int_{-\infty}^{\hat{y}} f_s(y|1) dy \cdot \int_{\hat{y}}^{+\infty} f_s(y|0) dy \cdot \left(\int_{-\infty}^{\hat{y}} f_s(y|0) dy \right)^{q-2} . \quad (3.15)$$

To find the erasure probability, we shall find the probability of correct reception, i. e., the probability that the threshold crossing occurs only in the subchannel, through which the user has transmitted a symbol. This probability is described by the relation:

$$p_{cor} \approx \int_{\hat{y}}^{+\infty} f_s(y|1)dy \cdot \left(\int_{-\infty}^{\hat{y}} f_s(y|0)dy \right)^{q-1}. \quad (3.16)$$

Since correct reception, error, and erasure form an exhaustive group of events, we may claim that the erasure probability is

$$p_{ers} = 1 - p_{cor} - p_{err} \quad (3.17)$$

Note that the obtained expressions are approximate (due to the aforementioned assumptions). More exact expressions can be easily obtained using the same method. However in this case the obtained expressions will have a much more cumbersome form.

4.1 DHA FH OFDMA system with a MAXP receiver: system model and probabilistic description

In the previous section a threshold reception has been considered; i. e. a receiver, equipped with a subchannel number generator synchronized with that of the user under consideration, was to compare values of the projections of the signals received from the subchannels with a certain threshold and take a decision on the symbol sent by the user under consideration. Hereinafter a far more simple and intuitive reception strategy will be used; i. e. the receiver is to compute the projections of the signals from the respective subchannels and to choose the subchannel with a maximum projection. In what follows we shall refer to this receiver as a MAXimum Projection receiver (a MAXP receiver). The block diagram of the DHA FH CDMA system with a threshold receiver is shown in Figure 2.

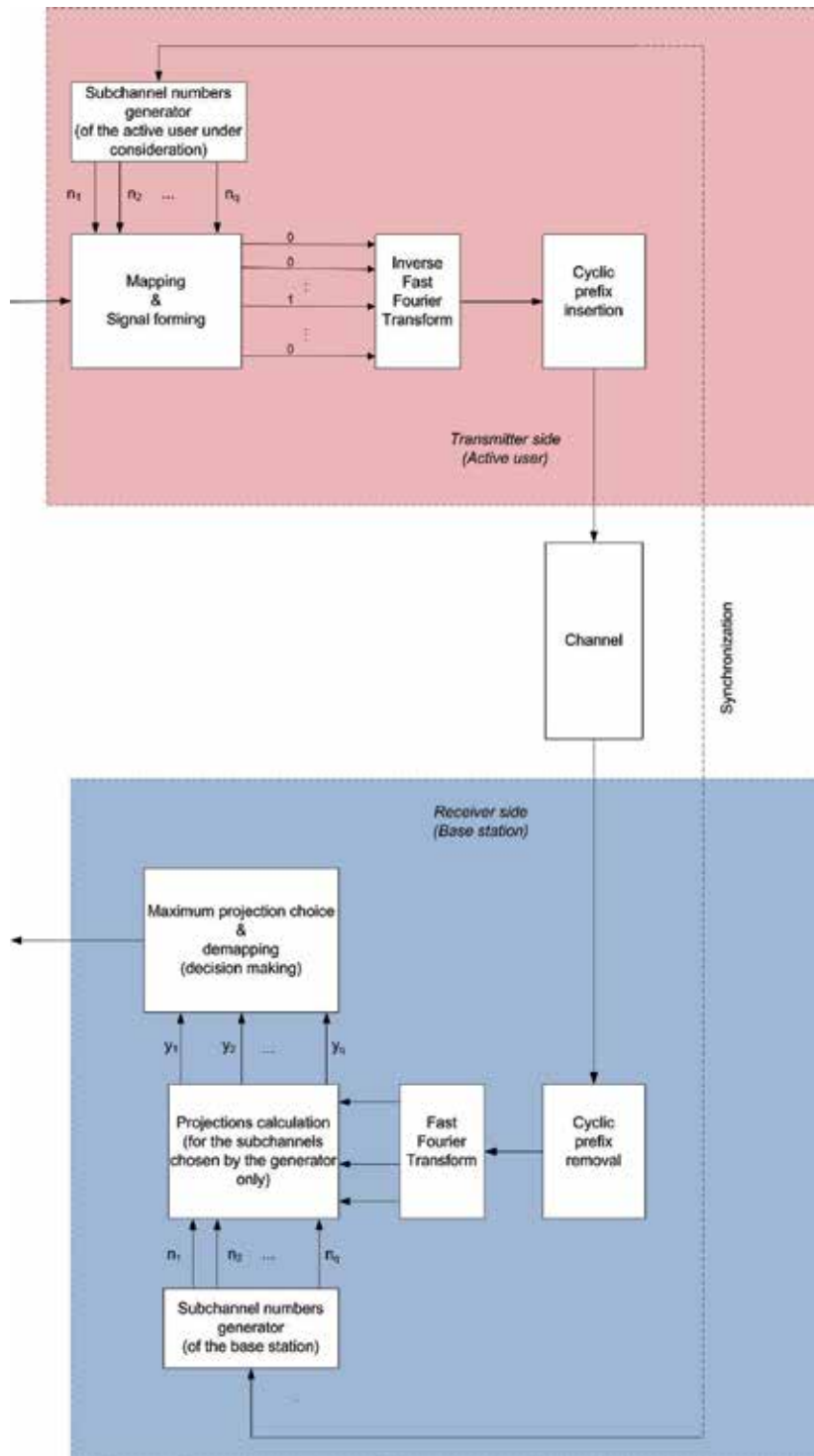


Fig. 2. DHA FH OFDMA system with a MAXP receiver: block diagram.

Note that in DHA FH CDMA with a threshold receiver an optimal threshold value is to be precomputed in advance. Moreover, as can be seen from the previous paragraphs, the optimal threshold value depends on the number of active users and SNR. In DHA FH CDMA with a MAXP receiver, on the other hand, neither additional computation nor any kind of side information is needed. It should be noted, however, that for DHA FH CDMA system with a threshold receiver and DHA FH CDMA system with a MAXP receiver different types of outer codes are to be used. In a DHA FH CDMA system with a threshold receiver outer codes capable of correcting erasures (a number of low density codes suited for the task were introduced recently) are to be used, whereas in a DHA FH CDMA system with a MAXP receiver only error correction is needed (woven and woven turbo codes seem to be the best solution in the case).

Let us consider a difference:

$$\delta_{j^*j} = y_{j^*} - y_j = a_{j^*} + \rho_{j^*j} + n, \tag{4.1}$$

here y_{j^*} is the projection of the output of the j^* -th subchannel (i. e. the subchannel, via which the user under consideration has actually transmitted a symbol); y_j is the projection of the output of the j -th subchannel ($j \in S, j \neq j^*$).

Note that for parameters that adequately describe modern multiple access systems, the probability of a collision of multiplicity greater than two is much less than the probability of a collision of multiplicity two. Therefore, hereinafter we are considering the case of a collision of multiplicity two only. Correspondingly we are to consider several distinct situations:

- a. A collision has occurred both in the j^* -th subchannel and in the j -th subchannel (see Figure 3).

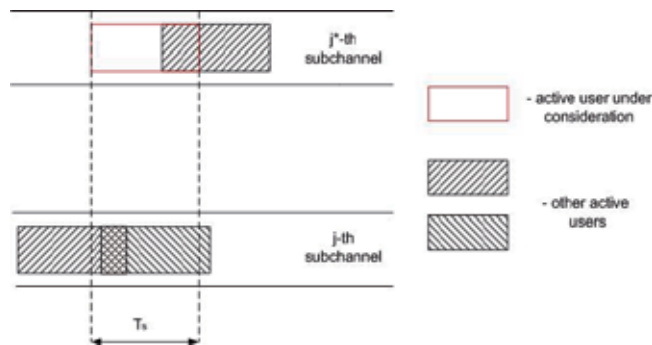


Fig. 3. "case a." (three interfering signals): diagram.

Then ρ_{j^*j} is given by:

$$\rho_{j^*j}(c^*, s, c) = \lambda \cos(\alpha) - \mu \cos(\beta) - \kappa \cos(\varphi). \tag{4.2}$$

- b. A collision has occurred in the j^* -th subchannel and a user has transmitted a symbol via the j -th subchannel. (see Figure 4).

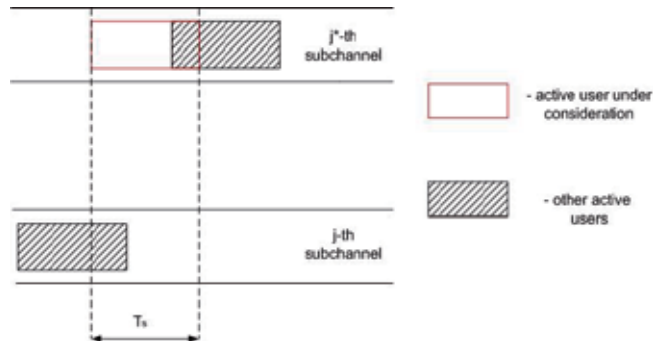


Fig. 4. "case b." (two interfering signals): diagram

Then ρ_{j^*j} is given by:

$$\rho_{j^*j}(c^*, s, \bar{c}) = \lambda \cos(\alpha) - \mu \cos(\beta). \tag{4.3}$$

- c. A collision has occurred in the j^* -th subchannel and none of the users has transmitted a symbol via the j -th subchannel (see Figure 5).

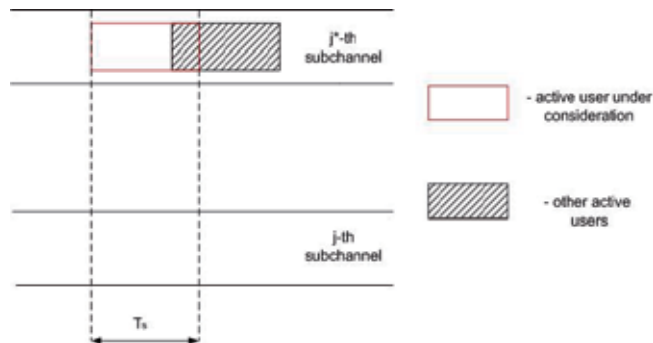


Fig. 5. "case c." (one interfering signal): diagram.

Then ρ_{j^*j} is given by:

$$\rho_{j^*j}(c^*, \bar{s}, \bar{c}) = \lambda \cos(\alpha). \tag{4.4}$$

- d. A user has transmitted a symbol via the j -th subchannel and no collision has occurred either in the j -th subchannel or in the j^* -th subchannel (see Figure 6).

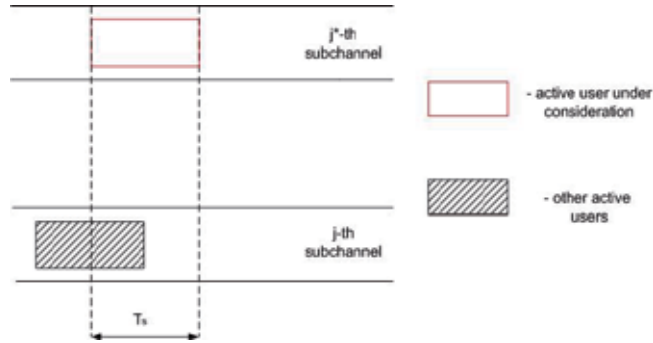


Fig. 6. "case d." (one interfering signal): diagram.

Then ρ_{j^*j} is given by:

$$\rho_{j^*j}(\bar{c}^*, s, \bar{c}) = -\mu \cos(\beta). \tag{4.5}$$

- e. A collision has occurred in the j -th subchannel and no collision has occurred in the j^* -th subchannel (see Figure 7).

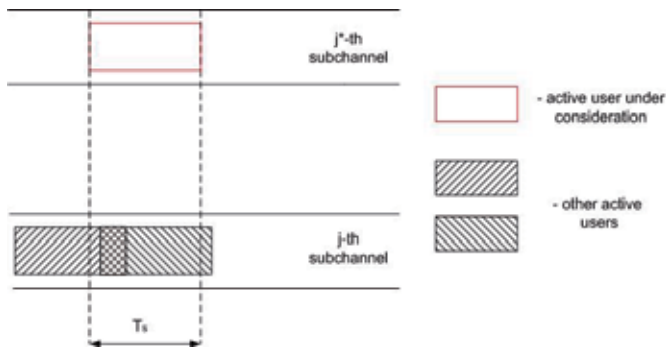


Fig. 7. "case e." (two interfering signals): diagram.

Then ρ_{j^*j} is given by:

$$\rho_{j^*j}(\bar{c}^*, s, c) = -\mu \cos(\beta) - \eta \cos(\varphi). \tag{4.6}$$

- f. No collision has occurred in the j^* -th subchannel and none of the users has transmitted a symbol via the j -th subchannel (see Figure 8).

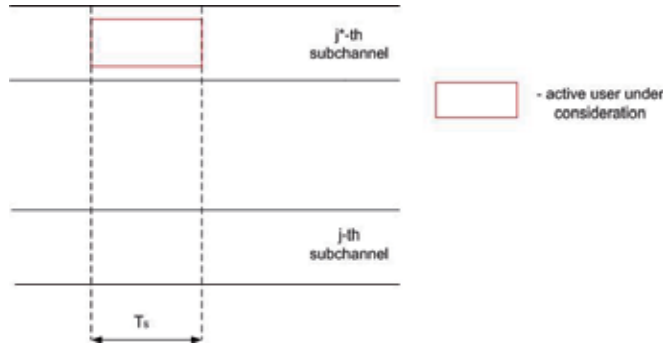


Fig. 8. "case f." (no interfering signals): diagram.

Then ρ_{j^*j} is given by:

$$\rho_{j^*j} = 0.$$

Note that the distribution of ρ_{j^*j} does not depend on the sign of the component since all the phases are distributed uniformly on $[0, 2\pi]$. Therefore $\rho_{j^*j}(c^*, \bar{s}, \bar{c})$ and $\rho_{j^*j}(\bar{c}^*, s, \bar{c})$ have the same distribution.

Moreover the probability density function of differences

$$\delta_{j^*j}(c^*, \bar{s}, \bar{c}) = a_{j^*} + \lambda \cos(\alpha) + n \quad \text{and} \quad \delta_{j^*j}(\bar{c}^*, s, \bar{c}) = a_{j^*} - \mu \cos(\beta) + n$$

can be obtained using the same method we have used to obtain the projection y_{j^*} and is given by

$$f^1(y, a, \sigma) = f_{\delta_{j^*j}(c^*, \bar{s}, \bar{c})}(y, a, \sigma) = f_{\delta_{j^*j}(\bar{c}^*, s, \bar{c})}(y, a, \sigma) = \sum_{k=1}^{\infty} \frac{1}{(2k+1)2^{2k}(k!)^2} \frac{d^{2k} \eta(y, a, \sigma \sqrt{2})}{dy^{2k}} \quad (4.7)$$

here $\eta(\xi, a, \sigma \sqrt{2})$ is the probability density function of a normal distribution with mean a and standard deviation $\sigma \sqrt{2}$

Analogously $\rho_{j^*j}(c^*, s, \bar{c})$ and $\rho_{j^*j}(\bar{c}^*, s, c)$ have the same distribution. Since all the components in (4.3) and (4.6) are independent the characteristic function is simply the product of the characteristic functions of the components:

$$g^2(\xi) = g^1(\xi) \cdot g^1(\xi) = 1 + \sum_{m=1}^{\infty} \sum_{k=1}^{\infty} (i)^{2k+2m} \frac{\xi^{2k+2m}}{(2k+1)(2m+1)2^{2k+2m}(k!m!)^2}$$

$$t = k + m$$

$$g^2(\xi) = 1 + \sum_{t=1}^{\infty} \frac{\xi^{2t}}{2^{2t}} \left(\sum_{k=1}^t \frac{1}{(2k+1)(2t-2k+1)(k!(t-k)!)} \right)$$

The probability density function of differences $\delta_{j,j}^*(c^*, s, \bar{c}) = a_{j^*} + \lambda \cos(\alpha) - \mu \cos(\beta) + n$ and $\delta_{j,j}(\bar{c}^*, s, c) = a_{j^*} - \mu \cos(\beta) - \eta \cos(\varphi) + n$ is given by:

$$\begin{aligned} f^2(y, a, \sigma) &= f_{\delta_{j,j}^*(c^*, s, \bar{c})}(y, a, \sigma) = f_{\delta_{j,j}(\bar{c}^*, s, c)}(y, a, \sigma) = \int_{-\infty}^{\infty} e^{-i\xi y} g^2(\xi) \cdot \chi(\xi, a, \sigma\sqrt{2}) d\xi, \\ f^2(y, a, \sigma) &= \sum_{t=0}^{\infty} \left(\frac{d^{2t} \eta(y, a, \sigma\sqrt{2})}{dy^{2t}} \frac{1}{2^{2t}} \left(\sum_{k=1}^t \frac{1}{(2k+1)(2t-2k+1)(k!(t-k)!)} \right) \right). \end{aligned} \quad (4.8)$$

Similarly the characteristic function of $\delta_{j,j}(c^*, s, c) = a_{j^*} + \lambda \cos(\alpha) - \mu \cos(\beta) - \kappa \cos(\varphi) + n$ is given by:

$$g^2(\xi) = g^1(\xi) \cdot g^1(\xi) \cdot g^1(\xi) = 1 + \sum_{k=1}^{\infty} \sum_{m=1}^{\infty} \sum_{w=1}^{\infty} (i)^{2k+2m+2w} \frac{\xi^{2k+2m+2w}}{(2k+1)(2m+1)(2w+1)2^{2k+2m+2w} (k!m!w!)^2}.$$

And the probability density function of difference $\delta_{j,j}^*(c^*, s, c)$ is

$$\begin{aligned} f^3(y, a, \sigma) &= f_{\delta_{j,j}^*(c^*, s, c)}(y, a, \sigma) = \\ &= \sum_{t=0}^{\infty} \left(\frac{d^{2t} \eta(y, a, \sigma\sqrt{2})}{dy^{2t}} \frac{1}{2^{2t}} \left(\sum_{k=1}^t \sum_{m=1}^k \frac{1}{(2k+1)(2m+1)(2t-2k-2m+1)(k!m!(t-k-m)!)} \right) \right). \end{aligned} \quad (4.9)$$

Note that difference $\delta_{j,j}^*(c^*, s, c) = a_{j^*} + n$ is simply a Gaussian viable.

4.2 DHA FH OFDMA system with a MAXP reception: error probability

To find the error probability let us consider the probability of correct reception. Correct reception is possible if (and only if) $\delta_{j,j} > 0 \forall j \in S, j \neq j^*$. As can be seen from what has been said the distribution of the differences $\delta_{j,j}$ depend on how many active users are there in the respective subchannels. Moreover, as has already been mentioned, we shall confine ourselves to the case of collisions of multiplicity two (in the subchannels chosen by the subchannel number generator of the active user under consideration). Let us consider the following situation: in the rest $q-1$ subchannels (i. e. in all the subchannels chosen by the subchannel number generator of the active user under consideration but for the one in use) there are exactly a subchannels where a collision has occurred (i. e. in each of the a subchannels 2 users were transmitting) b subchannels where users were transmitting but

no collision had occurred (i. e. there was 1 active user in each subchannel) and $c = q - 1 - a - b$ subchannels where no users were transmitting any data.

The probability of such a situation is given by:

$$p(a, b, q, Q, \Xi) = \frac{(q-1)!}{a!b!(q-1-a-b)!} (Q-q)^{\Xi-2a-b} \cdot \sum_{a=0}^{\lfloor \frac{\Xi}{2} \rfloor} \sum_{b=0}^{\Xi-2a} \frac{(q-1)!}{a!b!(q-1-a-b)!} (Q-q)^{\Xi-2a-b} \quad (4.10)$$

where Ξ is the total number of signals that can be transmitted via all the subchannels but for the one, via which the user under consideration has transmitted (see Appendix B.)

As has been already mentioned if the total number of active users amounts to K the number of signals that can interfere with the signal transmitted by the user under consideration is $K = 2 \cdot (K - 1)$ due to the transmission asynchrony. Thus, we are to consider two distinct cases:

- I. A collision has occurred in the subchannel, via which the user has transmitted a signal (this case obviously corresponds to the cases a.)-c.) from the previous section)
- II. No collision has occurred in the subchannel, via which the user has transmitted a signal (this case corresponds to the cases d.)-f.) from the previous section)

Since we are considering collisions of multiplicity two only in case II, the number of interfering users is given by $\Xi = 2(K - 1)$ and in case I by $\Xi = 2(K - 1) - 1$

To obtain the conditional probability note that in the abovementioned case, if a collision has occurred in the subchannel in use, we obtain a differences with pdf f^3 , b differences with pdf f^2 and $c = q - 1 - a - b$ differences with pdf f^1 . Thus, the conditional probability of error for the situation in question is given by:

$$p_e(a, b, q | \zeta = 1) = \left[1 - \left(\int_0^{+\infty} f^3(y, a, \sigma) dy \right)^a \left(\int_0^{+\infty} f^2(y, a, \sigma) dy \right)^b \left(\int_0^{+\infty} f^1(y, a, \sigma) dy \right)^{q-1-a-b} \right] \quad (4.11)$$

If there is no collision in the subchannel in use we obtain a differences with pdf f^2 , b differences with pdf f^1 and $c = q - 1 - a - b$ differences with pdf f^0 . The conditional probability is then given by:

$$p_e(a, b, q | \zeta = 0) = \left[1 - \left(\int_0^{+\infty} f^2(y, a, \sigma) dy \right)^a \left(\int_0^{+\infty} f^1(y, a, \sigma) dy \right)^b \left(\int_0^{+\infty} f^0(y, a, \sigma) dy \right)^{q-1-a-b} \right] \quad (4.12)$$

Thus, the probability of error is given by:

$$\begin{aligned}
 p_{err} \approx & \sum_{a=0}^{\lfloor \frac{K-2}{2} \rfloor} \sum_{b=0}^{2 \cdot (K-1-a)-1} (p_e(a,b,q|\zeta=1) p_i p(a,b,q,Q,2 \cdot (K-1)-1)) + \\
 & \text{for } K > 2 \quad (4.13) \\
 & + \sum_{a=0}^{\lfloor \frac{K-1}{2} \rfloor} \sum_{b=0}^{2 \cdot (K-1-a)} (p_e(a,b,q|\zeta=0) (1-p_i) p(a,b,q,Q,2 \cdot (K-1)))
 \end{aligned}$$

where p_i is the probability of collision (see (3.2)).

5. Conclusions and future work

Hereinabove a novel class of FH CDMA systems has been introduced: these are Dynamic Hopset Allocation FH CDMA systems. Two models with different reception strategies were considered: the DHA FH CDMA system with a threshold receiver and the DHA FH CDMA with a MAXP receiver. For both models a probabilistic description has been given using the approach based on characteristic function apparatus (for the DHA FH CDMA system with a threshold reception both a nonlinear equation for optimal threshold value and analytical expressions for error and erasure probabilities have been given; for the DHA FH CDMA with a MAXP receiver an analytical expression for the probability of error has been given).

However, even though several simplifying assumptions were used the obtained expressions are still complicated. Thus, obtaining rougher but less cumbersome expressions for the probability density functions of the random variables in question and respectively obtaining upper and lower bounds for error and erasure probabilities is one of the most important tasks. Moreover, it is to be mentioned that the expressions in question were obtained for the AWGN channel. Generalizing the obtained results for fading channel models (say, Raleigh, Nakagami ect.) is also a very important task. Obviously power control at the receiver side is unacceptable in this case. However, even in case of open loop nearly ideal power control it is to be taken into account that the power of a real life transmitter is bounded i. e. even in this case expressions for error and erasure probabilities will be different from those obtained for the AWGN channel.

6. Appendix A

Let us show that the probability of collisions of multiplicities greater than two is much less than the probability of a multiplicity-two collision. To this end, consider the process of choosing subchannels for transmission by users as a sequence of independent trials. Due to asynchronicity, during the time when a user transmits a symbol, each other active user chooses two subchannels. Thus, the process of choosing subchannels for transmission by other active users is equivalent to a series of $N = 2(K - 1)$ trials with "success" probability $p = 1/Q$ (in this case, it is the probability that there is chosen the subchannel which is used by the user under consideration). Therefore, the probability that a collision of multiplicity $m = k+1$ occurs in a given subchannel is the probability that in a series of $N = 2(K - 1)$ trials with "success" probability $p = 1/Q$ there are precisely k successes. This probability is given by the Bernoulli formula:

$$p_j(m) = C_N^k \cdot \left(\frac{1}{Q}\right)^k \cdot \left(1 - \frac{1}{Q}\right)^{N-k},$$

where $p_j(1)$ is the probability of no collision. Consider the ratio:

$$\kappa = \frac{p_j(m > 2)}{p_j(2)}.$$

It is seen from the aforesaid that:

$$\kappa = \frac{p_j(m > 2)}{p_j(2)} = \frac{\sum_{k=2}^N C_N^k \cdot \left(\frac{1}{Q}\right)^k \cdot \left(1 - \frac{1}{Q}\right)^{N-k}}{C_N^1 \cdot \left(\frac{1}{Q}\right)^1 \cdot \left(1 - \frac{1}{Q}\right)^{N-1}} = \frac{\sum_{k=2}^N C_N^k \cdot (Q-1)^{N-k}}{N \cdot (Q-1)^{N-1}}, \quad (6.1)$$

hence we get:

$$\kappa = \frac{\sum_{k=2}^N C_N^k \cdot (Q-1)^{-k+1}}{N}. \quad (6.2)$$

For each term in this expansion, we may write:

$$\frac{C_N^k \cdot (Q-1)^{-k+1}}{N} = \frac{N!}{(N-k)! \cdot (k)!} \cdot \frac{(Q-1)^{-k+1}}{N} = \frac{N \cdot (N-1) \cdot \dots \cdot (N-k+1)}{N \cdot (Q-1)^{k-1} \cdot (k)!} \ll \left(\frac{N-1}{(Q-1) \cdot 2}\right)^{k-1}. \quad (6.3)$$

thus, it is obvious that:

$$\kappa \ll \sum_{k=2}^N \left(\frac{N-1}{(Q-1) \cdot 2}\right)^{k-1}. \quad (6.4)$$

For any Q such that $Q > \frac{N-1}{2}$ (and in real-world systems we have $Q \gg N$), the expression on the right-hand side is a sum of a decreasing geometric progression starting with the second term:

$$\kappa \ll \sum_{k=1}^N \left(\frac{N-1}{(Q-1) \cdot 2}\right)^{k-1} - 1 \ll \sum_{k=1}^{\infty} \left(\frac{N-1}{(Q-1) \cdot 2}\right)^{k-1} - 1 = \frac{1}{1 - \frac{N-1}{(Q-1) \cdot 2}} - 1 \quad (6.5)$$

Note that $\frac{1}{1 - \frac{N-1}{(Q-1) \cdot 2}} - 1 \leq 1 \quad \forall Q, Q > \frac{N}{2}$.

As we have already noted, in real-world systems we have $Q \gg N$. Therefore, we may claim that for any parameters that adequately describe modern systems, the formulated statement certainly holds.

7. Appendix B

To obtain the probability of such a situation let us find the number of all sets complying with the abovementioned condition. To simplify the process let us treat the process of random subchannel choice performed by each of the active users in terms of assigning the interfering signals from other active users to the subchannels (the latter procedure is analogous to the classical examples with balls randomly placed into boxes). Let us again consider the subset of $q-1$ subchannels (these are all the subchannels chosen by the subchannel numbers generator but for the one, via which the user under consideration has transmitted) where there are exactly a subchannels, to which 2 signals are assigned, b subchannels, to which 1 signal is assigned, and the rest of the subchannels are empty (i. e. no signal has been assigned to none of these subchannels). The number of ways to perform such an assignment is given by

$$\tilde{N}(a, b, q-1) = \frac{(q-1)!}{a!b!(q-1-a-b)!} \tag{7.1}$$

Now let us consider the process of the symbol transmission by the user under consideration. In what follows we shall assume that there are Ξ interfering signals and that the assignment for all the subchannels chosen by the subchannel numbers generator (but for the one, via which the user under consideration has transmitted) is performed in the very way that has been discussed above. Thus we still have to assign $\tilde{k} = \Xi - 2a - b$ signals to $\Theta = Q - q$ subchannels (these are all the subchannels but for those chosen by the subchannel numbers generator of the user under consideration). However, from now on we needn't confine ourselves to the case of collisions of multiplicity two. The process of "assigning" the remaining subchannels to the signals boils down to a series of $\tilde{k} = \Xi - 2a - b$ trails, each of which is a random choice of one of $\Theta = Q - q$ subchannels. Thus the number of all the possible outcomes is

$$\hat{N}(q, Q, \Xi | a, b) = (Q - q)^{\Xi - 2a - b} \tag{7.2}$$

And the number of all the sets meeting the abovementioned requirements is given by

$$N(a, b, q, Q, \Xi) = \tilde{N}(a, b, q-1) \hat{N}(q, Q, \Xi | a, b) = \frac{(q-1)!}{a!b!(q-1-a-b)!} (Q - q)^{\Xi - 2a - b} \tag{7.3}$$

Apparently the probability of the occurrence of the aforesaid situation is the fraction of all the sets meeting the abovementioned requirements in the total number of sets. The latter is to be computed by summing $N(a, b, q, Q, \Xi)$ over all possible values of a and b :

$$p(a, b, q, Q, \Xi) = \frac{\frac{(q-1)!}{a!b!(q-1-a-b)!} (Q-q)^{\Xi-2a-b}}{\sum_{a=0}^{\lfloor \frac{\Xi}{2} \rfloor} \sum_{b=0}^{\Xi-2a} \frac{(q-1)!}{a!b!(q-1-a-b)!} (Q-q)^{\Xi-2a-b}}. \quad (7.4)$$

8. References

- Feller W., (1971). *An Introduction to Probability Theory and Its Applications vol.2*, Wiley and Sons, ISBN: 0471257095 / 0-471-25709-5, NY.
- Lukacs E., (1987). *Characteristic Functions, A Charles Griffin Book*, ISBN: 0195205782, London.
- Watson G. N., (1945). *Theory of Bessel Functions*, Cambridge Press, ISBN: 0521483913, Cambridge.
- Zigangirov K. Sh. (2004), *Theory of Code Division Multiple Access Communication*, IEEE Press, ISBN: 0471457124, Piscataway, New Jersey.
- Zyablov V. V. & Osipov D. S., (2008). On the optimum choice of a threshold in a frequency hopping OFDMA system. *Problems of Information Transmission*, Vol. 44, No. 2, 2008, pp. 91-98, ISSN 0032-9460.

Performance analysis of multi-server queueing system operating under control of a random environment

Che Soong Kim¹, Alexander Dudin², Valentina Klimenok²,
and Valentina Khramova²

¹*Sangji University
Korea*

²*Belarusian State University
Belarus*

1. Introduction

Since the early 1900th the Erlang multi-server queueing systems with losses (B -model or $M/M/N/0$ system) and with an infinite size buffer (C -model or $M/M/N$ system) provided good mathematical tools for capacity planning and performance evaluation in the classic telephone networks for many years. Good quality of the loss probability forecasting in real world networks based on the formulas obtained for the $M/M/N/0$ system and the delay prediction based on the formula obtained for the $M/M/N$ system was a rather surprising because the requirement that inter-arrival and service times have an exponential distribution, which is imposed in the $M/M/N/0$ and $M/M/N$ models, seems to be too strict. The interest of mathematicians to the fact of good matching of the calculated under debatable assumptions characteristics to their measured value in real world systems have lead to the following two results.

By efforts of many mathematicians (A. Ya. Khinchin and B. I. Grigelionis first of all), it was proved that the superposition of a large number of independent flows having uniformly small intensity approaches to the stationary Poisson input when the number of the superposed inputs tends to infinity. It explains the fact that the flows in classic telephone networks (where flows are composed by small individual flows from independent subscribers) have the exponentially distributed inter-arrival times.

Concerning the service time distribution, situation was more complicated. The real-life measurements have shown that the service (conversation) time can not be well approximated by means of the exponentially distributed random variable. So, due to the good matching of results obtained for the $M/M/N/0$ queue performance characteristics to characteristics of real systems modelled by such a queue, the hypothesis has arisen that the stationary state distribution in the $M/M/N/0$ queue is the same as the one in the $M/G/N/0$

queue conditional that the average service times in both models coincide. This property was called the invariant (or insensitivity) property of the model with respect to the service time distribution. The work [10] by B. A. Sevastjanov is the first one where this property was proven strictly.

So, the question why the Erlang's models give very good results for a practice was highlighted. The special books containing the tables for a loss probability under the given values of the number N of channels and intensities of the input and service exist. Different design problems (for a fixed value of permissible loss probability, to find the maximal intensity of the flow, which can be served by the line consisting of a fixed number of channels under the fixed average service time, or to find the necessary number of channels sufficient for transmission of the flow with a fixed intensity, etc) are solved by means of these tables.

However, the flows in the modern telecommunication networks have lost the nice properties of their predecessors in the old classic networks. In opposite to the stationary Poisson input (stationary ordinary input with no aftereffect), the modern real life flows are non-stationary, group and correlated. The *BMAP* (*Batch Markovian Arrival Process*) arrival process was introduced as a versatile Markovian point process (*VMPP*) by M.F. Neuts in the 70th. The original development of *VMPP* contained extensive notations; however these notations were simplified greatly in [7] and ever since this process bears the name *BMAP*. The class of *BMAP*s includes many input flows considered previously, such as stationary Poisson (M), Erlangian (E_k), Hyper-Markovian (HM), Phase-Type (PH), Interrupted Poisson Process (*IPP*), Markov Modulated Poisson Process (*MMPP*). Generally speaking, the *BMAP* is correlated, so it is ideal to model correlated and (or) bursty traffic in modern telecommunication networks.

As it was mentioned above, the question why the inter-arrival times in the classical networks have the exponential distribution was answered in literature. However, Erlang's assumption that the service time distribution has the exponential distribution is not supported by the real networks measurements. In the case of the $M/M/N/0$ system, good fitting of performance measures of this system with the respective measures of real world systems is easy explained by Sevastjanov's result. But in the case of the $M/M/N$ system, it was necessary to generalize results by Erlang to the cases of another, than exponential, service time distributions. This work was started by Erlang who offered so called Erlang's distribution. He introduced Erlangian of order k distribution as a distribution of a sum of k independent identically exponentially distributed random variables (phases). Further, so called phase type (PH) distribution was introduced into consideration as the straightforward generalization of Erlangian distribution, see, e.g., [8]. PH distribution includes as the special cases the exponential, Erlangian, Hyper-exponential, Coxian distributions. In our chapter we assume that service times at the fixed operation mode of the system have PH distribution.

It follows from discussion above that it is interesting to extend investigation of Erlang's models to the case of the *BMAP* input and PH type service process. This work was started by M. Combe in [1] and V. Klimenok in [5] where the *BMAP*/ M / N and *BMAP*/ M / N / 0 models, respectively, were investigated.

In paper [2], we investigated the *BMAP*/ PH / N / 0 model having no buffer. It was shown there that the stationary distribution of the system states essentially depends on the shape of

the service time distribution and so Sevastjanov's invariant property does not hold true in the case of the general *BMAP* arrival process. Here we analyze the *BMAP/PH/N/L* system with a finite buffer and the *BMAP/PH/N* system with infinite buffer. Simultaneously, we make one more essential generalization of the model under study. Motivation of this generalization is as follows.

Even if one will use such general models of the arrival and service process as the *BMAP* and *PH*, he may fail in application to practical systems. The reason is the following. Assumption that the input flow is described by the *BMAP* allows to take into consideration a burstiness, an effect of correlation in the arrival process and variation of inter-arrival times. Assumption that the service process is described by the *PH* distribution allows to take into consideration variation of service times. But the *BMAP* arrival process and *PH* service process are assumed to be stationary and independent of each other within the borders of the models of *BMAP/PH/N/L* type, $0 \leq L \leq \infty$. While in many real world systems the input and service processes are not absolutely stable and may be mutually dependent. They may be influenced by some external factors, e.g., the different level of the noise in the transmission channel, hardware degradation and recovering, change of the distance by a mobile user from the base station, parallel transmission of high priority information, etc. Information transmission channel modeled by means of the *BMAP/PH/N/L* queueing system can be a part of complex communication network. The rest of the network may essentially vary characteristics of the arrival and service process in this system by means of: (i) changing the bandwidth of the channel (due to reliability factors or the needs to provide good quality of service in another parts of the network when congestion occurs); (ii) changing the mean arrival rate due breakdowns, overflow or underflow of alternative information transmission channels. Thus, to get the mathematical tool for adequate modeling such information transmission channels, more complicated queues than the *BMAP/PH/N/L* queueing system should be analyzed. These queues, in addition to the account of complicated internal structure of the arrival and service processes by means of considering the *BMAP* and *PH*, must take into account the influence of random external factors. In some extent, it can be done by means of analyzing the models of queues operating in a random environment. Such an analysis is the topic of this chapter.

Importance of investigation of the queues operating in a random environment (*RE*) drastically increased in the last years due to the following reason. The flows of information in the modern communication networks are essentially heterogeneous. Some types of information are very sensitive with respect to a delay and an jitter but tolerant with respect to losses. Another ones are tolerant with respect to the delay but very sensitive with respect to the loss of the packets. So, different schemes of the dynamic bandwidth sharing among these types exist and are developing. They assume that, in the case of congestion, transmission of the delay tolerant flows is temporarily postponed to provide better conditions for transmission of the delay sensitive flows. Analysis of such schemes requires the probabilistic analysis of the multi-dimensional processes describing transmission process of the different flows. This analysis is often impossible due to the mathematical complexity. In such a case, it is reasonable to decompose a simultaneous consideration of all flows to separate analysis of the processes of transmission of the delay sensitive and the delay tolerant flows. To this end, we model transmission of the delay sensitive flows in terms of the queues with the controlled service or (and) arrival rate where the service or the

arrival rate can be changed depending on the queue length or the waiting time. Redistribution of a bandwidth to avoid congestion for the delay sensitive flows causes a variation, at random moments, of an available bandwidth for the delay tolerant flows. Correspondingly, the queues operating in a random environment naturally arise as the mathematical model for the delay tolerant flows transmission.

Mention that the *BMAP/PH/N/0* model operating in the *RE* was recently investigated in [4]. Short overview of the recent research of queues operating in the *RE* can be found there. In this chapter, we consider the models *BMAP/PH/N/L* and *BMAP/PH/N* operating in the *RE*.

2. The Mathematical Model

We consider the queueing system having N identical servers. The system behavior depends on the state of the stochastic process (random environment) $r_t, t \geq 0$, which is assumed to be an irreducible continuous time Markov chain with the state space $\{1, \dots, R\}$, $R \geq 2$, and the infinitesimal generator Q .

The input flow into the system is the following modification of the *BMAP*. In this input flow, the arrival of batches is directed by the process $\nu_t, t \geq 0$, (the underlying process) with the state space $\{0, 1, \dots, W\}$. Under the fixed state r of the *RE*, this process behaves as an irreducible continuous time Markov chain. Intensities of transitions of the chain $\nu_t, t \geq 0$, which are accompanied by arrival of k -size batch, are described by the matrices $D_k^{(r)}, k \geq 0$,

$r = \overline{1, R}$, with the generating function $D^{(r)}(z) = \sum_{k=0}^{\infty} D_k^{(r)} z^k, |z| \leq 1$. The matrix $D^{(r)}(1)$ is an

irreducible generator for all $r = \overline{1, R}$. Under the fixed state r of the random environment,

the average intensity $\lambda^{(r)}$ (fundamental rate) of the *BMAP* is defined as

$\lambda^{(r)} = \boldsymbol{\theta}^{(r)} (D^{(r)}(z))' \Big|_{z=1} \mathbf{e}$, and the intensity $\lambda_b^{(r)}$ of batch arrivals is defined as

$\lambda_b^{(r)} = \boldsymbol{\theta}^{(r)} (-D_0^{(r)}) \mathbf{e}$. Here the row vector $\boldsymbol{\theta}^{(r)}$ is the solution to the equations

$\boldsymbol{\theta}^{(r)} D^{(r)}(1) = \mathbf{0}, \boldsymbol{\theta}^{(r)} \mathbf{e} = 1$, \mathbf{e} is a column vector of appropriate size consisting of 1's. The

variation coefficient $c_{var}^{(r)}$ of intervals between batch arrivals is given by

$$\left(c_{var}^{(r)}\right)^2 = 2\lambda_b^{(r)} \boldsymbol{\theta}^{(r)} (-D_0^{(r)})^{-1} \mathbf{e} - 1,$$

while the correlation coefficient $c_{cor}^{(r)}$ of intervals between successive batch arrivals is calculated as

$$c_{cor}^{(r)} = \left(\lambda_b^{(r)} \boldsymbol{\theta}^{(r)} (-D_0^{(r)})^{-1} (D^{(r)}(1) - D_0^{(r)}) (-D_0^{(r)})^{-1} \mathbf{e} - 1\right) / \left(c_{var}^{(r)}\right)^2.$$

At the epochs of the process $r_t, t \geq 0$, transitions, the state of the process $\nu_t, t \geq 0$, is not changed, but the intensities of its transitions are immediately changed.

The service process is defined by the modification of the *PH*-type service time distribution. Service time is interpreted as the time until the irreducible continuous time Markov chain $m_t, t \geq 0$, with the state space $\{0, 1, \dots, M + 1\}$ reaches the absorbing state $M + 1$. Under the fixed value r of the random environment, transitions of the chain $m_t, t \geq 0$, within the state space $\{1, \dots, M\}$ are defined by an irreducible sub-generator $S^{(r)}$ while the intensities of transition into the absorbing state are defined by the vector $S_0^{(r)} = -S^{(r)}\mathbf{e}$. At the service beginning epoch, the state of the process $m_t, t \geq 0$, is chosen according to the probabilistic row vector $\beta^{(r)}, r = \overline{1, R}$. It is assumed that the state of the process $m_t, t \geq 0$, is not changed at the epoch of the process $r_t, t \geq 0$, transitions. Just the exponentially distributed sojourn time of the process $m_t, t \geq 0$, in the current state is re-started with a new intensity defined by the sub-generator corresponding to the new state of the random environment $r_t, t \geq 0$.

The system under consideration has $L, 0 \leq L \leq \infty$, waiting positions. In the case of an infinite buffer ($L = \infty$) all customers are always admitted to the system. In the case of a finite L , the system behaves as follows. If the system has all servers being busy at a batch arrival epoch, the batch looks for the available waiting position, and occupies it in case of success. If the system has all servers and all waiting positions being busy, the batch leaves the system forever and is considered to be lost. Due to a possibility of the batch arrivals, it can occur that there are free servers or waiting positions in the system at an arrival epoch, however the number of these positions is less than the number of the customers in an arriving batch. In such situation the acceptance of the customers to the system is realized according to the partial admission (*PA*) discipline (only a part of the batch corresponding to the number of free servers is allowed to enter the system while the rest of the batch is lost), the complete rejection (*CR*) discipline (a whole batch leaves the system if the number of free servers is less than the number of customers in the batch), complete admission (*CA*) discipline (a part of the batch corresponding to a number of free servers starts the service immediately while the rest of the batch waits for a service in the system in some special waiting space). All these disciplines are popular in the real life systems and got a lot of attention in the literature. Here, we consider all these disciplines.

Our aim is to calculate the stationary state distribution and main performance measures of the described queueing model.

For the use in the sequel, let us introduce the following notation:

- \mathbf{e}_n ($\mathbf{0}_n$) is a column (row) vector of size n , consisting of 1's (0's). Suffix may be omitted if the dimension of the vector is clear from context;
- $I(\mathbf{O})$ is an identity (zero) matrix of appropriate dimension (when needed the dimension of this matrix is identified with a suffix);
- $diag\{a_k, k = \overline{1, K}\}$ is a diagonal matrix with diagonal entries or blocks a_k ;
- \otimes and \oplus are symbols of the Kronecker product and sum of matrices;
- $\Omega^{\otimes l} = \underbrace{\Omega \otimes \dots \otimes \Omega}_l, l \geq 1, \Omega^{\otimes 0} = \mathbf{1}, \quad \Omega^{\oplus l} = \sum_{m=0}^{l-1} I_{n^m} \otimes \Omega \otimes I_{n^{l-m-1}}, l \geq 1$, where n is the dimension of square matrix Ω ;

- $D(z) = \sum_{k=0}^{\infty} \text{diag}\{D_k^{(r)}, r = \overline{1, R}\} z^k;$
- $\mathcal{D}_k^{(n)} = \text{diag}\{D_k^{(r)} \otimes I_{M^n}, r = \overline{1, R}\}, n = \overline{0, N}, k \geq 0;$
- $\mathcal{D}^{(n)}(z) = \sum_{k=0}^{\infty} \mathcal{D}_k^{(n)} z^k, n = \overline{0, N};$
- $\mathcal{B}_l^{(n)} = \text{diag}\{I_{\overline{W}} \otimes I_{M^n} \otimes (\boldsymbol{\beta}^{(r)})^{\otimes l}, r = \overline{1, R}\}, n = \overline{1, N}, \overline{W} = W + 1;$
- $\mathcal{S}^{(n)} = \text{diag}\{I_{\overline{W}} \otimes (\mathbf{S}^{(r)})^{\oplus n}, r = \overline{1, R}\}, n = \overline{1, N};$
- $\mathcal{S} = \text{diag}\{\mathbf{S}^{(r)}, r = \overline{1, R}\};$
- $\mathcal{S}_0^{(n)} = \text{diag}\{I_{\overline{W}} \otimes (\mathbf{S}_0^{(r)})^{\oplus n}, r = \overline{1, R}\}, n = \overline{1, N};$
- $\overline{\mathcal{S}}_0^{(N)} = \text{diag}\{I_{\overline{W}} \otimes (\mathbf{S}_0^{(r)} \boldsymbol{\beta}^{(r)})^{\oplus N}, r = \overline{1, R}\};$
- $\mathcal{C}^{(n)} = Q \otimes I_{\overline{W}} \otimes I_{M^n} + \mathcal{D}_0^{(n)} + \mathcal{S}^{(n)}, n = \overline{0, N};$
- $\overline{\mathcal{C}}^{(n)} = Q \otimes I_{\overline{W}} \otimes I_{M^{\min(n, N)}} + \mathcal{D}_0^{(\min(n, N))} + \sum_{k=N+L-n+1}^{\infty} \mathcal{D}_k^{(\min(n, N))} + \mathcal{S}^{(\min(n, N))}, n = \overline{0, N};$
- $\overline{\mathcal{C}}^{(N+L)} = Q \otimes I_{\overline{W}} \otimes I_{M^N} + \sum_{k=0}^{\infty} \mathcal{D}_k^{(N)} + \mathcal{S}^{(N)}.$

3. Process of the System States

It is easy to see that operation of the considered queueing model is described in terms of the regular irreducible continuous-time Markov chain

$$\xi_t = \{n_t, r_t, v_t, m_t^{(1)}, \dots, m_t^{(\min\{n_t, N\})}\}, t \geq 0,$$

where

- n_t is the number of customers in the system, where $n_t = \overline{0, N+L}$ in case of *PA* and *CR* disciplines and $n_t \geq 0$ in case of *CA* discipline;
- r_t is the state of the random environment, $r_t = \overline{1, R};$
- v_t is the state of the *BMAP* underlying process, $v_t = \overline{0, W};$
- $m_t^{(n)}$ is the phase of *PH* service process in the n th busy server, $m_t^{(n)} = \overline{1, M},$
 $n_t = \overline{1, N},$ (we assume here that the busy servers are numerated in order of their occupying, i.e. the server, which begins the service, is appointed the maximal number among all busy servers; when some server finishes the service, the servers are correspondingly enumerated) at epoch $t, t \geq 0.$

Let us enumerate the states of the chain $\xi_t, t \geq 0,$ in the lexicographic order and form the row vectors \mathbf{p}_n of probabilities corresponding to the state n of the first component of the process $\xi_t, t \geq 0.$ Denote also $\mathbf{p} = (\mathbf{p}_0, \mathbf{p}_1, \mathbf{p}_2, \dots).$

It is well known that the vector \mathbf{p} satisfies the system of the linear algebraic equations (so called equilibrium equations or Chapman-Kolmogorov equations) of the form:

$$\mathbf{p}A = \mathbf{0}, \quad \mathbf{p}\mathbf{e} = 1, \tag{1}$$

where A is the infinitesimal generator of the Markov chain $\xi_t, t \geq 0$.

Structure of this generator and methods of system (1) solution vary depending on the admission discipline.

3.1. The Case of Partial Admission Discipline

Lemma 1. Infinitesimal generator A of the Markov chain $\xi_t, t \geq 0$, in the case of partial admission discipline has the following block structure:

$$A = (A_{n,n'})_{n,n'=0,\overline{N+L}} = \begin{pmatrix} \mathcal{C}^{(0)} & \Psi_{1,1}^{(0)} & \dots & \Psi_{N-1,N-1}^{(0)} & \Psi_{N,N}^{(0)} & \Psi_{N+1,N}^{(0)} & \dots & \Psi_{N+L-1,N}^{(0)} & \hat{\Psi}_{N+L,N}^{(0)} \\ \mathcal{S}_0^{(1)} & \mathcal{C}^{(1)} & \dots & \Psi_{N-2,N-2}^{(1)} & \Psi_{N-1,N-1}^{(1)} & \Psi_{N,N-1}^{(1)} & \dots & \Psi_{N+L-2,N-1}^{(1)} & \hat{\Psi}_{N+L-1,N-1}^{(1)} \\ O & \mathcal{S}_0^{(2)} & \dots & \Psi_{N-3,N-3}^{(2)} & \Psi_{N-2,N-2}^{(2)} & \Psi_{N-1,N-2}^{(2)} & \dots & \Psi_{N+L-3,N-2}^{(2)} & \hat{\Psi}_{N+L-2,N-2}^{(2)} \\ \vdots & \vdots & \ddots & \vdots & \vdots & \vdots & \ddots & \vdots & \vdots \\ O & O & \dots & \mathcal{C}^{(N-1)} & \Psi_{1,1}^{(N-1)} & \Psi_{2,1}^{(N-1)} & \dots & \Psi_{L,1}^{(N-1)} & \hat{\Psi}_{L+1,1}^{(N-1)} \\ O & O & \dots & \mathcal{S}_0^{(N)} & \mathcal{C}^{(N)} & \mathcal{D}_1^{(N)} & \dots & \mathcal{D}_{L-1}^{(N)} & \hat{\mathcal{D}}_L^{(N)} \\ O & O & \dots & O & \overline{\mathcal{S}}_0^{(N)} & \mathcal{C}^{(N)} & \dots & \mathcal{D}_{L-2}^{(N)} & \hat{\mathcal{D}}_{L-1}^{(N)} \\ \vdots & \vdots & \ddots & \vdots & \vdots & \vdots & \ddots & \vdots & \vdots \\ O & O & \dots & O & O & O & \dots & \overline{\mathcal{S}}_0^{(N)} & \overline{\mathcal{C}}^{(N+L)} \end{pmatrix}$$

where

$$\Psi_{m,m'}^{(k)} = \mathcal{D}_m^{(k)} \mathcal{B}_{m'}^{(k)}, \quad k = \overline{0, N-1}, \quad m \geq 1, \quad m' = \overline{1, N},$$

$$\hat{\Psi}_{m_1, m'}^{(k)} = \sum_{m=m_1}^{\infty} \Psi_{m,m'}^{(k)}, \quad \hat{\mathcal{D}}_{m_1}^{(k)} = \sum_{m=m_1}^{\infty} \mathcal{D}_m^{(k)}.$$

Proof of the Lemma follows from analysis of Markov chain $\xi_t, t \geq 0$, transitions during an infinitesimal interval. Block entries of the generator have the following meaning. The non-diagonal entries of the matrix $\mathcal{C}^{(k)}$ define intensity of transition of the components $\{r_t, \nu_t, m_t^{(1)}, \dots, m_t^{(n_t)}\}$ of the Markov chain $\xi_t, t \geq 0$, which do not lead to the change of the number k of busy servers. The diagonal entries of the matrix $\mathcal{C}^{(k)}$ are negative and define, up to the sign, intensity of leaving the corresponding states of the Markov chain $\xi_t, t \geq 0$. The entries of the matrix $\Psi_{m,m'}^{(k)} = \mathcal{D}_m^{(k)} \mathcal{B}_{m'}^{(k)}$ define intensity of transitions of the components $\{r_t, \nu_t, m_t^{(1)}, \dots, m_t^{(n_t)}\}$ of the Markov chain $\xi_t, t \geq 0$, which are accompanied by arrival of m

customers and occupying m' servers conditional the number of busy servers is k . The entries of the matrix $S_0^{(k)}$ define intensity of transitions, which are accompanied by a departure of a customer, conditional the number of busy servers is k .

To solve system (1) with the matrix A defined by Lemma 1, we use the effective numerically stable procedure developed in [2] that exploits the special structure of the matrix A (it is upper block Hessenberg) and probabilistic meaning of the unknown vector \mathbf{p} . This procedure is given by the following statement.

Theorem 1. In case of partial admission, the stationary probability vectors $\mathbf{p}_i, i = \overline{0, N+L}$, are computed as follows:

$$\mathbf{p}_l = \mathbf{p}_0 F_l, l = \overline{1, N+L},$$

where the matrices F_l are calculated recurrently:

$$F_l = \left(\bar{A}_{0,l} + \sum_{i=1}^{l-1} F_i \bar{A}_{i,l} \right) \left(-\bar{A}_{l,l} \right)^{-1}, l = \overline{1, N+L-1},$$

$$F_{N+L} = \left(A_{0,N+L} + \sum_{i=1}^{N+L-1} F_i A_{i,N+L} \right) \left(-A_{N+L,N+L} \right)^{-1},$$

the matrices $\bar{A}_{l,N+L}$ are calculated from the backward recursions:

$$\bar{A}_{l,N+L} = A_{i,N+L}, i = \overline{0, N+L},$$

$$\bar{A}_{i,l} = A_{i,l} + \bar{A}_{i,l+1} G_l, i = \overline{0, l}, l = N+L-1, N+L-2, \dots, 0,$$

the matrices $G_l, l = \overline{0, N+L-1}$, are calculated from the backward recursion:

$$G_i = \left(-A_{i+1,i+1} - \sum_{l=1}^{N+L-i-1} A_{i+1,i+l+1} G_{i+l} G_{i+l-1} \dots G_{i+1} \right)^{-1} A_{i+1,i},$$

$$i = N+L-1, N+L-2, \dots, 0,$$

the vector \mathbf{p}_0 is calculated as the unique solution to the following system of linear algebraic equations:

$$\mathbf{p}_0 \bar{A}_{0,0} = 0, \quad \mathbf{p}_0 \left(\sum_{l=1}^{N+L} F_l \mathbf{e} + \mathbf{e} \right) = 1.$$

3.2. The Case of Complete Rejection Discipline

Lemma 2. Infinitesimal generator A of the Markov chain $\xi_t, t \geq 0$, in the case of complete rejection discipline has the following block structure:

$$A = \left(A_{n,n'} \right)_{n,n'=\overline{0, N+L}} =$$

$$= \begin{pmatrix} \bar{C}^{(0)} & \Psi_{1,1}^{(0)} & \dots & \Psi_{N-1,N-1}^{(0)} & \Psi_{N,N}^{(0)} & \Psi_{N+1,N}^{(0)} & \dots & \Psi_{N+L-1,N}^{(0)} & \Psi_{N+L,N}^{(0)} \\ \mathcal{S}_0^{(1)} & \bar{C}^{(1)} & \dots & \Psi_{N-2,N-2}^{(1)} & \Psi_{N-1,N-1}^{(1)} & \Psi_{N,N-1}^{(1)} & \dots & \Psi_{N+L-2,N-1}^{(1)} & \Psi_{N+L-1,N-1}^{(1)} \\ O & \mathcal{S}_0^{(2)} & \dots & \Psi_{N-3,N-3}^{(2)} & \Psi_{N-2,N-2}^{(2)} & \Psi_{N-1,N-2}^{(2)} & \dots & \Psi_{N+L-3,N-2}^{(2)} & \Psi_{N+L-2,N-2}^{(2)} \\ \vdots & \vdots & \ddots & \vdots & \vdots & \vdots & \ddots & \vdots & \vdots \\ O & O & \dots & \bar{C}^{(N-1)} & \Psi_{1,1}^{(N-1)} & \Psi_{2,1}^{(N-1)} & \dots & \Psi_{L,1}^{(N-1)} & \Psi_{L+1,1}^{(N-1)} \\ O & O & \dots & \mathcal{S}_0^{(N)} & \bar{C}^{(N)} & \mathcal{D}_1^{(N)} & \dots & \mathcal{D}_{L-1}^{(N)} & \mathcal{D}_L^{(N)} \\ O & O & \dots & O & \bar{\mathcal{S}}_0^{(N)} & \bar{C}^{(N)} & \dots & \mathcal{D}_{L-2}^{(N)} & \mathcal{D}_{L-1}^{(N)} \\ \vdots & \vdots & \ddots & \vdots & \vdots & \vdots & \ddots & \vdots & \vdots \\ O & O & \dots & O & O & O & \dots & \bar{\mathcal{S}}_0^{(N)} & \bar{C}^{(N+L)} \end{pmatrix}.$$

The proof of the Lemma is analogous to the proof of the previous Lemma and takes into account the fact that the number of customers in the system does not change when the number of customers in an arriving batch exceeds the number of free servers.

To solve system (1) with the matrix A defined by Lemma 2, we also use the procedure described by Theorem 1.

3.3. The Case of Complete Admission Discipline

Lemma 3. Infinitesimal generator A of the Markov chain $\xi_t, t \geq 0$, in the case of complete admission discipline has the following block structure:

$$A = (A_{n,n'})_{n,n' \geq 0} =$$

$$= \begin{pmatrix} C^{(0)} & \Psi_{1,1}^{(0)} & \dots & \Psi_{N,N}^{(0)} & \Psi_{N+1,N}^{(0)} & \dots & \Psi_{N+L-1,N}^{(0)} & \Psi_{N+L,N}^{(0)} & \Psi_{N+L+1,N}^{(0)} & \dots \\ \mathcal{S}_0^{(1)} & C^{(1)} & \dots & \Psi_{N-1,N-1}^{(1)} & \Psi_{N,N-1}^{(1)} & \dots & \Psi_{N+L-2,N-1}^{(1)} & \Psi_{N+L-1,N-1}^{(1)} & \Psi_{N+L,N-1}^{(1)} & \dots \\ O & \mathcal{S}_0^{(2)} & \dots & \Psi_{N-2,N-2}^{(2)} & \Psi_{N-1,N-2}^{(2)} & \dots & \Psi_{N+L-3,N-2}^{(2)} & \Psi_{N+L-2,N-2}^{(2)} & \Psi_{N+L-1,N-2}^{(2)} & \dots \\ \vdots & \vdots & \ddots & \vdots & \vdots & \ddots & \vdots & \vdots & \vdots & \vdots \\ O & O & \dots & \Psi_{1,1}^{(N-1)} & \Psi_{2,1}^{(N-1)} & \dots & \Psi_{L,1}^{(N-1)} & \Psi_{L+1,1}^{(N-1)} & \Psi_{L+2,1}^{(N-1)} & \dots \\ O & O & \dots & C^{(N)} & \mathcal{D}_1^{(N)} & \dots & \mathcal{D}_{L-1}^{(N)} & \mathcal{D}_L^{(N)} & \mathcal{D}_{L+1}^{(N)} & \dots \\ O & O & \dots & \bar{\mathcal{S}}_0^{(N)} & C^{(N)} & \dots & \mathcal{D}_{L-2}^{(N)} & \mathcal{D}_{L-1}^{(N)} & \mathcal{D}_L^{(N)} & \dots \\ \vdots & \vdots & \ddots & \vdots & \vdots & \ddots & \vdots & \vdots & \vdots & \dots \\ O & O & \dots & O & O & \dots & C^{(N)} & \mathcal{D}_1^{(N)} & \mathcal{D}_2^{(N)} & \dots \\ O & O & \dots & O & O & \dots & \bar{\mathcal{S}}_0^{(N)} & \bar{C}^{(N+L)} & O & \dots \\ O & O & \dots & O & O & \dots & O & \bar{\mathcal{S}}_0^{(N)} & \bar{C}^{(N+L)} & \dots \\ \vdots & \vdots & \ddots & \vdots & \vdots & \ddots & \vdots & \vdots & \vdots & \ddots \end{pmatrix}.$$

Essential difference of complete admission discipline is that the state space of the Markov chain $\xi_t, t \geq 0$, is infinite and this makes its analysis more complicated. However, the block

rows, except the first $N + L$ boundary block rows, have only two non-zero blocks and this Markov chain behaves as Quasi-Death process when the state of the first component n_t of the Markov chain $\xi_t, t \geq 0$, is greater than $N + L$. It allows to construct effective stable algorithm for calculation of the stationary distribution of this Markov chain. Note, that although the state space of the Markov chain $\xi_t, t \geq 0$, is infinite, this Markov chain is ergodic under the standard assumptions about the parameters of the *BMAP* input, the *PH* type service and the random environment. The algorithm for calculation of the stationary distribution is given in the following statement.

Theorem 2. In case of complete admission discipline, the stationary probability vectors $\mathbf{p}_l, l \geq 0$, are calculated as follows:

$$\mathbf{p}_l = \mathbf{p}_0 F_l, l \geq 1,$$

where the matrices F_l are calculated recurrently

$$F_l = \left(\bar{A}_{0,l} + \sum_{i=1}^{l-1} F_i \bar{A}_{i,l} \right) \left(-\bar{A}_{l,l} \right)^{-1}, l \geq 1,$$

the matrices $\bar{A}_{i,l}$ are calculated as:

$$\bar{A}_{i,l} = A_{i,l} + \sum_{k=1}^{\infty} A_{i,l+k} G^{\max\{0, l+k-N-L\}} G_{\min\{N+L, l+k\}-1} G_{\min\{N+L, l+k\}-2} \dots G_l, \quad i = 0, \dots, l, \quad l \geq 1,$$

the matrix G has a form

$$G = -\left(\bar{C}^{(N+L)} \right)^{-1} \bar{S}_0^{(N)},$$

the matrices $G_i, i = \overline{0, N+L-1}$, are calculated from the backward recursion

$$G_i = -\left(A_{i+1, i+1} + \sum_{l=i+2}^{\infty} A_{i+1, l} G^{\max\{0, l-N-L\}} \cdot G_{\min\{N+L, l\}-1} \cdot G_{\min\{N+L, l\}-2} \dots \cdot G_{i+1} \right)^{-1} A_{i+1, i},$$

the vector \mathbf{p}_0 is the unique solution of the system:

$$\mathbf{p}_0 \bar{A}_{0,0} = 0, \quad \mathbf{p}_0 \left(\sum_{l=1}^{\infty} F_l \mathbf{e} + \mathbf{e} \right) = 1.$$

The proof of the Theorem follows from the theory of multi-dimensional Markov chains with continuous time, see [6]. It is worth to note that Neuts' matrix G , which is usually found numerically as solution to matrix equation, see [9], here is obtained in the explicit form.

3.4. The Case of an Infinite Size of a Buffer ($L=\infty$)

The system under consideration in this section has an infinite waiting space. If an arriving batch of customers sees idle servers, a part of the batch corresponding to the number of free servers occupy these servers while the rest of the batch joins the queue. If the system has all servers being busy at a batch arrival epoch, all customer of the batch go to the queue.

Lemma 3. Infinitesimal generator A of the Markov chain $\xi_t, t \geq 0$, has the following block structure:

$$A = (A_{n,n'})_{n,n' \geq 0} = \begin{pmatrix} \mathcal{C}^{(0)} & \Psi_{1,1}^{(0)} & \Psi_{2,2}^{(0)} & \dots & \Psi_{N-1,N-1}^{(0)} & \Psi_{N,N}^{(0)} & \Psi_{N+1,N}^{(0)} & \Psi_{N+2,N}^{(0)} & \dots \\ \mathcal{S}_0^{(1)} & \mathcal{C}^{(1)} & \Psi_{1,1}^{(1)} & \dots & \Psi_{N-2,N-2}^{(1)} & \Psi_{N-1,N-1}^{(1)} & \Psi_{N,N-1}^{(1)} & \Psi_{N+1,N-1}^{(1)} & \dots \\ O & \mathcal{S}_0^{(2)} & \mathcal{C}^{(2)} & \dots & \Psi_{N-3,N-3}^{(2)} & \Psi_{N-2,N-2}^{(2)} & \Psi_{N-1,N-2}^{(2)} & \Psi_{N,N-2}^{(2)} & \dots \\ \vdots & \vdots & \vdots & \ddots & \vdots & \vdots & \vdots & \vdots & \ddots \\ O & O & O & \dots & \mathcal{C}^{(N-1)} & \Psi_{1,1}^{(N-1)} & \Psi_{2,1}^{(N-1)} & \Psi_{3,1}^{(N-1)} & \dots \\ O & O & O & \dots & \mathcal{S}_0^{(N)} & \mathcal{C}^{(N)} & \mathcal{D}_1^{(N)} & \mathcal{D}_2^{(N)} & \dots \\ O & O & O & \dots & O & \overline{\mathcal{S}}_0^{(N)} & \mathcal{C}^{(N)} & \mathcal{D}_1^{(N)} & \dots \\ O & O & O & \dots & O & O & \overline{\mathcal{S}}_0^{(N)} & \mathcal{C}^{(N)} & \dots \\ \vdots & \vdots & \vdots & \dots & \vdots & \vdots & \vdots & \vdots & \ddots \end{pmatrix}. \quad (2)$$

In what follows we perform the steady state analysis of the Markov chain having generator of form (2). To this end, we use the results for continuous time multi-dimensional Markov chain (QTMC) presented in [6].

Theorem 3. The necessary and sufficient condition for existence of the Markov chain $\xi_t, t \geq 0$, stationary distribution is the fulfillment of the inequality

$$\rho = \lambda / \bar{\mu} < 1, \quad (3)$$

where

$$\begin{aligned} \lambda &= \mathbf{x}_1 D'(z) \Big|_{z=1} \mathbf{e}, \\ \bar{\mu} &= \mathbf{x}_2 \text{diag} \left\{ \left(\mathbf{S}_0^{(r)} \right)^{\oplus N}, r = \overline{1, R} \right\} \mathbf{e}, \end{aligned} \quad (4)$$

the vectors $\mathbf{x}_n, n = 1, 2$, are the unique solutions to the following systems of linear algebraic equations:

$$\mathbf{x}_1 (Q \otimes I_{\overline{W}} + D(1)) = \mathbf{0}, \quad \mathbf{x}_1 \mathbf{e} = 1, \quad (5)$$

$$\mathbf{x}_2 \left(Q \otimes I_{M^N} + \text{diag} \left\{ \left(S^{(r)} + \mathbf{S}_0^{(r)} \beta^{(r)} \right)^{\oplus N}, r = \overline{1, R} \right\} \right) = \mathbf{0}, \quad \mathbf{x}_2 \mathbf{e} = 1. \quad (6)$$

Proof. Using the results of [6], we directly obtain the desired condition in the form of inequality

$$\mathbf{x} \left[\mathcal{C}^{(N)} z + z \mathcal{D}^{(N)}(z) \right]_{z=1}^{\prime} \mathbf{e} < 0, \tag{7}$$

where \mathbf{x} is the unique solution to the system

$$\mathbf{x} \left(Q \otimes I_{\overline{WM}^N} + \mathcal{D}^{(N)}(1) + \mathcal{S}^{(N)} + \overline{\mathcal{S}}_0^{(N)} \right) = \mathbf{0}, \quad \mathbf{x} \mathbf{e} = 1. \tag{8}$$

It is easy to show that inequality (7) is reduced to the following inequality:

$$\mathbf{x}_1 D'(z) \Big|_{z=1} \mathbf{e} < \mathbf{x}_2 \text{diag} \left\{ \left(\mathbf{S}_0^{(r)} \right)^{\oplus N}, r = \overline{1, R} \right\} \mathbf{e}, \tag{9}$$

where $\mathbf{x}_1 = \mathbf{x} \left(I_{R\overline{W}} \otimes \mathbf{e}_{M^N} \right)$, $\mathbf{x}_2 = \mathbf{x} \left(I_R \otimes \mathbf{e}_{\overline{W}} \otimes I_{M^N} \right)$.

To get the equations for the row vectors \mathbf{x}_1 and \mathbf{x}_2 , we multiply equation (8) by the matrices $I_{R\overline{W}} \otimes \mathbf{e}_{M^N}$ and $I_R \otimes \mathbf{e}_{\overline{W}} \otimes I_{M^N}$ respectively. After multiplication and some algebra we obtain equations (5), (6) for the vectors \mathbf{x}_1 and \mathbf{x}_2 . So, inequality (9) is equivalent to inequality (3) and the theorem is proved.

The value ρ has a meaning of the system load. In what follows we assume inequality (3) be fulfilled.

To solve system (1) with the matrix A defined by (2), we use the effective numerically stable procedure [6] based on the account special structure of the matrix A , notion of the censored Markov chain and probabilistic meaning of the unknown vector \mathbf{p} . For more detail see [6]. This procedure is given by the following statement.

Theorem 4. The stationary probability vectors $\mathbf{p}_l, l \geq 0$, are calculated as follows:

$$\mathbf{p}_l = \mathbf{p}_0 F_l, l \geq 1,$$

where the matrices F_l are calculated recurrently:

$$F_l = \left(\overline{A}_{0,l} + \sum_{i=1}^{l-1} F_i \overline{A}_{i,l} \right) \left(-\overline{A}_{l,l} \right)^{-1}, l \geq 1,$$

the matrices $\overline{A}_{i,l}$ are calculated as:

$$\begin{aligned} \overline{A}_{i,l} &= A_{i,l} + \overline{A}_{i,l+1} G_l, \quad 0 \leq i \leq l < N, \\ \overline{A}_{i,l} &= A_{i,l} + \overline{A}_{i,l+1} G, \quad l \geq \max\{i, N\}, \quad i \geq 0, \end{aligned}$$

the matrix G is calculated from the equation

$$G = \left(-\sum_{l=1}^{\infty} A_{N+1, N+l} G^{l-1} \right)^{-1} A_{N+1, N},$$

the matrices $G_i, i = \overline{0, N-1}$, are calculated from the backward recursion:

$$G_i = - \left(A_{i+1, i+1} + \sum_{l=i+2}^{\infty} A_{i+1, l} G^{\max\{0, l-N\}} \cdot G_{\min\{N, l\}-1} \cdot G_{\min\{N, l\}-2} \cdots \cdot G_{i+1} \right)^{-1} A_{i+1, i},$$

the vector \mathbf{p}_0 is calculated as the unique solution to the following system of linear algebraic equations:

$$\mathbf{p}_0 \bar{A}_{0,0} = \mathbf{0}, \quad \mathbf{p}_0 \left(\sum_{l=1}^{\infty} F_l \mathbf{e} + \mathbf{e} \right) = 1.$$

4. Performance Measures

Having the probability vector \mathbf{p} been computed, we are able to calculate performance measures of the considered model. The main performance measure in the case of a finite buffer is the probability P_{loss} that an arbitrary customer will be lost (the loss probability).

Theorem 5. The loss probability P_{loss} is calculated as follows

(i) in the case of *PA* discipline

$$P_{loss} = 1 - \frac{1}{\lambda} \sum_{i=0}^{N+L-1} \mathbf{p}_i \sum_{k=0}^{N+L-i} (k+i-N-L) \mathcal{D}_k^{(i)} \mathbf{e}, \quad (10)$$

(ii) in the case of *CR* discipline

$$P_{loss} = 1 - \frac{1}{\lambda} \sum_{i=0}^{N+L-1} \mathbf{p}_i \sum_{k=0}^{N+L-i} k \mathcal{D}_k^{(i)} \mathbf{e}, \quad (11)$$

(iii) in the case of *CA* discipline

$$P_{loss} = 1 - \frac{1}{\lambda} \sum_{i=0}^{N+L-1} \mathbf{p}_i \sum_{k=0}^{\infty} k \mathcal{D}_k^{(i)} \mathbf{e}. \quad (12)$$

Proofs of formulae (10) - (12) are analogous. So, we will prove only formula (10). According to a formula of the total probability, the probability P_{loss} is calculated as

$$P_{loss} = 1 - \sum_{i=0}^{N+L-1} \sum_{k=1}^{\infty} P_k D_i^{(k)} R^{(i,k)} \quad (13)$$

where P_k is a probability that an arbitrary customer arrives in a batch consisting of k customers; $D_i^{(k)}$ is a probability to see i servers being busy at the epoch of the k -size batch arrival; $R^{(i,k)}$ is a probability that an arbitrary customer will not be lost conditional it arrives in a batch consisting of k customers and i servers are busy at the arrival epoch.

It can be shown that

$$P_i^{(k)} = \frac{\mathbf{p}_i \mathcal{D}_k^{(i)} \mathbf{e}}{\mathbf{x}_1 \mathcal{D}_k^{(0)} \mathbf{e}}, \quad i = \overline{0, N+L-1}, k \geq 1, \quad (14)$$

$$P_k = \frac{k \mathbf{x}_1 \mathcal{D}_k^{(0)} \mathbf{e}}{\mathbf{x}_1 D(z) \Big|_{z=1} \mathbf{e}} = k \frac{\mathbf{x}_1 \mathcal{D}_k^{(0)} \mathbf{e}}{\lambda}, \quad k \geq 1, \quad (15)$$

$$R^{(i,k)} = \begin{cases} 1, & k \leq N+L-i, \\ \frac{N+L-i}{k}, & k > N+L-i, \quad i = \overline{0, N+L-1}. \end{cases} \quad (16)$$

By substituting (14)-(16) into (13) after some algebra we get (10). \square

Some performance measures for the case $L = \infty$ are presented below.

- The probability to see i customers in the system

$$p_i = \overline{\mathbf{p}_i \mathbf{e}}, \quad i \geq 0;$$

- The mean number of customers in the system

$$L_{queue} = \sum_{i=0}^{\infty} i \overline{\mathbf{p}_i \mathbf{e}};$$

- The probability to see n busy servers

$$p_n = \overline{\mathbf{p}_n \mathbf{e}}, \quad n = \overline{0, N-1}, \quad p_N = \sum_{n=N}^{\infty} \overline{\mathbf{p}_n \mathbf{e}};$$

- The mean number of busy servers

$$N_{busy} = \sum_{n=1}^N n \overline{\mathbf{p}_n \mathbf{e}} + N \sum_{n=N}^{\infty} \overline{\mathbf{p}_n \mathbf{e}};$$

- The mean number N_{idle} of idle servers

$$N_{idle} = N - N_{busy};$$

• The vector $\hat{\mathbf{p}}_n$ whose $(\overline{W}(r-1) + \nu + 1)$ -th entry is the joint probability to see n busy servers, the random environment in the state r and the process ν_i in the state ν

$$\hat{\mathbf{p}}_n = \overline{\mathbf{p}_n (I_{R\overline{W}} \otimes \mathbf{e}_{M^n})}, \quad n = \overline{0, N-1}, \quad \hat{\mathbf{p}}_N = \sum_{n=N}^{\infty} \overline{\mathbf{p}_n (I_{R\overline{W}} \otimes \mathbf{e}_{M^n})};$$

• The vector of conditional means of the number of busy servers under the fixed states of the random environment

$$\mathbf{n} = \sum_{n=1}^{\infty} \min\{n, N\} \hat{\mathbf{p}}_n (I_R \otimes \mathbf{e}_{\overline{V}}) \text{diag}\{q_r^{-1}, r = \overline{1, R}\};$$

• The vector $\mathbf{p}^{(a)}(n)$ whose $(\overline{W}(r-1) + \nu + 1)$ -th entry is the joint probability that an arbitrary arriving call sees n busy servers and the random environment in the state r and the state of the process ν_t becomes ν after the arrival epoch

$$\mathbf{p}^{(a)}(n) = \lambda^{-1} \hat{\mathbf{p}}_n D'(z) \Big|_{z=1}, n = \overline{0, N};$$

• The probability $p^{(a)}(n)$ that an arbitrary arriving call sees n busy servers

$$p^{(a)}(n) = \mathbf{p}^{(a)}(n) \mathbf{e}, n = \overline{0, N};$$

• The vector $\mathbf{p}_b^{(a)}(n)$ whose $(\overline{W}(r-1) + \nu + 1)$ -th entry is the joint probability that an arbitrary arriving batch of size k sees n busy servers and the random environment in the state r and the state of the process ν_t becomes ν after the arrival epoch

$$\mathbf{p}_b^{(a)}(k, n) = \lambda_b^{-1} \hat{\mathbf{p}}_n \text{diag}\{D_k^{(r)}, r = \overline{1, R}\}, n = \overline{0, N}, k \geq 1,$$

where $\lambda_b = \mathbf{x}(D(1) - D(0)) \mathbf{e}$;

• The probability $p_b^{(a)}(k, n)$ that an arbitrary arriving batch of size k sees n busy servers

$$p_b^{(a)}(k, n) = \mathbf{p}_b^{(a)}(k, n) \mathbf{e}, n = \overline{0, N}, k \geq 1;$$

• The vector $\mathbf{p}_b^{(a)}(n)$ whose $(\overline{W}(r-1) + \nu + 1)$ -th entry is the joint probability that an arbitrary arriving batch sees n busy servers and the random environment in the state r and the state of the process ν_t becomes ν after the arrival epoch

$$\mathbf{p}_b^{(a)}(n) = \lambda_b^{-1} \hat{\mathbf{p}}_n (D(1) - D(0)), n = \overline{0, N};$$

• The probability $p_b^{(a)}(n)$ that an arbitrary arriving batch sees n busy servers

$$p_b^{(a)}(n) = \mathbf{p}_b^{(a)}(n) \mathbf{e}, n = \overline{0, N};$$

• The probability P_{imm} that an arbitrary customer will enter the service immediately upon arrival (without visiting a buffer)

$$P_{imm} = \lambda^{-1} \sum_{i=0}^{N-1} \mathbf{p}_i \sum_{k=0}^{N-i} (k+i-N) \mathcal{D}_k^{(i)} \mathbf{e}.$$

5. Actual Sojourn Time

Let $v_a(s)$, $Re s > 0$, be the Laplace-Stieltjes transform (LST) of the sojourn time distribution and \bar{v}_a be the mean sojourn time of the arbitrary customer in the system.

Theorem 6. The Laplace-Stieltjes transform $v_a(s)$ is calculated as follows

$$v_a(s) = \frac{1}{\lambda} \left\{ \sum_{i=0}^{N-1} \mathbf{p}_i \sum_{k=1}^{\infty} \min\{k, N-i\} \mathcal{D}_k^{(i)} (I_R \otimes \mathbf{e}_{\bar{W}_m^i}) + \right. \tag{17}$$

$$\left. + \sum_{i=0}^{\infty} \mathbf{p}_i \sum_{k=\max\{1, N-i+1\}}^{\infty} \mathcal{D}_k^{(\min\{i, N\})} \mathcal{B}^{(\max\{0, N-i\})} \sum_{l=\max\{1, N-i+1\}}^k (\mathcal{F}(s))^{i-N+l} (I_R \otimes \mathbf{e}_{M^N}) \right\} \mathcal{H}(s) \mathbf{e}_R,$$

where

$$\begin{aligned} \mathcal{H}(s) &= -diag\{\boldsymbol{\beta}^{(r)}, r = \overline{1, R}\} (sI - (Q \otimes I_M + \mathcal{S}))^{-1} diag\{\mathbf{S}_0^{(r)}, r = \overline{1, R}\}, \\ \mathcal{F}(s) &= -\left(sI - \left(Q \otimes I_{M^N} + diag\left\{ (S^{(r)})^{\oplus N}, r = \overline{1, R} \right\} \right) \right)^{-1} diag\left\{ (\mathbf{S}_0^{(r)} \boldsymbol{\beta}^{(r)})^{\oplus N}, r = \overline{1, R} \right\}, \\ \mathcal{B}^{(n)} &= diag\left\{ \mathbf{e}_{\bar{W}} \otimes I_{M^{N-n}} \otimes (\boldsymbol{\beta}^{(r)})^{\oplus n}, r = \overline{1, R} \right\}, \quad n = \overline{0, N}, \\ \mathcal{S} &= diag\{S^{(r)}, r = \overline{1, R}\}. \end{aligned}$$

Proof. We derive the expression for the LST $v_a(s)$ by means of the method of collective marks (method of additional event, method of catastrophes) for references see, e.g. [3], [11]. To this end, we interpret the variable s as the intensity of some virtual stationary Poisson flow of catastrophes. So, $v_a(s)$ has the meaning of probability that no one catastrophe arrives during the sojourn time of an arbitrary customer. Then, the proof of the theorem follows from the formula of total probability if we analyze the states of the system at an arbitrary customer arrival epoch and take into account the probabilistic meaning of the involved matrices. The matrix $\mathcal{H}(s)$ is the matrix LST of an arbitrary customer service time distribution. It is the R -size square matrix whose (r, r') entry is a probability that during the service time of a customer a catastrophe does not arrive and the process $r_t, t \geq 0$, transits from the state r to the state $r', r, r' = \overline{1, R}$. It is defined by the formula:

$$\mathcal{H}(s) = diag\{\boldsymbol{\beta}^{(r)}, r = \overline{1, R}\} \int_0^{\infty} e^{-st} e^{(Q \otimes I_M + diag\{S^{(r)}, r = \overline{1, R}\})t} dt diag\{\mathbf{S}_0^{(r)}, r = \overline{1, R}\}.$$

Analogously, the entries of the matrix LST $\mathcal{F}(s)$ are the probabilities of no catastrophe arrival and corresponding transitions of the process $\{r_t, m_t^{(1)}, \dots, m_t^{(N)}\}, t \geq 0$, during the time

interval from an arbitrary moment when all N servers are busy till the first epoch when one of these servers finishes the service of a customer. This matrix is defined by the formula:

$$\mathcal{F}(s) = \int_0^\infty e^{-st} e^{(Q \otimes I_{M^N} + \text{diag}\{(S^{(r)})^{\otimes N}, r = \overline{1, R}\})t} dt \text{diag}\left\{(\mathbf{S}_0^{(r)} \boldsymbol{\beta}^{(r)})^{\otimes N}, r = \overline{1, R}\right\}.$$

Theorem 7. The mean sojourn time \bar{v}_a of an arbitrary customer in the system is calculated by

$$\begin{aligned} \bar{v}_a = & -\frac{1}{\lambda} \left\{ \sum_{i=0}^\infty \mathbf{p}_i \sum_{k=\max\{1, N-i+1\}}^\infty \mathcal{D}_k^{(\min\{i, N\})} \mathcal{B}^{(\max\{0, N-i\})} \sum_{l=\max\{1, N-i+1\}}^k \sum_{m=0}^{i+l-N-1} (\mathcal{F}(0))^m \mathcal{F}'(0) (I_R \otimes \mathbf{e}_{M^N}) + \right. \\ & \left. + \sum_{i=0}^{N-1} \mathbf{p}_i \sum_{k=1}^\infty \min\{k, N-i\} \mathcal{D}_k^{(i)} (I_R \otimes \mathbf{e}_{\overline{WM}^i}) \mathcal{H}'(0) + \right. \\ & \left. + \sum_{i=0}^\infty \mathbf{p}_i \sum_{k=\max\{1, N-i+1\}}^\infty \mathcal{D}_k^{(\min\{i, N\})} \mathcal{B}^{(\max\{0, N-i\})} \sum_{l=\max\{1, N-i+1\}}^k (\mathcal{F}(0))^{i-N+l} (I_R \otimes \mathbf{e}_{M^N}) \mathcal{H}'(0) \right\} \mathbf{e}_R \end{aligned} \quad (18)$$

where

$$\begin{aligned} \mathcal{H}'(0) &= -\text{diag}\left\{\boldsymbol{\beta}^{(r)}, r = \overline{1, R}\right\} [Q \otimes I_M + \mathcal{S}]^{-2} \text{diag}\left\{S_0^{(r)}, r = \overline{1, R}\right\}, \\ \mathcal{F}'(0) &= -\left[Q \otimes I_{M^N} + \text{diag}\left\{(S^{(r)})^{\otimes N}, r = \overline{1, R}\right\}\right]^{-2} \text{diag}\left\{(\mathbf{S}_0^{(r)} \boldsymbol{\beta}^{(r)})^{\otimes N}, r = \overline{1, R}\right\}. \end{aligned}$$

Proof. To get expression (18) for \bar{v}_a we differentiate (17) at the point $s=0$ and use the formula $\bar{v}_a = -\bar{v}'_a(0)$.

6. Numerical Examples

The goal of the numerical experiments is to demonstrate the feasibility of the proposed algorithms for computing the stationary distributions of the number of customers and the sojourn time in the system and to give some insight into behavior of the considered queueing systems. In particular, the following issues are addressed:

- Comparison of the mean sojourn time of an arbitrary customer and the probability of immediate access to the servers in the systems with varying traffic intensities and different coefficients of correlation in the $BMAP$ s (experiment #1);
- Comparison of the mean sojourn time of an arbitrary customer and the probability of immediate access to the servers in the original system in a RE and in more simple queueing systems for different system loads (experiments #2);
- Demonstration of possible positive effect of redistribution of traffic between the peak traffic periods and normal traffic periods (experiment #3);
- Comparison of the exact value of performance measures of the system in a RE and their simple engineering approximations in cases of slowly and quickly varying RE (experiment #4);
- Investigation of the rate of convergence of the mean sojourn time and the probability of immediate access in the system with the finite buffer to corresponding

performance measures of the system with an infinite buffer when the buffer size increases (experiment #5);

- Demonstration of the possibility to apply the presented results for optimization of the number of servers in the system (experiment #6).

In numerical examples, we consider the systems operating in the *RE* which has two states ($R = 2$). The generator of the random environment is $Q = \begin{pmatrix} -5 & 5 \\ 15 & -15 \end{pmatrix}$. The stationary distribution of the *RE* states is defined by the vector $\mathbf{q} = (0.75, 0.25)$. The number of servers is $N = 3$.

In the presented examples, we will use several different *MAP* s and *BMAP* s for description of the arrival process and two *PH* type distributions for description of the service processes under the fixed value of the *RE*. For the use in the sequel, let us define these processes.

We consider four arrival processes *MAP*_{*r*}, $r = \overline{1,4}$. *MAP*_{*r*} is defined by the matrices $D_0^{(r)}$, $D_1^{(r)}$, $r = \overline{1,4}$, where

$$\begin{aligned}
 D_0^{(1)} &= \begin{pmatrix} -3.9 & 0.15 & 0.15 \\ 0.13 & -0.6 & 0.1 \\ 0.15 & 0.14 & -0.5 \end{pmatrix}, & D_1^{(1)} &= \begin{pmatrix} 3.5 & 0.08 & 0.02 \\ 0.03 & 0.3 & 0.04 \\ 0.02 & 0.06 & 0.13 \end{pmatrix}; \\
 D_0^{(2)} &= \begin{pmatrix} -6.4 & 0.1 & 0.1 \\ 0.04 & -0.6 & 0.1 \\ 0.07 & 0.1 & -0.44 \end{pmatrix}, & D_1^{(2)} &= \begin{pmatrix} 6.06 & 0.12 & 0.02 \\ 0.01 & 0.4 & 0.05 \\ 0.01 & 0.06 & 0.2 \end{pmatrix}; \\
 D_0^{(3)} &= \begin{pmatrix} -2.9 & 0.73 & 0.77 \\ 0.87 & -3.06 & 0.53 \\ 0.85 & 0.5 & -2 \end{pmatrix}, & D_1^{(3)} &= \begin{pmatrix} 0.68 & 0.45 & 0.27 \\ 0.48 & 1.08 & 0.1 \\ 0.35 & 0.05 & 0.25 \end{pmatrix}; \\
 D_0^{(4)} &= \begin{pmatrix} -1.3 & 0.21 & 0.17 \\ 0.16 & -2.04 & 0.21 \\ 0.01 & 0.16 & -1.3 \end{pmatrix}, & D_1^{(4)} &= \begin{pmatrix} 0.46 & 0.32 & 0.14 \\ 0.13 & 1.34 & 0.2 \\ 0.02 & 0.01 & 1.1 \end{pmatrix}.
 \end{aligned}$$

All these *MAP* s have fundamental rate $\lambda^{(r)} = 1.25$. The *MAP*₁ has the squared variation coefficient $(c_{var}^{(1)})^2 = 4$ and the coefficient of correlation of the lengths of successive inter-arrival times $c_{cor}^{(1)} = 0.2$. For the rest of the *MAP* s, the corresponding parameters are:

$$(c_{var}^{(2)})^2 = 4, \quad c_{cor}^{(2)} = 0.3; \quad (c_{var}^{(3)})^2 = 1.097, \quad c_{cor}^{(3)} = 0.0052; \quad (c_{var}^{(4)})^2 = 1.037, \quad c_{cor}^{(4)} = 0.0065.$$

Based on these *MAP* s, we construct batch flows *BMAP* s as follows. If the *MAP* is defined by the matrices $D_0^{(r)}$, and $D_1^{(r)}$, $r = \overline{1,4}$, then the *BMAP* having the maximal size of a batch equal to K is defined by the matrices $D_0^{(r)}$, $D_k^{(r)} = D_1^{(r)} q^{k-1} (1-q) / (1-q^K)$, $k = \overline{1, K}$, $r = \overline{1, R}$, where $q = 0.9$.

Following this way, we construct the $BMAP_1, BMAP_2, BMAP_3, BMAP_4$ flows based on the $MAP_1, MAP_2, MAP_3, MAP_4$ correspondingly, with $K = 5$. Note that the coefficients of variation and correlation of all $BMAP$ s are the same as these coefficients for the corresponding MAP s. Fundamental rate $\lambda^{(r)}$ and the mean batch size $\bar{k}^{(r)}$ of the $BMAP$ s are the following: $\lambda^{(1)} = \lambda^{(2)} = \lambda^{(3)} = \lambda^{(4)} = 3.488$, $\bar{k}^{(1)} = \bar{k}^{(2)} = \bar{k}^{(3)} = \bar{k}^{(4)} = 1.989$.

The $PH_r, r = 1, 2$, service processes are defined by the vectors $\beta^{(1)} = (1, 0)$, $\beta^{(2)} = (0.2, 0.8)$ and the matrices

$$S^{(1)} = \begin{pmatrix} -4 & 4 \\ 0 & -4 \end{pmatrix}, \quad S^{(2)} = \begin{pmatrix} -10 & 2 \\ 2 & -20 \end{pmatrix}.$$

The mean rates of service are $\mu^{(1)} = 2, \mu^{(2)} = 14$. The coefficients of variation of the service time distribution are defined by $(c_{var}^{(1)})^2 = 0.5, (c_{var}^{(2)})^2 = 1.24$.

In the **first experiment**, we compare the dependence of \bar{v}_a and P_{imm} on the system load ρ for the $BMAP$ s with different correlations.

In the experiment we use service processes defined by PH_1 and PH_2 and four different input flows which are described by $BMAP_1, BMAP_2, BMAP_3$ and $BMAP_4$ having the same mean fundamental rate equal to 3.488 but different correlation coefficients.

We consider three queueing systems which have different combinations of the $BMAP$ s under the first and second states of the RE .

The input flow in the first system is defined by $BMAP_1$ and $BMAP_2$. These $BMAP$ s have large coefficients of correlation $c_{cor}^{(1)} = 0.2$ and $c_{cor}^{(2)} = 0.3$.

The input flow in the second system is defined by $BMAP_3$ and $BMAP_4$. These $BMAP$ s have small coefficients of correlation $c_{cor}^{(3)} = 0.0052$ and $c_{cor}^{(4)} = 0.0065$.

In the third system the input is defined by $BMAP_1$ and $BMAP_4$. The correlation coefficients of these $BMAP$ s differ significantly.

Figures 1 and 2 show the dependence of the mean sojourn time \bar{v}_a and the probability P_{imm} on the system load ρ for all these systems. Variation of the value of ρ in all experiments is performed by means of multiplying the entries of the matrices, which define the corresponding $BMAP$, by some varying factor γ . This implies the increase of the fundamental rate of all the $BMAP$ by a factor γ . Service time distributions are not modified. It is clear from Figure 1 that correlation in $BMAP$ has a great impact on the sojourn time in the system. An increase of correlation at least in one of the $BMAP$ s describing input in the system implies an increase of the sojourn time in the system in all range of the system load.

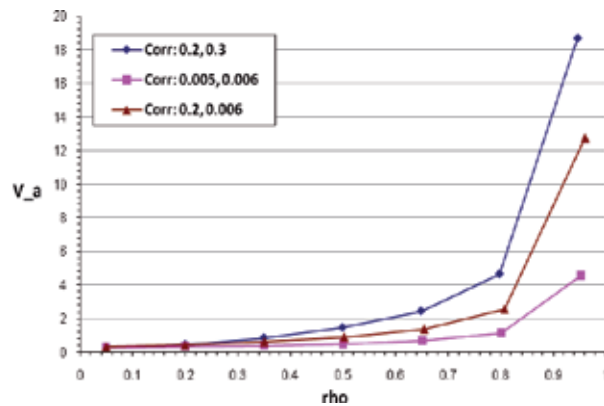


Fig. 1. Mean sojourn time in the system as a function of the system load for different correlations in the *BMAP* s

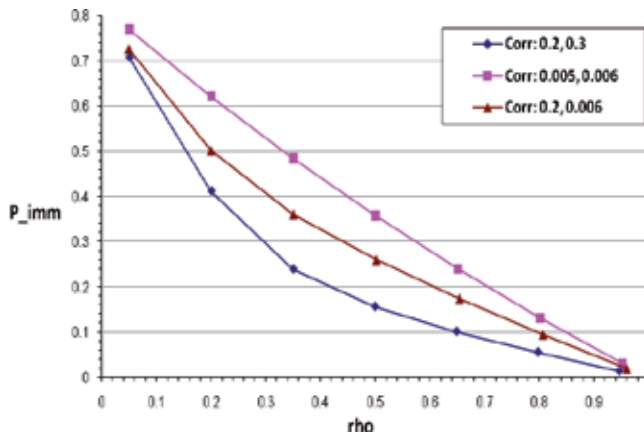


Fig. 2. Probability of immediate access to the servers in the system as a function of the system load for different correlations in the *BMAP* s

In the **second experiment** we compare the values \bar{v}_a and P_{imm} in the *BMAP/PH/N* system operating in the *RE* and in more simple queueing systems which can be considered as its simplified analogs. The first type analog is the $M^X/PH/N$ system in the *RE* where, under the fixed value of the *RE*, the input flow is a group stationary Poisson with the same batch size distribution and intensity equal to fundamental rate of the corresponding *BMAP* in the original system. The second type analog is the system $M^X/M/N$ with parameters of arrival and service processes which are obtained by means of averaging, according to stationary distribution of the *RE*, parameters of the original system.

Input flow is described by $BMAP_1$ and $BMAP_2$. Service processes are PH_1 and PH_2 .

Figures 3 and 4 show the dependence of the the mean sojourn time \bar{v}_a and the probability P_{imm} on the value of ρ .

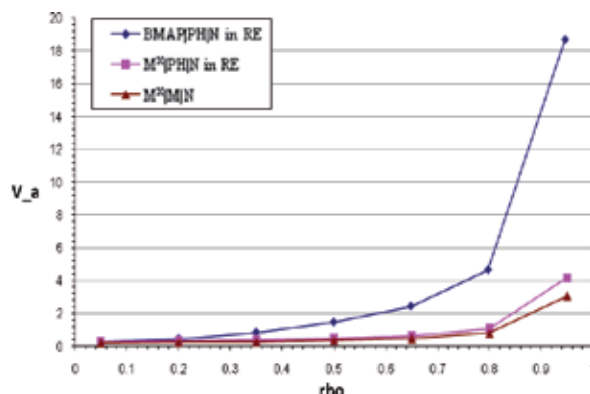


Fig. 3. Mean sojourn time in original system and more simple queueing systems

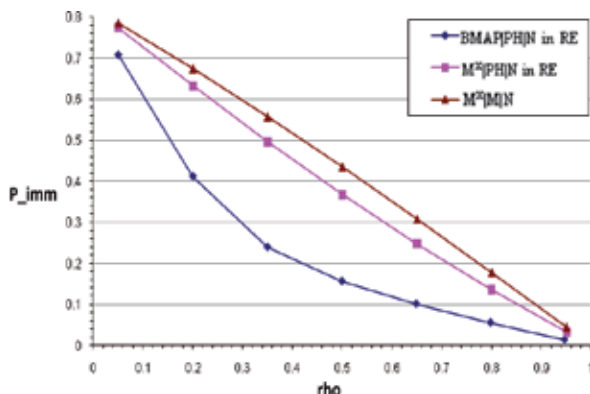


Fig. 4. Probability of immediate access to the servers in original system and more simple queueing systems

It can be seen from *Figures 3 and 4* that an approximation of the mean sojourn time and the probability that an arbitrary call reaches the server immediately by means of their values in some specially constructed more simple queueing system can be rather bad.

The idea of the **third experiment** is the following. Let us assume that the *RE* has two states. One state corresponds to the peak traffic periods, the second one corresponds to the normal traffic periods. Service times during these periods are defined by PH_1 and PH_2 distributions. Arrivals during these periods are defined by the stationary Poisson flow with the rates λ_1 and λ_2 correspondingly and initially we assume that $\lambda_1 \gg \lambda_2$. It is intuitively clear that if it is possible to redistribute the arrival processes (i.e., to reduce the arrival rate during the peak periods and to increase it correspondingly during the normal traffic periods) without changing the total average arrival rate, the mean sojourn time in the system can be reduced. In real life system such a redistribution is sometimes possible, e.g., by means of controlling tariffs during the peak traffic periods. The goal of this experiment is to show that this intuitive consideration is correct and to illustrate the effect of the redistribution.

We assume that the averaged arrival rate λ should be 12.5 and consider four different situations: a huge difference of arrival rates $\lambda_1 = 50\lambda_2$, a very big difference $\lambda_1 = 10\lambda_2$, a big difference $\lambda_1 = 3\lambda_2$ and equal arrival rates $\lambda_1 = \lambda_2$. The generator of the random environment is $Q = \begin{pmatrix} -15 & 15 \\ 5 & -5 \end{pmatrix}$.

It can be seen from *Figures 5 and 6* that the smoothing of the peak rates can cause essential decrease of the mean sojourn time and the increase of the probability that an arbitrary call reaches the server immediately upon arrival in the system.

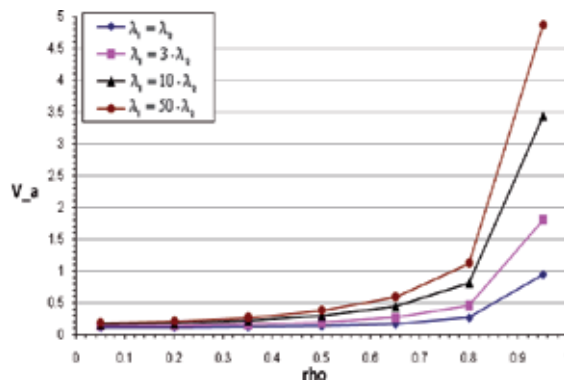


Fig. 5. Mean sojourn time as a function of system load for different relations of arrival rates

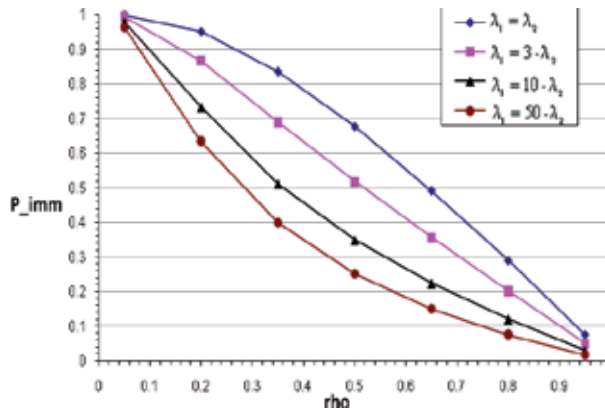


Fig. 6. Probability of immediate access to the servers as a function of system load for different relations of arrival rates

In the second experiment, we have seen that an approximation of the system performance measures by means of their values in more simple queueing system can be bad. However, it is intuitively clear the following. If the random environment is "very slow" (the rate of the RE is much less then the rates of the input flow and the service processes), an approximation called below as "mixed system" can be applied successfully. This approximation consists of calculation of the system characteristics under the fixed states of

the RE and their averaging by the RE distribution. If the random environment is "very fast", approximation called below as "mixed parameters" can be successfully applied. This approximation consists of averaging parameters of the arrival and service processes by the distribution of the RE and calculation of performance measures in $BMAP/PH/N$ system with the averaged arrival and service rates.

In the **fourth experiment**, we show numerically that sometimes the described approximations make sense. However, in situations when environment is neither "very slow" nor "very fast", these approximations can be very poor. We consider the RE s with different rate which are characterized by the generators of the form $Q^{(k)} = \begin{pmatrix} -5 & 5 \\ 15 & -15 \end{pmatrix} \cdot 10^k$.

We vary the parameter k from -7 to 4 what corresponds to the variation of the RE rate from "very slow" to "very fast". In this and further experiments, the input flow is described by the $BMAP_1$ and $BMAP_2$ and the service process is defined by the PH_1 and PH_2 . The results are presented in *Figures 7, 8 and 9*. In application of "mixed system" approximation, the averaged arrival rates under both states of the RE are equal to 3.488. The averaged service rate is equal to 2 at the first state of the RE and is equal to 14 at the second state. The mean sojourn times of an arbitrary customer at these states are equal to 3.5297 and 0.0998, respectively; the probabilities of immediate access to the servers are equal to 0.2021 and 0.81399; the mean numbers of customers in the system are equal to 12.311 and 0.3482. The averaged, according to the stationary distribution of the RE , mean sojourn time of an arbitrary customer is equal to 2.6722 and the probability that an arbitrary arriving customer sees an idle server is equal to 0.355. In application of "mixed parameters" approximation, the averaged, according to the stationary distribution of the RE , arrival rate is equal to 3.778 while the averaged service rate is equal to 4.0625. The value of the mean sojourn time of an arbitrary customer in the system with averaged arrival and service rates is equal to 0.7541, the probability of immediate access to the servers is equal to 0.4168, the mean number of customers in the system is equal to 2.849.

Figures 7, 8 and 9 confirm the hypothesis that the first type approximation ("mixed system") is good in case of "very slow" RE and the second one ("mixed parameters") can be applied to case of "very fast" RE . But sometimes the second type approximation is not very good (see *Figures 8*) because it is not quite clear how to make averaging of service intensity. Simple averaging of service rates under the different states of the RE may be not correct when the load of the system is not high because there are time intervals when the system is empty and no service is provided. It is worth to note also that there is an interval for RE rate (interval $k \in [-3, 0]$) where one should not use the values of the system performance measures calculated based on the considered approximating models. The use of these values can lead to the large relative error. Thus, *Figures 7, 8 and 9* confirm the importance of investigation implemented in this chapter. Simple engineering approximations can lead to unsatisfactory performance evaluation and capacity planning in real world systems.

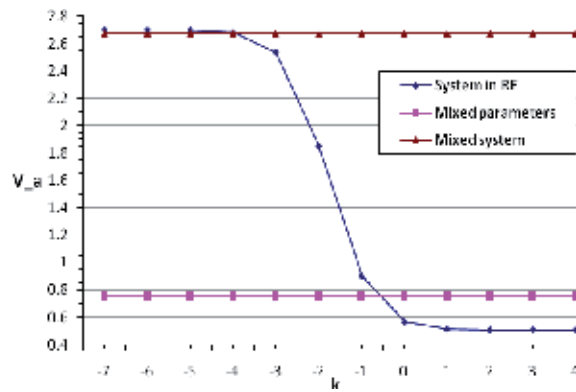


Fig. 7. Mean sojourn time of an arbitrary customer as a function of the RE rate

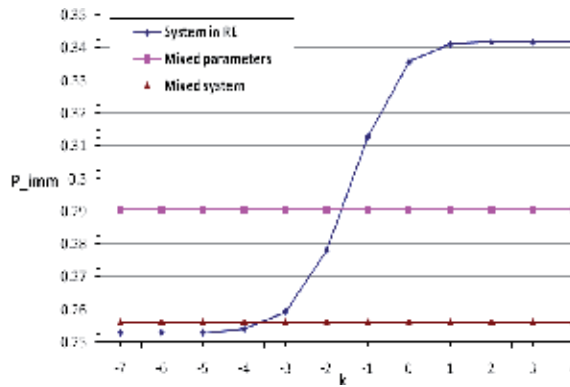


Fig. 8. Probability of immediate access to the servers as a function of the RE rate

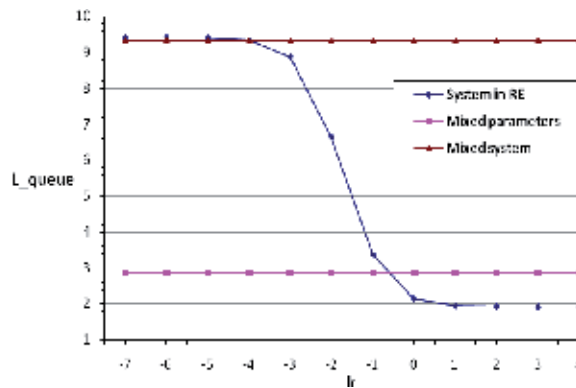


Fig. 9. The mean number of customers in the system L_{queue} as a function of the RE rate

In the **fifth experiment** we compare the mean number of customers, probability of immediate access to the servers and loss probability in the $BMAP/PH/N$ and

BMAP/PH/N/L systems operating in the *RE* for different values L of the buffer capacity and different customers admission discipline.

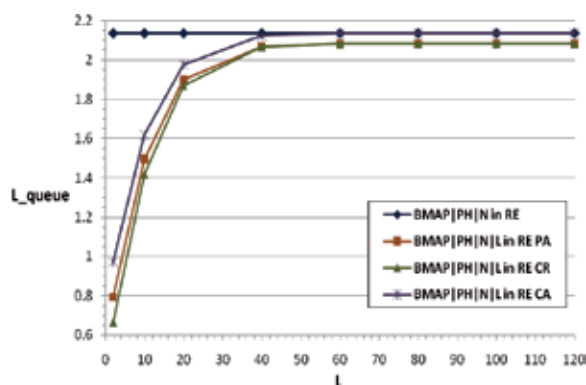


Fig. 10. Mean number of customers in the system as a function of the buffer capacity L

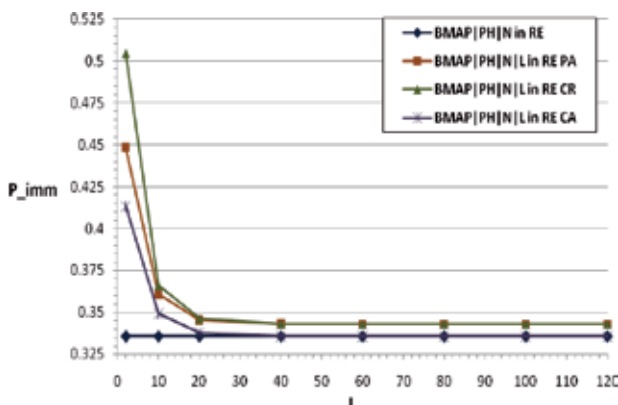


Fig. 11. Probability of immediate access to the servers as a function of the buffer capacity L

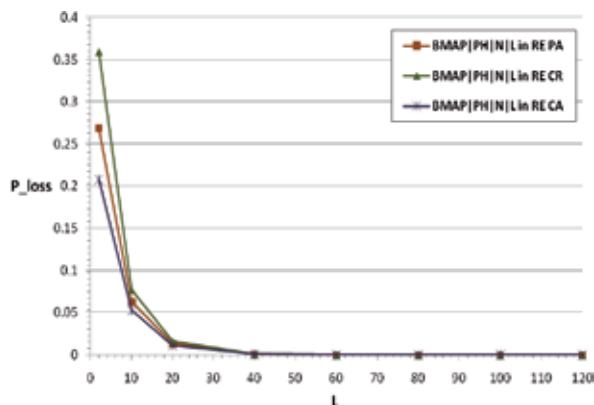


Fig. 12. Loss probability as a function of the buffer capacity L

Looking at *Figures 10-12*, it should be noted that the rate of convergence of the curves corresponding to the disciplines *PA* and *CR* to their limits defined by the system with an infinite buffer is not very high. When we further increase the value *L*, we discover that even for the buffer capacity *L* about 5000, the difference is not negligible. So, estimation of performance measures of the system with an infinite buffer by the respective measures of the system with a finite buffer can be not very good. This explains why we made the separate analysis of the system with an infinite buffer.

Finally, in the **sixth experiment** we consider the next optimization problem:

$$J(N) = c_1 \bar{v}_a + c_2 N \rightarrow \max_N, \tag{19}$$

where

- \bar{v}_a is the mean sojourn time in the system,
- N is the number of servers,
- c_1 is the charge for an unit of customer sojourn time in the system,
- c_2 is the cost of a server maintenance per unit of time.

It is clear that this problem is not trivial. When the number of servers is small, the cost of servers maintenance is also small, but the mean sojourn time is large. If we increase the number of servers, the mean sojourn time decreases while the cost of servers maintenance increases.

Let us assume that the cost coefficients be fixed as $c_1 = 5$ and $c_2 = 3$. Service time distribution at both states of the *RE* is exponential with intensities $\mu^{(1)} = 1$, $\mu^{(2)} = 7$.

On *Figure 13*, dependence of the cost criterion $J(N)$ on N is presented along with the dependences of the summands $c_1 \bar{v}_a$ and $c_2 N$.

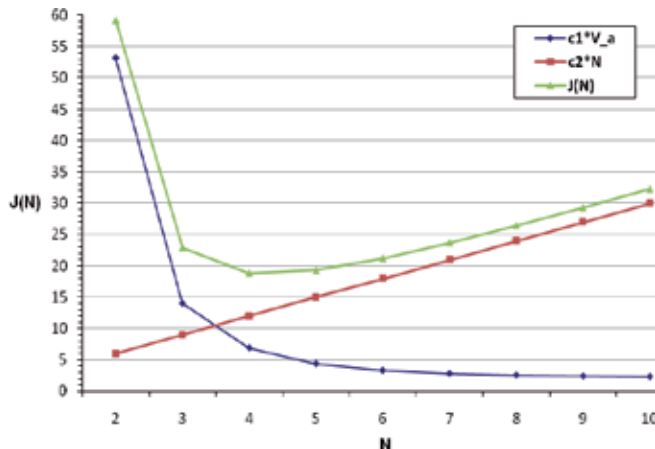


Fig. 13. Criterion $J(N)$ as a function of number of servers in the system

Based on *Figure 13*, one can conclude that our analysis allows effectively solve the problems of the system design and that the optimal value of the cost criterion (in this example it is provided by $N = 4$) can be significantly smaller than the values of the cost criterion for other values on N .

7. Conclusion

The $BMAP/PH/N/L$ system operating in a finite state space Markovian random environment is investigated for the finite and infinite buffer capacity. The joint stationary distribution of the number of the customers in the system, the state of the random environment, and the states of the underlying processes of arrival and service processes is calculated. The analytic formulas for performance measures of the system are derived. The Laplace-Stieltjes transform of sojourn time distribution is derived and the mean sojourn time is calculated. Selected results of numerical study are presented. They show an impact of the correlation in arrival process, illustrate the poor quality of the system characteristics approximation by means of more simple models, confirm the positive effect of the traffic redistribution between the peak and normal operation periods. The results can be used for the optimal design, capacity planning, and performance evaluation of real world systems in which operation of the system can be changed depending on some external factors.

Acknowledgement

This work was supported by the Korea Research Foundation Grant Funded by the Korean Government (MOEHRD)(KRF-2008-313-D01211).

8. References

- Combe, M. (1994) Queueing models with dependence structure. *Amsterdam: CWI*, p. 165.
- Kim, C.S., Klimenok, V.I., Orlovsky, D.S., Dudin, A.N. (2005) Lack of invariant property of the Erlang loss model in case of MAP input. *Queueing Systems*, Vol. 49. pp. 187-213.
- Kasten, H., Runnenburg, J.Th. (1956) Priority in waiting line problems. *Mathematisch Centrum, Amsterdam, Holland*. Dec. 1956.
- Kim, C.S., Dudin, A.N, Klimenok, V.I., Khramova, V.V. (2009) Erlang loss queueing system with batch arrivals operating in a random environment. *Computers and Operations Research*, Vol. 36, pp. 674-967.
- Klimenok, V.I. (1999) Characteristics calculation for multi-server queue with losses and bursty traffic. *Automatic Control and Computer Sciences*, Vol. 12, pp. 393-415.
- Klimenok, V.I., Dudin, A.N. (2006) Multi-dimensional asymptotically quasi-Toeplitz Markov chains and their application in queueing theory. *Queueing Systems*, Vol. 54 pp. 245-259.
- Lucantoni, D. (1991) New results on the single server queue with a batch Markovian arrival process. *Comm. Stat. Stochastic Models*, Vol. 7: pp. 1-46.
- Nuets, M.F. (1981) Matrix-Geometric Solutions in Stochastic Models. *John Hopkins Univ. Press, Baltimore*, 1981.
- Neuts, M.F. (1989) Structured Stochastic Matrices of $M/G/1$ Type and Their Applications. *Marcel Dekker, New York*, 1989.

- Sevastjanov, B.A. (1959) Erlang formula in telephone systems under the arbitrary distribution of conversations duration. *In: Proc. Of 3rd All-Union Mathematical Congress (Academy of Science, Moscow), 1959, Vol. 4, pp. 68-70.*
- Van Danzig, D. (1955) Chaines de Markof dans les ensembles abstraits applications aux processus avec regions absorbantes et au problem des boucles. *Ann. De l'Inst. H. Poincare 14 (fasc. 3), pp. 145-199.*

Interdomain QoS paths finding based on overlay topology and QoS negotiation approach

Șerban Georgică Obreja and Eugen Borcoci
*University Politehnica Bucharest
Romania*

1. Introduction

The real time multimedia services, delivered on Internet networks, raised new challenges for the network regarding the end to end (E2E) quality of services (QoS) control in order to ensure the proper delivery of the services from content provider (source) to content consumer (destination). But, despite a lot of studies and research done, the actual traffic processing in real Internet deployments is still mostly best effort. Several approaches have been proposed, focused on provisioning aspects – usually solved in the management plane – and then performing monitoring and adjustments in the control plane: e.g., well known dynamic techniques have been standardized, like IntServ, Diffserv, or combinations. Offering multimedia services in multi-domain heterogeneous environments is an additional challenge at network/ transport level. Service management is important here for provisioning, offering, handling, and fulfilling variety of services. Appropriate means are needed to enable a large number of providers in order to extend their QoS offerings over multiple domains. To this aim, an integrated management system can be a solution to preserve each domain independency while offering integration at a higher (overlay) layer in order to achieve E2E controllable behaviour.

This chapter deals with the problem of establishing QoS enabled aggregated multi-domain paths, to be later used for many individual streams. A general framework is described exposing the ideas of overlay topologies solutions. Then a simple but extendable procedure is proposed, running at management level, to find (through communication between domain managers) several potential inter-domain end to end paths. Then, using a resource negotiation process performed also in the management plane, QoS enabled aggregated pipes, spanning several IP domains, are established. All these functions are performed at an overlay level, based on abstract characterization of intra and inter-domain capabilities delivered by an intra-domain resource manager. This is important in the sense that each domain (or, Autonomous System – AS) can preserve its own independency in terms of resource management. The subsystem is part of an integrated management multi-domain system, dedicated to end to end distribution of multimedia streams.

The QoS path finding solution presented here is not like a traditional routing process: it is not implemented on routers, and it does not choose a route between network devices, but between two or more nodes of an overlay virtual topology described at inter-domain level.

Together with the intra-domain QoS routing available inside each network domain we will obtain an E2E QoS routing solution.

We recall that in our context, QoS enabled aggregated pipes are established (at request of a Service Provider entity), in advanced to the real traffic flow transportation. These are mid-long term virtual links. Related to this, the main advantage of the proposed solution is that, by separating the process of path finding from the QoS negotiation, the path searching process doesn't need to work real time. So, one can find several paths in very complex overlay topologies. Also, the overlay topology is made simple by virtualisation: each domain (including its manager) is considered as an abstract node in the virtual topology. Therefore the solution is scalable and capable to work in cases of large topologies, being no need for a hierarchical approach.

This Chapter is organized as follows: the Section 2 contains the state of the art in QoS inter-domain routing; the Section 3 shortly describes the general Enthroned architecture focusing on the service management at the network level. The Section 4 introduces the proposed QoS inter-domain path finding solution. Section 5 presents details about the implementation and Section 6 contains conclusions, possibilities of extensions and open issues.

2. State of the art

Because our approach deals with QoS path finding and routing, a short overview of the available approaches for QoS routing is presented below [13][14][15][17][18]. We distinguish between intra - and inter-domain QoS problems.

The intra-domain QoS routing solutions could be divided in two major approaches.

Classically, intra-domain QoS routing protocols run on the routers and find paths with QoS constraints from source to destination. While having the advantage of being an Internet philosophy compliant solution , i.e., completely distributed and dynamic, this approach does not offer at the domain level an image of the available resources. For mid-long term paths with QoS guarantees a centralized solution is better. This introduces a domain central manager having knowledge of the total resource allocation inside the domain. To find the routes it could use an algorithm to determine QoS routes between source and destination. In this case the QoS routing process would be run by a dedicated module of the domain manager. Note that such a solution would centralize completely the routing and would not benefit from Internet intra-domain routing protocols. Other approach is that the manager can collect information from routers which are capable to compute QoS constrained paths. The main thing is that the resulted routes are installed on the network equipments at the initiative of the manager which commands such actions to a network controller. Usually the QoS routing process is triggered by a new request addressed to the manager for a QoS path through the domain.

For inter-domain QoS routing also we can distinguish between two kinds of approaches. The first one proposes enhancements for the BGP protocol in order to support QoS features. The BGP advertises QoS related information between autonomous systems (ASes), and the routing table is build taking into consideration this additional QoS information. The Q-BGP protocol, proposed in MESCAL project [20], is such an example.

Another category of inter-domain QoS routing solutions are based on the overlay network idea [13][14]. An overlay network is built, which abstracts each domain with a node, represented by the domain service manager, or with several nodes represented by the egress

routers from that domain. Then protocols are defined between nodes for exchanging QoS information and, based on this information, QoS routing algorithms are used to choose the QoS capable path. In [13] a Virtual Topology (VT) solution is proposed. The VT is formed by a set of virtual links that map the current link state of the domain without showing internal details of the physical network topology. Then a Push and a Pull model for building the VT at each node are considered and analyzed. In the Push model each AS advertises their VT to their neighbor ASes. This model is suited for small topologies. In the Pull model the VT is requested when needed, and only from the ASes situated along the path between source and destinations, path which is determined using BGP routing information. If BGP kept several routes between source and destination than the VTs for each domain situated along the founded paths are requested. Based on this VTs information the QoS route from source to destination is calculated. After that an end to end QoS negotiation protocol is used to negotiate the QoS resources along the path.

One problem with these solutions is that they suppose that the ASes make available for others their virtual resource topology information. This requirement could be not accepted by the actual network providers, due to their confidentiality policy regarding their resource availability.

Also, these solutions are based on an end to end QoS negotiation process. After the QoS path is found, the negotiation process is started. The QoS routing process previously performed in advance would increase the chance of negotiation success, but the overall process implies two QoS -related searching processes: building the QoS topology and secondly negotiation in order to reserve resources.

This chapter proposes a simpler approach by separating the process of path searching in a virtual topology (built by abstracting each domain with a node) from the process of QoS negotiation (QoS searching path). By combining these two processes we will obtain a QoS inter-domain routing solution.

This solution has been developed and integrated in an E2E QoS management system [2][8][9][10]. The system was proposed and implemented by an European consortium in the FP6 European project ENTHRONE [2][3][4][5], and continued with ENTHRONE II [6][7][8]. The ENTHRONE project developed an integrated management solution to solve the end-to-end QoS - enabled transportation of multimedia flows over heterogeneous networks, from content sources to terminals. It proposes an integrated management solution that covers the entire audio-visual service distribution chain, including protected content handling, distribution across networks and reception at user terminals.

The overlay QoS path finding solution is based on the overlay network topology abstracting each pair (IP domain + manager) with a node. The overlay network graph in this case is only a connectivity one, with no information about the resources available intra and inter-domain. Several alternative inter-domain paths are computed, at overlay level, for each destination domain. Then, the end to end QoS negotiation mechanism is used to ask for and to reserve resources. Together they will act as a QoS inter-domain routing algorithm.

3. Enthroned End to End QoS Management System

As mentioned before the ENTHRONE project, IST 507637 (continued with ENTHRONE II, IST 038463) European project, had as main objective the delivery of real time multimedia flows with end to end quality of services (QoS) guarantees, over IP based networks. To

achieve this goal, a complex architecture has been proposed, which cover the entire audio-visual service distribution chain, including content generation, protection, distribution across QoS-enabled heterogeneous networks, and delivery of content at user terminals [2][3][4][5][6][7]. A complete business model has been considered, containing actors (entities) such as: Service Providers (SP), Content Providers (CP), Network Providers (NP), Customers (Content Consumers - CC), etc.

3.1 Enthroned basic concepts

ENTHRONE has defined an E2E QoS multi-domain Enthroned Integrated Management Supervisor (EIMS). It considers all actors mentioned above and their contractual service related relationships, Service Level Agreements (SLA) and Service Level Specifications (SLS), as defined in [2][3][4][5][6][7]. One of the main EIMS components is the service management (SM). It is independent of particular management systems used by different NPs in their domains, and it is implemented in a distributed way, each network domain containing Service Management entities. They are present in different amounts in SP, CP, NP, CC entities, depending on the entity role in the E2E chain. The SM located in NPs should cooperate with each IP domain manager and also with other actors in the E2E chain. Figure 1 shows the general architecture and emphasizes the cascaded model for pSLS negotiation.

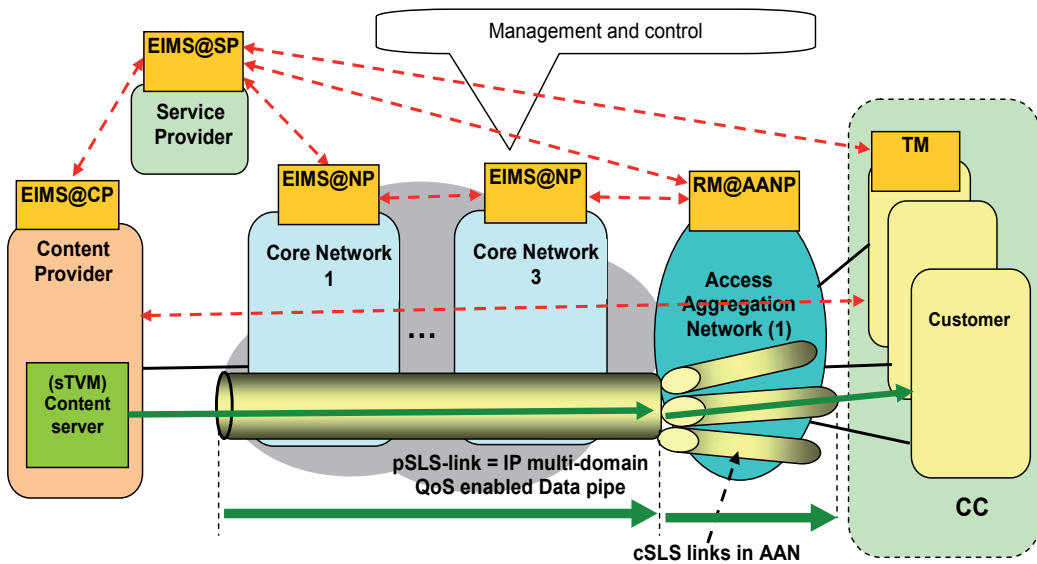


Fig. 1. Forwarded cascaded model for pSLS negotiation

Legend:

EIMS@CP, EIMS@SP, EIMS@NP – ENTHRONED Integrated Management Supervisor at: Content Provider (CP), Service Provider (SP) and Network Provider (NP)

sTVM – Source TV and Multimedia Processor (Content server)

AAN – Access Aggregation Network; *AANP* – AAN Provider

RM@AANP – Resource Manager of AAN (it is ENTHRONED compliant), *TM* Terminal Manager

ENTHRONE supposes a multi-domain network composed of several IP domains and access networks (AN) at the edges. The CPs, SP, CCs, etc., are connected to these networks. The QoS transport concepts of ENTHRONE are shortly described below.

First, QoS enabled aggregated pipes, to be negotiated based on forecasted data (and later installed in the network), span the core network, which is part of the multi-domain network. They are mid-long term logical pipes built by the Service Management entities. The aggregated QoS enabled pipe, called pSLS pipe (we also will use the term pSLS-link), is identified by the associated pSLS agreement (Provider SLS) established between the Network Providers, in order to reserve the requested resources. Each pSLS-link belongs to a given QoS class, [20].

Then, slices/tracks of pSLS-links are used for individual flows based on individual cSLA/SLS contracts, concluded after CC requests addressed to the SP. An individual QoS enabled pipe is identified by a cSLS agreement, which is established between the manager of the Service Provider (EIMS@SP) and a CC for reserving the necessary resources for the requested quality of service. Several cSLSs pipes are included at the core network level by an aggregated pSLS pipe, belonging to the same QoS class.

In the data plane of core IP domains, Diffserv or MPLS can be used to enforce service differentiation corresponding to the QoS class defined. In the ANs, the traffic streams addressed to the users (Content Consumers) is treated similar to the intserv, i.e. individual resource reservations and invocations are made for each user.

3.2 Service Management at Network Provider

The EIMS architecture at NP (EIMS@NP) contains four functional planes: the Service Plane (SPI) establishes appropriate SLAs/SLSs among the operators/ providers/customers. The Management Plane (MPI) performs long term actions related to resource and traffic management. The Control Plane (CPI) performs the short term actions for resource and traffic engineering and control, including routing. In a multi-domain environment the MPI and CPI are logically divided in two sub-planes: inter-domain and intra-domain. Therefore, each domain may have its own management and control policies and mechanisms. The Data Plane (DPI) is responsible to transfer the multimedia data and to set the DiffServ traffic control mechanisms to assure the desired level of QoS.

One main task of the EIMS@NP is to find, negotiate and establish QoS enabled pipes, from a Content Server (CS), belonging to a Content Provider, to a region where potential clients are located. Each pipe is established and identified by a chain of pSLS agreements, between successive NP managers. The forwarded cascaded model is used to build the pSLS pipes [5]. The pipes are unidirectional ones. An E2E negotiation protocol is used to negotiate the pSLS pipe construction across multiple network domains [5].

The process of establishing a pSLS-link/pipe is triggered by the SP. It decides, based on market analyses and users recorded requirements, to build a set of QoS enabled pipes, with QoS parameters described by a pSLS agreement. It starts a new negotiation session for each pSLS pipe establishment. It sends a pSLS_Subscribe_request to the EIMS@NP manager of the Content Consumer network domain. The EIMS@NP manager performs the QoS specific tasks such as admission control (AC), routing and service provisioning. To this aim it splits the pSLS request into intra-domain respectively inter-domain pSLS request. It also performs intra-domain routing to find the intra-domain route for the requested pSLS, and then it performs intra-domain AC. If these actions are successfully accomplished, and if the pSLS

pipe is an inter-domain one, then the manager uses the routing agent to find the ingress point in the next domain, does inter-domain AC and then send a pSLS Subscribe request towards the next domain. This negotiation is continued in the chain and up to the destination domain, i.e., the domain of the CC access network. If the negotiation ends successfully the QoS enabled pipe is considered logically established along the path from source to destination.

The Figure 2 shows the signalling message sequence associated to the pSLS-link negotiation. The actual installation and configuration of routers is considered in ENTHRONE a separate action and is done in invocation phase in a similar signalling way, plus the “vertical” commands given by EIMS@NP to the intra-domain resource manager.

After the pSLS pipe is active (i.e. subscribed and invoked) the Service Provider is ready to offer the new service to the users from the access network situated at the end of the pipe. Now the process of cSLS individual agreements establishment, for this new pSLS pipe, could be started.

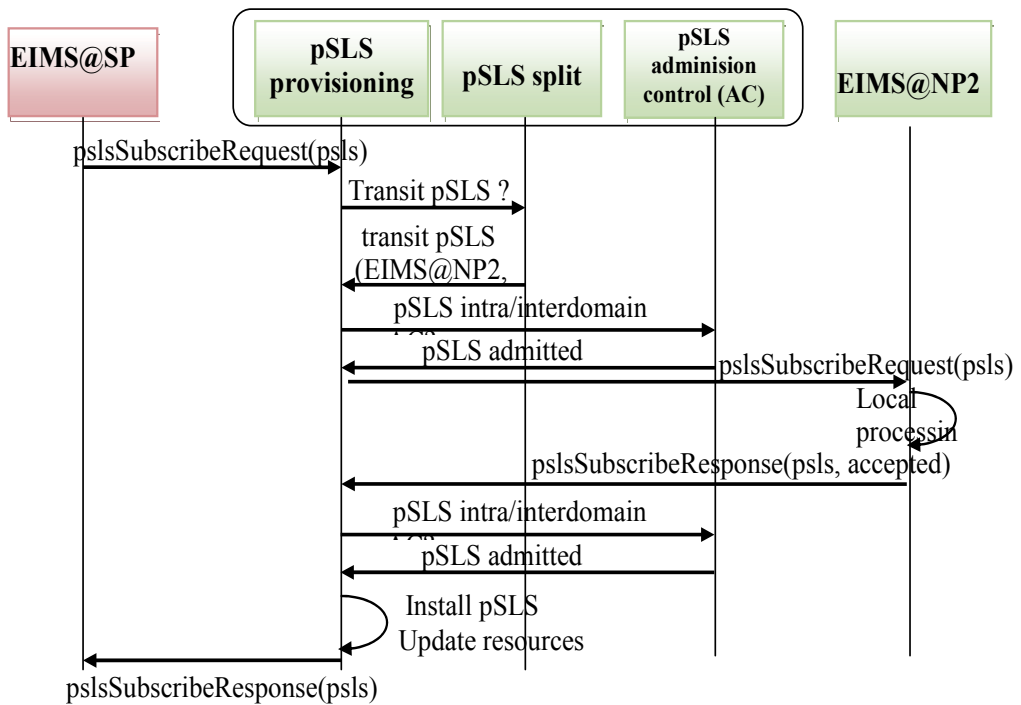


Fig. 2. pSLS negotiation for QoS enabled path establishment (negotiation and installation)

4. Finding an end to end path with guaranteed quality

4.1 General considerations

The main concepts of ENTRONE as stated in [8] are:

- E2E QoS over multiple domains is a main target of EIMS.
- But each AS has complete autonomy regarding the network resources, including off-line traffic engineering (TE), network dimensioning and dynamic routing.

Each Network Service Manager (cooperating with Intra-domain network resources manager) is supposed to know about its network resources in terms of QoS capabilities. ENTHRONE assumes that each AS manager has an abstract view of its network and output links towards neighbours in a form of a set of virtual pipes (called Traffic Trunks in ENTHRONE I, see [5][6]) each such pipe belonging to a given QoS class.

A solution to the route finding problem is to define/use routing protocols with QoS constraints called QoS routing protocols. They can find a path between source and destination satisfying QoS constraints.

While finding the QoS path is only a first step, then maintaining the QoS with a given level of guarantees during the data transfer requires additional actions of resource management, including AC applied to new calls.

EIMS@NP management system performs these tasks. It is a centralized manager knowing the topology and resources of a domain: otherwise, if using Diffserv only, in the core one cannot hope to have guaranteed QoS. Being a central management node for a network domain, a centralized QoS routing solution is appropriate inside the domain.

On the other side the multiple domain pSLS-links should also belong to some QoS classes and therefore inter-domain QoS aware routing information is necessary to increase the chances of successful pSLS establishment when negotiating the pSLSes. Several approaches are possible for inter-domain provisioning of QoS-enabled routing for ENTHRONE system, and they will be presented in the next sections. These solutions are based on the overlay topology approach.

4.2 Overlay QoS virtual topologies

The overlay solutions come out of the ideas expressed in the section above. Also this approach has been considered in [13] [14] which propose a Virtual Topology Service (VTS) offering multiple domains QoS enabled virtual pipes. The VTS abstracts the physical network details of each AS and can be integrated with BGP. Note that the pSLS links already proposed in the ENTHRONE project are similar.

Therefore one can define two separate types of network services providers: NP itself owning and responsible of the network infrastructure, which is actually an Infrastructure Provider; the overlay (virtual) network services provider (ONSP), which in our case is represented by EIMS@NP, which establishes agreements with other similar providers the final target being to offer QoS enabled pSLS-links.

In the ENTHRONE system each AS can assure QoS enabled paths towards some destination network prefixes while implementing its own network technology: DiffServ, MPLS, etc. Each AS is seen in an abstract way as an *Overlay Network Topology (ONT)* expressed in terms of TTs (traffic trunks) characterized by the bandwidth, latency, jitter, etc. The *Overlay Network Service (ONS)* is responsible for getting the ONT of each AS on a path in order to give to the source AS information related to QoS towards a given destination. The End to End Negotiation Service, which is supported by the EIMS@NP, will then negotiate the pSLS contracts with the chosen domains in order to reserve resources and then to invoke them. The ONS can be modeled in two ways, [13][14]: a proactive (*Push*) model and a reactive one (also called *pull* or *on demand*) model in order to obtaining the overlay (virtual) topologies of other ASes.

In the proactive case every AS advertises its ONT to other ASes without being requested for, while the reactive model assumes that overlay topologies are obtained on demand by an AS which is interested to reach a given destination prefix.

The proactive (push) model has the advantage offered by traditional IP proactive routing protocols: the ONTs of other ASes are already available at a given AS because they are periodically advertised among AS managers; therefore latency in offering a route to a new request is small. The advertisement can also be done at each AS manager initiative, so this model allows promotion of some routes to other domains. This can be subject of policies. The dynamicity is high (advertisements can be event driven). But the proactive model is more complex than the reactive model. Scalability problems may exist, because of high control traffic volume and also flooding the neighbor ASes with (maybe) not needed information. The managers will keep information on some routes that are of no interest for them (yet).

The reactive (on-demand) model is simpler than the proactive model, because an AS will query each domain of a given path to get the ONTs. No advertising mechanism is necessary. The scalability is higher because only the ONTs of the chosen routes will be obtained. Studies show that the mean E2E communication in the Internet traverses between 3 and 4 domains. Therefore the number of domains to be queried to obtain the ONTs is small. The pull model latency when finding a path is higher (need time for queries and calculations). The updates of ONT knowledge is not event driven because the lack of an advertisement mechanism. In [13], a notification message is proposed to solve this problem, i.e., to allow a domain to notify other domains about local events. Then the source domain can invoke the VTS to obtain a new set of ONTs.

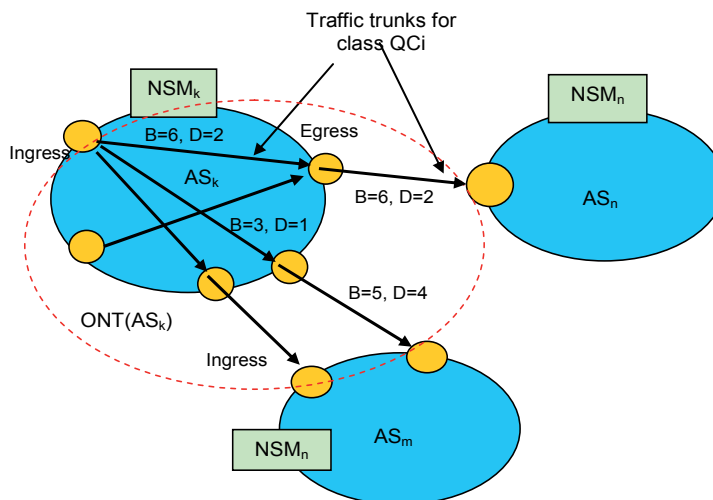


Fig. 3. Overlay network topology of AS_k - example

4.3 Proactive approach

Each AS Manager (e.g. NSM@NP manager in ENTHRONE case) knows its ONT. Figure 3 presents a graphic diagram showing several ASes. The ONT of AS_k includes all unidirectional TTs of AS_k . One TT can be internal to AS_k or external, linking the AS_k with

other neighbor domains. One external TT is defined from an egress point (router) of the domain up to the input of an ingress router of a neighbor domain. Each TT belongs to a given QoS class and may be characterized by parameters like bandwidth (B), delay (D), etc. It is the responsibility of the AS manager to find out these values by using internal mechanisms. Two styles, different in terms of flexibility, can be applied in the proactive solution, as described below:

1) *Maximum flexibility: Proactive ONT advertisements*

Each AS Manager advertises its ONT to the neighbors, and also the ONTs learned from other domains. In such a way (similar to the procedures used in the link-state routing protocols) each AS manager will become aware of the inter-domain overlay virtual topology and, applying some constrained routing algorithm, can select its paths to given destinations. The Figure 4 shows this process.

This solution is based on flooding so it exposes scalability problems. It can be useful for “regional” scenarios in which the number of ASes is not high. In [13] it is mentioned that a regional scenario may be formed by “condominiums of domains”; group of domains which agreed on advertising overlay topologies to each other. All the ASes making part of the same condominium will eventually know the overlay topologies of other ASes. In such regions of domains one could apply different business policies/rules and create new relationships to make the interactions more customer-oriented.

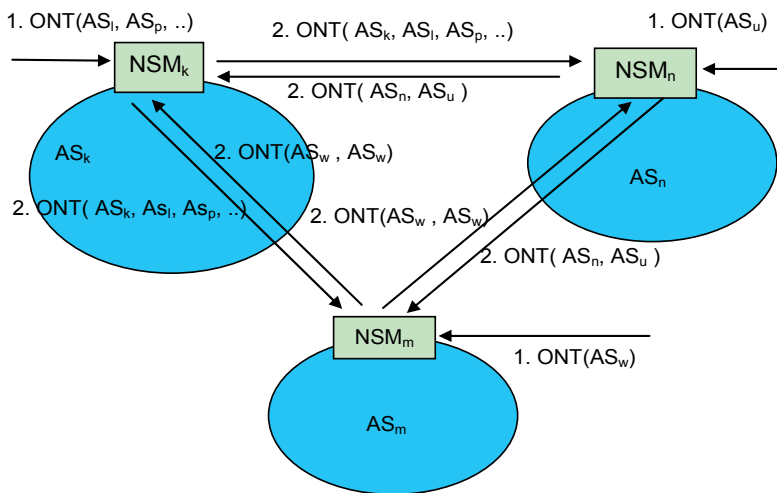


Fig. 4. ONT advertisement

2) *Minimum flexibility: Proactive vector paths advertisements*

At the other extreme there is a solution in which each AS knows its ONT and some path vectors (in the BGP meaning) reported by other ASes. In such case the advertisements do not contain ONTs but vector paths (in the sense of BGP, but having additional QoS information). Each AS wanting to reach a given destination will compute the best path(s) using its ONT and paths reported by other ASes (based on constrained routing algorithm). The degree of freedom in path selection is minimum in the sense that a given AS manager

can only select among paths proposed by the other domains and maybe benefit from its own ONT. But the scalability is better. The Figure 6 shows this solution in a simplified manner.

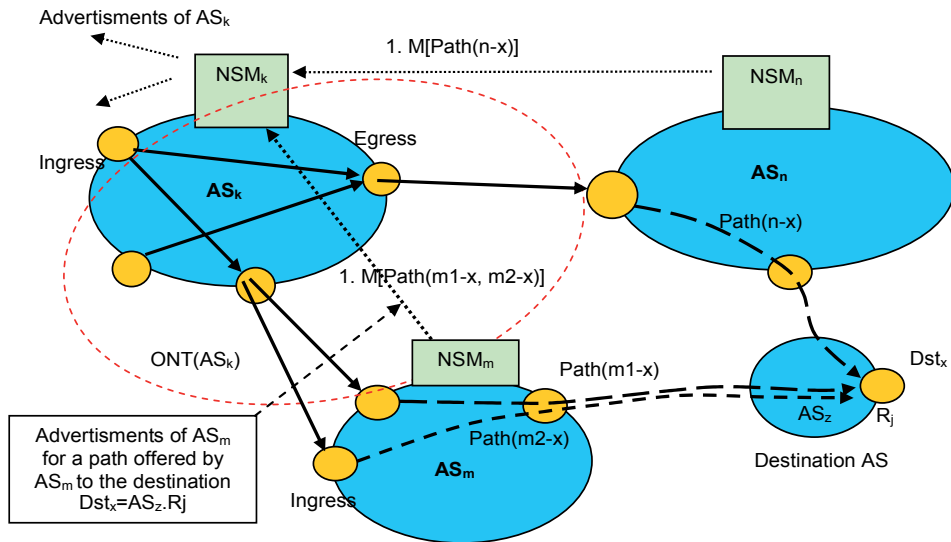


Fig. 5. Phase 1: Path advertisements from ASm, ASn sent to ASk for destination ASz.Rj

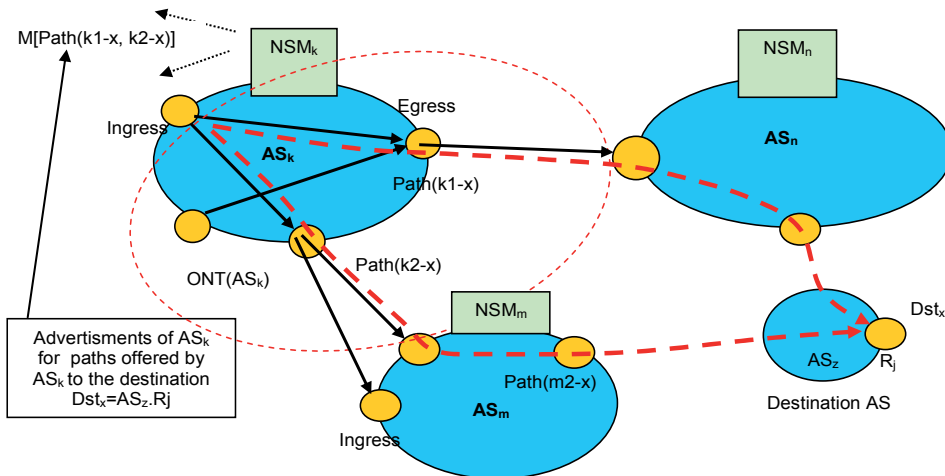


Fig. 6. Phase 2: Paths computed and selected by ASk

We distinguish two phases:

- ASK receives from the ASn advertisements messages having the generic form $M[\text{Path}(n-x)]$, indicating a path vector to destination - ASz domain, Router R_j . In a similar way, other messages are received from other domains. Note that actually these messages are not synchronized.

AS_k uses its own ONT values and computes one or more “best” or “equivalent” paths for each QoS class, Figure 6 shows two such paths computed and selected as acceptable (to be also advertised to other domains)

4.4 On demand approach

The domains do not advertise their overlay topologies to the neighbouring domains. The ONT is obtained by each domain at request if it wants to know the ONTs of other domains. When a given AS needs to find an E2E QoS-enabled inter-domain route, it queries its BGP local table and determines the possible routes towards the destination. BGP delivers a list of ASes to follow for a path to destination. Then the initiator domain can query each domain on the path chain towards the destination and gets the ONT of the domains specifically for that route. Based on this the initiator domain can get more routes to the destination than BGP offers.

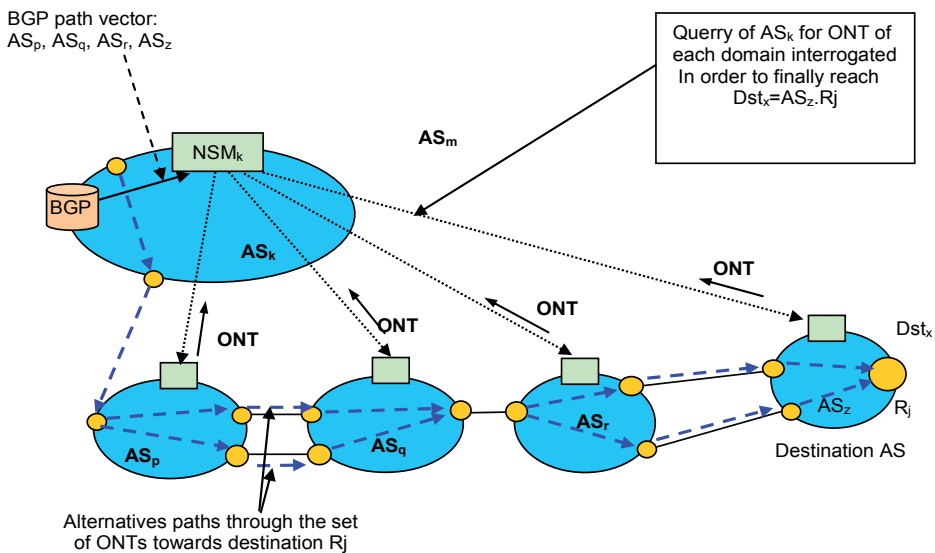


Fig. 7. Hub model to obtain the ONTs in the on-demand model

Figure 7 shows an example in which the domain AS_k needs to reach a destination AS_z with a required QoS set of values for this path.

The manager of the domain AS_k queries its local BGP table and finds the BGP route to the destination AS_z, through AS_p, AS_q, AS_r. The AS_k manager invokes the overlay topology service (OTS) to obtain the ONT of each domain. Figure 7 presents for this a hub model. Note that there can be more than one BGP path to the destination AS_z. Therefore AS_k can recursively query each domain in each path and find the best path towards the destination.

After obtaining all the ONTs of each possible route towards domain AS_z, the source domain AS_k can use a Constraint Shortest Path (CSP) algorithm to find the best route that fits the QoS requirements. The path calculation can be done using only one attribute or more than one (bandwidth, latency, loss). It may happen that after obtaining the ONTs of each route towards a destination, the AS_k can realize that there is no route that satisfies the QoS

requirements. A solution to this is proposed in [13]: to make use of the Internet hierarchy to collect more alternative routes towards a given destination. Taking into account the hierarchy of ASes in the world, going upwards this hierarchy may produce several routes which have been not advertised initially by BGP.

Suppose that the stub domain AS_k is multi-homed with domains AS_q and AS_p and it has received two BGP routes from its providers to reach prefixes at domain AS_z. The first route is AS_q, AS_r, AS_z and the second is AS_p, AS_z. Then, to increase the number of paths to query for ONTs, the OTS can invoke its providers and asks other BGP routes that were not initially advertised. In this case, domain AS_p would return to domain AS_k the paths AS_u, AS_z and AS_z towards AS_z,

So, AS_k will have one more route available. In general this procedure can be used when a domain is multi-homed

4.5 The proposed overlay inter-domain QoS path finding solution

We proposed a simplified version [1], which takes into account the following assumption regarding the specific characteristics of the Enthroned system:

- The number of E2E QoS enabled pipes is not very large because they are long term aggregated pipes.
- The number of NP entities is much lower than the number of routers.
- The EIMS@NPs are implemented on powerful and reliable machines, having enough computing and storage capabilities.
- The inter-domain core IP topology is stable during the inter-domain routing process; this is fulfilled within the assumptions of this work.

This solution is also based on the idea of Overlay Virtual Network (OVN) similar as in [13], but the OVN consists only of network domains (autonomous systems) abstracted as nodes. Each node will be represented by an EIMS@NP in this Overlay Virtual Network. This virtual network contains only information on connectivity between the domains, represented by the EIMS@NP nodes, or additionally static information regarding the inter-domain QoS parameters: links bandwidth, maximum jitter and delay, mean jitter and delay, etc.

This overlay virtual connectivity topology (OVCT) can be learned statically (offline) or dynamically.

The statically approach considers that the OVCT is built on a dedicated server – a topology server, like in the Domain Name Service (DNS). When a Network Provider wants to enter in the Enthroned system, then its EIMS@NP should register on this topology server. The topology server will return the Overlay Virtual Connectivity Topology. So we will consider that each EIMS@NP has the knowledge of this connectivity topology.

In the dynamic case each EIMS@NP, if it wants to build the OVCT, will query its directly linked (at data plane level) neighbour domains' managers. It is supposed that it has the knowledge of such neighbours.

Each queried EIMS@NP returns only the list of its neighbours. At receipt of such information, the querier EIMS@NP updates its topology database (note that this process is not a flooding one as in OSPF). Then it queries the new nodes learned and so on. The process continues until the querier node EIMS@NP learns the whole graph of "international" topology.

As we mentioned above the graph contains as nodes the EIMS@NPs which means that is made from the Network Service Managers of Enthroned capable domains, as shown in Figure 8.

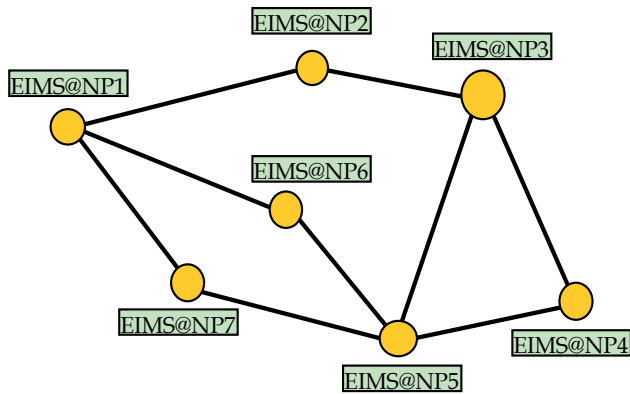


Fig. 8. Overlay Virtual Connectivity Network

If the Enthroned system will be implemented at large scale the number of nodes in the graph will be large, which means that the time required calculating the routing table will be also large. But because the topology structure changes events (adding new EIMS domains) are not frequent (it might happen at weeks, months), the topology construction process could run at large time intervals (once a day for example). In this case the routes calculation is triggered also at large time intervals, which means that there are no real time constraints. Another consequence is that the messages used to build the OVCT will not overload significantly the network. Enthroned capable domains can be separated by normal domains, with no Enthroned capabilities. In this case we consider that static initially QoS enabled pipes are built between Enthroned capable domains, pipes crossing the Enthroned non capable domains. The domains (Enthroned non capable) will be transparent for the Enthroned domains.

On the graph learned each EIMS@NP can compute several paths between different sources and destinations, thus being capable to offer alternative routes to the negotiation function.

The number of hops is used as a primary metric for the path choosing process. By the "hop" term we refer to a node in the Overlay Virtual Topology.

The process of route selection is as follows:

- When a request for a new pSLS arrived at one EIMS@NP, this will select the best path to the destination (the next EIMS@NP node that belong to this path), based on the overlay routing table.
- After the next hop is selected, the EIMS@NP will check if it has an intra-domain QoS enabled path for this route, i.e., between an appropriate ingress router and an egress router to the chosen next hop domain. If there is no such QoS enabled route, the next hop EIMS@NP node is selected from the overlay routing table.
- In case that a QoS enabled route intra-domain is found, the EIMS@NP, based on mechanisms defined in Enthroned, triggers a request for a new pSLS or a modified pSLS negotiation to the chosen EIMS@NP neighbor.
- This process continues until the destination is reached. If the negotiation ends with success than the pSLS pipe with guaranteed QoS parameters is found. If the process fails then the EIMS@NP will choose another overlay path to the destination and starts a new negotiation.

In Figure 9 the messages sequence for pSLS negotiation process in the case of multiple paths towards the destination is shown. The Service Provider decides to build a pSLS enabled pipe between a source located in the NP1 domain and a destination located in NP5 domain. We consider for this example that the working overlay topology is the one given in Figure 8. One can see that we have four possible routes between NP1 and NP5 domains. The first two of them, in terms of cost value, are the routes through NP6 and NP7 respectively. In Figure 9 it is illustrated the case when the pSLS negotiation along the route NP1-NP6-NP5 fails, due to admission control rejection in NP6 domain, either on intra-domain pipe inside NP6 domain, or on the inter-domain pipe between the NP6 and NP5 domains.

When it receives the rejection response at the pSLS subscription request the NP1 domain checks for an alternate route towards the NP5 domain. It finds the route through the NP7 domain and starts a new negotiation using this new route. This negotiation ends successfully, so the QoS enabled pipe between NP1 and NP5 will follow the route NP1-NP7-NP5.

This solution has the advantage of being simple and that it not require at an AS the knowledge of current traffic trunks for the other network domains as in [13].

A drawback of our solution (proposed above) is a larger failure probability in negotiating a segment (therefore a longer mean time for negotiation process), if comparing with solutions which calculate the QoS path before the negotiation process. The latter approach increases the probability that the negotiation finished with success at the first try.

The path finding process described above is not based on BGP information at all. BGP is used only for best effort traffic. The process of QoS routing takes place at service management level. But it is possible in principle to use such BGP information.

5. Routing Tables

5.1 Design Details

As mentioned before this solution is based on the knowledge of the overlay network connectivity topology. The topology can be kept in a form of a square matrix. The dimension M is equal to the number of nodes in the overlay topology network. Each entry rij , has an integer value. A zero value means that there is no direct connectivity between the nodes i and j . A value different from zero, value 1 for example, implies that there is a direct connection between the two nodes: Lij represents the link between nodes i and j (more precisely, between the two domains there are some linked routers). Because the matrix is a sparse one it can be easily compress in order to be stored in case that the dimension M is large.

Based on this overlay topology each EIMS@NP builds a routing table which contains, for each destination node in the network, several possible paths to this destination node, and the costs associated with each of these paths. Because in the routing table several entries will exists for each destination, the QoS negotiation process will be able to be carried on successively on multiple paths, increasing the probability that a path fulfilling the QoS requirements is found.

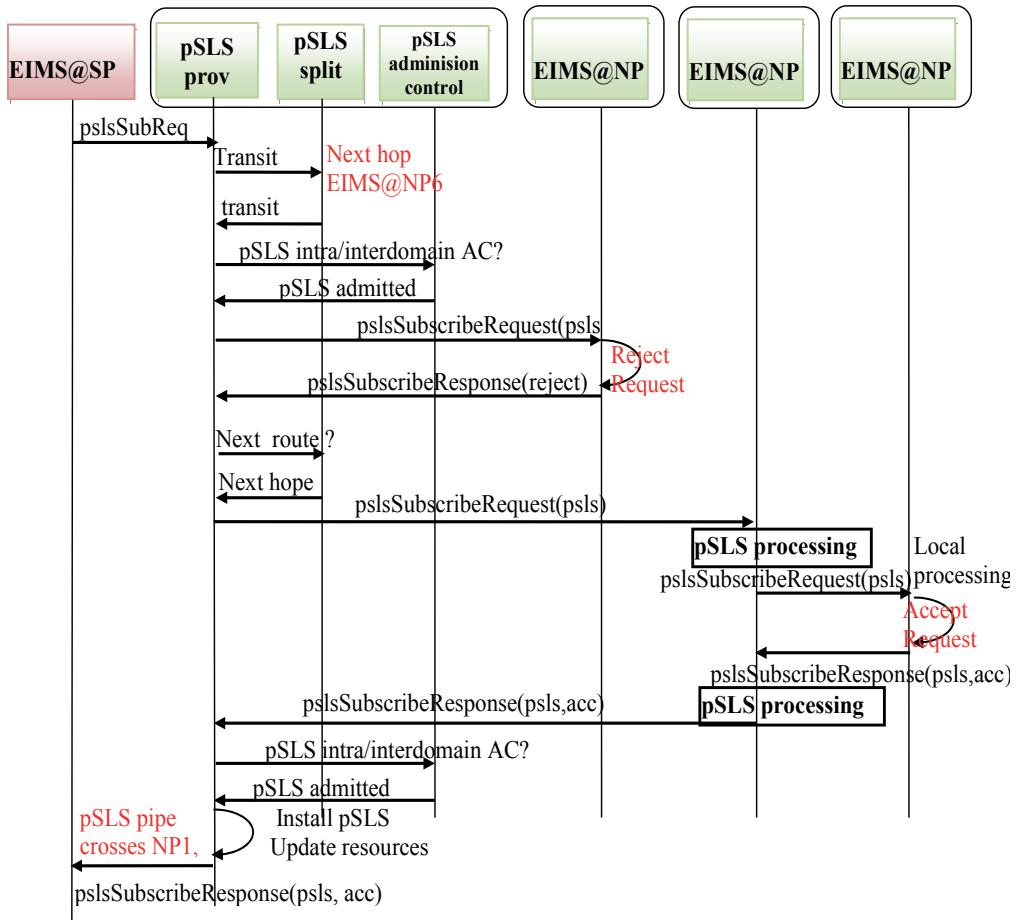


Fig. 9. MSC for QoS negotiation in case of multiple paths towards a given destination

Because the number of possible paths from source to a certain destination could be high we have limited it to the first four ones, with the lowest costs. If the number of neighbours are less than four, than the number of possible routes towards a destination is limited to this number. It is used the same principle as in the case of distance vector protocols. In the case when there are several paths to the same destination EIMS@NP node, using as first next hop the same node, in the routing table we will store the best cost of all the possible paths going through that node.

This is not a limitation because in our case the routing decision is taken hop by hop so the source node has no idea what route to the destination will be chosen at the node where the paths are splitting. An EIMS@NP does not need to keep the whole path information (but the total cost only) because it cannot influence the route chosen decision at the next hops along the path.

Let's suppose that the EIMS@NPk node has the neighbour nodes EIMS@NPm, EIMS@NPn, EIMS@NPp. The routing table from EIMS@NPk node to EIMS@NP1 node will be:

Destination	EIMS@NP ₁	EIMS@NP ₁	EIMS@NP ₁
Nex Hop	EIMS@NP _m	EIMS@NP _p	EIMS@NP _n
Cost (Nb of hops)	5	0	3

Table 1. Routing table at node K for node L destination

The EIMS@NP at node k builds such a record for each node in the overlay network. This process, of searching several possible paths for each possible destination, in this overlay network topology, is an expensive one in terms of calculation. But based on the assumptions presented above, which are realistic ones, if such a management system will be implemented in the network domains, this routing table building process will be run only on topology updates, which means at very long time intervals. Such a process will put low computing overhead on the Service Manager. Also, it could be scheduled to run on intervals with low management activity [5]. Taking this in consideration, it could be considered that the routing table is a static one, and the route search process reduces to a simple database search one. We do not need to run the searching algorithm for each pSLS subscription request. It is enough to search, in the routing table, the route to the destination with the smallest cost, and forward the request to the chosen next node. If the negotiation for QoS parameters along this path failed, then we will chose the next path, in terms of cost, from the routing table.

5.2 Possible Improvements

It is said that the solution did not take into consideration any QoS parameters, in the first phase, for path building process. This task left for the QoS negotiation process.

A possible improvement is to take into account some general data about the QoS parameters, in the path finding phase. For example, based on agreements with Service Managers of some domains, or based on some general QoS parameters of the domains, the Policy Based Management module could associate different costs for the links in the topology matrix. It is supposed that domains agreed to share these parameters, such as: the min/mean/max delay and jitter, introduced by the domain. In such a way the Policy module could influence the routing decision process. In this case the matrix element \mathbf{rij} could have the value \mathbf{Cij} if the link \mathbf{Lij} exists. The value \mathbf{Cij} is the cost for the link \mathbf{Lij} , and could be established by weighting appropriately the general QoS parameters mentioned above. These weights could be established by the domain administrator and transmitted to the Policy module.

The cost of a link could be also modified based on statistics regarding the acceptance or rejection rate of previous negotiated pSLS pipes. For example, if some domain with a good link cost rejects several times the requesting domain could modify the costs of the links crossing that domain.

When the path cost is computed it could be taken into account the existence of resource price agreements between some domains. These agreements could be negotiated using pull model, based on some statistics. For example an EIMS@NP node has two different paths towards a destination with similar path costs. It chose the path with a better cost, but it also could periodically request resource price information from both neighbour nodes crossed by the two paths. If the second node has available resources and is interested to carry traffic from the source domain, it will propose a better resource price as a response to resource

price requests. So the EIMS@NP source node could modify the routing table by improving the path cost for the second path, and the future pSLS pipe requests will be routed through the second path. Such a resource price communication could be easily implemented because the EIMS@NP managers are built as web-services, which implies very flexible communication capabilities.

5.3 Overlay topology building

For our solution we have chosen to build the overlay topology by means of successive interrogations of all the available nodes. The node which decides to build/refresh overlay the topology starts to interrogate all the other overlay nodes about their neighbours. It starts with its direct connected neighbours and then continues interrogating the new found neighbours, and so on.

For the EIMS@NP implementation we have used the web service technology. The interfaces between the EIMS@NP modules are implemented using WSDL language. The interdomain path finding WSDL interface it is used by EIMS@NP to interact with other EIMS@NPs in order to build the overlay topology used to search for interdomain overlay paths.

The interdomain path finding WSDL interface has defined the following messages:

- `getEimsNeighborsRequest ()`
- `getEimsNeighborsResponse(EimsNeighborsArray eimsNeighbors)`
- `getDomainQoSRequest ()`
- `getDomainQoSResponse(DomainQoS qos)`

The first two messages are used by the Overlay Path Building module from EIMS@NP subsystem to build the overlay topology. The response message contains an array with all the neighbours of the interrogated domain, and their associated data about the web services addresses, identification, IP addresses.

The next two messages are used to get general information about the QoS parameters of the domain: min/max/mean delay and jitter, mean transit cost, max bandwidth. These values refer to the transit parameters for the domain. We have considered that such information could be offered by each domain without affecting its confidentiality policy. These parameters are used to establish the cost associated with a link between two neighbour domains. For establishing the cost we have weighted the normalized values for these parameters. The weights were chosen arbitrarily, such as their sum to be one. No studies have been done to find the optimal values.

The format of messages parameters are given in table 2.

```

<wsdl:types>
<xsd:schema
targetNamespace="http://webservice.enthrone.org/eims/
xmlns:xsd="http://www.w3.org/2001/XMLSchema"
/InterdomainPath/datatype">
<xsd:complexType name="EndPoint">
<xsd:sequence>
<xsd:element name="IPAddress" type="xsd:string"/>
<xsd:element name="NetMask" type="xsd:string"/>
</xsd:sequence>
</xsd:complexType>
<xsd:complexType name="Neighbor">
<xsd:sequence>
<xsd:element name="id" type="xsd:string"/>
<xsd:element name="OverlayPathWebserv" type="xsd:string"/>
<xsd:element name="Address" type="tns:EndPoint"/>
</xsd:sequence>
</xsd:complexType>
<xsd:complexType name="DomainQoS">
<xsd:sequence>
<xsd:element name="minDelay" type="xsd:int"/>
<xsd:element name="maxDelay" type="xsd:int"/>
<xsd:element name="meanDelay" type="xsd:int"/>
<xsd:element name="minJitter" type="xsd:int"/>
<xsd:element name="maxJitter" type="xsd:int"/>
<xsd:element name="meanDelay" type="xsd:int"/>
<xsd:element name="meanCost" type="xsd:int"/>
<xsd:element name="maxBandwidth" type="xsd:int"/>
</xsd:sequence>
</xsd:complexType>
</xsd:schema>
</wsdl:types>

```

Table 2. Data type section for the interdomain path finding WSDL interface

In order to be able to perform the pSLS negotiation and to obtain the overlay topology we have defined several database tables used to store the data required by the above mentioned operations. These tables are shortly described next:

- **Overlay_topology table** – it contains data about each EIMS node in the topology, such as the addresses of the web-services available, the IP address, the domain identifier, and the QoS parameters. It is updated by the Inter-domain Overlay Path module at each overlay topology building cycle. It is used by the overlay routing process to build the overlay topology matrix used in the overlay route searching process.
- **Eims_neighbors table** – stores information about the neighbours for each EIMS node contained in the overlay_topology table. It is also updated by the Inter-domain Overlay Path module at each overlay topology building cycle.
- **Overlay_interdomain_routes table** – is used to store several alternative routes towards a destination overlay node. The number of alternative routes is limited to four. It is managed by the overlay routing process.
- **Local_eims table** – stores information about the local NetSrvMgr@NP such as: IP address, web services ports, domain Id. It is managed by the system administrator.
- **Border_routers table** – stores information about the local domains border routers. It contains the border routers IP address and neighbour EIMS reached through this border router. It is managed by the system administrator.

- **Access_networks table** – stores information about the access networks for the local domain. It contains the access network IP address and the border router IP address. It is managed by the system administrator.
- **Local Eims_neighbors table** - stores information about the EIMS neighbours for the local domain. It contains information about the border routers used to connect the local domains and the neighbors, border router IP address, web service port addresses, etc. It is managed by the system administrator.
- **Domain_qos_parameters table** – it is used to store global QoS parameters about the domain. It is managed also by the system administrator.

5.4 Functionality tests

This solution was implemented on the test-bed built at our university in the Enthroned project framework [21] [22]. The test-bed consists of three Autonomous Systems, each managed by a Network Service Manager (EIMS@NP). The EIMS@NP managers are implemented using web services technology. Between domains the BGP protocol is used to route the best effort traffic. A Network Manager is used to install the pSLS pipes on network devices. Also the test-bed has a Service Provider EIMS Manager, and the other modules required by the Enthroned system. The connectivity tests involved only the Network Provider managers and Service Provider manager.

The EIMS@SP was used to trigger pSLS subscribe requests, between a Content Provider and one of the available Access Networks, until the resources on the lowest cost path between the chosen source and destination, were exhausted. Then it has been triggered additional requests between the same source and destination. These new requests were admitted but the pSLS pipes were built along the next cheapest path between the chosen end points.

Because the testbed is a small one, is difficult to evaluate the performances of the proposed solution for a large number of domains. We have measured how fast, a request for getting the neighbours EIMS from a network domain, is served. We have obtained a mean time less than 0.1s per request. If we take for example a topology consisting of 1000 domains then, because we can consider that the total processing time is increasing linearly with the number of domains, the total processing time required to obtain the overlay topology is about 100s. We can increase it with 50% to take into account that at a large number of domains the local processing time, between two interrogations could be higher. So we could consider that for 1000 domains the topology building process takes about 150s, which is an acceptable value. Also, the solution used to build the overlay topology implies a large number of messages to be exchanged in order to build the topology. Each node should communicate with the other nodes. But the messages exchanged are small, because each of them contains only a few data about the neighbors of the interrogated node. If it have been adopted a link state like protocol to build the topology, then the messages would have been very big in case of large number of domains, so the amount of signaling data in the network would have been bigger. Also in our case we don't have convergence problems.

It has not been evaluated till now the time needed to compute several paths towards all the destinations nodes in the overlay topology.

The testbed used is not appropriate to test the scalability for the path finding process performed in the first phase. It could only be used to see that routing table is built correctly,

containing several paths towards each destination domain in the topology. Then, several requests for QoS enabled pSLS pipes have been triggered. These pipes were built along the first path specified in the routing table. When the resources on this path were exhausted, during the negotiation process, the next route was used for the following pSLS pipe. These tests proved that the solution is able to find QoS enabled pipes, in a multi domain environment.

6. Conclusion

This chapter has proposed a simple solution for solving the problem of QoS enabled inter-domain path finding, applicable when Network Service Management systems exist in each domain capable of constructing mid-long term pSLS pipes with imposed QoS parameters.

Because the solution does not require at a domain the knowledge of other domain resources, it could be attractive and accepted by the real life network providers. Another advantage is that it does not burden a given domain manager with the need of knowing the available traffic trunks of other network domains. Also, by separating the process of path finding from the QoS negotiation, the path searching process doesn't need to work real time. So we can find several paths in very complex overlay topologies. Also, by simplifying the overlay topology, considering only the domain managers as topology nodes, the solution might work for very complex topologies, being no need for an hierarchical approach.

The solution has as a main disadvantage that it does work only in the presence of a QoS negotiation system capable. It is based on this feature to check the QoS constraints on the paths founded in the overlay topology. Another disadvantage is that, it may not find the best QoS enabled path, as could be the case with other solutions.

The solution has proved to be simple to implement and is well suited for ENTHRONE Integrated Management System. It is also naturally extensible for more sophisticated techniques in QoS capable paths finding.

Further studies and simulations will be done in order to validate this solution for a real network environment. Also, it has been supposed that, because the path finding process could be run offline and the topology is a simplified one, a non hierarchical solution could be adopted for Internet. Simulations should be done to establish the amount of resources need by such a process.

7. References

- [1] S.G. Obreja, E. Borcoci, Overlay Topology Based Inter-domain QoS Paths Building. AICT apos;08. *Fourth Advanced International Conference on Telecommunications Proceedings*, Volume , Issue , 8-13 June 2008 Page(s):64 - 70
- [2] ENTHRONE I Deliverable 05 IMS Architecture Definition and Specification, June 2004.
- [3] A. Kourtis, H. Asgari, A. Mehaoua, E. Borcoci, S. Eccles, E. Le Doeuff, P. Bretillon, J. Lauterjung, M. Stiernerling, Overall Network Architecture, *D21 ENTHRONE Deliverable*, May 2004.
- [4] T.Ahmed - ed. Et al., End-to-end QoS Signaling & Policy-based Management Architectures, *ENTHRONE IST Project Public Deliverable D23F*, September 2005, <http://www.enthrone.org>.

- [5] H. Asgari, ed., et al., Specification of protocols, algorithm, and components, the architecture, and design of SLS Management, *ENTHRONE IST Project Public Deliverable D24F*, July 2005, <http://www.enthrone.org>
- [6] P. Bretillon ed., et. al, Overall system architecture, *ENTHRONE II Deliverable D01*, February 2007
- [7] P.Souto ed., et al, EIMS for ENTHRONE, *ENTHRONE II Deliverable D03f*, March 2007
- [8] E. Borcoci, Ş. G. Obreja eds., et al, Service Management and QoS provisioning, *ENTHRONE II Deliverable D18f*, March 2008.
- [9] Project P1008, Inter-operator interfaces for ensuring end-to-end IP QoS, Selected Scenarios and requirements for end-to-end IP QoS management, Deliverable 2, January 2001.
- [10] P. Trimintzios, I. Andrikopoulos, G. Pavlou, P. Flegkas, D. Griffin, P. Georgatsos, D. Goderis, Y. T'Joens, L. Georgiadis, C. Jacquenet, R. Egan, A Management and Control Architecture for Providing IP Differentiated Services in MPLS-Based Networks, *IEEE Comm. Magazine*, May 2001, pp. 80-88.
- [11] E. Marilly et. al, SLAs: A Main Challenge for Next Generation Networks, *2nd European Conference on Universal Multiservice Networks Proceedings*, ECUMN'2002 April 8-10, 2002.
- [12] T. Engel, H. Granzer, B.F. Koch, M. Winter, P. Sampatakos I.S. Venieris, H. Hussmann, F. Ricciato, S. Salsano, AQUILA: Adaptive Resource Control for QoS Using an IP-Based Layered Architecture, *IEEE Communications Magazine*, January 2003, pp. 46-53. See also <http://www-st.inf.tu-dresden.de/aquila/>
- [13] Fabio L. Verdi, Mauricio F. Magalhaes Using Virtualization to Provide Interdomain QoS-enabled Routing, *Journal of Networks*, April 2007.
- [14] Z. Li, P. Mohapatra, and C. Chuah, Virtual Multi-Homing: On the Feasibility of Combining Overlay Routing with BGP Routing, *University of California at Davis Technical Report: CSE-2005-2*, 2005.
- [15] Z. Wang and J. Crowcroft, Quality of Service Routing for supporting multimedia applications, *IEEE Journal of Selected Areas in Communication (JSAC)*, 14 (7) (1996), pp. 1228-1234.
- [16] D. Eppstein, "Finding k-shortest paths", *SIAM Journal on Computing*, 28 (2) (1998), pp. 652-673.
- [17] D. Griffin, J. Spencer, J. Griem, M. Boucadair, P. Morand, M. Howarth, N. Wang, G. Pavlou, A. Asgari, P. Georgatso, Interdomain routing through QoS-class planes, *Communications Magazine*, IEEE, Feb. 2007
- [18] S.P. Romano, ed., Resource Management in SLA Networks, *D2.3 CADENUS Deliverable*, May 2003.
- [19] T. Ahmed, A. Asgari, A. Mehaoua, E. Borcoci, L. Berti-Équille, G. Kourmentzas, End-to-End QoS Provisioning Through an Integrated Management System for Multimedia Content Delivery, *Computer Communication Journal*, May 2005.
- [20] E. Borcoci, A. Asgari, N. Butler, T. Ahmed, A. Mehaoua, G. Kourmentzas, S. Eccles, Service Management for End-to-End QoS Multimedia Content Delivery in Heterogeneous Environment, *AICT Conference Proceedings*, July 2005, Lisbon.
- [21] T. Ahmed, ed. et al., Pilot and services integration and tests, *ENTHRONE II Deliverable D27*, March 2008
- [22] M. Mushtaq, T. Ahmed ed. et al., Trials and evaluation, *ENTHRONE II Deliverable D28*, November 2008

Dual Linearly Polarized Microstrip Array Antenna

M. S. R Mohd Shah, M. Z. A Abdul Aziz and M. K. Suaidi
*Faculty of Electronic and Computer Engineering,
Universiti Teknikal Malaysia Melaka,
Hang Tuah Jaya, Ayer keroh, 75450, Melaka.
Malaysia*

M. K. A Rahim,
*Radio Communication
engineering,
Faculty of Electrical Engineering,
Universiti Teknologi Malaysia,
81300 Skudai, Malaysia.*

1. Introduction

The wireless communications systems have been greatly expand to the high performance applications. Nowadays, most of the wireless communications systems offers high data rate transmission and keep growing for higher data rates technology. Then, the communication devices were design to be small in size, low power consumption, low profile and practical.

2. Important

Recently, Multiple Input Multiple Output (MIMO) has become popular research topic among researchers for development of a new wireless communications technology. The system capacity can be increase with deployment of MIMO technique in the communications system. Thus, the used of high frequency bandwidth can be avoid since this method required high cost implementation. High transmitted power also is not required because all transmitted branch will transmit same power in MIMO system. There are three major studies in MIMO which are research on array antenna and adaptive signal processing, research on information theory and coding algorithm and research on MIMO channel propagation (Nirmal et al., 2004).

MIMO channel capacity can be increase with the increase of number of transmitter and receiver. When the number of the antennas used is fixed, the channel capacity is related to the spatial correlation and the diversity gain from antenna spacing configuration at

transmitter or receiver. The spatial correlation in MIMO system is always exploited by using diversity technique such as frequency diversity, space diversity, time diversity and polarization diversity. Polarization diversity can be achieved by deploying two or more different polarized antenna at transmitter or receiver. The transmitted signal with different polarized in MIMO channel will improved the un-correlation channel between transmitter and receiver (Collins, Brain. S, 2000)(Manoj. N et al.,2006)(Byoungsun. L, 2006).

A few technique have been introduce to obtain dual polarized antenna such as aperture-coupled microstrip antenna, two port corporate feed network and two or more probe feeds technique. The aperture coupled microstrip antenna was developed by using cross slot aperture at the plane between feed line plane and ground plane. Each aperture excite the patch in single direction and two orthogonal modes can be excited from the cross aperture (Ghorbanifar &Waterhouse., 2004)(S. B. Chakraby et al., 2000). Besides, the used of T, H and U slot configuration can offer better isolation between the two ports (Sami Hienonen et al., 1999)(S. Gao et al., 2003)(S. Gao & A. Sambell, 2005)(B. Lee, S. Kwon& J. Choi, 2001). A good isolation between ports will lead to good axial ratio if the circular polarized is used. Thus, the combination of the slots and slots modifications has been widely investigated by the researchers as report in (S. K. Padhi et al., 2003)(A. A. Serra et al., 2007)(Kin-Lu Wong et al., 2002) (B. Lindmark, 1997). Higher gain for these technique can be achieve by using number of patch and array feed network (M. Arezoomand et al., 2005)(J. Choi & T. Kim, 2000). This technique requires relatively complicated feed arrangement or multilayer construction in order to reduce the coupling between two feed lines (W.-C. Liu et al., 2004).

Two port feed network technique will excite two independent dominant mode from the patch with fed at the dual central point. Thus, the patches mode will degenerates at the far fields and produce the orthogonal and linear polarized at angles of designed (LJ du Toit & JH Cloete, 1987). A patches with corner fed also can excite two orthogonal polarized with equal amplitude and in phase. The corner fed method produce higher isolation as compared to edge centre fed method (Shun-Shi Zhong et al., 2002) (ShiChang Gao & Shunsui Zhong, 1998)(S. C. Gao et al., 2001).

Dual linear polarized antenna can also develop by using square patch with two feed probes. Each feed probe will generate one polarized signal primarily such as horizontally and vertically polarization (K. Woelders & Johan Granholm, 1997). The cross polarization at far field will cause the field generate by the patches is not purely orthogonal. These problem can be reduce by integrate bend slots in the square patch and reducing the antenna size as well (W.-C. Liu et al., 2004)(Keyoor Gosalia & Gianluca Lazzi, 2003).

Most of the dual polarized microstrip antenna was design to generate signals with vertical and horizontal polarized or +45 and -45 polarized. Vertical and horizontal polarized can be excite from patch with vertical and horizontal in position. However, +45 and -45 polarized signal excite from the patch which are slant at the angle of +45 and -45 from the principle plane. This topic will discussed the design of ± 45 dual polarized microstrip antenna with a single port at the single layer substrate. The further investigate also will be done to investigate the dual polarized signal excitation for array technique.

All the design will used 1.6 mm FR4 substrate with $\epsilon_r = 4.7$ and $\tan\delta = 0.019$. First, the design simulation and measurement of single patch slant at ± 45 will be presented. Then, further investigation for array implementation also will be discussed later. The Computer Simulation Technology (CST) Studio 2006 was used as CAD tools and fabrication was done by using chemical etching technique.

3. Design specification

As this design was intended to confirm the basic concept, it was decided to build the antenna using a best and successful approach. The specification such as the dielectric substrate and impedance matching will be meeting and find. Appropriate components will choose including the SMA/coaxial connector and FR4 board. A single element of square geometry $+45^\circ$ and -45° slanted polarized as shown in Figure 3.2 and Figure 3.3 can be designed for the lowest resonant frequency using transmission line model.

The substrate used is FR4 with a dielectric constant of 4.7 and a thickness of 1.6 mm. The loss tangent of the substrate is 0.019. After all dimensions have been calculated, the design would then be simulated in CST Studio Suite 2006 software to obtain the return loss, radiation pattern, and VWSR.

3.1 Transmission line model

The method used that allows the design of square microstrip patch antenna is the transmission line model. A square microstrip antenna fed to excite only one dominant mode (TM_{10} or TM_{01}) has a single resonance which may be modeled as this method. These values are designated R_a , L_a , C_a as shown in Fig 1. This figure represents the inset fed patch antenna which the arrangement of feed is shown in Figure 2. At resonance the relationship between the resonant frequency f_0 and the patch model values L_a and C_a are;

$$f_0^2 = \frac{1}{L_a C_a} \quad \text{Equation 3.1}$$

When the patch is resonant the inductive and capacitive reactance of L_a and C_a cancel each other, and the maximum value of resistance occurs. If the patch is probe fed and thick, the impedance at resonance will have a series inductive reactance term L_s ;

$$Z_{in} = R_a + j f_0 L_s \quad \text{Equation 3.2}$$

In order to obtain the values of L_a and C_a from measured or computed data one must subtract the series inductive reactance from the impedance. The value of two points either side of resonant frequency is obtained.

$$f_1 = f_0 - \Delta f_1 \quad \text{Equation 3.3}$$

$$f_2 = f_0 + \Delta f_2 \quad \text{Equation 3.4}$$

With the subtraction of the series inductance, the reactance now changes sign either side of f_0 . The admittance at each frequency may be expressed as;

$$Y_1 = \frac{1}{R_a} + j f_1 C_a + \frac{1}{j f_1 L_a} = G_1 + j B_1 \quad \text{Equation 3.5}$$

$$Y_2 = \frac{1}{R_a} + j f_2 C_a + \frac{1}{j f_2 L_a} = G_2 + j B_2 \quad \text{Equation 3.6}$$

The conductance G_1 and G_2 in the equivalent circuit of the patch antenna will account for the losses through radiated power, and the susceptance B_1 and B_2 will give a measure of the reactive power store in neighborhood of the radiating slots. Since the slots are identical $G_1 = G_2 = G$, the expression of B_1 and B_2 is;

$$B_1 = f_1 C_a - \frac{1}{f_1 L_a} \tag{Equation 3.7}$$

$$B_2 = f_2 C_a - \frac{1}{f_2 L_a} \tag{Equation 3.8}$$

Solving the equations for C the expression can be obtained as;

$$C_a = \frac{f_1 B_1 - f_2 B_2}{f_1^2 - f_2^2} \tag{Equation 3.9}$$

The susceptance, B can be obtained by equation below;

$$B = k_0 \Delta l \frac{\sqrt{\epsilon_{eff}}}{Z_0} \tag{Equation 3.10}$$

Where; Δl = Extended incremental length
 ϵ_{eff} = Effective dielectric constant

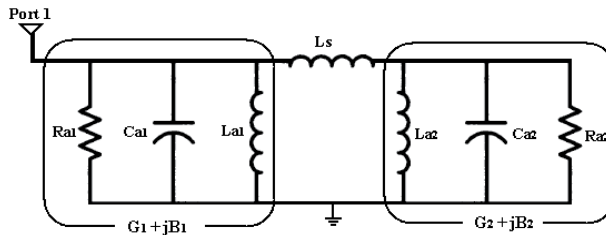


Fig. 3.1. Equivalent circuit for proposed microstrip patch antenna

3.2 Microstrip patch design

3.2.1 Square Patch

The design of the square shape patch follows the equation for designing the rectangular shape patch. The same length and width of the patch of the antenna was made to ease the design steps. Inset feeding is introduced into the design to offset the feeding location to the point where matched impedance can be achieved. The design calculation for the square patch has been discussed in this section. The parameters that needed to be calculated are the length of the patch, the inset feed and the feed line's length as shown in Fig 3.2.

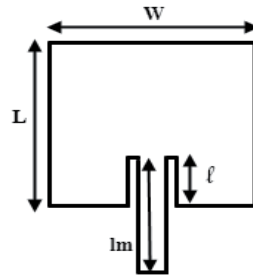


Fig. 3.2. Layout of the square patch.

The calculated parameters of the patch have been calculated as shown in Table 3.1. The input impedance level of the patch can be control by adjusting the length of the inset. Variations in the inset length do not produce any change in resonant frequency, but a variation in the inset width will result in a change in resonant frequency (M. Ramesh & K. B. Yip, 2003). The feed line is made to be a quarter wavelength of the operating frequency. The width of patch can be determined using the equation 3.11.

$$W = \frac{1}{2f_r \sqrt{\mu_0 \epsilon_0}} \sqrt{\frac{2}{\epsilon_r + 1}} \quad \text{Equation 3.11}$$

The ϵ_0 and the μ_0 are the permittivity and the permeability in free space respectively. The equation $\frac{1}{\sqrt{\mu_0 \epsilon_0}}$ can also be interpreted as the speed of light, c which is 3×10^8 m/s. The symbol f is the resonant frequency that the antenna intended to be operating and ϵ_r is the permittivity of the dielectric. The patch's length can be calculated using the equations 3.12. The length's extension, ΔL and the effective permittivity, ϵ_{reff} have to be calculated before calculating the length of the microstrip patch as shown in equation 3.13 and 3.14. The h is the height of the substrate while the W is the width of the patch as calculated before.

$$L = \frac{1}{2f_r \sqrt{\epsilon_{\text{reff}}} \sqrt{\mu_0 \epsilon_0}} - 2\Delta L \quad \text{Equation 3.12}$$

$$\Delta L = 0.412h \frac{(\epsilon_{\text{reff}} + 0.3) \left(\frac{W}{h} + 0.264\right)}{(\epsilon_{\text{reff}} - 0.258) \left(\frac{W}{h} + 0.8\right)} \quad \text{Equation 3.13}$$

$$\epsilon_{\text{reff}} = \frac{\epsilon_r + 1}{2} + \frac{\epsilon_r - 1}{2} \left[1 + 12 \frac{h}{W} \right]^{-\frac{1}{2}} \quad \text{Equation 3.14}$$

where:

f = Operating frequency	μ_0 = Permeability in free space
ϵ_r = Permittivity of the dielectric	W = Patch's width
ϵ_0 = Permittivity in free space	h = Thickness of the dielectric
ϵ_{reff} = Effective permittivity of the dielectric	

The type of feeding technique that will be used is the inset feed technique. It is one of the best feeding techniques and it is also easy to control the input impedance of the antenna. The input impedance level of the patch can be control by adjusting the length of the inset. The calculation of the inset fed is shown in the equations 3.19 which show the resonant input resistance for the microstrip patch.

$$\lambda_0 = \frac{c}{f} \tag{Equation 3.15}$$

$$\lambda_g = \frac{\lambda_0}{\sqrt{\epsilon_{reff}}} \tag{Equation 3.16}$$

$$G_1 = \frac{W}{120\lambda_0} \left[1 - \frac{1}{24} (k_0 h)^2 \right] \tag{Equation 3.17}$$

where:

$$k_0 = \frac{2\pi}{\lambda_g} \tag{Equation 3.18}$$

So, for resonant input resistance, R_{in}

$$R_{in}(L = \ell) = \frac{1}{2G_1} \left(\cos^2 \frac{\pi}{L} y_0 \right) \tag{Equation 3.19}$$

L is the length of the patch, ℓ is the length of the inset, and G_1 is the conductance of the microstrip radiator. As reported in frequency (M. Ramesh & K. B. Yip, 2003), the calculations for finding the inset length can be simplified as shown in the equation 3.20. This equation is valid for ϵ_r from 2 to 10. Using the equation below helps to ease the calculation for the inset length of the microstrip antenna.

$$\ell = 10^{-4} \left(\frac{0.001699\epsilon_r^7 + 0.13761\epsilon_r^6 - 6.1783\epsilon_r^5 + 93.187\epsilon_r^4 - 682.69\epsilon_r^3 + 2561.9\epsilon_r^2 - 4043\epsilon_r + 6697}{2} \right)^{\frac{L}{2}} \tag{Equation 3.20}$$

where: ϵ_r = Permittivity of the dielectric
 L = Length of the microstrip patch

The summary of the calculated characteristics of the designed patch antenna is shown on Table 3.1. All calculation for square patch dimension is applied onto CST Studio Suite 2006.

Patch characteristics	Dimension (mm)
Microstrip line width (w_0)	3.00
Patch width (W)	37.00
Effective dielectric constant (ϵ_{eff})	4.35
Extended incremental length (ΔL)=	0.732
Patch effective length (L_{eff})=	29.94
Patch actual length (L)	28.48

Table 3.1. summary of patch characteristics

Figures 3.3 show simulation result of return loss for single element obtained by using CST Studio Suite software. According to this figure, the result of the return loss of a single patch design has a good result at frequency of 2.4GHz which is -31.88dB which could be considered as a good result. Where at the resonant frequency of 2.4GHz which is the intended design frequency has a value of -10dB. The bandwidth obtained from the simulation of this microstrip antenna is 108.7 MHz which in percentage value is 4.05%.

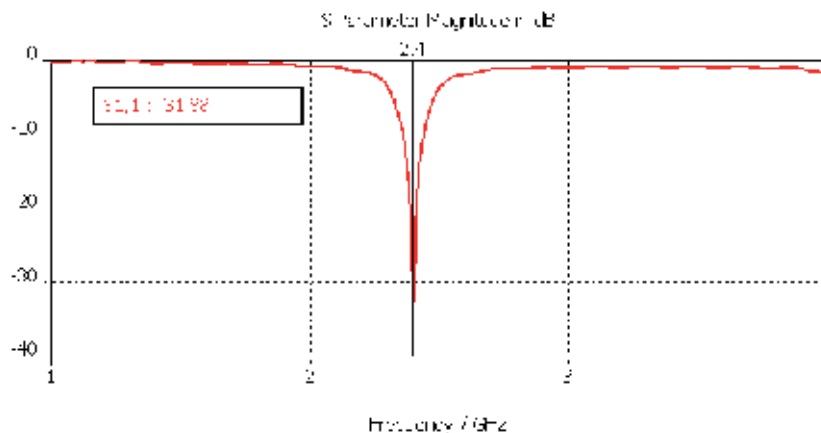


Fig. 3.3. Return loss simulation results of a single patch design.

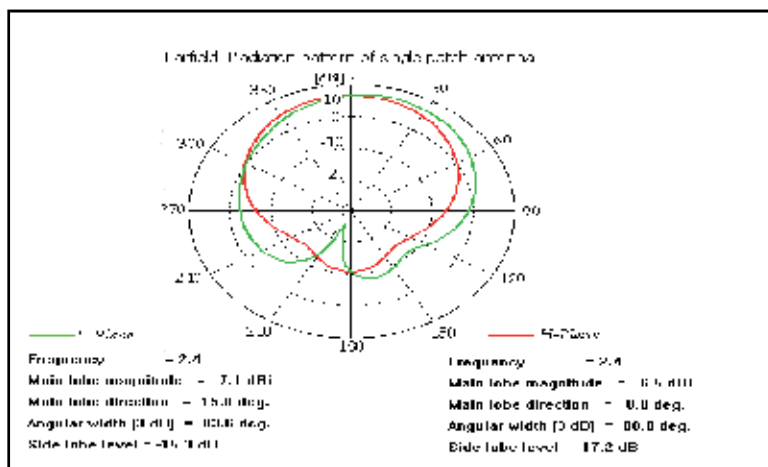


Fig. 3.4. E-plane and H-plane for single patch design

From the radiation pattern as shown in Fig 3, the normalized value of the radiation pattern which 50Ω input impedance will give half power beamwidth value. Half power beamwidth is a measurement of angular spread of the radiated energy. From this radiation pattern, the values at 3 dB for E-plane and H-plane are 94.9° and 99.6° respectively. The summary of the simulation results for single element patch design is shown in Table 3.2. Half power beamwidth for both E and H-Plane, directivity and gain that has extracted from radiation pattern are also shown in this table.

Type	Single patch
Return loss	-31.88 dB
Bandwidth	108.7 MHz (4.05%)
Directivity	6.11 dBi
Gain	2.56 dB
HPBW (E-Plane)	83.6°
HPBW (H-Plane)	80.0°

Table 3.2. Summary of simulation results for single patch antenna.

3.2.2 Square patch slanted +45° and -45° polarized

To gain insight into the behavior of dual polarized antenna, a single inset feed was designed for geometry slanted at +45° and -45° linear polarized. As indicated in the introduction, all work was carried out at 2.4 GHz which is implementing onto WLAN application.

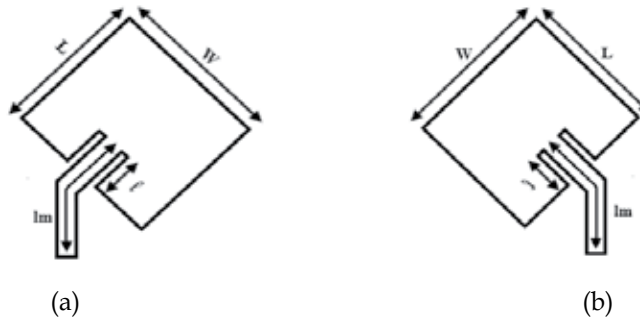


Fig. 3.5. (a) Layout of the +45° slanted polarization patch antenna
(b) Layout of the -45° slanted polarization patch antenna

The basic single linear +45° and -45° polarized microstrip antenna configuration is shown in Fig 3.5. The baseline configuration uses a square patch inset-feed technique on the top layer. All dimensions of a single patch +45° and -45° polarized microstrip antenna such as length, width and inset are calculated exactly using equation 3.11-3.20. Then, a single element patch is rotated at 45° for antenna slanted at +45° and 45° to produce polarized needed.

Hence, the width and length of single patch used in slant 45° and -45° are the same which its width, W and length, L equal to 27.67 mm. However, the inset length, l is changed due to the band element connected to the square patch. Since slant 45° and -45° have perpendicular polarizations, the antennas do not have much effect on each other and give similar results in terms of return loss and bandwidth. The simulation of return loss and bandwidth of the design single 45° and -45° polarization are shown in Fig 3.6. All plots contain impedance data that has been normalized to 50 Ω . The resonant frequency was 2.4 GHz with return loss of -12.84 dB for single 45° and -16.24 dB for single -45°.

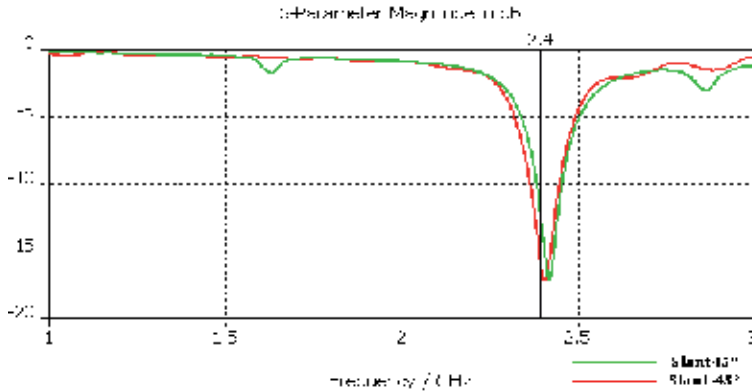


Fig. 3.6. Return Loss [dB] for 45° and -45° polarized antenna

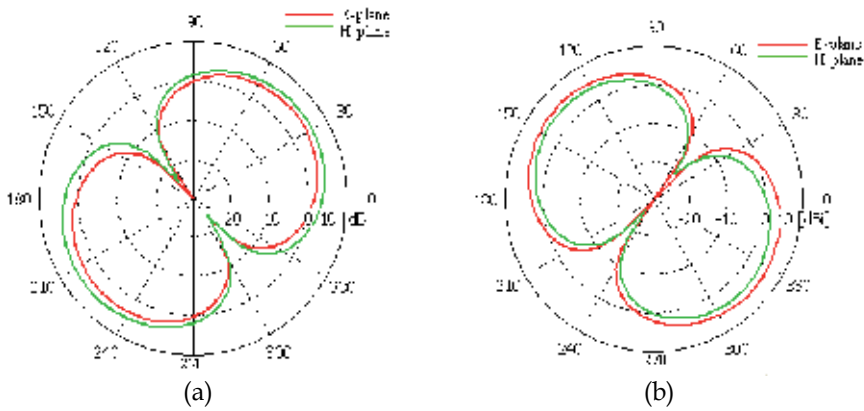


Fig. 3.7. (a) E and H-plane of the +45° slanted polarization patch antenna
 (b) E and H-plane of the -45° slanted polarization patch antenna

From the radiation pattern as shown in Fig 3.7, the normalized value of the radiation pattern will give half power beamwidth value. The summary of the simulation results for single element patch design is shown in Table 3.3. Half power beamwidth for both E and H-Plane, directivity and gain that has extracted from radiation pattern are also shown in the table.

Type	Single 45°	Single -45°
Return loss	-16.84 dB	-16.8 dB
Bandwidth	87 MHz (3.7%)	86 MHz (3.6%)
Directivity	5.69 dBi	5.71 dBi
Gain	2.56 dB	2.61 dB
HPBW (E-Plane)	83.4°	89.8°
HPBW (H-Plane)	89.8°	82.5°

Table 3.3: summary of simulation results for single 45° and -45° patch antenna.

3.3 Dual Polarized Array Antenna

3.3.1 1x2 Dual Polarized Array Antenna

After designed the slanted polarized for each $+45^\circ$ and -45° , the combination for both layouts can give the dual polarized radiation in term of array. A parallel or corporate feed configuration was used to build up the array. In parallel feed, the patch elements were fed in parallel by using transmission lines. The transmission lines were divided into two branches according to the number of patch elements. The impedances of the line were translated into length and width by using AWR Simulator. Fig 3.8, Fig 3.9, and show the circuit layout of the 1x2 array antennas with different position of the patch. In this project, the position of the patch is considered at 45° and -45° to obtain dual linearly polarized.

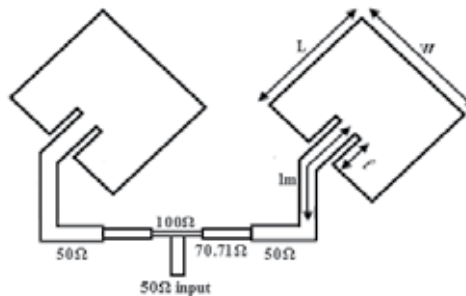


Fig. 3.8. Layout of the 1x2 $+45^\circ$ polarized array antenna

In Fig 3.8 a single $+45^\circ$ polarized was combined using corporate feed network to produce an array antenna. The comparison result between single element and 1x2 array antenna was describe clearly in terms of return loss, radiation pattern and gain. Same like Fig 3.9, this structure was built using single -45° polarized and combines with two elements to achieve polarization slant at -45° .

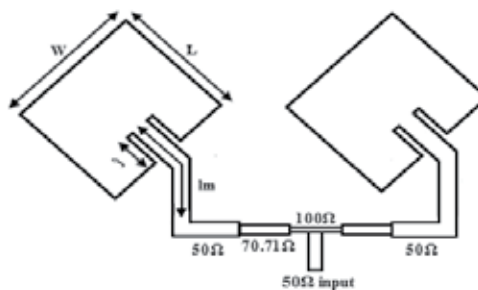


Fig. 3.9. Layout of the 1x2 -45° polarized array antenna

The simulation results for 1x2 array antennas slanted at 45° polarization were 103 MHz and -28.11 dB for bandwidth and return loss respectively. While, the simulation result for 1x2 array antennas slanted at -45° polarizations were 103 MHz and -31.82 dB for bandwidth and return loss respectively. Fig 3.10 show simulation result for 45° and -45° polarized 1x2 array antenna.

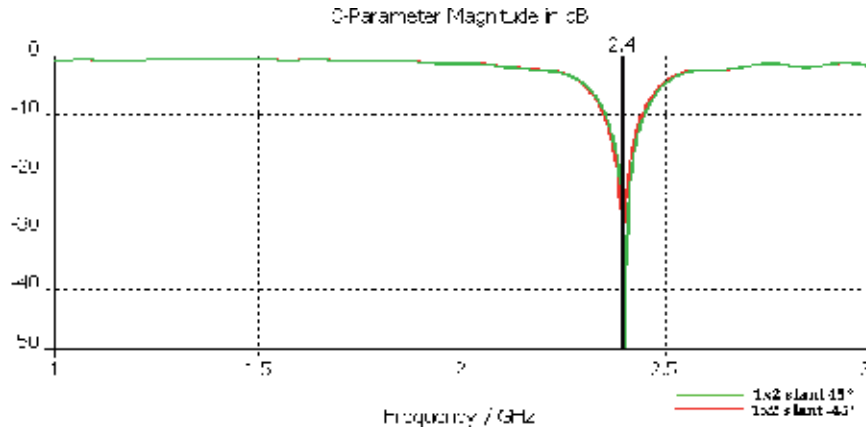


Fig. 3.10. Return Loss for 45° and -45° polarized 1x2 array antenna.

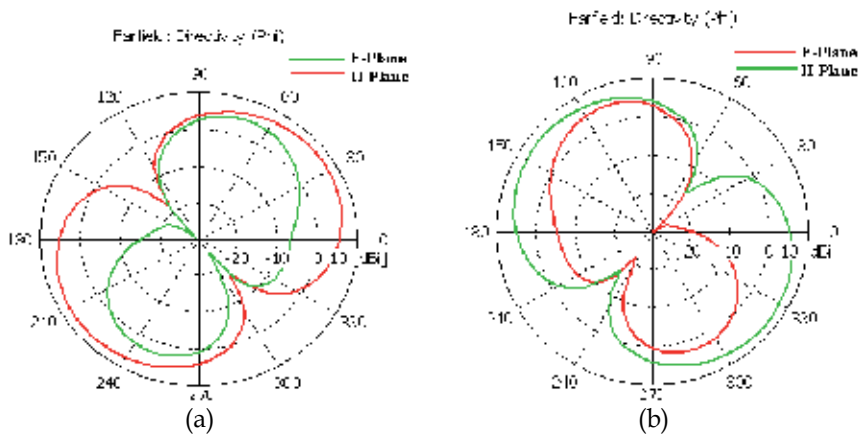


Fig. 3.11. (a) E and H-plane of the +45° slanted polarization patch antenna
(b) E and H-plane of the -45° slanted polarization patch antenna

The resulting radiation pattern of the E-plane and the H-plane of the two element antenna array is shown in Figure 3.11 (a) and (b), respectively. It is clear from these figures that the array antenna demonstrates a more directive pattern with better half power beamwidth and gain compared to that of individual patch.

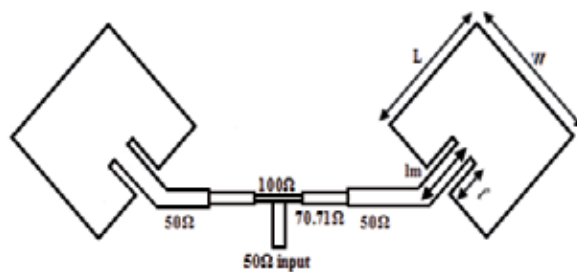


Fig. 3.12. Layout of the dual polarized 1x2 array antenna

Using built single patch slant at 45° and -45° polarization; 2-element array patch had designed and simulated in CST Studio Suite 2006 as shown in Fig 3.12. The array network is used to combine the 2 element of single patch antennas. A microstrip feed line has connected to the patch from the edge of the substrate.

An array of 1x2 dual polarized array antenna is build from combination of slant $+45^\circ$ and slant -45° . In order to combine, corporate feed again is involved to connect a single $+45^\circ$ and -45° polarized. According to the layout in figure 3.12, the antenna exhibits to have radiation of dual polarization pattern. The simulated return loss of the 1x2 dual polarization array antennas are shown in Fig 3.13. The simulation results for 1x2 dual polarization array antennas were 82.5 MHz and -21.31 dB for bandwidth and return loss respectively.

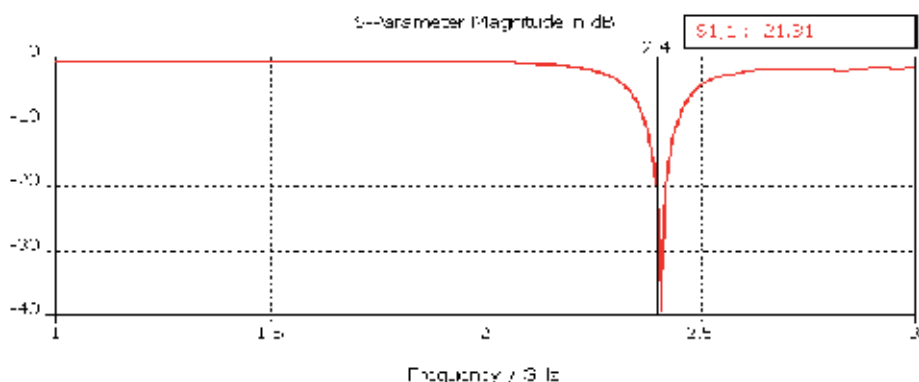


Fig. 3.13. Return Loss for dual polarization 1x2 array antenna.

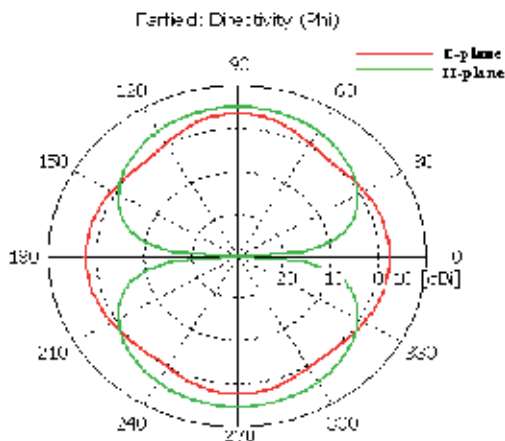


Fig. 3.14. Simulation radiation pattern of 1x2 dual polarization array antennas.

Fig 3.14 show the radiation pattern of the 1x2 dual polarization array antennas for E-plane and H-plane respectively. Overall, this design give better gain and directivity compared 1x2 array at slant 45° and -45° polarization antennas. The simulation of HPBW for E-plane is about 61.1° ; while at H plane is about 89.9° . All simulation data for 1x2 array antenna designs are tabulated in Table 3.4.

Design	Return Loss (dB)	BW (%)	Gain	Directivity	HPBW (E-Plane)	HPBW (H-Plane)
45° polarized	-28.11	4.29 (102.3MHz)	2.98	7.82	57.5	89.8
-45° polarized	-31.82	4.29 (102.3MHz)	2.96	7.71	54.9	90
Dual-polarized	-17.72	4.42	3.09	8.18	61.1	89.9

Table 3.4. Simulation results for 1x2 array antennas

3.3.2 1x4 Dual Polarized Array Antenna

Based on the pervious design of 1x2 dual linear polarized a 1x4, 2x2 and 2x4 arrays was designed and simulated. The initial dimensions for dual linear polarization are the same as the single polarization element. The patch and feed dimensions were maintained from the 1x2 dual linear polarized designs when designing 1x4 arrays antenna. 1x4 array antennas had designed and simulated in CST Studio Suite 2006. A microstrip feed line has connected to the patch from the edge of the substrate. As mention before, the design center frequency is 2.4 GHz applied for WLAN application. The most important results of the array design that should be achieved are the return loss result, bandwidth result, radiation pattern results and gain result. The much element used for designing dual polarized the higher gain and performance can be achieved.

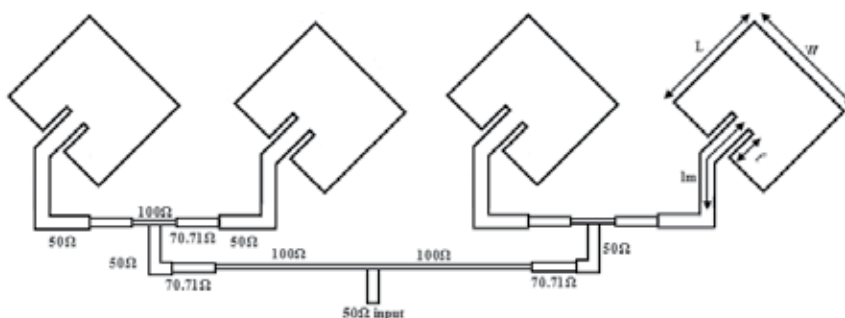


Fig. 3.15. Layout of the 1x4 +45° polarized array antenna

In Fig 3.15, two set of 1x2 array antenna slant at +45° polarized was combined using corporate feed network to produce an array antenna. The comparison result between single element and 1x2 array antenna was describe clearly in terms of return loss, radiation pattern and gain. Same like Fig 3.16, this structure was built using single -45° polarized and combines with two elements to achieve polarization slant at -45°.

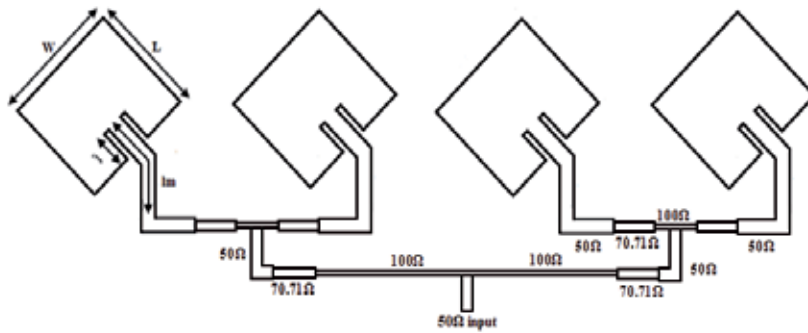


Fig. 3.16. Layout of the 1x4 -45° polarized array antenna

An array of 1x4 dual polarized array antenna is build from combination of 1x2 array antenna slant +45° and slant -45°. According to the layout in Fig 3.17, the antenna exhibits to have better radiation pattern and return loss compared to 1x2 dual polarized array antennas.

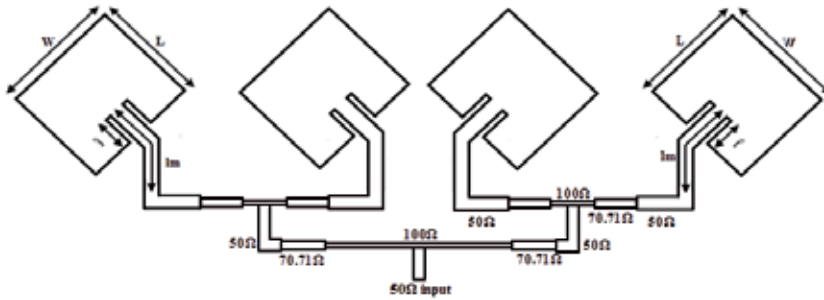


Fig. 3.17. Layout of the 1x4 dual liner polarized array antenna.

The simulated return loss of the 1x4 microstrip array is shown in Fig 3.18. The simulation results for 1x4 array antennas were 79.4 MHz and -25.74 dB for bandwidth and return loss respectively. Fig 3.19 shows the radiation pattern for 1x4 array antenna. Note in this radiation pattern is has consist of mutual coupling between the radiating elements.

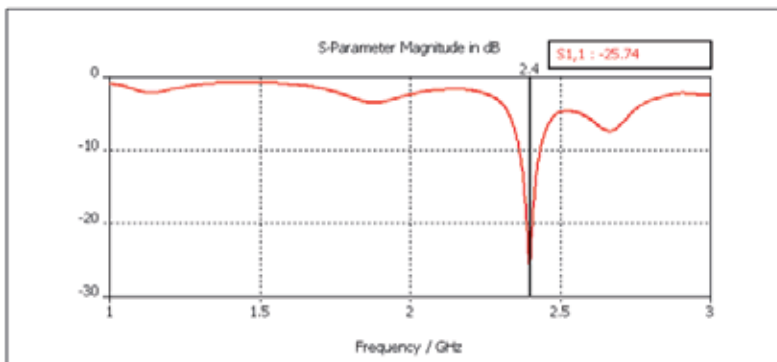


Fig. 3.18. Return Loss for dual polarization 1x4 array antenna.

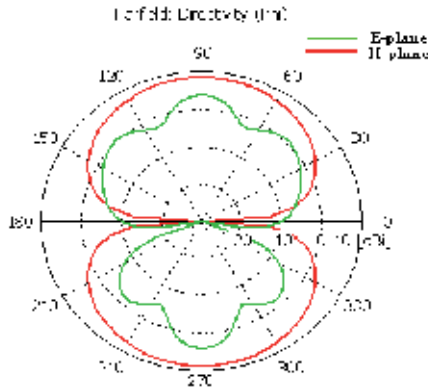


Fig. 3.19. Simulation radiation pattern of 1x4 dual polarization array antennas.

The simulation radiation pattern of the 1x4 dual polarization array antennas for E-plane and H-plane are shown, respectively. The HPBW achieved for the E-plane and the H-plane is about 524.6° and 89° respectively. The HPBW shows that at H-plane cut is better compared to E-plane cut. Moreover, there is a null appears in E-plane pattern result of 1x4 array patch design which decreases the HPBW lower than 2x2 dual polarization array antenna. At 2.4 GHz as shown in figure 4.24, the antenna directivity is about 8.673 dBi while antenna gain is about 5.01 dB.

3.3.3 2x2 Dual Polarized Array Antenna

As seen in Fig 3.20, the 2x2 dual linear polarized designs are fed by coax probe. This was integrated with 1x2 dual polarized array antenna and feed at centre of the quarter wave transmission line using coaxial technique. Compared with the expected result for a single element design, this result can be considered as a better result where a single microstrip element produces a very low gain. The most important results of the array design that should be achieved are the return loss, bandwidth, radiation pattern and gain result.

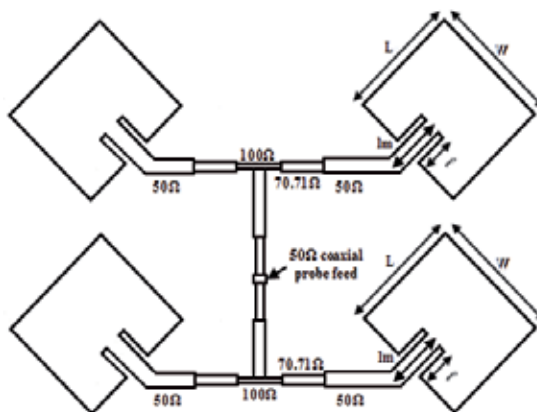


Fig. 3.20. Layout of the 2x2 dual linear polarized array antenna.

The simulated return loss of the 2x2 microstrip array is shown in Fig 3.21. As mention in pervious chapter the design was used coax probe compare to other design use transmission line technique. The square patch dimension was maintained from the single element design. The simulation results for 2x2 array antennas were 89 MHz and -37.45 dB for bandwidth and return loss.

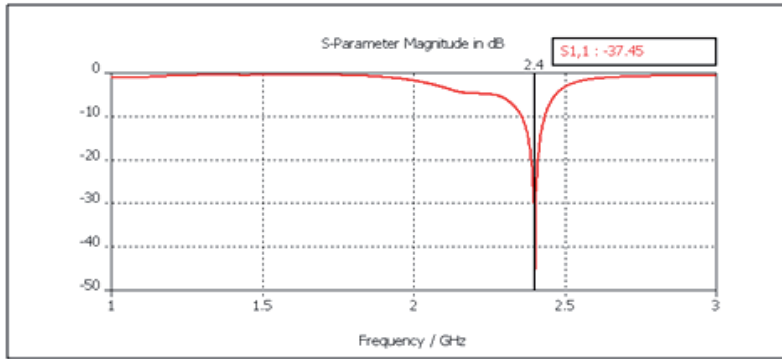


Fig. 3.21. Return Loss for dual polarization 1x4 array antenna.

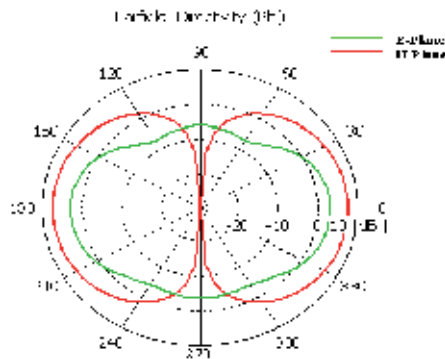


Fig. 3.22. Simulation radiation pattern of 2x2 dual polarization array antennas.

According to Fig 3.22, the antenna gain for this design is better comparing 1x2 array antennas which 1.2 dB higher. This radiation pattern show the E-Plane and H-Plane for 2x2 dual polarization array antenna. The HPBW show that at H-Plane cut is better compared to E-Plane cut. Moreover, there is a null appears in E-Plane pattern result of 2x2 array patch design. This may due to mutual coupling occurred in arrays, beside that each four elements in the array design configuration is facing the back of each other, which also influence in the null that appeared in the radiation pattern results.

3.4 Measurement result

3.4.1 Dual Polarized 1x2 Array Antenna measurement result

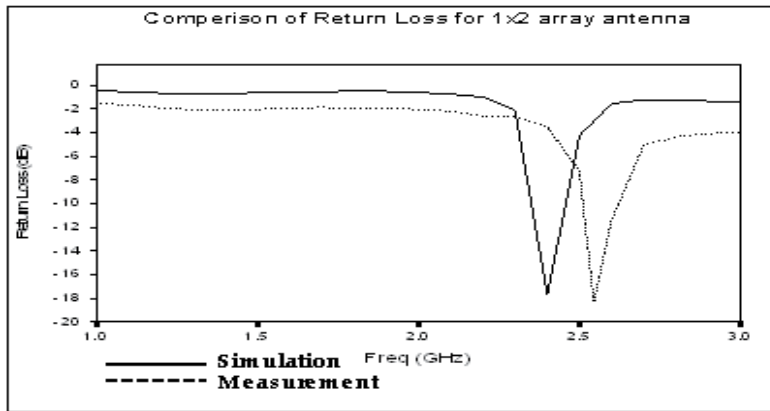


Fig. 3.23. Return Loss [dB] for 1x2 dual linear polarized array antenna.

The comparison between simulated and measured result was shown in Fig 3.23. The measured of return loss slightly different at desired frequency compare to simulated result. This because due to error on fabrication process. Since, the simulation result of the return loss has a value of -17.72dB at resonant frequency of 2.4GHz. While the fabrication results of the return loss has a value of -18.28dB at resonant frequency of 2.53GHz.

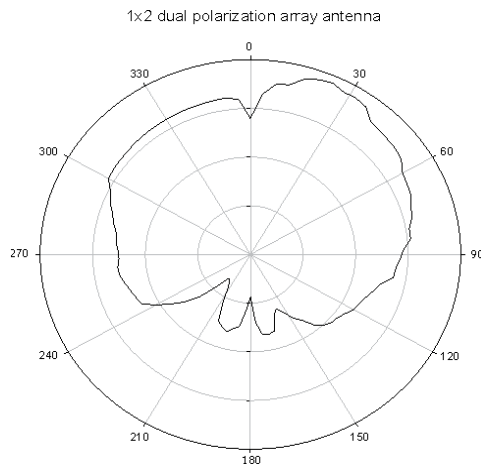


Fig. 3.24. 1x2 array antenna radiation pattern fabrication results

The radiation pattern for this antenna is presented in Fig 3.24, where it can be seen that the pattern seem like radiating in slant 45° and -45° . The gain of this antenna is 2.83 dB, which is lower than 0.26 dB from simulation result.

3.4.2 Dual Polarized 1x4 Array Antenna measurement result

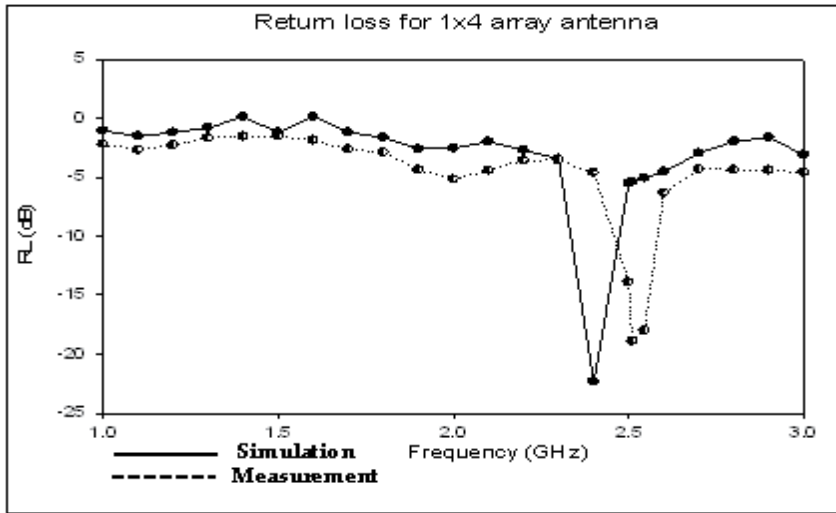


Fig. 3.25. Return Loss [dB] for 1x4 dual linear polarized array antenna.

According to Fig 3.25, the result of the return loss of the 4-element array patch design has a good result at frequency of 2.5 GHz which is -23 dB. This result could be considered as a good result. Where at the resonant frequency of 2.45GHz which is the intended design frequency has a value of -9.8dB. However, the bandwidth of measurement value is lower than simulation which is only 3.03%.

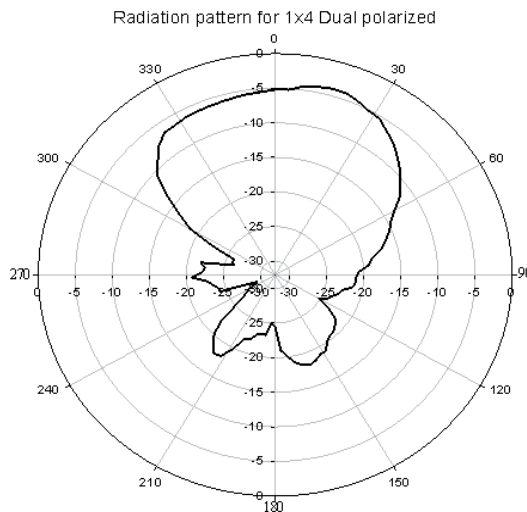


Fig. 3.26. 1x4 array antenna radiation pattern fabrication results

Fig 3.26 show the measurement radiation pattern of the 1x4 dual polarization array antennas. The HPBW achieved for the antenna is about 54.6°. At 2.4 GHz as shown in this pattern, the antenna gain is about 4.37 dB. From the measurement result, one can considered

that there is a variation in the resonant frequency which shift to 2.5 GHz compared to the simulation result. According to this variation, the other measurement method like radiation pattern of both the electrical field and magnetic field, gain and directivity will be applied using the resonant frequency of the return loss fabrication result. Since, the resonant frequency of 2.5 GHz has the best value compared to the intended resonant frequency of the design which is 2.4 GHz.

3.4.3 Dual Polarized 2x2 Array Antenna measurement result

The measurement result of return loss for 1x4 microstrip array is shown in Fig 3.27. The measurement results for 1x4 array antennas were 3.615% and -23.74 dB for bandwidth and return loss respectively. The resonant frequency for fabrication result has shifted by 2.49 GHz which is 5.4% from the simulation resonant frequency. The root cause of the shift is could be due to the FR4 board has ϵ_r that varies from 4.0 to 4.8. In practical world, a material which has varying ϵ_r along a length/width/height, will affect resonant frequency to shift. The other factors affecting etching accuracy such as chemical used, surface finish and metallization thickness also could be the reason for the resonant frequency shifting.

According to Fig 3.28, the beam pattern for 2x2 dual-polarizations has lower sidelobe level compared to 1x2 and 1x4 antennas, but the bandwidth at resonant frequency was very narrow. The narrow bandwidth characteristic of 2x2 antennas can be improved by adjusting the distance of array network, which is quarter wavelength between the patches. This enhancement was achieved without any significant degradation of the beam patterns and bandwidths. The HPBW achieved for the antenna is about 87°. At 2.4 GHz as shown in Fig 3.28, the antenna gain is about 3.57 dB.

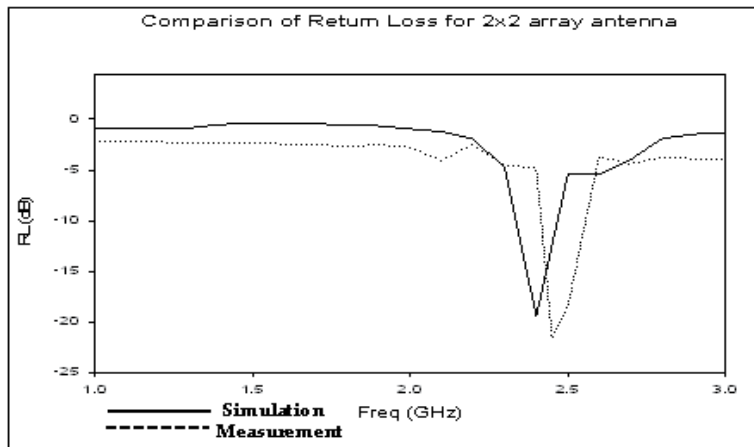


Fig. 3.27. Return Loss [dB] for 2x2 dual linear polarized array antenna.

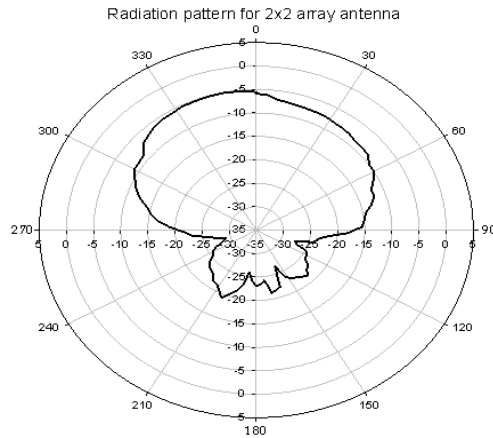


Fig. 3.28. 2x2 array antenna radiation pattern fabrication results

3.4.5 Comparison of the simulation and measurement result

Table 3.5 shows a comparison between simulation and fabrication results of the radiation pattern. According to the variation that occurred in the return loss result, the radiation pattern results were measured by adjusting the resonant frequency at 2.53GHz instead of 2.44 GHz. From this table, one can notice that the HPBW for simulation and fabrication results are in a good agreement.

The gain of the single element antenna was almost 2.21 dBi, and the gain of 1x2 arrays was 2.83 dBi. By designing more patches, which were 2x2 and 1x4 array antennas, the enhancement of gain achieved were 3.57 dBi and 4.37 dBi, respectively. The radiation pattern for 2x2 dual-polarizations has lower sidelobe level compared to 1x2 and 1x4 antennas, but the bandwidth at resonant frequency was very narrow. The narrow bandwidth characteristic of 2x2 antennas can be improved by adjusting the distance of radiation, which is quarter wavelength between the patches. This enhancement was achieved without any significant degradation of the radiation patterns and bandwidths.

	1 x 2		1 x 4		2 x 2	
	Sim	Meas	Sim	Meas	Sim	Meas
Resonant Freq(GHz)	2.4	2.54	2.4	2.51	2.4	2.48
Return loss (dB)	-17.6	-17.3	-21.1	-18.19	-19.4	-21.03
VSWR	1.35	1.18	1.37	1.16	1.24	1.17
BW (%)	4.42	3.45	4.41	4.77	5.46	3.61
Gain	3.09	2.83	5.01	4.37	4.29	3.57

Table 3.5. A comparison of the radiation pattern results for simulation and fabrication

4. Conclusion

A high gain of 3 design microstrip patch antennas oriented at 45° and -45° was proposed to obtain dual polarization. The antennas were operated at resonant frequency, around 2.4GHz with low VSWR. The return loss, radiation pattern and antenna gain have been observed for single, 1x2, 1x4 and 2x2 dual-polarization microstrip patches array antennas. It can be concluded that the responses from the 2x2 and 1x4 patches were better compared to the 1x2 array antenna and single patches antenna. Although the results from the measurement were not exactly the same as in the simulation, there were still acceptable since the percentage error was very small due to the manual fabrication process.

5. References

- Nirmal Kumar Das, Takashi Inoue, Tetsuki Taniguchi and Yoshio Karasawa (2004). An experiment on MIMO system having three orthogonal polarization diversity branches in multipath-rich environment, *Proceeding of Vehicular Technology Conferenc*, pp.1528-1532.vol2, ISBN: 0-7803-8521-7, Tokyo, 26-29 Sept 2004, Japan.
- Collins Brian S. (2000). Polarization-diversity antennas for compact base stations. *Microwave journal*, January, 2000.
- Narayanan Manoj, Amir Faizal & S. Santosh Palai.(2006). Multi Polarization Antenna Structures for Efficient MIMO Systems Employing Software Radio Design Methodology, *Proceeding of RF & Microwave Conf*, pp 390-392, ISBN 0-7803-9745-2, Putrajaya, 12-14 Sept, Malaysia
- Byoungsun. L, Sewoong Kwon, Hyun.Y, Jewoo. L, Jeho. S.(2006). Modeling the indoor channel for the MIMO system using Dual Polarization Antenna, *Proceeding of the 9th EuMA*, pp.334-337, ISBN 2-9600551-5-5, September, Manchester, U.K
- K. Ghorbani and R. B. Waterhouse. (2004). Dual Polarized Wide-Band Aperture Stacked Patch Antennas. *IEEE Transactions on Antennas and Propagation*, pp.2171-2174.vol. 52, no. 8, ISSN: 0018-926X, August 2004.
- S. B. Chakrabarty, F. Klefenz, A. Dreher. (2000). Dual Polarized Wide-Band Stacked Microstrip Antenna with Aperture coupling for SAR application. *Proceeding of Antennas and Propagation Society International Symposium*, pp 2216-2219, ISBN: 0-7803-6369-8, Salt Lake City, 16-21 July 2000, UT.
- S. Hienonen, A. Letho, Annti V.R (1999). Simple broadband dual-polarized aperture-coupled microstrip antenna. *Proceeding of Antennas and Propagation Society International Symposium*, pp 1228-1231, ISBN: 0-7803-5639-x, Orlando, 11-16 July, Florida
- S. Gao, L. W. Li, M. S. Leong, and T. S. Yeo (2003). A broad-band dual-polarized microstrip patch antenna with aperture coupling. *IEEE Transactions on Antennas and Propagation*, pp. 898-900.vol. 51, no. 4, ISSN: 0018-926X, April 2003.
- S. Gao & A. Sambell (2005). Dual polarized Broad- Band Microstrip Antenna fed by Proximity coupling. *IEEE Transactions on Antennas and Propagation*, pp. 526-530.vol. 53, no. 1, ISSN: 0018-926X, January 2005.
- B. Lee, S. Kwon & J. Choi (2001). Polarisation diversity microstrip base station antenna at 2 GHz using T-shaped aperture- coupled feeds. *Microwaves, Antennas and Propagation, IEE Proceedings*, pp. 334-338. Vol 148, no. 5, ISSN: 1350-2417, October 2001

- S. K. Padhi, N. C. Karmakar, Sr., C. L. Law & S. Aditya, Sr. (2003). A dual Polarized aperture coupled circular patch antenna using a C- shaped coupling slot. *IEEE Transactions on Antennas and Propagation*, pp. 3295-3298.vol. 51, no. 12, ISSN: 0018-926X, December 2003.
- A. A. Serra, P. Nepa, G. Manara, G. Tribellini & S. Cioci (2007). A wide-band dual polarized stacked patch antenna. *IEEE Antennas and Wireless Propagation Letters*, pp. 141-143.vol. 6, no. 1, ISSN: 1536-1225, 2005.
- Kin-Lu Wong, Hao-Chun Tung & Tzung-Wern Chiou (2002). Broadband dual-polarized aperture-coupled patch antennas with modified H-shaped coupling slots. *IEEE Transactions on Antennas and Propagation*, pp. 188-191.vol. 50, no. 2, ISSN: 0018-926X, February 2002.
- B. Lindmark (1997). A novel dual polarized aperture coupled patch element with a single layer feed network and high isolation. *Proceeding of Antennas and Propagation Society International Symposium*, pp. 2190-2193. vol.4, ISBN: 0-7803-4178-3, 13-18 July, 1997.
- M. Arezoomand, H. Aziminezhad, F. Hakamizadeh & S. Sadat (2005). A dual polarized aperture coupled microstrip antenna for GSM 900 MHz systems. *Proceeding of international Symposium on Telecommunications*, pp. 539-543, 10-11 September, 2005, Iran.
- J. Choi & T. Kim (2000). Microstrip array antenna for PCS and IMT-2000 base station. *Proceeding of Microwave Conference, 2000 Asia-Pacific*, pp. 25-28. 2000.
- W.-C. Liu, C.-C. Huang and C.-M. Wu (2004). Dual-polarised single-layer slotted patch antenna. *IEE Electronics Letters*, pp. 717-718. vol. 40. no.12, 10 June 2004.
- LJ du Toit & JH Cloete (1987). Dual polarized linear microstrip patch array. *Proceeding of Antennas and Propagation Society International Symposium*, pp. 810- 813. Vol.25, Jun 1987.
- Shun-Shi Zhong, Xue-Xia Yang, Shi-Chang Gao & Jun-Hai Cui (2002). Corner-fed microstrip antenna element and arrays for dual-polarization operation. *IEEE Transactions on Antennas and Propagation*, pp. 1473-1480.vol. 50, no. 10, ISSN: 0018-926X, October 2002.
- Shi-Chang Gao & Shun-Shi Zhong (1998). A dual-polarized microstrip antenna array with high isolation fed by coplanar network. *Microwave and Optical Technology Letters*. pp. 214-216, vol.19, no.3, 20 October 1998.
- S. C. Gao, L. W. Li, T. S. Yeo & M . S. Leong (2001). Low cost, dual linearly polarized microstrip patch array. *IEE Proceeding of Microwave Antenna and Propagation*, pp. 21-24. vol. 148, no.1, ISSN: 1350-2417, February 2001.
- Kim Woelders & Johan Granholm (1997). Cross-Polarization and sidelobe suppression in dual linear polarization antenna arrays, *IEEE Transactions on Antennas and Propagation*, pp. 1727-1740.vol. 45, no. 12, ISSN: 0018-926X, December 1997.
- Keyoor Gosalia & Gianluca Lazzi (2003), Reduced size, dual-polarized microstrip patch antenna for wireless communications. *IEEE Transactions on Antennas and Propagation*, pp. 2182-2186.vol. 51, no. 9, ISSN: 0018-926X, September 2003.
- M. Ramesh, K. B. Yip (2003), Design Inset Fed Microstrip Antenna, *Microwaves and RF Letters*, vol.42, no. 12, Dec. 2003.

A Time-Delay Suppression Technique for Digital PWM Control Circuit

Yoichi Ishizuka
Nagasaki University
Japan

1. Introduction

Recently, power management has been introduced to improve the power efficiency of Micro Processing Unit (MPUs), Field Programmable Gate Array (FPGAs) and Digital Signal Processor (DSPs). The power management system includes a full operation mode, standby mode, and sleep mode. The clock frequency, core voltage and/or core current are changed in each mode accordingly. As a result, the output current of the point-of-load (POL) DC-DC converters is intermittent and has a high slew rate. A low output voltage, a large output current and a high speed response are required for the POL. In such a condition for the control circuit, highly accurate and high-speed control demands that the tolerance of the output voltage becomes internally severe, advanced by speed-up and lowering of the voltage of the MPUs, FPGAs and DSPs. A general control method is pulse width modulation (PWM) control with PID. Generally, such control circuits are composed with analog circuits and/or simple combination digital circuits.

In these days, robustness or flexible controls for versatile conditions are demanded which cannot accomplished with analog control circuit. For the control purpose, DPWM control is a one of appropriate technique (Edward Lam, Robert Bell, and Donald Ashley (2003), A.V.Peterchev and S.R.Sanders (2003), B.J.Patella, A.Prodic, A.Zirger and D.Maksimovic

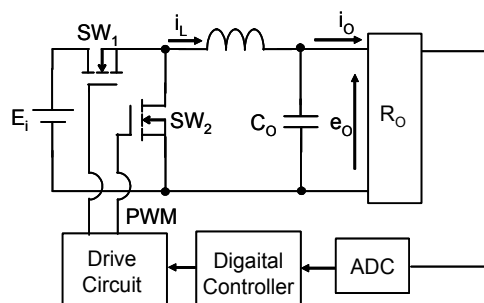


Fig. 1. Common digital control DC-DC converter.

(2004), D.Maksimovic, R.Zane, and R. Erickson (2004), S.Saggini, D.Trevisan and P.Mattavelli (2007), S.Saggini, E.Orietti, P.Mattavelli, A.Pizzutelli and Bianco(2008)).

Digital control or DPWM can accomplish robust and flexible power control with soft-tuned parameters and will become popular control technique.

Although, there are some disadvantages in cost and speed, against analog control circuit.

Especially, A/D converter circuit, which doesn't need for analog control, is the one of the key circuits which effects on cost and speed. Generally, A/D converter is located in front of digital controller as shown in Figure 1. Therefore, the transition speed of A/D converter directly effects on the response speed of the control circuit. And, the cost and speed are always trade off problem. This problem is especially serious in POL DC-DC converter which is required to design the control circuit in relatively low-cost and high speed control response. Moreover, generally, there is sample-and-hold circuit in front of A/D converter which degrades the response speed.

A delay in any feedback system degrades the stability and damping of the system. Especially, in DPWM, if a total of the delays described in above become larger than on-term of one switching period, a factor of A/D converter becomes V_q/Z shown in Figure 2 where V_q is a coefficient constant.

An objective of this paper is to design high speed and low cost voltage sensing circuit for DPWM control circuit for DC-DC converter. And, also real-time PID control method is proposed. In Sec. II, the details of proposed system are described. In Sec. III, the some characteristics of the system are confirmed with experimental results. Finally, in Sec. IV, the summary is described.

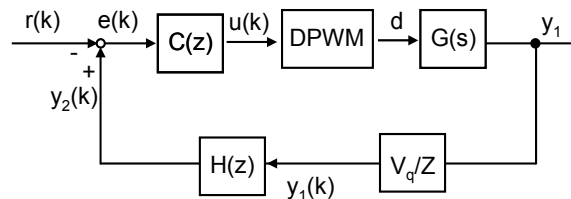


Fig. 2. Control System.

2. Proposed System

We propose a scheme of a digital control and DPWM circuit for DC-DC converter without A/D converter shown in Figs.3 and 4, respectively. In this proposed control circuit, most components are digital components. Analog components for the control circuit are essentially only D/A converter and analog comparator. Theoretical waveforms of each part are shown in Figure 5. The control circuit is composed of three major blocks.

2.1 Analog-Timing Converter (ATC)

The first block is ATC block which detects the output voltage e_o and outputs the detected signal to latch register. The maximum output value of D/A converter DAC is set as a sum of the output reference voltage of DC-DC converter V_{ref} and margin $\alpha(>0)$. A digital staircase waveform data, pre-stored in memory Memory1, is output to DAC synchronized with a system clock, and converted analog staircase waveforms V_{ref}' is compared with e_o . As soon as $V_{ref}' > e_o$, the comparator outputs high.

2.2 PID Control with Look-up Table

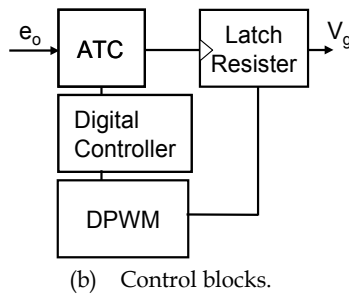
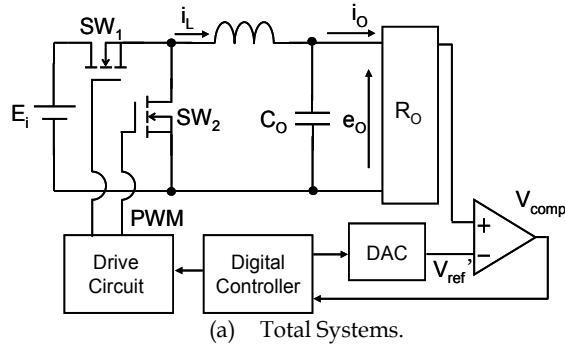


Fig. 3. Proposed DPWM Control DC-DC converter

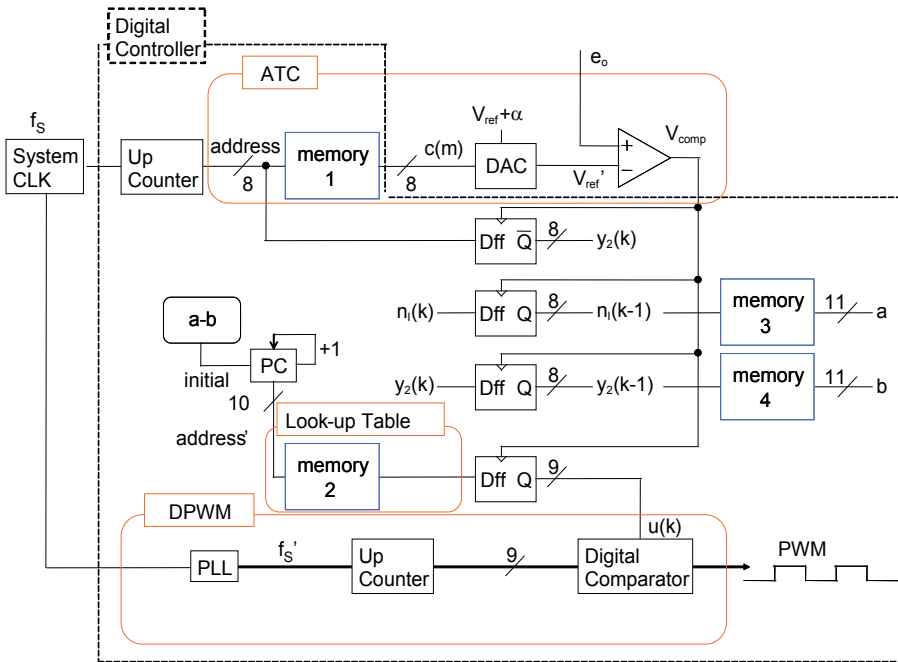


Fig. 4. Proposed digital control circuit.

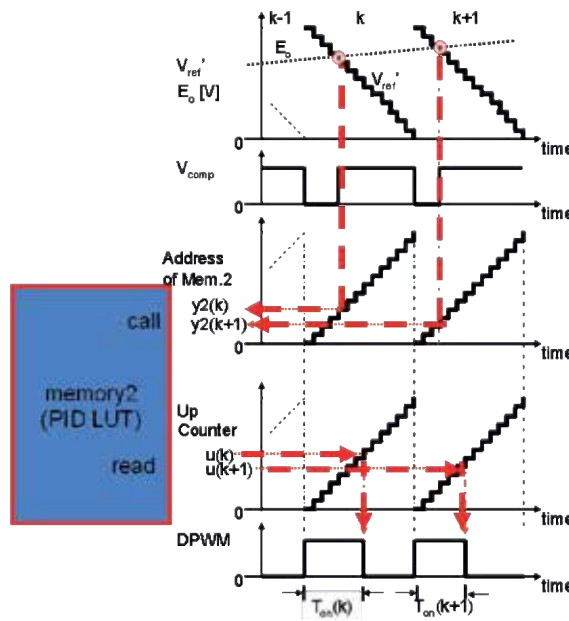


Fig. 5. Theoretical waveforms.

$u(k)$ which is output from Memory2 is calculated by general PID digital control laws as

$$u(k) = u_{Ref} + K_P e(k) + K_I n_I(k) + K_D (e(k) - e(k-1)) \tag{1}$$

where u_{Ref} is a reference value of $u(k)$, $e(k)$ is a digitalized error value between r which is digitalized reference voltage V_{ref} in switching term k , and $n_I(k) = n_I(k-1) + e(k)$ (G. F. Franklin, J. D. Powell and M. L. Workman (1997)). K_P , K_I and K_D are a proportional gain, an integral gain and a derivative gain, respectively. Equation (1) can be transformed to

$$u(k) = u_{Ref} - (K_P + K_I)r + A\{y_2(k) + \frac{K_I}{A}n_I(k-1) - \frac{K_D}{A}y_2(k-1)\} \tag{2}$$

where $A = K_P + K_I + K_D$ and $y_2(k)$ is digitalized output voltage e_o in switching period k . In Figure 4,

$$a = \frac{K_I}{A}n_I(k-1) \tag{3}$$

$$b = \frac{K_D}{A}y_2(k-1) \tag{4}$$

Memory3 and Memory4 store a and b , respectively.

In Eq. (2), $a - b$ in the term k is pre-calculated in the term $k-1$ and the obtained value becomes the initial value of programmable counter PC of the term k . And, $address'$ which indicates address of Memory2 is incremented with system clock and $u(k)$ is called from Memory2, simultaneously.

$$address' = y_2(k) + a - b \tag{5}$$

From (2) and (5),

$$u(k) = u_{Ref} - (K_P + K_I)r + A\{address'\} \tag{6}$$

Therefore, $u(k)$ is determined as soon as $y_2(k)$ is detected.

2.3 DPWM

In this system, on-term $T_{on}(k)$ of DPWM signal is decided by $u(k)$, which is normalized $T_{on}(k)$, and system clock frequency f_s' as

$$T_{on}(k) = u(k) / f_s' \tag{7}$$

$u(k)$ is decided by latched value of Memory2.

In parallel with the processing of ATC block, the $u(k)$ is called with system clock and latched by ATC output as trigger.

3. Sensing Resolution

3.1 Resolution Increasing

As described in previous section, all blocks are synchronized with only one clock source.

From this advantage, all blocks are modified in easy way.

In this paper, voltage sense resolution increase of output voltage is proposed.

In proposed system, R-2R ladder type D/A converter is used. The output voltage is set between $V_{ref}^+ (= V_{ref} + \alpha)$ and V_{ref}^- . Therefore,

$$V_{ref}' = \frac{c(m)}{2^n} (V_{ref}^+ - V_{ref}^-) + V_{ref} \tag{2.8}$$

where n is bits. Also, least significant bit (LSB) voltage a_{LSB} becomes

$$a_{LSB} = \frac{1}{2^n} (V_{ref}^+ - V_{ref}^-) \tag{2.9}$$

In this paper, V_{ref}' is set to $V_{ref} / 2$. Almost $n+1$ bits resolution can be realized by n bits digital system as shown in Table 1.

3.2 Sensing Time Delay

With this method, sensing time is increased. To avoid the time delay, the reference voltage waveform data pre-set in memory1 V_{ref}' is modified as shown in Figure 6.

	bits	Reference voltage		LSB voltage value
	n[bit]	$V_{ref}^+[V]$	$V_{ref}^-[V]$	$a_{LSB}[mV]$
[3]	8	1.7	0	6.64
[3] with 9bits	9	1.7	0	3.32

Table 1. Relations between parameter and quantization error of D/A Converter

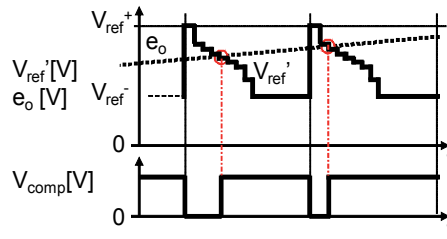


Fig. 6. Modified reference voltage waveforms

4. Prototype Circuit Experiments

4.1 Experimental Conditions

Some experiments are performed to verify the scheme. The proposed controller with prototype circuit is shown in Figure 7. The digital controller part is designed in FPGA Altera Stratix with Quartus II. 149 logic elements and 1 PLL block are used. All memory blocks, Memory1, Memory2, Memory3 and Memory4, are including in the logic elements. Intersil CA3338MZ is used as 8bit DAC. National Semiconductor LMV7219 is used as an analog comparator.

The DC-DC converter topology is basically same as Figure 3. The experimental conditions are shown in Table 2.

4.2 Experimental Results

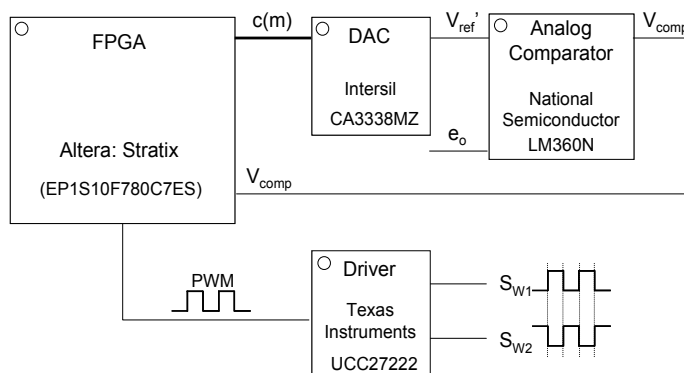


Fig. 7. Prototype proposed control circuit.

The static experimental waveforms are shown in Figure 8.

From this result, it is able to confirm that the output voltage sensing is done within the on-width of PWM signal.

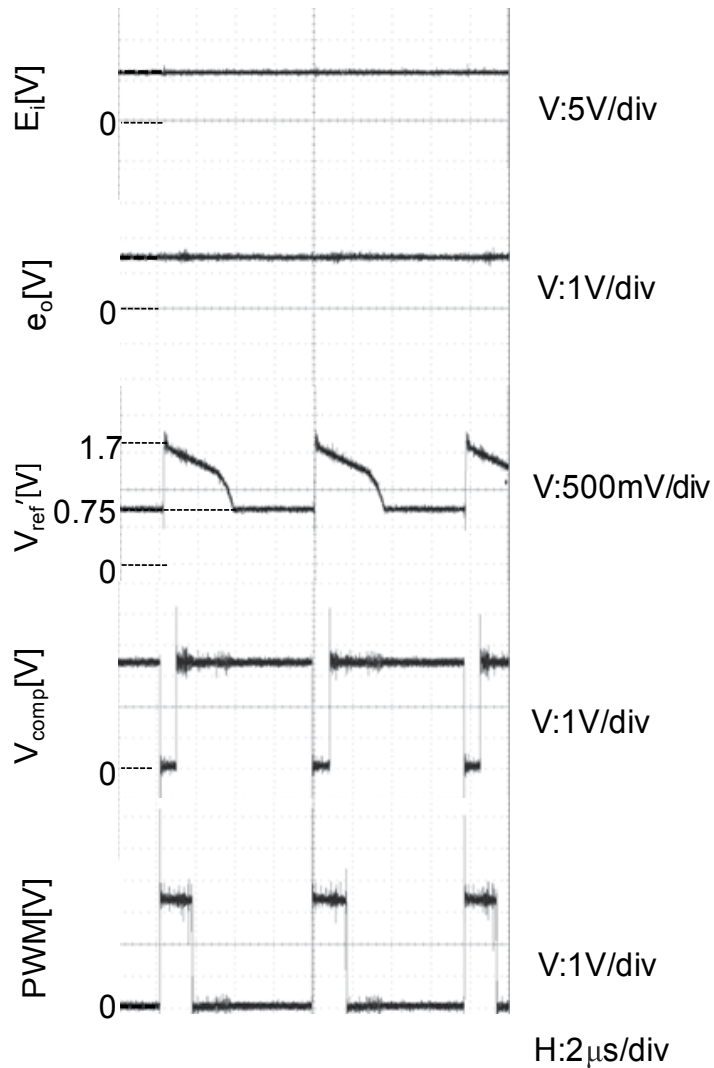


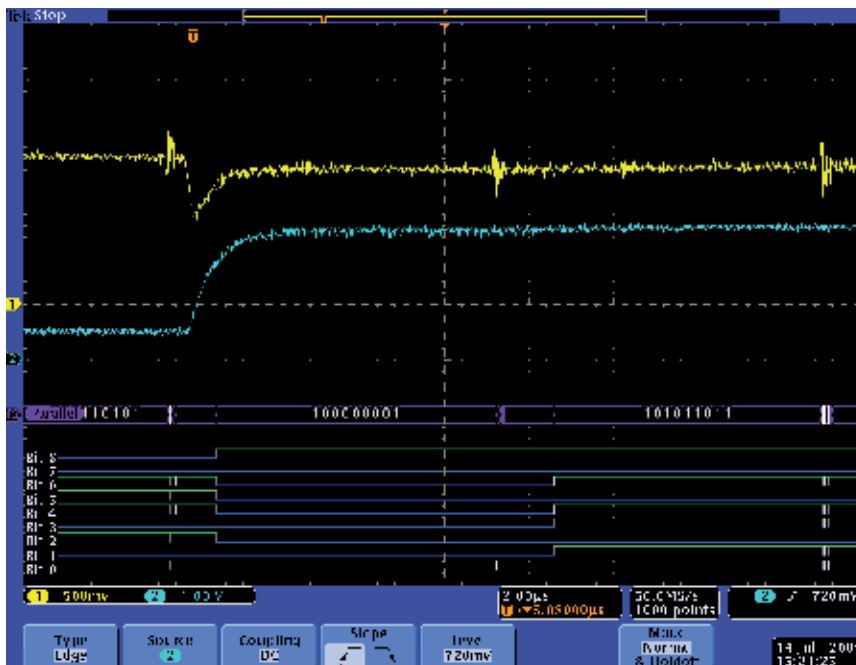
Fig. 8. Experimental waveforms

4.3 Dynamic Characteristics

Figure 9 and 10 show dynamic characteristics with load current i_o changing between 0.5A and 2.5A, respectively. The mixed-signal oscilloscope Textronix MSO4034 is used to measure analog and digital signal, coinstantaneously. The load current changing is

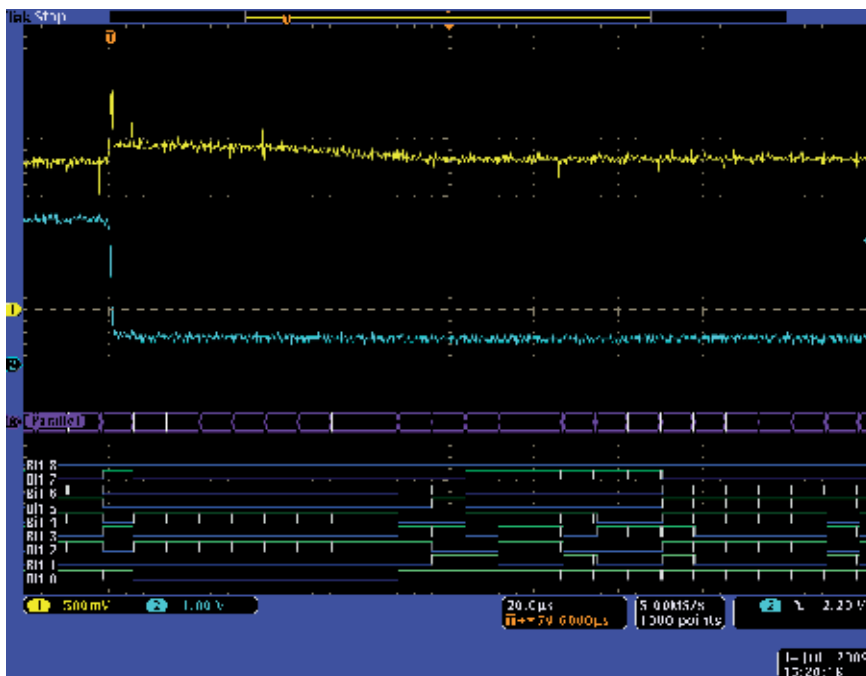


(a) H: 20µs/div.

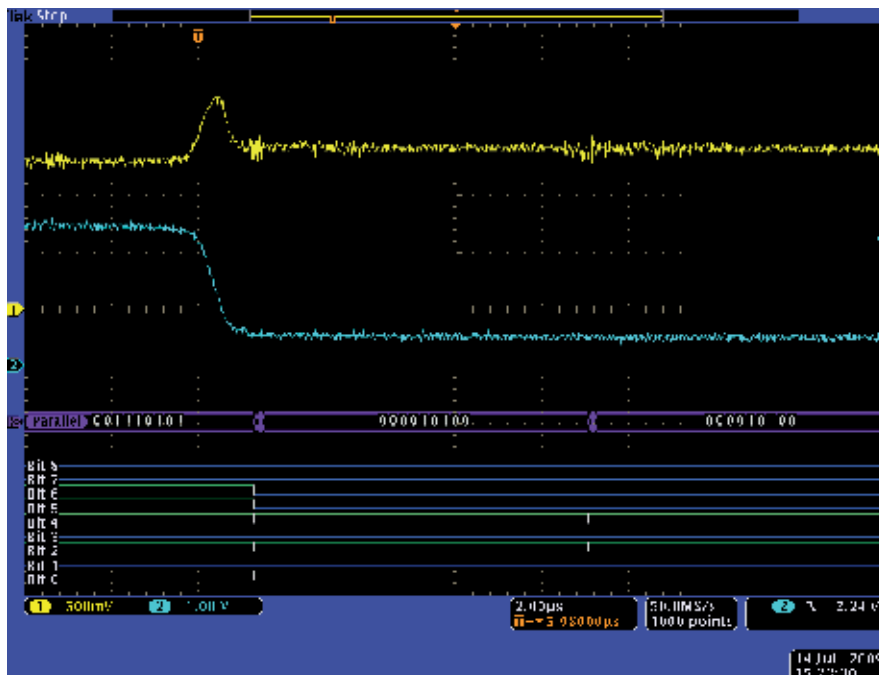


(b) H: 2µs/div.

Fig. 9. Dynamic characteristics (from 0.5A to 2.5A)



(a) H: 20µs/div.



(b) H: 2µs/div.

Fig. 10. Dynamic characteristics (from 2.5A to 0.5A).

performed with 1kHz driven power MOSFET parallelly-connected to load resistance. Yellow and Blue line shows the output voltage and the output current, respectively. The 9 bits pulse waveforms shown at the bottom of Figure 9 are calculated DPWM of FPGA.

Figure 9 shows the sudden load current increasing results. From these results, after the 1 μ s voltage drop, the output voltage immediately recovers to the reference voltage.

Figure 10 shows the sudden load current decreasing results. From these results, after the 1 μ s voltage rising, the output voltage immediately recovers to the reference voltage.

5. Conclusion

This paper describes a digital PWM controller IC without A/D converters. The analog timing converter (ATC) is proposed for output voltage sensing. In this system, analog circuit are realized with an comparator and an D/A converter.

6. References

- A. Ichinose, Y. Ishizuka, and H. Matsuo (2006). A Fast Response DC-DC Converter with DPWM Control, *Technical Report of IEICE*, vol. 105, no. 538, EE2005-58, 67-71
- Y. Ishizuka, M. Ueno, I. Nishikawa, A. Ichinose, and H. Matsuo (2007). A Low-Delay Digital PWM Control Circuit for DC-DC Converters, *IEEE Applied Power Electronics Conference (APEC'07)*, 579-584
- M. Nishi, Y. Asako, Y. Ishizuka, and H. Matsuo (2008). A control circuit composition and several characteristics of the proposed DPWM controlled POL, *Technical Report of IEICE*, vol. 107, no. 430, EE2007-46, 13-18
- Edward Lam, Robert Bell, and Donald Ashley (2003). Revolutionary Advances in Distributed Power Systems, *Proc. IEEE APEC '03*, 1.5
- A.V.Peterchev, and S.R.Sanders (2003): "Quantization Resolution and Limit Cycling in Digitally Controlled PWM", *IEEE Trans. on Power Electronics*, Vol. 18, No. 1, 301-308
- B.J.Patella, A.Prodic, A.Zirger, and D.Maksimovic (2004). High-frequency digital PWM controller IC for DC-DC converters, *IEEE Transactions on Power Electronics*, Vol. 18
- D.Maksimovic, R.Zane, and R. Erickson: "Impact of Digital Control in Power Electronics", *IEEE International Symposium on Power Semiconductor Devices & ICs, Kitakyushu, Japan*, 13-22
- Kaiwei Yao (2004). High-Frequency and High-Performance VRM Design for the Next Generation of Processors, *Doctor thesis of Virginia Polytechnic Institute and State University*
- S.Saggini, D.Trevisan, and P.Mattavelli (2007). Hysteresis-Based Mixed-Signal Voltage-Mode Control for dc-dc Converters, *IEEE Power Electronics Conference (PESC'07)*, Orlando, Florida
- S.Saggini, E.Orietti, P.Mattavelli, A.Pizzutelli and Bianco (2008). Fully-Digital Hysteretic Voltage-Mode Control for dc-dc Converters based on Asynchronous Sampling, *IEEE Applied Power Electronics Conference (APEC'08)*, Issue , 24-28, 503 - 509
- G.F.Franklin, J.D.Powell, and M.L.Workman (1997). *Digital Control of Dynamic Systems*, Addison Wesley Longman Press, Menlo Park. CA

Layer 2 Quality of Service Architectures

Christos Bouras^{1,2}, Vaggelis Kapoulas¹, Vassilis Papapanagiotou^{1,2},
Leonidas Pouloupoulos^{2,3}, Dimitris Primpas^{1,2} and Kostas Stamos^{1,2}

¹*Research Academic Computer Technology Institute, Greece*

²*Computer Engineering and Informatics Dept., University of Patras, Greece*

³*Greek Research and Academic Network - GRNET, Greece*

1. Introduction

Quality of Service (QoS) provisioning has become indispensable in today's networks. Most existing QoS solutions are deployed in Layer 3 (network layer). In order to provide end-to-end QoS guarantees in these networks, the need for Layer 2 QoS deployment as well as the cooperation between any existing Layer 3 QoS deployment must be studied. QoS provisioning in Layer 2 is very important to networks that are primarily based on Layer 2 infrastructure as it is the only way to provide QoS on the network. Furthermore, networks based on both Layer 2 and Layer 3 network devices could benefit from a more integrated approach in end-to-end QoS provisioning that includes both Layer 2 and Layer 3.

In today's broadband networks, congestion does not necessarily occur at the edge of the network (the link interconnecting the subscriber to the network core): congestion is equally likely to occur at the edge and in the core of the network. A common congestion cause of in broadband networks is the capacity mismatch in different parts of the network core. This calls for protection measures at the network perimeter and unified or interoperable QoS schema across all network (both layer 2 and layer 3).

Moreover, Layer 2 QoS is lightweight, easily implemented and independent of Layer 3. Because of its independency, it can also be applied to non-IP networks where any QoS provisioning was impossible or very difficult. In this chapter, we examine the cooperation between Layer 2 and Layer 3 QoS in IP networks. When discussing Layer 2 devices and procedures in this chapter, we are specifically referring to Ethernet technology switches, which have become the dominating Layer 2 technology during the past years and have largely substituted older technologies at the same layer, such as ATM and Frame Relay.

Layer 2 Ethernet switches rely on 802.1p standard to provide QoS. The standard 802.1p is part of the IEEE 802.1Q (IEEE, 2005) which defines the architecture of virtual bridged LANs (VLANs). This architecture uses tagged frames inserted in Ethernet frames after the source address field. One of the tag fields, the Tag Control Information, is used by 802.1p in order to differentiate between the classes of service. More specifically, the 3 most significant bits of the Tag Control Information field known as Priority Code Point (PCP) are used to define frame priority. Taking advantage of PCP, QoS in Layer 2 can be applied.

Layer 2 QoS experiments with Ethernet switches have been conducted and described in (Ubik & Vojtech, 2003). In (Ubik & Vojtech, 2003) 4 Layer 2 QoS experiments are conducted

and effects on link throughput and packet loss are shown. Other researchers such as (Liotopoulos & Guizani, 2002) have dealt with Layer 2 QoS in ATM networks. An interesting application of L2 Ethernet QoS has been studied in the field of avionics networks with the demand for low latency and jitter in (Wernicke, 2006) and (Jacobs et al., 2004), while 802.1p has been studied as an approach for the improvement of traffic performance originating from collaborative systems applications in (Perez et al., 2006).

In the next sections of this chapter, we discuss the issue of Layer 2 QoS deployment, and in particular we present in detail:

- The cooperation of Layer 2 QoS with possibly pre-existing Layer 3 QoS architectures in MAN broadband networks.
- The architecture for Layer 2 QoS deployments, with analysis of the authors' experience at GRNET as a case study.
- The status of Layer 2 QoS support in various vendors' equipment according to our experience.

2. Integration of Layer 2 and Layer 3 architectures

Quality of Service support was initially enabled on routing devices using the available fields in the IP header. Therefore, a comprehensive architecture has to take this into account and be able to accommodate the addition of more devices, which do not route packets, in the overall QoS architecture. For example, Layer 2 Ethernet switches rely on 802.1p standard to provide QoS. An example of a network where the need for integrated Layer 2 and Layer 3 QoS provisioning has been investigated is the Greek Research Network (GRNET, 2009a), which is described in detail in the next section of this chapter.

In general, the integration of Layer 2 and Layer 3 QoS architectures can take several forms, depending on the purpose for which the switching and/or routing devices are used (access, core), their functionality (since several devices have capabilities that tend to blur the L2/L3 distinction, for example switches that can inspect the IP header), the policies of the network domain and other factors. A basic distinction of the most common choices is provided below:

- Layer 2 devices at the edge (access) of the network and routing devices (possibly using MPLS) in the core: A very common case, this scenario is studied in detail in the next sections of this chapter, as it largely describes the structure of GRNET.
- A combination of Layer 2 and Layer 3 across the network, with switching devices comprising L2 MANs: Sometimes it is convenient to build "islands" where traffic is simply switched and not routed. This approach is usually accompanied with extensive VLAN usage for traffic management purposes. Part of the GRNET network has been built with this philosophy, and its practical implications are described in the relative section of the chapter.
- Switched-based network, with Layer 3 devices at the periphery: A growing tendency in high speed modern networks has been towards connectivity at lower layers, bypassing expensive routing functions. In this case, L2 QoS takes center stage in the planning of a QoS architecture.

In all cases, a proper QoS architecture has to include the basic steps of classification, policing, marking and scheduling. The design of the network and the specific mix of devices

and requirements will determine whether both Layer 2 and Layer 3 devices perform all of these functions, or whether these functions are distributed.

A network that serves several clients at its periphery will generally have to consider the traffic sources untrustworthy, in terms of proper packet classification and marking. Therefore, the edge devices of the network will have to take up this role. Classification typically requires packet inspection and is therefore more suited for higher-layer devices, although several switching devices do support some form of inspection of encapsulated higher layer headers. If that is not the case, then traffic might have to be classified when it first traverses suitable equipment. This means that incoming traffic might not be subjected to prioritized treatment immediately upon arriving at the borders of the network.

3. Layer 2 QoS case studies

GRNET is the Greek National Research and Education Network (NREN) (GRNET, 2009a). GRNET is a mixed IP- and Ethernet-based network, operating at Gigabit speeds. Together with the high-speed LANs of its subscribers (universities and research institutes) and the European academic and research backbone, GEANT, GRNET forms a set of hierarchically-federated networks.

However, because part of its backbone consists of switch based MANs, this architecture had to be extended in order to encompass Layer 2 (Ethernet) devices, which should appropriately implement QoS policies and QoS signaling/metering as well.

The GRNET backbone consists of network nodes in 8 major Greek cities, namely, Athens (2 PoPs), Thessaloniki, Patras, Ioannina, Xanthi, Heraklion, Larisa and Syros as shown in Fig. 1, a screenshot from the GRNET's GoogleMaps Topology Visualization (GRNET, 2009b).

The WAN network is built on DWDM links with 2.5Gbps capacity (STM-16 lambdas). The access interfaces of the routers are using Gigabit Ethernet technology and connect the 130 subscribers of GRNET which consist of universities, technological educational institutes, research institutes, two content providers (the Greek National Television and the Greek Parliament) and the school network. During the last few months the major Greek Universities upgraded their connection speed to GRNET from 1-Gbps to 10-Gbps. In addition to the WAN, GRNET also has 2 distinct MAN networks. The Athens MAN is router-based (Fig. 2), whereas the Crete MAN is switch-based (Fig. 3), with a router in the main aggregation site (Heraklio).

The Greek Research and Academic Network (GRNET, 2009a) has deployed for several years a Layer 3 QoS service based upon the features provided by the MPLS technology deployed in the core of the GRNET network, and DiffServ architecture. This architecture allows the support of multiple classes of service. The focus is on three separate classes of service, namely IP Premium for absolute performance guarantees, best effort for the usual treatment of traffic packets and Less than Best Effort (LBE) for non-critical traffic that can be dropped first in case of congestion. IP Premium service is a circuit-like subscriber-to-subscriber service, where both subscriber end-networks and the necessary bandwidth allocation are known at request time. IP Premium service is provided using a provisioning tool called ANStool (Varvitsiotis et al., 2005; GRNET, 2009c). LBE is provided unprovisioned, which means that each subscriber decides on its own and uses this service simply by marking the packets appropriately. In order to provide the QoS service, the Layer 3 network equipment (routers) has to perform traffic marking, classification, policing and shaping. Per-flow

functions are performed at the edge routers of GRNET network, while core routers only perform per-traffic class functions, based on the MPLS Exp field.

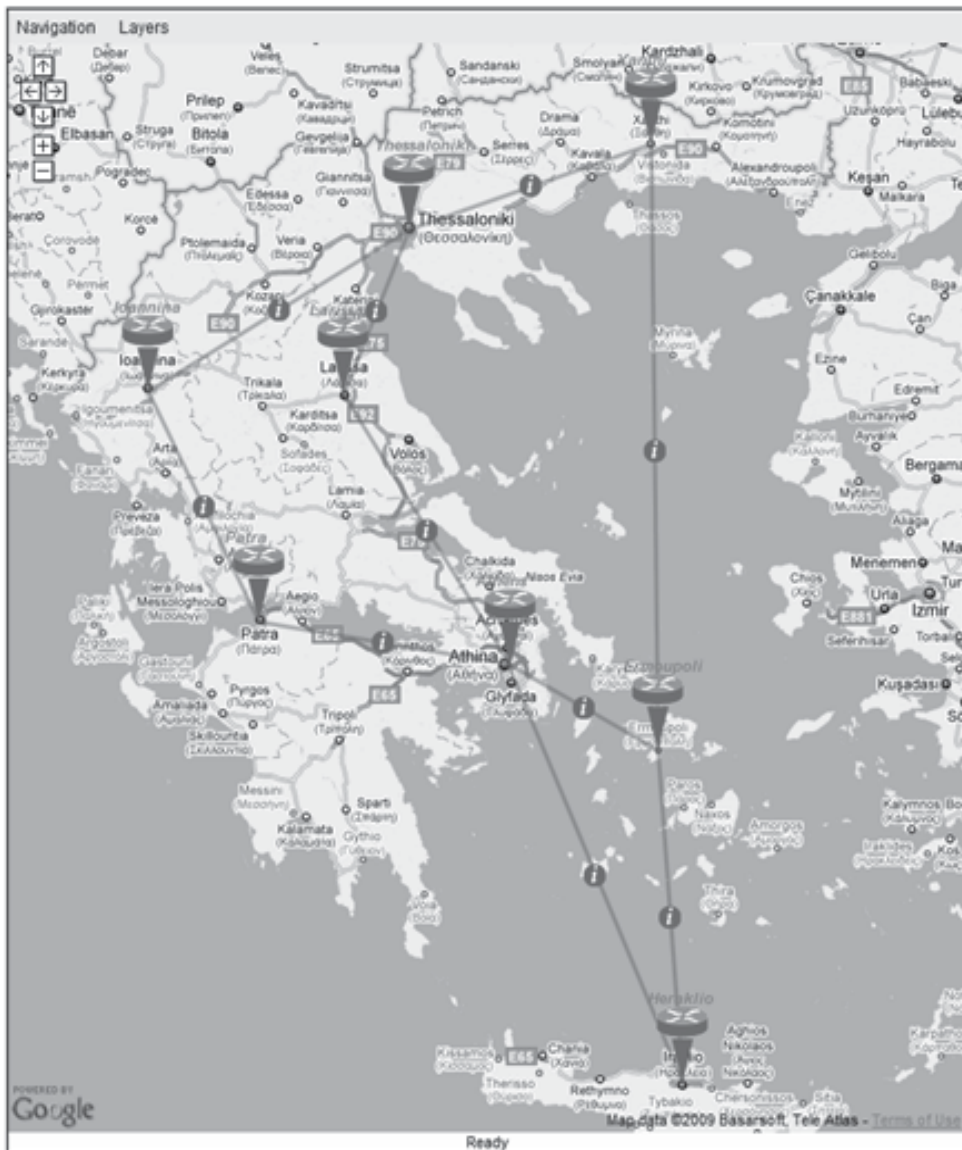


Fig. 1. GRNET's Layer 3 Country Network Topology

The above service design has several implications for traffic between two GRNET clients (such as institutions, universities or other research organizations). It means that traffic coming out of GRNET network ("output" for GRNET edge routers) has been subjected to the specified QoS mechanisms. However, traffic coming into the GRNET network ("input" for GRNET edge routers) receives no treatment up to the point of reaching the edge Layer 3 device (router) of the GRNET network.

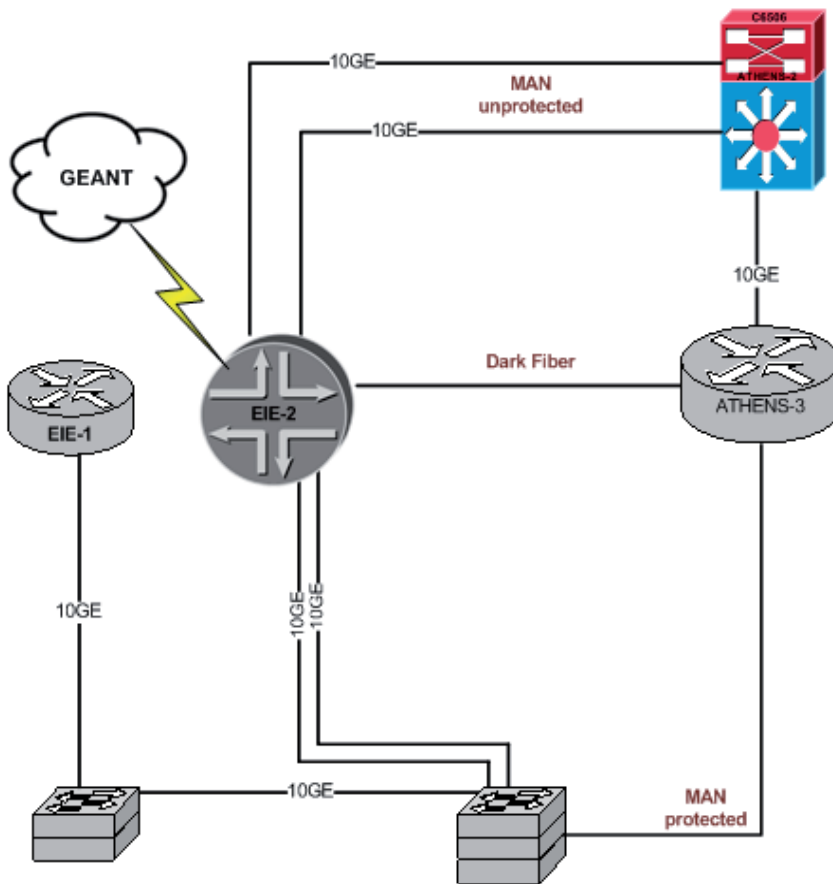


Fig. 2. Athens' MAN

In the most common case (except Crete's MAN), traffic between the GRNET client and the GRNET edge router will go through one or more Layer 2 devices (Ethernet switches). For the simple case where only one Layer2 device is located between GRNET and the subscriber, we use scripting to query the speed and bandwidth settings at each L-2 border interface. We then reflect the speed setting of the border interface into a traffic shaping queue for the respective VLAN at the L-3 border. Using this technique, we make sure that the congestion points occur only at the L-3 border.

With the advent of hybrid networks and the tendency to carry high speed network traffic at the lowest layer possible (in order to avoid handling it with costly Layer 3 equipment), this part of current and future network is bound to expand. Whether this Layer 2 part of the network forms multiple paths between the connected Layer 3 devices (in which case the need for spanning tree algorithms arises in the common Ethernet case) determines in large part the complexity of the Layer 2 QoS solution that will have to be adopted.

Therefore, in designing and implementing the service described in this chapter, we took into account the current need for controlling traffic behavior at the edge of the GRNET network (where it slips from current Layer 3 QoS model) and we also considered the increasing importance of that part of the network to the overall network architecture in the future.

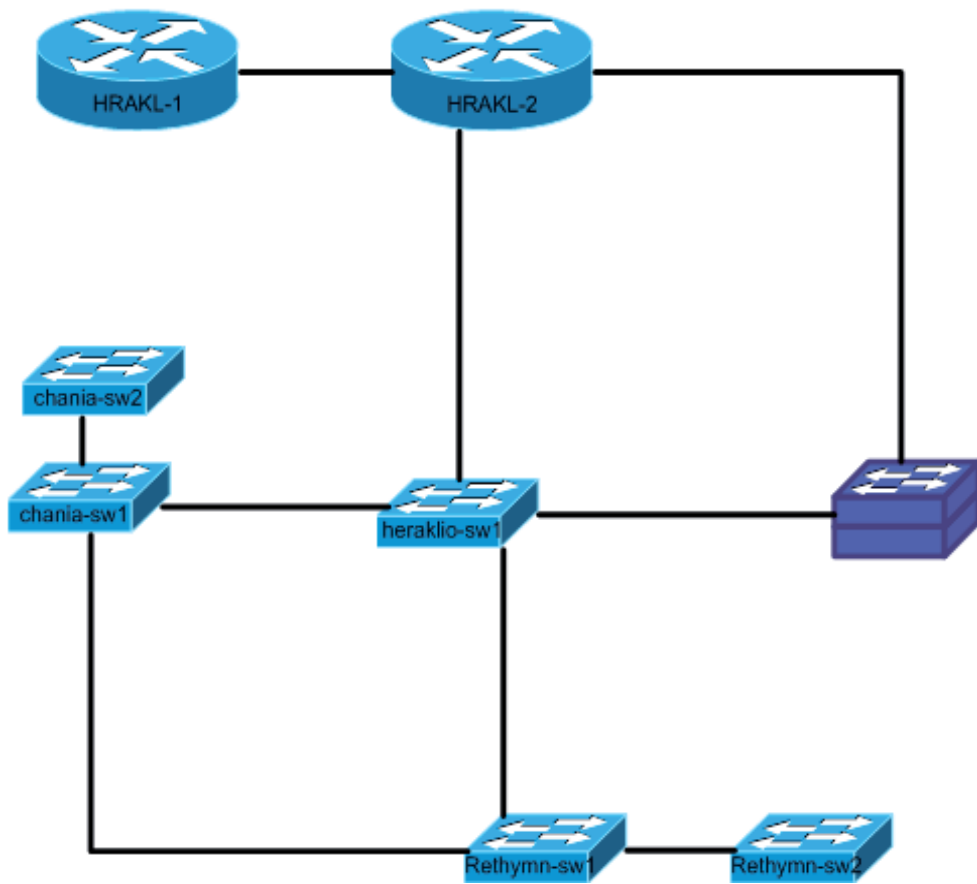


Fig. 3. L2 Crete's MAN

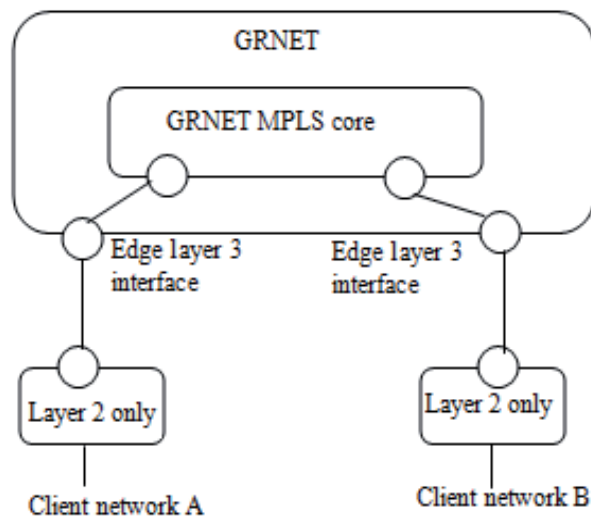


Fig. 4. Schematic of GRNET core/edge/L2-only edge network parts

3.1 Implementation Issues

IEEE 802.1Q (also known as VLAN tagging) defines a 3-bit field called Class of Service (CoS), which can be used in order to differentiate traffic. Table 1 shows the 8 possible values of the CoS field and their original purpose.

CoS	Acronym	Purpose
0	BE	Best effort
1	BK	Background
2	-	Spare
3	EE	Excellent Effort
4	CL	Controlled Load
5	VI	"Video" < 100 ms latency and jitter
6	VO	"Voice" < 10 ms latency and jitter
7	NC	Network control

Table 1. CoS field values

For the purposes of our deployment, we have adopted the usage of CoS value 5 for marking premium traffic (which requires quality of service), CoS 0 for best-effort traffic and CoS 1 for less than best effort traffic. Traffic is marked as less than best effort when it is of minor importance, and is allowed to occupy at most 1% of the total bandwidth. The usage of CoS value 5, indicates that the default DSCP-to-CoS mapping scheme is followed, bearing in mind that in GRNET IP Premium is marked with DSCP 46 as denoted in (Varvitsiotis et al., 2005). In the case of the GRNET (GRNET, 2009a) network, end to end traffic between client network interconnected through GRNET will traverse a combination of Layer 2 (switches) and Layer 3 devices (routers). To this end, the policies of the edge routers of the GRNET network must be adapted so that ethernet frames belonging to premium traffic are marked with CoS 5 at the output. Additionally, the port of the subscriber's switch which is connected on the edge router has to be configured in order to trust the values of CoS of the received traffic streams. Because CoS is part of the standard 802.1Q (IEEE, 2005), the port on which the edge router is connected must be in trunk mode. When a port is in trunk mode it uses the tagged frames of 802.1Q (IEEE, 2005) to communicate, which contain CoS and other information about virtual bridged local area networks (VLANs).

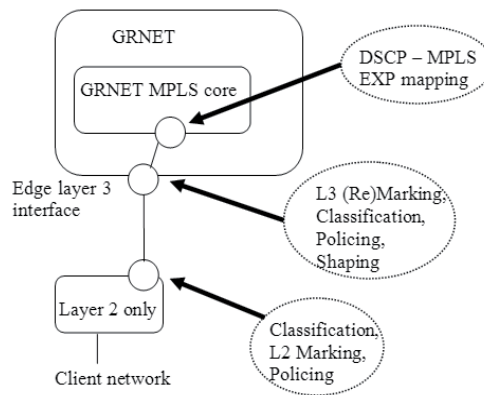


Fig. 5. Schematic of L3 and L2 QoS actions

The procedure of deploying Layer 2 Quality of Service is quite similar to the one of Layer 3 QoS. Classification procedure is applied in incoming packets along with policing functions. Next, if traffic is in profile it is marked accordingly, else the packet is marked down or dropped. Next, the packets enter the switch's queues according to their markings.

Queue management and scheduling are the most important issues in configuring Layer 2 Quality of Service. L2 Ethernet switches support a number of ingress and egress queues (switches in our testbed support 2 ingress queues and 4 egress queues). Scheduling in our equipment (Cisco Systems devices) is performed using the Shaped Round Robin (SRR) algorithm. The ingress queues can only be shared whereas the egress queues can also be shaped. When queues are shared their bandwidth is guaranteed to configured weights but is not limited to it. When a queue is empty, the other queues in shared mode share its unused bandwidth. When a queue is shaped it is guaranteed a percentage of bandwidth but it is rate limited to that amount. By default, from the ingress queues the second one is used to handle high priority traffic, and from the egress queues the first one is the high priority queue and it cannot be changed. Additionally, the high priority egress queue is by default shaped to occupy 1/25 of total bandwidth, and when a queue is shaped any sharing settings are overridden. When the expedited output queue is enabled (as in our experiments, using the command `priority queue-out`), the expedited queue is serviced first until it is empty and then the other queues are serviced in a round-robin manner. More information can be found in (Cisco, 2009). In the GRNET network the edge routers shape the traffic on the output, so there is no need to shape the queues on the switches, however in our experiments, we use policies to limit the bandwidth when needed. Additionally, in the GRNET network the switch trusts the CoS of the packets coming from a GRNET edge router. By contrast, in our experiments traffic was classified by the switch and the DSCP field (46 for premium traffic, 0 for best-effort) was set, as in testing equipment policies that set CoS are not supported.

In order to verify the proper configuration and operation of the Layer 2 QoS service, extensive experimentation was performed in both laboratory and production environments (Bouras et al., 2008). The conducted experiments acknowledged and proved that the activation of L2 QoS does benefit the overall result that was previously produced by only L3 QoS in GRNET's network.

An additional step is the enhancement of the GRNET QoS provisioning tool (GRNET, 2009c) with the necessary functionality and features in order to manage the L2 QoS service as well. In this direction, a module was developed and integrated into GRNET's QoS provisioning tool. This service is unprovisioned and does not require any type of interaction of GRNET's customers with the Layer 2 module. Of course, for the proper operation of the end-to-end QoS provisioning, GRNET's clients must submit a Layer 3 request in the first place.

The Layer 2 module of the QoS provisioning tool provides the network administrator with the appropriate vendor-specific configuration, which in turn is applied to the network switches. A view of the switches' list is presented in Fig. 6.

When a switch is selected, the administrator must activate QoS at the switch by selecting "Standard CPE QoS configuration" as shown in Fig. 7, an option that provides the appropriate configuration. Finally, the requested interfaces are selected. Once the Layer 3 configuration is applied to router and the Layer 2 configuration is applied to the switch, the customer is given end-to-end QoS.

ihu-asw.grnet.gr	Extreme	Extreme 450
iibeaa-asw.grnet.gr	Extreme	Extreme 450
ilsp-asw.grnet.gr	Extreme	Extreme 450
ionio-asw.grnet.gr	Cisco	catalyst37xxStack
iptil-asw.grnet.gr	Cisco	catalyst37xxStack
kape-asw.grnet.gr	Extreme	Extreme 450
maich-asw.grnet.gr	Cisco	catalyst3512XL
noa-asw.grnet.gr	Cisco	catalyst37xxStack
ntua-asw.grnet.gr	Extreme	Extreme 450
oipp-asw.grnet.gr	Extreme	Extreme 450
panteion-asw.grnet.gr	Cisco	catalyst3512XL
pasteur-asw.grnet.gr	Extreme	Extreme 450
selete-asw.grnet.gr	Extreme	Extreme 450
teiath-asw.grnet.gr	Cisco	catalyst297024TS

Fig. 6. View of network switches

L2 QoS configuration

Standard CPE QoS Configuration

teilar-asw.grnet.gr

Uplink interface(s)

GigabitEthernet0/25 - *** Uplink to grnet ***

Access interfaces

GigabitEthernet0/24 - *** tei-lar ***

Fig. 7. Switch QoS configuration options

The interoperability between Layer 3 QoS and Layer 2 QoS takes actual place at the border router and in particular, at the interface which is connected to the Layer 2 device. As the majority of GRNET's switches are multilayer (mls), meaning that it is possible to classify based either on DSCP or CoS, there are two options concerning the marking of packets or frames performed by the border router at the egress:

- CoS marking: For each packet with a given DSCP value, mark the frame with the corresponding CoS value as indicated in Table 2.
- DSCP marking: For each packet with a given DSCP value keep this value intact.

Regarding the switch, at the ingress of its interfaces, the DSCP and CoS values of the packets and frames received respectively are trusted as marked by the router. At this point it should be mentioned that the majority of vendors, by default, disable the trusting of DSCP and CoS values at the ingress interfaces of Layer 2 devices. In order to achieve integration between Layer 3 and Layer 2 for QoS, trusting of DSCP and/or CoS values should be enabled. Thus internal DSCP-to-CoS mapping at the switch is avoided. However, this should be performed in combination to very strict policies so as to avoid abuse of the QoS service.

GRNET's switches provides the flexibility to classify incoming traffic based either on DSCP or CoS. CoS classification is preferred as it can provide backwards compatibility with some no-mls capable switches.

DSCP	CoS	Description
46,47,40	5	IP Premium
0	0	Best Effort
8	1	Less than Best Effort

Table 2. DSCP-to-CoS mapping

3.2 Multiple L2 paths in Crete's MAN

An exception to the more common structure of the GRNET network described above is the part of the GRNET network at the island of Crete, which forms the Crete's MAN. It consists exclusively of L2 Ethernet switches which are aggregated to the only L3 device, a router at the city of Heraklio connected to the rest of GRNET (Fig. 3). Some of the L2 interfaces are therefore considered part of the GRNET core network (the ones which form the MAN itself), while the rest connect to client networks, similarly to the common case discussed in previous sections. Therefore, for the latter case, the existing L2 approach can be still utilized. The core L2 devices form a ring consisting of 3 Ethernet switches (Cisco 3750), with several client networks connected on each one of them. Traffic between the client networks in Crete and towards the rest of the GRNET network is carried in VLANs in order to form isolated VPNs. A related limitation of the current Cisco L2 equipment is that it does not support QoS classification of traffic on VLAN ports, but only on physical ports.

Each VLAN has its own spanning tree which directs the traffic accordingly, and which can be quickly adjusted using Rapid Spanning Tree Protocol (RSTP) for link failure recovery and load balancing. In the case of a link failure, VLAN traffic using the failed link will be redirected due to the corresponding spanning tree protocol switching a blocking link's state to forwarding. This means that assuming the worst case scenario, a core L2 link will have to be able to carry the whole of the traffic traversing the core of Crete's L2 MAN. Under such an assumption, the worst-case dimensioning algorithm will have to allow premium traffic reservations up to the specified allocated percentage for the whole of the L2 MAN

(conversely this can be expressed as the requirement that the allocated percentage should be calculated by adding all allowed traffic reservations through the MAN). The premium allocated percentage can follow the guidelines set by L3 allocations for L3 links of similar bandwidth. The symmetry of Crete' MAN regarding link capacity simplifies this calculation. The worst case assumption has also been the selected approach for premium reservations at the L3 part of the network, and is therefore a natural extension for this case.

4. Status of Layer 2 QoS support

Many vendors have presented Layer 2 devices (switches) with increased capabilities, which are able to inspect Ethernet frames and support CoS or DSCP based differentiation. In this chapter we discuss the approaches chosen by each of the main switching equipment vendors where we have enabled Layer 2 QoS capabilities.

Cisco is possibly the most important vendor of network equipment and, as discussed above, GRNET has traditionally based its network infrastructure largely on Cisco equipment and in particular Cisco Catalyst switches. L2 QoS has been extensively tested on Catalyst 2970 and Catalyst 3750 series that comprise a large part of GRNET's access network and some parts of its core MAN networks as described above (Bouras et al., 2008).

GRNET includes many switches from Extreme Networks, and namely SummitX450 and SummitX350 type switches, which also support L2 QoS (Extreme Networks, 2008). In particular, Policy-based Quality of Service (QoS) is implemented in ExtremeXOS, the operating system used by Extreme Networks switches, and it allows the user to specify different service levels for traffic traversing the switch. The hardware implementation varies depending on the platform, for example some Extreme Networks BlackDiamond series switches contain separate hardware queues on every physical port, while other switches such as the Summit series contain two default queues and several more configurable queues on a switch-wide level. When two or more queues are contending for transmission on the same physical port, the switch makes sure to prioritize usage of the port with regard to the respective queue management parameters. Extreme Networks consider Layer 2 QoS to be applicable in a number of traffic requirements, and provide specific guidelines for applications such as voice, video, critical databases, web browsing and file server applications. Configuration is based on the concept of QoS profiles, which encompass a list of parameters (depending on the specific hardware implementation, this list generally varies between different families of products), such as the maximum amount of packet buffer memory available and the relative weight assigned, or the maximum bandwidth that can be transmitted, the minimum bandwidth reserved and the level of priority.

L2 QoS support by Extreme Networks switches has been extensively tested by GRNET in both laboratory and production environments. The GRNET network is in a position to successfully integrate Extreme Networks switches in a production network comprised of devices from multiple vendors and has verified their interoperability.

Moreover, during the last few months there have been conducted a series of tests concerning the interoperability between Layer 2 and Layer 3 devices. The majority of GRNET's Layer 3 devices is CISCO GSR (12xxx) Series Routers (IOS), while there has been a Juniper T1600 (JunOS 9.4) in production for the last 6 months. Juniper seemed to be much more flexible and granular than Cisco concerning QoS provisioning and setup (Juniper Networks, 2009).

There have been tests with all the combination of equipment showing that GRNET is capable of providing end-to-end QoS regardless of vendor.

5. Conclusions

In this chapter we have provided a wide overview of the existing solutions and deployments for QoS provisioning at Layer 2, with an emphasis on Ethernet-based deployments, which is the dominant Layer 2 technology. We have discussed the integration of existing Layer 3 QoS deployments with the introduction of Layer 2 devices (switches) with relevant capabilities, the implementation issues from a case study implemented in Greece at the GRNET network, and we have presented the current status of Layer 2 QoS support for various equipment vendors.

Our future work includes extensive interoperability testing, including Layer 2 QoS solutions by Cisco, Extreme Networks, Juniper Networks and more vendors such as Nortel. Such interoperability testing has to include all combinations of vendor equipment and Layer 2 - Layer 3 interactions. Furthermore, large scale testing and results from production availability of the services are going to be conducted and analyzed for further service refinement.

6. References

- Bouras C., Kapoulas V., Papapanagiotou V., Pouloupoulos L., Primpas D., Stamos K., (2008). Extending QoS support from Layer 3 to Layer 2, *Proceedings of 15th International Conference on Telecommunications*, St. Petersburg, Russia, 16 - 19 June 2008
- Cisco (2009). Catalyst 2970 Switch Software Configuration Guide. Chapter 27: Understanding QoS.
http://www.cisco.com/en/US/docs/switches/lan/catalyst2970/software/release/12.1_14_ea1/configuration/guide/2970SCG.pdf
- Ek Niclas (1999) Department of Electrical Engineering, Helsinki University of Technology. IEEE 802.1 P,Q - QoS on the MAC level, <http://www.tml.tkk.fi/Opinnot/Tik-110.551/1999/papers/08IEEE802.1QosInMAC/qos.html>
- Extreme Networks, (2008). ExtremeXOS Concepts Guide, Software Version 12.1, May 2008
- GRNET (2009a). Greek Research Network (GRNET) www.grnet.gr
- GRNET (2009b) <http://netmon.grnet.gr/networkmap/gmindex.php>
- GRNET (2009c). GRNET's Advanced Network Services Provisioning Tool
<http://anstool2.grnet.gr>
- IEEE (2005). IEEE Standard for Local and Metropolitan area networks, Virtual Bridged Local Area Networks 802.1Q. <http://standards.ieee.org/getieee802/download/802.1Q-2005.pdf>
- Jacobs A.; Wernicke J.; Oral S.; Gordon B.; George A., (2004). Experimental characterization of QoS in commercial Ethernet switches for statistically bounded latency in aircraft networks, *Proceedings of 29th Annual IEEE International Conference on Local Computer Networks*, 2004, 16-18 Nov. 2004 Page(s): 190 - 197
- Juniper Networks (2009). JUNOS Configuration Guide, Class of Service
<http://www.juniper.net/techpubs/software/junos/junos93/swconfig-cos/swconfig-cos.pdf>

- Liotopoulos F.K., & Guizani M. (2002). Implementing layer-2, connection-oriented QoS on a 3-stage Clos switch architecture., *Proceedings of Global Telecommunications Conference, 2002, GLOBECOM '02*. IEEE Volume 3, Issue , 17-21 Nov. 2002 Page(s): 2741 - 2746 vol.3
- Perez, J.A., Zarate, V.H., Cabrera, C., and Janecek, J., (2006). A Network and Data Link Layer Infrastructure Design to Improve QoS for Real Time Collaborative Systems, *Proceedings of International Conference on Internet and Web Applications and Services/Advanced International Conference on Telecommunications, 2006*., AICT-ICIW apos;06. 19-25 Feb. 2006 Page(s): 19 - 19
- Ubik S. & Vojtech J. (2003). QoS in Layer 2 Networks with Cisco Catalyst 3550, CESNET Technical Report 3/2003
- Varvitsiotis A., Siris V., Primpas D., Fotiadis G., Liakopoulos A., & Bouras C., (2005). Techniques for DiffServ-based QoS in Hierarchically Federated MAN Networks - the GRNET Case, *Proceedings of The 14th IEEE Workshop on Local and Metropolitan Area Networks (LANMAN 2005)*, Chania. Island of Crete, Greece, , 18 - 21 September 2005.
- Wernicke John, (2006). Simulative Analysis of QoS in Avionics Networks for Reliably Low Latency, *Journal of Undergraduate Research*., Volume 7, Issue 2 - January/February 2006.

Secrecy on the Physical Layer in Wireless Networks

Eduard A. Jorswieck, Anne Wolf, and Sabrina Gerbracht*
Technische Universität Dresden
Germany

1. Introduction

This chapter provides a comprehensive state-of-the-art description of the emerging field of physical layer security. We will consider wireless security from an information theoretic view, which allows us to talk about provable secrecy and to derive ultimate secrecy limits. Our main focus is on the optimization of transmit strategies and resource allocation schemes under secrecy constraints.

We will consider the following scenario, which is illustrated in Figure 1: Alice wants to send a private message to Bob, which should be kept perfectly secret from Eve. Eve listens and tries to decode the message that Alice sends to Bob.



Fig. 1. Communication system with a transmitter (Alice), a legitimate receiver (Bob) and an eavesdropper (Eve).

In this communication system, Alice is the transmitter, Bob is the intended or legitimate receiver, and Eve is the eavesdropper. We assume that Bob and Eve perfectly know their individual channel realization and that Alice has full channel state information (CSI), i.e., she knows all channel realizations perfectly. This assumption, which is essential for our further discussion, seems to be unrealistic in the wiretap setting in which Eve probably only listens. However, this assumption will be justified, if Bob and Eve are both users in a cellular environment using up- and downlink transmission.

Within this chapter, we give an overview on the research problems and current results concerning secrecy on the physical layer. In the first section, we describe the attacker model and some conventional cryptographic methods. Afterwards, we introduce the wiretap channel and define the secrecy on the physical layer. In the second part of the chapter, we present results for the achievable secrecy rates or the secrecy capacity in various single-user systems including single-antenna, multi-antenna and multi-carrier systems and provide power allocation strategies for secrecy rate optimizations. In the third section, we extend these results to

*Part of this work is supported by DFG under grant Jo 801/2-1.

multi-user systems. We study basic elements that can be used to model more complex networks and give an overview on current research results on the secrecy capacity regions or the secrecy rate regions. The chapter is completed with a discussion of the results and open research problems.

1.1 Attacker Model

We consider a wireless communication system and focus on a cellular system. The transmitter has perfect CSI for the channels to all potential receivers, irrespective of the fact, whether the receiver is a legitimate receiver or an eavesdropper. The receivers only know their own channels perfectly using channel estimation based on pilot signals. Every user of the system has knowledge of the structure of the system, including all technical details, e.g., codebooks and transmit strategies.

system	<ul style="list-style-type: none"> • wireless communication (cellular system)
transmitter	
knowledge?	<ul style="list-style-type: none"> • perfect CSI for the channels to both, the legitimate receiver and the eavesdropper • structure of the system (including all technical details, e.g., codebooks and transmit strategies)
legitimate receiver	
knowledge?	<ul style="list-style-type: none"> • only perfect CSI for his own channel • structure of the system (including all technical details, e.g., codebooks and transmit strategies)
eavesdropper	
who?	<ul style="list-style-type: none"> • member of the system
objective?	<ul style="list-style-type: none"> • passive attack, eavesdrops the communication between transmitter and legitimate receiver, undermines confidentiality of communication (without interfering)
how?	<ul style="list-style-type: none"> • within range of transmitter • tries to decode the intercepted message
knowledge?	<ul style="list-style-type: none"> • only perfect CSI for his own channel • structure of the system (including all technical details, e.g., codebooks and transmit strategies)

Table 1. Attacker model at a glance.

The attacker is a passive attacker. He wants to undermine the confidentiality by eavesdropping the communication of one or more legitimate users of the system without interfering the communication between transmitter and receivers. For this reason, we use the terms attacker and eavesdropper synonymously. The attacker himself is also a user of the system. He is in reach of the transmitter and tries to decode the intercepted message. He has perfect CSI for the channel from the transmitter to himself, but he does not know the channel between the transmitter and the legitimate receiver. Since the eavesdropper is a user of the system, the transmitter knows the channel to the attacker and is able to fend the attack.

An overview of all important facts of the attacker model can be found in Table 1.

1.2 Cryptography

Currently, the mostly used method to ensure confidentiality in communication systems is the end-to-end cryptography (Schneier, 1996). What all cryptographic algorithms have in common is the fundamental attacker model. The sender, namely Alice, wants to send a message to the receiver, called Bob. Eve, the eavesdropper, should not obtain any knowledge of the message content. In order to achieve this, Alice performs a number of mathematical operations on the original message, predetermined by the cryptographic algorithm and the encryption key. Bob, who knows which algorithm was used, decrypts the cipher message with his key. Eve may know the algorithm, but as long as she does not know the key, it is difficult for her to decipher the message.

There are two basic concepts in the field of cryptography, the symmetric and the asymmetric cryptography. One of the main differences between both concepts is located in the key management.

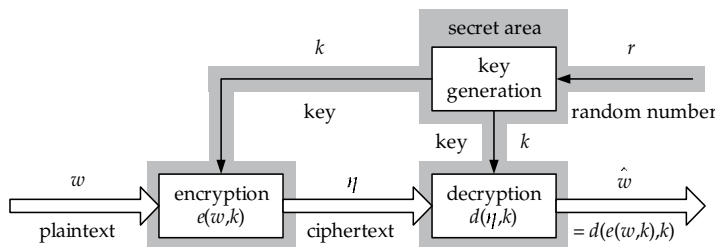


Fig. 2. The basic concept of symmetric cryptography, including key generation, key management, encryption and decryption.

The classical method of symmetric cryptography requires identical keys at sender and receiver, as it can be seen in Figure 2. The difficulty is to transmit the key from Alice to Bob (or vice versa) in a secure and secret way before the communication. In order to avoid this problem, Whitfield Diffie and Martin Hellman invented in 1976 the basic principles of asymmetric cryptography, also called public-key cryptography (Diffie & Hellman, 1976). Diffie and Hellman implemented a key exchange protocol. The first real cryptographic algorithm was designed by Ronald L. Rivest, Adi Shamir, and Leonard Adleman in 1977 at the Massachusetts Institute of Technology (MIT), named RSA by the initial letters of the three inventors (Rivest et al., 1978).

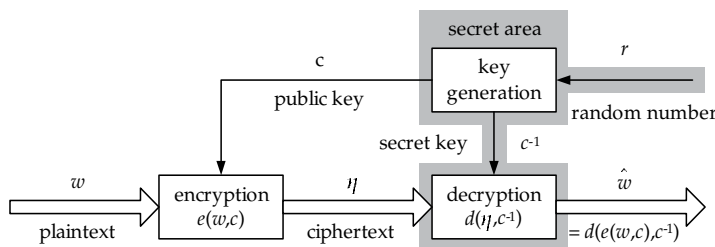


Fig. 3. The basic concept of asymmetric cryptography, including key generation, key management, encryption and decryption.

As the name public-key cryptography suggests, Alice und Bob do not share the same key anymore. Figure 3 shows that Bob initially generates a key pair consisting of a public key and

a private key. Alice, and everyone else, can now encrypt a message, which she would like to send to Bob, with the published key, whereas only Bob is able to decrypt the ciphertext with his private key that he has kept secret. Because of this concept, it is no longer necessary to exchange the encryption key secretly.

Today, we mostly use a mixture of these both concepts. The main message is encrypted by a symmetric encryption algorithm, whereas the symmetric key is enciphered by public-key cryptography. By this method, we can combine the advantages of both concepts: the fast computable encryption and decryption of the symmetric cryptography with the very simple key management of the asymmetric cryptography.

Since all cryptographic algorithms are assigned to the application layer, it is in the user's hand to ensure the secrecy of his data. In this chapter we want to present a possibility to enhance the security of the transmitted information without the requirement of cryptographic protocols and the engagement of the user. This type of secrecy is realized on the physical layer.

1.3 Notation

We use the following mathematical notations throughout the chapter:

- $[\cdot]^+ = \max(0, \cdot)$.
- \mathbf{A}^\dagger is the adjoint matrix of the matrix \mathbf{A} , i.e., the conjugate transpose matrix of \mathbf{A} .
- $\mathbf{A} \succeq 0$ means that the matrix $\mathbf{A} \in \mathbb{C}^{n \times n}$ is positive semidefinite, where we use the following definition for positive semidefiniteness, which automatically implies that \mathbf{A} is Hermitian: $\mathbf{z}^\dagger \mathbf{A} \mathbf{z}$ is real and $\mathbf{z}^\dagger \mathbf{A} \mathbf{z} \geq 0$ for all complex vectors $\mathbf{z} \in \mathbb{C}^n$.
- $|x|$ is the absolute value of a (complex) variable x .
- $\|\mathbf{x}\|$ is the Euclidean norm of a (real or complex) vector \mathbf{x} with $\|\mathbf{x}\| = \sqrt{\mathbf{x}^\dagger \mathbf{x}} = \sqrt{\sum_{i=1}^n |x_i|^2}$, if we assume a vector of length n .
- Vectors and matrices are denoted by lower and upper case bold symbols, respectively.
- Vectors are column vectors if not stated otherwise.

1.4 The Wiretap Channel

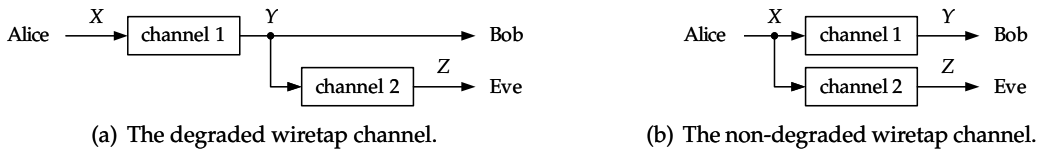


Fig. 4. Two models for the wiretap channel.

The first important results in this research area were presented by Wyner and by Csiszár and Körner. They provided the theoretical basis and introduced two basic system models that are still used today: the wiretap channel (Wyner, 1975), which was later referred to as degraded wiretap channel, and the non-degraded wiretap channel (Csiszár & Körner, 1978). Both system models are depicted in Figure 4.

From a system theoretic view, the models are characterized by random variables at the channel inputs and channel outputs. For the channel input of channel 1 (Alice), we use the random variable X . The channel output of channel 1 (Bob) and channel 2 (Eve) are referred to as Y and Z , respectively. The corresponding channel input or output alphabets are written as \mathcal{X} , \mathcal{Y} and \mathcal{Z} .

In Wyner's degraded wiretap channel, Bob receives a signal that was transmitted over channel 1, the so-called main channel, whereas Eve observes a signal that was additionally sent over channel 2, the so-called wiretapper channel. Therefore, Eve's received signal is always a degraded or noisier version of Bob's received signal, i.e., the random variables form a Markov chain $X \rightarrow Y \rightarrow Z$. This fact simplifies the analysis and derivation of ultimate secrecy limits in Wyner's model compared to the model of Csiszár and Körner. In the non-degraded wiretap channel of Csiszár and Körner, the channels to Bob and Eve are supposed to be independent from each other. In principle, this model does not allow a statement, which channel is the better one. However, it is more suitable for the discussion of secrecy in mobile communication systems.

1.5 Secrecy on the Physical Layer from an Information Theoretic View

From an information theoretic view, the system can be characterized as follows. A message from the message set $\mathcal{W} = \{1, 2, \dots, M\}$ with $M = 2^{n R_S}$ is to be transmitted in n channel uses while ensuring information theoretic security. The messages are chosen at random and thus are modeled by a random variable W with alphabet \mathcal{W} . Then, the message is encoded by the encoding function

$$f_{\text{enc}} : \mathcal{W} \rightarrow \mathcal{X}^n, \quad w \mapsto \mathbf{x}^{(n)},$$

which takes the channel state information at the transmitter into account. Since the messages are random, the input to the channel is random too, and is modeled by the random vector $\mathbf{X}^{(n)}$. The output of the channel at the legitimate receiver is denoted by $\mathbf{Y}^{(n)}$. It is decoded by the decoding function

$$f_{\text{dec}} : \mathcal{Y}^n \rightarrow \mathcal{W}, \quad \mathbf{y}^{(n)} \mapsto \hat{w},$$

which takes the channel state information at the receiver into account. An (M, n) -code comprises a message set \mathcal{W} , an encoding function f_{enc} and a decoding function f_{dec} .

The average decoding error probability $P_e^{(n)}$ of such a code is defined as

$$P_e^{(n)} = \frac{1}{M} \sum_{w=1}^M \Pr(f_{\text{dec}}(\mathbf{Y}^{(n)}) \neq w \mid \mathbf{X}^{(n)} = f_{\text{enc}}(w)),$$

which is the real decoding error probability, if the messages are uniformly distributed.

The level of secrecy is measured by the uncertainty of Eve about the message W , which was sent by Alice, under the condition that Eve receives $\mathbf{Z}^{(n)}$. This measure is called equivocation rate and is given with the conditional entropy function H by

$$R_e^{(n)} = \frac{1}{n} H(W \mid \mathbf{Z}^{(n)}). \quad (1)$$

We are interested in secure data transmissions with an achievable secrecy rate R_S . A secrecy rate R_S is said to be achievable over the wiretap channel if for any $\epsilon > 0$, there exists an integer $n(\epsilon)$ and a sequence of (M, n) -codes of rate

$$R_S = \frac{1}{n} \log_2 M, \quad (2)$$

such that for all $n \geq n(\epsilon)$, the average decoding error probability becomes arbitrarily small, i.e.,

$$P_e^{(n)} \leq \epsilon, \quad (3)$$

and the security constraint

$$\frac{1}{n} H(W|Z^{(n)}) \geq R_S - \epsilon \quad (4)$$

is fulfilled.

For perfect secrecy, i.e., $\epsilon = 0$, the secrecy capacity C_S is the supremum of all achievable rates that guarantee the secrecy of the transmitted data. This means, it can be proven that it is the tightest upper bound on the amount of information that can be reliably transmitted to the receiver and perfectly kept secret from the eavesdropper.

By now, we only focus on Gaussian wiretap channels and Gaussian wiretap channels with an additional attenuation of the transmit signal. For the degraded Gaussian wiretap channel, which was introduced by (Leung-Yan-Cheong & Hellman, 1978) and whose structure is equal to that of Wyner's wiretap channel (cf. Figure 4), the secrecy capacity is given by the maximum difference of mutual informations:

$$C_S = \max_{f_X \in \mathcal{F}} [I(X; Y) - I(X; Z)], \quad (5)$$

where \mathcal{F} is the set of all probability density functions (pdfs) at the channel input under power constraint at the transmitter. Since Eve always receives a degraded version of Bob's signal, the secrecy capacity in (5) is always non-negative. For the non-degraded Gaussian wiretap channel, which is structured like the model of Csiszár and Körner (cf. Figure 4), the secrecy capacity is given by a slightly modified term:

$$C_S = \max_{f_X \in \mathcal{F}} [I(X; Y) - I(X; Z)]^+, \quad (6)$$

i.e., the secrecy capacity C_S is set to zero, if Eve has a better channel realization than Bob. In the following, we will use the non-degraded system model, if it is not stated otherwise. The mutual information terms $I(X; Y)$ and $I(X; Z)$ are concave in f_X . This allows us to formulate a lower bound R_S for the secrecy capacity C_S :

$$C_S = \max_{f_X \in \mathcal{F}} [I(X; Y) - I(X; Z)]^+ \geq \underbrace{\left[\max_{f_X \in \mathcal{F}} (I(X; Y)) \right]}_{\text{channel capacity from Alice to Bob}} - \underbrace{\left[\max_{f_X \in \mathcal{F}} (I(X; Z)) \right]}_{\text{channel capacity from Alice to Eve}} = R_S. \quad (7)$$

Note that the secrecy rate R_S is defined with the difference of the channel capacities from Alice to Bob and from Alice to Eve. This lower bound R_S is often used for a simplified calculation of achievable secrecy rates since it is known how to maximize the mutual information terms. For some scenarios, it has already been proven that the secrecy rate R_S equals the secrecy capacity C_S , e.g., for the single-user system with multiple antennas (see Section 2.3) or for the MISO and MIMO broadcast channel (see Section 3.1).

1.6 The Basic System Model and Preliminaries

Now, we consider Gaussian channels with an additional attenuation of the transmit signal. As a basis for all system models, which are used throughout this chapter, we introduce the following system model for each channel use:

$$\begin{aligned} y &= h \cdot x + \phi \quad \text{and} \\ z &= g \cdot x + \psi \end{aligned} \tag{8}$$

with Alice's transmit signal x , channel coefficients h and g to model the signal attenuation for the channels from Alice to Bob and from Alice to Eve, additive white Gaussian noise ϕ and ψ and signals y and z at the receivers of Bob and Eve, respectively. Figure 5 illustrates how the basic system model is independently used n times to transmit the codeword of length n that is chosen for the message.

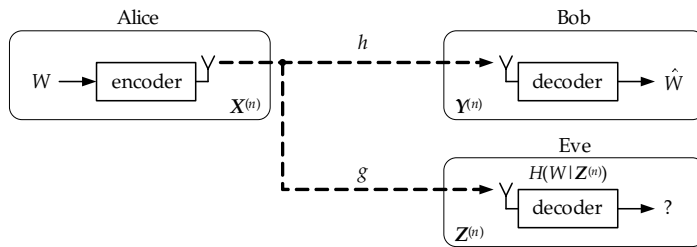


Fig. 5. The basic system model.

For the system model, we make the following assumptions:

- The variables ϕ , ψ and x are stochastically independent.
- The noise variables ϕ and ψ are circular symmetric complex Gaussian distributed with zero mean and variance σ^2 . We write $\phi, \psi \sim \mathcal{CN}(0, \sigma^2)$.
- At the transmitter, we have a power constraint P , i.e., for a codeword x of length n

$$\frac{1}{n} \sum_{i=1}^n |x_i|^2 \leq P. \tag{9}$$

In order to achieve the channel capacities in (7), the variable x has to be circular symmetric complex Gaussian distributed with zero mean and variance P . We write $x \sim \mathcal{CN}(0, P)$.

- We define the so called channel gains α and β by

$$\alpha = |h|^2 \quad \text{and} \quad \beta = |g|^2. \tag{10}$$

In this model, Bob's and Eve's signal-to-noise ratio (SNR) is given by $\frac{\alpha P}{\sigma^2}$ and $\frac{\beta P}{\sigma^2}$, respectively. Therewith, the secrecy rate R_S can be quantified in bit per complex symbol (bpcs) and expressed as a function of the transmit power constraint P :

$$R_S(P) = \left[\log_2 \left(1 + \frac{\alpha P}{\sigma^2} \right) - \log_2 \left(1 + \frac{\beta P}{\sigma^2} \right) \right]^+ \quad \text{[bpcs]}, \tag{11}$$

where a Gaussian codebook maximizes both mutual information terms in (7). This is the secrecy rate of the non-degraded Gaussian wiretap channel with channel gains α and β .

Based on the model above, we define a system with slow quasi-static block flat fading. In order to model flat fading, the channel coefficients h and g in (8) become random variables, which we call channel states. We assume slow quasi-static block fading, i.e., the channel states are random but remain constant for a sufficiently long time to transmit a whole codeword. The next channel state is independent of all other channel states before and is identically distributed.

For every channel state, the secrecy rate can be calculated according to (11). Therefore, the secrecy rate is called instantaneous secrecy rate. Depending on the statistics assumed for the channel coefficients, we can calculate average or outage secrecy rates as defined in (Bloch et al., 2008). In the following sections, we present instantaneous secrecy rates for given channel coefficients and average secrecy rates, where we make the following assumptions for the distribution of the channel states: The channel coefficients h and g are stochastically independent of each other, the transmit signal, and the noise variables. They are circular symmetric complex Gaussian distributed with zero mean and variance 1. We write $h, g \sim \mathcal{CN}(0, 1)$. This means, we add Rayleigh fading to the Gaussian wiretap channel.

The interesting observation in (Bloch et al., 2008) for wiretapped fading channels is that even if the average channel quality between transmitter and eavesdropper is better than the average channel between transmitter and intended receiver, the average secrecy capacity can still be positive.

1.7 Extension to a Multi-Carrier or a Multi-Antenna System Model

The system model in Section 1.6 can be extended to a multi-carrier or a multi-antenna system model:

- For an ideal multi-carrier system with L carriers, the system model in (8) is used L times in parallel. For each carrier ℓ , we have the same assumptions and the same relations between the variables as listed in Section 1.6. Besides, the transmit signals and the noise variables are assumed to be independent between the L carriers. For corresponding variables, we assume an identical distribution. If we assume random channel coefficients, the L parallel channel coefficients for the channels from Alice to Bob are correlated in general. The same applies to the L parallel channel coefficients for the channels from Alice to Eve. The power constraint P at the transmitter becomes a sum power constraint over all L carriers, i.e., $\sum_{\ell=1}^L P_{\ell} = P$.
- In multi-antenna (multiple-input multiple-output, MIMO) systems, we assume that Alice has m_A transmit antennas, Bob has m_B receive antennas, and Eve has m_E receive antennas. Then, the system model in Section 1.6 is expanded by using vectors and matrices instead of scalars. The assumptions and relations between the variables mentioned in this context in Section 1.6 are still valid or can be formulated analogously. Each noise vector consists of independent and identically distributed components. However, the channels from Alice to Bob can be spatially correlated. The same applies to the channels from Alice to Eve. The power constraint P at the transmitter becomes a sum power constraint over all antennas, which is written as $\text{trace}(\mathbf{Q}) = P$ with the covariance matrix \mathbf{Q} of the transmit signal vector \mathbf{x} .

In the multi-carrier or multi-antenna scenario, Alice has more degrees of freedom than before. Now, she can vary the power allocation (under the sum power constraint) over L carriers or m_A antennas to achieve a high secrecy rate for the data transmission to Bob. Note that both models can be combined to have a MIMO multi-carrier system. In the following parts of

Section 2, we will derive an optimal power allocation that maximizes the achievable secrecy rate to Bob for multi-carrier or multi-antenna scenarios.

The channel capacities, which we use in the secrecy rate formula in (11) or in secrecy rate expressions derived from it, are concave functions in P or Q . But the difference of two concave functions generally is neither convex nor concave. Therefore, finding the optimal power allocation over L carriers or m_A antennas under a sum power constraint is a difficult, non-convex optimization problem.

1.8 Extension to a Multi-User Scenario

So far, we have considered a single-user scenario, where Alice wants to transmit a private message to Bob, and Eve is a passive eavesdropper who wants to decode this message. Now, we want to introduce a multi-user scenario with one transmitter (Alice) and K receivers. Alice wants to transmit private messages to each of the K users and to keep these messages secret from all other users. In such a system, we have K secrecy rates or a K -dimensional secrecy rate region. In this chapter, we will confine ourselves to the 2-user scenario with the receivers Bob and Eve, who are now both: legitimate receiver of one message and potential eavesdropper of the other.

In some multi-user scenarios that we present in Section 3, the signals for the different users can interfere. For the evaluation of the achievable secrecy rates for the 2-user case, we slightly modify the definition of the secrecy rate in (7). For the individual secrecy rates, we use the signal-to-interference-and-noise ratio (SINR) for the legitimate user, where the complete interference from the other user's signal is simply treated as additional noise, and the signal-to-noise ratio (SNR) for the eavesdropper. Under power constraint $P_B + P_E = P$, Alice allocates power P_B and P_E for the data transmission to Bob and Eve, respectively. This results in the following expression for the achievable secrecy rate R_{S_B} for the transmission to Bob:

$$R_{S_B}(P_B, P_E) = \left[\log_2 \left(1 + \frac{\alpha P_B}{\sigma^2 + \alpha P_E} \right) - \log_2 \left(1 + \frac{\beta P_B}{\sigma^2} \right) \right]^+ \quad [\text{bps}]. \quad (12)$$

This is a worst-case assumption since we assume that Eve performs successive interference cancellation (SIC), i.e., first, she is able to detect her own data, afterwards she subtracts it from her received signal and tries to decode the message for Bob.

The achievable secrecy rate for the transmission to Eve can be formulated in the same way:

$$R_{S_E}(P_B, P_E) = \left[\log_2 \left(1 + \frac{\beta P_E}{\sigma^2 + \beta P_B} \right) - \log_2 \left(1 + \frac{\alpha P_E}{\sigma^2} \right) \right]^+ \quad [\text{bps}]. \quad (13)$$

2. Secrecy Capacity in Single-User Systems

2.1 Single-Antenna Systems

For a single-user single-antenna system, we have already presented the secrecy rate in Section 1.6. For this single-input single-output (SISO) system, the secrecy rate given in (11) is exactly the secrecy capacity given in (6). In this scenario, Alice only has the choice to transmit the message to Bob or not, according to the channel coefficients for the channels to Bob and Eve. In a completely static system, this would result in a constant secrecy rate that is either positive or zero all the time. But in a time-varying system where we assume slow quasi-static block flat fading, the situation changes from block to block: we have instantaneous channel realizations and thus instantaneous secrecy rates, which can be averaged in time.

2.2 Multi-Carrier Systems

In this section, we extend the basic model from Section 1.6 to the multi-carrier wiretap channel, where Alice wants to send a private message to Bob in a system with L parallel carriers. This message should be kept secret from the eavesdropper Eve. This is a single-antenna scenario since every member of the system has only one transmit or receive antenna. We study the resource allocation under the secrecy constraint and a sum power constraint over all carriers.

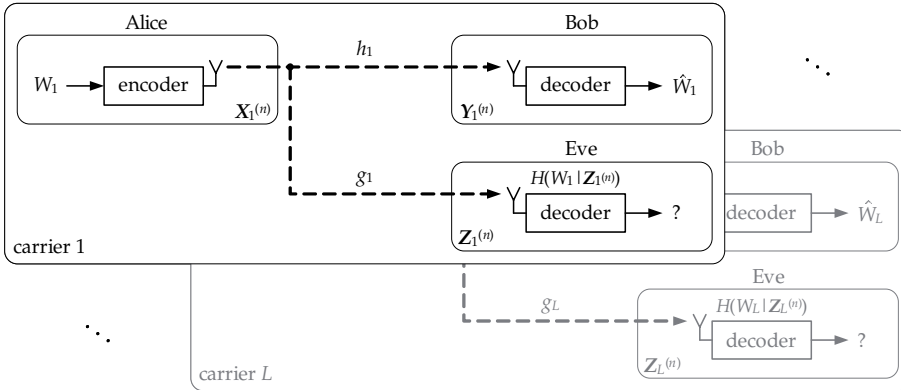


Fig. 6. The multi-carrier wiretap channel with L carriers.

The system model is modified as described in Section 1.7 and illustrated in Figure 6. On carrier ℓ with $1 \leq \ell \leq L$, Bob and Eve observe the received signals y_ℓ and z_ℓ , respectively:

$$\begin{aligned}
 y_\ell &= h_\ell x_\ell + \phi_\ell \quad \text{and} \\
 z_\ell &= g_\ell x_\ell + \psi_\ell
 \end{aligned}
 \tag{14}$$

with Alice' transmit signal x_ℓ , channel coefficients h_ℓ, g_ℓ , and noise variables ϕ_ℓ and ψ_ℓ . The assumptions listed for the basic system model in Section 1.6 also apply to this model. The channel gains α_ℓ, β_ℓ are defined according to equation (10).

In this multi-carrier system, the secrecy rate is the sum over all secrecy rates per carrier, which can be computed according to (7), and is given by

$$R_S(\mathbf{P}_B) = \sum_{\ell=1}^L \left[\log_2 \left(1 + \frac{\alpha_\ell P_{B\ell}}{\sigma^2} \right) - \log_2 \left(1 + \frac{\beta_\ell P_{B\ell}}{\sigma^2} \right) \right]^+ \quad [\text{bps}], \tag{15}$$

where $P_{B\ell}$ is the power that Alice allocates to carrier ℓ in order to transmit the message to Bob. The power allocation over all carriers can be written in a vector $\mathbf{P}_B = (P_{B1}, \dots, P_{BL})$.

We derive the single-user optimal power allocation for maximizing the secrecy rate in this multi-carrier system under sum power constraint P over all carriers:

$$\max_{\mathbf{P}_B} R_S(\mathbf{P}_B) \quad \text{subject to} \quad \sum_{\ell=1}^L P_{B\ell} \leq P \quad \text{and} \quad P_{B\ell} \geq 0. \tag{16}$$

This is a non-convex optimization problem with objective function R_S .

The optimal power allocation that solves (16) is to allocate zero power to all carriers with $\alpha_\ell \leq \beta_\ell$:

$$\forall \ell \in \{1, 2, \dots, L\}: \quad \alpha_\ell \leq \beta_\ell \implies P_{B\ell} = 0. \tag{17}$$

The proof is based on the necessary Karush-Kuhn-Tucker (KKT) optimality conditions (Jorswieck & Wolf, 2008). Furthermore, it was shown that the remaining optimization problem

$$\max_{\mathbf{P}_B} R_S(\mathbf{P}_B) \quad \text{subject to} \quad \sum_{\ell=1}^L P_{B\ell} \leq P, \quad P_{B\ell} \geq 0 \quad \text{and} \quad P_{B\ell} = 0 \text{ for } \alpha_\ell \leq \beta_\ell \quad (18)$$

is convex (see (Boyd & Vandenberghe, 2004) for general convex optimization theory). The optimal power allocation is a type of waterfilling (see (Cover & Thomas, 2006) for standard waterfilling). We give the solution in implicit form with

$$P_{B\ell} = \begin{cases} 0 & \text{if } \alpha_\ell \leq \beta_\ell \\ \left[-\frac{\sigma^2(\alpha_\ell + \beta_\ell)}{2\alpha_\ell\beta_\ell} + \sqrt{\frac{\sigma^4(\alpha_\ell - \beta_\ell)^2}{4(\alpha_\ell\beta_\ell)^2} + \frac{1}{\mu} \frac{\sigma^2(\alpha_\ell - \beta_\ell)}{\ln(2)\alpha_\ell\beta_\ell}} \right]^+ & \text{otherwise} \end{cases} \quad (19)$$

and $\mu > 0$ such that

$$\sum_{\ell=1}^L P_{B\ell} = P. \quad (20)$$

However, the typical order of the channels is different from standard waterfilling. For small SNR, the carriers are ordered according to $(\alpha_\ell - \beta_\ell)$, i.e., the carrier with largest $(\alpha_\ell - \beta_\ell)$ is supported first, whereas for high SNR, the carriers are ordered according to $\frac{\alpha_\ell}{\beta_\ell}$.

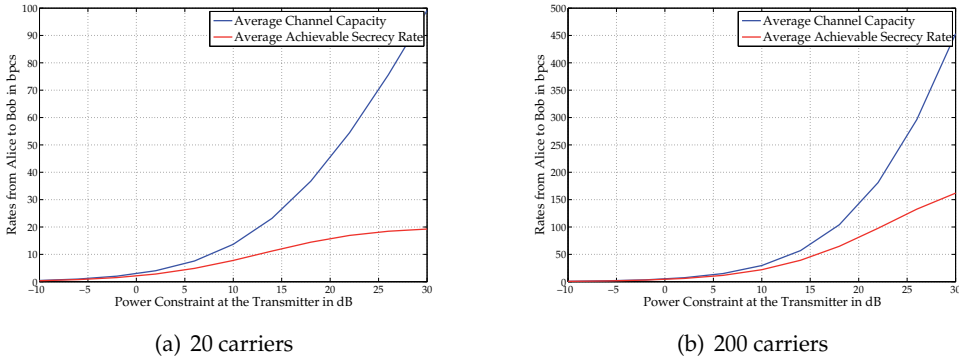


Fig. 7. Average channel capacities and average achievable secrecy rates for transmission from Alice to Bob in a multi-carrier system with 20 and 200 independent carriers.

In Figure 7, we compare the average achievable secrecy rate with the average channel capacity of the single-user multi-carrier channel for different numbers of carriers. The main observation is that the high SNR channel capacity grows without bound whereas the secrecy rate is bounded because the mutual information between the transmitter and the eavesdropper is subtracted from the rate. If the number of carriers is increased, the asymptotic behavior will remain the same. However, the high SNR bound is shifted to the right. We see that in multi-carrier systems with a large number of carriers (and corresponding multipath fading), the costs of security are decreased, i.e., the high SNR bound is increased.

2.3 Multi-Antenna Systems

In this section, we extend the basic model from Section 1.6 to the multi-antenna wiretap channel. As in the scenarios above, Alice wants to send a private message to Bob, which should be kept secret from the eavesdropper Eve. Now, we consider a multi-antenna system, where Alice has m_A transmit antennas, Bob and Eve have m_B and m_E receive antennas, respectively. We study the resource allocation under the secrecy constraint and a sum power constraint over all transmit antennas.

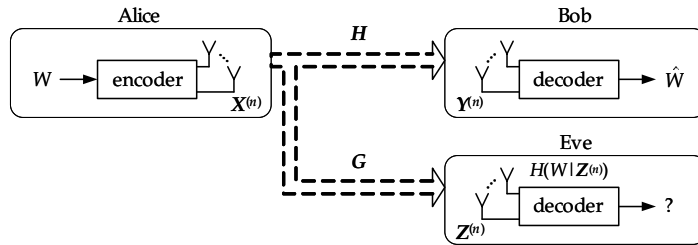


Fig. 8. The multi-antenna wiretap channel.

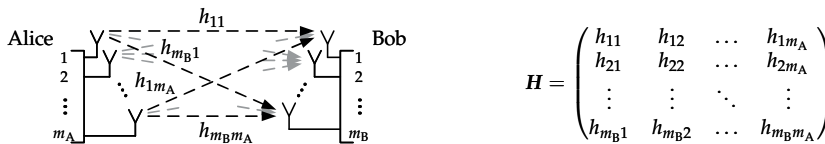


Fig. 9. The structure of a channel matrix using the example of channel matrix H for the channels from Alice to Bob.

The system model, which is depicted in Figure 8, is modified as described in Section 1.7. It can be described by

$$\begin{aligned} \mathbf{y} &= \mathbf{H} \cdot \mathbf{x} + \phi \quad \text{and} \\ \mathbf{z} &= \mathbf{G} \cdot \mathbf{x} + \psi. \end{aligned} \tag{21}$$

The complex channel coefficients are written as the components of H and G , which are channel matrices of dimension $[m_B \times m_A]$ and $[m_E \times m_A]$, respectively. Figure 9 illustrates the structure of such a channel matrix. Alice's transmit signals are written in a column vector x of dimension $[m_A \times 1]$. The noise variables ϕ and ψ are column vectors of dimension $[m_B \times 1]$ and $[m_E \times 1]$, respectively, with independent components. Bob's and Eve's received signals y and z are column vectors of dimension $[m_B \times 1]$ and $[m_E \times 1]$, respectively. The assumptions listed for the basic system model in Section 1.6 analogously apply to this model. The transmit vector x , and the noise vectors ϕ and ψ are stochastically independent, i.e., the components of one vector are stochastically independent of the components of the other vectors. The noise vectors are composed of independent and circular symmetric complex Gaussian distributed components. Their covariance matrices are normalized to the identity matrix. For fading scenarios, the channel matrices H and G are assumed to be stochastically independent of each other, the transmit vector x , and the noise vectors ϕ and ψ .

In this multi-antenna system, the secrecy rate, which is the secrecy capacity for this scenario (Oggier & Hassibi, 2008), is given by

$$R_S(\mathbf{Q}) = \left[\log_2 \det(\mathbf{I}_{m_B} + \mathbf{H}\mathbf{Q}\mathbf{H}^\dagger) - \log_2 \det(\mathbf{I}_{m_E} + \mathbf{G}\mathbf{Q}\mathbf{G}^\dagger) \right]^+ \quad [\text{bps}]. \quad (22)$$

\mathbf{I}_{m_B} and \mathbf{I}_{m_E} are identity matrices of dimension $[m_B \times m_B]$ and $[m_E \times m_E]$, respectively. \mathbf{Q} is the covariance matrix of the input signal vector \mathbf{x} , i.e., $\mathbf{Q} = \text{Cov}(\mathbf{x}) = \mathbb{E}(\mathbf{x}\mathbf{x}^\dagger)$.

We derive the single-user optimal power allocation for maximizing the secrecy rate in this multi-antenna system under sum power constraint P over all transmit antennas:

$$\max_{\mathbf{Q}} R_S(\mathbf{Q}) \quad \text{subject to} \quad \text{trace}(\mathbf{Q}) \leq P \quad \text{and} \quad \mathbf{Q} \succeq 0. \quad (23)$$

This is a non-convex optimization problem, which we analyze for some special cases.

Multiple-Input Single-Output (MISO) Systems

In the MISO case, where Bob and Eve have only one receive antenna each, the channel matrices \mathbf{H} and \mathbf{G} in (21) reduce to row vectors \mathbf{h} and \mathbf{g} of dimension $[1 \times m_A]$:

$$\mathbf{h} = (h_1, \dots, h_{m_A}) \quad \text{and} \quad \mathbf{g} = (g_1, \dots, g_{m_A}). \quad (24)$$

The secrecy rate in (22) can be written as

$$R_S(\mathbf{Q}) = \left[\log_2(1 + \mathbf{h}\mathbf{Q}\mathbf{h}^\dagger) - \log_2(1 + \mathbf{g}\mathbf{Q}\mathbf{g}^\dagger) \right]^+ \quad [\text{bps}]. \quad (25)$$

This scenario was analytically solved in (Li et al., 2007). The authors used an invertible coordinate transformation with a unitary transformation matrix

$$\mathbf{T} = \left(\begin{array}{c|c} \frac{\mathbf{h}^\dagger}{\|\mathbf{h}\|}, & \frac{(\mathbf{g} - \frac{\|\mathbf{g}\|}{\|\mathbf{h}\|}\zeta\mathbf{h})^\dagger}{\|\mathbf{g}\|\sqrt{1-\zeta^\dagger\zeta}}, \quad \text{further } (m_A - 2) \text{ columns} \end{array} \right) \quad \text{with} \quad \zeta = \frac{\mathbf{g}\mathbf{h}^\dagger}{\|\mathbf{g}\|\|\mathbf{h}\|}, \quad (26)$$

where the last $(m_A - 2)$ columns are an orthonormal basis for the $(m_A - 2)$ dimensions and orthogonal to the first two columns. Therewith, the transformed channel vectors $\mathbf{h}\mathbf{T}$ and $\mathbf{g}\mathbf{T}$ have zeros in the subspace spanned by the last $(m_A - 2)$ columns of \mathbf{T} . Focussing only on the subspace spanned by the first two columns of \mathbf{T} the transformed channel vectors $\mathbf{h}\mathbf{T}$ and $\mathbf{g}\mathbf{T}$ can be represented by $\bar{\mathbf{h}}$ and $\bar{\mathbf{g}}$ with

$$\bar{\mathbf{h}} = \|\mathbf{h}\| (1, 0) \quad \text{and} \quad \bar{\mathbf{g}} = \|\mathbf{g}\| (\zeta, \sqrt{1 - \zeta^\dagger\zeta}). \quad (27)$$

In the transformed space, the covariance matrix with the optimal power allocation for the optimization problem derived from (23) for the MISO scenario is

$$\bar{\mathbf{Q}} = P\bar{\mathbf{q}}\bar{\mathbf{q}}^\dagger, \quad (28)$$

where $\bar{\mathbf{q}}$ is the generalized eigenvector corresponding to the largest generalized eigenvalue of the two matrices $(\mathbf{I}_2 + P\bar{\mathbf{h}}^\dagger\bar{\mathbf{h}})$ and $(\mathbf{I}_2 + P\bar{\mathbf{g}}^\dagger\bar{\mathbf{g}})$. The covariance matrix \mathbf{Q} has unit-rank, which means that only one data stream is supported at the transmitter and beamforming can be applied with vector $\bar{\mathbf{q}}$. Finally, the optimal covariance matrix \mathbf{Q} in the original space is

obtained by adding zeros for the subspace spanned by the last $(m_A - 2)$ columns of \mathbf{T} and the inverse coordinate transformation.

In Figure 10, the difference between the average achievable secrecy rate and the average channel capacity of the single-user MISO scenario is illustrated for different numbers of transmit antennas.

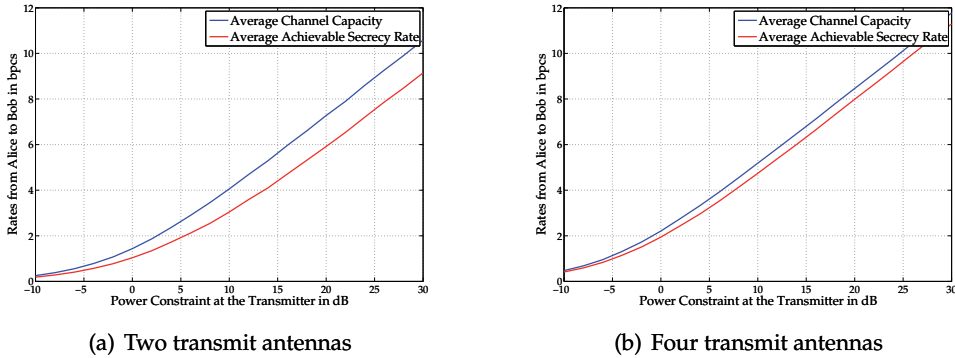


Fig. 10. Average channel capacities and average achievable secrecy rates in a MISO system with two and four transmit antennas and uncorrelated channels.

Single-Input Multiple-Output (SIMO) Systems

In the SIMO case, where Alice has only one transmit antenna and Bob and Eve have an arbitrary number of receive antennas, the channel matrices \mathbf{H} and \mathbf{G} in (21) reduce to column vectors of dimension $[m_B \times 1]$ and $[m_E \times 1]$, respectively:

$$\mathbf{h} = (h_1, \dots, h_{m_B})^T \quad \text{and} \quad \mathbf{g} = (g_1, \dots, g_{m_E})^T. \quad (29)$$

Similar to the single-antenna (SISO) case in Section 2.1, Alice has only the choice either to transmit the message to Bob with power P or not. This SIMO scenario can be transformed in an equivalent SISO scenario with modified channel statistics. Bob and Eve can apply matched filters at the receivers. In the equivalent SISO scenario, Bob's SNR is $\frac{\|\mathbf{h}\|^2 P}{\sigma^2}$ and Eve's SNR is $\frac{\|\mathbf{g}\|^2 P}{\sigma^2}$, where P is the transmit power constraint and σ^2 is the noise variance for each receive antenna.

Some Special Multiple-Input Multiple-Output (MIMO) Systems

In the MIMO 2-2-1 scenario, where Alice has two transmit antennas, Bob has two receive antennas, whereas Eve has only one single receive antenna, the channel matrices \mathbf{H} and \mathbf{G} in (21) reduce to a matrix \mathbf{H} of dimension $[2 \times 2]$ and a row vector \mathbf{g} of dimension $[1 \times 2]$. The optimization problem derived from (23) for the MIMO 2-2-1 scenario was analytically solved in (Shafiee et al., 2008). The authors transformed the problem into a Rayleigh quotient problem, whose solution is the optimal covariance matrix \mathbf{Q} :

$$\mathbf{Q} = P\mathbf{q}\mathbf{q}^\dagger, \quad (30)$$

where \mathbf{q} is the eigenvector that corresponds to the largest eigenvalue of the matrix $(\mathbf{I}_2 + P\mathbf{g}^\dagger\mathbf{g})^{-1/2}(\mathbf{I}_2 + P\mathbf{H}^\dagger\mathbf{H})(\mathbf{I}_2 + P\mathbf{g}^\dagger\mathbf{g})^{-1/2}$.

For the general MIMO scenario, where each user can have an arbitrary number of antennas, it has been proven in (Oggier & Hassibi, 2008) that the secrecy rate in (22) is equal to the secrecy capacity of the system in (21).

In (Liu, Hou & Serali, 2009), the authors presented a global optimization algorithm called branch-and-bound with reformulation and linearization technique (BB/RLT). This method guarantees finding a global optimal solution for the non-convex optimization problem in (23). Another characterization of the optimal transmit covariance matrix \mathbf{Q} is derived in (Liu, Liu, Poor & Shamai (Shitz), 2009). This approach is discussed in the multi-user context in Section 3.1.

3. Secrecy Rate Region in Multi-User Systems

In this section, we extend some of the previously presented results to the multi-user case. Due to the fact that there is more than one user, we will not use anymore the terms secrecy rate and secrecy capacity, but secrecy rate region and secrecy capacity region.

In the literature, the case of one confidential (private) and one public message is often discussed. We focus on the case, where only confidential messages are sent. For convenience, we confine ourselves to systems with only two users. The extension to more than two users can be done straightforward.

3.1 Broadcast Channels

The broadcast channel (BC) is the logical extension of the basic system presented in Section 1.6 to the multi-user scenario. In this channel model, Alice additionally sends a message to Eve that should be concealed from Bob. This new system setting is shown in Figure 11.

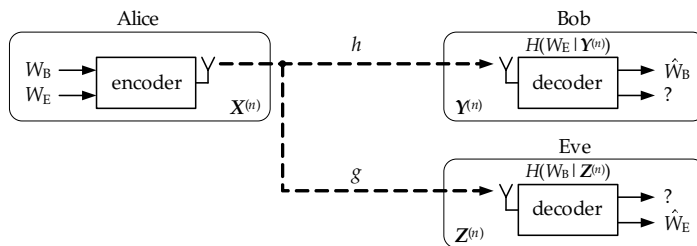


Fig. 11. The basic model of the broadcast channel with two confidential messages.

The extensions of the basic model discussed in Section 2 can also be applied to the broadcast channel. Based on the results of the single-user multi-carrier scenario in Section 2.2, we consider now a cellular broadcast channel with two users, namely Bob and Eve and reuse the system model shown in Figure 6.

The system model is equivalent to the model given in (14)

$$\begin{aligned}
 y_\ell &= h_\ell x_\ell + \phi_\ell \quad \text{and} \\
 z_\ell &= g_\ell x_\ell + \psi_\ell,
 \end{aligned}
 \tag{31}$$

but now Bob and Eve eavesdrop each other. The assumptions listed in Section 1.6 also apply to this model. The channel gains α_ℓ and β_ℓ are defined according to (10).

On carrier ℓ , Alice allocates power $P_{B\ell}$ for data transmission to Bob and $P_{E\ell}$ for data transmission to Eve. The sum power constraint translates to

$$\sum_{\ell=1}^L (P_{B\ell} + P_{E\ell}) \leq P. \quad (32)$$

We collect the power allocation for Bob and Eve in appropriate vectors, i.e., $\mathbf{P}_B = (P_{B1}, \dots, P_{BL})$ and $\mathbf{P}_E = (P_{E1}, \dots, P_{EL})$.

The achievable secrecy rates per carrier are modified according to the explanations in Section 1.7 and 1.8. The achievable secrecy rates for data transmission to Bob and Eve are the sum over all secrecy rates per carrier and given by

$$\begin{aligned} R_{SB}(\mathbf{P}_B, \mathbf{P}_E) &= \sum_{\ell=1}^L \left[\log_2 \left(1 + \frac{\alpha_\ell P_{B\ell}}{\sigma^2 + \alpha_\ell P_{E\ell}} \right) - \log_2 \left(1 + \frac{\beta_\ell P_{B\ell}}{\sigma^2} \right) \right]^+ \quad [\text{bps}] \quad \text{and} \\ R_{SE}(\mathbf{P}_B, \mathbf{P}_E) &= \sum_{\ell=1}^L \left[\log_2 \left(1 + \frac{\beta_\ell P_{E\ell}}{\sigma^2 + \beta_\ell P_{B\ell}} \right) - \log_2 \left(1 + \frac{\alpha_\ell P_{E\ell}}{\sigma^2} \right) \right]^+ \quad [\text{bps}]. \end{aligned} \quad (33)$$

The system operator might be interested in the sum of the individual secrecy rates in (33). The sum secrecy rate is defined as

$$R_S^{(\text{sum})}(\mathbf{P}_B, \mathbf{P}_E) = R_{SB}(\mathbf{P}_B, \mathbf{P}_E) + R_{SE}(\mathbf{P}_B, \mathbf{P}_E). \quad (34)$$

The corresponding programming problem maximizes the sum secrecy rate in (34):

$$\max_{\mathbf{P}_B, \mathbf{P}_E} R_S^{(\text{sum})}(\mathbf{P}_B, \mathbf{P}_E) \quad \text{subject to} \quad \sum_{\ell=1}^L (P_{B\ell} + P_{E\ell}) \leq P, \quad P_{B\ell} \geq 0 \quad \text{and} \quad P_{E\ell} \geq 0. \quad (35)$$

In (Jorswieck & Wolf, 2008), it was shown that it is optimal to support only the best user per carrier. From that fact and the power constraint $P_{A\ell} = P_{B\ell} + P_{E\ell}$ per carrier follows the user allocation per carrier, which is

$$P_{B\ell} = \begin{cases} P_{A\ell} & \text{if } \alpha_\ell > \beta_\ell \\ 0 & \text{otherwise} \end{cases} \quad \text{and} \quad P_{E\ell} = \begin{cases} 0 & \text{if } \alpha_\ell \geq \beta_\ell \\ P_{A\ell} & \text{otherwise} \end{cases}. \quad (36)$$

Then, the power allocation per carrier is derived from equation (19) by replacing $(\alpha_\ell - \beta_\ell)$ by $(\max(\alpha_\ell, \beta_\ell) - \min(\alpha_\ell, \beta_\ell))$.

Note that the case $\alpha_\ell = \beta_\ell$ can be ignored in the fading scenario, if we assume a continuous distribution for the channel coefficients and hence the channel gains, since $\Pr(\alpha_\ell = \beta_\ell) = 0$. Moreover, for the spectral power allocation in (19), it is all the same, which user is assumed to be supported. The algorithm allocates zero power to this carrier and therefore the secrecy rate on this carrier will be zero.

The previously described sum secrecy rate maximization for the broadcast channel can be easily extended to the weighted sum secrecy rate maximization as discussed in (Jorswieck & Gerbracht, 2009). The weighted sum secrecy rate is given by

$$R_S^{(\text{wsum})}(\mathbf{P}_B, \mathbf{P}_E, \lambda) = \lambda R_{SB}(\mathbf{P}_B, \mathbf{P}_E) + (1 - \lambda) R_{SE}(\mathbf{P}_B, \mathbf{P}_E) \quad (37)$$

with $0 \leq \lambda \leq 1$. Herewith, the system operator is able to fulfill certain Quality of Service (QoS) constraints.

The programming problem that maximizes the weighted sum secrecy rate is given by

$$\max_{\mathbf{P}_B, \mathbf{P}_E, \lambda} R_S^{(\text{wsum})}(\mathbf{P}_B, \mathbf{P}_E, \lambda) \quad \text{subject to} \quad \sum_{\ell=1}^L (P_{B\ell} + P_{E\ell}) \leq P, \quad P_{B\ell} \geq 0 \quad \text{and} \quad P_{E\ell} \geq 0.$$

The user allocation is equivalent to the case without weighting factor in (36). It is optimal to support only the best user per carrier.

Furthermore, the spectral power allocation, which is similar to the one in the single-user multi-carrier scenario in Section 2.2, is a kind of waterfilling. The optimal power allocation is given by

$$P_{A\ell} = \begin{cases} \left[-\frac{\sigma^2(\alpha_\ell + \beta_\ell)}{2\alpha_\ell\beta_\ell} + \sqrt{\frac{\sigma^4(\alpha_\ell - \beta_\ell)^2}{4\alpha_\ell^2\beta_\ell^2} + \frac{\lambda}{\mu} \frac{\sigma^2(\alpha_\ell - \beta_\ell)}{\ln(2)\alpha_\ell\beta_\ell}} \right]^+ & \text{if } \ell \in \mathcal{L}_1 \\ \left[-\frac{\sigma^2(\alpha_\ell + \beta_\ell)}{2\alpha_\ell\beta_\ell} + \sqrt{\frac{\sigma^4(\beta_\ell - \alpha_\ell)^2}{4\alpha_\ell^2\beta_\ell^2} + \frac{1-\lambda}{\mu} \frac{\sigma^2(\beta_\ell - \alpha_\ell)}{\ln(2)\alpha_\ell\beta_\ell}} \right]^+ & \text{if } \ell \in \mathcal{L}_2 \end{cases},$$

where $\mathcal{L}_1 = \{\ell \in \{1, \dots, L\} : \alpha_\ell > \beta_\ell\}$, $\mathcal{L}_2 = \{1, \dots, L\} \setminus \mathcal{L}_1$ and $\mu > 0$ such that

$$\sum_{\ell=1}^L P_{A\ell} = P. \tag{38}$$

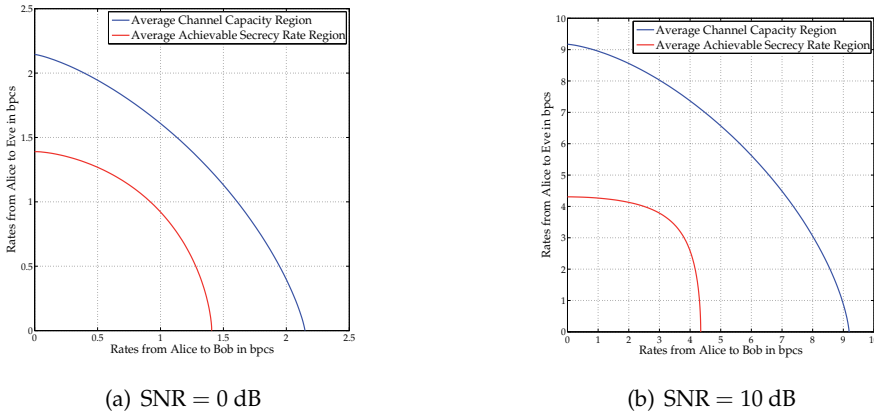


Fig. 12. The average channel capacity region and the average achievable secrecy rate region for the multi-carrier broadcast channel with eight carriers and two users.

Figure 12 shows the achievable average secrecy rate region for the broadcast channel with eight carriers compared to the average channel capacity region, which was found by exhaustive search. We observe that the gap between the achievable secrecy rate region and the capacity region grows with increasing SNR. For $\text{SNR} \rightarrow \infty$, we know that the secrecy rate region does not grow without bound. It is limited by the second term in the equations in (33).

Now, we present the secrecy capacity region for the real-valued MIMO broadcast channel, which can be found in (Liu, Liu, Poor & Shamai (Shitz), 2009). The system model is given by

$$\begin{aligned} \mathbf{Y} &= \mathbf{H}\mathbf{x} + \mathbf{\Phi} \quad \text{and} \\ \mathbf{Z} &= \mathbf{G}\mathbf{x} + \mathbf{\Psi}, \end{aligned} \tag{39}$$

where \mathbf{H} and \mathbf{G} are real channel matrices of size $[m_B \times m_A]$ and $[m_E \times m_A]$, respectively. The noise is modeled by vectors of dimension $[m_B \times 1]$ and $[m_E \times 1]$. For the distribution of the noise vectors, we assume $\Phi, \Psi \sim \mathcal{N}(0, \mathbf{I}_{m_k})$ with $k \in \{B, E\}$. The channel input \mathbf{x} is a vector of the size $[m_A \times 1]$. Furthermore, we have an average power constraint, defined by $\mathbb{E}(\|\mathbf{x}\|^2) \leq P$.

The achievable secrecy rates are given by

$$\begin{aligned}
 R_{SB}(\mathbf{Q}_B) &= \left[\frac{1}{2} \log_2 \det \left(\frac{\mathbf{I}_{m_B} + \mathbf{H}\mathbf{Q}_B\mathbf{H}^T}{\mathbf{I}_{m_E} + \mathbf{G}\mathbf{Q}_B\mathbf{G}^T} \right) \right]^+ \text{ [bps]} \quad \text{and} \\
 R_{SE}(\mathbf{Q}_B, \mathbf{Q}_E) &= \left[\frac{1}{2} \log_2 \det \left(\frac{\mathbf{I}_{m_E} + \mathbf{G}(\mathbf{Q}_B + \mathbf{Q}_E)\mathbf{G}^T}{\mathbf{I}_{m_E} + \mathbf{G}\mathbf{Q}_B\mathbf{G}^T} \right) - \frac{1}{2} \log_2 \det \left(\frac{\mathbf{I}_{m_B} + \mathbf{H}(\mathbf{Q}_B + \mathbf{Q}_E)\mathbf{H}^T}{\mathbf{I}_{m_B} + \mathbf{H}\mathbf{Q}_B\mathbf{H}^T} \right) \right]^+ \text{ [bps]},
 \end{aligned} \tag{40}$$

where \mathbf{Q}_B and \mathbf{Q}_E are the covariance matrices for the transmission to Bob and to Eve, respectively. They are positive semidefinite matrices with $\text{trace}(\mathbf{Q}_B + \mathbf{Q}_E) \leq P$.

For this system model, it has been shown in (Liu, Liu, Poor & Shamai (Shitz), 2009) that the secrecy capacity region is given by

$$\mathcal{R} = \bigcup_{0 \leq \text{trace}(\mathbf{Q}_B + \mathbf{Q}_E) \leq P} (R_{SB}(\mathbf{Q}_B), R_{SE}(\mathbf{Q}_B, \mathbf{Q}_E)). \tag{41}$$

Even though the secrecy capacity region has been proven for the MIMO and the MISO broadcast channel (Liang et al., 2009), it is still an open problem to find the secrecy capacity region for the single-antenna case. So far, there are no results known about the optimal transmit strategies in MIMO and MISO broadcast channels.

3.2 Multiple Access Channels

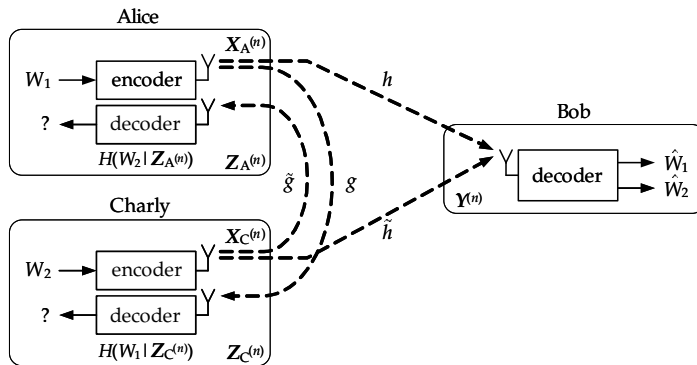


Fig. 13. The multiple access channel (one example).

The multiple access channel (MAC) is difficult to analyze in a system setting concerning secrecy on the physical layer. The conventional channel model for the MAC consists of two

or more transmitters, e.g., mobile devices, and only one receiver, e.g., the base station. In this model, there is nobody who could eavesdrop the sent messages in accordance with the attacker model in Section 1.1. However, if the uplink transmission (MAC) and the downlink transmission (BC) are studied together, every user in the system can eavesdrop all other users. But from the transmitter’s point of view, the channel model would always be a broadcast channel, where all other mobile devices and the base station serve as receivers.

There are currently a lot of research activities concerning the MAC in the secrecy context. One of the models assumed for the MAC in this case is depicted in Figure 13 and studied in (Liang et al., 2009). Another channel model is described in (Tekin & Yener, 2006). It deals with the degraded MAC, where the eavesdropper obtains a degraded version of the receiver’s signal.

3.3 Interference Channels

In this section, we will present two results for the interference channel (IFC). The first one will be a weak interference, single-antenna channel, whereas the second one is a multi-antenna interference channel. For both channel models, we need an additional sender, called Charly, as it can be seen in Figure 14.

Alice wants to send a private message to Bob, which should be kept secret from Eve. Furthermore, Charly wants to send a confidential message to Eve, which should be concealed from Bob. These communication channels have the channel coefficients h and g . The interference or eavesdropper channels from Alice to Eve and from Charly to Bob have the coefficients \tilde{g} and \tilde{h} , respectively.

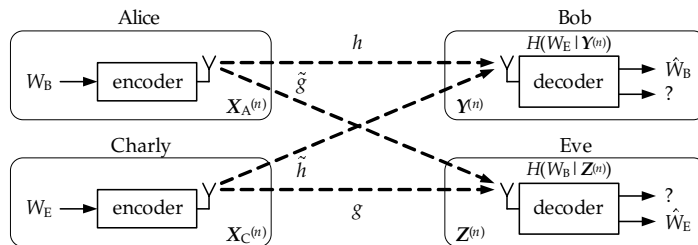


Fig. 14. The interference channel.

The basic system model from Section 1.6 has to be modified to be suitable for the interference channel. Nevertheless, the assumptions listed for the basic system model also apply to this model. For the interference channel, the system model, which was studied in (Zhang & Gursoy, 2009), is given by

$$\begin{aligned}
 y &= hx_A + \tilde{h}x_C + \phi \quad \text{and} \\
 z &= gx_C + \tilde{g}x_A + \psi,
 \end{aligned}
 \tag{42}$$

where h, g, \tilde{h} and \tilde{g} are deterministic channel coefficients. x_A and x_C are the channel inputs at the transmitters. ϕ and ψ are independent and circular symmetric complex Gaussian random variables with $\mathcal{CN}(0, \sigma^2)$. The channel causes weak interference, i.e., $\frac{\tilde{\alpha}}{\alpha} < 1$ and $\frac{\tilde{\beta}}{\beta} < 1$, where the channel gains $\tilde{\alpha}$ and $\tilde{\beta}$ of the eavesdropper channels are defined according to (10) by $\tilde{\alpha} = |\tilde{h}|^2$ and $\tilde{\beta} = |\tilde{g}|^2$. The individual power constraint at the transmitters are given by

$$\mathbb{E}(|x_A|^2) \leq P_A \quad \text{and} \quad \mathbb{E}(|x_C|^2) \leq P_C.
 \tag{43}$$

The system model has to be modified according to Section 1.8. The consideration of interference results in the achievable secrecy rates given by

$$\begin{aligned} R_{SB}(P_B, P_E) &= \left[\log_2 \left(1 + \frac{\alpha P_B}{\sigma^2 + \tilde{\alpha} P_E} \right) - \log_2 \left(1 + \frac{\tilde{\beta} P_B}{\sigma^2} \right) \right]^+ \quad [\text{bps}] \quad \text{and} \\ R_{SE}(P_B, P_E) &= \left[\log_2 \left(1 + \frac{\beta P_E}{\sigma^2 + \tilde{\beta} P_B} \right) - \log_2 \left(1 + \frac{\tilde{\alpha} P_E}{\sigma^2} \right) \right]^+ \quad [\text{bps}], \end{aligned} \quad (44)$$

where P_B is the power allocated by Alice for data transmission to Bob and P_E is the power allocated by Charly for data transmission to Eve.

The achievable secrecy rate region is given by

$$\mathcal{R} = \bigcup_{\substack{0 \leq P_B \leq P_A, \\ 0 \leq P_E \leq P_C}} (R_{SB}(P_B, P_E), R_{SE}(P_B, P_E)). \quad (45)$$

Now, we present some results for the multi-antenna interference channel, which are discussed in (Jorswieck & Mochaourab, 2009) in a game-theoretic context. Both transmitters use m_A and m_C antennas, whereas Eve and Bob receive the messages with only one antenna each. The system model is modified according to Sections 1.7 and 1.8 and is described by

$$\begin{aligned} y &= \mathbf{h} \cdot \mathbf{x}_A + \tilde{\mathbf{h}} \cdot \mathbf{x}_C + \phi \quad \text{and} \\ z &= \mathbf{g} \cdot \mathbf{x}_C + \tilde{\mathbf{g}} \cdot \mathbf{x}_A + \psi, \end{aligned} \quad (46)$$

where \mathbf{h} and $\tilde{\mathbf{g}}$ are row vectors of dimension $[1 \times m_A]$ and $\tilde{\mathbf{h}}$ and \mathbf{g} are row vectors of dimension $[1 \times m_C]$ with complex channel coefficients. \mathbf{x}_A and \mathbf{x}_C are vectors of dimension $[m_A \times 1]$ and $[m_C \times 1]$ and are independent, circular symmetric, and complex Gaussian distributed, i.e., $\mathbf{x}_A \sim \mathcal{CN}(0, \mathbf{v}_A \mathbf{v}_A^\dagger)$ and $\mathbf{x}_C \sim \mathcal{CN}(0, \mathbf{v}_C \mathbf{v}_C^\dagger)$. The beamforming vectors \mathbf{v}_A and \mathbf{v}_C are of dimensions $[m_A \times 1]$ and $[m_C \times 1]$ with $\|\mathbf{v}_A\|^2 = \|\mathbf{v}_C\|^2 = 1$. ϕ and ψ are independent white Gaussian noise with variance σ^2 , i.e., $\phi, \psi \sim \mathcal{CN}(0, \sigma^2)$. Both transmitters have a power constraint P .

The achievable secrecy rate pair for the Gaussian MISO IFC is given by

$$\begin{aligned} R_{SB}(\mathbf{v}_A, \mathbf{v}_C) &= \left[\log_2 \left(1 + \frac{|\mathbf{h} \cdot \mathbf{v}_A|^2 P}{\sigma^2 + |\tilde{\mathbf{h}} \cdot \mathbf{v}_C|^2 P} \right) - \log_2 \left(1 + \frac{|\tilde{\mathbf{g}} \cdot \mathbf{v}_A|^2 P}{\sigma^2} \right) \right]^+ \quad [\text{bps}] \quad \text{and} \\ R_{SE}(\mathbf{v}_A, \mathbf{v}_C) &= \left[\log_2 \left(1 + \frac{|\mathbf{g} \cdot \mathbf{v}_C|^2 P}{\sigma^2 + |\tilde{\mathbf{g}} \cdot \mathbf{v}_A|^2 P} \right) - \log_2 \left(1 + \frac{|\tilde{\mathbf{h}} \cdot \mathbf{v}_C|^2 P}{\sigma^2} \right) \right]^+ \quad [\text{bps}]. \end{aligned} \quad (47)$$

The efficient beamforming vectors are described in the following. According to (Jorswieck & Mochaourab, 2009), we denote the maximum ratio transmission beamforming vector of user k as $\mathbf{v}_k^{(MRT)}$ and the zero-forcing beamforming vector as $\mathbf{v}_k^{(ZF)}$, where $k \in \{A, C\}$. We obtain

$$\begin{aligned} \mathbf{v}_A(\lambda_A) &= \frac{\lambda_A \cdot \mathbf{v}_A^{(MRT)} + (1 - \lambda_A) \cdot \mathbf{v}_A^{(ZF)}}{\left\| \lambda_A \cdot \mathbf{v}_A^{(MRT)} + (1 - \lambda_A) \cdot \mathbf{v}_A^{(ZF)} \right\|} \quad \text{and} \\ \mathbf{v}_C(\lambda_C) &= \frac{\lambda_C \cdot \mathbf{v}_C^{(MRT)} + (1 - \lambda_C) \cdot \mathbf{v}_C^{(ZF)}}{\left\| \lambda_C \cdot \mathbf{v}_C^{(MRT)} + (1 - \lambda_C) \cdot \mathbf{v}_C^{(ZF)} \right\|} \end{aligned} \quad (48)$$

with transmit strategies $0 \leq \lambda_A, \lambda_C \leq 1$.

The maximization of the secrecy rate from Alice to Bob depends on the given interference caused by Charly. The rate can be described as the best response, if λ_C is given:

$$\lambda_A^*(\lambda_C) = \arg \max_{0 \leq \lambda_A \leq 1} R_{SB}(\lambda_A, \lambda_C). \quad (49)$$

Equivalently, Charly's best response to Alice' transmit strategy is given by

$$\lambda_C^*(\lambda_A) = \arg \max_{0 \leq \lambda_C \leq 1} R_{SE}(\lambda_A, \lambda_C). \quad (50)$$

From Alice' and Charly's point of view, the interference channel equals the broadcast channel. Because of this fact, they do not have the possibility to influence, but to react to the interference generated by each other. The optimal solution for the maximization problems in (49) and (50) can be found by an iterative algorithm described in (Jorswieck & Mochaourab, 2009). This optimum is not the best solution, which is possible in this scenario. It is an achievable and stable point, the so-called Nash Equilibrium, that will be reached, if Alice and Charly do not cooperate. Another approach to solve these non-convex optimization problems is to use a monotonic optimization framework. This has been proven useful for the MISO interference channel in (Jorswieck & Larsson, 2009) in order to optimize the transmit strategies.

4. Discussion and Open Problems

The information theoretic description of secrecy capacities and secrecy capacity regions (Liang et al., 2009) is an important research area to support a better understanding of security on the physical layer. Based on the secrecy capacity expressions or achievable secrecy rates, the transmit strategies, including power allocation, beamforming and subcarrier allocation, are optimized in order to choose a certain operating point. In this chapter, we focus on the optimization of the physical layer transmit strategies for typical wireless communication scenarios.

In single-user scenarios, the system design is more complicated with additional secrecy constraints, since the secrecy capacity expressions are in general not concave or convex in the transmit strategies. The secrecy rate terms usually consist of a difference of two parts. The first one corresponds to the amount of data that can be reliably transmitted to the intended user and it is therefore concave in the transmit strategies. The second one corresponds to the amount of data that is overheard by the eavesdropper and it is thus also concave in the transmit strategies. The resulting transmit optimization problems are non-convex optimization problems since the difference of two concave functions is not necessarily convex or concave. However, in the multi-carrier case, the problem can be reduced to a convex optimization problem that can be efficiently computed. We conjecture that also the multiple antenna (MIMO) scenario will be completely solved in the very next future.

In multi-user scenarios, the secrecy rate regions of all four elements of network information theory, the broadcast, the multiple access, the relay, and the interference channel were recently studied. The attacker models of the MAC and the relay case are more difficult than the well-motivated ones of the broadcast and the interference channel. Therefore, we focus on the broadcast and interference channel. The resource allocation for the parallel broadcast channel without secrecy is involved due to a hard combinatorial problem – the matching of carriers to users. Interestingly, with secrecy constraints, the resulting programming problem is much simpler and the optimal power and resource allocation can be solved efficiently. A similar

observation in the context of interference channels with beamforming and without cooperation shows that the secrecy constraint leads to a more altruistic and less selfish behavior. In both cases, the additional term in the utility functions simplifies and improves the resulting transmit optimization.

In addition to the resource allocation and transmit optimization problems discussed in this chapter, there are many important practical issues to be solved. The assumption to have perfect CSI at the transmitter(s) and receiver(s) is idealistic. The impact of channel estimation errors and limited feedback on the achievable secrecy rates needs to be analyzed. The assumption to apply Gaussian codebooks is idealistic, too. Finite modulation and coding schemes lead to more difficult bit and power allocation problems at the transmitter. Recent results in the development of channel codes for secure communications are not discussed in this chapter due to length constraints. However, there is interesting current work on the analysis and development of channel codes that are able to achieve the secrecy capacity. Finally, the attacker model studied in this chapter is important but not the only one possible. Future work will also consider malicious user behavior as well as byzantine attacks. There are many interesting open problems in the broad area of physical layer security in wireless communications.

Acknowledgement

The authors want to thank Martin Mittelbach for his review of this chapter, critical comments and productive discussions.

5. References

- Bloch, M., Barros, J., Rodrigues, M. R. D. & Laughlin, S. W. M. (2008). Wireless Information-Theoretic Security, *IEEE Transactions on Information Theory* **54**(6): 2515–2534.
- Boyd, S. & Vandenberghe, L. (2004). *Convex Optimization*, Cambridge University Press.
URL: <http://www.stanford.edu/boyd/cvxbook/>
- Cover, T. M. & Thomas, J. A. (2006). *Elements of Information Theory*, Wiley & Sons.
- Csiszár, I. & Körner, J. (1978). Broadcast Channels with Confidential Messages, *IEEE Transactions on Information Theory* **24**(3): 339–348.
- Diffie, W. & Hellman, M. E. (1976). New directions in cryptography, *IEEE Transactions on Information Theory* **22**(6): 644–654.
- Jorswieck, E. A. & Gerbracht, S. (2009). Secrecy Rate Region of Downlink OFDM Systems: Efficient Resource Allocation, *14th International OFDM-Workshop (InOWo)*, Hamburg, Germany.
- Jorswieck, E. A. & Larsson, E. (2009). Monotonic Optimization Framework for the MISO IFC, *IEEE International Conference on Acoustics, Speech and Signal Processing (ICASSP)*, pp. 3633–3636.
- Jorswieck, E. A. & Mochaourab, R. (2009). Secrecy Rate Region of MISO Interference Channel: Pareto Boundary and Non-Cooperative Games, *International ITG Workshop on Smart Antennas*, Berlin, Germany.
- Jorswieck, E. A. & Wolf, A. (2008). Resource Allocation for the Wire-tap Multi-carrier Broadcast Channel, *Proceedings of International Workshop on Multiple Access Communications (MACOM)*, Saint Petersburg, Russia.
- Leung-Yan-Cheong, S. & Hellman, M. (1978). The Gaussian wire-tap channel, *IEEE Transactions on Information Theory* **24**(4): 451–456.

- Li, Z., Trappe, W. & Yates, R. (2007). Secret Communication via Multi-antenna Transmission, *41st Annual Conference on Information Sciences and Systems (CISS)*, pp. 905–910.
- Liang, Y., Poor, H. V. & Shamai (Shitz), S. (2009). *Information Theoretic Security*, Vol. 5 of *Foundations and Trends in Communications and Information Theory*, now publishers, pp. 355–580.
- Liu, J., Hou, Y. T. & Sherali, H. D. (2009). Optimal power allocation for achieving perfect secrecy capacity in MIMO wire-tap channels, *43rd Annual Conference on Information Sciences and Systems (CISS)*, pp. 606–611.
- Liu, R., Liu, T., Poor, H. V. & Shamai (Shitz), S. (2009). Multiple-Input Multiple-Output Gaussian Broadcast Channels with Confidential Messages, *CoRR* **abs/0903.3786**. submitted.
- Oggier, F. & Hassibi, B. (2008). The Secrecy Capacity of the MIMO Wiretap Channel, *IEEE International Symposium on Information Theory (ISIT)*, pp. 524–528.
- Rivest, R. L., Shamir, A. & Adleman, L. (1978). A method for obtaining digital signatures and public-key cryptosystems, *Communications of the ACM* **21**(2): 120–126.
- Schneier, B. (1996). *Applied Cryptography*, Wiley & Sons.
- Shafiee, S., Liu, N. & Ulukus, S. (2008). Secrecy Capacity of the 2-2-1 Gaussian MIMO Wire-tap Channel, *3rd International Symposium on Communications, Control and Signal Processing (ISCCSP)*, pp. 207–212.
- Tekin, E. & Yener, A. (2006). The Gaussian Multiple Access Wire-Tap Channel with Collective Secrecy Constraints, *IEEE International Symposium on Information Theory (ISIT)*, pp. 1164–1168.
- Wyner, A. D. (1975). The Wire-tap Channel, *Bell System Technical Journal* **54**(8): 1355–1387.
- Zhang, J. & Gursoy, M. C. (2009). Low-SNR Analysis of Interference Channels under Secrecy Constraints, *CoRR* **abs/0901.3132**. submitted.

Performance Analysis of Time-of-Arrival Mobile Positioning in Wireless Cellular CDMA Networks

M. A. Landolsi, A. H. Muqaibel, A. S. Al-Ahmari, H.-R. Khan
and R. A. Al-Nimnim

*EE Department, King Fahd University of Petroleum & Minerals
KFUPM, P.O. Box 1413, Dhahran 31261, Saudi Arabia*

1. Introduction

Recently, wireless mobile communication systems have experienced a tremendous growth and became an integral part of people's daily life worldwide. This global predominance of wireless communications has been ever more pronounced with the success of new generations of wireless communication standards that support a rich set of value-added features in addition to basic phone services. Among these features is the possibility to offer radiolocation services whereby the mobile system (MS) position is determined by combining relevant information (such as signal time of arrival or angle of arrival) from different base stations (BSs) having radio links with the intended mobile. This positioning capability can support many services ranging from medical emergency help, security and law enforcement, on-the-road assistance, location-dependent commercial advertisement, etc. As such, mobile radiolocation has been mandated by several of the recently introduced wireless standards, and is being widely deployed by cellular network operators worldwide (Rappaport et al., 1996).

With the deployment of the 3rd generation wireless cellular standards such as the Universal Mobile Telecommunication System (UMTS) (Dahlman et al., 2000), the use of wideband code division multiple access (CDMA) signals is poised to offer highly accurate positioning capabilities with time-of-arrival (TOA) information owing to the fine timing resolution of the high chip rate wideband spread-spectrum waveforms used. There are however some impairments such as multi-path fading, multi-user interference and noise, that can affect the performance of mobile positioning schemes. In particular, because of the need to use signal detection at several base stations in mobile positioning, the problem of near-far interference at remote base stations (whereby a far-away mobile weak signal can be overwhelmed by strong signals from close-in mobiles) can constitute a major limiting factor. In CDMA networks, this is further exacerbated by power control (Viterbi, 1995). Indeed, power control loops operate in such a way to maintain the received power from different users at the same level at their respective *servicing* base station. However, at other non-servicing base stations (not actively involved in a call with the intended mobile), the mobile received power level can be extremely low, thereby giving rise to a problem of signal hearability, which, in turn,

will affect the accuracy of the mobile positioning algorithms (Gosh & Love, 1998). A thorough analysis of these different aspects under realistic channel modeling and network traffic loading conditions is therefore necessary in order to obtain an accurate assessment of the achievable positioning performance.

In this work, we study the accuracy of mobile radiolocation under near-far interference, and show that it can vary considerably depending on the mobile link quality with the base stations involved in position determination. We first present a detailed performance analysis of mobile TOA estimation in broadband CDMA wireless cellular networks at the different base stations surrounding the mobile terminal. In most previous works, the proposed radiolocation algorithms have simplistically assumed that the time-of-arrival measurements are Gaussian-distributed, with a fixed known variance that is commonly set irrespective of the actual RF channel and interference conditions or other system parameters. Moreover, the same TOA variance is typically assigned for all base stations involved in positioning, which is an inaccurate and overly optimistic assumption, as our results will show. Instead, our approach is the use of complete statistics for the mobile timing estimation errors, derived by taking into account realistic system parameters at the different base stations of interest.

Since precise TOA estimation in CDMA receivers is typically implemented by delay-locked loop (DLL) tracking systems (Viterbi, 1995), a detailed study of the DLL TOA tracking is introduced under fading and multi-user interference conditions assuming a cellular model with multiple tiers of base stations, and it is shown that the DLL tracking performance can vary widely depending on the level of multiple-access interference and RF propagation conditions of the links between the mobile and base stations. Using the TOA data collected at the base stations involved in mobile positioning, a numerically-efficient, quasi-optimum algorithm, based on Approximate Maximum Likelihood (AML) estimation (Chan et al., 2006), is presented, and a generalization of this algorithm is also derived under the realistic assumption of un-equal TOA estimation errors at the different base stations.

Based on our analysis, the impact of mobile link condition and its relative position with respect to the base stations involved in its positioning is fully quantified for a number of scenarios depending on the near-far interference environment and the level of Soft Handoff (SHO) connectivity of the mobile with the base stations. Our results show that positioning accuracy is greatly improved when the mobile station is in 2-way, and particularly in 3-way SHO (i.e., with two and three base stations, respectively), compared to single connectivity with only the home serving base station.

The rest of the chapter is organized as follows. First, in Section 2, we present an overview of radiolocation techniques, focusing in particular on network-based approaches with TOA processing suitable for cellular systems. The system modeling and analysis of near-far interference in CDMA networks is presented in Section 3, followed by a detailed analysis of the performance of delay-locked loops for time-of-arrival tracking in Section 4. Then, in Section 5, the approximate maximum likelihood positioning algorithm is presented, and various illustrative examples and numerical results are discussed in Section 6, followed by summary and final conclusions in Section 7.

2. Wireless Network-Based Mobile Radiolocation

2.1 Overview

The concept of wireless radiolocation refers to the determination of the geographic position information of a mobile user in terms of its geographic coordinates with respect to a reference point. Wireless location is also commonly referred to as mobile positioning, radiolocation, or localization. Position location techniques can be classified into two main categories: handset-based and network-based. A well known example of handset-based radiolocation is the Global Positioning System (GPS) and other similar systems (Kaplan, 1996). The other category consists of network-based techniques that utilize the existing wireless cellular networks to obtain location information (Sayed, et al., 2005). In this work, we mainly focus on the network-based approach which integrates seamlessly with the widely deployed mobile cellular infrastructures throughout the world. The basic architecture of such systems is illustrated in Figure 1.

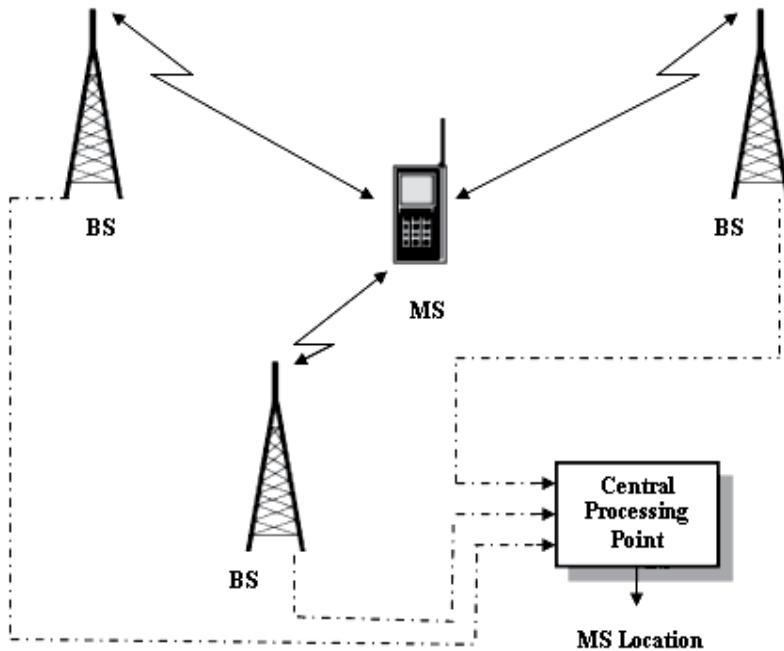


Fig. 1. Network-based wireless mobile radiolocation

The network-based positioning schemes rely on data collected by several base stations surrounding the mobile station of interest, and can be based on the mobile's signal strength (SS), angle of arrival (AOA), time of arrivals (TOA) or time difference of arrival (TDOA) measurements. Using these measurements, specific geometric and/or statistical signal processing algorithms are used to determine the mobile location. Hybrid methods involving more than one of type of measurements can also be used (Sayed, et al., 2005). In general, locating a mobile in two-dimensions requires a minimum of three sets of measurements from corresponding base stations, although for AOA methods, two base stations are

sufficient. However, in the presence of noisy measurements, statistical signal processing algorithms using data collected from multiple base stations are preferred in order to resolve the ambiguities arising from multiple crossings of the lines of position, and to improve the positioning accuracy.

2.2 Time-of-Arrival Mobile Radiolocation

TOA-based techniques offer several advantages compared to the other methods, including low cost and ease of use. The TOA data is readily available from timing synchronization mechanisms at the different base stations, without requiring complex hardware as with the Angle-of-Arrival methods. In particular, with the widespread deployment of the latest 3G CDMA-based wireless cellular networks, the spread-spectrum signaling waveforms offer high time resolution and good robustness vis-à-vis the radio channel impairments (fading, shadowing, and near-far interference), and are therefore well-suited to aid in achieving the required accuracy in position location services.

In the TOA-based mobile radiolocation approach, the distance between an MS and a BS is measured by finding the one-way propagation delay under direct line-of-sight (LOS) propagation conditions. The TOA measurements at the different base stations are therefore directly proportional to the mobile-base distance separation. The involved base stations are assumed to have a common timing reference, with a known mobile transmission time. Geometrically, the mobile position will trace a circle centered at the base stations. By using three base stations to resolve ambiguities, the mobile position is given by the intersection of these circles as illustrated in Figure 2. It should be pointed out that, in the presence of noisy TOA data due to interference and synchronization errors, the three circles may not intersect at a single point. Therefore, the geometric approach will not produce a single intersection point, and “statistical” techniques are typically adopted to process the noisy data, as will be further discussed subsequently when we introduce the AML algorithm.

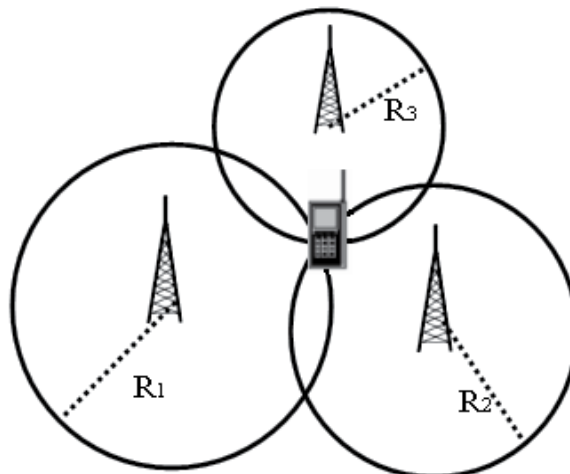


Fig. 2. TOA radiolocation based on intersection of base station centered circles

3. Near-Far Interference Analysis

3.1 Signal and System Models

Consider a cellular CDMA network employing signaling schemes with quaternary phase-shift keying (QPSK) modulation and complex spreading (conforming to 3G/UTMS standards (Dahlman et al., 2000)). At the transmitter, the complex baseband signal for a given mobile user is given by

$$\tilde{s}(t) = \sum_{m=-\infty}^{\infty} s_m h(t - mT_c) \quad (1)$$

where $\{s_m\}$ are the complex spreading chip symbols, and T_c the chip duration. The information data bits are omitted here for simplicity as this will be applicable for a pure pilot signal that can be used for positioning purposes. The impulse response $h(t)$ of the pulse-shaping filter is assumed to be a root-raised cosine filter with roll-off factor 22%, as recommended in the UMTS standard. As will be seen next, the Fourier transform $H(f)$ of the filter impulse response $h(t)$ will have a major impact on the other-user interference in cellular CDMA networks.

For wireless fading channels, the received signal at the output of the radio frequency (RF) receiver filter is written as

$$r(t) = \sqrt{P} \operatorname{Re} \left\{ \sum_{i=1}^M \tilde{s}(t - \tau_i(t)) a_i(t) e^{j2\pi f_c t} \right\} + n(t) \quad (2)$$

where P is the received signal power, M is the number of resolvable multipath signals, with a_i and τ_i denoting the i -th path complex Gaussian tap factor (with a Rayleigh-fading magnitude) and its propagation delay, respectively, and f_c is the carrier frequency. The noise signal $n(t)$ models the total noise-plus-interference terms and is assumed to be zero-mean Gaussian random process. For the different resolvable multipath signal epochs, we mainly focus on the first arriving signal which will be tracked to estimate its TOA. The combined multiple-access interference (MAI) terms from both same-cell and other-cell users can be modeled as being Gaussian distributed, which is a valid assumption for a large number of users. In this case, it can be shown that the total composite power spectral density (PSD), I_0 , that captures the effect of both thermal noise and MAI terms (assumed to be statistically independent) is given by (Viterbi, 1995)

$$I_0 = N_0 \int_{-\infty}^{\infty} |H(f)|^2 df + \frac{\rho_0}{T_c} \int_{-\infty}^{\infty} |H(f)|^4 df = N_0 + \frac{\rho_0}{T_c} \int_{-\infty}^{\infty} |H(f)|^4 df \quad (3)$$

where N_0 is due to the thermal noise component and the factor ρ_0 represents both same-cell and other-cell MAI terms. The function $H(f)$ denotes the Fourier transfer of the chip shaping filter impulse response $h(t)$. The MAI PSD term is typically the dominant factor in CDMA systems, and will depend on network loading, fraction of inter-cell to intra-cell MAI, channel pathloss and shadowing models. For typical system parameters of interest, it is

found that the ρ_0 MAI factor is approximately $1.6(K_u-1)$, where K_u is the number of users per cell (Viterbi, 1995).

3.2 Near-Far Interference and Soft Handoff Impact

We consider a cellular network with a central cell and two tiers of surrounding cells as illustrated in Figure 3, where mobiles are assumed to be uniformly distributed across the coverage area.

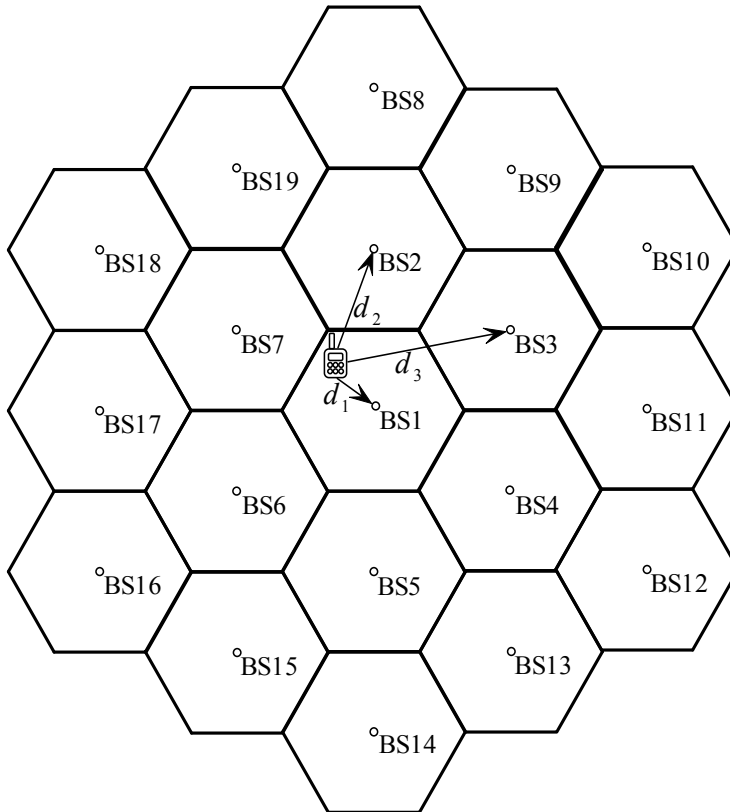


Fig. 3. Cellular network model, with center cell and two tiers of interfering cells.

The mobile received power at a given base station, BS_i , is multiplied by an attenuation factor, α , that reflects distance path loss, $p(d)$, and log-normal shadowing factor, ξ , according to (Viterbi, 1995):

$$\alpha(d_{BS_i}, \xi_{BS_i}) = p(d_{BS_i}) 10^{\xi_{BS_i}/10} \quad (4)$$

The path-loss factor is assumed to follow the model:

$$p(d) = 10n \log_{10}(d) \quad (5)$$

where n is the path loss exponent and d the mobile's relative position with respect to the base station. For a given mobile location, shadowing vis-à-vis the different base stations is typically assumed to be partially correlated, log-normally-distributed, and given by (Viterbi, 1995):

$$\xi_{BS_i} = a\xi_c + b\xi_i \quad (6)$$

where ξ_c and ξ_i denote the common and independent terms, respectively, and $a^2 + b^2 = 1$. With closed-loop CDMA power control, a given mobile will have the same received power at its home (serving) base station compared with other intra-cell mobiles. On the other hand, at the neighboring base stations, the mobile will be received at much lower power due to the so-called near-far problem (which cannot be mitigated due to the lack of "inter-cell" power control). However, when the mobile is in soft-handoff with other neighboring base stations, its received power is relatively close to that at the home cell, and this greatly improve radiolocation accuracy, as will be discussed next.

Since TOA estimation accuracy depends on the timing synchronization mechanism, which is in turn affected by the received interference levels at the different base stations, the near-far interference at the non-serving base stations will have a major impact on the final mobile positioning accuracy. To illustrate this point, we consider a system where the mobile is served by the center base station BS_1 and is radio-located using TOA data from three or more base stations BS_1, BS_2, \dots, BS_7 (sorted in a descending order from BS_1 that receives the highest average received power). The near-far interference impact can be conveniently assessed by defining the ratio of its average received power at BS_i compared to BS_1 (for which the power will be normalized to 1, and used as a reference value). We then define the following:

$$\beta_i = P_i / P_1 \quad (7)$$

where P_i is the received power at BS_i and $\beta_1 = 1 \geq \beta_2 \geq \beta_3 \geq \dots \geq \beta_7$. A wide fluctuation in the β factors is expected depending on the mobile position relative to the base stations of interest. It should be noted that, due to power control, all mobiles will be received at equal power ($\beta=1$) at their respective home serving base stations, but much lower values of β are expected at far-away base stations (because of the near-far problem). This however will depend on the relative position of the mobile with respect to the other base stations (i.e., its proximity to the cell border). Soft Handoff (SHO) is one of the salient features of CDMA cellular systems which allow the mobile to be simultaneously connected to more than one serving base station. In fact, the possibility of SHO calls enables a stronger signal reception at multiple base stations, and this will in turn improve positioning accuracy.

To further investigate this point, we consider different scenarios denoted by Cases 1, 2, and 3, respectively. Case 1 refers to a mobile in close proximity (within half the cell radius, R) of its serving BS_1 , with a signal at least 10dB above that at the other nearest two base stations. Case 2 represents a two-way soft handover scenario, with the mobile power at BS_2 within 3dB from that at BS_1 . Finally, Case 3 corresponds to a 3-way soft handover situation where

the mobile signal at both BS₂ and BS₃ is within 3dB compared to BS₁. The numbers chosen here merely serve to illustrate the variability in received signal power (and its subsequent impact on TOA estimation accuracy), but do not attempt to model the specific thresholds and soft handover mechanisms used in CDMA standards.

Table 1 and Table 2 give the different β factors for the three cases of interest, and for different values for the pathloss and shadowing models, where a typical 50% correlation factor is assumed ($a=b$). For the numerical results, we assumed typical parameters for the radio propagation channel model. A two-segment pathloss model with breakpoint at distance $d_0=200\text{m}$ and exponents $n=2$ and 4, respectively, was used, with a load of 20 users per cell, and a cell radius of 2Km. The relative power factors given in Table 1 and Table 2 clearly show that large variations occur across the base stations depending on the mobile soft handoff conditions and its proximity to one or more base station, and this will impact the accuracy of signal estimation at the different base stations as will be discussed next.

	β_1	β_2	β_3	β_4	β_5	β_6	β_7
Case 1 (mobile close to home BS)	1	0.0216	0.0113	0.0069	0.0045	0.0031	0.0021
Case 2 (mobile in two-way SHO)	1	0.6982	0.2215	0.1202	0.0735	0.0485	0.0331
Case 3 (mobile in three-way SHO)	1	0.7922	0.6353	0.2993	0.1701	0.1065	0.0706

Table 1. Relative received power factors for various mobile soft-handoff link conditions. Shadowing s.t.d $\sigma=8\text{dB}$.

	β_1	β_2	β_3	β_4	β_5	β_6	β_7
Case 1 (mobile close to home BS)	1	0.0248	0.0125	0.0072	0.0045	0.0030	0.0020
Case 2 (mobile in two-way SHO)	1	0.7000	0.2281	0.1258	0.0761	0.0486	0.0322
Case 3 (mobile in three-way SHO)	1	0.7985	0.6443	0.3403	0.1953	0.1252	0.0808

Table 2. Relative received power factors for various mobile soft-handoff link conditions. Shadowing s.t.d $\sigma=12\text{dB}$.

4. Signal Time-of-Arrival Estimation

4.1. Delay-Locked Loop Time Tracking

Timing synchronization for CDMA signals is typically implemented in two steps consisting of an initial coarse timing acquisition (within an uncertainty range on the order of one-chip interval), followed by fine time tracking achieved by a delay-locked loop (DLL) mechanism (Viterbi, 1995). In this work, we assume that the initial timing acquisition has been achieved, and focus on the more accurate DLL tracking as the main signal timing estimation mechanism. For each base station involved in mobile positioning, a DLL device continuously attempts to bring the local code timing estimate in perfect alignment with the

incoming mobile signal. However, this timing estimation will be subject to error due to noise, fading and multiple-access interference. In the following, we consider TOA estimation based on a non-coherent DLL (NC-DLL) scheme. In practice, the NC-DLL is preferred over a coherent structure because of its insensitivity to carrier phase error and data modulation. Figure 4 depicts a block diagram showing the different processing stages of a NC-DLL code tracking loop. Because QPSK spreading is used, the NC-DLL employs both I & Q branches where the I & Q received signals, after down conversion and chip matched filtering, are fed to two early & late branches which correlate the spread-spectrum waveforms with advanced and delayed code sequence replicas. The outputs obtained at the I & Q channels of the early & late branches can be obtained as (Viterbi, 1995)

$$Y_{I\pm} = AN\sqrt{PT_c}R(\tau \pm \delta)\cos\theta \quad (8)$$

$$Y_{Q\pm} = AN\sqrt{PT_c}R(\tau \pm \delta)\sin\theta \quad (9)$$

where A is the fading signal envelope modeled as a Rayleigh random variable, and θ is its uniform phase. δ is the early & late timing offset (typically set to $T_c/2$), P is the signal power, and N is the number of accumulated chips. The function $R(\tau)$ is a correlation function given by the convolution of the impulse responses of the pulse-shaping filter and its matched filter (Viterbi, 1995):

$$R(\tau) = h(\tau) * h(-\tau) = \int_{-\infty}^{\infty} |H(f)|^2 \cos(2\pi f\tau) df \quad (10)$$

The DLL I & Q correlator outputs are combined as shown in Figure 4, and a resulting discriminator metric ΔZ is low-pass filtered to form an error signal used to drive a numerically-controlled oscillator (NCO) that controls the code timing adjustment. The DLL discriminator output can be obtained as (Viterbi, 1995):

$$\Delta Z = \beta AS(\varepsilon) + \eta \quad (11)$$

where β is the power reduction factor reflecting the impact of DLL operation at different base stations (compared to the main serving base station, as discussed previously). The term η represents the combined Gaussian noise term with variance I_0 . The function $S(\varepsilon)$ is known as the normalized DLL S-curve, and is given by

$$S(\varepsilon) = R^2(\varepsilon - \delta) - R^2(\varepsilon + \delta) \quad (12)$$

where ε is the normalized timing error given by

$$\varepsilon = (\tau - \hat{\tau})/T_c \quad (13)$$

with τ denoting the correct TOA and $\hat{\tau}$ the estimated one.

A common figure of merit for assessing the DLL performance is based on the tracking jitter variance. For additive white Gaussian (AWGN) channels, a simple upper-bound approximation for the tracking jitter variance, valid for linearized first-order DLL models, is derived in (Viterbi, 1995) as

$$\sigma_\epsilon \approx \frac{2I_0^2 + 4NE_c I_0}{N^2 E_c^2 \kappa^2} \tag{14}$$

where E_c is the received chip energy, κ is the slope of the S-curve at the origin, and I_0 is the variance of the thermal noise & MAI terms. However, there is no simple equivalent result for the case of frequency-selective multipath fading channels considered in this work, and the above approximation is only valid for high mobile received Signal-to-Noise Ratio (SNR) conditions, which is not necessarily the case at the remote base stations (other than the home serving one), as discussed previously. In this work, we resort to a more accurate performance analysis valid for all SNR conditions and based on the computation of the full statistics (probability density function) of the DLL tracking loop, as discussed next.

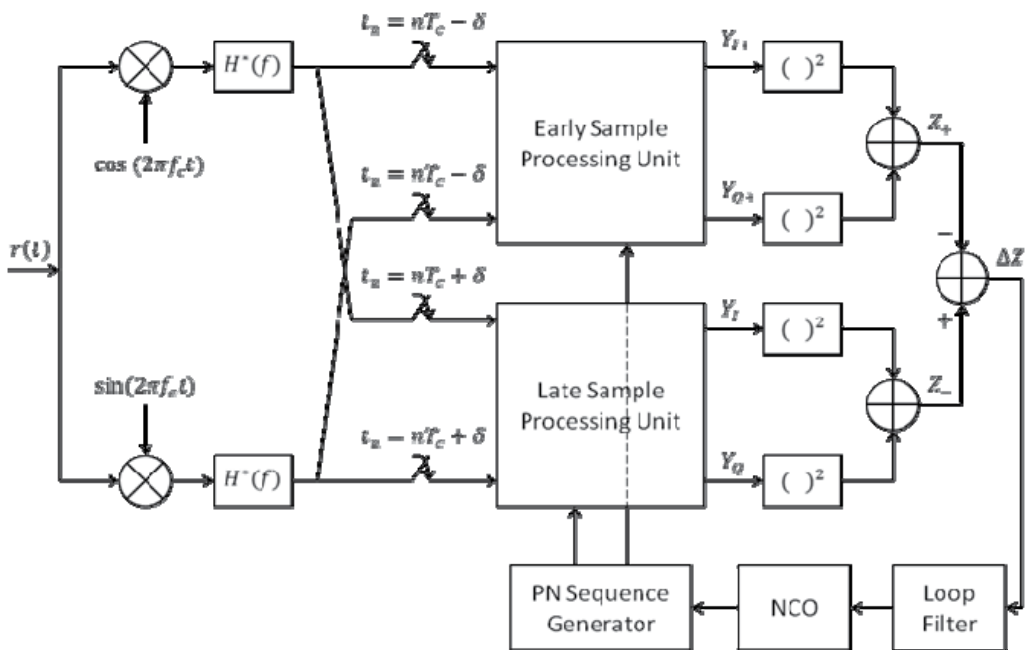


Fig. 4. DLL system used for CDMA signal timing synchronization and TOA estimation

4.2. DLL Tracking Error Statistics

For the purpose of analyzing the impact of TOA estimation error on mobile positioning accuracy, we need to obtain accurate statistics for the TOA measurements at each of the base stations involved in tracking the given mobile TOA. Hypothetical distributions (Gaussian models) are commonly assumed for the TOA timing estimation error. The same variance is

usually assigned to the TOA error at all base stations involved in mobile positioning, and this variance is sometimes set rather arbitrarily. In this work, we use results based on a more rigorous analysis with full derivation of the TOA error probability density function (PDF). The results are obtained following the approach presented in (Su & Yen, 1997) and extended to quadrature-spread CDMA signals in (Khan, 2009). Assuming a discrete-time model, the analysis is based on a discrete-time Markov model for the residual DLL error, according to the following equation:

$$\varepsilon_k = \varepsilon_{k-1} - K_{NCO} \left[\beta A_{k-1}^2 S(\varepsilon_{k-1}) + \eta_{k-1} \right] \quad (15)$$

where K_{NCO} is the NCO gain, and η_k is the additive Gaussian noise term. It can be seen that the residual tracking error follows a discrete-time Markov process for which the first order probability distribution can be obtained using the Kolmogorov-Chapman equation (Su & Yen, 1997):

$$p_k(\varepsilon) = \int_{-\infty}^{\infty} f_{k-1}(\varepsilon | x) p_{k-1}(x | \varepsilon_0) dx \quad (16)$$

where ε_0 is the initial timing error, $p_{k-1}(x | \varepsilon_0)$ is the PDF of x given ε_0 , and $f_{k-1}(\varepsilon | x)$ is the transition pdf of ε_k given x . Through detailed analysis, one can calculate the exact expressions $f_{k-1}(\varepsilon | x)$ under assumption of a Rayleigh fading channel. Using numerical integration, it is then possible to iterate the Kolmogorov-Chapman equation to get the PDF of the TOA estimation error. The lengthy details of this derivation are not included here, but can be found in (Khan, 2009).

The procedure outlined above can be done for different scenarios reflecting mobile TOA estimation at a given base station of interest. For our purpose, we analyze the performance of TOA DLL tracking at the different base stations for each one of the three cases described in Section 3. The results are shown in Figures 5 through 7, where it is clearly seen that the TOA residual error behavior can vary widely depending on the mobile position vis-à-vis the tracking base station. For example, in Figure 5 which corresponds to a mobile very close to its home serving base station, the residual error at the home base station is well-confined and nearly Gaussian-distributed (with a standard deviation found to be on the order of $0.15T_c$), whereas for the other two base stations, the timing errors remain nearly uniformly-distributed with a standard deviation of $0.29T_c$ (which shows that the DLL loops at those base stations are not effectively tracking the mobile signal TOA). On the other hand, in Figure 6 and Figure 7 corresponding to 2-way and 3-way SHO, respectively, the mobile time tracking performance at BS2 and BS3 is markedly better, with distributions approaching that of the home BS1. It is to be noted that the number of users per cell (assumed the same for all cells, for simplicity) can also have a major impact on the timing estimation accuracy, regardless of the mobile position scenario (i.e., for all different cases discussed previously). Indeed, as shown in Figure 8, when the number of users increases, the tracking error PDFs are more wide-spread, and have an increasing error s.t.d (given with a normalization factor of $1/T_c$).

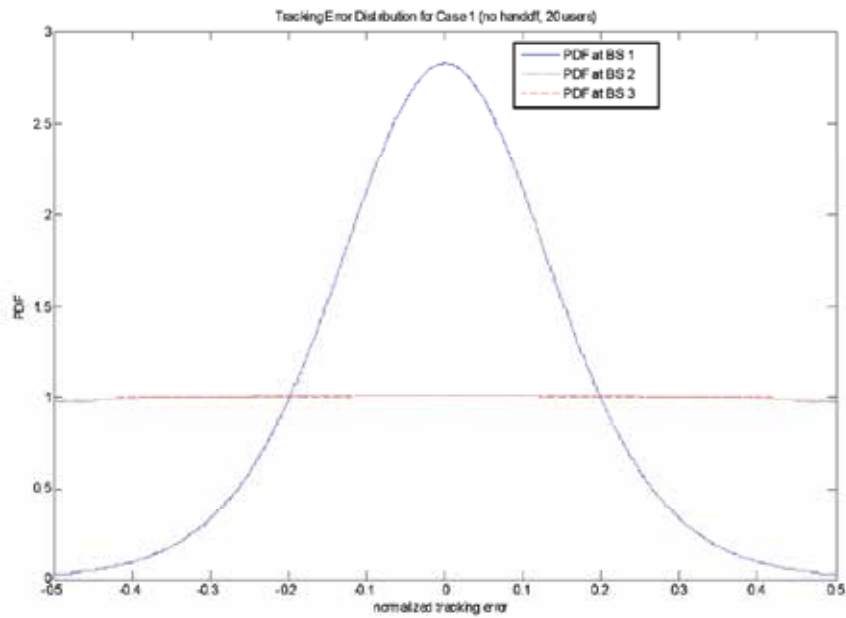


Fig. 5. Mobile TOA Tracking error PDF at BS1, BS2, BS3 for Case 1 (MS without handoff)

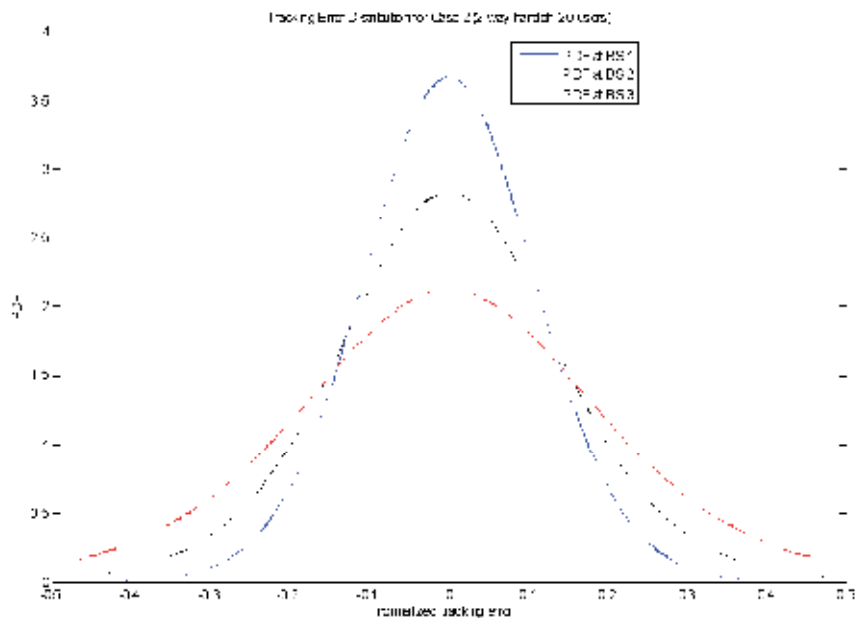


Fig. 6. Mobile TOA tracking error PDF at BS1, BS2, BS3 for Case 2 (MS in 2-way soft handoff)

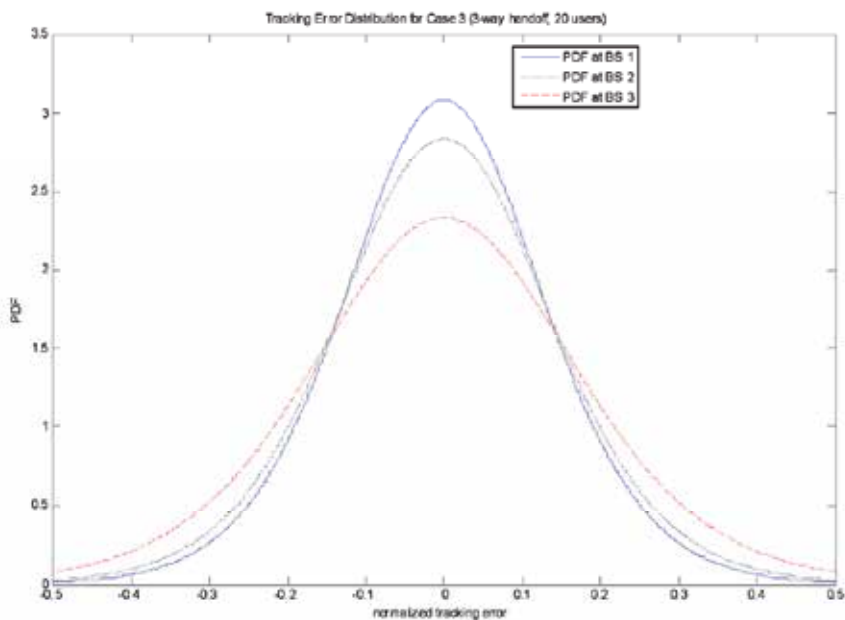


Fig. 7. Mobile TOA time tracking error PDF at BS1, BS2, BS3 for Case 3 (MS in 3-way soft handoff)

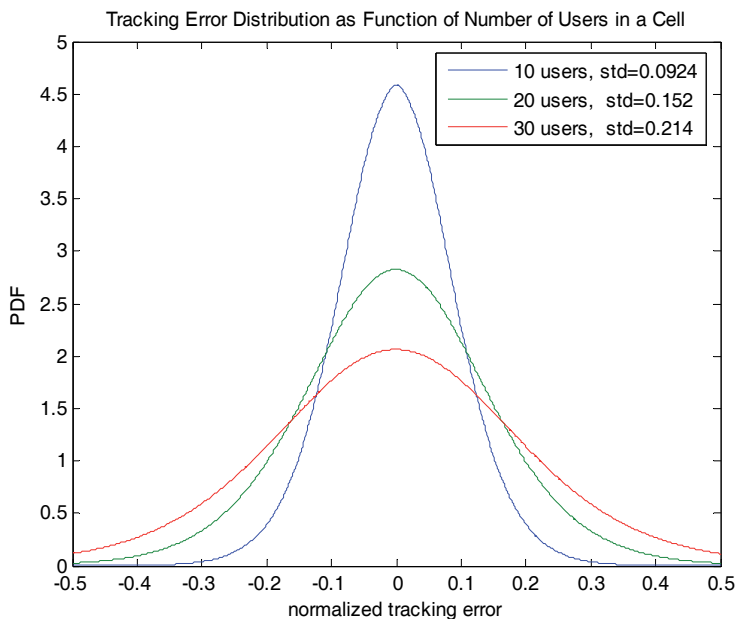


Fig. 8. Illustration of the impact of the number of users on the TOA tracking error probability density function.

5. TOA Processing for Mobile Positioning

5.1. Approximate Maximum Likelihood Algorithm

In time-of-arrival radiolocation techniques, the distance is calculated as the propagation time multiplied by the speed of light c . Line-of-sight (LOS) propagation is assumed, whereby the mobile signal travels on a direct path at the constant speed of light in free space. It is further assumed that the base stations are synchronized and the mobile transmission time is known (set to zero for simplicity). The TOA measurements, produced at each base station, are therefore directly proportional to the mobile-base distance separation. Geometrically, circles centered at the base stations can be drawn with the calculated distance as the radius. With the help of three base stations, the mobile location can be found geometrically as the intersection of the corresponding circles. However, in the presence of noise and interference, the three circles may not intersect at a single point. Therefore, the geometric approach is not suitable, and several other “statistical” techniques have been proposed (Caffrey, 1999), (Sayed et al., 2005) to process the noisy data. Many of these are based on iterative algorithms using least-squares or gradient search minimization. On the other hand, since the positioning equations involved are typically nonlinear, some traditional approaches based on linearization followed by a gradient search were proposed (Niezgoda & Ho, 1994). However, these approaches suffer from sensitivity to initialization errors and convergence problems. More recently, some researchers introduced new closed-form linear techniques (Caffrey & Stuber, 2000), (Chan & Ho, 1994), but the drawback of these methods is that optimum location estimates can only be found at high SNR values, which may not always be the case in practice.

Another interesting solution was proposed by (Chan et al., 2006) and shown to have near-optimum performance, with the added advantage of reduced complexity. Their method uses an Approximate Maximum Likelihood (AML) algorithm, which we adopt in this study. In the following, we give a general overview of the AML algorithm processing steps, and introduce a modification tailored towards the case of unequal TOA variances at the different base stations, and relevant to mobile radiolocation under near-far interference conditions (which is the focus of this work), as will be outlined subsequently. Based on the assumed cellular geometry, the true distances between the BSs and MS are given by

$$R_i = \sqrt{(x - x_i)^2 + (y - y_i)^2} \quad i=1,2,\dots,N_{\text{BS}} \quad (17)$$

where N_{BS} is the number of involved BSs. The measured distances, l_i , is given by

$$l_i = R_i + \varepsilon_i \quad i=1,2,\dots,N_{\text{BS}} \quad (18)$$

where ε_i is the DLL timing error. In matrix form, this is written as

$$\mathbf{l} = \mathbf{R} + \boldsymbol{\varepsilon} \quad (19)$$

Dividing by c to get the measured TOA vector \mathbf{T} , we obtain

$$\mathbf{T} = \frac{\mathbf{R}}{c} + \frac{\boldsymbol{\varepsilon}}{c} = \mathbf{T}^0 + \mathbf{e} \quad (20)$$

where

$$\mathbf{R} = [R_1 \dots R_N]^t = \mathbf{R}(\boldsymbol{\Theta}) \quad (21)$$

and

$$\mathbf{e} = [e_1 \dots e_N]^t \quad (22)$$

is the vector of additive measurement noise, and \mathbf{T}^0 is the vector of true TOAs. The original AML algorithm proposed by (Chan et al., 2006) assumes that all BSs have an equal error variance. Hence, the elements of \mathbf{e} are assumed to be independent, zero-mean Gaussian random variables with covariance matrix

$$\mathbf{Q} = E\{\mathbf{e}\mathbf{e}^t\} = \sigma^2 \mathbf{I} \quad (23)$$

The AML algorithm can be generalized to account for different values of the error variance at different BSs. If the variance of the error can be estimated at each BS, one can use this information to improve the localization performance by giving more trust to BSs with lower error variance. In this case the elements of \mathbf{e} are assumed to be independent, zero mean Gaussian random variables with covariance matrix:

$$\mathbf{Q} = E\{\mathbf{e}\mathbf{e}^t\} = \text{diag}[\sigma_1^2 \dots \sigma_N^2] \quad (24)$$

The conditional probability density function (PDF) of \mathbf{T} given $\boldsymbol{\Theta}$ is given by

$$f(\mathbf{T}|\boldsymbol{\Theta}) = (2\pi)^{-\frac{N_{BS}}{2}} (\det \mathbf{Q})^{-\frac{1}{2}} \exp\left\{-\frac{J}{2}\right\} \quad (25)$$

where

$$J = \left[\mathbf{T} - \frac{\mathbf{R}(\boldsymbol{\Theta})}{c} \right]^t \mathbf{Q}^{-1} \left[\mathbf{T} - \frac{\mathbf{R}(\boldsymbol{\Theta})}{c} \right] = [e_1 \dots e_N] \begin{bmatrix} \sigma_1^2 & \dots & 0 \\ \vdots & \ddots & \vdots \\ 0 & \dots & \sigma_N^2 \end{bmatrix}^{-1} \begin{bmatrix} e_1 \\ \vdots \\ e_N \end{bmatrix} = \sum_{i=1}^{N_{BS}} \frac{1}{\sigma_i^2}. \quad (26)$$

The ML estimate of the MS position (x, y) is the $\boldsymbol{\Theta}$ that minimizes J (Trees, 1968). Minimizing J is done by setting its gradient with respect to $\boldsymbol{\Theta}$ to zero. Considering first the derivative with respect to the position variable x , we have

$$\frac{\partial J}{\partial x} = \sum_{i=1}^{N_{BS}} \frac{1}{\sigma_i^2} \frac{\partial e_i^2}{\partial x} = \sum_{i=1}^{N_{BS}} \frac{1}{\sigma_i^2} 2e_i \cdot \frac{\partial e_i}{\partial x} \quad (27)$$

By expressing the timing error in terms of the difference between the true TOA and measured one, this gives

$$\frac{\partial e_i}{\partial x} = \frac{\partial}{\partial x} \left(T - \frac{R_i}{c} \right) = -\frac{1}{c} \cdot \frac{\partial R_i}{\partial x} \quad (28)$$

Utilizing Equation (17), we may write

$$\frac{\partial R_i}{\partial x} = \frac{1}{2} \cdot \left(2 \frac{(x - x_i)}{R_i} \right) = \frac{(x - x_i)}{R_i} \quad (29)$$

Substituting the result in Equation (28) yields

$$\frac{\partial e_i}{\partial x} = -\frac{1}{c} \cdot \frac{(x - x_i)}{R_i} \quad (30)$$

Substituting in Equation (27), we get

$$\begin{aligned} \frac{\partial J}{\partial x} &= -\frac{1}{c} \cdot \sum_{i=1}^{N_{BS}} \frac{1}{\sigma_i^2} \cdot 2e_i \cdot \frac{(x - x_i)}{R_i} \\ &= \frac{2}{c^2} \cdot \sum_{i=1}^{N_{BS}} \frac{1}{\sigma_i^2} \cdot \frac{(R_i - l_i) \cdot (x - x_i)}{R_i} \end{aligned} \quad (31)$$

The above steps starting with Equation (27) can be repeated for $\partial J / \partial y$ in a straightforward manner. Finally, by setting the gradient of J with respect to Θ to zero, we get the two ML equations

$$\begin{aligned} \sum_{i=1}^{N_{BS}} \frac{1}{\sigma_i^2} \cdot \frac{(R_i - l_i) \cdot (x - x_i)}{R_i} &= 0 \\ \sum_{i=1}^{N_{BS}} \frac{1}{\sigma_i^2} \cdot \frac{(R_i - l_i) \cdot (y - y_i)}{R_i} &= 0 \end{aligned} \quad (32)$$

The above equations can be expressed in matrix notation as

$$2 \begin{bmatrix} \sum g_i x_i & \sum g_i y_i \\ \sum h_i x_i & \sum h_i y_i \end{bmatrix} \begin{bmatrix} x \\ y \end{bmatrix} = \begin{bmatrix} \sum g_i (s + K_i - l_i^2) \\ \sum h_i (s + K_i - l_i^2) \end{bmatrix} \quad (33)$$

where

$$s = x^2 + y^2 \quad (34)$$

$$K_i = x_i^2 + y_i^2 \quad (35)$$

$$g_i = \frac{x - x_i}{\sigma_i^2 \cdot R_i \cdot (R_i + l_i)} \quad (36)$$

$$h_i = \frac{y - y_i}{\sigma_i^2 \cdot R_i \cdot (R_i + l_i)} \quad (37)$$

In a more compact form, Equation (34) can be re-written as

$$\mathbf{A}\Theta = \mathbf{b} \quad (38)$$

with the matrix \mathbf{A} and vector \mathbf{b} being functions of Θ . A suboptimal solution based on a linear model (Chan & Ho, 1994) can be used as a first initial estimate of Θ , which will in turn give starting values of \mathbf{A} and \mathbf{b} . Then, solving Equation (33) produces a new value of Θ to update \mathbf{A} and \mathbf{b} , and subsequently Θ . This iterative procedure first gives an approximate maximum likelihood (AML) estimator, which can then be iterated a number of times to obtain a final solution. The final solution takes the Θ that gives the smallest J in Equation (26). This ensures that the AML will not diverge. In fact, simulation results presented in (Chan et al., 2006) show that the AML can nearly achieve the Cramer-Rao lower bound (CRLB) with a small number of iterations (typically on the order of five updates are found to be sufficient). It should be noted that, for the special case of equal measurement variance assumption (as in the original AML), the common σ term drops from Equation (32). However, with the modified AML in Equation (33), the quantities g_i and h_i will be different for different BSs, and this is found to yield some improvement in performance as will be discussed next.

5.2. Positioning Accuracy with the Modified AML Algorithm

To illustrate the impact of the modified AML that takes into account the unequal error variances, we consider an example of three BSs with different measurement error statistics for mobiles located in three different regions, as described in the different cases of Section 3. Figure 9 shows the geometry of the layout used for this purpose, where distances are shown in meters. The dense scatter points represents a total of 10^5 noisy mobile locations generated according to the TOA statistics for the different cases of interest which are referred to as MS1, MS2, MS3, corresponding to mobiles classified in Section 3 as Case 1, 2, and 3, respectively. For each mobile location, the AML and modified AML algorithms are executed to obtain the estimated mobile coordinates, and by comparing with the known mobile position, the resulting positioning error can be computed. The different parameters for the radio channel and relative received power factors used are based on the results given in Table 1 of Section 3.

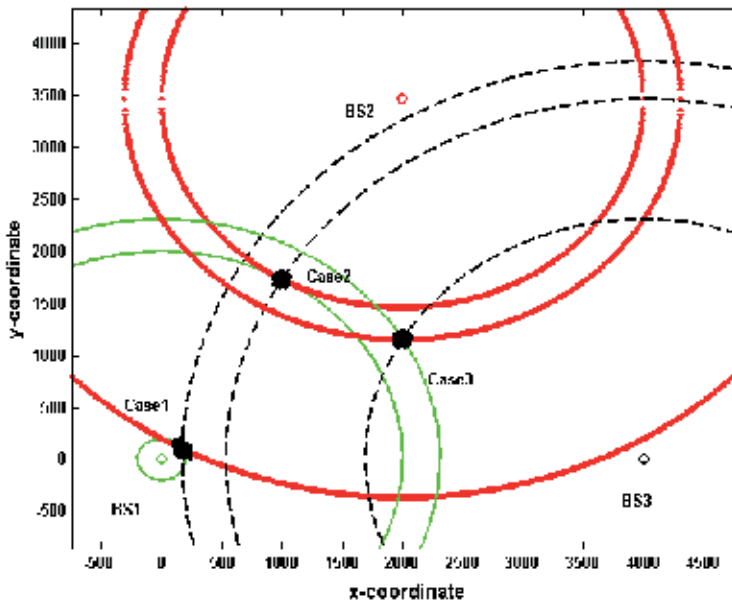


Fig. 9. Layout of the mobile localization geometry used to test the accuracy of the AML algorithm.

Various aspects of mobile positioning performance are illustrated in Figure 10 based on the cumulative distribution function (CDF) of the radiolocation error. First, it can be seen that the modified AML which takes into account the differences in TOA noise statistics at the various base stations (as proposed in this work) outperforms, albeit slightly, the conventional AML which assumes equal TOA noise variance at all base stations. This is more pronounced for mobiles categorized as MS1 (i.e., which are in close proximity to their home base stations). The other major observation from Figure 10 is that a large difference in radiolocation accuracy is present depending on the mobile relative position with respect to the base stations. It is clearly seen that MS2 and particularly MS3 mobiles, corresponding to mobiles in 2-way and 3-way soft handoff, respectively, achieve much better performance as opposed to MS1. This is due to the poor TOA accuracy at BS2 and BS3 for the latter case, owing to the overwhelming near-far interference experienced by the mobile at the remote base stations, as discussed in Section 4. As an example, the probability of the residual positioning error being less than 20m is almost one for MS3 mobiles, while it is on the order of 70% for MS2, and only 50% for MS1-type mobiles. Similar observations also hold for other distances. Therefore, as highlighted throughout this study, the accuracy of mobile positioning is best when the mobile is in close proximity to a border cell region where soft handoff connectivity is established with one or two more cells involved in its positioning in addition to its home serving cell.

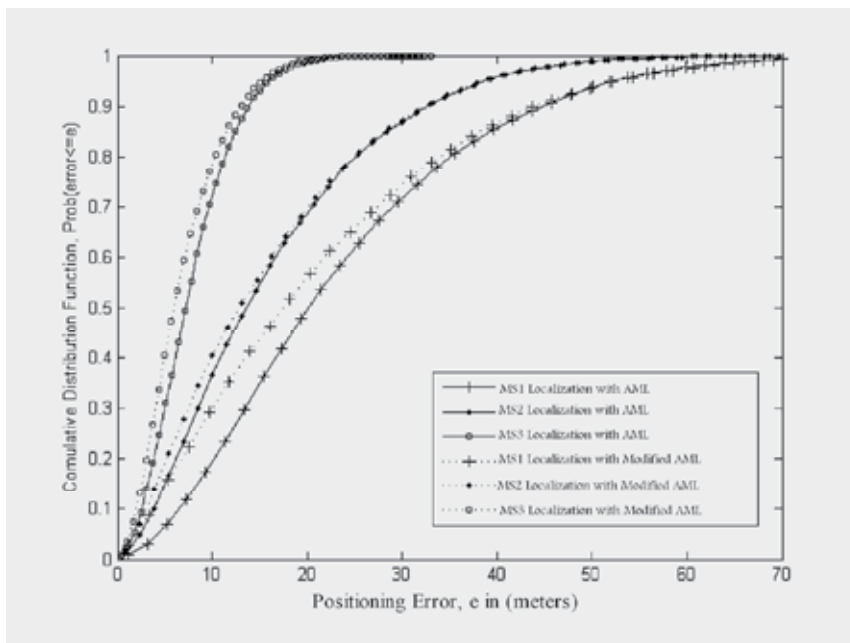


Fig. 10. Illustration of mobile positioning accuracy with the Approximate Maximum Likelihood Algorithm.

6. Conclusion

This study dealt with the performance analysis of time-of-arrival (TOA) techniques for mobile positioning in CDMA wireless cellular networks. Since several base stations are typically needed for mobile radiolocation, the problem of weak signal hearability at remote base stations is a major challenge, and a detailed analysis of this issue was presented by taking into account the near-far interference usually present in CDMA cellular networks.

TOA-based positioning methods are well-suited for wide deployment of radiolocation services since the synchronization circuits that can extract timing information are readily available at the base stations receiving the mobile signal. For CDMA signals, the delay-locked loop (DLL) is commonly used as a TOA estimation device, and a detailed analysis of DLL-based TOA tracking was presented taking into account the cellular network layout, cell loading and other-user interference, as well as RF channel shadowing and pathloss that affect received signal strength at the different base stations. In particular, it was shown that the TOA tracking error statistics can vary considerably depending on the mobile link conditions with respect to the base stations involved in its positioning, and soft handoff (SHO) links with two or three base stations for mobiles close to border-cell regions were found to improve the precision of mobile TOA tracking.

Using TOA information, a mobile radiolocation positioning algorithm based on a computationally-efficient, near-optimum approximate maximum likelihood (AML) processing was presented, and a generalization to the case of unequal timing error variances at the different base stations was also derived. Numerical results were presented to quantify

the achievable positioning accuracy of the AML algorithms, and it was also shown that SHO radio links with two or particularly three base stations have a clear impact on the precision of mobile radiolocation. Finally, it should be noted that the problem of non-line-of-sight (NLOS) propagation, which constitutes another major challenge to mobile positioning accuracy, was not included in this study, and would be addressed in future work.

Acknowledgment

This work was gratefully supported by King Abdulaziz City for Science & Technology and King Fahd University of Petroleum & Minerals, Saudi Arabia.

7. References

- Caffrey, J. J. (1999). *Wireless Location in CDMA Cellular Radio Systems*. Kluwer Academic Publishers.
- Caffrey, J. J. & Stuber, G. L. (2000). Effects of multiple access interference on the non-coherent delay lock loop. *IEEE Transactions on Communications*, Vol. 48, (December 2000) 2109-2119.
- Chan, Y-T.; Hang, H. & Ching, P-C. (2006). Exact and approximate maximum likelihood localization algorithms. *IEEE Transactions on Vehicular Technology*, vol. 55, No. 1, (January 2006) 10-16.
- Chan, Y. T. & Ho, K. C. (1994). A simple and efficient estimator for hyperbolic location. *IEEE Transactions on Signal Processing*, Vol. 42, No. 8, (August 1994) 1905-1915.
- Chan, Y. T.; Yau, C. H. & Ching P. C. (2006). Exact and approximate maximum likelihood localization algorithms. *IEEE Transactions on Vehicular Technology*, Vol. 55, No. 1, (January 2006) 10-16.
- Dahlman, E.; Gudmundson, B.; Nilsson, M. & Skold, A. (2000). UMTS/IMT-2000 based on wideband CDMA. *IEEE Communications Magazine*, (September 2000) 70-80.
- Gosh, A. & Love, R. (1998). Mobile station location in a DS-CDMA system, *Proceedings of IEEE VTC*, Vol. 1, pp. 254-258.
- Kaplan, E. (1996). *Understanding GPS: Principles and Applications*. Norwood, MA: Artech House.
- Khan, H. R. (2009). *DLL Code Tracking for CDMA Signals under Fading and Multiple Access Interference*, M.S. Thesis, King Fahd University of Petroleum & Minerals, February 2009.
- Niezgoda, G. H. & Ho, K. C. (1994). Geolocation by combined range difference and range rate measurements, *Proceedings of International Conference Acoustics, Speech, Signal Process (ICASSP'94)*, Adelaide, Australia, Vol. 2, 1994, pp. 357-360.
- Rappaport, T.; Reed, J. & Wornor, B. (1996). Position location using wireless communications on highways of the future. *IEEE Communications Magazine*, (October 1996) 33-41.
- Sayed, A. H.; Tarighat, A. & Khajehnouri, N. (2005). Network-Based Wireless Location. *IEEE Signal Processing Magazine*, (July 2005) 24-40.
- Su, S. L. & Yen, N. Y. (1997). Performance of digital code tracking loops for direct-sequence spread-spectrum signals in mobile radio channels. *IEEE Transactions on Communications*, Vol. 45, (May 1997) 596-604.
- Trees, H. L. V. (1968). *Detection, Estimation, and Modulation Theory: Part 1*, Wiley, New York.
- Viterbi, A. J. (1995). *CDMA: Principles of Spread Spectrum Communication*, Addison-Wesley.

Mobility and Handoff Management in Wireless Networks

Jaydip Sen
Tata Consultancy Services
INDIA

1. Introduction

With the increasing demands for new data and real-time services, wireless networks should support calls with different traffic characteristics and different Quality of Service (QoS) guarantees. In addition, various wireless technologies and networks exist currently that can satisfy different needs and requirements of mobile users. Since these different wireless networks act as complementary to each other in terms of their capabilities and suitability for different applications, integration of these networks will enable the mobile users to be always connected to the best available access network depending on their requirements. This integration of heterogeneous networks will, however, lead to heterogeneities in access technologies and network protocols. To meet the requirements of mobile users under this heterogeneous environment, a common infrastructure to interconnect multiple access networks will be needed. Although IP has been recognized to be the de facto protocol for next-generation integrated wireless, for inter-operation between different communication protocols, an adaptive protocol stack is also required to be developed that will adapt itself to the different characteristics and properties of the networks (Akyildiz et al., 2004a). Finally, adaptive and intelligent terminal devices and smart base stations (BSs) with multiple air interfaces will enable users to seamlessly switch between different access technologies.

For efficient delivery of services to the mobile users, the next-generation wireless networks require new mechanisms of *mobility management* where the location of every user is proactively determined before the service is delivered. Moreover, for designing an adaptive communication protocol, various existing mobility management schemes are to be seamlessly integrated. In this chapter, the design issues of a number of mobility management schemes have been presented. Each of these schemes utilizes IP-based technologies to enable efficient roaming in heterogeneous network (Chiussi et al., 2002). Efficient handoff mechanisms are essential for ensuring seamless connectivity and uninterrupted service delivery. A number of handoff schemes in a heterogeneous networking environment are also presented in this chapter.

The chapter is organized as follows. Section 2 introduces the concept of mobility management and its two important components- *location management* and *handoff management*. Section 3 presents various network layer protocols for macro-mobility and micro-mobility. Section 4 discusses various link layer protocols for location management.

Section 5 introduces the concept of handoff. Different types of handoff mechanisms are classified, and the delays associated with a handoff procedure are identified. Some important cross-layer handoff mechanisms are also discussed in detail. Section 6 presents *media independent handover* (MIH) services as proposed in IEEE 802.21 standards. It also discusses how MIH services can be utilized for designing seamless mobility protocols in next-generation heterogeneous wireless networks. Section 7 discusses security issues in handover protocols. Section 8 identifies some open areas of research in mobility management. Section 9 concludes the chapter.

2. Mobility Management

With the convergence of the Internet and wireless mobile communications and with the rapid growth in the number of mobile subscribers, mobility management emerges as one of the most important and challenging problems for wireless mobile communication over the Internet. Mobility management enables the serving networks to locate a mobile subscriber's point of attachment for delivering data packets (i.e. location management), and maintain a mobile subscriber's connection as it continues to change its point of attachment (i.e. handoff management). The issues and functionalities of these activities are discussed in this section.

2.1 Location management

Location management enables the networks to track the locations of mobile nodes. Location management has two major sub-tasks: (i) *location registration*, and (ii) *call delivery* or *paging*. In location registration procedure, the mobile node periodically sends specific signals to inform the network of its current location so that the location database is kept updated. The call delivery procedure is invoked after the completion of the location registration. Based on the information that has been registered in the network during the location registration, the call delivery procedure queries the network about the exact location of the mobile device so that a call may be delivered successfully. The design of a location management scheme must address the following issues: (i) minimization of signaling overhead and latency in the service delivery, (ii) meeting the guaranteed quality of service (QoS) of applications, and (iii) in a fully overlapping area where several wireless networks co-exist, an efficient and robust algorithm must be designed so as to select the network through which a mobile device should perform registration, deciding on where and how frequently the location information should be stored, and how to determine the exact location of a mobile device within a specific time frame.

2.2 Handoff management

Handoff management is the process by which a mobile node keeps its connection active when it moves from one access point to another. There are three stages in a handoff process. First, the initiation of handoff is triggered by either the mobile device, or a network agent, or the changing network conditions. The second stage is for a new connection generation, where the network must find new resources for the handoff connection and perform any additional routing operations. Finally, data-flow control needs to maintain the delivery of the data from the old connection path to the new connection path according to the agreed-upon QoS guarantees. Depending on the movement of the mobile device, it may undergo

various types of handoff. In a broad sense, handoffs may be of two types: (i) intra-system handoff (horizontal handoff) and (ii) inter-system handoff (vertical handoff). Handoffs in homogeneous networks are referred to as intra-system handoffs. This type of handoff occurs when the signal strength of the serving BS goes below a certain threshold value. An inter-system handoff between heterogeneous networks may arise in the following scenarios (Mohanty, 2006) - (i) when a user moves out of the serving network and enters an overlying network, (ii) when a user connected to a network chooses to handoff to an underlying or overlaid network for his/her service requirements, (iii) when the overall load on the network is required to be distributed among different systems.

The design of handoff management techniques in all-IP based next-generation wireless networks must address the following issues: (i) signaling overhead and power requirement for processing handoff messages should be minimized, (ii) QoS guarantees must be made, (iii) network resources should be efficiently used, and (iv) the handoff mechanism should be scalable, reliable and robust.

2.3 Mobility management at different layers

A number of mobility management mechanisms in homogeneous networks have been presented and discussed in (Akyildiz et al., 1999). Mobility management in heterogeneous networks is a much more complex issue and usually involves different layers of the TCP/IP protocol stack. Several mobility management protocols have been proposed in the literature for next-generation all-IP wireless networks. Depending on the layers of communication protocol they primarily use, these mechanisms can be classified into three categories - protocols at the network layer, protocols at the link layer and the cross-layer protocols. Network layer mobility protocols use messages at the IP layer, and are agnostic of the underlying wireless access technologies (Misra et al., 2002). Link layer mobility mechanisms provide mobility-related features in the underlying radio systems. Additional gateways are usually required to be deployed to handle the inter-operating issues when roaming across heterogeneous access networks. In link layer protocols, handoff signals are transmitted through wireless links, and therefore, these protocols are tightly-coupled with specific wireless technologies. Mobility supported at the link layer is also called *access mobility* or *link layer mobility* (Chiussi et al., 2002). The cross-layer protocols are more common for handoff management. These protocols aim to achieve network layer handoff with the help of communication and signaling from the link layer. By receiving and analyzing, in advance, the signal strength reports and the information regarding the direction of movement of the mobile node from the link layer, the system gets ready for a network layer handoff so that packet loss is minimized and latency is reduced.

3. Network Layer Mobility Management Mechanisms

Over the past several years, a number of IP mobility management protocols have been proposed. Different mobility management frameworks can be broadly distinguished into two categories - device mobility management protocol for localized or *micro-mobility* and protocols for inter-domain or *macro mobility*. The movement of a mobile node (MN) between two subnets within one domain is referred to as micro-mobility. For example, the movement of MN from subnet *B* to subnet *C* in Figure 1 is an example of micro-mobility. An example of micro-mobility in UMTS Terrestrial Radio Access Networks (UTRAN) is movement of an

MN from one BS to another, both BSs belonging to the same *random access network (RAN)*, while in WLAN it is a node movement between two *access points (APs)*. The movement of devices between two network domains is referred to as *macro-mobility*. For example, the movement of MN from domain 1 to domain 2 in Figure 1 is an example of macro-mobility. A domain represents an administrative body, which may include different access networks, such as WLAN, second-generation (2G), and third-generation (3G) networks (Akyildiz et al., 2004b). Next-generation all-IP wireless network will include various heterogeneous networks, each of them using possibly different access technologies. Therefore, satisfactory macro-mobility solution supporting all these technologies is needed.

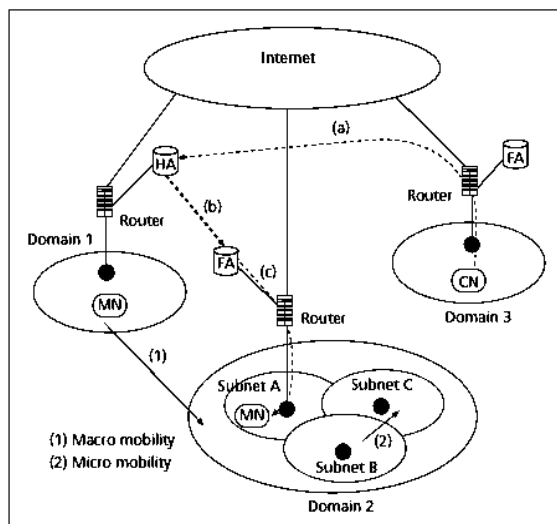


Fig. 1. Mobile IP Architecture [Source: (Akyildiz et al., 2004)]

3.1 Macro-mobility protocols

Mobile IP is the most widely used protocol for macro-mobility management. In addition to Mobile IP, three macro-mobility architectures are discussed in the section. These protocols are: Session Initiation Protocol (SIP)-based mobility management, multi-tier hybrid SIP and Mobile IP protocol, and network inter-working agent-based mobility protocol.

Mobile IP: Mobile IP (Perkins, 2008) is the most well-known macro mobility scheme that solves the problem of node mobility by redirecting the packets for the MN to its current location. It introduces seven elements: (i) *Mobile node (MN)* – a device or a router that can change its point of attachment to the Internet, (ii) *Correspondent node (CN)* – the partner with which MN communicates, (iii) *Home network (HN)* – the subnet to which MN belongs, (iv) *Foreign network (FN)* – the current subnet in which the MN is visiting, (v) *Home agent (HA)* – provides services for the MN and is located in the HN, (vi) *Foreign agent (FA)* – provides services to the MN while it visits in the FN, (vii) *Care-of-address (CoA)* – defines the current location of the MN; all packets sent to the MN are delivered to the CoA. Mobile IP protocol has three steps: (i) agent discovery, (ii) registration, and (iii) routing and tunneling.

Agent discovery: An MN is able to detect whether it has moved into a new subnet by two methods – agent advertisement and agent solicitation. In the agent advertisement method, FAs and HAs advertise their presence periodically using agent advertisement messages.

These advertisement messages can be seen as beacon broadcasts into the subnets. An MN in a subnet can receive agent advertisements. If no agent advertisement messages are found or the inter-arrival time is too high, the MN may send agent solicitations. After the step of agent advertisement or solicitation, the MN receives a CoA. The CoA may be either an FA or a co-located CoA (Perkins, 2008). A co-located CoA is found by using Dynamic Host Configuration Protocol (DHCP) or Point-to-Point Protocol (PPP).

Registration: After the MN receives its CoA, it registers it with the HA. The main objective of the registration is to inform the HA about the current location of MN. The registration may be done in two ways depending on the location of the CoA. If the CoA is the FA, the MN sends its registration request to the FA which in turn forwards it to the HA. If the CoA is co-located, the MN may send the request directly to the HA.

Routing and tunneling: When a CN sends an IP packet to the MN, the packet is intercepted by the HA. The HA encapsulates the packet and tunnels it to the MN's CoA. With FA CoA, the encapsulated packet reaches the FA serving the MN. The FA decapsulates the packet and forwards it to the MN. With co-located CoA, the encapsulated packets reach the MN, which decapsulates them. In Figure 1, the tunneling (step b) ends at the MN instead of at the FA.

Paging Extension for Mobile IP: For saving battery power at MNs, IP paging mechanism has been proposed (Haverinen & Malinen, 2000). Paging typically includes transmitting a request for an MN to a set of locations, in one of which the MN is expected to be present. The set of locations is called a paging area and it consists of a set of neighboring base stations. A network that supports paging allows the MNs to operate in two different states – an active state and a standby state. In an active state, the MN is tracked at the finest granularity such as its current base station (resulting in no need for paging). In the standby state, the MN is tracked at a much coarser granularity such as a paging area. The MN updates the network less frequently in stand by mode (every paging area change) than in active state (every base station). The cost of paging, however, is the complexity of the algorithms and the protocols required to implement the procedures, and the delay incurred for locating an MN.

Drawbacks of Mobile IP: The Mobile IP has the following shortcomings:

- The packets sent from a CN to an MN are received by the HA before being tunneled to the MN. However, packets from the MN are sent directly to the CN. This inefficient mechanism of non-optimized Mobile IP is called *triangular routing*. It results in longer routes and more delay in packet delivery.
- When an MN moves across two different subnets, the new CoA cannot inform the old CoA about MN's current location. Packets tunneled to the old CoA are lost.
- Mobile IP is not an efficient mechanism in a highly mobile scenario as it requires an MN to send a location update to the HA whenever it changes its subnet. The signaling cost for location updates and the associated delay may be very high if the distance between the visited network and the home network is large.

Optimization in Mobile IP: In (Perkins & Johnson, 2001), an optimization technique has been proposed to solve the problem of triangular routing. The idea is to inform the CN about the current location of the MN so as to bypass the HA. The CN can learn the location of the CoAs of the MN by caching them in a binding cache in the CN. When a CN sends packets to an MN, it first checks if it has a binding cache entry for the MN. If there is an entry, the CN tunnels the packets directly to the CoA. If no binding cache entry is available, the CN sends the packets to the HA, which in turn tunnels them to the CoA. In optimized Mobile IP, the packets tunneled by the HA to the old CoA are not lost in transit. When an MN registers

with a new FA, it requests the new FA to notify the previous FA about its movement. As the old FA now knows the location of the current FA, it can forward the packets to the new FA.

SIP-Based Mobility Management: In (Salsano et al., 2008), a *Session Initiation Protocol (SIP)*-based solution, called *mobility management using SIP extension (MMUSE)*, has been proposed that supports vertical handoffs in next-generation wireless networks. SIP has been chosen by the Third Generation Partnership Project (3GPP) as the signaling protocol to set up and control real-time multimedia sessions. In MMUSE, a *mobile host (MH)* is assumed to be equipped with multiple network interfaces; each of them is assigned a separate IP address when connected to different *access networks (ANs)*. The MH uses the SIP protocol to set up multimedia sessions. The architecture of the scheme is depicted in Figure 2. The *session border controller (SBC)* is a device that is typically located at the border of an IP network, and manages all the sessions for that network. A new entity, called the *mobility management server (MMS)* resides within the SBC. The MMS cooperates with another entity - *mobility management client (MMC)* that resides in each MH. Both the *SIP user agents (UAs)* on the MH and on the *corresponding host (CH)* remain unaware of all the handoff procedures, which are handled by the MMC and the MMS. On the MH, the UA sees only the MMC as its outbound proxy and forwards the normal SIP signaling and media flows to it. MMC relays the packets to the MMS/SBC. From there on, the packets follow the path determined by the usual SIP routing procedure. Every time the MH moves across two ANs, a location update SIP message is sent to the MMS. This is done over the new network so that the procedure can be completed even if the old network is suddenly not available. If the MMS receives a call addressed to one of its served MHs, it forwards the call to the correct interface. When the MH changes its AN while it is engaged in a call, the procedure is almost identical. However, in this case, the MMC sends to the MMS an SIP message that contains the additional information required to identify the call to be shifted to new interface. To minimize the handoff duration, the *real-time transport protocol (RTP)* flow coming from the MH during the handoff is duplicated using the MMC. When the MMC starts the handoff procedures, it sends the handover request to the MMS and at the same time, it starts duplicating the RTP packets over both interfaces. As soon as the MMS receives the handover message, the packets coming from the new interface are already available. The MMS performs the switching and sends the reply back to the MMC. When the MMC receives the reply message, it stops duplicating the packets.

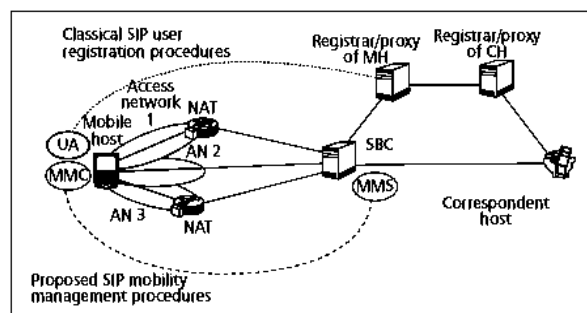


Fig.2. Architecture of MMUSE [Source: (Salsano et al., 2008)]

Multi-Layer Mobility Management using Hybrid SIP and Mobile IP: In (Politis et al., 2003), two mobility management architectures based on SIP and Mobile IP are presented.

The two approaches provide mobility in two different layers: application and network layers respectively. The scheme is therefore called multi-layer mobility management scheme. The SIP-based protocol uses SIP in combination with IP encapsulation mechanisms on CHs to support mobility for all types of traffic from/to the MH. The second approach performs separation of traffic and employs SIP in combination with *network address translation* (NAT) mechanisms to support mobility for real-time traffic over UDP. The mobility for non-real-time traffic (mainly TCP-based applications) is supported by Mobile IP. In the SIP-based approach, if the MH moves during a session, the SIP UA sends a SIP re-INVITE request message to each of its CHs. If a CH runs a TCP session, IP encapsulation is used to forward packets to MH. However, if a CH runs a UDP session, the packets are sent directly to the MH's new address. The MH completes the handoff by sending a SIP REGISTER message to the SIP server. For the hybrid SIP/Mobile IP scheme, the inter-domain mobility is based on the synergy of SIP with Mobile IP. Traffic from/to an MH is separated on the domain edge routers. SIP signaling is used to support inter-domain mobility for real-time (RTP over UDP) traffic, while Mobile IP supports non-real-time traffic.

Network Inter-Working Agent-Based Mobility Management: In (Akyildiz et al., 2005) an architecture has been proposed for next-generation all-IP wireless systems. Different wireless networks are integrated through an entity called the *network inter-working agent* (NIA). In Figure 3, an NIA integrates one WLAN, one cellular network, and one satellite network. NIA also handles authentication, billing, and mobility management issues during inter-system (inter-domain) roaming. Two types of movement of an MH are considered: movement between different subnets of one domain (intra-domain mobility) and movement between different access networks belonging to different domains (inter-domain mobility). For inter-domain mobility, a novel cross-layer mobility management protocol is proposed, which makes an early detection of the possibility of an inter-domain handoff and allows authentication, authorization and registration of the MH in the new domain before the actual handoff. These interoperability operations are executed by the NIA.

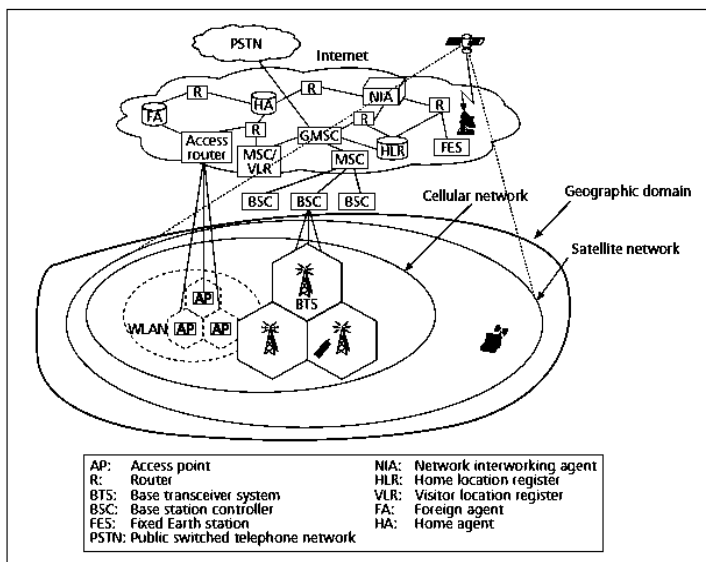


Fig. 3. NIA-Based Mobility Management Architecture [Source: (Akyildiz et al., 2005)]

3.2 Micro-mobility protocols

Over the past several years a number of IP micro-mobility protocols have been proposed, designed and implemented that complement the base Mobile IP (Campbell & Gomez, 2001) by providing fast, seamless and local handoff control. IP micro-mobility protocols are designed for environments where MHs changes their point of attachment to the network so frequently that the base Mobile IP mechanism introduces significant network overhead in terms of increased delay, packet loss and signaling. For example, many real-time wireless applications, e.g. VOIP, would experience noticeable degradation of service with frequent handoff. Establishment of new tunnels can introduce additional delays in the handoff process, causing packet loss and delayed delivery of data to applications. This delay is inherent in the round-trip incurred by the Mobile IP as the registration request is sent to the HA and the response sent back to the FA. Route optimization (Perkins & Johnson, 2001) can improve service quality but it cannot eliminate poor performance when an MH moves while communicating with a distant CH. Micro-mobility protocols aim to handle local movement (e.g., within a domain) of MHs without interaction with the Mobile IP-enabled Internet. This reduces delay and packet loss during handoff and eliminates registration between MHs and possibly distant HAs when MHs remain inside their local coverage areas. Eliminating registration in this manner also reduces the signaling load experienced by the network.

The micro-mobility management schemes can be broadly divided into two groups: (i) tunnel-based schemes and (ii) routing-based schemes. In tunnel-based approaches, the location database is maintained in a distributed form by a set of FAs in the access network. Each FA reads the incoming packet's original destination address and searches its visitor list for a corresponding entry. If an entry exists, it is the address of next lower level FA. The sequence of visitor list entries corresponding to a particular MH constitutes the MH's location information and determines the route taken by downlink packets. Mobile IP regional registration (MIP-RR) (Fogelstroem et al., 2006), hierarchical Mobile IP (HMIP) (Soliman et al., 2008), and intra-domain mobility management protocol (IDMP) (Misra et al., 2002) are tunnel-based micro-mobility protocol.

Routing-based approaches forward packets to an MH's point of attachment using mobile-specific routes. These schemes introduce implicit (snooping data) or explicit signaling to update mobile-specific routes. In the case of Cellular IP, MHs attached to an access network use the IP address of the gateway as their Mobile IP CoA. The gateway decapsulates packets and forwards them to a BS. Inside the access network, MHs are identified by their home address and data packets are routed using mobile-specific routing without tunneling. Cellular IP (CIP) (Campbell et al., 2000) and handoff-aware wireless access Internet infrastructure (HAWAII) (Ramjee et al., 2002) are routing-based micro-mobility protocols.

Mobile IP Regional Registration: In Mobile IP, an MN registers with its HA each time it changes its CoA. If the distance between the visited network and the home network of the MN is large, the signaling delay for these registrations may be long. MIP-RR (Fogelstroem et al., 2006) attempts to minimize the number of signaling messages to the home network and reduce the signaling delay by performing registrations locally in a regional network. This reduces the load on the home network, and speeds up the process of handover. The scheme introduces a new network node called the *gateway foreign agent* (GFA). The address of the GFA is advertised by the FAs in a visited domain. When an MN first arrives at this visited domain, it performs a home registration - that is, a registration with its HA. At this time, the MN registers the address of the GFA as its CoA. When the MN moves between different

FAs within the same visited domain, it only needs to make a regional registration to the GFA. When the MN moves from one regional network to another, it performs a home registration with its HA. The packets for the MN are first intercepted by its HA, which tunnels them to the registered GFA. The GFA checks its visitor list and forwards the packets to the corresponding FA of the MN. The FA further relays the packets to the MN. The use of the GFA avoids any signaling traffic to the HA as long as the MN is within a regional network.

Hierarchical Mobile IPv6: The basic idea of hierarchical Mobile IP (Soliman et al., 2008) (HMIP) is the same as that of regional registration scheme. HMIP introduces a new Mobile IP node called the *mobility anchor point* (MAP). An MN is assigned two CoAs - regional CoA (RCoA) and on-link CoA (LCoA). The MN obtains the RCoA from the visited networks. RCoA is an address on the MAP's subnet. The LCoA is the CoA that is based on the prefix advertised by the *access router* (AR). The AR is the default router of the MN and receives all outbound traffic from it. When an MN enters a new network, it receives router advertisement that contains the available MAPs and their distances from the MN. The MN selects a MAP, gets the RCoA in the MAP's domain and the LCoA from the AR. The MN sends a binding update to the MAP. The MAP records the binding and inserts it in its binding cache (foreign registration). The MAP sends the binding update message also to the MN's HA and to the CNs (home registration). When MN is outside its home network, the incoming data to MN goes through MAP hierarchy. Messages from CN or HA are received by the MAP, which tunnels them to LCoA. As the MN roams locally, it gets a new LCoA from its new AR. The RCoA remains unchanged as long as the MN is within the same network.

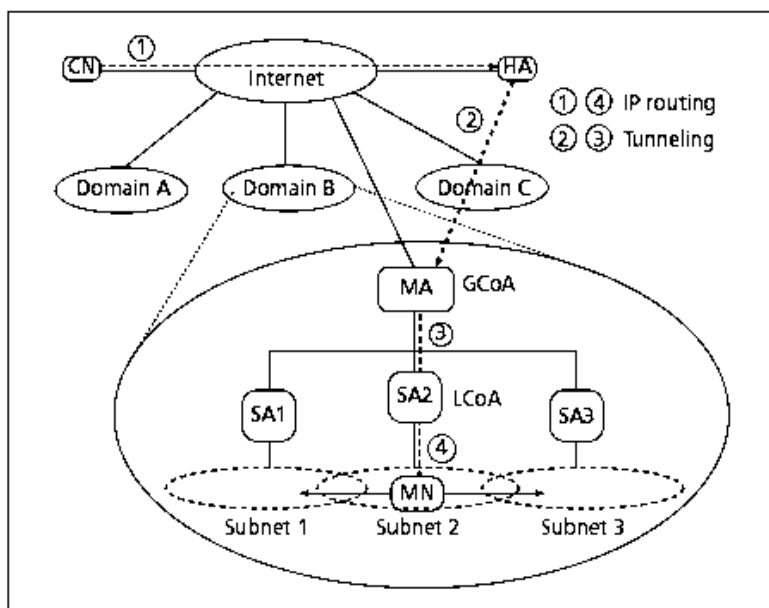


Fig. 4. The Architecture of IDMP [Source: (Akyildiz et al., 2004)]

Intra-Domain Mobility Management Protocol: Intra-domain mobility management protocol (IDMP) (Misra et al., 2002) is a two-level, hierarchical, multi-CoA, intra-domain mobility management protocol. The first level of the hierarchy consists of different mobility domains. The second level consists of IP subnets within each domain. This hierarchical approach localizes the scope of intra-domain location update messages and thereby reduces both the global signaling load and update latency. The two-level hierarchical architecture defined by IDMP is shown in Figure 4. IDMP consists of two types of entities: (i) *mobility agent* (MA) and (ii) *subnet agent* (SA). The MA provides a domain-wide stable access point for an MN. An SA handles the mobility of MNs within a subnet. Similar to HMIP, each MN can get two CoAs - global CoA (GCoA) and local CoA (LCoA). The GCoA specifies the domain to which the MN is currently attached. The LCoA identifies the MN's present subnet. The packets destined to an MN are first received by the HA. The HA tunnels the packets to the MA using the MN's GCoA. The MA first decapsulates the packets, determines the current LCoA of the MN using its internal table, and tunnels them to the LCoA. The encapsulated packets are received by the SA. Finally, the SA decapsulates the packets and forwards them to the MN. When the MN moves from one subnet to another inside the same domain, it is assigned a new LCoA. The MN registers the address of the new LCoA with its MA. Till the registration of the new LCoA is complete, the MA forwards all packets for the MN to the old LCoA. This results in packet drops. A fast handoff procedure has been proposed to avoid this packet loss (Misra et al., 2002). It eliminates intra-domain update delay by anticipating the handover in connectivity between the networks and the MNs. The anticipation of MN's movement is based on a link layer trigger which initiates a network layer handoff before the link layer handoff completes. Once the MN senses a handoff, it sends a request to the MA to multicast the packets to its SAs. The MA multicasts incoming packets to each neighboring SAs. Each SA buffers the packets in order to prevent any loss of packets in transit during the handoff. After the MN finishes registration, the new SA transfers all buffered packets to the MN.

Cellular IP: Cellular IP (Campbell et al., 2000) is a mobility management protocol that provides access to a Mobile IP-enabled Internet for fast moving MHs. The architecture of Cellular IP is shown in Figure 5. It consists of three major components: (i) cellular IP node or the base station (BS), (ii) cellular IP gateway (GW), and (iii) cellular IP mobile host (MH). A Cellular IP network consists of interconnected BSs. The BSs route IP packets inside the cellular network and communicate with MHs via wireless interface. The GW is a cellular IP node that is connected to a regular IP network by at least one of its interfaces. The BSs periodically emit beacon signals. MHs use these beacon signals to locate the nearest BSs. All IP packets transmitted by an MH are routed from the BS to the GW by hop-by-hop shortest path routing, regardless of the destination address. The BSs maintain route cache. Packets transmitted by the MH create and update entries in BS's cache. An entry maps the MH's IP address to the neighbor from which the packet arrived to the host. The chain of cached mappings referring to an MH constitutes a reverse path for downlink packets for the MH. To prevent timing out of these mappings, an MH periodically transmits control packets. MHs that are not actively transmitting or receiving data themselves may still remain reachable by maintaining paging caches. MHs listen to the beacons transmitted by BSs and initiate handoff based on signal strength. To perform a handoff, an MH tunes its radio to the new BS and sends a *route update* packet. This creates routing cache mappings on route to the new BS. Handoff latency is the time that elapses between the handoff and the arrival of the

first packet through the new route. The mappings associated with the old BS are cleared after the expiry of a timer. Before the timeout, both the old and new downlink routes remain valid and packets are delivered through both the BSs. This feature used in Cellular IP semi-soft handoff algorithms improves handoff performance.

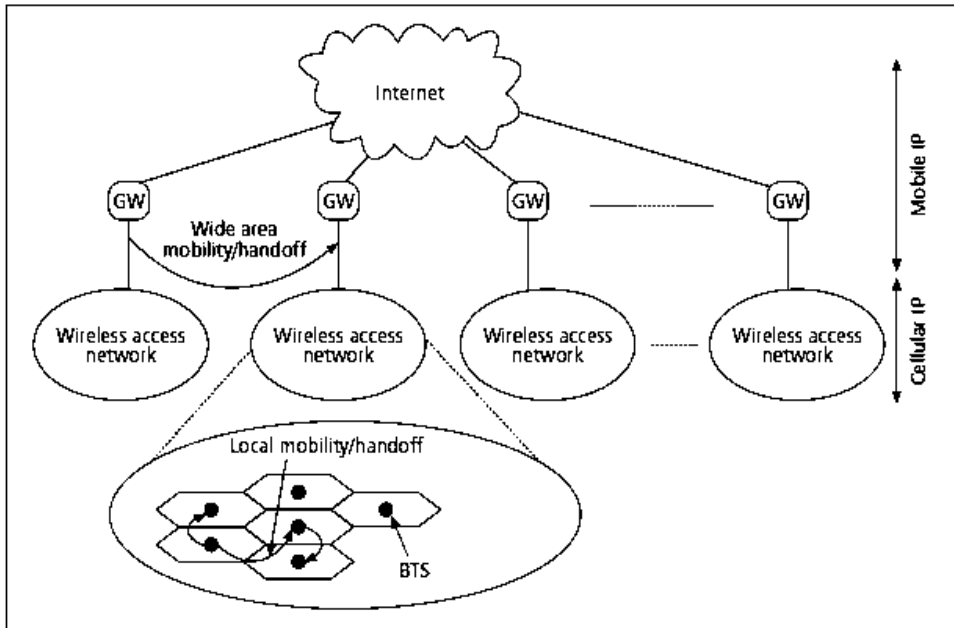


Fig. 5. Architecture of Cellular IP [Source: (Akyildiz et al., 2004)]

Handoff Aware Wireless Access Internet Infrastructure: Handoff-Aware Wireless Access Internet Infrastructure (HAWAII) (Ramjee et al., 2002) is a domain-based approach for supporting mobility. The network architecture of HAWAII is shown in Figure 6. Mobility management within a domain is handled by a gateway called a *domain root router* (DRR). Each MH is assumed to have an IP address and a home domain. While moving in its home domain, the MN retains its IP address. The packets destined to the MH reach the DRR based on the subnet address of the domain and are then forwarded to the MH. The paths to MH are established dynamically. When the MH is in a foreign domain, packets for the MH are intercepted by its HA. The HA tunnels the packets to the DRR of the MH. The DRR routes the packets to the MH using the host-based routing entries. If the MH moves across different subnets in the same domain, the route from the DRR to the BS serving the MN is modified, while the other paths remain unchanged. This causes a reduction in signaling message and handoff latency during intra-domain handoff. In traditional Mobile IP, the MH is directly attached either to the HA (i.e. the home domain router) or the FA (i.e. the foreign domain router). Thus, every handoff causes a change in the IP address for the MH, resulting in lack of scalability. HAWAII also supports IP paging. It uses IP multicasting to page idle MHs when packets destined to an MH arrive at the domain root router and no recent routing information is available.

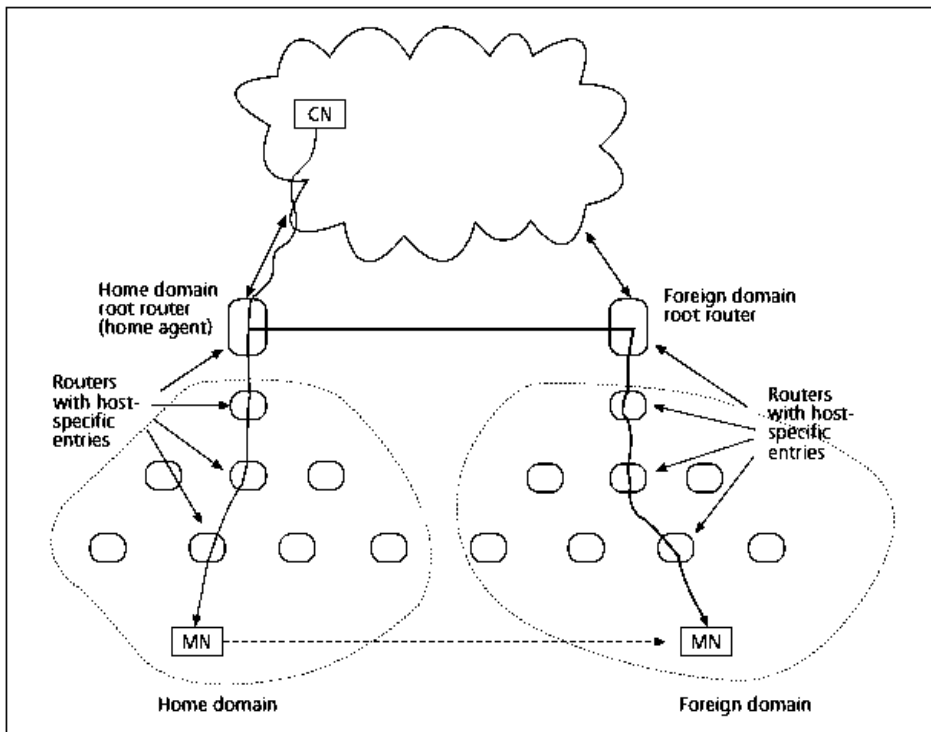


Fig. 6. Architecture of HAWAII Protocol [Source: (Akyildiz et al., 2004)]

Summary: Various network layer micro-mobility management schemes have been compared based on their features (Chiussi et al., 2002; Ramjee et al., 1999; Campbell et al., 2002). Each protocol uses the concept of domain root router. In all the protocols, signaling traffic is largely localized in a domain so as to reduce the global signaling traffic overhead. Routing-based schemes utilize the robustness of IP forwarding mechanism. Mobile-specific address lookup tables are maintained by all the mobility agents within a domain. In tunnel-based schemes, registration of the mobile nodes and encapsulation of the IP packets are performed in a local or hierarchical manner. Routing-based schemes avoid tunneling overhead, but suffer from the high cost of propagating host-specific routes in all routers within the domain. Moreover, the root node in routing schemes is a potential single point of failure (Chiussi et al., 2002). Tunnel-based schemes are modular and scalable. However, they introduce more cost and delays (Campbell et al., 2002).

4. Link Layer Mobility Management Mechanisms

Link layer mobility management mechanisms deal with issues related to inter-system roaming between heterogeneous access networks with different radio technologies and network management protocols. Two important considerations for designing inter-system roaming standards are: (i) the protocols for air interface and (ii) the mobile application part (MAP). In situations where a mobile node enters one wireless access network from another that support the same air interface protocols and MAP, the services are seamlessly migrated.

However, when the MAPs are different for the two networks, additional network entities need to be placed and signaling traffic are to be transmitted for inter-working. Since each network has its own mobility management protocols, the new inter-working entities should not replace existing systems. Rather, the entities should coexist and inter-work.

4.1 Location management protocols

For next-generation heterogeneous wireless networks, the inter-working and inter-operating function is suggested to accommodate roaming between dissimilar networks (Pandya et al., 1997). For existing practical systems, several solutions are proposed for some specific pairs of inter-working systems. In these schemes, the inter-operating function is implemented in either some additional inter-working unit with the help of dual-mode handsets (Phillips & Namee, 1998), or a dual-mode home location register (HLR) (Garg & Wilkes, 1996) to take care of the transformation of signaling formats, authentication, and retrieval of user profiles. Recent research efforts attempt to design general location management mechanisms for the integration and inter-working of heterogeneous networks. The research activities can be grouped into two categories: location management for adjacent dissimilar systems with partially overlapping coverage at the boundaries (Akyildiz & Wang, 2002; Wang & Akyildiz, 2001; ETSI, 2002) and location management in multi-tier systems where service areas of heterogeneous networks are fully overlapped (Lin & Chlamtac, 1996). All these solutions propose additional entities that take care of inter-working issues.

Location Management for Adjacent Networks: Researchers have addressed the issues of location management in two adjacent networks with overlapping areas (Akyildiz & Wang, 2002; Wang & Akyildiz, 2001; ETSI, 2002). Some of the protocols are discussed briefly.

Gateway Location Register Protocol: To enable inter-system roaming, a new level has been introduced in the hierarchy of location management entities for UMTS/ IMT-2000 networks. The new level consists of a *gateway location register* (GLR) (ETSI, 2002). The GLR is a gateway that enables inter-working between two networks by suitably converting signaling and data formats. It is located between the *visitor location register* (VLR) and the *serving GPRS support node* (SGSN) and the *home location register* (HLR). When a subscriber roams, the GLR plays the role of the HLR toward the VLR and SGSN in a *visited public land mobile network* (VPLMN), and the role of the VLR and SGSN to the HLR in a *home public land mobile network* (HPLMN). The GLR protocol assists the operators in lowering costs and optimizing roaming traffic. However, the protocol is not designed for ongoing call connection during inter-system roaming (Wang & Akyildiz, 2001). The incoming calls are routed to the home network even when the MN is roaming. This makes the protocol inefficient.

Boundary Location Register Protocol: In (Akyildiz & Wang, 2002), a location management mechanism has been proposed for heterogeneous network environment. It involves a mechanism for inter-system location updates and paging. Inter-system location update is implemented by using the concept of a *boundary location area* (BLA) existing at the boundary between two systems - X and Y in Figure 7. The BLA is controlled by a *boundary interworking unit* (BIU), which is connected to the *mobile switching centers* (MSCs) in both the systems. The BIU queries the user's service information, converts the message formats, checks the compatibility of the air interfaces and performs authentication of mobile users. When an MN is inside its BLA, it sends a location registration request to the new system. A distance-based location update mechanism reports MN's location when its distance from the boundary is less than a pre-defined threshold. An entity called a *boundary location register*

(BLR) is used for inter-system paging. The BLR maintains in its cache the location information of the MN and its roaming information when it crosses an intersystem boundary. During the inter-system paging process, only one system (X or Y) is searched. The associated MAP protocol is designed for mobile nodes with ongoing connections during inter-system roaming (Wang & Akyildiz, 2001). Instead of performing location registration after a mobile node arrives at the new system, the BLR protocol enables the node to update its location and user information actively before it enters the new system. In this way, the incoming calls to the MN during its inter-system roaming are delivered to the node.

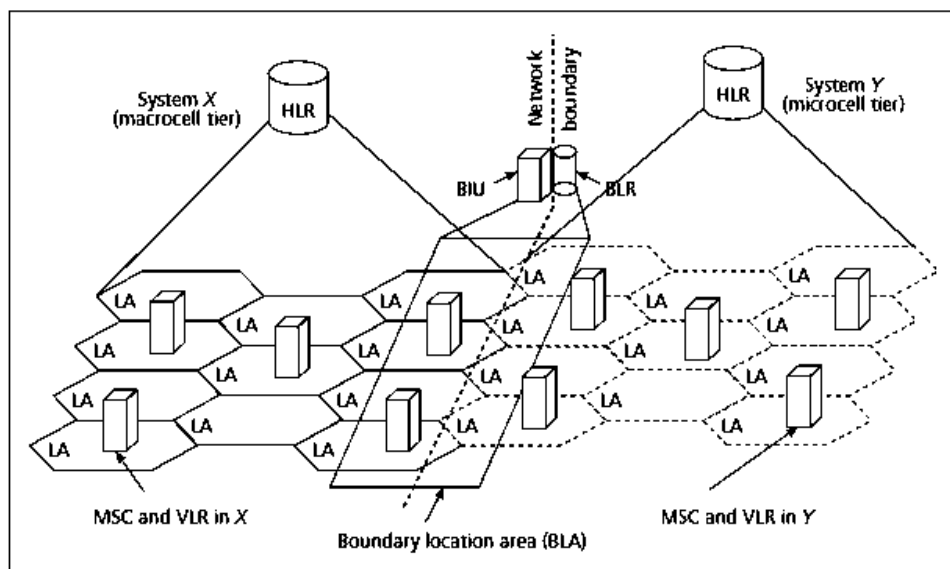


Fig. 7. The Boundary Location Register Protocol [Source: (Akyildiz et al. 2004)]

Location Management in Heterogeneous Networks: An MN is reachable via multiple networks when their service areas are fully overlapped. Since heterogeneous networks use different signaling formats, authentication procedures, and registration messages, it is difficult to merge heterogeneous HLRs into a single HLR. A multi-tier HLR (MHLR) is proposed in (Lin & Chalmtac, 1996), where a *tier manager* is connected to all the HLRs. Two types of location registration are possible: (i) single registration (SR) and (ii) multiple registrations (MR). Under SR scheme, an MN associates with the lowest tier of the MHLR, and receives services at low cost and high bandwidth. Under MR method, the MN registers on multiple tiers simultaneously. The individual tiers perform their own roaming management. The tier manager keeps track of the currently visited high-tier and low-tier VLRs of the MN. It has been found that MR scheme involves less signaling overhead (Lin & Chlamtac, 1996). However, since the current tier of the MN is not known to the MHLR, it incurs a high loss when a wrong tier is selected.

Summary: To summarize, all link layer-based mobility management schemes require additional inter-working entities for enabling information exchange between different systems. These inter-working entities are different depending on the systems, e.g., the GLR/BLR for inter-system location management, the MHLR for a multi-tier PCS system, and the gateways in the integrated UMTS/WLAN system. The interworking entities

perform the following functions: (i) format translation of the signaling messages and data packets and address translation between networks, (ii) retrieval of user profile from the home network, (iii) acting as a gateway for signal transmission and route setup, (iv) recording of mobility-related information during inter-system roaming, (v) negotiating QoS when an MN enters a new network, and (vi) performing authentication during inter-system movement. Different approaches for mobility management at the link layer address the following issues: (i) the location where the inter-working entities are put, (ii) the degree of coupling (loose or tight) of the entities, (iii) the timing of location registration and handoff initiation, (iv) the way location and handoff management is performed.

5. Handoff Management Protocols

Handoff or handover is a process by which an MN moves from one point of network attachment to another. Handovers can be classified as either homogeneous or heterogeneous. A heterogeneous handover occurs when an MN either moves between networks with different access technologies, or between different domains. As the diversity of available networks increases, it is important that mobility technologies become agnostic to link layer technologies, and can operate in an optimized and secure fashion without incurring unreasonable delay and complexity (Dutta et al., 2008). Supporting handovers across heterogeneous access networks, such as IEEE 802.11 (Wi-Fi), global system for mobile communications (GSM), code-division multiple access (CDMA), and worldwide interoperability for microwave access (WiMAX) is a challenge, as each has different quality of service (QoS), security, and bandwidth characteristics. Similarly, movement between different administrative domains poses a challenge since MNs need to perform access authentication and authorization in the new domain. Thus, it is desirable to devise a mobility optimization technique that can reduce these delays and is not tightly coupled to a specific mobility protocol. In this section, we describe different types of handovers and investigate the components that contribute to a handover delay. Some inter-technology and media-independent handover frameworks are then described.

5.1 Taxonomy of handoff mechanisms

Different types of handovers may be classified based on three parameters as follows: (i) subnets, (ii) administrative domains, and (iii) access technologies (Dutta et al., 2008).

Inter-technology: this type of handover is possible with an MN that is equipped with multiple interfaces supporting different technologies. An inter-technology handover occurs when the two points of attachment use different access technologies. During the handoff, the MN may move out of the range of one network (e.g., Wi-Fi) into that of a different one (e.g., CDMA). This is also known as *vertical handover*.

Intra-technology: this type of handoff occurs when an MN moves between points of attachments supporting the same access technology, such as between two Wi-Fi access points. An intra-technology handover may happen due to intra-subnet or inter-subnet movement and thus may involve the layer 3 trigger.

Inter-domain: when the points of attachment of an MN belong to different domains, this type of handoff takes place. A domain is defined as a set of network resources managed by a single administrative entity that authenticates and authorizes access for the MNs. An

administrative entity may be a service provider or an enterprise. An inter-domain handover possibly involves an inter-subnet handover also.

Intra-domain: handovers of this type occurs when the movement of an MN is confined within an administrative domain. Intra-domain movement may also involve intra-subnet, inter-subnet, intra-technology, and/or inter-technology handovers as well.

Inter-subnet: an inter-subnet handover occurs when the two points of attachment belong to different subnets. The MN acquires a new IP address and possibly undergoes a new security procedure. A handover of this type may occur along with either an inter- or an intra-domain handover and also with either an inter- or an intra-technology handover.

Intra-subnet: an intra-subnet handover occurs when the two points of attachment belong to the same subnet. This is typically a link layer handover between two access points in a WLAN networks, or between different cell sectors in cellular networks. It is administered by the radio network and requires no additional authentication and security procedures.

5.2 Delays in handoff

All the layers in the communication protocol stack contribute to the delay in a handoff.

Link layer delay: depending on the access technology, an MN may go through several steps with each step adding its contribution to the overall delay before a new link is established. For example, a Wi-Fi link goes through the process of scanning, authentication, and association before being attached to a new access point. For intra-subnet handovers, where network layer configurations are necessary, link layer contributes the maximum to the overall delay.

Network layer delay: after completion of the link layer procedures, it may be necessary to initiate a network layer transition. A network layer transition may involve steps such as: acquiring a new IP address, detecting a duplicate address, address resolution protocol (ARP) update, and subnet-level authentication.

Application layer delay: the delay of this type is due to reestablishment and modification of the application layer properties such as IP address while using *session initiation protocol* (SIP). The authentication and authorization procedure such as *extensible authentication protocol* (EAP) includes several round-trip messages between the MN and the *authentication authorization and accounting* (AAA) server causing delay in handoff.

5.3 Research work on handoff mechanisms

This section presents some of the existing handoff mechanisms proposed in the literature.

In (Hasswa et al., 2005), a vertical handoff decision function is proposed for roaming across heterogeneous wireless networks. An optimization scheme for vertical hand off has been proposed in (Zhu & McNair, 2004). In (Park et al., 2003), a seamless vertical handoff scheme is proposed between a WLAN and a CDMA 2000-based cellular network. A vertical handoff scheme between a UMTS and a WLAN network is proposed in (Zhang et al., 2003). A *connection manager* detects the changes in wireless networks and makes the handoff decision. When the MN moves from the UMTS to the WLAN network, the objective of the handoff is to have better QoS because of the higher bandwidth of WLAN. However, in case of handoff from WLAN to UMTS, the handoff is initiated just before the connection to WLAN breaks.

In (Efthymiou et al., 1998), a protocol for *inter-segment handover* (ISHO) is proposed in an integrated space/terrestrial UMTS environment. A backward mobile-assisted handover

incorporating signalling diversity is chosen as the most appropriate handover scheme. Based on the *generic radio-access network* (GRAN) concept and by using a satellite-UMTS network architecture and functional model, the derivation of an ISHO protocol is presented. In (McNair et al., 2000), a handoff technique is introduced that supports mobility between networks with different handover protocols. Three types of handoffs are presented: (i) *network-controlled handoff* (NCHO), (ii) *mobile-assisted handoff* (MAHO), and (iii) *mobile-controlled handoff* (MCHO). Under NCHO or MAHO, the network generates a new connection, finds new resources for the handoff and performs any additional routing operations. For MCHO, the MN finds the new resources and the networks approves.

In (Stemm & Katz, 1998), a vertical handoff scheme is designed for wireless overlay networks, where heterogeneous networks in a hierarchical structure have fully overlapping service areas. The BSs send out periodic beacons similar to Mobile IP FA advertisements. The MN listens to these packets and decides which BS would forward packets, which BS should buffer packets for a handoff, and which BS should belong to the multicast group.

In (Buddhikot et al., 2003), the issues of integration of WLAN and 3G networks have been addressed to offer seamless connectivity. Two approaches have been identified: (i) a tightly-coupled approach and (ii) a loosely-coupled approach. In the tightly-coupled approach, the gateway of 802.11 network appears to the upstream 3G core as either a *packet control function* (PCF), in case of a CDMA2000 core network, or as a *serving GPRS service node* (SGSN), in case of a UMTS network. The 802.11 gateway hides the details of the 802.11 network to the 3G core, and implements all the protocols required in a 3G access network. In the loosely-coupled scheme, the same 802.11 gateway is used. However, the gateway connects to the Internet and does not have any direct link to the 3G network elements such as *packet data service nodes* (PDSNs), *gateway GPRS service nodes* (GGSNs) or 3G core network switches. In this case, the data paths in 802.11 and 3G networks are different. The high speed 802.11 traffic is never injected into the 3G network but the end user still achieves seamless access.

5.4 Cross-layer handoff mechanisms

The cross-layer protocols for mobility management are mainly applied for handoff. Most of these mechanisms use link layer information to make an efficient network layer handoff. The utilization of link layer information reduces the delay in movement detection of the MN so that the overall handoff delay is minimized.

In (Yokota et al., 2002), a low-latency handoff algorithm for a WLAN has been proposed that uses access points and a dedicated *medium access control* (MAC) bridge. A seamless handoff architecture for Mobile IP, called S-MIP is presented in (Hsieh et al., 2003) that combines a location tracking scheme with the HMIP handoff. A vertical handoff mechanism between IEEE 802.11 (WLAN) and IEEE 802.16e (Mobile WiMAX) networks in a wireless mesh backbone is proposed in (Zhang, 2008). In (Dutta et al., 2008), a media-independent pre-authentication scheme has been proposed. These four handoff schemes are discussed below.

Link Layer-Assisted Fast Handoff over WLAN: In the Mobile IP protocol, the MN movement can be detected from advertisements of the FAs that differ from the previously received advertisement. The new CoA is registered with the HA. However, data packets are not forwarded to the new FA before the registration is complete. This interruption may degrade the QoS especially in real-time applications. To tackle this issue, a handoff mechanism is proposed in which APs in a WLAN and a dedicated MAC bridge are jointly used to eliminate packet loss (Yokota et al., 2002). The authors have noted that the delay in

Mobile IP handoff is contributed by two elements: (i) the delay in movement detection of the MN, and (ii) delay due to signaling for registration. The proposed mechanism reduces the movement detection delay. It has two parts: (i) handoff for the forward direction (i.e. mobile-terminated data) and (ii) handoff for the reverse direction (i.e. mobile-originated data). The APs in the WLAN have the capability to notify the MAC address of an MN that moves into their coverage areas. The MAC bridge is configured in a way that it sends only those MAC frames whose destination addresses are registered in the filtering database (DB).

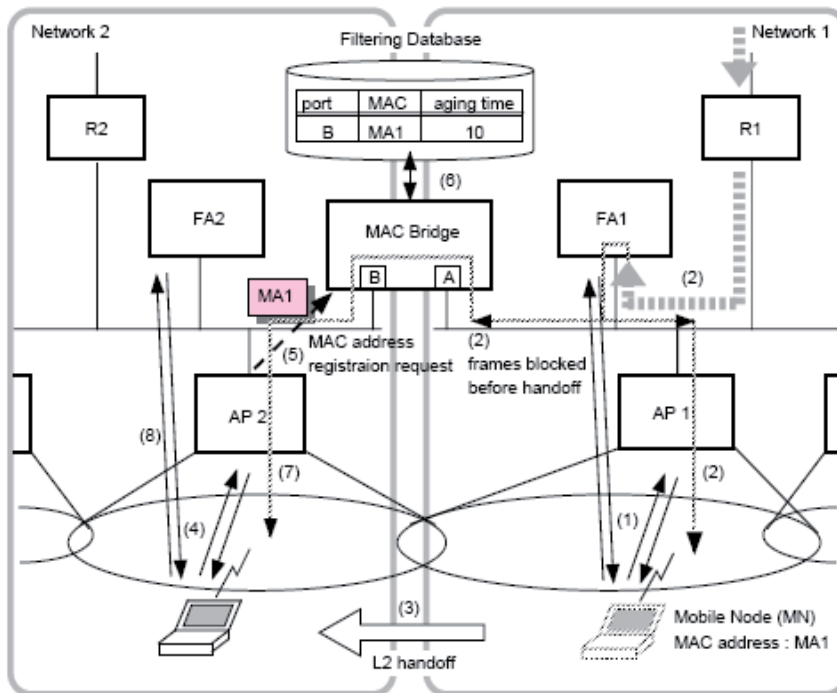


Fig. 8. Handoff Scenario in Forward Direction [Source: (Yokota et al., 2002)]

The handoff in the forward direction happens as follows. In Figure 8, the MN establishes an association with an access point- AP1, and registers the CoA with HA. The packets destined to the MN are encapsulated by the HA and tunneled to FA1- the FA of the MN. FA1 decapsulates the packets and sends them directly to the MN. When the signal strength of the channel of communication between AP1 and the MN falls below a threshold, MN attempts to find a new AP. The MN establishes association with a new AP- AP2. AP2 places the MAC address of the MN in a *MAC address registration request message* and broadcasts it on the local segment. The MAC bridge receives the address registration request. It then makes an entry of the MAC address contained in the message and the port on which the message was received into the filtering DB. When the MAC bridge receives a MAC frame on a port, it refers to the filtering DB to see if the destination MAC address is registered. If the address is registered, the MAC bridge sends it out to the corresponding port. Packets from FA1 are thus bridged from port A to the port B of the MAC bridge, and delivered to the Network 2, to which the MN is now connected. The MN detects its movement as it receives new *agent advertisements* from FA2 and registers the new CoA with the HA. When the registration is

complete, packets destined for the MN are tunneled to FA2 and delivered to the MN. Since no packets are bridged from that time onward, the entry for the MN in the filtering DB must be removed upon expiration of its aging time. Thus, the MN receives packets even before Mobile IP registration is over.

If the MAC bridge relays only those frames whose source MAC addresses are registered in the filtering DB to the network to which MN was previously attached, then it can reduce transmission interruption in the reverse direction as well. However, the transmission interruption in the reverse direction is possible if the MAC bridge has only two ports. The MAC bridge with two ports checks the source MAC address of an incoming frame from one port with the filtering DB, and transfers it to the other port. However, if the MAC bridge has more than two ports, the direction in which the frame should be transferred will depend on the speed of the MN and how fast the Mobile IP registration process completes. By taking into account that the next hop of a frame sent by the MN is always the default router of the network where the MN has been registered, the authors have proposed a fast handoff method in the reverse direction by registering the MAC address of the default router in the filtering DB. The algorithm exploits the Mobile IP agent advertisement message which are periodically broadcasted by the FAs and received by the MN. The scheme has been evaluated in an actual network environment to measure the time required for forward and reverse handoffs on UDP and TCP traffic. The latency due to Mobile IP handoff has been found to be equal to that of a link layer handoff (Yokota et al., 2002).

Seamless Handoff Architecture for Mobile IP: Seamless Handoff Architecture for Mobile IP (S-MIP) is an architecture which minimizes the handoff latency in a large indoor environment (Hsieh et al., 2003). The architecture of S-MIP is depicted in Figure 9. It is an extension of the HMIP architecture with an additional entity called *decision engine* (DE). The DE is identical to MAP in HMIP, and makes the handoff decision for its network domain. The MAP separates the mobility type into micro-mobility and macro-mobility. The *new access router* (nAR) and the *old access router* (oAR) retain the same functionality and meaning as in HMIP. Through periodic feedback information from the ARs, the DE maintains a global view of the connection state of any MN in its network domain. DE also tracks the movement patterns of all MNs in its domain using the signal strength information received from the link layer and the IDs of the ARs.

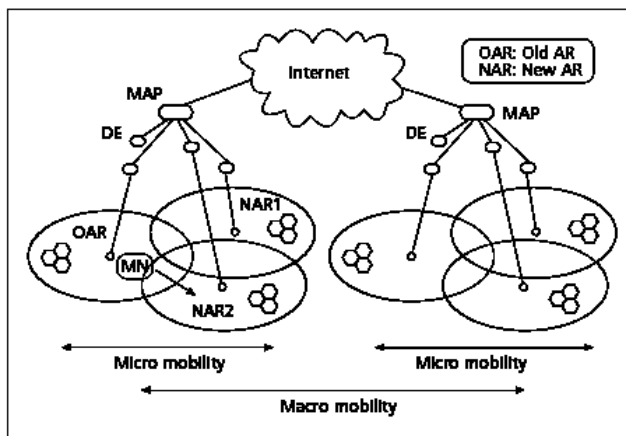


Fig. 9. Architecture of the S-MIP Scheme [Source: (Hsieh et al., 2003)]

In HMIP and fast handoff mechanisms, the packet loss occurs either within the MAP and the ARs (segment packet loss), or between the last ARs and the MN (edge packet loss). While edge packet losses occur due to the mobility of an MN and transmission errors, the segment-packet loss is due to the non-deterministic nature of handoffs and the resulting switching of the data stream at the MAP after the receipt of the MAP *binding update*. The design of S-MIP minimizes the edge packet and segment packet losses. Edge packet loss is minimized by keeping the anchor point for the forwarding mechanism as close to the MN as possible. Hence it is located at the AR that bridges the wireless network and the wired network. Segment packet loss is minimized by using a newly developed *synchronized packet simulcast* (SPS) scheme and a hybrid handoff mechanism. The SPS simulcasts packets to the current network where the MN is attached to and to the potential access network that the MN is asked to switch onto. The hybrid handoff strategy is MN-initiated, but network determined. The decision as to which access network to handoff is formulated from the movement tracking mechanism which is based on a synchronized feedback. The authors have provided a combination of simulation results and mathematical analysis to argue that S-MIP is capable of providing zero-packet loss handoff with latency similar to that of a link layer delay in a WLAN environment.

A Vertical Handoff Scheme between WLAN and Mobile WiMAX Networks: In (Zhang, 2008), a vertical handoff scheme has been proposed between 802.11(WLAN) and 802.16e (Mobile WiMAX) networks. The framework has been discussed with a *wireless mesh network* (WMN) that provides high speed, scalable and ubiquitous wireless Internet services. A *wireless mesh router* (WMR) is a gateway that has routing capabilities to support mesh networking. Each WMR is assumed to have 802.11e functions, 802.16e BS functions with *point-to-multi-point mode* (PMP), routing capabilities, and 802.16e subscriber station (SS) functions with mesh mode. The MNs can connect only via mesh routers to access the Internet using two types of links: the IEEE 802.11e and IEEE 802.16e links. The IEEE 802.16e links between MNs and mesh routers operate in the PMP mode, while the IEEE 802.16e links among neighboring mesh routers operate in the mesh mode. Figure 10 illustrates the system. The links between the WMRs are 802.16e mesh links. The WMR which is connected to the Internet with wired line is called *mesh gateway* (MGW). The MNs with dual network interfaces can connect to the Internet through the WMRs by an 802.11e link or 802.16e link. The WMRs which are connected directly or indirectly with one MGW form a domain or subnet. The MNs connect to the WMRs using 802.11e link for high data rate and small coverage area and 802.16e links for higher data rate and large coverage.

An MN initially sets up a connection with a WMR. The WMR forwards the IP packets from the MN to the MGW through one or more WMRs. The MGW transmits the IP packets to the CN in the Internet. IP packets from the CN are routed through the reverse route to the CN. The CN may be located in the same domain as the MN. In this case, the WMRs forward the IP packets for them. While an MN is inside the area doubly covered by the WLAN and WiMAX, a proper vertical handoff is needed if the WLAN network is congested or if the MN is roaming across the edge of the WLAN coverage. The author has proposed a vertical handoff scheme for this scenario. The algorithm has four steps: (i) new network interface scanning, (ii) new access router discovery, (iii) new network entry, and (iv) routing information updating. After completion of these stages, the MN can transmit or receive information data packets through the new network interface.

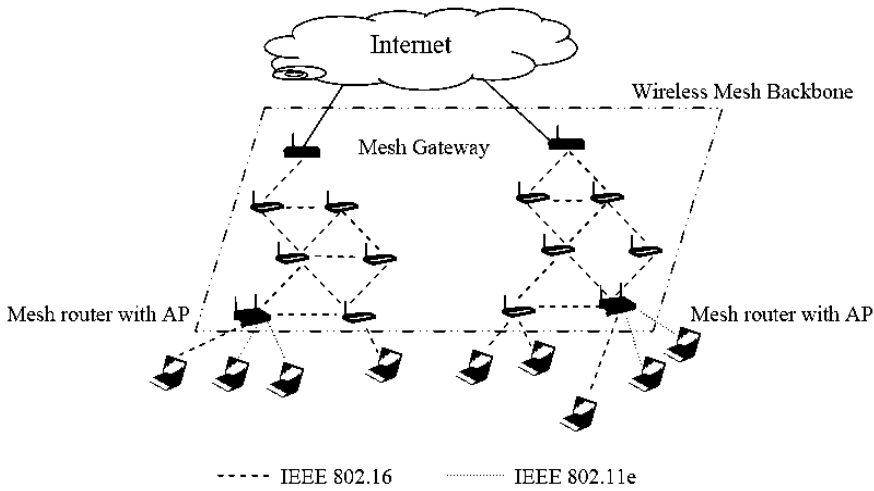


Fig. 10. Architecture of the Wireless Mesh Network [Source: (Zhang, 2008)]

In Figure 11, two domains are served by service providers A and B respectively. The WMRs in the same and different domains are called *intra-mesh routers* and *inter-mesh routers* respectively. If the CN is in the same domain as the MN, the IP packets are routed through the intra-mesh routers only. When the MN moves to another domain, the packets from the CN are routed via the HA. Four scenarios are considered for MN mobility.

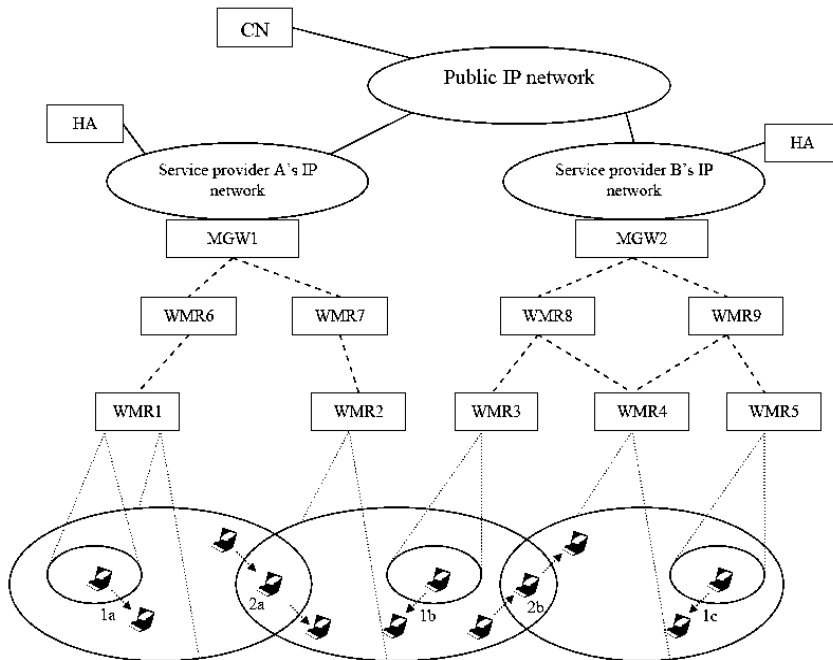


Fig. 11. Macro-Mobility and Micro-Mobility Scenario [Source: (Zhang, 2008)]

Scenario 1: the MN is connected to the WLAN. It moves out of WLAN and connects to the WiMAX. The movements 1a, 1b, 1c depict this situation. The WMR does not change, only the medium access interface changes in case of 1a. The handoff occurs between intra-mesh routers in 1c and between inter-mesh routers in case 1b.

Scenario 2: the MN is currently connected to the WiMAX. It moves into the WLAN and either connects to the WLAN or continues with the WiMAX connection depending on the network conditions, user preference, or application QoS requirements.

Scenario 3: the MN is located in the double-coverage area (i.e. area covered by WLAN and WiMAX) and is currently stationary. If the WLAN is congested, the MN can switch to the WiMAX if it can provide more bandwidth for the MN to transmit its data packets.

Scenario 4: A horizontal handoff occurs when the MN moves in 2a and 2b. In (Kim et al., 2005), a scheme called *last packet marking* (LPM) has been proposed for case 2a. The MIPSHOP (Mobility for IP: Performance, Signaling and Handoff Optimization) working group of the Internet Engineering Task Force (IETF) has developed Mobile IPv6 fast handoff over 802.16e networks for case 2b (Jang et al., 2008).

Media Independent Pre-Authentication for Secure Inter-Domain Handover: A *media-independent pre-authentication* (MPA) scheme has been proposed in (Dutta et al., 2008). It is a mobile-assisted, secure handover optimization scheme that works over any link layer and with any mobility management protocol. With MPA, an MN securely obtains an IP address and other configuration parameters for a *candidate target network* (CTN) - the network to which the mobile node is being handed off. The MN is also able to send and receive IP packets using the IP address before it attaches to the CTN. In this way, the MN completes the binding update and use the new CoA before performing a handover at the link layer.

MPA provides four basic procedures that optimize handover for an MN. The serving network is the network that currently serves the MN. The first procedure - *pre-authentication* establishes a security association with the CTN to secure subsequent protocol signaling. The second procedure - *pre-configuration* securely executes a configuration protocol to obtain an IP address and other parameters from the CTN. The third procedure executes a *tunnel management protocol* that establishes a *proactive handover tunnel* (PHT) between the MN and an access router in the CTN over which binding updates as well as data packets, can travel. Finally, the fourth procedure deletes the PHT before attaching to the CTN and reassigns the inner address of the deleted tunnel to its physical interface after the MN attaches to the target network. The final two procedures are collectively referred to as *secure proactive handover*. Through the third procedure the MN completes higher-layer handover before starting link layer handover. This means that the MN is able to perform all the higher-layer configuration and authentication procedures before link layer connectivity to the CTN is established. This can significantly reduce the handover delays.

Summary: As a macro-mobility management protocol, Mobile IP is simple, but it has several shortcomings such as triangular routing, high-global signaling load, and high handoff latency. Although, the route optimization mechanism eliminates triangular routing, the high handoff latency still remains. The micro-mobility management mechanisms are not suitable for inter-domain mobility. Most of these solutions assume one domain to be one wireless access network or under one administrative domain. Although IDMP (Misra et al., 2002) defines a domain based on geographic proximity where one domain consists of networks with different access technologies in a particular geographic region, there is no procedure specified for inter-system authentication, format transformation, and so on. In a

heterogeneous environment where users have freedom to move between different domains, the global signaling load and corresponding handoff delay will increase significantly, adversely affecting the network performance. The S-MIP approach (Hsieh et al., 2003) demonstrates that along with the hierarchical architecture and procedures for fast handoff, the link layer information used to determine the mobility pattern of the MHs can greatly improve intra-domain handoff performance. However, the protocol cannot be extended to support mobility between different domains, because the coverage area of one domain might be completely covered by another domain in the hierarchical heterogeneous environment; for example, a WLAN domain is mostly covered completely by the overlaying 2G/3G network.

6. IEEE 802.21- Media Independent Handover Services

A novel solution that ensures interoperability between several types of wireless access network is given by the developing IEEE 802.21 standard (Eastwood et al., 2008). The work on the standard began in 2004 and is expected to be finalized around 2010. The IEEE 802.21 is focused on handover facilitation between different wireless networks in heterogeneous environments. The standard names this type of vertical handover as Media Independent Handover (MIH). In MIH, the handover procedures can use the information gathered from both the mobile terminals and the network infrastructure. At the same time, several factors may determine the handover decision, e.g., service continuity, application class and QoS, negotiation of QoS, security, power management, handover policy etc. IEEE 802.21 facilitates, speeds, and thereby increases the success rate of inter-technology handover decision making and other pre-execution processes. These processes include inter-technology candidate network discovery, target network selection, target network preparation, and handover execution timing and initiation. IEEE 802.21 defines three services to facilitate inter-technology handovers: (i) *media independent information service* (MIIS), (ii) *media independent command service* (MICS), and (iii) *media independent event service* (MIES). MIIS provides information about the neighboring networks, their capabilities and available services. MICS allows effective management and control of different link interfaces on multimodal device and enables both mobile- and network-initiated handovers. It supports querying of target networks about the status of the rapidly changing resources. Some MICS commands are part of the signaling between inter-*radio access technology* (RAT) gateways. MIES provides events triggered by changes in the link characteristics and status. This interface provides service primitives to the upper layers that are independent of the access technology.

One of the most important aspects of MIH is the fact that it allows for *network controlled handovers* and *user controlled handovers*. The advantages of the network controlled handover lies in the lower user battery consumption since the monitoring of various network conditions is done by the networks themselves. However, it incurs a huge signaling overhead and a high processing load in the network elements. In user controlled handover, the user collects necessary data and initiates the appropriate actions. The disadvantage of this approach is the high battery power consumption.

6.1 Mobility using IEEE 802.21 in a heterogeneous IMT-advanced (4G) network

The telecommunication industry is defining a new generation of mobile wireless technologies, called *fourth generation* (4G). In this regard, the International Telecommunications Union- Radio Standardization Sector (ITU-R) has defined the concept of IMT-Advanced that targets peak data rates of about 100 Mb/s for highly mobile access (at speeds of up to 250 km/hr), and 1 Gb/s for low mobility (pedestrian speeds or fixed) access. The IEEE is developing extensions to both IEEE 802.11 and 802.16 to meet IMT-Advanced requirements. The evolving standard of IEEE 802.16m aims to achieve a data rate of 100 Mb/s in a highly mobile (25 km/hr) scenario. These data rate and mobility capabilities make 802.16m a candidate for the high mobility portion of the IMT-Advanced standard requirements. Another working group of IEEE 802.11n is working towards designing a *very high throughput* (VHT) radio capable of data rates up to 1 Gb/s at stationary or pedestrian speeds. Together, 802.16m and 802.11n will satisfy both the low-mobility and fully mobile user velocity vs. data rate requirements for IMT-Advanced systems. If IEEE proposes a combination of 802.11m and 802.11n for IMT-Advanced standard, an interworking mechanism must be designed for tying up these two systems. In (Eastwood et al., 2008), the authors have proposed a mobility management approach in 4G using IEEE 802.21 Media Independent Handover (MIH) services.

7. Security in Handoff Procedures

Whenever an MN connects to a point of network access, it establishes a security context with the service provider. During the handover process, some or all the network entities involved in the security mechanism may change. Thus the current security context changes as well. The MN and the network have to ensure that they still communicate with each other and they agree upon the keys to protect their communication.

However, during handovers in networks like GSM/GPRS and UMTS no authentication is used. This makes the handover procedures vulnerable to a hijacking attack. An attacker can masquerade as an authentic mobile station (MS) just by sending message at the right frequency and time slot during handover. As long as the attacker does not know the encryption and/or integrity keys currently being used, he cannot insert valid traffic into the channel. However, if an attacker can gain access to the key(s) (e.g. because of a missing protection on the backbone network), he can impersonate the MS. In fact, in GSM/GPRS, UMTS and WLAN networks, no standard protection mechanism in the backbone network has been specified. Many GSM operators do not protect the radio link between their fixed networks and the BSs. In UMTS, during a handover, the keys used to protect the traffic between the MS and the previous BS are reused in communication with the next BS. While the keys are being transmitted, they can be intercepted by an adversary, if the wireless link is not protected.

Usually an authentication process happens before location updates and call setups. The same mechanisms cannot however, be applied in establishing connection during a handover process because of the stringent time constraint. In GSM, for example, the time between the handover command and the handover complete or handover failure message is restricted to 0.5- 1.5 s. The generation of an authentication response, however, takes about 0.5 s at the MS side. Thus an authentication overhead will cause connection disruption.

As we have seen earlier in this chapter, efficient cell prediction mechanisms can reduce the signaling overhead between the MS and the old BS. The free time slots may be used to forward authentication traffic between the MS, the old BS and the new BS. The MS can pre-compute an authentication challenge and the encryption and integrity protection keys before the actual change of channel. When the MS and the new BS establish connection, the MS sends the pre-computed authentication response for the new BS to check. If the checking yields positive results, a *handover complete* message is sent and the old BS releases its resources. Otherwise, a *handover failure* happens and the MS falls back to the old channel.

8. Some Open Issues in Mobility and Handover Management

Future wireless networks will be based on all-IP framework and heterogeneous access technologies. Design of efficient mobility management mechanisms will be playing ever important role in providing seamless services. Following issues will play dominant roles.

QoS issues – next-generation all-IP wireless networks will have to provide guaranteed QoS to mobile terminals. QoS provisioning in a heterogeneous wireless and mobile networks will bring in new problems to mobility management, such as location management for efficient access and timely service delivery, QoS negotiation during inter-system handoff, etc.

User terminals – the design of a single user terminal that is able to autonomously operate in different heterogeneous access networks will be another important factor. This terminal will have to exploit various surrounding information (e.g., communication with localization systems, cross-layering with network entities etc.) in order to provide richer user services (e.g. location/situation/context-aware multimedia services). This will also put strong emphasis on the concept of cognitive radio and cognitive algorithms for terminal re-configurability.

Location and handoff management in wireless overlay networks – future wireless networks will be inherently hierarchical where access networks have different coverage areas. Mobility management in wireless overlay networks will be a very important issue.

Mobile services – sophisticated 4G service discovery mechanisms will combine the location/situation information and context-awareness in order to deliver users' services in a best possible manner. Additionally, future mobile services will require more complex personal and session mobility management to provision personalized services through different personalized operating environments to a single user terminal address. Whether SIP should be the core 4G protocol, and whether the service delivering framework be the network layer-based or application layer-based is still an open question.

Cross-Layer optimization – design of efficient cross-layer-based approaches will play a key role in developing new mobility management schemes.

Other issues – fault-tolerance, availability of network services, enhanced security, intelligent packet and call routing, intelligent gateway discovery and selection procedures and design of a unified protocol stack and vertical protocol integration mechanisms are some of the other important issues in next-generation heterogeneous networks.

9. Conclusion

In this chapter, a comprehensive discussion has been made on mobility management in next-generation wireless networks. Issues in location registration and handoff management

have been identified and several existing mechanisms have been presented. Since global roaming will be an increasing trend in future, attention has been paid on mechanisms which are applicable in heterogeneous networks. Media Independent Handover Services of IEEE 802.21 standard as an enabler for handover has also been presented. Security and authentication issues in next-generation heterogeneous networks are discussed briefly. Finally, the chapter concludes by highlighting some open areas of research in mobility management.

10. References

- Akyildiz, I.F., McNair, J., Ho, J.S.M., Uzunalioglu, H., and Wang, W. (1999). Mobility management in next-generation wireless systems, *Proceedings of the IEEE*, Vol 87, No 8, Aug 1999, pp. 1347-1384.
- Akyildiz, I.F., and Wang, W. (2002). A dynamic location management scheme for next-generation multitier PCS systems. *IEEE Transactions in Wireless Communications*, Vol 1, No 1, Jan 2002, pp. 178-89.
- Akyildiz, I.F., Altunbasak, Y., and Sivakumar, R. (2004a). AdaptNet: an adaptive protocol suite for the next-generation wireless Internet. *IEEE Communications Magazine*, Vol 42, No 3, Mar 2004, pp. 128-136.
- Akyildiz, I.F., Xie, J., and Mohanty, S. (2004b). A survey of mobility management in next-generation all-IP-based wireless systems. *IEEE Wireless Communications Magazine*, Vol 11, No 4, Aug 2004, pp. 16-28.
- Akyildiz, I.F., Mohanty, S., and Xie, J. (2005). A ubiquitous mobile communication architecture for next-generation heterogeneous wireless systems. *IEEE Communications Magazine*, Vol 43, No 6, Jun 2005, pp. 29-36.
- Buddhikot, M., Chandranmenon, G., Han, S., Lee, Y.W., Miller, S., and Salgarelli, L. (2003). Integration of 802.11 and Third-Generation Wireless Data Networks, *Proceedings of IEEE INFOCOM*, Vol 1, Mar-Apr 2003, pp. 503-512.
- Campbell, A.T., Gomez, J., Kim, S., Valko, A.G., Chieh-Yih Wan, and Turanyi, Z.R. (2000). Design, implementation, and evaluation of cellular IP. *IEEE Personal Communications*, Vol 7, No 4, Aug 2000, pp. 42-49.
- Campbell, A.T. and Gomez, J. (2001). IP micro-mobility protocols. *ACM SIGMOBILE Mobile Computing and Communications Review*, Vol 4, No 4, Oct 2001, pp. 45-54.
- Campbell, A.T., Gomez, J., Kim, S., Chieh-Yih Wan, Turanyi, Z.R., and Valko, A.G. (2002). Comparison of IP micromobility protocols. *IEEE Wireless Communications*, Vol 9, No 1, Feb 2002, pp. 72-82.
- Chiussi, F.M., Khotimsky, D.A., and Krishnan, S. (2002). Mobility management in third-generation all-IP networks. *IEEE Communications Magazine*, Vol 40, No 9, Sep 2000, pp. 124-135.
- Dutta, A., Famolari, D., Das, S., Ohba, Y., Fajardo, V., Taniuchi, K., Lopez, R., and Schulzrinne, H. (2008). Media-independent pre-authentication supporting secure interdomain handover optimization. *IEEE Wireless Communications*, Vol 15, No 2, April 2008, pp. 55-64.
- Eastwood, L., Migaldi, S., Xie, Q., and Gupta, V. (2008). Mobility using IEEE 802.21 in a heterogeneous IEEE 802.16/802.11-based IMT-advanced (4G) network. *IEEE Wireless Communications*, Vol 15, No 2, Apr 2008, pp. 26-34.

- Efthymiou, N., Hu, Y.F., Sheriff, R. (1998). Performance of intersegment handover protocols in an integrated space/terrestrial-UMTS environment. *IEEE Transactions on Vehicular Technology*, Vol 47, No 4, Nov 1998, pp. 1179-1199.
- ETSI TS 129 120 V4.0.0 (2002). Universal Mobile Telecommunications Systems (UMTS); Mobile Application Part (MAP) Specification for Gateway Location Register (GLR); Stage 3, 3GPP/ETSI 2002.
- Fogelstroem, E., Jonsson, A., and Perkins, C. (2006). Mobile IPv4 regional registration. Internet draft, IETF, draft-ietf-mip4-reg-tunnel-04.txt, October 2006.
- Garg, V.K., and Wilkes, J.E. (1996). Interworking and interoperability issues for North American PCS. *IEEE Communications Magazine*, Vol 34, No 3, Mar 1996, pp. 94-99.
- Hasswa, A., Nasser, N., and Hassanein, H. (2005). Generic vertical handoff decision function for heterogeneous wireless networks, *Proceedings of IEEE and IFIP International Conference on Wireless and Optical Communications Networks (WOCN)*, March 2005, pp. 239-243.
- Haverinen, H., and Malinen, J. (2000). Mobile IP regional paging. Internet draft, IETF, draft-haverinen-mobileip-reg-paging-00.txt, June 2000.
- Hsieh, R., Zhou, Z.G., and Seneviratne, A. (2003). S-MIP: a seamless handoff architecture for Mobile IP, *Proceedings of IEEE INFOCOM*, Vol 3, Mar-Apr, 2003, pp. 1774-1784.
- Jang, H. J., Jee, J., Han, Y.H., Park, S.D., and Cha, J. (2008). Mobile IPv6 fast handovers over IEEE 802.16e networks. IETF Internet draft work in progress, June 2008.
- Kim, K., Kim, C., and Kim, T. (2005). A seamless handover mechanism for IEEE 802.16e broadband access, *Proceedings of International Conference on Computational Science (ICCS)*, Vol 3515, May 2005, pp. 527-534.
- Lin, Y-B., and Chlamtac, I. (1996). Heterogeneous personal communications services: integration of PCs systems. *IEEE Communications Magazine*, Vol 34, No 9, September 1996, pp. 106-113.
- McNair, J., Akyildiz, I.F., and Bender, M.D. (2000). An inter-system handoff technique for the IMT-2000 system, *Proceedings of IEEE INFOCOM*, Vol 1, 2000, pp. 208-216.
- Misra, A., Das, S., Dutta, A., and McAuley, A., and Das, S.K. (2002). IDMP-based fast handoffs and paging in IP-based 4G mobile networks. *IEEE Communications Magazine*, Vol 4, No 3, March 2002, pp. 138-145.
- Mohanty, S. (2006). A new architecture for 3G and WLAN integration and inter-system handover management. *Wireless Networks*, Vol 12, No 6, November 2006, pp. 733-745.
- Pandya, R., Grillo, D., Lycksell, E., Mieybegue, P., Okinaka, H., and Yabusaki, M. IMT-2000 standards: network aspects. *IEEE Personal Communications*, Vol 4, No 4, August 1997, pp. 20-29.
- Park, H., Yoon, S., Kim, T., Park, J., Do, M., and Lee, J. (2003). Vertical handoff procedure and algorithm between IEEE 802.11 WLAN and CDMA cellular network. *Lecture Notes in Computer Science (LNCS)*, No 2524, 2003, pp. 103-112.
- Perkins, C.E., and Johnson, D.B. (2001). Route optimization in Mobile IP. Internet draft, IETF, draft-ietf-mobileip-optim-11.txt, September 2001.
- Perkins, C.E. (2008). IP mobility support for IPv4, IETF RFC 3344, draft-ietf-mip4-rfc3344bis-07, October 2008.
- Phillips J., and Namee, G.M. (1998). *Personal wireless communication with DECT and PWT*, Artech House (Boston), 1998, ISBN: 0890068720.

- Politis, C., Chew, K.A., and Tafazolli, R. (2003). Multilayer mobility management for all-IP networks: pure SIP vs. hybrid SIP/mobile IP, *Proceedings of IEEE Vehicular Technology Conference (VTC)*, April 2003, Vol 4, pp. 2500-2504.
- Ramjee, R., La Porta, T., Thuel, S., Vardhan, K., and Wang, S.Y. (1999). HAWAII: a domain-based approach for supporting mobility in wide-area wireless networks, *Proceedings of ICNP*, Oct-Nov 1999, pp. 283-292.
- Salsano, S., Polidoro, A., Mingardi, C., Niccolini, S., and Veltri, L. (2008). SIP-based mobility management in next-generation networks. *IEEE Wireless Communications*, Vol 15, No 2, April 2008, pp. 92-99.
- Stemm, M., and Katz, R.H. (1998). Vertical handoffs in wireless overlay networks. *ACM Mobile Networks and Applications*, Vol 3, No 4, 1998, pp. 335-350.
- Soliman, H., Castelluccia, C., ElMalki, K., and Bellier, L. (2008). Hierarchical Mobile IPv6 mobility management (HMIPv6). IETF draft-ietf-mipshop-4140bis-05, October 2008.
- Wang, W., and Akyildiz, I.F. (2001). A new signaling protocol for intersystem roaming in next-generation wireless systems. *IEEE Journal on Selected Areas in Communications*, Vol 19, No 10, October 2001, pp. 2040-2052.
- Yokota, H., Idoue, A., Hasegawa, T., and Kato, T. (2002). Link layer assisted Mobile IP fast handoff method over wireless LAN networks, *Proceedings of ACM MOBICOM*, 2002, pp. 131-139.
- Zhang, Q., Guo, C., Guo, Z., and Zhu, W. (2003). Efficient mobility management for vertical handoff between WWAN and WLAN. *IEEE Communications Magazine*, Vol 41, No 11, November 2003, pp. 102-108.
- Zhang, Y. (2008). *Vertical handoff between 802.11 and 802.16 wireless access networks*. Master Thesis, Department of Electrical and Computer Engineering, University of Waterloo, Ontario, Canada.
- Zhu, F., and McNair, J. (2004). Optimizations for vertical handoff decision algorithms, *Proceedings of IEEE WCNC*, Vol 1, March 2004, pp. 867-872.

GPS Total Electron Content (TEC) Prediction at Ionosphere Layer over the Equatorial Region

Norsuzila Ya'acob¹, Mardina Abdullah^{1,2} and Mahamod Ismail^{1,2}

¹*Department of Electrical, Electronic and Systems Eng, Universiti Kebangsaan Malaysia*

²*Institute of Space Science, Universiti Kebangsaan Malaysia
Malaysia*

1. Introduction

Space weather is a fairly new field in science today and has very interesting effects on humans, environment and technology in general. Scientists are now studying space weather with a wide range of tools to try to learn more about the physical and chemical processes taking place in the upper atmosphere and beyond. One of these tools is Global Positioning System (GPS). GPS is currently one of the most popular global satellite positioning systems due to global availability of signal as well as performance. GPS is a satellite-based navigation radio system which is used to verify the position and time in space and on the Earth. GPS nowadays allows to measure positions in real time with an accuracy of few centimetres (Warnant et al., 2007). The advent of GPS has led to technical revolutions in navigation as well as in fields related to surveying. The GPS system - an all-weather satellite-based radio navigation system - can provide users on a world-wide basis with navigation, positioning, and time information which is not possible with conventional navigation and surveying methods.

Apart from geodesy and geophysical interest, GPS has great importance in scientific applications. The GPS satellites that are orbiting the Earth, at altitudes of about 20,200 km, transmit signals that propagate through the ionosphere that exists at about 60 -1500 km above the Earth's surface. The signals from the GPS satellites travel through the ionosphere on their way to receivers on the Earth's surface. The free electrons populating this region of the atmosphere affect the propagation of the signals, changing their velocity and direction of travel as shown at figure 1. Due to the inhomogeneity of the propagation medium in the ionosphere, the GPS signal does not travel along a perfectly straight line (Ioannides & Strangeways, 2000). The effects of the ionosphere can cause range-rate errors for users of the GPS satellites who require high accuracy measurements (Bradford & Spilker, 1996).

Ionosphere is highly variable in space and time (sunspot cycle, seasonal, and diurnal), with geographical location (polar, aurora zones, mid-latitudes and equatorial regions), and with certain solar-related ionospheric disturbances. Ionosphere research attracts significant attention from the GPS community because ionosphere range delay on GPS signals is a major error source in GPS positioning and navigation. The ionosphere has practical importance in GPS applications because it influences the transionospheric radio wave

propagation. Observed ionospheric behaviour varies over the Earth and can be generalized into aurora, mid-latitude and equatorial regions. Ionospheric delays of 38 ~ 52 m were observed at low-latitude region during high solar activity period at an elevation cut off angle of 10° (Komjathy et al., 2002). The equatorial ionosphere differs significantly from what is typically observed at mid-latitudes. The geographic bands 10° - 15° north and south of the magnetic equator are referred to as the equatorial anomaly region, due to the occurrence of Appleton anomaly (Doherty et al., 2002).

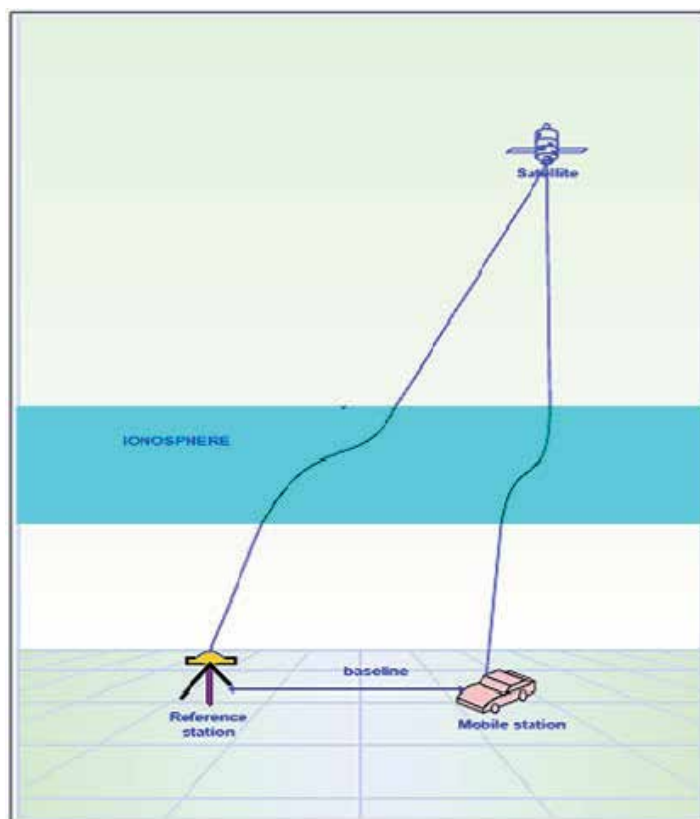


Fig. 1. Exaggerated view of GPS signal geometric paths

The parameter of ionosphere that produces most of the effects on radio signals is total electron content (TEC). By modelling TEC parameter, the evaluation of the ionospheric error and the correction of these ionospheric errors for differential GPS can be done. The ionosphere causes GPS signal delays to be proportional to TEC along the path from the GPS satellite to a receiver. TEC is defined by the integral of electron density in a 1 m^2 column along the signal transmission path. TEC is a key parameter in the mitigation of ionospheric effects on radio system. The TEC measurements obtained from dual frequency GPS receivers are one of the most important methods of investigating the Earth's ionosphere. The TEC itself is hard to accurately determine from the slant TEC because this depends on the sunspot activity, seasonal, diurnal and spatial variations and the line of sight which includes

knowledge of the elevation and azimuth of the satellite. The highest TEC in the world occurs in the equatorial region. In Malaysia there are few corresponding research done on the low latitude (equatorial) ionosphere.

Ionospheric research in the equator and tropical areas has sparked interests in several research groups. Ong and Kamarudin (2006) have conducted a research on the TEC distribution estimation with the Bent, IRI and Klobuchar modelling by using the GPS MASS station network. While Ho et al. (2002) reported on the typical hourly variations for quiet ionosphere over Malaysia for 24 hours on July 14, 2000. At Universiti Kebangsaan Malaysia (UKM) researchers have been analysing TEC since 1999. Abdullah et al. (2008) did an analysis of TEC determination over single GPS receiver station using Precise Point Positioning (PPP) technique. The ionosphere over Malaysia is unique because of its location near the equator line.

In this chapter, the focus is placed on the implementation of the method to the local area GPS reference network and the data analysis of its performance in ionospheric TEC predictions in support of GPS positioning and navigation. It investigated ionospheric TEC predictions using Dual frequency technique and TEC map using Bernese software (BGS) with PPP technique. For TEC dual frequency, it assessed the errors translated from the code-delay to the carrier-phase ionospheric observable by the so-called "Levelling Process", which was applied to reduce carrier-phase ambiguities from the data. The TEC data derived from GPS pseudorange measurements have a large uncertainty because the pseudorange has high noise level. In contrast, the noise level of carrier phase measurements is significantly lower than the pseudorange ones. To reduce the effect of pseudorange noise on TEC data, GPS pseudorange data can be smoothed by carrier phase measurements, for example, by using carrier phase smoothing technique, which is also often referred to as carrier phase levelling. Whereas, for TEC Map technique, GPS measurements from stations at the Equatorial region were used for producing maps. The Matlab and Bernese GPS software was used to derive TEC from GPS data.

This chapter describes the parameter of the ionosphere that produces most of the effects on GPS signal which is the TEC. TEC is measured to estimate the impact of ionosphere to the signal transmitted by GPS satellite to the receiver on Earth. It is a measure of the total amount of electrons along a particular Line of sight (LOS). Ionospheric delay correction is carried out through modelling the TEC along each satellite signal path due to high spatial variability of the ionosphere. Prediction of communication failures and radio interference additionally requires accurate information on TEC variations. Another technique to calculate TEC is by using Code's IGS TEC Map. It is based on spherical harmonic expansion parameterizations and computed based on the BGS Software and the output is in standard IONEX.

2. Total Electron Content (TEC) in Ionosphere

The TEC is defined as the total number of electrons integrated along the path from the receiver to each GPS. The TEC as an indicator of ionospheric variability that derived by the modified GPS signal through free electrons. TEC is measured in units of 10^{16} electrons meter per square area, where 10^{16} electrons/m² = 1 TEC unit (TECU) (Abdullah, 2009).

The nominal range is 10^{16} to 10^{19} with minima and maxima occurring at midnight and mid afternoon approximately. At night the TEC decays rather slowly due to recombination of

electrons and ions. Maximum TEC usually occurs in the early afternoon and minimum TEC usually occurs just before sunrise. Also daily TEC variations increase as one travels from north to south, as sunlight is more direct.

There are several methods to obtain the TEC over the reference station. In this work TEC was obtained from dual frequency method and the IGS (International GPS Service) TEC map.

2.1 Dual Frequency Model TEC

TEC is significant in determining scintillation and group delay of a radio wave through a medium. Ionospheric TEC is characterized by observing carrier phase delays of received radio signals transmitted from satellites located above the ionosphere, often using GPS satellites. GPS satellites transmit electromagnetic waves for positioning on two frequencies which is L1 (1575.42 MHz) and L2 (1227.60 MHz) allowing receivers equipped with dual frequency operation to be used. This enables us to extract the ionosphere TEC along the line of sight, from satellite to receiver.

In this work, the TEC is observed at the F layer because this region has the highest variability of free electrons, causing the greatest effect on GPS received signal compared to other layers. More than two-third of electron concentration are located at F2 layer. This method is conducted by going through several processes. Figure 2 shows the flow chart of work progress to achieve the objective of the project.

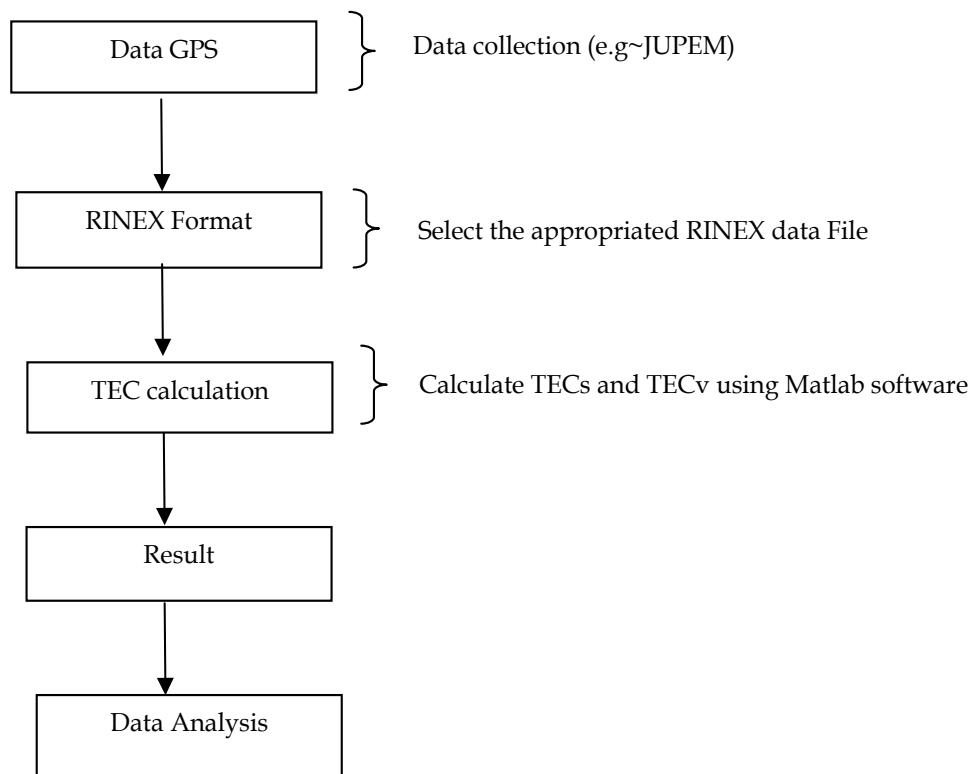


Fig. 2. Flow chart of TEC processing

The process of extracting data from RINEX (Receiver Independent Exchange) file was done by using Matlab programming language whereby the RINEX file was obtained from the GPS receiver as shown in figure 3. The program will analyse and extract the information needed in calculating the TEC from the observation and navigation RINEX file. The result will show the graph of elevation angle, different phase, different delay, slant TEC (TECs) and vertical TEC (TECv) versus time. This data of TECv were used since its value is not depending on the location of satellite receiver compared to TECs.

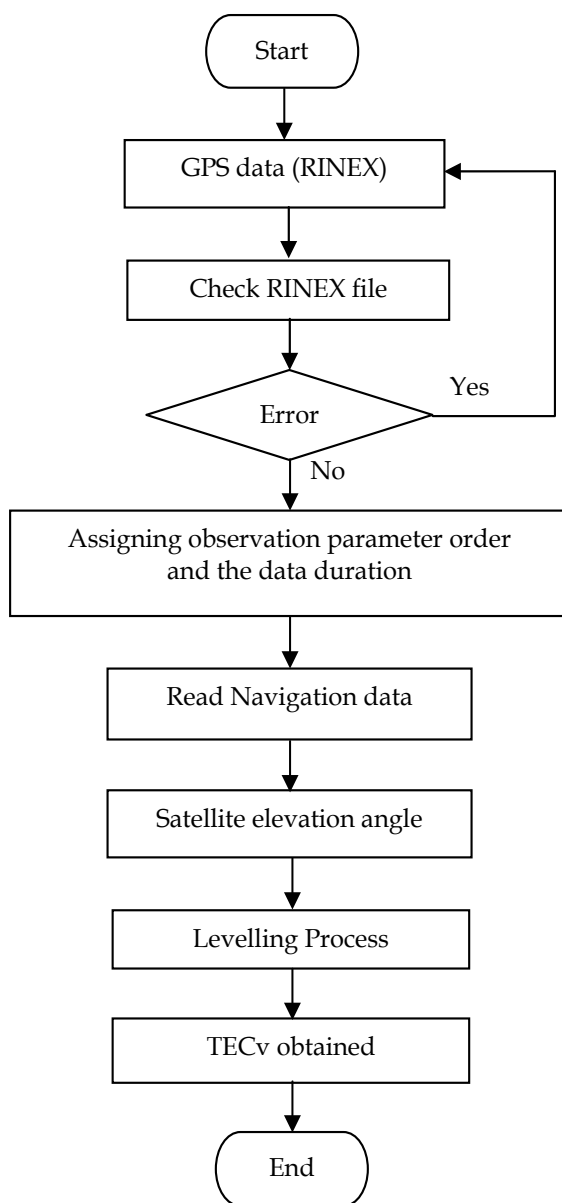


Fig. 3. Flowchart of TEC processing

2.1.1 Determination of TEC

Dual-frequency carrier phase and code-delay GPS observations are combined to obtain ionospheric observables related to the (TECs) along the satellite-receiver line of sight (LOS). Pseudorange is applicable to P(Y)-codes and C/A-codes. The pseudorange equation in units of length can be expressed as:

$$P_r^S = c(t_r - t^S) = c\tau_r^S = \rho_r^S + c(\delta t_r - \delta t^S) + I + T + mpp + \varepsilon \quad (1)$$

Where P_r^S is pseudorange measured at receiver; c is speed of light in vacuum, t^S is transmission time of signal measured by time frame of satellite, t_r is reception time of signal measured by the clock of receivers r ; τ_r^S is signal travelling time, ρ_r^S is LOS range from satellite antenna and receiver antenna, δt_r , δt^S is satellite and receiver clock error due to the difference in system time; I is ionospheric induced error; T is tropospheric induced error, mpL is multipath error and ε is noise or random error.

Carrier phase is the measurement of the phase difference between the carrier signal generated by the receiver's internal oscillator and the carrier signal transmitted from a satellite. The basic equation for the carrier phase measurement is:

$$L_r^S = \rho_r^S + c(\delta t_r - \delta t^S) - I + T + \lambda N_r^S + mpL + \varepsilon \quad (2)$$

Where L_r^S is phase measurement in units of length, N_r^S is integer ambiguity between the satellite and receiver, mpL is multipath error.

The true range or geometric range can be represented by:

$$\rho_r^S = \sqrt{(X^S - x_r)^2 + (Y^S - y_r)^2 + (Z^S - z_r)^2} \quad (3)$$

Where X , Y and Z are the satellite coordinates, x , y and z are the receiver coordinates. Dual band GPS receivers were considered in the measurable linear combination (LC). Dual frequency observations can be used to measure the ionosphere delay. This delay can then be removed from the measurements by combining the frequencies, L_1 and L_2 . Ionosphere delay can then be removed from the measurements by combining the frequencies and providing the Linear Combination (LC) solution. All observables have the dimension of length, terms due to noise and multipath are not explicitly shown, and higher-order ionospheric terms are ignored:

$$L_1 = \rho - I_1 + \lambda_1 N_1$$

$$L_2 = \rho - \left(f_1^2 / f_2^2\right) I_1 + \lambda_2 N_2$$

$$P_1 = \rho + I_1$$

$$P_2 = \rho + \left(f_1^2 / f_2^2 \right) I_1 \quad (4)$$

Where ρ is non dispersive delay, contains LOS, clocks and troposphere bias, I_1 is dispersive delay of first frequency and N_1, N_2 is integer ambiguities on L1 and L2.

The integrated TEC from the receiver to the satellite is proportional to the accumulated effect by the time the signal arrives at the receiver. This affects the GPS range observables: a delay is added to the code measurements and advance to the phase measurements. To achieve very precise positions from GPS, this ionospheric delay or advance must be taken into account. A GPS operates on two different frequencies f_1 and f_2 , which are derived from the fundamental frequency of = 10.23 MHz:

$$\begin{aligned} f_1 &= 154.f_0 = 1575.42 \text{ MHz and} \\ f_2 &= 120.f_0 = 1227.60 \text{ MHz} \end{aligned} \quad (5)$$

A dual-frequency GPS receiver can measure the difference in ionospheric delays between the L1 and L2 of the GPS frequencies, which are generally assumed to travel along the same path through the ionosphere. Thus, the group delay can be obtained as:

$$P_1 - P_2 = 40.3TEC \left(\frac{1}{f_2^2} - \frac{1}{f_1^2} \right) \quad (6)$$

Where P_1 and P_2 are the group path lengths corresponding to the high GPS frequency ($f_1=1575.42$ MHz) and the low GPS frequency ($f_2=1227.6$ MHz), respectively.

The TEC can also be obtained by writing Eq. (6) as

$$TEC = \frac{1}{40.3} \left(\frac{f_1 f_2}{f_1 - f_2} \right) (P_2 - P_1) \quad (7)$$

if dual frequency receiver measurements are available;

where (P_1 and P_2) are the pseudoranges measured in L1 and L2, respectively.

TEC can be divided into two parts. There are:

- (a) Slant TEC (TECs)
- (b) Vertical TEC (TECv)

Slant TEC is a measure of the total electron content of the ionosphere along the ray path from the satellite to the receiver, represented in figure 4. Although TECs is measured at differing elevation angles, usually the TECv is modelled. TECv enables TEC to be mapped across the surface of the Earth.

TEC measurements are taken from different GPS satellite observed at arbitrary elevation angles. This causes the GPS signals to cross largely different portion of the ionosphere. To compare the electron contents for paths with different elevation angles, the TECs must be transformed into equivalent vertical content or TECv by dividing it by the secant of the

elevation angle at a mean ionospheric height, which usually taken to be between 350 and 450 km. Generally by referring to figure 4, the slant TEC, TECs through a given sub-ionospheric point is obtained from Eq. (8).

2.1.2 Mapping Function

Precision monitoring of ionosphere will have profound implications in almost all areas of GPS user communities. The ionospheric mapping function is one of the first assumptions to consider typically when ionospheric corrections are estimated or applied from Global Navigation Satellite System (GNSS) data. The typical assumption in many GNSS imaging and navigation systems is to consider a fixed mapping function constant, and associated to a 2D distribution of electron content at a given effective height (typically some value between 300 and 500 km).

The line-of-sight TEC values were converted to TECv values using a simple mapping function and were associated to an ionospheric pierce point (IPP) latitude and longitude, assuming the ionosphere to be compressed into a thin shell at the peak ionospheric height of 350 km as illustrated in figure 4. The thin shell model was used and its height is the effective height which is taken as the ionospheric pierce point altitude. Generally, the ionosphere can be divided into several layers in altitude according to electron density, which reaches its peak value at about 350 km in altitude.

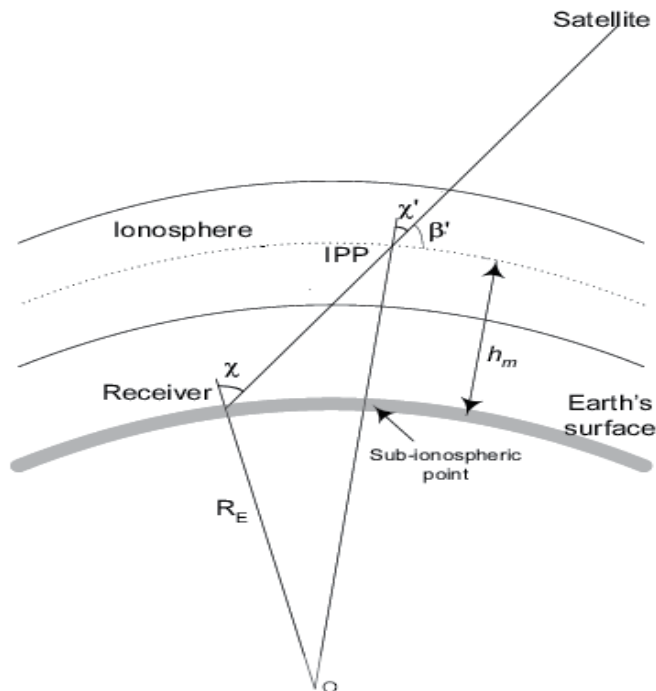


Fig. 4. Ionospheric Single Model (SLM)

Source: Schaer 1996

The thin layer model currently used in GPS has deficiencies resulting from conversion of slant TEC to effective vertical TEC. The deficiencies come from in appropriate attribution of the thin shell height. This conversion introduces a few errors in the middle latitude where electron density is small. But it many result in obvious error at low latitude with large electron density and great gradient (Horvath, 2000). Usually, the ionospheric delay resulting from observation noises, less than 1 TECU, is omitted. It is assumed that, in the two-dimensional spherical shell model, the majority of electron density is concentrated in a thin layer with a height of 350-450 km above the surface of the Earth. Generally by referring to figure 4, TECs through a given sub-ionospheric point is obtained from Eq. (8)

$$TEC_V = TEC_S (\cos \chi')$$
(8)

Where TECs is the value of slant TEC, χ' is the difference between 90° and zenith angle (90°- χ). In some literature this is called the elevation-dependent single layer (or thin shell) model mapping function, SLM where can be written as

$$F(\chi) = \frac{TEC(\chi)}{TEC(0)} = \frac{1}{\cos \chi' \text{ (or } \sin \beta')} = \frac{1}{\sqrt{1 - \sin^2 \chi'}}$$
(9)

$$\sin \chi' = \frac{R_e}{R_e + h_m} \sin \chi$$
(10)

Where R_e is the mean earth radius, h_m is the height of maximum electron density, and χ and χ' are the zenith angles at the receiver site and at the IPP (or β' is the elevation angle at IPP), respectively. χ can be calculated from a known satellite position and the approximate coordinates of the receiver location. For h_m , in general the value is taken as the height corresponding to the maximum electron density at the F2 peak. The peak altitude ranges from 250 to 350 km at mid-latitudes and from 350 to 500 km at equatorial latitudes. Typical value for R_e and h_m are set to 6371 and 450 km, respectively. The more precise mapping function according to Schaer et al. (1996) and currently applied in the IGS Global TEC map is the modified single layer model, M-SLM. This is defined as;

$$\sin \chi' = \frac{R_e}{R_e + h_m} \sin(\alpha \chi)$$
(11)

where α is correction factor which is close to unity. The value is chosen to be 0.9782 when using R_e and h_m as 6371 and 506.7 km, respectively and assuming a maximum zenith angle of 80°.

$F(\chi)$ is also known as the slant or obliquity factor in the Klobuchar model and varies from 1 to slightly above 3 at $h_m = 350$ km. For low elevation angles slant TEC can reach until 3 times the value of TEC at zenith. However the oblique-to-zenithal thin shell conversion including the determination of h_m is still being developed further. It has also been suggested that h_m should be taken to be between 600 and 1200 km which is greater than the commonly adopted value. If this is correct, assuming a lower value could produce an error of 15 to 30% or more in TEC.

2.1.3 Carrier phase levelling process

GPS signals can be used to extract ionospheric parameters such as TEC. For single frequency GPS users, models of the ionosphere such as the Klobuchar model (Klobuchar, 1987), which is also known as the GPS broadcast model, have been constructed utilizing ionospheric parameters given in the GPS broadcast message. It is represented by a third degree polynomial where the coefficients of the polynomial are transmitted as part of the broadcast message header. The TEC can also be obtained as in Eq. (7), if dual frequency receiver measurements are available. As the TEC between the satellite and the user depends on the satellite elevation angle, this measurement is called TECs. The TEC varies with times and over the space, and it depends on the solar activity, user location and the PRN elevation angle.

In practice, calculation of TEC by the above means, using pseudorange data only, can produce a noisy result. It is desirable to also use the relative phase delay between the two carrier frequencies in order to obtain a more precise result. Differential carrier phase gives a precise measure of relative TEC variations but because the actual number of cycles of phase is not known, absolute TEC cannot be found unless pseudorange is also used. Pseudorange gives the absolute scale for TEC while differential phase increases measurement precision. The TEC data derived from GPS pseudorange measurements have a large uncertainty because the pseudorange has high noise level. In contrast, the noise level of carrier phase measurements is significantly lower than the pseudorange ones. To reduce the effect of pseudorange noise on TEC data, GPS pseudorange data can be smoothed by carrier phase measurements. For example is by using carrier phase smoothing technique, which is also often referred to as carrier phase levelling. Carrier phase levelling or phase smoothing is essentially some combination of the noisy code pseudorange with the comparatively smooth varying carrier phase. The carrier phase contains much smaller measurement error than pseudoranges, so that ionospheric TECs can be obtained by carrier phase smoothing the pseudoranges (Hansen et al., 2000). This was done as shown below:

Firstly, the phase observations, measured in cycles, are scaled to units of length by multiplying with the wavelength. Because the phase measurements are ambiguous, so the phase derived slant delay, obtained from geometry free linear combination, L_4 calculated from Eq. (12) was scaled to zero relative range error at the first epoch. This eliminates the integer ambiguity provided there are no cycle slips.

$$L_4 = L_1 - L_2 = \left(1 - f_1^2 / f_2^2\right) I_1 + \left(\lambda_1 N_1 - \lambda_2 N_2\right) \quad (12)$$

To eliminate the code multipath effect that is normally seen at both ends of the path or at low elevation angles, the code differential delay was fitted at the higher elevation angles.

This was done by defining a shift value and was added to the relative phase to fit the code differential delay. This results in the absolute differential delay and the remaining noise was discarded.

Figure 5 shows the differential delays determined using the above procedure. This smoothed differential delay (with less noise and multipath) was then translated to the absolute TECs by multiplying with a constant (see Eq. (7)). A mapping function, SLM is used together with Eq. (8) to convert TEC to the vertical from the slant value. For a good description on the determination of absolute TEC from dual frequency GPS measurements refer to Parkinson and Spilker (1996).

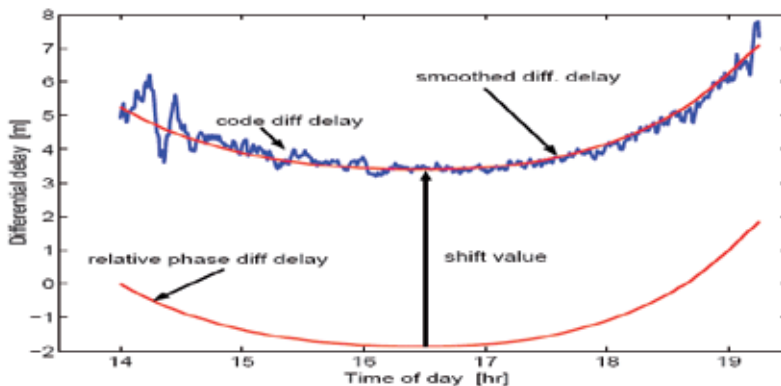


Fig. 5. Phase smoothed code differential delay

2.2 TEC Map

Bernese GPS Software (BGS) was used to map the ionosphere in this work. BGS is commonly used by scientists for research and education, survey agencies responsible for high-accuracy GNSS surveys, agencies responsible for maintaining arrays of permanent GPS receiver and also commercial users with complex applications demanding high accuracy, reliability and high productivity (Dach, 2007). TEC map has gained much attention in the recent years because of the ionospheric effects to the GPS-based navigation application. A range delay caused by the ionosphere during quiet and disturbed geomagnetic days can be approximated using the measurements of TEC map.

TEC ionospheric values and maps can be delivered by the International GPS Service (IGS). IGS has developed the global ionospheric gridded data representing the TEC over the whole globe. Analysis centres deliver their results of TECv and DCBs in the IONosphere Exchange (IONEX) format (Schaer et al., 1998).

In this new version of BGS, PPP was processed using BPE. BPE consists of data, user scripts and four process control file (PCF) where one of the PCF is PPP. PCF in PPP mode has been selected to run PPP. In this PPP.PCF, regional ionosphere model is generated and stored in Bernese ionosphere file and in IONEX file using GPS Estimation (GPSEST) program. GPSEST is the program that able to generate TEC maps in IONEX (Schaer et al., 1998). GPSEST program is used to model and estimate the ionosphere. In GPSEST program, geometry-free linear combination from the zero-difference code observations was used because it principally contains ionospheric information. Geometry-free linear combination of this un-differenced GPS observations is then applied in GPSEST to generate TEC map.

A MSLM was used for mapping the TEC, approximated by a spherical layer with infinitesimal thickness assuming that all free electrons are concentrated in altitude, H , above the spherical Earth. The altitude H of this idealized layer is set to 350 km. Based on this model, TEC values were calculated in geographic reference system which was able to produce the epoch-specific instantaneous regional maps of the ionosphere. Using MSLM noted above, a vertical TEC can be obtained at IPP. It can be shown that a single GPS receiver can probe the ionosphere in a radius of 960 km assuming 10° elevation cut-off angle and 450 km height.

This proved that PPP technique can be used to determine TEC over single station in Malaysia. With the new BGS version 5.0; PPP technique is now available to produce ionosphere maps. PPP is known as a valuable tool to provide an accurate position anywhere on Earth, also for investigating many geophysical processes at the millimetre level.

3. Analysis of TEC

The ionosphere GPS-TEC measurements were carried out using GPS receiver networks from Department of Survey and Mapping, JUPEM. GPS data on 8 November 2005 were analyzed for this initial analysis. The stations were at Wisma Tanah, Kuala Lumpur, ($3^\circ 10' 15.44''\text{N}$; $101^\circ 43' 03.35''\text{E}$) KTPK station and Universiti Teknologi Malaysia, Johor ($1^\circ 33' 56.934''\text{N}$, $103^\circ 38' 22.429''\text{E}$), UTMJ station as shown in figure 6. This analysis was based on one hour observations from 5:00 - 6:00 UT (13-14 PM (LT)) using GPS satellite PRN 23 for KTPK station and also using GPS satellite PRN 23 for UTMJ station. The GPS data was recorded in universal time (UT) system. The sampling time interval is 15 second and the cut-off elevation mask is 15° . GPS data used in this project were recorded on a quiet geomagnetic day where the geomagnetic index K_p is 1.



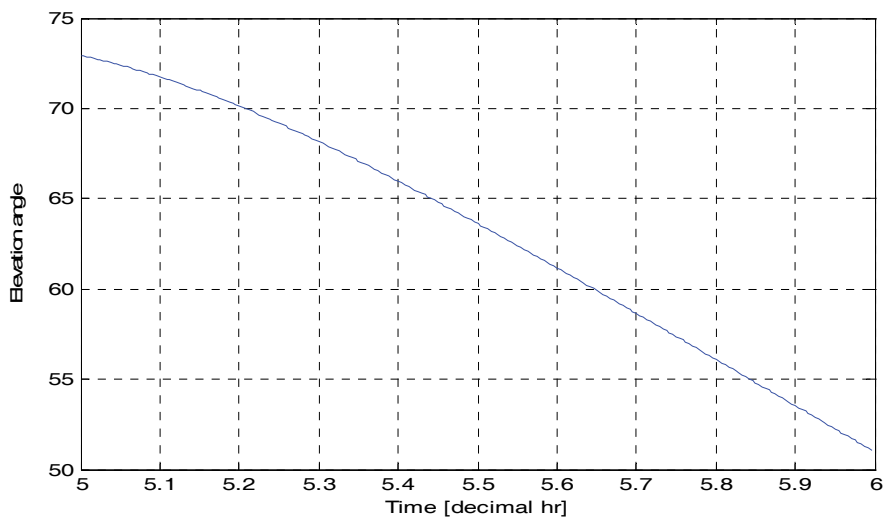
Fig. 6. MASS stations in Malaysia

Source: JUPEM 2009

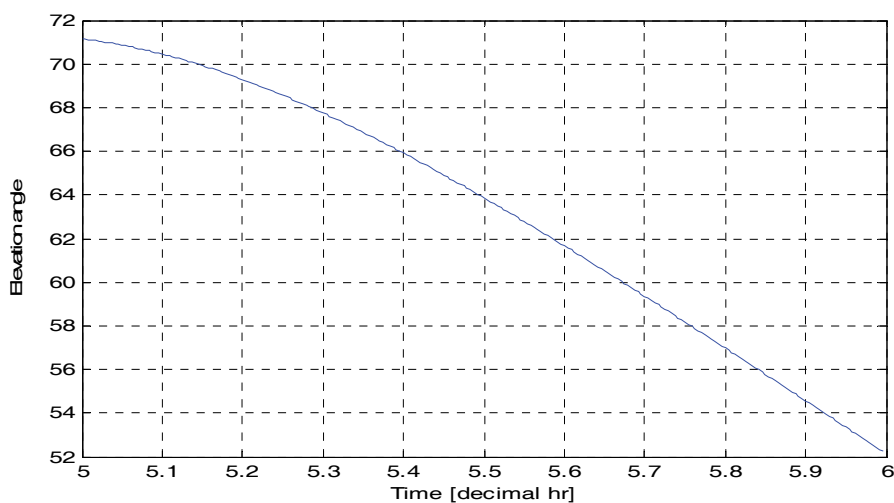
3.1 TEC Dual- frequency using levelling process

Figure 7 to 11 show representative cases of the different situations found in the analysis. The absolute slant TEC from the KTPK station and UTMJ station can be measured directly from this dual frequency method. This can be calculated by using pseudorange and carrier phase measurements from the satellites (e.g. PRN 23) used in this study. Figure 7 (a and b) shows

the elevation angle of GPS satellite PRN 23 at 5:00 – 6:00 (UT) for KTPK Station and 5:00 – 6:00 (UT) for UTMJ station. The elevation angle can be calculated from the GPS navigation data (or ephemeris). The elevation angle for KTPK and UTMJ station can be illustrated as below:



(a)



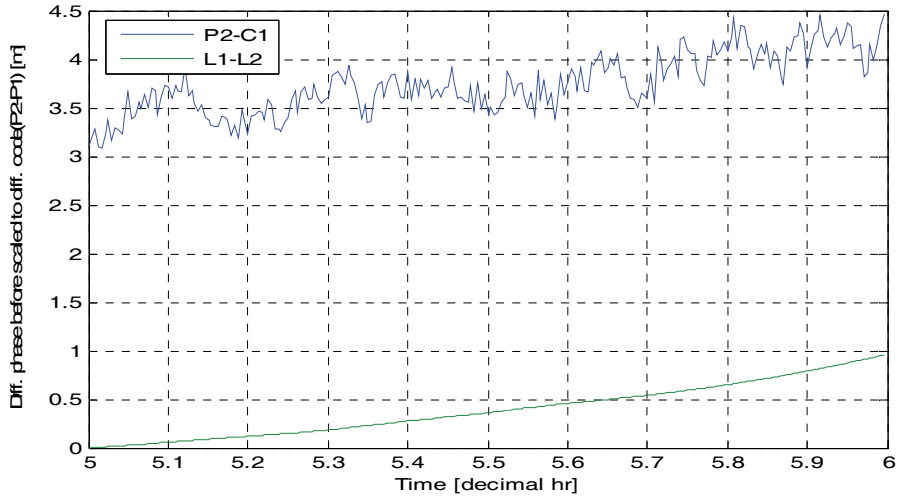
(b)

Fig. 7. (a) Elevation angle of GPS Satellite PRN 23, 5:00-6:00 (UT) (KTPK station)

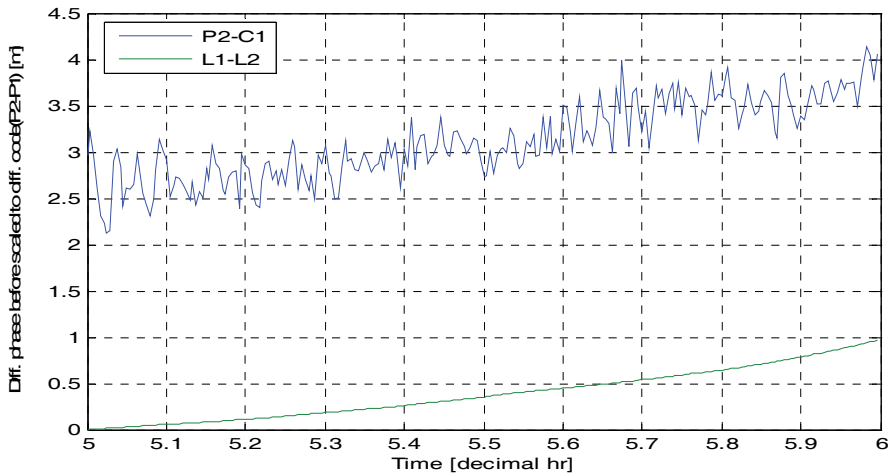
(b) Elevation angle of GPS Satellite PRN 23, 5:00-6:00 (UT) (UTMJ station)

Figure 8 (a and b) clearly indicate the code TEC and phase TEC of PRN 23 for elevation from 74° to 51° and 71° to 52°. The differential delay ($=P2-C1$) from code measurements is noisy

and influenced by multipath while the phase measurements, are ambiguous and less effected by the multipath, were used to smooth the code differential delay. Then the vertical TEC can be obtained. This eliminates the integer ambiguity provided there are no cycle slips.

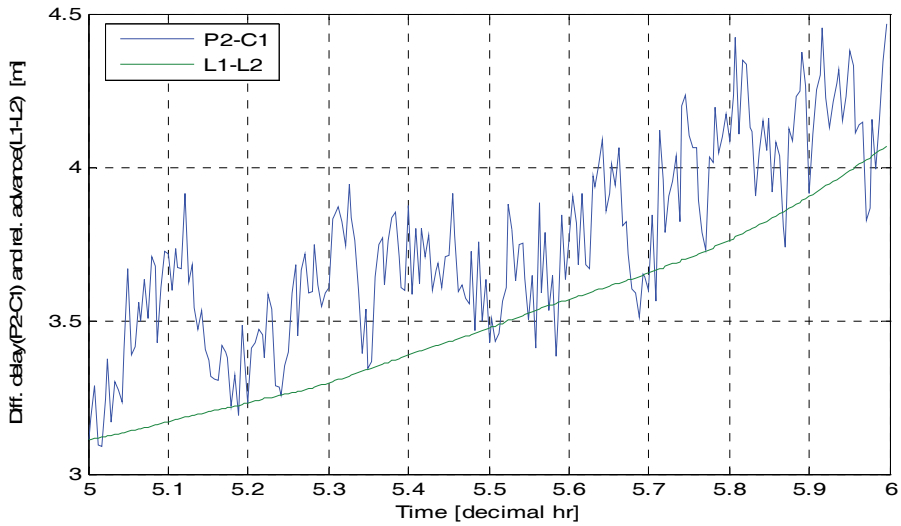


(a)

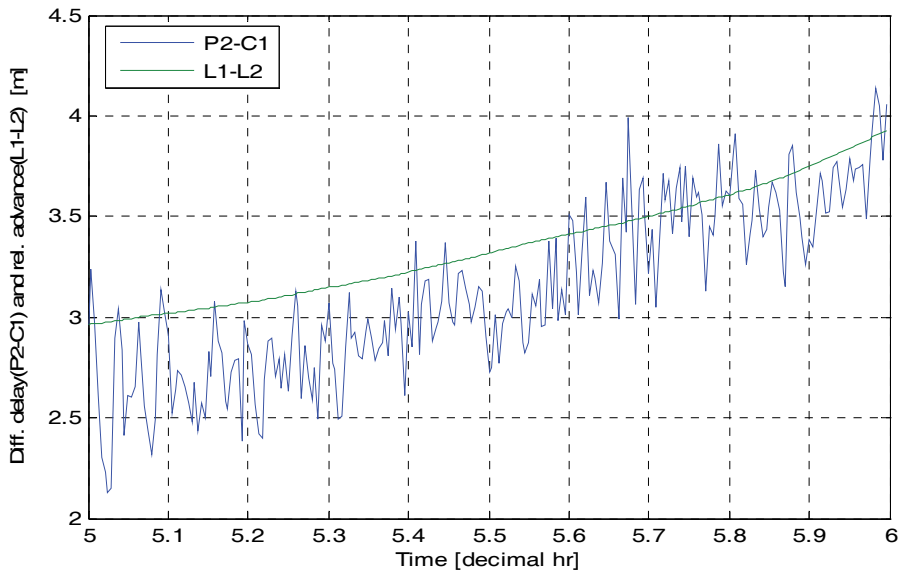


(b)

Fig. 8. (a) Different phase (L1-L2) before scale to different code (P2-C1) for GPS Satellite PRN 23, 5:00-6:00 (UT) (KTPK station)
 (b) Different phase (L1-L2) before scale to different code (P2-C1) for GPS Satellite PRN 23, 5:00-6:00 (UT) (UTMJ station)



(a)



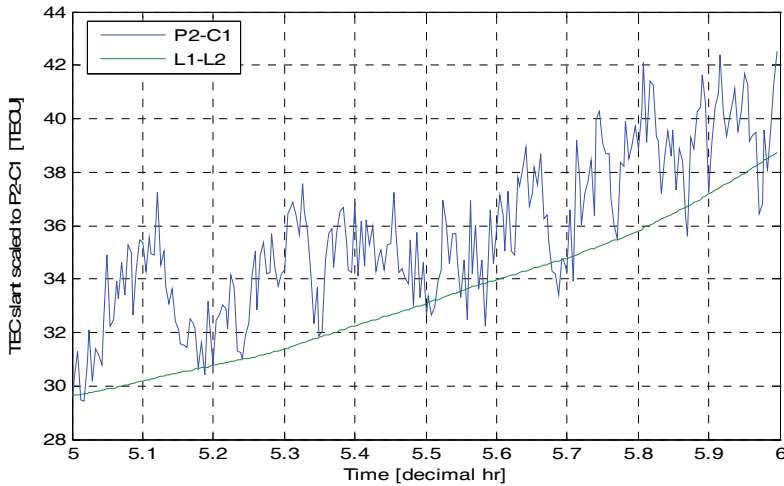
(b)

Fig. 9. (a) Relative range error computed from the differential carrier phase advance for GPS Satellite PRN 23, 5:00-6:00 UT (KTPK station)

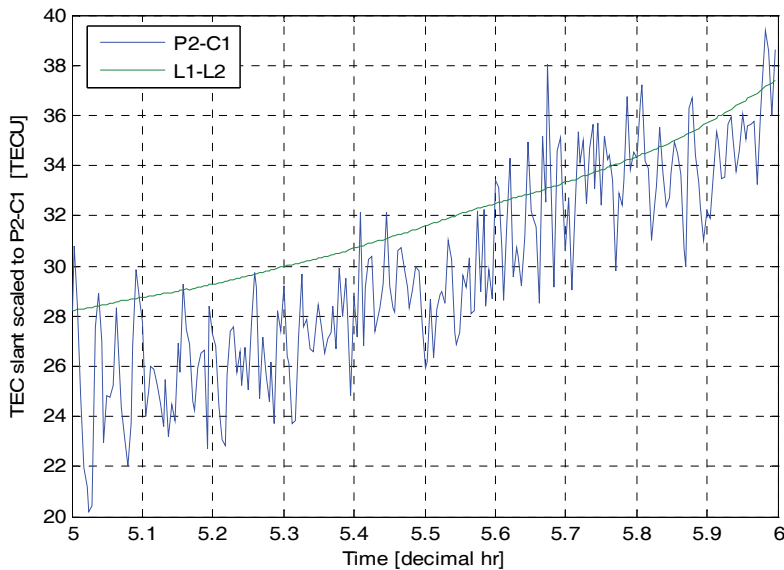
(b) Relative range error computed from the differential carrier phase advance for GPS Satellite PRN 23, 5:00-6:00 UT (UTMJ station)

Shown in figure 9 (a and b) are the absolute ionospheric range error obtained from differential group delay. At this stage, levelling process was applied to eliminate the code multipath effect especially at low elevation angles. This was done by defining a shift value

and adding it to the relative phase to fit the code differential delay. For the levelling process, it assumed the average at the elevation angle ($\pm 60^{\circ}$ - 90°) as reference and it can be seen in figure 7. This value was chosen because there is no multipath at the high elevation angle and during low elevation angle multipath where it can still be seen. After the differential carrier phase was converted to an absolute scale by fitting it to the differential group delay curve over the desirable, low multipath portion of each pass, the differential group delay data were simply discarded.



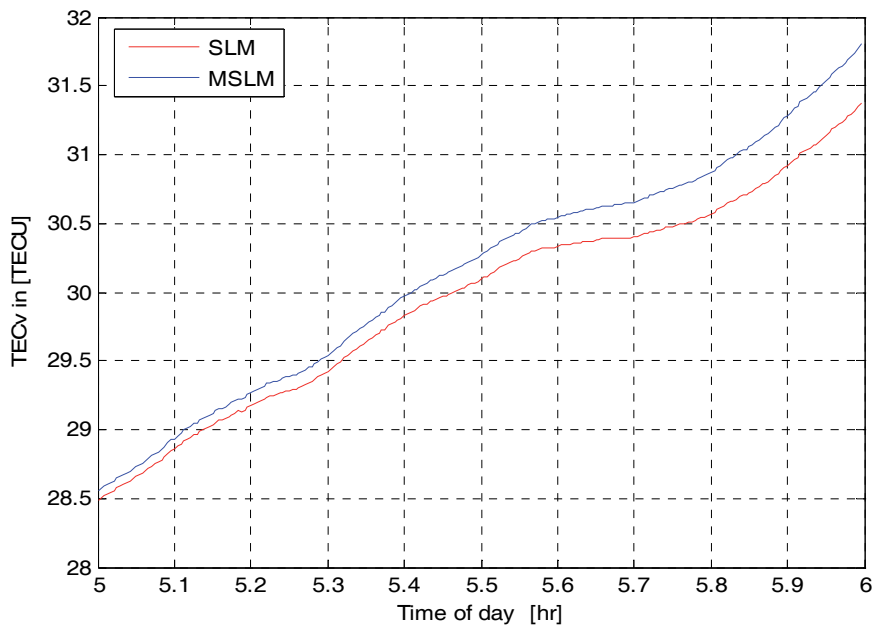
(a)



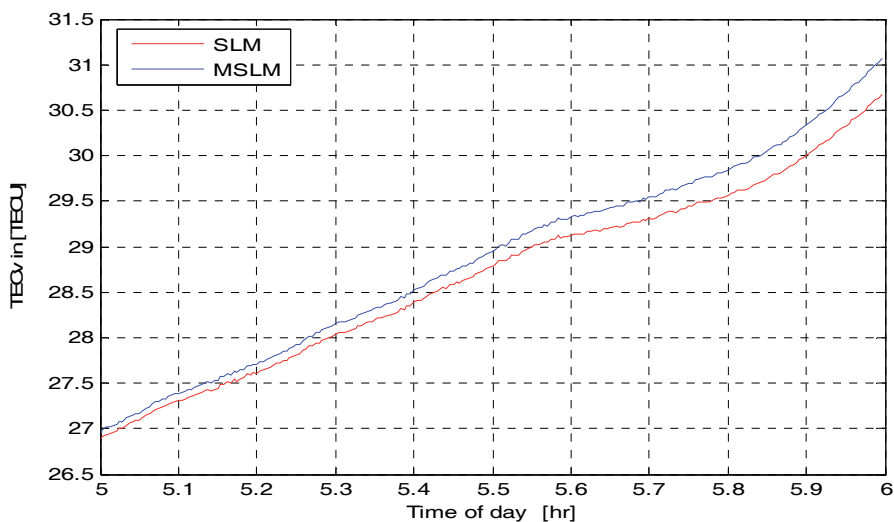
(b)

Fig. 10. (a) TEC slant scale to (P2- C1) TECU for PRN 23, 5:00-6:00 UT (KTPK station)
 (b) TEC slant scale to (P2- C1) TECU for PRN 23, 5:00-6:00 UT (UTMJ station)

This smoothed differential delay (with less noise and multipath) was then translated to the absolute slant TEC by multiplying it by a constant Eq. (7) as shown in figure 10 while figure 11 shows TEC vertical for GPS satellite PRN 23 for KTPK and PRN 23 for UTMJ station.



(a)



(b)

Fig. 11. (a) TEC SLM, TEC M-SLM, GPS Satellite PRN 23, 5:00-6:00 UT (KTKP station)
(b) TEC SLM, TEC M-SLM, GPS Satellite PRN 23, 5:00-6:00 UT (UTMJ station)

Figure 11 shows that SLM was used to convert the slant TEC to vertical TEC. The analysis at an equatorial region used SLM mapping function. The peak altitude ranges from 350 to 500 km at equatorial latitudes. However, from the figure it also shows that the MSLM which is TEC for SLM is small compared to MSLM. The vertical TEC values are precise, accurate and without multipath, unless the multipath environment is really terrible, in which case a small, residual amount of multipath can even be seen in the differential carrier phase.

3.2 TEC Map

TEC Map is computed with the BGS software using the PPP program and the output is in standard IONEX format. A MSLM was used for mapping the TEC, approximated by a spherical layer with infinitesimal thickness assuming that all free electrons are concentrated in altitude, H , above the spherical Earth. The altitude H of this idealized layer is set to 450 km. Based on this model, TEC values were calculated in geographic reference system which was able to produce the epoch-specific instantaneous regional maps of the ionosphere.

Using MSLM noted above, a vertical TEC can be obtained at IPP. It can be shown that a single GPS receiver can probe the ionosphere in a radius of 960 km assuming 10° elevation cut-off angle and 450 km height. In order to suit the geographic location to all observational epochs, region located between 0° to 7° north of geographic latitude and 90° to 110° longitude was selected. This map covers a 24 hour time period at intervals of 2 hours starting from 00.00.00 hour.

Figure 12 illustrates the longitudinal vertical TEC map for KTPK station on 8 November 2005 produced with PPP technique with two-hour intervals between each map, starting from 00:00 to 22:00 UT where local time (LT) is +8. Based on figure 12, TEC starts increasing at 00:00 UT at about 7 TECU and gradually increased reaching a maximum level of 28 TECU at 06:00 UT (14:00 LT) then decreased steadily until nearly 20:00 UT before sunrise and rate of ion production is low. It showed that the maximum value of TECU usually happens near midday while the minimum value of TECU occurs at night. The low TEC over equatorial region is mostly due to the Kp and Dst index.

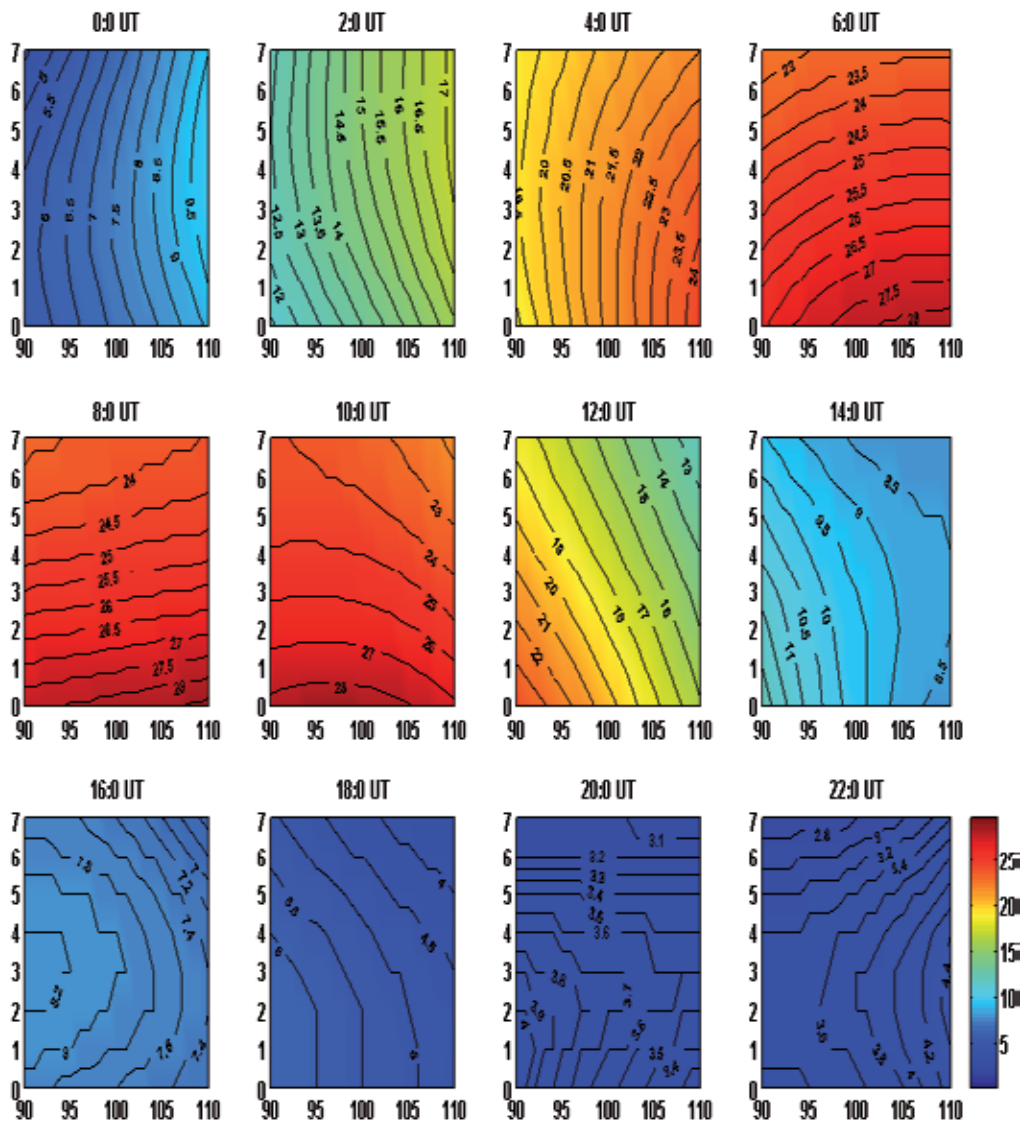


Fig. 12. TEC Map for KTPK station, 8 November 2005

A comparison was made with Global Ionosphere Maps (GIM) downloaded from Centre for Orbit Determination in Europe (CODE) as shown in figure 13. GIM from CODE was generated using data from about 150 GPS receivers around the globe. GIM used 5.0° and 2.5° in longitude and latitude of special resolution with two-hour intervals. For the comparison purpose, an area covering regional model was extracted from IGS maps. Both figures show the same pattern of longitudinal variation of TEC starting from 00:00 UT to 22:00 UT. It is noticeable however, that TEC from GIM is higher by about 0 to 5 TECU, as compared with the maps generated by PPP.

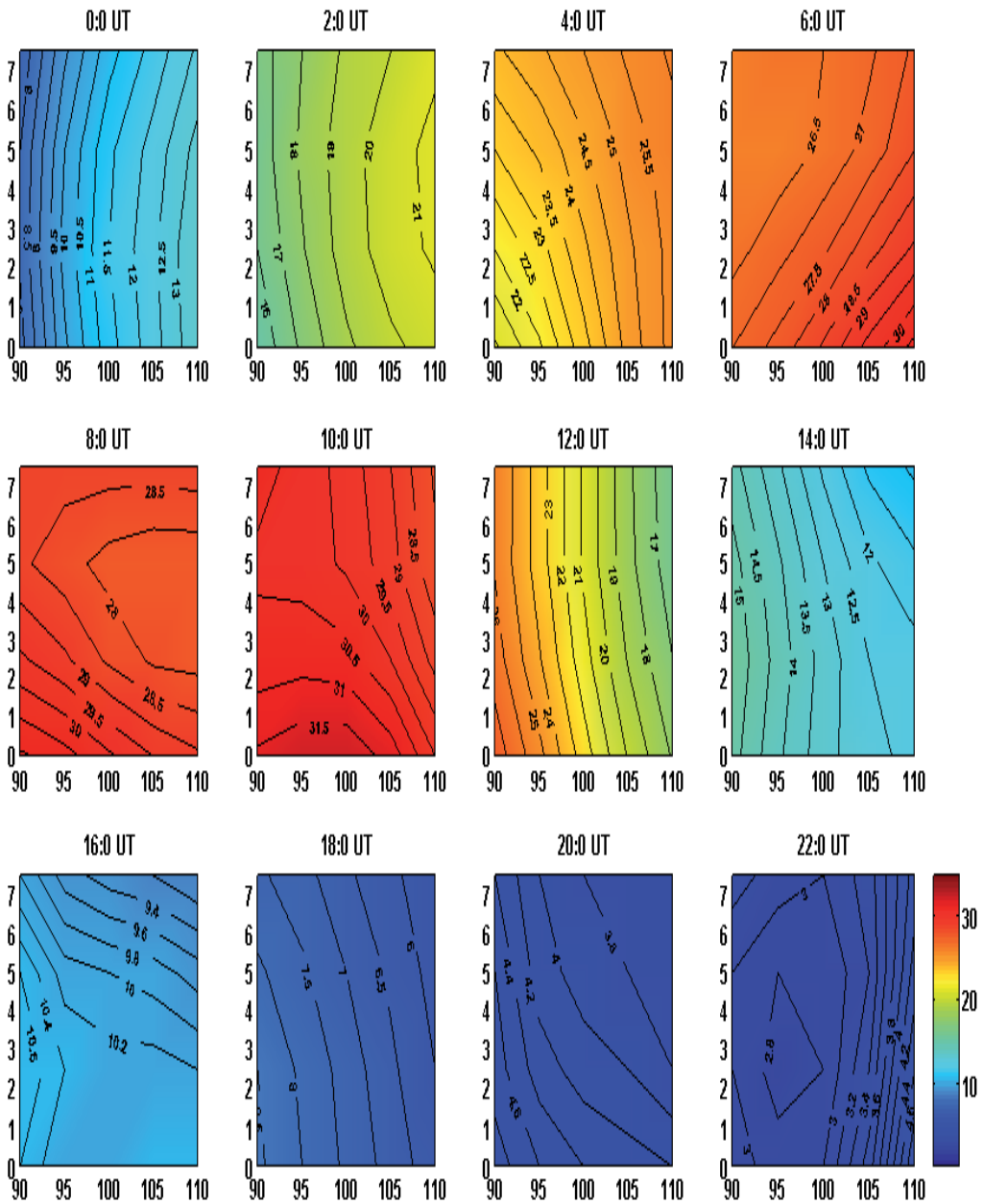


Fig. 13. TEC map from IGS, 8 November 2005

This data was 12 plotted as a 24 hour contour map as a function of longitude as illustrated in figure 12. The TEC above the reference station was extracted from interpolation of this data at every epoch (30s interval) as illustrated in figure 14.

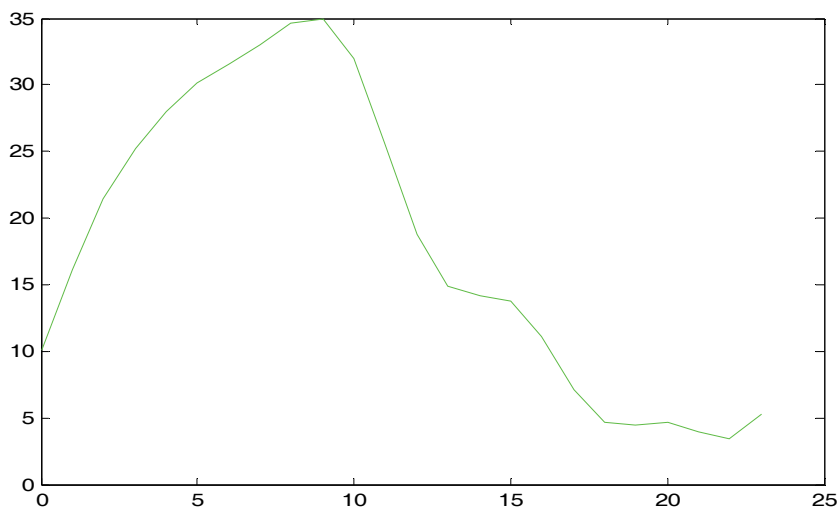


Fig. 14. TEC extracted from TEC map

The difference between the two maximum TEC is because there was no IGS station located in Malaysia. The diurnal profile of ionospheric variation from both figure showed a good agreement. This proved that PPP technique can be used to generate TEC map over single receiver station. Figure 15 clearly indicates the 3-D maps based on IONEX data. The IONEX data have been generated from the BGS software with PPP program. The effective height obtained for 450 km (MSLM) for KTPK station with TEC is 34 TECU.

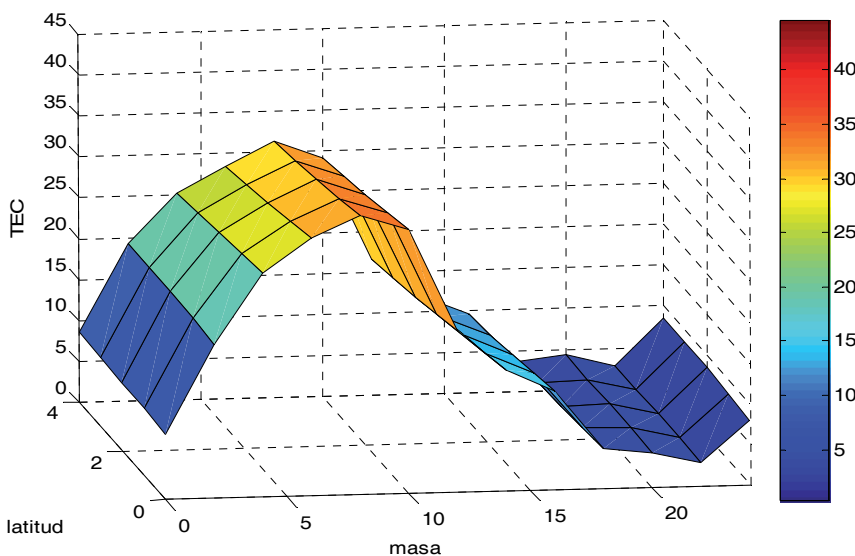


Fig. 15. 3-D MSLM for KTPK station

4. Future Work

The research has also identified several possibilities of GPS methodology including accuracy issues and further improvement on TEC that can be incorporated in future research. The following issues and directions have been noted:

- i). In this work, only two signal involve which is L1 and L2 to investigate ionospheric TEC. Further, it would be necessary to include new improved signal, which is L5 for more precise and accurate.
- ii). Utilize data taken from other satellite navigation systems such as GLONASS, Galileo, etc
- iii). More detailed work for different ionospheric condition needs to be verified and compared for other region such as high latitude, Antartic and Artic.

Implementing this suggested further work would extend the TEC measurements at any location with any ionospheric conditions. The outcome gives a different approach that could be considered also for current or future GNSS augmentation systems to overcome the ionospheric error.

5. Conclusion

In this chapter we have presented methods for processing TEC which utilize different techniques. Two scenario of obtaining TEC were studied such as TEC dual frequency and TEC Map. First, for TEC Dual Frequency, GPS carrier phase derived TEC provides a smooth but relative measurement of ionospheric TEC, while code derived TEC provides a noisy but absolute measurement. To mitigate inherent fluctuations in pseudorange due to bandwidth limited precision, receiver noise, cycle slip, multipath etc, Levelling Process was applied to reduce carrier-phase ambiguities from the data. As a result, the remaining noise is discarded.

Mean while for TEC Map, analysis results showed that TEC have similar variations, where the TEC values start to increase gradually from morning and reach its maximum at noon and decrease around afternoon. Bernese software, the scientific GPS software packages has already proved its ability to determine an accurate regional TEC map. The PPP technique can be used to generate the TEC map. TEC map are needed in order to characterize the ionospheric behaviour. The result proved that PPP technique can be performed at cm- level. Besides, extraction of TEC information can also be done.

Considering the variability of the ionosphere in the equatorial region, it is recommended to analyze other mapping functions to project the line-of-sight ionosphere delay into the vertical used in the proposed approach.

6. References

- Abdullah, M.; Strangeways, H.J. & Walsh, D.M.A. (2009). Improving ambiguity resolution rate with an accurate ionospheric differential correction. *Journal of Navigation*, Vol. 62, No. 1, pp. 151-166, ISSN: 0373-4633.

- Abdullah, M.; Bahari S.A. & Yatim, B. (2008). TEC determination over single GPS receiver station using PPP technique, *International Symposium on GPS/GNSS 2008*, November 11-14, 2008 Tokyo
- Bradford, W.P. & Spilker, J.J.J. (1996). *Global Positioning System: Theory and applications*, American Institute of Aeronautics and Astronautics, Vol. I and II Washington DC, USA.
- Doherty, P.H.; Dehel, T.; Klobuchar, J.A.; Delay, S.H.; Datta-Barua, S.; de Paula E.R. & Rodrigues, F.S. (2002). Ionospheric effects on low-latitude space based augmentation systems, *Proceedings of ION GPS 2002*, September 24-27, 2002, Portland, pp. 1321-1329, Oregon.
- Dach, R.; Hugentobler, U.; Fridez, P. & Meindl, M. (2007). *Manual of Bernese GPS Software Version 5.0*, Astronomical Institute, University of Bern.
- Hansen, A.; Blanch, J. & Walter, T. et al. (2000). Ionospheric correction analysis for WAAS quiet and stormy. *ION GPS*, Salt Lake City, Utah, September 19-22, 2000, pp 634-642, America.
- Horvath, I & Essex, E.A. (2000). Using observations from the GPS and TOPEX satellites to investigate night-time TEC enhancement at mid-latitudes in the southern hemisphere during a low sunspot number period, *Journal of Atmospheric and solar Terrestrial-Physics*, Vol. 62, No.5, pp. 371-391.
- Ho, Y.H.; Zain, A.F.M. & Abdullah, M. (2002). Hourly variations total electron content, TEC, for quiet ionosphere over Malaysia. *Proceeding of the Annual Workshop National Science Fellowship (NSF) 2001*, Petaling Jaya, pp. 77-79, Kuala Lumpur.
- Ioannides, R.T. & Strangeways, H.J. (2000). Ionosphere-induced errors in GPS range finding using MQP modelling, ray-tracing and nelder-mead optimization. *Millennium Conference on Antennas and Propagation*, AP2000, vol. II, Davos, pp. 404-408, Switzerland.
- JUPEM. (2009). MASS station. Malaysia [10 January 2009].
<http://www.jupem.gov/>
- Klobuchar, J.A. (1987). Ionospheric time-delay algorithm for single-frequency GPS users, *IEEE Transactions on aerospace and electronic systems*, Vol. 23, No. 3, pp. 325-331.
- Komjathy, A. (1997). *Global ionospheric total electron content mapping using the Global Positioning System*. Ph.D. dissertation. Department of Geodesy and Geomatics Engineering Technical Report No. 188. University of New Brunswick, Fredericton, New Brunswick, Canada. p 248.
- Ong, H. P. & Kamarudin, M.N. (2006). Calculation in Estimating Total Electron Content GPS. Universiti Teknologi Malaysia.
- Parkinson, B.W. (1996). *GPS error analysis, in Global Positioning System: theory and application*, Vol. 1, Edited by Parkinson & Spilker, American Institute of Aeronautics and Astronautics, Inc., Washington D.C., pp. 469-483.
- Schaer, S.; Markus, R.; Gerhard, B. & Timon, A.S. (1996). Daily Global Ionosphere Maps based on GPS Carrier Phase Data Routinely produced by the CODE Analysis Center, *Proceeding of the IGS Analysis Center Workshop*, Silver Spring, Maryland, pp. 181-192, USA.
- Schaer, S.; Gurtner, W. & Feltens, J. (1998). IONEX: The IONosphere map exchange format version 1, *Proceeding of IGS Analysis Center Workshop*, pp. 233-247.

Warnant, R.; Ivan, K.; Marinov, P.; Bavier, M. & Lejeune, S. (2007). Ionospheric and geomagnetic conditions during periods of degraded GPS position accuracy: 2.RTK events during disturbed and quiet geomagnetic conditions, *Advances in Space Research*, Vol. 39, No. 5., pp. 881-888.

Performance Evaluation Methods to Study IEEE 802.11 Broadband Wireless Networks under the PCF Mode

Vladimir Vishnevsky and Olga Semenova

*ZAO Research & Development Company "Information and Networking Technologies"
Russia*

1. Introduction

In the Chapter, we consider design concepts and protocols for metropolitan area wireless networks, realization methods for adaptive dynamic polling in these networks and investigation of their main performance characteristics by means of stochastic polling models.

Polling mechanism is widely used in the wireless metropolitan area networks (WMANs). In the wireless networks with PCF (Point Coordination Function), a base station polls subscriber stations accordingly to a polling table describing the order of polling. For IEEE 802.11 Wi-Fi networks, the polling is an option; for WiMAX networks (IEEE 802.16), it is basic. Using the PCF in the MANs allows to avoid the problem of hidden stations, efficiently schedule an order of station access to the wireless channel, flexibly control the radio cell operation and change its parameters correspondingly to the current situation by adjusting only the base station.

The methods to form and keep up the polling table are not specified in the standard thus the wireless network developers can freely decide on how to realize it. The specific polling mechanism and its parameters are the main factors determining the efficiency of the broadband wireless MAN with centralized control. In the Section, we give the description of the IEEE 802.11 protocols and the main directions of their development, including the recent versions IEEE 802.11n and IEEE 802.11 VHT. The much attention is given to development and modelling of the algorithms to poll subscriber stations, the schemes of adaptive dynamic polling (ADP). The adaptive dynamic polling is proposed to cut down the expenses of polling the empty subscriber stations and stations that stopped working for some reason. The adaptive dynamic polling is the prospective direction of developing the IEEE 802.11 broadband wireless networks.

We present the models of adaptive polling system and the system with threshold polling. With the adaptive polling order, the order of queue visit is cyclic but a server does not visit queues that were empty at the instant of polling in the previous cycle. Under the threshold polling, a queue is served only if its length exceeds the given threshold. Such service discipline is a possible way to assign a priority to a queue depending on the threshold value, and it allows server to give more attention to queues with high traffic intensity rather than spend time in queues with low traffic.

2. Performance evaluation of the broadband wireless networks

Polling mechanism is widely used in the metropolitan area wireless transmission networks. In the wireless networks with PCF (Point Coordination Function), a base station polls subscriber stations accordingly to a polling table describing the order of polling. For IEEE 802.11 Wi-Fi networks, the polling is an option; for WiMAX networks (IEEE 802.16), it is basic. In this Section, we consider design concepts and protocols for metropolitan area wireless networks, realization methods for adaptive dynamic polling in these networks.

2.1 Development of the broadband wireless networks: state of the art and prospects

In the recent years, the wireless transmission networks become the main direction of the network industry development. It was provided by both the rapid Internet development and the adoption of new progressive methods for coding, modulation and wireless data transmission. Recently, it is obvious that broadband wireless networks are without a rival with their efficiency of deployment, portability, price and area of potential applications.

Wireless technologies displace the wired one almost in all places where they can provide high-quality data transmission. The tendency is evidently continuing to the future since the wireless world is more comfortable. Nowadays, the wireless data transmission technologies have become ingrained in everyday life of millions of people and enterprises. The modern wireless networks allows solving variety of problems from the indoor network management to the distributed wireless networks within a city, a region or a country. Low cost, efficiency of deployment, wide performance capabilities to transmit data, IP telephony and video streams, all these make the wireless technologies the most rapidly developing telecommunication area. Rapid growth of the broadband wireless networks often called the "wireless revolution" in the field of data transmission networks is explained by a number of their own distinctive features, such as

- flexibility of a network topology enabling the dynamic change of the topology without time loss when mobile users connect to the network, move or disconnect;
- high data transmission rate (up to 54 Mbit/sec);
- rapidity of designing and realization which is significant because of the strict technical conditions to network construction;
- high unauthorized access protection level;
- high-priced laying or rent of the fiber optic or copper cable are not needed.

Recently, the wireless technologies provide effective solution of the following problems:

- mobile access to the Internet;
- organization of the wireless radiocommunication between workstations of a local area network (organization of the wireless access to a local area network resources);
- unification of local area networks and workstations into a single data transmission network and providing the remote access to the Internet for local area networks;
- last mile problem solution;
- interconnecting the automatic telephone systems with wireless channels of up to 54 Mbit/sec rate;
- creation of the land cellular radio modem data networks.

The mentioned features of the wireless technologies are substantially brought about by the fact that wireless networks operating within the range 2.4-6.4 GHz are based on the technology of broadband, or noise-type signal. The technology was initially used for the military purposes and recently it is efficiently used for civil radio networks.

The broadband wireless technologies use two radically different methods of frequency band utilization, they are Direct Sequence Spread Spectrum (DSSS) and Frequency Hopping Spread Spectrum (FHSS). Both methods imply the frequency band division into n subchannels. Under DSSS method, each data bit is coded as a sequence of n bits, and all those n bits are transmitted simultaneously through all n subchannels, and the coding algorithm is individual for each pair 'transmitter-receiver' so as to provide the transmission security. Under the FHSS method, a station transmits only through one of n subchannels at each time moment periodically changing the subchannel. Those change-overs (hops) happen simultaneously for both a transmitter and a receiver, and their sequence is pseudo-random and is known only for 'transmitter-receiver' pair that provide the transmission security as well.

Undoubtedly, each method has its own advantages and disadvantages. The DSSS method allows reaching the maximal throughput and due to the n -modular redundancy it, first, provides the narrow-band interference immunity, and, second, gives the opportunity to use the low power signal so as not to interfere with ordinary radio devices. On the other hand, the FHSS equipment is considerably simpler and cheaper and has the broadband interference immunity.

To work with the wireless networks, we need the special MAC (Media Access Control) protocols due to the fundamental differences from the cable medium, namely the lack of complete connection (the stations can be hidden from each other), the wireless medium is not protected from the outside signals and its signal propagation properties are asymmetric and variable by times. In order to provide the effective wireless medium access, the international standards, protocols and recommendations are developed which specify the physical and MAC layers of wireless networks: Bluetooth, ETSI Hiperlan and IEEE 802.11 for local area networks (LAN); IEEE 802.11 using the necessary amplifiers and parabolic antennae for metropolitan area networks (MAN), and finally, IEEE 802.16 and cellular telephony technologies modified for data and video images transmission (GPRS, UMTS and CDMA-2000) for MANs (Vishnevsky et al., 2009).

Among the LAN and MAN developers, the IEEE 802.11 protocol is very popular (referred to as Radio-Ethernet as well) adopted as an international standard in 1997 and having the following features:

- it can be used in both LANs and MANs;
- both DSSS and FHSS methods of the broadband wireless network deployment are regulated;
- the huge number of software and hardware of the large companies (such as CISCO Aironet, Lucent Technologies, Alvarion, etc.) in the world markets support the standard.

The IEEE 802.11 protocol determines two network development topology, they are topologies with infrastructure and so called ad-hoc-topology. With infrastructure topology, a wireless network has a single access point (or base station). An access point provides the synchronization and coordination for stations within the range, transmits broadcast packets and, what is of the great importance, can be a portal into the global network. Such topology is referred to as the Basic Service Set (BSS). To cover the wide area, it is possible to set up several access points working in different frequency channels and connected to the joint wired or wireless

backbone. Besides, the subscriber stations can be provided with a roaming between the access points. Such topology is called the Extended Service Set (ESS). The ad-hoc topology called the Independent Basic Service Set (IBSS) is the network performance scheme under which the numerous stations are connected directly avoiding connection to the special access point. This regime is effective when the wireless network infrastructure is not constructed (e.g., conference hall), or can not be constructed by some reason.

The IEEE 802.11 protocol specifies the data transmission rate equal to 1 or 3 Mbit/sec, with this the packet header and the service information can be transmitted at 1 Mbit/sec. Note that the transmission rate did not satisfy the users even when the protocol was adopted and approved. In order to make the wireless technology popular, cheap and, above all, to satisfy the modern strict conditions of business applications, the developers had to set up new standards which were the extensions of IEEE 802.11. Consider them in brief.

IEEE 802.11a. The IEEE 802.11a protocol exploits the radio frequency band of 5 GHz (5150-5250 MHz, 5250-5350 MHz and 5725-5850 MHz). In contrast to IEEE 802.11, the protocol applies not the spectrum broadening technologies but Orthogonal Frequency Division Multiplexing (OFDM), also referred to as multiple carrier modulation, which uses several carrier signals of different frequencies each transmitting a number of bites. This technology allows reaching the following data transmission rates: 6, 9, 12, 18, 24, 36, 48 and 54 Mbit/sec.

IEEE 802.11b. The IEEE 802.11b protocol involves the changes within the IEEE 802.11 physical layer. The network operates in 2.4 GHz radio frequency band. But the other signal modulation technology, Complementary Code Keying (CCK) allows reaching the rates 5.5 and 11 Mbit/sec and increases the connection stability in interference and multipath signal propagation conditions.

IEEE 802.11g. The IEEE 802.11g protocol as long as IEEE 802.11b operates in 2,4 GHz radio frequency band but applies the orthogonal frequency division multiplexing (OFDM) allowing to reach the data transmission rate equivalent to IEEE 802.11a (up to 54 Mbit/sec). Nevertheless, the protocol enables stations to get back to rates 1, 2, 5.5 and 11 Mbit/sec, i.e to CCK modulation. Therefore, the devices 802.11b and 802.11g are compatible within a segment of broadband wireless network.

Recently, the standard IEEE 802.11n describing the networks with data transmission rate 100Mbit/sec on the base of antenna system technology MIMO is going to be finished. The mobile version of the standard (IEEE 802.11p) and the addition IEEE 802.11e to provide the guaranteed quality of service (QoS).

In 2007, the generalized standard (see IEEE Std. 802.11-2007) was approved involving all standards finished before June, 2007. They are IEEE 802.11a/b/g mentioned above and additions IEEE802.11e/h/i/j.

The standard IEEE 802.11 is constantly being improved and developed to provide new customer services and to increase the data transmission rate and its quality. In 2009, it is planned to release a number of new standards being developed from 2003-2004. First of all, they are IEEE 802.11n and IEEE 802.11s. Though those standards are being finished, many companies have started production of devices and provide the wireless network operation based on the draft versions of those standards.

The other standards to be approved in 2009 are:

- standard IEEE 802.11u describing communications between IEEE 802.11 networks and outer networks;
- standard IEEE 802.11r regulating procedures of switching between subscriber stations for delay sensible applications like IP-telephony, etc.;

- standard IEEE 802.11p for operation in dynamic environment, and for fast moving wireless devices, in particular;
- standard IEEE 802.11v describing the wireless network control protocols;
- standard IEEE 802.11w regulating the methods to protect supervisory frames in a wireless network;
- standard IEEE802.11z describing the protocol for direct data exchanging between stations without using an access point.

The standard IEEE 802.11k should be also mentioned but it is not included into the generalized standard IEEE 802.11-2007 since its final version was released at the end of 2007 only. The standard regulates the mechanisms to exchange information about radio resource, radiochannel performance and load, noise level, etc.

The persistent growth of the transmission data volume, release of new applications, e.g. high definition video, impose heavy demands on wireless network throughput.

In spite of high data transmission rate in third generation mobile networks based on LTE technology and in networks IEEE 802.11n (up to 300 Mbit/sec), work on new technologies creation in the framework of IEEE 802.11 is continued. From 2007, the standard IEEE 802.11 VNT (Very High Throughput) has been started providing a base for very high throughput local wireless networks with nominal speed up to 500Mbit/sec within the frequency range 6 GHz. The standard is planned to be finished in 2012.

High network throughput is obtained by the MIMO technology application with 8 spaced antennas on both transmitting and receiving sides, by band enhancement up to 80 MHz through multiplexing of four channels of width 20 MHz, also by using OFDMA to organize frequency division multiple access as in IEEE 802.16. The developed standard supports compatibility with devices working under IEEE 802.11a/b/g/n.

In Russian Federation, the new technology and both hardware and software for very high throughput mesh-networks operating in the frequency range 60GHz (Vishnevsky & Frolov, 2009). As compared to existing mesh-networks, the proposed approach provides transmission rate up to 1000 Mbit/sec and makes the frequency planning and operating in duplex mode unnecessary.

In the 802.11 protocol, the fundamental mechanism to access the medium is called Distributed Coordination Function (DCF). This is a random access scheme, based on the Carrier Sense Multiple Access with Collision Avoidance (CSMA/CA) protocol. Retransmission of collided packets for each station is managed according to binary exponential backoff rules (Section 2.2). The alternative access mechanism as an option specified in IEEE 802.11 is point coordination function (PCF) under which the coordinator station manages the centralized polling of other stations (Section 2.3).

2.2 Medium access layer in IEEE 802.11. Distributed Coordination Function (DCF)

The IEEE 802.11 protocol is the part of IEEE 802 protocols for local area networks (LANs) and metropolitan area networks (MANs) involving the well-known protocols IEEE 802.3 (Ethernet LAN) and IEEE 802.5 (Token Ring LAN). The majority of IEEE 802 protocols determines the physical and data link layers of the Open Systems Interconnection (OSI) seven-level reference model of the International Organization for Standardization (ISO). Furthermore, the data link layer is represented as two sub-layers, the Logical Link Control (LLC) and Medium Access Control (MAC). Such division is conditioned by the fact that under the same LLC, the mechanisms providing MAC can be different. The IEEE 802.11 involves the functional

description of both MAC and PHY layers. Both layers possess significant features, e.g. the high packet loss rate due to noise and collisions, and the fact that wireless data transmission can suffer from the unauthorized access. Logical link control is not considered in the protocol since it is the same as in IEEE 802.2.

All questions on regulation of the wireless sharing by the network stations are determined on MAC-layer. The necessity of such regulation rules is quite obvious. Imagine the situation when each station of the wireless network sends data to the medium without observing any rules. As a result of such signals interference, the destination stations can not receive the data, and even understand the data were destined for them. Therefore, the stringent regulating rules are essential to determine the wireless medium multiple access. The multiple access rules can be compared to the rules of the road which regulate the road sharing by road users.

As it is mentioned above, there are four types of IEEE 802.11 MAC layer multiple access to wireless medium, they are Distributed Coordination Function (DCF), its extension Extended DCF (EDCF), Point Coordination Function (PCF) and Hybrid Coordination Function (HCF). Below, we consider these mechanisms in details.

The DCF is a method to organize peer-to-peer access to the wireless medium. The function is based on the Carrier Sense Multiple Access/Collision Avoidance (CSMA/CA). With this access, each station before sending a packet listens to the medium trying to detect the carrier signal and starts transmission only when the channel is idle. But in this case the probability that a packet collides with another one upon its transmission is high enough, when two or more stations find out the channel is idle and start transmission at the moment when some station is transmitting. In order to decrease the collision probability, the Collision Avoidance (CA) mechanism is applied. The mechanism is described as follows. A station detecting the channel idle waits for the prespecified time interval before it starts transmission. The time interval is random given by two intervals: the Distributed InterFrame Space (DIFS) and the random Backoff time. Consequently, each station waits for a random time before starting data transmission that essentially decreases the collision probability since the probability that at least two stations have the same backoff is negligible.

MAC-layer of the IEEE 802.11 protocol, its modification described in IEEE 802.11e thereof, specifies five types of a time interval between consecutive data transmissions, namely Interframe Space (IFS). The shortest one is SIFS (Short Interframe Space) used for special sequence of data exchange, e.g. ACK transmission to acknowledge a frame successful reception. The SIFS duration is specified by physical layer to give enough time for the system to switch from reception to transmission or inversely. The other intervals are given in duration increasing order: PIFS, used by stations with Point Coordination Function; DIFS, used by stations with Distributed Coordination Function; AIFS, used in Extended DCF (EDCF), and EIFS (Extended Interframe Space), used by stations after transmission error.

In order to provide stations with the equal access to the channel, it is necessary to determine the appropriate algorithm to choose the backoff time which is a number of basic time intervals called time-slots. To choose the random backoff, each station determines the Contention Window (CW) which is the range the backoff time is chosen from. The minimal CW is 31 time slots, and maximal one is 1023 time slots. The backoff is determined as:

$$Backoff = Random(CW) \cdot SlotTime,$$

where $Random(CW)$ is an integer uniformly chosen in the range $(0, CW - 1)$. At each time, the value CW depends on the number n of the attempts failed to send a packet and is given by

$$CW = CW_0 2^n,$$

where CW_0 is the minimal contention window, $0 \leq n \leq m$, and m is the maximal number of attempts allowed to send a packet. If the $m + 1$ -th attempt is failed the packet is discarded.

When a station tries to get an access to the channel, after the DIFS expires the backoff starts to count down. If the channel is idle during DIFS and the backoff, the station immediately starts transmission as the backoff counter reaches 0.

After the successful packet transmission, the CW is determined anew. If another station transmits during the backoff time, the backoff counter is frozen until the channel becomes idle (transmission is finished and DIFS expired). With this procedure, it is easy so see that the more times the station freezes its backoff counter the greater the probability that the packet waiting for transmission will not collide.

The described algorithm to get an access to the wireless medium guarantees the equal access for all stations in the network. But under such procedure, the probability of collision (that an arbitrary packet collides upon its transmission) is still non-zero. The collision probability could be reduced by extension of the maximal CW . But it leads to the greater backoff value which decreases the channel throughput. Therefore, the DCF uses the following algorithm to minimize collisions. After each successful frame reception, the destination station sends the ACK (ACKnowledgement) after SIFS to acknowledge the transmission was successful. If collision happens upon transmission the sender station does not get an ACK, so it finds out the transmission failed. The sender waits for ACK during EIFS, and if the ACK is not received the sender increases its CW . Thus, if the CW is 31 slots for the first transmission attempt for the second one it is 63, 127 for the third, 255 for the fourth, 511 for the fifth, and 1023 for other attempts. It can be seen that the CW is dynamically increased with collision number increasing, which allows reducing both the delay and the collision probability.

Note that the sender station can not receive the ACK frame indicating the transmission was success due to collision or signal distortion. And both reasons are not distinguishable for the sender station.

As it is mentioned above, all stations are equal to get an access to the wireless medium due to the contention mechanism, and no station has a priority to transmit data. This restricts DCF to provide Quality of Service (QoS). In IEEE 802.11e protocol, QoS is enabled by Enhanced DCF (EDCF). The EDCF mechanism is similar to DCF, but the difference concerns the CW size and the backoff counter to provide the priority access for various applications to wireless medium. For EDCF the traffic is divided into categories (TC, Traffic Categories) which differ from each other by priority to get an access to the transmission medium. Meanwhile, the medium access mechanism is the same as for DCF contention based.

Before a station detecting the channel idle starts transmission, it waits for AIFS (Arbitration InterFrame Space) and then counts down the backoff counter. The backoff counter is uniformly chosen in the range $[1, CW(TC) + 1]$ where $CW(TC)$ is the contention window for the given TC. TC priority is provided by using the different values of minimal and maximum CW and AIFS. Thus, the minimal value of AIFS is always DIFS but it can be increased depending on the TC.

In case of collisions which happen when two or more backoff counter drop to zero simultaneously and AIFS intervals are the same, the CW is increased. For EDCF, the new CW size is

determined as $newCW(TC) = ((oldCW(TC) + 1)PF) - 1$, where PF is the constant CW scaling factor depending on the TC. Note that for DCF we have $PF = 2$.

Thus in EDCA, the TC is assigned a priority by variation of the parameters CW_{min} , CW_{max} , AIFS, PF. Each station of the wireless network can have up to 8 TC queues for transmission. But in this case, the TC backoff counters within the same station can drop to zero simultaneously which is called the virtual collision. To avoid virtual collisions, the station uses the special queue scheduler which provides the higher priority TC with the priority access to the transmission medium.

The considered mechanism of transmission medium multiple access control have the same bottleneck, so-called problem of hidden stations. The situation happens when two stations can not listen to each other directly due to natural barriers. Such stations are called hidden. To avoid the problem, the DCF and EDCF mechanisms have the optional technique known as Request-To-Send/Clear-To-Send (RTS/CTS).

Accordingly to RTS/CTS, before transmitting a packet, a station operating in RTS/CTS mode "reserves" the channel by sending a special Request-To-Send short frame. An RTS frame involves the information on the forthcoming transmission and destination station and is available to all stations in the network (except ones hidden from the sender station). It allows the other stations to postpone transmission for the declared transmission time, and during this time the channel is considered "virtually busy". The destination station acknowledges the receipt of an RTS frame by sending back a Clear-To-Send (CTS) frame, after which normal packet transmission and ACK response occurs. Since collision may occur only on the RTS frame, and it is detected by the lack of CTS response, the RTS/CTS mechanism allows to increase the system performance by reducing the duration of a collision when long messages are transmitted.

The DCF and EDCF are simple and reliable mechanisms of multiple access to transmission medium in IEEE 802.11 broadband wireless networks. But they have two shortcomings: the lack of both QoS support and solution of the hidden stations problem. Thereby, the IEEE 802.11 protocol was supplemented with the alternative methods to multiple access control.

2.3 Point coordination function

The DCF mechanism described above is basic for IEEE 802.11 protocols and can be used in both ad-hoc wireless networks and infrastructure networks (having Access Point, AP). But for the infrastructure networks, there are more appropriate methods to control the transmission medium multiple access, namely, Point Coordination Function (PCF) and Hybrid Coordination Function (HCF). Note that PCF and HCF mechanisms are optional and applied for networks with AP only.

In case of PCF, one of stations (access point) is central and called the Point Coordinator (PC). The PC controls is imposed a responsibility to control the multiple access on the base of the specified polling algorithm or information on station priority. Thus, the PC polls all stations in the network listed in its polling table and organizes data transmission between network stations. As opposed to DCF where each station decides for itself when to start transmission, the PCF implies that only PC decides what station can get an access to the channel. It is significant to note that this approach completely avoids the contention access to the channel unlike DCF, makes collisions impossible and provide the priority access for time-sensitive applications. Thus, PCF can be used to organize collision-free priority access to the transmission medium.

The Point Coordination Function does not contradict the Distributed Coordination Function and rather supplements it. In fact, the PCF networks can use both PCF and traditional DCF. During network operating, the time intervals for PCF and DCF alternate.

In order to provide alternating the PCF and DCF modes, the access point which realizes PCF has to have a priority access to transmission medium. It is possible if an access to the channel is contention one (as for DCF) but the time interval for the access point to wait the response is less than DIFS. In this case, when the access point tries to get an access to the channel it waits the end of transmission as other stations do and since it has the minimal interframe space, it gets an access first. The interframe space for the access point is called PIFS (PCF Interframe Space), given that $SIFS < PIFS < DIFS$.

The DCF and PCF mechanisms are combined in so called superframe which is the sum of PCF interval of the contention-free access called CFP (Contention-Free Period) and the succeeding DCF interval of CP (Contention Period). The CP length should be enough to enable the transmission of at least one frame by using PCF mechanism. It is necessary for the association procedure but it is out of our topic. The superframe starts with the beacon frame, and all stations having received it postpone their transmissions for the time determined by the CFP. The beacons contain the information on the CFP duration and allow synchronizing the operation of all stations.

Under PCF, the access point sends data packets (DATA) destined for stations (if available) and asks (polls) all stations about the frames waiting for transmission by sending them the service frame CF-POLL (invitation to transmit). The access point polls stations accordingly to its polling list (polling table). The methods to form and keep up the polling table are not specified in the standard thus the wireless network developers can freely decide on how to realize it.

A station can transmit packets to the channel only when it receives the CF-POLL. Having received the CF-POLL, the station sends the short frame containing both data (if available) and acknowledgement of CF-POLL reception after SIFS. If there are no data to transmit, the station answers with NULL frame containing the header only. If the access point gets the answer frame, it waits for SIFS and polls the next station. Otherwise if there is now answer during PIFS, the access point considers the station inaccessible and polls the next station.

In order to cut expenses, an access point can combine the CF-POLL with data transmission (the frame DATA+CF-POLL). Similarly, the stations are allowed to combine acknowledgement frame with data transmission (the frame DATA+CF-ACK). Under the PCF, there are four types of a frame:

- DATA, data frame;
- CF-ACK, acknowledgement frame;
- CF-POLL, poll frame;
- DATA+CF-ACK, combined frame of data and acknowledgement;
- DATA+CF-POLL, combined frame of data and poll;
- DATA+CF-ACK+CF-POLL, combined frame of data, acknowledgement and poll;
- CF-ACK+CF-POLL, combined frame of acknowledgement and poll.

Along with the extended distributed function EDCF in the IEEE 802.11e protocol, the Hybrid Coordination Function (HCF) is determined. Similarly as the EDCF is extension of the DCF, the HCF extends the PCF.

Due to the fact that the PCF and HCF realize centralized non-collision priority access to transmission medium, they completely solve the problem of hidden stations and provide QoS. But regardless of their advantages, the PCF and HCF are harder to be realized than the DCF. Besides, the point coordination functions imply relatively large number of service frames (CF-POLL, etc.) that essentially increases overhead expenses of data transmission in the wireless medium. To organize the wireless network with PCF or HCF, all stations support these regimes and one station serves as an access point while the DCF allows organizing the ad-hoc network without access point. The distributed coordination functions are reasonable to be used in the simplest wireless networks without hidden stations and delay-sensitive applications.

2.4 Problem of hidden stations in wireless metropolitan area networks

In IEEE 802.11 broadband wireless network, the basic structure unit is a radio-cell having star-shape structure: the center is a base station with omnidirectional antenna which antennae of all subscriber stations are focused on presenting the radio bridges between wireless network and local cable networks.

In typical conditions of the wireless metropolitan area network, the subscriber stations do not have a radio visibility for each other (they are hidden from each other) and have to communicate through the retransmitting base station disposed on the high altitude (tower buildings, TV tower, etc.) and providing an access to the outer network. Thus, the broadband wireless metropolitan area networks have the mesh structure: a mesh is a radio cell and subscriber stations are connected with the high-speed backbone network.

Below we consider the operation of a radio cell in the broadband wireless metropolitan area network.

A radio cell has the following features:

- all subscriber stations are hidden from each other and their antennae are focused on the base station, i.e. data transmission between subscriber stations is possible through the base station only;
- the distances between the base station and subscriber ones are large enough (several kilometers) and different.

Each of the IEEE 802.11 protocols supports its own set of transmission rates. For IEEE 802.11b, they are the channel rates 1, 2, 5.5 and 11 Mbit/sec, for IEEE 802.11a they are 6, 9, 12, 18, 24, 48 and 54 Mbit/sec. A rate is a type of modulation which modulate the carrier radio signal or its part in the system with several carriers. The "faster" modulations are less noise-resistant, and otherwise. For this reason, the IEEE 802.11 based devices use more noise-resistant modulations, or lower transmission rates in cases of the signal depression and large number of losses when transmitting frames. It is obvious that a frame of n bits is transmitted longer by rate 1 Mbit/sec (hence it reserves a channel for a longer time) than by rate 11 Mbit/sec. In case when a subscriber station is far off or is placed in a nasty place, the radio signal it receives from the base station is weak, and the subscriber station automatically decrease the transmission rate. It results in decreasing of the network throughput. In case of PCF, the situation gets worse as it is impossible to control the subscriber station behavior. Remind, that accordingly to the DCF and EDCF mechanisms, the subscriber station decides by itself when to transmit data. Besides, regardless of data transmission directions within a radio cell, they come through the base station, thus it is logical to impose the base station on the radio cell control responsibility. It is easy to see that due to the above-mentioned features, it is not reasonable to use the distributed coordination functions in broadband wireless metropolitan area networks. Even though the

equipment supporting the centralized control is more complicated for development and production hence it is more expensive, it much more efficiently uses two most valuable resources of the broadband wireless network, they are frequency and throughput. The centralized control in the MANs allows to avoid the problem of hidden stations, efficiently schedule an order of station access to the wireless channel, flexibly control the radio cell operation and change its parameters correspondingly to the current situation by adjusting only the base station. The adaptive centralized control is a prospective direction of developing the IEEE 802.11 broadband wireless networks.

2.5 Adaptive dynamical polling in wireless networks

Since both the Point Coordination Function and Hybrid Coordination Function are based on the centralized control (polling), the main attention should be focused on the method of the centralized control realization. The specific polling mechanism and its parameters are the main factors determining the efficiency of the broadband wireless MAN with centralized control. The IEEE 802.11 standards allow the developers freely construct the methods of PCF and HCF realization. The standard does not specify: the method to poll the subscriber stations, method to construct and support the polling table, the policy to form queues of frames for transmission, and recommendations on the relation between DCF and PCF intervals in a superframe. Further, within the Section the main attention is given to development and modelling of the algorithms to poll subscriber stations, the schemes of adaptive dynamic polling (ADP).

For each subscriber station, the base station forms a queue of frames. Within a queue, the frames are ordered accordingly to the priority of traffic they belong to. Then the base station starts the polling cycle. As the cycle starts, it polls the first station in the polling list (polling table) sending frames from the corresponding queue to the station. Then the base station polls it sending the CF-POLL (or QoS CF-POLL) and receives the frames to be transmitted from the station (if available). As the base station finishes polling the subscriber one, it switches to polling the next station accordingly to the polling table. Note that PCF leads to the overhead expenses which can not be avoided during data exchange between the base station and the subscriber one, they are the time to switch to subscriber stations and service frames for polling them (CF-POLL, etc.).

The development the algorithm of adaptive dynamic polling lead to the following problems:

- choosing the method to poll the subscriber stations;
- choosing the policy to work with a subscriber station (receiving and transmission);
- development of methods to minimize the overhead expenses and;
- development of methods to optimize the system parameters.

Since the base station is substantially the central device in a radio cell of the broadband wireless MAN, it is reasonable to provide it with the complete functionality concerning the radio cell control, service of the queues, determination of the polling order and minimization of the overhead expenses. For the equipment developers, it means that the base station has to carry the majority of the network features. A subscriber station plays a passive role just answering the service frames from the base station.

Efficiency of the broadband wireless PCF network performance considerably depends on the method of polling mechanism realization. At the same time, the choosing of a cyclic polling type and a queue service discipline is determined by the method of the broadband wireless MAN (Metropolitan Area Network) application. Normally, there are two situations during the broadband wireless MAN operating. In the first one, uplink traffic from the base station to end

stations dominates over the downlink one. Such a traffic is typical while using a broadband wireless MAN cell as a "last mile" for Internet provider. In this case, each end station has its own segment of LAN (Local Area Network) that gets an access to Internet via the wireless network. The investigation of the real broadband wireless MAN (Vishnevsky, 2000) working as the "last mile" shows that traffic from the outer network to the local segment is much higher than the backward traffic.

In the second case, downlink traffic from an end station to the base one dominates over the uplink one. Such a traffic is typical while using the broadband wireless network as backbone network to transmit information from the objects "behind" the end stations to the outer network (usually, to an information data storage center). The situation takes place when the wireless network is used for the video monitoring systems, automatic process control systems, telemetering, systems of collection, storage and processing of data.

Further we say a cell works in the "last mile" mode if the downlink traffic is dominant and it works in the "data collection" mode if the uplink traffic is dominant.

The fundamental difference between two situations is that the base station (coordinator of the wireless network cell work) knows the parameters of the queue of frames to be transmitted to end stations in the case of dominating downlink traffic. Thus, the base station can choose the policy to work with an end station queue before it polls the station. In the second case, the base station knows nothing about the queues of frames to be transmitted when the uplink traffic is dominant. Hence, it needs to poll the end station first and then to decide on the policy to work with the queue.

When a cell works in the "data collection" mode we can neglect the data traffic from the base station to the end ones considering just uplink traffic from the end stations to the base one. In this case, the base station polls an end one first, that is connects to the end station and starts transmitting. Then, the base station makes an attempt to switch to the next end station accordingly to the polling table. Moreover, the base station does not know if the end station will respond to the poll and if it will have the frames for transmission. In order to cut down expenses of polling the empty end stations and stations that stopped working for some reason we propose not to poll those stations at the next polling cycle.

Thus the rule to poll the end stations could be as follows. The base station polls a subscriber one if it polled it in the previous cycle and the end station had frames for transmission or it was skipped. In the case the end station did not respond to the base one in the previous cycle or it was empty when being polled, it is skipped (not polled) by the base station in the current cycle. Since the base station can not estimate the number of frames in the queue to be transmitted in advance (before polling the end station) it is not reasonable to serve the queue until it is empty. Thus, we propose the discipline to serve the end station: the base station transmits only the frames which were present in the queue at the station polling epoch. The adequate model to investigate the performance characteristics of the broadband wireless network working in the "data collection" mode described above is the polling system with adaptive polling mechanism and gated service analyzed in Section 3 where we presented the analytical and simulation results.

When a cell works in the "last mile" mode, the data traffic from the end station to the base one can be neglected. So we consider just downlink data traffic from the base station to the end one. In this case, the base station sends frames from the queue to the corresponding end station. Then, it waits for the successful data transmission acknowledgment from the subscriber station (during PIFS) and starts sending frames from the next queue. Time to switch between queues is random so it is impossible to say in advance if the data are transmitted successfully. If the

queue of frames is short it is obvious that data transmission costs are high. So, it is better to serve the queue only if its length exceeds the given value called the threshold in order to cut down the expenses. To maximize the system throughput, the queues of each end station should be served until empty. But in the case when one or several queues are long enough, the frame mean waiting time in the queue is large that is unacceptable for some network applications. So, the most important system parameters are the mean queue length and the frame mean waiting time. These parameters can be estimated by means of stochastic model with exhaustive threshold service considered in Section 4.

3. Adaptive polling system

The polling systems are varieties of the queuing systems with multiple queues and one (or more) server(s) common to all queues that poll the queues and serve the queued customers. Classification of polling systems and methods to study them are presented in reviews (Levy & Sidi, 1990; Vishnevsky & Semenova, 2006) and books (Takagi, 1986; Borst, 1996; Vishnevsky & Semenova, 2006).

The adaptive polling mechanism assumes that the server polls not all queues in a cycle. The queues that were empty at the previous polling epoch are skipped (not visited) by the server and are visit in the next cycle only. Unfortunately, the exact analysis of adaptive polling systems is cumbersome, and in this Section, we provide an approximate analysis.

We consider the polling system with N queues (having unlimited waiting space) and a single server which is common for all queues. Each queue, say i , has a Poisson input of customers with parameter λ_i . Service times at queue i are independent and identically distributed with the distribution function $B_i(t)$ with the moments $b_i^{(r)} = \int_0^\infty t^r dB_i(t)$, $r \geq 1$, and Laplace-Stieltjes transform (LST) $\beta_i(s) = \int_0^\infty e^{-st} dB_i(t)$, $i = \overline{1, N}$.

The server visits queues in cyclic order from queue 1 to queue N accordingly to an adaptive scheme. A cycle is referred to as the time the server spends visiting (serving) queues 1 through N . With adaptive mechanism, the server skips (does not visit) queues which were visited in the previous cycle and were found empty at their polling moments. After being skipped, a queue is always visited in the next cycle.

If queue i is polled (or visited) by the server, the switchover time is incurred with distribution function $S_i(t)$ having the LST $\tilde{S}_i(s)$ and the moments $s_i^{(r)}$, $r \geq 1$, $r = \overline{1, N}$. A polling moment is referred to as a moment when the switchover time is finished and the server is ready to start working at a queue. The service discipline is gated, i. e. the server serves only those customers that presented at a queue at its polling instant. The customers arriving during the queue service time will be served in the next cycle.

If N queues were sequentially found empty at their polling moments, the server takes a vacation having the distribution function $F(t)$ with LST $\varphi(s)$, and moments $\varphi^{(k)}$, $k \geq 1$. After a vacation, server starts working at the queue that he stopped polling at and went for a vacation. The approach we use to investigate the model with several queues is based on the decomposition of the polling system to separate queues, further analysis of a queue as a queueing system with server's vacations, and then, application of the obtained results to the system with several queues. The analysis aims at deriving the first and second moments of the mean waiting time in a separate queue and is partially based on the results obtained in (Sumita, 1988) for the queueing system with server's vacations which are discussed in Section 3.1.

3.1 Analysis of a single queue

First, consider a single queue with server’s vacations. Within this subsection, we omit the lower index denoting the queue number. We assume that the vacation time depends on the fact whether the queue was empty at the moment the server finishes the previous vacation or it was not. If not, the vacation time has distribution function $H(t)$ with LST $h(s)$ and the moments $h^{(k)}$, $k \geq 1$. If the queue is empty when server finishes a vacation, the next vacation period is distributed with the function $\tilde{H}(t)$ having the LST $\tilde{h}(s)$, and the moments $\tilde{h}^{(k)}$, $k \geq 1$. To investigate the queue, consider the Markov chain describing the queue state at the end of vacations. Let t_k be the k th epoch when vacation is finished, $k \geq 1$, and i_{t_k} be the number of customers at the queue at the epoch t_k . It is easy to see that the process i_{t_k} , $k \geq 1$, presents the discrete-time Markov chain, and its one-step transition probabilities

$$p_{i,j} = P\{i_{t_{k+1}} = j | i_{t_k} = i\}, \quad i, j \geq 0,$$

have the form

$$p_{0,j} = \tilde{y}_j, \quad p_{i,j} = \sum_{l=0}^j a_l^{(i)} y_{j-l}, \quad i > 0, \quad j \geq 0,$$

where

$$a_l^{(i)} = \int_0^\infty \frac{(\lambda t)^l}{l!} e^{-\lambda t} dB^{(*i)}(t), \quad y_l = \int_0^\infty \frac{(\lambda t)^l}{l!} e^{-\lambda t} dH(t), \quad \tilde{y}_l = \int_0^\infty \frac{(\lambda t)^l}{l!} e^{-\lambda t} d\tilde{H}(t), \quad l \geq 0,$$

and $B^{(*i)}(t)$ is the i -fold convolution of the distribution function $B(t)$.

It can be shown that under the condition $\rho = \lambda b^{(1)} < 1$ fulfilled, the stationary state probabilities exist

$$q^{(j)} = \lim_{k \rightarrow \infty} P\{i_{t_k} = j\}, \quad j \geq 0.$$

These probabilities satisfy the following set of the balance equations, $j \geq 0$,

$$q^{(j)} = q^{(0)} \int_0^\infty \frac{(\lambda t)^j}{j!} e^{-\lambda t} d\tilde{H}(t) + \sum_{i=1}^\infty \int_0^\infty \frac{(\lambda t)^l}{l!} e^{-\lambda t} dB^{(*i)}(t) \int_0^\infty \frac{(\lambda t)^{j-l}}{(j-l)!} e^{-\lambda t} dH(t). \quad (1)$$

By multiplying the equations (1) by the corresponding powers of z and summing them up, it readily follows that the probability generating function (PGF) $Q(z) = \sum_{j=0}^\infty q^{(j)} z^j$ of the stationary probabilities satisfies the functional equation

$$Q(z) = (Q(\beta(\lambda - \lambda z)) - q^{(0)})h(\lambda - \lambda z) + q^{(0)}\tilde{h}(\lambda - \lambda z), \quad |z| \leq 1. \quad (2)$$

The equations of type (2) have been solved in (Sumita, 1988) on the base of the method to solve the functional equations like (2) described in (Kuczma, 1968) and the corresponding result is included into (Takagi, 1991), pp. 223-225.

Below, we briefly describe the solution of (2). Consider the sequence of functions $\eta_j(z)$, $j \geq 0$, which are defined recursively,

$$\eta_0(z) = z, \quad \eta_{j+1}(z) = \beta(\lambda - \lambda \eta_j(z)), \quad j \geq 0. \quad (3)$$

It was proven in (Sumita, 1988) that if $\rho = \lambda b^{(1)} < 1$, the sequence of functions $\eta_j(z)$, $j \geq 0$, converges uniformly to 1 as $j \rightarrow \infty$ for all z , $0 \leq z \leq 1$. By substitution $\eta_j(z)$ instead of z in (2), we get

$$Q(\eta_j(z)) = Q(\eta_{j+1}(z))h(\lambda - \lambda\eta_j(z)) + q^{(0)}(\tilde{h}(\lambda - \lambda\eta_j(z)) - h(\lambda - \lambda\eta_j(z))).$$

Continuing the substitution for $j = 0, 1, \dots, n-1$, we have

$$Q(z) = Q(\eta_n(z)) \prod_{j=0}^{n-1} h(\lambda - \lambda\eta_j(z)) + q^{(0)} \sum_{j=0}^{n-1} (\tilde{h}(\lambda - \lambda\eta_j(z)) - h(\lambda - \lambda\eta_j(z))) \prod_{k=0}^{j-1} h(\lambda - \lambda\eta_k(z)). \quad (4)$$

Here we assume that $\prod_{k=a}^b c_k = 1$ if $b < a$.

Now, let $n \rightarrow \infty$ in (4). Using the normalization condition $Q(1) = 1$, we obtain

$$Q(z) = \prod_{j=0}^{\infty} h(\lambda - \lambda\eta_j(z)) + q^{(0)} \sum_{j=0}^{\infty} (\tilde{h}(\lambda - \lambda\eta_j(z)) - h(\lambda - \lambda\eta_j(z))) \prod_{k=0}^{j-1} h(\lambda - \lambda\eta_k(z)). \quad (5)$$

Setting $z = 0$ at the latter equation, we get the relation for the probability $q^{(0)}$:

$$q^{(0)} = \prod_{j=0}^{\infty} h(\lambda - \lambda z^{(j)}) \left[1 - \sum_{j=0}^{\infty} (\tilde{h}(\lambda - \lambda z^{(j)}) - h(\lambda - \lambda z^{(j)})) \prod_{k=0}^{j-1} h(\lambda - \lambda z^{(k)}) \right]^{-1}, \quad (6)$$

where the quantities $z^{(j)} = \eta_j(0)$, $j \geq 0$, are given by the recursion

$$z^{(0)} = 0, \quad z^{(j+1)} = \beta(\lambda - \lambda z^{(j)}), \quad j \geq 0. \quad (7)$$

Finally, the equations (1), (5)–(7) give the probabilities $q^{(j)}$, $j \geq 0$.

To obtain the performance characteristics of the system with adaptive polling scheme, we need to derive formulas for the first three derivatives $Q'(1)$, $Q''(1)$, $Q'''(1)$ of the PGF $Q(z)$ at $z = 1$, which can be found by using (5). The formula (5) involves the LSTs $(\tilde{h}(\lambda - \lambda\eta_j(z)))$ and $h(\lambda - \lambda\eta_j(z))$, where the functions $\eta_j(z)$, $j \geq 0$, are given by recursion (3). Thus, in order to obtain the formulas for the derivatives $Q'(1)$, $Q''(1)$, $Q'''(1)$ of the PGF $Q(z)$, we have to find the explicit expressions for the derivatives of the functions $\eta_j(z)$, $j \geq 0$, at $z = 1$:

$$\eta_j(1) = 1, \quad \eta_j'(1) = \rho^j, \quad j \geq 0, \quad \eta_j''(1) = \lambda^2 b^{(2)} \rho^{j-1} \frac{1 - \rho^j}{1 - \rho}, \quad j \geq 0,$$

$$\eta_j'''(1) = \lambda^3 b^{(3)} \rho^{j-1} \frac{1 - \rho^{2j}}{1 - \rho^2} + 3\lambda^4 (b^{(2)})^2 \rho^{j-1} \frac{(1 - \rho^{j-1})(1 - \rho^j)}{(1 - \rho)(1 - \rho^2)}, \quad j \geq 0.$$

Using the formulas obtained above, we can calculate the derivatives of functions $h(\lambda - \lambda\eta_j(z))$, $j \geq 0$, at $z = 1$: $h(\lambda - \lambda\eta_j(z))|_{z=1} = 1$,

$$(h(\lambda - \lambda\eta_j(z)))'|_{z=1} = \lambda h^{(1)} \rho^j, \quad (h(\lambda - \lambda\eta_j(z)))''|_{z=1} = \lambda^2 h^{(2)} \rho^{2j} + \lambda^3 h^{(1)} b^{(2)} \rho^{j-1} \frac{1 - \rho^j}{1 - \rho},$$

$$\begin{aligned}
 (h(\lambda - \lambda\eta_j(z)))'''|_{z=1} &= \lambda^3 h^{(3)} \rho^{3j} + 3\lambda^4 h^{(2)} b^{(2)} \rho^{j-1} \frac{1 - \rho^j}{1 - \rho} + \\
 &+ \lambda h^{(1)} \rho^{j-1} \left[\lambda^3 b^{(3)} \frac{1 - \rho^{2j}}{1 - \rho^2} + 3\lambda^4 (b^{(2)})^2 \frac{(1 - \rho^{j-1})(1 - \rho^j)}{(1 - \rho)(1 - \rho^2)} \right].
 \end{aligned}$$

Finally, after cumbersome simplifications, the formulas for the derivatives $Q'(1)$, $Q''(1)$, $Q'''(1)$ of the PGF $Q(z)$ at $z = 1$ are obtained as

$$Q'(1) = \frac{\lambda h^{(1)}}{1 - \rho} + q^{(0)} \frac{\lambda(\tilde{h}^{(1)} - h^{(1)})}{1 - \rho}, \tag{8}$$

$$\begin{aligned}
 Q''(1) &= \frac{\lambda^2 h^{(2)}}{1 - \rho^2} + \frac{\lambda^3 h^{(1)} b^{(2)} + (\lambda h^{(1)})^2 2\rho}{(1 - \rho)(1 - \rho^2)} + q^{(0)} \left[\frac{\lambda^2 (\tilde{h}^{(2)} - h^{(2)})}{1 - \rho^2} + \right. \\
 &\quad \left. + (\tilde{h}^{(1)} - h^{(1)}) \frac{\lambda^3 b^{(2)} + 2\rho \lambda^2 h^{(1)}}{(1 - \rho)(1 - \rho^2)} \right], \tag{9}
 \end{aligned}$$

$$\begin{aligned}
 Q'''(1) &= \frac{\lambda^3 h^{(3)}}{1 - \rho^3} + \frac{\lambda^4 h^{(1)} b^{(3)}}{(1 - \rho)(1 - \rho^3)} + \frac{3\rho \lambda^4 h^{(2)} b^{(2)} + 3\rho(1 + 2\rho)\lambda^3 h^{(1)} h^{(2)}}{(1 - \rho^2)(1 - \rho^3)} + \tag{10} \\
 &+ \frac{3\rho \lambda^5 h^{(1)} (b^{(2)})^2 + 3\lambda^4 (1 + 2\rho^2) (h^{(1)})^2 b^{(2)}}{(1 - \rho)(1 - \rho^2)(1 - \rho^3)} + \frac{6\rho^3 (\lambda h^{(1)})^3}{(1 - \rho)(1 - \rho^2)(1 - \rho^3)} + q^{(0)} \left[\frac{\lambda^3 (\tilde{h}^{(3)} - h^{(3)})}{1 - \rho^3} + \right. \\
 &\quad + \frac{\lambda^4 (\tilde{h}^{(1)} - h^{(1)}) b^{(3)}}{(1 - \rho)(1 - \rho^3)} + \frac{3\rho \lambda^4 (\tilde{h}^{(2)} - h^{(2)}) b^{(2)}}{(1 - \rho^2)(1 - \rho^3)} + \\
 &\quad + \frac{3\rho^2 \lambda^3 (\tilde{h}^{(2)} - h^{(2)}) h^{(1)}}{(1 - \rho^2)(1 - \rho^3)} + \frac{3\rho(1 + \rho)\lambda^3 (\tilde{h}^{(1)} - h^{(1)}) h^{(2)}}{(1 - \rho^2)(1 - \rho^3)} + \\
 &\quad \left. + \frac{3\rho \lambda^5 (\tilde{h}^{(1)} - h^{(1)}) (b^{(2)})^2 + 3\lambda^4 (1 + 2\rho^2) ((\tilde{h}^{(1)} - h^{(1)}) h^{(1)} b^{(2)})}{(1 - \rho)(1 - \rho^2)(1 - \rho^3)} + \frac{6\rho^3 \lambda^3 (h^{(1)})^2 (\tilde{h}^{(1)} - h^{(1)})}{(1 - \rho)(1 - \rho^2)(1 - \rho^3)} \right].
 \end{aligned}$$

Let ζ be the duration of the queue service (between two successive server’s vacations). Using the relations obtained above, we can get the moments $\hat{\psi}^{(r)}$, $r = 1, 2, 3$ of ζ . The number of customers served between two successive server’s vacations is a random variable, say τ , which has the first three moments $L_1 = Q'(1)$, $L_2 = Q''(1) + Q'(1)$, $L_3 = Q'''(1) + 3L_2 - 2L_1$, and the service time of the k th customer in a service period is a random variable, say ξ_k , which has the moments $b^{(r)}$, $r = 1, 2, 3$. It is easy to see that $\zeta = \sum_{k=1}^{\tau} \xi_k$. The random variables ξ_k are mutually independent and independent of τ . Thus, ζ equals to the sum of a random number of the random variables. Using the technique of the conditional expectations, it can be shown that the moments $\hat{\psi}^{(r)}$, $r = 1, 2, 3$, of the random variable ζ are

$$\hat{\psi}^{(1)} = b^{(1)} L_1, \quad \hat{\psi}^{(2)} = b^{(2)} L_1 + (b^{(1)})^2 (L_2 - L_1), \tag{11}$$

$$\hat{\psi}^{(3)} = L_1 b^{(3)} + 3b^{(1)} b^{(2)} (L_2 - L_1) + (b^{(1)})^3 (L_3 - 3L_2 + 2L_1). \tag{12}$$

Denote by $\psi^{(r)}$, $r = 1, 2, 3$, the conditional moments of the distribution of ζ , duration of the queue service between two successive vacations, given that the queue is not empty. It is easy

to see that the conditional moments $\psi^{(r)}$, $r = 1, 2, 3$, are expressed in the terms of the moments $\hat{\psi}^{(r)}$, $r = 1, 2, 3$, as follows:

$$\psi^{(r)} = \frac{\hat{\psi}^{(r)}}{1 - q^{(0)}}, \quad r = 1, 2, 3.$$

Thus, the formulas (5)–(7) give the stationary distribution of $q^{(i)}$, $i \geq 0$, the number of customers in the queue at the epoch the server finishes a vacation, and the formulas (8)–(10) express the first three moments of that distribution.

Let $W(x)$, $x \geq 0$, be the distribution of the waiting time in the queue, and $w(s) = \int_0^\infty e^{-sx} dW(x)$ be its LST. It is easy to see that

$$w(s) = w^{(0)}(s) + w^{(1)}(s) + w^{(2)}(s),$$

where $w^{(0)}(s)$ is the LST of the waiting time of an arbitrary customer arrived to the system when the server was busy, $w^{(1)}(s)$ is the LST of the waiting time of an arbitrary customer arrived to the system when the server was on an ordinary vacation (with distribution $H(t)$), $w^{(2)}(s)$ is the LST of the waiting time of an arbitrary customer arrived to the system when the server was on a special vacation (with distribution $\tilde{H}(t)$).

Using the probabilistic sense of LST, one can verify the following formulas are valid

$$\begin{aligned} w^{(0)}(s) &= \tau^{-1} h(s) \frac{Q(\beta(\lambda(1 - \beta(s)))) - Q(\beta(s))}{s - \lambda(1 - \beta(s))}, \\ w^{(1)}(s) &= \tau^{-1} (Q(\beta(\lambda(1 - \beta(s)))) - q^{(0)}) \frac{h(\lambda(1 - \beta(s))) - h(s)}{s - \lambda(1 - \beta(s))}, \quad w^{(2)}(s) = \\ &= \tau^{-1} q^{(0)} \frac{\tilde{h}(\lambda(1 - \beta(s))) - \tilde{h}(s)}{s - \lambda(1 - \beta(s))}. \end{aligned}$$

These formulas lead to the following result.

Theorem 1. *The LST $w(s)$ of the waiting time is given by*

$$w(s) = \frac{\tau^{-1}}{s - \lambda(1 - \beta(s))} (Q(\beta(s))(1 - h(s)) + q^{(0)}(h(s) - \tilde{h}(s))).$$

By differentiating $w(s)$ at $s = 0$, we obtain the formula for the mean waiting time

$$W^{(1)} = \frac{v^{(2)}}{2v^{(1)}} + \frac{\lambda b^{(2)} + 2\rho h^{(1)}}{2(1 - \rho)} \quad (13)$$

and for second moment $W^{(2)}$ of the waiting time

$$W^{(2)} = \frac{v^{(3)}}{3v^{(1)}} + \frac{\lambda b^{(3)} + 3\lambda b^{(2)}h^{(1)} + 3\rho h^{(2)}}{3(1 - \rho)} + W^{(1)} \left(\frac{\lambda b^{(2)}}{1 - \rho} + \frac{2\rho^2 h^{(1)}}{1 - \rho^2} \right) \quad (14)$$

with $v^{(k)} = (1 - q^{(0)})h^{(k)} + q^{(0)}\tilde{h}^{(k)}$, $k = 1, 2, 3$.

3.2 Approximate analysis of the system with N queues

As it follows from (6)–(14), the key role in calculation of the performance characteristics of the system considered is played by the form of the functions $h(s)$ and $\tilde{h}(s)$, the LSTs of the distributions of vacation period after visiting an empty or non-empty queue, respectively. In order to apply the results obtained for the system with single queue to the polling system with N queues, we have to estimate those LSTs. It is easy to see that they depend on the time the server spends visiting other queues, and are unknown. Below, we elaborate a procedure of successive approximations to calculate the first and second moments of waiting time in each queue on the base of the analysis given in Section 3.1. Note that the unknown LSTs $h(s)$ and $\tilde{h}(s)$ of vacation duration are improved at each stage of the procedure. And below, we elaborate such a heuristic procedure.

In the procedure, we use the quantities $z_i^{(j)}$, $j \geq 0$, $q_i^{(0)}$, $\psi_i^{(r)}$, $r = 1, 2, 3$, and $W_i^{(r)}$, $r = 1, 2$, $i = \overline{1, N}$, given by formulas (6)–(14) where all LSTs and the corresponding moments are given the subscript i , the number of the queue.

Since a queue being polled and found empty will not be visited at the next cycle and will be polled again two cycles later, it seems reasonable to assume that the time when the server is away from the queue is equal to the double intervisit time as if the queue was visited each cycle (after being polled and found non-empty). Besides, we need to take into account the fact that, if all queues are found empty, they are all visited in the cycle following the server’s vacation. Thus, we assume that $\tilde{h}_i(w) = \tilde{\chi}_i(w)\tilde{S}_i(w)$, where $\tilde{\chi}_i(w) = (\chi_i(w))^2 + \bar{q}_i(\varphi(w + \lambda_i(1 - \beta_i(w)))r_i(w) - \chi_i(w))$, the functions $\chi_i(s)$ are given by formula (17),

$$\bar{q}_i = \prod_{j=1, j \neq i}^N q_j^{(0)}, \quad r_i(w) = \prod_{j=1, j \neq i}^N (q_j^{(0)} + (1 - q_j^{(0)})\psi_j(w))\tilde{S}_j(w).$$

It follows that the moments of the distribution functions $\tilde{H}(t)$ and $H(t)$ of a vacation period in the system with single queue considered in Section 3.1 are defined as

$$\tilde{h}_i^{(1)} = \tilde{\chi}_i^{(1)} + s_i, \quad \tilde{h}_i^{(2)} = \tilde{\chi}_i^{(2)} + s_i^{(2)} + 2\tilde{\chi}_i^{(1)}s_i, \quad \tilde{h}_i^{(3)} = \tilde{\chi}_i^{(3)} + s_i^{(3)} + 3\tilde{\chi}_i^{(2)}s_i + 3\tilde{\chi}_i^{(1)}s_i^{(2)},$$

where $\tilde{\chi}_i^{(l)}$, $i = \overline{1, 3}$, are calculated as

$$\tilde{\chi}_i^{(1)} = 2\chi_i^{(1)} + \bar{q}_i(\hat{\varphi}^{(1)} + r_i^{(1)} - \chi_i^{(1)}), \quad \tilde{\chi}_i^{(2)} = 2\chi_i^{(2)} + 2(\chi_i^{(1)})^2 + \bar{q}_i(\hat{\varphi}^{(2)} + 2\hat{\varphi}^{(1)}r_i^{(1)} + r_i^{(2)} - \chi_i^{(2)}),$$

$$\tilde{\chi}_i^{(3)} = 2\chi_i^{(3)} + 6\chi_i^{(1)}\chi_i^{(2)} + \bar{q}_i(\hat{\varphi}^{(3)} + 3\hat{\varphi}^{(2)}r_i^{(1)} + 3\hat{\varphi}^{(1)}r_i^{(2)} + r_i^{(3)} - \chi_i^{(3)}),$$

$\varphi^{(r)}$, $r = \overline{1, 3}$, are given by

$$\hat{\varphi}^{(1)} = \varphi^{(1)}(1 + \rho_i), \quad \hat{\varphi}^{(2)} = \varphi^{(2)}(1 + \rho_i)^2 + \varphi^{(1)}\lambda_i b_i^{(2)},$$

$$\hat{\varphi}^{(3)} = \varphi^{(3)}(1 + \rho_i)^3 + 3\varphi^{(2)}(1 + \rho_i)\lambda_i b_i^{(2)} + \varphi^{(1)}\lambda_i b_i^{(3)},$$

and the moments $r_i^{(l)}$ are defined as

$$r_i^{(1)} = \sum_{j=1, j \neq i}^N (q_j^{(0)}s_j^{(1)} + (1 - q_j^{(0)})a_j^{(1)}),$$

$$\begin{aligned}
 r_i^{(2)} &= \sum_{j=1, j \neq i}^N (q_j^{(0)} s_j^{(2)} + (1 - q_j^{(0)}) a_j^{(2)}) + \\
 &+ (q_j^{(0)} s_j^{(1)} + (1 - q_j^{(0)}) a_j^{(1)}) \sum_{k=1, k \neq i, k \neq j}^N (q_k^{(0)} s_k^{(1)} + (1 - q_k^{(0)}) a_k^{(1)}), \\
 r_i^{(3)} &= \sum_{j=1, j \neq i}^N (q_j^{(0)} s_j^{(3)} + (1 - q_j^{(0)}) a_j^{(3)} + 2(q_j^{(0)} s_j^{(2)} + (1 - q_j^{(0)}) a_j^{(2)}) \sum_{k=1, k \neq i, k \neq j}^N (q_k^{(0)} s_k^{(1)} + \\
 &+ (1 - q_k^{(0)}) a_k^{(1)}) + (q_j^{(0)} s_j^{(1)} + (1 - q_j^{(0)}) a_j^{(1)}) \sum_{k=1, k \neq i, k \neq j}^N (q_k^{(0)} s_k^{(2)} + (1 - q_k^{(0)}) a_k^{(2)} + \\
 &+ (q_k^{(0)} s_k^{(1)} + (1 - q_k^{(0)}) a_k^{(1)}) \sum_{m=1, m \neq i, m \neq j, m \neq k}^N (q_m^{(0)} s_m^{(1)} + (1 - q_m^{(0)}) a_m^{(1)})).
 \end{aligned}$$

Further, we discuss the problem of determining the LST $h(s)$.

On the first step of the procedure, assume that each queue is visited (polled) in each cycle and the server serves only one customer in a queue per a visit. From this assumption it follows that the initial form of the LST $h_i(s)$ of the vacation (intervisit time for queue i) could be

$$h_i(s) = \frac{\sigma_i}{s + \sigma_i}$$

with

$$(\sigma_i)^{-1} = \sum_{j=1, j \neq i}^N (b_j^{(1)} + s_j^{(1)}), \quad i = \overline{1, N}.$$

Then, the moments of the vacation period (intervisit time for queue i) are given by equations

$$h_i^{(1)} = \sigma_i^{-1}, \quad h_i^{(2)} = 2\sigma_i^{-2}, \quad h_i^{(3)} = 6\sigma_i^{-3}.$$

Using LSTs $h_i(s)$, $i = \overline{1, N}$, and the moments $h_i^{(r)}$, $r = \overline{1, 3}$, we calculate the values of $z_i^{(j)}$, $j \geq 0$, $q_i^{(0)}$, $\psi_i^{(r)}$, $r = 1, 2, 3$, $W_i^{(r)}$, $r = 1, 2$, $i = \overline{1, N}$, by the formulas (6)–(14) for each queue i , $i = \overline{1, N}$. Note that we can use the Lyapunov inequality to check the correctness of numerical calculation of the moments. For instance, the values $\psi_i^{(r)}$, $r = 1, 2, 3$, have to satisfy the inequalities

$$\psi_i^{(2)} \geq (\psi_i^{(1)})^2, \quad \psi_i^{(3)} \geq (\psi_i^{(1)})^3, \quad \psi_i^{(3)} \geq (\psi_i^{(2)})^{\frac{3}{2}}.$$

Having analyzed the moments $\psi_i^{(r)}$, $r = 1, 2, 3$, of queue i service period, we choose the form of the LST $\psi_i(s)$ as follows.

- If the value $c_\psi = \frac{\psi_i^{(2)}}{(\psi_i^{(1)})^2}$ is approximately equal to 1, we set $\psi_i(s) = \frac{1}{1 + s\psi_i^{(1)}}$, i.e. the vacation (intervisit time) is exponentially distributed.

- If $c_\psi \approx \frac{1}{k}$, where k is some positive integer, we set

$$\psi_i(s) = \left(\frac{1}{1 + s \frac{\psi_i^{(1)}}{k}} \right)^k,$$

i.e. the vacation has Erlang- k distribution.

- If $c_\psi > 1$, we suppose that a vacation has hyper-exponential distribution, i.e.

$$\psi_i(s) = p_i \frac{\mu_i^{(1)}}{\mu_i^{(1)} + s} + (1 - p_i) \frac{\mu_i^{(2)}}{\mu_i^{(2)} + s}. \tag{15}$$

The parameters $p_i, \mu_i^{(1)}, \mu_i^{(2)}$ are calculated through values $\psi_i^{(r)}, r = 1, 2, 3$, in the following way. First, calculate the values

$$v_l = \frac{\psi_i^{(l)}}{l!}, \quad l = 1, 2, 3, \quad f_1 = \frac{v_3 - v_1 v_2}{v_2 - (v_1)^2}, \quad f_2 = \frac{v_1 v_3 - (v_2)^2}{v_2 - (v_1)^2},$$

$$\mu_i^{(1)} = \frac{2}{f_1 + \sqrt{f_1^2 - 4f_2}}, \quad \mu_i^{(2)} = \frac{2}{f_1 - \sqrt{f_1^2 - 4f_2}}, \quad p_i = \frac{\mu_i^{(1)}(\mu_i^{(2)} v_1 - 1)}{\mu_i^{(2)} - \mu_i^{(1)}}.$$

If the inequalities $v_2 > v_1^2, v_3 > v_1 v_2, v_1 v_3 > v_2^2$ and $f_1^2 > 4f_2$, are fulfilled then we define the function $\psi_i(s)$ from (15). Otherwise, the values $\mu_i^{(1)}, \mu_i^{(2)}$ and p_i are chosen to satisfy the relations

$$p_i \neq \frac{2(\psi_i^{(1)})^2}{\psi_i^{(2)}}, \quad 0 \leq p_i \leq 1, \quad \mu_i^{(2)} = \frac{2\psi_i^{(1)}(1 - p_i) - \sqrt{2(1 - p_i)p_i(\psi_i^{(2)} - 2(\psi_i^{(1)})^2)}}{2(\psi_i^{(1)})^2 - \psi_i^{(2)} p_i},$$

$$\psi_i^{(1)} \mu_i^{(2)} - 1 + p_i > 0, \quad \mu_i^{(1)} = \frac{p_i \mu_i^{(2)}}{\psi_i^{(1)} \mu_i^{(2)} - (1 - p_i)}.$$

Note that the value p_i should be chosen to minimize $\left| \frac{6p_i}{(\mu_i^{(1)})^3} + \frac{6(1-p_i)}{(\mu_i^{(2)})^3} - \psi_i^{(3)} \right|$ for the better approximation (Kazimirsky, 2002).

- If $c_\psi < 1$ but c_ψ does not equal to $\frac{1}{k}$ approximately, the vacation period distribution can be approximated by the phase distribution.
- If $c_\psi \approx 0$, we use the following form:

$$\psi_i(s) = e^{-\psi_i^{(1)} s}.$$

Now, suppose the LSTs $\psi_i(s)$, $i = \overline{1, N}$, are known. Note that queues may have different forms of the LST of intervisit times (server's vacations).

Then, we make a simplifying assumption that the probability that queue i is found empty at an arbitrary polling epoch is independent of the state of the other queues. Note that this assumption may not be valid at all (e.g. if the other queues are empty, queue i gets more time for its customers to be served, hence the probability that the queue is empty is greater than in the case when all other queues are not empty). But this assumption makes it possible to investigate the model with adaptive polling analytically. Thus, we can rewrite the form of the LST $h_i(s)$ of vacation duration for queue i (its intervisit time) can be rewritten as

$$h_i(w) = \chi_i(w)\tilde{S}_i(w), \quad (16)$$

with

$$\chi_i(w) = \prod_{j=1, j \neq i}^N (q_j^{(0)} + (1 - q_j^{(0)})\psi_j(w)\tilde{S}_j(w)). \quad (17)$$

The derivation of (16)–(17) is based on the probabilistic interpretation of LST as the probability that a catastrophe from a Poisson input with parameter w does not occur during the period considered. A catastrophe does not occur during a vacation time for the queueing system with vacations corresponding to queue i if it does not occur during switchover time for this queue (with probability $\tilde{S}_i(w)$) and during the switchover and service periods for the rest of queues in the current cycle (with probability $\chi_i(w)$). The first term in (17) implies that a catastrophe does not occur during the switchover time to queue j and the following service period with probability 1, if the queue is not visited by the server, and with probability $\psi_j(w)\tilde{S}_j(w)$ if it was.

Formulas (16) and (17) result in the relations for the moments of the intervisit time for queue i :

$$h_i^{(1)} = \chi_i^{(1)} + s_i^{(1)}, \quad h_i^{(2)} = \chi_i^{(2)} + s_i^{(2)} + 2\chi_i^{(1)}s_i^{(1)}, \quad h_i^{(3)} = \chi_i^{(3)} + s_i^{(3)} + 3\chi_i^{(2)}s_i^{(1)} + 3\chi_i^{(1)}s_i^{(2)}, \quad (18)$$

where

$$\begin{aligned} \chi_i^{(1)} &= \sum_{j=1, j \neq i}^N (1 - q_j^{(0)})a_j^{(1)}, \quad \chi_i^{(2)} = \sum_{j=1, j \neq i}^N (1 - q_j^{(0)})a_j^{(2)} + \\ &+ \sum_{j=1, j \neq i}^N (1 - q_j^{(0)})a_j^{(1)} \sum_{k=1, k \neq i, k \neq j}^N (1 - q_k^{(0)})a_k^{(1)}, \\ \chi_i^{(3)} &= \sum_{j=1, j \neq i}^N (1 - q_j^{(0)})a_j^{(3)} + 2 \sum_{j=1, j \neq i}^N (1 - q_j^{(0)})a_j^{(2)} \sum_{k=1, k \neq i, k \neq j}^N (1 - q_k^{(0)})a_k^{(1)} + \\ &+ \sum_{j=1, j \neq i}^N (1 - q_j^{(0)})a_j^{(1)} \sum_{k=1, k \neq i, k \neq j}^N (1 - q_k^{(0)})a_k^{(1)} \sum_{m=1, m \neq i, m \neq j, m \neq k}^N (1 - q_m^{(0)})a_m^{(1)}, \end{aligned} \quad (20)$$

where, for $m = \overline{1, N}$,

$$a_m^{(1)} = s_m^{(1)} + \psi_m^{(1)}, \quad a_m^{(2)} = s_m^{(2)} + \psi_m^{(2)} + 2s_m^{(1)}\psi_m^{(1)}, \quad a_m^{(3)} = s_m^{(3)} + \psi_m^{(3)} + 3s_m^{(2)}\psi_m^{(1)} + 3s_m^{(1)}\psi_m^{(2)}.$$

Then using formulas (16)–(20) for the LSTs and the moments of the vacation duration (of intervisit time for a queue), we recalculate the values $q_i^{(0)}, \psi_i^{(r)}, r = 1, 2, 3, W_i^{(r)}, r = 1, 2, i = \overline{1, N}$, by formulas (6)–(14) for all $i, i = \overline{1, N}$.

The iterative procedure described above should be repeated until the values $q_i^{(0)}, \psi_i^{(r)}, r = 1, 2, 3, W_i^{(r)}, r = 1, 2, i = \overline{1, N}$, calculated at the succeeding steps coincide with the necessary accuracy. Thus, we get the moments, $W_i^{(r)}, r = 1, 2, i = \overline{1, N}$, of the waiting time in the queues.

3.3 Numerical results

Here we give numerical examples to illustrate how the algorithm works for polling systems with various numbers of queues and traffic intensity comparing to the simulation results obtained using the general-purpose simulation system GPSS World (Schriber, 1974). The object of modeling was represented by a regional broadband wireless network consisting of several devices operating with one base station. The rates of packet arrivals to the devices and the rate of processing them are different. The devices are polled cyclically. Packet servicing is gated, that is, only those packets are transmitted which were at the queue at the polling moment. The input flows are assumed to be of the Poisson nature, and the times of packet servicing and polling initialization are assumed to be exponentially distributed.

We assume for simulation that the system is in the stationary mode when at duplication of the number of the packets passing through the system none of the comparison parameters changes more than by 0.5%. In the experiments, more than three million of packets passed through the system.

Average packet service time, switchover time, etc. in the numerical examples are taken from the real IEEE 802.11a broadband wireless network under PCF mode with realistic packet sizes and load levels. Thus, the obtained results correspond to such networks and mean waiting times satisfy the real systems requirements.

Case N = 2. First, consider the symmetric system of two queues with the mean service times $b_1^{(1)} = b_2^{(1)} = 0.311$, the mean switchover times $s_1^{(1)} = s_2^{(1)} = 0.091$ and the mean time of server’s vacation $\varphi^{(1)} = 0.005$. The mean waiting time calculated by the Algorithm (column "A"). Simulation results (column "S") and relative error of comparison (column " Δ ") are shown in Table 1. The first column describes the customers input intensities and the corresponding traffic intensities. Two last lines of the Table present the results obtained for different mean server’s vacation times $\varphi^{(1)}$ given that $\lambda_1 = \lambda_2 = 0.5$.

	A	S	$\Delta, \%$
$\lambda_1 = \lambda_2 = 0.321, \rho = 0.2$	0.289	0.268	7.8
$\lambda_1 = \lambda_2 = 0.5, \rho = 0.311$	0.392	0.358	9.5
$\lambda_1 = \lambda_2 = 0.803, \rho = 0.5$	0.659	0.601	9.7
$\lambda_1 = \lambda_2 = 1.28, \rho = 0.8$	1.73	1.93	10.4
$\varphi^{(1)} = 0.05$	0.392	0.358	9.5
$\varphi^{(1)} = 0.1$	0.417	0.384	8.6

Table 1. System with two queues

Case N = 3. Now, consider the case of three queues with symmetric service $b_i^{(1)} = 0.044, s_i^{(1)} = 0.1, i = \overline{1, 3}, \varphi^{(1)} = 0.1$. The mean waiting times $W_i^{(1)}, i = \overline{1, 3}$ obtained by using the algorithm and simulation are presented in Table 2 for various customer input intensities. The last two lines contain results for fully symmetric system (all $\lambda_i, i = \overline{1, 3}$ are the same).

Case N = 5. And, finally, consider the case of five queues with $\lambda_1 = 1, \lambda_2 = 2, \lambda_3 = 0.5, \lambda_4 = 6, \lambda_5 = 0.5, b_i^{(1)} = 0.05, s_i^{(1)} = 0.05, i = \overline{1,5}, \varphi^{(1)} = 0.05$. We vary the input intensity by multiplying all λ_i by α which takes values 0.285, 0.714, 1, and 1.143. Thus, the traffic intensity, ρ , varies from 0.2 to 0.8. The results are given in Table 3. The last four lines present results for the fully symmetric system with $\lambda_i = 2$ multiplied by the same values of α .

	A	S	$\Delta, \%$		A	S	$\Delta, \%$
$\lambda_1 = 2.5$	0.342	0.365	6.3	$\lambda_1 = 4.375$	0.658	0.698	5.7
$\lambda_2 = 6$	0.335	0.361	7.2	$\lambda_2 = 10.5$	0.781	0.834	3.0
$\lambda_3 = 0.5$	0.410	0.440	6.8	$\lambda_3 = 0.875$	0.778	0.805	3.4
Symmetric system							
$\lambda_i = 3, i = \overline{1,3}$	0.387	0.382	1.3	$\lambda_i = 5.25, i = \overline{1,3}$	0.702	0.771	8.9

Table 2. System with three queues

		A	S	$\Delta, \%$			A	S	$\Delta, \%$
$\alpha = 0.285$ $\rho = 0.2$	$W_1^{(1)}$	0.203	0.220	7.7	$\alpha = 1$ $\rho = 0.7$	$W_1^{(1)}$	0.714	0.672	6.2
	$W_2^{(1)}$	0.199	0.215	7.4		$W_2^{(1)}$	0.661	0.618	7.0
	$W_3^{(1)}$	0.205	0.222	7.7		$W_3^{(1)}$	0.776	0.738	5.1
	$W_4^{(1)}$	0.197	0.203	3.0		$W_4^{(1)}$	0.705	0.679	3.8
	$W_5^{(1)}$	0.205	0.224	8.5		$W_5^{(1)}$	0.776	0.745	4.2
$\alpha = 0.714$ $\rho = 0.5$	$W_1^{(1)}$	1.036	0.974	6.4	$\alpha = 1.143$ $\rho = 0.8$	$W_1^{(1)}$	0.374	0.398	6.0
	$W_2^{(1)}$	0.353	0.370	4.6		$W_2^{(1)}$	0.967	0.934	3.5
	$W_3^{(1)}$	0.393	0.419	6.2		$W_3^{(1)}$	1.153	1.080	6.8
	$W_4^{(1)}$	0.340	0.355	4.2		$W_4^{(1)}$	1.152	1.120	2.9
	$W_5^{(1)}$	0.393	0.422	6.9		$W_5^{(1)}$	1.153	1.090	5.8
Symmetric system									
$\rho = 0.2$	$W_i^{(1)}$	0.207	0.216	4.2	$\rho = 0.7$	$W_i^{(1)}$	0.759	0.686	10.6
$\rho = 0.5$	$W_i^{(1)}$	0.455	0.391	16.4	$\rho = 0.8$	$W_i^{(1)}$	1.003	1.040	3.6

Table 3. System with five queues

The results for non-symmetric service ($b_1^{(1)} = 0.07, b_2^{(1)} = 0.015, b_3^{(1)} = 0.1, b_4^{(1)} = 0.025, b_5^{(1)} = 0.4$) are given in Table 4.

Below, we discuss the results in brief. For the symmetric systems with $N = 2$ and $N = 3$, the relative error of comparison grows as the traffic intensity ρ grows. But the situation is different in case $N = 5$: the approximate and simulation results coincide up to 5% for low and high traffic intensity, but for $\rho = 0.5$ and $\rho = 0.7$, the error becomes unacceptable (grater than 10%). For the system with five queues, the dependence of the relative error on the total traffic intensity, or the traffic intensity to a queue, is not well-understood. In case of non-symmetric system with five queues (Tables 3 and 4), the results can not be well explained. In case of non-symmetric input of customers (Table 3), the coincidence gets better as ρ increases, but when we make the service non-symmetric (Table 4), it holds only for queues with relatively high traffic intensities, namely, queues 4 and 5, as long as the results for the rest of queues behave the different way (the relative error grows as the values of $\rho_i, i = \overline{1,3}$, grow). Note that in Table 3, the results for queues 3 and 5 have to be the same as the queues are identical but the simulation results differ up to 1%, which is the simulation error.

		A	S	$\Delta, \%$			A	S	$\Delta, \%$
$\alpha = 0.4,$ $\rho = 0.2$	$W_1^{(1)}$	0.251	0.250	0.4	$\alpha = 1,$ $\rho = 0.5$	$W_1^{(1)}$	0.570	0.506	12.7
	$W_2^{(1)}$	0.248	0.244	1.6		$W_2^{(1)}$	0.535	0.475	12.7
	$W_3^{(1)}$	0.251	0.254	1.2		$W_3^{(1)}$	0.592	0.548	7.9
	$W_4^{(1)}$	0.244	0.228	7.0		$W_4^{(1)}$	0.516	0.455	13.4
	$W_5^{(1)}$	0.223	0.254	12.2		$W_5^{(1)}$	0.538	0.559	3.8
$\alpha = 0.6,$ $\rho = 0.3$	$W_1^{(1)}$	0.318	0.314	1.3	$\alpha = 1.4,$ $\rho = 0.7$	$W_1^{(1)}$	1.016	0.902	12.6
	$W_2^{(1)}$	0.311	0.302	3.0		$W_2^{(1)}$	0.901	0.831	8.4
	$W_3^{(1)}$	0.322	0.325	0.9		$W_3^{(1)}$	1.095	0.994	10.2
	$W_4^{(1)}$	0.305	0.281	8.5		$W_4^{(1)}$	0.938	0.896	4.7
	$W_5^{(1)}$	0.281	0.325	13.5		$W_5^{(1)}$	1.082	1.080	0.2

Table 4. System with five queues and non-symmetric service

To complete the numerical analysis, we compare two polling schemes in the system working in "data collection" mode described in Section 2.5. The comparison is based on the radio cell model with parameters $N = 4$, input intensities $\lambda_1 = \lambda_2 = 1500, \lambda_3 = \lambda_4 = \lambda$ take values from 1 to 200 with step 10, mean service times are $b_1^{(1)} = b_2^{(1)} = b_4^{(1)} = 1/4500, b_3^{(1)} = 1/3000$ and the mean switch-over times are $s_1^{(1)} = s_2^{(1)} = s_3^{(1)} = s_4^{(1)} = 1/1500$. The obtained results are shown on Fig. 1. The figure shows that adaptive dynamical polling can make significant profit when some stations have light traffic, since the waiting times are the same for classical cyclic polling system and one with adaptive polling in case of heavy traffic.

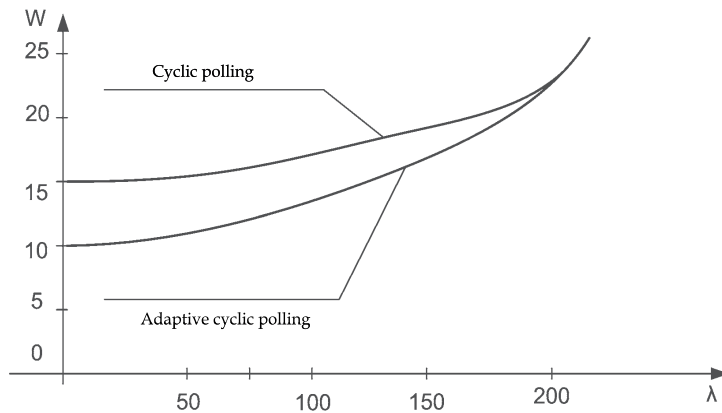


Fig. 1. The dependence of the mean waiting time on λ under the adaptive cyclic polling

4. System with exhaustive threshold service

In this Section, we present the polling system modelling a radio-cell working in the "last mile" mode as described in Section 2.5. We consider the polling system described in Section 3, but we assume that the service at a queue is exhaustive (the queue is served until empty).

The server visit a queue only if the queue length exceeds the given threshold (k_i for queue i), $k_i \geq 0, i = \overline{1, N}$. Before starting service at the queue i , the server needs a random time exponentially

distributed with the parameter s_i to prepare for work. This time can be considered the time to switch to queue i which is incurred only if the queue is served. The queue also has a finite waiting space h_i ($h_i \geq k_i$).

The service time in queue i is exponentially distributed with parameter μ_i , $i = \overline{1, N}$. The queue is served until it becomes empty, then the server moves to the nearest queue which has the sufficient number of customers (having reached its threshold). If the numbers of customers in all queues are insufficient to get service (less than k_i for queue i), the server stops polling until the number of customers in any queue reaches the threshold.

4.1 Stationary distribution of the system states and the performance characteristics

A system state at an arbitrary time t in a steady-state is presented by a random process

$$\xi(t) = (m(t), i(t), \mathbf{n}(t)), \quad t \geq 0,$$

where $m(t) = 0$, if at time t the server is idle, $m(t) = 1$, if at time t the server switches to a queue, $m(t) = 2$, if at time t the server serves the customers, $t \geq 0$; $i(t)$ is the number of queue which server is attended at time t , $i(t) = 0$, if the server is idle; $\mathbf{n}(t)$ is a vector

$$\mathbf{n}(t) = (n_1(t), n_2(t), \dots, n_N(t)),$$

$n_j(t)$ is the number of customers at queue j at time t , $j = \overline{1, N}$.

The stochastic process $\xi(t)$, $t \geq 0$, is Markovian. Introduce the stationary state probabilities of the process $\xi(t)$, $t \geq 0$ for $\mathbf{r} = (r_1, r_2, \dots, r_N)$, $i = \overline{1, N}$,

$$a(\mathbf{r}) = \lim_{t \rightarrow \infty} P\{m(t) = 0, i(t) = 0, \mathbf{n}(t) = \mathbf{r}\}, 0 \leq r_m < k_m, m = \overline{1, N},$$

$$p_i(\mathbf{r}) = \lim_{t \rightarrow \infty} P\{m(t) = 1, i(t) = i, \mathbf{n}(t) = \mathbf{r}\}, r_m = \overline{0, h_m}, m = \overline{1, N}, m \neq i, r_i = \overline{k_i, h_i},$$

$$q_i(\mathbf{r}) = \lim_{t \rightarrow \infty} P\{m(t) = 2, i(t) = i, \mathbf{n}(t) = \mathbf{r}\}, 0, \overline{h_m}, m = \overline{1, N}, m \neq i, r_i \in \overline{1, h_i}.$$

The balance equations for the stationary probabilities are

$$\lambda a(\mathbf{r}) = \sum_{j=1}^N \lambda_j a(\mathbf{r} - \mathbf{e}_j) I_{\{r_j > 0\}} + \sum_{j=1}^N \mu_j q_j(\mathbf{r} + \mathbf{e}_j) I_{\{r_j = 0\}}, \quad r_1 < k_1, \dots, r_N < k_N, \quad (21)$$

$$\left(\sum_{m=1}^N \lambda_m I_{\{r_m < h_m\}} + \mu_i \right) q_i(\mathbf{r}) = \sum_{j=1}^N \lambda_j q_i(\mathbf{r} - \mathbf{e}_j) I_{\{r_j > \delta_{ij}\}} + \mu_i q_i(\mathbf{r} + \mathbf{e}_i) I_{\{r_i < h_i\}} + s_i p_i(\mathbf{r}) I_{\{r_i \geq k_i\}}, \quad (22)$$

$$\left(\sum_{m=1}^N \lambda_m I_{\{r_m < h_m\}} + s_i \right) p_i(\mathbf{r}) = \sum_{j=1}^N \lambda_j p_i(\mathbf{r} - \mathbf{e}_j) I_{\{r_j > k_i \delta_{ij}\}} + \mu_{i-1} q_{i-1}(\mathbf{r} + \mathbf{e}_{i-1}) I_{\{r_{i-1} = 0\}} + \quad (23)$$

$$+ \lambda_i a(r_1, \dots, r_{i-1}, k_i - 1, r_{i+1}, \dots, r_N) I_{\{r_1 < k_1, \dots, r_{i-1} < k_{i-1}, r_i = k_i, r_{i+1} < k_{i+1}, \dots, r_N < k_N\}} +$$

$$+ \sum_{j=1}^{i-2} \mu_j q_j(\mathbf{r} + \mathbf{e}_j) I_{\{r_j = 0, r_{j+1} < k_{j+1}, \dots, r_{i-1} < k_{i-1}\}} +$$

$$+ \sum_{j=i+1}^N \mu_j q_j(\mathbf{r} + \mathbf{e}_j) I_{\{r_j = 0, r_{j+1} < k_{j+1}, \dots, r_N < k_N, r_1 < k_1, \dots, r_{i-1} < k_{i-1}\}},$$

$$0 \leq r_m \leq h_m, \quad m = \overline{1, N}, \quad m \neq i, \quad k_i \leq r_i \leq h_i, \quad i = \overline{1, N}.$$

By replacing one of the equations of system (21)–(23) by normalization condition

$$\sum_{\mathbf{r} \in \Lambda} a(\mathbf{r}) + \sum_{i=1}^N \sum_{\mathbf{r} \in \Pi_i} q_i(\mathbf{r}) + \sum_{i=1}^N \sum_{\mathbf{r} \in \chi_i} p_i(\mathbf{r}) = 1,$$

with $\Lambda = \{(r_1, \dots, r_N) : r_m < k_m, m = \overline{1, N}\}$, $\Pi_i = \{(r_1, \dots, r_N) : 0 < r_i \leq h_i, 0 \leq r_m \leq h_m, m = \overline{1, N}, m \neq i\}$, $\chi_i = \{(r_1, \dots, r_N) : k_i \leq r_i \leq h_i, 0 \leq r_m \leq h_m, m = \overline{1, N}, m \neq i\}$, $i = \overline{1, N}$, we get a system of equations for $\sum_{i=1}^N (2h_i - k_i + 1) \prod_{j=1, j \neq i}^N (h_j + 1) + \prod_{j=1}^N k_j$ unknowns.

Having calculated the stationary state distribution, we can readily derive the following performance characteristics:

1. Mean length of queue j at time when queue i is served (excluding a customer being served): $L_j^i = \sum_{\mathbf{r} \in \Pi_i} (r_j - \delta_{ij}) q_i(\mathbf{r})$, $i, j = \overline{1, N}$;
2. Mean length of queue j at time when the server switches to queue i : $S_j^i = \sum_{\mathbf{r} \in \chi_i} r_j p_i(\mathbf{r})$, $i, j = \overline{1, N}$;
3. Mean length of queue j at time when the server is idle: $U_j = \sum_{\mathbf{r} \in \Lambda} r_j a(\mathbf{r})$, $j = \overline{1, N}$;
4. Mean length of queue j at arbitrary time: $L_j = \sum_{i=1}^N (L_j^i + S_j^i) + U_j$, $j = \overline{1, N}$;
5. The mean fraction of time the server is idle: $\bar{a} = \sum_{\mathbf{r} \in \Lambda} a(\mathbf{r})$.

Since the waiting space in the system is limited, some arriving customers can be lost. The probability P_{lost}^j that an arbitrary customer arriving to queue j is lost equals to the probability that an arbitrary time all h_j waiting places are occupied,

$$P_{lost}^j = \sum_{i=1, i \neq j}^N \sum_{\mathbf{r} \in \Pi_i} q_i(\mathbf{r}) I_{\{r_j=h_j\}} + \sum_{i=1}^N \sum_{\mathbf{r} \in \chi_i} p_i(\mathbf{r}) I_{\{r_j=h_j\}}, \quad j = \overline{1, N}.$$

The mean waiting time in queue j can be obtained by Little’s law $W_j = L_j / \lambda_j$.

Consider the model of the broadband wireless network radio cell working in the "last mile" mode with adaptive polling mechanism. The model parameters are the following: $N = 4$, $\lambda_1 = \lambda_2 = 1500$, $\lambda_3 = \lambda_4 = \lambda$ take the values 30, 60, 100. The service intensities $\mu_1 = \mu_3 = \mu_4 = 4500$, $\mu_2 = 3000$, the intensities of switching between queues $s_1 = s_2 = s_3 = s_4 = 1500$. The Fig. 2 shows the dependence of the frame mean waiting time on the threshold value $k_i = k$ ($i = \overline{1, 4}$) assumed to be the same for all the queues. We see that the optimal value k varies from curve to curve. The less the queues are loaded the greater the k minimizing the mean waiting time. If the system has queues with low traffic it is reasonable to increase their service thresholds. As a result, the frame mean waiting time in queues with low traffic increases but it decreases for queues with high traffic so it can reduce the weighted sum of the mean waiting times in the system. The optimal threshold choosing can be a troublesome problem in practise since the threshold value depends on the relation between numbers of stations with light traffic and heavy traffic, station parameters, etc.

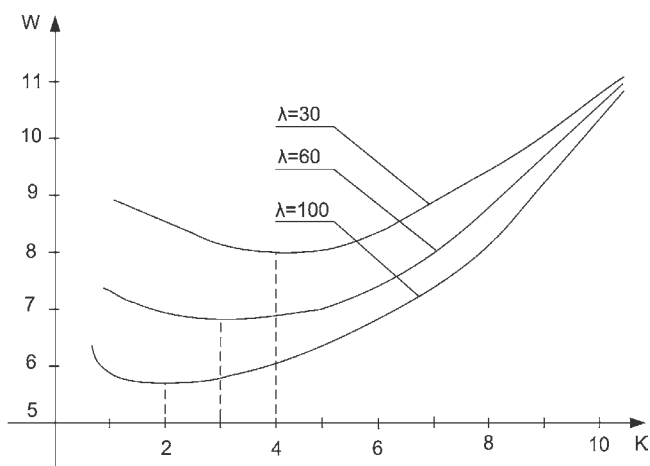


Fig. 2. The dependence of the mean waiting time on the threshold

5. References

- Borst, S.C. (1996). *Polling Systems*, Stichting Mathematisch Centrum, ISBN 90-6196-467-9, Amsterdam.
- IEEE Std 802.11-2007. Part 11: Wireless LAN Medium Access Control (MAC) and Physical Layer (PHY) Specifications, June 2007.
- Kazimirsky, A. (2002). On approximation of arrival flows with MAPs of order two, *Proceedings of IST'2002*, pp. 35-40, Minsk, November 2002. (in Russian)
- Kuczma, M. (1968). *Functional Equations in a Single Variable*, Polish Scientific Publishers, Warsaw.
- Levy, H. & Sidi, M. (1990). Polling systems: applications, modeling and optimization. *IEEE Transactions on Communications*, 38, 1750-1760. ISSN 0090-6778.
- Schriber, T.J. (1974). *Simulation Using GPSS*, John Wiley & Sons.
- Sumita, S. (1988). Performance analysis of interprocessor communications in an electronic switching system with distributed control. *Performance Evaluation*, 9, 83-91, ISSN 0166-5316.
- Takagi, H. (1986). *Analysis of Polling Systems*, MIT Press, Cambridge, ISBN 978-0262200578.
- Takagi, H. (1991). *Queueing Analysis: A Foundation of Performance Evaluation*, Vol. 1, North-Holland, ISBN 978-0444817709.
- Vishnevsky, V.M. (2000). Wireless networks for broadband access to the Internet. *Elektrosvyaz'*, 10, 9-13, ISSN 0013-5771. (in Russian)
- Vishnevsky V.M. & Frolov, S.A. (2009). Application for an invention No. 2007136908 of 03.02.2009 "Method of development of the very high throughput broadband wireless mesh networks".
- Vishnevskii, V.M. & Semenova, O.V. (2006). Mathematical methods to study the polling systems. *Automation and Remote Control*, 67, 173-220, ISSN 0005-1179.

- Vishnevskii, V.M. & Semenova, O.V. (2007). *Polling Systems: Theory and Applications for Broadband Wireless Networks*, Moscow, Technosphaera, ISBN 978-5-94836-166-6. (in Russian)
- Vishnevsky, V.M.; Portnoy, S.L. & Shakhnovich, I.V. (2009). *Encyclopaedia WiMAX. Way to 4G*, Moscow, Technosphaera. (in Russian)

Next Generation Optical Access Networks: from TDM to WDM

Ll. Gutierrez¹, P. Garfias¹, M. De Andrade¹,
C. Cervelló-Pastor¹ and S. Sallent²

*Technical University of Catalonia (UPC)¹ and i2cat Foundation²
Spain*

1. Introduction

Network infrastructure plays a key role in the success of added services and in user satisfaction. It is widely accepted that Passive Optical Networks (PON) are the most promising, cost-effective, and high-performance access network solutions. Access networks are also commonly referred to as either 'the last mile' by the operators, or 'the first mile of the network' in IEEE terminology. The term 'mile' is often related to the path portion that is used to reach the user from a network node, however access networks go as far as 20 km depending on the technology used.

An access network comprises connections between different subscribers and a Central Office (CO), which is attached to the metro or core network. The wired technology deployed varies significantly from one country to another, i.e. Digital Subscriber line (xDSL), based on copper wires; Hybrid Fiber-coax (HFC), and optical fiber.

The trends for Next Generation Access Networks (NGA) based on PON are: Wavelength Division Multiplexing (WDM), 10 Gb/s or more, and longer reach/higher splits. NGA must be able to cope with challenges, such as delivering diverse broadband services and facilitating the integration of different technologies. Moreover, NGA should provide higher bandwidths or further reduce the cost of existing delivering services, and serve as backhaul of wireless access networks (WiFi, WiMAX). The last one constitutes a relevant issue for the convergence between wireless and wired technologies.

1.1 Optical access networks - Fiber-to-the -x

Single-mode fiber's properties, such as low loss and extremely wide inherent bandwidth, make it the ideal candidate to meet the capacity challenges for today's and for the foreseeable future. This kind of fiber is often used in core and metropolitan networks, and nowadays their penetration in the access domain is increasing as well (Koonen, 2006).

The Passive Optical Network (PON) is the most interesting solution, basically because there is no active equipment installed in the field - a very satisfying feature for incumbent operators, and also because the equipment and the feeder fibers are shared amongst users.

The application of PON technology to provide broadband connectivity to subscribers in the access network is called fiber-to-the-x (FTTx). Depending on how deep the fiber penetrates into the first mile, FTTx can be classified as: FTTB (Business/Building), FTTC/Cab (Curb/Cabinet), FTTN (Neighborhood/Node), FTTP (Premises), and FTTH (Home). There is no final agreement in the terminology to be used all over the world, but the most common terms in the market are: FTTN/B and FTTH. The FTTN/B describes a PON where the fiber arrives directly from the CO to the building (or business premises) and the signal is converted and carried to the user dependencies by using copper or coaxial cables. Figure 1 depicts a FTTN/B, where the optical signal is converted to electrical signal in the very last mile of the network, and then is carried by means of a vDSL network up to the subscriber's premises.

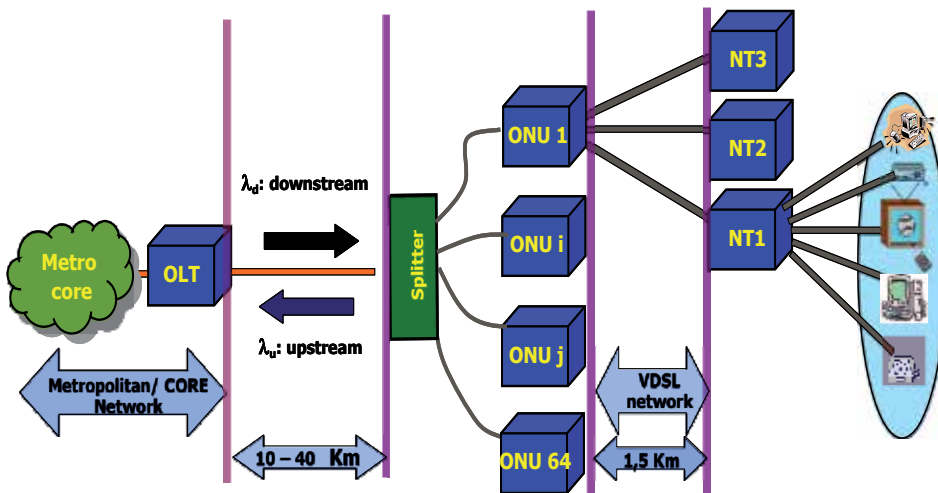


Fig. 1. FTTN/B network

FTTH refers to the reach of the fiber wire till the subscriber premises. It consists of an Optical Line Termination (OLT) at the service provider's CO, and a number of terminals near the end-user's device called Optical Network Unit (ONU) or Optical Network Terminal (ONT). PON can use single or multiple fibers for upstream and downstream traffic, with or without WDM, being a single fiber-single channel tree the most common topology [Figure 1].

The downstream channel is a broadcast channel, and the upstream channel is often shared amongst users' devices – their access must be arbitrated in order to avoid collisions amongst stations. Each ONU transmits a burst of data that cannot be interfered by any other burst sent from another ONU. For that reason, users' bursts are separated by a configurable guard-time. Such single full-duplex channel-single fiber solutions are commonly referred to as TDM-PON.

The worldwide market reflected that, by the end of 2008, PON networks, mainly FTTB/N and FTTH, were deployed on a large scale in Asia (78.5%) - APAC countries - and North America (13.5%). The market in Europe was far behind that of the APAC countries or America, scoring about 8%. However, there are many initiatives that aim to deploy PON

networks all around and it is expected that such deployment will even grow faster in a short period of time in Europe. (Lakic & Hajduczenia, 2007).

2. Legacy TDM-PON

Two main FTTH-PON standards are currently deployed around the world: Ethernet-based PON (EPON), approved in 2004 (IEEE 802.3ah, 2004); and Gigabit-capable PON (GPON), born in 2003 (ITU-T G.984.[1-4], 2003). In both solutions, the equipment installed in the field is fully passive, covering distances of up to 20 km, using a point-to-multipoint topology, providing wider bandwidth to the end user, and allowing video broadcasting (digital and/or analogue). The split-ratio (users per fiber) is variable – commonly, an average of 32 to 64 users.

In fact, the basic physical features for both standards are very similar – what makes them more different is the MAC protocol and the data encapsulation scheme. While EPON carries bursts of pure Ethernet frames, GPON encapsulates data using Generic Encapsulation Method (GEM). Fair and efficient bandwidth allocation to users is a key issue that is out of the scope of the standards.

2.1 The EPON standard: IEEE 802.3ah - Ethernet in the First Mile

The EPON is a point-to-multipoint network, whose topology is basically a single fiber-single channel tree. The bit rate is symmetric, up to 1 Gb/s – therefore, the maximum bandwidth allocated to each ONU is typically around 70 Mb/s, though it depends on the number of active ONUs and the users’ traffic profiles. The EPON standard focuses on defining the physical and the MAC layer as shown in Figure 2. In (Kramer, 2005) the author explains such standard deeply.

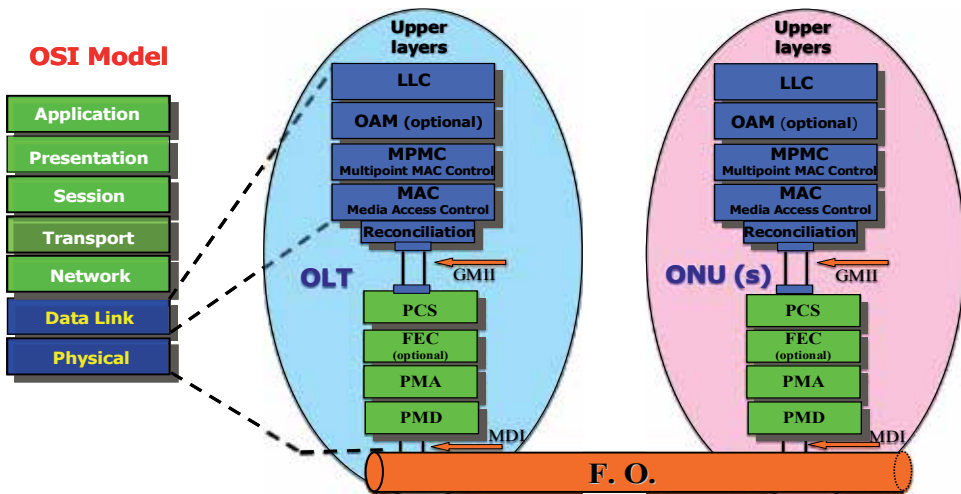


Fig. 2. architecture model of an EPON

Ethernet frames cannot be segmented before their transmission in an EPON. Therefore, the transmission of a frame will be deferred to the next cycle in case it does not fit in the current

assigned timeslot. The guard-time between bursts and the segmentation-less feature has a considerable impact on the network performance.

EPONs are composed by two types of active terminals: the OLT and the ONU. The signal is split by a passive optical splitter at the far end of the network. It is also possible to cascade the splitters, but it would lead to additional power losses. In such cases, it is important to consider that the optical power budget (power loss across the network path) should not be overtaken. In general, it can be said that the more passive devices taken in the network trunk, the less split ratio and/or the less distance covered.

2.1.1 The MAC layer

The MAC Control Layer is divided in two sublayers: the MPCP (Multi-Point MAC Control) and the Reconciliation sublayer as depicted in Figure 2.

The MPCP is devoted to control the access to the upstream channel amongst the subscribers, perform a discovery process, and allocate bandwidth to each ONU. MPCP is a request-permit protocol. Two main control messages are defined:

- GATE: sent by the OLT to the particular ONU, indicating the time and the bandwidth allocated to it
- REPORT: sent by the ONU to the OLT, indicating the queues occupation in order to request bandwidth for the next cycle

In each cycle, every ONU is polled, so that a REPORT message must be sent to the OLT even if its queues are empty and no bandwidth is requested. Moreover, the OLT periodically sends control messages to discover new ONUs aiming to join the network – the so-called ‘autodiscovery’ mode.

The algorithm to allocate the bandwidth to each ONU is an important issue to consider. However, attention must be paid to the fact that such algorithm is not defined by the standard – it is instead left open to the implementer. Section 5 is devoted to a brief survey on such algorithms, i.e. the scheduling framework and the allocation computation itself. The efficiency of such mechanism impacts directly the QoS perceived by the user.

2.2 The GPON standard. Gigabit in the access network

GPON was developed by the Full Service Access Network (FSAN) group. It is somehow based on the former ATM access networks (APON, BPON), but GPON’s data encapsulation (GEM) is more generic, and accepts different network protocols, such as ATM, Ethernet and IP.

The GPON is a point-to-multipoint network as well, with two types of active terminals: the OLT and the ONT/ONU. The user’s equipment is called ONT or ONU if no users are directly connected to the device. Finally, the network path itself is known as ODN (Optical Device Network) and it is usually integrated by fiber and a passive optical splitter.

2.2.1 The MAC layer

The basic transmission unit is called T-CONT (Transmission Container). The bandwidth is guaranteed by allocating timeslots to the ONU in order to transport the T-CONT of each communication. The bandwidth allocation algorithm is also of the request-permit type and it is performed at the OLT. The ONU requests bandwidth each cycle, and the OLT allocates

the guaranteed transmission window in the cycle to each active ONU. Two operations modes are possible:

- SR (Status Reporting)-DBA, where the ONU requests bandwidth to the OLT;
- and NSR (Non Status Reporting)-DBA, where the OLT monitors the incoming traffic flows but no information is sent to the OLT from the ONUs.

2.2.2 Service provisioning

The GPON standard specifies the services supported more accurately. They match very closely those defined in ATM networks:

- Asymmetric: Digital broadcast services, VOD, file download, etc.
- Symmetric: e-mail, file exchange, distance learning, telemedicine, etc.
- Synchronous: POTS, ISDN and circuit emulation (E1, T1). Such service is typically of the narrow band but more strict and time bounded.

2.3 Comparison amongst both standards

A summary of both standards is shown in Table 1. There is a common concern that the ATM-oriented technology – BPON, GPON – performs very well when the traffic is of the real time and emulation service, i.e. T1/E1 type; while Ethernet-oriented networks perform better when the traffic is mostly composed by pure data applications, i.e. Internet. Nonetheless, it is not so simple to make a definitive statement about the performance, mainly because the data collected depends on many parameters, and more importantly, on the implementation. Reference (Hajduczenia et al., 2007) concludes that in comparable system set-ups, GPON performs slightly better than EPON, but it is not yet a definitive statement.

Item		ITU G.984	IEEE 802.3 ah
MAC Layer	Service	Full services (Ethernet, TDM, POTS)	Ethernet data
	Frame	GEM frame	Ethernet frame
PHY Layer	Distance	10 / 20 km (logical: 60 km)	10 / 20 km
	Split ratio	64 (logical: 128)	64 max.
	Upstream (bit rate)	155 Mb/s, 622 Mb/s, 1.25 Gb/s	1.25 Gb/s
	Downstream (bit rate)	1.25 Gb/s, 2.5 Gb/s	1.25 Gb/s
	Bandwidth	Same as above (NRZ coding)	1Gbit/s (8B10B coding)
	Opt. Loss	15 / 20 / 25 dB	15 / 20 dB
	Wave-length	Down : 1480-1500 nm Up : 1260-1360 nm	Down : 1480-1500 nm Up : 1260-1360 nm
Efficiency	95%	89%	

Table 1. Comparison between legacy GPON and EPON

From the table above, it is important to remark that the power budget limits drastically the range of the network and the split ratio, which is typically 64 or less in both standards.

2.4 Summary

EPON is a natural extension of the LAN systems – it bridges the gap between the LAN and Ethernet based MAN/WAN structures. GPON, on the other hand, uses a novel encapsulation mechanism, GEM. It is important to emphasize that the GPON has the ability to fragment and reassemble frame fragments, including Ethernet frames. The upstream channel format shown by both standards is depicted in Figure 3(a) and (b).

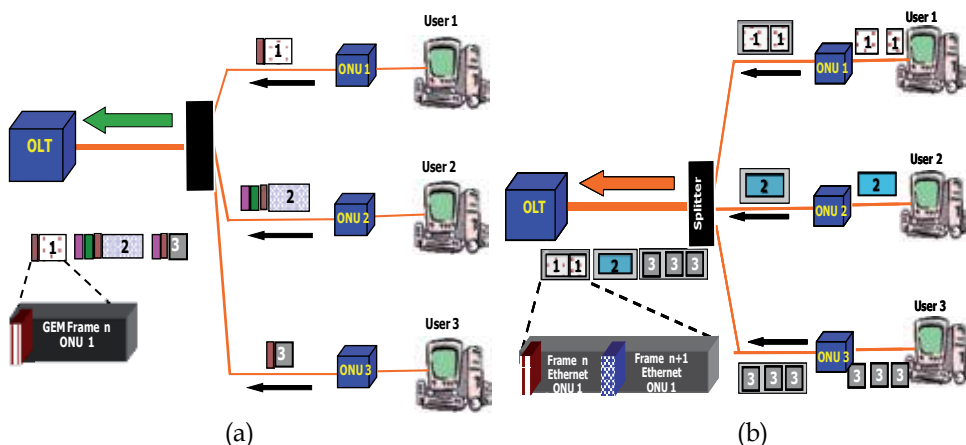


Fig. 3. Upstream channel transmission (a) GPON. (b) EPON

Optical devices determine the resulting system price. EPON hardware parameters are very relaxed, and therefore are more cost effective. On the other hand, GPON systems, due to their more strict hardware requirements, are more expensive.

Moreover, EPON networks are widely deployed in the APAC regions – by the end of March 2007 there were approximately 8 million subscriber ports and 16 million CO port capacity deployed, while GPON networks was mainly on the trial phase (Hajduczenia et al., 2007). In contrast, other reports predict that GPON will overtake EPON as the pre-dominant technology in a short or mid term. Some equipment manufacturers have announced the introduction of a new family of GPON integrated access device (IAD) semiconductors that are expected to offer high levels of integrations and better throughput performance.

The growth rate of PON deployments are of the order of 3 to 4 million subscriber ports every 6 months, mainly in the APAC countries (Japan, Korea, China, etc.); GPON is expected to grow first in Europe.

3. Next Generation Access networks (NGA)

Technological advances, especially in optical transmission devices, boost the upgrading of current TDM-PON to the NGA. Benefits expected are (Heron et al., 2009):

- High Capacity, up to several gigabits per seconds
- Increased reach, allowing to include more homes and/or to reduce the number of COs
- Wireless and wireline integration, with wireless nodes deployed deeper in the network

- Operation improvement, broadband services or evolved existent services
- Moreover, NGA are more cost-effective than the current ones, specially because CAPEX and OPEX are significantly reduced.

The 10G-EPON standard (IEEE 802.3av) was approved on September 2009, whereas the schedule for the 10G GPON is to be approved in 2010.

3.1 Next Generation 10G EPON. IEEE 802.3av

The next-generation TDM-EPON is upgraded up to 10 Gb/s by the IEEE 802.3av standard. The standard pursues the objectives listed below:

- To support subscriber access networks using point-to-multipoint topologies.
- To standardise two different single mode (SM) fiber data rate channels: symmetric - 10 Gb/s both down and up; and asymmetric - 10 Gb/s in the downstream channel and 1 Gb/s in the upstream channel.
- To have a BER better than 10^{-12} at the PHY service interface.
- To define up to 3 optical power budgets that support split ratios of 1:16 and 1:32, and distances of at least 20 km.
- To maintain a complete backward compatibility with legacy standards.

The goal is to upgrade the channel capacity for both upstream and downstream channels gracefully, while maintaining the logical layer intact, taking advantage of the already existing MPCP and DBA agent specifications. Moreover, 10G-EPON keeps on utilizing the analog video delivery systems before such delivery shifts gradually to an IP-based distribution system.

3.1.1 The 10G EPON. Physical layer

In this section, the main enhancements of the PHY layer are briefly explained. Table 2 illustrates the acronyms used to designate the new EPON power budgets:

Power Budget class	Power insertion loss	Downstream	Upstream	Split -ratio	Range (Km)
PR10	20 dB (low)	10 Gb/s	10 Gb/s	1:16	10
PR20	24 dB (medium)	10 Gb/s	10 Gb/s	1:16 (1) 1:32 (2)	20 (1) 10 (2)
PR30	29 dB (high)	10 Gb/s	10 Gb/s	1:32	20
PRX 10	20 dB (low)	10 Gb/s	1 Gb/s	1:16	10
PRX20	24 dB (medium)	10 Gb/s	1 Gb/s	1:16 (1) 1:32 (2)	20 (1) 10 (2)
PRX30	29 dB (high)	10 Gb/s	1 Gb/s	1:32	20

Table 2. 10G EPON acronyms and Power Budget classes

Notice that the physical-medium-dependent (PMD) and Power-Budget-Class (PBC) naming nomenclature for 10 Gb/s EPONs, is different than those for legacy EPON. Table 3 illustrates the differences between legacy TDM- EPON and 10G EPON in detail.

3.1.2 Wavelength allocation

The downstream 1 Gb/s and 10 Gb/s data streams will be WDM overlaid thus creating indeed two independent P2MP domains.

- The 1 Gb/s downstream link remains centered at 1490 ± 10 nm
- The 10 Gb/s downstream link uses 1575-1580 nm wavelength band.

	1G EPON	10G EPON
channel coding	8B10B	64B66B
Data rate (DS / US)	1 Gb/s 1 Gb/s symmetric	- 10 Gb/s 10 Gb/s symmetric - 10 Gb/s 1 Gb/s asymmetric
Upstream (λ)	1260 - 1360 nm	1260 - 1280 nm
Downstream (λ)	1480 - 1500	1575 - 1580
# of PBC	2	3
Split ratio	1:16	1:16 / 1:32
FEC	RSS (255,239) (optional)	RS (255,223) (mandatory)

Table 3. Differences between 1G and 10G EPON

For the symmetric line-rate scenario, WDM channel multiplexing in the upstream channel is discouraged due to increased cost for the ONU. The 10-Gb/s upstream channel will use the optical window centered at 1310 nm, which is the currently the allocated window for 1 Gb/s upstream channel.

The OLT should operate in a dual rate mode; therefore, an overlay dual stack structure will need to be implemented from the PMD up to the Reconciliation sublayer. An OLT supporting both downstream channels may multiplex the outputs of two transmitters using DWDM coupler, while the optical filters at an ONU are tuned to receive one downstream wavelength.

3.1.3 The 10G EPON MAC layer. The MPCP protocol

The MPCP protocol is essentially the same in both 1G and 10G EPON networks. It should also be considered that, for the coexistence of various line rates, the DBA in the OLT will be responsible for scheduling not one but two mutually cross-dependent EPON systems, sharing a single upstream channel but expecting only minor changes to the MPCP protocol. As in legacy TDM-PONs, the DBA is out of the scope of the IEEE802.3av standard, and thus left vendor-dependent.

3.2 Next Generation 10G GPON (NG-GPON)

The FSAN Group has been very active in upgrading the legacy GPON. The basic requirement of NG-GPON is to offer higher capacities than GPON while maximizing the re-use of protocols, components and infrastructure. It is mandatory to maintain the compatibility and the coexistence with the legacy GPON systems already deployed. Such upgrade will focus mainly on the physical layer - upgrading the rate to 10 Gb/s - but also on the optimization of Ethernet service delivery.

3.2.1 Wavelength allocation

To reach such goal the ITU community first developed the standard G.984.5 (ITU-T G.984.5, 2007) to reserve wavelengths for the next-generation applications. Summarizing, the G.984.5 entails:

- Wavelength ranges to be reserved for future use. Service signals are overlaid via WDM on an operating GPON system. Three optional enhancement bands (options 1, 2 and 3) are specified as depicted in Figure 4.
- Blocking filters to be supported at GPON ONT/ONU to ensure that next-generation ONUs could be installed on currently deployed GPON, side by side with legacy GPON ONT/ONU.
- GPON upstream wavelength reduction options, to free spectrum in the O band for future services.
- And of course, allowing operators to gradually migrate from a working GPON ONT/ONU to a NG-GPON ONT/ONU without disrupting existing customers.

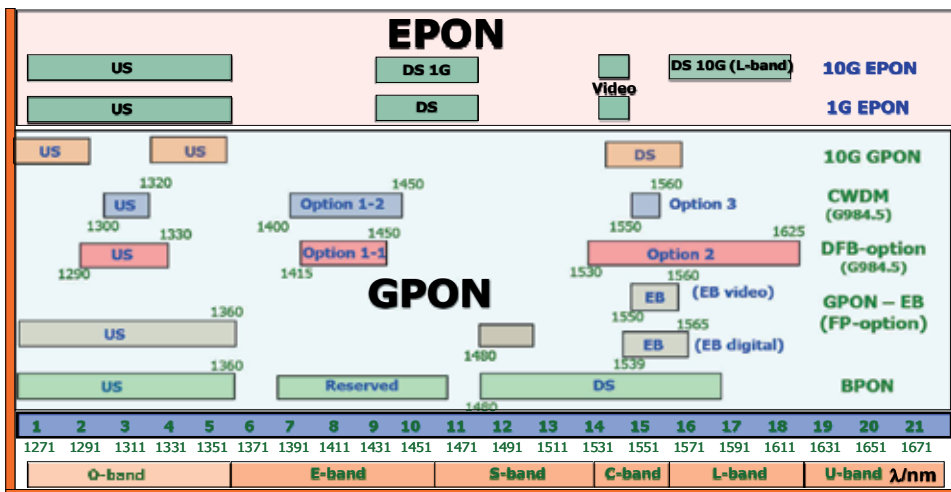


Fig. 4. Joint wavelength allocation proposals of 10G EPON and 10G GPON

3.2.2 10G GPON evolution

Two evolution stages will compose GPON evolution: in the first step, NG-GPON1 (expected in year 2010) will be fully compatible with legacy GPON. Its two expected goals are:

- A GPON supporting 10 Gb/s downstream, and 2.5 Gb/s upstream (referred to as XGPON1).
- A GPON supporting symmetric service, 10 Gb/s downstream, and 10 Gb/s upstream (referred to as XGPON2).
- A WDM option to overlay multiple GPONs and/or point-to-point overlays with different wavelengths (i.e. WDM) on the same fiber infrastructure.

NG-GPON1 stage will be compliant with G984.5, therefore GPON legacy ONTs/ONUs could be replaced one by one by new 10G GPON ONTs/ONUs or even added to an existent ODN.

Some voices propose a WDM-PON as an alternative solution to avoid the technical hurdles of the NG-GPON. Among others, WDM-PON has clear advantages because it combines the traditional PON low infrastructure cost, with the use of “colorless” optics, thus reducing management complexity.

Finally, the second step called NG-GPON2 is expected to come later (by 2015). It aims to develop a new GPON (probably disruptive) that does not require coexistence with Legacy service. Other technologies may be considered, like higher line rate, DWDM, OFDM, and others (Kani et al., 2009).

3.3. 10G EPON/GPON convergence

Finally, the xPON industry supports the development of a framework that will allow 10G PON standard networks to converge. Such goal is extremely interesting in order to reduce costs, thus increasing the 10G PON deployment worldwide.

The convergence may be achieved in two ways:

- Firstly, by aligning the 10G optics of an ITU NG-PON system with the optical layer specification of the emerging IEEE 10G EPON. In fact, optical layer specifications now being used by IEEE are more aligned with ITU optical budget rules than ever.
- Secondly, it will be also possible to develop an open extensible interface to the MAC control channel – for instance, an enhanced interface might be added to the 802.3av systems that allows the convergence with the ITU standards.

4. New Trends: the WDM-PON and Long-reach PON

The new Internet media services, such as symmetrical HD real time applications, videoconferencing, and broadcast, among others, followed by the new type of communications, like point-to-point or multipoint-to-point, increase drastically the end-user bandwidth demand. This bandwidth has an exponential growth that should cope with deployments of next generation optical access networks. The evolution of legacy PON technologies (GPON/EPON) should provide huge network resources and cost-effective solutions to fulfill the new user applications and network provider demands.

Requirements of Long-Reach NGA are listed below:

- Extend the geographical reach to a minimum of 100 Km
- Increase the split ratio up to 128 or more, reducing the cost per subscriber
- Increase the downlink and uplink throughput (evolution to 10 Gb/s)
- Be transparent or compatible as much as possible with current legacy PONs
- Reduce the CAPEX and OPEX (operation, deployment, and maintenance).

Finally, it is also desirable for NGAs to be deployed in a reasonable temporal horizon, 2010 to 2015, using available technologies (lasers, APD, amplifiers, new modulation schemes).

Several proposals are being launched by the standardization bodies (mainly ITU and IEEE), as well as research projects and position research papers; however, few approaches cover the previous requirements in their totality. The Long Reach Optical Access Network (LROAN) objective is to increase the reach of Optical Access Network under a common umbrella. It was proposed as an extension of the PLANET ACTS project, developed in the late 90s with a split ratio of 2048 users over 100 Km at 2.5 Gb/s downstream rate, and 311 Mb/s upstream rate (Van de Voorde et al., 2000).

4.1 LR-PON based on the legacy GPON

The recent standard G984.6 (ITU-T G.984.6, 2008) defines a new enhancement of the legacy GPON by extending the optical budget, and thus allowing the deployment of a longer reach and a higher split ratio. The increase of the reach in GPON is achieved using mid-span optical amplifier extenders, transponders or single side extenders.

The amendment allows a mid-span reach extension by adding an active device to the passive ODN (Regenerator or Optical Amplifier) in the fiber link, between the OLT and ONT, achieving a longer range of up to 60 km [see Figure 5].

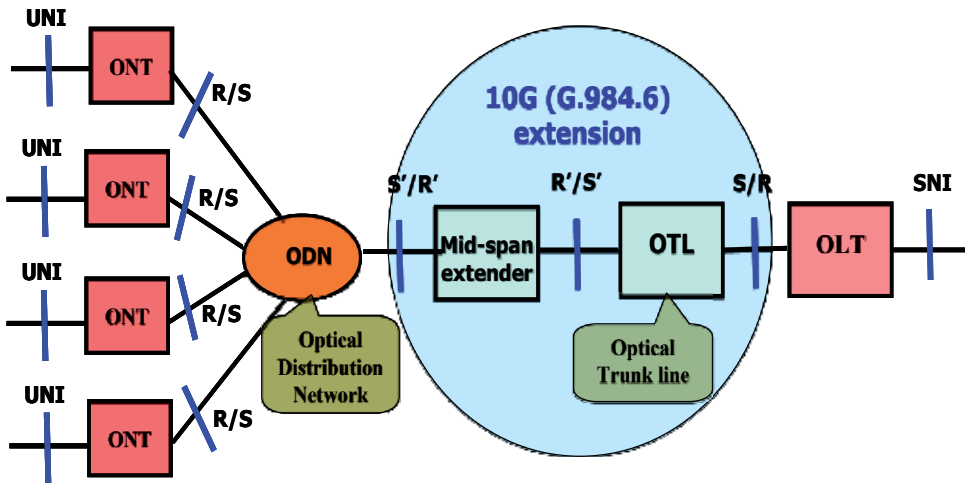


Fig. 5. GPON extension architecture (ITU-T G.984.6, 2008)

The remote OLT is connected with the mid-span extender through an Optical Trunk Line (OTL). In the same way, the ONUs are connected to mid-span using an optical distribution network (ODN) through the R/S and S'/R' interfaces. Reach extended (GPON-RE) adds a long point-to-point trunk line (OTL) to a point-to-multipoint GPON ODN. GPON-RE avoids metro network equipment, installing the OLT in the remote central office. Such proposal reduces the number of central offices, and at the same time it applies the same split independently of their topology and geography, simplifying the OAM operation.

Other approaches should maintain compatibility with existing OLTs to the maximum possible extent. The extension of the reach of the PON or alternatively the split ratio of the PON is penalized by adding an active device, thus converting the existent PON into an active PON.

The reach extender must be compatible with existing GPON 2.4/1.2 Gb/s rated ONT equipment and ODN (power budget class B+). In the past, however, the extender supporting a more capable ODN had already been defined as class C+ in the amendment G.984.2.

The mid-span can be built with SOA amplifiers operating in the O band (1310 nm) and the S band (1490nm). New devices such as wavelength filters and optical filters will be used to extend the reach of the OTL up to 50 km and to increase the loss budget up to 54 dB. Optical amplifiers, however, are expensive and not transparent – therefore, a 3R regenerator is needed. A 3R-RE is composed by OLT and ONT transceivers: it re-amplifies, re-shapes and re-times the signal. Nevertheless, such solution is not compatible with the legacy GPON.

4.2 Long Reach WDM PON

WDM-PON is the application of wavelength-division multiplexing that uses individual wavelength for each PON network. ONUs have light sources at different tuned wavelengths coexisting in the same fiber, increasing the total network bandwidth and the number of users served in the optical access network. Related to communications mode, the WDM-PON may use point-to-point communications, point-to-multipoint (like EPON/GPON trees by each wavelength), or hybrid solutions. In the point-to-point, no dynamic bandwidth allocation mechanisms are needed. The point-to-multipoint uses a WDM/TDM, achieving high resource utilization efficiency.

At the same time, the ONU/ONT in a WDM-PONs are classified as: colorless or colored. In the former one, the optical user terminal is wavelength-seeded from the remote OLT located in the central office, using the same wavelength path for downstream and upstream channels. In this case, the upstream optical flow is modulated using FSK, inverse return-to-zero (RZ), or intensity modulation (IM) (Shea & Mitchell, 2009), (Martinez et al., 2008). Such device is the preferred one because network management is gracefully reduced.

The splitter is replaced by a wavelength selective filter implemented with an arrayed waveguide grating (AWG) when the ONU is color-sensitive and the communication mode is of the point-to-multipoint type.

Long reach WDM-PON is feasible using low-loss AWG - in this case, the link budget is 28 dB, the splitting ratio is up to 64, and the reach increases to up to 80 km. The reference (Mukherjee, 2006) explains largely the current WDM technology.

4.3 Long Reach DWDM-CDM PON

DWDM-CDM PON combines the code and wavelength-division multiplexing, achieving ultra-long range due to coding gain, high bandwidth and bidirectional transmission on the same wavelength and with a single fiber.

Typical figures are 16λ DWDM-CDM PON, with a power budget of 42 dB at 100 km, with 32 orthogonal codes (32 users).

Some of this long reach schemes provide high split ratio, long reach -greater than 60 km- and high symmetrical and asymmetrical bandwidth (10/2.5 Gbps) (Iwamura et al., 2007).

4.4 Current research in WDM / Long-reach networks: a survey

A proposal for a long-range architecture was implemented by the ACTS (Advanced Communications and Technologies and Services) project, called Photonic Local Access NETWORK (PLANET) (Van de Voorde et al., 2000). The splitting factor was 2048 with a span of 100 km in the PLANET project. The span comprehends a maximum feeder length of 90 km and a drop section of 10 km. The transport system supported on this SuperPON architecture was based on an asynchronous transfer mode (ATM) cell. A bit rate of 2.5 Gb/s was distributed to the optical network units (ONU) by time-division multiplexing (TDM) in the downstream direction, whereas a time-division multiple access (TDMA) protocol was used to share the 311 Mb/s upstream bit rate. In order to compensate the fiber and splitting ratio losses, some optical amplifiers were housed in optical repeater units (ORUs) located at the feeder section and between the feeder and the drop sections.

Another related proposal on LR-PON is the SuperPON architecture based on GPON by British Telecom. This is a GPON over 135 km consistent with the standards of ITU-T. The

channels are 2488 Gb/s downstream and 1244 Gb/s upstream, using ~1490 nm and 1552,924 nm wavelengths. Advanced 40- λ dense-wavelength-division-multiplexing (DWDM) equipment is used to extend the physical reach and to provide fiber gain. Each wavelength can support a split of 64 (1×8 followed by 1×8), so that a fully populated system could support 2560 ONUs. The combined loss of the splitters and the last 10 km of the fiber is 23 dB.

The Hybrid DWDM-PON (Shea & Mitchell, 2009) by University College presents the extension in the reach toward 100 km and an upstream bit rate of 10 Gb/s. It can potentially support 17 TDM PONs operating at different wavelengths – each with up to 256 customers, giving an aggregate number of 4352 customers in total. It uses 100-GHz channel spacing, and divides the C-band into two, with one half (1529–1541 nm) carrying downstream channels and the other (1547.2–1560.1 nm) carrying upstream channels.

Further implementations using DWDM in the backhaul to increase the fiber efficiency are demonstrated in the EU project PIEMAN (Shea & Mitchell, 2007). In this architecture, the network has a 100-km reach with a 32 wavelength DWDM backhaul. Each 10 Gb/s wavelength is uniquely allocated to a PON with a 512-way split, enabling the network to support (32×512) up to 16,384 users with an average bandwidth of ~20 Mb/s. By using dynamic bandwidth allocation and 10 Gb/s-components in the ONU, it is possible for each user to burst at 10 Gb/s. [see table 4]

Project	Reach (Km)	# λ	DS/UP (Gb/s)	# ONTs
PLANET	100	1	2.5/0.311	2.048
Super-PON	135	40	2.5/1.25	2.560
Hybrid PON	100	17	10/10	$17 \times 256 = 4.352$
PIEMAN	100	32	10/10	$32 \times 512 = 16.384$
SUCCESS	25	4×16	1.25/1.25	4×16
SARDANA	100	>1	10/10	1000

Table 4. Long Reach-PON projects

One of the most promising recent WDM-PON network, is the so-called SUCCESS network (Kazovsky et al., 2007). The SUCCESS-HPON architecture is based on a topology consisting of a collector ring and several distribution stars connecting a central office (CO) and several optical networking units (ONUs). It uses Coarse WDM (CWDM) and dense WDM (DWDM) technologies. Each ONU has its own dedicated wavelength for both upstream and downstream transmissions on a DWDM grid to communicate with the OLT. The communication is a half-duplex communication – the tunable transmitters at the OLT are used for both downstream and upstream modulated frames by ONU's. Furthermore, a scheduling algorithm has been developed to keep track of the status of all shared resources and arrange them properly in both time and wavelength domains, including the control for both tunable transmitters and tunable receivers. The research is also focused on the evaluation performance of two scheduling algorithms: 1) batching earliest departure first (BEDF); and 2) sequential scheduling with schedule time framing (S3F).

Lastly, there are also important investments in optical technologies in Europe. The current FP7 framework of the CE launched in 2007 funds several projects related to optical technologies. Amongst others, is interesting to consider the project called Single-fiber Advanced Ring Dense Access Network Architecture (SARDANA) – its goals are quite ambitious: up to 1024 users per PON, 10 Gb/s data rate, remote passive amplification and

wavelength-agnostic customer equipment. Finally, it also aims to score well in traffic balancing, as well as being highly scalable and allowing cascading (Prat, 2008).

5. Dynamic Bandwidth Allocation (DBA) and QoS provisioning in EPON

One of the main challenges of a TDM-PON is to schedule the transmissions and the bandwidth allocation in the upstream shared channel efficiently. The issue of developing appropriate scheduling algorithms was an important topic of research in the past. Goals of the scheduler are: be efficient; support the QoS of each traffic flow requirements; allocate fair bandwidth to users reducing delay and jitter; and finally, it must be computationally simple enough.

To guarantee the efficiency and scalability of EPON in terms of resource management, numerous contributions have been presented. There are two main strategies: the fixed bandwidth allocation (FBA), and the dynamic bandwidth allocation (DBA). The first one allocates the same transmission slots to every ONU in every service cycle. It is a simple scheme but it does not perform optimally. On the contrary, the dynamic policy allocates the transmission in the upstream channel based on each ONU's requested bandwidth, consequently the dynamic scheme provides a more fair, efficient and flexible bandwidth allocation.

5.1 DBA algorithms legacy EPON network

The DBA of the EPON should accomplish QoS requirements to deliver different services, such as multimedia traffic. DBA algorithms proposed so far for EPONs deal with different criteria and can be categorized as shown in Figure 6.

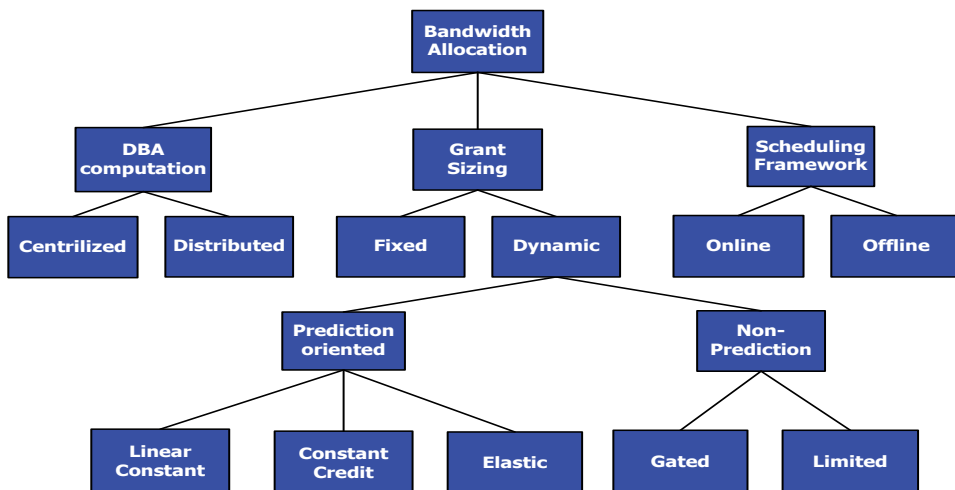


Fig. 6. Bandwidth Allocation Criteria

DBA algorithms may be either centralized or distributed. Besides, the dynamic grant sizing -bandwidth allocation- might be based on a prediction oriented or non-prediction oriented approaches.

Some examples of algorithms prediction-oriented are: (Hee-Jung Byun et al., 2003), (Yuanqiu Luo & Ansari, 2005), (Yongqing Zhu et al., 2006) and (Lannoo et al., 2007). Finally, authors in reference (Kramer et al., 2002b) proposed different DBAs explained in the IPACT section below.

On the other hand, the scheduling framework determines the way scheduling decisions are made. There are two main frameworks to consider: online and offline scheduling. With online scheduling, the OLT makes scheduling decisions “on-the-fly” based on individual requests and without global knowledge of the network. On the other hand, offline scheduling requires a full knowledge of the network status, thus its scheduling decisions are computed after having received the requests from all of the ONUs. (McGarry et al., 2006). In many settings, the online scheme performs better than the offline scheduling, but with less control of channel transmission times.

5.2 Centralised vs. distributed scheduling

The OLT computes the bandwidth allocation in the centralised scheduling, which is the most common approach. On the other hand, the distributed approach contemplates the participation of both OLT and ONUs. Bandwidth allocation is calculated by ONU though it is also authorized by OLT.

In what follows, we present a description of a centralized DBA, the Interleaved Polling with Adaptive Cycle Time (IPACT), and a distributed DBA, Dynamic Distributed Scheduler for EPON (DDSPON), and a performance comparison among them.

5.2.1 IPACT

The IPACT is one of the early works that became very popular in the literature (Kramer et al., 2002b). The cycle period adjusts to the bandwidth requirements of the ONUs, and the definition of a maximum transmission window does not allow ONUs with high traffic level to monopolize the bandwidth resource.

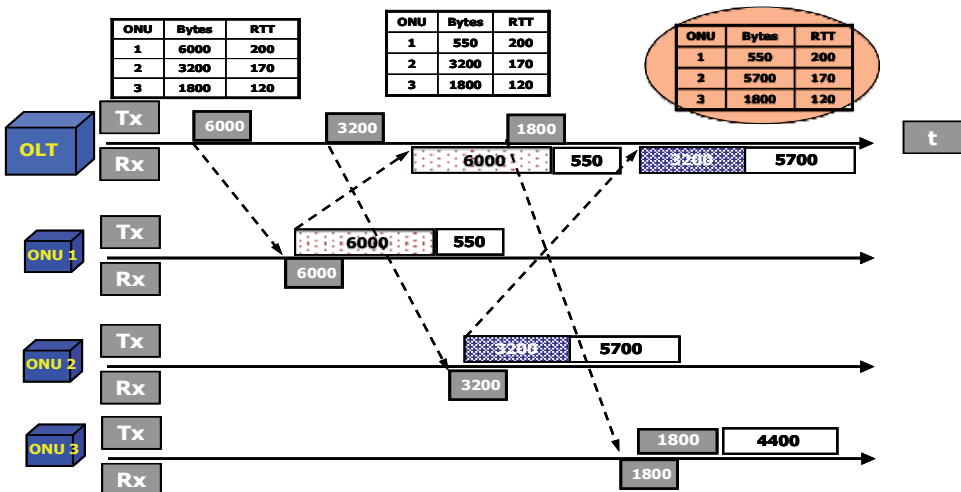


Fig. 7. Interleaving Polling mechanism in IPACT (Kramer et al., 2002b).

What is more interesting in this proposal is that IPACT uses an interleaved polling approach, in which the next ONU is polled before the transmission of the previous one is finished in order to utilize the channel efficiently, as depicted in Figure 7.

The IPACT grant sizing is performed using five different alternatives: fixed, limited, gated, constant credit, linear credit and elastic. Summarizing, the prediction-oriented DBAs are: constant credit, linear credit and elastic. The credit approach - constant or linear - grants the ONU's requested bandwidth plus an extra amount of bandwidth; while the elastic approach basically limits the maximum cycle time. The rest of the options - fixed, limited and gated- are non prediction-oriented DBAs. The limited approach allocates no more than a predefined amount of bandwidth to an ONU; and the gated one grants the requested bandwidth without any limitation. Finally, the authors demonstrate that the limited discipline is more efficient than the gated one and it has been the most preferred one to compare with in the literature.

5.2.2. DDSPON

The DDSPON (De Andrade et al., 2007) is a DBA developed by some of the authors of this chapter. This DBA requires an MPCP extension, because some extra information must be supplied and therefore carried in control messages - mainly the weight vector (Φ). This data vector allows ONUs to compute its transmission window size. Such parameter represents a proportional weight set up according to each ONU's guaranteed bandwidth agreement. The ONU computes the required bandwidth (R_i) and its current weight Φ_i , and then reports such value to the OLT in a report message. The interleaving polling mechanism is applied here as well as IPACT does [see Figure 8].

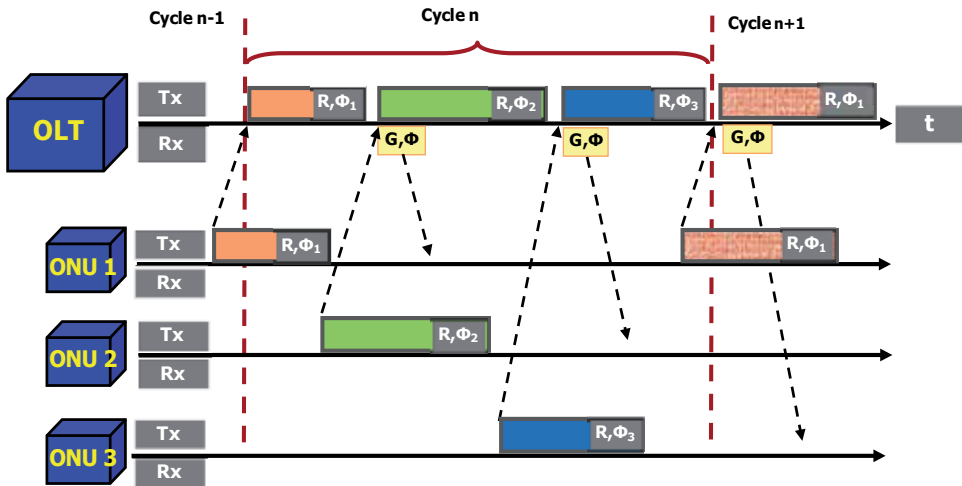


Fig. 8. DDSPON Polling Mechanism.

The average transmission window size of ONU_i is computed by the equation below:

$$W_i = \frac{\Phi_i}{\sum_{j=1}^N \Phi_j} W_{MAX}; [N : \text{of ONUs}] \tag{1}$$

where W_{MAX} is the maximum transmission window size (bits) that corresponds to the maximum cycle time (T_{MAX}).

$$W_{MAX} = T_{MAX} * \text{Upstream rate} \quad (2)$$

The DDSPON process is as follows:

- The OLT receives a report messages from ONU_i along the cycle n containing the window size ($R_i(n)$) computed by itself as in equation 5, and the weight (Φ_i)

ONU_1	ONU_2	ONU_3	ONU_N
$\Phi_1(n)$	$\Phi_2(n)$	$\Phi_3(n)$	$\Phi_N(n)$

- The OLT sends the Gate message to the ONU in the next cycle ($n+1$) including the weight vector Φ (with weights of all other ONUs) and the time to start the ONU's transmission. Then, the ONU_i transmits the data according to the value of $R_i(n)$ previously computed, and calculates the new values of $R_i(n+1)$ and $\Phi_i(n+1)$.

$$W_i(n+1) = \frac{\Phi_i^{conf}}{\Phi_i^{conf} + \sum_{j=1, j \neq i}^N \Phi_j(n)} W_{MAX} \quad (3)$$

And $R_i(n+1)$ is computed

$$R_i(n+1) = \min(W_i(n+1), Q_i); [Q_i : \text{queue size}] \quad (4)$$

Finally, the new weight for next cycle $n+1$ is calculated based on the request value for cycle $n+1$:

$$\Phi_i(n+1) = \frac{R_i(n+1) [\Phi_i^{conf} + \sum_{j=1, j \neq i}^N \Phi_j(n)]}{W_{MAX}} \quad (5)$$

Notice that each ONU schedules the size of its transmission window dynamically. DDSPON is executed in an online framework because the scheduling process is executed without the need of waiting the reports from the rest of the ONUs. Moreover, by getting the weight vector, each ONU is able to get an 'idea' of the rest of the ONUs' loads, which is characteristic in offline DBAs.

5.2.3. Performance evaluation

This section illustrates the performance evaluation of DBA algorithms. First we define the power ratio as in equation (Kleinrock, 1975):

$$P = \frac{\phi_{max}}{D}; \quad \phi_{max} : \text{throughput} \quad (6)$$

D: delay

The power ratio evaluates the DBA’s efficiency. Therefore the performance is evaluated by computing: packet delay, average queue size and throughput for different setting scenarios from low to high offered loads.

The comparison between DDSPON versus the IPACT was conducted by event-driven simulations using the OPNET Modeler simulator. These simulations considered an ideal channel and identical network parameters. To be more accurate, the distance parameter was modified through the different scenarios of simulations from long (20 km) to short distances (5 km), and the traffic model considered was self-similar in order to obtain more realistic results.

The setting scenario consists of 16 ONUs with the same nominal weight (1/16), 1 Gb/s line rate, 8 μseg. guard interval, large buffer size to avoid packet drops, and finally single traffic class per ONU.

The main results obtained are presented below. Firstly, Table 5 below presents the average queue size and packet delay for different offered loads and in the long distance scenario.

Offered load	Average queue size (bytes)		Average packet delay (ms)	
	IPACT scenario 1	DDSPON scenario 1	IPACT scenario 1	DDSPON scenario 1
0,05	942	694	0,286	0,29025
0,2	1809	1890	0,373	0,41108
0,4	3292	3497	0,567	0,62216
0,6	7078	6766	1,050	1,00087
0,8	157538	59307	19,095	7,09164
1	425367	148205	41,337	14,3108

Table 5. Queue and delay size (average) for 20 Km

Figure 9a presents the average packet delay, and Figure 9b presents the average queue size for different distances in a high loaded scenario (H=0.8). Notice that results provided have important implications, for instance the IPACT requires larger buffer size to avoid the packets loss than DDSPON.

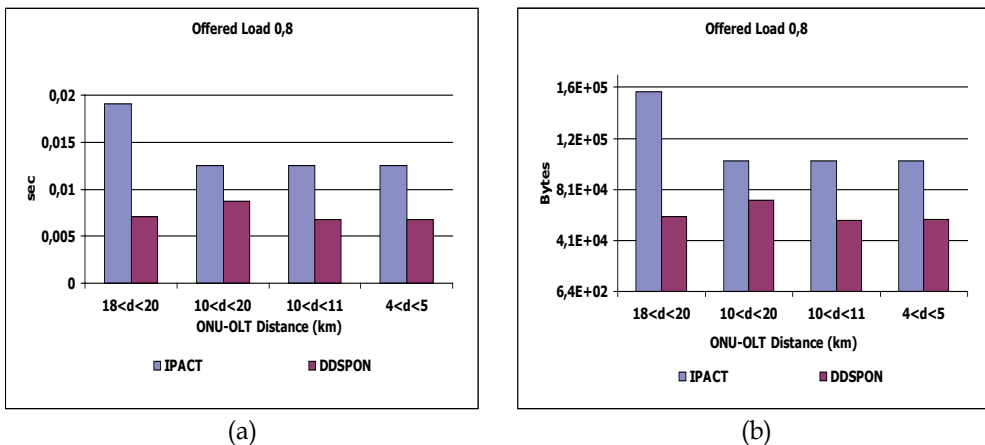


Fig. 9. Average comparison between IPACT and DDSPON. (a) packet delay (b) queue size.

It is interesting to consider in the figures above that DDSPON presents an increase in both, the average queue size and average packet delay, when the setting scenario is heterogeneous, i.e. ONUs are far distributed between 10 and 20 km, this variation is roughly about 21% higher (for loads of 0,8) than the results obtained in the homogeneous scenario. Figure 10 clearly shows that IPACT's average packet delay is worse than the DDSPON's one. The percentage of improvement of DDSPON over IPACT goes from 30.6% to 65.4% for the different distance ranges.

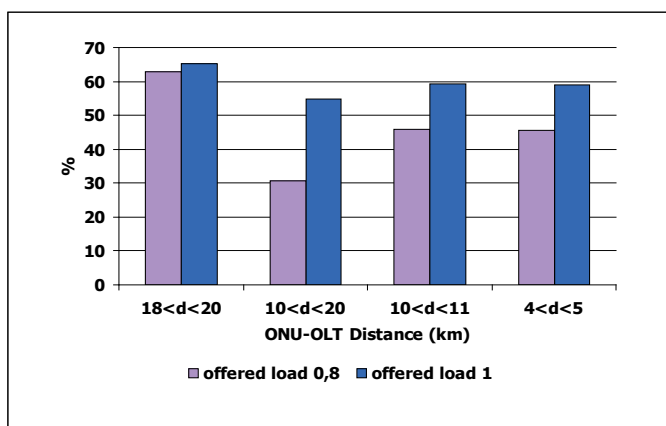


Fig. 10. Average packet delay percentage difference: DDSPON over IPACT.

To conclude, the DDSPON remains stable versus IPACT with the variation of distances, and the most remarkable is that DDSPON presents significant improvements versus the IPACT in all simulations performed, being more relevant in highly loaded scenarios.

5.3 QoS provisioning in an EPON

The bandwidth allocated to each ONU is guaranteed by the DBA (inter-ONU scheduling), but the QoS is guaranteed internally by the ONU, the so-called intra-ONU scheduling process. The EPON follows the IEEE QoS policy defined in the standards IEEE 802.1P/Q. There are up to eight sub-queues in each ONU depending on the traffic type; the intra-ONU scheduling is of the strict type, hence, queues are served in order of priority. Such procedure does not perform optimally in light load networks, so many algorithms, such as (Hsueh et al., 2003), (Kramer et al., 2002a), (Jing Xie et al., 2004), (Kramer et al., 2004) or (Yuanqiu Luo & Ansari, 2005) among others, propose to maximise intra-ONU scheduling.

According to the QoS policy, (McGarry et al., 2004) classifies DBA algorithms into two categories: algorithms with statistical multiplexing (no QoS guaranteed), and algorithms with quality of service. The latter is further separated into algorithms with absolute QoS assurances, i.e. those that follow the integrated services paradigm; and algorithms with relative QoS assurances, which provide different QoS levels according to the traffic classes, i.e. differentiated services.

DBA algorithms introducing the support of differentiated services use strict priority scheduling. Some of the examples developed in the past can be listed: (i) in (Choi & Huh, 2002), where bandwidth is allocated according to traffic priority requests; (ii) in (Kramer et al., 2002a), which combines IPACT and strict priority queuing in order to support QoS; (iii)

(Assi et al., 2003) introduced an approach that consists of distributing the fairly excessive bandwidth amongst the highly loaded ONUs. It takes also into consideration different traffic classes, so that requested bandwidth consists of high, medium and low priority; and (iv)in (Jing Xie et al., 2004), the authors propose the division of the frame, but in this case the frame is divided into multiple subframes according to the different traffic classes, in order to reduce the delay of high priority and medium priority classes; the size is variable depending on the request, and through the definition of weights for each class, it is possible to avoid bandwidth monopolization.

The aforementioned algorithms are the main contributions regarding DBA with differentiated QoS support; more references can be found in (Zheng & Mouftah, 2009). Furthermore, QoS contributions in DBAs are summarized in (McGarry et al., 2008).

5.4 Enhanced DBA algorithm for WDM-EPON networks

To provide higher bandwidth in PONs, a WDM technique can be performed incorporating multiple wavelengths in either, the upstream or downstream direction so a WDM-PON has many advantages such as increasing network capacity, in terms of bandwidth or user scalability.

The new challenge for WDM-EPON is to allocate bandwidth to ONUs in both time and wavelength domains, maximizing the whole network efficiency. Therefore, DBA algorithms initially designated for EPON require modifications to exploit the multichannel architecture. The bandwidth management problem can be split into two sub-problems: grant sizing (bandwidth allocation) and grant scheduling (wavelength selection). Such algorithms hereinafter are known as Dynamic-Wavelength and Bandwidth Allocation (DWBA).

Grant sizing is not analyzed anymore because any of the aforementioned DBAs may be used. Instead, two main approaches cope with grant scheduling by: improving a former DBAs, e.g. SIPACT (Clarke et al., 2006); or developing new mechanisms, for instance, applying a well-known scheduling theory (Pinedo, 2002). The backward compatibility of the MPCP is mandatory, but some extensions to the MPCP must be considered to deal with the wavelength discovery and scheduling.

The reference (McGarry et al., 2008) introduces the concept of just-in-time (JIT) which is a hybrid scheduling framework between offline and online. The OLT schedules the grant based on the report messages accumulated since the last channel became available. The ONUs that have not been allocated to a wavelength yet, are scheduled together across all wavelengths as soon as a wavelength becomes available. The online JIT scheduling framework gives the OLT more opportunity to make better scheduling decisions.

The simplest grant scheduling policy is to assign the next available supported channel (NASC) to the ONU which means that the OLT must know which upstream channel will first turn idle according to its polling table; such policy is not optimal in all cases and it does not consider ONUs that support different wavelengths.

The approach of selecting the wavelength by using the scheduling theory seems much better policy (McGarry et al., 2008), e.g. Shortest Path First (SPT), Longest Path First (LPT), and Least Flexible Job First (LFJ) amongst others (Pinedo, 2002). LFJ first schedules transmissions to the ONUs that support the fewest number of wavelength channels at the earliest available supported channel. The LFJ policy is optimal because it minimizes under certain conditions the length of the schedule.

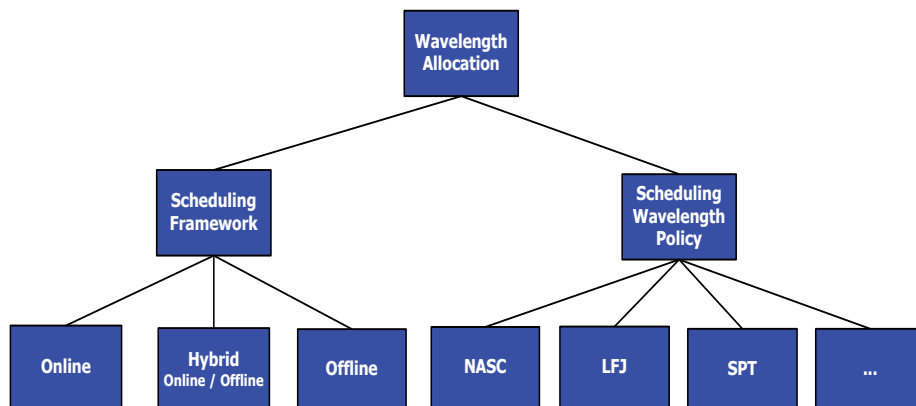


Fig. 11. Wavelength allocation scheduling

Figure 11 classifies the scheduling framework and the scheduling wavelength policies explained above.

5.4.1 Survey of DWBA

As an evolution of IPACT in WDM, some variants of IPACT are addressed in different proposals, e.g. in (Kae Hsiang Kwong et al., 2004). The authors propose an algorithm so-called WDM IPACT with a single polling table (WDM IPACT-ST). The grant scheduling is of the NASC type and the grant sizing is performed according the IPACT (with fixed, limited or gated approach). This approach requires new devices at both ends of the fiber links to support simultaneous transmissions over multiple wavelengths.

In (Clarke et al., 2006), the authors developed a DBA called Simultaneous and Interleaving Polling with Adaptive Cycle Time (SIPACT). SIPACT allows different architectures to poll ONUs, either intra-wavelength (on the same wavelength) or inter-wavelength (amongst different wavelengths), simultaneously but depending on the set of wavelengths supported by each individual ONU.

The authors in (Dhaini et al., 2007) presented several DWBA variants also based on former EPON DBAs algorithms and compared their performance. The three different approaches compared depend on the weight of the individual ONU, the two more interesting ones consider “on the fly” (online) mechanisms. Simulations performed showed that such approach presents a better throughput and delay performance.

Finally, the recent proposal (McGarry et al., 2008) addressed the queuing delay and channel utilization through the scheduling theory, which is concerned to scheduling a set of jobs with specific processing times to be executed on a set of machines. In this case, the ONUs represent the jobs, the grant size is represented by the processing time, and the channels are represented by machines.

6. Conclusions

This chapter discoursed on optical fiber based access networks. While the current backbone networks support high capacities; the last mile for the access network remains a bottleneck. New enhancements of the legacy standards are coming soon allowing the upgrade the

upstream/downstream channel line rate to 10 Gb/s. Such new standards are intended to be compatible with existent Legacy TDM-PONs.

But the more important step towards NGA is the implementation of the WDM technology. There are huge research efforts worldwide in developing metro and access networks based on WDM, using either DWDM or CWDM. The research is focused on improving the optical devices as well as in developing new architectures to handle the multi-wavelength channel efficiently. Such solutions are not only based on the type of network -such as WDM-PON or 10G PON- but also on hybrid technologies such those presented in section 4.

Moreover, incumbent operators are interested in the so-called Long Reach-PON (LR-PON) that will help the growing process of PON deployment. LR-PON is a very cost-effective solution because the CAPEX and the OPEX of the network are lower mainly due to the fact that the number of equipment interfaces, network elements, and nodes are reduced, and moreover, the network management complexity is also simplified.

The allocation of bandwidth to users in the upstream shared channel of the network is addressed by appropriate DBAs. Among them we present IPACT and DDSPON, which are representatives of centralized and distributed DBAs, respectively. The results provided demonstrate that DDSPON is more efficient than IPACT. New DBAs for WDM-PON networks are a key issue to manage and fairly distribute the resources. Proposals presented in section 5, especially those based in the scheduling theory are very promising, but further research should still be carried out.

Furthermore, the new goals are directed to support scalable networks and to help the coexistence between legacy and next-generation PONs.

7. References

- Assi, C.M.; Yinghua Ye; Sudhir Dixit & Ali, M.A. (2003). Dynamic bandwidth allocation for quality-of-service over Ethernet PONs. *IEEE Journal on Selected Areas in Communications*, Vol.21, No.9, pp. 1467-1477.
- Choi, S. & Huh, J. (2002). Dynamic Bandwidth Allocation Algorithm for Multimedia Services over Ethernet PONs. *ETRI Journal*, Vol.24, No.6, pp. 465-468.
- Clarke, F.; Sarkar, S. & Mukherjee, B. (2006). Simultaneous and interleaved polling: an upstream protocol for WDM-PON. *Optical Fiber Communication Conference, 2006 and the 2006 National Fiber Optic Engineers Conference. OFC 2006*, pp. 3.
- De Andrade, M.; Gutierrez, L. & Sallent, S. (2007). DDSPON: A Distributed Dynamic Scheduling for EPON. *IEEE International Conference on Signal Processing and Communications, 2007. ICSPC 2007*, pp. 840-843.
- Dhaini, A.R.; Assi, C.M.; Maier, M. & Shami, A. (2007). Dynamic Wavelength and Bandwidth Allocation in Hybrid TDM/WDM EPON Networks. *Journal of Lightwave Technology*, Vol.25, No.1, pp. 277-286.
- Hajduczenia, M.; da Silva, H.J.A. & Monteiro, P.P. (2007). 10G EPON Development Process. *ICTON '07. 9th International Conference on Transparent Optical Networks*, Vol.1, pp. 276-282.
- Hee-Jung Byun; Ji-Myung Nho & Jong-Tae Lim (2003). Dynamic bandwidth allocation algorithm in Ethernet passive optical networks. *Electronics Letters*, Vol.39, No.13, pp. 1001-1002.

- Heron, R.; Storry C. & Patel S (2009). Future Directions in Fiber Access Networks. *Proceedings NOC, Valladolid (Spain)*.
- Hsueh, ; An, ; Kim, & Kazovsky, (2003). A new media access control protocol with quality of service and fairness guarantee in ethernet-based passive optical networks. *Proceedings of the 7th joint conference on information sciences*, pp. 1392.
- IEEE 802.3ah (2004). IEEE Standard for Information Technology. "Ethernet in the First Mile".
- ITU-T G.984.[1-4] (2003). ITU - T Recommendations Gigabit-capable PON (GPON).
- ITU-T G.984.5 (2007). ITU - T Recommendations Gigabit-capable PON (GPON).
- ITU-T G.984.6 (2008). ITU - T Recommendations Gigabit-capable PON (GPON).
- Iwamura, H.; Gupta, C.; Kashima, M.; Tamai, H.; Watanabe, R.; Ushikubo, T. & Kamijoh, T. (2007). 42dB Loss Budget Hybrid DWDM-CDM-PON without Optical Amplifier. *Conference on Optical Fiber Communication and the National Fiber Optic Engineers Conference, 2007. OFC/NFOEC 2007*, pp. 1-3.
- Jing Xie; Shengming Jiang & Yuming Jiang (2004). A class-based dynamic bandwidth allocation scheme for EPONs. *The Ninth International Conference on Communications Systems, 2004. ICCS 2004*, pp. 356-360.
- Kae Hsiang Kwong; Harle, D. & Andonovic, I. (2004). Dynamic bandwidth allocation algorithm for differentiated services over WDM EPONs. *The Ninth International Conference on Communications Systems, 2004. ICCS 2004*, pp. 116-120.
- Kani, J.; Bourgard, F.; Cui, A.; Rafel, A.; Campbell, M.; Davey R. & Rodrigues, S. (2009). Next-Generation PON - Part I: Technology Roadmap and General Requirements. *IEEE Communications Magazine*, Vol.47, No.11, pp. 43-49.
- Kazovsky, L.G.; Wei-Tao Shaw; Gutierrez, D.; Ning Cheng & Shing-Wa Wong (2007). Next-Generation Optical Access Networks. *Journal of Lightwave Technology*, Vol.25, No.11, pp. 3428-3442.
- Kleinrock, L. (1975). *Queueing systems*. John Wiley & Sons, 0471491101; New York.
- Koonen, T. (2006). Fiber to the Home/Fiber to the Premises: What, Where, and When? *Proceedings of the IEEE*, Vol.94, No.5, pp. 911-934.
- Kramer, G.; Banerjee, A.; Singhal, N.K.; Mukherjee, B.; Sudhir Dixit & Yinghua Ye (2004). Fair queueing with service envelopes (FQSE): a cousin-fair hierarchical scheduler for subscriber access networks. *IEEE Journal on Selected Areas in Communications*, Vol.22, No.8, pp. 1497-1513.
- Kramer, G.; Mukherjee, B.; Dixit, S.; Ye, Y. & Hirth, R. (2002a). Supporting differentiated classes of service in Ethernet passive optical networks. *Journal of Optical Networking*, Vol.1, No.8, pp. 280-298.
- Kramer, G.; Mukherjee, B. & Pesavento, G. (2002b). Interleaved Polling with Adaptive Cycle Time (IPACT): A Dynamic Bandwidth Distribution Scheme in an Optical Access Network. *Photonic Network Communications*, Vol.4, No.1, pp. 89-107.
- Kramer, G. (2005). *Ethernet passive optical networks*. McGraw-Hill, 0071445625, New York.
- Lacic, B. & Hajduczenia, M. (2007). On optimized Passive Optical Network (PON) deployment. *Second International Conference on Access Networks & Workshops, 2007. AccessNets '07*, pp. 1-8.
- Lannoo, B.; Verslegers, L.; Colle, D.; Pickavet, M.; Demeester, P. & Gagnaire, M. (2007). Thorough analysis of the IPACT dynamic bandwidth allocation algorithm for EPONs. *Fourth International Conference on Broadband Communications, Networks and Systems*, pp. 486-494.

- Martinez, J.J.; Gregorio, J.I.G.; Lucia, A.L.; Velasco, A.V.; Aguado, J.C. & Binue, M.A.L. (2008). Novel WDM-PON Architecture Based on a Spectrally Efficient IM-FSK Scheme Using DMLs and RSOAs. *Journal of Lightwave Technology*, Vol.26, No.3, pp. 350-356.
- McGarry, M.P.; Reisslein, M. & Maier, M. (2008). Ethernet passive optical network architectures and dynamic bandwidth allocation algorithms. *Communications Surveys & Tutorials, IEEE*, Vol.10, No.3, pp. 46-60.
- McGarry, M.P.; Maier, M. & Reisslein, M. (2004). Ethernet PONs: a survey of dynamic bandwidth allocation (DBA) algorithms. *IEEE Communications Magazine*, Vol.42, No.8, pp. 8-15.
- McGarry, M.P.; Reisslein, M.; Colbourn, C.J.; Maier, M.; Aurzada, F. & Scheutzow, M. (2008). Just-in-Time Scheduling for Multichannel EPONs. *Journal of Lightwave Technology*, Vol.26, No.10, pp. 1204-1216.
- McGarry, M.P.; Reisslein, M. & Maier, M. (2006). WDM Ethernet passive optical networks. *IEEE Communications Magazine*, Vol.44, No.2, pp. 15-22.
- Mukherjee, B. (2006). *Optical WDM networks*. Springer, 0387290559, New York.
- Pinedo, M. (2002). *Scheduling: theory, algorithms, and systems*. Prentice-Hall, 0130281387, Upper Saddle River.
- Prat, J. (2008). *Next-Generation FTTH passive optical networks: research towards unlimited bandwidth access*. Springer, 9781402084690, London.
- Shea, D.P. & Mitchell, J.E. (2009). Architecture to integrate multiple PONs with long reach DWDM backhaul. *IEEE Journal on Selected Areas in Communications*, Vol.27, No.2, pp. 126-133.
- Shea, D.P. & Mitchell, J.E. (2007). Long-Reach Optical Access Technologies. *IEEE Network*, Vol.21, No.5, pp. 5-11.
- Van de Voorde, I.; Martin, C.M.; Vandewege, I. & Oiu, X.Z. (2000). The superPON demonstrator: an exploration of possible evolution paths for optical access networks. *IEEE Communications Magazine*, Vol.38, No.2, pp. 74-82.
- Yongqing Zhu; Maode Ma & Tee Hiang Cheng (2006). IPACT with Grant Estimation for EPON. *10th IEEE Singapore International Conference on Communication systems, 2006. ICCS 2006*, pp. 1-5.
- Yuanqiu Luo & Ansari, N. (2005). Bandwidth allocation for multiservice access on EPONs. *IEEE Communications Magazine*, Vol.43, No.2, pp. 16-21.
- Zheng, J. & Mouftah, H.T. (2009). A survey of dynamic bandwidth allocation algorithms for Ethernet Passive Optical Networks. *Optical Switching and Networking*, Vol. In Press, Corrected Proof.

Building energy efficiency design for telecommunication base stations in Guangzhou

Yi Chen, Yufeng Zhang and Qinglin Meng

*State Key Laboratory of Subtropical Building Science, Department of Architecture, South China University of Technology
China*

1. Introduction

Telecommunication base stations (TBSs), which are the basis of the telecommunications network, consume more energy than other public buildings due to their high inner heat density and special operating schedule. The number of mobile phone users in China exceeds 500 million, and the telecommunications network has become the largest in the world, consisting of more than 100,000 TBSs. The annual energy consumption of the network is 20 billion kWh, one third of which is used by TBSs. Guangzhou, as one of the fastest developing cities in China, has more than one thousand existing TBSs and the total annual electricity bills are in the tens of millions of RMB, 25% of which is the cost of air conditioning. With the rapid growth of telecommunications, energy conservation for TBSs is gaining greater attention in China.

Previous studies on energy conservation in TBSs mainly focused on improvement of efficient air-conditioning systems (Nakao et al., 1988; Maeda et al., 2005; Choi et al., 2007), indoor airflow optimization (Hayama & Nakao, 1989; Dan & Matti, 2000), use of renewable energy (Makhkamdjano, 2006), and other energy saving and monitoring techniques (Schmidt & Shaukatullah, 2003). There are very limited studies on building energy efficiency design of TBS. Building energy efficiency design, which is known as passive cooling technology, is very popular in the traditional buildings and well inherited and applied in the modern buildings in Southern China. Compared with the active one, such as air-conditioning, passive cooling technology has notable advantages on utilizing natural cooling capacities with no or few energy consumption. Many studies report building energy efficiency designs of walls, roof, glazing, shading and natural ventilation for residential buildings (Feng, 2004), institutional buildings (Athanasios et al., 2007) and high rise apartments (Cheung et al., 2005), however, no such studies were performed on TBS buildings. Nakao et al. (Nakao et al., 1988) studied a thermal control wall for TBS, which can lose heat by using a two-phase loop-type thermo-siphon system integrated inside the wall. The heat transmission coefficient of the wall was found to be one to ten times of the ordinary wall and the annual energy saving was estimated to be 20%. The study proposes a new energy efficiency design of wall for TBS, however, no other designs, such as shading or natural ventilation were mentioned.

This chapter reports the study on building energy efficiency design for TBSs in Guangzhou. Through field investigation of a typical TBS in Guangzhou, the basic information of TBS was achieved, the key factors influencing energy consumption of TBS were determined and several building energy efficiency designs were proposed. The effect on the annual cooling load for each energy efficiency design was analyzed and a combined effect was achieved for several combinations of the designs by building simulation. The building energy efficiency design strategy for TBS in Guangzhou was concluded. It was found that ventilation design is the primary choice for energy efficiency TBS building design. A new ventilation cooling technology (VCT) was proposed. Based on the field investigation, the application feasibility of VCT was studied systematically and the optimization of airflow organization for VCT was analyzed.

2. Field investigation

2.1. Climate conditions in Guangzhou

Guangzhou is located at latitude 23°08'N and longitude 113°19'E. Summer is hot and humid and winter is warm. The average air dry-bulb temperature is 28.4 °C in July and 13.3 °C in January. The mean daily temperature variation is 7.5 °C. The relative humidity is about 83% in summer and 70% in winter. The average annual rainfall is about 1705 mm of which 80% falls between April and September. The long, hot and humid summer in Guangzhou creates a huge demand for energy for cooling.

2.2. Field investigation methods

A typical TBS in Guangzhou was chosen for investigation. The TBS is located on the top of a library, with dimensions of 4.66 m long × 4.66 m wide × 2.8 m high. The plan view of the typical TBS is shown in Figure 1. The structure and conductive thermal resistance of the building envelopes of the typical TBS are shown in Table 1. Two air conditioners are installed for cooling with a temperature set point of 25 °C. The telecommunication equipment and the air conditioners work continuously, 24 h per day and 365 days per year. There is no window on the walls, mainly for the safety of the telecommunication equipment.

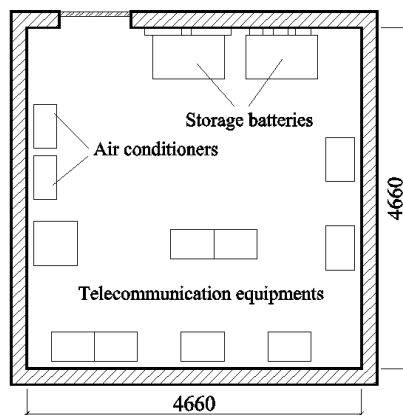
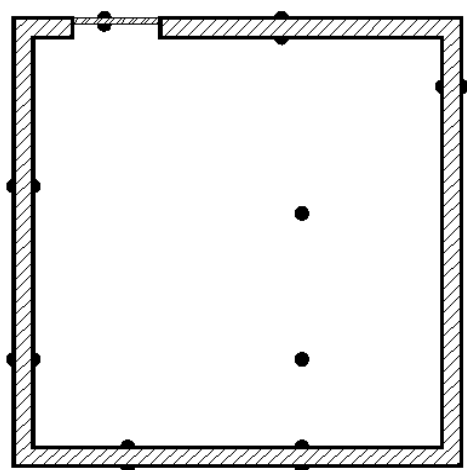


Fig. 1. Plan view of a typical TBS.

Building envelope	Structure	Conductive thermal resistance ($\text{m}^2\text{K}/\text{W}$)
Walls	External cement/sand plaster (20mm) Lime-sand brick (180mm) Internal gypsum plaster (20mm)	0.210
Roof	Polyurethane foam plastics (50mm) Internal gypsum plaster (20mm)	1.376
Floor	External cement/sand plaster (20mm) Reinforced concrete (100mm) Internal gypsum plaster (20mm)	0.104

Table 1. Structure and conductive thermal resistance of the building envelopes of the typical TBS.

The thermal characteristics of the building envelopes, the heat dissipation of the telecommunication equipments and the performance of the air conditioners were investigated through physical measurements. The measurements were carried out during the winter in Guangzhou from 18:00 h on January 8 to 13:00 h on January 10 (44 h in total). Measurements taken included the interior and exterior surface temperatures of the walls, roof and floor (Figure 2), the exterior surface temperature of the equipments, the velocity and temperature of the air exhausted from the equipments (Figure 3), the ambient room air temperature, and the return and supply air velocities and temperatures of the air conditioners. The temperature was measured using thermocouples with an accuracy of ± 0.5 °C and recorded by a data logger at 5 min intervals. Air velocity was measured by a heated-sphere anemometer with a range of 0.1-30 m/s and an accuracy of $\pm 5\%$. The energy consumption of the TBS was measured using a power meter.



- measuring positions of the walls
- measuring positions of the roof and floor

Fig. 2. The measuring positions on the building envelopes.

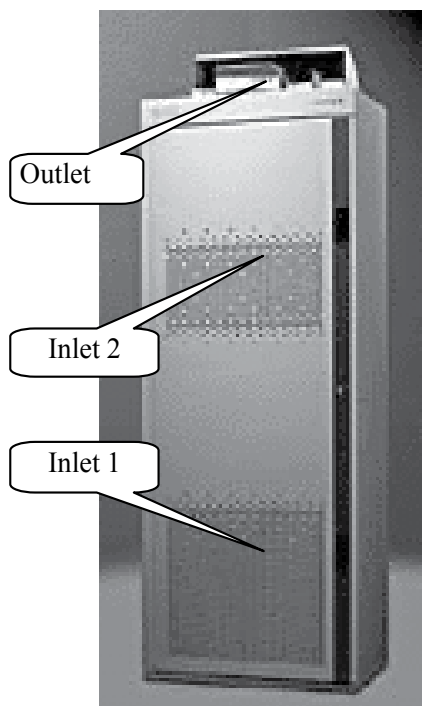


Fig. 3. Telecommunication equipment measurements.

2.3. Field investigation results

2.3.1. Inner heat source

Heat loss of the telecommunication equipments is the main inner heat source for the TBS, which can be transported by convective and radiative ways. The convective heat loss was calculated by using the airflow rate, ambient room air temperature (i.e. inlet air temperature) and outlet air temperature. The radiative heat loss was calculated by using the exterior surface temperature of the equipments and the interior surface temperatures of the envelopes. It was found that the total heat loss of the equipments was maintained constant at a level of 4.35 kW, regardless of communication work loads or outdoor weather conditions. The density of the inner heat source was about 200 W/m², which is much larger than the normal public buildings.

2.3.2. Thermal performance of building envelopes

Figure 4 shows the measured results of the south wall. Outdoor air temperature obtained from the local meteorological observatory in Guangzhou is included in Figure 4 as well. The interior surface temperature, mainly influenced by the indoor air temperature, was comparatively stable (around 25 °C). The exterior surface temperature, affected by the outdoor air temperature and solar radiation, fluctuated greatly with time from 12.5 to 37.5 °C. The mean outdoor air temperature was 12.8 °C and the highest was only 18.3 °C during the measuring period.

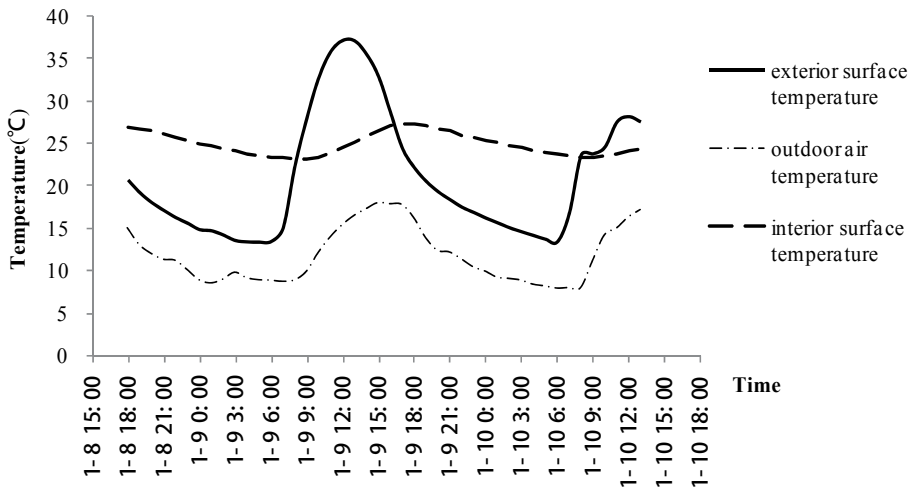


Fig. 4. Temperatures of interior and exterior surface of the southern wall and outdoor air temperature change with time.

It was decided to use the steady state heat transfer equation to make an initial observation on the variation of the heat transfer amount and direction, rather than the dynamic equation, which is relative complicated. The steady state heat transfer equation is:

$$Q = (\theta_e - \theta_i) / R \times S \tag{1}$$

where Q is the total heat transfer (W), θ_e is the exterior surface temperature ($^{\circ}\text{C}$), θ_i is the interior surface temperature ($^{\circ}\text{C}$), R is the conductive thermal resistance ($\text{m}^2\text{K}/\text{W}$) and S is the area (m^2) of the building envelopes. Based on the thermal characteristics (see Table 1) and the measured temperatures, heat transfer of each building envelope was calculated and shown in Figure 5.

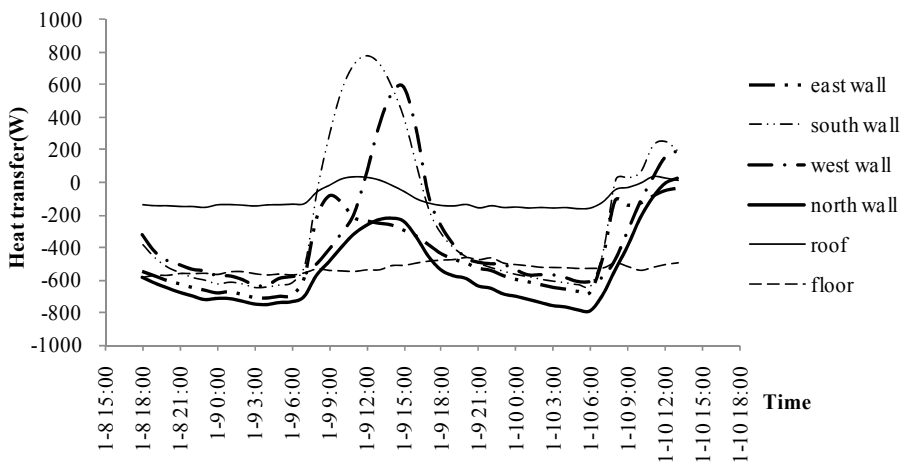


Fig. 5. Heat transfer change with time for each building envelope.

The variation of heat transfer with time was slight for the roof and floor, and large for the walls, especially for the south wall. Guangzhou is located in the northern hemisphere and the sun lies in the southern sky during the measurement, so the south wall gained more heat from solar radiation than the roof and the other walls, resulting in the largest heat transfer change with time. The heat gain (heat transfer from outdoor to indoor) was highest at noon for the south wall and roof and at 15:00 for the west wall. The heat loss (heat transfer from indoor to outdoor) was highest at 7:00 for all the envelopes.

The heat transfers of all the building envelopes were summed up and the change of the total heat transfer with time is shown in Figure 6. In the period of the investigation, the time for the building envelopes to gain heat is only 2 h and to lose heat in the rest of 42 h. Moreover, the maximum of hourly heat loss (3444 W) is far more than the one for heat gain (114 W). The building envelopes of the TBS works in most of time together with the air conditioners to discharge the inner heat generated by the telecommunication equipments and gains heat in only very short time due to the strong solar radiation.

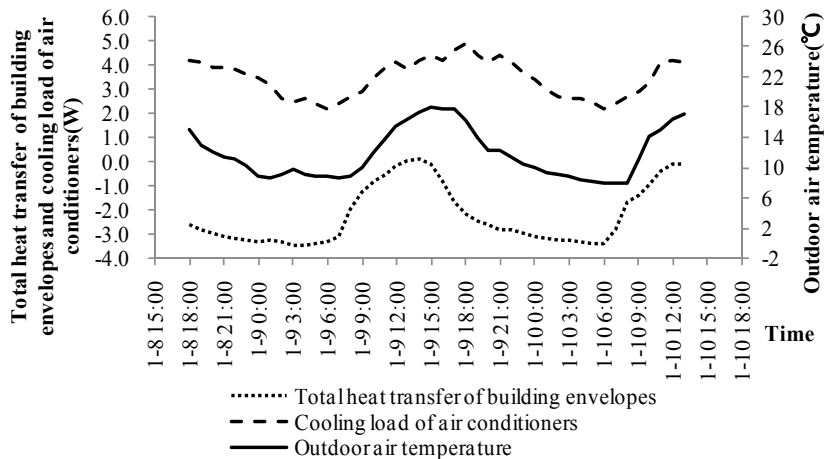


Fig. 6. Total heat transfer of building envelopes, cooling load of air conditioners and outdoor air temperature.

The cooling load of the air conditioners was calculated by using the measured results of the return and supply air temperature and airflow rate. The change tendencies with time are very similar for the cooling load of the air conditioners, the total heat transfer of the building envelopes and outdoor air temperature (see Figure 6). The lower the outdoor air temperature, the more the heat discharged by the building envelopes and the lower the cooling load of the air conditioners. Enhancement of the heat transfer of the building envelopes could save energy by decreasing the cooling load and shortening runtime of the air conditioners.

Figure 7 shows the measured results for the single-phase electrical power of the TBS. Electrical power was maintained at a low level from 5:10 pm to 5:45 pm on Jan 8. That is because the door was open during this period, and the heat was dissipated through the open door by natural ventilation. This shows that internal heat can be removed directly by ventilation, and thus the energy consumption for the air conditioning can be significantly reduced.

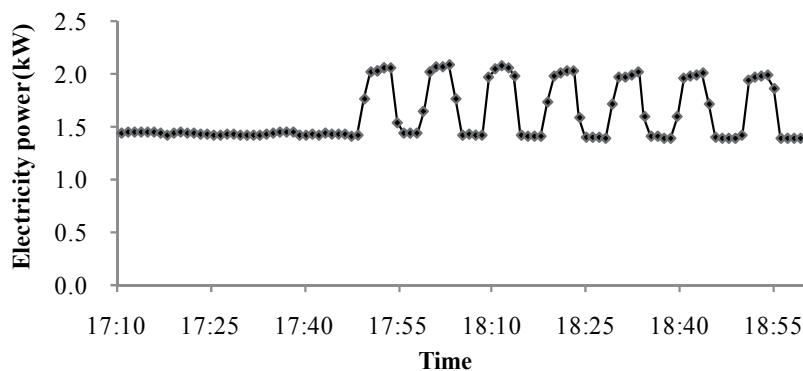


Fig. 7. Single-phase electrical power variation of the TBS with time.

The basic information of the TBS, including the thermal characteristics of the building envelopes, the inner heat density, the indoor air temperature set point, the operating schedule of equipments and air conditioners were achieved and the thermal performance of the building envelopes during the measuring period was studied by the field investigation. Based on this information, building simulation was applied to study the thermal performance of the TBS for a whole year and estimate the energy saving potentials for each building energy efficiency design.

3. Building simulation

3.1 Simulation methods

A dynamic thermal simulation program named DeST was applied to estimate the annual cooling load of the typical TBS. DeST was originally developed in 1989 by Tsinghua University in China based on the IISABRE simulation environment (Hong, et al. 1997) and validated by comparison with both well-known international thermal simulation programs (Bloomfield, 1994) and experimental results (Zhang, et al. 2004). DeST has become a reliable simulation program and is widely applied in building design and for national standards in many countries (Yan, et al. 2004).

Figure 8 shows the model of the typical TBS in DeST created according to the real plan of the TBS. The parameters for the simulations were set according to the basic information achieved by the field investigation. The structure and thermal characteristics of the building envelopes were set as in Table 1. The telecommunication equipments run all day with a total heat of 4.35 kW. The heat density of the lighting and the people were ignored due to the limited period of occupancy. The air conditioners operated continuously with a temperature set point of 25 °C and a relative humidity set range between 5% and 85%. The ventilation rate between the outdoor air and the TBS room was 0.5 h⁻¹. The absorption coefficient of solar radiation of the exterior surfaces of the walls and roof was 0.7. Outdoor climate data was set according to typical Guangzhou annual meteorological data.

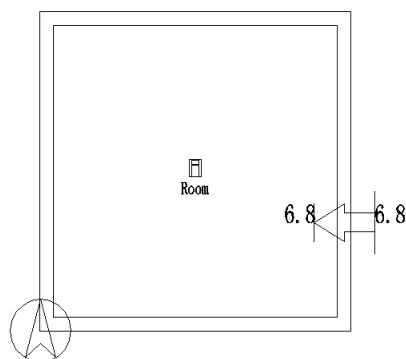


Fig. 8. Building simulation model for the typical TBS.

3.2 Simulation results and discussion

Simulation on the performance of the investigated TBS shows that the accumulation of annual cooling load is 36891 kWh. It can be seen that 97% of the inner heat source becomes the cooling load of the air conditioners and only 3% is discharged by the building envelopes in the investigated TBS. Well building energy efficiency design, which enhances the heat dissipation by the building envelopes, can save energy consumption of cooling. Heat transfer coefficient and solar absorptance are the key factors determining heat transfer of building envelope. In addition, shading and ventilation, which are widely used in the hot and humid region of China, are considered as the potential energy efficiency designs for TBS as well.

3.2.1. Temperature set point adjustment

Thermal performance of building energy efficiency design is affected by many factors, such as inner heat density, operating schedule and environmental requirements. The information of these factors were obtained by the field investigation and directly inputted as the known conditions into building simulation, except for the indoor temperature set point. The temperature set point for the air conditioners in a typical TBS is 25 °C, which takes human comfort requirements into consideration. In practice, the time for which people are present in the TBS is so short that the comfort requirements can be ignored, and the indoor temperature set point of the TBS can be raised to 30 °C according to the environmental requirements of the telecommunication equipment (Standardization Institute of Posts and Telecommunications, 1995). The performance of the TBS with the adjustment of temperature set point was simulated and the results show that the annual cooling load is decreased by 21% compared with the one without adjustment. Meanwhile, the role of building envelopes becomes more important and their heat dissipation accounts for 23% of inner heat source. The following analysis on the building energy efficiency design is based on the model with the temperature set point adjustment.

3.2.2. Design of heat transfer coefficient

The heat transfer coefficients of the walls and roof can be varied from 0.5 to 6W/m² K when choosing different local materials and structures in Guangzhou. The simulation results show that (see Figure 9) the relationship between the annual cooling load and the change of heat

transfer coefficient is linearly and an increase in heat transfer coefficient is beneficial to the reduction of cooling load. The concept of better insulation saving more energy is not applicable to the special kind of buildings such as TBS in Guangzhou. The annual cooling load was found to be less sensitive to the change of heat transfer coefficient of the roof due to the strong solar radiation absorption of the roof during a whole year. Considering the practical available materials and structures in Guangzhou and safety of the communication equipments, the walls and roof were determined as 60mm reinforced concrete walls with plaster and 50mm reinforced concrete roof with plaster. The percentage saving in annual cooling load achieved by the designs is 11.8% and 3.1% separately.

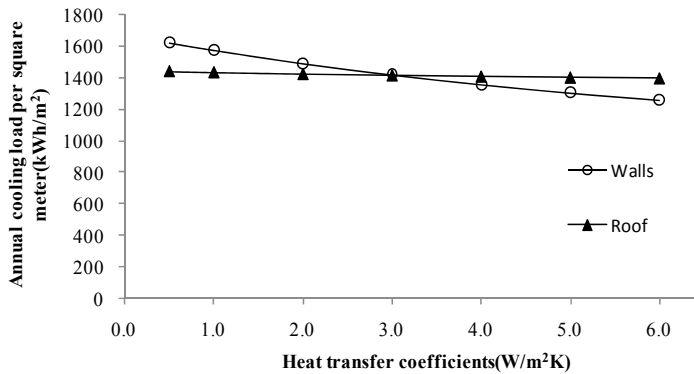


Fig. 9. Effect of heat transfer coefficients of walls and roof on annual cooling load.

3.2.3. Design of solar absorptance

The solar absorptance of the outside surface of the external walls and roof was changed from 0.7 to 0.1 to represent different external finishes. It was found that the annual cooling load has a linear relationship to the solar absorptance of the external surfaces, and the lower the solar absorptance, the higher the saving that can be achieved (see Figure 10). A reduction in solar absorptance from 0.7 to 0.1 can achieve a 7.5% and 1% saving in annual cooling load for the walls and roof separately. The design of shading on the walls or roof can be included into the design of solar absorptance by transforming the shading coefficient into the resulting solar absorptance.

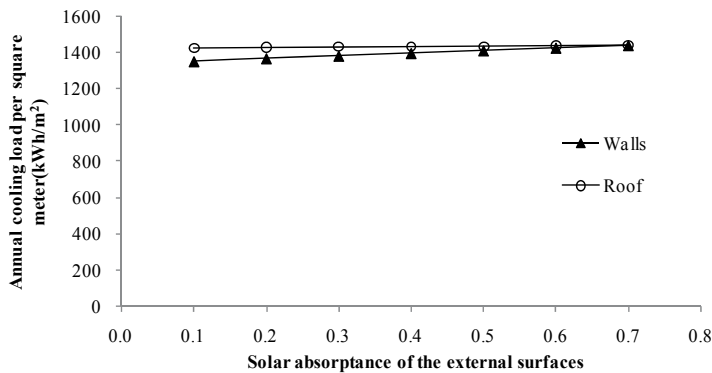


Fig. 10. Effect of solar absorptance of exterior surface of walls and roof on annual cooling load.

3.2.4. Ventilation design

The frequency distribution of outdoor air dry-bulb temperature in a typical year in Guangzhou is shown in Figure 11. The percentage of the time when outdoor air temperature is lower than the indoor temperature set point of TBS (30 °C) is more than 90%, which indicates a great potential of energy saving can be achieved by ventilation. Air exchange rate has a significant impact on cooling saving. The ventilation rate between the outdoor air and the TBS room when applying VCT was changed from 0.5 h⁻¹ to 300 h⁻¹ and the annual cooling load was simulated, and is shown in Figure 12. The ventilation rate has a significant effect on the annual cooling load. When the ventilation rate increases from 0.5 h⁻¹ to 50 h⁻¹, the annual cooling load per square meter decreases from 1439 kWh/m² to 514 kWh/m² and the rate of decline is 64%. As the ventilation rate continues to increase, the annual cooling load does not reduce significantly, which indicates that a reasonable ventilation rate for VCT is 50 h⁻¹. The increase of air exchange rate can be achieved in practice by design of mechanical ventilation.

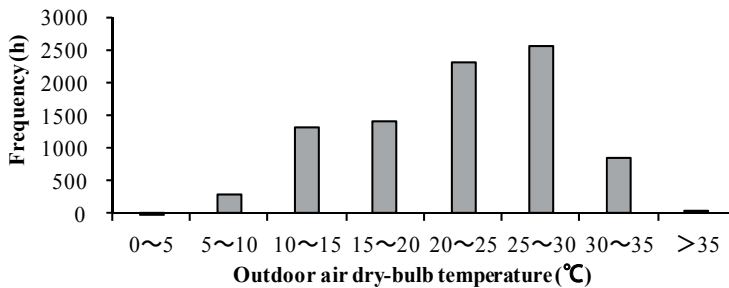


Fig. 11. Frequency distribution of outdoor air dry-bulb temperature in Guangzhou.

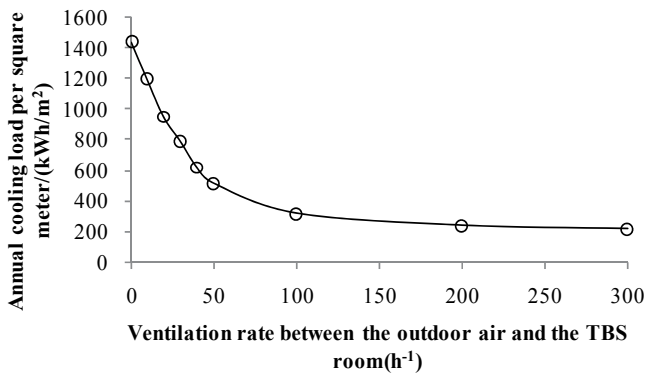


Fig. 12. Effect of ventilation rate on annual cooling load.

The internal heat in the TBS remains constant while the outdoor air temperature changes are comparatively large, and thus the time when the outdoor cold air can be used changes along with the outdoor air temperature. Figure 13 shows that the runtime of the air conditioners is greatly shortened by applying VCT. The air conditioners need to run year-round in a TBS without VCT, while they run mainly on a part-time basis from May to October in the TBS with applied VCT. The annual runtime of the air conditioners amounts to 2509 h, which accounts for only 29% of the total of 8760 h. Thus significant energy savings are made.

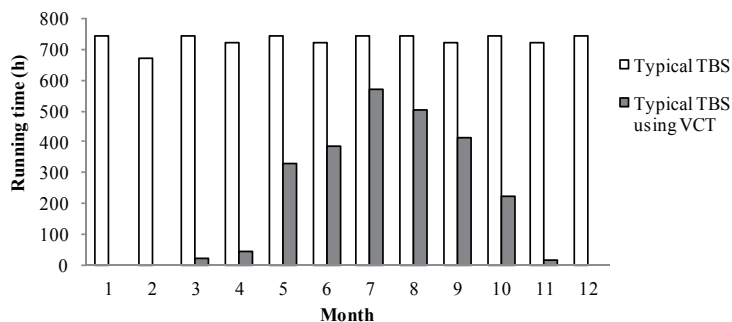


Fig. 13. Monthly runtime of air conditioners in a typical TBS and in a typical TBS using VCT.

3.2.5. Combinations of building energy efficiency designs

The savings of annual cooling load from various building energy efficiency designs are shown in Figure 14. It can be seen that ventilation design achieves the highest saving of more than 64.2%, followed by an 13.4% saving from heat transfer coefficient design of walls. The savings by using other energy efficient designs are less than 10%. The combination of the energy efficiency designs are always preferred and applied in practice to achieve a better thermal performance of a building. As the impact on energy saving may be strengthened or weakened by the combination, several possible combinations of the building energy efficiency designs were analyzed by using building simulation. The combined effect is approximately equal to the sum of the effect of each design for the combination of the designs of walls and roof (see Figure 15), which is because the impact of walls on cooling load can be considered independent from the one of roof. The combined effect is significantly greater than the sum for the combination of heat transfer coefficient design and solar absorptance design, which can be explained as followings: Not only the heat loss, but also the heat gain will increase with heat transfer coefficient design, and the latter one can be weakened by solar absorptance design, resulting in a higher energy saving. The combinations of ventilation design with others do not work much better than ventilation design, which is because that the most of inner heat source will be taken away through well ventilation and the impact of heat transfer of walls and roof becomes very slight.

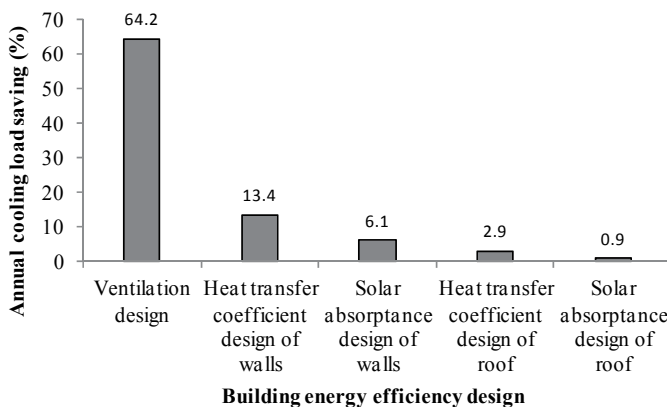


Fig. 14. Annual cooling load saving from various building energy efficiency design.

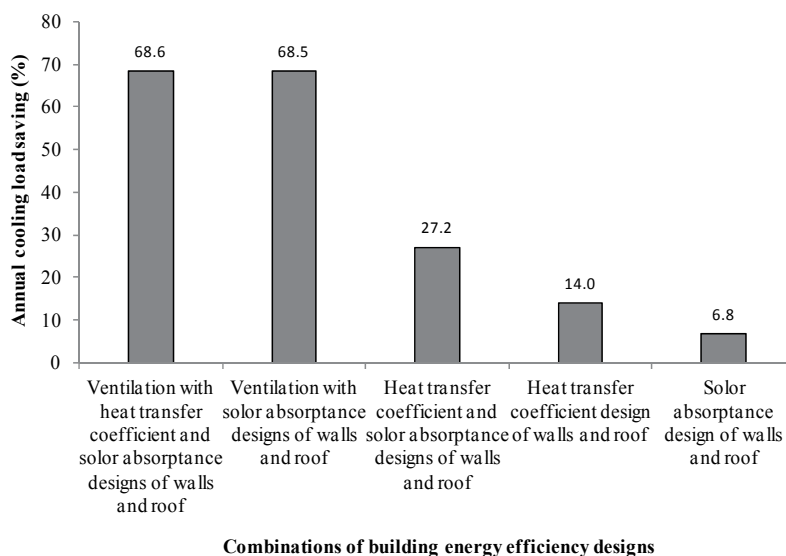


Fig. 15. Annual cooling load saving for combinations of building energy efficiency designs.

4. Study of ventilation cooling technology

It was found that ventilation design is the primary choice for energy efficiency TBS building design. However, there are no studies on TBS ventilation design for energy conservation to date. The envelopes of the existing TBSs are well sealed without any ventilation and the significant cooling capacity of outdoor air in winter, spring, autumn and morning and evening in summer is neglected, resulting in huge energy costs for air conditioning. To make full use of the natural outdoor cooling resources, a new ventilation cooling technology (VCT) was proposed. By applying VCT, the outdoor cold air is imported by fans to dissipate the internal heat of telecommunication equipment directly. The fans, which consume much less electrical power, are substituted for the air conditioners for environmental control when the temperature and humidity of the outdoor air meet the equipment requirements. The runtime of the air conditioners is thus greatly shortened, resulting in remarkable energy savings.

However, there are several practical problems for the application of VCT to the TBS such as: a control strategy for the fans and air conditioners for an environment with guaranteed temperature and humidity to ensure reliable operation of the equipment; the temperature and humidity of the environment itself in the TBS; chemically and mechanically active substances and their conditions in the TBS; the condensation risk on the internal surfaces of the building envelopes; additional costs for reconstruction and the payoff period. Therefore, a feasibility analysis for VCT relative to the above problems should also be carried out.

4.1 Feasibility analysis

4.1.1 Control strategy

Figure 16 shows a schematic drawing of the VCT applied in the typical TBS. The fans and filters are installed on the exterior walls. Air conditioners are also installed as auxiliary

cooling equipment to guarantee the environmental temperature and humidity requirements. There are three situations where the fans and air conditioners are controlled by the control system, i.e.: the fans and air conditioners are both switched off; the fans are switched off and the air conditioners are turned on; and the fans are switched on and the air conditioners are turned off. Figure 17 shows the control strategy for the VCT. If the indoor temperature T_i is lower than the temperature set point of T_{acs} , the fans and air conditioners are both switched off. Otherwise, if the outdoor temperature T_o is higher than the set point of T_{fs} or the indoor relative humidity Φ_i is higher than the set point of Φ_s , the air conditioners are turned on and the fans are switched off. However, if T_o is lower than T_{fs} and Φ_i is lower than Φ_s the air conditioners are turned off and the fans are switched on. These cycles are repeated at regular intervals.

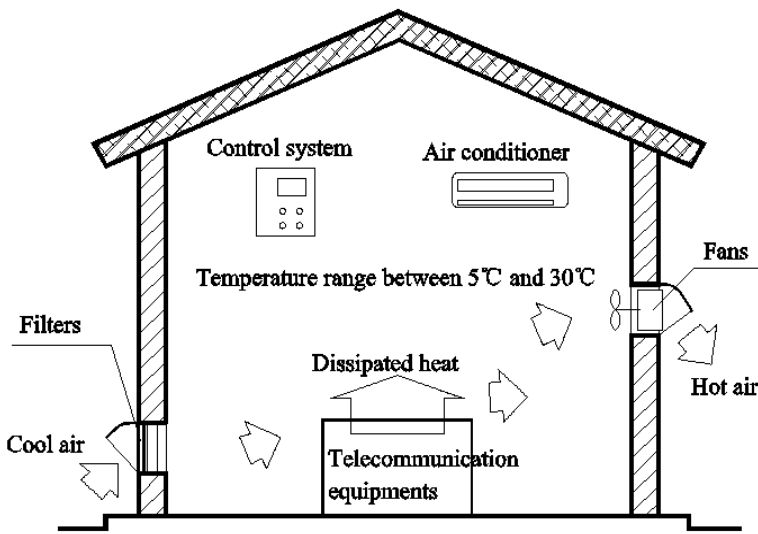


Fig. 16. Schematic drawing of VCT.

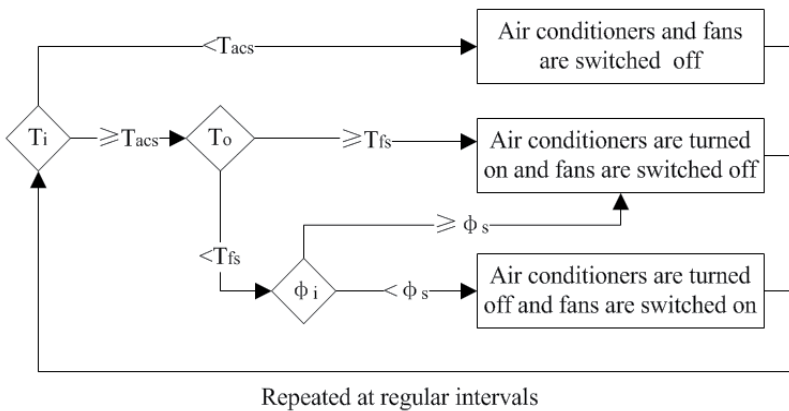


Fig. 17. Control strategy for VCT.

4.1.2 Temperature and humidity environment

The simulation results indicate that the time percentage for an indoor air temperature between 25 °C and 30 °C accounts for 60%, while temperatures between 20 °C and 25 °C account for 20% and those between 5 °C and 20 °C account for 20% (Figure 18). The telecommunication equipment in the typical TBS, called RBS2202, is designed for normal operation in the climatic/mechanical conditions of class 3.1 of ETSI EN 300 019-1-3 (European Telecommunications Standards Institute, 2004). Relative humidity conditions for environmental class 3.1 range from 5% to 85%. The indoor air temperature is much higher than the outdoor air temperature; consequently, the air relative humidity decreases markedly when air is transported into the room. The relative humidity of the air in the TBS is lower than 85% over the majority of the year. The relative humidity set range of air conditioners is from 5% to 85% in the building simulation model, i.e. the room air is humidified when the relative humidity is less than 5% and is dehumidified when the relative humidity exceeds 85%. The simulation results show that there is no need for the room air to be humidified year-round and no need for it to be dehumidified for the vast majority of the year. The dehumidification load is only 6.5 kWh annually. Under the control of the VCT control system, the fans will be turned off and the air conditioners will be switched on automatically to dehumidify the air when the indoor relative humidity exceeds the limit of the range, and consequently the humidity conditions are guaranteed.

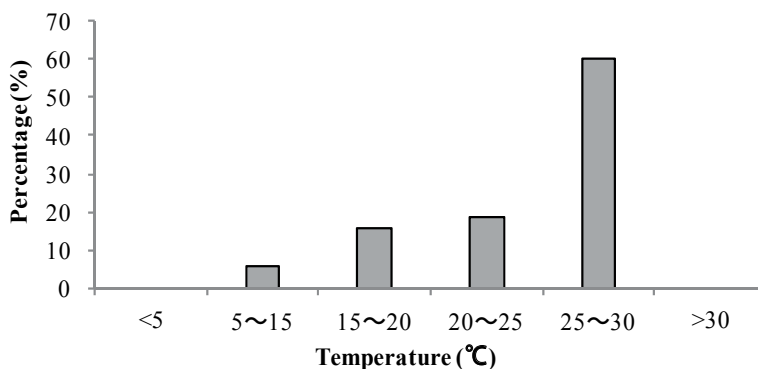


Fig. 18. Time percentage of the indoor air temperature.

4.1.3 Chemically and mechanically active substance conditions

Table 2 shows the atmospheric environment in Guangzhou in recent years and the relative conditions of the chemically and mechanically active substances used in the equipment (European Telecommunications Standards Institute, 2004). The sulphur dioxide and nitrogen oxide content levels meet the acceptable chemically active substance conditions for the equipment. Considering the maximum sedimentation dust content of 8.41 mg/m²h in recent years, filters with filtration efficiency of 85% will be able to maintain an acceptable indoor sedimentation dust content under these conditions. Lower resistance, lower wind pressure loss, ease of maintenance and long cycles for replacement of the filter materials should also be considered during filter selection.

Environmental parameter	Year	Sulphur dioxide	Nitrogen oxides	Dust sedimentation
		(mg/m ³)	(mg/m ³)	(mg/m ² h)
Atmospheric environment in Guangzhou	2001	0.051	0.071	8.41
	2002	0.058	0.068	7.98
	2003	0.059	0.072	8.31
	2004	0.077	0.073	8.21
	2005	0.053	0.068	7.37
	2006	0.054	0.067	7.81
Active substances conditions in equipment		0.3	0.5	1.5

Table 2. Atmospheric environment in Guangzhou in recent years and active substance conditions in equipment.

4.1.4 Condensation risk on the interior surfaces of the building

Water condensation on the interior surfaces of the building envelopes may have negative effects on the telecommunication equipment. Condensation occurs when the interior surface temperature is lower than the air dew-point temperature. The greater the difference there is between the interior surface temperature and the air dew-point temperature, the lower is the possibility of condensation. The air dew-point temperatures were obtained from typical annual meteorological data for Guangzhou and the interior surface temperature was calculated using the building simulation model. Taking the north wall, whose interior surface temperature is the lowest, for analysis, Figure 19 shows that the interior surface temperature is higher than the air dew-point temperature from 1.7 °C to 24.7 °C. Therefore, the condensation risk is quite small.

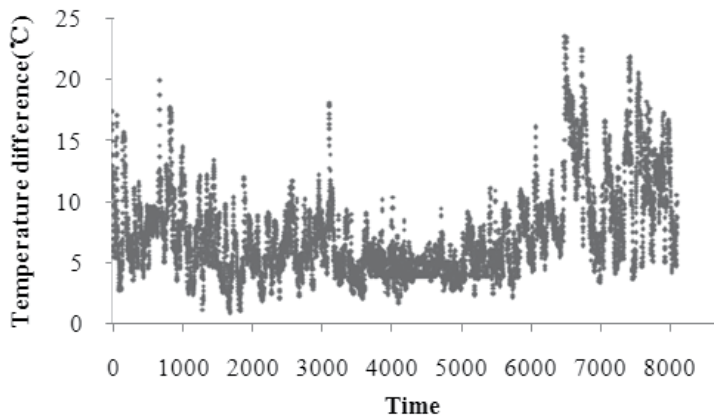


Fig. 19. Difference between the north wall interior surface temperature and the air dew-point temperature.

4.1.5 Cost-effectiveness analysis

The ventilation rate between the outdoor air and the TBS room reaches 50 h^{-1} when fans with total power of 0.22 kW are installed. Because of the high internal heat density, the time when the fans and air conditioners are both turned off is very short. Therefore it can be assumed that the fans run when the air conditioners are switched off (see Figure 13). Table 3 shows that the energy conservation is about 49% for application of VCT to the typical TBS. Additional cost for reconstruction is not more than 5000 RMB, which includes the costs of the fans, filters, ventilation control system and temperature and humidity detectors. Additional maintenance costs for replacing the filter materials are only some hundred RMB annually. The payoff period for the VCT is less than two years, based on a rate of 0.8 Yuan per kilowatt-hour of electricity. The majority of the TBSs in Guangzhou can be reconstructed. Provided that one thousand TBSs are reconstructed and VCT is applied, more than 3 million RMB will be saved annually in electricity bills.

	Typical TBS	Typical TBS using VCT
Annual cooling load of air conditioners (kWh)	31267	11182
Coefficient of performance of air conditioners	3.4	3.4
Power consumption of air conditioners (kWh)	9196	3289
Total power of fans (kW)	0	0.22
Runtime of fans (h)	0	6251
Power consumption of fans (kWh)	0	1375
Total power consumptions (kWh)	9196	4664
Annual Energy conservation (%)	0	49

Table 3. Annual energy conservation of VCT.

4.2 Optimization of airflow organization

The installation location of the fans and openings and the layout of the equipment all influence the temperature and air velocity distribution in the TBS, and therefore influence the heat dissipation of the equipment. Computational fluid dynamics (CFD) simulation provides detailed spatial distributions of the air velocity, air pressure, temperature, contaminant concentration and turbulence by numerically solving the governing conservation equations of fluid flows. It is a reliable tool for the evaluation of thermal environments. A CFD code, PHOENICS, was applied to simulate the temperature and air velocity distributions for the different cases of airflow organization in the typical TBS.

4.2.1 CFD model

Figure 20 shows the model of the typical TBS in PHOENICS created according to the real plan and dimensions of the TBS. The parameters for the simulations were set according to the field investigation results. The simulations were performed under steady state conditions using a k- ϵ turbulent model. A mesh of $0.1\text{ m} \times 0.1\text{ m} \times 0.1\text{ m}$ blocks was used.

The key boundary conditions needed for the calculation comprise:

Openings: External air temperature was set to $22\text{ }^{\circ}\text{C}$, which is the mean air temperature of Guangzhou according to typical annual meteorological data. External pressure was zero relative to the indoor atmospheric pressure.

Fans: The fan delivery was set according to the ventilation rate of 50 h^{-1} .

Envelopes: The walls, floor and roof were assumed to be adiabatic.

Cabinet model: The cabinet model was created according to the actual cabinet. Each cabinet has two inlets, one outlet and two heat sources. Each heat source was assigned a fixed total heat flux of 271.9 W and the total heat flux for all heat sources in the TBS amounted to 4.35 kW . The wind speed of the outlet was set at the measured value of 1.83 m/s . The actual cabinet and the cabinet model are shown in Figure 21.

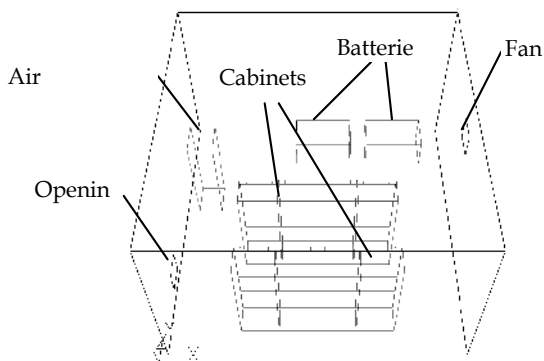


Fig. 20. Model of the typical TBS in PHOENICS.

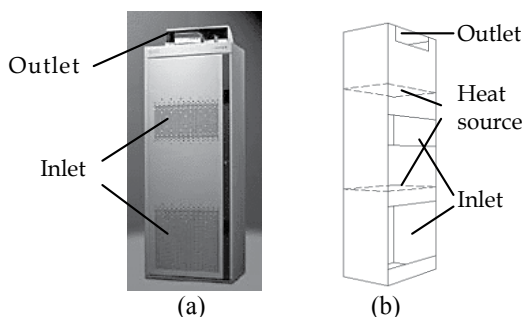


Fig. 21. Actual cabinet (a) and cabinet model (b)

4.2.2 Airflow organization

There are cabinets, batteries, air conditioners, fans and openings in the typical TBS with applied VCT. Taking the convenience of the reconstruction into consideration, the sizes of the openings and the fans should be minimized. The fans and openings are installed on the

exterior walls. The cabinets are relocated for facilitation of the airflow. Several airflow organization cases are proposed as follows:

Case 1: One opening and one fan with dimensions of $0.4\text{ m} \times 0.4\text{ m}$ are installed, where the opening is 0.2 m high and the fan is 1.8 m high.

Case 2: One opening and one fan with dimensions of $0.4\text{ m} \times 0.4\text{ m}$ are installed, where the opening is 1.8 m high and the fan is 0.2 m high.

Case 3: One opening and one fan with dimensions of $0.4\text{ m} \times 0.4\text{ m}$ are installed, where the opening and the fan are both 0.6 m high.

Case 4: Two openings and two fans with dimensions of $0.3\text{ m} \times 0.3\text{ m}$ are installed, where the openings are 0.2 m high and the fans are 1.8 m high.

The total deliveries of the fans in all cases mentioned above were set according to the ventilation rate of 50 h^{-1} . The layout of each case is shown in Figure 22.

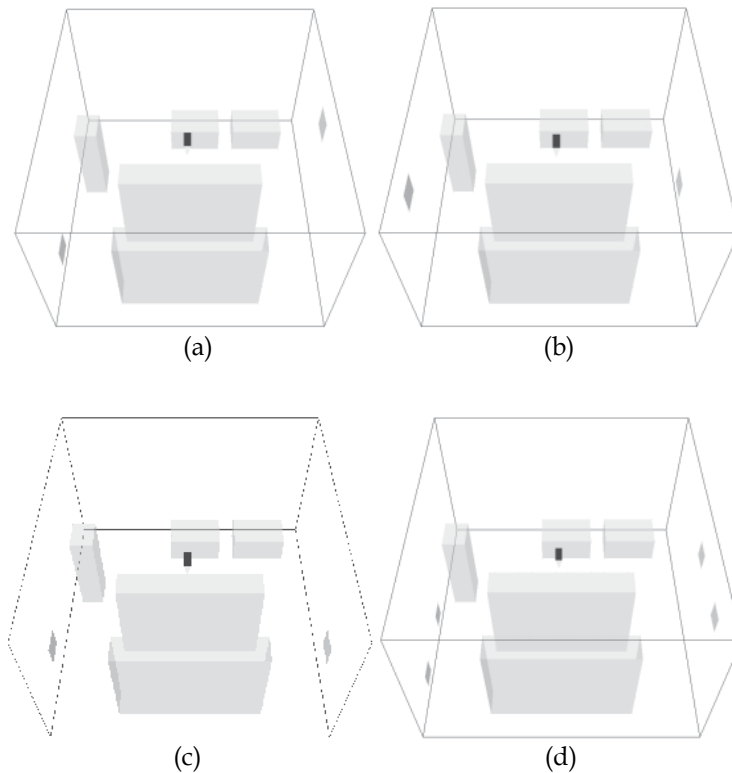


Fig. 22. Layout of each case: (a) Case 1, (b) Case 2, (c) Case 3 and (d) Case 4.

4.2.3 Results and discussion

As cold air is taken into the cabinet through the inlets and dissipated from the outlet, the average temperature of the inlets of all the cabinets for each case is used to evaluate the heat dissipation efficiency. Figure 23 illustrates the contour of indoor temperature of each case at

$z = 0.3$ m. The average temperature of the inlets of each cabinet and of all the cabinets for each case are presented in Figure 24. In Case 2, the cold air is mixed with the hot air exhaust from the cabinets, and the heat dissipation efficiency is greatly reduced. In Case 3, the cool air is quickly dissipated to the outdoors without sufficient heat exchange with the indoor air. In Case 4, due to the additional openings and fans, which are uniformly distributed in the region of the cabinets, the average temperature of the inlets of all cabinets drops by 1.1 °C compared with Case 1. In this study, Case 4 serves as the optimal design.

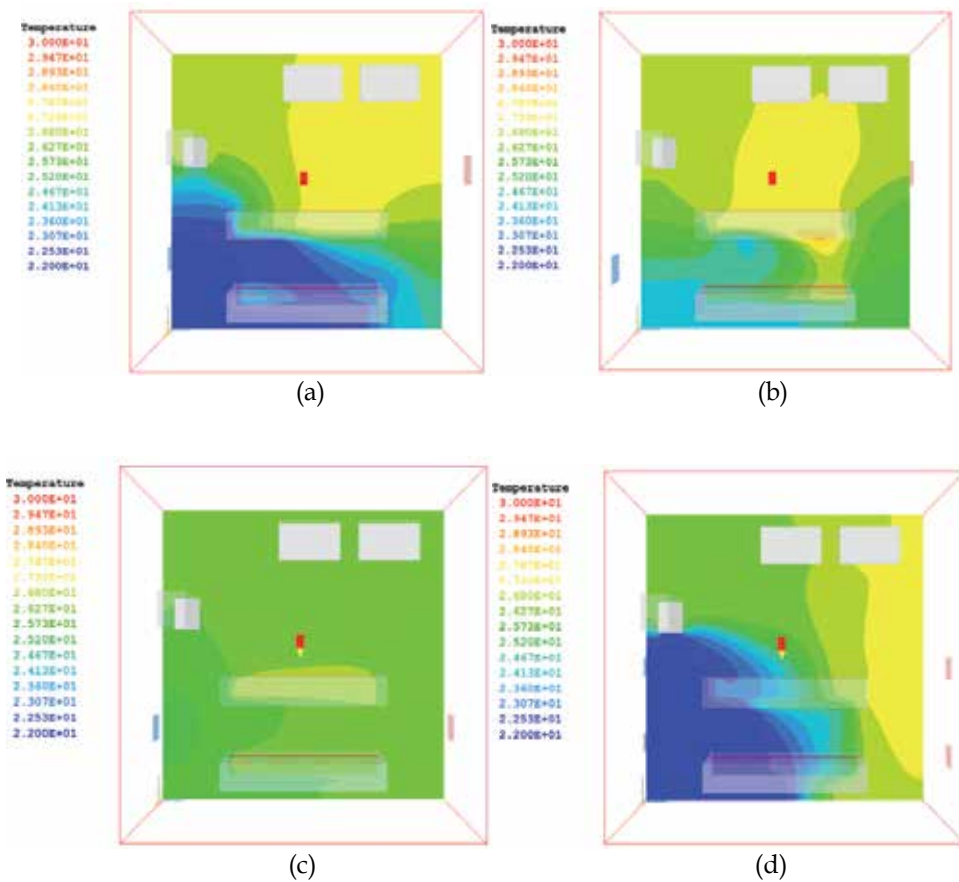


Fig. 23. Contour of indoor temperature (°C) of each case at $z=0.3$ m: (a) Case 1, (b) Case 2, (c) Case 3 and (d) Case 4.

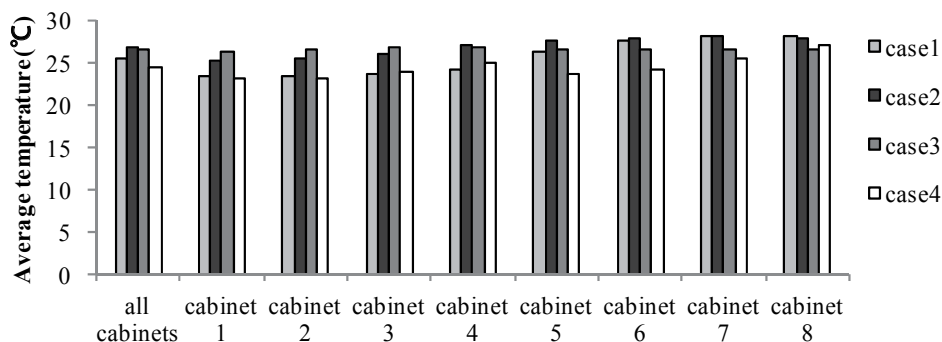


Fig. 24. Average temperature of the inlets of each cabinet and of all cabinets for each case.

Based on the above comparison, the following results are generated:

- 1) The openings should not be set too close to the fans to avoid short circuits.
- 2) The openings should not be set at the height of the outlets of the cabinets, and the fans should not be set at the height of the inlets of the cabinets to avoid mixing of cold and hot air.
- 3) The openings and fans when uniformly distributed in the region of the cabinets can provide a uniform temperature field and better heat dissipation efficiency.
- 4) Results show that optimization of the airflow organization has a strong influence on the heat dissipation efficiency for VCT.

5. Conclusions

TBS buildings have large numbers, high energy consumptions and great potentials on energy conservation. Through field investigation of a typical TBS in Guangzhou, the basic information of TBS was achieved, the key factors influencing energy consumption of TBS were determined and several building energy efficiency designs were proposed. The effect on annual cooling load was analyzed for each building energy efficiency design and the combined effect were achieved for several combinations of the designs by building simulation. The building energy efficiency design strategy for TBS in Guangzhou can be concluded as followings: The indoor air temperature set point of TBS should be elevated to 30 °C regardless of human thermal comfort requirement. Ventilation design is the prior choice for building energy efficiency design of TBS, and other designs are not necessarily considered when ventilation design is applied. For the TBS which is not feasible to apply ventilation design due to practical problems, the combination of designs of high heat transfer coefficient and low solar absorptance walls and roof is strongly recommended.

Study of ventilation cooling technology (VCT) was proposed. The application feasibility of VCT was analysed systematically. The results show that the temperature and humidity requirements of the equipment can be fully met under the linked control of the fans and air conditioners. The chemically and mechanically active substance conditions can be met by using filters with filtration efficiency of 85%. The condensation risk on the interior surfaces of the building envelopes is quite low. The energy conservation achieved by the use of VCT is about 49%, and the payoff period is less than two years. The application of VCT in the TBSs in Guangzhou is feasible, and obvious economic and social benefits will be achieved if VCT can be broadly applied. The PHOENICS CFD code was applied to simulate the

temperature and air velocity distribution for several different airflow organization cases in the typical TBS. The simulation results show that optimization of airflow organization has a strong influence on the efficiency of heat dissipation for VCT.

Acknowledgments

The authors are thankful for the financial support and cooperation of Guangzhou Mobile Communication Corporation. We especially thank the Department of Building Science of the School of Architecture in Tsinghua University for important contributions to the testing.

6. References

- Nakao, M.; Hayama, H. & Uekusa, T. (1988). An efficient cooling system for telecommunication equipment rooms, *Proceedings of the 10th International Telecommunications Energy Conference*, pp. 344-349, San Diego, Canada, October 1988
- Maeda, Y.; Seshimo, Y. & Okazaki, T. (2005). Study of a cooling system for the telecommunication base site, *ASHRAE Transactions*, Vol. 111, No. 2, pp. 746-755, 2005
- Choi, J.; Jeon, J. & Kim, Y. (2007). Cooling performance of a hybrid refrigeration system designed for telecommunication equipment rooms, *Applied Thermal Engineering*, Vol. 27, No. 11-12, pp. 2026-2032, August 2007
- Hayama, H. & Nakao, M. (1989). Air flow systems for telecommunications equipment rooms, *Proceedings of the 11th International Telecommunications Energy Conference*, pp. 1-7, Florence, Italy, October 1989
- Dan, N. & Matti, K. (2000). Application of CFD technique in thermal design of a telecommunication base station, *Proceedings of 9th International Flotherm User Conference*, Orlando, USA, October 2000
- Makhkamdjanov, B.M. (2006). Technological model of the independent power supply with converters of renewable energy for base station of mobile communication, *Proceedings of Internet, 2006 2nd IEEE/IFIP International Conference*, Central Asia, pp. 1-4. Sept. 2006
- Schmidt, R.R. & Shaukatullah, H. (2003). Computer and telecommunications equipment room cooling: a review of literature, *IEEE Transactions on components and packaging technologies*, vol. 26, No. 1, pp. 89-98, March 2003
- Feng, Y. (2004). Thermal design standards for energy efficiency of residential buildings in hot summer/cold winter zones, *Energy and Buildings*, Vol. 36, No. 12, pp. 1309-1312, December 2004
- Athanassios, T.; Andreas, K.A. & Panagiota, K. (2007). Simulation of facade and envelope design options for a new institutional building, *Solar Energy*, Vol. 81, No. 9, pp. 1088-1103, September 2007
- Cheung, C.K.; Fuller, R.J. & Luther, M.B. (2005). Energy-efficient envelope design for high-rise apartments, *Energy and Buildings*, Vol. 37, No. 1, pp. 37-48, January 2005
- Nakao, M.; Ohshima, K. & Jitsukawa, H. (1988). Thermal control wall for telecommunication equipment rooms, *Proceedings of the 10th International Telecommunications Energy Conference*, San Diego, Canada, pp. 280-284, October 1988

- Hong, T.; Zhang, J. & Jiang, Y. (1997). IISABRE: an integrated building simulation environment, *Building and Environment*, Vol. 32, No. 3, pp. 219-224. May 1997
- Bloomfield, D.P. (1994). Final report of IEA Annex 21 (Calculation of Energy and Environmental performance of buildings), *CRC Publications*, London, 1994.
- Zhang, X.; Xie, X.; Yan, D. & Jiang, Y. (2004). Building environment design simulation software DeST (3): validation of dynamic simulation results of building thermal progress, *HV & AC*, Vol. 34, No.9, pp. 37-50, 2004 (in Chinese)
- Yan, D.; Xie, X.; Song, F. & Jiang, Y. (2004). Building environment design simulation software DeST (1): an overview of developments and information of building simulation and DeST, *HV & AC*, Vol. 34, No.7, pp.48-56, 2004 (in Chinese)
- Standardization Institute of Posts and Telecommunications. (1995). *Environmental conditions for telecommunication base rooms, GF 014-1995*, 1995, China (in Chinese)
- European Telecommunications Standards Institute. (2004). *Equipment Engineering (EE); Environmental conditions and environmental tests for telecommunications equipment; part1-3: classification of environmental conditions; stationary use at weather protected locations, ETSI EN 300 019-1-3*, 650 Route des Lucioles, F-06921 Sophia Antipolis Cedex, France, 2004. [Online]. Available: www.etsi.org.

Dynamic Space-Code Multiple Access (DSCMA) System: A Double Interference Cancellation Multiple Access Scheme in Wireless Communications System

Chee Kyun Ng¹, Nor Kamariah Noordin¹, Borhanuddin Mohd Ali¹,
and Sudhanshu Shekhar Jamuar²

¹*Department of Computer and Communication Systems Engineering,
Faculty of Engineering, Universiti Putra Malaysia, Malaysia.*

²*Department of Electrical Engineering,
Faculty of Engineering, Universiti Malaya, Malaysia.*

1. Introduction

It is well known that cellular mobile phone systems have evolved from 1G and 2G that use frequency and time division multiple access (FDMA and TDMA) systems respectively, to code division multiple access (CDMA) of third generation (3G) systems (Chen et al., 2006). Furthermore, the exploitation of spatial diversity from the emergence of advance antenna technologies such as smart antenna and space time signal processing have given rise to induce another multiple access scheme called space division multiple access (SDMA) systems (Fang, 2002). Among these schemes, the system capacity and spectrum efficiency are the key factors to compare the performances of various mobile communication systems.

Since radio frequency (RF) spectrum is a limited resource, these techniques have approached their fundamental limitations. Flexible utilization of such resources in space, time and code has led to great improvement in system capacity. For a given bandwidth, the system capacity for narrowband radio systems such as FDMA and TDMA is dimension or bandwidth limited. In contrast, the system capacity of CDMA and SDMA systems is interference limited. Any reduction in interference in CDMA and SDMA systems converts directly and linearly into increased capacity (Yu et al., 2004), (Chen et al., 2008).

Multiple access schemes such as FDMA and TDMA increase their system capacity and spectrum efficiency by dividing the different network planning phases more clearly into individual parts to allow different frequencies to be used at different time moments (Castaeda & Lara, 2008). In CDMA systems, the same frequency is used simultaneously in adjacent cells and the interference level should be taken into account in the coverage-planning phase (Niemela & Lempiainen, 2003). Furthermore, cell splitting and sectorisation to form SDMA systems with use of directional antenna could also result in increase of system capacity and spectrum efficiency over the omnidirectional antenna system (Godara,

1997). Although these approaches do significantly increase the system capacity and spectrum efficiency, each scheme basically is attempting a more efficient use of the same resource.

It is well known that CDMA system is characterized as being interference limited. Independent simultaneous transmissions by mobile users at different locations in a cell give rise to the near-far phenomenon. To combat the near-far problem, power control is used to ensure equal signal levels are received from all mobile users at different location (Hashem & Sousa, 1997). Therefore, power control is considered the most important system requirement for CDMA systems to increase the system capacity on the reverse link by overcoming the near-far problem (Cameron & Woerner, 1996), (Uthansakul, 2002). Since all the cells can operate with the same channel in CDMA cellular network, a significant source of interference apart from traffic in its own cell is the traffic from neighbouring cells. Thus, the system capacity of CDMA systems is determined by the amount of co-channel interference that it can tolerate, which is comprised of intra-cell interference and inter-cell interference (Wu et al., 1998). If the traffic load in neighbouring cells is reduced, more traffic can be accepted in the observed cell (Chatovich & Jabbari, 1999). However, because of power control from observed cell base station (BS), transmitting a high power level in reverse link may result in high interference to neighbouring cell BS (Hashem & Sousa, 1997). Therefore, in CDMA systems, if the capacity of a single cell increases it creates higher interference to its neighbouring cells and thus impacts their capacity.

Other approach that shows a promise for substantial capacity enhancement is the use of spatial filtering with exploitation of smart antenna at cell site BS (Zheng et al., 1996). Hence, the deployment of SDMA system has been recognised as one of the most promising techniques for controlling co-channel interference in cellular systems, leading to the required system capacity improvement (Liberti & Rappaport, 1998). The beamforming ability of smart antenna technology has been adapted to increase the gain of the desired signal while null interference sources resulting in the improvement of the system capacity (Huang et al., 2001). The narrow beams from smart antenna are steered toward desired users in order to filter out interference caused by co-channel users located in the same cell and from adjacent cells (Galvan-Tejada & Gardiner, 2001).

However, in order to achieve an ideal SDMA system, smart antenna must carefully form its radiation patterns to capture the desired user and to nullify sufficiently interfering users. Therefore, the smart antenna requires high accuracy in propagation channel response estimation (Cho et al., 2002). If there are N elements antenna array used in a smart antenna system, it is only possible to accommodate $N - 1$ users in reverse link (Rapajic, 1998), (Kim et al., 2001). Actually in the randomness of mobile users distribution, this is not always possible to eliminate interferers by null-steering in the corresponding arrival directions. Hence, there will be a probability of two or more mobile users located near to each other. This means that the co-channel interferences will occur among these mobile users when adaptive beams steering smart antenna are employed. On the other hand, the present of sidelobes from smart antenna system will further reduce the signal to interference ratio (SIR) performance of each mobile user. Hence, more sidelobes interferences are radiated in the direction of the desired user main lobe pattern. These sidelobes interferences can significantly reduce the system capacity if multiple beams are synthesized from smart antenna to accommodate the density of mobile users in a particular area.

The wireless channel usually characterized by the path loss, shadowing and fading (Feuerstein et al., 1994). In urban areas, multipath propagation is common, whereby the receiver observes a number of copies of the transmitted signal, each with a different time delay (Adachi et al., 2005). This provides a form of multipath fading. In a digital communication system, the delay-spread of multipath propagation could also cause inter-symbol interference (ISI) (Lien & Cherniakov, 1998). The characteristics of the spreading sequences in CDMA system provide a crucial effect on the performance of the whole communication systems. This signature sequences in general determine how much interference is received at a receiver from other mobile users and influence the extraction capability of the desired signal from noise-like spectrum (Xie & Rahardja, 2005). On the other hand, since the reverse link of a CDMA system is usually asynchronous, in the sense that the arrival times for each mobile user signal are different (Thompson et al., 1996), (Choi et al., 2007). Therefore, the spreading sequences of CDMA systems are characterized with ISI as well as multiple access interference (MAI) (Peterson et al., 1995), (Guo & Wang, 2008). In multipath propagation environment, multiple copies of transmitted signal arrive at receiver with different time delay will cause ISI. A MAI occurs if the orthogonality among spreading sequences is lost (Ishida et al., 2000). The MAI is caused by asynchronous in a CDMA system where each mobile user will observe interference from all other mobile users in the system, since the transmitted signal will not be orthogonal in delay-spread environment (Thompson et al., 1996). Traditional CDMA spreading sequences such as m-sequence (Golomb, 1992), Gold codes (Gold, 1967), and Kasami codes (Kasami, 1966), exhibit non-zero cross-correlation which results in high MAI in asynchronous reverse link transmission. Another family of orthogonal codes is constituted by Walsh codes (Harmuth, 1970) and orthogonal Gold codes (Popovic, 1997), do retain their orthogonality in the case of perfect synchronization, but also exhibit non-zero cross-correlation in asynchronous transmission (Wei et al., 2005). Recently, an attractive family of large area synchronized (LAS) CDMA spreading sequences is introduced in (Li, 2003) has exhibited zero correlation zone (ZCZ) or interference free window (IFW) near zero delay time offset, resulting in zero ISI and MAI within the IFW. The LAS spreading sequence is constituted by the combination of Large Area (LA) code (Li, 1999) and Loosely Synchronous (LS) code (Stańczak et al., 2001). More specifically, the interference-free in CDMA system only become possible when the maximum channel-induced delay-spread is within the designed IFW duration. However, in the system design especially using omnidirectional antenna, not all multipath signal components arrive within IFW time offset. Since the total duration of IFW expressed in terms of the number of chip intervals depend on the minimum zero padding implanted between non-zero pulses interval, thus the number of minimum zero padding must be increased to maximum delay-spread of the channel in LAS sequence in order to accommodate all multipath signal components. This implies that the duty ratio of LAS spreading sequences is low when the number of minimum zero padding is increased. Therefore, a specific drawback of LAS-CDMA is that its relatively efficient orthogonal codes demanded in wireless systems are limited, and hence reduce its spectrum efficiency. Besides that, the implementation of LAS sequences is very complex that additional components are necessary.

There have been many multiple access systems for the cellular system designed to improve its system performance. Several works have been carried out to show the improvement in the system capacity using the joint multiple access system. A careful selection of joints

multiple access from two or more individual systems can determine the fitness of the joint system. Interference-limited systems such as CDMA and SDMA are susceptible to time of arrival (TOA) and angle of arrival (AOA) of individual user signals. Thus, a non-uniform traffic can severely degrade the performance of CDMA and SDMA systems. In this chapter, a joint multiple access of CDMA and SDMA system is proposed. The performance of this joint multiple access system is also vulnerable to the non-uniform traffic. Although the performance of this joint multiple access system has been previously studied in several papers (Liberti & Rappaport, 1994), (Naquib et al., 1994), (Buracchini et al., 1996) and (Ng & Sousa, 1998), none of them considers to evaluate the most realistic of system performance in this joint multiple access.

In this chapter, a new approach called dynamic space-code multiple access (DSCMA) system arising from the combination of CDMA and SDMA systems is designed, and its system performances are then investigated. An innovative approach to eliminate the existing interferences in DSCMA system is introduced. The spreading sequences of Large Area Synchronous Even Ternary (LAS-ET), which exhibited an interference free window (IFW) in their correlation, are exploited here. The spatial signature from smart antenna narrower beam is exploited to drive all the multipath propagation signals to arrive within the IFW in reverse link transmission. The size of IFW is adaptable with the size of smart antenna beamwidth through dynamic space-code (DSC) algorithm. Therefore, the result of combined dominant signature from DSCMA system will yield a perfect interference cancellation so that the system capacity increases dramatically.

2. The Properties of Orthogonal CDMA Sequences

Traditional ways of separating multiple access signals in time or frequency such as TDMA and FDMA are relatively simple by making sure that the signals are orthogonal and non-interfering. However, in CDMA different mobile users occupy the same bandwidth at the same time. They are separated from each other through the use of a set of orthogonal sequences. Two waveforms x and y are said to be orthogonal to each other if their cross-correlation, $R_{xy}(0)$ over T period is zero in time shift τ (Lee, 1998), where

$$R_{xy}(\tau) = \lim_{T \rightarrow \infty} \frac{1}{2T} \int_{-T}^T x(t)y(t+\tau)dt \quad (1)$$

In discrete time, the two sequences x and y are orthogonal if their cross product $R_{xy}(0)$ over T period is zero (Wang et al., 2007). The cross product of $R_{xy}(\tau)$ is defined as

$$R_{xy}(\tau) = \sum_{\tau=-T}^T x(t)y(t+\tau) \quad (2)$$

As an example, the following two sequences or codes, x and y are orthogonal.

$$x = [-1, -1, +1, +1] \quad (3)$$

$$y = [-1, +1, +1, -1] \quad (4)$$

Hence, their cross-correlation is zero.

$$R_{xy}(0) = (-1)(-1) + (-1)(+1) + (+1)(+1) + (+1)(-1) = 0 \quad (5)$$

In order for the set of codes to be used in a multiple access scheme, an additional property is needed. In addition to the zero cross-correlation property, each code in the set of orthogonal codes must have an equal number of +1s and -1s (Faruque, 1996). This second property gives that particular code the pseudorandom nature. A direct sequence CDMA (DS-SS) system spread the baseband data by directly multiplying the baseband data pulses with a pseudorandom or PN sequence that is produced by a PN code generator. A single pulse or symbol of the PN waveform is called a chip, where the chip rate is much higher than the data bit rate (Lee, 1991).

2.1 Welch Bound in CDMA Systems

The CDMA system is a multiple access scheme in which several independent users access a common communication channel by modulating their data symbols with preassigned spreading sequences. The receiver observes the sum of the transmitted signals in additive white Gaussian noise (AWGN) channel. The decoder for a given mobile user treats the sum of the interfering signals from other mobile users as noise. The spreading sequences are chosen to create good single user channels for the individual coding systems. In fact, however, the channel created by the spreading sequences is susceptible to MAI (Rupf & Massey, 1994). In 1974, Welch in (Welch, 1974) had shown that the lower bound for the acceptable sidelobes of auto-correlation and cross-correlation functions are set around $SF^{-\frac{1}{2}}$, where SF is the spreading factor or processing gain of the system. This lower bound is called as Welch bound (Li, 2003). Signature sequences that maximize the sum capacity in the uplink of CDMA systems in AWGN channel are known to satisfy Welch's bound on the total squared correlation with equality (Heath et al., 2004).

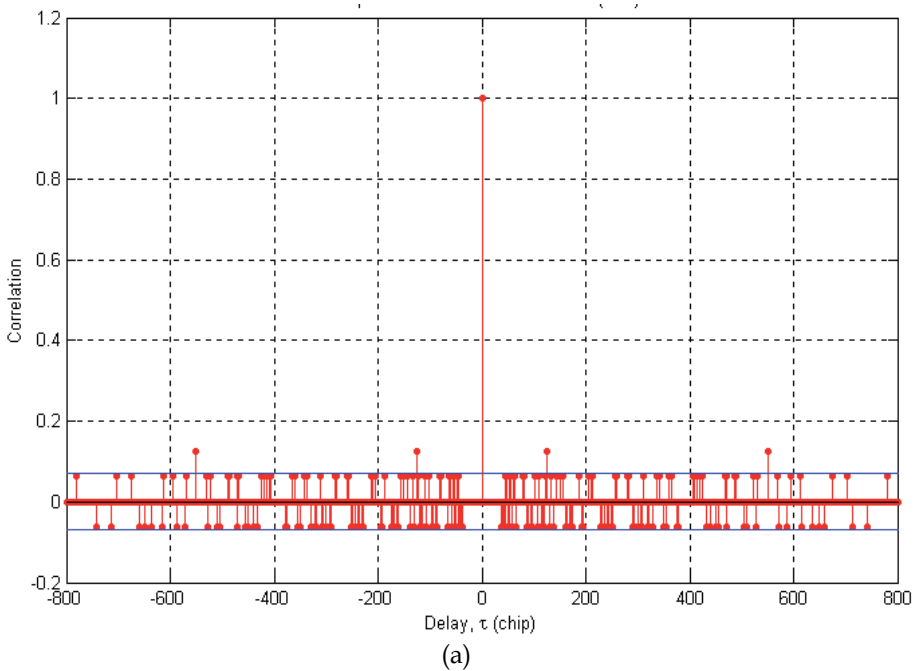
2.2 LAS-ET Sequences

The original LAS codes proposed in (Li, 1999) are synthesized by seeding LS codes in LA codes to improve it spectrum efficiency. An N_p LA codes are synthesized in such a manner that the N_p non-zero ± 1 pulses from m -sequences oriented are positioned as shown in Table 1. This arrangement forms a configuration of $LA(N_p, K_0, L_c)$ where K_0 is the minimum number of zero padding in pulse interval of non-zero pulses which determine the size of IFW delay-spread in term of chips, while having a total code length of L_c chips.

	0	38	78	120	164	210	258	308	360	414	470	530	592	660	732	808	847
C1	+	+	+	+	+	+	+	+	+	+	+	+	+	+	+	+	+
C2	+	+	+	+	-	-	-	-	+	-	+	-	-	+	+	-	+
C3	+	+	+	-	-	-	-	+	-	+	-	-	+	+	-	+	+
C4	+	+	-	-	-	-	+	-	+	-	-	+	+	-	+	+	+
C5	+	-	-	-	-	+	-	-	-	-	+	+	-	+	+	+	+
C6	+	-	-	-	+	-	+	-	-	+	+	-	+	+	+	-	+
C7	+	-	-	+	-	+	-	-	+	+	-	+	+	+	-	-	+
C8	+	-	+	-	+	-	-	+	+	-	+	+	+	-	-	-	+
C9	+	+	-	+	-	-	+	+	-	+	+	+	-	-	-	-	+
C10	+	-	+	-	-	+	+	-	+	+	+	-	-	-	-	-	+
C11	+	+	-	-	+	+	-	+	+	+	-	-	-	-	+	-	+
C12	+	-	-	+	+	-	+	+	+	-	-	-	-	+	-	+	+
C13	+	-	+	+	-	+	+	+	-	-	-	-	+	-	+	-	+
C14	+	+	+	-	+	+	+	-	-	-	-	+	-	+	-	-	+
C15	+	+	-	+	+	+	-	-	-	-	+	-	+	-	-	+	+
C16	+	-	+	+	+	-	-	-	-	+	-	+	-	-	+	+	+

Table 1. The arrangement of 16 $LA(16,38,847)$ sequences

In order to exploit the characteristics of LA sequences proposed in (Li, 1999) without altering the size of its IFW, a modified version of the sequence such LAS-ET sequences (Ng et al., 2009) is employed in DSCMA instead of LAS-CDMA sequences proposed in (Li, 2003) which exhibit a small IFW. Figure 1 shows the correlation properties of the $LAS - ET(16,38,818)$ sequences. As can be seen in these figures, the correlation properties of $LAS - ET(16,38,818)$ sequences are similar to the original proposed $LA(16,38,847)$ sequences which exhibited a large IFW around the origin. The cross-correlation value of $LAS - ET(16,38,818)$ sequence in zero delay spread is 4.03×10^{-17} .



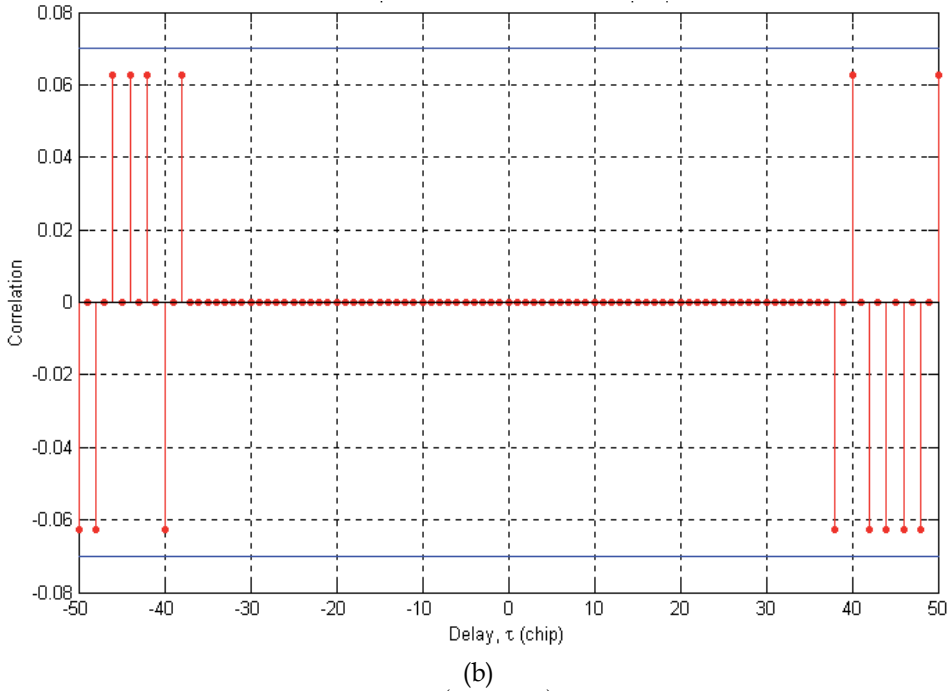


Fig. 1. Correlation properties of $LAS - ET(16,38,818)$ sequence; (a) auto-correlation and (b) cross-correlation.

3. Reverse Link Capacity of SDMA System

The conventional SDMA systems increase its capacity by spatial filtering the interferences. The system continuously adapts its narrower beam from smart antenna system to steer each mobile user with the main lobe while isolating interferences with nulls. Hence, SDMA is allowed to reuse the limited radio resources (frequency, time and code) within a cell. From Equation (1) in (Ng et al., 2008), the nulls' AOA, ψ_{nulls} of the SDMA radiation pattern occur at

$$\psi_{nulls} = \cos^{-1} \left[2 \left(\frac{h}{N_e} - \frac{\alpha}{2\pi} \right) \right] \quad (6)$$

where N_e is the number of elements in smart antenna system, α is progressively phase shift, and h is any integer but not equal to 0, $n, 2n, \dots$

Figures 2a and 2b show the typical SDMA system for $N_e = 8$ and 32 respectively with 90° AOA of the desired user. For $N_e = 8$, the nulls to accommodate interfering users are occurred at $41.41^\circ, 60^\circ, 75.52^\circ, 104.48^\circ, 120^\circ$ and 138.59° , while the nulls for $N_e = 32$ are occurred at $20.36^\circ, 28.96^\circ, 35.66^\circ, 41.41^\circ, 46.57^\circ, 51.32^\circ, 55.77^\circ, 60^\circ, 64.06^\circ, 67.98^\circ, 71.79^\circ, 75.52^\circ, 79.19^\circ, 82.82^\circ, 86.42^\circ, 90^\circ, 93.58^\circ, 97.18^\circ, 100.81^\circ, 104.48^\circ, 108.21^\circ, 112.02^\circ, 115.94^\circ, 120^\circ,$

124.23°, 128.68°, 133.43°, 138.59°, 144.34°, 151.05° and 159.64°. These figures show that the system capacity, K of SDMA system is direct proportional to the number of antenna elements in smart antenna with expression below (Rapajic, 1998)

$$K = N_e - 1 \quad (7)$$

The interfering users are only allowed to be located at null AOAs, otherwise co-channel interferences between mobile users will occur. Any additional mobile user into this system after the limited nulls are fully occupied will also cause co-channel interference to other mobile users.

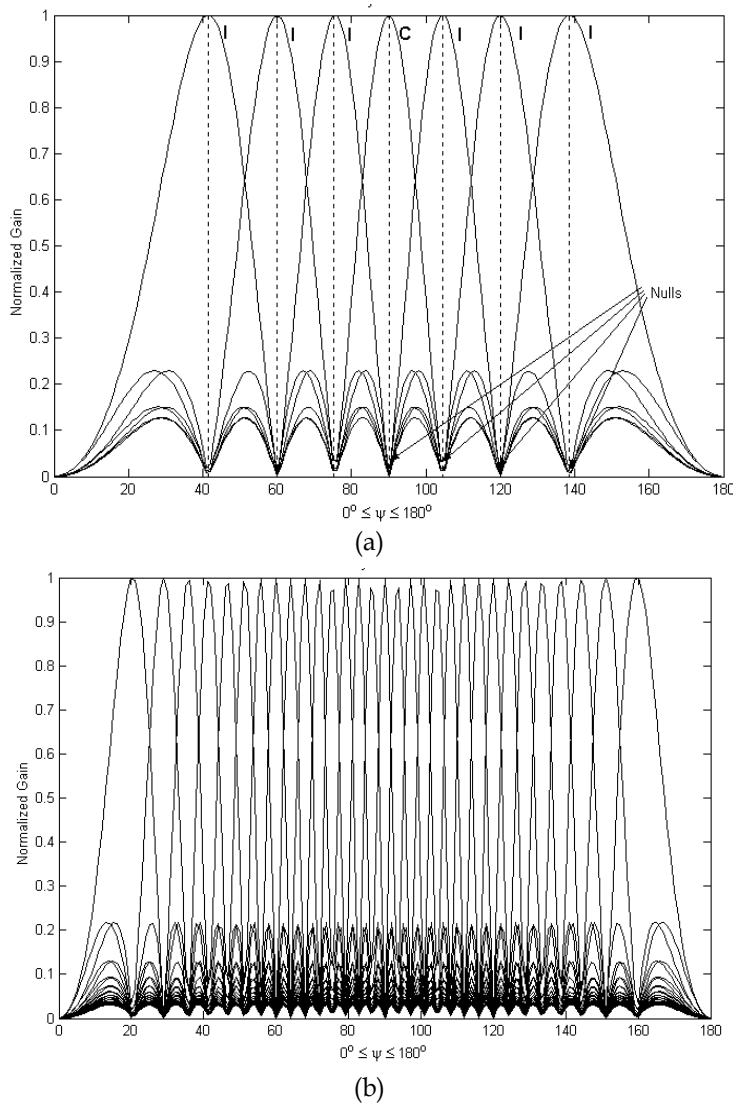


Fig. 2. Radiation pattern of SDMA system for (a) $N_e = 8$ and (b) $N_e = 32$.

It has been reported that smart antenna can synthesize a high directive beam toward the desired user while nulling the interfering users to increase capacity. However, fully nulling the interfering users in SDMA system do not take place because there are two major interference sources, which are side-lobes and co-channel interferences. The interfering users will not always locate at the nulls of the desired user radiation pattern especially in randomly distributed traffic environment as shown in Figure 3.

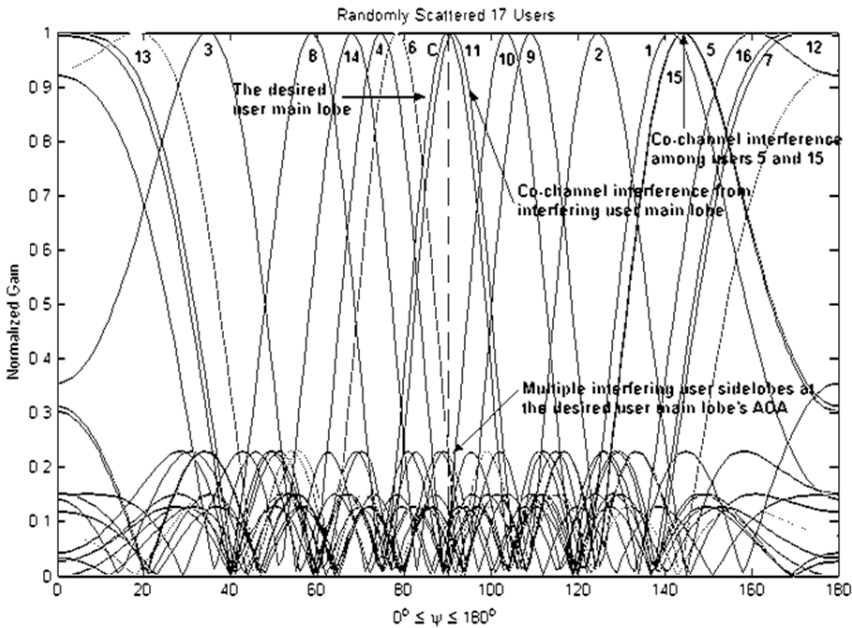


Fig. 3. Co-channel and side-lobes interferences to the desired user, C from randomly located interfering users of 1, 2, 3, 4,....., 16

4. Dynamic Space Code Multiple Access (DSCMA) System

Non-uniformly distributed traffic usually degrades the performance of CDMA and SDMA systems severely in the reverse link. The imperfect correlation properties of the traditional CDMA spreading sequences result in ISI and MAI at non-zero delay spread. The random positions of mobile users will cause MAI among them in the SDMA system, where positions at nulls of the desired user radiation pattern are rarely achieved. Therefore, the non-uniform traffic causes loss of orthogonality to distinguish each mobile user in the conventional interference limited systems.

Here, a promising solution to deploy the BS with smart antenna system to perform the joint multiple access of CDMA and SDMA systems is proposed. The CDMA and SDMA systems are adapted to each other dynamically to form DSCMA system. This proposed multiple access scheme is a novel interference cancellation scheme that employ the spreading sequences of CDMA system into spatial signatures of SDMA system through DSC algorithm. In DSC algorithm, the size of dedicated IFW from LAS-ET spread sequence is

adapted dynamically to the size of half power synthesized beamwidth from smart antenna beamforming system as shown in Figure 4. In this joint multiple access scheme, each user is assigned an LAS-ET sequence within a high directivity beam. Hence, the integration of these two signature schemes, spatial filtering and spreading sequence, creates a dominant signature scheme called DSC signature. Therefore, by using this dominant signature scheme, the inherent interferences in CDMA and SDMA systems environment can be eliminated.

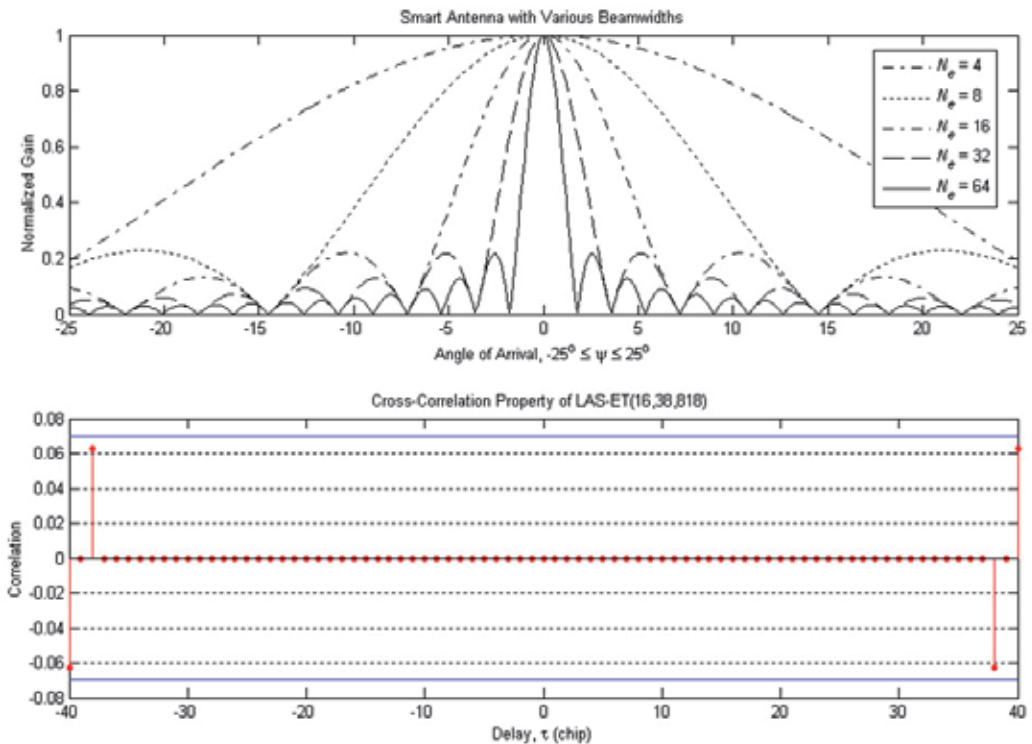


Fig. 4. Performance of various beamwidths in smart antenna system over IFW region from correlation property of $LAS-ET(16,38,818)$ sequences.

As shown in previous section, the co-channel interference between two mobile users in SDMA system occurs when both of them are located close to each other. For example, assuming that the desired user, C is located at AOA of 90° to the smart antenna axis while other mobile users are randomly located within the AOA of 0° to 180° as shown in Figure 3. It is observed that the 11th user's beam is located very near to C with only 0.6° separation. This phenomenon causes co-channel interference between them while other mobile users also contribute interferences to C through their sidelobes radiation pattern. It is possible to mitigate these co-channel interferences by CDMA spreading sequences. However, all traditional CDMA spreading sequences are self-interference systems when all signals from each mobile user arrive at the BS in asynchronous manner. The auto-correlation and cross-correlation properties of traditional CDMA sequences are not orthogonal at non-zero delay

spread, $\tau > 0$. Thus, it shows that interference occur among the mobile users in asynchronous transmission environment.

Therefore, it is necessary to prefer spreading sequences that exhibit zero correlation between each other to drive all the asynchronous signal components to drop within the smart antenna's narrow beam maximum propagation delay spread. Hence, a spreading sequence that exhibits large size of IFW is required to accommodate large beamwidth of smart antenna radiation pattern. Considering Figure 3 again, there is group of beams with their AOA respectively to accommodate 17 randomly distributed mobile users. Each beam is assigned to different mobile user with an LAS sequence order, $C_1, C_2, C_3, C_4, C_5, \dots, C_m$, where m is the maximum number of total available sequence. These sequences are assigned to mobile users in chronological order upon their arrival and can be reused dynamically whenever needed.

To illustrate how directive beam can improve the reverse link in a single cell of DSCMA system, consider the case in which each mobile user has an omnidirectional antenna, and the BS tracks each mobile user in the cell using a directive beam. Assume that the beam pattern, $G(\psi)$ in formed such that the pattern has a maximum gain in the AOA of the desired user. Such a directive pattern can be formed using an N_e elements smart antenna array. Assume that K users in the single cell of DSCMA system are non-uniformly distributed throughout a cell. On the reverse link, the power received from the desired user signal is $P_{r,0}$ with maximum gain of $G_0(\psi_0)$. The received powers from $K - 1$ interfering users are given by $P_{r,i}$ for $i = 1, 2, \dots, K - 1$. Then the average total received interference power, I seen at the desired user AOA, ψ_0 at the BS is given by

$$I = E \left\{ \sum_{i=1}^{K-1} G_i(\psi_0) P_{r,i} \right\} \quad (8)$$

where $G_i(\psi_0)$ is the i th interference gain level of smart antenna radiation pattern seen at the AOA of the desired user. The value of $G_i(\psi_0)$ can be obtained from Equation (1) in (Ng et al., 2008) and is given as

$$G_i(\psi_0) = \frac{1}{N_e} \left| \frac{\sin N_e(\pi k \cos \psi_0 + \alpha_i/2)}{\sin(\pi k \cos \psi_0 + \alpha_i/2)} \right| \quad (9)$$

where k is given as 0.5 for half wavelength spacing between elements to avoid the appearance of grating lobe in the system, and parameter α_i is the phase shift of the smart antenna to steer the beam in ψ_i direction of i th interfering user. If the perfect power control is applied such that the received power at the BS antenna from each mobile user is the same, then $P_{r,i} = P_c$ for each of K users, and hence the average interference power seen by the desired user is given by

$$I = P_c E \left\{ \sum_{i=1}^{K-1} G_i(\psi_0) \right\} \quad (10)$$

5. Reverse Link Interferences in DSCMA System

In DSCMA system, a BS equipped with smart antenna transmits signal to each mobile user in forward link transmission using a synthesized narrow beam and a dedicated spreading sequence. The signal is perfectly synchronized at transmission so that it arrives at mobile receiver in synchronism with zero delay spread. Consequently, due to the orthogonalities of both spatial signature and spreading sequence in zero delay spread among the K users in a cell, each mobile receiver can demodulate its own signal without interference from other transmitted signals that share the same channel.

However, this synchronism in forward link transmission cannot be maintained in reverse link transmission where all the signals from K users are rather arrived at BS in asynchronized manner. Thus, the signals from the other mobile users appear as additive interference to the desired user signal if the orthogonalities of both spatial signature and spreading sequence among them are loss in non-zero delay-spread. The reverse link interferences are twofold: the interference arising from $K - 1$ users in the same cell or can be known as intra-cell interference, and the interference arising from mobile users in neighbouring cells or also called as inter-cell interference. Hence, the system capacity of DSCMA is examined by considering both intra-cell and inter-cell interference environments in reverse link transmission.

5.1 Intra-cell Interference

Suppose that each cell has K randomly distributed mobile users. With the use of perfect instantaneous power control, all K user signals are arriving at the BS with the same power level S within the same cell. Therefore, the intra-cell interference, I_{intra} from $K - 1$ interfering users is given as

$$I_{intra} = (K - 1)S \quad (11)$$

In DSCMA system, the $K - 1$ interferences power level are not same in the AOA of the desired user, ψ_0 . Nevertheless, the interfering signals from $K - 1$ users are still received at the same power level S from their respective AOA through perfect power control. Most of these interfering signals contribute merely side-lobe interferences with $G_i(\psi_0) < S$ in ψ_0 direction. Some of the interfering signals are also received at the same power level, $G_i(\psi_0) = S$ when they are at the same AOA of the desired user.

The arbitrarily interferences level, $G_i(\psi_0)$ as shown in Figure 3 with 16 interfering users can be analogously as multiple dots along the line of radiation pattern as shown in Figure 5. This is assuming that all radiation patterns for all mobile users are same. Hence, from (9) and (11), the intra-cell interference in AOA of mobile user C , $I_{intra}(\psi_0)$ yields to

$$I_{intra}(\psi_0) = S \cdot \sum_{i=1}^{K-1} G_i(\psi_0) = \frac{S}{N} \cdot \sum_{i=1}^{K-1} \left| \frac{\sin N(\pi k \cos(\psi_0) + \alpha_i / 2)}{\sin(\pi k \cos(\psi_0) + \alpha_i / 2)} \right| \quad (12)$$

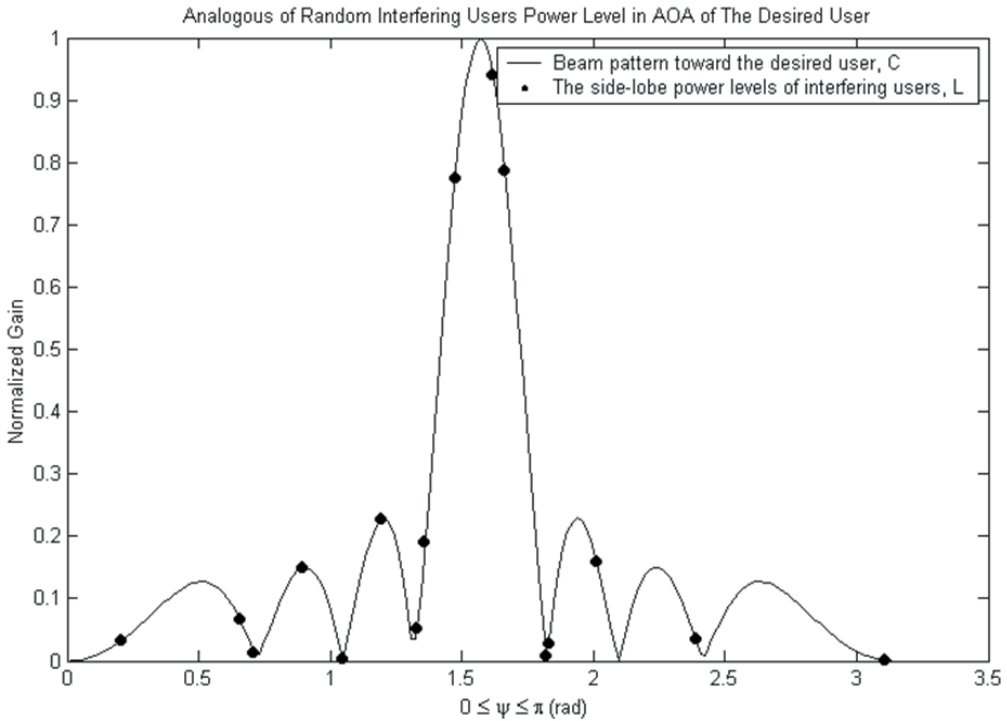


Fig. 5. The analogously random side-lobes interferences from 16 interfering users in AOA of the desired user

5.2 Inter-cell Interference

In the multi-cell of DSCMA system, the interference analysis in reverse link becomes complicated. This is because the mobile users are power controlled by their own cell BS. The membership of the user is determined by the maximum pilot signal power among the cells and not the minimum distance from a cell BS. The mobile users are connected to a BS that offers the lowest signal attenuation rather than the closest BS (Gilhousen et al., 1991). Because of power control, the interference level received from mobile users in neighbouring cells depends on two factors: attenuation in the path to the desired user's cell BS, and attenuation in the path to the mobile user's cell BS. Thus, in the fourth power law of distance, the user's transmitted power P_t can be expressed as (Chatovich & Jabbari, 1999)

$$P_t = P_r r^4 10^{(\zeta/10)} \tag{13}$$

where P_r is the received signal power at its BS, ζ is the log-normal Gaussian random variable with zero mean and standard deviation, σ of 8 dB, and r is the distance from the mobile user to BS. Since only average power levels are considered, the effects of multipath fading are ignored. To evaluate inter-cell interference, $I_{inter}(\psi_0)$ in DSCMA, consider an

interfering user located in m th neighbouring cell at a distance r_m from its base station BS_m and r_0 from the desired user base station BS_0 as shown in Figure 6.

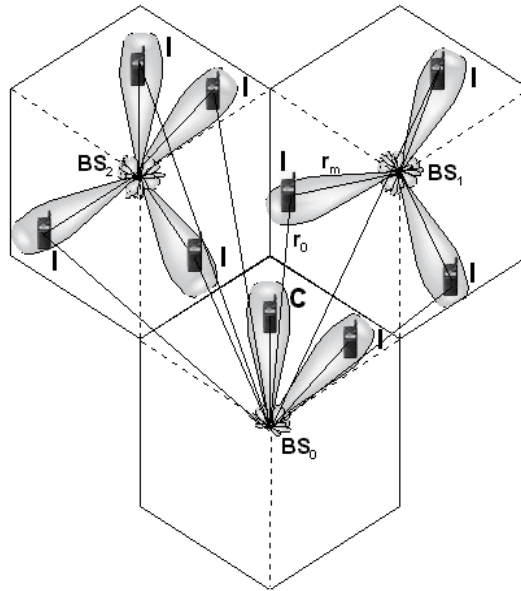


Fig. 6. Inter-cell interference environment model.

If P_t is its transmit power, the received power S at its BS is given by

$$S = \frac{P_t G_m(\psi_m)}{10^{(\zeta_m/10)} r_m^4} \tag{14}$$

where $G_m(\psi_m)$ is the antenna gain in the AOA of the interfering user to its cell BS_m , and ζ_m is the Gaussian random variable representing the shadowing process in its cell. Then the interference I received at BS_0 is given by

$$I = \frac{P_t G_0(\psi_{mi})}{10^{(\zeta_0/10)} r_0^4} \tag{15}$$

where $G_0(\psi_{mi})$ is the antenna gain of BS_0 in the AOA of the i th interfering user from m th neighbouring cell to BS_0 , and ζ_0 is the Gaussian random variable representing the shadowing process in the desired user cell.

Hence, from (14) and (15), the interference to signal ratio, I/S is given by

$$\frac{I}{S} = \left(\frac{r_m}{r_0}\right)^4 \cdot \left(\frac{G_0(\psi_{mi})}{G_m(\psi_m)}\right) \cdot 10^{(\zeta_m - \zeta_0)/10} \tag{16}$$

where the first term is due to the attenuation caused by distance and blockage to the given BS, while the third term is the effect of power control to compensate for the corresponding attenuation to its BS. Since ζ_m and ζ_0 are independent their difference has zero mean and variance $2\sigma^2$ (Cooper & Nettleton, 1978). The second term reveals the total antenna gain received in the AOA of the interfering user to the BS_0 , and its value is less than unity. In DSCMA, this second term will only has a maximum value when an interfering user from a neighbouring cell is located at the same AOA of the desired user, ψ_0 . Then $G_0(\psi_{mi})$ in (16) will become

$$G_0(\psi_{mi}) = \frac{1}{N_e} \cdot \sum_{m=1}^6 \sum_{i=1}^{K-1} \left| \frac{\sin N_e (\pi k \cos(\psi_{mi}) + \alpha_0 / 2)}{\sin(\pi k \cos(\psi_{mi}) + \alpha_0 / 2)} \right| \quad (17)$$

For all values of the parameters in (16), I/S is less than unity. If its value is not less than unity then the user would switch to the other cell BS. Therefore, $I_{inter}(\psi_0)$ in DSCMA is found by summing (16) for all mobile users in the first tier neighbouring cells

$$I_{inter}(\psi_{mi}) = \sum_{m=1}^6 \sum_{i=1}^{K-1} S \cdot \left(\frac{r_{mi}}{r_{0i}} \right)^4 \cdot \left(\frac{G_0(\psi_{mi})}{G_m(\psi_m)} \right) \cdot 10^{(\zeta_{mi} - \zeta_{0i})/10} \quad (18)$$

where $G_m(\psi_m) = 1$ which the gain to theirs mobile user is 1.

6. DSCMA System Signalling

To simplify the derivation, only the baseband signal of transmitted signal is being considered. Hence, in DSCMA system, the transmitted signal from the i th user, $s_i(t)$ that occupies the i th spreading sequence for $i = 1, 2, \dots, K - 1$ can be written as

$$s_i(t) = \sqrt{P} d_i(t) c_i(t) \quad 0 \leq t \leq T \quad (19)$$

Assuming that the desired user is user 0 and all the other $K - 1$ users are interfering users. The received signal, $r(t)$ is a sum of the transmitted signals from all K users and corrupted by its additive complex Gaussian thermal noise, $n(t)$ in an AWGN channel. The signal of each mobile user arrives at a different propagation delay, τ_i . Thus, the received signal at the BS equipped with smart antenna beamforming network in the AOA of user 0 can be expressed as

$$r(\psi_0, t) = \sum_{i=0}^{K-1} s_i(t - \tau_i) \sqrt{G_i(\psi_0)} + n(t) = \sum_{i=0}^{K-1} \sqrt{P} \sqrt{G_i(\psi_0)} d_i(t - \tau_i) c_i(t - \tau_i) + n(t) \quad (20)$$

where $G_i(\psi_0)$ denotes as i th radiation pattern gain of i th user in the AOA of user 0. This equation signifies the combination of CDMA and SDMA by the terms $G_i(\psi_0)$. When

$G_0(\psi_0)$ is normalized to 1, the generated $G_i(\psi_0)$ will be less than 1 if the i th interfering user is not located at the same AOA as user 0. For a conventional CDMA system, $G_i(\psi_0)$ will take the value of 1. This signal is then despread with the spreading sequence of user 0 at the receiver. A correlation-based detector is used to obtain the appropriate decision, z_0 which can be derived as

$$z_0 = \int_0^T r(\psi_0, t) c_0(t - \tau_0 - \tau_e) dt \tag{21}$$

where τ_e is the sequence synchronization error, which degrades the auto-correlation properties. If perfect synchronization is assumed as in the case of directional antenna, where the multipath fading effect is neglected, then $\tau_0 = \tau_e = 0$. Thus, Equation (21) leads to

$$\begin{aligned} z_0 &= \int_0^T r(\psi_0, t) c_0(t) dt \\ &= \int_0^T \left[\begin{aligned} &\sqrt{P} \sqrt{G_0(\psi_0)} d_0(t) c_0^2(t) + \sum_{i=1}^{K-1} \sqrt{P} \sqrt{G_i(\psi_0)} d_i(t - \tau_i) c_i(t - \tau_i) c_0(t) \\ &+ n(t) c_0(t) \end{aligned} \right] dt \\ &= S + I + \eta \end{aligned} \tag{22}$$

7. Probability of Error Evaluation in DSCMA System over AWGN Channel

A bit error rate (BER) expression for DSCMA is derived over MAI from the other $K - 1$ users in an AWGN channel. The derivation is performed at the baseband level, which will simplify the analysis. From the previous section, the first term of (22), S is the transmitted signal of user 0, where

$$S = \int_0^T \sqrt{P} \sqrt{G_0(\psi_0)} d_0(t) c_0^2(t) dt \tag{23}$$

Considering that $G_0(\psi_0) = 1$, $c_0^2(t) = 1$ and $d_0 = \pm 1$, thus Equation (23) becomes

$$S = \pm \sqrt{PT} \tag{24}$$

The term η in (22) is the noise component due to $n(t)$ in AWGN channel, which corresponds to the despread term of $n(t)$ attributes to

$$\eta = \int_0^T n(t) c_0(t) dt \tag{25}$$

Since $n(t)$ is the zero mean AWGN having a variance of $\sigma^2 = N_0/2$, thus η is also a zero mean Gaussian variable and a variance of $Var[\eta]$, which is derived as

$$\begin{aligned} Var[\eta] &= E[\eta^2] \\ &= E\left[\int_0^T n(t)c_0(t)dt \int_0^T n(u)c_0(u)du\right] \\ &= \int_0^T \int_0^T E[n(t)n(u)]c_0(t)c_0(u)dtdu \end{aligned} \quad (26)$$

But $E[n(t)n(u)]$ is the auto-correlation of $n(t)$, where

$$E[n(t)n(u)] = \frac{N_0}{2} \delta(t-u) \quad (27)$$

Therefore, the variance of (26) becomes

$$\begin{aligned} Var[\eta] &= \frac{N_0}{2} \int_0^T \int_0^T \delta(t-u)c_0(t)c_0(u)dtdu \\ &= \frac{N_0}{2} \int_0^T c_0^2(u)du \\ &= \frac{N_0 T}{2} \end{aligned} \quad (28)$$

The term I in (22) is the MAI component of the $K - 1$ interferers, which is given by

$$I = \sum_{i=1}^{K-1} \sqrt{P} \sqrt{G_i(\psi_0)} \int_0^T d_i(t - \tau_i) c_i(t - \tau_i) c_0(t) dt \quad (29)$$

Since $\int_0^T c_i(t - \tau_i) c_0(t) dt$ is cross-correlation between sequences c_i and c_0 , thus

$$\int_0^T c_i(t - \tau_i) c_0(t) dt = R_{i,0} T \quad (30)$$

and $d_i(t - \tau_i) = \pm 1$, therefore I is reduced to

$$I = \pm \sqrt{PT} \sum_{i=1}^{K-1} \sqrt{G_i(\psi_0)} R_{i,0} \quad (31)$$

The signal to interference plus noise ratio (SINR) is then given as

$$SINR = \frac{S^2}{Var[\eta] + I^2} \quad (32)$$

Therefore, from (24), (28) and (31), the SINR for the DSCMA system can be expressed as

$$\begin{aligned}
 SINR &= \frac{PT^2}{\frac{N_0T}{2} + PT^2 \sum_{i=1}^{K-1} G_i(\psi_0)R_{i,0}^2} \\
 &= \left[\frac{\frac{N_0T}{2} + PT^2 \sum_{i=1}^{K-1} G_i(\psi_0)R_{i,0}^2}{PT^2} \right]^{-1} \\
 &= \left[\frac{N_0}{2PT} + \sum_{i=1}^{K-1} G_i(\psi_0)R_{i,0}^2 \right]^{-1}
 \end{aligned} \tag{33}$$

Since the amplitude of each mobile user's signal is \sqrt{P} , then the energy per bit is $E_b = PT$. The Equation (33) leads to

$$SINR = \left[\frac{1}{2E_b/N_0} + \sum_{i=1}^{K-1} G_i(\psi_0)R_{i,0}^2 \right]^{-1} \tag{34}$$

Assuming that the combining noise and interference components have a Gaussian distribution, then the BER is given as

$$BER = Q(\sqrt{SINR}) = Q\left(\left[\frac{1}{2E_b/N_0} + \sum_{i=1}^{K-1} G_i(\psi_0)R_{i,0}^2 \right]^{\frac{1}{2}} \right) \tag{35}$$

where $Q(x)$ is the Gaussian Q-function.

For the interference limited of DSCMA system where thermal noise is not a factor due to

$$\frac{E_b}{N_0} = SF \frac{E_c}{N_0} \tag{36}$$

where the resultant of E_b/N_0 is large enough to cause the thermal noise become negligible. Therefore, Equation (35) is reduced to

$$BER = Q\left(\left[\sum_{i=1}^{K-1} G_i(\psi_0)R_{i,0}^2 \right]^{\frac{1}{2}} \right) \tag{37}$$

which is a expression of BER performance in DSCMA over AWGN channel.

8. BER Performance and System Capacity in DSCMA System

Two different types of BS antenna, omnidirectional antenna and smart antenna are exploited for BER performance comparison through simulation. The system simulation will evaluate the BER performance of DSC algorithm in DSCMA by considering interference from both intra-cell and inter-cell interferences. The BER expressions over these interferences have been derived in the previous section. From these BER expressions the system capacity in DSCMA can be estimated by looking at the number of mobile users that the system can support at 0.001 BER ($BER < 10^{-3}$). Since the cell is split into three sectors, the inter-cell interference sources are only considered from two neighbouring cells for each sector. The system chip rate is 1.2288 Mcps resulting at a data rate of 4.8 Kbps for sequence length of about 256 chips per bit. This data rate is used to transmit the multimedia type data. The data transmission will go through a wireless channel with fourth power of distance loss and 8 dB shadowing. The voice activity factor is not taken into consideration in this simulation. The system parameters for the system simulation are summarised in Table 2.

Cell radius, R	Unity
Number of sectors per cell	3
Number of interfering neighbouring cells per sector	2
Type of data	Multimedia
Spreading factor, SF	About 256
System chip rate, W	1.2288 Mcps
Data rate, R	4.8 Kbps
Path loss exponent, μ	4.0
Standard deviation of shadowing, ζ	8 dB

Table 2. Summary of the system parameters

The radiation pattern of a smart antenna represents gains of different AOA along a 120° azimuth span sector. It is assumed that K separate narrow beams and K different spreading sequences can be generated from BS and directed to each of K users within a sector of interest. Assume that a sector antenna beamwidth is 120° in the three sectors per cell configuration. This beamwidth size attributes to a maximum excess delay, τ_{max} of 142 chips for chip rate, R_c of 1.2288 Mcps in separation of 10 Km. Thus, the correlation property, $R_{i,0}$ of the spreading sequences between i th interfering user and the desired user is randomly taken within 142 chips delay spread. Nevertheless, when the smart antenna is exploited, the beamwidth becomes narrower as a function of the number of elements, N_e . Hence, the maximum excess delay, τ_{max} of this narrower beam will be reduced. The maximum excess delay, τ_{max} for the smart antenna system with different number of elements, N_e has been shown in Table 3.

Number of elements, N_e	Beamwidth, BW ($^\circ$)	Maximum angular spread, γ_{\max} ($^\circ$)	Maximum excess delay, τ_{\max}	
			(μs)	(chip)
1	120	60	115	142
4	25.5	12.75	15.1	18.5
8	12.75	6.375	7.45	9.15
16	6.375	3.19	3.7	4.56
32	3.19	1.59	1.85	2.27
64	1.59	0.8	0.93	1.14

Table 3. Performance of smart antenna for various N_e

This table showed that the narrower beam of a smart antenna will reduce the TOA of a transmitted signal. This implies that the maximum excess delay of a channel can be reduced when more elements in a smart antenna system is exploited. To analyse the system performance in DSCMA, all the simulations are executed by considering smart antenna systems with $N_e = 4, 8, 16, 32, 64$ in the channel models of AWGN, Rayleigh fading, and fading with diversity gain. The simulations also consider spreading sequences such as m -sequence, Gold, Walsh-Hadamard and LAS-ET for performance comparison in DSCMA system. For the simulation in AWGN channel, Equation (37) from previous section is used to analyse the BER performance in DSCMA system.

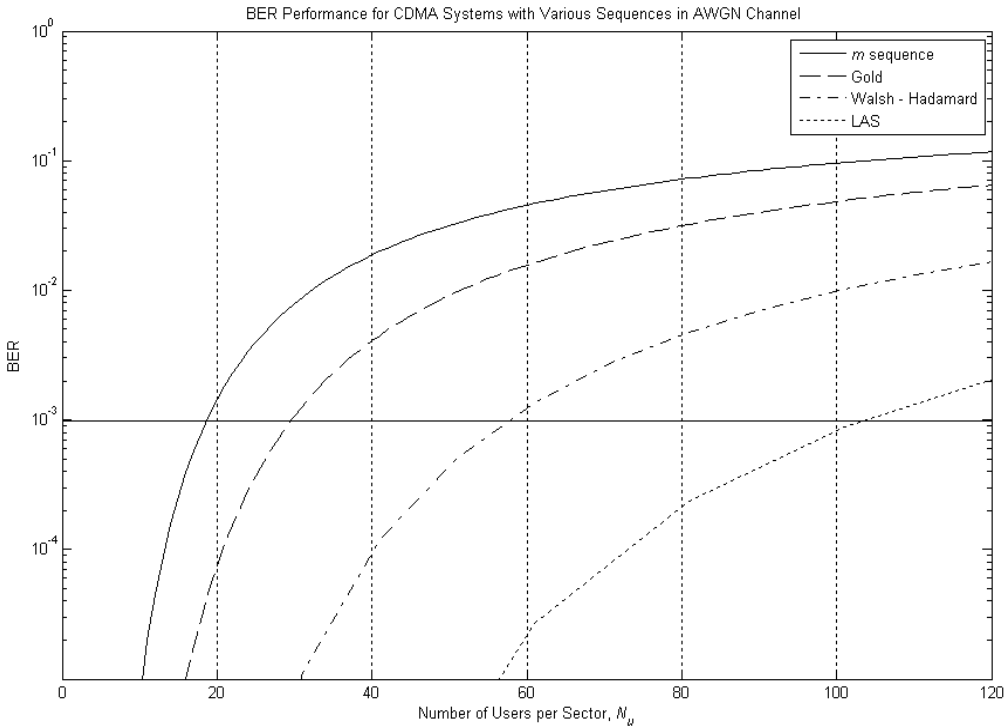


Fig. 7. BER performance of CDMA system for various spreading sequences

For comparison purposes, the BER of conventional CDMA and SDMA systems will be the first to be evaluated. In the CDMA system, the omnidirectional antenna gain, $G_i(\psi_0)$ for all mobile users are normalized to one in the whole sector. Therefore, the BER of the CDMA system is evaluated based on the correlation property of the spreading sequences. Figure 7 shows the BER performance of CDMA system for various spreading sequences. The system capacity of the CDMA system for these spreading sequences for $BER < 10^{-3}$ are shown in Table 4.

Sequences	Capacity, N_u ($BER < 10^{-3}$)
<i>m</i> -sequence	18
Gold	29
Walsh-Hadamard	58
LAS-ET	104

Table 4. System capacity of CDMA system for various spreading sequences

On the other hand, in the SDMA system, the correlation property, $R_{i,0}^2$ is normalized to one because it is not a factor of improvement in the conventional SDMA system. The only parameter that is used to evaluate BER performance of SDMA system is the antenna gain of interfering users, $G_i(\psi_0)$ in the direction of the desired user. These antenna gains of interfering users are taken randomly from the radiation pattern of smart antenna within the 120° sector. Figure 8 shows the BER performance of the conventional SDMA for various antenna beamwidths. The SDMA system capacity of $BER < 10^{-3}$ for various beamwidths is given in Table 5.

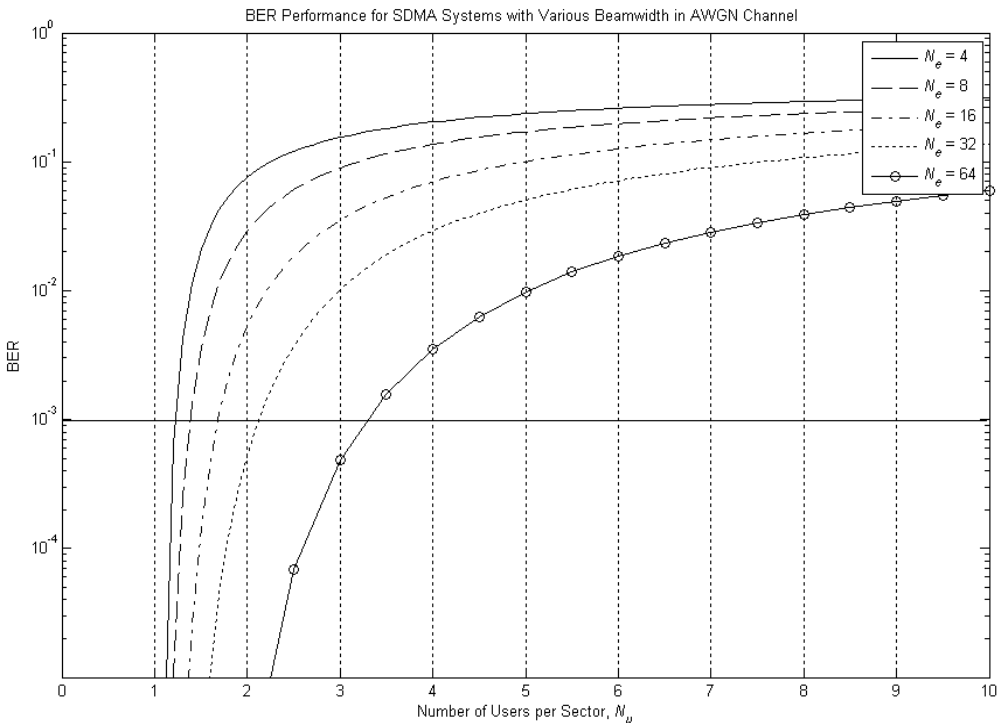


Fig. 8. BER performance of SDMA system for various numbers of elements

Number of elements, N_e	Capacity, N_u (BER < 10^{-3})
4	1
8	1
16	1
32	2
64	3

Table 5. System capacity of SDMA system for various numbers of elements

In the AWGN channel, it is necessary for DSCMA to perform in perfect synchronous manner to obtain the orthogonality among the mobile users in zero delay spread. However, perfect synchronisms rarely exist because each mobile user signal arrives at BS receiver with different delay. Therefore, the orthogonality between spreading sequences is no longer held in non-zero delay spread.

The BER performance of the DSCMA system in AWGN channel for various spreading sequences, vis m -sequence, Gold, Walsh-Hadamard and LAS-ET sequences are shown in Figures 9a - 9d respectively. In each figure, the BER performance is evaluated by exploiting the smart antenna with different number of elements, $N_e = 4, 8, 16, 32$ and 64 elements. Additionally, the system capacity of the DSCMA system based on $BER < 10^{-3}$ for these spreading sequences are shown in Tables 6a - 6d respectively.

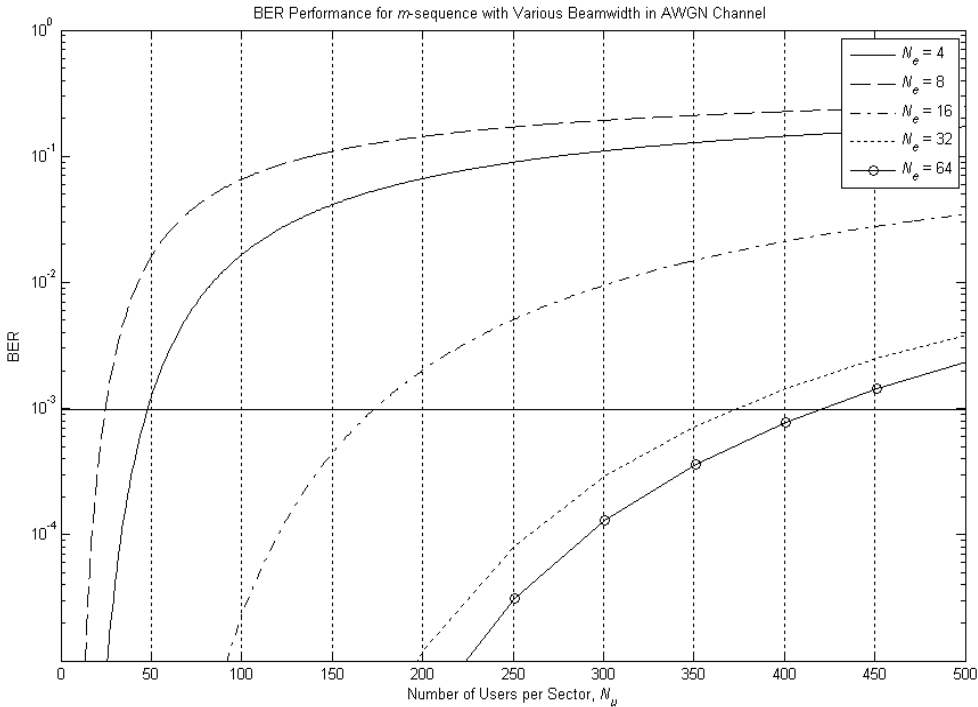


Fig. 9a. DSCMA system BER performance for m -sequence with different number of antenna elements, N_e in AWGN channel

Number of elements, N_e	Capacity, N_u (BER < 10^{-3})
4	48
8	25
16	173
32	374
64	420

Table 6a. DSCMA system capacity of BER < 10^{-3} for m -sequence with different number of antenna elements, N_e in AWGN channel

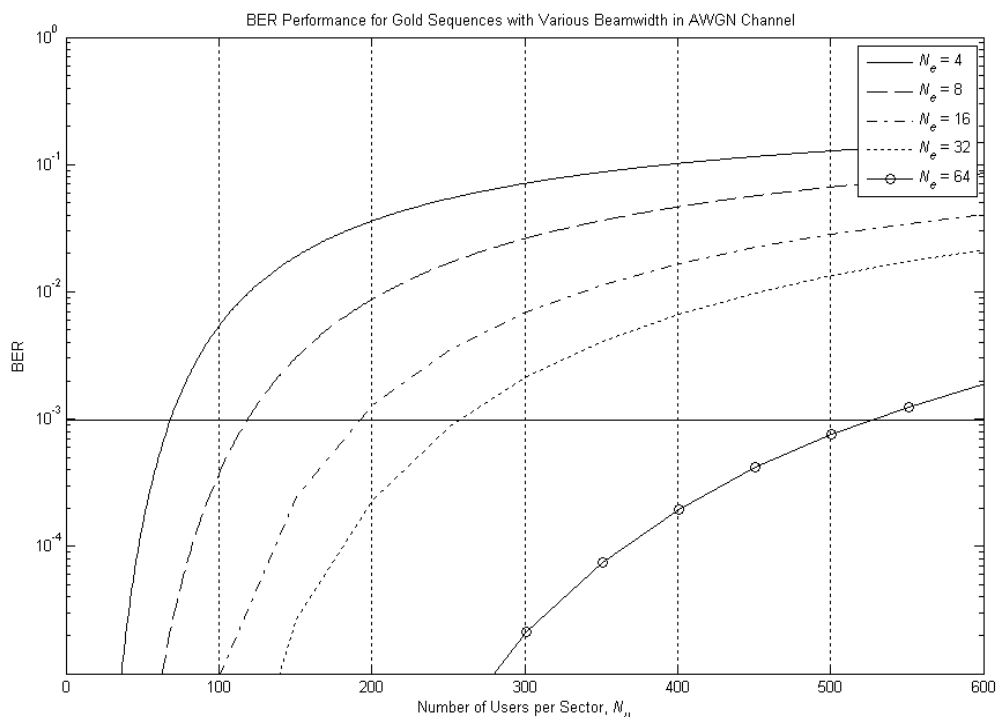


Fig. 9b. DSCMA system BER performance for Gold sequence with different number of antenna elements, N_e in AWGN channel

Number of elements, N_e	Capacity, N_u (BER < 10^{-3})
4	69
8	119
16	194
32	259
64	530

Table 6b. DSCMA system capacity of BER < 10^{-3} for Gold sequence with different number of antenna elements, N_e in AWGN channel

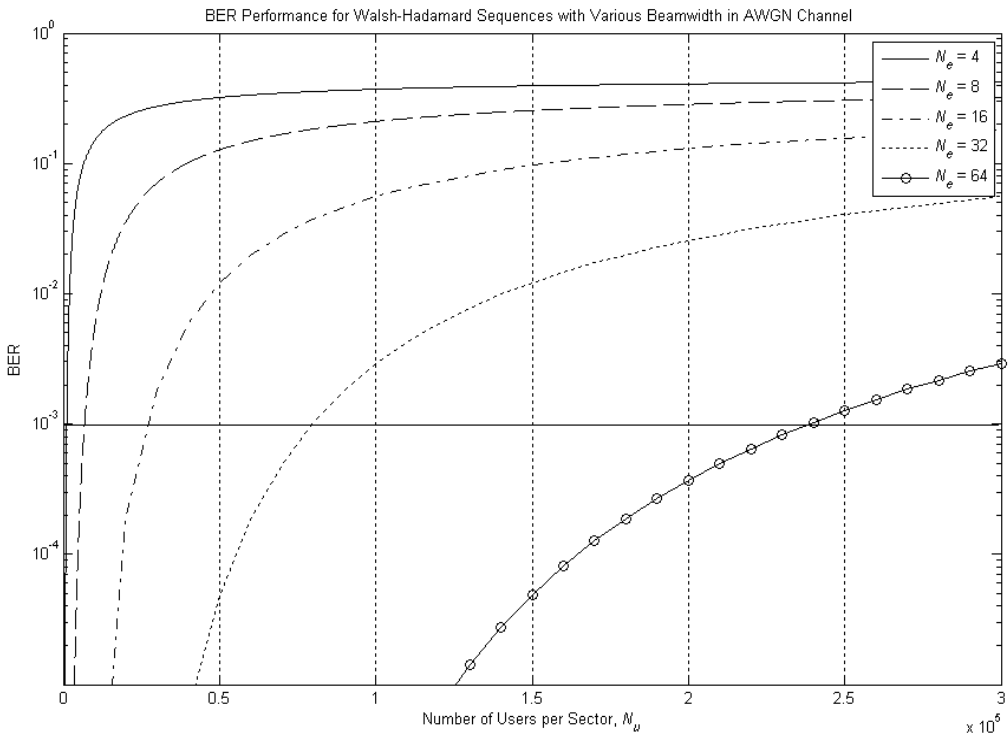


Fig. 9c. DSCMA system BER performance for Walsh-Hadamard sequence with different number of antenna elements, N_e in AWGN channel

Number of elements, N_e	Capacity, N_u (BER < 10^{-3})
4	1147
8	6.85×10^3
16	2.75×10^4
32	8×10^4
64	2.4×10^5

Table 6c. DSCMA system capacity of BER < 10^{-3} for Walsh-Hadamard sequence with different number of antenna elements, N_e in AWGN channel

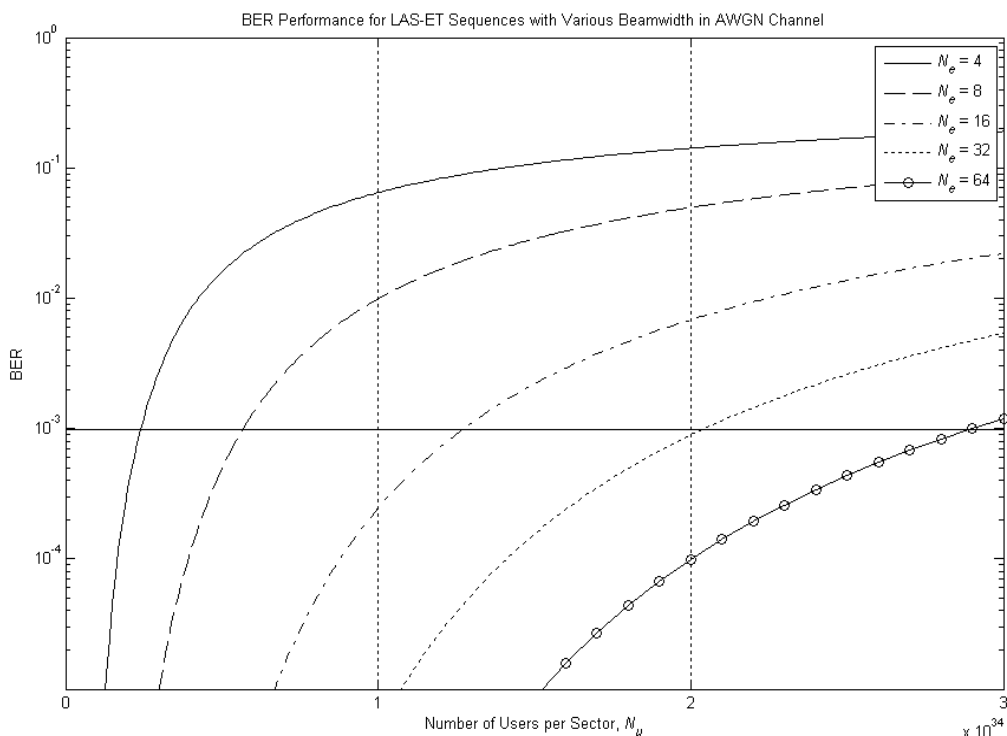


Fig. 9d. DSCMA system BER performance for LAS-ET sequence with different number of antenna elements, N_e in AWGN channel

Number of elements, N_e	Capacity, N_u (BER < 10^{-3})
4	2.4×10^{33}
8	5.67×10^{33}
16	1.27×10^{34}
32	2.04×10^{34}
64	2.9×10^{34}

Table 6d. DSCMA system capacity of BER < 10^{-3} for LAS-ET sequence with different number of antenna elements, N_e in AWGN channel

All the evaluated system capacities in DSCMA system here are based on the interference level that the system can tolerant. Hence, these attained results are not the ideal system capacity performance. There are some other factors need to be considered in conforming to this issue such as the totally bandwidth available, the number of spreading sequences that can be synthesized, and the limitation of system signal processing. Therefore, all the attained results are only suited for the comparison purpose and are not representing the real scenario.

In general, it shows that the DSCMA system performance is improved with spreading sequences of m -sequence, Gold, Walsh-Hadamard and LAS-ET in ascending order as in

conventional CDMA system. This is because the mean square correlation property, $E(R_{i,0}^2)$ for $i = 1, 2, 3, \dots, K - 1$ between $(K - 1)$ interfering users and the desired user are decreased in ascending order from these spreading sequences. Further improvement is exhibited when the number of elements, N_e in smart antenna is increased as in conventional SDMA system. This is because the interference gain factor, $G_i(\psi_0)$ for $i = 1, 2, 3, \dots, K - 1$ in the direction of the desired user, ψ_0 is reduced due to the fact that the sidelobe levels of interfering users radiation pattern presented in ψ_0 direction is decreased while the number of nulls increase when the number of elements in smart antenna is increase.

All the energies from higher number of antenna elements, N_e are transformed into high gain in the main lobe of smart antenna. It can be seen that there is considerable improvement when the beamwidth of the smart antenna become narrower. The narrower beam from higher number of antenna elements, N_e also contributes to the interference reduction due to the fact that the probability of users' beam interfere to each other is low in narrower beam compared to wider beam. Therefore, higher system capacity can be observed in DSCMA when number of elements, N_e is increased. And this improvement can achieve as high as 2.9×10^{34} users per sector when LAS-ET sequences together with DSC algorithm are used. On the other hand, this is interesting to find that in traditional spreading sequences, their system performances suppose to be appeared in randomness because of non-uniform distribution in their correlation property within the concerned delay-spread. This is obviously occurred in m -sequences.

9. Conclusion

It can be concluded that non-uniform traffics can severely degrade the performance of CDMA and SDMA cellular systems. The DSCMA system described in this chapter is a double signatures system that can distinguish more users by cancelling the existing interference in multipath environment. This multiple access system uses LAS-ET sequences to create IFW near zero delay spread in its cross-correlation function. In order to ensure all the signal components drop within the IFW, a narrow beam with higher directivity smart antenna system is exploited. The size of IFW is adapted to the smart antenna half-power beamwidth using DSC algorithm. Therefore, all the interferences induced in non-uniform traffics can be dramatically reduced in DSCMA system and thus resulting in higher system capacity.

10. References

- Adachi, F., Garg, D., Takaoka, S. & Takeda, K. (2005). Broadband CDMA techniques, *IEEE Wireless Communications*, vol. 12, no. 2, pp. 8 - 18.
- Buracchini, E. et al. (1996). Performance Analysis of A Mobile System Based on Combined SDMA/CDMA Access Technique, *IEEE 4th International Symposium on Spread Spectrum Techniques and Applications Proceedings*, vol. 1, pp. 370 - 374.
- Cameron, R. & Woerner, B. (1996). Performance Analysis of CDMA with Imperfect Power Control, *IEEE Transactions on Communications*, vol. 44, pp. 777 - 781.

- Castaeda-Camacho, J. & Lara-Rodriguez, D. (2008). Teletraffic Analysis of an Overlaid System Using CDMA and TDMA With Cell Coverage Area Restriction, *IEEE Transactions on Vehicular Technology*, vol. 57, no. 2, pp. 828 - 846.
- Chatovich, A. & Jabbari, B. (1999). Effect of Non-uniform Traffic Load on Erlang Capacity of CDMA, *IEEE 49th Vehicular Technology Conference Proceedings*, vol. 1, pp. 816 - 820.
- Chen, H. H., Chiu, H. W. & Guizani, M. (2006). Orthogonal Complementary Codes for Interference-Free CDMA Technologies, *IEEE Wireless Communications*, vol. 13, no. 1, pp. 68 - 79.
- Chen, H. H., Chiu, H. W. & Guizani, M. (2008). On Next Generation CDMA Technologies: The REAL Approach for Perfect Orthogonal Code Generation, *IEEE Transactions on Vehicular Technology*, vol. 57, no. 5, pp. 2822 - 2833.
- Cho, K. et al. (2002). Novel Smart Antennas for Applying SDMA to Cellular Mobile Communication Systems, *IEEE Antennas and Propagation Society International Symposium Proceedings*, vol. 4, pp. 652 - 655.
- Choi, W., Andrews, J. G. & Heath, R. W. (2007). Multiuser Antenna Partitioning for Cellular MIMO-CDMA Systems, *IEEE Transactions on Vehicular Technology*, vol. 56, no. 5, Part 1, pp. 2448 - 2456.
- Cooper, G. R. & Nettleton, R. W. (1978). A Spread Spectrum Technique for High Capacity Mobile Communications, *IEEE Transactions on Vehicular Technology*, vol. VT-27, pp. 264 - 275.
- Fang, X. (2002). More Realistic Analysis for Blocking Probability in SDMA Systems, *IEEE Proceedings Communications*, vol. 149, no. 3, pp. 152 - 156.
- Faruque, S. (1996). *Cellular Mobile Systems Engineering*, Norwood, MA, Artech House.
- Feuerstein, M. et al. (1994). Path Loss, Delay Spread, and Outage Models as Functions of Antenna Height for Microcellular System Design, *IEEE Transactions on Vehicular Technology*, vol. 43, no. 3, pp. 487 - 498.
- Galvan-Tejada, G. M. & Gardiner, J. G. (2001). Theoretical Model to Determine the Blocking Probability for SDMA Systems, *IEEE Transactions on Vehicular Technology*, vol. 50, no. 5, pp. 1279 - 1288.
- Gilhousen, K. S. et al. (1991). On The Capacity of A Cellular CDMA System, *IEEE Transactions on Vehicular Technology*, vol. 42, no. 2, pp. 303 - 312.
- Godara, L. C. (1997). Applications of Antenna Arrays to Mobile Communications, Part I: Performance Improvement, Feasibility, and System Considerations, *Proceedings of the IEEE*, vol. 85, no. 7, pp. 1031 - 1060.
- Gold, R. (1967). Optimal Binary Sequences for Spread Spectrum Multiplexing, *IEEE Transactions on Information Theory*, vol. 13, no. 4, pp. 619 - 621.
- Golomb, S. W. (1992). *Shift Register Sequences*, Aegean Park Press.
- Guo, D. & Wang, C. C. (2008). Multiuser Detection of Sparsely Spread CDMA. *IEEE Journal on Selected Areas in Communications*, vol. 26, no. 3, pp. 421 - 431.
- Harmuth H. F. (1970). *Transmission of Information by Orthogonal Functions*, Springer-Verlag.
- Hashem, B. & Sousa, E. (1997). On the Capacity of a Cellular DS/CDMA System under Slow Multipath Fading and Fixed Step Power Control, *IEEE 6th International Conference on Universal Personal Communications Record*, vol. 2, pp. 352 - 355.

- Heath, R. W. et al. (2004). Construction of Equiangular Signatures for Synchronous CDMA Systems, *IEEE 8th International Symposium on Spread Spectrum Techniques and Applications Proceeding*, pp. 708 - 712.
- Huang, C. et al. (2001). A Joint Multiple Access Scheme for Uplink Channels of CDMA Systems, *International Conferences on Info-tech and Info-net (ICII 2001) Proceedings*, vol. 2, pp. 323 - 328.
- Ishida, Y. et al. (2000). Wideband CDMA Base Station with Co-channel Interference Canceller, *IEEE 51st Vehicular Technology Conference (VTC 2000-Spring) Proceedings*, vol. 1, pp. 293 - 297, Tokyo.
- Kasami T. (1966). Weight Distribution Formula for Some Class of Cyclic Codes, *Technical Report R-285 (AD 632574)*, Coordinated Science Laboratory, Univ. of Illinois, Urbana.
- Kim, S. W. et al. (2001). Performance of Smart Antennas with Adaptive Combining at Handsets for the CDMA2000 System, *International Conference on Third Generation Wireless and Beyond Proceeding*, San Francisco, pp. 882 - 887.
- Lee, W. C. Y. (1991). Overview of Cellular CDMA, *IEEE Transactions on Vehicular Technology*, vol. 40, no. 2, pp. 291 - 302.
- Lee, W. C. Y. (1998). *Mobile Communications Engineering*, McGraw Hill.
- Li, D. (1999). A High Spectrum Efficient Multiple Access Code, *Fifth Asia-Pacific Conference on Communications and Fourth Optoelectronics and Communications Conference (APCC/OECC '99) Proceedings*, vol. 1, pp. 598 - 605.
- Li, D. (2003). The Perspectives of Large Area Synchronous CDMA Technology for the Fourth-Generation Mobile Radio, *IEEE Communications Magazine*, vol. 41, no. 3, pp. 114 - 118.
- Liberti, J. C. Jr. & Rappaport, T. S. (1994). Analytical Results for Capacity Improvements in CDMA, *IEEE Transactions on Vehicular Technology*, vol. 43, no. 3, pp. 680 - 690.
- Liberti, J. C. Jr. & Rappaport, T. S. (1998). *Smart Antennas for Wireless Communications*, Prentice Hall PTR, Upper Saddle River, NJ.
- Lien, S. Y. & Cherniakov, M. (1998). Analytical Approach for Multipath Delay Spread Power Distribution, *IEEE Global Telecommunications Conference (GLOBECOM 98) Proceedings*, The Bridge to Global Integration, vol. 6, pp. 3680 - 3685.
- Naguib, A. F. et al. (1994). Capacity Improvement with Base-Station Antenna Arrays in Cellular CDMA, *IEEE Transactions on Vehicular Technology*, vol. 43, no. 3, pp. 691 - 698.
- Ng, B. & Sousa, E. S. (1998). Performance Enhancement of DS-CDMA System for Wireless Local Loop, *IEEE International Telecommunications Symposium (ITS) Proceedings*, vol.1, pp. 78 - 82.
- Ng, C. K., Noordin, N. K., Khatun, S., Mohd Ali, B., Jamuar, S. S. & Ismail, M. (2008). Directional Diversity of Smart Antenna in LAS CDMA Systems, *Wireless Personal Communications*, Springer Netherlands, vol. 46, pp. 305 - 316.
- Ng, C. K., Noordin, N. K., Mohd Ali, B., Jamuar, S. S. & Ismail, M. (2009). Spectrum Efficiency Enhancement in Dynamic Space Coded Multiple Access (DSCMA) System, *Wireless Personal Communications*, Springer Netherlands, 0929-6212 (Print) 1572-834X (Online), DOI 10.1007/s11277-009-9682-7.

- Niemela, J. & Lempiainen, J. (2003). Impact of the Base Station Antenna Beamwidth on Capacity in WCDMA Cellular Networks, *The 57th IEEE Semiannual Vehicular Technology Conference (VTC 2003-Spring) Proceedings*, vol. 1, pp. 88 - 84.
- Peterson, R. L. et al. (1995). *Introduction to Spread Spectrum Communications*, Prentice Hall International Edition.
- Popovic, B. M. (1997). Efficient Despreaders for Multi-code CDMA Systems, *IEEE 6th International Conference on Universal Personal Communications Record*, vol. 2, pp. 516 - 520.
- Rapajic, P. B. (1998). Information Capacity of The Space Division Multiple Access Mobile Communication System, *IEEE 5th International Symposium on Spread Spectrum Techniques and Applications Proceedings*, vol. 3, pp. 946 - 950.
- Rupf, M. & Massey, J. L. (1994). Optimum Sequence Multisets for Synchronous Code-Division Multiple-Access Channels, *IEEE Transactions on Information Theory*, vol. 40, no. 4, pp. 1261 - 1266.
- Stańczak, S. et al. (2001). Are LAS-Codes a Miracle?," *IEEE GLOBECOM '01 Proceedings*, vol. 1, (San Antonio, Texas), pp. 589 - 593, November 2001.
- Thompson, J. S. et al. (1996). Smart Antenna Arrays for CDMA Systems, *IEEE Personal Communications*, pp. 16 - 25.
- Uthansakul, P. & Uthansakul M. (2002). Number of Elements in Smart Antenna System Effects on Both Perfect and Imperfect Power Control for Reverse Link of CDMA Cellular System, *The International Technical Conference on Circuits/Systems, Computer and Communications Proceedings*, Thailand.
- Wang, X., Ahonen, T. & Nurmi, J. (2007). Applying CDMA Technique to Network-on-Chip, *IEEE Transactions on Very Large Scale Integration (VLSI) Systems*, vol. 15, no. 10, pp. 1091 - 1100.
- Wei, H. et al. (2005). Interference-Free Broadband Single and Multicarrier DS-SSMA, *IEEE Communications Magazine*, vol. 43, no. 2, pp. 68 - 73.
- Welch, L. R. (1974). Lower Bounds on the Maximum Cross Correlation of Signals, *IEEE Transactions on Information Theory*, vol. IT-20, pp. 397 - 399.
- Wu, J. S. et al. (1998). Hot-Spot Traffic Relief with A Tilted Antenna in CDMA Cellular Networks, *IEEE Transactions on Vehicular Technology*, vol. 47, no. 1, pp. 1 - 9.
- Xie, S. & Rahardja, S. (2005). Performance Evaluation for Quaternary DS-SSMA Communications with Complex Signature Sequences over Rayleigh-Fading Channels, *IEEE Transactions on Wireless Communications*, vol. 4, no. 1, pp. 266 - 277.
- Yu, J. et al. (2004). Reverse-Link Capacity of Power-Controlled CDMA Systems with Beamforming, *IEEE Transactions on Vehicular Technology*, vol. 53, no. 5, pp. 1423 - 1433.
- Zheng, Z. et al. (1996). Capacity Improvement with Base Station Antenna Arrays in Cellular CDMA, *IEEE 46th Vehicular Technology Conference, Mobile Technology for the Human Race Proceedings*, vol. 2, pp. 1303 - 1306.

Video Streaming in Evolving Networks under Fuzzy Logic Control

Martin Fleury, Emmanuel Jammeh, Rouzbeh Razavi,
Sandro Moiron and Mohammed Ghanbari
*University of Essex
United Kingdom*

1. Introduction

Internet Protocol TV (IPTV) and other video streaming services are expected to dominate the bandwidth capacity of evolving telecommunications networks. In fact, managed, all-IP networks are under construction with video largely in mind. In these networks, a variety of broadband access networks will form the final link to the home across which video is streamed from proprietary servers. Co-existing with these networks or as an extension of them, the traditional, best-effort Internet will continue to support applications such as video-on-demand, Peer-to-Peer (P2P) streaming, and video clip selection.

This Chapter will begin by broadly surveying research and development of video streaming across evolving telecommunications networks under the categories of best-effort and managed networks. In particular, the Chapter will introduce the different forms of control that are necessary to ensure the quality of the delivered video, whether live or pre-encoded video, when for the latter bitrate transcoding may be required. The concentration will be on single-layer unicast distribution though simulcast, bandwidth reservation, multicast, and other forms of delivery will be touched upon.

With the growth in computational power, rate-distortion (R-D) control has emerged as an effective way to optimise the output encoded bitstream. In R-D control, the optimal choice of compression rate (and hence codec output bitstream rate) relative to improvement in video quality is sought. (The choice is generally found through the method of pre-set Lagrangian multipliers with trial codec settings repeatedly tested to find the best result.) Though attempts have been made to integrate R-D control and network congestion control (Chou & Miao, 2006), often congestion control has been considered separately as best-effort networks are prone to fluctuations in available bandwidth. In all-IP networks, though traffic in the core of the network will be switched, the variety of access network types poses a problem to servers that may be oblivious of the final hop technology. When broadband wireless (IEEE 802.16 d,e, WiMAX (Fleury et al., 2009)) access links are involved error control is especially important.

The Chapter will then specialise to consider in what ways fuzzy logic controllers (FLCs) have been applied to rate control and congestion control. A feature of this Chapter will be consideration given to the growing prominence of type-2 fuzzy logic in networked

multimedia control, bringing greater robustness in the face of unforeseen network conditions. To illustrate the application of fuzzy logic control, the Chapter will include two case studies. One of these will show how type-2 logic can improve upon type-1 logic, both of which forms of congestion control improve upon traditional controllers respectively within managed networks and within the Internet. The design of the controllers is illustrated for non-specialists, showing how type-2 controllers extend type-1 FLCs. From the results of simulations, FLCs in a managed network are shown to be superior to traditional congestion controllers. Transcoding is presented as an effective way to apply fuzzy logic control.

With the advent of IPTV, statistical multiplexing has again become an important issue for managed networks. Unlike traditional broadcast channels, network distribution may involve changes in available bandwidth and streaming conditions because of the variety of possible access types and coexisting traffic. In the second case study, an FLC is used to integrate two video complexity measures to achieve an effective combination of video or TV channels. The intention is dynamically to reduce the bandwidth allocation to channels that are already of high enough quality and increase the quality of streams with potentially greater coding complexity. Simulation results are presented to show the value of the approach applying the state-of-the-art H.264 codec. This case study will also include a review of other forms of statistical multiplexing.

2. Video streaming

2.1 Streaming basics

In video streaming, the compressed video bitstream is transmitted across a network to the end user's decoder (prior to display) without the need for storage other than in temporary buffering. Its advantage over progressive download from a network point-of-view is that the throughput is only that required to render the video at the user's display. Download risks overloading the network by too high a throughput. If download is not progressive, then the user has to wait an intolerable time before (say) viewing a 2 hr movie. There are also issues of commercial confidentiality if the video is stored on the user's machine.

Downloading video does permit Variable Bitrate (VBR) to be transported. In VBR, the codec quantization parameter (QP) is fixed leading to a constant quality. The alternative is to set a target bit rate for Constant Bitrate (CBR) video and allow fluctuating quality but with a gain in controllability. The main problem with VBR is that due to a strong variation in the number of bits allocated to each of the frame types (Lakshman et al., 1998) the rate is highly variable (Van der Auwera & Reisslein, 2009). Long video streams are also not statistically stationary in time, which causes a problem when attempting to model video input to a network. This variability is accentuated in the H.264/Advanced Video Codec (AVC) (Schwarz, 2007) and it is reported (Van der Auwera et al., 2008) that the variability is accentuated the more so in the Scalable Video (SVC) extension to H.264, with the result that prior smoothing of VBR streams is contemplated. (The reason for increased variability is attributable to the increased number of motion estimation modes in H.264/AVC and in H.264/SVC, the addition of hierarchical B-frames.)

In temporal smoothing, multiple encoded frames are accumulated so that the compressed bitstream can be packetized and sent at a desired average bitrate. This form of traffic shaping has the disadvantage for video streaming that end-to-end latency is increased by the number of frames accumulated. For 'conversational' video services, which have an

additional latency introduced by the need to encode each frame, the effect on the viewer can be disconcerting. Ideally end-to-end latency should be no longer than 200 ms. For this reason, in services such as teleconferencing and videophone, CBR is preferable. However, for pre-encoded video at a significant cost in computational complexity (Salehi et al., 1998) it is also possible through optimal smoothing to send video frames (or rather their compressed bitstream) in advance of their decode time, provided it is known that overflow (or underflow) at the playback buffer will not occur. In the best-effort Internet, jitter introduced by cross-traffic congestion will disrupt these calculations but in those network cores in which ATM or virtual ATM is still in place optimal smoothing has a role. Unfortunately, the presence of access networks of differing types prior to the consumer's home, or reduced bandwidth links prior to campus and corporate networks introduces an ill-behaved section within the end-to-end path.

Video is known as a delay-sensitive service but in fact there are varying levels of intolerance, and a limit of 200 ms has been mentioned. However, for one-way streaming the delay requirements are less stringent. For example, channel swapping or VCR-like control is restricted to 500 ms intervals, because anchor or key frames at which switching can occur are placed at these intervals within a stream. Another form of delay is start-up delay, with Video-on-Demand (VoD) services hoping to make this imperceptible (< 20 ms), which is perhaps possible on the Internet if the Resource ReSerVation Protocol (RSVP) (Zhang et al., 1997) were to be widely deployed. Variation in delay (jitter) is also important in terms of media synchronization (between audio and video) (Blakowski & Steinmetz, 1996). However, there are also display deadlines to be met, implying that a jitter buffer should be dimensioned to absorb any variation in delivery (assuming Internet delivery). For reference frames (one used for predictive motion estimation), their data is still of value for decoding future frames even if they miss their display deadline. Too large a receiver buffer will lead to increased end-to-end latency and start-up delay, while too small a buffer may cause overflow. This is why adaptive buffers have been contemplated in the research literature (Kalman et al., 2002).

Video streaming is also known as a loss-tolerant service. However, this is misleading as the loss of more than 10% of packets will generally lead to a noticeable deterioration in the quality of the video unless: error-resilience measures have been taken; error control through some form of acknowledgements (ACKs) is used (as in the Windows Media system); Forward Error Correction (FEC) is in place; or error concealment can be applied. A combination of these methods is preferable as part of an error response strategy and unequal error protection (UEP) is possible. In UEP, protection is prioritized according to compressed video content or the structure of the video. Acknowledgments are possible but their impact on delay must always be judged. For example, in (Mao et al., 2003) layered streaming was attempted across an ad hoc network in which multi-hop routing and broken links can lead to high levels of delay. In layered streaming (Mao et al., 2003), a more important base layer allows a basic reconstruction of the video while one or more enhancement layers can improve the quality. However, because of the high risk of delay, in (Mao et al., 2003) it was only possible to send one ACK at most to secure the base layer.

Though FEC schemes with linear decoder complexity (Raptor codes, a variety of rateless erasure codes) have been developed (Shokrollahi, 2006), FEC generally leads to delay in encoding. Because of the additional delay involved in sending acknowledgments (or negative acknowledgments), when there is a long round-trip-time careful engineering needs

to be applied if rateless erasure coding is to be used. In rateless or Fountain coding (MacKay, 2005), additional redundant data can always be generated, while in conventional forms of channel coding such as Reed-Solomon, there is a threshold effect whereby if the channel noise or packet erasures pass the level of protection originally provided then all data are lost.

Error resilience techniques, the range of which have been expanded in the H.264 codec (Wenger, 2003), are based on source coding. Error resilience results in lower-delay and as such is suitable for real-time, interactive video streaming, especially video-telephony and video conferencing. However, due to the growing importance of broadband wireless access networks, error resilience is also needed to protect video streaming to the home. This is because physical-layer FEC is already present and, therefore, application-layer FEC may duplicate its role. The exception is if application-layer FEC can be designed to act as an outer code after inner coding at the physical layer, in the manner of concatenated channel coding. Compressed frame data is often split into a number of slices each consisting of a set of macroblocks. In the MPEG-2 codec, slices could only be constructed from a single row of macroblocks. Slice resynchronization markers ensure that if a slice is lost then the decoder is still able to continue with entropic decoding. Therefore, a slice is a unit of error resilience and it is normally assumed that one slice forms a packet, after packing into a Network Abstraction Layer unit (NALU) in H.264. Each NALU is encapsulated in a Real Time Protocol (RTP) packet. Consequently, for a given frame, the more slices the smaller the packet size and the less risk of packet loss through bit errors.

In H.264/AVC, by varying the way in which the macroblocks are assigned to a slice (or rather group of slices), Flexible Macroblock Ordering (FMO) gives a way of reconstructing a frame even if one or more slices are lost. Within a frame up to eight slice groups are possible. A simple FMO method is to continue a row of macroblocks to a second row, Figure 1a, but allow disjoint slice groups (Lambert et al., 2006). Regions of interest are supported, Figure 1b. Checkerboard slice group selection, Fig. 1c allows one slice group to aid in the reconstruction of the other slice group (if its packet is lost) by temporal (using motion vector averaging) or spatial interpolation. Assignment of macroblocks to a slice group can be general (type 6) but the other six types pre-define an assignment formula, thus reducing the coding overhead from providing a full assignment map.

Data partitioning in H.264/AVC separates the compressed bitstream into: A) configuration data and motion vectors; B) intra-coded transform coefficients; and C) inter-coded coefficients. This data form A, B, and C partitions which are packetized as separate NALUs. The arrangement allows a frame to be reconstructed even if the inter-coded macroblocks in partition C. are lost, provided the motion vectors in partition A survive. Partition A is normally strongly FEC-protected at the application layer or physical layer protection may be provided such as the hierarchical modulation scheme in (Barmada et al., 2005) for broadcast TV. Notice that in codecs prior to H.264, data partitioning was also applied but no separation into NALUs occurred. The advantage of integral partitioning is that additional resynchronization markers are available that reset entropic encoding. This mode of data partitioning is still available in H.264 and is applied to I-frames.

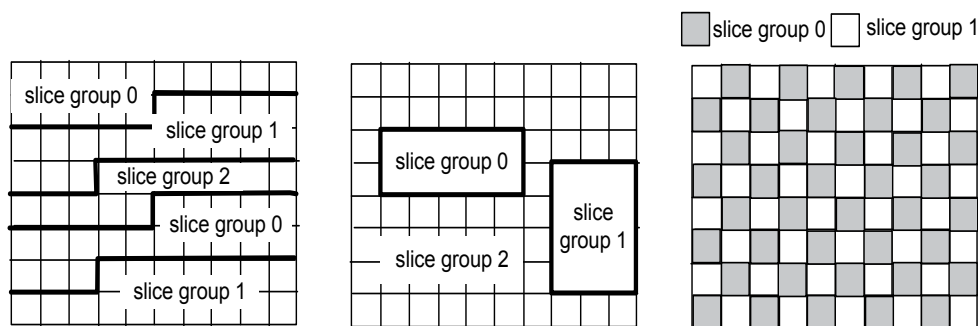


Fig. 1. Example FMO slice groups and types (after (Lambert, 2006) a) Continuing row (type 0) b) geometrical selection (type 2) c) checkerboard selection (type 1)

The insertion of intra-coded macroblocks into frames normally encoded through motion-compensated prediction allows temporal error propagation to be arrested if matching macroblocks in a previous frame are lost. Intra-refresh through periodic insertion of I-frames with all macroblocks encoded through spatial reference (intra-coded) is the usual way of catching error propagation. However, I-frames cause periodic increases in the datarate when encoding at a variable bitrate. They are also unnecessary if channel switching points and VCR functions are not required.

This brief review by no means exhausts the error-resilience facilities in H.264, with redundant frames, switching frames, and flexible reference frames also considered in (Stockhammer & Zia, 2007). We have referred to H.264/AVC anchor frames as I-frames for consistency with previous codecs. In fact, H.264 uses Instantaneous Decoder Refresh (IDR)-frames for the same purpose, whereas H.264 I-frames allow motion estimation reference beyond the Group of Pictures boundary.

Error concealment (Wang & Zou, 1998) is the process of concealing errors at the decoder. However, the form of error concealment is implementation dependent because of the complexity of these algorithms. In fact, for reasons of speed, previous frame replacement is often preferred. If lost frames are replaced by the last frame to arrive successfully there is a danger of freeze frame effects. When there is rapid motion or scene cuts then partial replacement of macroblocks from the previous frame will result in obvious blocky effects. For error concealment in H.264/AVC (Vars & Hannuksela, 2001) the motion vectors of correctly received slices are computed if the average motion activity is sufficient (more than a quarter pixel). Research in (Vars & Hannuksela, 2001) gives details of which motion vector to select to give the smoothest block transition. It is also possible to select the intra-coded frame method of spatial interpolation, which provides smooth and consistent edges at an increased computational cost. Experience shows a motion-vector-based method performs best except when there is high motion activity or frequent scene changes (Kim & Kim, 2002).

2.2 Streaming systems

In networked video delivery, systems are classically divided (Chou, 2007) into streaming and broadcast systems. In the former, video is pre-encoded before storage and access by a server, while in the latter there is no storage before server access and multicast over a network. A further distinction in this model is that in streaming a control path exists, whereas the presence of many receivers in a broadcast system means that feedback would

be impossible to manage. Feedback can be used for congestion control but it can also return VCR commands, typically through the Real Time Streaming Protocol (RTSP) (Schulzrinne et al., 1998). Nevertheless, it is possible to stream both pre-encoded and online or live video because, after feedback notification of congestion, the streaming rate can be changed through bitrate transcoding (Assunção & Ghanbari, 1997) (Sun et al., 2005). One problem that fast transcoding may face in the H.264 codec is error drift when transcoding I-frames (Lefol et al., 2006).

Scalable video also allows rate control as a response to network conditions or target device capability but a full discussion of the variety of multi-layer or scalable options such as Fine Grain Scalability (Radha et al., 2001), Multiple Description Coding (Wang, 2005), signal-to-noise ratio (SNR) scalability (Pesquet-Popescu et al., 2006) would require another chapter. Rich though the scalable options are commercial Internet operators seem to prefer simple schemes such as simulcast as used by RealVideo. In simulcast, multiple streams are stored (or encoded online) at different rates and selected according to network conditions. In H264/AVC, stream switching frames allow a smoother transition between low and higher quality stream at lower cost in bandwidth than through switching at I-frames.

At the target device, video is first buffered in a playout buffer, decoder or client buffer (there are various alternative names) prior to access by the decoder. This buffer will vary in size depending on the capabilities of the device. Large buffers are not advisable for battery-powered devices because of both active and passive energy consumption. Nevertheless some buffering is required to absorb variation of delay (jitter) over the network.

Because of motion-compensated prediction coding it is always necessary to store packets prior to decode, especially if VBR is in use. An additional render buffer, able to store a few frames prior to display, is also generally present. Apart from buffer overflow in the intermediate buffers of routers through congestion, buffer overflow at the playout buffer is also possible. Packets arriving too late for their display or decode deadlines may also be dropped. It is also possible, because of jitter, for buffer underflow to occur. In fact, in the Windows Media system (Chou, 2007) the receiver monitors the buffer level to detect network congestion. Again like RealVideo, Windows Media uses simulcast, with the receiver signaling the server to swap to a lower rate stream when it detects congestion. However, the Windows Media receiver or client is not only reliant on buffer monitoring, because packet loss at the receiver is also taken into account.

3. Congestion control

In this Section, the focus is on congestion control of single stream unicast for IPTV and other multimedia services. Because the main thrust in congestion control research is to provide an enhanced service through VBR delivery, this Section concentrates on that whereas in Section 4 on statistical multiplexing, multi-channel delivery of CBR streams is considered. The latter is likely to be a broadcast service.

3.1 IPTV and unicast streaming

Real-time video applications, such as IPTV, video-on-demand (VoD), and network-based video recorder interest telecommunication companies, because of their high bitrates, though they also risk overwhelming existing networks if it is not possible to control their flows. The unicast variety of IPTV is very attractive because it allows streaming of individual TV

programs at a time chosen by the end user. Broadly speaking, two types of heterogeneous delivery network exist: 1) the familiar Internet, with best-effort Internet Protocol (IP) routing, i.e. an unmanaged IP network; and 2) All-IP networks, which retain IP packet framing but, particularly in the network core, switch packets (across Clos switches) rather than employ packet routers, i.e. a managed IP network. These IP networks are generally referred to as converged networks, as they combine a traditional telephone service (through Voice-over-IP) with data delivery (normally high speed Internet access) and TV (through IPTV). The marketing term for such a combined service is 'triple-play' and if mobility is added then this term becomes 'quadruple-play'.

IPTV services are in active commercial development for converged telephony networks, such as British Telecom's 21st Century Network (21CN) (Geer, 2004) or the all-IP network of KPN in the Netherlands. Within the 21CN, video streaming is sourced either from proprietary servers or from an external Internet connection, with best-effort routing. Before distribution from the server to individual users, multiple videos streams will share a multimedia channel, an example being MPEG-2 Transport Stream which serves for H.264/AVC pre-encoded streams. These video streams could represent different TV channels that can be selected by the IPTV user. However, when the multimedia channel leaves the core network it is commonly delivered across an access network such as Asymmetric Digital Subscriber Line (ADSL) (Zheng & Liu, 2000), when different delivery conditions apply.

On the Internet, video streams must coexist with other data traffic, while in emerging All-IP networks multimedia traffic may predominate. In an All-IP network, as in the Internet, a capacity restriction may still exist at the connection between the network core and the access network, of which the technology can be cable (Vasudevan et al., 2008), broadband wireless (IEEE, 2004), or connections to the Video Serving Office (Han et al., 2008) from which video is typically distributed over Asymmetric Digital Subscriber Line (ADSL) connections. Note also that Internet traffic may be directed through an All-IP network by means of the common agency of IP framing.

In the Internet, a tight link (or more loosely a bottleneck), which commonly exists at the network edge before a corporate or campus network (Cisco, 2000), is the link of minimum available bandwidth on a network path. Strictly the term 'bottleneck' defines the bandwidth capacity of a network path, which while the path exists is a constant, though the term may also be loosely applied to a tight link. A tight link is a dynamic concept, as its location will vary firstly over time according to background traffic patterns and secondly according to the network path's route, which is not fixed because of dynamic routing on the Internet. These two factors can create uncertainty in any video streaming response. Available bandwidth is restricted by coexisting cross-traffic, which is most likely carried by the Transmission Control Protocol (TCP) and predominantly originates from web-servers or P2P file transfer (Xie et al., 2007). Transport-layer protocols like TCP, sitting above IP, are responsible for end-to-end negotiation of delivery between applications. On All-IP networks, coexisting traffic across a network sub-channel or pipe is more likely to arise from other proprietary video servers and be carried by the minimal User Datagram Protocol (UDP) as directed by congestion controllers. A pipe is a virtual bandwidth restriction imposed by quality-of-service requirements that must balance the requirements of other types of traffic and the capacity of the access network. As in the Internet, All-IP congestion controllers should be end-to-end over the network path, allowing a general solution in the sense that the nature of the access network

bottleneck may not be known in advance. In an All-IP network, statistical multiplexing of VBR video sources within a video pipe may increase its efficiency but there is no spare capacity for greedy acquisition of bandwidth by independently controlled video servers. We return to the subject of statistical multiplexing within the IPTV pipe in Section 4.

Congestion control is vital to avoid undue packet loss from the fragile compressed video stream. At the sub-frame level, because variable-length coding (VLC) prior to outputting the bitstream introduces a dependency between each encoded symbol, there is fragility that error resilience techniques such as decoder synchronization markers and reversible VLC only partially address. Because successive video frames are broadly similar (except at scene cuts and changes of camera shots), only the difference between successive frames is encoded in order to increase coding efficiency. Consequently, at the frame-level, removing temporal redundancy introduces a dependency on previously transmitted data that implies lost packets from reference frames will have an impact on future frames.

Unicast video streaming, which brings increased flexibility and choice to the viewer over multicast delivery, is achieved by determining the available bandwidth and adapting the video rate at a live video encoder or an intermediate transcoder. Fuzzy Logic Control (FLC) is suited to congestion control (Jammeh et al., 2007), because of the inherent looseness in the definition of congestion and the uncertainty in the network measurements available, together with the need for a real-time solution. Within video coding it has previously found an application (Grant et al., 1997) in maintaining a constant video rate by varying the encoder quantization parameter according to the output buffer state. This is a complex control problem without an analytical solution. Fuzzy logic is gaining acceptance in the video community, witness (Rezaei et al., 2008), but it turns out that further improvements are possible with interval type-2 (IT2) fuzzy logic.

3.2 Fuzzy logic control for congestion

In our application, FLC of congestion is a sender-based system for unicast flows. The receiver returns a feedback message indicating changes to the delay experienced by video stream packets crossing the Internet. This allows the sender to compute the network congestion level and from that the FLC estimates the response. The same controller also should be able to cope with a range of path delays and with video streams with differing characteristics in terms of scene complexity, motion, and scene cuts.

Traditional, type-1 FLC is not completely fuzzy, as the boundaries of its membership functions are fixed. This implies that there may be unforeseen traffic scenarios for which the existing membership functions do not suffice to model the uncertainties in the video stream congestion control task. IT2 FLC can address this problem by extending a Footprint-of-Uncertainty (FOU) on either side of an existing type-1 membership function. In IT2 fuzzy logic, the variation is assumed to be constant across the FOU, hence the designation 'interval'. Though the possibility of type-2 fuzzy systems has been known for some time (Zaddeh, 1975), only recently (Mendel, 2007) have algorithms become available to calculate an IT2 output control value at video rate. The first IT2 controllers (Hagras, 2007) are now emerging, in which conversion or retyping from fuzzy IT2 to fuzzy type-1 takes place before output. For video streaming there are important practical advantages. Not only does such a controller bring confidence that re-tuning will not be needed when arriving traffic displays unanticipated or un-modeled behavior but the off-line training period required to form the membership functions can be reduced.

We now compare type-1 FLC for congestion control of video streaming to an IT2 FLC and compare the performance in the presence of measurement noise that is artificially injected to test the relative robustness. The delivered video quality in terms of Peak Signal-to-Noise Ratio (PSNR) is equivalent to the successful type-1 FLC when the measurement noise is limited and under test results in a considerable improvement when the perturbations are large. We go on to compare the IT2 FLC to a non-adaptive approach and to congestion control by two well-known controllers, TCP-friendly Rate Control (TFRC) (Handley et al., 2003) and TCP Emulation at Receivers (TEAR) (Rhee et al., 2000), one sender-based and the other receiver based. These are tested by their ability to support multiple broadband connections over an all-IP network. However, firstly we introduce fuzzy logic control.

3.3 Fuzzy logic control

Figure 2 is a block diagram of FLC of congestion, with two inputs, the packet delay factor, df , and delay samples to form a trend (whether packet delay is increasing or decreasing). The formation of these inputs is described in Section 3.4. These inputs are converted to fuzzy form, whereby their membership of a fuzzy subset is determined by predetermined membership functions. This conversion takes place in the fuzzifier and trend test units of Figure 1. The fuzzy outputs are then combined in the inference engine through fuzzy logic. Fuzzy logic is expressed as a set of rules which take the form of linguistic expressions. These rules express experience of tuning the controller and, in the methodology, are captured in a knowledge database. The inference engine block is the intelligence of the controller, with the capability of emulating the human decision making process, based on fuzzy-logic, by means of the knowledge database and embedded rules for making those decisions. Lastly, the defuzzification block converts inferred fuzzy control decisions from the inference engine to a crisp or precise value, which is converted to a control signal. The control signal causes the quantization parameter of the video stream to be changed, thus adjusting the output bitstream.

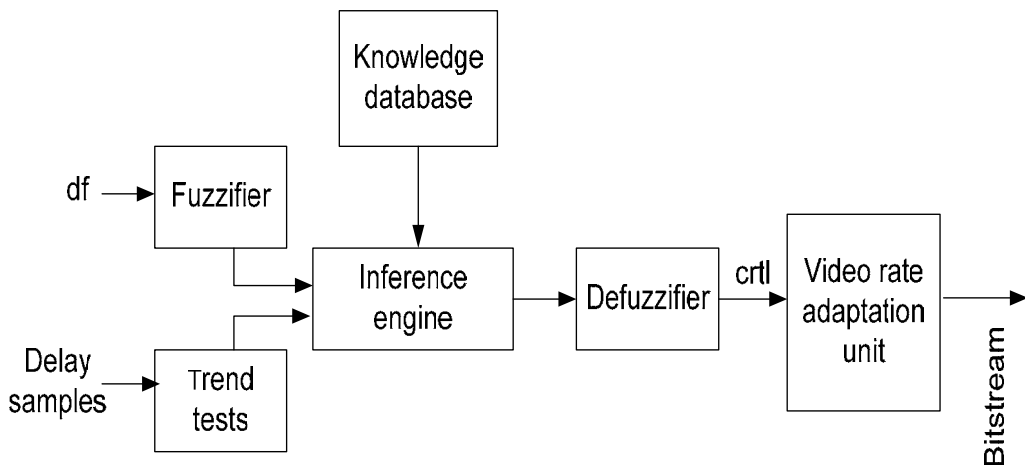


Fig. 2. FLC delay-based congestion controller

In a fuzzy subset, each member is an ordered pair, with the first element of the pair being a member of a set S and the second element being the possibility, in the interval $[0, 1]$, that the member is in the fuzzy subset. This should be compared with a Boolean subset in which every member of a set S is a member of the subset with probability taken from the set $\{0, 1\}$, in which a probability of 1 represents certain membership and 0 represents non-membership.

The FLC determines incipient congestion from one way packet queuing delay in intermediate router buffers. The queuing delay is a measure of network congestion, and the ratio of the average queuing delay to the maximum queuing delay is a measure of bottleneck link buffer fullness. For each received packet indexed by i

$$OWDi = Tr - Ts, \quad (1)$$

where Tr is the receive time of the current packet and Ts is the time the packet was sent. When it is appropriate, the computed $OWDi$ updates the minimum and maximum one-way delays ($OWDs$), $OWDmin$ and $OWDmax$, on a packet-by-packet basis. Subsequently, the maximum queuing delay is found as $maxQD = OWDmax - OWDmin$.

The queuing delay over the network path, QDi is computed from the measured delay and the minimum delay:

$$QDi = OWDi - OWDmin \quad (2)$$

and an exponentially-weighted average of the queuing delay for the i th received packet is formed by,

$$avgQDi = (1 - a) \times avgQDi-1 + a \times QDi \quad (3)$$

where $\alpha \leq 1$ is a forgetting constant. In tests, a was set to 0.1. A delay factor, Df , is computed from the average queuing delay and the maximum queuing delay,

$$Df = avgQDi / maxQD \quad (4)$$

where Df ranges between $[0,1]$ with 0 indicating no incipient congestion, 1 indicating full-blown congestion, with shades of incipient congestion between 0 and 1. Df is an early notification of congestion and is the first input to the FLC.

A trend analysis method is used to determine the general trend of the average delay. In each measurement epoch, a number k of queue delay samples are grouped into τ groups where $\tau = \sqrt{k}$. We use the pairwise comparison test (PCT) to determine the overall trend of the queueing delay as shown in (5).

$$T_{PCT} = \frac{\sum_{i=2}^{\tau} I(M^i > M^{i-1})}{\tau - 1} \quad (5)$$

where M^i is the median of group i and $I(X)$ is 1 if X holds and 0 otherwise. The value of T_{PCT} is sent back to the sender where a fuzzifier determines whether the level was increasing or not according to a membership function.

IT2 input membership functions for D_f and trend are constructed, Figure 3, as an extension of the type-1 FLC through an FOU at the boundaries of the formerly crisp (fixed) membership functions. Assuming the usual singleton input of D_f (or T_{PCT}), an interval set requires just an upper and lower value to be resolved to form the resulting FOU in the corresponding output set. For example, Figure 4 shows two IT2 membership functions for input sets A and B, each with an FOU. Singleton input X is a member of each with different degrees of membership. Strictly, an infinite number of membership functions (not all necessarily triangular) can exist within the FOUs of sets A and B, but IT2 sets allow the upper and outer firing levels to be taken, as shown in Figure 4. The minimum operator (\min) acts as a t -norm on the upper and lower firing levels to produce a firing interval.

The firing interval serves to bind the FOU in the output triangular membership function shown to the right in Figure 4. The lower trapezium outlines the FOU, which itself consists of an inner trapezoidal region that is fixed in extent. The minimum operator, also used by us as a t -norm, has the advantage that its implementation cost is less than a product t -norm. (A t -norm or triangular norm is a generalization of the intersection operation in classical logic.) Once the FOU firing interval is established, Center-of-Sets type reduction was applied by means of the Karnik-Mendel algorithm, which is summarized in (Mendel, 2007). Type reduction involves mapping the IT2 output set to a type-1 set. In practice, defuzzification of this type-1 output fuzzy set simply consists of averaging maximum and minimum values. The result of defuzzification is a crisp value that determines the change in the video rate.

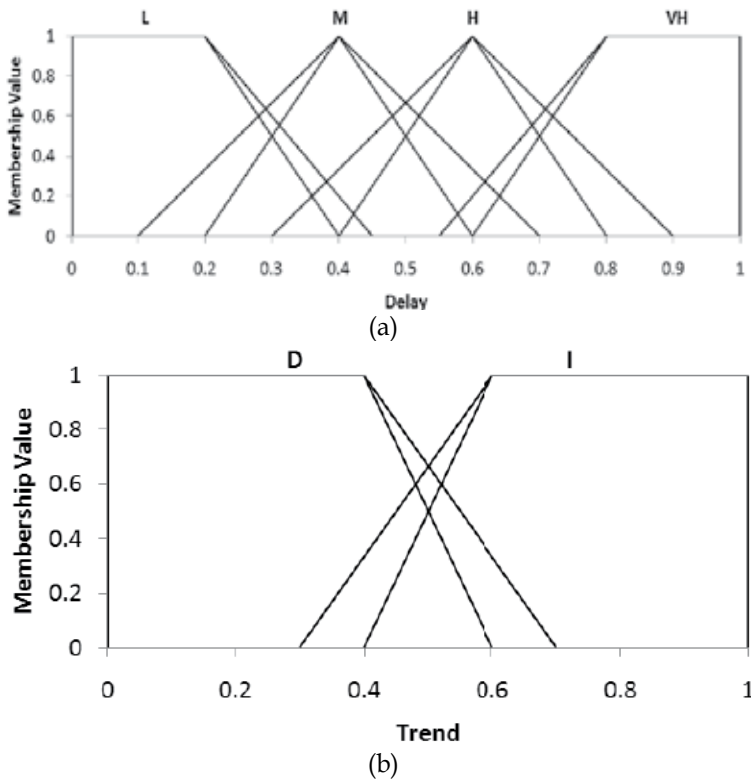


Fig. 3. IT2 FLCC (a) Delay factor (D_f) (b) Trend membership functions.

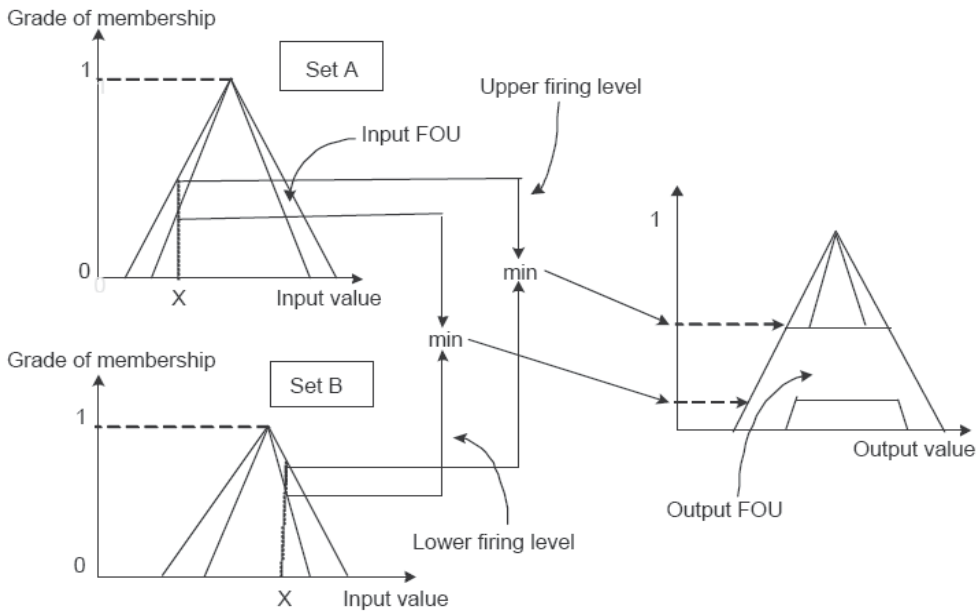


Fig. 4. IT2 FL calculation of output FOU

Figure 5 shows the streaming architecture in which fuzzy logic controls the sending bit rate. The congestion level determination (CLD) unit finds the congestion state of the network from measured delay and delay variation made by the timer module. The congestion state data are relayed to the sender. FLC employs this delay information to compute a new sending rate that is a reflection of the current sending rate and the level of network congestion. The video rate adaptation unit (either a bitrate transcoder adapting pre-encoded video or an encoder adapted through its quantization parameter) changes the sending rate to that computed by the fuzzy controller. The current implementation changes the quantization level of a frequency-domain transcoder (Assunção & Ghanbari, 2000) for VBR video. Full decode and re-encode is prohibitively time consuming. Prior approaches relied on estimation of the error introduced by re-quantization without taking account of the impact on motion estimation by reconstructing the picture and reusing information in the bitstream (Vetro et al., 2005), which still introduces delay, whereas partially (entropic) decoding and motion estimation in the transform domain is faster.

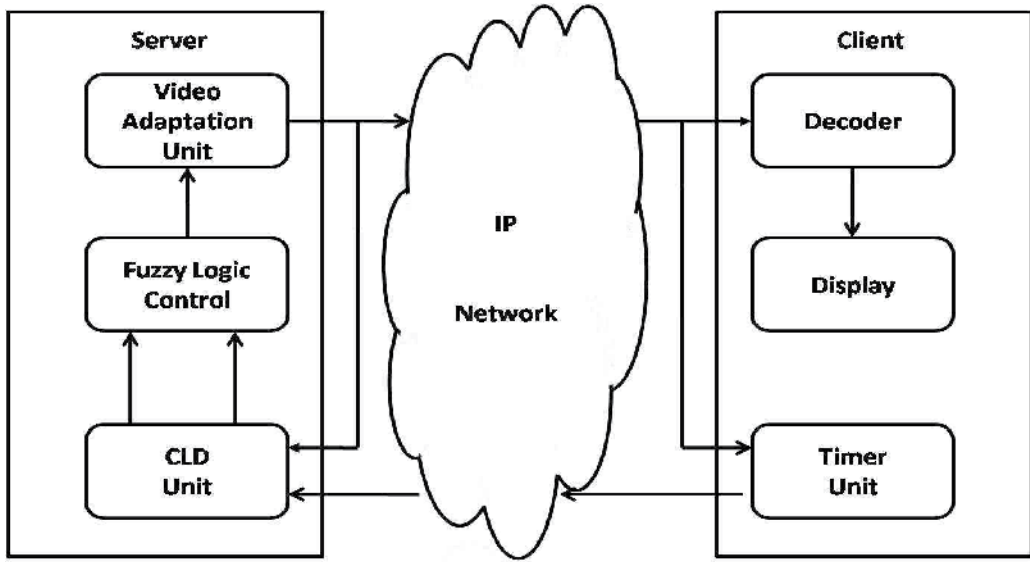


Fig. 5. Video server for all-IP network

Figure 6 shows one instance of server and client. VoD mode, IPTV or video clip services there are multiple video streams and multiple clients. Figure 6 assumes a bank of such servers delivered over an access network such as ADSL or ADSL2+, with downstream rates to 24 Mbps and beyond, one of the passive optical network types (PON) terminating in 100 Mbps Ethernet or coaxial cable, or broadband wireless such as IEEE 802.16 (WiMAX).

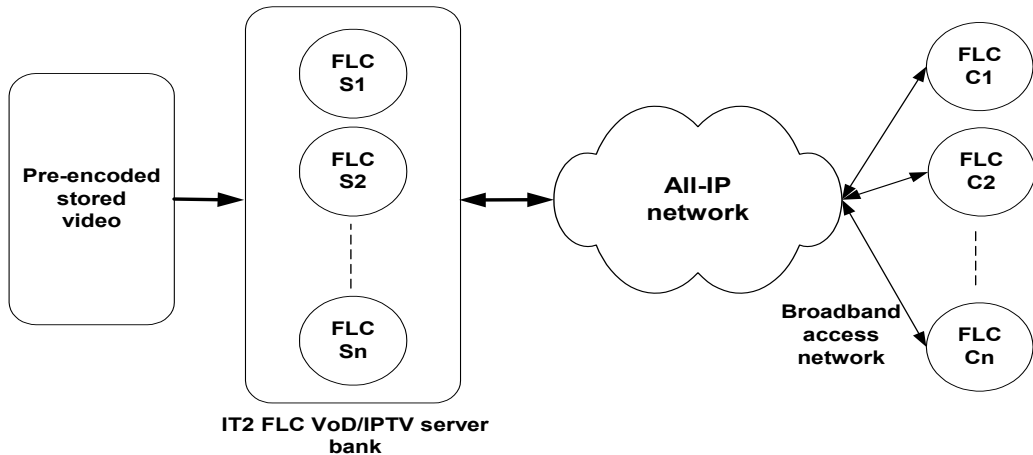


Fig. 6. VoD IPTV video delivery architecture

3.4 Evaluation

FLC congestion controller employs delay and its variation to gauge the state of the network. There is, however, inherent noise in the measurement of delay, including packet timestamps with limited resolution and unresolved clock drift between sender and receiver. These uncertainties in the input to an FLC will potentially impact its performance.

The well-known ns-2 network simulator (v. 2.32) was used, with the type-1 and IT2 FLC implemented as new protocols within ns-2. A normal distribution generated a random noise value with zero mean and a specified standard deviation, determined by the level of noise required and dynamically adjusted relative to the measured (simulated) value. For each simulation the level of additional noise was incrementally increased. At each incremental step, the performance of the two controllers was compared in terms of rate adaptation accuracy, packet loss rate, and delivered video quality (PSNR). Input was a 40 s MPEG-2 encoded video clip, showing a newsreader with a changing backdrop, with moderate movement. The VBR 25 frame/s Standard Interchange Format (SIF)-size clip had a Group of Pictures (GOP) structure of $N=12$, $M=3$ where N is the number of pictures (frames) between each Intra-coded picture and M is the number of pictures between each prediction-coded picture within the GOP (Ghanbari, 2003). For error resilience purposes, there was one slice per packet, resulting in 18 packets per frame. The FLC controllers adjusted their rate every frame. In this set of tests the encoded video was stored at a mean rate of 1 Mbps. The video streams were passed across a bottleneck link restricted to 400 kbps in capacity.

The results are gathered in Table 1, and Figs. 7–8. Below 30% additional noise, the two controllers do not significantly deviate. However, beyond 30% of additional noise, the IT2 FLC congestion controller showed significant improvement over the type-1 FLC in terms of reduced fluctuation in the sending rate and a reduced packet loss rate, both of which will be reflected in better average delivered video quality. The smoothness of the transmission rate (measured by a reduction in the standard deviation of the delay on a per-packet basis) is important in video transport as a fluctuating compressed bit-rate implies a fluctuation in video quality, which is more disconcerting to a viewer than a stream of consistent quality, even if that average quality was lower than that of a fluctuating stream. Figure 8 confirms that delivered average video quality is improved, though, for very high levels of measurement noise, the encoded video stream is so corrupt it matters little which FLC is in control, the quality is very poor. Detailed statistical examination of these results has confirmed their significance within 90% confidence intervals.

Noise level (%)	Type-1	Type-2
0	77.527	76.722
10	78.192	76.607
20	78.986	77.098
30	80.281	77.677
40	109.927	77.747
50	193.612	78.244
60	227.173	80.238
70	230.016	84.294
80	230.651	93.822
90	230.924	113.355
100	231.082	124.652

Table 1. Standard deviation of FLC type-1 and type-2 sending rates (kbps)

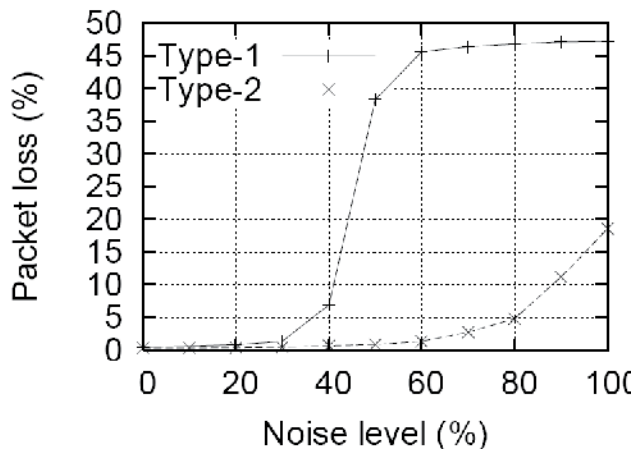


Fig. 7. Packet loss rate for an increasing noise level

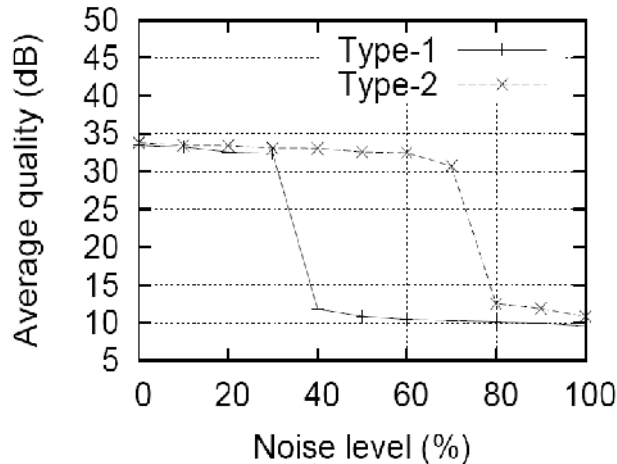


Fig. 8. Mean received video quality for an increasing noise level

Comparison was also made with the TFRC protocol, the subject of an RFC (Handley et al., 2003) and a prominent method of congestion control. The intention is that the average rate of TFRC should be equivalent to the dominant protocol in the Internet, TCP. However, the short term TFRC rate is intended to be less aggressive than TCP as sharp fluctuations in coding rate will result in variable quality at the receiver. In that way, it is hoped that TFRC will avoid causing congestion collapse by greedy acquisition of bandwidth. In TFRC, the sending rate is made a function of the measured packet loss rate during a single round-trip time (RTT) duration measured at the receiver. Unfortunately, if the TFRC feedback frequency is reduced TFRC tends to dominate co-existing flows (Rhee et al., 2000). The sender then calculates the sending rate according to the TCP throughput equation given in (Handley et al., 2003). As with IT2 FLC and TEAR, the UDP transport protocol is employed to avoid unbounded delays, which are possible with TCP transport.

No control			
No. of Sources	Loss rate (%)	Link use (%)	PSNR (dB)
25	0.0	100.0	-
30	16.66	120.0	-
35	28.56	140.0	-
40	37.49	160.0	-
45	44.44	180.0	-
50	49.99	200.0	-
TFRC			
No. of Sources	Loss rate (%)	Link use (%)	PSNR (dB)
25	1.50	101.48	36.08
30	1.81	101.80	35.11
35	2.11	102.80	33.78
40	2.39	102.44	33.07
45	2.65	102.78	31.34
50	2.91	102.96	30.18
TEAR			
No. of Sources	Loss rate (%)	Link use (%)	PSNR (dB)
25	2.50	102.52	33.27
30	3.51	103.60	32.34
35	4.61	104.80	31.56
40	5.75	106.08	30.70
45	6.86	107.36	29.61
50	7.91	108.56	28.78
IT2 FLC			
No. of Sources	Loss rate (%)	Link use (%)	PSNR (dB)
25	0.0	89.82	39.61
30	0.0016	99.96	37.90
35	0.0026	99.96	36.89
40	0.0029	99.96	35.44
45	0.0038	99.84	33.19
50	0.0048	99.82	31.40

Table 2. Performance comparison of congestion controllers

Unlike TFRC, TEAR is based on the Arithmetic Increase Multiplicative Decrease (AIMD) algorithm of TCP. Unlike TCP, TEAR avoids the oscillatory behavior of TCP by averaging its sending rate over a round, based on the time to send a congestion window's packets. TEAR's sending rate approximates that of an equivalent TCP source. Both TFRC and TEAR rely on measurements of the RTT, while TFRC is also adversely affected by inaccurate loss rate estimates (Rhee et al., 2007). Without a transcoder TFRC and TEAR require playout buffers to smooth out network delay. Therefore, PSNR is affected by loss rate only, assuming a large enough buffer to avoid overflow. FLC also reduces the video quality

through transcoding if there is insufficient bandwidth, but this avoids the need for long start-up delays and allows smaller buffers on mobile devices. In further comparison tests, the standard 'dumbbell' network topology was assumed with a bottleneck of 25 Mbps. The one-way delay, modeling the latency across the complete network path, was set to 40 ms, which is the same as the maximum delay across a country such as the U.K or France. Side link delay was set to 1 ms and the side link capacity was set to easily cope with the input video rate. The mean encoded video rate was again 1 Mbps. The buffer size on the intermediate routers was set to $RTT \times \text{bandwidth}$, to avoid overflow through too small a buffer. The router queuing discipline was drop-tail. The intention of these tests was to see how many video streams could be accommodated across the bottleneck link. In Table 2, the number of controlled video sources was incrementally increased.

The starting times of streaming the 'news clip' to each client was staggered, and then each clip was repeatedly sent over 200 ms. The first 40 s of results, was discarded as representing transient results. This method was chosen, rather than select from different video clips, because the side effects of the video clip type do not intrude.

As can be seen from Table 2, when there is no control, there is no packet loss until the capacity of the link is reached. Thereafter, the link utilization grows and, as might be expected, the packet loss rate rapidly climbs. Failure to estimate the available bandwidth causes both TFRC's and TEAR's mean link use to exceed the capacity of the bottleneck link. As the number of flows increases, it becomes increasingly difficult to control the flows and there is a steady upward trend in the overshoot. In respect to TEAR, this leads to considerable packet loss. The packet loss patterns are reflected in the resulting PSNRs, though there is no direct relationship because of the effect of motion estimation in the codec. It is surprising in that TEAR was developed after TFRC and in part as a reaction to it (Rhee et al., 2007). However, subsequent to the development of TEAR, TFRC has undergone some refinements such as TCP's self-clocking. However, from Table 2 it is apparent IT2 FLC congestion control does not suffer from the difficulties that TFRC and TEAR encounter. There is a very small loss rate due to moments when the time varying nature of VBR video results in the FLC overestimating the available bandwidth but this is significantly below the loss rates of the traditional controllers.

4. Statistical multiplexing

4.1 IPTV and statistical multiplexing

Fortunately, compressed video streams forming the TV channels making up the IPTV service will not necessarily have the same bandwidth requirements, as their content complexity will vary over time with changes in their spatial and temporal complexity. In the long term, for entertainment applications this variation is determined by the video genre, such as sport, cartoon, 'soap' and so on but there are also changes over a shorter time period caused by such factors as the type of video frame and whether there is a shot change or a scene cut. Consequently, multiple video streams as part of an IPTV service can each be adaptively allocated a proportion of the bandwidth capacity according to their content complexity.

As IPTV bandwidth may be constrained by a particular access network technology a practical solution, which has already been developed in the UK and Japan (Kasai et al., 2002), is to employ a transcoder bank to change the rates of video streams within the

multimedia channel. Transcoders can dynamically and selectively change the compression ratio of individual pre-encoded video streams within a multimedia channel. However it is accomplished, the process of adjusting the rates of individual video streams is called statistical multiplexing.

Transcoding is a normal procedure in statistical multiplexing (Eleftheriadis & Batra, 2006) whereby the input streams can be adapted to fit the video display terminal. The coding complexity measures are computed based respectively on the transform coefficient and motion vector information embedded in each input bitstream, representing the compressed video. This information can be easily obtained just after the first decoding stage of the transcoder, *i.e.* after entropic decompression.

Though research (He & Wu, 2008) has experimented with statistical multiplexing of VBR streams, the practical reality is that broadcasters may often employ a CBR multiplex of streams (Bóróczy et al., 1999) previously stored at a high quality. This is because CBR encoding allows planning of storage capacity and in video-on-demand schemes, it allows the bandwidth from a server to be tightly controlled. If the CBR video is not pre-encoded at a high rate (prior to transcoding) then dissolves, fast 'action' and scenes with camera motion (pans, zooms, tilts, ...) suffer. However, scenes with limited motion such as head-and-shoulder news sequences are not much affected by CBR encoding.

4.2 Statistical multiplexing gain

The revenue that can be potentially generated from combining video streams within a multimedia channel (Seeling & Reisslein, 2005) is related to the quality of the video delivered to the end users. In (Kuhn & Antkowiak, 2000) tests of a statistical multiplexor for Digital Video Broadcasting (DVB-T) (MPEG-2 encoded bitstreams) showed that multiplexing did not necessarily increase the number of TV channels that could be accommodated within a fixed bandwidth *but* did serve to avoid deep quality fades.

Allocating bandwidth to video streams simply on the basis of efficient usage and fair distribution of bandwidth (Jain et al., 2000) is not to be recommended, because the delivered video quality of some video streams will be more affected by a reduction in bandwidth than by others. Both unwarranted degradation of quality and unnecessarily high video quality may arise. This is also the reason why allocating bandwidth based on the past statistics of data rates may be ill-advised, as it fails to account for the impact of such allocations on the delivered video quality. R-D curves of video sequences significantly differ in their video quality at a particular CBR target bit-rate. Statistical multiplexing requires dynamic adjustment of the bandwidth share between several concurrent streams based upon the content complexity in order to equalize their delivered video quality. Ideally, the quality of all video streams will then fall within an acceptable range, being neither too high nor too low in quality.

From an R-D plot of three video sequences, Figure 9, it is apparent that there is a significant difference between the quality ratings of the videos. Therefore, the goal of statistical multiplexing is to adjust the quality between the streams relative to their content complexity rates over time. Good quality video normally falls within the range of 30-38 dB. At an initial target input rate of 1 Mbps, the quality of Mobile in Figure 9 is on the boundary of that range, while the quality of both Highway and Bridge-closed exceeds the range.

Statistical multiplexing techniques vary according to their complexity. In the research reported in (Wang & Vincent, 1996) a relatively simple form of statistical multiplexing was

applied in which the same quantization parameter was applied to all video frames within a multiplexed group to achieve a target bit rate. A binary chop search across the range of available quantization parameters was conducted. This procedure appeared to achieve its objective even though no direct account was taken of content complexity. The work in (Bórczy et al., 1999) was based on coding complexity statistics was applied to a set of R-D controlled MPEG-2 video encoders. Only spatial coding complexity was considered and, therefore, no control was needed to include temporal complexity, at a cost in accuracy. Because encoders were employed, a look-ahead scheme was needed. This suffers from the problem of video scene changes occurring within a GOP inspection window, as the complexity may change significantly within a GOP. Some allowance for this problem was made by a sliding window GOP prediction method. The alternative is to partially decode future frames, as occurs in (He & Wu, 2008) for VBR video. Unfortunately, in (He & Wu, 2008), only the temporal complexity measure is found by partial decode, while the spatial complexity is predicted from a previous frame.

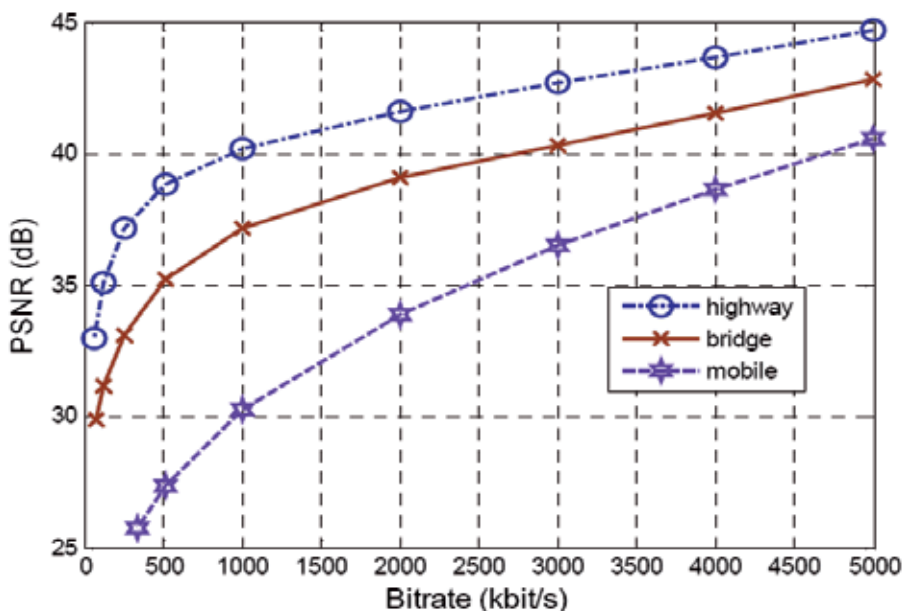


Fig. 9. R-D curves for three well-known video sequences.

In the statistical multiplexing system considered in this Chapter, R-D analysis is turned on in the H.264 encoder so that all rate decisions are optimized according to their effect on video quality. Moreover the problem of look ahead is resolved by directly transcoding each video stream GOP according to the joint estimation without the need for complex forward inspections of complexity (two-pass encoding) or potentially erroneous predictions.

4.3 Statistical multiplexing system

A top-level system diagram is presented in Figure 10. This is a suggested application of the scheme to illustrate a statistical multiplexing system. In this Figure, the statistical multiplexor receives n compressed bitstreams that pass through a bank of bit-rate

transcoders to adjust the combined bitrate according to the output channel constraints. The bandwidth share is defined by the statistical bandwidth manager which receives content complexity measure *parameters* from each transcoder and returns the appropriate bandwidth share a .

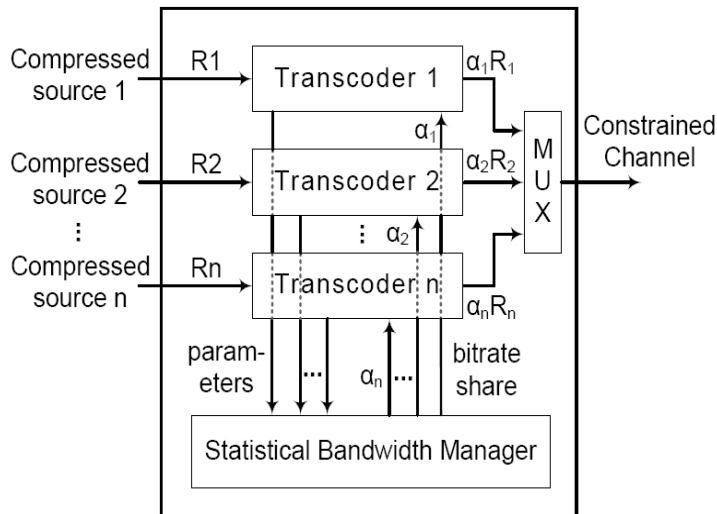


Fig. 10. A statistical multiplexor architecture

To reduce decision latency and to create a more direct way of judging the content complexity, metrics can be derived from the encoded bit-stream. Entropy decoding is required but this is a small overhead compared to a full decode. For example in the H.264/Advanced Video Codec (AVC), the Context Adaptive Variable Length (CAVLC) decode and bit-stream parsing on average take only 13% of the computational complexity of a full decode (Malvar et al., 2003).

Two metrics can be employed: temporal complexity index (TI) is indicated by a count of per frame non-zero motion vectors summed across a GOP, whereas spatial complexity can be found (Rosdiana & Ghanbari, 2000) by averaging a Scene Complexity Index (SCI) across the GOP. It is also possible to make decisions at scene change boundaries or through a GOP-sized sliding window at a cost in complexity but with a gain in reaction time. Because a large proportion of the bit-stream's length at higher video qualities is contributed to by quantized Discrete Cosine Transform (DCT) coefficients, the weighting given to the SCI metric is increased through the decision rules of an FLC. For a low bitrate service across a wireless channel then the impact of the motion vector coding would compete (Van der Auwera et al., 2007) with the quantized motion vectors, and it would become necessary to adjust the weighting between TI and SCI.

From the input video streams (coded in CBR mode) the average quantization parameter (QP) per frame is defined by the target bit rate. Consequently, multiple video streams sharing the channel can each be allocated a proportion of the bandwidth capacity according to their instantaneous spatial and temporal complexity. The target output rate of the video streams can be changed accordingly at a transcoder after each decision point (every GOP).

A FLC solves the problem of combining the two complexity indexes employed into a single bandwidth allocation ratio. Additionally, the FLC also receives notice of the bandwidth capacity. In the example illustrated in this Section, the final access link is assumed to be ADSL. However, ADSL is subject to burst errors following the Repetitive Electrical Impulse Noise (REIN) model (Luby et al., 2008). Once the FLC has determined the ratio allocated to each video stream sharing the IPTV multimedia sub-channel, the video bitstream rates are jointly adjusted by bitrate transcoders.

4.4 Experimental evaluation

For tests, 900 frames from the three well-known sequences of Figure 9 were selected with content complexity category estimated as difficult, medium, and easy. The JM v. 14.2 software implementation of the H.264/AVC codec was used with Common Intermediate Format (CIF)-30 Hz (frame/s) @ 5 Mbps, 4:2:0 sampling, and GOP size of 15. An IPPP... GOP structure was set with Instantaneous Decoder Refresh (IDR) frames configured. R-D control was set for the CBR output with initial quantization parameter (QP) at 28 and only 4x4 DCTs.

Figure 11 is a plot of the per GOP number of non-zero motion vectors over time. For ease of representation, an average of the first 20 GOPs is plotted, though naturally the entire 60 GOP sequences were examined. The TI measure for 'Mobile' fluctuates over time within this short excerpt, though recall that the TI emphasis is reduced in the FLC compared to the SCI. Figure 4 is a matching plot for the SCI over time. In general, the SCI is found as:

$$SCI = \frac{1}{1 + p + b} \left[IQ_I + \sum_{j=1}^p P_j QP_j + \sum_{i=1}^b B_j QB_i \right] \quad (6)$$

where p , b are the number of P and B pictures per GOP respectively and QI , QP and QB are the respective average (over the picture's macroblocks) quantizer step sizes for the I, P, and B pictures. I , P and B are the corresponding per picture type target bit-rates. Again, in Figure 12 it is the Mobile sequence that shows the most fluctuation. Alternative metrics are: 1) employing QP values into (6) to take account of the changing dynamic range of the allocations and 2) using the numbers of non-zero coefficients

Figure 13 shows the input PSNRs for the three sequences, showing fluctuations in behavior. As PSNR is best-suited to quality comparisons for the same video sequence coded at different rates, PSNR comparisons are made between equal allocation and statistical multiplexing and should not involve direct comparison of the quality between different video streams. Statistical multiplexing decisions are made on the basis of content complexity and do not involve PSNR.

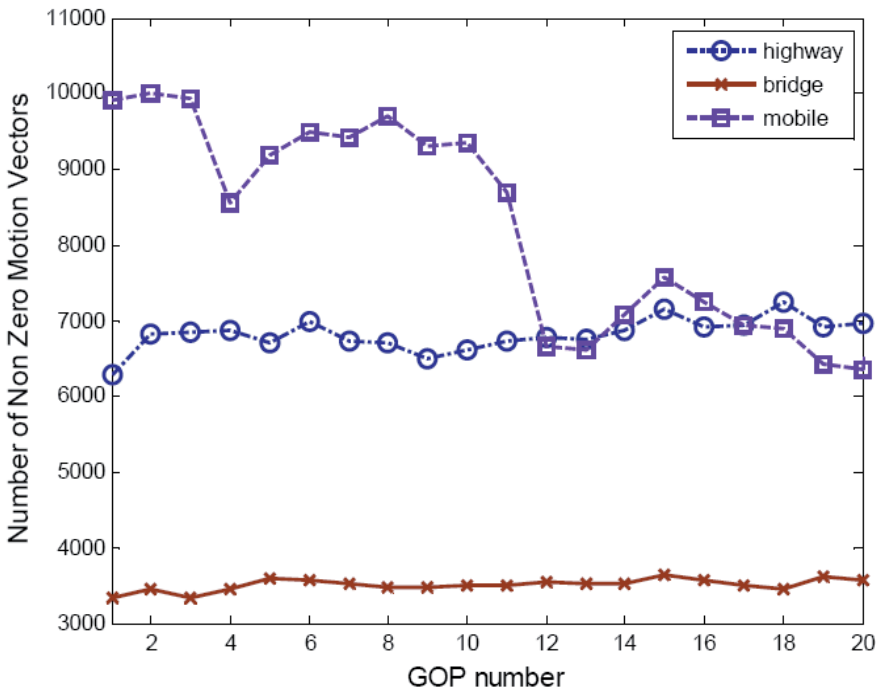


Fig. 11. Number of non-zero motion vectors on a GOP basis

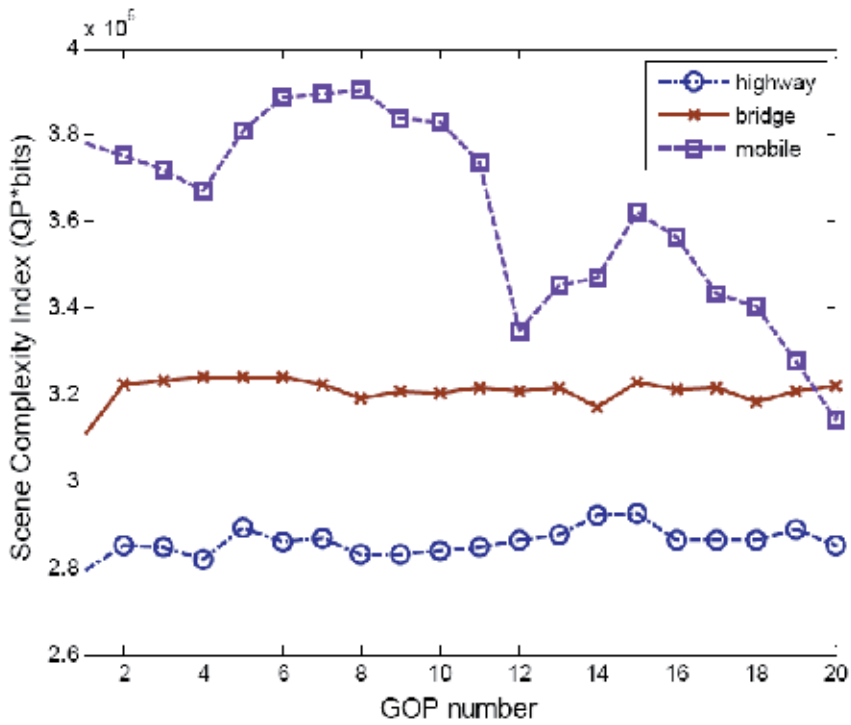


Fig. 12. Scene Complexity Index (SCI) on a GOP basis

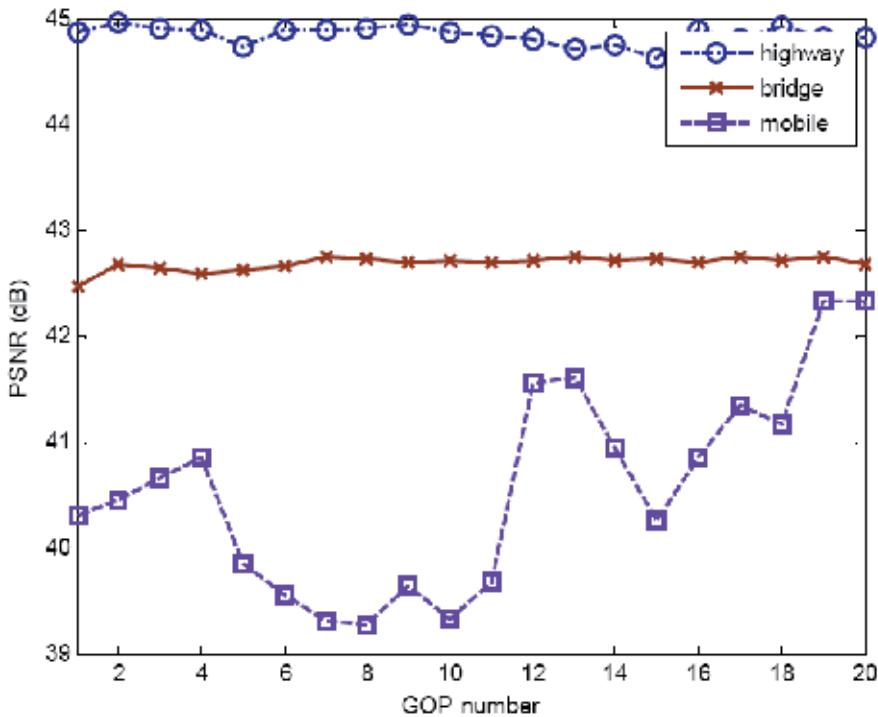


Fig. 13. PSNR fluctuation of input test sequences

In tests, packetisation was on the basis of one H.264 NALU per packet, with each row forming a slice to be encapsulated in a NALU. Error-free, fixed bandwidth (3 Mbps) allocation is firstly considered. (If the access link is cable or even a passive optical network (PON), the physical channel will be virtually error free and the bandwidth capacity will effectively be fixed.) Figure 14 shows the time-wise allocation of bandwidths after application of the FLC based on the SCI and TI metrics. The allocation follows approximately the content complexity of the test clips, in the sense that a more complex sequence receives a larger proportion of bandwidth. Figure 15 is a histogram of the per-frame frequencies for which the video sequences fell within the desired quality range (30-38 dB), compared to the same allocation if no adjustment to the initial CBR rates was made.

The allocation over time is illustrated for Highway in Figure 16. Table 3 summarizes the average video qualities resulting from the FLC and equal CBR allocations. It is apparent that for Mobile much of the time the FLC allocation results in a higher video quality than a CBR scheme would do, whereas for Highway and Bridge-closed, the video quality (which is already high) is somewhat reduced.

In (Luby et al., 2008), the REIN model for ADSL was applied to IPTV. This is a simple model of fixed-length error bursts, the duration of which was set to 8 ms. The bursts were randomly placed to achieve a loss rate in the range 5×10^{-2} to 5×10^{-3} . In (Luby et al., 2008), a larger error range was simulated but at the lower ends of that range the error rate was effectively close to being error free.

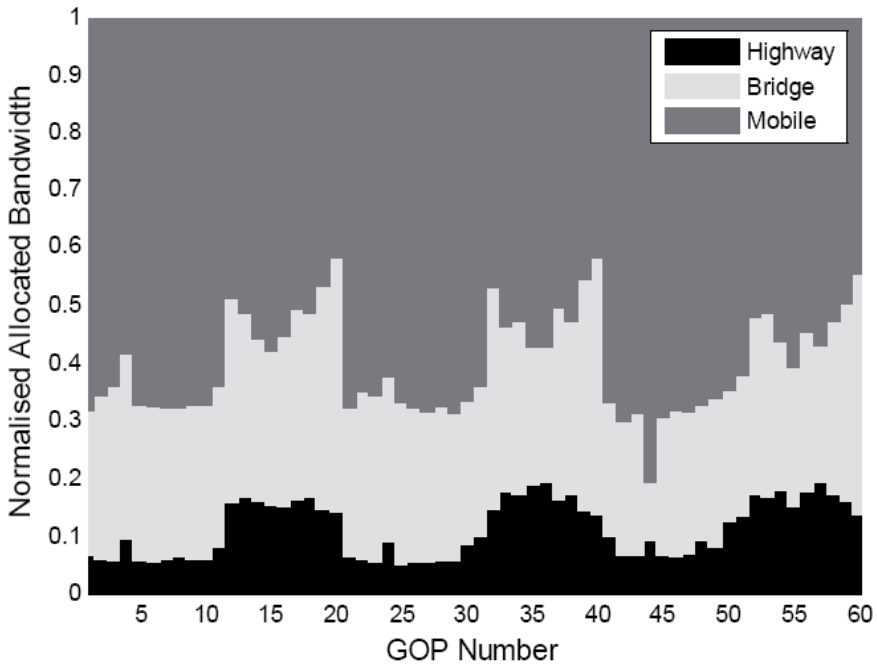


Fig. 14. Bandwidth allocation share per GOP with FLC controller

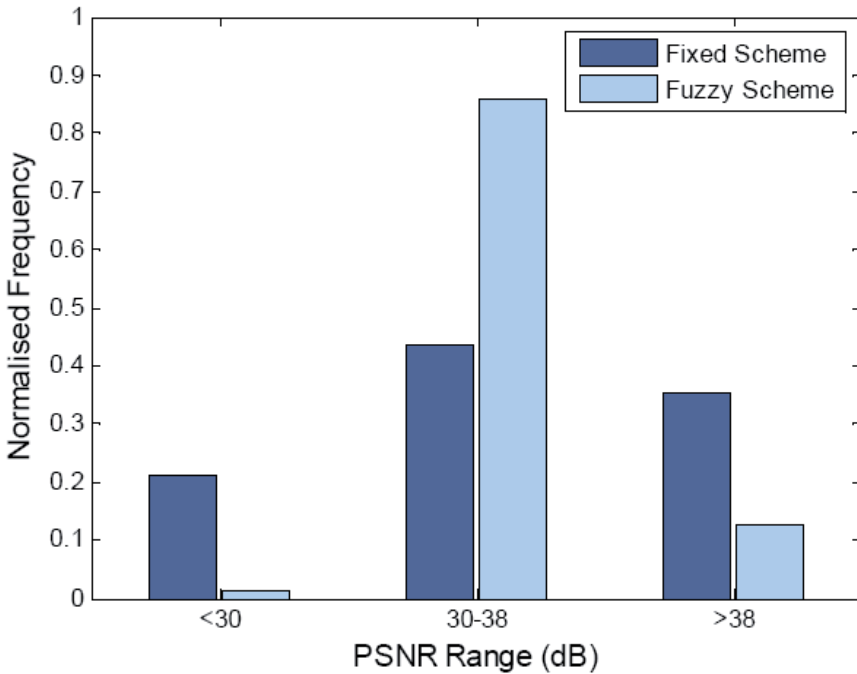


Fig. 15. Normalized per-frame frequencies of video quality for which the three test clips kept within a desired quality range for FLC and equal (fixed) CBR allocation bandwidth

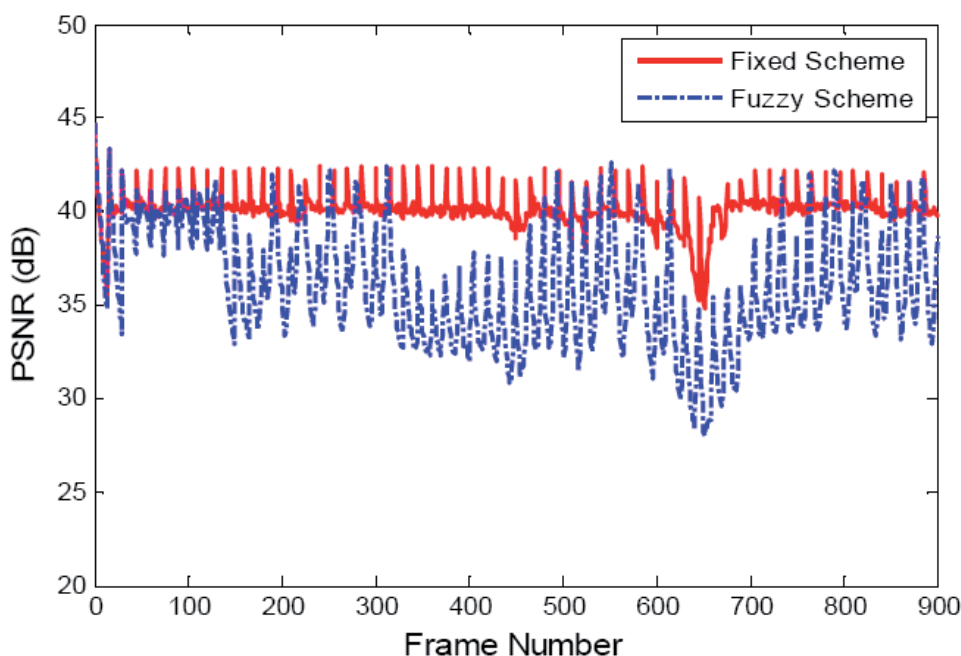


Fig. 16. Comparative video quality over time achieved for Highway between FLC and equal CBR (fixed) schemes

	FLC		CBR	
	Bitrate (kbps)	PSNR (dB)	Bitrate (kbps)	PSNR (dB)
Bridge	338.51	36.03	1000	40.60
Highway	857.01	36.62	1000	36.96
Mobile	1802.90	32.53	1000	29.61

Table 3. Summary results of comparative bandwidth allocation between FLC and equal CBR schemes with fixed available

The effect of physical channel degradation on video according to the REIN model for ADSL was ascertained for a fixed available bandwidth (of 3 Mbps), after subsequent distribution of the video streams to individual users. Figure 17 reports the relative video quality between equal CBR share and FLC allocation. In Figure 17, each data point is the result of forty runs in order to achieve convergence. In particular, the video quality of Mobile is improved by the FLC allocation. This Figure shows that the quality of difficult sequences like Mobile is improved at the expense of degradation on the easier sequences like Highway resulting in a balance between the quality of the quality of multiplexed video. At higher Bit Error Rates (BERs), Mobile's quality becomes poor in both schemes, though the CBR allocation can result in unwatchable TV. Perhaps, a weakness of the FLC allocation is that Highway also drops out of the desired quality range, though at high BERs.

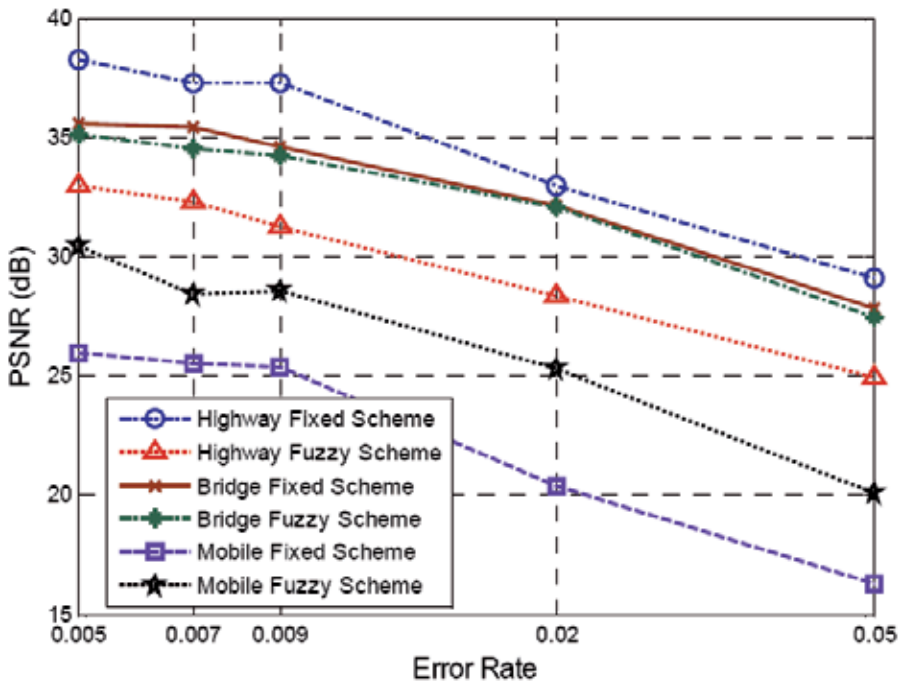


Fig. 17. Video quality according to FLC and equal CBR (fixed) schemes for the ADSL REIN model.

Statistical multiplexing aims to equalize the quality of a set of video streams sharing a common multimedia channel. The quality should also, as far as possible, fall within an acceptable range. The danger of statistical control of data rates is that it does not take account of the varying content complexity of video streams. However, dynamic adjustments can be jointly made to the target video data rates in response to prior input of spatial and temporal compression metrics. These can be extracted from the encoded bitstream just after entropic decode and simple parse operations. Fuzzy logic control subsequently serves to tune the impact of each of the metrics.

5. Concluding remarks

This Chapter has been an introduction to video streaming, from a particular perspective in which intelligent control methods increasingly handle congestion and allocation of bandwidth through statistical multiplexing. Though download undoubtedly has a role in activities such as multimedia podcasting and BitTorrent film downloads, there are always streaming alternatives, which in time may take over from the era of the download, with its inefficient bandwidth consumption. These alternatives range from: enhanced-quality IPTV; user-generated YouTube content; and P2P streaming systems such as PPLive and Coolstreaming, which have a strong following in China; and varieties of mobile TV, such as DVB-H. The demand for bandwidth is increasing as this year (2009) has seen the first High Definition mobile devices. This development is logical as a closer viewing distance strictly requires greater resolution. However, the move to higher resolution reduces the ability of

the user to store locally compressed video. In fact, the desire to own a DVD film just as books are owned and kept in a library may also decline.

6. References

- Assunção, P.A.A. & Ghanbari, M. (1997). Congestion Control of Video Traffic with Transcoder, *Int. Conf. on Image Processing*, pp. 523-527
- Assunção, P.A.A. & M. Ghanbari (2000). Buffer analysis and control in CBR video transcoding, *IEEE Trans. on Circuits and Systems for Video Technology*, Vol. 10, No. 1, pp. 83-92
- Barmada, B.; Ghandi, M. M.; Jones, E.; & Ghanbari, M. (Aug. 2005). Prioritized transmission of data partitioned H.264 video with hierarchical QAM, *IEEE Signal Proc. Lett.*, Vol. 12, No. 8, pp. 577-580
- Bőröczy, L.; Ngai, A. Y. & Westermann, E. F. (1999). Statistical multiplexing using MPEG-2 video encoders, *IBM J. of Research and Development*, Vol. 43, No. 4, pp. 511-520
- Blakowski, G. & Steinmetz, R. (Jan. 1996). A media synchronization survey: Reference model, specification, and case studies, *IEEE J. on Selected Areas in Comms.*, Vol. 14, No. 1, pp. 9-33
- Chou, P. A.; & Miao, Z. (April 2006) Rate-distortion optimized streaming of packetized media, *IEEE Trans. on Multimedia*, Vol. 8, No. 2, pp. 390-404
- Chou, P. A. (2007). Streaming media on demand and live broadcast, in P. A. Chou and M. van der Schaar (Eds.) *Multimedia in IP and Wireless Networks*, Academic Press, Burlington, MA, pp. 453-501
- Cisco Systems, Inc. (2000). *LAN design guide for the midmarket*, San Jose, CA
- Eleftheriadis, A. & Batra, P. (April 2006). Dynamic rate shaping of compressed digital video, *IEEE Trans. on Multimedia*, Vol. 8, No. 9, pp. 297-314
- Fleury, M.; Razavi, R.; Saleh, S.; Al-Jobouri, L. & Ghanbari, M. (2009). Enabling WiMAX video streaming, In *WiMAX, New Developments*, In-Tech Education and Publishing, Vienna, Austria
- Ghanbari, M. (2003). *Standard Codecs: Image Compression to Advanced Video Coding*, IET Press, London, UK
- Geer, D. (Nov. 2005). Building converged networks with IMS technology, *IEEE Computer*, Vol. 38, No. 11, pp. 14-16
- Grant, P. M.; Saw, Y.-S. & J. M. Hannah, J. M. (June 1997). Fuzzy rule-based MPEG rate prediction and control, *EURASIP ECAS Conf.*, pp. 211-214
- Hagras. H. (Feb. 2007). Type-2 FLCs: A new generation of fuzzy controllers, *IEEE Computational Intelligence*, pp. 30-43
- Han, S.; Lisle, S. & Nehib, G. (Feb. 2008). IPTV transport architecture alternatives and economic considerations, *IEEE Comms. Mag.*, Vol. 46, No. 2, pp. 70-77
- Handley, M.; Floyd, S.; Padyhe, J. & Widmer, J. (2003). TCP friendly rate control (TFRC): Protocol specification, IETF RFC 3448
- He, Z. & Wu, D. O. (Nov. 2008). Linear rate control and optimum statistical multiplexing for H.264 video broadcast, *IEEE Trans. Multimedia*, Vol. 10, No. 7, pp. 1237-1249
- IEEE 802.16-2004, (Oct. 2004). IEEE Standard for local and metropolitan area networks part 16: Air interface for fixed broadband wireless access systems

- Jain, R.; Kalyanaraman, S.; Goyal, R.; Fahmy, S. & Viswanathan, R. (Aug. 2000). ATM forum document number: ATM forum/96-1172 title: Erica switch algorithm: A complete description
- Jammeh, E. A.; Fleury, M. & Ghanbari, M. (April 2007). Delay-based congestion avoidance for video communication with fuzzy logic control, *17th Int. Workshop on Packet Video*
- Kalman, M.; Steinbach, E. & Girod, B. (Sept. 2002). Adaptive media playout for low delay video streaming over error-prone channels, *Int. Conf. on Image Processing*, pp. 841-851.
- Kasai, H. et al. (Oct. 2002). The development of a multimedia transcoding system for mobile access to video conferencing, *IEICE Trans. on Communications*, Vol. 10, No. 2, pp. 2171-2181
- Kim, I.-M. & Kim, H.-M. (2002). A new resource allocation scheme based on a PSNR criterion for wireless video transmission to stationary receivers over Gaussian channels., *IEEE Trans. on Wireless Commun.*, Vol. 2, No. 3, pp. 1320-1324
- Kuhn, M. & Antkowiak, J. (Apr. 2000). Statistical multiplex what does it mean for DVB-T?, *FKT Fachzeitschrift für Fernsehen, Film und elektronische Medien*
- Lakshman, T.; Ortega, A. & Reibman, A. (May 1998). VBR video: tradeoffs and potentials, *Proc. of the IEEE*, Vol. 86, No. 5, pp. 952-973
- Lambert, P.; de Neve, W.; Dhondt, Y. & van de Walle, R. (2006). Flexible macroblock ordering in H.264/AVC, *J. of Visual Communication*, Vol. 17, pp. 358-375
- Lefol, D.; Bull, D. & Canagarajah, N. (2006). Performance evaluation of transcoding algorithms for H.264, *IEEE Trans. on Consumer Electronics*, Vol. 52, No. 1, pp. 215-222
- Luby, M.; Stockhammer, T. & Watson, M. (May 2008). Application FEC in IPTV systems, *IEEE Commun. Mag.*, Vol. 46, No. 5, pp. 94-102
- Malvar, H.; Hallapuro, A.; Karczewicz, M. & Kerofsky, L. (July 2003). Low complexity transform and quantization in H.264/AVC, *IEEE Trans. on Circuits Syst. Video Technol.*, Vol. 13, No. 7, pp. 598-603
- Mackay, D. J. C. (2005). Fountain codes, *IEE Proc. on Communications*, Vol. 152, No. 6, pp. 1062-1068
- Mao, S.; Lin, S.; Panwar, S. S.; Wang, Y. & Celebi, E. (2003). Video transport over ad hoc networks: multistream coding with multipath transport, *IEEE J. on Selected Areas in Comms.*, Vol. 21, No. 4, pp. 1721-1737
- Mendel, J. M. (Feb. 2007) Type-2 fuzzy sets and systems: An overview, *IEEE Computational Intelligence*, pp. 20-29
- Pesquet-Popescu, B.; Li, S. & van der Schaar, M. (2007). Scalable video coding for adaptive streaming applications, in P. A. Chou and M. van der Schaar (Eds.) *Multimedia in IP and Wireless Networks*, Academic Press, Burlington, MA, pp. 117-158
- Radha, H.; van der Schaar, M.; Chen, Y. (Mar. 2001). The MPEG-4 Fine_Grained Scalable video coding method for multimedia streaming over IP, *IEEE Trans. on Multimedia*, Vol. 3, No. 1, pp. 53-68
- Rezaei, M.; Hanukse, M. M. & Gabbouj, M. (2008). Semi-fuzzy rate controller for variable bit rate video, *IEEE Trans. on Circuits and Systems for Video Technology*, Vol. 18, No. 5, pp. 633-645
- Rhee, I.; Ozdemir, V. & Yi, Y. (April 2000). TEAR: TCP emulation at receivers – flow control for multimedia streaming, *NCSU Technical Report*

- Rhee, I. & Xu, L. (2007) Limitations of equation-based congestion control, *IEEE/ACM Trans. on Networking*, Vol. 15, No. 4, pp. 852-865
- Rosdiana, R. & Ghanbari, M. (Mar. 2000). Picture complexity based rate allocation algorithm for transcoded video over ABR networks, *Electronics Letters*, Vol. 36, No. 6, pp. 521-522
- Salehi, J.; Zhang, Z.-L.; Kurose, J. & Towsley, D. (Aug. 1998). Supporting stored video: Reducing rate variability and end-to-end resource requirements through optimal smoothing, *IEEE/ACM Trans. on Networking*, Vol. 6, No. 4, pp. 397-410
- Schulzrinne, H.; Rao, A. & Lampeter, R. (April 1998) Real time streaming protocol (RTSP), proposed standard RFC 2326
- Seeling, P. & Reisslein, M. (Dec. 2005). The rate variability-distortion (VD) curve of encoded video and its impact on statistical multiplexing, *IEEE Trans. Broadcast.*, Vol. 51, No. 4, pp. 473-492
- Shokrollahi, A. (2006). Raptor codes, *IEEE Trans. on Information Theory*, Vol. 53, No. 1, pp. 2551-2567
- Stockhammer, T. & Zia, W. (2007). Error-resilient coding and decoding strategies for video communication, in P. A. Chou and M. van der Schaar (Eds.) *Multimedia in IP and Wireless Networks*, Academic Press, Burlington, MA, pp. 13-58
- Sun, H.; Chen, X. & Chiang, T. (2005). *Digital Video Transcoding for Transmission and Storage*, CRC Press, New York
- Van der Auwera, G.; Reisslein, M. & Karam, L. J. (Sept. 2007). Video texture and motion based modelling of rate variability-distortion (VD) curves, *IEEE Trans. on Multimedia*, Vol. 53, No. 3, pp. 637-648
- Van der Auwera, G.; David, P. D. & Reisslein, M. (Sept. 2008). Traffic and quality characterisation of single layer video streams with the H.264/MPEG-4 Advanced Video Coding Standard and Scalable Video Coding extension, *IEEE Trans. on Broadcasting*, Vol. 54, No. 3, pp. 698-718
- Van der Auwera, G. & Reisslein, M. (to appear Sept. 2009). Implications of smoothing on statistical multiplexing of H.264/AVC and SVC video streams, *IEEE Trans. on Broadcasting*.
- Vasudevan, S.; Liu, X. & Kollmansberger, K. (May 2008). IPTV Architectures for Cable Systems: An evolutionary approach, *IEEE Comms. Mag.*, Vol. 46, No. 5, pp. 102-109
- Vars, V. and Hannuksela, M. N. (2001). Non-normative error concealment algorithms, ITU-T SGI6 Doc., VCEG-N62
- Vetro, A.; Christopoulos, C. & Sun, H. (2005). Video transcoding architectures and techniques: An overview" *IEEE Signal Processing Mag.*, Vol. 20, pp. 18-29
- Wang, Y. & Zou, Q. F. (1998) Error control and concealment for video communication: A review. *Proceedings of the IEEE*, Vol. 86, No. 5, pp. 974-997.
- Wang, Y.; Reibman, A. R. & Lee, S. (2005). Multiple description coding for video delivery, *Proceedings of the IEEE*, Vol. 93, No. 1, pp. 57-70
- Wang, L. & Vincent, A. (Sept. 1996). Joint rate control for multi-program video coding, *IEEE Trans. Consumer Electron.*, Vol. 42, No. 3, pp. 300-305
- Wenger, S. (July, 2003) H264/AVC over IP, *IEEE Trans. on Circ. and Syst. for Video Technol.*, Vol. 13, No. 7, pp. 645-656
- Xie, G.; Zhang, G.; Yang, J.; Min, Y.; Issarny, V. & Conte, A. (June 2007). Survey on traffic of metro area network with measurement on-line, *Int. Teletraffic Congress*, pp. 666-677

- Zaddeh, L. A. (1975). The concept of linguistic variable and its application to approximate reasoning, *Information Sciences*, Vol. 8, pp. 199–249
- Zhang, L. et al. (Sept. 1997). Resource ReSerVation Protocol (RSVP), Request for Comment (RFC) 2205
- Zheng, H. & Liu, K. (July 2000). Multimedia services over digital subscriber lines, *IEEE Trans. Signal Processing*, Vol. 17, No. 4, pp. 44–60

The Development of Crosstalk-Free Scheduling Algorithms for Routing in Optical Multistage Interconnection Networks

Mohamed Othman, and Tg Dian Shahida Raja Mohd Auzar
*Department of Communication Technology and Network
Universiti Putra Malaysia
Malaysia*

1. Introduction

Advances in electro-optic technologies have made optical communication a promising networking alternative to meet the ever increasing demands of high-performance computing communication applications for high channel bandwidth, low communication latency and parallel processing as well. Optical Multistage Interconnection Network (OMIN) is popular in switching and communication applications and has been studied extensively as an important interconnecting scheme for communication and parallel computing systems. The OMIN is frequently proposed as connections in multiprocessor systems or in high bandwidth network switches. A major problem in OMIN is optical crosstalk. It is caused by coupling two signals within a Switching Element (SE). Crosstalk problem in a switch is the most prominent factor, which reduces the signal-to-noise ratio and restricts the size of a network.

Various methods to decrease the undesirable effect of crosstalk have been proposed, that apply the concept of dilation in either the space, time or wavelength domains. With the space domain approach, additional SE(s) and links are used to certify that at most only one input and one output of every SE will be active at any given time. With the time domain approach, two connections will be activated at different time slots if they share the same SE in any stage of the network. The last approach, the wavelength domain, different wavelengths are used for routing active connections by ensuring two wavelengths entering an SE to be far apart by routing or using wavelength converters. Whenever the limitation of the network size is reached, the time domain method may be used as a feasible way to trade the maximal bandwidth available to each particular input and output pair for enhanced connectivity. Again, it is useful when future technology let the transmission rate to expand faster than the network size or when the cost of expanding the bandwidth of each connection becomes as "cheap" as the cost of building a network of twice its original size.

The chapter covers the development of crosstalk-free scheduling algorithms for routing in an OMIN. The interest is on how to efficiently schedule messages using the time domain approach in order to avoid crosstalk. In the time domain approach, messages to be sent to the network are distributed into several groups for routing at different time slots. There are

two phases involved in the algorithm development; permutation decomposition phase to find messages with conflicting path (shares an SE) in the network and mapping these conflicts into some array before it can be selected for scheduling and scheduling algorithm phase to schedule messages according to some order for routing in the OMIN.

We begin this chapter with a brief introduction of MIN and OMIN, particularly the Optical Omega Network (OON) topology that will be used to represent OMIN, and the problem associated with routing permutations in OON in general and crosstalk as the main prominent factor that effect the performance of OON and OMIN at large. Next, we will also discuss commonly used approaches to solve crosstalk in OON including the strength and weaknesses of each approach. At the end of this chapter, we present recent research in crosstalk-free scheduling and their development based on the time domain approach.

2. Optical Multistage Interconnection Network

Multistage Interconnection Network (MIN) are a class of dynamic interconnection network that connects input devices to output devices through a number of switch stages, each stage consists of a set of SEs arranged in cascaded order, where each switch is a crossbar network (Feng, 1981). Frequently proposed as interconnection schemes in multiprocessor systems or in high bandwidth network switches, MIN has assumed importance in recent times, because of their cost-effectiveness. While crossbar networks have the advantage of establishing connections between every input port to any free output port, it requires N^2 switches to construct the network where N is the network size. MIN requires only $N(\log_2 N)/2$ switches for the same N (Dally, *et al.*, 2004 and Abdullah, *et al.*, 2006).

Depending on the interconnection scheme employed between two adjacent stages and the number of stages, various MINs have been proposed. MIN can be one-sided, where both inputs and outputs are on the same side, or two-sided, which usually have an input side and output side on opposite sides of the network. The two-sided MIN are generally divided into three classes, called blocking, rearrangeable and nonblocking network. In blocking networks, simultaneous connections of more than one input and output pair may result in link contention. Examples of blocking MIN are Baseline, Cube and Omega networks. Rearrangeable networks are a class of MIN where all possible connections can be performed between inputs and outputs by rearranging existing connections so that a connection path for a new input/output pair can always be established. The Benes network is an example of rearrangeable networks. The non-blocking class of MIN is a network that can handle all possible connections without blocking. The Clos network is an example of this class of MIN.

As optical technology advances, there are considerable interests in using optical technology for implementing interconnection networks and switches. As far as speed is concerned, with the introduction of optical switching, it is most feasible to apply MIN in the architecture for building electro-optical switches with a capacity at the rate of terabits per second. An OMIN can be implemented with either free-space optics or guided wave technology (Yang, *et al.*, 2000). It involve the switching of optical signals, rather than electronic signals as in conventional electronic systems. A hybrid OMIN can be built from electro-optic SEs such as common Lithium Niobate (LiNbO_3) directional coupler with two inputs and two outputs (Yang, *et al.*, 2000 and Lu, *et al.*, 2003). OMIN has been an attractive solution that offers a combination of high bandwidth, low error probability, and large transmission capacity in the design of high-speed communication networks and switches (Lu, *et al.*, 2003).

3. Optical Omega Network

An Optical Omega Network (OON) topology has altogether N inputs, N outputs and n stages where $n = \log_2 N$. Each stage has $N/2$ SEs with each SE has two inputs and two outputs connected in a certain pattern (Wu, *et al.*, 1980; Feng, 1981 and Dally, *et al.*, 2004). The inter-stage connection pattern in an Omega network is of shuffle-exchange connection pattern (Wu, *et al.*, 1981). To connect the source address to the destination address, the address is shifted one bit to the left circularly in each connection such as source to the first stage, one stage to the next stage. For instance, to connect between each stage in an 8×8 optical Omega network, each connection is shuffle-exchanged as shown in Figure 1(a).

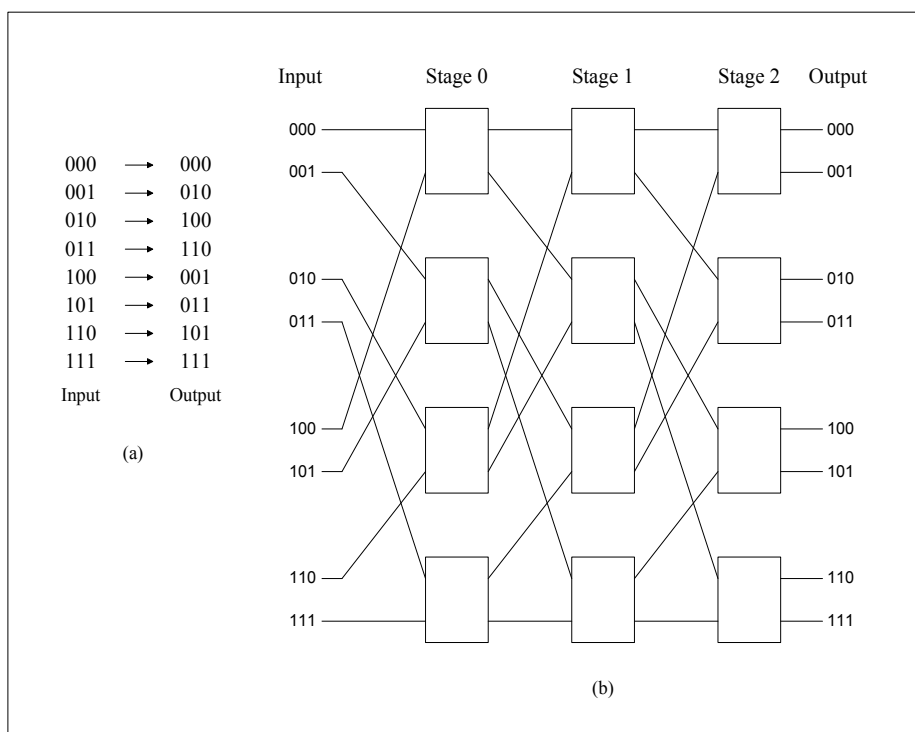


Fig. 1. (a) Shuffle-Exchange Inter-Stage Connection Pattern, and (b) An 8×8 Optical Omega Network

The shuffle-exchange connections have to be considered when scheduling a permutation for routing in the OON. The inter-stage connection pattern determines the routing mechanism in a network. It also limits the number of messages that can be routed simultaneously in a single time slot or pass, since no two signals are allowed to share an SE at any given time or crosstalk will occur. Figure 1(b) illustrates the general layout of the Omega network topology. OON is topologically equivalent to many other topologies such as the Baseline, Butterfly and Cube networks (Wu, *et al.*, 1980 and Feng, 1981). Since many other topologies are equivalent to the Omega network topology, performance results obtained for the Omega network are also applicable to other OMIN topologies (Abdullah, 2005).

Suppose an n -bit binary numbers from 0 to $N - 1$ (where $n = \log_2 N$ and N is the network size) is used to label the addresses of N input or output ports from top to bottom of the OON, the shuffle-exchange interconnection connects output port $s_0s_1s_2 \dots s_{n-1}$ from stage i to the input port $s_1s_2 \dots s_{n-1}s_0$ of stage $i + 1$, $0 \leq i < n - 1$. Every stage of switches in the OON is preceded by the shuffle-exchange interconnection including the N source inputs connected to the switches of the first stage. The switching connections in each SE can be of either straight or cross connection.

To route a message in an OON, the destination tag which is binary equivalent of the destination address, $(d_{n-1}d_{n-2} \dots d_1d_0)$ is used. The i^{th} bit d_i is used to control the routing at the i^{th} stage counted from the right with $0 \leq i \leq n - 1$. If $d_i = 0$, the input is connected to the upper output. Otherwise, if $d_i = 1$, it is connected to the lower output. In other words, message routing can be achieved simply by relaying messages to either the upper switch output link or the lower output link of the SEs according to the destination address. This unique characteristic of the OON are often referred to as self-routing (Chau, *et al.*, 2005 and Chau, *et al.*, 2007).

4. Optical Crosstalk in Optical Omega Network

Although electronic MIN and OMIN have many similarities, there are some fundamental differences between them. An SE can be connected using two types of logic states, namely the straight or cross connection as shown in Figure 2(a). Depending on the amount of voltage at the junction of the two waveguides, optical signals carried on either of the two inputs can be coupled to either of the two outputs. Figure 2(b) shows an illustration of the optical crosstalk occurrence within an SE connected with straight logic state. In the event of optical crosstalk occurrence, a small fraction of the input signal power may be detected at another output disregard of the actual signal injected to the appropriate output port. Consequently, the input signal will be distorted at the output due to loss and crosstalk accumulated along the connection path.

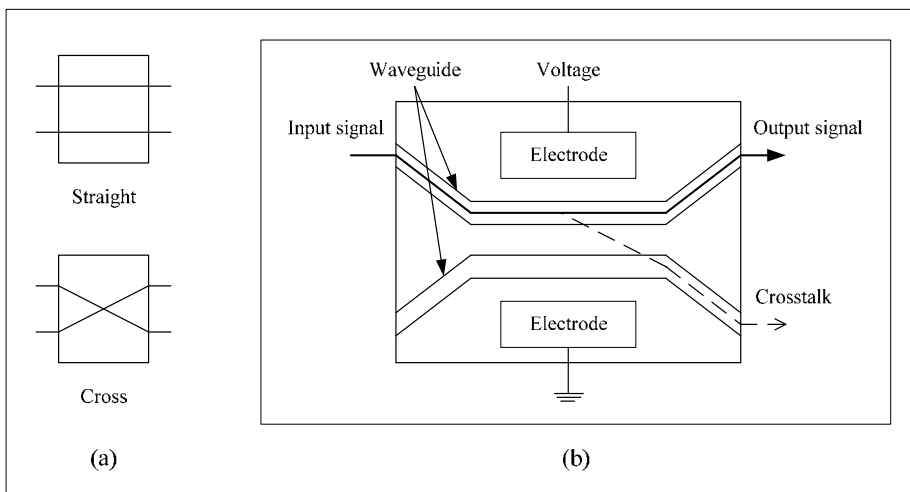


Fig. 2. (a) Straight or Cross Logic State of a 2x2 SE, and (b) Optical Crosstalk Effect in an Electro-Optic SE

Because routing in OON make use of both SE configuration shown in Figure 2(a), optical crosstalk has been the major drawback in achieving the most of network performance when routing permutations simultaneously. Therefore, it is not possible to route more than one message simultaneously, without optical crosstalk, over an SE in OON. Reducing the effect of optical crosstalk has been a challenging issue considering trade-offs between performance and hardware and software complexity. To solve optical crosstalk, many scheduling algorithms have been proposed for routing in OMIN based on a solution called the time domain approach, which divides the N optical inputs into several groups such that crosstalk-free connections can be established. In this chapter, we propose a solution that can further optimize and improve the performance of message scheduling for routing in OON using the time domain approach.

5. Time Domain Approach

In order to avoid crosstalk in OONs, several approaches based on network dilation have been proposed. The three approaches include the the space domain (Qiao, 1996), time domain (Qiao, *et al.*, 1994) and wavelength domain (Lu, *et al.*, 2004) dilation.

Space domain approach duplicates and combines a MIN to avoid crosstalk within individual SE. Using this approach, an $N \times N$ network is dilated into a network that is essentially equivalent to a $2N \times 2N$ network, but only half of the input and output ports used for routing. Based on this approach, a dilated Benes network has been proposed (Padmanabhan, *et al.*, 1987), where up to N connections can be established without sharing any SE. However, it uses more than double of the number of switches required for the same connectivity.

The wavelength domain (Vaez, *et al.*, 1998) implements an approach where the crosstalk between two signals passing through the same SE is suppressed. It is done by ensuring two wavelengths to be far apart by routing (Sharony, *et al.*, 1993) or by using wavelength converters (Qin, *et al.*, 2001). Thus, limits the efficiency of bandwidth utilization and/or increases cost and complexity (Lu, *et al.*, 2003 and Yang, *et al.*, 2004).

The time domain approach avoids optical crosstalk via network partitioning across the time dimension. The approach solves the crosstalk problem by allowing only one input and output link to be active at a time within each SE. A set of permutation connection is partitioned into several scheduling groups called semi-permutations in such a way that the entries within each group are crosstalk-free (Yang, *et al.*, 2000 and Lu, *et al.*, 2003). Each group is routed to its corresponding destination independent of the other groups in a different time slot. The main advantage of the time domain approach is that it does not involve additional cost of having more SEs as well as the cost for wavelength conversion as does the space and wavelength domain approaches.

5.1 Time Domain Approach Framework

Because routing messages simultaneously across the OON causes crosstalk, it is important to make sure a permutation is decomposed and scheduled in crosstalk-free order for routing messages. The general framework of the time domain approach consists of two phases including permutation decomposition in the first stage and message scheduling in the second as illustrated in Figure 3.

In permutation decomposition phase, the primary goal is to identify conflicts among all messages in the network. Permutation decomposition involves source and destination address generations, building the conflict matrix in order to discover message conflict for the permutation. In the message scheduling phase, based on the array of conflict generated, the messages are sorted and selected for scheduling into crosstalk-free groups called passes for routing to the intended destination, one group per time slot. Typically, messages are selected for scheduling according to some order unique to a particular scheduling algorithm. The output of each scheduling algorithm is the execution time for scheduling permutations and number of passes to route a permutation. Both the execution time and the number of passes are used to measure the performance of time domain scheduling algorithms.

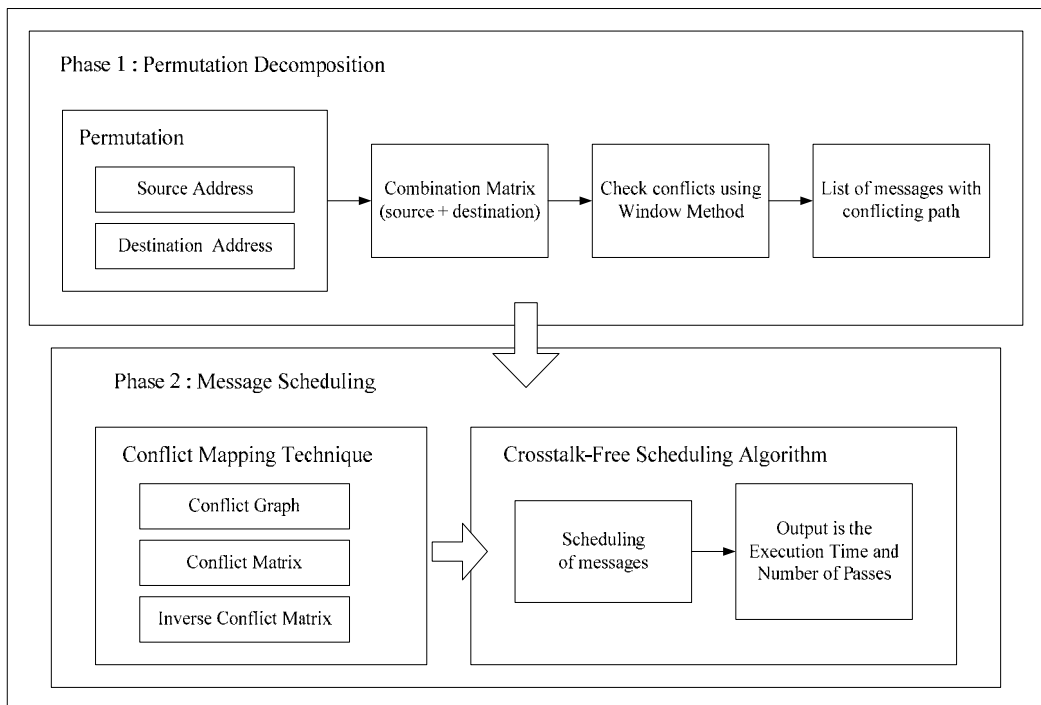


Fig. 3. Time Domain Approach Framework

5.2 Permutation Generation

Before a permutation can be divided into its crosstalk-free subsets, the source and destination addresses of the permutation are randomly generated. A permutation refers to a one-to-one mapping from a source node to a destination node in the OON. The network size, N is defined as a base-2 integer, 2^n where $n = \log_2 N$, ranging from the smallest size 4 to the largest size 1024 that represents the number of source nodes and destination nodes of the network. In each permutation generation, each source is connected to a random destination via unique one-to-one mapping. For example, when $N = 16$ it specifies that there are 16 unique source nodes mapped to 16 unique random destination nodes. This arbitrary source and destination address of the permutation generated is then combined in its binary form to build a combination matrix.

5.3 The Combination Matrix

To build the combination matrix, each source and destination address pair of a permutation will be represented separately in their n -digit binary structure, where $n = \log_2 N$. Then, both source and destination addresses from the pair are combined; with the source address put on the left followed by the destination address on the right. For example, combining the address of source '0' and destination '5' will result in binary 000101 with the first three digits from the left represent the source address while the last three digits represent the destination address. The combination matrix is useful when identifying conflicts in OON.

5.4 Conflict Discovery

5.4.1 Window Method

Based on the combination matrix, conflict patterns are checked using some pattern-checking method. Window Method (WM) is one example of a pattern-checking method where the combination matrix is divided into windows of the same size; and if any two messages have the same bit pattern between them in any of the windows, then it implies conflict between the message pair. Thus, the two messages must not be scheduled in the same group. In WM, an optical window of size $m - 1$ where $m = \log_2 N$ and N is the size of the optical network is applied to the columns of the combination matrix, from left to right excluding the first and the last columns. For each optical window, the bit pattern for each message is compared for similarity with the bit pattern of the rest of the other $N - 1$ message(s) sequentially starting from message 0 to $N - 1$. If the bit pattern is the same, it will be mapped into the array of conflict pattern.

5.4.2 Improved Window Method

Sequentially comparing bit patterns among all messages in each optical window was found to be time consuming especially when the network size, N is large and the number of optical window increases. To reduce the execution time contributed by the WM, the Improved WM (IWM) was proposed that eliminates checking for conflicts in the first optical window (Abdullah, 2005). This is because the first optical window has the same conflict pattern where the first $N/2$ inputs in sequence uses the same SEs as the second half of the other $N/2$ inputs. Therefore, inputs 0 to $(N/2 - 1)$ will have conflict with inputs $N/2$ to $(N - 1)$, which is always true for any size of network, N . The execution time is reduced approximately by $1/S$ as compared to the standard WM where S is the number of stages (Abdullah, 2005; Abdullah, *et al.*, 2005). In addition, the parallel IWM was developed on shared memory multiprocessors and the results shown drastic improvement in execution time (Othman, *et al.*, 2008).

5.4.3 Bitwise Window Method

Based on comparative analysis performed in (Abed, *et al.*, 2007), it was concluded that the time spent for identifying conflicts is very high compared to routing the messages. Table 1 shows the execution time of WM compared to the time executed for scheduling and routing.

Network Size	Routing + WM	WM	Routing
8	0.032	0.031	0.001
16	0.078	0.063	0.015
32	0.219	0.204	0.015
64	1.031	1.000	0.031
128	4.797	4.656	0.141
256	25.329	24.187	1.142
512	110.750	108.906	1.844
1024	519.922	499.046	20.876

Table 1. WM Execution Time (ms) (Abed, et al., 2007)

Based on the analysis, (Abed, 2007) then proposed the Bitwise Window Method (BWM) that significantly reduces the execution time of the WM. In the new BWM, each $(n - 1)$ -bit binary optical window of the standard WM where $n = \log_2 N$ and N is the network size, be transformed into its equivalent decimal representation using bitwise operations. As a result, the number of columns used to compare each message for similar bit pattern is reduced to n , instead of $(n^2 - n)$ for an $N \times N$ Omega network. Figure 4 illustrates the transformation steps for each optical window in BWM implementation.

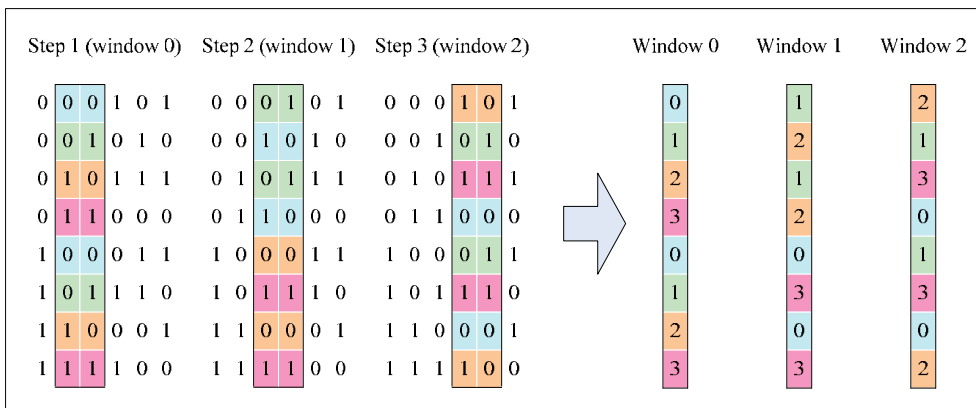


Fig. 4. Optical Window Transformation in BWM

5.5 Conflict Mapping

5.5.1 Conflict Graph

The conflict graph is one of the foremost technique proposed to map conflicts discovered using WM. By definition, the conflict graph of an N -permutation π (where N is the network size) is the graph $G(V, E)$ where V is a set of vertices $\{v_0 v_1 v_2 \dots v_{N-1}\}$ and E is a set of edges $\{(v_0, v_1), \dots, (v_i, v_j), \dots, (v_{N-2}, v_{N-1})\}$ (Shen, et al., 2001). Each vertex, $V = \{v_0 v_1 \dots v_{N-1}\}$ in the conflict graph represents a source node's address i.e. v_0 for source 000, v_1 for source 001 and so on for all nodes in the network. In the conflict graph, any two vertices v_i and v_j are connected by an edge, E to indicate conflict, if and only if they share a common SE at certain stage of the network.

5.5.2 Conflict Matrix

Another conflict-mapping technique that can be used to map conflict pattern identified using WM is called the conflict matrix, proposed by (Al-Shabi, 2005). The conflict matrix is defined as a square matrix, M with matrix size of $N \times N$ where N is the network size. Similar to the conflict graph, the conflict matrix can be generated based on the results from the WM, IWM or BWM. However, if there is an edge from some vertex i to some vertex j in the conflict graph, then the element $M_{i,j}$ in the conflict matrix is set to a value 1 to indicate conflict between the intersected messages, otherwise it is set to a value 0.

The conflict matrix is illustrated in Figure 5. Since the message 000 has conflict with messages 010, 100 and 111, elements $M_{000,010}$, $M_{000,100}$ and $M_{000,111}$ are set to the value 1 to indicate conflict in the conflict matrix. The rest of the intersections for message 000 i.e. the intersections between message 000 and messages 001, 011, 101 and 110 are set to 0 value, which means that these messages will not cause crosstalk with the message 000 during routing in the network.

Message	000	001	010	011	100	101	110	111
000	0	0	1	0	1	0	0	1
001	0	0	0	1	1	1	0	0
010	0	0	0	0	0	1	1	0
011	0	0	0	0	0	0	1	1
100	0	0	0	0	0	0	1	0
101	0	0	0	0	0	0	0	1
110	0	0	0	0	0	0	0	0
111	0	0	0	0	0	0	0	0

Fig. 5. The Conflict Matrix

6. Message Scheduling Algorithms

Among the algorithms developed by previous researchers to perform scheduling of the messages into crosstalk-free groups for routing in OON include the standard four Heuristic algorithms; Sequential Increasing, Sequential Decreasing, Degree Ascending and Degree Descending algorithm, Simulated Annealing (SA) algorithm, Genetic Algorithm (GA), Ant Colony Optimization (ACO) algorithm, Remove Last Pass (RLP) algorithm, Zero algorithm, Improved Zero (IZero) algorithm and Bitwise-Based algorithm. To evaluate the performance of the time domain scheduling algorithm, researchers have used two main parameters; the total execution time for scheduling permutations and the total number of passes to route a permutation (Katangur, *et al.*, 2002; Katangur, *et al.*, 2004; Chau, *et al.*, 2005; Abdullah, *et al.*, 2006 and Al-Shabi, *et al.*, 2008). Based on these parameters, we listed a summary of the performance analysis of the algorithms below:

- Among the four Heuristic algorithms, the Degree Descending algorithm gives the best result while the Degree Ascending algorithm gives the worst result in terms of

the number of passes obtained for a permutation (Katangur, *et al.*, 2002; Katangur, *et al.*, 2004 and Al-Shabi, *et al.*, 2008). In terms of the execution time, the Sequential Increase and Sequential Decrease algorithms gives best result compared to Degree Ascend and Degree Descend algorithms (Al-Shabi, *et al.*, 2008, Othman, *et al.*, 2008). It can be summarised that scheduling the messages based on their order of degrees achieved best results in the number of passes but consumes more time to calculate the degree for each message in the network. On the other hand, both Sequential Increase and Sequential Decrease algorithms achieve best in execution time but higher in the number of crosstalk-free passes obtained to route a given permutation.

- The SA algorithm is one of the time domain algorithms that perform best in terms of the number of passes for message routing without crosstalk. It is the second best among all time domain algorithms where the number of passes obtained by the SA algorithm result closely to that of the GA (Katangur, *et al.*, 2002) but slightly higher than the RLP algorithm (Chau, *et al.*, 2005). However, as much as the reduction in the execution time compared to the GA as demonstrated in (Katangur, *et al.*, 2002), the SA algorithm is also considered as one of the algorithms that consume longer time to compute a solution (Al-Shabi, *et al.*, 2008).
- Due to the complex procedures involved in the algorithm, the GA takes a very long time to calculate the number of passes especially for large network sizes and therefore considered less appropriate for message routing particularly in OON by previous researchers (Katangur, *et al.*, 2002; Chau, *et al.*, 2005 and Al-Shabi, *et al.*, 2008).
- The ACO algorithm successfully reduces the number of passes when limited crosstalk is allowed in the network. Unfortunately, when zero crosstalk is concerned, the number of passes is higher than the rest of the other algorithms (Katangur, *et al.*, 2004).
- RLP algorithm gives the best result when the number of passes is considered (Chau, *et al.*, 2005). However, the algorithm consumes longer execution time than other time domain algorithms. Apart from the algorithm's dependency to other algorithm to obtain the initial solution, the RLP algorithm also involves complex procedures when making scheduling decisions (Shahida, *et al.*, 2008d, Shahida, 2009).
- Based on the experimental results shown in (Al-Shabi, 2005; Al-Shabi, *et al.*, 2005 and Al-Shabi, *et al.*, 2008), Zero algorithms perform best in terms of the execution time for scheduling the permutations and result very closely to the Degree Descending algorithm in terms of the number of passes generated to route a permutation. However, it was found in (Abed, 2007) that crosstalk may still occur between messages scheduled in the same pass of a particular time slot using the original Zero algorithm.

- Improved the weaknesses found in the original Zero algorithm, IZero algorithm performed slightly higher in terms of its execution time for scheduling permutations compared to the original algorithm while maintaining the same result in the total number of passes to route a permutation (Abed, *et al.*, 2008; Shahida, *et al.*, 2008b; Shahida, *et al.*, 2008c).
- All Bitwise-Based algorithms have shown to successfully reduce the execution time of the original algorithm (Abed, 2007; Abed, *et al.*, 2007 and Abed, *et al.*, 2008), except that the number of passes obtained by the new algorithm is the same as before it is implemented using the Bitwise approach. Among all Zero-based algorithms, none of the previous researchers improved the performance of the algorithm in terms of the number of passes to route a permutation. Furthermore, since the Bitwise-Based algorithms used the same framework and procedures from the original algorithm, the BIZero algorithm is also not crosstalk-free.

7. Fast Zero Algorithm

Fast Zero (FastZ) algorithm (Shahida, *et al.*, 2008a; Shahida, *et al.*, 2008b and Shahida, *et al.*, 2008c), is among the latest time domain scheduling algorithm proposed to optimally minimize the execution time of Zero-based algorithms. Although various developments have been made towards the original Zero algorithm including the IZero and Bitwise IZero algorithms to refine the algorithm in different aspects, none of these developments affects the steps involved in the algorithm itself to improve the execution time of the algorithm. Through analysis, Zero-based algorithms involve a lot of iterative procedures in the algorithm's function for the summation of rows or columns, finding the intersections to refine the conflict matrix, multiple conflict-checking to ensure no conflicts when adding successful intersections to a group, reducing the matrix and calculating new summation for the reduced matrix.

FastZ algorithm consist of three algorithms namely Fast ZeroX (FastZ_X), Fast ZeroY (FastZ_Y) and Fast ZeroXY (FastZ_XY) algorithms. FastZ algorithm is also combined with the RLP algorithm to reduce the total number of passes obtained for a particular permutation and will be described in section 7.4.

7.1 Permutation Decomposition

Based on the time domain approach, scheduling depends very much on the pattern of conflicts among the messages. Conflict-mapping technique i.e. the conflict graph provides an easy access to refer conflicts between messages in the network before scheduling the messages. For instance, to determine if a message is routable in a particular group is as simple as referring to the conflict graph and check whether there is an edge connecting the message to the messages that is already scheduled in the same group. An efficient conflict-mapping technique affects the total execution time of an algorithm. Therefore, we proposed another technique called symmetric Conflict Matrix (sCM) to map conflicts in the network discovered using BWM. The new sCM is implemented in FastZ algorithm replacing the conflict matrix.

7.2 Symmetric Conflict Matrix

The sCM is defined as a square matrix, $S_{i,j}$ with matrix size of $N \times N$ where N is the network size. The sCM has the same data structure as the conflict matrix to indicate conflict or no conflict between a message pair, only that the entries in the sCM are symmetric to that of the conflict matrix with respect to the matrix's main diagonal of all 0's value. In other words, if an entry $M_{i,j} = 1$ (where $i = 0$ and $j = 4$) in the conflict matrix, see Figure 5, then entries $S_{i,j} = S_{j,i} = 1$ in the sCM as shown in Figure 6.

A great advantage using sCM compared to the conflict matrix is that the sCM provides a complete mapping of all possible conflicts in the network similar to the conflict graph. Scheduling algorithm can be simplified and more straightforward by comparing the intersection value of intersected messages to determine routability thus eliminates time-consuming procedures associated with multiple summation of the conflict matrix, finding intersections, and reducing the conflict matrix in Zero-based algorithms.

Message	000	001	010	011	100	101	110	111
000	0	0	1	0	1	0	0	1
001	0	0	0	1	1	1	0	0
010	1	0	0	0	0	1	1	0
011	0	1	0	0	0	0	1	1
100	1	1	0	0	0	0	1	0
101	0	1	1	0	0	0	0	1
110	0	0	1	1	1	0	0	0
111	1	0	0	1	0	1	0	0

Fig. 6. The Symmetric Conflict Matrix, sCM

7.3 Message Scheduling

The basis of Zero-based algorithms lies in the Unique Case and Refine functions executed after obtaining the row or column summations of the conflict matrix. However, these procedures are time-consuming, thus contribute to longer execution time to schedule messages for routing in the network. Using sCM, scheduling of messages is more straightforward simply by checking through the intersections between the entries in the sCM, without prior row or column summation of the conflict matrix.

For instance, to check if message 100 is routable in a group already scheduled with messages 000 and 101 based on the sCM in Figure 6, it is sufficient to make sure that $M_{100,000} = M_{100,101} = 0$. In this case, message 100 is not routable in the group since $M_{100,000} = 1$. Therefore, both the Unique Case and Refine functions are no longer necessary and can be removed in FastZ algorithm. Furthermore, the sCM need not be reduced to smaller matrix size since the sCM provides all the information needed for scheduling. Figure 7 shows the general flowchart of the FastZ algorithm.

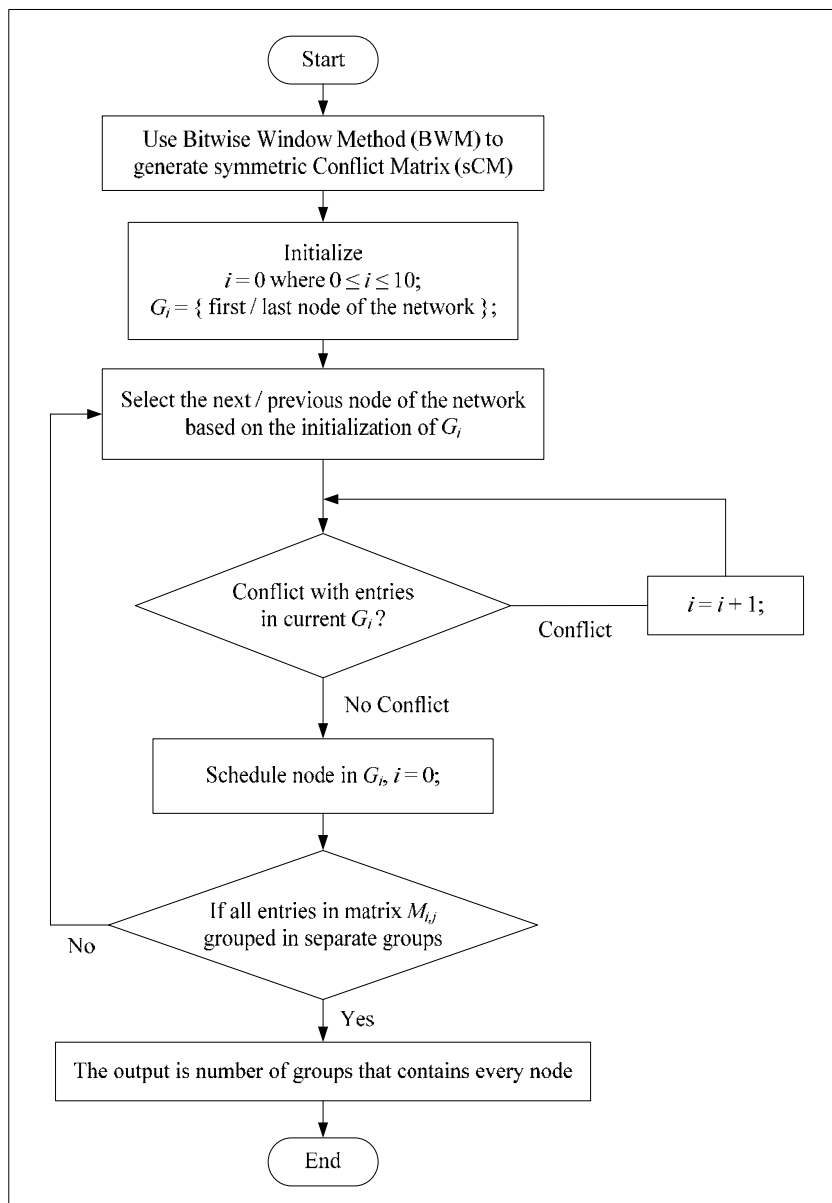


Fig. 7. General FastZ Algorithm Flowchart

FastZ algorithm consists of three algorithms; FastZ_X, FastZ_Y and FastZ_XY algorithms. The difference between these algorithms is in the selection of which message to be added to the first scheduling group during group initialization. For initialization, FastZ_X algorithm selects the first message in the network to the first group. The rest of the messages are selected for scheduling ascendingly, starting from the second message based on the message's source address. On the contrary, FastZ_Y algorithm chooses the last message, N in the network for initialization. FastZ_Y algorithm schedules the other messages

descendingly based on their addresses until all messages are scheduled into crosstalk-free groups. To schedule a permutation in the FastZ_{XY} algorithm, messages are scheduled using both FastZ_X and FastZ_Y algorithms sequentially. After both results are obtained, FastZ_{XY} algorithm compares both results and chooses whichever result that has the lowest total number of passes as its final result.

Apart from the algorithm's simplicity in routability and scheduling, FastZ algorithm is also crosstalk-free and therefore solved the weaknesses in Zero-based algorithms. Although IZero algorithm solved optical crosstalk in Zero algorithm, our analysis found that for some permutation involving the IZero algorithm's Unique Case function, crosstalk may still occur between messages scheduled in the same group. Therefore, the IZero algorithms and its predecessors are not crosstalk-free and only applicable for message scheduling in OMIN architecture where limited crosstalk is allowed.

7.4 Fast Zero Algorithm with RLP

We introduced the latest development of Zero-based algorithms; the FastZ algorithm with RLP or FastRLP in short. The algorithm is designed by integrating FastZ algorithm with the RLP algorithm proposed by (Xiao, 2004), with attempt to minimize the total number of passes for routing a given permutation. Based on analysis performed in (Chau, *et al.*, 2005), the RLP algorithm has shown to successfully schedule a permutation with less number of passes, than the Maximal Conflict Number (MCN) required for the permutation.

In FastRLP algorithm, messages are scheduled using FastZ algorithm to obtain initial scheduling groups called the initial solution. Depending on which algorithm used to obtain the initial solution, FastRLP algorithm can be divided into two algorithms. If the FastZ_X algorithm is used to obtain the initial solution, it is referred as the FastXRLP algorithm. Otherwise, if the FastZ_Y algorithm is used, then it is referred as the FastYRLP algorithm. After the initial solution is derived, RLP algorithm is used to remove the last pass by relaying messages to the unused paths of the previous passes. The RLP algorithm is executed if and only if the number of initial scheduling groups generated is more than two. This is because there is not a permutation that can be scheduled for routing in less than two groups without crosstalk in an OON regardless of the network size.

8. Numerical Results and Discussions

This section presents the experimental results obtained from the proposed algorithms. Each of the algorithms is simulated 10,000 times for each execution on different network sizes, N and presented in average for comparative analysis. Performance evaluation will be based on two types of parameters; the execution time and number of passes.

The execution time is defined as the time elapsed between the beginning and the end of its execution on a sequential computer measured in milliseconds (*ms*). The execution time calculated for each algorithm includes the time taken to generate random permutation addresses, execute window transformation, check for conflicts between the messages, mapping conflicts into the sCM and finally schedule the messages into the crosstalk-free groups for each permutation set. Minimum execution time reflects better performance of an algorithm.

Based on the time domain approach, transferring messages from source nodes to the intended destination nodes without crosstalk involves dividing the messages into

independent crosstalk-free groups called passes. These passes can be routed in one group at any given time. Less number of passes implies that more messages can be scheduled in the same pass for routing. Therefore, the number of passes obtained for an algorithm reflects the efficiency of the algorithm in terms of better scheduling strategy employed.

We divided and clustered the results of each algorithm into three categories; ZeroX, ZeroY and ZeroXY since they differ between each other in scheduling. Figure 8 and Figure 9 present the results for ZeroX algorithm, Figure 10 and Figure 11 present the result for ZeroY algorithm, while Figure 12 and Figure 13 present the result for ZeroXY algorithm in terms of the execution time and number of passes.

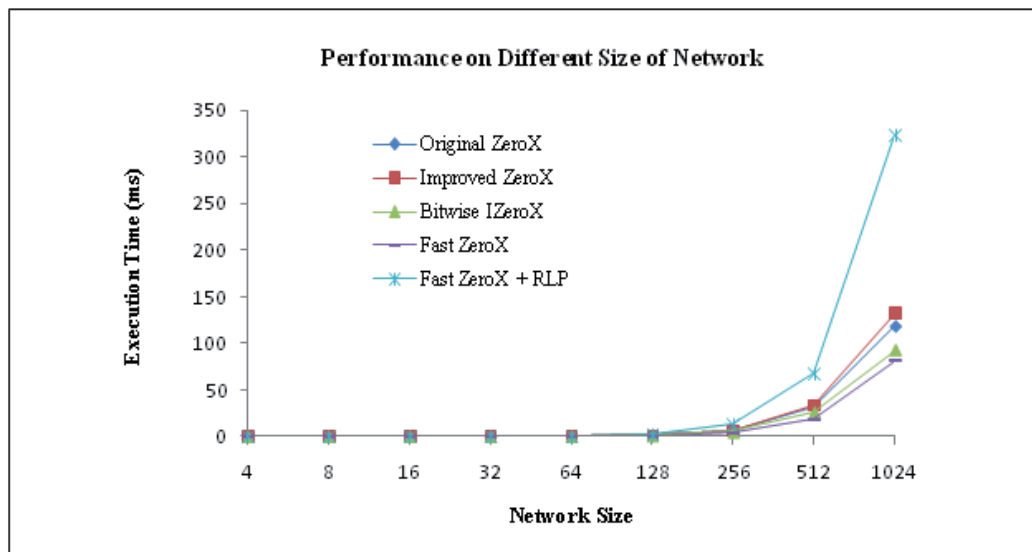


Fig. 8. Execution Time vs. Network Size of the ZeroX Algorithm

When the execution time is considered, it is evident that FastZ algorithm performs the best with the lowest average execution time consistently for all N , compared to all Zero-based algorithms (refer Figure 8, Figure 10 and Figure 12). Integrating FastZ and RLP algorithm result in higher execution time especially in large network, $N = 1024$ nodes. This is contributed by the RLP function embedded in the algorithm in order to reduce the number of passes.

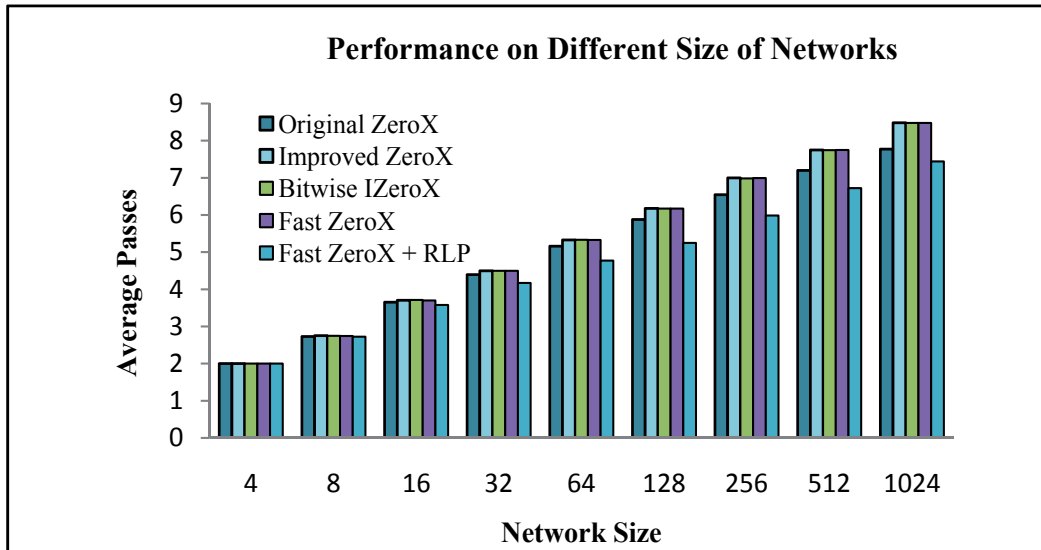


Fig. 9. Number of Passes vs. Network Sizes of the ZeroX Algorithm

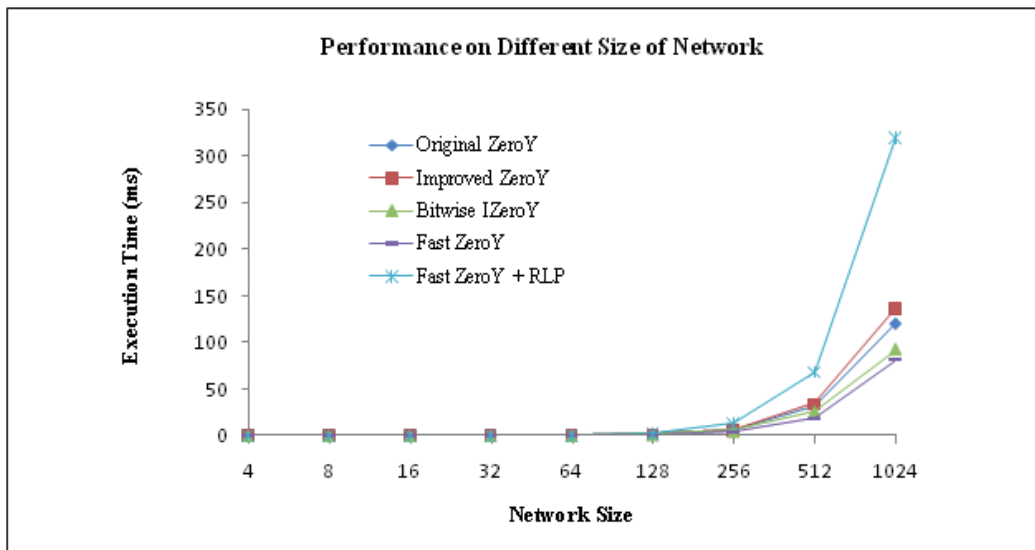


Fig. 10. Execution Time vs. Network Sizes of the ZeroY Algorithm

In terms of the number of passes generated for permutation routing, FastZ algorithm results closely to the IZero and BIZero algorithms. The increase in the number of passes of the FastZ algorithm compared to the original Zero algorithm was as expected. In terms of the elimination of crosstalk, the results in the number of passes are almost equal to that of the FastZ algorithm. This is mainly because the number of passes generated by FastZ algorithm may be the same as IZero and BIZero algorithms except which message(s) scheduled in each pass may be different when using FastZ algorithm.

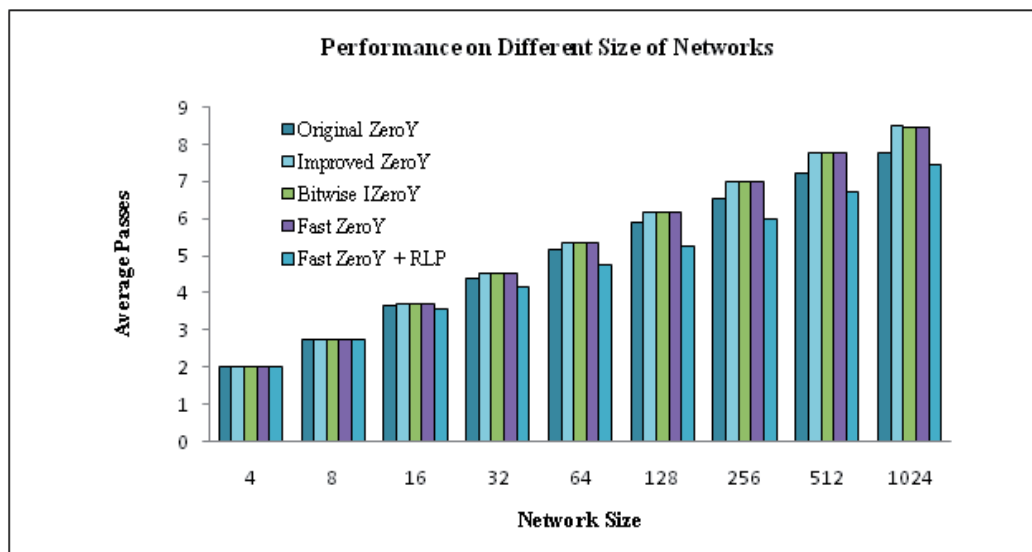


Fig. 11. Average Number of Passes vs. Network Sizes of the ZeroY Algorithm

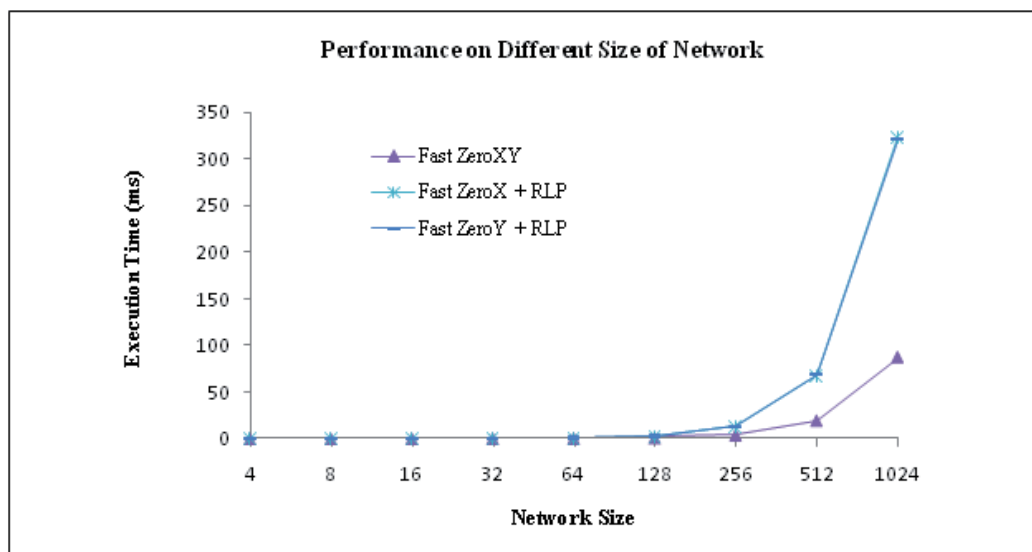


Fig. 12. Execution Time vs. Network Sizes of the ZeroXY Algorithm

Integrating the FastZ algorithm with RLP algorithm known as FastRLP algorithm has shown to successfully reduce the number of passes generated for a permutation starting from $N = 16$ onward (refer to Figure 9 and Figure 11). The results are not as significant for network size with small $N (<16)$ because in the time domain approach no more than one input/output link can be active at any given time. Therefore, the minimum number of passes for these network ranges is limited to two passes for a permutation where in this case the RLP algorithm will not be executed at all.

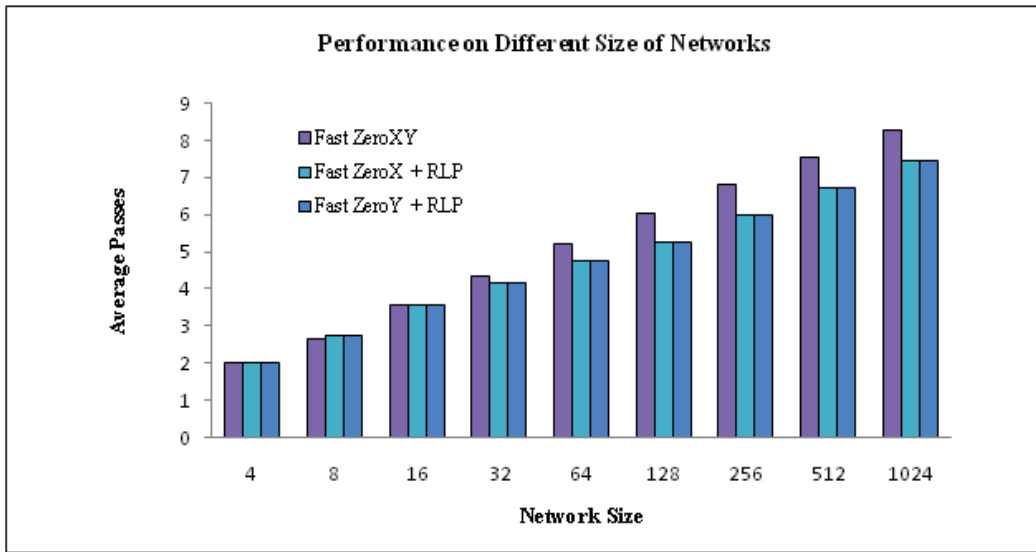


Fig. 13. Average Number of Passes vs. Network Sizes of the ZeroXY algorithm

When compared to FastZ_XY algorithm, FastRLP algorithm reduced the number of passes only when $N > 16$ as shown in Figure 13. This is because in FastZ_XY algorithm, it compares and chooses the minimum number of passes generated between FastZ_X and FastZ_Y algorithms in each execution. It was also proven in (Shahida, *et al.*, 2008a) that FastZ_XY algorithm has less number of passes compared to individual FastZ_X and FastZ_Y algorithm.

9. Conclusion and Future Works

Throughout this chapter, we have presented the development of crosstalk-free scheduling algorithms for routing in OON, a type of OMIN topology. We also presented two latest developments in crosstalk-free scheduling algorithms; FastZ and FastRLP algorithms. Using the proposed sCM to map conflicts in the network, both algorithms have proven to improve scheduling in terms of the execution time as well as the number of passes. Through simulation technique, FastZ algorithm reduced the execution time by 32% compared to previous Zero, IZero and BIZero algorithms without much difference in the number of passes generated. On the other hand, FastRLP algorithm reduced the number of passes by 11% in average compared to all Zero-based algorithms despite significant increase shown in the algorithm's execution time.

In future, we would suggest that the execution time of FastRLP algorithms be reduced using bitwise operations. The idea of sCM can also be applied to any other time domain algorithms to map conflicts identified between the messages in the network. Next, FastZ and FastRLP algorithms can be implemented in parallel to achieve exponential improvement in the algorithm's execution time. Finally, it is worth to consider the design to support for multicast communication in the network. In this case, the multilayer architecture can be incorporated with the single layer design of the OON topology.

10. References

- Abed, F. (2007). *Bitwise-Based Routing Algorithms in Optical Multistage Interconnection Networks*, Master Thesis, Universiti Putra Malaysia.
- Abed, F. & Othman, M. (2007). Efficient Window Method in Optical Multistage Interconnection Networks. *Proceedings of the IEEE International Conference on Telecommunications and Malaysia International Conference on Communications*, pp. 181-185.
- Abed, F. & Othman, M. (2008). Fast Method to Find Conflicts in Optical Multistage Interconnection Networks. *International Journal of The Computer, The Internet and Management*, Vol. 16, No. 1, pp. 18-25.
- Abdullah, M. (2005). *Efficient Sequential and Parallel Routing Algorithms in Optical Multistage Interconnection Networks*, Master Thesis, Universiti Putra Malaysia.
- Abdullah, M.; Othman, M. & Johari, R. (2005). Efficient Parallel Routing Algorithms in Optical Multistage Interconnection Network, *Proceeding of IEEE International Conference on Communication Networks*, pp. 505-509.
- Abdullah, M.; Othman, M. & Johari, R. (2006). An Efficient Approach for Message Routing in Optical Omega Network. *International Journal of The Computer, The Internet and Management*, Vol. 14, No. 1, pp. 50-60.
- Al-Shabi, M. A. (2005). *Zero Algorithms for Avoiding Crosstalk in Optical Multistage Interconnection Network*. PhD Thesis, Universiti Putra Malaysia.
- Al-Shabi, M. A. and Othman, M. (2008). A New Algorithm for Routing and Scheduling in Optical Omega Network. *International Journal of The Computer, The Internet and Management*, Vol. 16, No. 1, pp. 26-31.
- Chao, H. J. & Liu, B. (2007). *High Performance Switches and Routers*. Wiley-IEEE Press.
- Chau, S. C.; Xiao, T. & Fu, A. W. C. (2005). Routing and Scheduling for a Novel Optical Multistage Interconnection Networks. *Lecture Notes in Computer Science*, Vol. 3648, pp. 984-993.
- Dally, W. J. & Towles, B. (2004). *Principles and Practices of Interconnection Networks*. Morgan Kaufmann Publishers, San Francisco.
- Feng, T. Y. (1981). A Survey of Interconnection Networks. *Journal of Computer*, Vol. 14, pp. 12-27.
- Katangur, A. K. (2001). *Message Routing and Scheduling in Optical Multistage Networks Using Simulated Annealing*, Master Thesis, Georgia State University.
- Katangur, A. K.; Pan, Y. & Fraser, M. D. (2002). Message Routing and Scheduling in Optical Multistage Networks Using Simulated Annealing. *Proceedings of the International Parallel and Distributed Processing Symposium*, pp. 201-208.
- Katangur, A. K.; Akkaladevi, S.; Pan, Y. & Fraser, M. D. (2004). Applying Ant Colony Optimization to Routing Optical Multistage Interconnection Networks with Limited Crosstalk. *Proceedings of the 18th International Parallel and Distributed Processing Symposium*, pp. 163-170.
- Lu, E. & Zheng, S. Q. (2003). High-Speed Crosstalk-Free Routing for Optical Multistage Interconnection Networks. *Proceedings of the 12th International Conference on Computer Communications and Networks*, pp. 249-254.
- Lu, E. & Zheng, S. Q. (2004). Parallel Routing and Wavelength Assignment for Optical Multistage Interconnection Networks. *Proceeding of the International Conference on Parallel Processing*, pp. 214-221.

- Othman, M. & Abed, F. (2008). Fast Four Heuristic Routing Algorithms in Optical Multistage Interconnection Switch Networks. *Research Journal of Information and Communication Technology*, Vol. 2, No. 1, pp. 40-48.
- Othman, M.; Abdullah, M. & Johari, R. (2008). Parallel Optical Window Algorithm Applied to Optical Multistage Interconnection Switch Networks. *MathDigest*, Vol. 1, No. 2, pp. 36-39.
- Padmanabhan, K. & Netravali, A. N. (1987). Dilated Networks for Photonic Switching. *IEEE Transactions on Communications*, Vol. 35, No. 12, pp. 1357-1365.
- Qiao, C.; Melhem, R.; Chiarulli, D. M. & Levitan, S. P. (1994). A Time Domain Approach for Avoiding Crosstalk in Optical Blocking Multistage Interconnection Networks. *Journal of Lightwave Technology*, Vol. 12, No. 10, pp. 1854-1862.
- Qiao, C. (1996). Analysis of Space-Time Tradeoffs in Photonic Switching Networks. *Proceedings of the IEEE INFOCOM*, pp. 822-829.
- Qin, X. & Yang, Y. (2001). Permutation Capacity of WDM Switching Networks with Limited-Range Wavelength Conversion. *Proceedings of IEEE International Conference on Parallel Processing Workshops on Optical Networks*, pp. 271-276.
- Sharony, J.; Cheung, K. W. & Stern, T. E. (1993). The Wavelength Dilation Concept in Lightwave Networks - Implementation and System Considerations. *Journal of Lightwave Technology*, Vol. 11, No. 5/6, pp. 900-907.
- Shahida, T. D., Othman, M. & Khazani, M. (2008a). A Fast and Efficient Crosstalk-Free Algorithm for Routing in Optical Multistage Interconnection Networks. *Proceeding of the 5th IFIP International Conference on Wireless and Optical Communications Networks*, pp. 1-5.
- Shahida, T. D., Othman, M. & Khazani, M. (2008b). Fast ZeroX Algorithm for Efficient Message Routing in Optical Multistage Interconnection Networks. *Proceedings of the International Conference on Computer and Communication Engineering (ICCCE'08)*, pp. 275-279.
- Shahida, T. D., Othman, M. & Khazani, M. (2008c). Fast ZeroY Algorithm for Efficient Message Routing in Optical Multistage Interconnection Networks. *Proceedings of the 3rd International Symposium on Information Technology 2008 (ITSim'08)*, pp. 2369-2374.
- Shahida, T. D., Othman, M. & Khazani, M. (2008d). Integrating RLP and Fast Zero Algorithm to Improve Routing Performance in Optical Multistage Interconnection Networks. *Proceedings of the International Symposium on High Capacity Optical Networks and Enabling Technologies 2008 (HONET'08)*, pp. 34-38.
- Shahida, T. D., (2009). *Crosstalk-Free Scheduling Algorithms for Routing in Optical Multistage Interconnection Networks*. Master Thesis, Universiti Putra Malaysia.
- Shen, X.; Yang, F. & Pan, Y. (2001). Equivalent Permutation Capabilities Between Time-Division Optical Omega Networks and Non-Optical Extra-Stage Omega Networks. *IEEE/ACM Transactions on Networking*, Vol. 9, No. 4, pp. 518-524.
- Wu, C. L. & Feng, T. Y. (1980). On a Class of Multistage Interconnection Networks. *IEEE Transactions on Computers*, Vol. 29, No. 8, pp. 694-702.
- Wu, C. L. & Feng, T. Y. (1981). The Universality of the Shuffle-Exchange Network. *IEEE Transactions on Computers*, Vol. 30, No. 5, pp. 324-332.
- Xiao, T. (2004). *Message Routing and Scheduling in Optical Multistage Interconnection Networks*. Master Thesis, The University of Guelph.

- Yang, Y.; Wang, J. & Pan, Y. (2000). Permutation Capability of Optical Multistage Interconnection Networks. *Journal of Parallel and Distributed Computing*, Vol. 60, No. 1, pp. 72-91.
- Yang, Y. & Wang, J. (2004). Designing WDM Optical Interconnects with Full Connectivity by Using Limited Wavelength Conversion. *IEEE Transactions on Computers*, Vol. 53, No. 12, pp. 1547-1556.
- Vaez, M. M. & Lea C. T. (1998). Space-Wavelength Tradeoff in the Design of Nonblocking Directional-Coupler-Based Networks Under Crosstalk Constraint. *Journal of Lightwave Technology*, Vol. 8, No. 16, pp. 1373-1379.

Traditional float charges: are they suited to stationary antimony-free lead acid batteries?

T. M. Phuong Nguyen^{1,2}, Guillaume Dillenseger²
Christian Glaize² and Jean Alzieu¹

¹ EDF R&D site des Renardières
77818 Moret sur Loing, France

² Institut d'Electronique du Sud
Université Montpellier II, 34090 Montpellier, France

1. Introduction

The self-discharge phenomenon caused by side reactions such as corrosion, water decomposition and recombination is unavoidable in lead acid batteries. Self-discharge rates depend on several factors such as the state of charge, the temperature, grid alloys, etc. These rates are not equal between negative and positive electrodes and are independent of each other. In lead-acid batteries with antimony, the self-discharge rate of the negative electrode is several times stronger than the self-discharge rate of the positive electrode, depending mainly on the battery age and the antimony content in the alloy of the positive grid.

In order to compensate for the self-discharge of lead-acid batteries, a current whose value exceeds the self-discharge of the negative electrode has to be supplied. This is traditionally achieved by applying a constant voltage whose value is slightly higher than the battery open circuit voltage. This is called "float charge". It has to be kept in mind that the float polarization increases gas evolution rates at both electrodes.

In antimony-free lead-acid batteries, e.g. VRLA batteries, the self-discharge rate of the negative electrode is largely reduced and usually becomes lower than the self-discharge rate of the positive electrode. The question is: are traditional float charges really suited to antimony-free lead-acid batteries? Practical situations on field as well as experimental results say no. Standby VRLA batteries maintained under a constant float voltage to compensate self-discharge encounter the problem of short service life, when our results show that traditional float charge currents are far over what is needed to maintain the VRLA battery state of charge.

In order to reduce overcharge, intermittent charges (open-circuit and periodical charges) have been used instead of float charges and have given positive results in reducing thermal runaway and increasing the battery life span. Nevertheless, corrosion of the positive grid is also high during open-circuit periods of intermittent charges. Indeed, it is revealed in the literature that corrosion is minimum when the positive polarization is between 40 and 80 mV.

In this chapter, taking into account this minimum corrosion, a new method of maintaining the charge of antimony-free lead-acid batteries using low currents and periodic charges is

developed and tested. This is called "Low-current" method. This method is derived from the intermittent charge: open-circuit periods are replaced by constant low current periods whose values are about 5 to 10 times smaller than traditional float current values.

Laboratory experiments are focused on studying rates of self-discharge at open circuit and state of charge evolutions of lead-acid batteries in three different cases: float charge, low-current charge and open circuit. The new low-current method, associated to an improved storage architecture system is now used in several electrical substations and hydraulic power plants at Electricité de France (EDF). This association is intended to provide long life span and high reliability to VRLA batteries.

2. Lead acid batteries in stationary applications

Secondary reactions such as corrosion, water decomposition and oxygen recombination are the main cause of self-discharge of stationary lead-acid batteries. Maintaining the charge of standby batteries is necessary to compensate self-discharge. However, if the maintaining-charge current is too high, it can accelerate these side reactions, which can thus become the cause of several failures of standby batteries. An appreciated method of maintaining the charge for stationary lead acid batteries is a trade-off between their state of charge and state of health.

2.1 Secondary reactions as causes of self-discharge

The self-discharge phenomenon in stationary lead-acid batteries is due to the simultaneous presence of main reactions, i.e. charge and discharge of active materials and unavoidable side reactions such as corrosion, water decomposition and oxygen recombination. At open circuit, the battery voltage does not only correspond to the equilibrium voltage of principal reactions but depends on the mixed voltage of both main and side reactions (Berndt, 1997). Its value is between the equilibrium voltage value of the principal reactions and the one of the secondary reactions. Water electrolysis is one of the principal secondary reactions and its potential difference is 0.7 to 0.75 V lower than the potential difference of the charge-discharge reactions (depending on electrolyte density and temperature). In these conditions, at open circuit, secondary reactions are produced at the expense of principal reactions; the battery is thus discharged or "self-discharged". However, the influence of these secondary reactions is quite weak as the kinetics of oxygen and hydrogen evolutions are very slow. The battery potential difference at open circuit is smaller but very close to the potential difference of principal reactions.

The self-discharge caused by secondary reactions concerns only the positive or the negative electrode. The self-discharge of the negative electrode is mainly related to the evolution of hydrogen and to the reduction of oxygen while the self-discharge of the positive electrode is principally associated to the evolution of oxygen and to the corrosion of positive grids.

2.1.1 Self-discharge reactions at the negative electrode

1. Self-discharge due to hydrogen evolution

H₂ evolution: $2\text{H}_3\text{O}^+ + 2\text{e}^- \rightarrow \text{H}_2 + 2\text{H}_2\text{O}$

Discharge of Pb: $\text{Pb} \rightarrow \text{Pb}^{2+} + 2\text{e}^{-}$

Overall reaction: $\text{Pb} + \text{H}_2\text{SO}_4 \rightarrow \text{H}_2 + \text{PbSO}_4$ Reaction 1

2. Self-discharge due to oxygen reduction

O_2 reduction: $\frac{1}{2}\text{O}_2 + 2\text{H}_3\text{O}^+ + 2\text{e}^{-} \rightarrow 3\text{H}_2\text{O}$

Discharge of Pb: $\text{Pb} \rightarrow \text{Pb}^{2+} + 2\text{e}^{-}$

Overall reaction: $\text{Pb} + \frac{1}{2}\text{O}_2 + \text{H}_2\text{SO}_4 \rightarrow \text{PbSO}_4 + \text{H}_2\text{O}$ Reaction 2

Thus, in the presence of sulfuric acid, Reaction 1 and Reaction 2 cause self-discharge of the negative electrode with lead sulfate PbSO_4 as the final product.

2.1.2 Self-discharge reactions at the positive electrode

1. Self-discharge due to oxygen evolution

O_2 evolution: $3\text{H}_2\text{O} \rightarrow \frac{1}{2}\text{O}_2 + 2\text{H}_3\text{O}^+ + 2\text{e}^{-}$

Discharge of PbO_2 : $\text{PbO}_2 + \text{H}_2\text{SO}_4 + 2\text{H}_3\text{O}^+ + 2\text{e}^{-} \rightarrow \text{PbSO}_4 + 4\text{H}_2\text{O}$

Overall reaction: $\text{PbO}_2 + \text{H}_2\text{SO}_4 \rightarrow \frac{1}{2}\text{O}_2 + \text{PbSO}_4 + \text{H}_2\text{O}$ Reaction 3

2. Self-discharge due to corrosion

When the active material (PbO_2) supplies the O^{2-} ions to neutralize the Pb^{2+} ions:

Grid corrosion: $\text{Pb} \Rightarrow \text{Pb}^{2+} + 2\text{e}^{-}$
 $\text{Pb} + \text{O}^{2-} \Rightarrow \text{PbO} + 2\text{e}^{-}$ Reaction 4

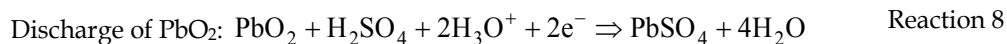
Discharge of PbO_2 : $\text{PbO}_2 + \text{H}_2\text{SO}_4 + 2\text{e}^{-} \Rightarrow \text{PbSO}_4 + \text{O}^{2-} + \text{H}_2\text{O}$ Reaction 5

Combining Reaction 4 and Reaction 5, we have:

$\text{Pb} + \text{PbO}_2 + \text{H}_2\text{SO}_4 \Rightarrow \text{PbO} + \text{PbSO}_4 + \text{H}_2\text{O}$ Reaction 6

Once the PbO_2 active material loses O^{2-} for corrosion, it will pick up O^{2-} ions of H_2O (H_2O content of the electrolyte, i.e. $2\text{H}_3\text{O}^+$ and O^{2-}) to neutralize its charge. Corrosion consumes water.

When the grid is on contact with the electrolyte:



Combining Reaction 7 and Reaction 8, we have:



The formed lead oxide (PbO) in Reaction 6 is converted into lead sulfate according to Reaction 10 as soon as it gets in contact with sulfuric acid:



It is clear that side reactions taking place at negative and positive electrodes are independent of one another and self-discharge rates are not equal between the positive and the negative electrodes.

Self-discharge rates depend on a lot of factors such as temperature, grid alloys and the battery state of charge.

Generally, the approximation holds true that a temperature increase of 10 K (degrees Centigrade) the reaction rate doubles. In electrochemical reactions, this means that equivalent currents are doubled, e.g. a temperature increase of 20 K means a current increase by a factor of 4; a rise in temperature of 30 K corresponds to a factor of 8 (Berndt, 1997).

In lead-acid batteries with antimony grid alloys, the self-discharge rate of the negative electrode is several times stronger than the self-discharge rate of the positive electrode, depending mainly on the antimony content in the alloy of the positive grid and the battery age. Indeed, at charge, the Sb metal, whose equilibrium potential is above that of the negative electrode, dissolves (corrodes) progressively from the positive grid, diffuses through the electrolyte and is precipitated (reduced) at the negative electrode. As this contaminated electrode has a lower hydrogen overvoltage, this results in a greater hydrogen gassing rate (Berndt, 1997). The more aged battery is, the more serious this "antimony affect" is. In antimony-free lead-acid batteries, e.g. VRLA batteries with Pb/Ca grid alloys, the self-discharge of the negative electrode is largely reduced. It should be kept in mind that the electrode with stronger self-discharge rate limits the capacity of the cell.

The self-discharge rate depends also on the battery state of charge as it affects gassing reactions. It is clear that the self-discharge is easier when more active materials are available, or in other words hydrogen H₂ and oxygen O₂ evolution cannot occur at a surface covered by lead sulfate PbSO₄.

2.2 Traditional method of maintaining the charge – float charge: a trade-off between state of charge and state of health

In order to compensate for the self-discharge of lead-acid batteries, a current whose value exceeds the self-discharge of the limit-capacity electrode has to be supplied. Traditionally, a voltage whose value is slightly higher than the battery open circuit voltage is applied to compensate for the difference between mixed potentials and equilibrium potentials of the principal reactions. This is called “float charge”.

In reality, equilibrium potentials depend on a lot of factors such as temperature, electrolyte density, grid alloys (Berndt, 1997, Bode, 1977). Moreover, as a constant voltage is applied between two terminals of a cell, the potential distribution is not properly shared between the negative and the positive electrode (Berndt and Teutsch, 1996, Ruetschi, 2003, Brecht, 1998, Martinez and Novak, 1990, Misra et al., 1994), cf. figure 3. In batteries with cells in a series configuration, the phenomenon of voltage scattering on cells is also present (Hawkins et al., 1995, Berndt, 1997, Misra et al., 1994, Rossinot et al., 2003), cf. figure 4. In addition, it should be kept in mind that the float polarization increases gas evolution rates at both electrodes. It is very difficult or even impossible to choose a value of float voltage, which can take into account all of these phenomena without paying the piper. Convenient practical values for float voltage have been empirically determined. To get rid of the risk of undercharge, batteries in float charge are permanently overcharged.

2.2.1 Bimodal float voltage distribution between the negative and positive electrodes – difference between vented batteries and VRLA batteries

The electrode reactions on float charge are described in detail by Berndt and Teutsch (Berndt and Teutsch, 1996). During float charge, hydrogen evolution, oxygen evolution and grid corrosion proceed certainly as presented in figure 1.

In maintaining the voltage above the open-circuit value, the float current serves to compensate for the electrode discharge caused by these side reactions. When this float current is too low, i.e. the positive potential is slightly below its equilibrium value, or the negative electrode potential is slightly above its equilibrium value, the discharge of the electrodes would occur. Otherwise, the battery is completely charged or overcharged. In general, batteries in float charges are permanently overcharged. The float current, i.e. overcharged current, feeds electrons to secondary reactions.

Berndt and Teutsch presented the model used for float charge describing the single cell behaviors at overcharge in (Berndt and Teutsch, 1996). Under normal float conditions as the battery is already completely charged, the charge and discharge reactions of the active materials do not occur. The equal float current flow through both electrodes can be written, cf. figure 2:

At the positive electrode: $I_{\text{float}} = I_{\text{O}_2 \text{ ev.}} + I_{\text{corr.}}$

At the negative electrode: $I_{\text{float}} = I_{\text{H}_2 \text{ ev.}} + I_{\text{O}_2 \text{ re.}}$

The balance reaction: $I_{\text{float}} = I_{\text{O}_2 \text{ ev.}} + I_{\text{corr.}} = I_{\text{H}_2 \text{ ev.}} + I_{\text{O}_2 \text{ re.}}$

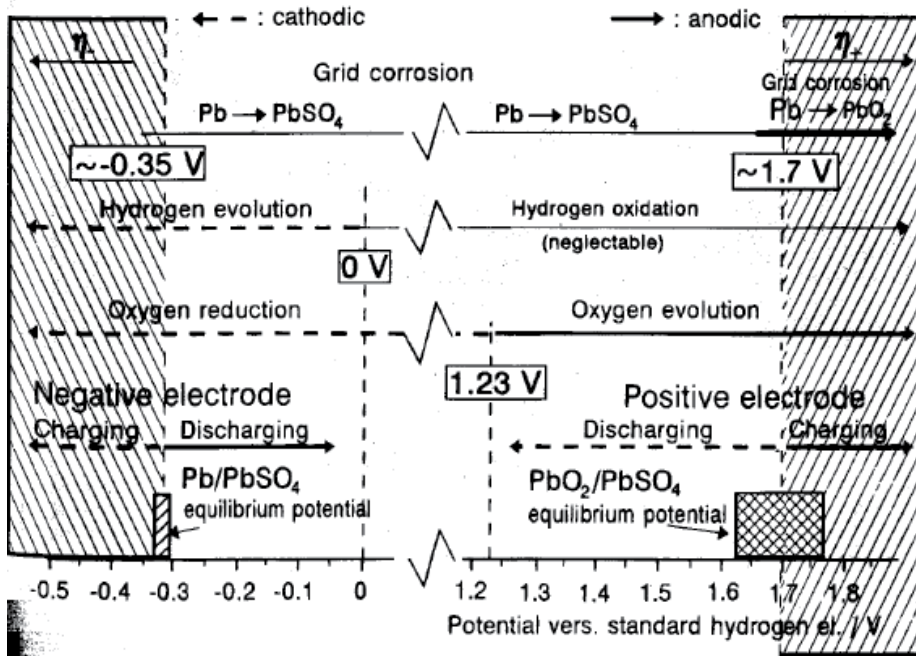


Fig. 1. Reactions that occur in lead acid batteries dependent on electrode potential. Equilibrium potentials of charge-discharge reactions (Pb/PbSO₄ and PbSO₄/PbO₂) are presented in columns, because they depend on the acid concentration. (Berndt and Teutsch, 1996)

In general for electrochemical reactions, the current is an exponential function of the electrode potential, cf. Eq.(1). At high overvoltage, current/voltage curve forms a straight line, called “Tafel line”.

$$\eta_a = \frac{RT}{\alpha nF} \ln(|i|) - \frac{RT}{\alpha nF} \ln(i_0) = a + b \log(|i|) \tag{1}$$

This is applied also for the H₂ and O₂ gas-evolving reaction in lead acid batteries, since they are polarized by more than 0.3 V already at the battery open-circuit voltage, cf. figure 1. Tafel lines for hydrogen and oxygen evolution have been confirmed in literatures. A slope *b* of about 0.12 V per current decade is nearly always found for hydrogen evolution, while the corresponding slope for oxygen evolution is between 0.07 and 0.14 V per current decade (Berndt, 1997, Bode, 1977). Feder and Carosella revealed that at float charge of a vented lead acid battery, the negative electrode is polarized more than the positive electrode (Feder and Carosella, 1994).

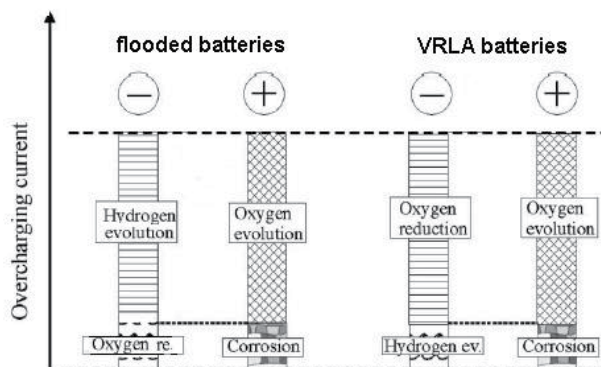


Fig. 2. Description of equal float current flows through both electrodes in the normal conditions at flooded batteries and VRLA batteries (supposing that the recombination efficiency at the VRLA battery is 100%)

In the case of VRLA batteries, the principal reactions at the negative electrode during float charge are hydrogen evolution and oxygen reduction. As the rate of H₂ evolution reaction is low thanks to the utility of antimony free grid alloys, essential float current is for the oxygen recombination. The rate of the oxygen reduction reaction is determined by the rate of oxygen diffusion from the positive electrode to the negative electrode, which does not depend on the electrode potential. If the diffusion of oxygen is sufficiently fast, which is the case in VRLA batteries, the oxygen recombination will occur, as the potential condition - inferior to 1.23V - is already satisfied at the negative electrode. The negative electrode is thus only polarized by the hydrogen evolution reaction. Therefore, in VRLA batteries the positive electrode takes essential polarization and the negative electrode can be depolarized during float charges, cf. figure 3.

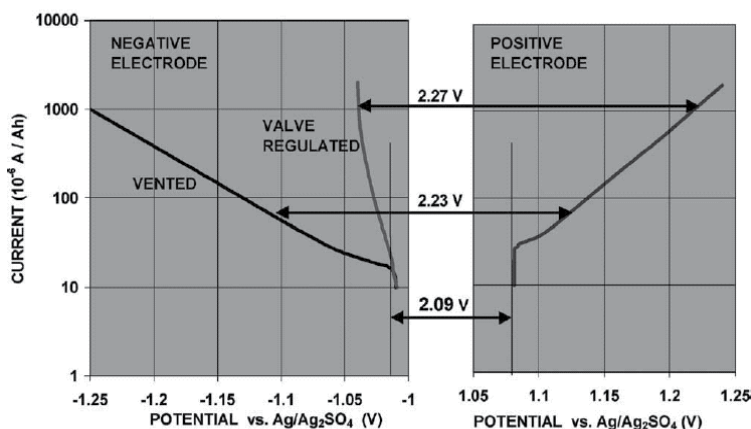


Fig. 3. Polarization curves of positive and negative electrodes, when measured against silver-silver sulfate reference electrodes. This figure demonstrates that the positive electrodes of valve-regulated batteries are subjected to much higher potentials than the positive electrodes in vented batteries (Ruetschi, 2003)

2.2.2 Cells in series configuration – scattering problem

In general, in order to obtain a desirable voltage value, one battery is composed of several cells connected in series configuration. A usual phenomenon observed in these assemblies is the voltage scattering between individual cells (Berndt, 1997, Misra et al., 1994, Rossinot et al., 2003, Hawkins et al., 1995). One example given by Berndt (Berndt, 1997) shows that for a mean float voltage of 2.38V per cell, a normal distribution curve with a standard deviation of $\pm 33\text{mV}$ and a difference between the maximum and the minimum values of 170mV are noticed. There are many reasons producing the voltage scattering. Some of them are found in industrial installations, despite the rigorous manufacturing process control and special industrial conditions (Rossinot et al., 2003).

It is revealed above that the polarization is not properly symmetrical for negative and positive electrodes. The voltage scattering thus reflects the voltage dispersion of negative electrode in flooded batteries (Feder and Carosella, 1994) and of the positive electrode in VRLA batteries (Berndt and Teutsch, 1996, Hawkins et al., 1995).

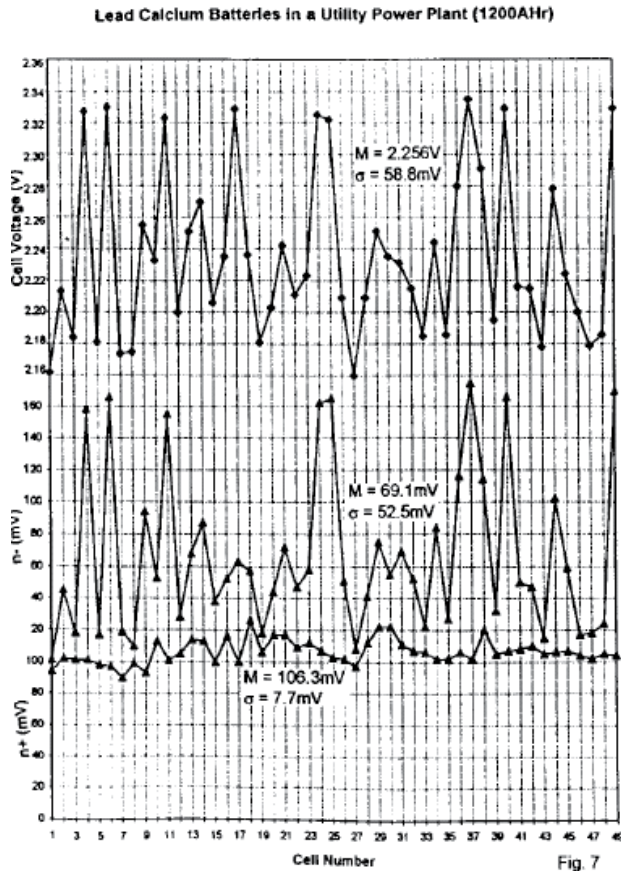


Fig. 4. Distribution of 113 V on 50 vented cells Pb-Ca in series configuration for 9 years of float charge. η^- and η^+ are potentials of the negative and positive electrodes. Voltage dispersion appears obviously at the negative electrodes and its presence is far smaller at the positive electrodes (Feder and Carosella, 1994)

2.3 Secondary reactions as causes of failure modes

At float charges, if both electrodes are well polarized, i.e. float potentials exceed the equilibrium ones; float currents will serve only to produce side reactions. The higher the float current is, the stronger the rates of side reactions are, especially the rates of gas evolution reactions.

Secondary reactions are not only the cause of self-discharge, but also the cause of main failure modes of stationary lead acid batteries under constant float voltages. Flooded and VRLA technologies can be affected by corrosion, including creeping, and degradation of positive electrodes (Berndt, 1997, Ruetschi, 2004, Stevenson, 1996, Wagner, 1995, Feder, 2001, Nakamura et al., 1996, Brissaud et al., 1997, Cooper and Moseley, 2003). VRLA batteries are moreover subjected to electrolyte dry-out and thermal runaway (Nakamura et al., 1996, Wagner, 1995, Berndt, 1997, Elgh, 1994, Cooper and Moseley, 2003).

2.3.1 Corrosion

Corrosion is the cause of different failure modes (Pavlov, 1993, Shiomi et al., 2003, Kosai et al., 1997, Peters, 1996, Ruetschi, 2004, Garche, 1995, Wagner, 1995, Misra and Williamson, 1995, Willihnganz, 1968):

- The oxides, corrosion products, take more volume than the metallic grid. The result is an expansion of the positive grid into three dimensions, in particular into the dimension of each bar of the grid. Under such mechanical stresses, the grid bars get longer and the grid dimension increases, this is called “grid growth” or “grid creeping”. This distortion can provoke internal short-circuits when the grown grid comes into contact with the negative top-bar, cf. figure 5.
- The formation of an electric passivation layer (barrier layer) at the interface between a positive grid and its active material prevents electrical contact between them. The passivation layer is sometimes said to be a closely structured PbSO_4 layer (high-resistance layer) formed at the grid active-material interface, or lower oxides of lead, such as PbO , that are generated in a high-pH environment.
- When the grid growth becomes excessive, apart from the passivation layer other causes of gradual loss of contact between the active material and the grid are noticed. The first one is the displacement of the active material away from the grid as it is not able to follow the grown grid. The second one is the gradual disappearance of the metallic grid, i.e. the grid is consumed by corrosion and can no longer take the role of electric conductor, cf. figure 6.

VRLA batteries under float charges, along with their grid design and their characteristic of the oxygen recombination, seriously suffer the corrosion consequences. Usually, 4% grid growth over the battery lifetime is the design limit. In most VRLA batteries, the grid sections are smaller; grid growth rates thus should be higher. There is some evidence that designs with absorbed and limited amounts of electrolyte are less tolerant to growth and, therefore, suffer greater capacity losses (Peters, 1996). Moreover, in VRLA batteries, in order to lower the self-discharge rate, Pb-Sb alloys are replaced by Pb-Ca alloys, where the electric passivation of the positive grid alloy, called the “antimony-free effect” usually occurs (Rocca and Steinmetz, 2003, Kosai et al., 1997). In addition, the operation potential of the positive electrode under float charge is higher in VRLA designs, cf. 2.2.1. For instance, the potential of the positive electrode is likely to be 50 to 100 mV higher than in a flooded battery (Peters, 1996). Different publications have demonstrated that there is a zone of positive polarization

where the corrosion is minimum, c.f. 3.2. According to Brecht et al. (Brecht et al., 1989), the corrosion rate is minimum when the positive polarization is between 30 and 70 mV and increases to almost double at 150 mV. Therefore, the increase of the grid growth due to corrosion is further encouraged in VRLA batteries under float charges.



Fig. 5. Due to corrosion, short-circuit took place and caused explosion accident in a standby tubular battery: (a) positive plate lengths were increased and touched the negative collective bar, (b) positive plates were distorted; the positive terminal obviously became more higher than the negative terminal; battery was destroyed after explosion (Source: EDF)



Fig. 6. Corroded positive plate of a starter battery, at the end of 5 years of service life in a passenger car (Ruetschi, 2004)

2.3.2 Water loss

Water electrolysis, i.e. evolutions of hydrogen at the negative electrode and of oxygen at the positive electrode, as well as positive grid corrosion cause water loss of the electrolyte, cf. 2.2.1. In VRLA batteries, despite of the recombination of oxygen at the negative electrode, water loss always occurs. This is due to the evolution of hydrogen, which cannot be re-oxidized to water at the positive electrode, at least not at a significant rate. Other causes of water loss such as container leakages, water evaporation, which are not mentioned in this chapter, aggravate the situation.

Dry-out

Water loss is not a problem as long as the electrolyte level can be refilled like in the case of flooded batteries. However, in the cases where maintenance intervals are not being properly respected or float charge rates are too high, water loss can reduce the capacity of the battery and finally limit the battery lifetime. Water loss induces a higher acid concentration, which results in an increase of the electrode equilibrium potentials. This means that oxygen and hydrogen overvoltages at open-circuit increase which lead to the growth of gas evolutions or of self-discharge rates. This would require an increase of float currents and of charge currents. If this demand is ignored, an insufficient state of charge and sulfation of plates can occur. If the electrolyte level is below the plate edges, the part of the plates above the acid level cannot be charged properly and this part of the plates will then undergo sulfation as well (Ruetschi, 2004). A dangerous case can happen when there is short-circuit in a non-electrolyte area; ignition of hydrogen can take place and provoke an explosion (cf. figure 5). In the case of VRLA batteries, as water cannot be refilled, water loss can become a serious problem, especially at high temperatures or excessive float voltages. Electrolyte “dry-out” is often observed. Apart of the increase of gas evolutions as mentioned above, the electrolyte decrease leads also to a decrease in the contraction of separator, when the electrolyte content is under 90 % (Nakamura et al., 1996). As separators in actual batteries initially retain about 95% of the electrolyte, separator shrinkage is not appreciable. This shrinkage can bring later to poor contacts between the plates and the separators, increasing the internal resistance. The increase of acid concentration due to water loss can induce also an increase of the oxygen recombination efficiency (Wagner, 1995). This chemical reaction of oxygen reduction is a strong heat source. Oxygen evolution is higher with the increase of acid concentration. Excessive recombination efficiency can increase dramatically the temperature of the battery and can lead to a so-called “thermal runaway”.

Thermal runaway

Thermal runaway is a current phenomenon observed at VRLA batteries (Pavlov, 1997, Giess, 1997, Culpin, 2004, Berndt, 1997, Hu et al., 2006). It is defined as an unstable state of operation where heat generation increases faster than heat can dissipate (Berndt, 1997). It is also described as an increase of charge current or float current that occurs as a result of an increase of the cell temperature from an initial applied constant potential. In other words, thermal runaway is usually considered to be the result of positive feedback of current and temperature when a cell is subjected to float charge at constant potential (Culpin, 2004). The initial float current flowing through the cell causes an increase in cell temperature that causes an increase in current that further increases the temperature until both current and temperature reach high values.

Two main source of heat during charging are the reversible heat effect of the cell reactions and the Joule heating caused by the charge current. The internal oxygen cycle represents a special form of Joule heating and is a strong heat source (Berndt, 1997).

The important parameters that mainly influence the internal oxygen cycle are the applied float voltage, the ambient temperature and the separator dry-out or the electrolyte saturation level in the separator pore volume. High float voltages and high temperatures induce more water loss, which in turn reduces the electrolyte saturation in the separator pore volume. The lower is the saturation the more favorable is the condition for the internal oxygen cycle to take place.

According to J. Hu et al. (Hu et al., 2006), when the saturation is low, there is more gas space in the AGM separator for oxygen generated from the positive plates to transport to the negative plates, where the oxygen recombination occurs. Oxygen reduction shifts the potential of the negative electrode to a less negative value. Since the applied voltage was unchanged, the potential of the positive electrode shifts more positively, which in turn leads to the generation of more oxygen on the positive plates. So the float current response becomes increasingly high. The thermal runaway occurs. In fact, the increased current at a constant float voltage is mainly used for oxygen evolution on the positive plates and the oxidation of Pb by O₂ on the negative plates to produce PbSO₄ (cf. reaction of self-discharge by O₂ reduction).

According to B. Culpin (Culpin, 2004), at high saturations, oxygen transport by the pressure-assisted route gives good recombination efficiencies of the order of 95 ÷ 97%, but only at low float currents. At low saturations oxygen transport is mainly by pure diffusion and the recombination efficiency is high even at high current. This high recombination current generates much more heat than when gassing overvoltage occurs and thermal runaway takes place.

Both authors show that the battery is out of control and thermal runaway occurs at a specific saturation of the separator around 80 ÷ 85 % even at low applied float voltages.

B. Culpin resumed the thermal runaway procedure in three stages:

- Stage 1: recombination efficiency is low; water loss is high, temperature and current rise slowly due to the small and slowly increasing internal resistance and low recombination efficiency.
- Stage 2: the recombination efficiency, even at high currents is high because of the change in oxygen transport mechanism through the separator. Heat generation increases rapidly because of a combination of increased recombination rate and increased internal resistance of the separator.
- Stage 3: the current rapidly decreases to zero as a result of the rapid increase in separator resistance. In fact, the internal resistance increases rapidly when the saturation is below 80 %, e.g. at 40% saturation the separator has a resistance 30 times of that in a fully saturated state.

3. New method of maintaining the charge for improving battery life span – low current method

3.1 Heritage of intermittent charges

In order to limit the overcharge problem, instead of continuous charge, periodic charges (ON phases) are applied and the rest of the time the battery is kept on open circuit or open-circuit voltage (OFF phases) (Reid and Glasa, 1987). This is called intermittent float or intermittent charge. This method is executed based on the principle that a battery on open-circuit for a given time (from some seconds to some weeks) loses a part of its capacity, which can be restored by a charge.

Different researches have shown positive results of intermittent charge vs. float charge concerning reduced average overcharge (Rossinot et al., 2001, Muneret et al., 2000), increased efficiency of charge phases (Rossinot et al., 2001) and reduced thermal runaway in VRLA batteries (Giess, 2001). However, if the intermittent charge parameters (threshold voltages, charge voltage or current, duration of ON phases and OFF phases...) are not

optimized, the risk of under charge, especially under charge of the negative electrode of VRLA batteries is frequent (Muneret et al., 2000). Improving intermittent charge parameters is still an open subject of research.

Characteristic	(Gun et al., 1997)	(Reid and Glasa, 1987)	(Kita et al., 1993)	(Giess, 2001)	(Rossinot et al., 2001)
Phase OFF	Open-circuit	2.17V/cell	Open-circuit	2.15V/cell	Open-circuit
Duration	≈ 15 s	-	≈ 2 months	108 h	≈ 1100 s
Fin condition	End-voltage	-	End-voltage	-	End-voltage
			2.125 V/cell		2.16V/cell
Phase ON	Constant current	Constant voltage	12 Ah charged	Constant voltage	Constant current
Fin condition		2.375 V/cell		2.25V/cell	23.8 mA/Ah
					End-voltage
					2.34V/cell
$\alpha = \text{duration ON}/(\text{ON} + \text{OFF})$	0.0625	0.5	≈ 0.1 to 0.03	0.357	0.0054

Table 1. Bibliography summary of characteristics of intermittent charges for VRLA batteries (Dillenseger, 2004)

3.2 Benefit of corrosion minimum

Reference	Analysis type	Minimum span (mV)	η^+ min (mV)
(Lander, 1956)	Grid without active material, few hours	$30 < \eta^+ < 200$	"flat"
(Ruetschi and Angstadt, 1964)	Grid without active material, few hours	$100 < \eta^+ < 250$	180
(Willihnganz, 1968)	Service life (accelerated), some years	$50 < \eta^+ < 100$	No defined
(Brecht et al., 1989, Brecht et al., 1990)	Grid growth (accelerated), some years	$30 < \eta^+ < 70$	40
(Berndt and Teutsch, 1996)	Review of literature	$40 < \eta^+ < 80$	60
(Ruetschi, 2004)	Review of literature	$20 < \eta^+ < 80$	60

Table 2. Bibliography summary of positive polarization (η^+) associated to a corrosion minimum (Dillenseger, 2004)

Different publications about corrosion phenomenon of the positive electrode have demonstrated that there is a potential zone where corrosion is at a minimum (cf. Table 2). This minimum would be at positive polarizations (η^+) between zero (at open-circuit) and polarizations at float charges ($\eta^+ \approx 100$ mV). According to Brecht et al. (Brecht et al., 1990) this minimum zone is situated in the range of [30;70] mV. This also shows that neither open-circuit periods of intermittent charges nor overcharge by traditional float charges can place the positive electrode potential in the minimum corrosion zone.

3.3 Principle of the new maintaining charge method

Taking into account this minimum corrosion zone, a new method for maintaining the charge of standby lead acid batteries, called "Low-current" method, has been developed at EDF (Nguyen et al., 2008, Dillenseger, 2004, Alzieu and Dillenseger, 2006). This method is derived from the intermittent charge: open-circuit periods are replaced by constant low current periods. These constant currents, whose values are smaller than traditional float currents, are intended to compensate, at least partially, self-discharge currents, and preferably place the battery in the minimum corrosion zone.

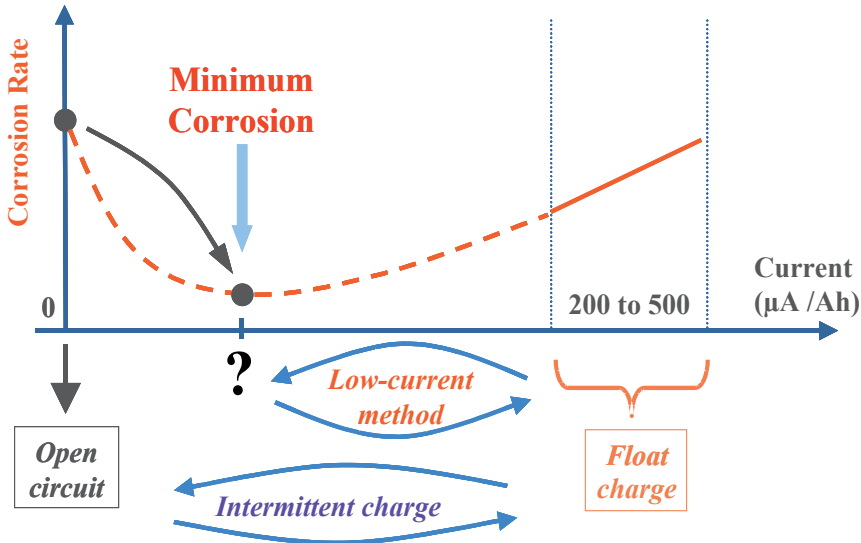


Fig. 7. Low-current method is derived from intermittent charge: open circuit periods are replaced by low currents, whose values are smaller than float current (200 to 500 $\mu\text{A}/\text{Ah}$). Battery should be in the minimum corrosion zone

The choice of piloting the current instead of the voltage to supply low positive polarizations relates to the fact that maintaining a voltage with a value very close to the battery open voltage is difficult and can accidentally discharge the battery (Giess, 2001). Moreover, the scattering phenomenon when a voltage is applied to the battery consisting of cells in series configuration is unavoidable. Monitoring the voltage share for each cell is difficult and expensive while applying a current ensures that every cell receives a given current value. Although these low currents alone are not supposed to maintain a full state of charge, they can compensate most of the self-discharge. They thus enable the intervals between recharge phases to be considerably extended so that water losses and corrosion associated to these charges are reduced.

Expected results are: (i) a slow down of the corrosion rate of positive grids, (ii) a reduction of the need of periodical charges.

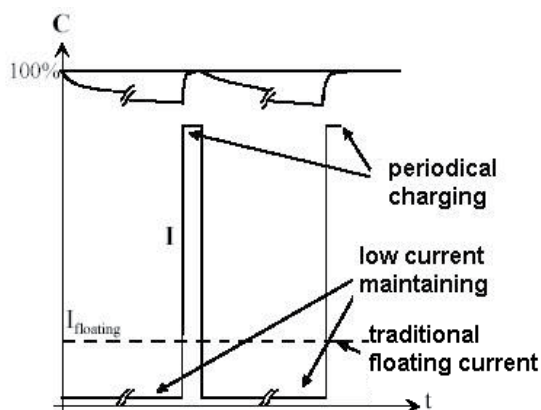


Fig. 8. Principle of new charge strategy using low-current and periodical charges

4. Experimental

Laboratory experiments aim to evaluate the state of charge of batteries subjected (1) to open circuit, (2) to float charges and (3) to polarizations whose values are intermediate between zero and float polarizations, i.e. low current charges. Several current values below float currents have been tested.

Two methods to evaluate the battery state of charge were used:

- Measurement of lead sulfate content in the battery active materials by a chemical titration. This procedure requires the destruction of the battery
- Battery capacity measurement by discharge tests.

We started different experiments with antimony-free vented SLI batteries, Exide 40 Ah/12V L01033C24A. During the experiments, capacity measurement results of these batteries showed a high degree of dispersion, which we attributed to the fact that they are not suitable for repetitive charge-discharge cycles. We then continued these experiments with VRLA AGM batteries, EnerSys 400 Ah/2 V

Low currents were applied using METRIX power supplies AX 502 2.5A – 30 V. As their accuracy does not allow a fine control of currents as low as a few mA, these power supplies were used as voltage regulators and the low currents were set using resistors in series.

Positive polarizations were evaluated using a lead acid battery reference electrode, which was first charged and then stabilized at open circuit. A current path between the tested cell and the reference electrode was provided by a tube filled with immobilized electrolyte.

The discharge-charge cycles were performed with BITRODE Battery Charge and Test System, Module Type LCN 100A – 5V.

Voltages, currents, positive polarizations and temperatures were recorded with Personal Daq 56™ USB Acquisition Systems.

4.1 Lead sulfate content measurement by chemical titration

Batteries used for lead sulfate measurements were antimony-free vented SLI batteries, Exide L01033C24A, 40 Ah-12V. The plates were pulled out of the batteries and rinsed with distilled water for 1 week before picking up active material samples. Lead sulfate contents on the later samples were measured chemically: the successive formation of complexes is

achieved using nitric acid, acetic acid, xylenol orange and titriplex III (EDTA). The last complex is reached using a titrated solution of EDTA. The final stage of this reaction induces a color change: violet to yellow. Sulfate content was calculated from the sample mass and the quantity of EDTA used.

Four batteries were subjected first to open circuit during 231 days, then to low currents of 25, 50, 100 and 200 $\mu\text{A}/\text{Ah}$ during 356 days at room temperature ($23 \pm 4^\circ\text{C}$) and were finally opened to analyze their lead sulfate content.

4.2 Capacity measurement by discharge test

Before beginning the experiments, we had a preliminary remark that the measurements of self-discharge, even after several months at open circuit, represent only a weak portion of the capacity, e.g. about 10%. The expected results concern differences between reduced rates of self-discharge. These results were supposed to be a few percent of the nominal capacity, which is less than the natural dispersion we generally observe in capacity measurements (e.g. between several batteries taken at random from the same lot of fabrication).

Two methods are *a priori* possible:

- Testing with a big enough number of batteries to obtain precise and meaningful statistical averages. We haven't chosen this method because the number of batteries required is too big for our test facilities.
- Comparing the capacity results of every single battery subjected to n months of self-discharge or float charge or low-current charge to its own capacity measured after a full charge. This is the chosen method.

Battery used for capacity measurements was VRLA AGM EnerSys 400Ah/2V. Four batteries of this technology were taken from the field and replaced by new ones after 6-year service, which corresponds to their mid-life (they are designed to last 12 years or more). In order to stabilize their capacities, these batteries were first subjected to 15 discharge-charge cycles, with discharges at C/10 - 1.8V stop voltage and IU_i charges (C/10 until 2.4 V then 2.4 V for 5 hours then C/80 without voltage restriction for 2 hours). The last capacity obtained is the reference capacity. They were then subjected to tests at room temperature ($18 \pm 3^\circ\text{C}$): open circuit, low-currents of 29 and 105 $\mu\text{A}/\text{Ah}$ and float charge at 2.27V (current response is 414 $\mu\text{A}/\text{Ah}$). After 6 months, these batteries were discharged with the same rate (C/10) to determine their final capacities.

5. Results & Discussion

5.1 Lead sulfate content measurement

Table 3 gives the results of PbSO_4 contents at initial state (after 231 days on open-circuit), and PbSO_4 final contents (after 356 days more at open-circuit and at constant low currents varying from 25 to 200 $\mu\text{A}/\text{Ah}$). Sulfate content variations during 356 days are the difference between final and initial sulfate contents.

From the obtained % of mass of PbSO_4 contents, the % of mol of PbSO_4 contents can be calculated as follows.

At the negative electrode we have:

$$PbSO_4(\%mass) = \frac{PbSO_4(\%mol) \times PbSO_4(g)}{PbSO_4(\%mol) \times PbSO_4(g) + [1 - PbSO_4(\%mol)] \times Pb(g)} \quad (2)$$

so:

$$PbSO_4(\%mol) = \frac{PbSO_4(\%mass) \times Pb(g)}{PbSO_4(g) - PbSO_4(\%mass) \times [PbSO_4(g) + Pb(g)]} \quad (3)$$

Executed service during 356 days	Applied Current (μA/Ah)	Obtained PbSO ₄ content (% mass)		Calculated PbSO ₄ content (% mol)		PbSO ₄ content variation during service (% mol)	
		NAM	PAM	NAM	PAM	NAM	PAM
Initial state (231 days at open circuit)	-	16	30	11.5	24.4	-	-
Self-discharge (Open-circuit)	0	21	45	15.4	37.3	3.9	12.9
Low current	25	16.8	24.0	12.1	19.4	0.6	-5
Low current	50	11.5	19.1	8.1	15.4	-3.4	-9
Low current	100	1.9	8.6	1.3	6.8	-10.2	-17.6
Low current	200	1.4	4.8	1	3.8	-10.5	-20.6

Table 3. After 231 days at open circuit, four batteries were subjected to low-currents during 356 days at room temperature 23 ± 4°C. Contents of lead sulfate were measured at the negative active material (NAM) and the positive active material (PAM). Active material samples were taken from the middle of the negative and positive plates.

Calculating the same way at the positive electrode:

$$PbSO_4(\%mol) = \frac{PbSO_4(\%mass) \times PbO_2(g)}{PbSO_4(g) - PbSO_4(\%mass) \times [PbSO_4(g) + PbO_2(g)]} \quad (4)$$

From the variations of sulfate contents and the duration of the experiments, equivalent currents can be calculated using the first Faraday’s law, they are called “Effective current”:

$$\text{Effective current: } I_{\text{Effect}} = PbSO_4(\%mol) \times \frac{m}{M} \times \frac{nF}{t} \quad (5)$$

According to the Exide manufacturer, the masses of active materials of L01033C24A, 40 Ah-12V battery are 365g of PbO₂ and 300g of Pb.

The Effective current at open circuit (I_{Effect}^0) is the self-discharge current ($I_{\text{selfdischarge}}$). It will be presented with a negative value in Table 4, as the battery is discharging.

$$I_{\text{Effect}}^0 = I_{\text{selfdischarge}} \quad (6)$$

Applying Eq. (5) to the battery at open circuit, we have self-discharge currents of the

negative electrode (I_{Effect}^{0-}) and of the positive electrode (I_{Effect}^{0+}):

$$I_{\text{Effect}}^{0-} = I_{\text{selfdischarge}}^{-} = 0.039 \times \frac{300}{207} \times \frac{2 \times 96500}{356 \times 24 \times 3600} = 0.00035 \text{ A} = 9 \text{ } \mu\text{A} / \text{Ah}$$

$$I_{\text{Effect}}^{0+} = I_{\text{selfdischarge}}^{+} = 0.129 \times \frac{365}{239} \times \frac{2 \times 96500}{356 \times 24 \times 3600} = 0.0012 \text{ A} = 30 \text{ } \mu\text{A} / \text{Ah}$$

“Current Balance” is the result theoretically expected when applying a current to the battery. So it is the subtraction of the applied low current and the self-discharge current.

$$\text{Current Balance: } I_{\text{Balance}} = I_{\text{Applied}} - I_{\text{selfdischarge}} \quad (7)$$

Executed service during 356 days	Applied Current I_{Applied} ($\mu\text{A}/\text{Ah}$)	Effective current I_{Effect} ($\mu\text{A}/\text{Ah}$)		Calculated Current Balance I_{Balance} ($\mu\text{A}/\text{Ah}$)		Calculated rate of side reactions $I_{\text{Side-reac}}$ ($\mu\text{A}/\text{Ah}$)	
		NAM	PAM	NAM	PAM	NAM	PAM
Initial state (231 days at open circuit)	-	-	-	-	-	-	-
Self-discharge (Open-circuit)	0	-9	-30	-9	-30	-9	-30
Low current	25	-1.4	12	16	-5	-26.4	-13
idem	50	8	22	41	20	-42	-28
idem	100	23	42.6	91	70	-77	-57.4
idem	200	24	50	191	170	-176	-150

Table 4. Equivalent currents obtained from the variations of sulfate level and the duration of the experiments, calculated current balances and side reaction rates.

Side reactions are always present inside the lead acid cell at open circuit as well as under low currents. At open circuit, the side reaction rate is the self-discharge current. Under low currents, side reaction rates can be calculated by subtracting the effective currents to the applied current.

$$\text{Side reaction rate under low currents: } I_{\text{Side-reac}} = I_{\text{Effective}} - I_{\text{Applied}} \quad (8)$$

In figure 9, Effective Currents (EC) are compared to Current Balances (CB) and Side Reaction Rates (SRR) for negative and positive plates.

At open-circuit in figure 9, variations of sulfate content in mole percent are +3.9% for the NAM and +12.9% for the PAM (Nguyen et al., 2008). One can calculate from these sulfate content variations the self-discharge currents during 356 days of the experiment: $-9 \mu\text{A}/\text{Ah}$ and $-30 \mu\text{A}/\text{Ah}$ for the negative and positive electrodes respectively. The self-discharge rate of the positive electrode is more than three times faster than the self-discharge rate of the negative electrode.

The lowest current we tested, 25 $\mu\text{A}/\text{Ah}$, induces a drastic change in the sulfate content evolution inside the active materials. The sulfate content in the NAM remains almost constant (0.6 % increase) while the sulfate content in the PAM decreases by 5%. So, the positive plate behaves worse than the negative plate at open-circuit but it has a better behavior as soon as the battery receives the lowest applied current.

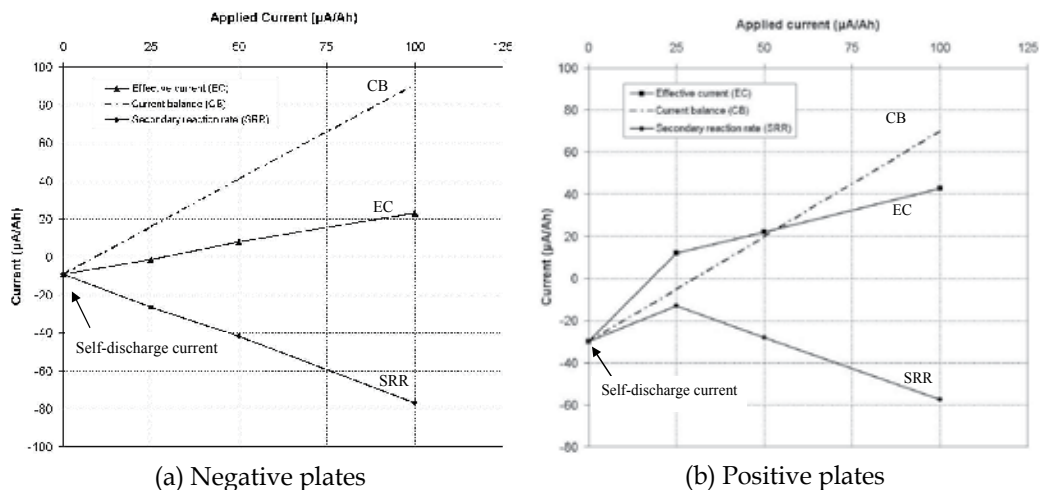


Fig. 9. Equivalent currents calculated from the variations of sulfate levels vs. applied currents: (a) negative plates, (b) positive plates. Current balance (CB) is the subtraction of the applied low currents and the self-discharge currents. Effective current (EC) is the equivalent currents corresponding to the sulfate content variations. Side reaction rate (SRR) is the subtraction of the effective currents and the applied currents

a. Negative plates

Figure 9 (a) shows the calculated current balances and the effective currents for the negative plates.

According to the lead sulfate content variation at 25 $\mu\text{A}/\text{Ah}$, the effective current for NAM is -1.4 $\mu\text{A}/\text{Ah}$. This negative value means that the low current compensates only partially the self-discharge. The current balance at 25 $\mu\text{A}/\text{Ah}$ is: $25 - 9 = 16 \mu\text{A}/\text{Ah}$.

The difference between the current balance and the effective current can be associated to losses of the applied current. Another explanation could be an increase of the secondary reactions involved in the self-discharge process under the polarization resulting from the applied current. These two hypotheses are in fact the same as secondary reactions involved in the self-discharge process and in losses during charging are identical: mainly hydrogen evolution and some oxygen recombination.

b. Positive plates

Figure 9 (b) shows the calculated current balances and the effective resulting currents for the positive plates.

A surprising result is observed at the 25 $\mu\text{A}/\text{Ah}$ applied current. The effective current (12 $\mu\text{A}/\text{Ah}$), is higher than the calculated current balance (-5 $\mu\text{A}/\text{Ah}$). Of course, one cannot

have an efficiency that is higher than 100%. The low current effect is then not only a compensation of the self-discharge process, but a modification and/or a rate reduction of the secondary reactions involved in this process. Indeed, one observes a minimum of the side reaction rate at 25 $\mu\text{A}/\text{Ah}$ (cf. figure 9).

Secondary reactions at the positive electrode are the oxygen evolution and the positive grid corrosion.

Oxygen evolution takes place at open-circuit, charge and discharge potentials. This reaction is known to increase its rate with positive polarization, so it cannot be the reason of the reduction of the self-discharge process observed in this case.

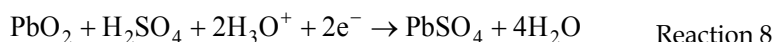
On the contrary, corrosion can slow down under positive polarizations. This phenomenon is well known in the field of corrosion of metals as anodic protection, or more generally as corrosion passivation.

In the case of lead acid batteries, it is also well known that corrosion reactions are different at open-circuit and during charging. More exactly, corrosion reactions of the positive grid consist of two steps:

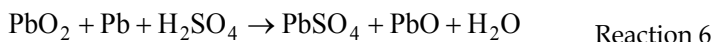


In which, O^{2-} ions are brought by migration from the active material across oxidation layers. Only the first step, Reaction 11, operates at open-circuit while these both steps occur during charging.

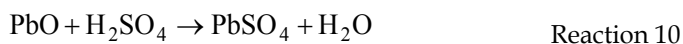
Indeed, at open-circuit, divalent lead (Pb^{2+}) is the stable state for lead. Only the first step of the corrosion reaction occurs but not the second step (Reaction 12, in which Pb^{2+} would oxidize into Pb^{4+}), because Pb^{4+} is not the thermodynamically stable state for lead. As at open-circuit the two electrons of Reaction 11 cannot be evacuated by the external circuit, they are used by reduction of Pb^{4+} into Pb^{2+} in the discharge reaction of the positive active material:



The combination of Reaction 11 and Reaction 8 is then:



When PbO is not protected with a dense PbO_2 layer, it reacts chemically with sulfuric acid to form PbSO_4 as follows:



The overall corrosion reaction at open-circuit is then:



When this reaction occurs, usually in prolonged open-circuit conditions, positive grids are no more protected. Indeed, the formation of lead sulfate in the corrosion layers leads to mechanical stress, causing the formation of cracks and the destruction of the protective layer.

During charging (under low currents), Reaction 12 takes place. Under positive polarization, Pb^{4+} (in PbO_2) is indeed the stable species of lead. PbO_2 produced in Reaction 12 is formed in the outer part of the corrosion layer. As it is dense, issued from the dense inner layer, and stable in sulfuric acid solution, it takes the role of protecting the PbO inner layer and the positive grid from the electrolyte (Ruetschi, 2004, Berndt, 1997, Garche, 1995).

Under positive polarizations, grid corrosion, which is part of the self-discharge process of the positive electrode, is then slowed down by the formation of a protective layer of dense PbO_2 . Therefore, for the positive electrode, this can be the reason why the effective current is sensibly higher than the calculated current balance, as long as corrosion is important part of the positive self-discharge process. Benefit of $25 \mu\text{A}/\text{Ah}$ low current is then triple:

(i) Compensation of the self-discharge:

For intermittent charge, in the prospect of replacing open-circuit periods by low current periods, it is obvious that periodical charges would no longer be necessary or at least would be required less frequently.

(ii) Slowing down of the corrosion rate:

As mentioned previously, several authors indicate a minimum corrosion zone. This minimum is generally situated at positive polarizations in the [30, 80] mV range. Indeed, at $25 \mu\text{A}/\text{Ah}$, the strong effect observed can be attributed to an important reduction of the corrosion rate. But in this case the positive polarization is in the order of 2 mV much lower than the preceding published values. It must be noticed that our results, obtained from long duration tests (over 19 months) at room temperature, differ from these published results, generally obtained at accelerated conditions.

(iii) Reduction of water consumption:

It concerns water involved in corrosion reactions. In these reactions, the oxygen is taken from the positive active material. In turn, the active material takes oxygen from water of the electrolyte. The oxygen, finally locked in the corrosion product layers, cannot be recombined to reform water. So, the decrease of water consumption due to corrosion is important for the battery life span.

5.2 Capacity measurement

Table 5 gives the capacities of VRLA batteries before (C_{ref}) and after (C_{fin}) 6 months at open-circuit, at low currents of 29 and $105 \mu\text{A}/\text{Ah}$, and at 2.27V float charge. These experiments were done at room temperature ($18 \pm 3^\circ\text{C}$). The battery at open-circuit for 6 months lost $(264 - 327)/327 = -19.3\%$ of its capacity compared to its reference capacity; the capacity of the battery subjected to $105 \mu\text{A}/\text{Ah}$ increased by $(329 - 313)/329 = +5.1\%$.

Figure 10 (a) shows the capacity variations given for each battery in percent of their

reference capacities. These percentages are also the state of charge variations induced by the applied currents during the 6 months of experiments. The capacity variations are converted to the equivalent currents or as named above the effective currents. These effective currents are presented as a function of the applied current in figure 10 (b). The currents balances and the side reaction rates are calculated as the same way in the section 5.1. At open-circuit, the capacity reduction of 63 Ah after 6 months allows calculating the average self-discharge current, which is 36 $\mu\text{A}/\text{Ah}$.

Battery	Reference capacity C_{ref} (Ah)	Applied Current during 6 months at room temperature $18 \pm 3^\circ\text{C}$ ($\mu\text{A}/\text{Ah}$)	Final capacity C_{fin} (Ah)	Capacity Variation $(C_{\text{fin}} - C_{\text{ref}})/C_{\text{ref}}$ (%)
B115	340.0	~ 414 (float charge at 2.27V)	379.0	11.8
B116	313.0	105	329.0	5.1
B117	318.0	29	308.0	-3.1
B118	327.0	0	264.0	-19.3

Table 5. Capacities of the VRLA batteries, which were subjected to open circuit, to 29 and 105 $\mu\text{A}/\text{Ah}$ low-currents and to 2.27 V float charge during 6 months at room temperature ($18 \pm 3^\circ\text{C}$) as well as their reference capacities before this service.

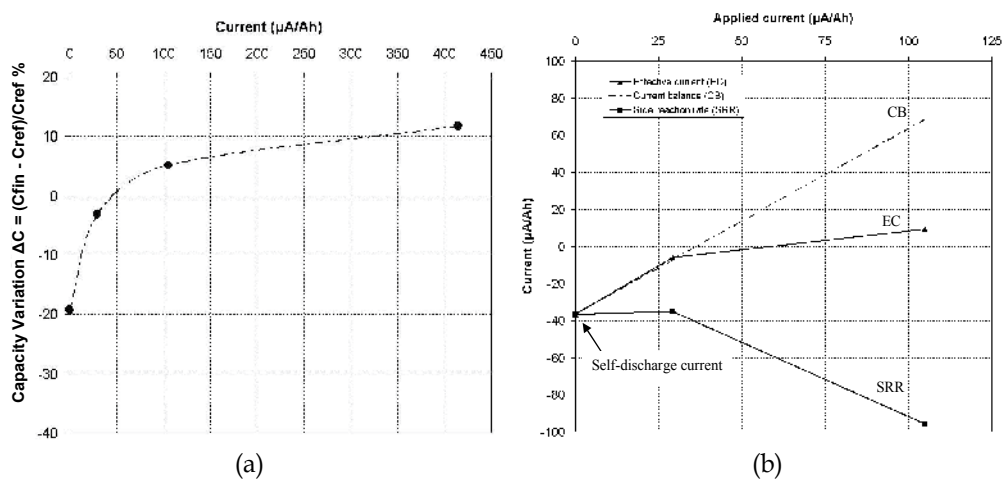


Fig. 10. VRLA Batteries were tested during 6 months at room temperature ($18 \pm 3^\circ\text{C}$). (a) Relative capacity variations (state of charge variations) vs. applied currents. (b) Equivalent currents calculated from the capacity variations vs. applied currents.

The capacity variation has a strong increase for the lowest applied current (29 $\mu\text{A}/\text{Ah}$). It appears that this low current, whose value is 80 % of the average self-discharge current (36 $\mu\text{A}/\text{Ah}$), compensates 84 % of the self-discharge. Such a high efficiency (superior to 100%) suggests that these VRLA batteries could be positive limited at this mid-life state. Further experiments confirmed that these batteries were indeed positive limited.

Increases of the battery state of charge at the low current of 105 $\mu\text{A}/\text{Ah}$ and at float current of 414 $\mu\text{A}/\text{Ah}$ indicate that the charge procedure we used does not lead to a real full charge. Charge is then completed slowly at currents beyond 50 $\mu\text{A}/\text{Ah}$. The reference capacity is

supposed to be the maximum capacity the battery is able to discharge after a full charge. But what is a full charge? We all know that absolute full charge of a lead acid battery does not exist. It is an asymptotic state. What we generally call a full charge is in fact the result of a compromise between the search of a high state of charge and the time we can spend on this operation. In practice it is considered that the end of charge is reached, when there is no charging current or voltage evolution during at least 2 hours. Our "full charge" procedure for VRLA batteries was a classical IUi charge. According to the results above, we must consider that our charge procedures were not sufficient to reach states of charge as high as after a few months of float charge or even of low current charge.

According to experiment results, we supposed that when combined with low currents in the order of 25 to 50 $\mu\text{A}/\text{Ah}$, a refresh charge every 6 months or every single year is sufficient to maintain antimony-free batteries in a good state of charge. Higher currents, as traditional float currents (10 times higher), are not necessary and not suited, as they would increase corrosion and water loss. We consider using a refresh charge only when the battery has been subjected to a discharge service.

6. New management system for standby antimony-free battery

Valve regulated lead acid batteries - VRLA batteries - have been developed and used for about 30 years in standby applications. They have shown several advantages compared to flooded lead acid batteries: spill-proof, reduced weight, free from excessive gas evolution or acid spillage, reduced maintenance and reduced cost. However, limitations have been also observed concerning system reliability and battery service life.

Several reliability prediction methods have been used such as complete discharge test (Piller et al., 2001), open-circuit voltage measurement (Bullock et al., 1997), conductance testing (Kniveton, 1995), internal resistance and impedance measurements (Hariprakash et al., 2004, Huet, 1998, Karden et al., 2000, Rodrigues et al., 2000, Shukla et al., 1998, Piller et al., 2001). Among these, the complete discharge test is well known as the most reliable one but it requires service interruption. This has driven EDF R&D to develop the "Stationary Multibat" system, which consists of a new design of the electrochemical storage and an adapted electronic battery management system (Desanti and Schweitz, 2006). This system, combining redundancy and automated periodical capacity measurements, increases reliability and allows a real time monitoring of the battery state of health. Redundancy not only ensures the continuity of service in the case of a cell failure, but also enables complete discharges to be periodically performed without service interruption.

Standby VRLA batteries maintained under a constant float voltage to compensate self-discharge encounter the problem of short service life, e.g. about 3-4 years compared to the so-called 20-year design and to the 20-year lifetime of conventional lead acid batteries in similar conditions (Misra, 2007). Indeed, VRLA batteries under float charges are permanently overcharged and different failure modes have been observed, such as corrosion of positive grid alloys, electrolyte dry-out and thermal runaway (Berndt, 1997, Feder, 2001, Ruetschi, 2004, Wagner, 1995, Dai et al., 2006).

A new management system for standby VRLA batteries has been developed at EDF using the Stationary Multibat system (Desanti and Schweitz, 2006) to ensure system reliability and the Low-current method (Nguyen et al., 2008) to improve the battery life span.

Figure 11 (a) describes a simplified schematic diagram of the Stationary Multibat system.

Three battery-pack strings in parallel instead of one pack are used in order to improve the system reliability. In case of a cell failure such as an open circuit, the system loses only one battery-pack string, i.e. one-third of the total capacity. This configuration also allows each string to be discharged completely across the test resistance to evaluate its real state of health. Each battery string is periodically (e.g. every 6 months) discharged and charged.

Fig. (b) describes how to integrate and to operate Low-current method of maintaining the charge on the Stationary Multibat system:

- A resistance branch is added to reduce the traditional float current with a factor of 5 to 10. In standby state, Programmable Logic Controllers (PLC) K_1 and K_2 are open; the battery is maintained at charge with a low current via the resistance R .
- On backup demand, a voltage drop appears on the DC bus, the battery immediately provides electricity to the DC load via the diode D . Then PLC K_1 closes; the battery directly supplies power to DC load.
- During the periodical discharge test (e.g. every 6 months) to evaluate the battery state of health, PLC K_2 closes and K_1 stays open. The battery-pack string is discharged across the test resistance. The low current, still provided to the battery pack string, is a parasitic but negligible effect ($< 0.1\%$). Next, the charge is operated via K_1 . The charge current is controlled by a Pulse Wave Modulation (PWM). When the charge finishes, K_1 re-opens, the battery is re-maintained the charge with a low current via R .

All those operations are done sequentially and automatically so that no intervention is required from the maintenance.

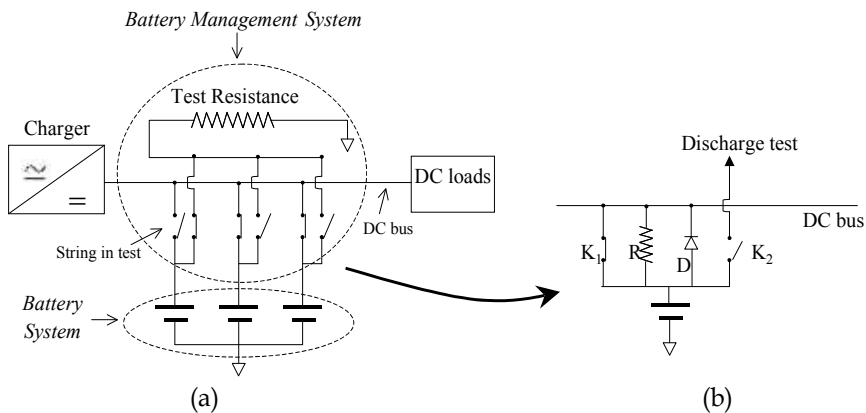


Fig. 11. (a) Simplified schematic diagram of the Stationary Multibat system. (b) Zoom on the power electronic components of one of the three battery-pack strings using Low-current method.

This system is expected to fulfill three targets:

- Increasing the system reliability by a redundancy in the design of the battery system and by an assessment method to control battery state of health.
- Improving battery life spans by the Low-current method, leading to reduced corrosion and water loss.
- Decreasing maintenance costs.

7. Conclusion

Antimony-free lead-acid batteries were tested for several months at open-circuit, float charge and intermediate rates of charge – called “Low-current” in this chapter. The following conclusions can be drawn from this study:

- In antimony-free lead acid batteries, the self-discharge rate of the positive electrode is higher than that of the negative electrode.
- Low-currents beyond 25 $\mu\text{A}/\text{Ah}$ appear to be able to maintain the state of charge for both positive and negative plates.
- The effect of 25 $\mu\text{A}/\text{Ah}$ low current on the positive active material is much higher than a simple compensation of the self-discharge. This can be explained by a passivation phenomenon of the positive grid corrosion. In other words, it constitutes an anodic protection of the positive grid.
- The use of low-current periods in place of open-circuit periods in the intermittent charging method should increase the life span of VRLA batteries, as it both lowers the water consumption and the corrosion rate of positive grids.

Combining the Low-current method, battery redundancy and automated periodical capacity measurements, VRLA batteries should provide long life spans and high reliability. Several management systems of this kind are being experimentally used at EDF.

Acknowledgment

The authors gratefully acknowledge financial support from the Association Nationale de la Recherche Technique (ANRT - France).

8. References

- ALZIEU, J. & DILLENSEGER, G. (2006) Method for maintaining the charge of a lead storage battery. France, Electricite de France.
- BERNDT, D. (1997) *Maintenance-Free batteries*, Taunton, Somerset, New York, Chichester, Toronto, Brisbane, Singapore, Research studies press LTD, John Wiley & Sons INC.
- BERNDT, D. & TEUTSCH, U. (1996) Float charging of VRLA batteries: A balancing act between secondary reactions. *Journal of Electrochemical Society*, 143.
- BODE, H. (1977) *Lead Acid batteries*, New York, London, Sydney, Toronto, John Wiley & Sons.
- BRECHT, W. B. (1998) Strategies for overcoming the adverse effects of imbalances in the second order reactions in valve regulated lead acid cells. *Telecommunications Energy Conference, 1998. INTELEC. Twentieth International*.
- BRECHT, W. B., FEDER, D. O., MCANDREWS, J. M. & WILLIAMSON, A. J. (1989) The effect of positive polarization on grid growth, cell performance and life. II. *Telecommunications Energy Conference, 1989. INTELEC '89. Conference Proceedings., Eleventh International*.
- BRECHT, W. B., FEDER, D. O., MCANDREWS, J. M. & WILLIAMSON, A. J. (1990) Low float technology battery. United States, C & D Charter Power Systems, Inc. (Plymouth Meeting, PA).

- BRISAUD, C., REUMONT, G., SMAHA, J. P. & FOCT, J. (1997) Structural and morphological study of damage in lead/acid batteries during cycling and floating tests. *Journal of Power Sources*, 64, 117-122.
- BULLOCK, K. R., WEEKS, M. C., BOSE, C. S. C. & MURUGESAMOORTHY, K. A. (1997) A predictive model of the reliabilities and the distributions of the acid concentrations, open-circuit voltages and capacities of valve-regulated lead/acid batteries during storage. *Journal of Power Sources*, 64, 139-145.
- COOPER, A. & MOSELEY, P. T. (2003) Progress in overcoming the failure modes peculiar to VRLA batteries. *Journal of Power Sources*, 113, 200-208.
- CULPIN, B. (2004) Thermal runaway in valve-regulated lead-acid cells and the effect of separator structure. *Journal of Power Sources*, 133, 79-86.
- DAI, C., YI, T., WANG, D. & HU, X. (2006) Effects of lead-foam grids on performance of VRLA battery. *Journal of Power Sources*, 158, 885-890.
- DESANTI, J. D. & SCHWEITZ, G. (2006) Decreasing Owning Costs of MV/LV Substations Backup Batteries. *Telecommunications Energy Conference, 2006. INTELEC '06. 28th Annual International*.
- DILLENSEGER, G. (2004) Caractérisation de nouveaux modes de maintien en charge pour batteries stationnaires de secours. *Sciences et Techniques du Languedoc*. Montpellier, Université de Montpellier II.
- ELGH, R. (1994) Tests on valve regulated lead acid batteries at different environmental temperatures and float voltages. *Telecommunications Energy Conference, 1994. INTELEC '94., 16th International*.
- FEDER, D. O. (2001) 1950-2001: more than one-half century of learning how to live with each new generation of telecommunication standby batteries. *Telecommunications Energy Conference, 2001. INTELEC 2001. Twenty-Third International*.
- FEDER, D. O. & CAROSELLA, G. (1994) The never ending pursuit of float voltage uniformity in stationary reserve battery plants. *Telecommunications Energy Conference, 1994. INTELEC '94., 16th International*.
- GARCHE, J. (1995) Corrosion of lead and lead alloys: influence of the active mass and of the polarization conditions. *Journal of Power Sources*, 53, 85-92.
- GIESS, H. (1997) Investigation of thermal phenomena in VRLA/AGM stationary lead/acid batteries with a thermal video imaging system. *Journal of Power Sources*, 67, 49-59.
- GIESS, H. (2001) The operation of VRLA monoblocs with an on/off float charge regime. *Telecommunications Energy Conference, 2001. INTELEC 2001. Twenty-Third International*.
- GUN, J. P., FIORINA, J. N., FRAISSE, M. & MABBOUX, H. (1997) Increasing UPS battery life main failure modes, charging and monitoring solutions. *Telecommunications Energy Conference, 1997. INTELEC 97., 19th International*.
- HARIPRAKASH, B., MARTHA, S. K., JAİKUMAR, A. & SHUKLA, A. K. (2004) On-line monitoring of lead-acid batteries by galvanostatic non-destructive technique. *Journal of Power Sources*, 137, 128-133.
- HAWKINS, J. M., MOORE, L. E. E. & BARLING, L. O. (1995) Aspects of the float and temperature behaviour of lead-acid batteries in telecommunications applications. *Telecommunications Energy Conference, 1995. INTELEC '95., 17th International*.
- HU, J., GUO, Y. & ZHOU, X. (2006) Thermal runaway of valve-regulated lead-acid batteries. *Journal of Applied Electrochemistry*, 36, 1083-1089.

- HUET, F. (1998) A review of impedance measurements for determination of the state-of-charge or state-of-health of secondary batteries. *Journal of Power Sources*, 70, 59-69.
- KARDEN, E., BULLER, S. & DE DONCKER, R. W. (2000) A method for measurement and interpretation of impedance spectra for industrial batteries. *Journal of Power Sources*, 85, 72-78.
- KITA, A., MATSUI, T., KASAI, Y. & KISHIMOTO, K. (1993) Uninterruptible power system. United States, Yuasa Battery Company Limited (Takatsuki, JP).
- KNIVETON, M. W. (1995) Reducing the cost of maintaining valve-regulated lead/acid batteries in telecommunications applications. *Journal of Power Sources*, 53, 149-152.
- KOSAI, M., YASUKAWA, S., OSUMI, S. & TSUBOTA, M. (1997) Effect of antimony on premature capacity loss of lead/acid batteries. *Journal of Power Sources*, 67, 43-48.
- LANDER, J. J. (1956) Further studies on the anodic corrosion of lead in H₂SO₄ solutions. *Journal of the Electrochemical Society*, 103, 1-8.
- MARTINEZ, T. G. & NOVAK, A. F. S. (1990) Increased float voltage and the effects of negative self-discharge on flooded lead calcium telecommunications cells. *Telecommunications Energy Conference, 1990. INTELEC '90., 12th International*.
- MISRA, S. S. (2007) Advances in VRLA battery technology for telecommunications. *Journal of Power Sources*, 168, 40-48.
- MISRA, S. S., NOVESKE, T. M. & WILLIAMSON, A. J. (1994) Maintenance and reliability of standby battery systems: flooded vs. valve regulated lead acid battery. *Telecommunications Energy Conference, 1994. INTELEC '94., 16th International*.
- MISRA, S. S. & WILLIAMSON, A. J. (1995) Impact of grid corrosion in valve regulated lead-acid battery on standby float service. *Telecommunications Energy Conference, 1995. INTELEC '95., 17th International*.
- MUNERET, X., COUX, M. & LENAIN, P. (2000) Analysis of the partial charge reactions within a standby VRLA battery leading to an understanding of intermittent charging techniques. *Telecommunications Energy Conference, 2000. INTELEC. Twenty-second International*.
- NAKAMURA, K., SHIOMI, M., TAKAHASHI, K. & TSUBOTA, M. (1996) Failure modes of valve-regulated lead/acid batteries. *Journal of Power Sources*, 59, 153-157.
- NGUYEN, T. M. P., DILLESEGER, G., GLAIZE, C. & ALZIEU, J. (2008) Between floating and intermittent floating: Low-current self-discharge under compensation. *Telecommunications Energy Conference, 2008. INTELEC 2008. IEEE 30th International*.
- PAVLOV, D. (1993) Premature capacity loss (PCL) of the positive lead/acid battery plate: a new concept to describe the phenomenon. *Journal of Power Sources*, 42, 345-363.
- PAVLOV, D. (1997) Energy balance of the closed oxygen cycle and processes causing thermal runaway in valve-regulated lead/acid batteries. *Journal of Power Sources*, 64, 131-137.
- PETERS, K. (1996) Review of factors that affect the deep cycling performance of valve-regulated lead/acid batteries. *Journal of Power Sources*, 59, 9-13.
- PILLER, S., PERRIN, M. & JOSSEN, A. (2001) Methods for state-of-charge determination and their applications. *Journal of Power Sources*, 96, 113-120.
- REID, D. P. & GLASA, I. (1987) A new concept: intermittent charging of lead acid batteries in telecommunication systems. *Telecommunications Energy Conference, 1987. INTELEC '87*.

- ROCCA, E. & STEINMETZ, J. (2003) Passivation phenomenon of low antimony alloys in deep discharge conditions of lead-acid batteries. *Journal of Electroanalytical Chemistry*, 543, 153-160.
- RODRIGUES, S., MUNICHANDRAIAH, N. & SHUKLA, A. K. (2000) A review of state-of-charge indication of batteries by means of a.c. impedance measurements. *Journal of Power Sources*, 87, 12-20.
- ROSSINOT, E., LEFROU, C., DALARD, F. & CUN, J. P. (2001) Batteries in standby applications: comparison of alternate mode versus floating. *Journal of Power Sources*, 101, 27-34.
- ROSSINOT, E., LEFROU, C. & GUN, J. P. (2003) A study of the scattering of valve-regulated lead acid battery characteristics. *Journal of Power Sources*, 114, 160-169.
- RUETSCHI, P. (2003) Silver-silver sulfate reference electrodes for use in lead-acid batteries. *Journal of Power Sources*, 116, 53-60.
- RUETSCHI, P. (2004) Aging mechanisms and service life of lead-acid batteries. *Journal of Power Sources*, 127, 33-44.
- RUETSCHI, P. & ANGSTADT, R. T. (1964) Anodic oxidation of lead at constant potential. *Journal of the Electrochemical Society*, 111, 1323-1330.
- SHIOMI, M., OKADA, Y., TSUBOI, Y., OSUMI, S. & TSUBOTA, M. (2003) Study of PCL mechanism: Influence of grid/PAM state on PCL. *Journal of Power Sources*, 113, 271-276.
- SHUKLA, A. K., GANESH KUMAR, V., MUNICHANDRAIAH, N. & SRINATH, T. S. (1998) A method to monitor valve-regulated lead acid cells. *Journal of Power Sources*, 74, 234-239.
- STEVENSON, P. (1996) Durée de vie des accumulateurs étanches. *REE, N°1*, 57-60.
- WAGNER, R. (1995) Failure modes of valve-regulated lead/acid batteries in different applications. *Journal of Power Sources*, 53, 153-162.
- WILLIHNGANZ, E. (1968) Accelerated testing of stationary batteries. *Electrochemical Technology*, 115, 338-341.

Neighbor Discovery: Security Challenges in Wireless Ad hoc and Sensor Networks

Mohammad Sayad Haghghi and Kamal Mohamedpour
K.N. Toosi University of Technology
Iran

1. Introduction

Wireless ad hoc and sensor networks are infrastructureless systems with self-configuration capabilities. Neighbor discovery protocols are fundamental requirements in the construction of self-organizing networks. Each computer (node) must discover who its neighbors are in order to be able to coordinate with them for any later communication. This goal is usually accomplished through broadcasting methods in the initial phases of network deployment.

Along with the development of neighbor discovery protocols, security threats also introduced and some researchers discovered new forms of attacks for neighbor discovery scenarios. Authors in this field have given different definitions on what a neighbor is and to what extent an adversary is equipped. We will first clarify these differences by making some categorizations and definitions before proceeding to the introduction of attacks and solutions.

After the introduction of initial concepts, we classify the attacks into two general groups and explain the solutions for each of the groups numerating the pros and cons of them. We will review the current external attacks solutions for the neighbor verification problem first and start with the early simple methods which tried to defeat the relaying attacks (like the wormhole one) using distance estimation methods. This family of protocols relied on time stamps which needed tight clock synchronization among the nodes and was quite impractical in distributed networks specially the sensor ones. After that, we introduce the descendants of that family of protocols which resolved the clock synchronization problem by using challenge-response-like methods.

Then, the recent efforts on formal description of the time-based and time- and location-based neighbor discovery protocols are explained. These researches led to the conclusion that time-based protocols can only secure the neighbor discovery under some strict conditions. Time- and location-based protocols are generally more secure than the time-based ones alone.

Next, we will argue why all of these protocols are vulnerable to the internal attacks and introduce other methods for defeating internal adversaries. Describing the mostly cryptographic solutions in this domain, we outline their pros and cons. As we will see, almost all of these protocols are either unable to resist the invasion of an internal adversary equipped with both powerful transmitter and sensitive receiver, or need an initial setup

phase in which the network is assumed to be secure. Adding the lack of mobility support to the specifications of this family of solutions, we move on to present our solution for a special type of internal attack which statistically tries to block the sensitive broadcasting internal adversary in mobile dense networks. This approach works based on the inherent characteristics of the dense networks and only the medium access control protocol parameters are changed. Therefore, it imposes a very low cost to the system to create higher levels of robustness.

At the end a conclusion is made which suggests combinational methods to be employed in the neighbor verification protocols to achieve an acceptable level of security against both the internal and external attackers.

1.1 Fundamental Concepts and Definitions

In wireless ad hoc networks, computers (nodes) are usually stand-alone entities working in cooperation with each other in order to fulfill a desired task (Rubinstein et al., 2006). In such networks, nodes are located centimeters to hundred meters away from each other but can communicate through their wireless transceivers.

Sensor networks can be thought to be a subgroup of ad hoc networks with some specific characteristics. They are usually deployed (densely) in an area to sense or monitor quantities of desired form (Akyildiz et al., 2002). For example in a battlefield, enemy movements can be detected and localized by a distributed sensor network. Unlike the ad hoc networks, the messages created by sensor nodes are always destined to be received by a single target named "Sink". The sensors cooperate to deliver the messages to the sink in a multi-hop manner.

The unattended nature of sensor networks and the high number of nodes creates some constraints for the designer. Each node must survive days or even years with a single source of power. Therefore, the protocols must not be too power consuming and should minimize both the amount of processing and the number of transmissions. The processing power and the amount of RAM¹ and ROM² of a sensor node are also quite limited. So, generally, designing a secure protocol is much harder in the sensor networks than in the ad hoc ones.

It is obvious that before a distributed cooperative network begins to work, nodes need to know their neighbors to form local structures. Any long-distance communication must be made in a multi-hop manner. The transmission radii of the nodes are limited and hence, each node should pass the messages to one/some of its neighbors in order to participate in the delivery of messages.

Neighbor discovery means determining whether a wireless device (node) is directly reachable without the assistance of any other device according to the predesigned rules of the network or not. Neighborhood can be unidirectional or bidirectional depending on whether only one side is able to deliver its messages to the other side or both sides are capable of doing so.

A neighbor-discovery attacker tries to deceptively convince the nodes to believe that they are neighbors of a specific set of nodes (possibly including the adversary herself), when they are actually not. There are various types of attacks on neighbor discovery scenarios. The effectiveness level of an attack depends on whether the adversary is a part of the network or

¹Random Access Memory

²Read-Only Memory

not. In the next sub-section, we make some definitions on adversaries' types and their level of capability.

1.2 Types and Capabilities of Adversaries

To describe the current solutions for the neighbor verification problem in the rest of this chapter better, we categorize them into two groups based on their resistance to internal (intrusive) or external (non-intrusive) attacks.

In external attacks the adversary is not able to compromise the nodes and hence, does not have access to the private information like the cryptographic keys and communication codes stored in the memory of the nodes whereas in the internal ones has (Khelladi et al., 2005).

Usually, an external attacker is only able to overhear (eavesdrop), relay (replay) or block (jam) the packets. On the other side, an internal attacker is capable of masquerading himself as a legal node and thus can imitate all the behaviors of a healthy node. Having the private cryptographic keys, she can even generate fake (but authenticated) messages to obtain a higher number of neighbors to what a traditional healthy node does. It is rather obvious that the second type of adversary is much more powerful than the first one.

1.3 Effective Attacks on Neighbor Discovery

In this part, we briefly introduce the currently known neighbor-discovery-related attacks in ad hoc and sensor networks. There are a few general attacks which have effects on neighbor discovery, and a few others which specifically address the neighbor-discovery-related issues.

One of the oldest external passive attacks is eavesdropping. Regardless of the protocol architecture, an adversary is always able to overhear wireless communications. There is little chance for the designer to block eavesdropping. However keyed cryptographic operators (like the encryption ones) are quite useful in keeping the external adversaries from extracting sensitive information out of the transmitted signal (Zhu et al., 2006)(Du et al., 2005)(Du et al., 2006). Neighbor discovery protocols are no exception. The protocol designer must seal the places where the information might leak during wireless transmissions.

The active invasions that target the availability of network services are called Denial of Service (DoS) attacks. DoS attacks can be planned to work on any layer of the network protocol stack depending on how much weak that layer is. Jamming can be well categorized into the physical layer DoS attacks group. There are only a few non-perfect classic solutions like spread spectrum communication for this attack (Pickholtz et al., 1982). Other types of DoS attack also exist among which some try to excessively overload a badly designed protocol run on a resource-limited machine (Djenouri et al., 2005). So, one can easily conclude that in sensor networks, designing a DoS-resilient neighbor discovery protocol is more complicated than in ad hoc networks. Ignoring the heuristic solutions, the classic countermeasures for protocol-related DoS attacks are easy-to-compute checksums and ciphers that reject massive fake messages.

Relaying and replaying are two other simple but powerful attacks (Papadimitratos et al., 2008). In the replay attack, an adversary uses an old packet which was previously generated by a healthy node in order to deceive another healthy node in the future. To overcome this problem researchers have suggested using timestamps (in clock-synchronized networks) and nonces (Du et al., 2006)(Shokri et al., 2008).

Relaying attacks are harder to detect. The adversary relays the healthy nodes' packets instantaneously (either at the physical layer or in a store-and-forward manner) in another part of the network. Wormhole attack is a well-known representative of this family. In the wormhole (tunneling) attack, two (or more) adversarial nodes try to transfer information through a dedicated channel between themselves and then use it in another part of the network (Hu et al., 2006). This attack can be implemented both by internal and external adversarial nodes. In the external form, they simply relay the packets either in a store-and-forward manner or instantaneously at the physical layer. In the internal form, they also have the opportunity to alter the packet contents intelligently before forwarding.

Every neighbor discovery protocol is composed of a series of packet transmissions. In a weak protocol, these attacks can be launched to relay neighbor discovery packets to other areas of the network, in order to convince distant nodes to believe that they are true neighbors. Figure 1 shows two healthy nodes *A* and *B*, and two adversarial nodes *C* and *D*. *A* and *B* cannot see each other directly since their transmission radii (shown with circles around them) are small compared to their distance. However, *C* and *D* can relay the neighbor-discovery-related packets to create a virtual link.

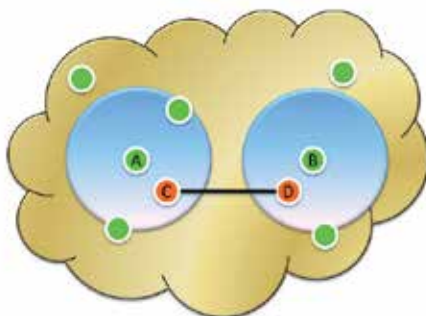


Fig. 1. The wormhole attack: Two adversarial nodes *C* and *D*, relay the packets between healthy nodes *A* and *B*, to deceptively convince them to believe that they are in the vicinity of each other

Hello flooding is a broadcast-type attack that was originally designed for sensor networks (Karlof et al., 2003). However, its concept can be adopted in the ad hoc networks too. Most of the neighbor discovery protocols (as well as the routing protocols) use a broadcasted packet called "Hello" or "Beacon" to announce a node's presence to its neighbors. Nodes receiving this message assume that the sending node is one of their neighbors. An internal attacker can launch a hello flooding attack by simply broadcasting the hello message with very high power. This way she tries to convince a lot of nodes that she is one of their neighbors and the victims add her to their table of neighbors. If the adversary is well equipped, she might even have a low noise sensitive receiver which enables her to receive distant weak signals and thus turn this attack into a bidirectional one. Figure 2. shows the adversarial and healthy transmission ranges.

This attack was initially designed for the internal attackers. However a simple repeater-like external adversary can also launch a similar attack through boosting a healthy node's transmission power and acting as a "man in the middle". Fortunately, as we will see, there are more solutions for the external threats than the internal ones.

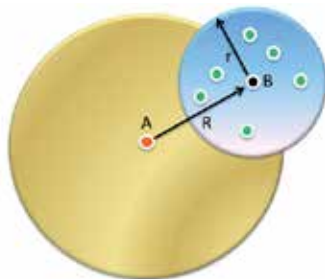


Fig. 2. A broadcast-type attack (hello flooding) diagram in a network with regular transmission range of r . The adversary (A) transmits messages with high power pretending to be a neighbor of B whereas she is actually R meters away ($R > r$)

Broadcast attacks can also be implemented in routing protocols in the route discovery phase (e.g. Routing Request (RREQ) message broadcasting) to shorten the adversary's path to the destination and thus putting her into most of the routes.

2. Neighbor Discovery External Attacks Countermeasures

If the maximum transmission range of a healthy node is r , then a secure neighbor discovery protocol must reject any claiming neighbor farther than this distance. The most challenging threat in designing externally resistant neighbor discovery protocols is the wormhole (or relaying) attack and the easiest way to block this attack is estimating the distance between the nodes.

The very early methods of neighbor verification relied on the round trip propagation time (RTT) measurement to estimate the approximate distance between two nodes and compare it with a maximum allowable value. Brands et al. were pioneers in using this method with their one-bit exchange proposal (Brands et al., 1993). The distance bounding method they proposed was a cryptographic protocol that put an upper-bound on the distance between two users (nodes for example) and did not let the protocol be manipulated. This scheme was able to resist man-in-the-middle like attacks, however, Singelee et al. later claimed that Brands' scheme is unable to stop what they called "terrorist fraud attack" which is an internal attack in our terminology (Singelee et al., 2005). After the introduction of distance bounding concept, similar protocols with names like "Echo protocol" (Sastry et al., 2003) appeared which were all based on the same basic idea of round trip time measurement.

In (Hu et al., 2003), to prevent wormhole attacks in ad hoc networks, a method called "packet leashes" was introduced and an idea similar to the signal trip delay measurement was repeated. The authors proposed two types of methods which could resist the (external) wormhole attacks: geographical leashes and temporal leashes. Geographical leashes fall into the category of time-and-location based protocols which we will introduce in the next parts. However, it does not actually use the timing data directly. It assumes that the sender sends its location (with the maximum relative error equal to δ) along with the timestamp showing the transmission time (with a maximum relative error of Δ). If the nodes move with a maximum speed of v , then this method gives an upper bound on the distance which is found by $d \leq ||loc_s - loc_r|| + 2v(t_r - t_s) + \delta$.

The authors also proposed a time-based approach which they called "temporal leashes". In this approach the transmission time is (authentically) written in the packet and the receiver

can then decide on the distance from the duration of signal flight. To authenticate the timestamp (and location in the previous part), digital signatures and the hash-chain-based (tree) authentication methods have been used. However the original idea comes from TESLA authentication method (Perrig et al., 2000).

Regardless of the protocol types, for both parties to be able to measure the distance, each must have the chance to challenge the other. So, at least three messages must be exchanged. For unidirectional neighbor discovery, exchanging two messages suffices (Sayad et al., 2008). Korkmaz addressed the RTT measurement, focusing on the difference of signal propagation speed in the healthy nodes and adversaries' channels (Korkmaz, 2005). In this method, a combination of power and delay-related criteria has been used. The simplified diagram of Korkmaz protocol is depicted in Figure 3. Here, "M" is an authenticated request message and "ACK" is its reply containing P_{r_m} , P_{t_a} and $t'_{t_a} - t'_{r_m}$ which is the processing delay in B.

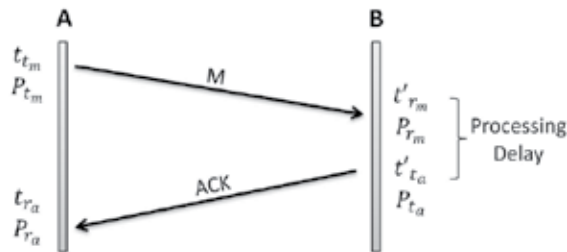


Fig. 3. Korkmaz's neighbor discovery protocol

If the worst case signal propagation speed between two nodes with distance R is s , and the maximum speed of signal propagation in the adversaries' media is v_{adv} ($v_{adv} > s$), then the upper and lower bound estimates of the RTT are found as $[\frac{2R}{v_{adv}}, \frac{2R}{s}]$. Any claiming neighbor with measured RTT lower than $\frac{2R}{v_{adv}}$ is accepted while anyone with a RTT larger than $\frac{2R}{s}$ is rejected. Not all the measurements which fall in this interval are accepted. If the actual speed of signal propagation in the network is x , then Korkmaz proposes using a hard decision making threshold for the RTT samples falling in the abovementioned interval. The following formula normalizes the measured RTT.

$$\epsilon_c = \frac{\frac{2R}{s} - RTT}{\frac{2R}{s} - \frac{2R}{v_{adv}}} \tag{1}$$

The hard decision making threshold is the acceptable level of confidence i.e. for $\epsilon_c \geq L_c$ we assume that the two nodes are neighbors and for $\epsilon_c \leq L_c$ we assume they are not. This threshold is equivalent to an effective distance $R_{eff} = x(1/s - L_c(1/s - 1/c))R$. Obviously, this distance can be either smaller or larger than R . So this type of decision making is always prone to either rejecting correct neighbors or accepting some incorrect ones which opens a vulnerability window for the system. To mitigate this flaw, Korkmaz proposed to combine the RTT-measurement-based method with a power-measurement-based one. Generally, the relationship between the distance, transmitted and received signal strengths is:

$$d = k \left(\frac{P_t}{P_r} \right)^{n-1} \tag{2}$$

where k and n are constants and are determined by the characteristics of channel and communicating devices. Since the ACK message contains the measured power fields, A can easily compute the distance (d) using equation (2). However, since k and n fluctuate in the real world scenarios it is proposed to verify the following equilibrium instead:

$$\frac{P_{tm}}{P_{rm}} = \frac{P_{ta}}{P_{ra}} \quad (3)$$

Korkmaz claims that if the nodes are not actual neighbors i.e. they communicate through relaying adversaries, then the values of P_{rm} and P_{ra} will be altered depending on the transmission power used during relaying and the distance between the adversaries and legitimate nodes, and hence, the above equilibrium does not hold. However, it can be easily verified that if the relaying adversaries collaborate with each other, this countermeasure is easily neutralized. For example in Figure 1, if C tells D to send the signal received from A , to B with the same power she received (and vice versa), then eq. (2) is satisfied. Also it should be emphasized that this method only addresses probabilistic security facing external attacks. Obviously B , as an internal attacker can deceive A if she lies about the processing time.

As an alternative approach, a few authors suggested searching for graph abnormalities to detect the relaying attackers either in a distributed or centralized manner. Maheshwari et al. proposed a distributed geometrical algorithm to search for graph abnormalities in wireless networks (Maheshwari et al., 2007). The core idea of their work was to find impossible cases which do not occur in healthy graphs. If two nodes are claimed not to be neighbors then the number of their independent neighbors (those neighbors of the two nodes who cannot see each other) is quite limited. For example consider Figure 4 in which two healthy nodes a and b are at their farthest possible range of neighborhood. In this case, the nodes which are considered to be neighbors of both of them can only be found in the intersection of the two coverage areas (the hatched area). Mashewari et al. have proved that no more than two independent neighbors can be found in the hatched area in this case. So if a third common neighbor comes in, then it must be covered by one of the previous common neighbors. The number of independent common neighbors decreases even more when the two nodes further move away from each other. So if the adversaries launch a wormhole attack like the one in Figure 5, then two independent nodes a and b which are far from each other, will have three common independent neighbors e , f and g and according to the argument we made there can be no more than two common independent neighbors in this case and hence, a fraud has been detected.

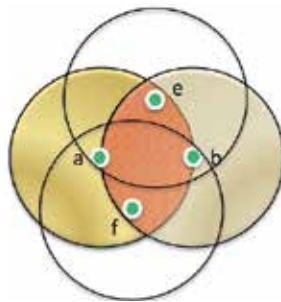


Fig. 4. Mashewari et al.'s diagram to demonstrate the maximum number of independent common neighbors of two nearly independent nodes

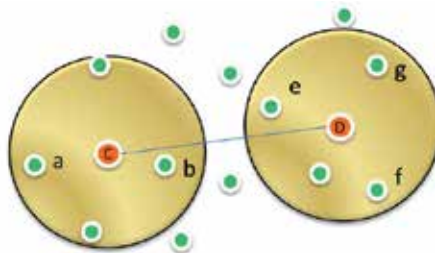


Fig. 5. A sample wormhole attack which is detected by Mashewari et al.'s forbidden structure search

However this was a simple example and the authors have extended this one-hop graph-based idea to a k-hop one to obtain a higher wormhole attack detection probability.

In a combined work of distance measurement and graph abnormality detection, Shokri et al. proposed what they called a practical secure neighbor verification protocol for sensor networks (Shokri et al., 2008). The core idea of their measurement part contribution relies on having two different transceivers (one Radio Frequency (RF) and one Ultra Sonic (US)) which is a bit similar to the echo protocol approach (Sastry et al., 2003). Since the sensors have simple processors of microsecond clock precision, the RF transceiver is used for clock synchronization-like purposes (or simply measuring the difference of time). Distance measurement with RF signals requires a nanosecond clock precision. So the RTT measurement (and consequently the distance measurement) is done more accurately using the slow-propagating US signals with the precision at hand.

This method is actually composed of three smaller sub-protocols. Assuming that all pairs of the nodes already have a symmetric shared key (like K_{AB} between A and B), each initiating node A , sends a request message to (arbitrary) node B over the RF channel. B replies to this request with another message. Then A broadcasts a message through its ultrasonic transmitter to reveal its nonce whose hash was previously sent at the request transmission phase. This is similar to the delayed authentication methods (like TESLA method (Perrig et al., 2000)) which bind the authenticity of the next step to the previous one. At last an ACK is sent to each of the candidates (like B). The whole message exchange of sub-protocol 1 is depicted in Figure 6. Notice that $E_K(\cdot)$ denotes an encryption with key K , and N_{AB} and N_A are two nonces. $MAC_K\{\cdot\}$ means that the whole message is protected with a message authentication code under key K . Node B 's side times are measured with its own clock which is not necessarily synchronized with A . At the end of this phase, B can compute its distance to A using $\hat{d}_{AB} = s \cdot [t'_{rng,B} - t_{rng,A} - (t'_{req,B} - t_{req,A})]$ where s is the speed of slowly propagating ultrasonic signal.

After this stage, the nodes exchange their local table of distances as the second step of the protocol so that each obtains a local view of the network topology. At the third stage, each node starts to run a series of tests on the information obtained in the previous stages. First of all, a node eliminates those links with distances outside the acceptable range. Second, the symmetry of the links is verified meaning that an arbitrary node A checks the $d_{AB} = d_{BA}$ equality for any candidate B . Third, for any claiming neighbor, the testing node tries to find two other candidates in the table and then, knowing the distances between them, it assumes hypothetical (but wisely selected) positions for these three candidates so that the triangular inequalities hold for each possible set of three nodes (including itself). At last, it verifies

whether the four nodes form a convex quadrilateral³ or not. The authors have shown that the above criteria, prevent wormhole attacks with two colluding adversaries and also resist well facing wormhole attacks with more than two adversaries.

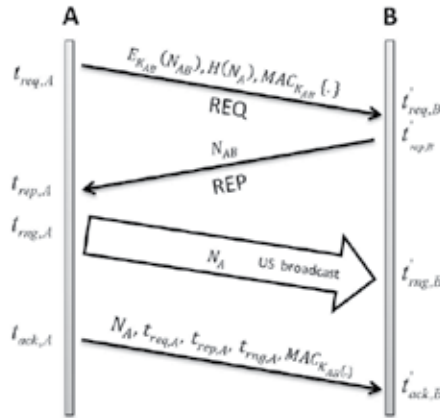


Fig. 6. The sub-protocol 1 (distance measurement) of Shokri et al.'s method

Although Shokri's protocol has novel contributions and combined many ideas like delayed authentication and geometrical tests, it suffers from some design flaws. In an infrastructureless wireless network, neighbor discovery is the first protocol which is run i.e. there is no information about the existence of the nearby nodes prior to starting the protocol. So there are no agreed mutual cryptographic keys and hence *A* cannot send authenticated messages to a node like *B* which is not even known to be in its vicinity. Sensor nodes are extremely resource-limited devices and in a network with thousands of sensors, it is practically impossible to store a large number of symmetric keys in a node's memory and this has been a challenging security problem thus far (Chan et al., 2003)(Du et al., 2005)(Zhu et al., 2003 & 2006). Using LEAP (Zhu et al., 2003) or LEAP+-like (Zhu et al., 2006) key distribution methods selected by the authors, is problematic since these protocols themselves have neighbor discovery protocols in their initial setup phase and static networks do not need multiple-time independent neighbor discoveries. Besides, LEAP+ itself is capable of blocking wormhole attacks after the key establishment phase. With a rather high number of message transmissions (which includes the hidden stage of table exchanges) and a high number of link verification computations, this solution is not very energy conserving. Also the use of two transceivers (RF and US) is in contradiction to the basic assumption in sensor networks design which is cost effectiveness. It should be mentioned that this protocol is unidirectional in our terminology and is designed to prevent external wormhole attacks in static networks, thus has limited functionality facing internal attackers and also in highly mobile networks. However, compared to the older centralized approaches for graph abnormality detection (Rasmussen et al., 2007), both of the abovementioned distributed approaches are valuable.

³A convex quadrilateral with four vertexes *A*, *B*, *C* and *D* is characterized by $(\overrightarrow{AB} \times \overrightarrow{BC})(\overrightarrow{BC} \times \overrightarrow{CD})(\overrightarrow{CD} \times \overrightarrow{DA})(\overrightarrow{DA} \times \overrightarrow{AB}) > 0$

Poturalski et al., in a series of evolutionary papers and technical reports, tried to classify neighbor discovery protocols into two generic time-based and time-and-location-based classes and provide systematic rules to formally verify the security of these protocols against external attacks (Poturalski et al., 2007) (Poturalski et al., 2008). In their initial technical report, they formally derived a so-called impossibility result for the time-based neighbor discovery protocols stating that it is impossible for a neighbor discovery protocol which solely relies on signal propagation time measurements to provide seamless security (Poturalski et al., 2007). Figure 7 demonstrates the “impossibility result” informally. If the maximum allowable distance of two healthy neighbors is r , then the maximum signal travel time would be r/s where s is the speed of signal propagation in the channel. If two nodes cannot reach each other directly, either due to a large distance (Figure 7c) or a barrier (Figure 7b) then one or more relaying adversaries can deliver the messages and as long as the time of signal flight is less than r/s , this relay will not be detected. However, if the imposed delay of a relay is more than r/s (i.e. $\Delta_{relay} > r/s$) then time-based protocols can become secure. It is also shown that designing secure time-and-location based protocols is possible since the receiving nodes have the sender’s location (in an authentic manner carried by the message) and compute the valid distance themselves and then compare it with the one obtained from time measurements to detect probable attacks.

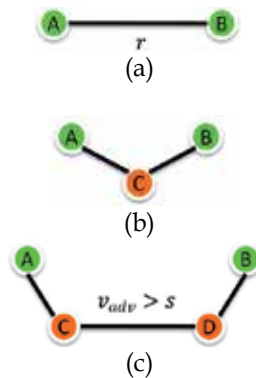


Fig. 7. There is no possibility for B (or A) to always distinguish between these three paths in a propagation time measuring protocol as long as the propagation delay does not exceed r/s . v_{adv} is the signal propagation speed in the adversaries’ channel which is higher than s .

Later, each of the two classes of protocols proposed by Poturalski et al., was divided into two groups; Beacon (B) and Challenge/Response (CR) protocols (Poturalski et al., 2008). In B-protocols, a node broadcasts some information without having the response of the other side. The receivers are supposed to add the sender to their list of neighbors after some processing and hence, this method is unidirectional. On the other side, CR-protocols support the minimum three-phase message exchange requirement for a bidirectional neighbor discovery. However the samples the authors have mentioned for the CR protocols are not really bidirectional (although they could be as in their original framework). In Poturalski’s examples, CR protocols create the chance of challenge for one side only, and all the other nodes must run the same protocol themselves to complete the neighbor discovery task.

The authors claimed a secure neighbor discovery protocol is characterized with two properties: “correctness” i.e. if the protocol declares two nodes neighbors at some time, they must indeed be neighbors at that time, and “availability” meaning that if two nodes remain neighbors for some time (T_P) then the protocol must detect this neighborhood.

They defined seven types of events to describe their rules and protocols with. Table 1 summarizes six of them which we will deal with, along with their description.

Receive(A;t;m)	A receives the first bit of message m at t
Bcast(A;t;m)	A broadcasts message m at t
Fresh(A;t;n)	Nonce n is freshly generated by A at t
Neighbor(A;t;B;C;t')	At t , A declares B has been a neighbor of C at t' (unidirectional)
NDstart(A;t)	A starts a neighbor discovery with all the nodes at t
NDstart(A;t;B)	A starts a neighbor discovery with B at t

Table 1. Some of the events symbols and their description in Poturalski et al.’s literature.

Based on these definitions, they formally defined security requirements for the four possible groups of neighbor discovery protocols and presented a sample pseudo-code for each group satisfying those set of requirements. To unify the demonstrations, we have converted the codes to message diagrams. Figure 8 and Figure 9 show Poturalski’s sample protocols for beacon time-based (B/T) and beacon time and location-based (B/TL) neighbor discovery protocols respectively. In Figure 10 and Figure 11, challenge-response versions of these protocols are depicted. Notice that some of the messages in these figures are actually intended to be received by a single node. However to comply with the broadcast-type message transmission symbol shown in Table 1 (and in the pseudo codes), they are drawn with broadcast-like arrows.

In all of these figures, $len\{\cdot\}$ stands for an operator giving the length of a message transmission (in seconds for example), r is a node regular transmission range and s is the signal propagation speed in the network communication channel.

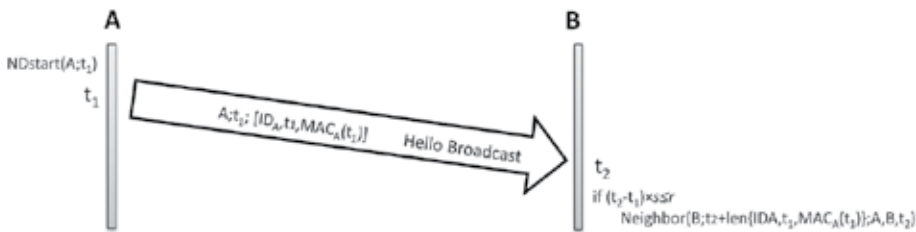


Fig. 8. A beacon and time-based protocol pseudo code (B/T)

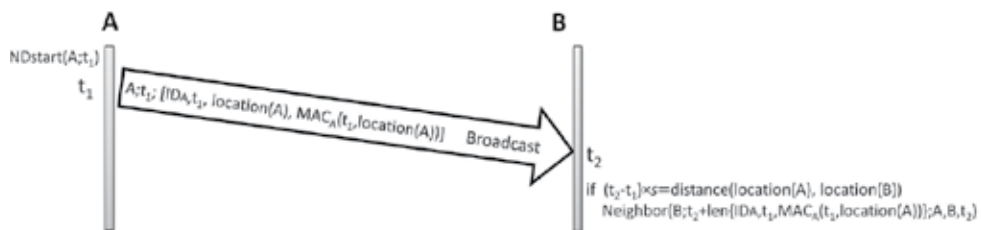


Fig. 9. A beacon and time-and-location-based protocol pseudo code (B/TL)

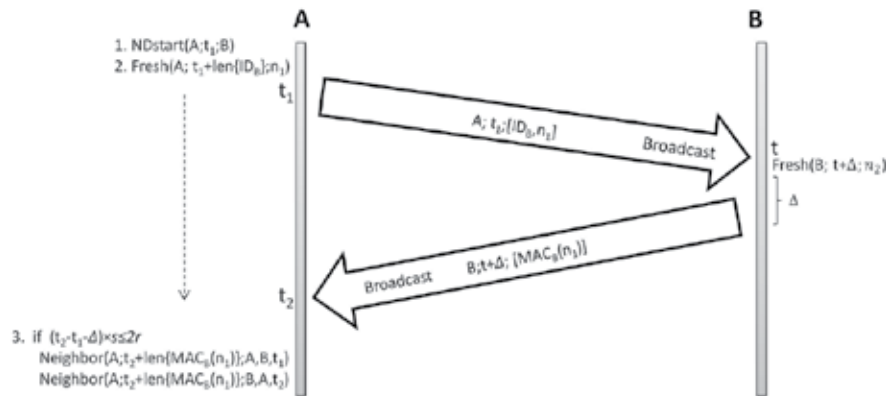


Fig. 10. A challenge-response time-based protocol pseudo code (CR/T)

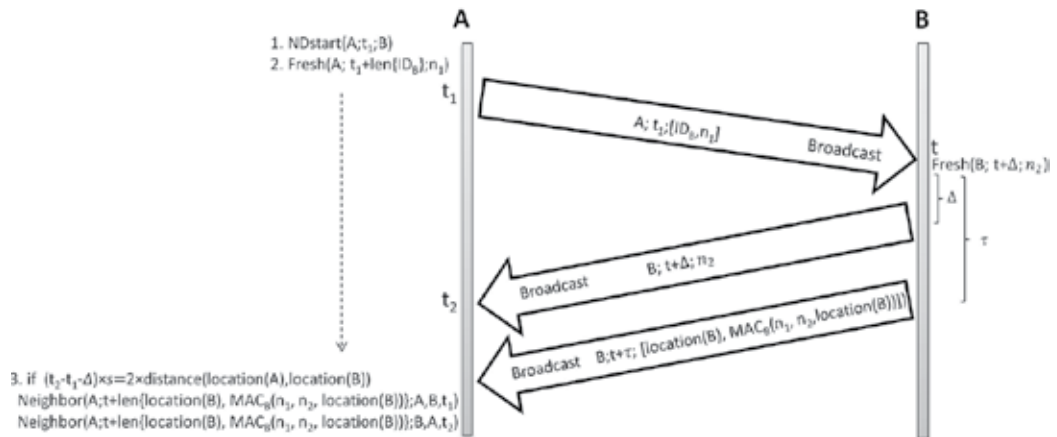


Fig. 11. A challenge-response time-and-location-based protocol pseudo code (CR/TL)

As we described in the previous parts, if there are no challenges and responses the adversaries can easily relay the broadcasted beacon packets to other parts of the network. Also notice that the protocols times are written from a third-party's point of view. In practice, B and A have time synchronization problems too, which even widens the vulnerability window more in beacon-based protocols.

In all of these sample protocols, nodes need to verify the authentication codes attached to the end of messages which in turn makes the protocols dependent on another key distribution protocol (involving either storage of all the keys in the memory of the nodes that makes it only suitable for ad hoc networks or employment of a key agreement protocol which inherently needs a neighbor discovery protocol itself).

Regardless of these practical issues, each of these simplified representatives of neighbor discovery protocols has been proven to satisfy Poturalski's mathematical security requirements under some specific conditions. Beacon time-based (B/T) protocols are secure if the adversary's relaying delay is greater than or equal to $r \cdot s^{-1}$. This is a rather obvious constraint since with less than this bound, the adversary can relay some messages without adding too much delay and keep the overall propagation and relaying delays below the acceptable threshold $r \cdot s^{-1}$ (refer to Figure 7). It can also be verified that the availability

property is also satisfied with $T_{pB/T} = \text{len}\{\text{ID}_A, t, \text{MAC}_A(t)\} + r \cdot s^{-1}$ i.e. if two nodes remain neighbors for this amount of time (and the B/T neighbor discovery is started) then, this neighborhood will be definitely detected by the protocol. Similarly, for a TL protocol to be secure, the designer must take a communication media whose signal propagation speed is close to the maximum possible speed in an adversary's channel (or simply the light speed ($s=c=v_{adv}$)). If less than this speed is used (i.e. $v_{adv} > s$), even though A has both B 's and its own locations, a pair of adversaries can simply launch the wormhole attack keeping the overall RTT equal to $2 \times \text{distance}(A,B)/s$ which is sufficient to satisfy the protocol criterion. The security conditions of other protocols can be found similarly. Table 2 summarizes the conditions under which each of the four groups of neighbor discovery protocols is secure.

Protocol Type	Security Constraints Applied
B/T	<ol style="list-style-type: none"> 1. $\Delta_{relay} \geq r \cdot s^{-1}$ 2. $T_{pB/T} = \text{len}\{\text{ID}_A, t, \text{MAC}_A(t)\} + r \cdot s^{-1}$
CR/T	<ol style="list-style-type: none"> 1. $\Delta_{relay} \geq 2r \cdot s^{-1}$ 2. $T_{pCR/T} = \text{len}\{\text{ID}_B, n\} + \text{len}\{\text{MAC}_B(n)\} + 2r \cdot s^{-1}$
B/TL	<ol style="list-style-type: none"> 1. $\Delta_{relay} \geq 0$ 2. $s = v_{adv}$
CR/TL	<ol style="list-style-type: none"> 3. $T_{pCR/TL} = \infty$ (depending on distance)

Table 2. Conditions for each class of neighbor discovery protocols to support Poturalski's formal description of security requirements

We investigated some of the main external-attack-related researches and the positive and negative aspects of them in this section. In the next section we focus on the internal attacks' countermeasures which are different from the previous methods in nature and mostly are cryptographic solutions.

3. Neighbor Discovery Internal Attacks Countermeasures

There are a few internal attacks affecting the performance of neighbor discovery protocols. Needless to say some of the external attacks have the internal form too. For example, in a wormhole attack, two internal relaying adversaries can even alternate the packet contents in order to deceive healthy entities. Unfortunately compared to the external attacks described in the previous section, the number of these attacks is not limited at all. This is because these attacks are more related to the protocol-specific features than the nature of neighbor discovery. As there are many variants for each neighbor discovery protocol family, the internal attacks are also numerous. However, there are a few common attacks that can conceptually cover some of these threats, and, among them, broadcast attacks are more outstanding.

Almost all the algorithms which use a broadcasted data are susceptible to being invaded by the broadcast-type attackers. In the sensor networks hello flooding case, a loud advertisement can convince many surrounding nodes that the adversary is one of their neighbors. This attack can be launched in the routing algorithms too e.g. the adversary can rebroadcast the received RREQ packet with high power to be a part of the best routes to the destination with a high probability. Notice that unlike the previous part, in internal attacks,

the adversary is a legitimate node i.e. a node is captured and compromised by an adversary and all of its cryptographic keys and private information are known to the adversaries.

Broadcast attacks had been previously addressed with different names somewhat but Karlof and Wagner were the first who introduced this attack specially in sensor networks (Karlof et al., 2003). Consider a simple form of neighbor discovery in which a well-equipped internal (legitimate) adversary tries to broadcast a packet called hello (beacon) and every node that hears this packet adds the sender to its neighbors list. Since one side of the protocol which sends the authenticated messages is adversary herself, it is impossible to rely on either time or location information given by the other party. So generally to defeat an internal attacker every node must rely on its own data. The same argument holds true for the CR protocols. If the adversary gives false (but authenticated) location information to the other party, then colluding with other relaying adversaries she can easily bypass the normal security checkpoints.

As a solution for the broadcast-type attacks, Karlof et al. proposed to verify bidirectionality of the links (Karlof et al., 2003). They assumed that the adversary has a high-power transmitter but an ordinary receiver and thus is unable to capture distant weak signals. If the receiver (*B*) sends valuable information in reply to the broadcasted message (hello), on which the adversary (*A*) must rely for future communications, then she will be defeated since she cannot hear *B*. The initial raw idea of verifying bidirectionality of the links was not developed much by the authors, however, it was mentioned that this countermeasure is useless if the adversary has both a high-power transmitter and a sensitive receiver.

In sensor networks, some authors then tried to limit the nodes communication ranges through cryptographic methods (Du et al., 2005)(Lin et al., 2005)(Zhu et al., 2006). The early methods, tried to pre-load a large number of pairwise keys in each node's memory (key pre-distribution). But for sensor networks, this was an impractical solution since the amount of memory each sensor has is quite limited. Probabilistic key pre-distribution schemes were proposed to solve this problem. In these methods, after the deployment, every node tries to find some common keys with its neighbors through a so-called mutual key discovery protocol (Eschenauer et al., 2002). However these solutions had problems too. The common key discovery was itself another protocol which was needed to be secured. Besides probabilistic approaches do not always guarantee providing a common key. So another approach was adopted which was letting the nodes themselves establish the keys after deployment (Lin et al., 2005)(Zhu et al., 2006). This implies the use of a negotiation protocol between the nodes when they are deployed. It is rather obvious that to protect these negotiations against external attackers the messages must be encrypted with some key and since the mutual keys are not known at this phase yet, usually a pre-loaded global key is used.

A general assumption made by these methods is that compromising a node takes time but to stop an attacker who can capture and compromise the nodes, the whole negotiation should not take more than T_{\min} seconds. To prevent further attacks, nodes themselves delete the global key from their memory after T_{\min} seconds.

Secure Cell Relay (SCR) is one of the distributed key establishment/routing protocols which resists broadcast attacks (Lin et al. 2005)(Du et al., 2006). It uses a three-way handshake protocol to avoid the unidirectional link problem. There are two versions of this protocol but the most recent one in which the location information has also been used is depicted in

Figure 12. In this figure, K is the global shared key, E_K the encrypting operator, and N_0 is a nonce. K_B^b is defined as the B 's broadcast key and K_{AB} is the private key between A and B used for later communications. At the end of this process, B adds A to its neighbors list and stores K_{AB} and K_B^b in a table for the future. After completion of the protocol for every node, all the nodes delete the global key from their memory.

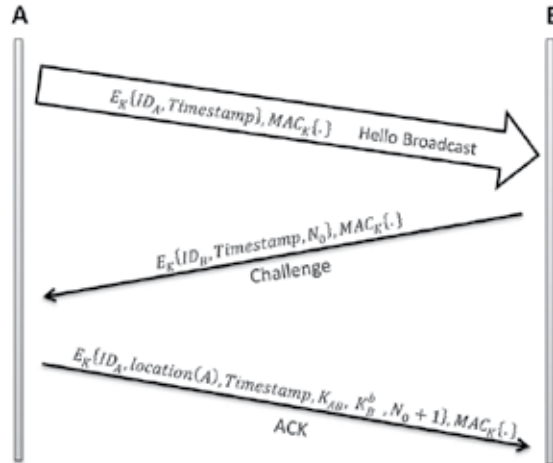


Fig. 12. Secure Cell Relay (SCR) neighbor discovery protocol message diagram

But SCR neighbor discovery protocol is weak in many aspects. The use of time stamps forces the designer to somehow maintain a synchronized clock which is problematic in distributed networks. Besides with a good design, in a three-phase message exchange protocol, both nodes can add each other to their neighbors list because both of the parties had the chance to challenge the other one. However, SCR messages need to be modified to provide this feature. Also notice that after erasing the global key K , there is no chance for a node to update its neighbors list. This property makes the protocol unsuitable for mobile scenarios. LEAP (Zhu et al., 2003) and then LEAP+ (Zhu et al., 2006) are key distribution protocols for sensor networks which also block the broadcasting adversary. The main goal of LEAP+ was to create four sets of keys for each node; one set of pairwise keys for inter-neighbor communications, one key for local broadcasting, one globally-shared network key and one key to communicate with the sink. As the local broadcast key is made from the local pairwise keys and dealing with the attack the two others are not needed, we only focus on the construction of pairwise keys.

Here again the assumption of an adversary-free immune network after the initial deployment is necessary. So we assume that for an interval which is at least T_{\min} seconds there is no internal attacker present in the network. To prevent external attacks during this period, there is a globally shared key pre-loaded into memory of the nodes.

If f_k is a one-way keyed pseudo-random function (like encryption operators) with key k , then the pairwise key construction in LEAP+ can be summarized as shown in Figure 13.

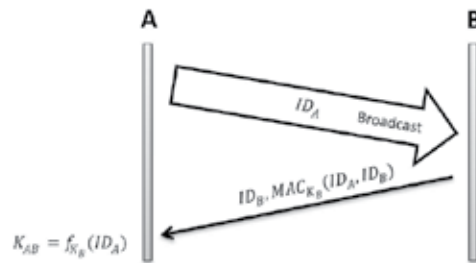


Fig. 13. The simplified form of key establishment in LEAP+ protocol at the initial deployment phase

"A" finds the pairwise key by computing $K_{AB} = f_{K_B}(ID_A)$ where K_B is found by applying the global key to the one-way function with B's ID as the input argument ($K_B = f_K(ID_B)$). Once this process is done for every node, the global key is erased from the memory along with K_B . After the pairwise key establishment phase, all the communications are done in an encrypted manner with the previously generated keys. Since the adversary is supposed to capture a node not sooner than T_{min} seconds, she is unable to send meaningful messages to nodes farther than the communication range of a normal node. So, broadcast attacks are thwarted this way. Also, the adversary cannot make new pairwise keys anymore since the required global key is missing in the memory of the captured node.

Although this protocol performs well in terms of resource consumption and complexity, it has drawbacks too. A closer look at the protocol reveals that B's presence in this challenge-response-like protocol is not as strong as it should be. The only role of B is announcing its presence by sending back its ID. It does not even generate any random number to maintain the freshness of the key. Although it has been assumed that the network is devoid of any internal adversaries for at least T_{min} seconds (since for example it takes at least T_{min} seconds to intrude into a tamper-resistant device memory), this is not a valid assumption for the external ones. If external adversaries are present before the nodes deployment, they are able to launch relay-based attacks which simply means, in the above protocol, B could be a relayed distant node. After T_{min} seconds, the adversary intrudes into A's memory and at the end, she has a large-range communication capability for which she had planned before. It is also obvious that due to the erasure of the global key after T_{min} seconds, nodes are unable to restart the neighbor discovery protocol in the future and thus, this protocol does not support mobility. Any mobility-supporting security framework must allow periodical updates of the neighbors list. This implicitly involves participation of either time or a random number (nonce) in the protocol to block replay attacks. The authors have virtually limited the range one node can communicate in, through cryptographic methods. With the erasure of global key (and the static network the authors assumed) the probable future neighbor discoveries are limited to the detection of lost connections due to power depletions or failures.

In (Sayad et al., 2008), as an alternative solution, especially in sensor networks in which broadcast attacks are more devastating, we proposed a probabilistic robust design framework for the internal broadcast attacks which has a very low complexity and can even be combined with any other secure neighbor discovery protocol. To define a probabilistic robustness, we shall first differentiate three general attack profiles.

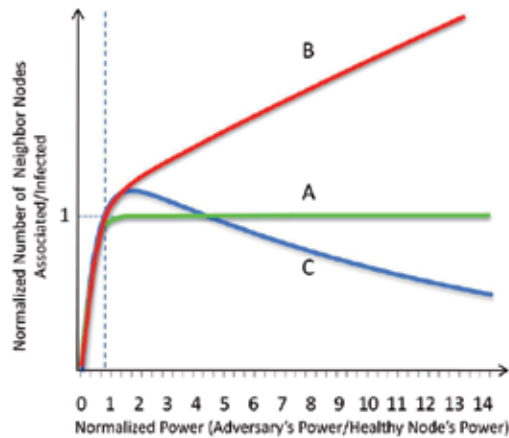


Fig. 14. (A) An optimal secure neighbor discovery protocol broadcast attack profile (B) An unprotected neighbor discovery protocol broadcast attack profile (C) A broadcast attack-resilient neighbor discovery profile

As shown in Figure 14., facing broadcast-type attacks, the behavior of neighbor discovery protocols can be categorized into three different profiles. When the transmission power of a node or sensor increases, the number of neighbors is also increased (conforming with the different transmission ranges nodes have based on their available power resources), but if the power of a node goes beyond a threshold corresponding to the maximum allowable transmission range, then these three family of protocols behave differently. Regarding the broadcast attacks, type A profile is the desired optimal secure neighbor discovery protocol i.e. if an adversary tries to increase her power in order to obtain more neighbors, she will not succeed. Complex cryptographic solutions may be put in this group.

Type B profile shows the performance of an unprotected neighbor discovery protocol. The adversary's payoff increases as its power goes up. In type C which is actually the focus of our work, the maximum payoff (possible number of neighbors) of the adversary is not as low as an optimal secure solution but definitely bounded. In this approach, the designer tries to simplify the protocol in expense of losing some (but not all) of the security. This is a general framework however and the amount of penalty paid for simplicity depends on the designer's approach. It is worth mentioning that the initial parts of all these three profiles are similar, because as long as an adversary's behavior falls in the class of healthy nodes' behavior, she receives the same amount of payoff as a normal node does. So, there is no instant solution which can decrease the payoff of an internal adversary to less than that of a healthy node.

We propose that one can wisely manipulate Medium Access Control (MAC) protocol parameters to achieve a type-C resistivity against broadcast attacks in sensor networks without consuming too much energy. In a compromised network, when an adversary that is equipped with both powerful transmitter and sensitive receiver, broadcasts a hello-like request or beacon (hello flooding), a lot of nodes receive it almost simultaneously. In a two (or more) way handshake protocol, these nodes will start to compete to grab the channel and send the reply messages in order to announce their presence. Healthy nodes have small transmission and reception ranges. Therefore, roughly speaking, those nodes located farther than the carrier sense range of each other will try to send the reply messages back almost

simultaneously. The main idea is to tune the channel access and transmission parameters so that the responses of these distant nodes collide with each other at the adversary's receiver due to the high density in arrival. If these reply messages contain valuable information which is vital for future communications, then as the adversary is unable to decode the reply messages correctly, she is obliged to reduce her power. This is somehow similar to the well-known hidden node effect in wireless ad hoc networks. Figure 15. shows the attacker and sample distant nodes colonies along with their corresponding transmission ranges.

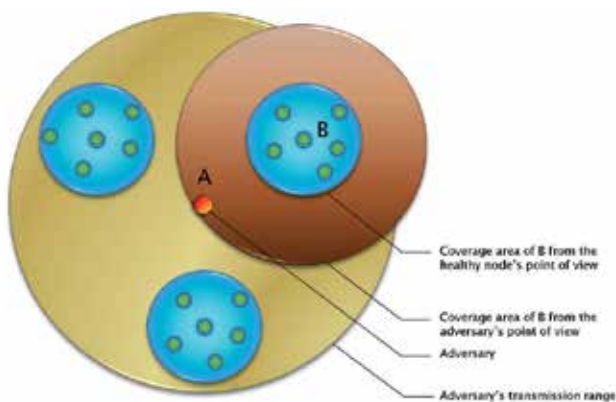


Fig. 15. Transmission ranges of normal and adversary nodes in Sayad et al.'s framework. Adversary's high transmission power attracts many healthy nodes. However, far healthy nodes do not see each other and hence start to transmit reply packets simultaneously

As in the neighbor discovery phase no infrastructure is already formed, a random channel accessing method is preferred. So one can expect that this approach would be a probabilistic one at the end. Although the design framework introduced is quite general, we give an instance protocol in which the notion of important information delivery in the reply packets transmission phase is contrived. The sample protocol in Figure 16 tries to establish a mutual key between the two nodes using Diffie-Hellman key agreement protocol (Diffie & Hellman, 1976) while following the framework rules.

It should be noticed that neighbor discovery message collisions must be minimized in a healthy scenario i.e. since the only difference between healthy and adversary nodes is their transmission ranges, high-colluding protocol design for the adversary might also affect the normal behavior of the network and this is to be avoided. In our example, this leads to a trade-off problem.

To make a demonstration of the above proposal's efficiency, for channel accessing, IEEE 802.15.4 WPAN standard was chosen (IEEE 802.15.4, 2006). However, some modifications were made to the protocol to adapt its neighbor discovery to the classic three-phase type, and the minimum and maximum back-off exponents were considered as the parameters to be tuned. With a node distribution density of 0.01 (1 node in 100m²), the attack profile for different values of the minimum back-off exponent is shown in Figure 17.

As it can be clearly seen, this method behaves like a type-C attack-resistant protocol. With the maximum back-off exponent set to eight and the identical reply packets which were seven back-off periods long, the minimum back-off exponent was swept. With this configuration, the adversary's payoff increases as the minimum back-off exponent goes up.

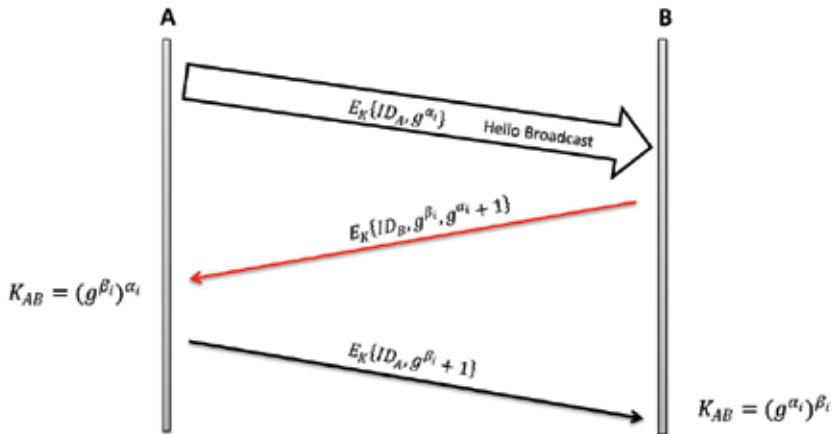


Fig. 16. An example of Sayad et al.’s framework. Reply message includes a part of the common key which will be used for future communications

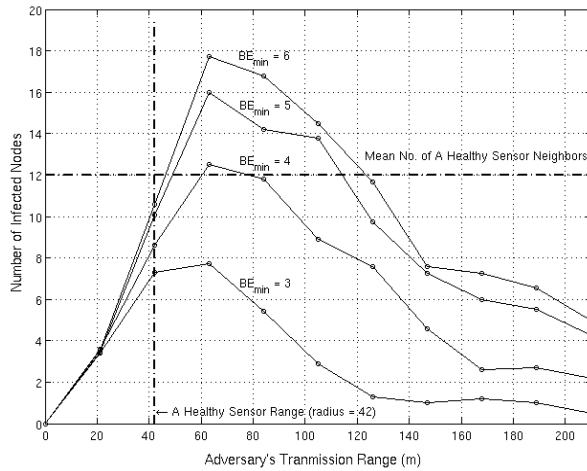


Fig. 17. The broadcast attack profiles on Sayad et al.’s sample protocol. The adversary receives a negative feedback from the network in response to her greediness in obtaining more neighbors

Notice that we also have to keep the healthy neighbor discovery scenario as intact as possible i.e. any profile closer to the intersection of the mean number of a healthy node’s neighbors line and the normal transmission range line is preferred. With a high minimum back-off exponent, the profile approaches the ideal point for healthy scenarios, however, the maximum (but still restricted) payoff of the adversary is also increased. Now it is up to the network designer to set how much security (with respect to the broadcast attacks) should be sacrificed for sake of gaining more efficiency.

The abovementioned design framework is a concept which can be freely combined with the other neighbor discovery protocols and since it has a very low cost, is quite applicable in resource-limited sensor networks. Unlike the cryptographic methods (and many other

described protocols), this framework supports (high) mobility of the nodes. Besides, in this approach, the limiting assumption about the initial adversary-free period of the network operation at the time of nodes deployment has been removed.

4. Conclusion

In this chapter, we introduced many of the current threats and solutions for the neighbor discovery problem in wireless ad hoc and sensor networks. Separating the attacks into internal and external ones, depending on how much the protocols are resistant to each of these attacks, we categorized them into two groups as well.

Many of the current solutions focus on the external relay-based attacks while little effort has been made to mitigate the internal attackers' damage. Most of the current solutions for the internal attacks are cryptographic which are either resource consuming or do not support mobility.

Numerating all the solutions, we proposed a probabilistic countermeasure for the internal broadcast attacks. It is obvious that combinational attacks require combinational solutions. Our design framework for the internal broadcast attacks can be combined with nearly all the other solutions to provide higher levels of security facing both internal and external attacks.

Acknowledgement

This work has been financially supported by Iran Telecommunication Research Center (ITRC). The authors also wish to thank Prof. Vijay Varadharajan from Macquarie University and Alireza Mohammadi-nodooshan from K.N.Toosi University of Technology for their scientific support.

5. References

- Akyildiz, F.; Ian, W.S., Sankarasubramaniam, Y. and Cayirci, E. (2002). A survey on sensor networks, *IEEE Communication Magazine*, vol. 40, Aug. 2002., pp. 102-114
- Brands, S.; Chaum, D. (1993). Distance-bounding protocols, *Proceedings of Eurocrypt '93: Workshop on the theory and application of cryptographic techniques on Advances in cryptology*, pp. 344-360, May 1993, Springer
- Chan, H. ; Perrig, A. & Song, D. (2003). *Random key predistribution schemes for sensor networks*, *Proceedings of IEEE Security and Privacy Symposium*, pp. 197-213, 2003
- Diffie, W.; Hellman, M.E. (1976). New directions in cryptography, *IEEE Transactions on Information Theory*, vol. 22, No.6, Nov. 1976, pp. 644-654
- Djenouri, D.; Khelladi, L., Jamel, D. and Badache, N. (2005). A survey of security issues in wireless ad hoc and sensor networks, *IEEE Communication Surveys*, vol. 7, 4th quarter 2005, pp. 2-28
- Du, W.; Deng, J., Han, W.S., Varshney, P.K., Katz, J., Khalili, A. (2005). *A pairwise key predistribution scheme for wireless sensor networks*. ACM Transactions on Information and System Security (TISSEC), 2005 , pp. 228-258, 2005, ACM Press
- Du, X. ; Xiao, Y., Chen, H.H. (2006). Secure cell relay routing protocol for sensor networks: Research Articles, Vol. 6, No. 3, *Wireless Communications and Mobile Computing*, May 2006, pp. 375-391

- Eschenauer, L.; Gligor, V. (2002). A Key Management Scheme for Distributed Sensor Networks, *Proceedings of ACM Conference on Computer and Communications Security*, pp. 41-47, USA, Apr. 2002, Washington DC
- Hu, Y.C.; Perrig, A., Johnson, D.B. (2006). Wormhole attacks in wireless networks, *IEEE Journal on Selected Areas in Communications*, Vol. 24, No. 2, Feb. 2006, pp. 370-380
- IEEE 802.15.4 Standard (2006). Wireless Medium Access Control (MAC) and Physical Layer (PHY) Specifications for Low-Rate Wireless Personal Area Networks (WPANs), *IEEE*, Sep. 2006
- Karlof, C.; Wagner, D. (2003). Secure Routing in Sensor Networks: Attacks and Countermeasures, *Elsevier Ad hoc Networks*, Vol. 1, No. 2-3, Sep. 2003, pp. 293-315
- Korkmaz, T. (2005). Verifying Physical Presence of Neighbors against Replay-based Attacks in Wireless Networks, *International Journal of Information Technology*, Vol. 11, No. 2, 2005., pp. 9-20
- Lin, F.; Du, X. (2005). Secure cell relay routing protocol for sensor networks, *Proceedings of IEEE Computing and Communications Conference*, pp. 477-482, Apr. 2005
- Maheshwari, R.; Gao, J. & Das, S.R. (2007). Detecting wormhole attacks in wireless networks using connectivity information, *Proceedings of IEEE International Conference on Computer Communications*, pp. 107-115, May 2007
- Papadimitratos, P.; Poturalski, M., Schaller, P., Lafourcade, P., Basin, D., Capkun, S., Hubaux, J.P., (2008). Secure neighborhood discovery: a fundamental element for mobile ad hoc networking, *IEEE Communication Magazine*, vol. 46, No. 2, Aug. 2002., pp. 102-114
- Perrig, A.; Canetti, R., Song, D., Tygar, D. (2000). Efficient Authentication and Signing of Multicast Streams over Lossy Channels, *Proceedings of IEEE Symposium on Security and Privacy*, May 2000
- Pickholtz, R.L.; Schilling, D.L. & Milstein, B. (1982). Theory of spread spectrum communications: a tutorial, *IEEE Transactions on Communications*, Vol. 20, No. 5, May 1982, pp. 855-884
- Poturalski, M.; Papadimitratos, P., Hubaux, J.P. (2008). Towards provable secure neighbor discovery in wireless networks, *LCA Report (EPFL University)*, Oct. 2008
- Poturalski, M.; Papadimitratos, P., Hubaux, J.P., (2007). Secure Neighbor Discovery in Wireless Networks: Formal Investigation of Possibility, *LCA Report (EPFL University)*, 2007
- Rasmussen, K.B.; Capkun, S. (2007). Implications of radio fingerprinting on the security of sensor networks, *Proceedings of International Conference on Security and Privacy for Emerging Areas in Communication Networks*, pp. 331-340, Sep. 2007
- Rubinstein, M.G.; Moraes, I.M., Campista, M.E.M., Costa, L.H.M.K., Duarte O.C.M.B. (2006). A survey on wireless ad hoc networks, In: *Mobile and Wireless Communication Networks (from International Federation for Information Processing (IFIP))*, Guy Pujolle (Ed.), Vol. 211, pp. 1-33, Springer, Boston
- Sastry, N.; Shankar, U. & Wagner, D. (2003). Secure verification of location claims, *Proceedings of ACM workshop on Wireless Security*, pp. 1-10, 2003, ACM Press
- Sayad Haghighi, M.; Mohamedpour, K. (2008). Securing wireless sensor networks against broadcast attacks, *Proceedings of International Symposium on Telecommunications*, pp. 49-54, Aug. 2008

- Shokri, R.; Poturalski, M., Ravot, G., Papadimitratos, P., Hubaux, J.P. (2008). A low-cost secure neighbor verification protocol for wireless sensor networks, *LCA Report (EPFL University)*, Oct. 2008
- Singelee, D.; Preneel, B. (2005), Location verification using secure distance bounding protocols, *Proceedings of IEEE International Conference on Mobile Ad hoc and Sensor Systems Conference*, pp. 840-846, Nov. 2005
- Zhu, S.; Setia, S. & Jajodia, S. (2003). *LEAP: efficient security mechanisms for large-scale distributed sensor networks*, *Proceedings of ACM conference on Computer and Communications Security*, pp. 62-72, May 2003
- Zhu, S.; Setia, S. & Jajodia, S. (2006). LEAP+: Efficient security mechanisms for large-scale distributed sensor networks, *ACM Transactions on Sensor Networks*, Vol. 2, No. 4, Nov. 2006, pp. 500-528

New Trends in Network Anomaly Detection

Yasser Yasami¹ and Saadat Pourmouzaffari
Amirkabir University of Technology
Iran

1. Introduction

Computer networks are complex interacting systems composed of individual entities such as various devices, workstations and servers. Nowadays, *Internet Protocol* (IP) is used as a dominant layer 3 protocol. The evolving nature of IP networks makes it difficult to fully understand the dynamics of the systems and networks. To obtain a basic understanding of the performance and behavior of these complex networks, large amount of information need to be collected and processed. Often, network performance information is not directly available, and the information obtained must be synthesized to obtain an understanding of the ensemble behavior.

Traditional signature-based intrusion detection techniques use patterns of well-known attacks to match and identify known intrusions. The main drawback of these techniques is inability to detect the newly invented attacks. To obtain sufficient information about complex network traffic and compensate for the weaknesses of traditional *Intrusion Detection Systems* (IDS), *Anomaly Detection Algorithms* (ADA) are used [G.Maselli & L.Deri, 2003; K. Hwang et al., 2004; A. Lazarevic et al., 2003]. These algorithms can be employed as a useful mechanism to analyze network anomalies and detect misbehaviors issued by users, or even unknown signature viruses and worms.

There are two main approaches to study or characterize the ensemble behavior of the network [M. Thottan & C. Ji, 2003]: the first is inference of the overall network behavior and the second is to analyze behavior of the individual entities or nodes. The approaches used to address the anomaly detection problem depend on the nature of the data that is available for the analysis. Network data can be obtained at multiple levels of granularity such as network-level or end-user-level. The methods presented in this chapter are host-based ADA's and are categorized in the latter approach.

In this chapter, we present some ADA's developed based on some classification methods. The goal of this chapter is to classify each user's behavior as anomalous or normal actions in an unsupervised fashion. Four different algorithms are discussed and compared based on some defined measures.

The experiments are performed on a real evaluation network test bed. Instances are captured in eight consecutive weeks, three weeks of training and five weeks of testing. Some

¹ Yasser Yasami is currently an instructor of computer science & engineering at Payam Nour University.

ARP anomaly criteria are defined. These criteria are applied to the three weeks training instances for generating normal ARP traffic.

Performance evaluation of the approaches is conducted by five performance measures: Sensitivity, Specificity, Negative Likelihood Ratio, Positive Predictive Value, and Negative Predictive Value. Finally some comparisons are performed based on the defined measures.

2. Background and Related Works

Network anomaly detection is a vibrant research area. ARP anomaly detection in particular has been of great interest. Some methods for anomaly detection are based on switch characteristics, such as performance and backplane [D. Ármannsson et al., 2005]. In such methods switch characteristics must be known. Our knowledge is limited to theoretical backplane speed mentioned in datasheets. But, because switch processing power, especially when forwarding and flooding small packets, does not equal to that of theory and performance of switches in high load, small packet traffic degrade dramatically, so using such algorithm, encounters functional limitations.

In other researches [D. Whyte et al., 2005], feature-based approaches for host-based analysis of ARP anomaly detection have been suggested. To achieve more accuracy on the results, more inputs factors to these algorithms are needed to be defined. Furthermore, the proposed factors have correlation with each other. None of these works include any suggestion about correlation between the factors, which affect on their precision.

The proposed algorithm in [Shekhar R. Gaddam et al., 2007] is a supervised ADA. We are not provided with a set of anomalous and normal labeled training instances, mostly. So, supervised algorithms such as the one proposed in [Shekhar R. Gaddam et al., 2007] are confronted with limitations in practical applications. Furthermore, the majority of the works proposed in [N. Ye et al., 2004; D. Mutz et al., 2006; S. Kumar & E.H. Spafford, 1994; C. Kruegel & G. Vigna, 2003] evaluate the performance of anomaly detection methods on the measurements drawn from one application domain, thereby addressing the problem of anomaly detection on limited data instances collected from a single application domain. There are some other approaches that apply machine learning techniques like symbolic dynamics [A. Ray, 2004], multivariate analysis [N. Ye, et al., 2002], neural-networks [Z. Zhang et al., 2001], self-organizing maps [S.T. Sarasamma et al., 2005], fuzzy classifiers [J. Gomez & D.D. Gupta, 2001] and others [H.S. Javitz & A. Valdes, 1991; I. Levin, 2000; D.Y. Yeung & C. Chow, 2002; R. Agarwal & M.V. Joshi, 2000; G. Qu et al., 2005]. Almost all of these anomaly detection approaches apply single machine learning techniques while recent advances in machine learning show that selection, fusion and cascading [A. Verikas et al., 1999; J. Kittler et al., 1998; L.I. Kuncheva, 2002] of multiple machine learning approaches have a better performance yield over individual approaches.

3. Network Anomalies

Network anomalies typically refer to circumstances when network operations deviate from normal network behavior. The anomalies can arise due to various causes such as malfunctioning network devices, bad configuration in network services and operating systems, network overload, malicious denial of service attacks, ill advised applications installed by users, high level users' effort to discover network and gather information about

it and its devices, and network intrusions that disrupt the normal delivery of network services. These anomalous events will disrupt the normal behavior of some measurable network data. The definition of normal network behavior for measured network data is dependent on several network specific factors such as dynamics of the network being studied in terms of traffic volume, the type of network data available, and types of applications running on the network. Accurate modeling of normal network behavior is still an active field of research, especially the online modeling of network traffic.

Some of intrusions and malicious usages don't have significant effects on network traffic (i.e. ARP Spoofing). So such misbehavior is not addressed in this chapter. Other types of attacks are based on broadcasting large number of packets with abnormal behavior, as in the case of DoS attacks. Abnormality is generally different from large number of packets, although large number of packets introduces abnormality to network traffic, too. High percentage of packets, degrade network performance. There are other types of attacks which apply broadcast traffic for detecting live hosts in network. Network anomalies can be caused by some unintentional and curious motivations, too. To detect these anomalies an algorithm is introduced in this chapter. The main objective of the ADA's is detection of zero-day worms and viruses broadcasting ARP requests to find vulnerable hosts. Besides, the approach will be very effective in preventing unwanted traffic, too.

4. Anomaly Detection by Stochastic Learning Automata

In this section the proposed method based on *Stochastic Learning Automata* (SLA) is described. A learning algorithm that constructs host-based learning models of normal ARP behavior from attack-free network ARP traffic is presented. Behavior that deviates from the learned normal model signals possible novel attacks.

4.1 Formal Description of SLA

An *automaton* is a machine or control mechanism designed to automatically follow a predetermined sequence of operations. The *stochastic* emphasizes the adaptive nature of the automaton. This adaptation is the result of *learning* process.

Formally, the automaton can be represented by quintuple $\{\Phi, \alpha, \beta, F(\cdot, \cdot), H(\cdot, \cdot)\}$ [K. S. Narendra & M. A. L. Thathachar, 1989], where :

- Φ is a set of internal *states*. At any instant n , the state $\phi(n)$ is an element of the finite set Φ which is as follow:

$$\Phi = \{\phi_i \mid \forall i, 1 \leq i \leq s\} \quad (1)$$

- α is a set of actions (or outputs of the automaton). The *output* or *action* of an automaton at the instant n , denoted by $\alpha(n)$, is an element of the finite set α . Description of α is as below:

$$\alpha = \{\alpha_i \mid \forall i, 1 \leq i \leq r\} \quad (2)$$

- β is a set of responses (or inputs from the environment). The input from the environment $\beta(n)$ is an element of the set β which could be either a finite set or an infinite set, such as an interval on the real line:

$$\beta = \{\beta_i \mid \forall i, 1 \leq i \leq m\} \text{ or } \beta = \{(a,b)\} \quad (3)$$

- $F(\bullet, \bullet): \Phi \times \beta \rightarrow \Phi$ is a function that maps the current state and input into the next state. F can be deterministic or stochastic:

$$\phi(n+1) = F[\phi(n), \beta(n)] \quad (4)$$

- $H(\bullet, \bullet): \Phi \times \beta \rightarrow \alpha$ is a function that maps the current state and input into the current output. If the current output depends on only the current state, the automaton is referred to as state-output automaton. In this case, the function $H(\bullet, \bullet)$ is replaced by an output function $G(\bullet): \Phi \rightarrow \alpha$, which can be either deterministic or stochastic:

$$\alpha(n) = G[\phi(n)] \quad (5)$$

The automaton applied for our application is of type of the later case.

4.2 General Reinforcement Scheme

In order to describe the reinforcement scheme, $p(n)$ is defined as a vector of action probabilities :

$$P_i(n) = P(\alpha(n) = \alpha_i), \quad 1 < i < r \quad (6)$$

Updating action probabilities can be represented as follow:

$$P(n+1) = T[p(n), \alpha(n), \beta(n)] \quad (7)$$

where T is a mapping. This formula says the next action probability $p(n+1)$ is updated based on the current probability $p(n)$, the input from the environment and the resulting action.

The general scheme for updating action probabilities for an r -action automaton in an environment with $\beta = \{0, 1\}$ is as follow:

if $\alpha(n) = \alpha_i$, when $\beta = 0$:

$$p_j(n+1) = p_j(n) - g_j(p(n)), \quad \forall j, j \neq i \quad (8.a.1)$$

$$p_i(n+1) = p_i(n) + \sum_{\substack{k=1 \\ k \neq i}}^r g_k(p(n)) \quad (8.a.2)$$

and when $\beta = 1$:

$$P_j(n+1) = p_j(n) + h_j(p(n)), \quad \forall j, j \neq i \quad (8.b.1)$$

$$p_i(n+1) = p_i(n) - \sum_{\substack{k=1 \\ k \neq i}}^r h_k(p(n)) \quad (8.b.2)$$

Where g_k and h_k , $k = 1, 2, \dots, r$ are continuous, nonnegative functions with the following assumptions :

$$0 < g_k(p(n)) < p_k(n) \quad (9.a)$$

$$0 < \sum_{\substack{k=1 \\ k \neq i}}^r p_k(n) + h_k(p(n)) < 1, \quad 1 < i < r, \quad 0 < p_k < 1 \quad (9.b)$$

4.3 Why Using SLA

Nowadays in *Intrusion Detection* researches, efforts are mainly focused on misuse detection direction, since it is strait forward and easy to implement. But it has some inherent disadvantages. It is difficult to gather required information on known attack (content of TCP packets must be checked while maybe not enough). The most severe disadvantage is that it possibly can not detect attempts to new and unforeseen vulnerabilities.

These disadvantages make *Anomaly Detection* approaches a vibrant research area. Here we will make some effort to do host-based anomaly detection.

In order to model normal user's behavior, we believe that a good model should be able to give a reasonable explanation of the real system. Here SLA is used to satisfy this condition. Our reasons are as follow:

1. A computer user of a system should have some kind of routine behavior, especially for long-term computer users. This is what anomaly detection is based on.
2. Each computer user should be in some kind of state, when using computer. This state corresponds to what he currently mainly wants to do. For example, at one time, the user wants to browse web sites for shopping, at another time, he wants to make programming, etc. In each state, the user will mainly do some correspondent actions which are different with other states. So from statistic aspect, the distribution of every kind of connections or commands in each state will be different from other states.
3. Transition from one state to another can be treated roughly as state transition process of *Finite State Machine*. For the *Steady State Duration* time, we treat it as Gaussian (Normal) distribution, since human doing a task is not without remembering, so exponential distribution can not be used. On state transition decision, because human usually make decision on which task he will do next based on the previous several tasks he has done, so we treat the transition probability with conditional transition.

So from above three aspects, we believe SLA can be used for modeling of computer user's behavior in an understandable and accurate way.

4.4 Modeling Normal Behavior of ARP Traffic with SLA

For each node of network one automaton is learned from attack-free network ARP traffic.

In this approach, there is one state corresponding to each node in the network. So that, the set of internal states for each node learning automaton is defined as follow:

$$\Phi = \{IP_i \mid 0 \leq i \leq s\} \quad (10)$$

Where IP_i is the IP address of node i and s is the number of existing nodes in the network.

The set of actions (or outputs of the automaton) is a set of triples as follow:

$$\alpha = \{(IP_i, \varepsilon_i, \sigma_i^2) \mid \forall i, 1 \leq i \leq r\} \quad (11)$$

Where IP_i is the state identity and ε_i and σ_i^2 are the Average and Variance of steady state duration, respectively which are defined as below:

$$\varepsilon_i = \frac{\sum_{j=1}^{n_i} t_{ij}}{n_i} \quad (12)$$

$$\sigma_i^2 = E[t_i^2] - E[t_i]^2 \quad (13)$$

Where t_{ij} is the elapsed time after j^{th} ARP request with destination IP address corresponding to i until next ARP request with source IP address i issues. n_i is the number of occurrence of the i (i.e., the number of ARP requests issued with destination IP address corresponding to state i).

$E[t_i]$ and $E[t_i^2]$ in the second expression are expected values (mean) of the random variables t_i (steady state duration of state i) and t_i^2 , respectively.

There is one action (output) for each state of the automaton, so we have ($r = s$).

The environment (network in our model) interacts with this automaton by introducing ARP requests to it. β , the set of responses (or inputs from environment) is defined as follow:

$$\beta = \{req_i \mid 0 \leq i \leq m\} \quad (14)$$

Where req_i is ARP request with destination IP address i . As stated earlier, the normal model is learned for each node x in the network. Therefore, the source IP address of all of the members of set β is same as the node whose normal model is under learning. It is obvious that m in this definition is equal to the number of nodes. We have ($m = s$).

Each ARP request causes a transition from one state (the state corresponding to destination IP address of the previous ARP request) to another state (the state corresponding to the ARP request destination IP address). The formal description of transition function (F) is as stated below:

$$IP_{n+1} = F(IP_n, req_{n+1}) \quad (15)$$

The transition function F of the automaton is deterministic and the result of this function is uniquely specified for each state. For each special state X and req_Y issued from the environment, the automaton changes its state from X to Y and this is deterministic.

The current output of the model is dependant on only current state, so the automaton is state-output. The formal description of output function is as below:

$$G(IP_n) = (IP_n, \varepsilon_n, \sigma_n^2) \quad (16)$$

This function is stochastic and nondeterministic, because the output set α is updated whenever the environment interacts with the automaton (whenever an ARP request issues). The elements of the set G are denoted by g_{ij} . The value of this element represents the probability that the action performed by the automaton is $(IP_j, \varepsilon_j, \sigma_j^2)$ given the automaton is in state IP_i :

$$G_{ij} = P[\alpha(n) = (IP_j, \varepsilon_j, \sigma_j^2) \mid \Phi(n) = IP_i], \quad 1 < i, j < s \quad (17)$$

In short the automaton takes an input from the environment and produces an action based on this.

The automaton is a variable-structure one. Although, transition function F is deterministic and does not change over time, but the output function is stochastic and its value changes over time.

4.5 The Reinforcement Scheme of the Proposed Model

The reinforcement scheme is the basis of learning process for learning automata. The formal definition of reinforcement scheme can be obtained by substitution of functions in Equation (8) as follow:

If $\Phi(n) = IP_n$ and the environment issues req_n then award function will be as:

$$g_k(p(n)) = \frac{a}{n+1} \quad (18)$$

If $\Phi(n) = IP_n$ and the environment issues $req_m, m \neq n$ then penalty function will be as:

$$h_k(p(n)) = \frac{b}{n+1} \quad (19)$$

Therefore, the formal definition of the reinforcement scheme is given as:

if $\alpha(n) = IP_n$, when environment response is req_n :

$$p_j(n+1) = p_j(n) - \frac{a}{n+1}, \quad \forall j, j \neq i \quad (20.a.1)$$

$$p_i(n+1) = p_i(n) + \frac{(r-1)a}{n+1} \quad (20.a.2)$$

and when environment response is $req_m, m \neq n$:

$$p_j(n+1) = p_j(n) + \frac{b}{n+1}, \quad \forall j, j \neq i \quad (20.b.1)$$

$$p_i(n+1) = p_i(n) - \frac{(r-1)b}{n+1} \quad (20.b.2)$$

4.6 Anomaly Detection

The purposed algorithm constructs a learning model of normal ARP traffic for each existing host in the network. The model resulted from this learning process is named as *normal model*. Discussion of producing normal ARP traffic will come, latter. Online network traffic is compared by the normal model in a process referred to as "*matching process*". Any deviation from the normal model is an indication of anomaly which is quantified as *Anomaly Score* (AS) parameter. The algorithm makes decisions on normality or abnormality of each node by means of the calculated AS parameter in matching process.

An important parameter in anomaly detection is an accurate threshold value. An indication of normality is used for this purpose, referred to as *Normal Score* (NS). This parameter is described latter.

- Anomaly Score (AS)

We apply AS as an anomaly indicator of a node ARP traffic and obtain it from weighted summation of *Partial Anomaly Scores* (PAS'es) as the following equation denotes:

$$AS = K_s A_s + \sum_{n=2}^N \frac{K_j^n A_j^n}{P_{ij}} \quad (21)$$

Where N in the above equation is the number of previous environment responses (ARP requests issued in matching process) affecting on the AS value and decision making on normality or abnormality of the corresponding node, j is the state in the learning model which the node will be in after n^{th} ARP request and A_j^n is the PAS, explained latter.

A_s is the PAS corresponding to the state which the node will be inside after the first ARP request ($(N-1)^{\text{th}}$ previous ARP request) and can be stated formally as follow:

$$A_s = A_i^1, \quad 1 \leq i \leq r \quad (22)$$

K_j^n is coefficient of the participating term in weighted summation of AS and is dependent on state j in learning model, such that occurrence of a state with low probability has more effect on AS than occurrence of a state with high probability. So the purposed value for this parameter is simply the inverted state probability:

$$K_j^n = P_j(n)^{-1} \quad (23)$$

This justification can be described for transition probability residing in denominator. $P_{ij}(n)$ is conditional probability of transition from state i to state j caused by n^{th} ARP request (environment response req_j^n), given the sequence of observed transitions in matching process. It can be formally described as follow:

$$P_{ij}(n) = P(T_{ij} | T_{i_1 i_2} T_{i_2 i_3} \dots T_{i_{n-2} i_{n-1}}) \quad (24)$$

Where, T_{ij} is transition from state i to state j , $T_{i_1 i_2} T_{i_2 i_3} \dots T_{i_{n-2} i_{n-1}}$ is sequence of transitions in matching process, I_x indexes correspond to states where the node will be in after n^{th} ARP

request in matching process (after $req_{I_i}^n$), as I_1 and I_{n-1} indexes correspond to states S and i , respectively. This conditional probability is calculated in learning process as follow:

$$P_{ij}(n) = \frac{P(T_{I_1 I_2} T_{I_2 I_3} \dots T_{I_{n-2} I_{n-1}} T_{ij})}{P(T_{I_1 I_2} T_{I_2 I_3} \dots T_{I_{n-2} I_{n-1}})} \tag{25}$$

- Partial Anomaly Score (PAS)

Defined as deviation from average steady state duration in a state:

$$A_j^n = \begin{cases} \frac{(\varepsilon_j^n - t_j^n)^2}{(\sigma_j^n)^2}, & \text{if } t_j^n < \varepsilon_j^n \\ 0, & \text{if } t_j^n \geq \varepsilon_j^n \end{cases} \tag{26}$$

Where t_j^n is the time interval between n^{th} and $(n+1)^{\text{th}}$ ARP requests in matching process, such that the node will be in state j after n^{th} ARP request.

Steady state duration values, greater than average value (ε_j^n) for each state, indicate normal behaviors, so its effect does not participate in AS.

There are some states in learning model which environment doesn't interact with them (there is not any req_i for such states labeled with i). For such states we have:

$$\alpha_i = (IP_i, \varepsilon_i, \sigma_i^2) = (IP_i, 0, 0) \tag{27.a}$$

$$P_i(n) = 0 \tag{27.b}$$

A similar problem exists about sequences of transitions with these conditions. Minimum state probability among probabilities of all of the existent states is used for probability of such states and minimum probability among sequences of transitions corresponding to the node for the probability of such sequences of transitions, as formally stated below:

$$P_i(n) = \text{MIN} \{P_k(n) \mid 1 \leq k \leq r\} \tag{28.a}$$

$$P_{ij}(n) = \text{MIN} \{P_{ik}(n) \mid 1 \leq k \leq r\} \tag{28.b}$$

Also, we considered statistical parameters of each state i satisfying conditions stated in equation (27) (parameters ε_i , and σ_i^2), as follow:

$$\varepsilon_i^n = \text{MAX} \{ \varepsilon_k^n \mid 1 \leq k \leq r \} \tag{29.a}$$

$$\sigma_i^n = \text{MIN} \{ \sigma_k^n \mid 1 \leq k \leq r \} \tag{29.b}$$

It means taking the worst case value for these parameters.

- Normal Score (NS)

NS, as hinted above, is an indicator of normality degree and is a function of partial NS'es (PNS). We define PNS_i as normality score at i^{th} time interval in learning process. NS is calculated as the following equation states:

$$NS = \text{MAX} \{PNS_i\} \quad (30)$$

For calculating PNS_i , we use the same method as used for calculation of AS, but in this case for normal ARP traffic. We get this normal traffic from purified traffic in different time intervals and calculate PNS for each interval. It is obvious that to obtain a right value for NS from PNS 's, these time intervals should be of the same length.

- Threshold calculations

An estimation of ARP traffic normality is required for a right threshold values. The NS value gives this estimation to the hand. It is an indication of maximum value of AS without being detected as abnormal. AS_i values calculated in matching process, satisfying the inequality $NS_i \leq Th_i < AS_i$ for threshold value of Th_i of node i , are detected as abnormal. Making decisions on Th values affect on *False Negative* and *False Positive* and accuracy of algorithm. There are various ways to this problem. One most simple and feasible way is to get threshold k times of NS . For example, the chosen value for k is 1.2 in [Kai Hwang, Hua Liu & Ying Chen, 2004].

5. Anomaly Detection by K-Means and ID3 Decision Trees

5.1 Anomaly Detection by K-Means Algorithm

The K-Means algorithm [R. Duda et al., 2000] groups N data points into k disjoint clusters, where k is a predefined parameter such that $k < N$. The steps in the K-Means clustering-based anomaly detection method are as follows:

1. Select k random instances from the training data subset as the centroids of the clusters C_1, C_2, \dots, C_k .
2. For each training instance X :
 - a. Compute the Euclidean distance:

$$D(C_i, X), i = 1 \dots k.$$

Find cluster C_q that is closest to X .

- b. Assign X to C_q . Update the centroid of C_q . (The centroid of a cluster is the arithmetic mean of the instances in the cluster.)
3. Repeat Step 2 until the centroids of clusters C_1, C_2, \dots, C_k stabilize in terms of mean-squared-error criterion. Finally, the algorithm aims at minimizing an *objective function* (here, squared error function). The objective function J :

$$J = \sum_{j=1}^k \sum_{i=1}^N \|X_i^{(j)} - c_j\|^2 \quad (31)$$

where the term:

$$\|X_i^{(j)} - c_j\|^2$$

is a chosen distance measure between a data point $X_i^{(j)}$ and the cluster centre c_j , is an indicator of the distance of the N data points from their respective cluster centers.

5.2 Anomaly Detection by ID3 Decision Trees

The ID3 decision tree learning algorithm [T. Mitchell, 1997] computes the *Information Gain* G on each attribute A , as:

$$G(S, A) = Entropy(S) - \sum_{v \in \text{values}(A)} \frac{|S_v|}{|S|} Entropy(S_v) \quad (32)$$

where S is the total input space and S_v is the subset of S for which attribute A has a value v . The *Entropy*(S) over c classes is given by:

$$Entropy(S) = \sum_{i=1}^c -p_i \log_2(p_i) \quad (33)$$

where p_i represents the probability of class "i". The probability of class i is calculated as follow:

$$p_i = \frac{N_i}{\sum_{j=1}^c N_j} \quad (34)$$

where, N_x is the number of training instances in class x .

The attribute with the highest information gain, say B , is chosen as the root node of the tree. Next, a new decision tree is recursively constructed over each value of B using the training subspace $S - \{S_B\}$. A leaf-node or a decision-node is formed when all the instances within the available training subspace are from the same class. The algorithm constructs the ID3 decision tree with the normal purified traffic. Anomaly detection is performed using this tree by traversing the tree with features of test instance. If the traverse reaches a leaf node, the test instance will be detected as normal; else it will be detected as abnormal.

5.3 Anomaly Detection by Combined K-Means Clustering & ID3 Decision Trees

We are provided with a normal (purified) training data set X_i where each instance represents an n -dimensional vector. The approach has two phases: training and testing. During training phase, K-Means-based anomaly detection method is first applied to partition the training space into k disjoint clusters C_1, C_2, \dots, C_k . Then ID3 decision tree is trained with instances in each K-Means cluster. The K-Means clustering method ensures that each training instance is associated with only one cluster. However, if there are any subgroups or overlaps within a cluster, the ID3 decision tree trained on that cluster refines the decision boundaries by partitioning the instances with a set of if-then rules over the feature space.

The combined application of the two algorithms overcomes some limitations of each algorithm when applied individually. For example, selection of a right value for parameter k in the K-Means clustering algorithm can affect on the overall accuracy of the algorithm. Considerably little values of k , compared to inherent number of natural subgroupings

within the training data will lead to overlapping subgroups within clusters. This problem is compensated by ID3 decision tree constructed in each cluster.

The testing phase of the algorithm includes two phases: the candidate selection phase and candidate combination phase. In the first phase, AS from K-Means clustering and decisions from ID3 decision tree are extracted. In the second phase, the final AS is gotten from combined results of K-Means clustering and ID3 decision tree. The algorithms applied for candidate selection and candidate combination is explained below.

5.4 The Candidate Selection Phase

Steps of the candidate selection algorithm are as follow:

1. For each test instance Z_i , $1 \leq i \leq n$:
 - a. Compute Euclidean distance:

$$D(Z_i, r_j), j = 1 < j < n,$$

and find f clusters closest to Z_i .

- b. Compute K-Means AS and extract decisions of ID3 decision trees for f nearest candidate clusters.
2. Return Anomaly Score Matrix for Z_i .

The algorithm gets test instances Z_i , $1 \leq i \leq n$, and the parameter f as inputs and gives matrix $AS[f \times 2]$ for each test instance Z_i . f is a user defined parameter. If DT_1, DT_2, \dots, DT_k be the ID3 decision trees on clusters C_1, C_2, \dots, C_k formed by applying the K-Means method on the training instances, and r_1, r_2, \dots, r_k be the centroids of clusters C_1, C_2, \dots, C_k , respectively, then given a test instance Z_i , the candidate selection procedure extracts AS'es from f candidate clusters G_1, G_2, \dots, G_k . The selected f candidate clusters are f clusters in C_1, C_2, \dots, C_k that are nearest to Z_i in terms of Euclidean distance between Z_i and the cluster centroids.

Let l_1, l_2, \dots, l_f be the centroids of candidate clusters G_1, G_2, \dots, G_f and the Euclidean distances between the test vector Z_i and the f candidate clusters is as follow:

$$D(Z_i, l_j) = d_j, 1 \leq j \leq f \quad (35)$$

the AS for each of the f candidate clusters is calculated by K-Means clustering as follow:

$$AS_j = P(C_j) \times \left[1 - \frac{d_j}{\sum_{a=1}^k D(Z_i, r_a)} \right], 1 \leq i \leq n, 1 \leq j \leq f \quad (36)$$

$P(C_j)$ in the above equation is probability of cluster C_j and is calculated as the following equation indicates:

$$P(C_j) = \frac{N_{C_j}}{\sum_{i=1}^k N_{C_i}} \quad (37)$$

where the nominator in the above equation is the number of training instances of cluster C_j and the denominator is the total number of training instances.

Term:

$$1 - \frac{d_j}{\sum_{a=1}^k D(Z_i, r_i)}$$

in equation (36) is referred to as *Scaling Factor* (SF). It scales $P(C_j)$ by weighing it against the ratio of the Euclidean distance between the cluster j and Z_i , and the sum of Euclidean distances between Z_i and the clusters C_1, C_2, \dots, C_k . The SF penalizes the probability of cluster C_j with its distance from the test vector Z_i , such that little distance D_j yields a high AS_j and vice versa. The decision from the ID3 decision trees associated with the f candidate clusters are either "0" or "1" representing normal or abnormal test instances, respectively. This output is depended on that the decision trees can be traversed reaching to a leaf node.

For each test instance Z_i , the candidate selection phase outputs a matrix $AS[f \times 2]$ with AS calculated by K-Means clustering algorithm and decision extracted from ID3 decision tree. The final AS resulted from combined application of the two algorithms is extracted by Candidate Combination. A detailed explanation of this algorithm follows.

5.5 The Candidate Combination Algorithm

Candidate Combination algorithm take as input the output of Candidate Selection algorithm, the AS matrix including the AS_j , $1 < j < f$, values of the K-means clustering algorithm and the decisions of ID3 decision trees over f candidate clusters. The algorithm then order the f candidate clusters G_1, G_2, \dots, G_k in AS matrix such that the distances d_1, d_2, \dots, d_f between Z and the candidate clusters G_1, G_2, \dots, G_f , respectively, satisfy $d_1 < d_2 < \dots < d_f$. The first AS_j value of the K-means clustering algorithm in the ordered AS matrix satisfying each of the below conditions, is selected as the final AS value of the combined K-Means clustering and ID3 decision tree algorithm. The conditions are:

$$AS_j \leq 0.5 \ \& \ DT_j = 0$$

$$AS_j > 0.5 \ \& \ DT_j = 1$$

Where $DT_j = "0"$ or $DT_j = "1"$, means ID3 decision tree of cluster j classifies the test instance as normal or abnormal, respectively. Finally, for each test instance Z_i , an AS value in continuous closed interval $[0,1]$ is yielded from the combined application of the two algorithms. The Threshold Rule is used for classification of the test instance Z_i as an anomalous or normal instance. The threshold rule for classifying a test instance Z_i that belongs to cluster C_r is as follow:

$$\text{Assign } Z \rightarrow 1 \text{ if } AS > \tau,$$

$$\text{Otherwise } Z \rightarrow 0.$$

where τ is a predefined threshold.

6. Evaluation Test Bed Network and Data Set

Our test bed network in this research work was a typical network with about 900 active devices. With exception of a few servers, all of hosts run different Microsoft Windows platforms like windows 98, 2K, XP and 2003 Server. The network is connected to Internet via a 2Mbps link and about 200 stations and 5 servers are connected to internet concurrently. Internet access was enabled for majority of hosts.

The captured data set contains approximately, eight weeks, three weeks of training and two weeks of test data. The main resources of abnormalities in our evaluation test bed network are malicious softwares, malfunctioning network devices, ill-advised applications, scanning tools and high level user's efforts for network discovery. To capture network traffic we used a computer connected to the core switch of the network. Capturing traffic and some statistical parameters from it, is performed in real-time interaction with our prototype, by setting the sniffing machine's NIC in sniffing mode. A sniffing tool in VC++ powered by WinPcap application programming interface has been developed for traffic capturing. The implementations have been performed by Matlab V.7.5.0.342.

Some anomaly criteria are defined and applied to the captured ARP traffic to generate normal training instances. These anomaly criteria are as follow:

- ARP rate: this criterion is defined as the overall number of ARP requests divided by the length of time over which these were observed.
- Burstiness: if we define the maximum instantaneous ARP request rate for a device to be the inverse of the shortest observed inter-request time between two consecutive requests from that device, burstiness can be defined as the ratio of maximum request rate to the ARP rate. The burstiness characteristics of ARP traffic for our evaluation test bed network are illustrated in figure (1). This diagram shows that most devices in normal operation do not send ARP request broadcasts in bursts.

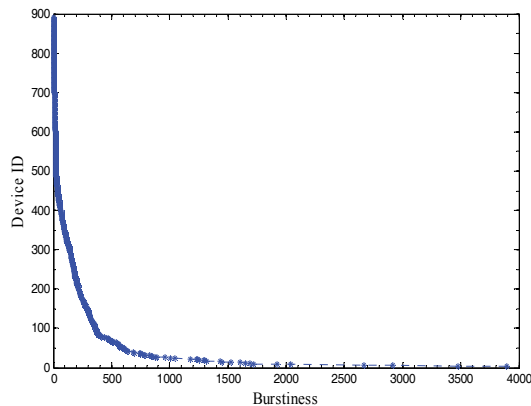


Fig. 1. Burstiness characteristics of ARP traffic for our test network.

- Sequential scans: sequential scan is defined as ARP requests with sequential destination IP addresses. ARP requests in normal conditions have not sequential destination IP addresses.
- Dark space: is defined as ARP requests with destination IP addresses not included in address space of network.

- Repetitive Requests: this criterion is defined as ARP Requests within time intervals smaller than expiration time of corresponding entries in ARP tables. ARP tables maintained by each host or network device are updated when an ARP request is issued. This caching mechanism prevents repetitive ARP requests.

7. Evaluation & experimental results

Our evaluation is based on the following criteria:

- *Sensitivity*: probability that a test result will be positive when there is anomaly (*True Positive* or TP).
- *Specificity*: probability that a test result will be negative when there is not anomaly (*True Negative* or TN).
- *Negative likelihood ratio*: ratio between the probability of a negative test result given the presence of the anomaly and the probability of a negative test result given the absence of the anomaly, i.e. Negative likelihood ratio = False negative rate / True negative rate = (1-Sensitivity) / Specificity.
- *Positive predictive value*: probability that the anomaly is present when the test is positive.
- *Negative predictive value*: probability that the anomaly is not present when the test is negative.

ARP traffic has been applied to detect network abnormalities in the approach, as stated before. In K-Means clustering, ID3 Decision trees, and the combinatorial approach of these two algorithms we are provided with training and test data set $X_i, 1 \leq i \leq N$, where X_i represents a 9-dimensional vector as follow:

$$X_i = (S_{i1}, D_{i1}, \Delta T_{i1}, S_{i2}, D_{i2}, \Delta T_{i2}, S_{i3}, D_{i3}, \Delta T_{i3}) \tag{38}$$

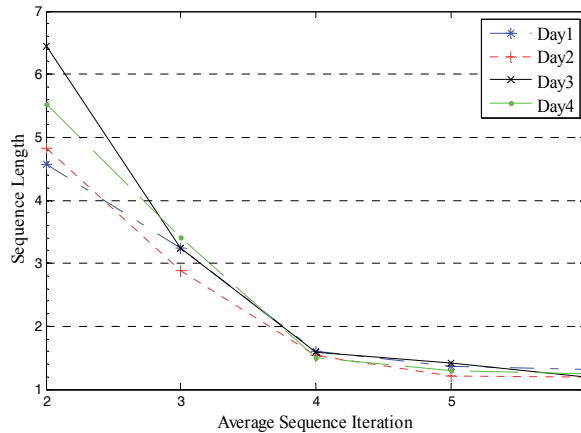


Fig. 2. Iteration of sequences with different length.

S_{ix} 'es and D_{ix} 'es in the data instance X_i are source and destination IP addresses of ARP requests. We have used three successive ARP request characteristics in each data instance X_i . ΔT_{ix} is the discretely quantized time interval between two successive ARP requests. The main reason for using characteristics of multiple ARP requests in each data instance X_i , is

that user activities include some sequential activities which are depended on the state the user is in and what he mainly wants to do in that state. So, individual ARP requests can not be applied for detecting abnormalities. Figure (2) presents average iteration of ARP requests sequences with different length within four different days. As it is obvious from this figure, there is an egregious difference between iteration of sequences of length 3, 4 such that iteration of sequences of length 4 is as close to 1 as desired. So, we have used three successive ARP requests in each data instance X_i .

The experimental results within five successive weeks are represented in table (1). The experiments are based on five evaluation measures, described above. The Sensitivity, Specificity, Negative Likelihood Ratio, Positive Predictive Value, and Negative Predictive Value characteristics of K-Means clustering, ID3 Decision tree, SLA-based and the combinatorial K-Means+ID3 is illustrated in figures (3) to (7). These figures show that:

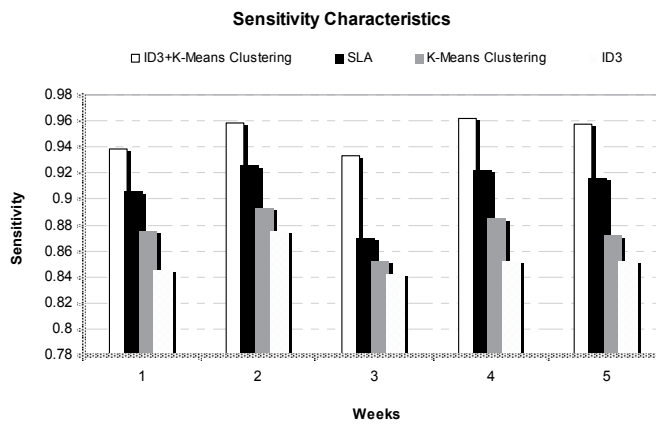


Fig. 3. Comparison of Sensitivity characteristics.

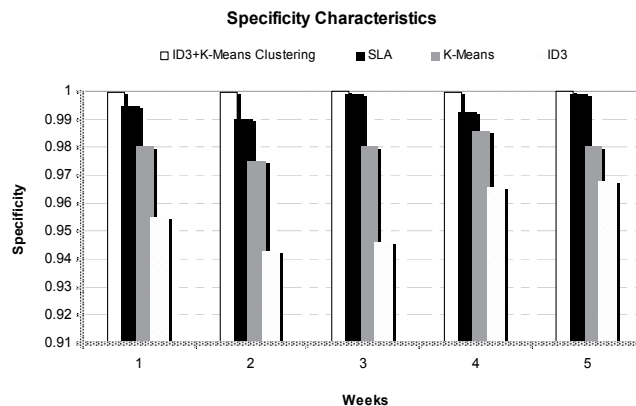


Fig. 4. Comparison of specificity characteristics.

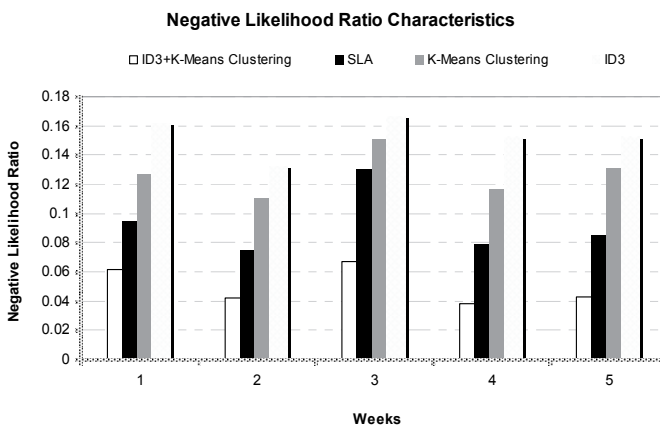


Fig. 5. Comparison of negative likelihood ratio characteristics.

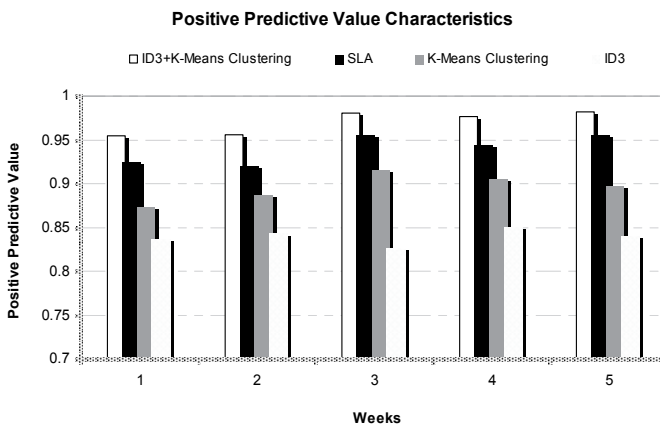


Fig. 6. Comparison of positive predictive value characteristics.

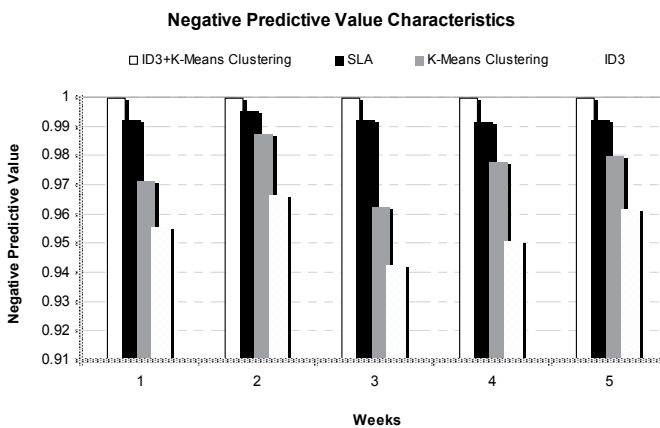


Fig. 7. Comparison of negative predictive value characteristics.

Week	1	2	3	4	5
Total Number of Test Instances	679100	856200	987000	598400	832700
The Number of Abnormality Instances	4500	10900	3400	5900	4200
Sensitivity	0.938326	0.958148	0.933155	0.961538	0.957303
Specificity	0.999704	0.99942	0.999929	0.999747	0.999903
Negative Likelihood Ratio	0.061692	0.041876	0.06685	0.038471	0.042701
Positive Predictive Value	0.955157	0.956444	0.980337	0.976563	0.981567
Negative Predictive Value	0.999585	0.999444	0.999746	0.999578	0.999771

Table 1. Evaluation results of the K-means+ID3 in five weeks.

- 1) K-Means+ID3 method has better performance than the other methods in terms of all defined measures.
- 2) The performance of the SLA-based approach is in-between the combinatorial approach and each of individual K-Means and ID3.
- 3) Individual K-Means has better performance than individual ID3.

Malicious softwares by issuing a large number of ARP packets in little time intervals had large effects on traffic abnormalities. They assigned high percentage of triggered alarms to themselves. Bad-configured applications were the main origins of abnormality after malicious softwares. Curious users' activities, malfunctioning or bad configured network devices, and etc. affect on network traffic abnormalities but had a lower portion in it.

8. Conclusion

This chapter presented some anomaly detection approaches for classification of anomalous and normal activities in computer network ARP traffic. The proposed approaches use some well-known machine learning methods: the SLA, K-Means clustering and the ID3 decision tree learning approaches. As described, in SLA-based approach a learning algorithm has been used for modeling of normal ARP traffic behavior. Making decisions on abnormal behavior of each device in the network is based on comparison of online behavior of each host by its normal model. In the combinatorial approach based on K-means and ID3 decision trees, the K-Means method was first applied to partition the training instances into k disjoint clusters. The ID3 decision tree built on each cluster learns the subgroups within the cluster and partitions the decision space into finer classification regions; thereby improving the overall classification performance. This combinatorial method was compared with the individual K-Means and ID3 methods and the other proposed approaches based on SLA in terms of the overall classification performance defined over five different performance measures. Results on real evaluation test bed network data sets show that: the proposed method outperforms the individual K-Means and the ID3 compared to the other approaches. The performance of SLA is in-between the proposed combinatorial K-Means+ID3 and individual K-Means and ID3, in terms of all the five performance measures over the real network ARP traffic data set.

Further research should be carried out to evaluate the performance of the proposed approaches with other combinatorial approaches which can be developed by different clustering approaches.

Acknowledgements

This work was partially supported by the Payam Nour University and Iran Information Technology Research Center.

9. References

- A. Lazarevic, A. Ozgur, L. Ertöz, J. Srivastava, and V. Kumar, "A Comparative Study of Anomaly Detection Schemes in Network Intrusion Detection", *Proceedings of SIAM Int'l Conference Data Mining*, May 2003.
- A. Ray, "Symbolic Dynamic Analysis of Complex Systems for Anomaly Detection", *Signal Processing*, vol. 84, no. 7, pp. 1115- 1130, 2004.
- A. Verikas, A. Lipnickas, K. Malmqvist, M. Bacauskiene, and A. Gelzinis, "Soft Combination of Neural Classifiers: A Comparative Study", *Pattern Recognition Letters*, vol. 20, pp. 429-444, 1999.
- C. Kruegel and G. Vigna, "Anomaly Detection of Web-Based Attacks", *Proceedings of ACM Conference Computer and Communication Security*, Oct. 2003.
- D. Ármannsson, G. Hjálmtýsson, P. D. Smith, L.Mathy; "Controlling the Effects of Anomalous ARP Behaviour on Ethernet Networks", *Proceedings of the 2005 ACM conference on Emerging network experiment and technology*, 2005, pp. 50-60.
- D. Mutz, F. Valeur, G. Vigna, and C. Kruegel, "Anomalous System Call Detection," *ACM Trans. Information and System Security*, vol. 9, no. 1, pp. 61-93, Feb. 2006.
- D. Whyte, E. Kranakis, P. Van Oorschot, "ARP-Based Detection of Scanning Worms within an Enterprise Network", *Proceedings of Annual Computer Security Applications Conference (ACSAC 2005)*, Tucson, AZ, Dec. 5-9, 2005.
- D. Y. Yeung and C. Chow, "Parzen-Window Network Intrusion Detectors", *Proceedings of 16th Int'l Conf. Pattern Recognition*, vol. 4, pp. 385- 388, Aug. 2002.
- G. Maselli, L.Deri, "Design and Implementation of an Anomaly Detection System: an Empirical Approach", *Proceedings of Terena TNC 2003*, May 2003, Zagreb, Croatia.
- G. Qu, S. Hariri, and M. Yousif, "A New Dependency and Correlation Analysis for Features", *IEEE Trans. Knowledge and Data Eng.*, vol. 17, no. 9, pp. 1199-1207, Sept. 2005.
- H. S. Javitz and A. Valdes, "The SRI IDES Statistical Anomaly Detector", *Proceedings of IEEE Symp. Security and Privacy*, pp. 316-326, May 1991.
- I. Levin, "KDD-99 Classifier Learning Contest: LLSOFT's Results Overview", *SIGKDD Explorations*, vol. 1, pp. 67-75, Jan. 2000.
- J. Gomez and D.D. Gupta, "Evolving Fuzzy Classifiers for Intrusion Detection", *Proceedings of 2002 IEEE Workshop Information Assurance*, June 2001.
- J. Kittler, M. Hatef, R.P.W. Duin, and J. Matas, "On Combining Classifiers", *IEEE Trans. Pattern Analysis and Machine Intelligence*, vol. 20, no. 3, pp. 226-239, Mar. 1998.
- K. Hwang, H. Liu, and Y. Chen, "Protecting Network-Centric Systems with Joint Anomaly and Intrusion Detection over Internet Episodes", *IEEE IPDPS- 2005*, Oct.8, 2004.
- K. S. Narendra, M. A. L. Thathachar, *Learning Automata: an introduction*, Prentice-Hall, 1989.
- Kai Hwang, Hua Liu, Ying Chen, "Cooperative Anomaly and Intrusion Detection for Alert Correlation in Networked Computing Systems", *IEEE Trans. Dependable and Secure Computing*, November 24, 2004.

- L. I. Kuncheva, "Switching between Selection and Fusion in Combining Classifiers: An Experiment", *IEEE Trans. Systems, Man, and Cybernetics*, vol. 32, no. 2, pp. 146-156, Apr. 2002.
- M. Thottan and C. Ji, "Anomaly Detection in IP Networks", *IEEE Trans. Signal Processing*, vol. 51, no. 8, pp. 2191-2204, 2003.
- N. Ye, S. M. Emran, Q. Chen, and S. Vilbert, "Multivariate Statistical Analysis of Audit Trails for Host-Based Intrusion Detection", *IEEE Trans. Computers*, vol. 51, no. 7, pp. 810-820, 2002.
- N. Ye, Y. Zhang, and C.M. Borrer, "Robustness of the Markov-Chain Model for Cyber-Attack Detection", *IEEE Trans. Reliability*, vol. 53, no. 1, pp. 116-123, 2004.
- R. Agarwal and M.V. Joshi, "PNrule: A New Framework for Learning Classifier Models in Data Mining (A Case-Study in Network Intrusion Detection)", *Technical Report DSTO-GD-0286*, Dept. of Computer Science, Univ. of Minnesota, 2000.
- R. Duda, P. Hart, and D. Stork, *Pattern Classification*, second ed. Wiley Publishers, Oct. 2000.
- S. Kumar and E.H. Spafford, "A Pattern Matching Model for Misuse Intrusion Detection", *Proceedings of 17th Nat'l Computer Security Conf.*, pp. 11-21, Oct. 1994.
- S. T. Sarasamma, Q. A. Zhu, and J. Huff, "Hierarchical Kohonen Net for Anomaly Detection in Network Security", *IEEE Trans. Systems, Man, and Cybernetics-Part B*, vol. 35, no. 2, Apr. 2005.
- Shekhar R. Gaddam, Vir V. Phoha, Kiran S. Balagani, "K-Means+ID3: A Novel Method for Supervised Anomaly Detection by Cascading K-Means Clustering and ID3 Decision Tree Learning Methods", *IEEE Transactions on Knowledge and Data Engineering*, Vol. 19, No. 3, March 2007.
- T. Mitchell, *Machine Learning*. McGraw-Hill, 1997.
- Z. Zhang, J. Li, C.N. Manikopoulos, J. Jorgenson, and J. Ucles, "HIDE: A Hierarchical Network Intrusion Detection System Using Statistical Preprocessing and Neural Network Classification", *Proceedings of 2001 IEEE Workshop Information Assurance*, pp. 85-90, June 2001.

An Efficient Energy Aware Routing Protocol for Real Time Traffics in Wireless Sensor Networks

Amir Hossein Mohajerzadeh¹ and Mohammad Hossein Yaghmaee²,

¹*Department of computer engineering, Ferdowsi university of Mashhad, Mashhad, Iran, ah.mohajerzadeh@stu-mail.um.ac.ir*

²*Department of computer engineering, Ferdowsi university of Mashhad, Mashhad, Iran, hyaghmae@ferdowsi.um.ac.ir*

1. Introduction

Wireless Sensor Networks (WSN) have recently been extensively deployed and researched. They are composed of a high number of small and simple nodes where most of them have to function as a router in an ad hoc manner. Because of limited energy sources in sensor network node, routing protocols should save the energy as much as possible. Energy consumption has a direct influence on network lifetime. From the Quality of Service (QoS) point of view, in many applications such as real time one, it is necessary to consider application QoS requirements. In this paper we propose an energy aware routing protocol for real time traffics in wireless sensor networks. The proposed protocol considers both energy and delay metrics to find an optimal path with minimum energy consumption and minimum end to end delay. Simulation results show that the proposed protocol is successful in low energy consumption and satisfying low end to end delay which makes it suitable for real time applications.

In the recent years, many researches have been conducted on wireless sensor networks. A wireless sensor network consists of sensor nodes that communicate with each other using wireless links. Wireless sensor networks contain hundreds or thousands of sensor nodes that can both send and forward data (Akyldiz et al., 2002), (Tubaishat & Madria, 2003). The WSNs are used to monitor physical or environmental conditions, such as temperature, sound, vibration, pressure, motion or pollutants, at different locations. Each node in WSNs consists of different parts including: sensors, processor unit (usually a small microcontroller), energy source (usually a battery) and communication unit. The communication part of a sensor node uses wireless communication devices, to be able to send and forward data using a wireless link.

During past few years, WSNs have found many different applications. Typical applications of WSNs include monitoring, tracking, and controlling. Some of the specific applications of WSNs are: habitat monitoring, object tracking, nuclear reactor controlling, fire detection and traffic monitoring. Small sensor nodes could also be used for medical applications (Mann, 1997), e.g., for the surveillance of elderly people. In this application, sensor devices monitor vital function and report them to the family doctor or directly to the ambulance in case of an

emergency like a heart attack. Some sensor nodes could also be implanted into the body in order to detect diseases like cancer in an early. WSNs are also used in commercial and industrial applications to monitor data that would be difficult or expensive to monitor using wired sensors. In the field of home automation (Kidd et al, 1999) sensor nodes could be located in every room to measure the temperature. Sensor nodes could at the same time monitor more than only temperature. They could also detect movements within rooms and report this information to the alarm equipment in case of absent occupants. Sensor networks have also been used for many real time applications. Each application has unique QoS requirements (Younis et al., 2004). For example, real time applications need low delay in data delivery (Akkaya & Younis, 2003). Sensor network's protocols should run appropriate algorithm to satisfy application QoS requirements. Routing protocols also should use appropriate algorithm to find routes with ability to satisfy application QoS requirements. The sensor nodes in WSNs have many limited sources of energy and computing. The main constraint of these networks is the amount of energy consumption. The lifetime of a sensor network depends on its node's energy. In most of sensor networks there is no way to charge node's battery; therefore efficient use of available energy sources is essential. With respect to all above mentioned points, the protocols in wireless sensor network should consider energy constraint in all network's layers. Also routing protocols should use efficient algorithms that consume energy optimally. Due to the inherent characteristics that distinguish WSNs from other networks, routing in wireless sensor networks is very challenging (Qiangfeng et al, 2004). Some of the routing challenges and design issues that affect the routing process in WSNs are: node deployment, energy consumption without losing accuracy, data reporting method, node/link heterogeneity, fault tolerance, scalability, network dynamics, transmission media, connectivity, coverage, data aggregation and quality of service.

Recently, many new routing protocols have been proposed for the routing in WSNs. These routing mechanisms have taken into consideration the inherent features of WSNs along with the application and architecture requirements. The task of finding and maintaining routes in WSNs is nontrivial since energy restrictions and sudden changes in node status cause frequent and unpredictable topological changes. To minimize energy consumption, energy aware routing techniques have been proposed in the different literatures. They employ some well-known routing tactics such as data aggregation, in-network processing, clustering, different node role assignment and data-centric methods. In real time applications, data should be delivered within a certain period of time from the moment it is sensed, or it will be useless. Therefore, bounded latency for data delivery in real time applications is too important. However, in many applications, conservation of energy, which is directly related to network lifetime, is considered relatively more important than the quality of data sent. As energy is depleted, the network may be required to reduce the quality of results in order to reduce energy dissipation in the nodes and hence lengthen the total network lifetime. Hence, energy-aware routing protocols are required to capture this requirement.

In this paper an efficient energy aware routing protocol for real time traffics in wireless sensor networks has been proposed. The proposed routing protocol is energy aware so its main goal is to consume energy optimally. The proposed routing protocol can find the best route which not only has the optimal energy consumption but also has the minimum end to end delay. The routing algorithm in the proposed protocol, considers a cost function which

helps the algorithm to assign a cost to each route. This cost function could be determined based on the application requirements. The proposed algorithm finds the best route depends on its cost. By using a cost function, the proposed routing algorithm selects an optimal route with possible lowest cost. The cost function is based on energy consumption and end to end delay. The end to end delay consists of transmission delay and queuing delay. In the proposed algorithm, there is an attempt to minimize end to end delay by minimizing transmission delay. As transmission delay is directly related to the route length, the minimum transmission delay can be achieved by minimizing route length between source and sink nodes. The proposed routing protocol uses a neighbor discovery algorithm to find its neighbors uniquely. As most of routing algorithms need to send data to a specific neighbor, neighbor discovery is very important. The proposed neighbor discovery algorithm uses three input parameters includes: node identifier (ID), received signal strength and a random number. Simulation results show that it can discover the neighbor uniquely.

The remainder of this paper is organized as follow. The second section, discusses the related researches in this field. Section 3 describes the proposed energy aware routing protocol in details. In section 4 the proposed neighbor discovery mechanism is explained. Section 5 is dedicated to the simulation results. Finally section 6 concludes the paper.

2. Related Works

past few years, many routing protocols have been developed for wireless sensor networks. As the energy is an important constraint of the WSNs, so the energy aware routing algorithms are too important. In the rest of this section we review some of the general routing protocols proposed for wireless sensor networks. Directed Diffusion (Intanagonwiwat et al, 2000) is a well known routing algorithm for wireless sensor networks. This algorithm is not complicated and directly diffuses the data related to sensor nodes. This procedure guarantees high data delivery rate and low delay for communications. Directed Diffusion consumes more energy to forward and receive redundant data. Sink sends interests to each network nodes and determines their job. When a node senses an event, it sends appropriate event related information to sink. SPEED (He et al, 2003) is a well known algorithm for transmitting real time traffics in wireless sensor networks. It considers energy consumption in its routing procedure. SPEED is a highly efficient and scalable protocol for sensor networks where the resources of each node are scarce. SPEED can be used in both data link and network layers. It is a flat routing algorithm. By guaranteeing data forwarding rate, it can support real time communications. It acts locally and uses neighbor information for routing. SPEED uses interesting mechanism layer for route maintenance and recovery that uses both data link and network layer. Reactive Energy Decision Routing Protocol (REDRP) (Wang et al, 2007) is another routing algorithm for WSNs that its main goal is optimal energy consumption. This algorithm attempts to distribute traffic in the entire network fairly. Using this mechanism, it decreases total network energy consumption. REDRP is routing reactively, and uses residual node energy in routing procedure. It uses local information to routing, but nodes have a global ID which is unique for the entire network. This algorithm is divided into 4 steps. In the first step, sink sends a control packet to all network nodes. The nodes estimate their distance to sink relatively by using this packet. Next step is route discovery. Routing is performed on

demand in REDRP. This means that the routes are established reactively. After route establishment in route discovery step, data is forwarded to sink by using those routes. In route recovery step if a route is damaged, it will be recovered or a new route will be established. Real time Power Aware framework (RPTAW) (Toscano et al, 2007) considers both energy and QoS metrics. This algorithm acts hierarchically. By changing cluster structure and creating new node which is called Relay Node that its job is forwarding information from cluster to sink, its goals are achieved. This algorithm claims that by using data aggregation functions, energy consumption is reduced. Furthermore it can manage quality of service depending on efficiency of routing protocol used. In (Vidhyapriya & Vanathi, 2007), (Huiifang et al, 2006), (Hassanein & Lou, 2006) and (Shin, 2007), different reliable energy aware routing protocols for wireless sensor networks have been presented.

3. Proposed Protocol

In this section, we describe the proposed energy aware routing protocol in details. The proposed protocol uses a flat routing algorithm (Qiangfeng et al, 2004) which is done proactively. This means that the routes are established before traffic transmission. The algorithm is run to find the least cost route between source and sink nodes. The proposed routing algorithm is divided into 3 phases which are: route discovery phase, data transmission phase and route recovery phase. The last phase is only done when the topology has been changed. Each node has a unique identifier (ID) which is determined in the route discovery phase. The nodes also have a routing table which includes 3 fields: ID, signal strength and route cost. There is a record for each neighbor of a node in its routing table. The routing table is created in route discovery phase. This table is used in data transmission phase to send traffic from source to sink. In the following subsections, we describe the functions of each phase in details.

3.1. Route Discovery Phase

The sink node as the initiator of this phase broadcasts a packet to all its neighbors. This packet is called Route Discover packet. The structure of Route Discover packet is shown in figure 1. As shown in this figure, each Route Discover packet consists of three fields which are: message type, sender ID and best route cost. The message type field determines the type of packet. The sender ID field determines the value of sender's ID. The best route cost field determines the cost of optimal route between sender node and sink.

Message type	Sender ID	Best route cost
--------------	-----------	-----------------

Fig. 1. Structure of Route Discover packet

Usually the value of sender ID field in all Route Discover packets which are sent by the sink node is equal to zero. As the cost of optimal route between sink node and itself is always zero, so the value of best route cost field is equal to zero.

After receiving the Route Discover packet, each node follows these steps:

1. The node increments the value of sender ID field in the received packet and compares the result with its ID. If the result is bigger than the node's ID, the received packet is dropped. Otherwise the node's ID is replaced by the value of the

result. When the node doesn't have any ID, the node's ID is equal to: sender ID +1. If packet is accepted the steps are continued as follows:

2. The node creates a new record for new received packet in its routing table. The ID field of the routing table is set to the value of sender ID field of the received packet.
3. The forwarding cost of packet which is sent directly from node i to j is calculated using the following cost function (1):

$$Cost_{ij} = \alpha.F(dist_{ij}) + \beta.G(energy_j) \quad (1)$$

In function (1), F and G are two functions which their inputs are equal to the distance between nodes i and j ($dist_{ij}$) and the residual energy of node j ($energy_j$), respectively. Furthermore, α and β are two constant coefficients. By adding the value of best route cost field exists in the received packet with the value of $Cost_{ij}$, the node could be able to obtain the new value of route cost. Each node to transmit its data toward sink, selects the optimal route which has least cost. If the new discovered route has a lower cost than the existing least cost route, the node replace the new discovered route as its best route to the sink. In this case, the sender of packet is chosen as the next hop node. As the routing strategy is hop by hop, so each node only stores information about its next hops.

4. To determine the distance between sender and receiver, the signal strength of received packet is measured. This value is stored in the signal strength field of the routing table. Using the signal strength, the distance between two nodes could be determined. Furthermore, using the distance, the transmission delay between two nodes is obtained. The end to end delay is determined using the transmission delay.
5. If in steps 2, 3 and 4 any changes occur in the values of node properties, the node should send a Route Discover packet to its neighbors containing the new value of the parameters.

In the proposed algorithm, each node receives Route-Discover packet from all its neighbors. It selects the lowest neighbor's ID as its ID. When all nodes send the Route-Discover packets, the value of best cost route field in their routing table is set to the value of least cost route. At the end of route discovery phase, each node knows the cost of sending data from itself to the sink node.

To make Route Discovery phase more clear an example is given in the following. Consider a wireless sensor network with a random topology. Suppose that there is a unique sink node in the network. The sink node as the initiator of this phase sends Route Discover packet to all its neighbors. The sink ID field in these packets is set to zero; therefore as describe above, the value of ID for all neighbors will be equal to 1. In figure 2, the node ID of all 3 sink's neighbors will be set to 1. For each neighbor, the cost of route between it and sink node depends on its distance to sink.

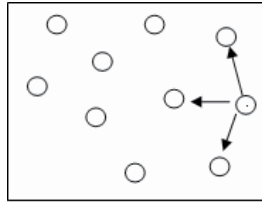


Fig. 2. Sink as the initiator node of route discovery phase, sends first packets

As shown in figure 3.a, suppose that the upper neighbor of sink receives the Route Discover packet. The node obtains its ID from received packet ID and then sends the Route Discover packet to its neighbors. As the next hop for this node is the sink node, so the value of route cost field in the Route Discover packet is equal to the cost between it and the sink node. As the Route Discover packets are broadcast to all neighbors, so the sink node will also receive this packet from its upper neighbor, but as the sender ID of the received packet is bigger than the sink's ID, the sink node doesn't process the received Route Discover packet. Now consider the Square node shown in figure 3.b. When it broadcasts Route Discover packet to its neighbors, the Diamond node will receive this packet.

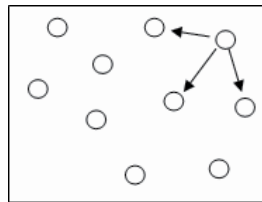


Fig. 3.a. The upper node sends Route Discover packet to its neighbors

In figure 3.b the diamond node has already received the Route Discover packet from the Triangle node. So its current ID is equal to 2. For the Diamond node, the next hop node in the least cost route toward sink is the Triangle node. So when Diamond node receives the Route Discovery packet from the Square node, its ID doesn't change. But the least cost route between Diamond node and sink node may be changed. The cost of route between Diamond node and sink node is equal to the sum of cost between Diamond node to Square node and Square node to sink node.

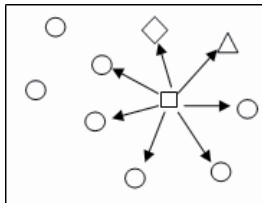


Fig. 3.b. The Square node sends Route Discover packet to its neighbors

If cost of route from Square node is less than that of Triangle node, the least cost route and next hop node of Diamond node will be changed. Note that in the Route Discovery phase the cost of routes is propagated between all nodes using Route Discover packets. This procedure is continued while all the nodes obtain their least cost route.

3.2. Data Transmission Phase

When a node detected an event, it should send data related to that event to the sink. As mentioned before, the routes are established in the route discovery phase. All nodes know their least cost route to the sink. So, using the optimal path the node will be able to send its data to the sink. Each node knows its next hop node in its least cost route. When a node detected an event or received any data, it sends them to the sink node via its next hop node.

3.3. Route Recovery Phase

This phase is executed periodically. The length of time periods depends on the node's mobility. If a node dies, it will never participate in the routing procedure in the next period. Therefore, the dead nodes are not belonging to any established route. If the next hop node is failed, the data are sent using a backup node. All nodes in the network know the cost of forwarding information through their neighbors. When the least cost route is failed then the node forwards data using the second least cost route. As the information about all the possible routes from a node to sink is stored in the node routing table, so it is easy to find the first and second least cost routes. When the reminding energy of a node is less than a predetermined threshold, it will inform this situation to all its neighbors. If a node realizes that its next hope node doesn't have any sufficient energy, it uses its second least cost route to send its data

4. Proposed Neighbour Discovery Phase

In this section, we explain the operation of proposed neighbor discovery phase. Most of routing algorithms need to send data to a specific neighbor. In essence, wireless links are broadcast links which means, when a node sends a packet, all the nodes placed in its communication range will receive it. In this situation, every node needs a mechanism that makes it enable to send data to a particular neighbor so that the other neighbors wouldn't process those data.

All energy aware routing protocols need neighbor discovery mechanism. Proposed approach uses a hop by hop routing algorithm; route to the sink is selected by each node via choosing next hop, meanwhile different routes are picked out by considering different next hop nodes. Most of routing algorithms use hop by hop strategy which is more efficient. All nodes which use hop by hop routing algorithm need information only about their next hop, which means they just need local information. When an algorithm needs to have a global view of the entire network, it absolutely must pay much more in contrast with the situation with only local view. Neighbor discovery algorithms collect local information about node's neighbors. To distinguish nodes from each other, we can assign a unique identifier to each node. This identifier makes enable the other nodes to select one node uniquely. By considering this deployment, all the node neighbors will receive the data, but only one node that is identified by the packet destination identifier field will process data. The node's identifier could be local or global. When a node's identifier is global, the node could be identified by the other nodes uniquely. But as we mentioned before, this type of identifying is too expensive. When a node uses local identifier, it can only distinguish its neighbors. As the proposed algorithm needs network's nodes to distinguish their neighbors uniquely, so it doesn't need global identifier and the local identifier is sufficient. In the following, we propose a new neighbor discovery mechanism for distinguishing node's neighbors.

In the proposed neighbor discovery mechanism, each node estimates its distance to the sender using received signal strength. This parameter can be used for distinguishing node's neighbors. In the route discovery phase many packets are transmitted between nodes. Using the signal strength of these packets, the receiver can estimate its distance to the sender node. Therefore at the end of route discovery phase all nodes know their distance to their neighbors. As discussed in section 3, in the route discovery phase an ID is assigned to each node. This ID is not unique in the entire network. The nodes with equal ID have the same number of hops to the sink. The proposed neighbor discovery algorithm uses both node ID and received signal strength to distinguish neighbors with a suitable accuracy rate. We believe that by using the distance between two nodes and the node ID, we can distinguish the neighbors with a high accuracy. If by using these two parameters, the node couldn't distinguish all its neighbors, this means that more than some of its neighbors have the same distance and ID. In this case, the proposed mechanism uses a random number to discern them.

When a node detects a collision, this means that it has more than one neighbor with the same distance and ID. It sends a Collision Recovery packet to the neighbors. In this packet the sending node advertises that only the nodes which detected any collision should process it and the other neighbors should ignore it. When the nodes which detected collision receive this packet, they create a random number between 0 and MAX (usually MAX is a big number, e.g., 100000) and send it for the node that has sent the Collision Recovery packet, using Collision Recovery Reply packet. Both sender and receiver, store this random number in their routing table in an appropriate record. This random number makes distinguishing action complete. By using distance (signal strength), ID and if needed the random number, it is possible to distinguish neighbors from each other. When a node wants to send a packet to one of its neighbors, it should use all of 3 mentioned parameters in the packet. All neighbors receive the packet, but only the neighbor which can find a match and has the same properties will process the packet and the other nodes will ignore it. To evaluate the performance of the proposed neighbor discovery phase, we implemented it in a simulator. Table 1, shows the simulations results. As mentioned before, the collision is only occurred when a node has more than one neighbor with the same distance and ID.

Simulation trials	Area (square)	Number of nodes	Communication range (m)	Number of detected collision
1	50*50	200	5	0
2	100*100	200	5	0
3	100*100	500	5	2
4	500*500	1000	20	23
5	10*10	100	1	12

Table 1. Number of collision occurred in different experiments.

The results shown in table 1, confirm that by increasing the density of nodes in the network, the probability of collision is also increased. We should emphasis here that, by using the third parameter (random number) as explained earlier, the distinguishing rate may be reach to 100%. When the mechanism uses the first two parameters (node ID and signal strength) the overhead is always zero, but when the third parameters is applied, only 2 packets should be transmitted in the network, that can be disregarded relative to number of packets transmitted in other phases.

5. Simulation Results

In this section, using computer simulation, we evaluate the performance of the proposed energy aware routing protocol with that of SPEED protocol. Before evaluating the performance, we describe the environment of our simulation. After that we analyze the simulation results and compare the performance of the proposed protocol with that of SPEED protocol.

5.1. Simulation Environment

We developed a simulation software using C++ language. To compare the performance of both protocols, we implemented the proposed protocol as well as the SPEED protocol in our simulation software. The simulated network topology consists of 100 fixed sensor nodes which are randomly deployed in a $200m \times 200m$ area. Each node is able to send data in a range of 40m. There is one sink node at point (0, 0). The location of sink node can be changed in many scenarios. We consider many different scenarios to evaluate different aspect of the proposed algorithm.

5.2. Results Analyze

In figure 4, for both proposed algorithm and SPEED algorithm, the average energy consumption of all nodes is plotted versus number of events. Less energy consumption means longer lifetime for the network. Horizontal axis shows the number of events which are occurred in the network terrain. Events are occurred in a random place in the network. Vertical axis shows the average energy consumption of the network nodes. The scale of vertical axis is $0.00005 J$. Based on results shown in figure 4, it is obviously observable that the average energy consumption of the network nodes in the proposed protocol is less than that of SPEED protocol. When the number of events is less than 200, the energy consumption of two protocols is nearly equal. But when number of events is more than 200, the proposed protocol consumes less energy than SPEED. It is necessary to note here that the main goal of proposed algorithm is to decrease energy consumption.

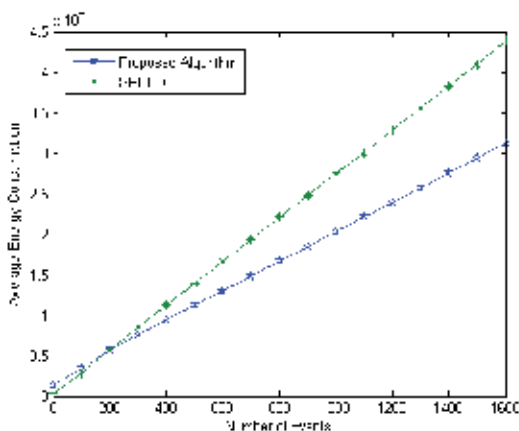


Fig. 4. The comparison of average energy consumption between two protocols, number of nodes =100.

In the next trial, we increased the number of nodes to 200. The results are shown in figure 5. As shown in this figure, when the number of events is less than 500, the average energy consumption of the SPEED protocol is less than the proposed protocol. Note that the proposed protocol uses a proactive routing algorithm; it means that the routes are established in advance before data transmission. So, when the number of events is low, the average energy consumption of the proposed protocol is more than SPEED.

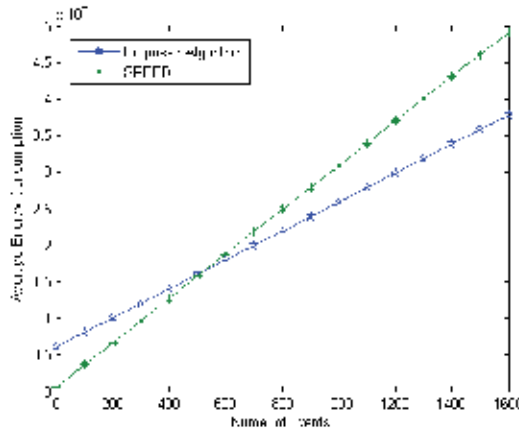


Fig. 5. The comparison of average energy consumption between two protocols, number of nodes =200.

In figure 6, for a network with different amount of nodes, the energy consumption of two protocols is shown. Horizontal axis shows the amount of network nodes and the vertical axis shows total network energy consumption.

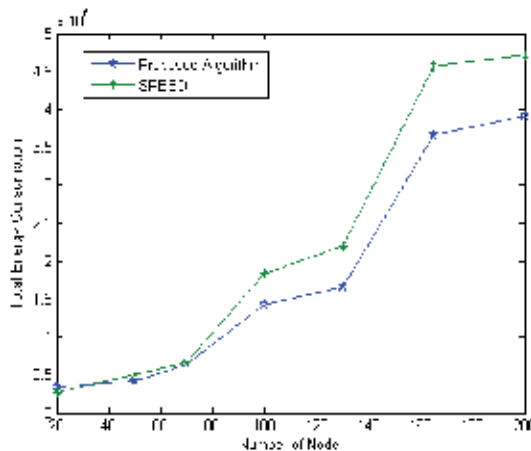


Fig. 6. The total network energy consumption for different amount of network nodes.

Total network energy consumption is calculated as the sum of energy consumption in all network nodes. It could be seen in figure 6 that for different number of nodes, the total

energy consumption of the proposed protocol is less than SPEED. Furthermore, it is obviously observable that by increasing the number of nodes, the performance of proposed protocol is also increased. In figure 7, for both two protocols, the number of dead nodes is plotted versus the number of events. If the energy of a node is finished, it will be dead. When a wireless sensor network has high number of alive nodes, it will live longer. Note that a wireless sensor network with higher number of nodes can perform its functions better. Figure 7 shows that the number of dead nodes in the proposed protocol is always less than SPEED.

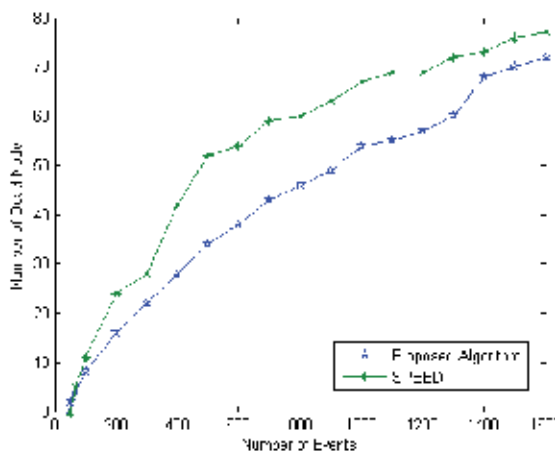


Fig. 7. Comparing the number of dead nodes between two protocols

Based on results shown in figures 4-7, it is clear that the proposed protocol has better performance in comparison with the traditional SPEED protocol. Simulation results show that the average energy consumption of the proposed protocol is lower than that of SPEED protocol. In the next simulation trials, we evaluate the delay performance of the proposed protocol. As we mentioned earlier, by decreasing the transmission delay, it is possible to decrease the end to end delay. Figure 8 shows the simulation results related to delay performance of both protocols. Results show that the path traversed by packet using proposed protocol has less delay than that of SPEED protocol. Horizontal axis illustrates the place where the event has occurred. Note that events occur in points with equal width and length. For example, number 200 in horizontal axis means that the event has occurred at point (200,200). The vertical axis shows the path delay which is related to the length of the route that a packet traverses between source node to the sink. As the queuing delay is negligible, we ignore it. Results shown in figure 8 clear that the end to end delay of the proposed protocol is less than that of SPEED protocol. Figure 9 shows the end to end delay, in the case that the number of nodes in network has been increased to 200 nodes. Based on results shown in figures 8,9, it is clear that the proposed protocol has lower delay than the SPEED protocol so it is more suitable for real time applications. As discussed in section 1, two main objectives of the proposed protocol are to minimize energy consumption and to choose a route with minimum end to end delay. The simulation results show that the proposed protocol has achieved to both of its goals.

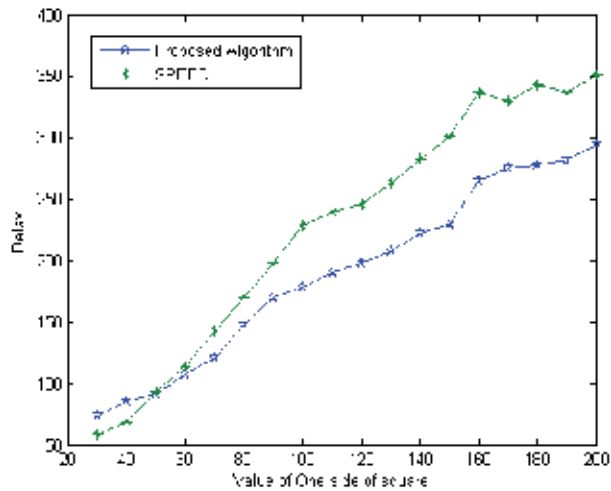


Fig. 8. End to end delay between source and sink, number of nodes=100

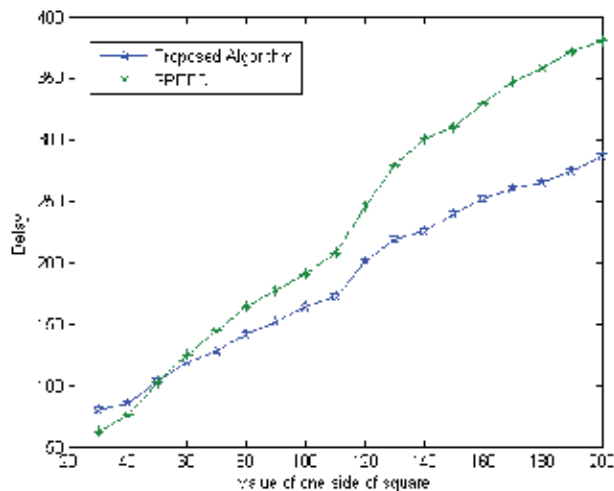


Fig. 9. End to end delay between source and sink, number of nodes=200

5.3. Real Time Traffics

To make the proposed routing protocol more scalable and more suitable for real time traffics, we used the clustering techniques. In this case, the network is divided to some clusters. For this purpose, sensor nodes are grouped into clusters by using one of the clustering techniques (Abbasi & Younis, 2007). Sensor nodes are only responsible for probing the environment to detect an event. Every cluster has a cluster head that manages the other members in the cluster. Clusters can be formed based on many criteria such as communication range, number and type of sensors and geographical location. We assume that all nodes are stationary and the cluster head is located within the communication range of all the cluster members. The Routing in Hierarchical routing protocols is divided into two

parts. First, routing between cluster members and cluster head. And second, routing between cluster heads and the sink. In this section we emphasis on first routing type. To forward traffic toward sink node, each cluster head should be able to route data to other cluster heads. The cluster head is responsible to find best route for all its members in terms of energy consumption and the end to-end delay requirement. We consider two types of traffics: real time and non-real time. Real time traffics have hard constraint on the value of end to end delay while non real time traffics don't have any specific delay constraint. Both real-time and non-real-time traffic coexist in the network. As delay constraints are associated only with real-time data, the cluster head is responsible to find the best path for this kind of traffics so that the end to end delay requirement are meet for real-time traffics. Each sensor node uses different queues for the two different types of traffic. Furthermore, each node has a classifier, which checks the type of the incoming packet and sends it to the appropriate queue. There is also a scheduler, which determines the order of packets to be transmitted from the queues. The cluster heads use the proposed cost function to find the best path which not only can meet the delay requirement but also consumes the minimum energy. We use a modified version of Djikstra routing algorithm. The cluster head is responsible to find the best route for all of its members. It will select the more suitable route that has enough resources for transmitting real time traffic from nominee routes with lowest energy consumption based on modified Djikstra algorithm.. After finding the best route, the cluster head sends the routing information to all of its members. So, each sensor node in each cluster knows the best path between itself and its cluster head for transmitting real time traffic. The cluster heads use an existing routing algorithm to transmit traffic toward the sink node. Non real time traffics are sent using Gossiping algorithm (Haas et al, 2006). In the simulation, we set the size of each cluster to $40m \times 40m$. Each cluster consists of some nodes. In figures 10(a,b,c), for both SPEED and the proposed protocols and for a cluster with 20 nodes, the average energy consumption, the energy consumption per node and the end to end delay are given, In this experiment, real time traffic is produced in constant rate but production rate of non real time traffic is variable.. Figure 10(a) shows the average energy consumption versus number of events occurred in the cluster. It can be seen that the proposed routing protocol consumes less energy in comparison with the traditional SPEED protocol. In figure 10(b), the energy consumption of each node is given. In figure 10(c), the end to end delay of real time traffics are plotted versus different number of non real time packets. As it can be seen, for the proposed routing protocol, the increasing in non real time traffic density doesn't have any serious affect in the end to end delay performance of real time traffics. In the next simulation trial, we increased the number of sensor nodes in a cluster to 40 nodes and produced both real time and non real time traffic with variable rate. In figure 11(a,b,c), the results are shown. Based on results given in figures 10,11, it is clear that the proposed routing protocol has better delay and energy consumption performance than the existing SPEED protocol.

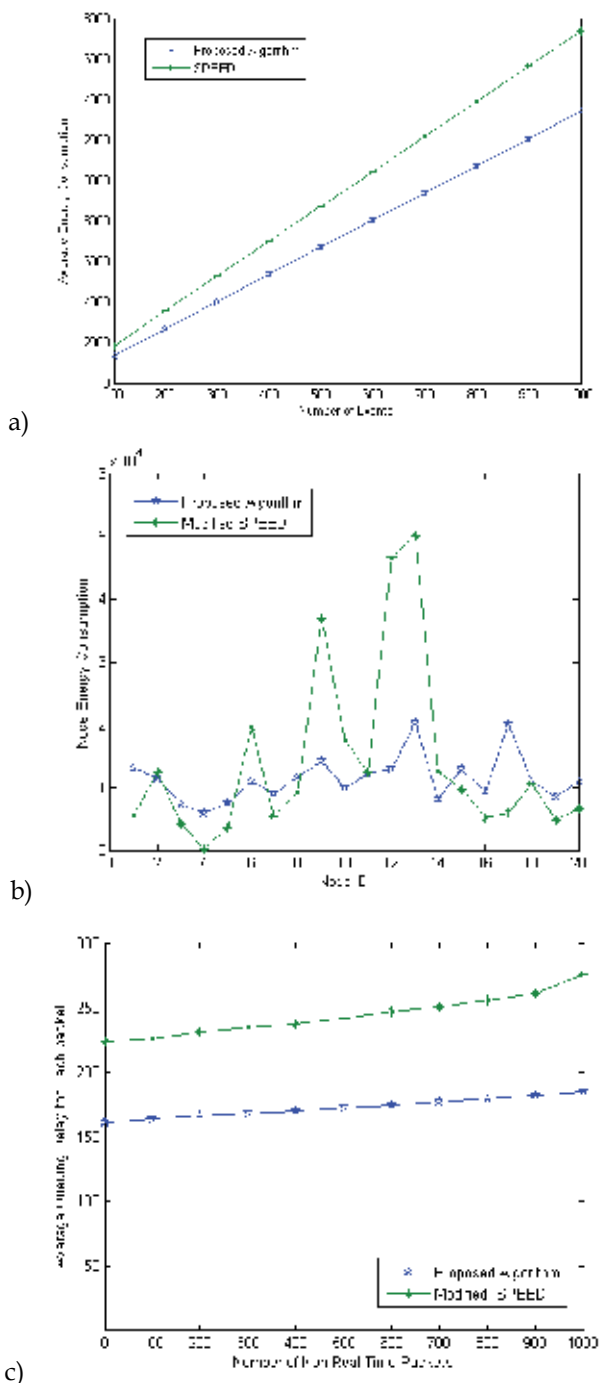


Fig. 10. Performance evaluation of two protocols for real time traffics: (a) average energy consumption, (b) energy consumption of each node and (c) end to end delay (number of nodes in cluster = 20 nodes)

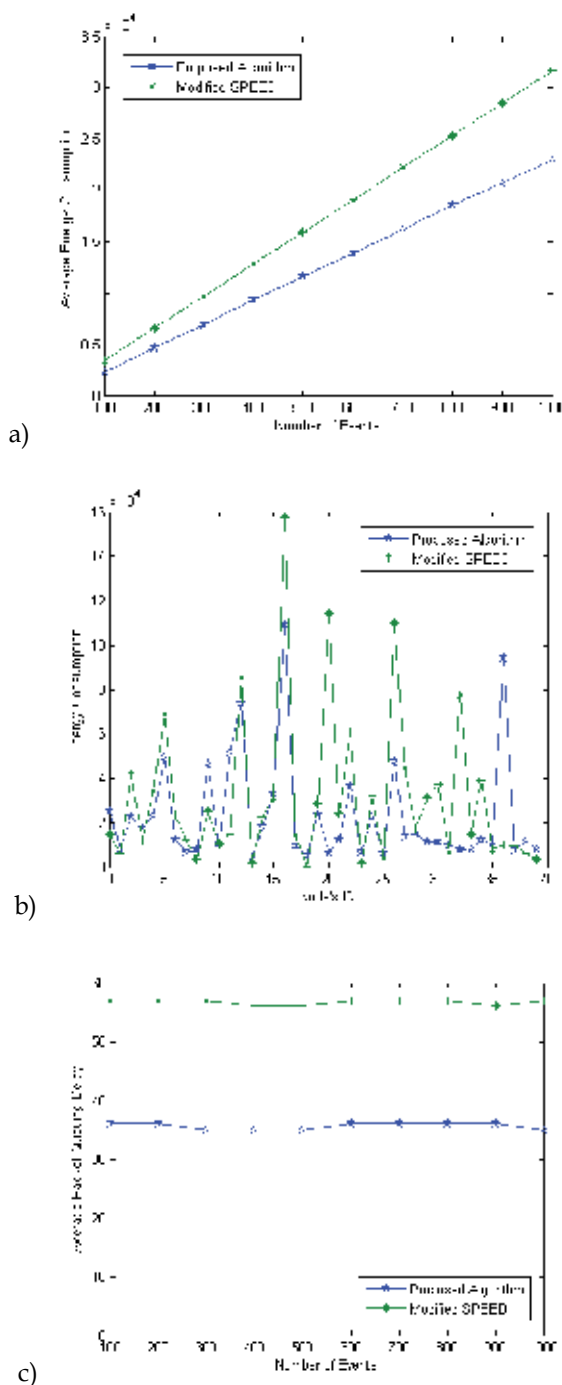


Fig. 11. Performance evaluation of two protocols for real time traffics: (a) average energy consumption, (b) energy consumption of each node and (c) end to end delay (number of nodes in cluster = 40 nodes)

6. Conclusion

Energy aware routing is most challenging issue in wireless sensor networks. Current research on routing of sensor data mostly focused on protocols that are energy aware to maximize the lifetime of the network, scalable for large number of sensor nodes and tolerant to sensor damage and battery exhaustion. In this paper an efficient energy aware routing protocol was proposed. The proposed routing protocol has two major goals which are low power consumption and low end to end delay. We evaluated the performance of the proposed protocol under different scenarios. Simulation results confirmed that the proposed protocol has more efficient energy consumption in comparison with the traditional SPEED protocol. Furthermore, the proposed routing protocol can find the optimal path with a low end to end delay. We believe that, by using data aggregation techniques the higher performance will be achievable. Also using other cost functions for route selection makes the proposed protocol suitable for other applications.

7. References

- Abbasi, A. A. & Younis, M. (2007). "A survey on clustering algorithms for wireless sensor networks", Volume 30, Issues 14-15, 15, Pages 2826-2841
- Akkaya, K. & Younis, M. (2003). "An Energy Aware QoS Routing Protocol for Wireless Sensor Networks.", ICDCS Workshop
- Akyildiz, I. F.; Su, W.; Sankarasubramaniam, W. & Cayirci, E. (2003). "A Survey On Sensor Networks.", IEEE Communication magazine, pp. 102-114.
- Haas, Z. J.; Halpern, J. Y & Li, L. (2006). "Gossip-based ad hoc routing". IEEE/ACM Transaction on Networking, 14(3):479-491
- Hassanein, H. & Jing L. (2006). "Reliable Energy Aware Routing In Wireless Sensor Networks", Second IEEE Workshop on Dependability and Security in Sensor Networks and Systems, 2006. DSSNS 2006., 24-28 April 2006 Page(s):54 - 64
- He, T.; Stankovic, J. A.; Lu, C. & Abdelzaher, T. (2003). "SPEED: A Stateless Protocol for Real Time Communication in Sensor Networks.", ICDCS
- Huifang C; Mineno, H.; Mizuno, T. (2006). "An Energy-Aware Routing Scheme with Node Relay Willingness in Wireless Sensor Networks", First International Conference Innovative Computing, Information and Control, 2006. ICICIC '06. Volume 1, 30-01 Aug. 2006 Page(s):397 - 400
- Intanagonwiwat, C.; Govindan, R. & Estrin, D. (2000). "Directed Diffusion: A scalable and robust communication paradigm for sensor networks.", Proceedings of the 16th Annual ACM/IEEE International Conference Mobile Computing and Networking, pp. 56-67
- Kidd, C. D.; Orr, R.; Abowd, G. D.; Atkeson, C. G.; Essa, I. A.; MacIntyre, B.; Mynatt, E. D.; Starner, T. & Newstetter, W. (1999). "The aware home: A living laboratory for ubiquitous computing research." In Cooperative Buildings, pages 191-198
- Mann, S. (1997). "Wearable computing: A first step toward personal imaging." IEEE Computer, 30(2):25-32
- Qiangfeng, Jiang, Manivannan, (2004) "Routing Protocols for Sensor Networks.", 1st IEEE Consumer Communications and Networking Conference, pp. 93-98

- Shin, K. Y.; Song, J.; Kim, J. W.; Yu, M. & Mah, P. S. (2007). " REAR: Reliable Energy Aware Routing Protocol for Wireless Sensor Networks", The 9th International Conference on Advanced Communication Technology, Volume 1, 12-14, Page(s):525 – 530
- Toscano, E.; Kaczynski, G. & Bello, L. L. (2007). "RTPAW: a Real Time Power Aware Framework for Wireless Sensor Networks.", WIP Proc, of the 13th IEEE Real Time and Embedded Technology and Applications Symposium, Bellevue, USA, April 2007, pp. 60-63
- Tubaishat, M. & Madria, S. (2003). "Sensor Networks: An Overview.", IEEE POTENTIALS April/May, pp20-23
- Vidhyapriya, R. & Vanathi, P. T. (2007). "Energy Aware Routing for Wireless Sensor Networks", Signal Processing, Communications and Networking, 2007. ICSCN '07. International Conference on 22-24, Page(s):545 – 550
- Wang, Y. H.; Hsu, C. P.; Lin, Y. C.; Kuo, C. S. & Ho, H. Y. (2007). "A Routing Method by Reactive Energy Decision in Wireless Sensor Networks.", 21st IEEE International Conference on Advanced Information Networking and Applications Workshops (AINAW'07)
- Younis, M.; Akkaya, K.; Eltoweissy, M. & Wadaa, A. (2004). "On Handling QoS Traffic in Wireless Sensor Networks.", Proceedings of the 37th Hawaii International Conference on System Sciences

Quality of Service Differentiation in WiMAX Networks

Pedro Neves¹, Susana Sargento², Francisco Fontes¹,
Thomas M. Bohnert³ and João Monteiro²

¹ *Portugal Telecom Inovação
Portugal*

² *University of Aveiro / Institute of Telecommunications
Portugal*

³ *SAP Research CEC Zurich
Switzerland*

1. Introduction

Broadband Wireless Access (BWA) based on the IEEE 802.16 standards [IEEE 802.16, 2004] [IEEE 802.16, 2005], also known as Worldwide Interoperability for Microwave Access (WiMAX), is gaining momentum as more and more field trials are transformed in commercial roll-outs. Very much likely, this is certainly a merit of the combined effort of the IEEE 802.16 standardization community, the WiMAX Forum [WiMAX Forum a, 2008] [WiMAX Forum b, 2008] and the research community. As of today, standards have matured, the WiMAX Forum has setup its certification program in order to foster interoperability, and the research community went through technological details up to an extent, such that many operators consider the risks associated with commercial deployment predictable.

Yet, WiMAX is still not deemed as globally established. This technology is very new and a competing system, namely Long-Term Evolution (LTE) [3GPP, 2009], is progressing in a similar pace. Which technology will finally make it through in the market, or will we have even several co-existing ones, is, among others, influenced by the research community. The better a technology is understood, the more likely it will be adopted by manufacturers, vendors and operators.

Key to scientific consideration is the availability of reliable simulation tools. This applies equally to WiMAX and any other technology and is embodied by an emerging business of commercial simulators like OPNET [OPNET] and Qualcomm [Qualcomm]. Unfortunately, these simulators are fairly expensive and/or their use is strictly licensed. As monetary considerations and openness frequently prevail, in particular in academia, NS-2 [NS-2], as open-source alternative, still retains its position.

Naturally, open-source software rarely approaches commercial standards, especially in terms of completeness and documentation. This is, for example, the case for the public available WiMAX module for NS-2. This module supports several WiMAX features but lacks a very essential one, Quality of Service (QoS) support. The lack of this feature

motivates the work presented in this chapter. This chapter describes a novel QoS framework for WiMAX with efficient service differentiation. The QoS framework is composed by a packet classification mechanism, as well as by a novel cross-layer scheduling algorithm based on user's prioritization and radio resources optimization [Monteiro, 2009].

Furthermore, in order to validate and evaluate the designed solution, a set of QoS oriented scenarios have been simulated in Network Simulator (NS-2) [NS2-NIST], demonstrating that the designed model is able to efficiently differentiate users in a competitive environment, differentiating between the traffic classes defined for WiMAX, mainly in throughput and delay metrics.

The reminder of this chapter is organized as follows. Section 2 briefly overviews WiMAX, focusing on the Medium Access Control (MAC) layer functionalities. Section 3 provides an overview about the WiMAX NS-2 module, focusing on its main features and limitations. Section 4 describes the proposed QoS model, including the packet classification mechanism and the scheduler, whereas Section 5 discusses the obtained simulation results for several scenarios. Finally, Section 6 concludes the chapter.

2. WiMAX High Level Description

Ubiquitous broadband Internet access is an important requirement to satisfy user demands and support a new set of real time services and applications. WiMAX, a Broadband Wireless Access (BWA) solution for Wireless Metropolitan Area Networks (WMAN), covering large distances with high throughputs, is a promising technology for Next Generation Networks. WiMAX supports both fixed and mobile users, based on IEEE 802.16-2004 [802.16, 2004] and IEEE 802.16e-2005 [802.16, 2005] standards, respectively. IEEE 802.16 system is connection oriented and provides Quality of Service (QoS) assurances through service flows and scheduling services. Therefore, all tasks are based on a connection, uniquely identified by a 16-bit Connection Identifier (CID), and no packets are allowed to traverse the wireless link without a specific connection allocated. A connection is, by definition, a unidirectional mapping between the WiMAX Base Station (BS) and the WiMAX Subscriber/Mobile Station (SS/MS) for transporting a service flow's traffic. Succinctly, scheduling services specify the policy used by the WiMAX BS and SS/MSs to manage the poll and grant procedures. Five scheduling services are defined to meet the QoS needs of the data flows carried over the air link:

- *Unsolicited Grant Service (UGS)*: designed for real-time service flows that generate fixed size data packets on a periodic basis, such as VoIP. The service offers fixed size unsolicited data grants (transmission opportunities) on a periodic basis. This eliminates the latency and overhead of requiring the SS/MS to send requests for transmission opportunities, and assures that grants are available to meet the flow's real-time needs;
- *real-time Polling Service (rtPS)*: designed for real-time service flows that generate variable size data packets on a periodic basis, such as video streaming. The service offers real-time, periodic, unicast request opportunities, which meet the flows real-time needs and allow the SS/MS to specify the size of the desired grant. In this case, the SS/MS is not allowed to use any contention request opportunities;

- *extended real-time Polling Service (ertPS)*: designed for real-time services that generate variable size data packets on a periodic basis, such as VoIP with silence suppression. This scheduling mechanism is based on UGS and rtPS. Unicast grants are provided to the MSs in an unsolicited manner, like in UGS, and therefore the latency of a bandwidth request message is saved. Instead of providing fixed allocations such as UGS, ertPS provides dynamics allocations;
- *non real-time Polling Service (nrtPS)*: designed for non-real-time service flows that require variable size data grants on a regular (but not strictly periodic) basis, such as high bandwidth File Transfer Protocol (FTP). The service offers unicast polls on a periodic basis but uses more space intervals than rtPS. This ensures that the flow receives request opportunities even during network congestion;
- *Best Effort (BE)*: designed for traffic where no throughput or delay guarantees are provided. The SS/MS sends requests for bandwidth in either random access slots or dedicated transmission opportunities. The occurrence of dedicated opportunities is subject to network load, and in contrast to the nrtPS, the SS/MS cannot rely on their presence.

A set of convergence sublayers are defined to map the upper layer packets into the 802.16-2004 system. The convergence sublayers support packet based protocols, such as Internet Protocol version 4 (IPv4) and Internet Protocol version 6 (IPv6), as well as cell based protocols, such as Asynchronous Transfer Mode (ATM). Both point-to-multipoint (PMP) and mesh modes of operation are supported by the standard, despite the mesh mode of operation is optional. During the WiMAX SS/MS network entry process, three pairs of management connections, with distinct QoS levels and hence reflecting three different QoS requirements, are established:

- Basic connection to transfer short, time-critical MAC management messages;
- Primary management connection to transfer longer, more delay tolerant management messages;
- Secondary management connection to transfer delay tolerant, standard-based management messages such as Dynamic Host Configuration Protocol (DHCP), Trivial File Transfer Protocol (TFTP) and Simple Network Management Protocol (SNMP).

Besides the aforementioned three pairs of management connections, a broadcast connection is configured by default and is used to transmit MAC management messages to all the SSs/MSs. Moreover, a multicast polling connection is used by the SSs/MSs to join multicast polling groups, allowing them to request bandwidth via polling. Finally, to satisfy the contracted services, transport connections are allocated for data packets.

With respect to the IEEE 802.16 protocol stack, it defines the Physical (PHY) and the Medium Access Control (MAC) layers. Internally, the MAC layer is divided in three sublayers: Service Specific Convergence Sublayer (CS), Common Part Sublayer (CPS) and Privacy Sublayer (PS). Figure 1 illustrates the IEEE 802.16 protocol stack, focusing on the MAC CS classification mechanism.

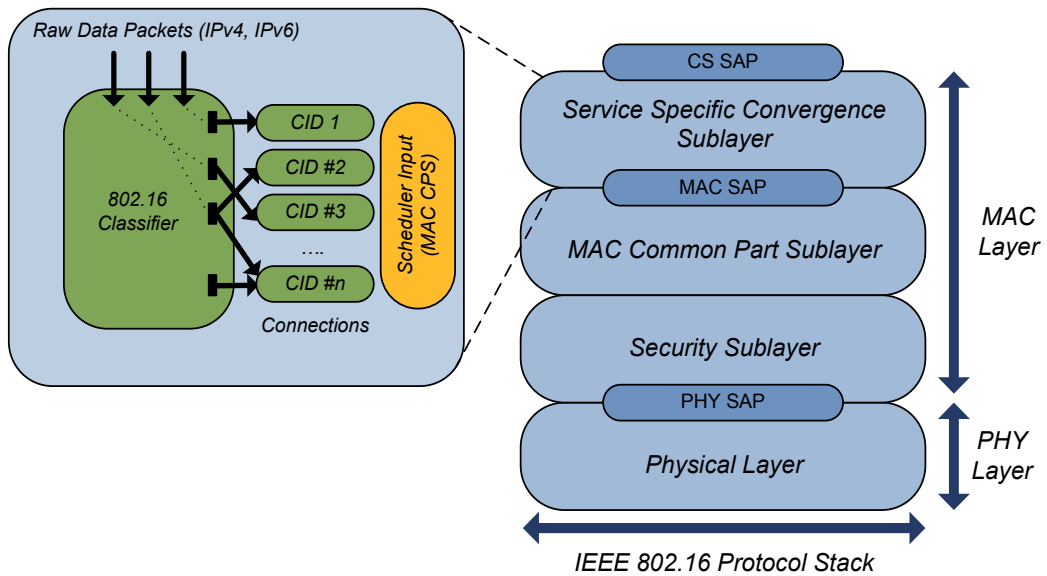


Fig. 1. IEEE 802.16 Protocol Stack

The interface between the 802.16 system and the upper layers from the protocol stack is provided by the CS, receiving the higher layer MAC Service Data Units (SDU) coming through the CS Service Access Point (SAP) and classifying them to the appropriate connection. The 802.16 classifier is a set of packet matching criteria applied to each packet. It consists of some protocol-specific fields, such as IP and MAC addresses, a classifier priority and a reference to a particular CID. Each connection has a specific service flow associated providing the necessary QoS requirements for that packet. If no classifier is found for a specific packet, a specific action must be taken. Since the classifier implementation is vendor dependent, the chosen decision depends on the algorithm implemented by the vendor – the packet can be discarded, sent on a default connection, or a new connection can be established for it, if enough resources are available. Downlink classifiers are applied by the WiMAX BS and uplink classifiers are applied by the WiMAX SS/MS. Two main types of CSs are defined within the standard for mapping services to and from the 802.16 system connections: the Packet Service Specific Convergence Sublayer (Packet CS) and the Asynchronous Transfer Mode Service Specific Convergence Sublayer (ATM CS). The Packet CS sublayer is defined for packet-based protocols, whereas the ATM CS is defined to support cell-based protocols.

The CPS is the second sublayer from the MAC layer. It receives classified packets arriving from the CS and is responsible for a set of functions, such as addressing, construction and transmission of the MAC PDUs, scheduling, bandwidth allocation, request mechanisms, contention resolution, among others. Finally, the PS is the third and last sublayer from the MAC layer and provides authentication, data encryption and security mechanisms.

Since the IEEE 802.16 standards are focused on defining the PHY and MAC layers for the air interface, the WiMAX Forum, in particular the Network Working Group (NWG), is specifying an “All-IP” end-to-end network architecture for IEEE 802.16 [WiMAX Forum a,

2008] [WiMAX Forum b, 2008]. The WiMAX Forum extends the IEEE 802.16 architecture by defining the Network Reference Model (NRM), which is a logical representation of the WiMAX network architecture, based on a set of functional entities and standardized interfaces, known as Reference Points (RPs) – R1 to R8. Using this model, multiple implementation options for a given functional entity are allowed, maintaining interoperability across them through the RPs. Three functional entities are defined: Connectivity Service Network (CSN), Access Service Network (ASN) and the Subscriber Station (SS)/Mobile Station (SS/MS). The WiMAX NRM is presented in Figure 2.

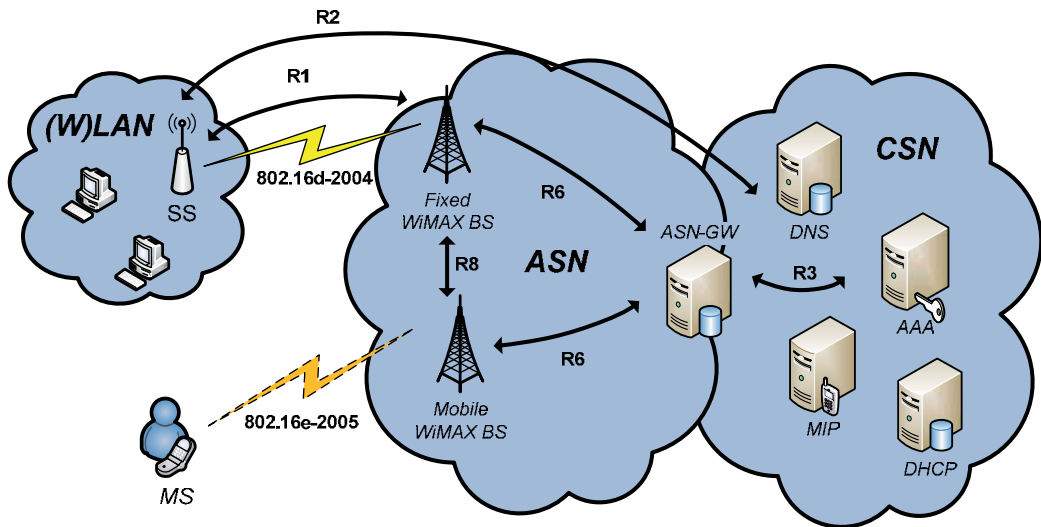


Fig. 2. WiMAX Network Reference Model

The SS and the MS are responsible for establishing radio connectivity with the WiMAX BS, for the fixed and mobile standards, respectively. The ASN is generally composed by several WiMAX BSs connected to one or more ASN-Gateways (ASN-GW); it establishes connectivity with the CSN. The ASN includes a set of functionalities in order to provide radio connectivity to WiMAX subscribers. Additionally, it also performs relay functions to the CSN in order to establish IP connectivity and authentication mechanisms. Finally, the CSN contains the DHCP, DNS, AAA (Authentication, Authorization, and Accounting) and MIP servers. Moreover, the CSN is responsible for establishing connectivity with the IP backbone.

After briefly describing WiMAX, the next section aims to depict the functionalities provided by default by the WiMAX QoS model implemented by the National Institute of Standards and Technology (NIST) [NS2-NIST] for the Network Simulator (NS2) [NS2].

3. NIST WiMAX QoS Model

The NS2 IEEE 802.16/WiMAX module [NS2-NIST] was developed by the NIST *Seamless and Secure Mobility Group* and henceforth the principal focus is on IEEE 802.16e/Mobile WiMAX.

Nevertheless, the overall architecture is set on top of a basic subset of IEEE 802.16-2004 [IEEE 802.16, 2004] and IEEE 802.16e-2005 [IEEE 802.16, 2005] common functionalities.

Out of the four specified physical (PHY) layers in the combined standard documents, a multi-carrier air interface using Orthogonal Frequency Division Multiplexing (OFDM) with 256 carriers was adopted, also known as WirelessMAN-OFDM, and Time Division Duplexing (TDD) was chosen as the duplexing technique. The 2 - 11 GHz licensed band provides lower transmission rates (75 Mbit/s) compared to the 10 - 66 GHz band, but it supports both Line-Of-Sight (LOS) and Non-Line-Of-Sight (NLOS) environments. Different modulations can be configured statically, such as Binary Phase Shift Keying (BPSK), Quadrature Phase Shift Keying (QPSK), 16-state Quadrature Amplitude Modulation (QAM) and 64-QAM, allowing the formation of varying robustness and efficient burst profiles. However, information coding is yet missing and hence the module does not support any Adaptive Modulation and Coding (AMC) scheme.

The TDD duplexing technique is illustrated in Figure 3, presenting both downlink and uplink subframes decomposition. The downlink subframe is composed by a Preamble used for synchronization, followed by the Frame Control Header (FCH). The FCH contains the Downlink MAP (DL-MAP) and Uplink MAP (UL-MAP) MAC management messages, indicating the location and burst profile of each downlink and uplink burst, respectively. Moreover, it contains the downlink and uplink channel descriptors (UCD and DCD management messages). Following the FCH, starts the downlink data bursts section. Downlink bursts are transmitted in order of decreasing robustness - QPSK followed by 16-QAM and finally 64-QAM. The WiMAX SSs/MSs listen to all the bursts that they are capable to decode, specifically bursts with profiles of equal or greater robustness compared with the one negotiated with the WiMAX BS during the connection setup phase. Thereafter the SS analyses the MAC header of each MAC Protocol Data Unit (PDU) inside each burst to check if the Connection Identifier (CID) belongs to it. At the end of the frame, the Transmit Transition Gap (TTG) is used to separate the downlink and the following uplink bursts. The TTG allows the WiMAX SS to switch from receive to transmit mode.

In the beginning of the uplink subframe there are two contention slots. The first contention slot is used by the WiMAX SSs/MSs for initial ranging (Initial Ranging), whereas the second contention slot is used by the WiMAX SSs/MSs to send bandwidth request PDUs to the BS (Request Contention). The remaining transmission slots are grouped by SSs/MSs. Each SS/MS has a specific slot allocated for uplink data transmission. The Subscriber Station Time Gap (SSTG) is a time interval used to separate the transmissions of the various SSs/MSs during the uplink subframe. Finally, the Receive Transition Gap (RTG) is used to separate the uplink and downlink bursts. The RTG allows the WiMAX SS/MS to switch from transmit to receive mode.

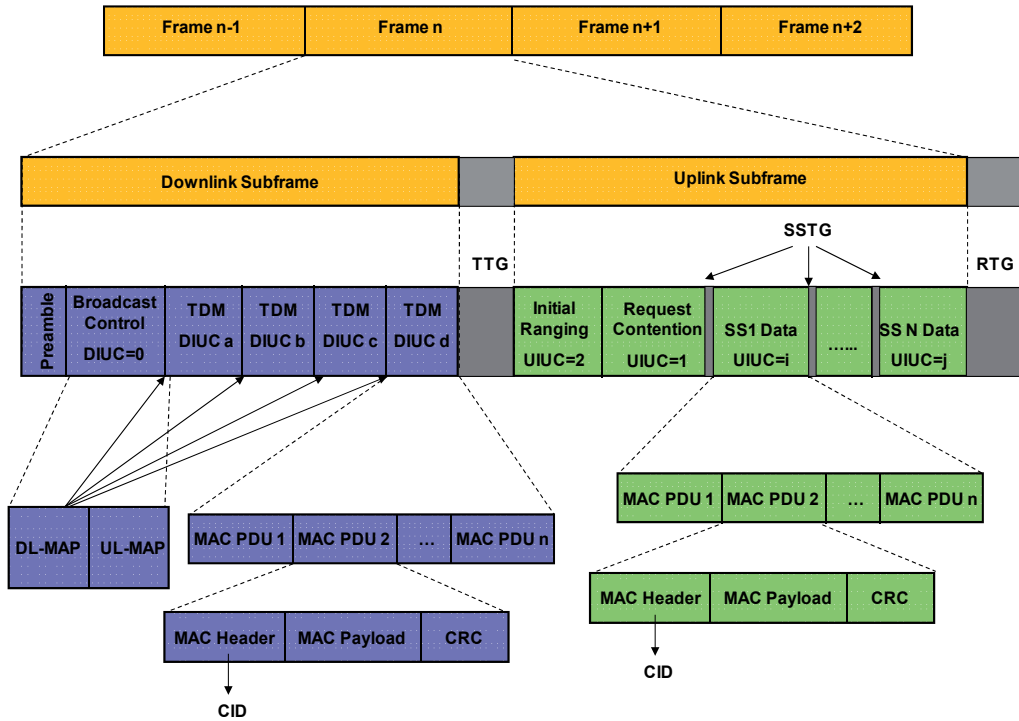


Fig. 3. WiMAX Frame Structure (Downlink and Uplink subframes)

The OFDM specific countermeasure to Inter Symbol Interference (ISI), the cyclic prefix, can also be configured, i.e. its length. Given these parameters, the module is able to compute the OFDM symbol duration, packet transmission time per modulation, maximum packet size per modulation and the number of OFDM symbols. As the implemented architecture is an extension of the NS-2 wireless networking sub-module, the standard NS-2 channel models and transmission power levels can be set accordingly to the NS-2 standard tools [NS2]. As for the PHY layer, the MAC layer supports only a subset of the IEEE 802.16 standard. For example, currently only the Packet Convergence Sublayer (Packet CS), as detailed in Section 2, is implemented. Although the module can be easily extended, the Packet CS is essentially a classifier, supporting the IP destination address as the classifier parameter. The connection oriented nature of IEEE 802.16 between MAC instances has also been implemented in the NIST model. As the IEEE 802.16 standard defines, each pair of WiMAX BS and SS establishes three management connections, Basic, Primary and Secondary. One of the drawbacks of the NIST implementation is that each MAC instance only supports one data transport connection. Additionally, out of Fragmentation, Packing and Automatic Repeat Request (ARQ), only the first, Fragmentation, is currently supported. With respect to mobility, channel scanning, communication parameters negotiation, initial ranging and registration, the provided implementation adheres largely to IEEE 802.16-2004 and IEEE 802.16e-2005 standards. Periodic ranging used to adjust coding and modulation is left out for now. Finally, the most crucial missing feature, which motivates this work, is the lack of a complete 802.16 compliant QoS model. The software has been prepared for future QoS integration but it was not implemented. Despite scheduling services, service flows and a

basic bandwidth request mechanism for BE (Best Effort) traffic is available, the current scheduler implements a simple Round-Robin discipline for the scheduler.

4. Proposed QoS Model

4.1 Packet Classification Mechanism

As defined in the 802.16 standard, packets received at the MAC layer, specifically at the Convergence Sublayer (CS), must be mapped to the correspondent Connection Identifier (CID), based on a set of packet matching criteria. In order to handle the incoming packets and the new QoS classes, we have modified the NIST CS module. Besides the existing connections (Basic, Primary, Secondary and Data connections), additional connections for UGS (Unsolicited Grant Service), rtPS (real time Polling Service), ertPS (extended real time Polling Service), nrtPS (non real time Polling Service) and BE (Best Effort) service classes have been established. The creation of these new connections required the addition of new CID ranges, providing each peer node a unique CID for these types of traffic.

To allow the creation of new connections between the WiMAX BS and the SSs/MSs, the *PeerNode* class in NIST was changed to have new members of type *Connection*, for receiving and sending packets of different traffic classes. These modifications were performed in the existing *DestClassifier* class. This new classifier is a subclass of the Service Data Unit Classifier (*SDUClassifier*) class, as shown in Figure 4. To improve the packet classification mechanism, the *QoSClassifier* class was implemented, also as a subclass of the *SDUClassifier* class.

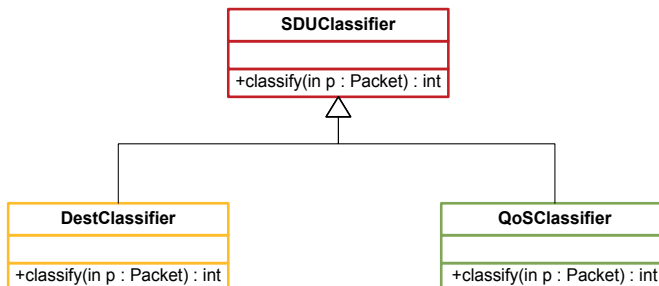


Fig. 4. Classifier Class Diagram

The most important method to implement the classification is the *classify()* method, called for all packets, which finds the appropriate *PeerNode* based on the destination address and QoS requirements. Thereafter, based on the packet type, the packet is sent to the appropriate connection queue on the scheduler, as illustrated in Figure 5. For example, if a broadcast packet is received on the BS classifier, a Broadcast CID is given; if the same packet is received on the SS/MS classifier, it will be classified with the Secondary Management CID. On the other hand, if a data packet arrives at the BS/SS classifier, it will be given a new transport CID and queue allocation correspondent to its traffic type.

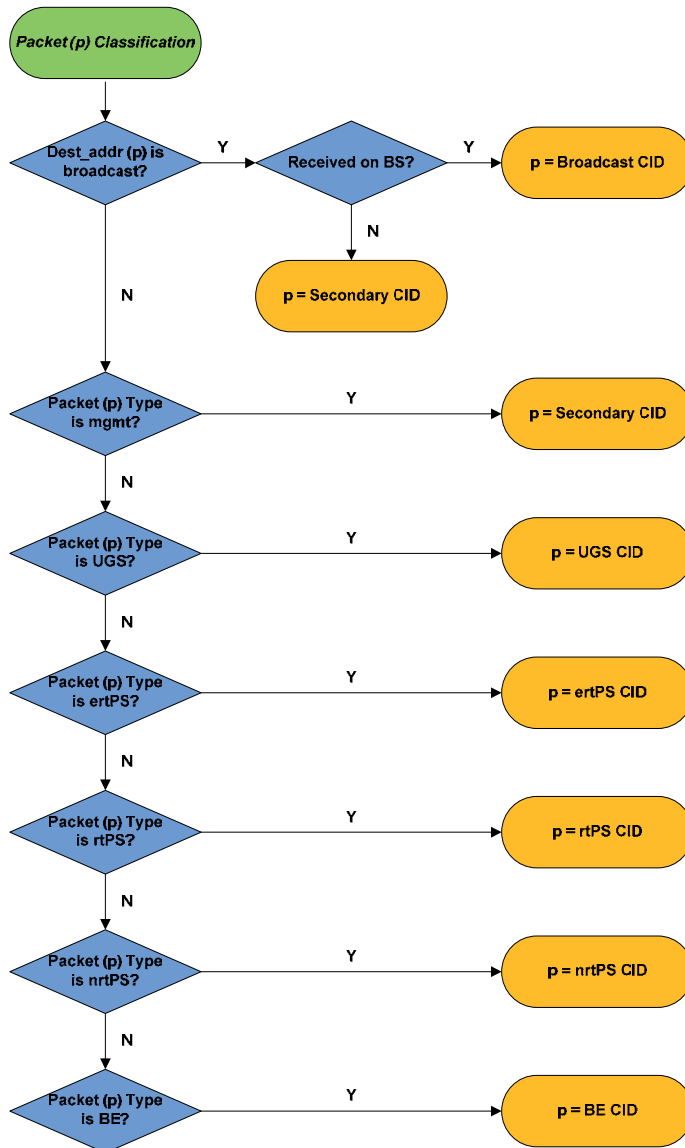


Fig. 5. Packet Classifier Diagram

Furthermore, new service classes were introduced in the model, as previously referred – UGS, ertPS, rtPS, nrtPS and BE. For each one of these service classes, a range of transport CIDs for the data connections was given. Apart from this association, modifications throughout the different functions that make use of the service classes were made. For instance, in the *Connection* function used by the WiMAX BS to initialize a new connection and assign the correspondent CID, the support for new connection types was added. In this case, a new type of connection is distinguished according to its type and respective CID.

4.2 Enhanced Scheduling Algorithm

The implemented BS scheduler enhances the simple Round Robin (RR) algorithm used in NS2-NIST/WiMAX module by adding a priority scheme – **priority Round Robin (PRR)**. Instead of equally distributing the available bandwidth between the registered SSs/MSs, the PRR scheduler prioritizes the most important service classes. Likewise, the SS/MS scheduler also uses a priority RR algorithm, distributing the available slots in the uplink direction. The proposed procedure is executed using a priority scheme to distinguish and transmit data packets in the following order of existing traffic type connections: UGS, ertPS, rtPS, nrtPS and BE. The new scheduler class – *QoSBSScheduler* – is also used as a subclass of the existing *BSScheduler*, as shown in Figure 6.

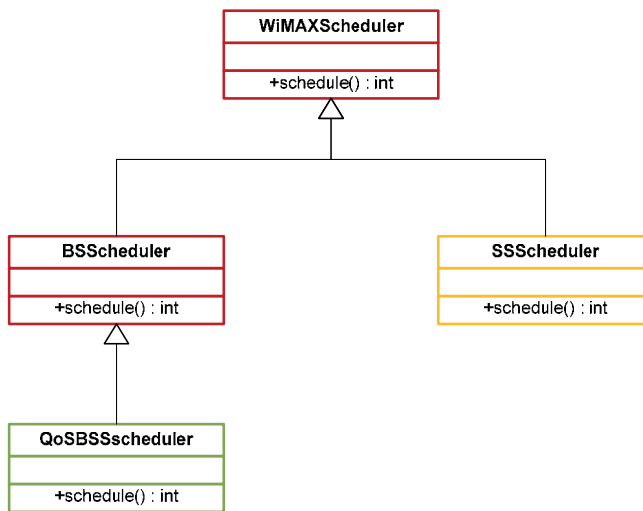


Fig. 6. Scheduler Class Diagram

5. Performance Evaluation

This section is devoted to the results and performance evaluation of the implemented QoS model. In order to evaluate the modifications to the existing NIST model, several simulation scenarios were implemented to test QoS using distinct network topologies. The obtained results use performance metrics, such as packet loss, latency, jitter and bandwidth usage, and also make use of differentiated traffic sources for each service class.

5.1 Simulation Scenario

The tested network topologies consider differentiated traffic going in the uplink direction from different hosts. Point-to-Point (PTP) and Point-to-Multipoint (PMP) scenarios, as illustrated in Figure 7, were considered. In the PTP case, four hosts directly connected to one WiMAX SS establish communication with the WiMAX BS, whereas in the PMP scenario, four WiMAX SSs communicate simultaneously with the WiMAX BS. Each host's traffic represents one connection flow in the uplink direction.

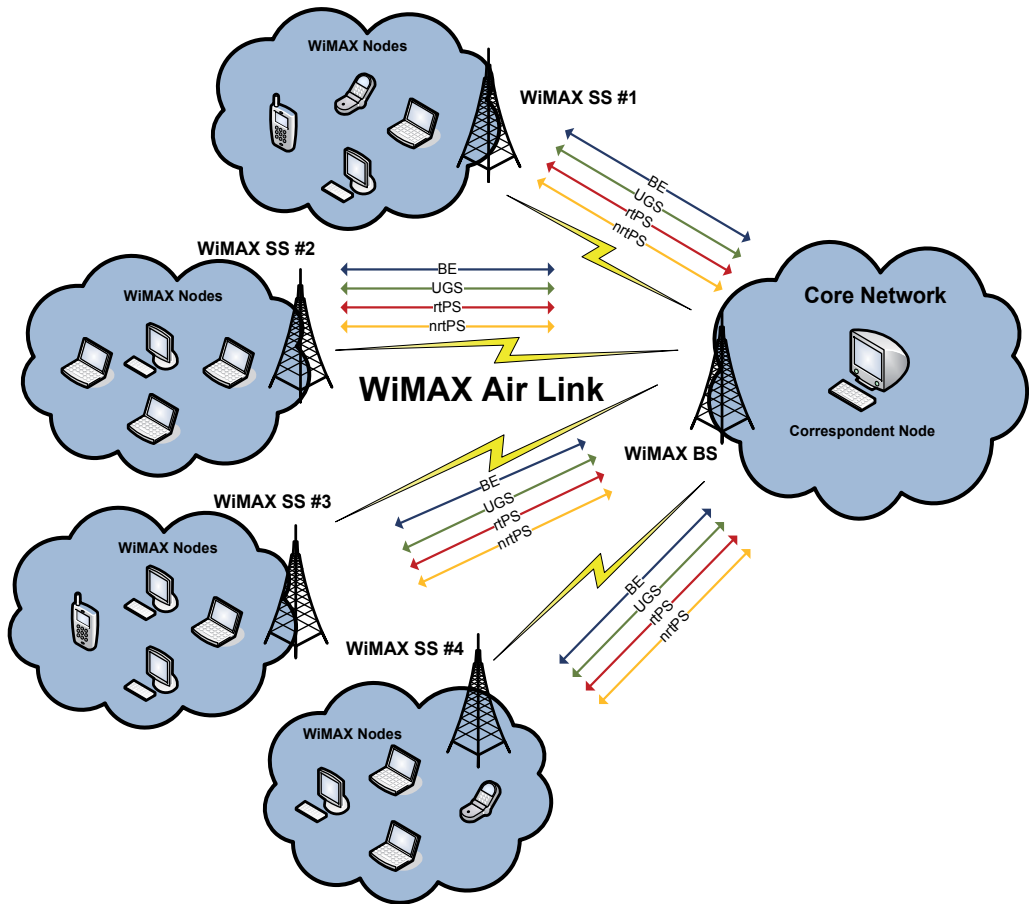


Fig. 7. Evaluation Scenario

In order to test the different network topologies, assuring differentiation between the different service classes, we defined and implemented new traffic sources. As an example, BE traffic generator contains a variable packet size and interval to emulate FTP/web traffic, and an UGS traffic generator contains a constant transmission rate. The different values adopted for these traffic generators are briefly presented in Table 1.

Service Class	Bitrate (Mbps)	Packet Size (Bytes)
BE	1	512 to 1024
UGS	1	300
rtPS	1	200 to 980
nrtPS	1	256 to 1024

Table 1. Service Classes Parameters

5.2 Simulation Results

Initial simulations made use of the PTP topology between the WiMAX BS and the WiMAX SS#1, presented in Figure 8, with four hosts connected to SS#1 and conveying differentiated traffic in the uplink direction. From this scenario we have also defined the WiMAX radio link parameters that would optimize the traffic transmission and subsequent simulation scenarios. The most important parameters are summarized in Table 2.

Modulation	Queue length	Bandwidth
64 QAM $\frac{3}{4}$	50 Packets	5 Mhz

Table 2. WiMAX Air Link Simulation Parameters

Initially, we tested a scenario in which four nodes, connected to each one of the WiMAX SSs, generate traffic competing for resources in the uplink direction. Each node has a traffic source dedicated to a specific WiMAX service class, specifically, UGS, rtPS, nrtPS and BE. The obtained throughput results are presented in Figure 8.

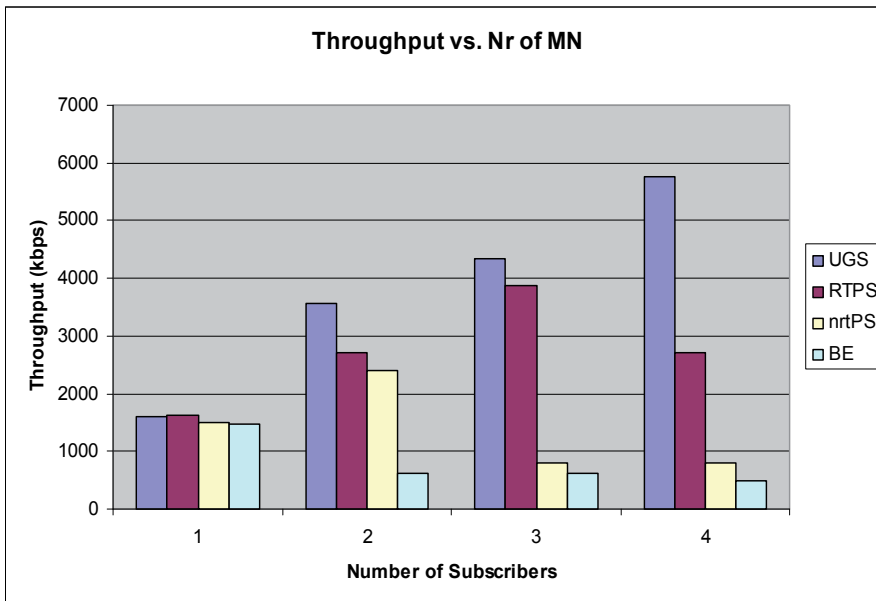


Fig. 8. Throughput vs. Number of WiMAX Subscribers Results

As depicted in Figure 8, the throughput values obtained for UGS services are quite satisfactory, with a reduced latency (Figure 9), jitter (Figure 10) and packet loss (Figure 11), when compared with the BE service. Therefore, packet differentiation is obtained, prioritizing the UGS related packets over the BE packets. Furthermore, one can see that with the increasing number of SSs, the obtained throughput is variable for each service class. Since the bandwidth is distributed into a higher number of WiMAX SSs, less bandwidth will be available for each one of them and, consequently, the less prioritized classes will be more degraded in terms of QoS.

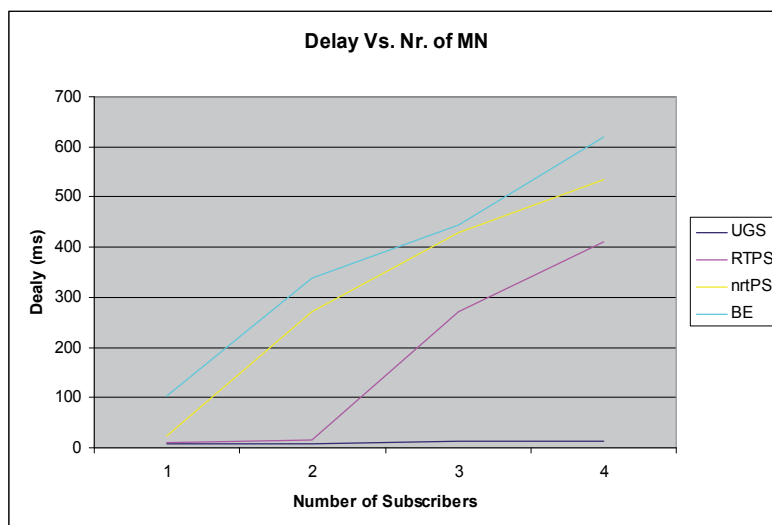


Fig. 9. Delay vs. Number of WiMAX Subscribers Results

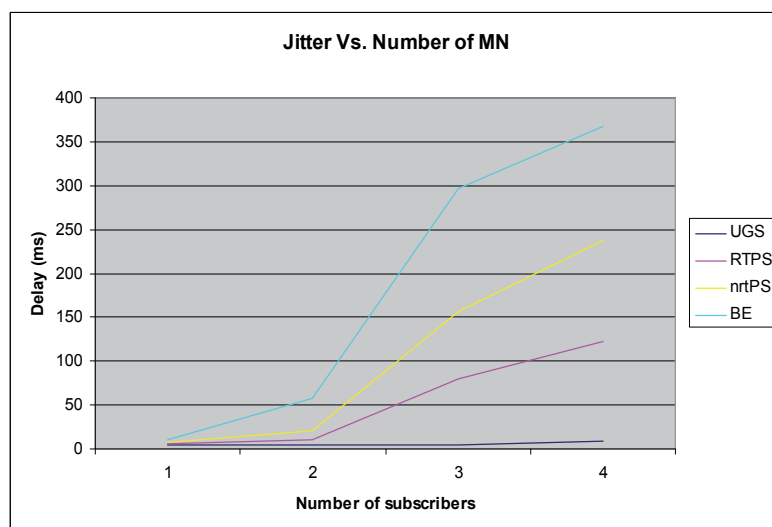


Fig. 10. Jitter vs. Number of WiMAX Subscribers Results

Analyzing the obtained results for the delay and jitter, presented in Figure 9 and Fig 10, respectively, it is visible that for the UGS traffic class these values always maintain reasonable and significantly very low values. Concerning the remaining traffic classes, with the increasing of subscribers, the delay and jitter values are, as expected, significantly affected.

With respect to the packet loss results, illustrated in Figure 11, the UGS service class remains almost unaffected, whereas the remaining service classes progressively drop more packets, due to the prioritization algorithm.

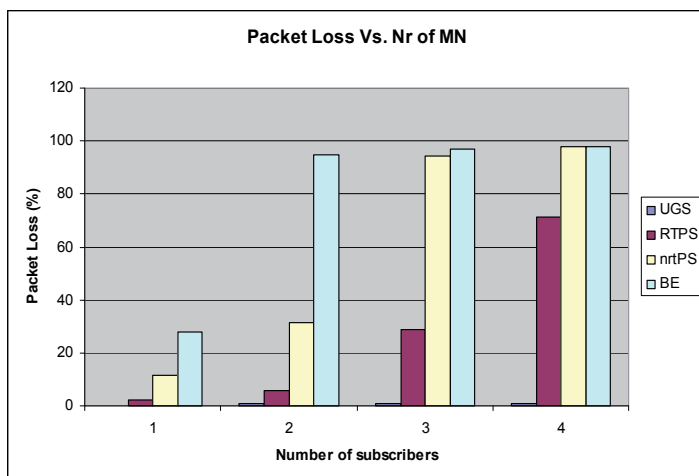


Fig. 11. Packet Loss vs. Number of WiMAX Subscribers Results

Finally, Figure 12 presents the bandwidth usage for each service class.

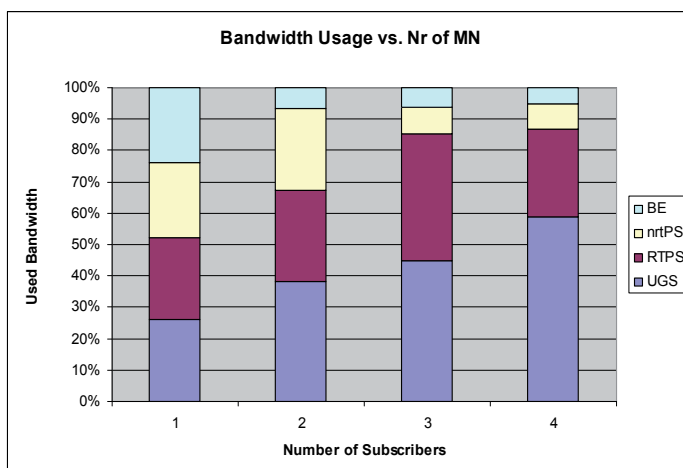


Fig. 12. Bandwidth Usage vs. Number of WiMAX Subscribers Results

It is visible a fair allocation of the available resources within each one of the service classes. When the number of WiMAX SSs increases, more bandwidth is allocated to the higher prioritized classes (e.g. UGS), avoiding starvation of the less prioritized classes (e.g. BE).

Summarizing, from the obtained results, one can see that the highest QoS demanding services achieve higher transmission throughput, penalizing the BE service. This differentiation is less visible for a single WiMAX SS, but increasing the number of WiMAX SSs, it is more clear the different treatment given to the packets that belong to different WiMAX scheduling services. This is explained by the fact that the BS has to distribute the available bandwidth between four SSs separately, leaving less available bandwidth for each one.

6. Conclusions

In this chapter we presented an enhancement for the NS2-NIST/WiMAX model in order to efficiently support QoS. Specifically, a packet classification mechanism and the associated scheduler, based on priority RR (PRR), have been designed, implemented and tested. Through the performance evaluation measurements with different topologies, point-to-point (PTP) and point-to-multipoint (PMP), it was possible to verify the differentiated behavior of the implemented WiMAX QoS classes. Based on the obtained results, we can conclude that there is a traffic differentiation visible by the different values obtained for the QoS parameters (latency, delay, bandwidth usage) in the test scenarios. Moreover, it was always assured a minimum transmission for all the service classes, although with different performances due to prioritization. The observed parameters degradation when using more subscribers is related to the priority RR implemented scheduler, in which less priority queues may not be served in the case of network overload or congestion.

7. References

- 3GPP, Evolved Universal Terrestrial Radio Access (E-UTRA) and Evolved Universal Terrestrial Radio Access Network (E-UTRAN) - Overall Description, TS 36.300, Stage 2, Release 9, Jun. 2009.
- IEEE 802.16, IEEE Standard for Local and Metropolitan Area Networks. Part 16: Air Interface for Fixed Broadband Wireless Access Systems, IEEE Std. 802.16-2004, Oct. 2004.
- IEEE 802.16, IEEE Standard for Local and Metropolitan Area Networks. Part 16: Air Interface for Fixed Broadband Wireless Access Systems. Amendment 2: Physical and Medium Access Control Layer for Combined Fixed and Mobile Operation in Licensed Bands, IEEE Std. 802.16e-2005, Dec. 2005.
- Monteiro J., Sargento S., Gomes A., Fontes F., Neves P., "IEEE 802.16 Packet Scheduling with Traffic Prioritization and Cross-Layer Optimization", The 1st International Conference on Mobile Lightweight Wireless Systems (MOBILIGHT), Athens, Greece, May 2009.
- NS2, <http://www.isi.edu/nsnam/ns/>
- NS2-NIST, <http://www.antd.nist.gov/seamlessandsecure/download.html>
- OPNET, <http://www.opnet.com>
- Qualcomm, <http://www.qualcomm.com>
- WiMAX Forum a, WiMAX End-to-End Network Systems Architecture Stage 2: Architecture Tenets, Reference Model and Reference Points, Release 1, Version 1.2, Jun. 2008.
- WiMAX Forum b, WiMAX End-to-End Network Systems Architecture Stage 3: Architecture Tenets, Reference Model and Reference Points, Release 1, Version 1.2, Jun. 2008.

Edited by Christos J Bouras

The main focus of the book is the advances in telecommunications modeling, policy, and technology. In particular, several chapters of the book deal with low-level network layers and present issues in optical communication technology and optical networks, including the deployment of optical hardware devices and the design of optical network architecture. Wireless networking is also covered, with a focus on WiFi and WiMAX technologies. The book also contains chapters that deal with transport issues, and namely protocols and policies for efficient and guaranteed transmission characteristics while transferring demanding data applications such as video. Finally, the book includes chapters that focus on the delivery of applications through common telecommunication channels such as the earth atmosphere. This book is useful for researchers working in the telecommunications field, in order to read a compact gathering of some of the latest efforts in related areas. It is also useful for educators that wish to get an up-to-date glimpse of telecommunications research and present it in an easily understandable and concise way. It is finally suitable for the engineers and other interested people that would benefit from an overview of ideas, experiments, algorithms and techniques that are presented throughout the book.

Photo by gintas77 / iStock

IntechOpen

